

Hobbs  
Roth

Intermediate Physics for Medicine and Biology

Russel K. Hobbie and Bradley J. Roth

Intended for advanced undergraduates and beginning graduate students in biophysics, biological physics, physiology, medical physics, cell biology, and biomedical engineering who have had prior course in physics and in calculus, this text bridges the gap between introductory physics and its application to the life sciences. Among the many topics treated in this wide-ranging book are forces in the skeletal system; fluid flow with examples from the circulatory system; the logistic equation; scaling; transport of neutral particles by diffusion and by solvent drag; membranes and various equipartition of energy in statistical mechanics; the chemical potential and free energy; biological magnets; beta, membrane and gated channels in membranes; nonlinear phenomena, including biological clocks and chaotic behavior; signal waves; detection of weak signals; radiological physics and the use of a tag in diagnosis and therapy; magnets; resonance imaging. The text includes many problems to test the student's understanding, and chapters include useful bibliographies for further reading. Its minimal prerequisites and wide coverage make it ideal for self-study, as well as a useful reference for workers in medical and biological research. The fourth edition will be updated throughout to reflect new developments; the discussion of theory will be more closely linked to experiment; a discussion of stochastic processes will be added; the discussions of anatomy and biology will be expanded.

Russel K. Hobbie • Bradley J. Roth

# Intermediate Physics for Medicine and Biology

*Fourth Edition*

Intermediate Physics for  
Medicine and Biology

Product



Springer.com

Fourth  
Edition



Springer

Intermediate Physics for Medicine and Biology  
Fourth Edition

Russell K. Hobbie  
Bradley J. Roth

# Intermediate Physics for Medicine and Biology

Fourth Edition

 Springer

Russell K. Hobbie  
Professor of Physics, Emeritus  
University of Minnesota  
Minneapolis, MN  
USA

Bradley J. Roth  
Oakland University  
Rochester, MI  
USA

Library of Congress Control Number: 2006938806

ISBN-10: 0-387-30942-X                      e-ISBN-10: 0-387-49885-0  
ISBN-13: 978-0-387-30942-2                e-ISBN-13: 978-0-387-49885-0

Printed on acid-free paper.

© 2007 Springer Science+Business Media, LLC

All rights reserved. This work may not be translated or copied in whole or in part without the written permission of the publisher (Springer Science+Business Media, LLC, 233 Spring Street, New York, NY 10013, USA), except for brief excerpts in connection with reviews or scholarly analysis. Use in connection with any form of information storage and retrieval, electronic adaptation, computer software, or by similar or dissimilar methodology now known or hereafter developed is forbidden.

The use in this publication of trade names, trademarks, service marks, and similar terms, even if they are not identified as such, is not to be taken as an expression of opinion as to whether or not they are subject to proprietary rights.

9 8 7 6 5 4 3 2 1

springer.com

# Intermediate Physics for Medicine and Biology

Russell K. Hobbie  
Professor of Physics, Emeritus  
University of Minnesota

Bradley J. Roth  
Associate Professor of Physics  
Oakland University

December 16, 2006

# Contents

<b>1</b>	<b>Mechanics</b>	<b>1</b>
1.1	Distances and Sizes . . . . .	1
1.2	Forces and Translational Equilibrium . . . . .	3
1.3	Rotational Equilibrium . . . . .	4
1.4	Vector Product . . . . .	5
1.5	Force in the Achilles Tendon . . . . .	6
1.6	Forces on the Hip . . . . .	7
1.7	The Use of a Cane . . . . .	9
1.8	Work . . . . .	10
1.9	Stress and Strain . . . . .	12
1.10	Shear . . . . .	13
1.11	Hydrostatics . . . . .	13
1.12	Buoyancy . . . . .	14
1.13	Compressibility . . . . .	15
1.14	Viscosity . . . . .	15
1.15	Viscous Flow in a Tube . . . . .	15
1.16	Pressure–Volume Work . . . . .	18
1.17	The Human Circulatory System . . . . .	19
1.18	Turbulent Flow and the Reynolds Number . . . . .	21
	Symbols Used . . . . .	23
	Problems . . . . .	24
	References . . . . .	29
<b>2</b>	<b>Exponential Growth and Decay</b>	<b>31</b>
2.1	Exponential Growth . . . . .	31
2.2	Exponential Decay . . . . .	33
2.3	Semilog Paper . . . . .	34
2.4	Variable Rates . . . . .	35
2.5	Clearance . . . . .	36
2.6	Multiple Decay Paths . . . . .	37
2.7	Decay Plus Input at a Constant Rate . . . . .	38
2.8	Decay with Multiple Half-Lives and Fitting Exponentials . . . . .	38
2.9	The Logistic Equation . . . . .	39
2.10	Log–log Plots, Power Laws, and Scaling . . . . .	39
	2.10.1 Log-log Plots and Power Laws . . . . .	39
	2.10.2 Food Consumption, Basal Metabolic Rate, and Scaling . . . . .	40

Symbols Used . . . . .	42
Problems . . . . .	42
References . . . . .	47
<b>3 Systems of Many Particles</b>	<b>49</b>
3.1 Gas Molecules in a Box . . . . .	50
3.2 Microstates and Macrostates . . . . .	51
3.3 The Energy of a System: The First Law of Thermodynamics . . . . .	53
3.4 Ensembles and the Basic Postulates . . . . .	54
3.5 Thermal Equilibrium . . . . .	56
3.6 Entropy . . . . .	58
3.7 The Boltzmann Factor . . . . .	58
3.8 The Nernst Equation . . . . .	59
3.9 The Pressure Variation in the Atmosphere . . . . .	60
3.10 Equipartition of Energy and Brownian Motion . . . . .	60
3.11 Heat Capacity . . . . .	61
3.12 Equilibrium When Particles Can Be Exchanged: The Chemical Potential . . . . .	61
3.13 Concentration Dependence of the Chemical Potential . . . . .	62
3.14 Systems That Can Exchange Volume . . . . .	63
3.15 Extensive Variables and Generalized Forces . . . . .	64
3.16 The General Thermodynamic Relationship . . . . .	64
3.17 The Gibbs Free Energy . . . . .	65
3.17.1 Gibbs Free Energy . . . . .	65
3.17.2 An Example: Chemical Reactions . . . . .	66
3.18 The Chemical Potential of a Solution . . . . .	67
3.19 Transformation of Randomness to Order . . . . .	69
Symbols Used . . . . .	70
Problems . . . . .	71
References . . . . .	79
<b>4 Transport in an Infinite Medium</b>	<b>81</b>
4.1 Flux, Fluence, and Continuity . . . . .	81
4.1.1 Definitions . . . . .	81
4.1.2 The Continuity Equation in One Dimension . . . . .	82
4.1.3 The Continuity Equation in Three Dimensions . . . . .	82
4.1.4 The Integral Form of the Continuity Equation . . . . .	83
4.1.5 The Differential Form of the Continuity Equation . . . . .	84
4.1.6 The Continuity Equation with a Chemical Reaction . . . . .	85
4.2 Drift or Solvent Drag . . . . .	85
4.3 Brownian Motion . . . . .	85
4.4 Motion in a Gas: Mean Free Path and Collision Time . . . . .	85
4.5 Motion in a Liquid . . . . .	86
4.6 Diffusion: Fick's First Law . . . . .	87
4.7 The Einstein Relationship Between Diffusion and Viscosity . . . . .	89
4.8 Fick's Second Law of Diffusion . . . . .	91
4.9 Time-Independent Solutions . . . . .	92
4.10 Example: Steady-State Diffusion to a Spherical Cell and End Effects . . . . .	94
4.10.1 Diffusion Through a Collection of Pores, Corrected . . . . .	95
4.10.2 Diffusion from a Sphere, Corrected . . . . .	95
4.10.3 How Many Pores Are Needed? . . . . .	96
4.10.4 Other Applications of the Model . . . . .	96
4.11 Example: A Spherical Cell Producing a Substance . . . . .	96
4.12 Drift and Diffusion in One Dimension . . . . .	98
4.13 A General Solution for the Particle Concentration as a Function of Time . . . . .	99
4.14 Diffusion as a Random Walk . . . . .	100
Symbols Used . . . . .	102
Problems . . . . .	102

References . . . . .	108
<b>5 Transport Through Neutral Membranes</b>	<b>111</b>
5.1 Membranes . . . . .	111
5.2 Osmotic Pressure in an Ideal Gas . . . . .	112
5.3 Osmotic Pressure in a Liquid . . . . .	114
5.4 Some Clinical Examples . . . . .	115
5.4.1 Edema Due to Heart Failure . . . . .	116
5.4.2 Nephrotic Syndrome, Liver Disease, and Ascites . . . . .	116
5.4.3 Edema of Inflammatory Reaction . . . . .	116
5.4.4 Headaches in Renal Dialysis . . . . .	116
5.4.5 Osmotic Diuresis . . . . .	116
5.4.6 Osmotic Fragility of Red Cells . . . . .	117
5.5 Volume Transport Through a Membrane . . . . .	117
5.6 Solute Transport Through a Membrane . . . . .	119
5.7 Example: The Artificial Kidney . . . . .	120
5.8 Countercurrent Transport . . . . .	121
5.9 A Continuum Model for Volume and Solute Transport in a Pore . . . . .	122
5.9.1 Volume Transport . . . . .	123
5.9.2 Solute Transport . . . . .	124
5.9.3 Summary . . . . .	127
5.9.4 Reflection Coefficient . . . . .	127
5.9.5 The Effect of Pore Walls on Diffusion . . . . .	128
5.9.6 Net Force on the Membrane . . . . .	128
Symbols Used . . . . .	129
Problems . . . . .	129
References . . . . .	133
<b>6 Impulses in Nerve and Muscle Cells</b>	<b>135</b>
6.1 Physiology of Nerve and Muscle Cells . . . . .	135
6.2 Coulomb's Law, Superposition, and the Electric Field . . . . .	137
6.3 Gauss's Law . . . . .	138
6.4 Potential Difference . . . . .	141
6.5 Conductors . . . . .	142
6.6 Capacitance . . . . .	143
6.7 Dielectrics . . . . .	143
6.8 Current and Ohm's Law . . . . .	145
6.9 The Application of Ohm's Law to Simple Circuits . . . . .	146
6.10 Charge Distribution in the Resting Nerve Cell . . . . .	148
6.11 The Cable Model for an Axon . . . . .	149
6.12 Electrotonus or Passive Spread . . . . .	153
6.13 The Hodgkin–Huxley Model for Membrane Current . . . . .	154
6.13.1 Voltage Clamp Experiments . . . . .	154
6.13.2 Potassium Conductance . . . . .	156
6.13.3 Sodium Conductance . . . . .	157
6.13.4 Leakage Current . . . . .	158
6.14 Voltage Changes in a Space-Clamped Axon . . . . .	158
6.15 Propagating Nerve Impulse . . . . .	159
6.16 Myelinated Fibers and Saltatory Conduction . . . . .	160
6.17 Membrane Capacitance . . . . .	163
6.18 Rhythmic Electrical Activity . . . . .	164
6.19 The Relationship Between Capacitance, Resistance, and Diffusion . . . . .	165
6.19.1 Capacitance and Resistance . . . . .	165
6.19.2 Capacitance and Diffusion . . . . .	165
Symbols Used . . . . .	167
Problems . . . . .	168
References . . . . .	175



<b>7</b>	<b>The Exterior Potential and the Electrocardiogram</b>	<b>177</b>
7.1	The Potential Outside a Long Cylindrical Axon . . . . .	177
7.2	The Exterior Potential is Small . . . . .	179
7.3	The Potential Far From the Axon . . . . .	180
7.4	The Exterior Potential for an Arbitrary Pulse . . . . .	181
7.5	Electrical Properties of the Heart . . . . .	184
7.6	The Current-Dipole Vector of the Heart as a Function of Time . . . . .	186
7.7	The Electrocardiographic Leads . . . . .	186
7.8	Some Electrocardiograms . . . . .	189
7.9	Refinements to the Model . . . . .	189
7.9.1	The Axon Has a Finite Radius . . . . .	190
7.9.2	Nonuniform Exterior Conductivity . . . . .	191
7.9.3	Anisotropic Conductivity: The Bidomain Model . . . . .	191
7.10	Electrical Stimulation . . . . .	192
7.11	The Electroencephalogram . . . . .	196
	Symbols Used . . . . .	196
	Problems . . . . .	197
	References . . . . .	201
<b>8</b>	<b>Biomagnetism</b>	<b>203</b>
8.1	The Magnetic Force on a Moving Charge . . . . .	203
8.2	The Magnetic Field of a Moving Charge or a Current . . . . .	205
8.2.1	The Divergence of the Magnetic Field Is Zero . . . . .	205
8.2.2	Ampere's Circuital Law . . . . .	205
8.2.3	The Biot-Savart Law . . . . .	206
8.2.4	The Displacement Current . . . . .	207
8.3	The Magnetic Field Around an Axon . . . . .	208
8.4	The Magnetocardiogram . . . . .	209
8.5	The Magnetoencephalogram . . . . .	211
8.6	Electromagnetic Induction . . . . .	213
8.7	Magnetic Stimulation . . . . .	214
8.8	Magnetic Materials and Biological Systems . . . . .	214
8.8.1	Magnetic Materials . . . . .	215
8.8.2	Measuring Magnetic Properties in People . . . . .	216
8.8.3	Magnetic Orientation . . . . .	217
8.9	Detection of Weak Magnetic Fields . . . . .	218
	Symbols Used . . . . .	219
	Problems . . . . .	220
	References . . . . .	224
<b>9</b>	<b>Electricity and Magnetism at the Cellular Level</b>	<b>227</b>
9.1	Donnan Equilibrium . . . . .	227
9.2	Potential Change at an Interface: The Gouy–Chapman Model . . . . .	229
9.3	Ions in Solution: The Debye–Hückel Model . . . . .	231
9.4	Saturation of the Dielectric . . . . .	233
9.5	Ion Movement in Solution: The Nernst–Planck Equation . . . . .	234
9.6	Zero Total Current in a Constant-Field Membrane: The Goldman Equations . . . . .	236
9.7	Membrane Channels . . . . .	238
9.8	Noise . . . . .	242
9.8.1	Shot Noise . . . . .	242
9.8.2	Johnson Noise . . . . .	242
9.9	Sensory Transducers . . . . .	243
9.10	Possible Effects of Weak External Electric and Magnetic Fields . . . . .	244
9.10.1	Introduction . . . . .	244
9.10.2	Effects of Strong Fields . . . . .	244
9.10.3	Fields in Homes are Weak . . . . .	244
9.10.4	Epidemiological Studies . . . . .	245

9.10.5	Laboratory Studies . . . . .	245
9.10.6	Reviews and Panel Reports . . . . .	245
9.10.7	Electric Fields in the Body . . . . .	246
9.10.8	Electric Fields in a Spherical Cell . . . . .	246
9.10.9	Electrical Interactions and Noise . . . . .	247
9.10.10	Magnetic Interactions and Noise . . . . .	247
	Symbols Used . . . . .	248
	Problems . . . . .	249
	References . . . . .	253
<b>10</b>	<b>Feedback and Control</b>	<b>255</b>
10.1	Steady-State Relationships Among Variables . . . . .	256
10.2	Determining the Operating Point . . . . .	257
10.3	Regulation of a Variable and Open-Loop Gain . . . . .	257
10.4	Approach to Equilibrium without Feedback . . . . .	259
10.5	Approach to Equilibrium in a Feedback Loop with One Time Constant . . . . .	259
10.6	A Feedback Loop with Two Time Constants . . . . .	262
10.7	Models Using Nonlinear Differential Equations . . . . .	263
10.7.1	Describing a Nonlinear System . . . . .	264
10.7.2	An Example of Phase Resetting: The Radial Isochron Clock . . . . .	265
10.7.3	Stopping an Oscillator . . . . .	268
10.8	Difference Equations and Chaotic Behavior . . . . .	268
10.8.1	The Logistic Map: Period Doubling and Deterministic Chaos . . . . .	269
10.8.2	The Bifurcation Diagram . . . . .	270
10.8.3	Quasiperiodicity . . . . .	271
10.9	A Feedback Loop with a Time Constant and a Fixed Delay . . . . .	272
10.10	Negative Feedback Loops: A Summary . . . . .	273
10.11	Additional Examples . . . . .	274
10.11.1	Cheyne–Stokes Respiration . . . . .	274
10.11.2	Hot Tubs and Heat Stroke . . . . .	274
10.11.3	Pupil Size . . . . .	274
10.11.4	Oscillating White-Blood-Cell Counts . . . . .	275
10.11.5	Waves in Excitable Media . . . . .	275
10.11.6	Period Doubling and Chaos in Heart Cells . . . . .	276
	Symbols Used . . . . .	277
	Problems . . . . .	277
	References . . . . .	283
<b>11</b>	<b>The Method of Least Squares and Signal Analysis</b>	<b>285</b>
11.1	The Method of Least Squares and Polynomial Regression . . . . .	285
11.1.1	The Simplest Example . . . . .	285
11.1.2	A Linear Fit . . . . .	286
11.1.3	A Polynomial Fit . . . . .	287
11.1.4	Variable Weighting . . . . .	288
11.2	Nonlinear Least Squares . . . . .	288
11.3	The Presence of Many Frequencies in a Periodic Function . . . . .	289
11.4	Fourier Series for Discrete Data . . . . .	290
11.4.1	Introducing the Fourier Series . . . . .	290
11.4.2	Equally Spaced Data Points Simplify the Equations . . . . .	290
11.4.3	The Standard Form for the Discrete Fourier Transform . . . . .	291
11.4.4	Complex Exponential Notation . . . . .	291
11.4.5	Example: The Square Wave . . . . .	292
11.4.6	Example: When the Sampling Time Is Not a Multiple of the Period of the Signal . . . . .	292
11.4.7	Example: Spontaneous Births . . . . .	293
11.4.8	Example: Photosynthesis in Plants . . . . .	294
11.4.9	Pitfalls of Discrete Sampling: Aliasing . . . . .	294
11.4.10	Fast Fourier Transform . . . . .	295

11.5	Fourier Series for a Periodic Function . . . . .	295
11.6	The Power Spectrum . . . . .	296
11.7	Correlation Functions . . . . .	298
11.7.1	Cross-Correlation of a Pulse . . . . .	298
11.7.2	Cross-Correlation of a Nonpulse Signal . . . . .	299
11.7.3	Cross-Correlation Example . . . . .	299
11.7.4	Autocorrelation . . . . .	299
11.7.5	Autocorrelation Examples . . . . .	299
11.8	The Autocorrelation Function and the Power Spectrum . . . . .	300
11.9	Nonperiodic Signals and Fourier Integrals . . . . .	301
11.9.1	Introduce Negative Frequencies and Make the Coefficients Half as Large . . . . .	301
11.9.2	Make the Period Infinite . . . . .	302
11.9.3	Complex Notation . . . . .	303
11.9.4	Example: The Exponential Pulse . . . . .	303
11.10	The Delta Function . . . . .	304
11.11	The Energy Spectrum of a Pulse and Parseval's Theorem . . . . .	304
11.11.1	Parseval's Theorem . . . . .	305
11.11.2	Example: The Exponential Pulse . . . . .	305
11.12	The Autocorrelation of a Pulse and Its Relation to the Energy Spectrum . . . . .	305
11.13	Noise . . . . .	306
11.14	Correlation Functions and Noisy Signals . . . . .	308
11.14.1	Detecting Signals in Noise . . . . .	308
11.14.2	Signal Averaging . . . . .	308
11.14.3	Power Spectral Density . . . . .	309
11.14.4	Units . . . . .	309
11.15	Frequency Response of a Linear System . . . . .	310
11.15.1	Example of Calculating the Frequency Response . . . . .	311
11.15.2	The Decibel . . . . .	311
11.15.3	Example: Impulse Response . . . . .	312
11.16	The Frequency Spectrum of Noise . . . . .	312
11.16.1	Johnson Noise . . . . .	312
11.16.2	Shot Noise . . . . .	315
11.16.3	$1/f$ Noise . . . . .	315
11.17	Testing Data for Chaotic Behavior . . . . .	316
11.17.1	Embedding . . . . .	316
11.17.2	Surrogate Data . . . . .	316
11.18	Stochastic Resonance . . . . .	317
11.18.1	Threshold Detection . . . . .	317
11.18.2	Feynman's Ratchet . . . . .	318
	Symbols Used . . . . .	319
	Problems . . . . .	319
	References . . . . .	323
<b>12</b>	<b>Images</b> . . . . .	<b>325</b>
12.1	The Convolution Integral and its Fourier Transform . . . . .	325
12.1.1	One Dimension . . . . .	325
12.1.2	Two Dimensions . . . . .	326
12.2	The Relationship Between the Object and the Image . . . . .	327
12.2.1	Point-Spread Function . . . . .	327
12.2.2	Optical-, Modulation-, and Phase-Transfer Functions . . . . .	328
12.2.3	Line- and Edge-Spread Functions . . . . .	329
12.3	Spatial Frequencies in an Image . . . . .	329
12.3.1	Summary . . . . .	331
12.4	Two-Dimensional Image Reconstruction from Projections by Fourier Transform . . . . .	331
12.5	Reconstruction from Projections by Filtered Back Projection . . . . .	332
12.6	An Example of Filtered Back Projection . . . . .	335
	Symbols Used . . . . .	337

Problems . . . . .	337
References . . . . .	340
<b>13 Sound and Ultrasound</b>	<b>343</b>
13.1 The Wave Equation . . . . .	343
13.1.1 Plane Waves in an Elastic Rod . . . . .	343
13.1.2 Plane Waves in a Fluid . . . . .	344
13.2 Properties of the Wave Equation . . . . .	345
13.3 Acoustic Impedance . . . . .	346
13.3.1 Relationships Between Pressure, Displacement and Velocity in a Plane Wave . . . . .	346
13.3.2 Reflection and Transmission of Sound at a Boundary . . . . .	346
13.4 Comparing Intensities: Decibels . . . . .	347
13.4.1 The Decibel . . . . .	347
13.4.2 Hearing Response . . . . .	347
13.5 The Ear and Hearing . . . . .	348
13.6 Attenuation . . . . .	349
13.7 Medical Uses of Ultrasound . . . . .	350
13.7.1 Ultrasound Transducers . . . . .	350
13.7.2 Pulse Echo Techniques . . . . .	352
13.8 The Doppler Effect . . . . .	353
Symbols Used . . . . .	354
Problems . . . . .	354
References . . . . .	357
<b>14 Atoms and Light</b>	<b>359</b>
14.1 The Nature of Light: Waves versus Photons . . . . .	359
14.2 Atomic Energy Levels and Atomic Spectra . . . . .	361
14.3 Molecular Energy Levels . . . . .	362
14.4 Scattering and Absorption of Radiation; Cross Section . . . . .	364
14.5 The Diffusion Approximation to Photon Transport . . . . .	367
14.5.1 General Theory . . . . .	367
14.5.2 Continuous Measurements . . . . .	368
14.5.3 Pulsed Measurements . . . . .	368
14.5.4 Refinements to the Model . . . . .	369
14.6 Biological Applications of Infrared Scattering . . . . .	369
14.6.1 Near Infrared (NIR) . . . . .	369
14.6.2 Optical Coherence Tomography (OCT) . . . . .	370
14.6.3 Raman Spectroscopy . . . . .	371
14.6.4 Far Infrared or Terahertz Radiation . . . . .	372
14.7 Thermal Radiation . . . . .	372
14.8 Infrared Radiation from the Body . . . . .	375
14.8.1 Atherosclerotic Coronary Heart Disease . . . . .	376
14.9 Blue and Ultraviolet Radiation . . . . .	377
14.9.1 Treatment of Neonatal Jaundice . . . . .	377
14.9.2 The Ultraviolet Spectrum . . . . .	377
14.9.3 Response of the Skin to Ultraviolet Light . . . . .	378
14.9.4 Ultraviolet Light Causes Skin Cancer . . . . .	380
14.9.5 Protection from Ultraviolet Light . . . . .	380
14.9.6 Ultraviolet Light Damages the Eye . . . . .	381
14.9.7 Ultraviolet Light Synthesizes Vitamin D . . . . .	381
14.9.8 Ultraviolet Light Therapy . . . . .	381
14.10 Heating Tissue with Light . . . . .	381
14.11 Radiometry and Photometry . . . . .	383
14.11.1 Radiometric Definitions . . . . .	383
14.11.2 Photometric Definitions . . . . .	387
14.11.3 Actinometric Definitions . . . . .	388
14.12 The Eye . . . . .	388

14.13 Quantum Effects in Dark-Adapted Vision . . . . .	390
Symbols Used . . . . .	392
Problems . . . . .	393
References . . . . .	397
<b>15 Interaction of Photons and Charged Particles with Matter</b>	<b>401</b>
15.1 Atomic Energy Levels and X-ray Absorption . . . . .	401
15.2 Photon Interactions . . . . .	403
15.2.1 Photoelectric Effect . . . . .	403
15.2.2 Compton and Incoherent Scattering . . . . .	403
15.2.3 Coherent Scattering . . . . .	403
15.2.4 Inelastic Scattering . . . . .	403
15.2.5 Pair Production . . . . .	403
15.2.6 Energy Dependence . . . . .	404
15.3 The Photoelectric Effect . . . . .	404
15.4 Compton Scattering . . . . .	405
15.4.1 Kinematics . . . . .	405
15.4.2 Cross Section: Klein–Nishina Formula . . . . .	406
15.4.3 Incoherent Scattering . . . . .	406
15.4.4 Energy Transferred to the Electron . . . . .	407
15.5 Coherent Scattering . . . . .	407
15.6 Pair Production . . . . .	407
15.7 The Photon Attenuation Coefficient . . . . .	408
15.8 Compounds and Mixtures . . . . .	410
15.9 Deexcitation of Atoms . . . . .	410
15.10 Energy Transfer from Photons to Electrons . . . . .	412
15.11 Charged-Particle Stopping Power . . . . .	414
15.11.1 Interaction with Target Electrons . . . . .	418
15.11.2 Scattering from the Nucleus . . . . .	421
15.11.3 Stopping of Electrons . . . . .	422
15.11.4 Compounds . . . . .	422
15.12 Linear Energy Transfer and Restricted Collision Stopping Power . . . . .	422
15.13 Range, Straggling, and Radiation Yield . . . . .	423
15.14 Track Structure . . . . .	424
15.15 Energy Transferred and Energy Imparted; Kerma and Absorbed Dose . . . . .	425
15.15.1 An Example . . . . .	425
15.15.2 Energy Transferred and Kerma . . . . .	427
15.15.3 Energy Imparted and Absorbed Dose . . . . .	427
15.15.4 Net Energy Transferred, Collision Kerma, and Radiative Kerma . . . . .	428
15.16 Charged-Particle Equilibrium . . . . .	428
15.16.1 Radiation Equilibrium . . . . .	428
15.16.2 Charged-particle Equilibrium . . . . .	428
15.17 Buildup . . . . .	429
Symbols Used . . . . .	430
Problems . . . . .	431
References . . . . .	434
<b>16 Medical Use of X Rays</b>	<b>437</b>
16.1 Production of X Rays . . . . .	437
16.1.1 Characteristic X Rays . . . . .	437
16.1.2 Bremsstrahlung . . . . .	438
16.2 Quantities to Describe Radiation Interactions . . . . .	439
16.2.1 Radiation Chemical Yield . . . . .	439
16.2.2 Mean Energy per Ion Pair . . . . .	439
16.2.3 Exposure . . . . .	440
16.3 Detectors . . . . .	440
16.3.1 Film and Screens . . . . .	440

16.3.2 Scintillation Detectors . . . . . 442

16.3.3 Gas Detectors . . . . . 444

16.3.4 Semiconductor Detectors . . . . . 445

16.3.5 Thermoluminescent Dosimeters . . . . . 445

16.3.6 Chemical Dosimetry . . . . . 445

16.3.7 Digital Detectors . . . . . 446

16.4 The Diagnostic Radiograph . . . . . 446

16.4.1 X-ray Tube and Filter . . . . . 446

16.4.2 Collimation . . . . . 447

16.4.3 Attenuation in the Patient: Contrast Material . . . . . 447

16.4.4 Antiscatter Grid . . . . . 450

16.4.5 Film–Screen Combination . . . . . 450

16.4.6 Computed and Direct Radiography . . . . . 450

16.5 Image Quality . . . . . 450

16.6 Angiography and Digital Subtraction Angiography . . . . . 453

16.7 Mammography . . . . . 453

16.8 Fluoroscopy . . . . . 454

16.9 Computed Tomography . . . . . 454

16.10 Biological Effects of Radiation . . . . . 457

16.10.1 Cell-Culture Experiments . . . . . 458

16.10.2 Chromosome Damage . . . . . 458

16.10.3 The Linear-quadratic Model . . . . . 460

16.10.4 The Bystander Effect . . . . . 460

16.10.5 Tissue Irradiation . . . . . 461

16.10.6 A Model for Tumor Eradication . . . . . 463

16.11 Radiation Therapy . . . . . 463

16.11.1 Classical Radiation Therapy . . . . . 464

16.11.2 Modern X-ray Therapy . . . . . 465

16.11.3 Charged Particles and Neutrons . . . . . 465

16.12 Dose Measurement . . . . . 467

16.13 The Risk of Radiation . . . . . 468

16.13.1 Equivalent and Effective Dose . . . . . 468

16.13.2 Comparison with Natural Background . . . . . 469

16.13.3 Calculating Risk . . . . . 470

16.13.4 Radon . . . . . 472

Symbols Used . . . . . 473

Problems . . . . . 474

References . . . . . 477

**17 Nuclear Physics and Nuclear Medicine 481**

17.1 Nuclear Systematics . . . . . 482

17.2 Nuclear Decay: Decay Rate and Half-Life . . . . . 484

17.3 Gamma Decay and Internal Conversion . . . . . 484

17.4 Beta Decay and Electron Capture . . . . . 485

17.5 Calculating the Absorbed Dose from Radioactive Nuclei within the Body . . . . . 488

17.6 Activity and Cumulated Activity . . . . . 489

17.6.1 The General Distribution Problem: Residence Time . . . . . 490

17.6.2 Immediate Uptake with No Biological Excretion . . . . . 490

17.6.3 Immediate Uptake with Exponential Biological Excretion . . . . . 490

17.6.4 Immediate Uptake Moving through Two Compartments . . . . . 491

17.6.5 More Complicated Situations . . . . . 491

17.6.6 Activity per Unit Mass . . . . . 492

17.7 Mean Energy Emitted per Unit of Cumulated Activity . . . . . 492

17.8 Calculation of the Absorbed Fraction . . . . . 493

17.8.1 Nonpenetrating Radiation . . . . . 493

17.8.2 Infinite Source in an Infinite Medium . . . . . 493

17.8.3 Point Source of Monoenergetic Photons in Empty Space . . . . . 494

17.8.4	Point Source of Monoenergetic Photons in an Infinite Isotropic Absorber . . . . .	494
17.8.5	More Complicated Cases—the MIRD Tables . . . . .	494
17.9	Radiopharmaceuticals and Tracers . . . . .	495
17.9.1	Physical Properties . . . . .	495
17.9.2	Biological Properties . . . . .	497
17.10	Sample Dose Calculation . . . . .	498
17.11	Auger Electrons . . . . .	500
17.12	Detectors; The Gamma Camera . . . . .	500
17.13	Single-Photon Emission Computed Tomography . . . . .	501
17.14	Positron Emission Tomography . . . . .	502
17.15	Brachytherapy and Internal Radiotherapy . . . . .	503
17.16	Radon . . . . .	505
	Symbols Used . . . . .	506
	Problems . . . . .	507
	References . . . . .	512
<b>18</b>	<b>Magnetic Resonance Imaging</b>	<b>515</b>
18.1	Magnetic Moments in an External Magnetic Field . . . . .	515
18.2	The Source of the Magnetic Moment . . . . .	516
18.3	The Magnetization . . . . .	517
18.4	Behavior of the Magnetization Vector . . . . .	518
18.5	A Rotating Coordinate System . . . . .	519
18.5.1	Transforming to the Rotating Coordinate System . . . . .	519
18.5.2	An Additional Oscillating Field . . . . .	520
18.5.3	Nutation . . . . .	521
18.5.4	$\pi$ and $\pi/2$ Pulses . . . . .	521
18.6	Relaxation Times . . . . .	522
18.7	Detecting the Magnetic Resonance Signal . . . . .	524
18.8	Some Useful Pulse Sequences . . . . .	525
18.8.1	Free-Induction-Decay (FID) Sequence . . . . .	525
18.8.2	Inversion-Recovery (IR) Sequence . . . . .	525
18.8.3	Spin-Echo (SE) Sequence . . . . .	526
18.8.4	Carr-Purcell (CP) Sequence . . . . .	526
18.8.5	Carr-Purcell-Meiboom-Gill (CPMG) Sequence . . . . .	527
18.9	Imaging . . . . .	527
18.9.1	Slice Selection . . . . .	528
18.9.2	Readout in the $x$ Direction . . . . .	529
18.9.3	Projection Reconstruction . . . . .	530
18.9.4	Phase Encoding . . . . .	530
18.9.5	Other Pulse Sequences . . . . .	531
18.9.6	Image Contrast and the Pulse Parameters . . . . .	533
18.9.7	Safety . . . . .	534
18.10	Chemical Shift . . . . .	534
18.11	Flow Effects . . . . .	535
18.12	Functional MRI . . . . .	536
18.13	Diffusion and Diffusion Tensor MRI . . . . .	536
	Symbols Used . . . . .	537
	Problems . . . . .	538
	References . . . . .	542
<b>A</b>	<b>Plane and Solid Angles</b>	<b>543</b>
A.1	Plane Angles . . . . .	543
A.2	Solid Angles . . . . .	543
<b>B</b>	<b>Vectors; Displacement, Velocity, and Acceleration</b>	<b>545</b>
B.1	Vectors and Vector Addition . . . . .	545
B.2	Components of Vectors . . . . .	546

B.3	Position, Velocity, and Acceleration . . . . .	546
<b>C</b>	<b>Properties of Exponents and Logarithms</b>	<b>549</b>
<b>D</b>	<b>Taylor's Series</b>	<b>551</b>
<b>E</b>	<b>Some Integrals of Sines and Cosines</b>	<b>555</b>
<b>F</b>	<b>Linear Differential Equations with Constant Coefficients</b>	<b>557</b>
F.1	First-order Equation . . . . .	558
F.2	Second-order Equation . . . . .	558
<b>G</b>	<b>The Mean and Standard Deviation</b>	<b>561</b>
<b>H</b>	<b>The Binomial Probability Distribution</b>	<b>563</b>
<b>I</b>	<b>The Gaussian Probability Distribution</b>	<b>567</b>
<b>J</b>	<b>The Poisson Distribution</b>	<b>571</b>
<b>K</b>	<b>Integrals Involving <math>e^{-ax^2}</math></b>	<b>575</b>
<b>L</b>	<b>Spherical and Cylindrical Coordinates</b>	<b>577</b>
<b>M</b>	<b>Joint Probability Distributions</b>	<b>579</b>
M.1	Discrete Variables . . . . .	579
M.2	Continuous Variables . . . . .	580
<b>N</b>	<b>Partial Derivatives</b>	<b>581</b>
<b>O</b>	<b>Some Fundamental Constants and Conversion Factors</b>	<b>583</b>
	<b>Index</b>	<b>585</b>



# Preface

From the Preface to the Third Edition, by Russell K. Hobbie:

Between 1971 and 1973 I audited all the courses medical students take in their first two years at the University of Minnesota. I was amazed at the amount of physics I found in these courses and how little of it is discussed in the general physics course.

I found a great discrepancy between the physics in some papers in the biological research literature and what I knew to be the level of understanding of most biology majors or premed students who have taken a year of physics. It was clear that an intermediate-level physics course would help these students. It would provide the physics they need and would relate it directly to the biological problems where it is useful.

This book is the result of my having taught such a course since 1973. It is intended to serve as a text for an intermediate course taught in a physics department and taken by a variety of majors. Since its primary content is physics, I hope that physics faculty who might shy away from teaching a conventional biophysics course will consider teaching it. I also hope that research workers in biology and medicine will find it a useful reference to brush up on the physics they need or to find a few pointers to the current literature in a number of areas of biophysics. (The bibliography in each chapter is by no means exhaustive; however, the references should lead you quickly into a field.) The course offered at the University of Minnesota is taken by undergraduates in a number of majors who want to see more physics with biological applications and by graduate students in physics, bio-

physical sciences, biomedical engineering, physiology, and cell biology.

Because the book is intended primarily for students who have taken only one year of physics, I have tried to adhere to the following principles in writing it:

1. Calculus is used without apology. When an important idea in calculus is used for the first time, it is reviewed in detail. These reviews are found in the appendices.
2. The reader is assumed to have taken physics and to know the basic vocabulary. However, I have tried to present a logical development from first principles, but shorter than what would be found in an introductory course. An exception is found in Chapters 14–18, where some results from quantum mechanics are used without deriving them from first principles. (My students have often expressed surprise at this change of pace.)
3. I have not intentionally left out steps in most derivations. Some readers may feel that the pace could be faster, particularly after a few chapters. My students have objected strongly when I have suggested stepping up the pace in class.
4. Each subject is approached in as simple a fashion as possible. I feel that sophisticated mathematics, such as vector analysis or complex exponential notation, often hides physical reality from the student. I have seen electrical engineering students who could not tell me what is happening in an RC circuit but could solve the equations with Laplace transforms.

The Fourth Edition follows the tradition of earlier editions. The book now has a second author: Bradley

J. Roth of Oakland University. Both of us have enjoyed this collaboration immensely. We have added a chapter on sound and ultrasound, deleting or shortening topics elsewhere, in order to keep the book only slightly longer than the Third Edition. Some of the deleted material is available at the book's website: <http://www.oakland.edu/~roth/hobbie.htm>.

The Fourth Edition has 44% more end-of-chapter problems than the Third Edition; most highlight biological applications of the physical principles. Many of the problems extend the material in the text. A solutions manual is available to those teaching the course. Instructors can use it as a reference or provide selected solutions to their students. The solutions manual makes it much easier for an instructor to guide an independent-study student. Information about the Solutions manual is available at the book's website.

*Chapter 1* reviews mechanics. Translational and rotational equilibrium are introduced, with the forces in the heel and hip joint as clinical examples. Stress and strain, hydrostatics, incompressible viscous flow, and the Poiseuille–Bernoulli equation are discussed, with examples from the circulatory system. The chapter concludes with a discussion of Reynolds number.

*Chapter 2* is essential to nearly every other chapter in the book. It discusses exponential growth and decay and gives examples from pharmacology and physiology (including clearance). The logistic equation is discussed. Students are also shown how to use semilog and log-log graph plots and to determine power-law coefficients using a spreadsheet. The chapter concludes with a brief discussion of scaling.

*Chapter 3* is a condensed treatment of statistical physics: average quantities, probability, thermal equilibrium, entropy, and the first and second laws of thermodynamics. Topics treated include the following: the Boltzmann factor and its corollary, the Nernst equation; the principle of equipartition of energy; the chemical potential; the general thermodynamic relationship; the Gibbs free energy; and the chemical potential of a solution. You can plow through this chapter if you are a slave to thoroughness, touch on the highlights, or use it as a reference as the topics are needed in later chapters.

*Chapter 4* treats diffusion and transport of solute in an infinite medium. Fick's first and second laws of diffusion are developed. Steady-state solutions in one, two and three dimensions are described. An important model is a spherical cell with pores providing transport through the cell membrane. It is shown that only a small number of pores are required to keep up with the rate of diffusion toward or away from the cell, so there is plenty of room on the cell surface for many different kinds of pores and receptor sites. The combination of diffusion and drift (or solvent drag) is also discussed. Finally, a simple random-walk model of diffusion is introduced.

*Chapter 5* discusses transport of fluid and neutral solutes through a membrane. This might be a cell mem-

brane, the basement membrane in the glomerulus of the kidney, or a capillary wall. The phenomenological transport equations including osmotic pressure are introduced as the first (linear) approximation to describe these flows. Countercurrent transport is described. Finally, a hydrodynamic model is developed for right-cylindrical pores. This model provides expressions for the phenomenological coefficients in terms of the pore radius and length. It is also used to calculate the net force on the membrane when there is flow.

After reviewing the electric field, electric potential, and circuits, *Chapter 6* describes the electrochemical changes that cause an impulse to travel along a nerve axon or along a muscle fiber before contraction. Two models are considered: electrotonus (when the membrane obeys Ohm's law) and the Hodgkin–Huxley model (when the membrane is nonlinear). Saltatory conduction in myelinated fibers is described. The dielectric properties of the membrane are modeled in terms of its molecular structure. Some simple changes to the membrane conductivity give rise to a periodically repeating action potential. Finally, a general relationship is developed between diffusive transport, resistance and capacitance for a given geometry.

*Chapter 7* shows how an electric potential is generated in the medium surrounding a nerve or muscle cell. This leads to the current dipole model for the electrocardiogram. The model is refined to account for the anisotropy of the electrical conductivity of the heart. We then discuss electrical stimulation, which is important for pacemakers, stimulating nerve and muscle cells, and defibrillation. Finally, the model is extended to the electroencephalogram.

*Chapter 8* shows how the currents in a conducting nerve or muscle cell generate a magnetic field, leading to the magnetocardiogram and the magnetoencephalogram. Some bacteria (and probably some higher organisms) contain magnetic particles used for determining spatial orientation in the earth's magnetic field. The mechanism by which these bacteria are oriented is described. The detection of weak magnetic fields and the use of changing magnetic fields to stimulate nerve or muscle cells are also discussed.

*Chapter 9* covers a number of topics at the cellular and membrane level. It begins with Donnan equilibrium, where the presence of an impermeant ion on only one side of a membrane leads to the buildup of a potential difference across the membrane, and the Gouy–Chapman model for how ions redistribute near the membrane to generate this potential difference. The Debye–Hückel model is a simple description of the neutralization of ions by surrounding counterions. The Nernst–Planck equation provides the basic model for describing combined diffusion and drift in an applied electric field. It also forms the basis for the Goldman–Hodgkin–Katz model for zero total current in a membrane with a constant electric field. Gated membrane channels are then discussed. Noise is inescapable in all signalling situations. After

developing the basic properties of shot noise and Johnson noise, we show how a properly adapted shark can detect very weak electric fields with a reasonable signal-to-noise ratio. The chapter concludes with a discussion of the basic physical principles that must be kept in mind when assessing the possibility of biological effects of weak electric and magnetic fields.

*Chapter 10* describes feedback systems in the body. It starts with the regulation of breathing rate to stabilize the carbon dioxide level in the blood, moves to linear feedback systems with one and two time constants, and then to nonlinear models. We show how nonlinear systems described by simple difference equations can exhibit chaotic behavior, and how chaotic behavior can arise in continuous systems as well. Examples of feedback systems include Cheyne-Stokes respiration, heat stroke, pupil size, oscillating white-blood-cell counts, waves in excitable media, and period doubling and chaos in the heart.

*Chapter 11* shows how the method of least squares underlies several important techniques for analyzing data. These range from simple curve fitting to discrete and continuous Fourier series, power spectra, correlation functions, and the Fourier transform. We then describe the frequency response of a linear system and the frequency spectrum of noise. We conclude with a brief discussion of testing data for chaotic behavior and the important concept of stochastic resonance.

Armed with the tools of the previous chapter, we turn to images in *Chapter 12*. Images are analyzed from the standpoint of linear systems and convolution. This leads to the use of Fourier analysis to describe the spatial frequencies in an image and the reconstruction of an image from its projections. Both Fourier techniques and filtered backprojection are discussed.

*Chapter 13* is new in the Fourth Edition. It discusses acoustics, hearing, and medical ultrasound.

*Chapter 14* discusses the visible, infrared, and ultraviolet regions of the electromagnetic spectrum. The scattering and absorption cross sections are introduced and are used here and in the next three chapters. We then describe the diffusion model for photon transport in turbid media. Biological examples of infrared scattering include the near infrared, optical coherence tomography, Raman scattering, and the far infrared. Thermal radiation emitted by the body can be detected; the emission of infrared radiation by the sun includes ultraviolet light, which injures skin. Protection from ultraviolet light is both possible and prudent. The definitions of various radiometric quantities have varied from one field of research to another. We present a coherent description of radiometric, photometric and actinometric definitions. We then turn to the eye, showing how spectacle lenses are used to correct errors of refraction. The chapter closes with a description of the quantum limitations to dark-adapted vision.

*Chapter 15*, like Chapter 3, has few biological examples but sets the stage for later work. It describes how photons and ionizing charged particles such as electrons lose energy in traversing matter. These interaction mechanisms, both in the body and in the detector, are fundamental to the formation of a radiographic image and to the use of radiation to treat cancer.

*Chapter 16* describes the use of x rays for medical diagnosis and treatment. It moves from production to detection, to the diagnostic radiograph. We discuss image quality and noise, followed by angiography, mammography, fluoroscopy, and computed tomography. After briefly reviewing radiobiology, we discuss therapy and dose measurement. The chapter closes with a section on the risks from radiation.

*Chapter 17* introduces nuclear physics and nuclear medicine. The different kinds of radioactive decay are described. Dose calculations are made using the fractional absorbed dose method recommended by the Medical Internal Radiation Dose committee of the Society of Nuclear Medicine. Auger electrons can magnify the dose delivered to a cell or to DNA. This can potentially provide new methods of treatment. Diagnostic imaging includes single photon emission tomography and positron emission tomography. Therapies include brachytherapy and internal radiotherapy. A section on the nuclear physics of radon closes the chapter.

*Chapter 18* develops the physics of magnetic resonance imaging. We show how the basic pulse sequences are formed and used for slice selection, readout, image reconstruction and to manipulate image contrast. We close with chemical shift imaging, flow effects, functional MRI, and diffusion and diffusion tensor MRI.

Biophysics is a very broad subject. Nearly every branch of physics has something to contribute, and the boundaries between physics and engineering are blurred. Each chapter could be much longer; we have attempted to provide the essential physical tools. Molecular biophysics has been almost completely ignored: excellent texts already exist, and this is not our area of expertise. This book has become long enough.

We would appreciate receiving any corrections or suggestions for improving the book.

Finally, thanks to our long-suffering families. We never understood what these common words really mean, nor the depth of our indebtedness, until we wrote the book.

Russell K. Hobbie  
Professor of Physics Emeritus, University of Minnesota  
(hobbie@umn.edu)

Bradley J. Roth  
Associate Professor of Physics, Oakland University  
(roth@oakland.edu)

# 1

## Mechanics

This chapter introduces some concepts from mechanics that are of biological or medical interest. We begin with a discussion of sizes important in biology. Then we turn to the forces on an object that is in equilibrium and calculate the forces experienced by various bones and muscles. In Sec. 1.8 we introduce the concept of mechanical work, which will recur throughout the book. The next two sections describe how materials deform when forces act on them. Sections 1.11 through 1.14 discuss the forces in stationary and moving fluids. These concepts are then applied to laminar viscous flow in a pipe, which is a model for the flow of blood and the flow of fluid through pores in cell membranes. The chapter ends with a discussion of the circulatory system.

### 1.1 Distances and Sizes

In biology and medicine, we study objects that span a wide range of sizes: from giant redwood trees to individual molecules. Therefore, we begin with a brief discussion of length scales. The basic unit of length in the metric system is the meter (m): about the height of a three-year-old child. For objects much larger or smaller than a meter, we add a prefix as shown in Table 1.1. For example, a kilometer is formed by adding the prefix “kilo”, which means times one thousand ( $10^3$  m = 1 km). Living organisms rarely if ever reach a size of 1 km; the tallest trees are about 0.1 km (100 m) high. A few animals (whales, dinosaurs) reach the size of tens of meters, but most organisms are a few meters or less in size.

The diversity of life becomes more obvious as we move down to smaller length scales. One one-hundredth of a meter is called a centimeter ( $1$  cm =  $10^{-2}$  m). The centimeter is still common in the medical literature, although it is going out of style among metric purists who prefer

TABLE 1.1. Common prefixes used in the metric system.

Prefix	Abbreviation	Multiply by
giga	G	$10^9$
mega	M	$10^6$
kilo	k	$10^3$
milli	m	$10^{-3}$
micro	$\mu$	$10^{-6}$
nano	n	$10^{-9}$
pico	p	$10^{-12}$
femto	f	$10^{-15}$
atto	a	$10^{-18}$

to use only prefixes that are factors of one thousand.<sup>1</sup> One one-thousandth of a meter is a millimeter ( $1$  mm =  $10^{-3}$  m), about the thickness of a dime. We can still see objects of this size, but we can’t study their detailed structure with the unaided eye.

The microscope enables us to study objects many times smaller than 1 mm. The natural unit for measuring such objects is  $10^{-6}$  m or  $10^{-3}$  mm, called a micrometer ( $1$   $\mu$ m =  $10^{-6}$  m). The nickname for the micrometer is the “micron.” Figure 1.1 shows the relative sizes of objects in the range of 1 mm to 1  $\mu$ m and encompasses the length scale of cell biology. Many small structures of our body are this size. For instance, our lungs consist of a branching network of tubes through which air flows. These tubes end in small, nearly spherical air sacs called *alveoli* [Fig. 1.1(b)]. Each alveolus has a diameter of about 250  $\mu$ m, and this size is set by the diffusion properties of air (Chapter 4). *Protozoans* are a type of small one-celled animal. A paramecium is a protozoan about

<sup>1</sup>We find that restricting ourselves to prefixes that are a multiple of 1000 makes it easier to remember relative sizes.

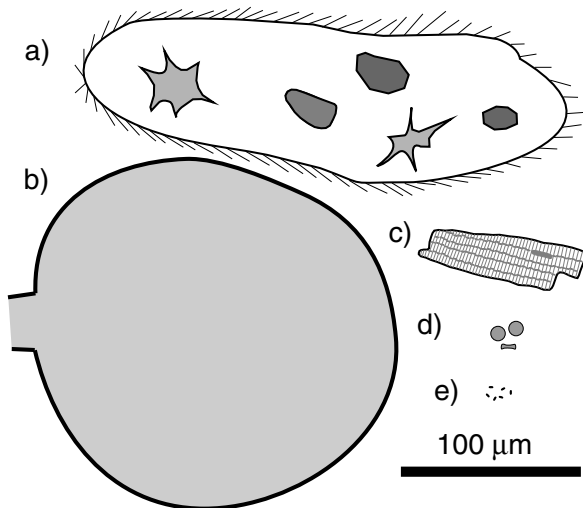


FIGURE 1.1. Objects ranging in size from 1 mm down to 1  $\mu\text{m}$ . (a) A paramecium, (b) an alveolus (air sac in the lung), (c) a cardiac cell, (d) red blood cells, and (e) *Escherichia coli* bacteria.

250  $\mu\text{m}$  long [Fig. 1.1(a)]. The cells in multicellular animals tend to be somewhat smaller than protozoans. For instance, the mammalian *cardiac cell* (a muscle cell found in the heart, Chapter 7) shown in Fig. 1.1(c) is about 100  $\mu\text{m}$  long and 20  $\mu\text{m}$  in diameter. Nerve cells have a long fiber-like extension called an *axon*. Axons come in a variety of sizes, from 1  $\mu\text{m}$  diameter up to tens of microns. The squid contains a giant axon nearly one millimeter in diameter. This axon played an important role in our understanding of how nerves work (Chapter 6).

Our red blood cells (*erythrocytes*) carry oxygen to all parts of our body. (Actually, red blood cells are not true cells at all, but rather “corpuscles”). Red blood cells are disk-shaped, with a diameter of about 8  $\mu\text{m}$  and a thickness of 2  $\mu\text{m}$  [Fig. 1.1(d)]. Blood flows through a branching network of vessels (Section 1.17), the smallest of which are *capillaries*. Each capillary has a diameter of about 8  $\mu\text{m}$ , meaning that the red blood cells can barely pass through it single-file.

One valuable skill in physics is the ability to make order-of-magnitude estimates, meaning to calculate something approximately right. For instance, suppose we want to calculate the number of cells in the body. This is a difficult calculation, because cells come in all sizes and shapes. But for some purposes we only need an approximate answer (say, within a factor of ten). For example: cells are roughly 10  $\mu\text{m}$  in size, so their volume is about  $(10 \mu\text{m})^3$ , or  $(10 \times 10^{-6})^3 = 10^{-15} \text{ m}^3$ . An adult is roughly 2 m tall and about 0.3 m wide, so our volume is about  $2 \text{ m} \times 0.3 \text{ m} \times 0.3 \text{ m}$ , or  $0.18 \text{ m}^3$ . We are made up almost entirely of cells, so the number of cells in our body is about  $(0.18 \text{ m}^3)/(10^{-15} \text{ m}^3)$ , or roughly  $2 \times 10^{14}$ . Some problems at the end of the chapter ask you to make similar order-of-magnitude calculations.

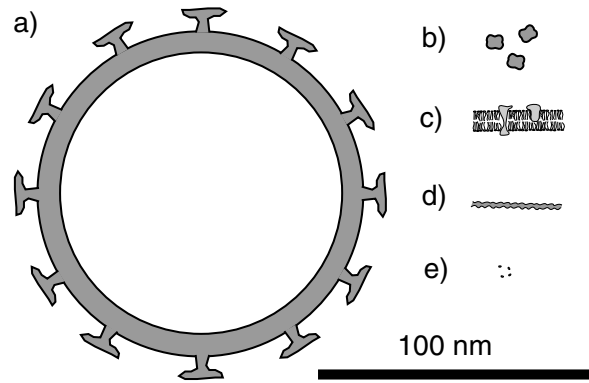


FIGURE 1.2. Objects ranging in size from 1  $\mu\text{m}$  down to 1 nm. (a) the human immunodeficiency virus (HIV), (b) hemoglobin molecules, (c) a cell membrane, (d) a DNA molecule, (e) glucose molecules.

Most cells are larger than a few microns. But many cells (called *eukaryotes*) are complex structures that contain *organelles* about this size. *Mitochondria*, organelles where many of the chemical processes providing cells with energy take place, are typically about 2  $\mu\text{m}$  long. *Proto-plasts*, organelles found in plant cells where photosynthesis changes light energy to chemical energy, are also about 2  $\mu\text{m}$  long.

The simplest cells are called *prokaryotes* and contain no subcellular structures. *Bacteria* are the most common prokaryotic cells. The bacterium *Escherichia coli*, or *E. coli*, is about 2  $\mu\text{m}$  long [Fig. 1.1(e)], and has been studied extensively.

To examine structures smaller than bacteria, we must measure lengths that are smaller than a micron. One-thousandth of a micron is called a nanometer (1 nm =  $10^{-9}$  m). Figure 1.2 shows objects having lengths from 1 nm to 1  $\mu\text{m}$ . *E. coli* bacteria, which seemed so tiny compared to cells in Fig. 1.1, are giants on the nanometer length scale, being 20 times longer than the 100 nm scale bar in Fig. 1.2. *Viruses* are tiny packets of genetic material encased in protein. On their own they are incapable of metabolism or reproduction, so some scientist don’t even consider them as living organisms. Yet, they can infect a cell and take control of its metabolic and reproductive functions. The length scale of viruses is one-tenth of a micron, or 100 nm. For instance, HIV (the virus that causes AIDS) is roughly spherical with a diameter of about 120 nm [Fig. 1.2(a)]. Some viruses, called *bacteriophages*, infect and destroy bacteria. Most viruses are too small to see in a light microscope. The resolution of a microscope is limited by the wavelength of light, which is about 500 nm (Chapter 14). Thus, with a microscope we can study cells in detail, we can see bacteria without much resolution, and we can barely see viruses, if we can see them at all.

Below 100 nm, we enter the world of individual molecules. *Proteins* are large, complex macromolecules that are vitally important for life. For example, hemoglobin is

the protein in red blood cells that binds to and carries oxygen. Hemoglobin is roughly spherical, about 6 nm in diameter [Fig. 1.2(b)]. Many biological functions occur in the cell *membrane* (see Chapter 5). Membranes are made up of layers of lipid (fat), often with proteins and other molecules embedded in them [Fig. 1.2(c)]. A typical cell membrane is about 10 nm thick. The molecule *adenosine triphosphate* (ATP), crucial for energy production and distribution in cells, is about 2 nm long (Chapter 3). Chemical energy is stored in molecules called *carbohydrates*. A common (and relatively small) carbohydrate is *glucose* ( $C_6H_{12}O_6$ ), which is about 1 nm long [Fig. 1.2(e)]. Genetic information is stored in long, helical strands of *deoxyribonucleic acid* (DNA). DNA is about 2.5 nm wide, and the helix completes a turn every 3.4 nm along its length [Fig. 1.2(d)].

At the 1-nm scale and below, we reach the world of small molecules and individual atoms. Water is the most common molecule in our body. It consists of two atoms of hydrogen and one of oxygen. The distance between adjacent atoms in water is about 0.1 nm. The distance 0.1 nm (100 pm) is used so much at atomic length scales that it has earned a nickname: the angstrom ( $\text{\AA}$ ). Like the cm, this unit is going out of fashion as the use of nanometer becomes more common. Individual atoms have diameters of 100 or 200 pm.

Below the level of 100 pm, we leave the realm of biology and enter the world of subatomic physics. The nuclei of atoms (Chapter 17) are very small, and their sizes are measured in femtometers ( $1 \text{ fm} = 10^{-15} \text{ m}$ ).

One cannot possibly memorize the size of all biological objects: there are simply too many. The best one can do is remember a few mileposts along the way. Table 1.2 contains a rough guide to how large a few important biological objects are. Think of these as rules of thumb. Given the diversity of life, one can certainly find exceptions to these rules, but if you memorize Table 1.2 you will have a rough framework to organize your thinking about size. To examine the relative sizes of objects in more detail, see Morrison *et al.* (1994) or Goodsell (1998).

## 1.2 Forces and Translational Equilibrium

There are several ways that we can introduce the idea of force, depending on the problem at hand and our philosophical bent. For our present purposes it will suffice to say that a force is a *push* or a *pull*, that forces have both a magnitude and a direction, and that they give rise to accelerations through Newton's second law,  $\mathbf{F} = m\mathbf{a}$ . Experiments show that forces add like *displacements*, so they can be represented by *vectors*. (Some of the properties of vectors are reviewed in Appendix B; others are introduced as needed.) Vectors will be denoted by boldfaced characters.

TABLE 1.2. Approximate sizes of biological objects.

Object	Size
Protozoa	100 $\mu\text{m}$
Cells	10 $\mu\text{m}$
Bacteria	1 $\mu\text{m}$
Viruses	100 nm
Macromolecules	10 nm
Molecules	1 nm
Atoms	100 pm

One finds experimentally that an object is in *translational equilibrium* if the vector sum of all the forces acting on the body is zero. *Equilibrium* means that the object either remains at rest or continues to move with a constant velocity. That is, it is not accelerated. *Translational* means that only changes of position are being considered; changes of orientation of the object with respect to the axes are ignored.

We must consider *all* the forces that act *on* the object. If the object is a person standing on both feet, the forces are the upward force of the floor on each foot and the downward force of gravity on the person (more accurately, the vector sum of the gravitational force on every cell in the person). We do *not* consider the downward force that the person's feet exert *on the floor*. It is also possible to replace the sum of the gravitational force on each cell of the body with a single downward gravitational force acting at one point, the *center of gravity* of the body.

The forces that add to zero to give translational equilibrium need not all act at one point on the object. If the object is a person's leg and the leg is at rest, there are three forces exerted on the leg by other objects (Fig. 1.3). Force  $\mathbf{F}_1$  is the push of the floor up on the bottom of the foot. The various pushes and pulls of the rest of the body

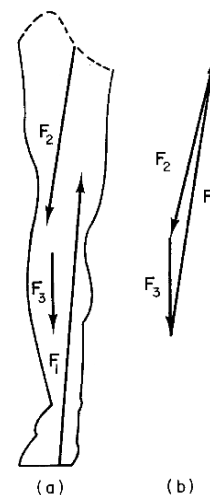


FIGURE 1.3. Forces on the leg in equilibrium. Each force is exerted by some other object. (a) The points of application are widely separated. (b) The sum of the forces is zero.

on the leg through the hip joint and surrounding muscles have been added together to give  $\mathbf{F}_2$ . The gravitational pull of the earth downward on the leg is  $\mathbf{F}_3$ . Force  $\mathbf{F}_1$  acts on the bottom of the leg,  $\mathbf{F}_2$  acts on the top, and  $\mathbf{F}_3$  acts somewhere in between. If the leg is in equilibrium the sum of these forces is zero, as shown in Fig. 1.3(b). Although the points of application of the forces can be ignored in considering translational equilibrium, they are important in determining whether or not the object is in rotational equilibrium. This is discussed shortly.

The Greek letter  $\Sigma$  (capital sigma) is usually used to mean a sum of things. With this notation, the condition for translational equilibrium can be written

$$\sum_i \mathbf{F}_i = 0. \quad (1.1)$$

The subscript  $i$  is used to label the different forces acting on the body. A notation this compact has a lot hidden in it. This is a vector equation, standing for three equations:

$$\begin{aligned} \sum_i F_{ix} &= 0, \\ \sum_i F_{iy} &= 0, \\ \sum_i F_{iz} &= 0. \end{aligned} \quad (1.2)$$

Often the subscript  $i$  is omitted and the equations are written as  $\sum F_x = 0$ ,  $\sum F_y = 0$ ,  $\sum F_z = 0$ . In this notation, a component is positive if it points along the positive axis and negative if it points the other way.

Sometimes, as in the next example, we draw forces in particular directions and assume that these directions are positive. If the subsequent algebra happens to give a solution that is negative, the force points opposite the direction assumed.

As an example, consider the person standing on both feet as in Fig. 1.4. The earth pulls down at some point with force  $\mathbf{W}$ . The floor pushes up on the right foot with force  $\mathbf{F}_1$  and on the left foot with force  $\mathbf{F}_2$ . To determine what the condition for translational equilibrium tells us

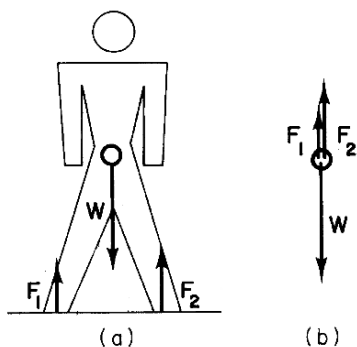


FIGURE 1.4. A person standing. (a) The forces on the person. (b) A free-body or force diagram.

about the forces, draw the force diagram or *free-body diagram* of Fig. 1.4(b). This diagram is an abstraction that ignores the points at which the forces are applied to the body. We can get away with this abstraction because we are considering only translation. When we consider rotational equilibrium, we will have to redraw the diagram showing the points at which the various forces act on the person. If all the forces are vertical, then there is only one component of each force to worry about, and the equilibrium condition gives  $F_1 + F_2 - W = 0$ , or  $F_1 + F_2 = W$ . The total force of the floor pushing up on both feet is equal to the pull of the earth down.

If there is a sideways force on each foot, translational equilibrium provides two conditions:  $F_{1x} + F_{2x} = 0$ , and  $F_{1y} + F_{2y} - W = 0$ .

This is all that can be learned from the condition for translational equilibrium. If the person stands on one foot, then  $F_1 = 0$  and  $F_2 = W$ . If the person stands with equal force on each foot, then  $F_1 = F_2 = W/2$ .

### 1.3 Rotational Equilibrium

If the object is in rotational equilibrium, then another condition must be placed upon the forces. Rotational equilibrium means that the object either does not rotate or continues to rotate at a constant rate (with a constant number of rotations per second). Consider the object of Fig. 1.5, which is a rigid rod pivoted at point  $X$  so that it can rotate in the plane of the paper. Forces  $\mathbf{F}_1$  and  $\mathbf{F}_2$  are applied to the rod in the plane of the paper at distances  $r_1$  and  $r_2$  from the pivot and perpendicular to the rod. The pivot exerts the force  $\mathbf{F}_3$  on the rod needed to maintain translational equilibrium. If both  $\mathbf{F}_1$  and  $\mathbf{F}_2$  are perpendicular to the rod, they are parallel. They must also be parallel to  $\mathbf{F}_3$ , and translational equilibrium requires that  $\mathbf{F}_3 = \mathbf{F}_1 + \mathbf{F}_2$ .

Experiment shows that there is no rotation of the rod if  $F_1 r_1 = F_2 r_2$ . The condition for rotational equilibrium can be stated in a form analogous to that for translational equilibrium if we define the *torque*,  $\tau$ , to be

$$\tau_i = r_i F_i. \quad (1.3)$$

With this definition goes an algebraic sign convention: the torque is positive if it tends to produce a counter-clockwise rotation. The rod is in rotational equilibrium if

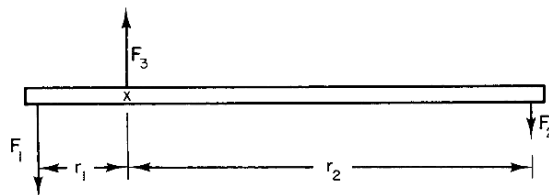


FIGURE 1.5. A rigid rod free to rotate about a pivot at point  $X$ .

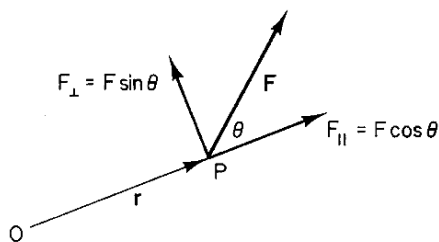


FIGURE 1.6. A force  $\mathbf{F}$  is applied to an object at point  $P$ . The object can rotate about point  $O$ . Vectors  $\mathbf{r}$  and  $\mathbf{F}$  determine the plane of the paper.

the algebraic sum of all the torques is zero:

$$\sum_i \tau_i = \sum_i r_i F_i = 0. \quad (1.4)$$

Note that  $\mathbf{F}_3$  contributes nothing to the torque because  $r_3$  is zero.

The torque is defined about a certain point,  $X$ . It depends on the distance from the point of application of each force to  $X$ .<sup>2</sup> As long as the object is in translational equilibrium, the torque can be evaluated around any point. This theorem, which we will not prove, often allows calculations to be simplified, because taking torques about certain points can cause some forces not to contribute to the torque equation.

The torque can also be calculated if the force is not at right angles to the rod. Imagine an object free to rotate about point  $O$  in Fig. 1.6. Force  $\mathbf{F}$  lies in the plane of the paper but is applied in some arbitrary direction at point  $P$ . The vectors  $\mathbf{r}$  and  $\mathbf{F}$  determine the plane of the paper if they are not parallel. Force  $\mathbf{F}$  can be resolved into two components: one parallel to  $\mathbf{r}$ ,  $F_{\parallel} = F \cos \theta$ , and the other perpendicular to  $\mathbf{r}$ ,  $F_{\perp} = F \sin \theta$ . The component parallel to  $\mathbf{r}$  will not cause any rotation about point  $O$ . (Pull on an open door parallel to the plane of the door; there is no rotation.) The torque is therefore

$$\tau = rF_{\perp} = rF \sin \theta. \quad (1.5)$$

The perpendicular distance from the line along which the force acts to point  $X$  is  $r \sin \theta$ . It is often called the *moment arm*, and the torque is the magnitude of the force multiplied by the moment arm.

The angle  $\theta$  is the angle of rotation from the direction of  $\mathbf{r}$  to the direction of  $\mathbf{F}$ . It is called positive if the rotation is counterclockwise. For the angle shown in Fig. 1.6  $\sin \theta$  has a positive value, and the torque is positive. Figure 1.7(a) shows an angle between  $90^\circ$  and  $180^\circ$  for which the torque and  $\sin \theta$  are still positive. Figure 1.7(b) shows an angle between  $180^\circ$  and  $360^\circ$ , for which both

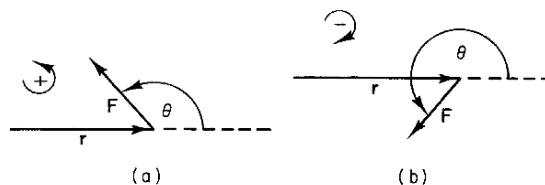


FIGURE 1.7. (a) When  $\theta$  is between  $0^\circ$  and  $180^\circ$ , both  $\sin \theta$  and the torque are positive. (b) When  $\theta$  is between  $180^\circ$  and  $360^\circ$ , both  $\sin \theta$  and the torque are negative.

the torque and  $\sin \theta$  are negative. In all cases, Eq. 1.5 gives the correct sign for the torque.

To summarize: the torque due to force  $\mathbf{F}$  applied to a body at point  $P$  must be calculated about some point  $O$ . If  $\mathbf{r}$  is the vector from  $O$  to  $P$ , the magnitude of the torque is equal to the magnitude of  $\mathbf{r}$  times the magnitude of  $\mathbf{F}$ , times the sine of the angle between  $\mathbf{r}$  and  $\mathbf{F}$ . The angle is measured counterclockwise from  $\mathbf{r}$  to  $\mathbf{F}$ .

## 1.4 Vector Product

Torque can be thought of as a vector,  $\boldsymbol{\tau}$ . Its magnitude is  $F r \sin \theta$ . The only direction uniquely defined by vectors  $\mathbf{r}$  and  $\mathbf{F}$  is perpendicular to the plane in which they lie. This is also the direction of an axis about which the torque would cause a rotation. However, there is ambiguity about which direction along this line to assign to the torque. The convention is to say that a positive torque points in the direction of the thumb of the right hand when the fingers curl in the direction of positive rotation from  $\mathbf{r}$  to  $\mathbf{F}$ .<sup>3</sup> When  $\mathbf{r}$  and  $\mathbf{F}$  point in the same direction, so that no plane is defined, the magnitude of the torque is zero.

The product of two vectors according to the foregoing rules is called the *cross product* or *vector product* of the two vectors. One can use a shorthand notation

$$\boldsymbol{\tau} = \mathbf{r} \times \mathbf{F}. \quad (1.6)$$

There is another way to write the cross product. If both  $\mathbf{r}$  and  $\mathbf{F}$  are resolved into components, as shown in Fig. 1.8, then the cross product can be calculated by applying the rules above to the components. Since  $\mathbf{F}_y$  is perpendicular to  $\mathbf{r}_x$  and parallel to  $\mathbf{r}_y$ , its only contribution is a counterclockwise torque  $r_x F_y$ . The only contribution from  $\mathbf{F}_x$  is a clockwise torque,  $-r_y F_x$ . The magnitude of the cross product is therefore

$$\tau = r_x F_y - r_y F_x. \quad (1.7)$$

<sup>2</sup>The discussion associated with Fig. 1.5 suggests that torque is taken about an axis, rather than a point. In a three-dimensional problem the torque is taken about a point.

<sup>3</sup>This arbitrariness in assigning the sense of  $\boldsymbol{\tau}$  means that it does not have quite all the properties that vectors usually have. It is called an axial vector or a pseudovector. It will not be necessary in this book to worry about the difference between a real vector and an axial vector.



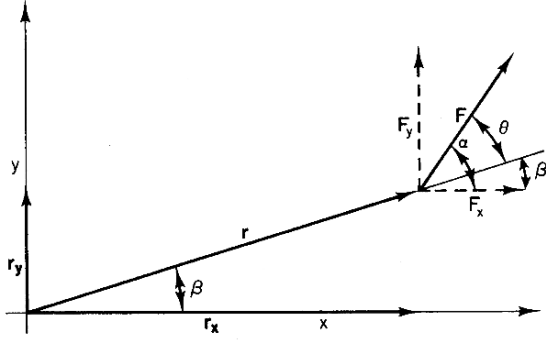


FIGURE 1.8. The cross product  $\mathbf{r} \times \mathbf{F}$  is calculated by resolving  $\mathbf{r}$  and  $\mathbf{F}$  into components.

Note that this is the (signed) sum of each component of the force multiplied by its moment arm.

The equivalence of this result to Eq. 1.5 can be verified by writing Eq. 1.7 as

$$\begin{aligned}\tau &= (r \cos \beta)(F \sin \alpha) - (r \sin \beta)(F \cos \alpha), \\ \tau &= rF (\sin \alpha \cos \beta - \cos \alpha \sin \beta).\end{aligned}$$

There is a trigonometric identity that

$$\sin(\alpha - \beta) = \sin \alpha \cos \beta - \cos \alpha \sin \beta.$$

Since  $\theta = \alpha - \beta$  (from Fig. 1.8), this is equivalent to  $\tau = rF \sin \theta$ .

When vectors  $\mathbf{r}$  and  $\mathbf{F}$  lie in the  $xy$  plane,  $\boldsymbol{\tau}$  points along the  $z$  axis. If  $\mathbf{r}$  and  $\mathbf{F}$  point in arbitrary directions, Eq. 1.7 gives the  $z$  component of  $\boldsymbol{\tau}$ . One can apply the same reasoning for other components and show that

$$\begin{aligned}\tau_x &= r_y F_z - r_z F_y, \\ \tau_y &= r_z F_x - r_x F_z, \\ \tau_z &= r_x F_y - r_y F_x.\end{aligned}\quad (1.8)$$

If you are familiar with the rules for evaluating determinants, you will see that this is equivalent to the notation

$$\boldsymbol{\tau} = \begin{vmatrix} \hat{\mathbf{x}} & \hat{\mathbf{y}} & \hat{\mathbf{z}} \\ r_x & r_y & r_z \\ F_x & F_y & F_z \end{vmatrix}.\quad (1.9)$$

## 1.5 Force in the Achilles Tendon

The equilibrium conditions can be used to understand many problems in clinical orthopedics. Two are discussed in this book: forces that sometimes cause the Achilles tendon at the back of the heel to break, and forces in the hip joint.

The Achilles tendon connects the calf muscles (the gastrocnemius and the soleus) to the calcaneus at the back of the heel (Fig. 1.9). To calculate the force exerted by

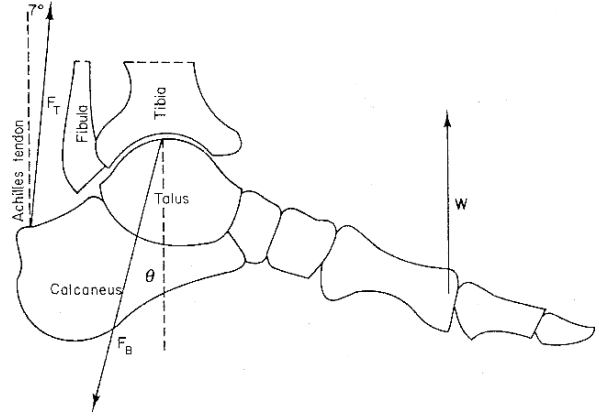


FIGURE 1.9. Simplified anatomy of the foot.

this tendon on the calcaneus when a person is standing on the ball of one foot, assume that the entire foot can be regarded as a rigid body. This is our first example of creating a *model* of the actual situation. We try to simplify the real situation to make the calculation possible while keeping the features that are important to what is happening. In this model the internal forces within the foot are being ignored.

Figure 1.10 shows the force exerted by the tendon on the foot ( $\mathbf{F}_T$ ), the force of the leg bones (tibia and fibula) on the foot ( $\mathbf{F}_B$ ), and the force of the floor upward, which is equal to the weight of the body ( $\mathbf{W}$ ). The weight of the foot is small compared to these forces and will be neglected. Measurements on a few people suggest that the angle the Achilles tendon makes with the vertical is about  $7^\circ$ .

Translational equilibrium requires that

$$\begin{aligned}F_T \cos(7^\circ) + W - F_B \cos \theta &= 0, \\ F_T \sin(7^\circ) - F_B \sin \theta &= 0.\end{aligned}\quad (1.10)$$

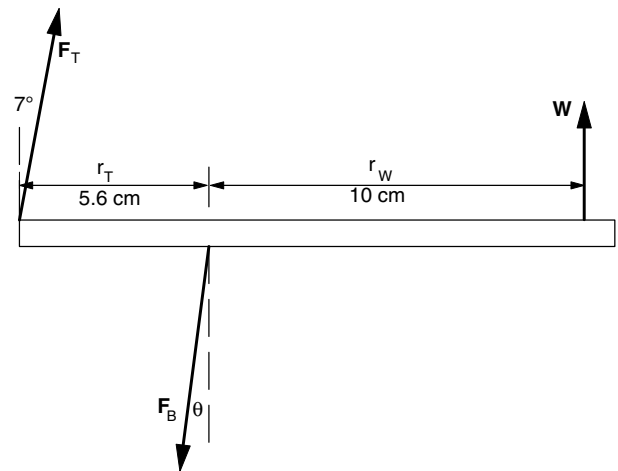


FIGURE 1.10. Forces on the foot, neglecting its own weight.

To write the condition for rotational equilibrium, we need to know the lengths of the appropriate vectors  $\mathbf{r}_T$  and  $\mathbf{r}_W$ , assuming that the torques are taken about the point where  $\mathbf{F}_B$  is applied to the foot. In our simple model we ignore the contributions of the horizontal components of any forces to the torque equation. This is not essential (if we are willing to make more detailed measurements), but it simplifies the equations and thereby makes the process clearer. The horizontal distances measured on one of the authors are  $r_T = 5.6$  cm and  $r_W = 10$  cm, as shown in Fig. 1.10. The torque equation is

$$10W - 5.6F_T \cos 7^\circ = 0. \quad (1.11)$$

This equation can be solved for the tension in the tendon:

$$F_T = \frac{10W}{5.6 \cos 7^\circ} = 1.8W. \quad (1.12)$$

This result can now be used in Eq. 1.10 to find  $F_{By} = F_B \cos \theta$ :

$$\begin{aligned} (1.8)(W)(0.993) + W &= F_B \cos \theta, \\ 2.8W &= F_B \cos \theta. \end{aligned} \quad (1.13)$$

From Eqs. 1.10 and 1.12, we get

$$\begin{aligned} (1.8)(W)(0.122) &= F_B \sin \theta, \\ 0.22W &= F_B \sin \theta. \end{aligned} \quad (1.14)$$

Equations 1.13 and 1.14 are squared and summed and the square root taken to give  $F_B = 2.8W$ , while they can be divided to give

$$\begin{aligned} \tan \theta &= \frac{0.22}{2.8} = 0.079, \\ \theta &= 4.5^\circ. \end{aligned}$$

The tension in the Achilles tendon is nearly twice the person's weight, while the force exerted on the leg by the talus is nearly three times the body weight. One can understand why the tendon might rupture.

## 1.6 Forces on the Hip

The forces in the hip joint can be several times the person's weight, and the use of a cane can be very effective in reducing them.

As a person walks, there are moments when only one foot is on the ground. There are then two forces acting on the body as a whole: the downward pull of the earth  $W$  and the upward push of the ground on the foot  $N$ . The pull of the earth may be regarded as acting at the center of gravity of the body [Halliday *et al.* (1992, Chap. 13)]. The center of gravity is located on the midline (if the limbs are placed symmetrically), usually in the lower abdomen [Williams and Lissner (1962), Chap. 5.] If torques are taken about the foot, then the center of gravity must

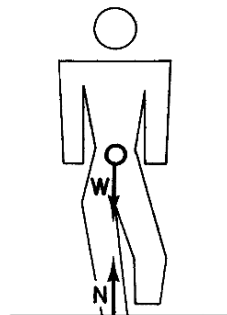


FIGURE 1.11. A person standing on one foot must place the foot under the center of gravity, which is on or near the midline.

be directly over the foot so that there will be no torque from either force. This situation is shown in Fig. 1.11. The condition for translational equilibrium requires that  $N = W$ .

The anatomy of the pelvis, hips, and leg is shown schematically in Fig. 1.12. Fourteen muscles and several ligaments connect the pelvis to the femur. Extensive measurements of the forces exerted by the abductor<sup>4</sup> muscles in the hip have been made by Inman (1947). If the leg is considered an isolated system as in Fig. 1.12, the following forces act:

- F**: The net force of the abductor muscles, acting on the greater trochanter. These muscles are primarily the gluteus medius and gluteus minimus, shown as a single band of muscle in Fig. 1.12.
- R**: The force of the acetabulum (the socket of the pelvis) on the head of the femur.
- N**: The upward force of the floor on the bottom of the foot (in this case, equal to  $W$ ).
- $W_L$** : The weight of the leg, acting vertically downward at the center of gravity of the leg.  $W_L \approx W/7$  [Williams and Lissner (1962), Chap. 5].

Inman found that **F** acts at about a  $70^\circ$  angle to the horizontal. In a typical adult, the distance from the greater trochanter to the midline is about 18 cm, the horizontal distance from the greater trochanter to the center of gravity of the leg is about 10 cm, and the distance from the greater trochanter to the middle of the head of the femur is about 7 cm.

A free-body diagram is shown in Fig. 1.13. The middle of the head of the femur will turn out to be very close to the intersection of the line along which **R** acts and a horizontal line drawn from the point where **F** acts. This means that if torques are taken about this intersection point (point  $O$ ), there will be no contributions from **R** or from the horizontal component of **F**. The intersection is

<sup>4</sup> To *abduct* means to move away from the midline of the body.

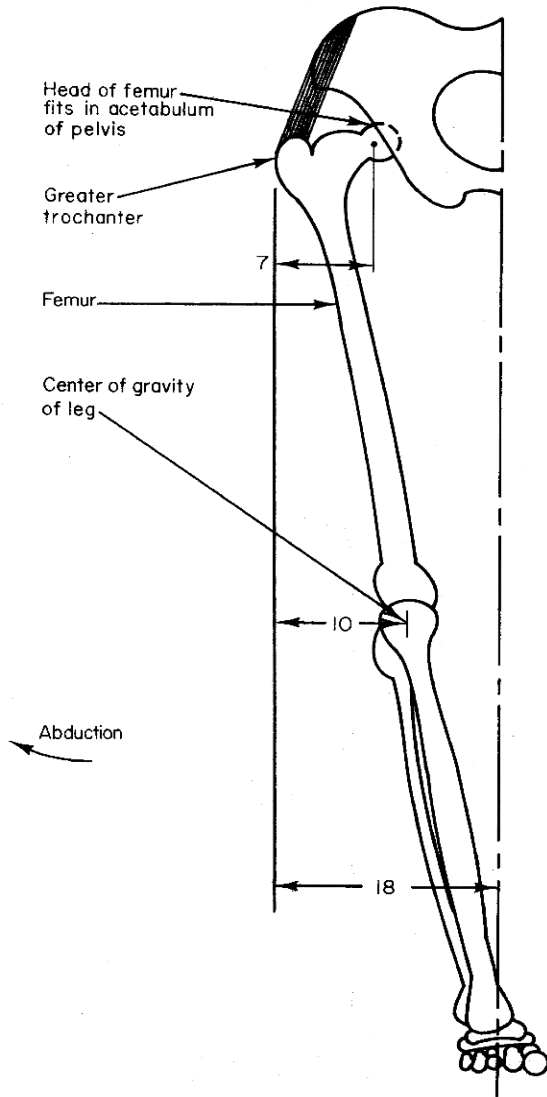


FIGURE 1.12. Pertinent features of the anatomy of the leg.

about 7 cm toward the midline from the point of application of  $\mathbf{F}$ . Since  $N = W$  and  $W_L \approx W/7$ , the equilibrium equations are

$$\sum F_y = F \sin(70^\circ) - R_y - W/7 + W = 0, \quad (1.15)$$

$$\sum F_x = F \cos(70^\circ) - R_x = 0, \quad (1.16)$$

$$\sum \tau = -F \sin(70^\circ)(7) - (W/7)(10 - 7) + W(18 - 7) = 0.$$

The last of these equations can be written as  $11W - \frac{3}{7}W - 6.6F = 0$ , from which  $F = 1.6W$ . The magnitude of the force in the abductor muscles is about 1.6 times the body weight.

Equations 1.15 and 1.16 can now be used to find  $R_x$  and  $R_y$ :

$$R_x = F \cos(70^\circ) = (1.6)(W)(0.342) = 0.55W,$$

$$R_y = F \sin(70^\circ) + \frac{6}{7}W = (1.6)(W)(0.94) + 0.86W = 2.36W.$$

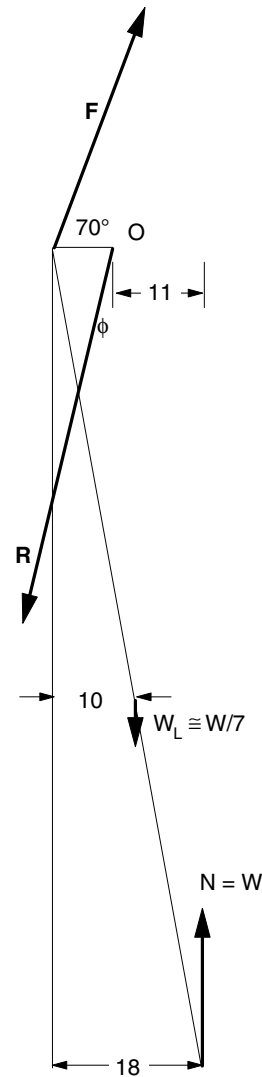


FIGURE 1.13. A free-body diagram of the forces acting on the leg. Torques are taken about point  $O$ , which is the intersection of a line along which  $\mathbf{R}$  acts and a horizontal line through the point at which  $\mathbf{F}$  is applied. This point is 7 cm toward the midline (medially) from the greater trochanter.

The angle that  $\mathbf{R}$  makes with the vertical is given by

$$\tan \phi = \frac{R_x}{R_y} = 0.23,$$

$$\phi = 13^\circ.$$

The magnitude of  $\mathbf{R}$  is  $R = (R_x^2 + R_y^2)^{1/2} = 2.4W$ .

If the patient had not had to put the foot under the center of gravity of the body, the moment arm of the only positive torque,  $11W$ , could have been much less, and this would have been balanced by a smaller value of  $F$ . This can be done by having the patient use a cane on the *opposite* side, so that the foot need not be right under the center of gravity. This will be explored in the next section. Conversely, if the patient were carrying a

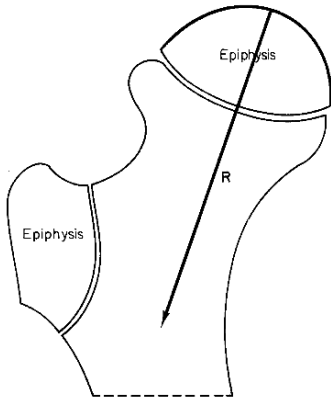


FIGURE 1.14. The femoral epiphysis and the direction of  $\mathbf{R}$ .

suitcase in the opposite hand, the center of mass would be moved away from the midline, the foot would still have to be placed under the center of mass, and the moment arm, and hence  $F$ , would be even larger (Problem 11).

One very interesting conclusion of Inman's study was that the force  $\mathbf{R}$  always acts along the neck of the femur in such a direction that the femoral epiphysis has very little sideways force on it. The epiphysis is the growing portion of the bone (Fig. 1.14) and is not very well attached to the rest of the bone. If there were an appreciable sideways force, the epiphysis would slip sideways, and indeed it sometimes does (Fig. 1.15). This is a serious problem, since if the blood supply to the epiphysis is compromised, there will be no more bone growth.

Suppose that, for some reason, the gluteal muscles are severed. The patient can no longer apply force  $\mathbf{F}$  to the greater trochanter; Eq. 1.16 shows that then  $R_x$  must be zero. This change in the direction of  $\mathbf{R}$  causes a rotation



FIGURE 1.15. X-ray of a slipped femoral epiphysis in an adolescent male. (Courtesy of the Department of Diagnostic Radiology, University of Minnesota.)

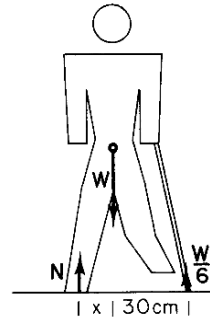


FIGURE 1.16. A person using a cane on the left side (front view) to favor the right hip.

of the epiphyseal plate and a gradual reshaping of the femur.

## 1.7 The Use of a Cane

A cane is beneficial if used on the side opposite to the affected hip (Fig. 1.16). We ignore the fact that the arm holding the cane has moved, thereby shifting slightly the center of mass, and we assume that the force of the ground on the cane is vertical. If we assume that the tip of the cane is about 30 cm (12 in.) from the midline and supports one-sixth of the body weight, then we can apply the equilibrium conditions to learn that  $N + \frac{1}{6}W - W = 0$ , so  $N = \frac{5}{6}W$ . Torques taken about the center of mass give  $(30)(\frac{W}{6}) - x(\frac{5}{6})W = 0$ ,  $x = 6$  cm. (Figure 1.16 is not to scale.)

Having the foot 6 cm from the midline reduces the force in the muscle and the joint. To find out how much, consider the force diagram in Fig. 1.17. The most difficult part of the problem is working out the various moment arms. Assume that the slight movement of the leg has not changed the point about which we take torques (point  $O$ ). Again,  $\mathbf{R}$  contributes no torque about this point. The horizontal distance of  $\mathbf{F}$  from this point is still 7 cm. The force of the ground on the leg is now  $5W/6$ , and its moment arm is  $18 - 6 - 7 = 5$  cm. The weight of the leg,  $W/7$ , acts at the center of mass of the leg, which is still  $\frac{10}{18}$  of the distance from the greater trochanter to the foot. Its horizontal position is therefore  $\frac{10}{18}$  of the horizontal distance from the greater trochanter to the foot:  $(10)(12)/18 = 6.67$  cm. The moment arm is  $7 - 6.67$  cm = 0.33 cm. The torque equation is

$$-F \sin(70^\circ)(7) + \left(\frac{W}{7}\right)(0.33) + \left(\frac{5W}{6}\right)(5) = 0.$$

It is solved by writing it as

$$-6.58F + 0.047W + 4.17W = 0,$$

$$F = 0.64W.$$

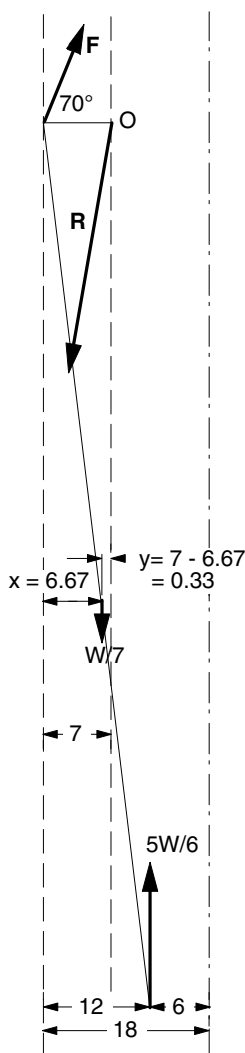


FIGURE 1.17. A force diagram for the leg when a cane is being used and the leg is 6 cm from the midline.

Even though the cane supports only one-sixth of the body weight,  $F$  has been reduced from  $1.6W$  to  $0.64W$  by the change in the moment arm.

The force of the acetabulum on the head of the femur can be determined from the conditions for translational equilibrium:

$$\begin{aligned}
 F \cos(70^\circ) - R_x &= 0, \\
 R_x &= 0.22W, \\
 F \sin(70^\circ) - R_y - \frac{W}{7} + \frac{5}{6}W &= 0, \\
 R_y &= 1.29W.
 \end{aligned}$$

The resultant force  $\mathbf{R}$  has magnitude  $(R_x^2 + R_y^2)^{1/2} = 1.3W$ . This compares to the value  $2.4W$  without the cane. The force in the joint has been reduced by slightly more than the body weight. It is interesting to read what an orthopedic surgeon had to say about the use of a cane. The following is from the presidential address of W. P.

Blount, M.D., to the Annual Meeting of the American Academy of Orthopedic Surgeons, January 30, 1956:

The patient with a wise orthopedic surgeon walks with crutches for six months after a fracture of the neck of the femur. He uses a stick for a longer time—the wiser the doctor, the longer the time. If his medical adviser, his physical therapist, his friends, and his pride finally drive him to abandon the cane while he still needs one, he limps. He limps in a subconscious effort to reduce the strain on the weakened hip. If there is restricted motion, he cannot shift his body weight, but he hurries to remove the weight from the painful hip joint when his pride makes him reduce the limp to a minimum. The excessive force pressing on the aging hip takes its toll in producing degenerative changes. He should not have thrown away the stick.<sup>5</sup>

## 1.8 Work

So far this chapter has considered only situations in which an object is in equilibrium. If the total force on the object is not zero, the object experiences an acceleration  $\mathbf{a}$  given by Newton's second law:

$$\mathbf{F} = m\mathbf{a}.$$

The study of how forces produce accelerations is called *dynamics*. It is an extensive field that will be discussed only briefly here.

Suppose an object moves along the  $x$  axis with velocity  $v_x$ . If it is subject to a force in the  $x$  direction  $F_x$ , it will be accelerated, and the velocity will change according to  $F_x = ma_x = m(dv_x/dt)$ . If  $F_x$  is known as a function of time, then this equation can be written as  $dv_x = (1/m)F_x(t)dt$ , and it can be integrated, at least numerically.

In this context it is useful to define the *kinetic energy*

$$E_k = \frac{1}{2}mv_x^2. \tag{1.17}$$

As long as  $F_x$  acts, the object is accelerated and the kinetic energy changes. We can gain some understanding of how it changes by noting that

$$\frac{d}{dt} \left( \frac{1}{2}mv_x^2 \right) = mv_x \frac{dv_x}{dt} = F_x v_x. \tag{1.18}$$

<sup>5</sup>Quoted with permission from W. P. Blount. Don't throw away the cane. *J. Bone Joint Surg.* **38A**: 695–708. Copyright © 1956 *J. Bone Joint Surg.* This article was first quoted to the physics community by G. B. Benedek and F.M.H. Villars. *Physics with Illustrative Examples from Medicine and Biology. Vol. 1. Mechanics.* Reading, MA, Addison-Wesley, 1973, pp. 3–8.

Therefore  $F_x v_x$  is the rate at which the kinetic energy is changing with time. It is called the *power* due to force  $F_x$ . The units of kinetic energy are  $\text{kg m}^2 \text{s}^{-2}$  or joules (J); the units of power are  $\text{J s}^{-1}$  or watts (W).

If  $v_x$  and  $F_x$  are both positive, the acceleration increases the object's velocity, the kinetic energy increases, and the power is positive. If  $v_x$  and  $F_x$  are both negative,  $v_x$  decreases—becomes more negative—but the magnitude of the velocity increases. The kinetic energy increases with time, and the power is positive. If  $v_x$  and  $F_x$  point in opposite directions, then the effect of the acceleration is to reduce the magnitude of  $v_x$ , the kinetic energy decreases, and the power is negative.

Equation 1.18 can be written as

$$\frac{d}{dt} \left( \frac{1}{2} m v_x^2 \right) = F_x \frac{dx}{dt}.$$

Both sides of this equation can be integrated with respect to  $t$ :

$$\int_{t_1}^{t_2} \frac{d}{dt} \left( \frac{1}{2} m v_x^2 \right) dt = \int_{t_1}^{t_2} F_x(t) \frac{dx}{dt} dt.$$

The indefinite integral corresponding to the left-hand side is the integral with respect to time of the derivative of  $\frac{1}{2} m v_x^2$  and is therefore  $\frac{1}{2} m v_x^2$ . If  $F_x$  is known not as a function of  $t$  but as a function of  $x$ , it is convenient to write the right-hand side as

$$\int_{x_1}^{x_2} F_x(x) dx = W.$$

This quantity is called the *work* done by force  $F_x$  on the object as it moves from  $x_1$  to  $x_2$ . The complete equation is therefore

$$\left[ \frac{1}{2} m v_x^2 \right]_2 - \left[ \frac{1}{2} m v_x^2 \right]_1 = \int_{x_1}^{x_2} F_x(x) dx = W. \quad (1.19)$$

The increase in kinetic energy of the body as it moves from position 1 (at time 1) to position 2 (at time 2) is equal to the work done *on* the body *by* the force  $F_x$ . The work done on the body by force  $F_x$  is the area under the curve of  $F_x$  vs  $x$ , between points  $x_1$  and  $x_2$ . This is shown in Fig. 1.18.

If several forces act on the body, then the acceleration is given by Newton's second law, where  $\mathbf{F}$  is the *total* force on the body. The change in kinetic energy is therefore the work done by the total force or the sum of the work done by each individual force.

When the force and displacement vectors point in any direction, the kinetic energy is defined to be

$$E_k = \frac{1}{2} m v^2 = \frac{1}{2} m (v_x^2 + v_y^2 + v_z^2). \quad (1.20)$$

Differentiating this expression with respect to time shows that the power is given by an extension of Eq. 1.18:

$$\frac{dE_k}{dt} = F_x v_x + F_y v_y + F_z v_z.$$

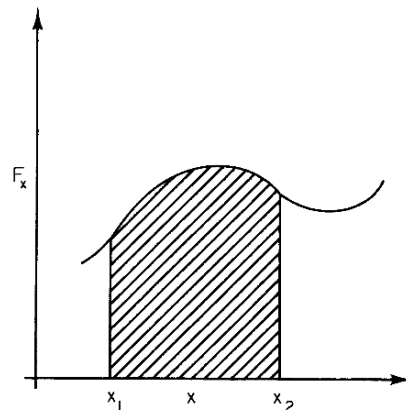


FIGURE 1.18. The work done by  $F_x$  is the shaded area under the curve between  $x_1$  and  $x_2$ .

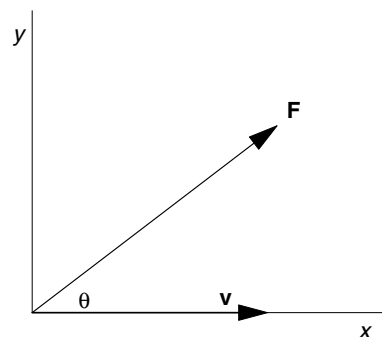


FIGURE 1.19. Aligning the axes so that  $\mathbf{v}$  is along the  $x$  axis and  $\mathbf{F}$  is in the  $xy$  plane shows that an alternative expression for  $\mathbf{F} \cdot \mathbf{v}$  is  $Fv \cos \theta$ .

This particular combination of vectors  $\mathbf{F}$  and  $\mathbf{v}$  is called the *scalar product* or *dot product*. It is written as  $\mathbf{F} \cdot \mathbf{v}$ .

There is another way to write the scalar product. If  $\mathbf{F}$  and  $\mathbf{v}$  are not parallel, they define a plane. Align the  $x$  axis with  $\mathbf{v}$  so that  $v_y$  and  $v_z$  are zero, and choose the direction of  $y$  so that  $\mathbf{F}$  is in the  $xy$  plane (Fig. 1.19). Then it is easy to see that  $\mathbf{F} \cdot \mathbf{v} = F_x v_x = Fv \cos \theta$ , where  $\theta$  is the angle between  $\mathbf{F}$  and  $\mathbf{v}$ .

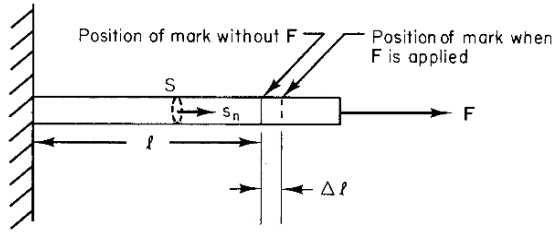
To summarize, the power is

$$P = \frac{dE_k}{dt} = \mathbf{F} \cdot \mathbf{v} = Fv \cos \theta = F_x v_x + F_y v_y + F_z v_z. \quad (1.21)$$

Equation 1.21 can be integrated in the same manner as above to obtain

$$\Delta E_k = \int F_x dx + \int F_y dy + \int F_z dz = \int \mathbf{F} \cdot d\mathbf{s}. \quad (1.22)$$

This is the general expression for the work done by force  $\mathbf{F}$  on a point mass that undergoes displacement  $\mathbf{s}$ .

FIGURE 1.20. A rod subject to a force  $\mathbf{F}$  along it.

## 1.9 Stress and Strain

Whenever a force acts on an object, it undergoes a change of shape or deformation. Often these deformations can be ignored, as they were in the previous sections. In other cases, such as the contraction of a muscle, the expansion of the lungs, or the propagation of a sound wave, the deformation is central to the problem and must be considered. This book will not develop the properties of deformable bodies extensively; nevertheless deformable body mechanics is important in many areas of biology [Fung (1993)]. We will develop the subject only enough to be able to consider viscous forces in fluids.

Consider a rod of cross-sectional area  $S$ . One end is anchored, and a force  $F$  is exerted on the other end parallel to the rod (Fig. 1.20). Effects of weight will be ignored. A *surface force* is transmitted across any surface defined by an imaginary cut perpendicular to the axis of the rod. A surface force is exerted by the substance to the right of the cut on the substance to the left (and vice versa, in accordance with Newton's third law: when object  $A$  exerts a force on object  $B$ , object  $B$  exerts an equal and opposite force on object  $A$ ). The surface force per unit area is called the *stress*. In this case, when the surface is perpendicular to the axis of the rod and the force is along the axis of the rod, it is called a *normal stress*:

$$s_n = \frac{F}{S}. \quad (1.23)$$

In the general case there can also be a component of stress parallel to the surface.

The *strain*  $\epsilon_n$  is the fractional change in the length of the rod:

$$\epsilon_n = \frac{\Delta l}{l}. \quad (1.24)$$

If increasing stress is applied to a typical substance, the strain increases linearly with the stress for small stresses. Then it increases even more rapidly. At higher strains it may be necessary to reduce the stress to maintain the same strain. Finally, at a high enough strain, the sample breaks. This is plotted in Fig. 1.21. Because of the double-valuedness of the strain as a function of stress, the strain is usually plotted as the independent variable, as on the right in Fig. 1.21.

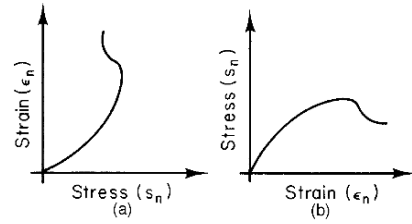


FIGURE 1.21. A typical stress–strain relationship. On the left, stress is the independent variable. On the right, strain is the independent variable. Strain is usually used as the independent variable because it is often a double-valued function of the stress.

In the linear region, the relationship between stress and strain is written as

$$s_n = E\epsilon_n. \quad (1.25)$$

The proportionality constant  $E$  is called *Young's modulus*. Since the strain is dimensionless,  $E$  has the dimensions of stress. Various units are  $\text{N m}^{-2}$  or pascal (Pa),  $\text{dyn cm}^{-2}$ , psi (pound per square inch), and bar ( $1 \text{ bar} = 14.5 \text{ psi} = 10^5 \text{ Pa} = 10^6 \text{ dyn cm}^{-2}$ ).

If the stress is increased enough, the bar breaks. The value of the stress when the bar breaks under tension is called the *tensile strength*. The material will also rupture under compressive stress; the rupture value is called the *compressive strength*. Table 1.3 gives values of Young's modulus, the tensile strength, and the compressive strength for steel, long bone (femur), and wood (walnut).

In some materials, the stress depends not only on the strain, but on the rate at which the strain is produced. It may take more stress to stretch the material rapidly than to stretch it slowly, and more stress to stretch it than

TABLE 1.3. Young's modulus, tensile strength, and compressive strength of various materials in Pa.

Material	$E$	Tensile strength	Compressive strength
Steel (approx.) <sup>a</sup>	$20 \times 10^{10}$	$50 \times 10^7$	
Femur (wet) <sup>b</sup>	$1.4 \times 10^{10}$	$8.3 \times 10^7$	$1.8 \times 10^7$
Walnut <sup>c</sup>	$0.8 \times 10^{10}$	$4.1 \times 10^7$	$5.2 \times 10^7$

<sup>a</sup>American Institute of Physics Handbook (1957). New York, McGraw-Hill, pp. 2-70.

<sup>b</sup>B. K. F. Kummer (1972), Biomechanics of bone. In Y. C. Fung, et al. eds., *Biomechanics—Its Foundations and Objectives*. Englewood Cliffs, NJ, Prentice-Hall, p. 237.

<sup>c</sup>U.S. Department of Agriculture (1955). *Wood Handbook*, Handbook No. 72. Washington, D.C., U.S. Government Printing Office, p. 74.

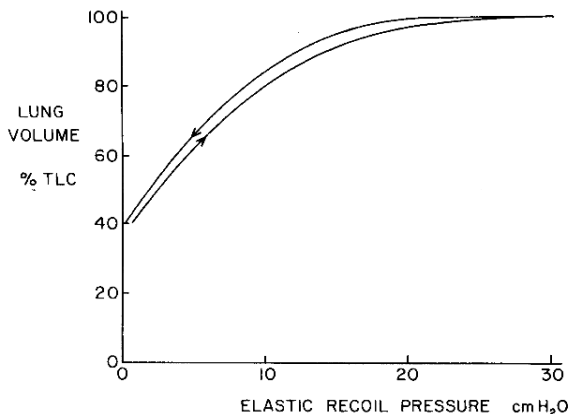


FIGURE 1.22. A pressure–volume curve for a normal lung, showing hysteresis. The elastic recoil pressure is the difference between the pressure in the alveoli (air sacs) of the lung and the thorax just outside the lung. From P. T. Macklem. *Tests of lung mechanics*. *N. Engl. J. Med.* **293**: 339–342. Copyright © 1975 Massachusetts Medical Society. All rights reserved. Drawing courtesy of Prof. Macklem.

to maintain a fixed strain. Such materials are called *viscoelastic*. They are often important biologically but will not be discussed here [Fung (1993)].

Still other materials exhibit *hysteresis*. The stress–strain relationship is different when the material is being stretched than when it is allowed to return to its unstretched state. This difference is observed even if the strain is changed so slowly that viscoelastic effects are unimportant. Figure 1.22 shows a pressure–volume curve for the lung. It is related to the stress–strain relationship for the lung tissue and shows hysteresis.

### 1.10 Shear

In a shear stress, the force is parallel to the surface across which it is transmitted.<sup>6</sup> In a shear strain, the deformation increases as one moves in a direction perpendicular to the deformation. Examples of shear stress and strain are shown in Fig. 1.23. The shear stress is

$$s_s = \frac{F}{S}, \tag{1.26}$$

and the shear strain is

$$\epsilon_s = \frac{\delta}{h}. \tag{1.27}$$

<sup>6</sup>This discussion of stress and strain has been made simpler than is often the case. In general, the force  $\mathbf{F}$  across any surface is a vector. It can be resolved into a component perpendicular to the surface and two components parallel to the surface. One can speak of nine components of stress:  $s_{xx}, s_{xy}, s_{xz}, s_{yx}, s_{yy}, s_{yz}, s_{zx}, s_{zy}, s_{zz}$ . The first subscript denotes the direction of the force and the second denotes the normal to the surface across which the force acts. Components  $s_{xx}, s_{yy}$  and  $s_{zz}$  are normal stresses; the others are shear stresses. It can be shown that  $s_{xy} = s_{yx}$ , and so forth.

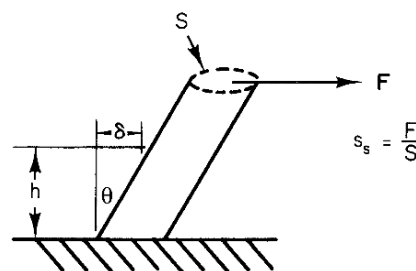


FIGURE 1.23. Shear stress and strain.

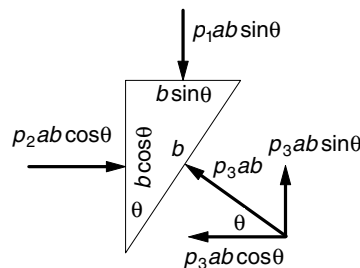


FIGURE 1.24. A volume element of fluid used to show that the pressure in a fluid at rest is the same in all directions.

It is possible to define a shear modulus  $G$  analogous to Young’s modulus when the shear strain is small:

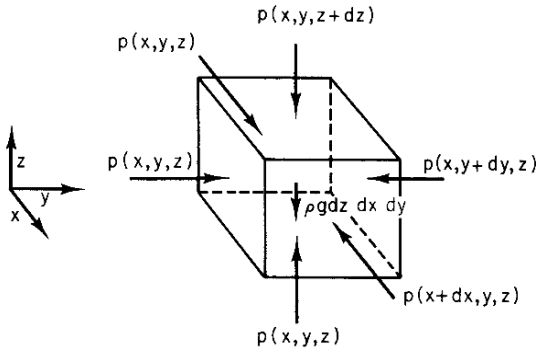
$$s_s = G\epsilon_s. \tag{1.28}$$

### 1.11 Hydrostatics

We now turn to some topics in the mechanics of fluids that will be useful for understanding several phenomena, including the circulation and fluid movement through membranes in Chapter 5. *Hydrostatics* is the description of fluids at rest. A fluid is a substance that will not support a shear when it is at rest. When the fluid is in motion, there can be a shear force called *viscosity*.

An immediate consequence of the definition of a fluid is that when the fluid is at rest, all the stress is normal. The normal stress is called the pressure. The pressure at any point in the fluid is the same in all directions. This can be demonstrated experimentally, and it can be derived from the conditions for equilibrium. Consider the small volume of fluid shown in Fig. 1.24. It has a length  $a$  perpendicular to the page. This volume is in equilibrium. Since the fluid at rest cannot support a shear, the pressure is perpendicular to each face, and there is no other force across each face. To prove this, assume that the pressures perpendicular to the three faces can be different, and call them  $p_1, p_2$ , and  $p_3$ . The force exerted across face 1 is  $p_1 ab \sin \theta$ , acting downward. The force across face 2 is  $p_2 ab \cos \theta$  acting to the right. Across face 3 it is  $p_3 ab$ , with vertical component  $p_3 ab \sin \theta$  and horizontal component  $p_3 ab \cos \theta$ . The vertical components sum to zero



FIGURE 1.25. The fluid in volume  $dx dy dz$  is in equilibrium.

only if  $p_1 = p_3$ , while the horizontal components sum to zero only if  $p_3 = p_2$ . Since this result is independent of the value of  $\theta$ , the pressure must be the same in every direction.

Next, consider how the pressure changes with position. Suppose that  $p$  depends on the coordinates  $p = p(x, y, z)$  and that the density of the fluid is  $\rho \text{ kg m}^{-3}$ . The only external force acting is gravity in the direction of the  $-z$  axis. The fluid in the volume  $dx dy dz$  of Fig. 1.25 is in equilibrium. In the  $y$  direction there is a force to the right across the left-hand face equal to  $p(x, y, z) dx dz$  and to the left across the right-hand face equal to  $-p(x, y + dy, z) dx dz$ . These are the only forces in the  $y$  direction, and their magnitudes must be the same. Therefore  $p$  does not change in the  $y$  direction. A similar argument shows that  $p$  does not change in the  $x$  direction. In the  $z$  direction there are three terms: the upward force across the bottom face, the downward force across the top face, and the pull of gravity. The weight of the fluid is its mass ( $\rho dx dy dz$ ) times the gravitational acceleration  $g$  ( $g = 9.8 \text{ m s}^{-2}$ ). The three forces must add to zero:

$$p(x, y, z) dx dy - p(x, y, z + dz) dx dy - \rho g dx dy dz = 0.$$

For small changes in height,  $dz$ , it is possible to approximate<sup>7</sup>  $p(x, y, z + dz)$  by  $p(x, y, z) + (dp/dz) dz$ . With this approximation, the equilibrium equation is

$$dx dy dz \left( -\frac{dp}{dz} - \rho g \right) = 0.$$

This equation can be satisfied only if

$$\frac{dp}{dz} = -\rho g. \quad (1.29)$$

This is a differential equation for  $p(z)$ . It is a particularly simple one, since the right-hand side is constant if  $\rho$  and

$g$  are constant:  $dp = -\rho g dz$ . Integrating this gives

$$\int dp = -\rho g \int dz, \\ p = -\rho g z + c.$$

The constant of integration is determined by knowing the value of  $p$  for some value of  $z$ . If  $p = p_0$  when  $z = 0$ , then  $p_0 = c$  and

$$p = p_0 - \rho g z. \quad (1.30)$$

With a constant gravitational force per unit volume acting on the fluid, the pressure decreases linearly with increasing height. The SI unit of pressure is  $\text{N m}^{-2}$  or pascal (Pa). The density is expressed in  $\text{kg m}^{-3}$ , so that  $\rho g$  has units of  $\text{N m}^{-3}$  and  $\rho g z$  is in  $\text{N m}^{-2}$ . Pressures are often given as equivalent values of  $z$  in some substance, for example, in millimeters of mercury (torr) or centimeters of water. In such cases, the value of  $z$  must be converted to an equivalent value of  $\rho g z$  before calculations involving anything besides pressure are done. The density of water is  $1 \text{ g cm}^{-3}$  or  $10^3 \text{ kg m}^{-3}$ . The density of mercury is  $13.6 \times 10^3 \text{ kg m}^{-3}$ , so  $1 \text{ torr} = 133 \text{ Pa}$ . Another common unit for pressure is the atmosphere (atm), equal to  $1.01 \times 10^5 \text{ Pa}$ . One atmosphere is approximately the atmospheric pressure at sea level.

## 1.12 Buoyancy

Buoyancy effects are important when an object is immersed in a fluid. We are all familiar with buoyant effects when swimming; they are also important in instruments such as the centrifuge. Consider an object of density  $\rho$  immersed in a fluid of density  $\rho_{\text{fluid}}$ . The net force on such an object is the sum of the gravitational force and a force arising from the pressure gradient in the fluid. To visualize this, consider a small object with sides  $dx$ ,  $dy$ ,  $dz$ . We have just seen that the pressure on the bottom face is greater than the pressure on the top face. Therefore there is an upward force on the cube. The total force on the object is then

$$F = \left( -\frac{dp}{dz} - \rho g \right) dx dy dz.$$

Since the pressure gradient in the fluid is  $-\rho_{\text{fluid}} g$ , the total force is

$$F = (\rho_{\text{fluid}} - \rho) g V, \quad (1.31)$$

where  $V$  is the volume of the object. The second term is the object's weight, directed downward. The first term is called the buoyant force and is directed upward. The buoyant force reduces the "effective weight" of the object and depends on the difference of densities of the object and the surrounding fluid.

Animals are made up primarily of water, so their density is approximately  $10^3 \text{ kg m}^{-3}$ . The buoyant force depends on the animal's environment. Terrestrial animals

<sup>7</sup>See Appendix D on Taylor's series for a more complete discussion of this approximation.

live in air, which has a density of  $1.2 \text{ kg m}^{-3}$ . The buoyant force on terrestrial animals is very small compared to their weight. Aquatic animals live in water, and their density is almost the same as the surrounding fluid. The buoyant force almost cancels the weight, so the animal is essentially “weightless.” Gravity plays a major role in the life of terrestrial animals, but only a minor role for aquatic animals. Denny (1993) explores the differences between terrestrial and aquatic animals in more detail.

## 1.13 Compressibility

Increasing the pressure on a fluid causes a deformation and a decrease in volume. The compressibility  $\kappa$  is defined as

$$\frac{\Delta V}{V} = -\kappa \Delta p. \quad (1.32)$$

Since  $\Delta V/V$  is dimensionless,  $\kappa$  has the units of inverse pressure,  $\text{N}^{-1} \text{ m}^2$  or  $\text{Pa}^{-1}$ . In many liquids the compressibility is quite small (e.g.,  $5 \times 10^{-10} \text{ Pa}^{-1}$  for water), and for many purposes, such as flow through pipes, compressibility can be ignored. Other effects, such as the transmission of sound through a fluid, depend on deformation, and compressibility cannot be ignored.

## 1.14 Viscosity

A fluid at rest does not support a shear. If the fluid is moving, a shear force can exist. At large velocities the flow of the fluid is turbulent and may be difficult or impossible to calculate. We will consider only cases in which the velocity is low enough so that the flow is smooth. This means that particles of dye introduced into the fluid to monitor its motion flow along smooth lines called *streamlines*. A streamline is tangent to the velocity vector of the fluid at every point along its path. There is no mixing of fluid across streamlines; the flow is *laminar* (in layers). Laminar flow is often used in rooms where dirt or bacterial contamination is to be avoided, such as operating rooms or manufacturing clean rooms. Clean air enters and passes through the room without mixing. Any contaminants picked up are carried out in the air.

A fluid can support a viscous shear stress if the shear strain is changing. One way to create such a situation is to immerse two parallel plates, each of area  $S$ , in the fluid, and to move one parallel to the other as in Fig. 1.26. If the fluid in contact with each plate sticks to the plate,<sup>8</sup> the fluid in contact with the lower plate is at rest and that in contact with the upper plate moves with the same velocity as the plate. Between the plates the fluid flows parallel to the plates, with a speed that depends

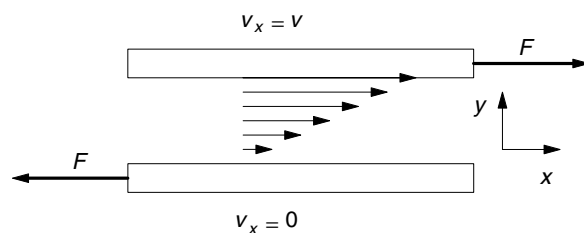


FIGURE 1.26. Forces  $\mathbf{F}$  and  $-\mathbf{F}$  are needed to make the top plate move in a viscous fluid while the bottom plate remains stationary. The velocity profile is also shown.

on position as shown in Fig. 1.26. The variation of velocity between the plates gives rise to a velocity gradient  $dv_x/dy$ . Note that this is the rate of change of the shear strain.

In order to keep the top plate moving and the bottom plate stationary, it is necessary to exert a force of magnitude  $F$  on each plate: to the right on the upper plate and to the left on the lower plate. The resulting shear stress or force per unit area is in many cases proportional to the velocity gradient:

$$\frac{F}{S} = \eta \frac{dv_x}{dy}. \quad (1.33)$$

The constant  $\eta$  is called the *coefficient of viscosity*. Often this equation is written with a minus sign, in which case  $\mathbf{F}$  is the force of the fluid on the plate rather than the plate on the fluid. The units of  $\eta$  are  $\text{N s m}^{-2}$  or  $\text{kg m}^{-1} \text{ s}^{-1}$  or  $\text{Pa s}$ . Older units are the  $\text{dyn s cm}^{-2}$  or poise, the centipoise, and the micropoise.  $1 \text{ poise} = 0.1 \text{ Pa s}$ . Equation 1.33 gives the force exerted by fluid above the plane at height  $y$  on the fluid below the plane. In the case of the parallel plates, the force from above on fluid in the slab between  $y$  and  $y + dy$  is the same in magnitude as (and opposite in direction to) the force exerted by the fluid below the slab. Therefore there is no net force on the fluid in the slab, and the fluid moves with constant velocity. Fluids that are described by Eq. 1.33 are called *Newtonian fluids*. Many fluids are not Newtonian.

Since  $dv_x/dy$  is the rate of change of the shear strain, Eq. 1.27, Eq. 1.33 can be written

$$s_s = \frac{F}{S} = \eta \frac{d\epsilon_s}{dt}.$$

The rate of change of the shear strain is also called the *shear rate*.

## 1.15 Viscous Flow in a Tube

Biological fluid dynamics is a well-developed area of study [Lighthill (1975); Mazumdar (1992); Vogel (1994)]. External biological fluid dynamics is concerned with locomotion—from single-celled organisms to swimming

<sup>8</sup>This is called the “no-slip” boundary condition. There are exceptions.

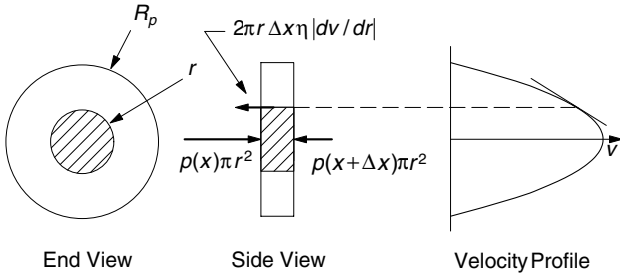


FIGURE 1.27. Longitudinal and transverse cross sections of the tube. Newton’s first law is applied to the shaded volume.

fish and flying birds. Internal biological fluid dynamics deals with mass transport within the organism. Two obvious examples are flow in the airways and the flow of blood.

Consider laminar viscous flow of fluid through a pipe of constant radius  $R_p$  and length  $\Delta x$ . Ignore for now the gravitational force. The pressure at the left end of a segment of pipe is  $p(x)$ ; at the right end it is  $p(x + \Delta x)$ . For now consider the special case in which none of the fluid is accelerated, so the total force on any volume element of the fluid is zero. The velocity profile must be as shown in Fig. 1.27: zero at the walls and a maximum at the center. Our problem is to determine  $v(r)$ .

Let us determine the forces acting on the shaded cylinder of fluid of radius  $r$  shown in Fig. 1.27. Since gravity is ignored, there are only three forces acting on the volume. The fluid on the left exerts a force  $\pi r^2 p(x)$  acting to the right in the direction of the positive  $x$  axis. The fluid on the right exerts a force  $-\pi r^2 p(x + \Delta x)$  (the minus sign because it points to the left). The slower-moving fluid outside the shaded region exerts a viscous drag force across the cylindrical surface at radius  $r$ . The area of the surface is  $2\pi r \Delta x$ . The force points to the left. Its magnitude is  $2\pi r \Delta x \eta |dv/dr|$ . Since  $dv/dr$  is negative, we obtain the correct sign by writing it as  $2\pi r \Delta x \eta (dv/dr)$ . Since the fluid is not accelerating, the forces sum to zero:

$$\pi r^2 [p(x) - p(x + \Delta x)] + 2\pi r \Delta x \eta (dv/dr) = 0, \quad (1.34)$$

which can be rearranged to give

$$\frac{dv}{dr} = \frac{r}{2\eta} \left( \frac{p(x + \Delta x) - p(x)}{\Delta x} \right) = \frac{dp}{dx} \frac{r}{2\eta}. \quad (1.35)$$

This can be integrated:

$$\int dv = \frac{1}{2\eta} \left( \frac{dp}{dx} \right) \int r dr, \\ v(r) = \frac{1}{4\eta} \left( \frac{dp}{dx} \right) r^2 + A. \quad (1.36)$$

For flow to the right  $dp/dx$  is negative. Therefore it is convenient to write  $\Delta p$  as the pressure drop from  $x$  to  $x + dx$ :  $\Delta p = p(x) - p(x + \Delta x)$ . Then the first term in Eq. 1.36 is  $-(1/4\eta)(\Delta p/\Delta x)r^2$ . The constant of integration can be

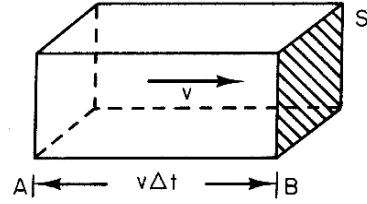


FIGURE 1.28. Flow of fluid across the plane at  $B$ .

determined assuming the “no-slip” boundary condition: that the velocity of the fluid immediately adjacent to a solid is the same as the velocity of the solid itself. Because the wall is at rest, the velocity of the fluid is zero at the wall ( $r = R_p$ ). The final result is

$$v(r) = \frac{1}{4\eta} \frac{\Delta p}{\Delta x} (R_p^2 - r^2). \quad (1.37)$$

The total flow rate or *volume flux* or *volume current*  $i$  is the volume of fluid per second moving through a cross section of the tube. Its units are  $\text{m}^3 \text{s}^{-1}$ . The *volume fluence rate* or *volume flux density*<sup>9</sup> or *current density*  $j_v$  is the volume per unit area per unit time across some small area in the tube. The units of  $j_v$  are  $\text{m}^3 \text{s}^{-1} \text{m}^{-2}$  or  $\text{m s}^{-1}$ .

In fact,  $j_v$  is just the velocity of the fluid at that point. To see this, consider the flow of an incompressible fluid during time  $\Delta t$ . In Fig. 1.28 the fluid moves to the right with velocity  $v$ . At  $t = 0$ , the fluid just to the left of plane  $B$  crosses the plane; at  $t = \Delta t$ , that fluid that was at  $A$  at  $t = 0$  crosses plane  $B$ . All the fluid between plane  $A$  and plane  $B$  crosses plane  $B$  during the time interval  $\Delta t$ . The volume fluence rate is

$$j_v = \frac{(\text{volume transported})}{(\text{area})(\text{time})} = \frac{Sv\Delta t}{S\Delta t} = v. \quad (1.38)$$

It may seem unnecessarily confusing to call the fluence rate or flux density  $j_v$  instead of  $v$ ; however, this notation corresponds to a more general notation in which  $j$  means the fluence rate or flux density of anything per unit area per unit time, and the subscript  $v$ ,  $s$ , or  $q$  tells us whether it is the fluence rate of volume, solute particles, or electric charge.

To find the volume current  $i$ ,  $j_v$  must be integrated over the cross-sectional area of the pipe. The volume of fluid crossing the washer-shaped area  $2\pi r dr$  is  $j_v 2\pi r dr = v 2\pi r dr$ . The total flux through the tube is therefore

$$i = \int_0^{R_p} j_v(r) 2\pi r dr, \\ i = \frac{2\pi}{4\eta} \frac{\Delta p}{\Delta x} \int_0^{R_p} (R_p^2 - r^2) r dr. \quad (1.39)$$

<sup>9</sup>Some authors call  $j_v$  the flux. The nomenclature used here is consistent throughout the book.

To integrate this, let  $u = R_p^2 - r^2$ . Then  $du = -2rdr$  and the integral is  $R_p^4/4$ . Therefore

$$i = \frac{\pi R_p^4}{8\eta} \frac{\Delta p}{\Delta x} \quad (1.40)$$

is the flux of a viscous fluid through a pipe of radius  $R_p$  due to a pressure gradient  $(\Delta p/\Delta x)$  along the pipe. The dependence of  $i$  on  $R_p^4$  means that small changes in diameter cause large changes in flow.

This relationship was determined experimentally in painstaking detail by a French physician, Jean Leonard Marie Poiseuille, in 1835. He wanted to understand the flow of blood through capillaries. His work and knowledge of blood circulation at that time have been described by Herrick (1942).

As an example of the use of Eq. 1.40, consider a pore of the following size, which might be found in the basement membrane of the glomerulus of the kidney:

$$\begin{aligned} R_p &= 5 \text{ nm}, \\ \Delta p &= 15.4 \text{ torr}, \\ \eta &= 1.4 \times 10^{-3} \text{ kg m}^{-1} \text{ s}^{-1}, \\ \Delta x &= 50 \text{ nm}. \end{aligned} \quad (1.41)$$

It is first necessary to convert 15.4 torr to Pa using Eq. 1.30 and the value of  $\rho$  for mercury,  $13.55 \times 10^3 \text{ kg m}^{-3}$ :

$$\begin{aligned} \Delta p &= \rho g \Delta z = (13.55 \times 10^3)(9.8)(15.4 \times 10^{-3}) \\ &= 2.04 \times 10^3 \text{ N m}^{-2}. \end{aligned}$$

Then Eq. 1.40 can be used:

$$i = \frac{(3.14)(5 \times 10^{-9})^4(2.04 \times 10^3)}{(8)(1.4 \times 10^{-3})(50 \times 10^{-9})} = 7.2 \times 10^{-21} \text{ m}^3 \text{ s}^{-1}.$$

Now consider the general case in which we have not only viscosity, but the fluid may be accelerated and gravity is important. We continue to write  $\Delta p$  as the pressure drop and consider four contributions, each of which will be discussed:

$$\begin{aligned} \Delta p &= \int_{x_1}^{x_2} (dp/dx) dx \\ &= \Delta p_{\text{visc}} + \Delta p_{\text{grav}} + \Delta p_{\text{accel1}} + \Delta p_{\text{accel2}}. \end{aligned} \quad (1.42)$$

For simplicity, we restrict the derivation to an incompressible fluid and a pipe of circular cross section where the radius can change. The distance along the pipe is  $x$  and the radius of the pipe is  $R_p(x)$ . Gravitational force acts on the fluid, and the height of the axis of the pipe above some reference plane is  $z$ , as shown in Fig. 1.29.

Because the fluid is incompressible, the total current  $i$  is independent of  $x$ . If the pipe narrows, the velocity increases. Assume that changes in pipe radius occur slowly enough so that the velocity profile remains parabolic at every point in the pipe and we can treat  $x$  as though it

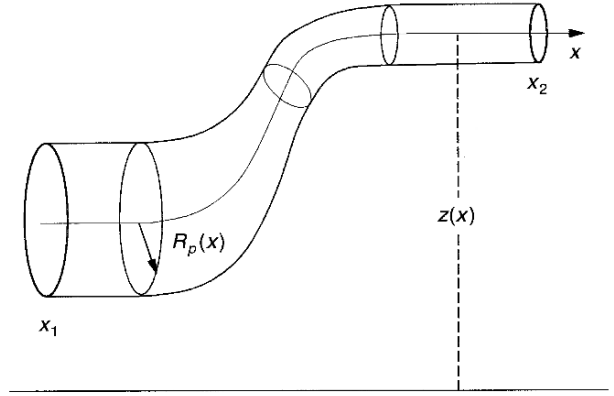


FIGURE 1.29. A pipe of circular cross section with radius and height varying along the pipe.

were a distance along the axis of the cylinder. If we define the average velocity as

$$\bar{v}(x) = \frac{i}{\pi R_p^2(x)}, \quad (1.43)$$

we can use Eq. 1.37 to rewrite the velocity profile as

$$v(r, x) = 2\bar{v} \left[ 1 - \frac{r^2}{R_p^2(x)} \right] = \frac{2i}{\pi R_p^2(x)} \left[ 1 - \frac{r^2}{R_p^2(x)} \right]. \quad (1.44)$$

The first term in Eq. 1.42 is the pressure to overcome viscous drag. We can rewrite Eq. 1.35 as

$$\frac{dp_{\text{visc}}}{dx} = \frac{2\eta}{r} \frac{dv}{dr}.$$

Using Eq. 1.44 we can write

$$\frac{dp_{\text{visc}}}{dx} = -\frac{8\eta i}{\pi R_p^4(x)}. \quad (1.45)$$

We saw this earlier, solved for  $i$  in a pipe of constant radius, as Eq. 1.40. The pressure drop is obtained by integration:

$$\begin{aligned} \Delta p_{\text{visc}} &= -\int_{x_1}^{x_2} dp_{\text{visc}} = -\int_{x_1}^{x_2} \left( \frac{dp_{\text{visc}}}{dx} \right) dx \\ &= +\frac{8\eta i}{\pi} \int_{x_1}^{x_2} \frac{dx}{R_p^4(x)}. \end{aligned} \quad (1.46)$$

To go further requires knowing  $R_p(x)$ .

The next term  $p_{\text{grav}}$  is the hydrostatic pressure change that we saw in Eq. 1.30:

$$\Delta p_{\text{grav}} = -\int_{x_1}^{x_2} dp_{\text{grav}} = -\int \frac{dp_{\text{grav}}}{dz} dz = \rho g(z_2 - z_1). \quad (1.47)$$

The last two terms of Eq. 1.42 are pressure differences required to accelerate the fluid. When the flow is steady—that is, the velocity depends only on position, and the

velocity at a fixed position does not change with time—there can still be an acceleration if the cross section of the pipe changes. The third term,  $\Delta p_{\text{accel1}}$ , provides the force for this acceleration. It can be derived as follows. Imagine a streamline in the fluid. No fluid crosses the streamline. Consider a small length of streamline  $ds$  and a small area  $dA$  perpendicular to it. Note that  $ds$  is a small displacement along a streamline, while  $dx$  is along the axis of the pipe. The edge of  $dA$  defines another set of streamlines that form a tube of flow, and  $dAds$  defines a small volume of fluid. Make  $ds$  and  $dA$  small enough so that  $v$  is nearly the same at all points within the volume. The mass of fluid in the volume is  $dm = \rho dAds$ . We ignore viscosity and gravity, so the only pressure difference is due to acceleration. The net force on the volume is

$$dF = -\frac{dp}{ds} ds dA. \quad (1.48)$$

This is equal to the mass times the acceleration  $dv/dt$ . The acceleration of the fluid in the element is then

$$\frac{dv}{dt} = \frac{dF}{dm} = \frac{-\left(\frac{dp}{ds}\right) ds dA}{\rho ds dA} = -\frac{1}{\rho} \left(\frac{dp}{ds}\right). \quad (1.49)$$

We are considering only velocity changes that occur because the fluid moves along a streamline to a different position. We use the chain rule to write

$$\frac{dv}{dt} = \left(\frac{dv}{ds}\right) \left(\frac{ds}{dt}\right) = v \left(\frac{dv}{ds}\right).$$

Combining these gives

$$\frac{dp_{\text{accel1}}}{ds} = -\rho v \left(\frac{dv}{ds}\right). \quad (1.50)$$

This can be integrated along the streamline to give

$$\begin{aligned} \Delta p_{\text{accel1}} &= -\int_{s_1}^{s_2} \left(\frac{dp_{\text{accel1}}}{ds}\right) ds = +\rho \int_{x_1}^{x_2} v \left(\frac{dv}{ds}\right) ds \\ &= \frac{\rho v_2^2}{2} - \frac{\rho v_1^2}{2}. \end{aligned} \quad (1.51)$$

The final term  $\Delta p_{\text{accel2}}$  is the pressure change required to accelerate the fluid between points 1 and 2 if the velocity of the fluid at a fixed position is changing with time. This happens, for example, to blood that is accelerated as it is ejected from the heart during systole, or to fluid that is sloshing back and forth in a U tube. To derive this term, again imagine a small length of streamline  $ds$  and a small area  $dA$  perpendicular to it. In addition to ignoring gravity and viscosity, we ignore changes in velocity because of changes in cross section. There is acceleration only if the velocity at a fixed location is changing. The acceleration is  $\partial v/\partial t$ . The derivative is written with  $\partial$ 's to signify the fact that we are considering only changes in the velocity with time that occur at a fixed position.

The net force required to accelerate this mass is provided by the pressure difference Eq. 1.48:

$$\begin{aligned} dF &= -dA dp_{\text{accel2}} = dm \left(\frac{\partial v}{\partial t}\right) = \rho \left(\frac{\partial v}{\partial t}\right) dA ds, \\ dp_{\text{accel2}} &= -\rho \left(\frac{\partial v}{\partial t}\right) ds, \\ \Delta p_{\text{accel2}} &= -\int_{s_1}^{s_2} dp_{\text{accel2}} = \rho \int_{s_1}^{s_2} \left(\frac{\partial v}{\partial t}\right) ds. \end{aligned} \quad (1.52)$$

All of these effects can be summarized in the *generalized Bernoulli equation*:

$$\begin{aligned} p_1 - p_2 = \Delta p &= \underbrace{\rho \int_{s_1}^{s_2} \frac{\partial v}{\partial t} ds}_{\Delta p_{\text{accel2}}} + \underbrace{\int_{s_1}^{s_2} \left(-\frac{dp_{\text{visc}}}{ds}\right) ds}_{\Delta p_{\text{visc}}} \\ &\quad + \underbrace{\frac{\rho v_2^2}{2} - \frac{\rho v_1^2}{2}}_{\Delta p_{\text{accel1}}} + \underbrace{\rho g (z_2 - z_1)}_{\Delta p_{\text{grav}}} \end{aligned} \quad (1.53)$$

Equation 1.53 is valid for nonuniform viscous flow that may be laminar or turbulent if the integral is taken along a streamline [see, for example, Synolakis and Badeer (1989)].

## 1.16 Pressure–Volume Work

An important example of work is that done in a biological system when the volume of a container (such as the lungs or the heart or a blood vessel) changes while the fluid within the container is exerting a force on the walls.

To deduce an expression for pressure–volume work, consider a cylinder of gas fitted with a piston, Fig. 1.30(a). If the piston has area  $S$ , the gas exerts a force  $F_g = pS$  on the piston. If no other force is exerted on the

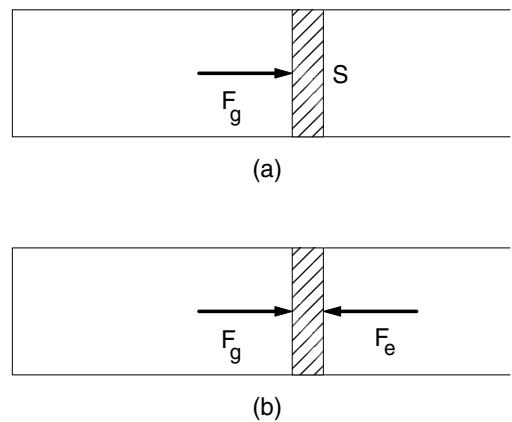


FIGURE 1.30. (a) A cylinder containing gas has a piston of area  $S$  at one end. (b) The force exerted on the piston by the gas is balanced by an external force if the piston is at rest.

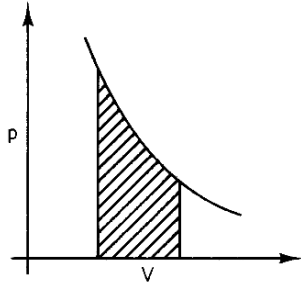


FIGURE 1.31. A plot of  $p$  vs  $V$ , showing the work done by the gas as it expands.

piston to restrain it, it will be accelerated to the right and gain kinetic energy as the gas does work on it:

$$(\text{work done by gas}) = F_g dx = pSdx = pdV. \quad (1.54)$$

If the piston is prevented from accelerating by an external force  $\mathbf{F}_e$  equal and opposite to that exerted by the gas [Fig. 1.28(b)], then the external force does work on the piston:

$$\begin{aligned} (\text{work done by external force}) &= -F_e dx & (1.55) \\ &= -pSdx = -pdV, \end{aligned}$$

which is the negative of the work done on the piston by the expanding gas. The result is that the kinetic energy of the piston does not change. The gas does work on the surroundings as it expands, increasing the energy of the surroundings; the surroundings, through the external force, do *negative* work on the gas; that is, they decrease the energy of the gas. (The meaning of “energy of the gas” and “energy of the surroundings” is discussed in Chapter 3.) If the gas is compressed, the situation is reversed: the surroundings do positive work on the gas and the gas does negative work on the surroundings.

For a large change in volume from  $V_1$  to  $V_2$ , the pressure may change as the volume changes. In that case the work done by the gas on the surroundings is

$$W_{\text{by gas}} = \int_{V_1}^{V_2} p dV. \quad (1.56)$$

This work is the shaded area in Fig. 1.31. If the gas is compressed, the change in volume is negative and the work done *by* the gas is negative.

Let us apply this model to the heart. Suppose that the left ventricle of the heart contracts at constant pressure, so that it changes volume by  $\Delta V = V_2 - V_1$ . (Since  $V_2 < V_1$  the quantity  $\Delta V$  is negative. A volume of blood  $-\Delta V$  is ejected into the aorta.) The work done by the heart wall on the blood is  $-p\Delta V$  and is positive, since  $\Delta V$  is negative.

As another example of pressure–volume work, we can develop a model to estimate the work necessary to breathe. Consider the model of the lungs and airways shown in Fig. 1.32. The pressure at the nose is the atmospheric pressure  $p$ . In the alveoli (air sacs) the pressure

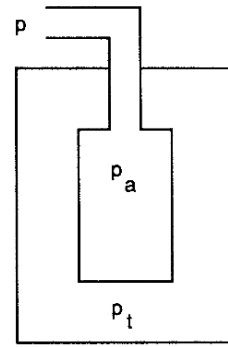


FIGURE 1.32. A model of the thorax, lungs, and airways that can be used to understand some features of breathing.

is  $p_a$ . If there is no flow taking place,  $p_a = p$ . For air to flow in,  $p_a$  must be less than  $p$ ; for it to flow out,  $p_a$  must be greater than atmospheric. The work done by the walls of the alveoli on the gas in them is  $-\int p_a dV$ . The net value of this integral for a respiratory cycle is positive. Perhaps the easiest way to see this is to imagine an inspiration, in which the alveolar pressure is  $p_a = p - \Delta p$  and the volume change is  $\Delta V$ . The work done on the gas is  $-(p - \Delta p)\Delta V$ . This is followed by an expiration at pressure  $p_a = p + \delta p$ , for which the work is  $-(p + \delta p)(\Delta V)$ . The net work done on the gas is  $(\Delta p + \delta p)\Delta V$ . The energy imparted to the gas shows up as a mixture of heating because of frictional losses and kinetic energy of the exhaled air.

There is another mechanism by which work is done in breathing. Refer again to Fig. 1.32. The pressure in the chest cavity (thorax) is  $p_t$ . (The pressure measured in mid-esophagus is a good estimate of  $p_t$ .) Because of contractile forces in the lung tissue,  $p_a > p_t$ . The quantity  $p_a - p_t$  is the “elastic recoil pressure” of Fig. 1.22. The gas in the alveoli and the fluid in the thorax both do work on the lung tissue. The latter has opposite sign, since a positive displacement  $dx$  of a portion of the alveolar wall is in the direction of the force exerted by the alveolar gas but is opposite to the direction of the force exerted by the thoracic fluid. The elastic recoil pressure, multiplied by  $dV$ , gives the net work done by both forces on the wall of the lung.

Figure 1.22 shows elastic recoil pressure versus lung volume. It is redrawn in Fig. 1.33. During inspiration (curve  $AB$ ), the elastic recoil pressure  $p_a - p_t$  is greater than that during expiration (curve  $BC$ ). The net work done on the lung wall during the respiratory cycle goes into frictional heating of the lung tissue.

## 1.17 The Human Circulatory System

The human circulatory system is responsible for pumping blood and its life-sustaining nutrients to all parts of

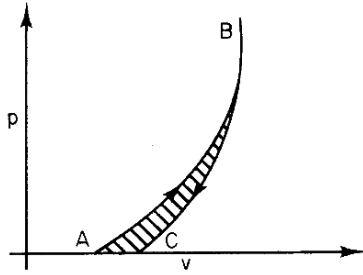


FIGURE 1.33. A hypothetical plot of the pressure–volume relationship for inhalation and exhalation.

the body [Vogel (1992)]. The circulatory system has two parts: the *systemic circulation* and the *pulmonary circulation*, as shown in Fig. 1.34. The left heart pumps blood into the systemic circulation: organs, muscles, etc. The right heart pumps blood through the lungs. As the heart beats, the pressure in the blood leaving the heart rises and falls. The maximum pressure during the cardiac cycle is the *systolic pressure*. The minimum is the *diastolic pressure*. (A blood pressure reading is in the form systolic/diastolic, measured in torr.) The blood flows from the aorta to several large arteries, to medium-sized arteries, to small arteries, to arterioles, and finally to the capillaries, where exchange with the tissues of oxygen, carbon dioxide, and nutrients takes place. The blood emerging from the capillaries is collected by venules, flows into increasingly larger veins, and finally returns to the heart through the vena cava.

At any given time, blood is flowing in only a fraction of the capillaries. The state of flow in the capillaries is continually changing to provide the amount of oxygen required by each organ. In skeletal muscle, terminal arterioles constrict and dilate to control distribution of blood to groups of capillaries. In smooth muscle and skin, a precapillary sphincter muscle controls the flow to each capillary [Patton *et al.* (1989), p. 860]. Since the blood is incompressible and is conserved,<sup>10</sup> the total volume flow  $i$  remains the same at all generations of branching in the vascular tree. Table 1.4 shows average values for the pressure and vessel sizes at different generations of branching. Most of the pressure drop occurs in the arterioles.

We define the *vascular resistance*  $R$  in a pipe or a segment of the circulatory system as the ratio of pressure difference across the pipe or segment to the flow through it:

$$R = \frac{\Delta p}{i}. \quad (1.57)$$

The units are Pa m<sup>-3</sup> s. Physiologists use the peripheral resistance unit (PRU), which is torr ml<sup>-1</sup> min. For Poiseuille flow the resistance can be calculated

<sup>10</sup>This is not strictly true. Some fluid leaves the capillaries and returns to the heart through the lymphatic system instead of the venous system. See Chapter 5.

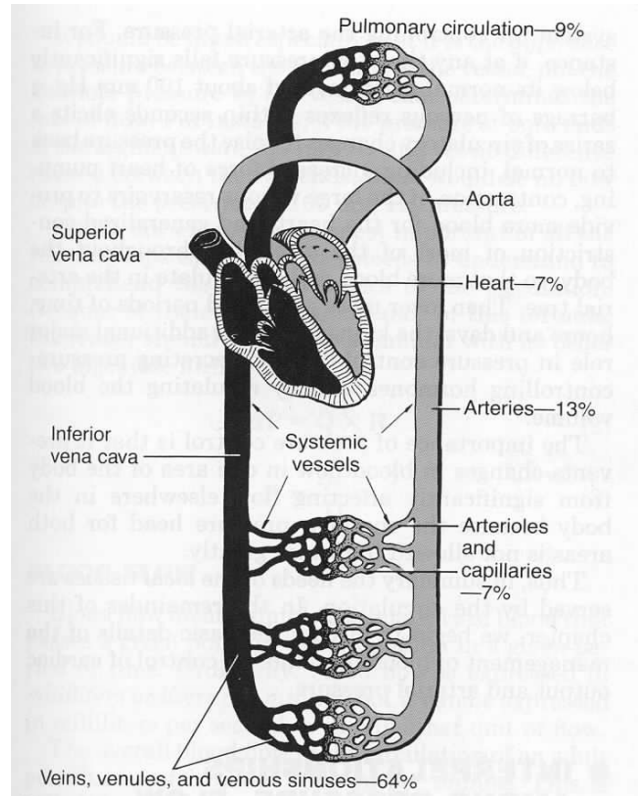


FIGURE 1.34. The human circulatory system. The subject is facing you, so the left chambers of the heart are on the right in the picture. The left heart pumps oxygenated blood (gray), and the right heart pumps deoxygenated blood (black). Reprinted from A.C. Guyton. *Textbook of Medical Physiology*, 8th ed. p. 151. © 1991 Elsevier, Inc. Used with permission of Elsevier.

from Eq. 1.40:

$$R = \frac{8\eta\Delta x}{\pi R_p^4}. \quad (1.58)$$

The resistance decreases rapidly as the radius of the vessel increases.

If vessels of different diameters are connected in series so that the flow  $i$  is the same through each one and the total pressure drop is the sum of the drops across each vessel, then the total resistance is the sum of the resistances of each vessel:

$$R_{\text{tot}} = R_1 + R_2 + R_3 + \dots \quad (1.59)$$

If there is branching so that several vessels are in parallel with the same pressure drop across each one, the total flow through all the branches equals the flow in the vessel feeding them. The total resistance is then given by

$$\frac{1}{R_{\text{tot}}} = \frac{1}{R_1} + \frac{1}{R_2} + \frac{1}{R_3} + \dots \quad (1.60)$$

For the most part, the capillaries are arranged in parallel. Even though the resistance of an individual capillary is large because of its small radius (Eq. 1.58), the resistance

TABLE 1.4. Typical values for the average pressure at the entrance to each generation of the major branches of the cardiovascular tree, the average blood volume in certain branches, and typical dimensions of the vessels.

Location	Average pressure (torr)	Blood volume <sup>a</sup> (ml)	Diameter <sup>b</sup> (mm)	Length <sup>b</sup> (mm)	Wall thickness <sup>b</sup> (mm)	Avg. velocity <sup>b</sup> (m s <sup>-1</sup> )	Reynolds number at maximum flow <sup>c</sup>
Systemic circulation							
Left atrium	5						
Left ventricle	100						
Aorta	100	156	20	500	2.00	$4.80 \times 10^{-1}$	9 400
Arteries	95	608	4	500	1.00	$4.50 \times 10^{-1}$	1 300
Arterioles	86	94	0.05	10	0.2	$5.00 \times 10^{-2}$	
Capillaries	30	260	0.008	1	0.001	$1.00 \times 10^{-3}$	
Venules	10	470	0.02	2	0.002	$2.00 \times 10^{-3}$	
Veins	4	2682	5	25	0.5	$1.00 \times 10^{-2}$	
Vena cava	3	125	30	500	1.5	$3.80 \times 10^{-1}$	3 000
Right atrium	3						
Pulmonary Circulation							
Right atrium	3						
Right ventricle	25						
Pulmonary artery	25	52					
Arteries	20	91					7 800
Arterioles	15	6					
Capillaries	10	104					
Veins	5	215					2 200
Left atrium	5						

<sup>a</sup>From R. Plonsey (1995). Physiologic Systems. In J. R. Bronzino, ed. *The Biomedical Engineering Handbook*, Boca Raton, CRC Press, pp. 9–10.

<sup>b</sup>From J. N. Mazumdar (1992). *Biofluid Mechanics*. Singapore, World Scientific, p. 38.

<sup>c</sup>From W. R. Milnor (1989). *Hemodynamics*, 2nd. ed. Baltimore, Williams & Wilkins, p. 148.

of the capillaries as a whole is relatively small because there are so many of them (see Problem 41).

The average flow from the heart is the stroke volume—the volume of blood ejected in each beat—multiplied by the number of beats per second. A typical value might be

$$i = (60 \text{ ml beat}^{-1})(80 \text{ beat min}^{-1}) = 4800 \text{ ml min}^{-1} \\ = 80 \times 10^{-6} \text{ m}^3 \text{ s}^{-1}.$$

The total resistance would then be the average pressure divided by the flow:

$$R = \frac{(100 \text{ torr})(133 \text{ Pa torr}^{-1})}{80 \times 10^{-6} \text{ m}^3 \text{ s}^{-1}} = 1.66 \times 10^8 \text{ Pa m}^{-3} \text{ s}.$$

The pressure in the left ventricle changes during the cardiac cycle. It can be plotted vs time. It can also be plotted vs ventricular volume, as in Fig. 1.35. The  $p$ - $V$  relationship moves counterclockwise around the curve during the cycle. Filling occurs at nearly zero pressure until the ventricle begins to distend when the volume exceeds 60 ml. There is then a period of contraction at

nearly constant volume that causes the ventricular pressure to rise until it exceeds the (diastolic) pressure in the aorta, and the aortic valve opens. The contraction continues, and the pressure rises further, but the ventricular volume decreases as blood flows into the aorta. The ventricle then relaxes. The aortic valve closes when the ventricular pressure drops below that in the aorta. The work done in one cycle is the area enclosed by the curve. For the curve shown, it is 6600 torr ml = 0.88 J. At 80 beats per minute the power is 1.2 W. In this drawing the stroke volume is 100–35 = 65 ml, and the cardiac output is

$$i = (65 \text{ ml beat}^{-1})(80 \text{ beats}/60 \text{ s}) = 87 \times 10^6 \text{ m}^3 \text{ s}^{-1}.$$

## 1.18 Turbulent Flow and the Reynolds Number

Many features of the circulation can be modeled by Poiseuille flow. However, at least four effects—in addition to those in Eq. 1.42—cause departures from Poiseuille



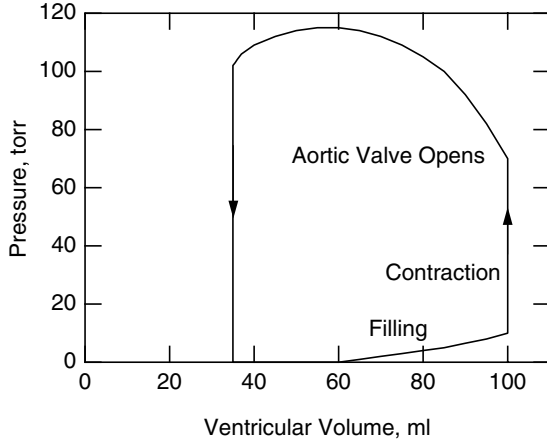


FIGURE 1.35. Pressure–volume relationship in the left ventricle. The curve is traversed counterclockwise with increasing time. The stroke volume is  $100 - 35 = 65$  ml. Systolic pressure is 118 torr, and diastolic pressure is 70 torr. The ventricular pressure drops below diastolic while the pressure in the arteries remains about 70 torr because the aortic valve has closed and prevents back flow

flow: (1) there may be turbulence; (2) there are departures from a parabolic velocity profile; (3) the vessel walls are elastic; and (4) the apparent viscosity depends on the both fraction of the blood volume occupied by red cells and on the size of the vessel.

The importance of turbulence (nonlaminar) flow is determined by a dimensionless number characteristic of the system called the *Reynolds number*  $N_R$ . It is defined by

$$N_R = \frac{LV\rho}{\eta}, \quad (1.61)$$

where  $L$  is a length characteristic of the problem,  $V$  a velocity characteristic of the problem,  $\rho$  the density, and  $\eta$  the viscosity of the fluid. When  $N_R$  is greater than a few thousand, turbulence usually occurs.

The Reynolds number arises in the following way. If we were to write Newton’s second law for a fluid (which we have not done) in terms of dimensionless primed variables such as  $\mathbf{r}' = \mathbf{r}/L$ ,  $\mathbf{v}' = \mathbf{v}/V$ , and  $t' = t/(L/V)$ , we would find that the equations depend on the properties of the fluid only through the combination  $N_R$  [Mazumdar (1992), p. 14]. With appropriate scaling of dimensions and times, flows with the same Reynolds number are identical.

There is ambiguity in defining the characteristic length and the characteristic velocity. Should one use the radius or the diameter of a tube? The maximum velocity or the average velocity? If one is solving the equations of motion, one knows what values of  $L$  and  $V$  were used to transform the equations. They are used to transform the solution back to “real world” coordinates. However, if one is making a statement such as “turbulence usually occurs for values of  $N_R$  greater than a few thousand,” there is ambiguity. On the other hand, the statement is

not very precise. Sometimes an additional subscript is used to specify how  $N_R$  was determined.

When  $N_R$  is large, inertial effects are important. External forces accelerate the fluid. This happens when the mass is large and the viscosity is small. As the viscosity increases (for fixed  $L$ ,  $V$ , and  $\rho$ ) the Reynolds number decreases. When the Reynolds number is small, viscous effects are important. The fluid is not accelerated, and external forces that cause the flow are balanced by viscous forces. Since viscosity is a form of internal friction in the fluid, work done on the system by the external forces is transformed into thermal energy. The low-Reynolds-number regime is so different from our everyday experience that the effects often seem counterintuitive. They are nicely described by Purcell (1977).

Here is an example of an estimate expressed in terms of the Reynolds number. A pressure difference  $\Delta p$  acts on a segment of fluid of length  $\Delta x$  undergoing Poiseuille flow. The difference between the force exerted on the segment of fluid by the fluid “upstream” and that exerted by the fluid “downstream” is  $\pi R_p^2 \Delta p$ . If the average speed of the fluid is  $\bar{v}$ , then the net work done on the segment by the fluid upstream and downstream in time  $\Delta t$  is  $W_{\text{visc}} = \pi R_p^2 \Delta p \bar{v} \Delta t$ . Since the fluid is not accelerated, this work is converted into thermal energy. We can solve Eq. 1.40 for  $\Delta p$  and use Eq. 1.43 to write

$$W_{\text{visc}} = \pi R_p^2 \Delta p \bar{v} \Delta t = 8\eta\pi\bar{v}^2 \Delta x \Delta t.$$

The kinetic energy of the moving fluid in a cylinder of length  $\bar{v}\Delta t$  is

$$E_k = \frac{mv^2}{2} = \frac{\rho\pi R_p^2(\bar{v}\Delta t)\bar{v}^2}{2} = \frac{\rho\pi R_p^2\bar{v}^3\Delta t}{2},$$

and the ratio of the kinetic energy to the work done is

$$\frac{E_k}{W_{\text{visc}}} = \frac{\rho\bar{v}R_p^2}{16\eta\Delta x} = \frac{1}{16\xi} \frac{\rho\bar{v}R_p}{\eta} = \frac{1}{16\xi} N_R.$$

(The last step was done by writing the  $\Delta x$  as  $\xi R_p$ .) This result shows that the ratio of kinetic energy to viscous work is proportional to the Reynolds number. Another example is given in the problems.

A large range of values of  $N_R$  occurs in the circulatory system. Typical values corresponding to the peak flow are given in Table 1.4. Blood flow is laminar except in the ascending aorta and main pulmonary artery, where turbulence may occur during peak flow.

There are two main causes of departures from the parabolic velocity profile. First, a red cell is about the same diameter as a capillary. Red cells in capillaries line up single file, each nearly blocking the capillary. The plasma flows in small volumes between each red cell, with a velocity profile that is nearly independent of radius. Second, the *entry region* causes deviations from Poiseuille flow in larger vessels.

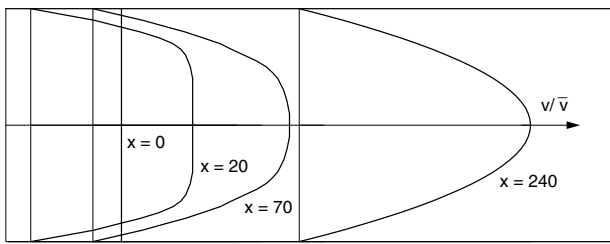


FIGURE 1.36. Velocity profiles in steady laminar flow at the entrance to a tube, showing the development of the parabolic velocity profile. The velocity is given as  $v/\bar{v}$ . At the entrance  $v/\bar{v} = 1$ . When the Poiseuille flow is fully developed,  $v/\bar{v}$  is 2 at the center of the tube. These curves are calculated from a graph by Cebeci and Bradshaw (1977) for laminar flow in a tube of radius 2 mm and a pressure gradient of  $20 \text{ torr m}^{-1}$ , carrying a fluid with a viscosity of  $3 \times 10^{-3} \text{ N s m}^{-2}$  and a density of  $10^3 \text{ kg m}^{-3}$ . The scales are different along the axis and radius of the tube; the tube radius is 2 mm and the entrance region is 240 mm long.

Suppose that blood flowing with a nearly flat velocity profile enters a vessel, as might happen when blood flowing in a large vessel enters the vessel of interest, which has a smaller radius. At the wall of the smaller vessel the flow is zero. Since the blood is incompressible, the *average* velocity is the same at all values of  $x$ , the distance along the vessel. (We assume the vessel has constant cross-sectional area.) However, the velocity profile  $v(r)$  changes with distance  $x$  along the vessel. At the entrance to the vessel ( $x = 0$ ) there is a very abrupt velocity change near the walls. As  $x$  increases a parabolic velocity profile is attained. The transition or entry region, is shown in Fig. 1.36. In the entry region the pressure gradient is different from the value for Poiseuille flow. The velocity profile cannot be calculated analytically in the entry region. Various numerical calculations have been made, and the results can be expressed in terms of scaled variables [see, for example, Cebeci and Bradshaw (1977)]. The Reynolds number used in these calculations was based on the diameter of the pipe,  $D = 2R_p$ , and the average velocity. The length of the entry region is

$$L = 0.05DN_{R,D} = 0.1R_pN_{R,D} = 0.2R_pN_{R,R_p}. \quad (1.62)$$

Blood pressure is, of course, pulsatile. This means that the average velocity and  $v(r)$  are changing with time and also departing from the parabolic profile. Also, at the peak pressure during systole, the aorta and arteries expand, storing some of the blood and releasing it gradually during the rest of the cardiac cycle. Pulsatile flow and the elasticity of vessel walls are discussed extensively by Caro *et al.* (1978) and by Milnor (1989).

Blood is not a Newtonian fluid. The viscosity depends strongly on the fraction of volume occupied by red cells (the hematocrit). In blood vessels of less than  $100 \mu\text{m}$  radius, the apparent viscosity decreases with tube radius.

Since a red cell barely fits in a capillary, the velocity profile in capillaries is not parabolic. Flow in arterioles and arteries is often modeled as individual particles surrounded by plasma and transported by laminar flow, each red cell staying at its own distance from the central axis. However, high-speed motion pictures show that the red cells often collide with other red cells and with the wall. [See the articles by Trowbridge (1982, 1983) and Trowbridge and Meadowcroft (1983), and also the Caro *et al.* and Milnor articles.]

## Symbols Used in Chapter 1

Symbol	Use	Units	First used on page
$\mathbf{a}, a$	Acceleration	$\text{m s}^{-2}$	3
$a, b$	Small distances	m	13
$c$	Constant of integration		14
$g$	Acceleration due to gravity	$\text{m s}^{-2}$	14
$h$	Small distance	m	13
$i$	Total volume flux or flow rate or current	$\text{m}^3 \text{ s}^{-1}$	16
$j_v$	Volume fluence rate or flux density (flow of volume per unit area per second)	$\text{m s}^{-1}$	16
$l$	Length of rod	m	12
$m$	Mass	kg	3
$p$	Pressure	Pa	13
$p_t$	Pressure in thorax	Pa	19
$p_a$	Pressure in alveoli	Pa	19
$\mathbf{r}$	Position	m	5
$r$	Distance from origin (radius) in polar coordinates	m	4
$\mathbf{s}$	Displacement	m	11
$s_n$	Normal stress	Pa	12
$s_s$	Shear stress	Pa	13
$s$	Distance along a streamline	m	18
$t$	Time	s	10
$v, \mathbf{v}$	Velocity	$\text{m s}^{-1}$	10
$x, y, z$	Coordinates	m	4
$\hat{\mathbf{x}}, \hat{\mathbf{y}}, \hat{\mathbf{z}}$	Unit vectors along the $x, y,$ and $z$ axes		6
$A$	Constant of integration		16
$dA$	Small area perpendicular to a streamline	$\text{m}^2$	18
$D$	Pipe diameter	m	23
$E$	Young's modulus	Pa	12
$E_k$	Kinetic energy	J	10
$F, \mathbf{F}$	Force	N	3
$G$	Shear modulus	Pa	13
$L$	Characteristic length	m	23
$N, \mathbf{N}$	Force	N	7
$N_R$	Reynolds number		22
$N_{R,D}$	Reynolds number based on diameter		23
$N_{R,R_p}$	Reynolds number based on pipe radius		23
$P$	Power	W	11
$R, \mathbf{R}$	Force	N	7

Symbol	Use	Units	First used on page
$R_p$	Radius of pipe	m	16
$R$	Vascular resistance	$\text{Pa m}^{-3} \text{ s}$	20
$S$	Cross-sectional area	$\text{m}^2$	12
$V$	Volume	$\text{m}^3$	15
$V$	Velocity	$\text{m s}^{-1}$	22
$W, \mathbf{W}$	Weight	N	4
$W$	Work	J	19
$\delta$	A small distance	m	13
$\epsilon_n$	Normal strain		12
$\epsilon_s$	Shear strain		13
$\eta$	Viscosity	$\text{Pa s}$	15
$\alpha, \beta, \theta, \phi$	Angle		5
$\kappa$	Compressibility	$\text{Pa}^{-1}$	15
$\rho$	Mass density	$\text{kg m}^{-3}$	14
$\tau, \boldsymbol{\tau}$	Torque	N m	4
$\xi$	Dimensionless ratio		22

## Problems

### Section 1.1

**Problem 1** Estimate the number of hemoglobin molecules in a red blood cell. Red blood cells are little more than bags of hemoglobin, so it is reasonable to assume that the hemoglobin takes up all the volume of the cell.

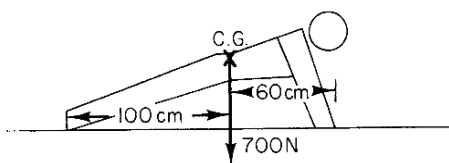
**Problem 2** Our genetic information or genome is stored in the parts of the DNA molecule called base pairs. Our genome contains about 3 billion ( $3 \times 10^9$ ) base pairs, and there are two copies in each cell. Along the DNA molecule, there is one base pair every one-third of a nanometer. How long would the DNA helix from one cell be if it were stretched out in a line? If the entire DNA molecule were wrapped up into a sphere, what would be the diameter of that sphere?

**Problem 3** Estimate the size of a box containing one air molecule. (Hint: What is the volume of one mole of gas at standard temperature and pressure?) Compare the size of the box to the size of an air molecule (about 0.1 nm).

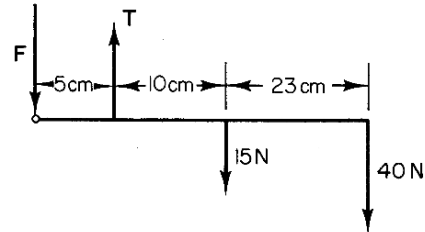
**Problem 4** Estimate the density of water ( $\text{H}_2\text{O}$ ) in  $\text{kg m}^{-3}$ . Useful information: an oxygen atom contains 8 protons and 8 neutrons. A hydrogen atom contains 1 proton and no neutrons. The mass of the electron is negligible.

### Section 1.3

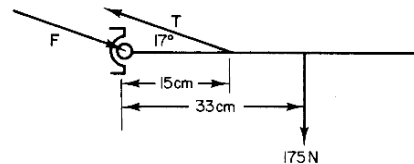
**Problem 5** A person with mass  $m = 70 \text{ kg}$  has a weight ( $mg$ ) of about 700 N. If the person is doing push-ups as shown, what are the vertical components of the forces exerted by the floor on the hands and feet?



**Problem 6** A person with upper arm vertical and forearm horizontal holds a mass of 4 kg. The mass of the forearm is 1.5 kg. Consider four forces acting on the forearm:  $\mathbf{F}$  by the bones and ligaments of the upper arm at the elbow,  $\mathbf{T}$  by the biceps, 40 N by the mass, and 15 N as the weight of the arm. The points of application are shown in the drawing. Calculate the vertical components of  $\mathbf{F}$  and  $\mathbf{T}$ .

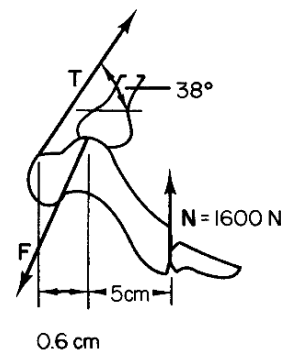


**Problem 7** When the arm is stretched out horizontally, it is held by the deltoid muscle. The situation is shown schematically. Determine  $\mathbf{T}$  and  $\mathbf{F}$ .



### Section 1.5

**Problem 8** When a person crouches, the geometry of the heel is as shown. Determine  $\mathbf{T}$  and  $\mathbf{F}$ . Assume all the forces act in the plane of the drawing.

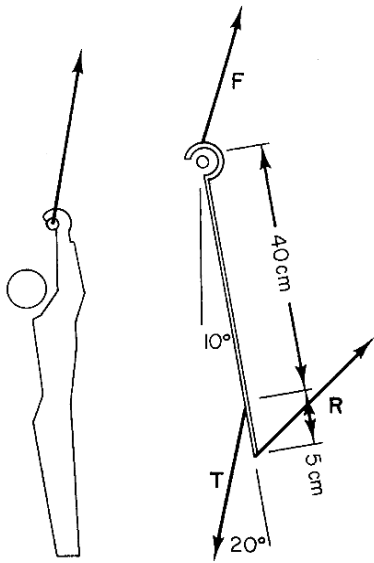


**Problem 9** A person of weight  $W$  is suspended by both hands from a high bar as shown. The center of mass is directly below the bar.

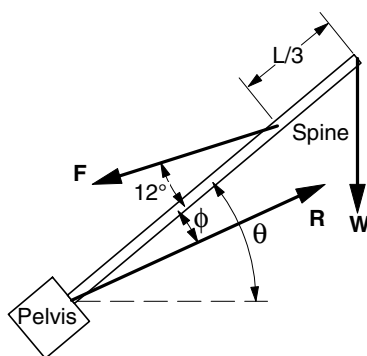
(a) Find the horizontal and vertical components  $F_x$  and  $F_y$ , where  $\mathbf{F}$  is the force exerted by the bar on each of the two hands.

(b) Given the additional information about the arm shown in the second drawing, calculate the components of  $\mathbf{R}$ , the force exerted by the humerus on the forearm through the elbow, and the tension  $\mathbf{T}$  in the biceps tendon. Neglect the weight of the arm, and assume that  $\mathbf{T}$

and  $\mathbf{R}$  are the only forces exerted on the forearm by the upper arm.



**Problem 10** Consider the forces on the spine when lifting. Approximate the spinal column as a stiff bar of length  $L$  that has three forces acting on it.  $\mathbf{W}$  is the downward force acting at the top of the spinal column (via the arms and shoulders), and equals the weight of the object being lifted.  $\mathbf{F}$  is the force applied by the erector spinae muscle, which attaches to the spine about one-third of the way from the top of the column. Assume this muscle acts at an angle of  $12^\circ$  to the spinal column.  $\mathbf{R}$  is the force the pelvis exerts on the spinal column. The weight of the trunk is neglected. Assume the spinal column makes an angle  $\theta$  with the horizontal.



- (a) Determine  $\mathbf{R}$  and  $\mathbf{F}$  in terms of  $\mathbf{W}$  and  $\theta$ .
- (b) The spinal column may be injured if  $\mathbf{R}$  is too large. Compare  $\mathbf{R}$  when  $\theta$  is  $0^\circ$  and  $90^\circ$ . This problem explains why people say to “lift with your legs, not with your back.”
- (c) Compare the angle  $\phi$  when  $\theta$  is  $0^\circ$  and  $90^\circ$ . If  $\phi$  is not close to zero, there will be considerable transverse force at the disks in the lower back, which is not a good situation.

Section 1.7

**Problem 11** Suppose that instead of using a cane, a person holds a suitcase of weight  $W/4$  in one hand,  $0.4\text{ m}$  from the midline. The person is standing on the opposite leg. Calculate the force exerted by the hip abductor muscles and by the acetabulum on that leg.

Section 1.9

**Problem 12** Young’s modulus for a spider’s thread is about  $0.2 \times 10^{10}\text{ Pa}$ , and the thread breaks when it undergoes a strain of about 50% [Köhler and Vollrath (1995)].

- (a) Calculate the tensile strength of the thread and compare it to the tensile strength of steel.
- (b) Calculate the strain that steel undergoes when it breaks. (Assume that a linear relationship between stress and strain holds until it breaks.) Compare the breaking strain to the spider’s thread.

**Problem 13** Assume an object undergoes a normal strain in all three directions:  $\epsilon_x = \Delta x/l_x$ ,  $\epsilon_y = \Delta y/l_y$ ,  $\epsilon_z = \Delta z/l_z$ . Relate the three strains to the change in volume of the object. Assume the strains are small.

Section 1.10

**Problem 14** Relate the shear strain to angle  $\theta$  in Fig. 1.23. How does this relationship simplify if  $\theta$  is small?

Section 1.11

**Problem 15** The inspirational pressure difference  $p_{in}$  that the lung can generate is about 86 torr. What would be the absolute maximum depth at which a person could breathe through a snorkel device? (A safe depth is only about half this maximum, since the lung ventilation becomes very small at the maximum depth. Assume the lungs are 30 cm below the mouth.)

**Problem 16** A person standing erect can in some cases be modeled by a column of water.

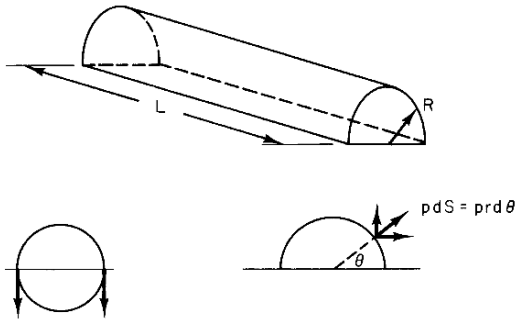
- (a) Calculate the hydrostatic pressure difference between a person’s head and foot in torr.
- (b) Explain why blood pressure is measured in the arm at the same vertical height as the heart.
- (c) Our body has adapted to having a larger hydrostatic pressure in our feet than in our head. Speculate on why you feel uncomfortable when you “stand on your head.”

**Problem 17** A medication dissolved in a saline solution is infused into a vein in the patient’s arm (IV infusion). The density of saline is the same as water. The pressure of the blood inside the vein is 5 torr above atmospheric pressure. How high above the insertion point must the container be hung so that there is sufficient hydrostatic pressure to force fluid into the vein?

**Problem 18** The walls of a cylindrical pipe that has an excess pressure  $p$  inside are subject to a tension force per unit length  $T$ . (Consider only the force per unit length in the walls of the cylinder, not the force in any end caps of the pipe.) The force per unit length in the walls can be calculated by considering a different pipe made up of two parts as shown in the figure: a semicircular half-cylinder of radius  $R$  and length  $L$  attached to a flat plate of width  $2R$  and length  $L$ . What is the force that the excess pressure exerts on the flat plate? Show that the tension force per unit length in the wall of the tube is  $f = pR$ . This is called the Law of Laplace. (Do not worry about any deformation.)

See if you can obtain the same answer by direct integration of the horizontal and vertical components of the force due to the excess pressure.

Sometimes a patient will have an aneurysm in which a portion of an artery will balloon out and possibly rupture. Comment on this phenomenon in light of the  $R$  dependence of the force per unit length [Hademenos (1995)].



**Problem 19** Find a relationship among the tension per unit length  $T$  across any element of the wall of a soap bubble, the excess pressure inside the bubble,  $\Delta p$ , and the radius of the bubble,  $R$ . (Hint: Use the same technique as for the previous problem.)

Section 1.12

**Problem 20** Suppose a fish has an average density of  $1030 \text{ kg m}^{-3}$ , compared to the density of the surrounding water,  $1000 \text{ kg m}^{-3}$ . One way the fish can keep from slowly sinking is by using an air bladder (the density of air is  $1.2 \text{ kg m}^{-3}$ ). What fraction of the fish's total volume must be air in order for the fish to be neutrally buoyant (the buoyant force is equal and opposite to the weight). Assume that the volume  $V$  of the fish's tissue is fixed, so in order to increase the volume  $U$  of the air bladder, the total volume of the fish  $V + U$  must increase.

**Problem 21** This problem explores the physics of a centrifuge. A cylinder of fluid of density  $\rho_{\text{fluid}}$  and length  $L$  is rotated at an angular velocity  $\omega$  ( $\text{rad s}^{-1}$ ) in a horizontal plane about a vertical axis through one end of the tube. Neglect gravity. An object moving in a circle with

constant angular velocity has an acceleration  $a = -r\omega^2$  toward the center of the circle. Find the pressure in the fluid as a function of distance from the axis of rotation, assuming the pressure is  $p_0$  at  $r = 0$ .

**Problem 22** Buoyancy plays an important role in the centrifuge. Consider a small cubic particle of density  $\rho$  immersed in a fluid of density  $\rho_{\text{fluid}}$ .

(a) Write Newton's second law for the particle, considering only the centripetal acceleration and the pressure exerted by the fluid (Problem 21). Find an expression for the "effective weight" of the particle (analogous to Eq. 1.31) in terms of  $\rho$ ,  $\rho_{\text{fluid}}$ ,  $\omega$ ,  $r$ , and the particle volume  $V$ . Your result is more general than you might expect: it is true for a particle of any shape [Wick and Tooby (1977)].

(b) Find the ratio of the "effective weight" derived in (a) to the "effective weight" due to gravity (Eq. 1.31).

(c) If the particle is 10 cm from the axis of a centrifuge spinning at 40 000 revolutions per minute, evaluate the ratio obtained in (b).

(d) The "density gradient" technique uses a sucrose solution of varying concentration to produce a fluid density that varies with  $r$ ,  $\rho_{\text{fluid}}(r)$ . Explain how in this case the centrifuge can be used to separate particles of different densities.

**Problem 23** For the centrifuge of Problem 22 assume there is one additional force: a viscous force proportional to the speed  $u$  of the particle relative to the fluid.

(a) Derive an expression for  $u$ , the "sedimentation velocity" assuming the particle is not accelerating relative to the fluid.

(b) The sedimentation velocity per unit acceleration,  $S$ , is a parameter commonly used in centrifuge work. Divide the expression obtained in (a) by the centripetal acceleration to obtain an expression for  $S$ . The common unit for  $S$  is the svedberg ( $1 \text{ Sv} = 10^{-13} \text{ s}$ ).

(c) Consider two particles with  $S = 50$  and  $70 \text{ Sv}$ . For the centrifuge of Problem 22(c), how long will it take for the particles to separate by 3 mm if they were initially at the same position? How long would this separation take if gravity were used instead of a centrifuge?

Section 1.13

**Problem 24** What is the compressibility of a gas for which  $pV = \text{const}$ ? Compare the compressibility of water to that of air at atmospheric pressure. What are the implications of this for the volume of the lungs of a swimmer diving deep below the water surface?

**Problem 25** Figure 1.20, showing a rod subject to a force along its length, is a simplification. Actually, the cross-sectional area of the rod shrinks as the rod lengthens. Let the axial strain and stress be along the  $z$  axis. They are related by Eq. 1.25,  $s_z = E\epsilon_z$ . The lateral strains  $\epsilon_x$  and  $\epsilon_y$  are related to  $s_z$  by  $s_z = -(E/\nu)\epsilon_x =$

$-(E/\nu)\epsilon_y$ , where  $\nu$  is called the “Poisson’s ratio” of the material.

(a) Use the result of Problem 13 to relate  $E$  and  $\nu$  to the fractional change in volume  $\Delta V/V$ .

(b) The change in volume caused by hydrostatic pressure is the sum of the volume changes caused by axial stresses in all three directions. Relate Poisson’s ratio to the compressibility.

(c) What value of  $\nu$  corresponds to an incompressible material?

(d) For an isotropic material,  $-1 < \nu < 0.5$ . How would a material with negative  $\nu$  behave?

Elliott et al. (2002) measured Poisson’s ratio for articular (joint) cartilage under tension and found  $1 < \nu < 2$ . This large value is possible because cartilage is anisotropic: its properties depend on direction.

### Section 1.14

**Problem 26** A sphere of radius  $R$  moving with speed  $v$  in laminar flow through a viscous fluid experiences a drag force  $F_{\text{visc}} = 6\pi\eta Rv$ . At higher speeds inertial effects (the acceleration of the fluid displaced by the sphere) become important, and the drag becomes proportional to  $v^2$  and to  $\rho$ , the density of the fluid. The force also depends on the radius of the sphere to some unknown power:  $F_{\text{drag}} = K\rho v^2 R^a$ , where  $K$  is a dimensionless constant.

(a) Make a dimensional analysis to find the power  $a$ .

(b) Find the critical velocity at which  $F_{\text{visc}} = F_{\text{drag}}$ .

**Problem 27** Consider fluid flowing between two slabs as shown in Fig. 1.26. Since the work done by the external force on the system in time  $dt$  is  $dW = Fvdt$ , the rate of doing work is  $P = dW/dt = Fv$ , where  $v$  is the speed of the moving plate. Find the power dissipated per unit volume of the fluid in terms of the velocity gradient.

**Problem 28** Consider a fluid that is flowing in the  $x$  direction, but with the velocity  $v_x$  changing in the  $y$  direction.

(a) Start with Newton’s second law. Analyze the forces on a small cube of fluid and derive the equation

$$\rho \frac{\partial v_x}{\partial t} + \rho v_x \frac{\partial v_x}{\partial x} = -\frac{\partial p}{\partial x} + \eta \frac{\partial^2 v_x}{\partial y^2}.$$

This is a simplified version of the Navier-Stokes equation that governs fluid flow.

(b) Which term in the equation is nonlinear (that is, if  $p$  and  $v_x$  are doubled, which term does not double)? A nonlinear equation is needed to describe complicated flows such as turbulence.

**Problem 29** Consider the simplified version of the Navier-Stokes equation in Problem 28. Assume the fluid speed is approximately  $V$  and all spatial changes occur over distances of order  $L$ . Take the ratio of the “inertial term”  $\rho v_x(\partial v_x/\partial x)$  to the “viscous term”  $\eta(\partial^2 v_x/\partial y^2)$  and show that you get the Reynolds number, Eq. 1.61.

### Section 1.15

**Problem 30** Consider laminar flow in a pipe of length  $\Delta x$  and radius  $R_p$ . Find the total viscous drag exerted by the pipe on the fluid.

**Problem 31** The maximum flow rate from the heart is  $500 \text{ ml s}^{-1}$ . If the aorta has a diameter of 2.5 cm and the flow is Poiseuille, what are the average velocity, the maximum velocity at the center of the vessel, and the pressure gradient along the vessel? Plot the velocity vs distance from the center of the vessel. As an approximation to the viscosity of blood, use  $\eta = 10^{-3} \text{ kg m}^{-1} \text{ s}^{-1}$ .

**Problem 32** The glomerular pore described in Eq. 1.41 has a flow  $i = 7.2 \times 10^{-21} \text{ m}^3 \text{ s}^{-1}$ . How many molecules of water per second flow through it? What is their average speed?

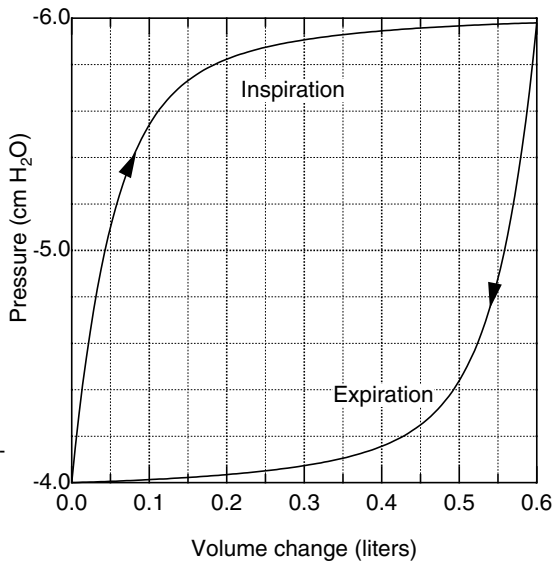
**Problem 33** A parent vessel of radius  $R_p$  branches into two daughter vessels of radii  $R_{d1}$  and  $R_{d2}$ . Find a relationship between the radii such that the shear stress on the vessel wall is the same in each vessel. (Hint: Use conservation of the volume flow.) This relationship is called “Murray’s Law”. Organisms may use shear stress to determine the appropriate size of vessels for fluid transport [LaBarbera (1990)].

**Problem 34** Sap flows up a tree at a speed of about  $1 \text{ mm s}^{-1}$  through its vascular system (xylem), which consists of cylindrical pores of  $20 \mu\text{m}$  radius. Assume the viscosity of sap is the same as the viscosity of water. What pressure difference between the bottom and top of a 100 m tall tree is needed to generate this flow? How does it compare to the hydrostatic pressure difference caused by gravity?

**Problem 35** Consider a small cube of incompressible fluid. Analyze the volume fluence rate for each face of the cube and show that the divergence of  $\mathbf{v}$  is zero. (The divergence is defined in Chapter 4.)

### Section 1.16

**Problem 36** The accompanying figure shows the negative pressure (below atmospheric) that must be maintained in the thorax during the respiratory cycle by a patient with airway obstruction in order to breathe. Viscous effects are included. Estimate the work in joules done by the body during a breath.



### Section 1.17

**Problem 37** The volume of blood in a typical person is 5 liters, and the volume current through the aorta is about  $5 \text{ liter min}^{-1}$ .

(a) What is the total volume current through all the systemic capillaries?

(b) What is the total volume current through all the pulmonary capillaries?

(c) How long does the blood take to make one complete circuit through the circulatory system?

**Problem 38** Find the conversion factor between PRU and  $\text{Pa m}^{-3} \text{ s}$ .

**Problem 39** Equation 1.58 relates the resistance of a vessel to its radius. In the circulatory system, the resistance of an arteriole increases when the smooth muscle surrounding the arteriole contracts, thereby decreasing its radius. By what factor does the resistance increase if the radius decreases by 10%?

**Problem 40** Derive the equations for resistance in a collection of vessels in series and in parallel. Remember that when several vessels are in series, the current is constant and the total pressure change is the sum of the pressure changes along the length of each vessel. When vessels are in parallel, each has the same pressure drop, but the current before the vessels branch is the sum of the currents in each branch.

**Problem 41** The velocity of the blood in the aorta is about  $0.5 \text{ m s}^{-1}$ , and the velocity of the blood in a capillary is about  $0.001 \text{ m s}^{-1}$ . We have only one aorta, with a diameter of 20 mm, but many capillaries in parallel, each with a diameter of  $8 \mu\text{m}$ . Estimate how many capillaries are typically open at any one time.

**Problem 42** Suppose a student asked you, “How can blood be moving more slowly in a capillary than in

the aorta? For an incompressible fluid, when the cross-sectional area along a pipe decreases, the velocity increases, so that the volume current  $i$  is the same. The capillary has a much smaller cross-sectional area than the aorta. Therefore, the blood should move faster in the capillary than in the aorta!” How would you respond to this student?

**Problem 43** For Poiseuille flow, find an expression for the maximum shear rate in each vessel from Eq. 1.44. Where in the vessel does it occur? Typical maximum shear rates are  $50 \text{ s}^{-1}$  in the aorta,  $150 \text{ s}^{-1}$  in the femoral artery, and  $400 \text{ s}^{-1}$  in an arteriole.

**Problem 44** A sphere of radius  $a$  moving through a fluid with speed  $v$  is subject to a viscous drag  $F_{\text{drag}} = 6\pi\eta av$ . Make an argument similar to that in the text to show that the ratio of kinetic energy of a sphere of fluid of the same size moving at the same speed to the viscous work done to displace the sphere by its own diameter is  $N_R/18$ .

**Problem 45** Find an expression for the entry length in terms of the tube size, the pressure gradient, and the properties of the fluid. Estimate the length of the entry region in the aorta, in an artery, and in an arteriole of radius  $20 \mu\text{m}$ . Use  $\eta = 10^{-3} \text{ kg m}^{-1} \text{ s}^{-1}$ .

**Problem 46** Estimate the tension per unit length and the stress in the walls of various blood vessels using the data in Table 1.4.

**Problem 47** Consider laminar viscous flow in the following situation, which models flow in the bronchi or a network of branching blood vessels. A vessel of radius  $R$  connects to  $N$  smaller vessels, each of radius  $xR$ .

(a) What is the relationship between total cross-sectional area of the smaller vessels and that of the larger vessel if the pressure gradient is the same in both sets of vessels?

(b) How do the pressure gradients compare if the total cross-sectional area is the same in both sets of vessels? (Neither assumption is realistic.)

**Problem 48** Compare the magnitude of the four terms in Eq. 1.42 in the following two cases. Ignore branching. Assume the vessels are vertical. Use  $\rho = 10^3 \text{ kg m}^{-3}$  and  $\eta = 10^{-3} \text{ Pa s}$ .

(a) The descending aorta. Assume the length is 35 cm, the radius is 1 cm (independent of distance along the aorta), the peak acceleration of the blood is  $1800 \text{ cm s}^{-2}$ , and the peak velocity (during the cardiac cycle) is  $70 \text{ cm s}^{-1}$  at the entrance and  $60 \text{ cm s}^{-1}$  at the exit. (These velocities are different because some of the blood leaves the aorta in major arteries.)

(b) An arteriole of radius  $50 \mu\text{m}$ , length 1 mm, and constant velocity of  $5 \text{ mm s}^{-1}$  at both entrance and exit.

**Problem 49** The viscosity of water (and therefore of blood) is a rapidly decreasing function of temperature.

Water at 5°C is twice as viscous as water at 35°C. Speculate on the implications of this extreme temperature dependence for the circulatory system of cold-blooded animals. [For a further discussion see Vogel (1994), pp. 27–31.]

### Section 1.18

**Problem 50** Estimate the Reynolds number for the following flows. In each case, determine whether the Reynolds number is high ( $\gg 1$ ) or low ( $\ll 1$ ).

(a) *E. coli* bacteria (length 2 microns) swim in water at speeds of about  $0.01 \text{ mm s}^{-1}$ .

(b) An Olympic swimmer (length 2 m) swims in water at speeds of up to  $2 \text{ m s}^{-1}$ .

(c) A bald eagle (wingspan = 2 m) flies in air (density =  $1.2 \text{ kg m}^{-3}$ , viscosity =  $1.8 \times 10^{-5} \text{ Pa s}$ ) at speeds of  $20 \text{ km hr}^{-1}$ .

**Problem 51** Estimate the Reynolds number of blood flow in a capillary, using the data in Table 1.4. How does this compare to that in the aorta?

## References

- Benedek, G. B., and F. M. H. Villars (2000). *Physics with Illustrative Examples from Medicine and Biology*. Vol. 1. *Mechanics*. New York, Springer-Verlag.
- Caro, C. G., T. J. Pedley, R. C. Schroter, and W. A. Seed (1978). *The Mechanics of the Circulation*. Oxford, Oxford University Press.
- Cebeci, T., and P. Bradshaw (1977). *Momentum Transfer in Boundary Layers*. Washington, Hemisphere.
- Denny, M. W. (1993). *Air and Water: The Biology and Physics of Life's Media*. Princeton, Princeton University Press.
- Elliott, D. M., D. A. Normoneva and L. A. Setton (2002). Direct measurement of the Poisson's ratio of human patella cartilage in tension. *J. Biomech. Eng.* **124**: 223–228.
- Fung, Y. C. (1993). *Biomechanics: Mechanical Properties of Living Tissue*. 2nd. ed. New York, Springer-Verlag.
- Goodsell, D. S. (1998). *The Machinery of Life*. New York, Springer-Verlag.
- Hademenos, G. J. (1995). The physics of cerebral aneurysms. *Physics Today*, Feb., 24–30.
- Halliday, D., R. Resnick, and K. S. Krane (1992). *Fundamentals of Physics*, 4th ed., Vol. 1. New York, Wiley.
- Herrick, J. F. (1942). Poiseuille's observations on blood flow lead to a new law in hydrodynamics. *Am. J. Phys.* **10**: 33–39.
- Inman, V. T. (1947). Functional aspects of the abductor muscles of the hip. *J. Bone Joint Surg.* **29**: 607–619.
- Köhler, T. and F. Vollrath (1995). Thread biomechanics in the two orb-weaving spiders, *Araneus diadematus* (Araneae, Araneidae) and *Uloborus walckenaerius* (Araneae, Uloboridae). *J. Exp. Zool.* **271**: 1–17.
- LaBarbera, M. (1990). Principles of design of fluid transport systems in zoology. *Science*. **249**: 992–1000.
- Lighthill, J. (1975). *Mathematical Biofluidynamics*. Philadelphia, Society for Industrial and Applied Mathematics.
- Macklem, P. T. (1975). Tests of lung mechanics. *N. Engl. J. Med.* **293**: 339–342.
- Mazumdar, J. N. (1992). *Biofluid Mechanics*. Singapore, World Scientific.
- Milnor, William R. (1989). *Hemodynamics*, 2nd ed. Baltimore, Williams & Wilkins.
- Morrison, P., P. Morrison, and the office of C. & R. Eames (1994). *Powers of Ten*. New York, Scientific American Library.
- Patton, H. D., A. F. Fuchs, B. Hille, A. M. Scher and R. Steiner, eds. (1989). *Textbook of Physiology*. 21st ed. Philadelphia, Saunders.
- Purcell, E. M. (1977). Life at low Reynolds number. *Am. J. Phys.* **45**: 3–11.
- Synolakis, C. E., and H. S. Badeer (1989). On combining the Bernoulli and Poiseuille equation—A plea to authors of college physics texts. *Am. J. Phys.* **57**(11): 1013–1019.
- Trowbridge, E. A. (1982). The fluid mechanics of blood: equilibrium and sedimentation. *Clin. Phys. Physiol. Meas.* **3**(4): 249–265.
- Trowbridge, E. A. (1983). The physics of arteriole blood flow. I. General theory. *Clin. Phys. Physiol. Meas.* **4**(2): 151–175.
- Trowbridge, E. A. and P. M. Meadowcroft (1983). The physics of arteriole blood flow. II. Comparison of theory with experiment. *Clin. Phys. Physiol. Meas.* **4**(2): 177–196.
- Vogel, S. V. (1992). *Vital Circuits: On Pumps, Pipes, and the Workings of Circulatory Systems*. Oxford, Oxford University Press.
- Vogel, S. V. (1994). *Life in Moving Fluids*. Princeton, Princeton University Press.
- Wick, G. L. and P. F. Tooby (1977). Centrifugal buoyancy forces. *Amer. J. Physics* **45**: 1074–1076.
- Williams, M., and H. R. Lissner (1962). *Biomechanics of Human Motion*. Philadelphia, Saunders.



# 2

## Exponential Growth and Decay

The exponential function is one of the most important and widely occurring functions in physics and biology. In biology, it may describe the growth of bacteria or animal populations, the decrease of the number of bacteria in response to a sterilization process, the growth of a tumor, or the absorption or excretion of a drug. (Exponential growth cannot continue forever because of limitations of nutrients, etc.) Knowledge of the exponential function makes it easier to understand birth and death rates, even when they are not constant. In physics, the exponential function describes the decay of radioactive nuclei, the emission of light by atoms, the absorption of light as it passes through matter, the change of voltage or current in some electrical circuits, the variation of temperature with time as a warm object cools, and the rate of some chemical reactions.

In this book, the exponential function will be needed to describe certain probability distributions, the concentration ratio of ions across a cell membrane, the flow of solute particles through membranes, the decay of a signal traveling along a nerve axon, and the return of some physiologic variables to their equilibrium values after they have been disturbed.

Because the exponential function is so important, and because we have seen many students who did not understand it even after having been exposed to it, the chapter starts with a gentle introduction to exponential growth (Sec. 2.1) and decay (Sec. 2.2). Section 2.3 shows how to analyze exponential data using semilogarithmic graph paper. The next section shows how to use semilogarithmic graph paper to find instantaneous growth or decay rates when the rate varies. Some would argue that the availability of computer programs that automatically produce logarithmic scales for plots makes these sections unnecessary. We feel that intelligent use of semilogarithmic and logarithmic (log-log) plots requires an understanding of the basic principles.

Variable rates are described in Sec. 2.4. Clearance, discussed in Sec. 2.5, is an exponential decay process that is important in physiology. Sometimes there are competing paths for exponential removal of a substance: multiple decay paths are introduced in Sec. 2.6. A very basic and simple model for many processes is the combination of input at a fixed rate accompanied by exponential decay, described in Sec. 2.7. Sometimes a substance exists in two forms, each with its own decay rate. One then must fit two or more exponentials to the set of data, as shown in Sec. 2.8.

Section 2.9 discusses the logistic equation, one possible model for a situation in which the growth rate decreases as the amount of substance increases. The chapter closes with a section on power-law relationships. While not exponential, they are included because data analysis can be done with log-log graph paper, a technique similar to that for semilog paper. If you feel mathematically secure, you may wish to skim the first four sections, but you will probably find the rest of the chapter worth reading.

### 2.1 Exponential Growth

*An exponential growth process is one in which the rate of increase of a quantity is proportional to the present value of that quantity.* The simplest example is a savings account. If the interest rate is 5% and if the interest is credited to the account once a year, the account increases in value by 5% of its present value each year. If the account starts out with \$100, then at the end of the first year, \$5 is credited to the account and the value becomes \$105. At the end of the second year, 5 percent of \$105 is credited to the account and the value grows by \$5.25 to \$110.25. The growth of such an account is shown in Table 2.1 and Fig. 2.1. These amounts can be calculated as follows. At the end of the first year, the original

TABLE 2.1. Growth of a savings account earning 5% interest compounded annually, when the initial investment is \$100.

Year	Amount	Year	Amount	Year	Amount
1	\$105.00	10	\$162.88	100	\$13,150.13
2	110.25	20	265.33	200	1,729,258.09
3	115.76	30	432.19	300	$2.27 \times 10^8$
4	121.55	40	704.00	400	$2.99 \times 10^{10}$
5	127.63	50	1146.74	500	$3.93 \times 10^{12}$
6	134.01	60	1867.92	600	$5.17 \times 10^{14}$
7	140.71	70	3042.64	700	$6.80 \times 10^{16}$
8	147.75	80	4956.14	800	$8.94 \times 10^{18}$
9	155.13	90	8073.04	900	$1.18 \times 10^{21}$

amount,  $y_0$ , has been augmented by  $(0.05)y_0$ :

$$y_1 = y_0(1 + 0.05).$$

During the second year, the amount  $y_1$  increases by 5%, so

$$y_2 = y_1(1.05) = y_0(1.05)(1.05) = y_0(1.05)^2.$$

After  $t$  years, the amount in the account is

$$y_t = y_0(1.05)^t.$$

In general, if the growth rate is  $b$  per compounding period, the amount after  $t$  periods is

$$y_t = y_0(1 + b)^t. \tag{2.1}$$

It is possible to keep the same annual growth (interest) rate, but to compound more often than once a year. Table 2.2 shows the effect of different compounding intervals on the amount, when the interest rate is 5%. The last two columns, for monthly compounding and for “instant

TABLE 2.2. Amount of an initial investment of \$100 at 5% annual interest, with different methods of compounding.

Month	Annual	Semiannual	Quarterly	Monthly	Instant
0	\$100.00	\$100.00	\$100.00	\$100.000	\$100.000
1	100.00	100.00	100.00	100.417	100.418
2	100.00	100.00	100.00	100.835	100.837
3	100.00	100.00	101.25	101.255	101.258
4	100.00	100.00	101.25	101.677	101.681
5	100.00	100.00	101.25	102.101	102.105
6	100.00	102.50	102.52	102.526	102.532
7	100.00	102.50	102.52	102.953	102.960
8	100.00	102.50	102.52	103.382	103.390
9	100.00	102.50	103.80	103.813	103.821
10	100.00	102.50	103.80	104.246	104.255
11	100.00	102.50	103.80	104.680	104.690
12	105.00	105.06	105.09	105.116	105.127

interest,” are listed to the nearest tenth of a cent to show the slight difference between them.

The table entries were calculated in the following way. Suppose that compounding is done  $N$  times a year. In  $t$  years, the number of compoundings is  $Nt$ . If the annual fractional rate of increase is  $b$ , the increase per compounding is  $b/N$ . For six months at 5% ( $b = 0.05$ ) the increase is 2.5, for three months it is 1.25, etc. The amount after  $t$  units of time (years) is, in analogy with Eq. 2.1,

$$y = y_0(1 + b/N)^{Nt}. \tag{2.2}$$

Recall (refer to Appendix C) that  $(a^b)^c = (a^b)^c$ . The expression for  $y$  can be written as

$$y = y_0[(1 + b/N)^N]^t. \tag{2.3}$$

Most calculus textbooks show that the quantity

$$(1 + b/N)^N \rightarrow e^b$$

as  $N$  becomes very large. (Rather than prove this fact here, we give numerical examples in Table 2.3 for two different values of  $b$ .) Therefore, Eq. 2.3 can be rewritten as

$$y = y_0e^{bt} = y_0 \exp(bt). \tag{2.4}$$

(The  $\exp$  notation is used when the argument is complicated.) To calculate the amount for instant interest, it is necessary only to multiply the fractional growth rate per unit time  $b$  by the length of the time interval and then

TABLE 2.3. Numerical examples of the convergence of  $(1 + b/N)^N$  to  $e^b$  as  $N$  becomes large.

$N$	$b = 1$	$b = 0.5$
10	2.594	1.0511
100	2.705	1.0513
1000	2.717	1.0513
$e^b$	2.718	1.0513

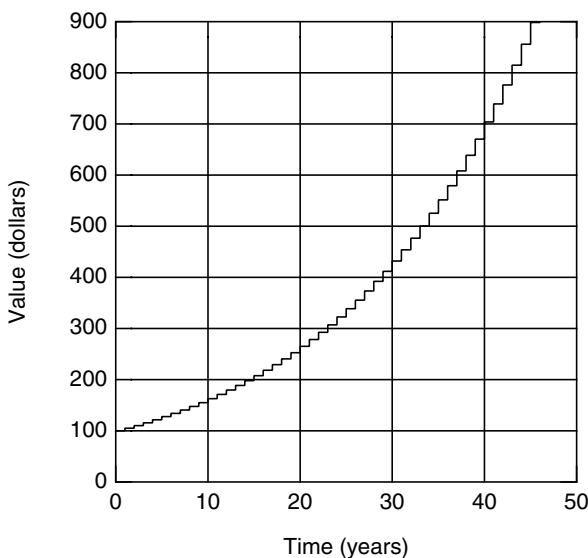


FIGURE 2.1. The amount in a savings account after  $t$  years, when the amount is compounded annually at 5% interest.

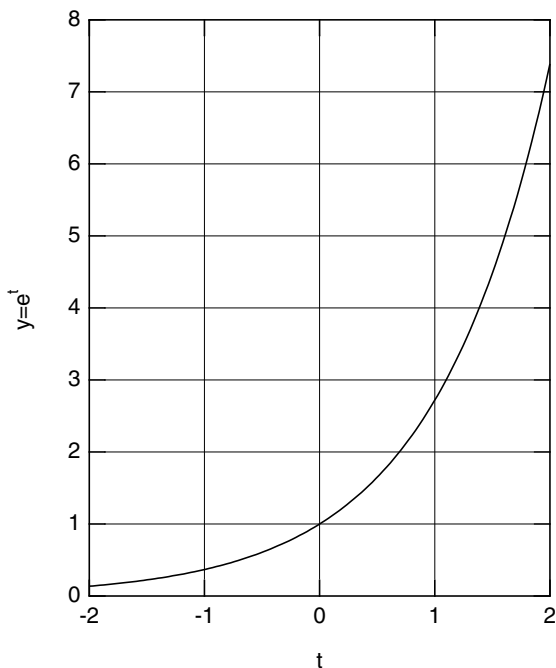


FIGURE 2.2. A graph of the exponential function  $y = e^t$ .

look up the exponential function of this amount in a table or evaluate it with a computer or calculator. The number  $e$  is approximately equal to  $2.71828\dots$  and is called the “base of the natural logarithms.” Like  $\pi$  ( $3.14159\dots$ )  $e$  has a long history [Maor (1994)].

The exponential function is plotted in Fig. 2.2. (The meaning of negative values of  $t$  will be considered in the next section.) This function increases more and more rapidly as  $t$  increases. This is expected, since the rate of growth is always proportional to the present amount. This is also reflected in the following property of the exponential function:

$$\frac{d}{dt}(e^{bt}) = be^{bt}. \quad (2.5)$$

This means that the function  $y = y_0e^{bx}$  has the property that

$$\frac{dy}{dt} = by. \quad (2.6)$$

Any constant multiple of the exponential function  $e^{bt}$  has the property that its rate of growth is  $b$  times the function itself. Whenever we see the exponential function, we know that it satisfies Eq. 2.6. Equation 2.6 is an example of a *differential equation*. If you learn how to solve only one differential equation, let it be Eq. 2.6. Whenever we have a problem in which the growth rate of something is proportional to the present amount, we can expect to have an exponential solution. Notice that for time intervals  $t$  that are not too large, Eq. 2.6 implies that  $\Delta y = (b\Delta t)y$ . This again says that the increase in  $y$  is proportional to  $y$  itself.

The independent variable in this discussion has been  $t$ . It can represent time, in which case  $b$  is the fractional

growth rate per unit time; distance, in which case  $b$  is the fractional growth per unit distance; or something else. We could, of course, use another symbol such as  $x$  for the independent variable, in which case we would have  $dy/dx = by$ ,  $y = y_0e^{bx}$ .

## 2.2 Exponential Decay

Figure 2.2 shows the exponential function for negative values of  $t$  as well as positive ones. (Remember that  $e^{-t} = 1/e^t$ .) To see what this means, consider a bank account in which no interest is credited, but from which 5% of what remains is taken each year. If the initial balance is \$100, \$5 is removed the first year to leave \$95.00. In the second year, 5% of \$95 or \$4.75 is removed. In the third year, 5% of \$90.25 or \$4.65 is removed. The annual decrease in  $y$  becomes less and less as  $y$  becomes less and less. The equations developed in the preceding section also describe this situation. It is only necessary to call  $b$  the fractional decay and allow it to have a negative value,  $-|b|$ . Equation 2.1 then has the form  $y = y_0(1 - |b|)^t$  and Eq. 2.4 is

$$y = y_0e^{-|b|t}. \quad (2.7)$$

Often  $b$  is regarded as being intrinsically positive, and Eq. 2.7 is written as

$$y = y_0e^{-bt}. \quad (2.8)$$

One could equally well write  $y = y_0e^{bt}$  and regard  $b$  as being negative.

The radioactive isotope  $^{99m}\text{Tc}$  (read as technetium-99) has a fractional decay rate  $b = 0.1155 \text{ h}^{-1}$ . If the number of atoms at  $t = 0$  is  $y_0$ , the fraction  $f = y/y_0$  remaining at later times decreases as shown in Fig. 2.3. The equation that describes this curve is

$$f = \frac{y}{y_0} = e^{-bt}, \quad (2.9)$$

where  $t$  is the elapsed time in hours and  $b = 0.1155 \text{ h}^{-1}$ . The product  $bt$  must be dimensionless, since it is in the exponent.

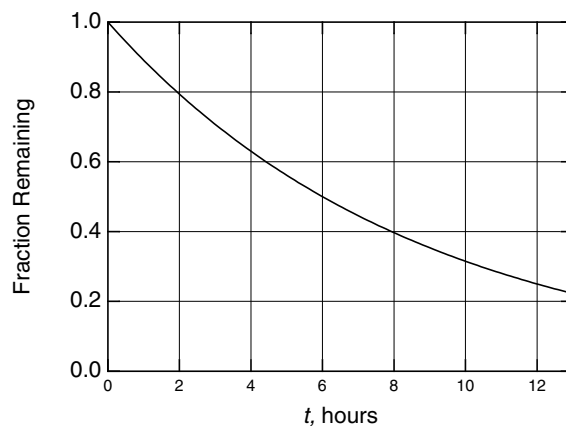


FIGURE 2.3. A plot of the fraction of nuclei of  $^{99m}\text{Tc}$  surviving at time  $t$ .

People often talk about the *half-life*  $T_{1/2}$ , which is the length of time required for  $f$  to decrease to one-half. From inspection of Fig. 2.3, the half-life is 6 h. This can also be determined from Eq. 2.9:

$$0.5 = e^{-bT_{1/2}}.$$

From a table of exponentials, one finds that  $e^{-x} = 0.5$  when  $x = 0.69315$ . This leads to the very useful relationship  $bT_{1/2} = 0.693$  or

$$T_{1/2} = \frac{0.693}{b}. \tag{2.10}$$

For the case of  $^{99m}\text{Tc}$ , the half-life is  $T_{1/2} = 0.693/0.1155 = 6$  h.

One can also speak of a *doubling time* if the exponent is positive. In that case  $2 = e^{bT_2}$ , from which

$$T_2 = \frac{0.693}{b}. \tag{2.11}$$

### 2.3 Semilog Paper

A special kind of graph paper, called *semilog paper*, makes the analysis of exponential growth and decay problems much simpler. If one takes logarithms (to any base) of Eq. 2.4 one has

$$\log y = \log y_0 + bt \log e. \tag{2.12}$$

If the dependent variable is considered to be  $u = \log y$ , and since  $\log y_0$  and  $\log e$  are constants, this equation is of the form

$$u = c_1 + c_2t. \tag{2.13}$$

The graph of  $u$  vs.  $t$  is a straight line with positive slope if  $b$  is positive and negative slope if  $b$  is negative.

On semilog paper the vertical axis is marked in a logarithmic fashion. The graph can be plotted without having to calculate any logarithms. Figure 2.4 shows a plot of the exponential function of Fig. 2.2, for both positive and negative values of  $t$ . First, note how to read the vertical axis. A given distance along the axis always corresponds to the same multiplicative factor. Each cycle represents a factor of 10. To use the paper, it is necessary first to mark off the decades with the desired values. In Fig. 2.4 the decades have been marked 0.1, 1, 10, 100. The 6 that lies between 0.1 and 1 is 0.6; the 6 between 1 and 10 is 6.0; the 6 between 10 and 100 represents 60; and so forth. The paper can be imagined to go vertically forever in either direction; one never reaches zero. Figure 2.4 has two examples marked on it with dashed lines. The first shows that for  $t = -1.0$ ,  $y = 0.36$ ; the second shows that for  $t = +1.5$ ,  $y = 4.5$ .

Semilog paper is most useful for plotting data that you suspect may have an exponential relationship. If the data plot as a straight line, your suspicions are confirmed.

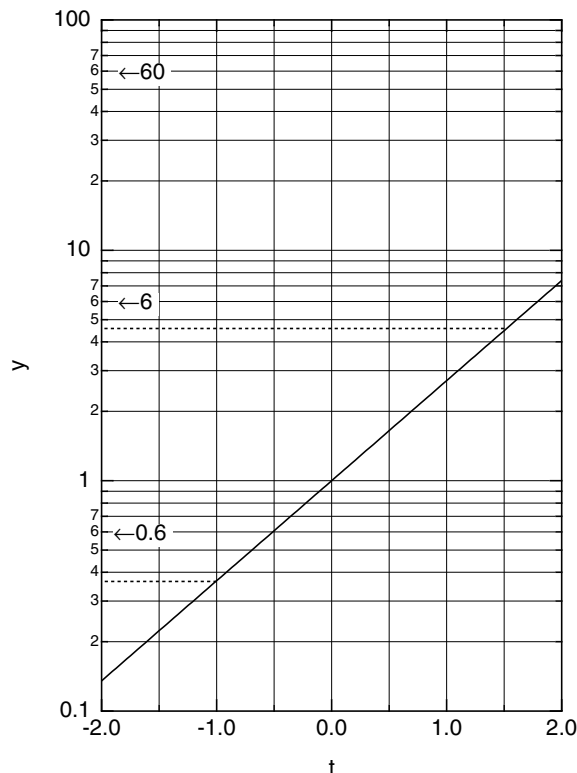


FIGURE 2.4. A plot of the exponential function on semilog paper.

From the straight line, you can determine the value of  $b$ . Figure 2.5 is a plot of the intensity of light that passed through an absorber in a hypothetical example. The independent variable is absorber thickness  $x$ . The decay is exponential, except for the last few points, which may be high because of experimental error. (As the intensity of the light decreases, it becomes harder to measure accurately.) We wish to determine the decay constant in  $y = y_0e^{-bx}$ . One way to do it would be to note (dashed line A in Fig. 2.5) that the half-distance is 0.145 cm, so that, from Eq. 2.10,

$$b = \frac{0.693}{0.145} = 4.8 \text{ cm}^{-1}.$$

This technique can be inaccurate because it is difficult to read the graph accurately. It is more accurate to use a portion of the curve for which  $y$  changes by a factor of 10 or 100. The general relationship is  $y = y_0e^{bx}$ , where the value of  $b$  can be positive or negative. If two different values of  $x$  are selected, one can write

$$\frac{y_2}{y_1} = \frac{y_0e^{bx_2}}{y_0e^{bx_1}} = e^{b(x_2-x_1)}.$$

If  $y_2/y_1 = 10$ , then this equation has the form  $10 = e^{bX_{10}}$  where  $X_{10} = x_2 - x_1$  when  $y_2/y_1 = 10$ . From a table of exponentials,  $bX_{10} = 2.303$ , so that

$$b = \frac{2.303}{X_{10}}. \tag{2.14}$$

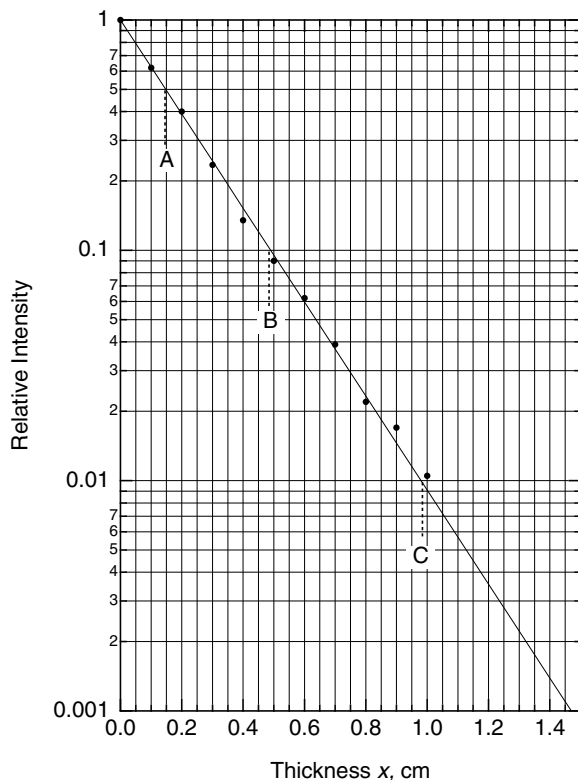


FIGURE 2.5. A semilogarithmic plot of the intensity of light after it has passed through an absorber of thickness  $x$ .

The same procedure can be used to find  $b$  using a factor of 100 change in  $y$ :

$$b = \frac{4.605}{X_{100}}. \quad (2.15)$$

If the curve represents a decaying exponential, then  $y_2/y_1 = 10$  when  $x_2 < x_1$ , so that  $X_{10} = x_2 - x_1$  is negative. Equation 2.14 then gives the negative value of  $b$ .

As an example, consider the exponential decay in Fig. 2.5. Using points  $B$  and  $C$ , we have  $x_1 = 0.97$ ,  $y_1 = 10^{-2}$ ,  $x_2 = 0.48$ ,  $y_2 = 10^{-1}$ ,  $X_{10} = 0.480 - 0.97 = -0.49$ . Therefore  $b = 2.303/(-0.49) = -4.7 \text{ cm}^{-1}$ , which is a more accurate determination than the one we made using the half-life.

## 2.4 Variable Rates

The equation  $dy/dx = by$  (or  $dy/dt = by$ ) says that  $y$  grows or decays at a rate that is proportional to  $y$ . The constant  $b$  is the fractional rate of growth or decay. It is possible to define the *fractional rate of growth or decay* even if it is not constant but is a function of  $x$ :

$$b(x) = \frac{1}{y} \frac{dy}{dx}. \quad (2.16)$$

Semilogarithmic graph paper can be used to analyze the curve even if  $b$  is not constant. Since  $d(\ln y)/dy = 1/y$ ,

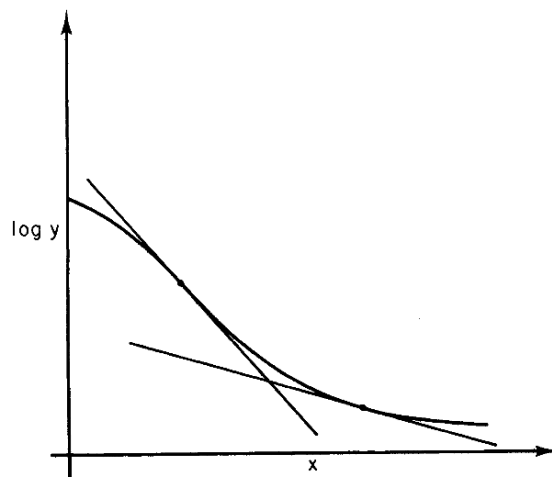


FIGURE 2.6. A semilogarithmic plot of  $y$  vs  $x$  when the decay rate is not constant. Each tangent line represents the instantaneous decay rate for that value of  $x$ .

the chain rule for evaluating derivatives gives

$$\frac{d}{dx} (\ln y) = \frac{1}{y} \frac{dy}{dx} = b.$$

This means that  $b(x)$  is the slope of a plot of  $\ln y$  vs.  $x$ . A semilogarithmic plot of  $y$  vs  $x$  is shown in Fig. 2.6. The straight line is tangent to the curve and decays with a constant rate equal to  $b(x)$  at the point of tangency. The value of  $b$  for the tangent line can be determined using the methods in the previous section. A second tangent line at a larger value of  $x$  in Fig. 2.6 has a smaller value of the decay rate.

If finite changes  $\Delta x$  and  $\Delta y$  have been measured, they may be used to estimate  $b(x)$  directly from Eq. 2.16. For example, suppose that  $y = 100,000$  people and that in  $\Delta x = 1$  year there is a change  $\Delta y = -37$ . In this case  $\Delta y$  is very small compared to  $y$ , so we can say that  $b = (1/y)(\Delta y/\Delta x) = -37 \times 10^{-5}$ . If the only cause of change in this population is deaths, the absolute value of  $b$  is called the *death rate*.

A plot of the number of people surviving in a population, all of whom have the same disease, can provide information about the prognosis for that disease. The death rate is equivalent to the decay constant. An example of such a plot is shown in Fig. 2.7. Curve  $A$  shows a disease for which the death rate is constant. Curve  $B$  shows a disease with an initially high death rate which decreases with time; if the patient survives the initial period, the prognosis is much better. Curve  $C$  shows a disease for which the death rate increases with time.

Surprisingly, there are a few diseases that have death rates independent of the duration of the disease (Zumoff 1966). Any discussion of mortality should be made in terms of the surviving population, since any further deaths must come from that group. Nonetheless, one often finds results in the literature reported in terms of

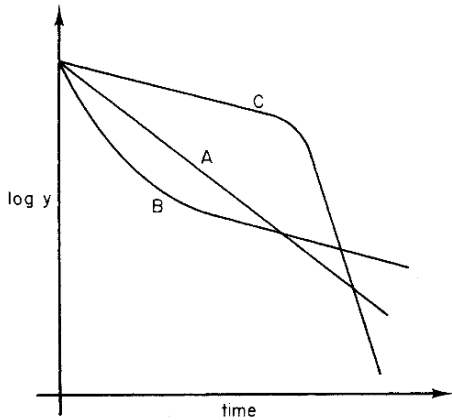


FIGURE 2.7. Semilogarithmic plots of the fraction of a population surviving in three different diseases. The death rates (decay constants) depend on the duration of the disease.

the cumulative fraction of patients who have died. Figure 2.8 shows the survival of patients with congestive heart failure for a period of nine years. The data are taken from the Framingham study [McKee *et al.* (1971)]; the death rate is constant during this period. For a more detailed discussion of various possible survival distributions, see Clark (1975).

As long as  $b$  has a constant value, it makes no difference what time is selected to be  $t = 0$ . To see this, suppose that the value of  $y$  decays exponentially with constant rate:  $y = y_0 e^{-bt}$ . Consider two different time scales, shifted with respect to each other so that  $t' = t_0 + t$ . In terms of the shifted time  $t'$ , the value of  $y$  is

$$y = y_0 e^{-bt} = y_0 e^{-b(t'-t_0)} = (y_0 e^{bt_0}) e^{-bt'}$$

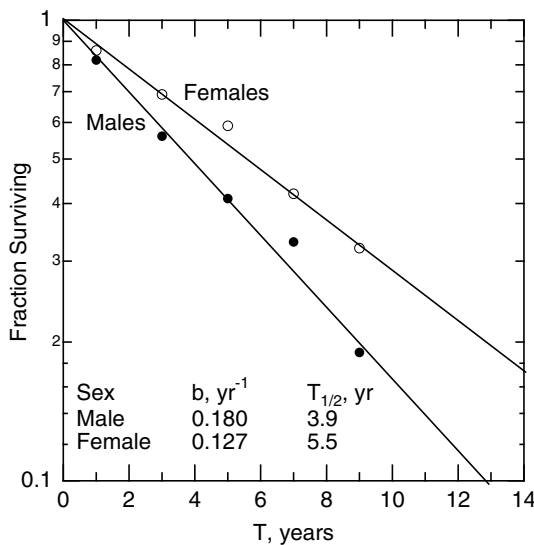


FIGURE 2.8. Survival of patients with congestive heart failure. Data are from McKee *et al.* (1971).

This has the same form as the original expression for  $y(t)$ . The value of  $y'_0$  is  $y_0 e^{bt_0}$ , which reflects the fact that  $t' = 0$  occurs at an earlier time than  $t = 0$ , so  $y'_0 > y_0$ .

If the decay rate is not constant, then the origin of time becomes quite important. Usually there is something about the problem that allows  $t = 0$  to be determined. Figure 2.9 shows survival after a heart attack (myocardial infarct). The time of the initial infarct defines  $t = 0$ ; if the origin had been started two or three years after the infarct, the large initial death rate would not have been seen.

As long as the rate of increase can be written as a function of the independent variable, Eq. 2.16 can be rewritten as  $dy/y = b(x)dx$ . This can be integrated:

$$\int_{y_1}^{y_2} \frac{dy}{y} = \int_{x_1}^{x_2} b(x) dx,$$

$$\ln(y_2/y_1) = \int_{x_1}^{x_2} b(x) dx,$$

$$\frac{y_2}{y_1} = \exp\left(\int_{x_1}^{x_2} b(x) dx\right). \quad (2.17)$$

If we can integrate the right-hand side analytically, numerically, or graphically, we can determine the ratio  $y_2/y_1$ .

## 2.5 Clearance

In some cases in physiology, the amount of a substance may decay exponentially because the rate of removal is proportional to the concentration of the substance (amount per unit volume) instead of to the total amount. For example, the rate at which the kidneys excrete a substance may be proportional to the concentration in the

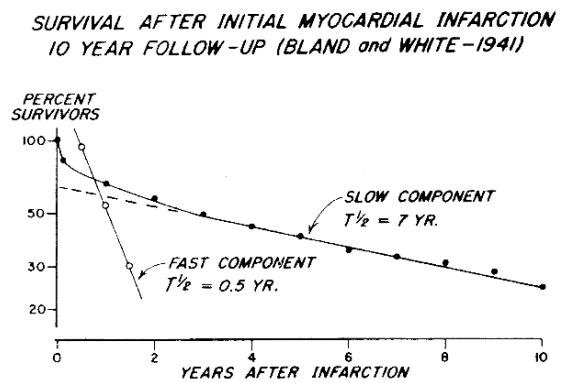


FIGURE 2.9. The fraction of patients surviving after a myocardial infarction (heart attack) at  $t = 0$ . The curve labeled “Fast Component” plots 10 times the difference between the survival curve and the extrapolated “Slow Component.” From B. Zumoff, H. Hart, and L. Hellman (1966). Considerations of mortality in certain chronic diseases. *Ann. Intern. Med.* 64: 595–601. Reproduced by permission of *Annals of Internal Medicine*. Drawing courtesy of Prof. Zumoff.

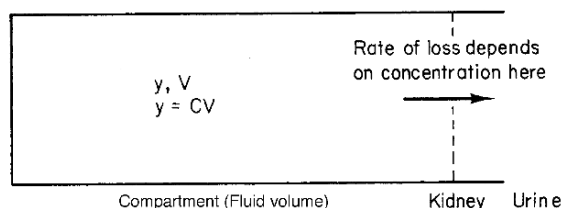


FIGURE 2.10. A case in which the rate of removal of a substance from a fluid compartment depends on the concentration, not on the total amount of substance in the compartment. Increasing the compartment volume with the same concentration of the substance would not change the rate of removal.

blood that passes through the kidneys, while the total amount depends on the total fluid volume in which the substance is distributed. This is shown schematically in Fig. 2.10. The large box on the left represents the total fluid volume  $V$ . It contains a total amount of some substance,  $y$ . If the fluid is well mixed, the concentration is  $C = y/V$ . The removal process takes place only at the dashed line, at a rate proportional to  $C$ . The equation describing the change of  $y$  is

$$\frac{dy}{dt} = -KC = -K\left(\frac{y}{V}\right). \quad (2.18)$$

The proportionality constant  $K$  is called the *clearance*. Its units are  $\text{m}^3 \text{s}^{-1}$ . The equation is the same as Eq. 2.6 if  $K/V$  is substituted for  $b$ . The solution is

$$y = y_0 e^{-(K/V)t}. \quad (2.19)$$

The basic concept of clearance is best remembered in terms of Fig. 2.10. Other definitions are found in the literature. It sometimes takes considerable thought to show that the definitions are equivalent. A common definition in physiology books is “*clearance is the volume of plasma from which  $y$  is completely removed per unit time.*” To see that this definition is equivalent, imagine that  $y$  is removed from the body by removing a volume  $V$  of the plasma in which the concentration of  $y$  is  $C$ . The rate of loss of  $y$  is the concentration times the rate of volume removal:

$$\frac{dy}{dt} = -\left|\frac{dV}{dt}\right|C. \quad (2.20)$$

( $dV/dt$  is negative for removal.) Comparison with Eq. 2.18 shows that  $|dV/dt| = K$ .

As long as the compartment containing the substance is well mixed, the concentration will decrease uniformly throughout the compartment as  $y$  is removed. The concentration also decreases exponentially:

$$C = C_0 e^{-(K/V)t}. \quad (2.21)$$

An example may help to clarify the distinction between  $b$  and  $K$ . Suppose that the substance is distributed in

a fluid volume  $V = 18 \text{ l}$ . The substance has an initial concentration  $C_0 = 3 \text{ mg l}^{-1}$  and the clearance is  $K = 2 \text{ l h}^{-1}$ . The total amount is  $y_0 = C_0 V = 3 \times 18 = 54 \text{ mg}$ . The fractional decay rate is  $b = K/V = 1/9 \text{ h}^{-1}$ . The equations for  $C$  and  $y$  are  $C = (3 \text{ mg l}^{-1})e^{-t/9}$ ,  $y = (54 \text{ mg})e^{-t/9}$ . At  $t = 0$  the initial rate of removal is  $-dy/dt = 54/9 = 6 \text{ mg h}^{-1}$ .

Now double the fluid volume to  $V = 36 \text{ l}$  without adding any more of the substance. The concentration falls to  $1.5 \text{ mg l}^{-1}$  although  $y_0$  is unchanged. The rate of removal is also cut in half, since it is proportional to  $K/V$  and the clearance is unchanged. The concentration and amount are now  $C = 1.5e^{-t/18}$ ,  $y = 54e^{-t/18}$ . The initial rate of removal is  $dy/dt = 54/18 = 3 \text{ mg h}^{-1}$ . It is half as large as above, because  $C$  is now half as large.

If more of the substance were added along with the additional fluid, the initial concentration would be unchanged, but  $y_0$  would be doubled. The fractional decay rate would still be  $K/V = 1/18 \text{ h}^{-1}$ :  $C = 3.0e^{-t/18}$ ,  $y = 108e^{-t/18}$ . The initial rate of disappearance would be  $dy/dt = 108/18 = 6 \text{ mg h}^{-1}$ . It is the same as in the first case, because the initial concentration is the same.

## 2.6 Multiple Decay Paths

It is possible to have several independent paths by which  $y$  can disappear. For example, there may be several competing ways by which a radioactive nucleus can decay; a radioactive isotope given to a patient may decay radioactively and be excreted biologically at the same time; a substance in the body can be excreted in the urine and metabolized by the liver; or patients may die of several different diseases.

In such situations the total decay rate  $b$  is the sum of the individual rates for each process, as long as the processes act independently and the rate of each is proportional to the present amount (or concentration) of  $y$ :

$$\begin{aligned} \frac{dy}{dt} &= -b_1 y - b_2 y - b_3 y - \dots \\ &= -(b_1 + b_2 + b_3 + \dots)y = -by. \end{aligned} \quad (2.22)$$

The equation for the disappearance of  $y$  is the same as before, with the total decay rate being the sum of the individual rates. The rate of disappearance of  $y$  by the  $i$ th process is *not*  $dy/dt$  but is  $-b_i y$ . Instead of decay rates, one can use half-lives. Since  $b = b_1 + b_2 + b_3 + \dots$ , the total half-life  $T$  is given by

$$\frac{0.693}{T} = \frac{0.693}{T_1} + \frac{0.693}{T_2} + \frac{0.693}{T_3} + \dots$$

or

$$\frac{1}{T} = \frac{1}{T_1} + \frac{1}{T_2} + \frac{1}{T_3} + \dots \quad (2.23)$$

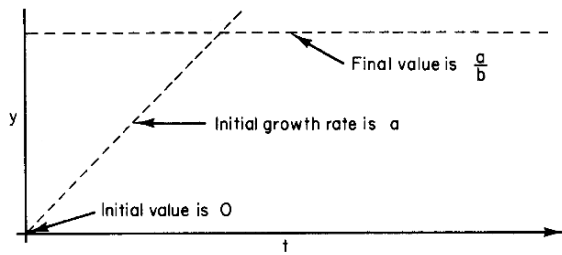


FIGURE 2.11. Sketch of the initial slope  $a$  and final value  $a/b$  of  $y$  when  $y(0) = 0$ .

## 2.7 Decay Plus Input at a Constant Rate

Suppose that in addition to the removal of  $y$  from the system at a rate  $-by$ ,  $y$  enters the system at a constant rate  $a$ , independent of  $y$  and  $t$ . The net rate of change of  $y$  is given by

$$\frac{dy}{dt} = a - by. \quad (2.24)$$

It is often easier to write down a differential equation describing a problem than it is to solve it. In this case the solution to the equation and the techniques for solving it are well known. However, a good deal can be learned about the solution by examining the equation itself. Suppose that  $y(0) = 0$ . Then the equation at  $t = 0$  is  $dy/dt = a$ , and  $y$  initially grows at a constant rate  $a$ . As  $y$  builds up, the rate of growth decreases from this value because of the  $-by$  term. Finally, when  $a - by = 0$ ,  $dy/dt$  is zero and  $y$  stops growing. This is enough information to make the sketch in Fig. 2.11.

The equation is solved in Appendix F. The solution is

$$y = \frac{a}{b} (1 - e^{-bt}). \quad (2.25)$$

The derivative of  $y$  is  $dy/dt = (\frac{a}{b})(-1)(-b)e^{-bt} = ae^{-bt}$ .

You can verify by substitution that Eq. 2.25 satisfies Eq. 2.24. The solution does have the properties sketched in Fig. 2.11, as you can see from Fig. 2.12. The initial value of  $dy/dt$  is  $a$ , and it decreases exponentially to zero. When  $t$  is large, the exponential term in  $y$  vanishes, leaving  $y = a/b$ .

## 2.8 Decay with Multiple Half-Lives and Fitting Exponentials

Sometimes  $y$  is a mixture of two or more quantities, each decaying at a constant rate. It might represent a mixture of radioactive isotopes, each decaying at its own rate. A biological example is the survival of patients after a myocardial infarct (Fig. 2.9). The death rate is not constant, and many models can be proposed to explain why. One possible model is that there are two distinct classes of

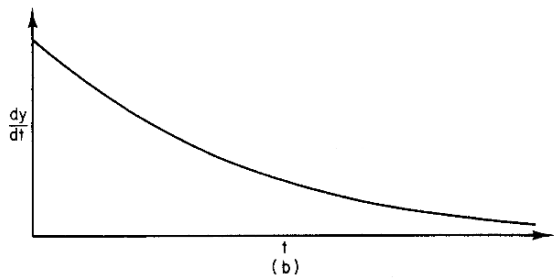
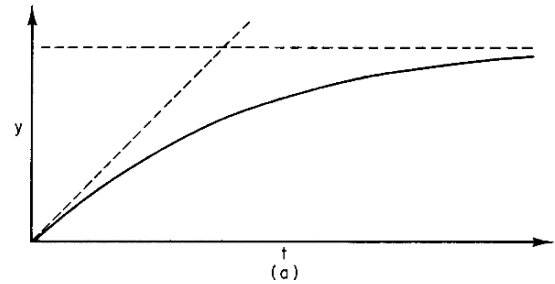


FIGURE 2.12. (a) Plot of  $y(t)$ . (b) Plot of  $dy/dt$ .

patients immediately after the infarct. Each class has an associated death rate that is constant. After three years, virtually none of the subgroup with the higher death rate remains. Another model is that the death rate is higher right after the infarct for all patients. This higher death rate is due to causes associated with the myocardial injury: irritability of the muscle, arrhythmias in the heart-beat, the weakening of the heart wall at the site of the infarct, and so forth. After many months, the heart has healed, scar tissue has replaced the necrotic (dead) muscle, and deaths from these causes no longer occur.

Whatever the cause, it is sometimes useful to fit a set of experimental data with a sum of exponentials. It should be clear from the discussion of survival after myocardial infarction that simply fitting with an exponential or a sum of exponentials does not prove anything about the decay mechanism.

If  $y$  consists of two quantities,  $y_1$  and  $y_2$ , each with its own decay rate, then

$$y = y_1 + y_2 = A_1 e^{-b_1 t} + A_2 e^{-b_2 t}. \quad (2.26)$$

Suppose that  $b_1 > b_2$ , so that  $y_1$  decays more rapidly than  $y_2$ . After enough time has elapsed,  $y_1$  will be much less than  $y_2$ , and its effect on a semilog plot will be negligible. A typical plot of  $y$  is curve  $A$  in Fig. 2.13. Line  $B$  can then be drawn through the data and used to determine  $A_2$  and  $b_2$ . This line is extrapolated back to earlier times, so that  $y_2$  can be subtracted from  $y$  to give an estimate for  $y_1$ . For example, at point  $C$  ( $t = 4$ ),  $y = 400$ ,  $y_2 = 300$ , and  $y_1 = 100$ . At  $t = 0$ ,  $y_1 = 1500 - 500 = 1000$ . For times greater than 5 s, the curves for  $y$  and  $y_2$  are close together, and error in reading the graph produces considerable scatter in  $y_1$ . When several values of  $y_1$  have



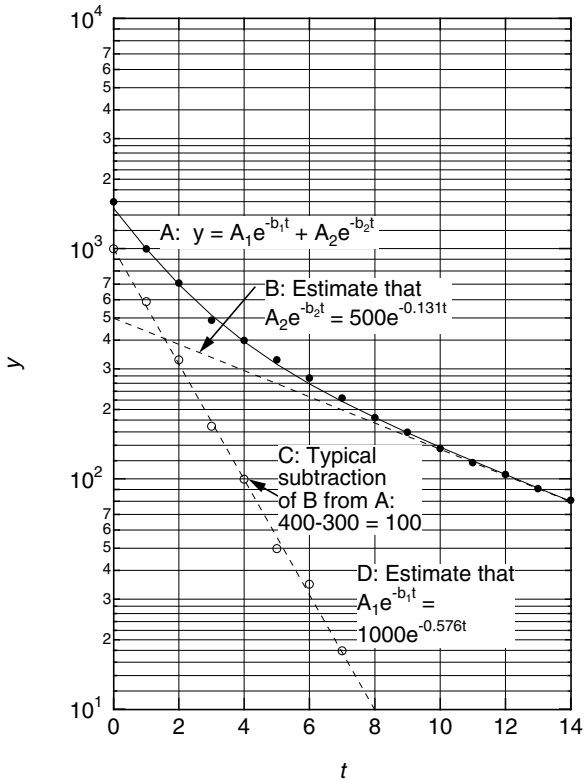


FIGURE 2.13. Fitting a curve with two exponentials.

been determined, line *D* is drawn, and parameters  $A_1$  and  $b_1$  are estimated.

This technique can be extended to several exponentials. However, it becomes increasingly difficult to extract meaningful parameters as more exponentials are used, because the estimated parameters for the short-lived terms are very sensitive to the initial guess for the parameters of the longest-lived term. For a discussion of this problem, see Riggs (1970), pp. 146–163.

## 2.9 The Logistic Equation

Exponential growth cannot go on forever. [This fact is often ignored by economists and politicians. Albert Bartlett has written extensively on this subject. You can find several references in *The American Journal of Physics* and *The Physics Teacher*. See the summary in Bartlett (2004).]

Sometimes a growing population will level off at some constant value. Other times the population will grow and then crash. One model that exhibits leveling off is the *logistic model*, described by the differential equation

$$\frac{dy}{dt} = b_0 y \left( 1 - \frac{y}{y_\infty} \right), \quad (2.27)$$

where  $b_0$  and  $y_\infty$  are constants. This equation has constant solutions  $y = 0$  and  $y = y_\infty$ . If  $y \ll y_\infty$ , then the

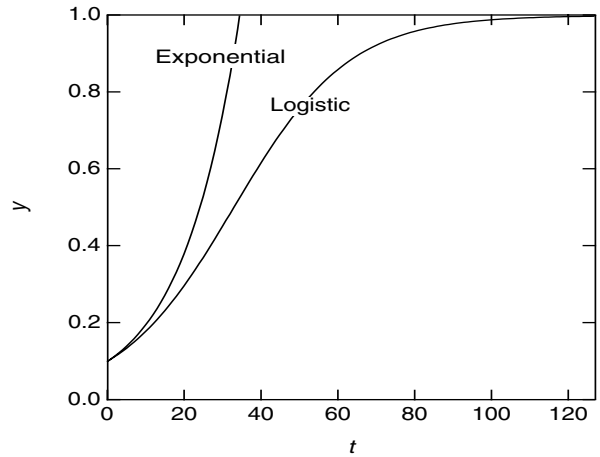


FIGURE 2.14. Plot of the solution of the logistic equation when  $y_0 = 0.1$ ,  $y_\infty = 1.0$ ,  $b_0 = 0.0667$ . Exponential growth with the same values of  $y_0$  and  $b_0$  is also shown.

equation is approximately  $dy/dt = b_0 y$  and  $y$  grows exponentially. As  $y$  becomes larger, the term in parentheses reduces the rate of increase of  $y$ , until  $y$  reaches the saturation value  $y_\infty$ . This might happen, for example, as the population begins to consume a significant fraction of the food supply, causing the birth rate to decrease or the mortality rate to increase.

If the initial value of  $y$  is  $y_0$ , the solution of Eq. 2.27 is

$$\begin{aligned} y(t) &= \frac{1}{\frac{1}{y_\infty} + \left( \frac{1}{y_0} - \frac{1}{y_\infty} \right) e^{-b_0 t}} \quad (2.28) \\ &= \frac{y_0 y_\infty}{y_0 + (y_\infty - y_0) e^{-b_0 t}}. \end{aligned}$$

You can easily verify that  $y(0) = y_0$  and  $y(\infty) = y_\infty$ . A plot of the solution is given in Fig. 2.14, along with exponential growth with the same value of  $b_0$ .

Another way to think of Eq. 2.27 is that it has the form  $dy/dt = b(y)y$ , where  $b(y) = b_0(1 - y/y_\infty)$  is now a function of the dependent variable  $y$  instead of the independent variable  $t$ . As  $y$  grows toward the asymptotic value, the growth rate  $b(y)$  decreases linearly to zero. The logistic model was an early and very important model for population growth. It provides good fits in a few cases, but there are now many more sophisticated models in population biology [Murray (2001)].

## 2.10 Log-log Plots, Power Laws, and Scaling

### 2.10.1 Log-log Plots and Power Laws

This section considers the use of plots in which both scales are logarithmic: log-log plots. They are useful when  $x$  and  $y$  are related by the function

$$y = Bx^n. \quad (2.29)$$

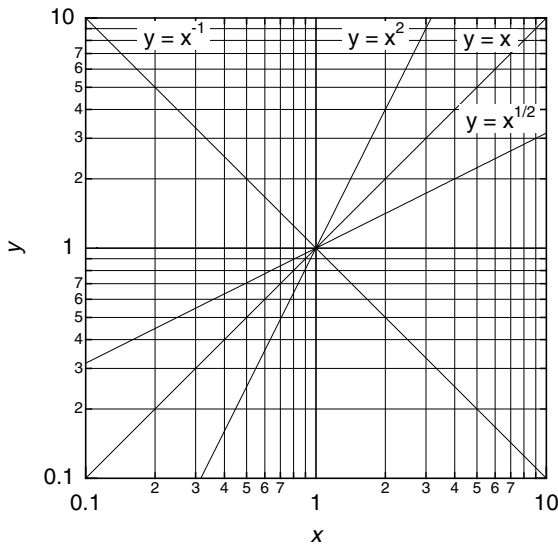


FIGURE 2.15. Log-log plots of  $y = x^n$  for different values of  $n$ . When  $x = 1$ ,  $y = 1$  in every case.

Notice the difference between this and the exponential function: here the independent variable  $x$  is *raised to a constant power*, while in the exponential case  $x$  (or  $t$ ) is *in the exponent*. It also leads to a discussion of *scaling*, whereby simple physical arguments lead to important conclusions about the variations between species in size, shape, metabolic rate, and the like.

By taking logarithms of both sides of Eq. 2.29, we get

$$\log y = \log B + n \log x. \quad (2.30)$$

This is a linear relationship between  $u = \log y$  and  $v = \log x$ :

$$u = \text{const} + nv. \quad (2.31)$$

Therefore a plot of  $u$  vs  $v$  is a straight line with slope  $n$ . The slope can be positive or negative and need not be an integer. Figure 2.15 shows plots of  $y = x$ ,  $y = x^2$ ,  $y = x^{1/2}$ , and  $y = x^{-1}$ . The slope can be determined from the graph by taking  $\Delta u / \Delta v$ . The value of  $B$  is determined either by substituting particular values of  $y$  and  $x$  in Eq. 2.29 after  $n$  is known, or by determining the value of  $y$  when  $x = 1$ , in which case  $x^n = 1$  for any value of  $n$ , so  $n$  need not be known.

Figure 2.16 shows how the curves change when  $B$  is changed while  $n = 1$ . The curves are all parallel to one another. Multiplying by  $B$  is equivalent to adding a constant to  $\log y$ .

If the expression is not of the form  $y = Bx^n$  but has an added term, it will not plot as a straight line on log-log paper. Figure 2.16 also shows a plot of  $y = x + 1$ , which is not a straight line. (Of course, for very large values of  $x$ ,  $\log(x + 1)$  becomes nearly indistinguishable from  $\log x$ , and the line appears straight.)

When the slope is constant,  $n$  can be determined from the slope  $\Delta u / \Delta v$  measured with a ruler on the log-log

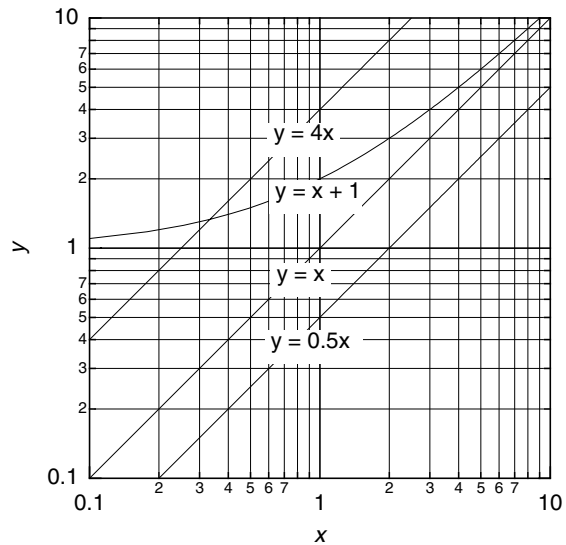


FIGURE 2.16. Log-log plots of  $y = Bx$ , showing how the curves shift on the paper as  $B$  changes. Since  $n = 1$  for all the curves, they all have the same slope. There is also a plot of  $y = x + 1$ , to show that a polynomial does not plot as a straight line.

paper. When determining the slope in this way *one must be sure that the length of a cycle is the same in each direction on the graph paper*. To repeat the warning: it is easy to get a rough idea of the exponent from inspection of the slope of the log-log plot in Fig. 2.15 because on commercial log-log graph paper the distance spanned by a decade or cycle is the same on both axes. Some magazines routinely show log-log plots in which the distance spanned by a decade is not the same on both axes. Moreover, commercial graphing software does not impose this constraint on log-log plots, so it is becoming less and less likely that you can determine the exponent by glancing at the plot. Be careful!

When using a spreadsheet or other graphing software, it is often useful to make an extra column that contains the calculated variable  $y_{\text{calc}} = Ax^m$  with the values for  $A$  and  $m$  stored in two cells of the spreadsheet. If you plot this column as a line, and your real data as points without a line, then you can change the parameters while inspecting the graph to find the values that give the best fit.

An example of the use of a log-log plot is Poiseuille flow of fluid through a tube versus tube radius when the pressure gradient along the tube is constant (Problem 35). It was shown in Chapter 1 that an  $r^4$  dependence is expected.

### 2.10.2 Food Consumption, Basal Metabolic Rate, and Scaling

Consider the relation of daily food consumption to body mass. This will introduce us to simple scaling arguments.

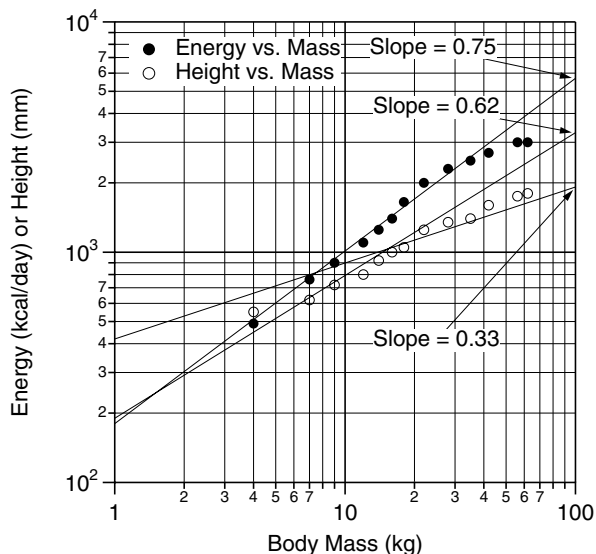


FIGURE 2.17. Plot of daily food requirement  $F$  and height  $H$  vs mass  $M$  for growing children. Data are from Kempe *et al.* (1970), p. 90.

As a first model, we might suppose that each kilogram of tissue has the same metabolic requirement, so that food consumption should be proportional to body mass. However, there is a problem with this argument. Most of the food that we consume is converted to heat. The various mechanisms to lose heat—radiation, convection and perspiration—are all roughly proportional to the surface area of the body rather than its mass. (This statement neglects the fact that considerable evaporation takes place through the lungs and that the body can control the rate of heat loss through sweating and shivering.) If all persons were the same shape, then the total surface area would be proportional to  $H^2$ , where  $H$  is the height. The total volume and mass would be proportional to  $H^3$ , so  $H$  would be proportional to  $M^{1/3}$ . Therefore the surface area would be proportional to  $(M^{1/3})^2$  or  $M^{2/3}$ . (See Problem 40 for a discussion of other possible dependences of surface area on mass.) Figure 2.17 plots  $H$  and the total daily food requirement  $F$  vs body mass  $M$  for growing children [Kempe, Silver, and O'Brien (1970), p. 90].

Neither of the models proposed above fits the data very well. At early ages  $H$  is more nearly proportional to  $M^{0.62}$  than to  $M^{1/3}$ . For older children, when the shape of the body has stopped changing, an  $M^{0.33}$  dependence does fit better. This better fit occurs for masses greater than 23 kg, which correspond to ages over 6 years. The slope of the  $F(M)$  curve is 0.75. This is less than the 1.0 of the model that food consumption is proportional to the mass and greater than the 0.67 of the model that food consumption is proportional to surface area.

This 3/4-power dependence is remarkable because it is seen across many species, from one-celled organisms to large mammals. It is called *Kleiber's law*. Peters (1983) quotes work by Hemmingsen (1960) that shows the stan-

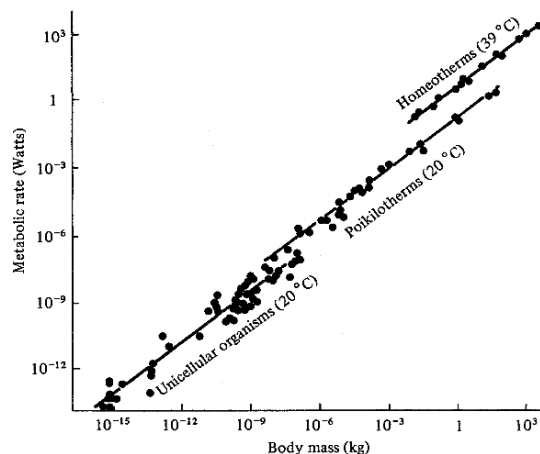


FIGURE 2.18. Plot of resting metabolic rate vs. body mass for many different organisms. Graph is from R. H. Peters (1983). *The Ecological Implications of Body Size*. Cambridge, Cambridge University Press. Modified from A. M. Hemmingsen (1960). Energy metabolism as related to body size and respiratory surfaces, and its evolution. *Reports of the Steno Memorial Hospital and Nordisk Insulin Laboratorium*. 9 (Part II): 6–110. Used with permission.

dard metabolic rates for many species can be fitted by the following. The standard metabolic rate is in watts and mass in kilograms. (*Standard* means as close to resting or basal as possible.) For unicellular organisms at 20°C,

$$R_{\text{unicellular}} = 0.018M^{0.751}. \quad (2.32a)$$

The range of masses extended from  $10^{-15}$  to  $10^{-6}$  kg. For poikilotherms (organisms such as fish whose body temperature is the same as the surroundings) at 20°C (masses from  $10^{-8}$  to  $10^2$  kg),

$$R_{\text{poikilotherm}} = 0.14M^{0.751}, \quad (2.32b)$$

and for homeotherms (animals that can maintain their body temperature independent of the surroundings) at 39°C (masses from  $10^{-2}$  to  $10^3$  kg),

$$R_{\text{homeotherm}} = 4.1M^{0.751}. \quad (2.32c)$$

Peters's graph is shown in Fig. 2.18.

The 3/4-power dependence has been widely accepted; however, some recent analyses of the data, such as White and Seymour (2003), support a 2/3 power dependence. Even more recent studies affirm a 3/4 power [Savage *et al.* (2004)].

A number of models have been proposed to explain a 3/4-power dependence [McMahon (1973); Peters (1983); West *et al.* (1999); Banavar *et al.* (1999)]. West *et al.* argue that the 3/4-power dependence is universal: they derive it from a model that supplies nutrients through a branching network that reaches all parts of the organism, minimizes the energy required for distribution,

and ends in capillaries (or terminal xylem in plants) that are all the same size. Whether it is universal is still debated [Kozłowski and Konarzewski (2004)]. West and Brown (2004) review quarter-power scaling in a variety of circumstances.

We will discuss temperature dependence in Chapter 3.

## Symbols Used in Chapter 2

Symbol	Use	Units	First used on page
$a$	Rate of input of a substance	$s^{-1}$	38
$b, b_0$	Rate of growth or decay	$s^{-1}, h^{-1}$	31
$c_1, c_2$	Constants		34
$f$	Fraction		33
$m, n$	Exponent in power law relationship		39
$t$	Time	s	32
$u$	Logarithm of dependent variable		34
$v$	Logarithm of independent variable		40
$x$	General independent variable		33
$y$	General dependent variable		32
$y$	Amount of substance in plasma	kg, mg	37
$x_0, y_0$	Initial value of $x$ or $y$		32
$y_\infty$	Saturation value of $y$		39
$A$	Constant		38
$B$	Constant		39
$C$	Concentration	$kg\ m^{-3}$ , etc.	37
$F$	Food requirement	$kcal\ day^{-1}$	41
$H$	Body height	m	41
$K$	Clearance	$m^3\ s^{-1}$	37
$M$	Body mass	kg	41
$N$	Number of compoundings per year		32
$R$	Standard metabolic rate	W	41
$T_{1/2}$	Half-life	s, etc.	34
$T_2$	Doubling time	s	34
$V$	Volume	$m^3$	37
$X_{10}$	Change in $x$ for a factor-of-10 change in $y$		34
$X_{100}$	Change in $x$ for a factor-of-100 change in $y$		35

## Problems

### Section 2.1

**Problem 1** Suppose that you are 20 years old and have an annual income of \$20,000. You plan to work for 40 years. If inflation takes place at a rate of 3% per year, what income would you need at age 60 to have the same

buying power you have now? Ignore taxes. Make the calculation assuming that (a) inflation is 3% and occurs once a year and (b) inflation is continuous but at a 3% annual rate.

**Problem 2** The number  $e$  is defined by  $\lim_{n \rightarrow \infty} (1 + 1/n)^n$ .

(a) Calculate values of  $(1 + 1/n)^n$  for  $n = 1, 2, 4, 8$ , and 16.

(b) Use the binomial formula  $(1 + a)^n = 1 + na + \frac{n(n-1)}{2!}a^2 + \frac{n(n-1)(n-2)}{3!}a^3 + \dots$  to obtain a series for  $e^x = \lim_{n \rightarrow \infty} (1 + x/n)^n$ . [See also Appendix D, Eq. D.3.]

**Problem 3** A child with acute lymphocytic leukemia (ALL) has approximately  $10^{12}$  leukemic cells when the disease is clinically apparent.

(a) If a cell is about  $8\ \mu m$  in diameter, estimate the total mass of leukemic cells.

(b) Curing the disease requires killing every single cell. The doubling time for the cells is about 5 days. If all cells were killed except for one, how long would it take for the disease to become apparent again?

(c) Suppose that chemotherapy reduces the number of cells to  $10^9$  and there are no changes of ALL cell properties (no mutations). How long a remission would you expect? What if the number were reduced to  $10^6$ ?

**Problem 4** Suppose that tumor cells within the body reproduce at rate  $r$ , so that the number is given by  $y = y_0 e^{rt}$ . Each time a chemotherapeutic agent is given it destroys a fraction  $f$  of the cells then existing. Make a semilog plot showing  $y$  as a function of time for several administrations of the drug, separated by time  $T$ . What different cases must you consider for the relation among  $f$ ,  $T$ , and  $r$ ?

**Problem 5** An exponentially growing culture of bacteria increases from  $10^6$  to  $5 \times 10^8$  cells in 6 h. What is the time between successive cell divisions if there is no cell mortality?

**Problem 6** The following data on railroad tracks were obtained from R. H. Romer [(1991). The mathematics of exponential growth—keep it simple, *Phys. Teach.* **9**: 344–345]:

Year	Miles of track
1860	30,626
1870	52,922
1880	93,262
1890	166,703

(a) What is the doubling time?

(b) Estimate the surface area of the contiguous United States. Assume that a railroad roadbed is 7 m wide. In what year would an extrapolation predict that the surface of the United States would be completely covered with railroad track?

Section 2.2

**Problem 7** A dose  $D$  of drug is given that causes the plasma concentration to rise from 0 to  $C_0$ . The concentration then falls according to  $C = C_0e^{-bt}$ . At time  $T$ , what dose must be given to raise the concentration to  $C_0$  again? What will happen if the original dose is administered over and over again at intervals of  $T$ ?

**Problem 8** Consider the atmosphere to be at constant temperature but to have a pressure  $p$  that varies with height  $y$ . A slab between  $y$  and  $y + dy$  has a different pressure on the top than on the bottom because of the weight of the air in the slab. (The weight of the air is the number of molecules  $N$  times  $mg$ , where  $m$  is the mass of a molecule and  $g$  is the gravitational acceleration.) Use the ideal gas law,  $pV = Nk_B T$  (where  $k_B$  is the Boltzmann constant and  $T$ , the absolute temperature, is constant), and the fact that the air is in equilibrium to write a differential equation for  $p$  as a function of  $y$ . The equation should be familiar. Show that  $p(y) = Ce^{-mgy/k_B T}$ .

**Problem 9** The mean life of a radioactive substance is defined by the equation

$$\tau = \frac{-\int_0^\infty t(dy/dt) dt}{-\int_0^\infty (dy/dt) dt}.$$

Show that if  $y = y_0e^{-bt}$ , then  $\tau = 1/b$ .

Section 2.3

**Problem 10** R. Guttman [(1996). *J. Gen. Physiol.* **49**: 1007] measured the temperature dependence of the current pulse necessary to excite the squid axon. He found that for pulses shorter than a certain length  $\tau$ , a fixed amount of electric charge was necessary to make the nerve fire; for longer pulses the current was fixed. This suggests that the axon integrates the current for a time  $\tau$  but not longer. The following data are for the integrating time  $\tau$  vs temperature  $T$  ( $^\circ\text{C}$ ). Find an empirical exponential relationship between  $T$  and  $\tau$ .

$T$ ( $^\circ\text{C}$ )	$\tau$ (ms)
5	4.1
10	3.4
15	1.9
20	1.4
25	0.7
30	0.6
35	0.4

**Problem 11** A normal rabbit was injected with  $1\text{ cm}^3$  of staphylococcus aureus culture containing  $10^8$  organisms. At various later times,  $0.2\text{ cm}^3$  of blood was taken from the rabbit's ear. The number of organisms per  $\text{cm}^3$  was calculated by diluting the material, smearing it on culture plates, and counting the number of colonies formed. The results are shown below. Plot these data and see if

they can be fitted by a single exponential. Can you also estimate the blood volume of the rabbit?

$t$ (min)	Bacteria (per $\text{cm}^3$ )
0	$5 \times 10^5$
3	$2 \times 10^5$
6	$5 \times 10^4$
10	$7 \times 10^3$
20	$3 \times 10^2$
30	$1.7 \times 10^2$

Section 2.4

**Problem 12** All members of a certain population are born at  $t = 0$ . The death rate in this population (deaths per unit population per unit time) is found to increase linearly with age  $t$ : (death rate) =  $a + bt$ . Find the population as a function of time if the initial population is  $y_0$ .

**Problem 13** The accompanying table gives death rates (in  $\text{yr}^{-1}$ ) as a function of age. Plot these data on linear graph paper and on semilog paper. Find a region over which the death rate rises approximately exponentially with age, and determine parameters to describe that region.

Age	Death Rate	Age	Death Rate
0	0.000 863	45	0.005 776
5	0.000 421	50	0.008 986
10	0.000 147	55	0.013 748
15	0.001 027	60	0.020 281
20	0.001 341	65	0.030 705
25	0.001 368	70	0.046 031
30	0.001 697	75	0.066 196
35	0.002 467	80	0.101 443
40	0.003 702	85	0.194 197

**Problem 14** Suppose that the amount of a resource at time  $t$  is  $y(t)$ . At  $t = 0$  the amount is  $y_0$ . The rate at which it is consumed is  $r = -dy/dt$ . Let  $r = r_0e^{bt}$ , that is, the rate of use increases exponentially with time. (For example, the world use of crude oil has been increasing about 7% per year since 1890.)

(a) Show that the amount remaining at time  $t$  is  $y(t) = y_0 - (r_0/b)(e^{bt} - 1)$ .

(b) If the present supply of the resource were used up at constant rate  $r_0$ , it would last for a time  $T_c$ . Show that when the rate of consumption grows exponentially at rate  $b$ , the resource lasts a time  $T_b = (1/b)\ln(1 + bT_c)$ .

(c) An advertisement in *Scientific American*, September 1978, p. 181, said, "There's still twice as much gas underground as we've used in the past 50 years—at our present rate of use, that's enough to last about 60 years." Calculate how long the gas would last if it were used at a rate that increases 7% per year.

(d) If the supply of gas were doubled, how would the answer to part (c) change?

(e) Repeat parts (c) and (d) if the growth rate is 3% per year.

**Problem 15** When we are dealing with death or component failure, we often write Eq. 2.17 in the form  $y(t) = y_0 \exp \left[ - \int_0^t m(t') dt' \right]$  and call  $m(t)$  the mortality function. Various forms for the mortality function can represent failure of computer components, batteries in pacemakers, or the death of organisms. (This is not the most general possible mortality model. For example, it ignores any interaction between organisms, so it cannot account for effects such as overcrowding or a limited supply of nutrients.)

(a) For human populations the mortality function is often written as  $m(t) = m_1 e^{-b_1 t} + m_2 + m_3 e^{+b_3 t}$ . What sort of processes does each of these terms represent?

(b) Assume that  $m_1$  and  $m_2$  are zero. Then  $m(t)$  is called the Gompertz mortality function. Obtain an expression for  $y(t)$  with the Gompertz mortality function. Time  $t_{\max}$  is sometimes defined to be the time when  $y(t) = 1$ . It depends on  $y_0$ . Obtain an expression for  $t_{\max}$ .

**Problem 16** The incidence of a disease is the number of new cases per unit time per unit population (or per 100,000). The prevalence of the disease is the number of cases per unit population. For each situation below, the size of the general population remains fixed at the constant value  $y$ , and the disease has been present for many years.

(a) The incidence of the disease is a constant,  $i$  cases per year. Each person has the disease for a fixed time of  $T$  years, after which the person is either cured or dies. What is the prevalence  $p$ ? Hint: The number who are sick at time  $t$  is the total number who became sick between  $t-T$  and  $t$ .

(b) The patients in part (a) who are sick die with a constant death rate  $b$ . What is the prevalence?

(c) A new epidemic begins at  $t = 0$ , and the incidence increases exponentially with time:  $i = i_0 e^{kt}$ . What is the prevalence if each person has the disease for  $T$  years?

## Section 2.5

**Problem 17** The creatinine clearance test measures a patient's kidney function. Creatinine is produced by muscle at a rate  $p$  g  $h^{-1}$ . The concentration in the blood is  $C$  g  $l^{-1}$ . The volume of urine collected in time  $T$  (usually 24 h) is  $V$  l. The creatinine concentration in the urine is  $U$  g  $l^{-1}$ . The clearance is  $K$ . The plasma volume is  $V_p$ . Assume that creatinine is stored only in the plasma.

(a) Draw a block diagram for the process and write a differential equation for  $C$ .

(b) Find an expression for the creatinine clearance  $K$  in terms of  $p$  and  $C$  when  $C$  is not changing with time.

(c) If  $C$  is constant all creatinine produced in time  $T$  appears in the urine. Find  $K$  in terms of  $C$ ,  $V$ ,  $U$ , and  $T$ .

(d) If  $p$  were somehow doubled, what would be the new steady-state value of  $C$ ? What would be the time constant for change to the new value?

**Problem 18** A liquid is injected in muscle and spreads throughout a spherical volume  $V = 4\pi r^3/3$ . The volume is well supplied with blood, so that the liquid is removed at a rate proportional to the remaining mass per unit volume. Let the mass be  $m$  and assume that  $r$  remains fixed. Find a differential equation for  $m(t)$  and show that  $m$  decays exponentially.

**Problem 19** A liquid is injected as in Problem 18, but this time a cyst is formed. The rate of removal of mass is proportional to both the pressure of liquid within the cyst, and to the surface area of the cyst, which is  $4\pi r^2$ . Assume that the cyst shrinks so that the pressure of liquid within the cyst remains constant. Find a differential equation for the rate of mass removal and show that  $dm/dt$  is proportional to  $m^{2/3}$ .

**Problem 20** The following data showing ethanol concentration in the blood vs time after ethanol ingestion are from L. J. Bennison and T. K. Li [(1976). *New Engl. J. Med.* **294**: 9–13]. Plot the data and discuss the process by which alcohol is metabolized.

$t$ (min)	Ethanol concentration(mg $dl^{-1}$ )
90	134
120	120
150	106
180	93
210	79
240	65
270	50

**Problem 21** Consider the following two-compartment model. Compartment 1 is damaged myocardium (heart muscle). Compartment 2 is the blood of volume  $V$ . At  $t = 0$  the patient has a heart attack and compartment 1 is created. It contains  $q$  molecules of some chemical which was released by the dead cells. Over the next several days the chemical moves from compartment 1 to compartment 2 at a rate  $i(t)$ , such that  $q = \int_0^\infty i(t) dt$ . The amount of substance in compartment 2 is  $y(t)$  and the concentration is  $C(t)$ . The only mode of removal from compartment 2 is clearance with clearance constant  $K$ .

(a) Write a differential equation for  $C(t)$  that may also involve  $i(t)$ .

(b) Integrate the equation and show that  $q$  can be determined by numerical integration if  $C(t)$  and  $K$  are known.

(c) Show that volume  $V$  need not be known if  $C(0) = C(\infty)$ .

## Section 2.6

**Problem 22** The radioactive nucleus  $^{64}\text{Cu}$  decays independently by three different paths. The relative decay rates of these three modes are in the ratio 2:2:1. The half-life is 12.8 h. Calculate the total decay rate  $b$ , and the three partial decay rates  $b_1$ ,  $b_2$ , and  $b_3$ .

**Problem 23** The following data were taken from Berg et al. (1982). At  $t = 0$ , a 70-kg subject was given an intra-

venous injection of 200 mg of phenobarbital. The initial concentration in the blood was  $6 \text{ mg l}^{-1}$ . The concentration decayed exponentially with a half-life of 110 h. The experiment was repeated, but this time the subject was fed 200 g of activated charcoal every 6 h. The concentration of phenobarbital again fell exponentially, but with a half-life of 45 h.

- What was the volume in which the phenobarbital was distributed?
- What was the clearance in the first experiment?
- What was the clearance due to charcoal?

## Section 2.7

**Problem 24** You are treating a severely ill patient with an intravenous antibiotic. You give a loading dose  $D$  mg, which distributes immediately through blood volume  $V$  to give a concentration  $C$   $\text{mg dl}^{-1}$  (1 deciliter = 0.1 liter). The half-life of this antibiotic in the blood is  $T$  h. If you are giving an intravenous glucose solution at a rate  $R$   $\text{ml h}^{-1}$ , what concentration of antibiotic should be in the glucose solution to maintain the concentration in the blood at the desired value?

**Problem 25** The solution to the differential equation  $dy/dt = a - by$  for the initial condition  $y(0) = 0$  is  $y = (a/b)(1 - e^{-bt})$ . Plot the solution for  $a = 5 \text{ g min}^{-1}$  and for  $b = 0.1, 0.5, \text{ and } 1.0 \text{ min}^{-1}$ . Discuss why the final value and the time to reach the final value change as they do. Also make a plot for  $b = 0.1$  and  $a = 10$  to see how that changes the situation.

**Problem 26** Derive an approximate expression for  $(a/b)(1 - e^{-bt})$  which is accurate for small times ( $t \ll 1/b$ ). Use the Taylor expansion for an exponential given in Appendix D.

**Problem 27** We can model the repayment of a mortgage with a differential equation. Suppose that  $y(t)$  is the amount still owed on the mortgage at time  $t$ , the rate of repayment per unit time is  $a$ ,  $b$  is the interest rate, and that the initial amount of the mortgage is  $y_0$ .

- Find the differential equation for  $y(t)$ .
- Try a solution of the form  $y(t) = a/b + Ce^{bt}$ , where  $C$  is a constant to be determined from the initial conditions. Find  $C$ , plot the solution, and determine the time required to pay off the mortgage.

**Problem 28** When an animal of mass  $m$  falls in air, two forces act on it: gravity,  $mg$ , and a force due to air friction. Assume that the frictional force is proportional to the speed  $v$ .

- Write a differential equation for  $v$  based on Newton's second law,  $F = m(dv/dt)$ .
- Solve this differential equation. (Hint: Compare your equation to Eq. 2.24.)

- Assume that the animal is spherical, with radius  $a$  and density  $\rho$ . Also, assume that the frictional force is proportional to the surface area of the animal. Determine the terminal speed (speed of descent in steady state) as a function of  $a$ .

- Use your result in part (c) to interpret the following quote by J. B. S. Haldane [1985]: "You can drop a mouse down a thousand-yard mine shaft; and arriving at the bottom, it gets a slight shock and walks away. A rat is killed, a man is broken, a horse splashes."

**Problem 29** In Problem 28, we assumed that the force of air friction is proportional to the speed  $v$ . For flow at high Reynolds numbers, a better approximation is that the force is proportional to  $v^2$ .

- Write the differential equation for  $v$  as a function of  $t$ .

- This differential equation is nonlinear because of the  $v^2$  term and thus difficult to solve analytically. However, the terminal speed can easily be obtained directly from the differential equation by setting  $dv/dt = 0$ . Find the terminal speed as a function of  $a$  (defined in Problem 28).

**Problem 30** A drug is infused into the body through an intravenous drip at a rate of  $100 \text{ mg h}^{-1}$ . The total amount of drug in the body is  $y$ . The drug distributes uniformly and instantaneously throughout the body in a compartment of volume  $V = 18 \text{ l}$ . It is cleared from the body by a single exponential process. In the steady state the total amount in the body is 200 mg.

- At noon ( $t = 0$ ) the intravenous line is removed. What is  $y(t)$  for  $t > 0$ ?
- What is the clearance of the drug?

## Section 2.8

**Problem 31** You are given the following data:

$x$	$y$	$x$	$y$
0	1.000	5	0.444
1	0.800	6	0.400
2	0.667	7	0.364
3	0.571	8	0.333
4	0.500	9	0.308
		10	0.286

Plot these data on semilog graph paper. Is this a single exponential? Is it two exponentials? Plot  $1/y$  vs  $x$ . Does this alter your answer?

## Section 2.9

**Problem 32** Suppose that the rate of consumption of a resource increases exponentially. (This might be petroleum, or the nutrient in a bacterial culture.) During the first doubling time the amount used is 1 unit. During the second doubling time it is 2 units, the next 4, etc. How does the amount consumed during a doubling time compare to the total amount consumed during all previous doubling times?

**Problem 33** Suppose that the rate of growth of  $y$  is described by  $dy/dt = b(y)y$ . Expand  $b(y)$  in a Taylor's series and relate the coefficients to the terms in the logistic equation.

**Problem 34** Consider a classic predator-prey problem. Let the number of foxes be  $F$  and the number of rabbits be  $R$ . The rabbits eat grass, which is plentiful. The foxes eat only rabbits. The number of foxes and rabbits can be modelled by the Lotka-Volterra equations

$$\begin{aligned} \frac{dR}{dt} &= aR - bRF \\ \frac{dF}{dt} &= -cF + dRF. \end{aligned}$$

(a) Describe the physical meaning of each term on the right-hand side of each equation. What does each of the constants  $a, b, c$ , and  $d$  denote?

(b) Solve for the steady-state values of  $F$  and  $R$ .

These differential equations are difficult to solve because they are nonlinear (see Chapter 10). Typically,  $R$  and  $F$  oscillate about the steady-state solutions found in part (b). For more information, see Murray (2001).

Section 2.10

**Problem 35** Plot the following data for Poiseuille flow on log-log graph paper. Fit the equation  $i = CR_p^n$  to the data by eye (or by trial and error using a spread sheet), and determine  $C$  and  $n$ .

$R_p$ ( $\mu\text{m}$ )	$i$ ( $\mu\text{m}^3 \text{ s}^{-1}$ )
5	0.000 10
7	0.000 38
10	0.001 6
15	0.008 1
20	0.026
30	0.13
50	1.0

**Problem 36** Below are the molecular weights and radii of some molecules. Use log-log graph paper to develop an empirical relationship between them.

Substance	$M$	$R$ (nm)
Water	18	0.15
Oxygen	32	0.20
Glucose	180	0.39
Mannitol	180	0.36
Sucrose	390	0.48
Raffinose	580	0.56
Inulin	5,000	1.25
Ribonuclease	13,500	1.8
$\beta$ -lactoglobulin	35,000	2.7
Hemoglobin	68,000	3.1
Albumin	68,000	3.7
Catalase	250,000	5.2

**Problem 37** How well does Eq. 2.32c explain the data of Fig. 2.17? Discuss any differences.

**Problem 38** Compare the mass and metabolic requirements (and hence waste output, including water vapor) of 180 people each weighing 70 kg with 12,600 chickens of average mass 1 kg.

**Problem 39** Figure 2.17 shows that in young children, height is more nearly proportional to  $M^{0.62}$  than to  $M^{1/3}$ . Find pictures of children and adults and compare ratios of height to width, to see what the differences are.

**Problem 40** Consider three models of an organism. The first is a sphere of radius  $R$ . The second is a cube of length  $L$ . These are crude models for animals. The third is a broad leaf of surface area  $A$  on each side and thickness  $t$ . Assume all have density  $\rho$ . In each case, calculate the surface area  $S$  as a function of mass,  $M$ . Ignore the surface area of the edge of the leaf. [For a comparison of scaling in leaves and animals, see Reich (2001). He shows that for broad leaves  $S \propto M^{1.1}$ .]

**Problem 41** If food consumption is proportional to  $M^{3/4}$  across species, how does the food consumption per unit mass scale with mass? Qualitatively compare the eating habits of hummingbirds to eagles and mice to elephants. [See Schmidt-Nielsen (1984), pp. 52–64.]

**Problem 42** In problem 41, you found how the specific metabolic rate (food consumption per unit mass) varies with mass. If all animal heart volumes and blood volumes are proportional to  $M$ , then the only way for the heart to increase the oxygen delivery to the body is by increasing the frequency of the heart rate. [Schmidt-Nielsen (1984), pp. 126–150.]

(a) Using the result from problem 41, if a 70 kg man has a heart rate of 80 beats  $\text{min}^{-1}$ , determine the heart rate of a guinea pig ( $M = 0.5$  kg).

(b) To a first approximation, all hearts beat about 800,000,000 times in a lifetime. A 30 g mouse lives about 3 years. Estimate the life span of a 3000 kg elephant.

(c) Humans live longer than their mass would indicate. Calculate the life span of a 70 kg human based on scaling, and compare it to a typical human life span.

**Problem 43** Let's examine how high animals can jump [Schmidt-Nielsen (1984), pp. 176–179]. Assume that the energy output of the jumping muscle is proportional to the body mass,  $M$ . The gravitational potential energy gained upon jumping to a height  $h$  is  $Mgh$  ( $g = 9.8 \text{ m s}^{-2}$ ). If a 3 g locust can jump 60 cm, how high can a 70 kg human jump? Use scaling arguments.

**Problem 44** In problem 43, you should have found that all animals can jump to about the same height (approximately 0.6 m), independent of their mass  $M$ .

(a) Equate the kinetic energy at the bottom of the jump ( $Mv^2/2$ , where  $v$  is the "take-off speed") to the potential energy  $Mgh$  at the top of the jump to find how the take-off speed scales with mass.

(b) Calculate the take-off speed.



(c) In order to reach this speed, the animal must accelerate upward over a distance  $L$ . If we assume a constant acceleration  $a$ , then  $a = v^2/(2L)$ . Assume  $L$  scales as the linear size of the animal (and assume all animals are basically the same shape but different size). How does the acceleration  $a$  scale with mass?

(d) For a 70 kg human,  $L$  is about  $1/3$  m. Calculate the acceleration (express your answer in terms of  $g$ ).

(e) Use your result from part (c) to estimate the acceleration for a 0.5 mg flea (again, express your answer in terms of  $g$ ).

(f) Speculate on the biological significance of the result in part (e) [See Schmidt-Nielsen (1984), pp. 180–181].

## References

- Banavar, J. R., A. Maritan, and A. Rinaldo (1999). Size and form in efficient transportation networks. *Nature*, **399**: 130–132.
- Bartlett, A. (2004). *The Essential Exponential! For the Future of Our Planet*. Lincoln, NE, Center for Science, Mathematics & Computer Education.
- Berg, M. J., W. G. Berlinger, M. J. Goldberg, R. Spector, and G. F. Johnson (1982). Acceleration of the body clearance of phenobarbital by oral activated charcoal. *N. Engl. J. Med.* **307**: 642–644.
- Clark, V. A. (1975). Survival distributions. *Ann. Rev. Biophys. Bioeng.* **4**: 431–438.
- Haldane, J. B. S. (1985). *On Being the Right Size and Other Essays*. Oxford, Oxford University Press.
- Hemmingsen, A. M. (1960). Energy metabolism as related to body size and respiratory surfaces, and its evolution. *Reports of the Steno Memorial Hospital and Nordisk Insulin Laboratorium* **9**: 6–110.
- Kempe, C. H., H. K. Silver, and D. O'Brien (1970). *Current Pediatric Diagnosis and Treatment*, 2nd ed. Los Altos, CA, Lange.
- Kozlowski, J., and M. Konarzewski (2004). Is West, Brown, and Enquist's model of allometric scaling mathematically correct and biologically relevant? *Funct. Ecol.* **18**: 283–289.
- Maor, E. (1994). *e: The Story of a Number*. Princeton, NJ, Princeton University Press.
- McKee, P. A., W. P. Castelli, P. M. McNamara, and W. B. Kannel (1971). The natural history of congestive heart failure: The Framingham study. *New Engl. J. Med.* **285**: 1441–1446.
- McMahon, T. (1973). Size and shape in biology. *Science* **179**: 1201–1204.
- Murray, J. D. (2001). *Mathematical Biology*. New York, Springer-Verlag.
- Peters, R. H. (1983). *The Ecological Implications of Body Size*. Cambridge, Cambridge University Press.
- Reich, P. (2001). Body size, geometry, longevity, and metabolism: do plant leaves behave like animal bodies? *Trends in Ecology and Evolution* **16**(12): 674–680.
- Riggs, D. S. (1970). *The Mathematical Approach to Physiological Problems*. Cambridge, MA, MIT Press.
- Savage, V. M., J. F. Gillooly, W. H. Woodruff, G. B. West, A. P. Allen, B. J. Enquist, and J. H. Brown (2004). The predominance of quarter-power scaling in biology. *Funct. Ecol.* **18**: 257–282.
- Schmidt-Nielsen, K. (1984). *Scaling: Why Is Animal Size So Important?* Cambridge, Cambridge University Press.
- West, G. B., J. H. Brown, and B. J. Enquist. (1999). The fourth dimension of life: Fractal geometry and allometric scaling of organisms. *Science*, **284**: 1677–1679. (see also Mackenzie's accompanying editorial on p. 1607 of the same issue of *Science*).
- West, G. B., and J. H. Brown. (2004). Life's universal scaling laws. *Physics Today*, **57**(9): 36–42.
- White, C. R., and R. S. Seymour. (2003). Mammalian basal metabolic rate is proportional to body mass<sup>2/3</sup>. *Proc. Nat. Acad. Sci.* **100**(7): 4046–4049.
- Zumoff, B., H. Hart, and L. Hellman (1966). Considerations of mortality in certain chronic diseases. *Ann. Intern. Med.* **64**: 595–601.

# 3

## Systems of Many Particles

It is possible to identify all the external forces acting on a simple system and use Newton's second law ( $\mathbf{F} = m\mathbf{a}$ ) to calculate how the system moves. (Applying this technique in a complicated case such as the femur may require the development of a simplified model, because so many muscles, other bones, and ligaments apply forces at so many different points.) In an atomic-size system consisting of a single atom or molecule, it is possible to use the quantum-mechanical equivalent of  $\mathbf{F} = m\mathbf{a}$ , the Schrödinger equation, to do the same thing. (The Schrödinger equation takes into account the wave properties that are important in small systems.)

In systems of many particles, such calculations become impossible. Consider, for example, how many particles there are in a cubic millimeter of blood. Table 3.1 shows some of the constituents of such a sample. To calculate the translational motion in three dimensions, it would be necessary to write three equations for each particle using Newton's second law. Suppose that at time  $t$  the force on a molecule is  $\mathbf{F}$ . Between  $t$  and  $t + \Delta t$ , the velocity of the particle changes according to the three equations

$$v_i(t + \Delta t) = v_i(t) + F_i\Delta t/m, \quad (i = x, y, z).$$

The three equations for the change of position of the particle are of the form  $x(t + \Delta t) = x(t) + v_x(t)\Delta t + F_x(t)(\Delta t)^2/(2m)$ . If  $\Delta t$  is small enough the last term can be neglected. Solving these equations requires at least six multiplications and six additions for each particle. For  $10^{19}$  particles, this means about  $10^{20}$  arithmetic operations per time interval. If a computer can do  $10^{12}$  operations per second, then the complete calculation for a single time interval will require  $10^8$  seconds or three years! Another limitation arises in the physics of the processes. It is now known that relatively simple systems can exhibit deterministic chaos: a collection of identical systems differing in their initial conditions by an infinitesimally small

TABLE 3.1. Some constituents of 1 mm<sup>3</sup> of blood.

Constituent	Concentration in customary units	Number in 1 mm <sup>3</sup> (= 10 <sup>-9</sup> m <sup>3</sup> = 10 <sup>-3</sup> cm <sup>3</sup> )
Water	1 g cm <sup>-3</sup>	$3.3 \times 10^{19}$
Sodium	3.2 mg cm <sup>-3</sup>	$8.3 \times 10^{16}$
Albumin	4.5 g dl <sup>-1</sup>	$3.9 \times 10^{14}$
Cholesterol	200 mg dl <sup>-1</sup>	$3.1 \times 10^{15}$
Glucose	100 mg dl <sup>-1</sup>	$3.3 \times 10^{15}$
Hemoglobin	15 g dl <sup>-1</sup>	$1.4 \times 10^{15}$
Erythrocytes	$5 \times 10^6$ mm <sup>-3</sup>	$5 \times 10^6$

amount can become completely different in their subsequent behavior in a surprisingly short period of time. It is impossible to trace the behavior of this many molecules on an individual basis.

Nor is it necessary. We do not care which water molecule is where. The properties of a system that are of interest are averages over many molecules: pressure, concentration, average speed, and so forth. These average macroscopic properties are studied in *statistical* or *thermal physics* or *statistical mechanics*.

Unfortunately, this chapter relies heavily on your ability to accept delayed gratification. It has only a few biological examples, but the material developed here is necessary for understanding some topics in most of the later chapters, especially Chapters 4–9 and 14–18. In addition to developing a statistical understanding of pressure, temperature, and concentration, this chapter derives four quantities or concepts that are used later:

1. The *Boltzmann factor*, which tells how concentrations of particles vary with potential energy (Sec. 3.7).

2. The *principle of equipartition of energy*, which underlies the diffusion process that is so important in the body (Sec. 3.10).
3. The *chemical potential*, which describes the condition for equilibrium of two systems for the exchange of particles, and how the particles flow when the systems are not in equilibrium (Secs. 3.12, 3.13, and 3.18).
4. The *Gibbs free energy*, which tells the direction in which a chemical reaction proceeds and allows us to understand how the cells in the body use energy (Sec. 3.17).

The first six sections form the basis for the rest of the chapter, developing the concepts of microstates, heat flow, temperature, and entropy. Sections 3.7 and 3.8 develop the Boltzmann factor and its corollary, the Nernst equation. Section 3.9 applies the Boltzmann factor to the air molecules in the atmosphere. Section 3.10 discusses the very important equipartition of energy theorem. Section 3.11 discusses heat capacity—the energy required to increase the temperature of a system.

The transport of particles between two systems is described most efficiently using the chemical potential. The chemical potential is introduced in Sec. 3.12, and an example of its use is shown in Sec. 3.13.

Section 3.14 considers systems that can exchange volume. An idealized example is two systems separated by a flexible membrane or a movable piston. The next two sections extend the idea of systems that exchange energy, particles, or volume to the exchange of other variables such as electric charge.

The Gibbs free energy, introduced in Sec. 3.17, is used to describe chemical reactions that take place at constant temperature and pressure. It is closely related to the chemical potential. The chemical potential of an ideal solution is derived in Sec. 3.18 and is used extensively in Chapter 5.

### 3.1 Gas Molecules in a Box

*Statistical physics* or *statistical mechanics* deals with average quantities such as pressure, temperature, and particle concentration and with probability distributions of variables such as velocity. Some of the properties of these averages can be illustrated by considering a simple example: the number of particles in each half of a box containing a fixed number of gas molecules. (This is a simple analog for the concentration.) We will not be concerned with the position and velocity of each molecule, since we have already decided not to use Newtonian mechanics. Nor will we ask for the velocity distribution at this time. This simplified example will describe only how many molecules are in the volume of interest. The number will fluctuate

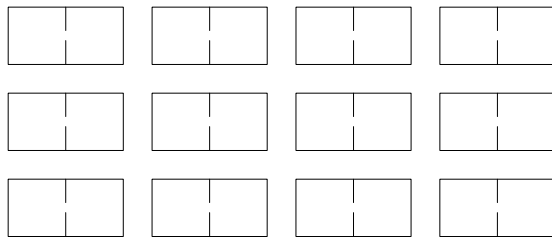


FIGURE 3.1. An ensemble of boxes, each divided in half by an imaginary partition.

with time. We will deal with probabilities:<sup>1</sup> if the number of particles in the volume is measured repeatedly, what values are obtained, and with what relative frequency?

If we were willing to use Newtonian mechanics, we could count periodically how many molecules are in the volume of interest. [This has actually been done for small numbers of particles. See Reif (1964), pp. 8–9.] For larger numbers of particles, it is easier to use statistical arguments to obtain the probabilities. The particles travel back and forth, colliding with the walls of the box and occasionally with one another. After some time has elapsed, all memory of the particles' original positions and velocities has been lost because of collisions with the walls of the box, which have microscopic inhomogeneities. Therefore, the result can be obtained by imagining a whole succession of completely different boxes, in which the particles have been placed at random. We can count the number of molecules in the volume of interest in each box. Such a collection of similar boxes is called an *ensemble*. Ensembles of similar systems will be central to the ideas of this chapter.

Imagine an ensemble of boxes, each divided in half as in Fig. 3.1. We want to know how often a certain number of particles is found in the left half. If one particle is in a box ( $N = 1$ ), two cases can be distinguished, depending on which half the particle is in. Call them L and R. Each case is equally likely to occur, since nothing distinguishes one half of a box from the other. If  $n$  is the number of particles in the left half, then case L corresponds to  $n = 1$  and case R corresponds to  $n = 0$ .

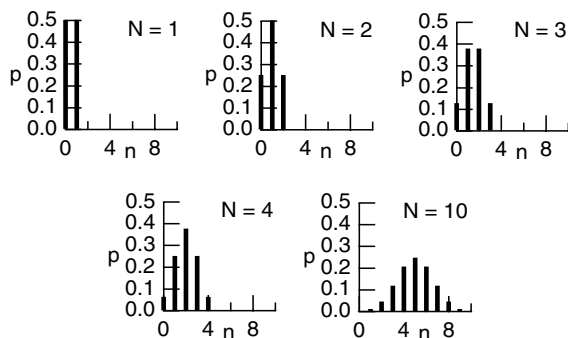
The probability of having a particular value of  $n$  is defined to be

$$P(n) = \frac{(\text{number of systems in the ensemble in which } n \text{ is found})}{(\text{total number of systems})} \quad (3.1)$$

in the limit as the number of systems becomes very large.

Because there are only two possible values of  $n$ , 0 or 1, and because each corresponds to one of the equally likely configurations,  $P(0) = 0.5$ ,  $P(1) = 0.5$ . The sum of the probabilities is 1. A histogram of  $P(n)$  for  $N = 1$  is given in Fig. 3.2(a). To recapitulate:  $n$  is the number of molecules in the left half of the box, and  $N$  is the

<sup>1</sup>A good book on probability is Weaver (1963).

FIGURE 3.2. Histograms of  $P(n; N)$  for different values of  $N$ .

total number of molecules in the entire box. Since  $N$  will change in the discussion below, we will call the probability  $P(n; N)$ . (The fixed parameters that determine the probability distribution are located after the semicolon.)

Now let  $N = 2$ . Each molecule can be on the left or the right with equal probability. The possible outcomes are listed in the following table, along with the corresponding values of  $n$  and  $P(n; 2)$ .

Molecule 1	Molecule 2	$n$	$P(n; 2)$
R	R	0	$\frac{1}{4}$
R	L	1	$\frac{1}{2}$
L	R	1	$\frac{1}{2}$
L	L	2	$\frac{1}{4}$

Each of the four outcomes is equally probable. To see this, note that L or R is equally likely for each molecule. In half of the boxes in the ensemble, the first molecule is found on the left. In half of these, the second molecule is also on the left. Therefore LL occurs in one-fourth of the systems in the ensemble. (This is not strictly true, because there can be fluctuations. If we throw a coin six times, we cannot say that heads will always occur three times. If we repeat the experiment many times, the average number of heads will be three.)

If three molecules are placed in each box, there are two possible locations for the first particle, two for the second, and two for the third. If the three particles are all independent, then there are  $2^3 = 8$  different ways to locate the particles in a box. If a box is divided in half, each of these ways has a probability of  $1/8$ .

Molecule 1	Molecule 2	Molecule 3	$n$	$P(n; 3)$
R	R	R	0	$\frac{1}{8}$
R	R	L	1	$\frac{3}{8}$
R	L	R	1	
L	R	R	1	
L	L	R	2	$\frac{3}{8}$
L	R	L	2	
R	L	L	2	
L	L	L	3	$\frac{1}{8}$

The cases of two and three molecules in the box are also plotted in Fig. 3.2.

In each case,  $P(n; N)$  has been determined by listing all the ways that the  $N$  particles can go into a box. This can become tedious if the number of particles is large. Furthermore, it does not provide a way to calculate  $P$  if the two volumes of the box are not equal. We will now introduce a more general technique that can be used for any number of particles and for any fractional volume of the box.

Each box is divided into two volumes,  $v$  and  $v'$ , with total volume  $V = v + v'$ . Call  $p$  the probability that a single particle is in volume  $v$ . The probability that the particle is in the remainder of the box,  $v'$ , is  $q$ :

$$p + q = 1. \quad (3.2)$$

As long as there is nothing to distinguish one part of a box from the other,  $p$  is the ratio of  $v$  to the total volume:

$$p = \frac{v}{V}. \quad (3.3)$$

By the same argument,  $q = v'/V$ . These values satisfy Eq. 3.2. If  $N$  particles are distributed between the two volumes of the box, the number in  $v$  is  $n$  and the number in  $v'$  is  $n' = N - n$ . The probability that  $n$  of the  $N$  particles are found in volume  $v$  is given by the *binomial probability distribution* (Appendix H):

$$P(n; N) = P(n; N, p) = \frac{N!}{n!(N-n)!} p^n (1-p)^{N-n}. \quad (3.4)$$

Table 3.2 shows the calculation of  $P(n; 10)$  using this equation. Histograms for  $N = 4$  and 10 are also plotted in Fig. 3.2. In each case there is a value of  $n$  for which  $P$  is a maximum. When  $N$  is even, this value is  $N/2$ ; when  $N$  is odd, the values on either side of  $N/2$  share the maximum value. The probability is significantly different from zero only for a few values of  $n$  on either side of the maximum.

A probability distribution, in the form of an expression, a table of values, or a histogram, usually gives all the information that is needed about the number of molecules in  $v$ ; it is not necessary to ask which molecules are in  $v$ . The number of molecules in  $v$  is not fixed but fluctuates about the number for which  $P$  is a maximum. For example, if  $N = 10$ , and we measure the number of molecules in the left half many times, we find  $n = 5$  only about 25% of the time. On the other hand, we find that  $n = 4, 5$ , or 6 about 65% of the time, while  $n = 3, 4, 5, 6$ , or 7 about 90% of the time.

## 3.2 Microstates and Macrostates

If we know “enough” about the detailed properties (such as position and momentum) of every particle in a

TABLE 3.2. Calculation of  $P(n; 10)$  using the binomial probability distribution. Note that  $0! = 1$ .

$P(0; 10) = \frac{10!}{0!10!} \left(\frac{1}{2}\right)^0 \left(\frac{1}{2}\right)^{10} = \left(\frac{1}{2}\right)^{10} = 0.001$
$P(1; 10) = \frac{10!}{1!9!} \left(\frac{1}{2}\right)^1 \left(\frac{1}{2}\right)^9 = 10 \left(\frac{1}{2}\right)^{10} = 0.010$
$P(2; 10) = \frac{10!}{2!8!} \left(\frac{1}{2}\right)^2 \left(\frac{1}{2}\right)^8 = 45 \left(\frac{1}{2}\right)^{10} = 0.044$
$P(3; 10) = \frac{10!}{3!7!} \left(\frac{1}{2}\right)^3 \left(\frac{1}{2}\right)^7 = 120 \left(\frac{1}{2}\right)^{10} = 0.117$
$P(4; 10) = \frac{10!}{4!6!} \left(\frac{1}{2}\right)^4 \left(\frac{1}{2}\right)^6 = 210 \left(\frac{1}{2}\right)^{10} = 0.205$
$P(5; 10) = \frac{10!}{5!5!} \left(\frac{1}{2}\right)^5 \left(\frac{1}{2}\right)^5 = 252 \left(\frac{1}{2}\right)^{10} = 0.246$
$P(6; 10) = \frac{10!}{6!4!} \left(\frac{1}{2}\right)^6 \left(\frac{1}{2}\right)^4 = 210 \left(\frac{1}{2}\right)^{10} = 0.205$
$P(7; 10) = \frac{10!}{7!3!} \left(\frac{1}{2}\right)^7 \left(\frac{1}{2}\right)^3 = 120 \left(\frac{1}{2}\right)^{10} = 0.117$
$P(8; 10) = \frac{10!}{8!2!} \left(\frac{1}{2}\right)^8 \left(\frac{1}{2}\right)^2 = 45 \left(\frac{1}{2}\right)^{10} = 0.044$
$P(9; 10) = \frac{10!}{9!1!} \left(\frac{1}{2}\right)^9 \left(\frac{1}{2}\right)^1 = 10 \left(\frac{1}{2}\right)^{10} = 0.010$
$P(10; 10) = \frac{10!}{10!0!} \left(\frac{1}{2}\right)^{10} \left(\frac{1}{2}\right)^0 = \left(\frac{1}{2}\right)^{10} = 0.001$

system,<sup>2</sup> then we say that the *microstate* of the system is specified. (The criterion for “enough” will be discussed shortly.) We may know less than this but know the *macrostate* of the system. (In an ideal gas, for example, the macrostate would be defined by knowing the number of molecules and volume, and the pressure, temperature, or total energy.) Usually there are many microstates corresponding to each macrostate. The large-scale average properties (such as pressure and number of particles per unit volume in the ideal gas) fluctuate slightly about well-defined mean values.

In the problem of how many molecules are in half of a box, the macrostate is specified if we know how many molecules there are, while a microstate would specify the position and momentum of every molecule. In other cases, internal motions of the molecule may be important, and it will be necessary to know more than just the position and momentum of each particle.

The relation between microstates and macrostates may be clarified by the following example, which contains the essential features, although it is oversimplified and somewhat artificial. A room is empty except for some toys on the floor. Specifying the location of each of the toys on the floor would specify the microstate of the system. If the toys are in the shaded corner in Fig. 3.3, the macrostate is “picked up”. If the toys are any place else in the room, the macrostate is “mess”. There are many more microstates

<sup>2</sup>A *system* is that part of the universe that we choose to examine. The *surroundings* are the rest of the universe. The system may or may not be isolated from the surroundings.

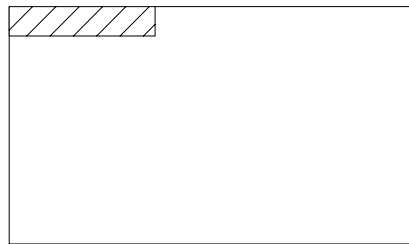


FIGURE 3.3. A room with toys. If all the toys are in the shaded area, the macrostate is “picked up.” Otherwise, the macrostate is “mess.”

corresponding to the macrostate “mess” than there are corresponding to the macrostate “picked up.” We know from experience that children tend to regard any microstate as equally satisfactory; the chances of spontaneously finding the macrostate “picked up” are relatively small.

A situation in which  $P$  is small is called *ordered* or *nonrandom*. A situation in which  $P$  is large is called *disordered* or *random*. Macrostate “mess” is more probable than macrostate “picked up” and is disordered or random.

The same idea can be applied to a box of gas molecules. Initially, the molecules are all kept in the left half of the box by a partition. If the partition is suddenly removed, a large number of additional microstates are suddenly available to the molecules. The macrostate in which they find themselves—all in the left half of the box, even though the partition has been removed—is very improbable or highly ordered. The molecules soon fill the entire box; it is quite unlikely that they will all be in the left half again if the number of molecules is very large. (Suppose that there are 80 molecules in the box. The probability that all are in the left half is  $\left(\frac{1}{2}\right)^{80} = 10^{-24}$ . If samples were taken  $10^6$  times per second, it would take  $10^{18}$  seconds to sample  $10^{24}$  boxes, one of which, on the average, would have all of the molecules in the left half. This is greater than the age of the universe.)

Just after the partition in the box was removed, the situation was very ordered. The system spontaneously approached a much more random situation in which nearly half the molecules were in each half of the box. The actual number  $n$  fluctuates about  $N/2$ , but in such a way that the average  $\langle n \rangle$  (taken, say, over several seconds) no longer changes with time. Typical fluctuations with a constant  $\langle n \rangle$  are shown in Fig. 3.4(a). When the average<sup>3</sup>

<sup>3</sup>There is a subtlety about the meaning of average that we are glossing over here. If we take a whole ensemble of identical systems, which were all prepared the same way, and measure  $n$  in each one, we have the *ensemble average*  $\bar{n}$ . This is calculated in the way described in Appendix G. If we watch one system over some long time interval, as in Fig. 3.4, we can take the *time average*  $\langle n \rangle$ . It is taken by recording values of  $n$  for a large number of discrete times in some interval. Strictly speaking, an equilibrium state is one in which the ensemble average is not changing with time.

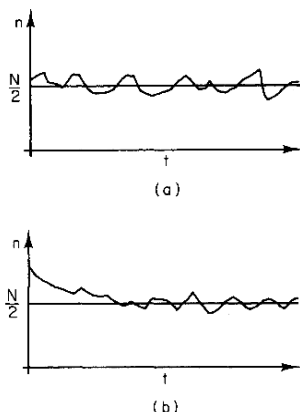


FIGURE 3.4. (a) Fluctuations of  $n$  about  $N/2$ . (b) The approach of the system to the equilibrium state after the partition is removed.

of the macroscopic parameters is not changing with time, we say that the system is in an *equilibrium state*. Figure 3.4(b) shows the system moving toward the equilibrium state after the partition is removed.

An equilibrium state is characterized by macroscopic parameters whose average values remain constant with time, although the parameters may fluctuate about the average value. It is also the most random (i.e., most probable) macrostate possible under the prescribed conditions. It is independent of the past history of the system and is specified by a few macroscopic parameters.<sup>4</sup>

The definition of a microstate of a system has so far been rather vague; we have not said precisely what is required to specify it. It is actually easier to specify the microstate of a system when using quantum mechanics than when using classical mechanics. When the energy of an individual particle in a system (such as one of the molecules in the box) is measured with sufficient accuracy, it is found that only certain discrete values of the energy occur. This is because of the wave nature of the particles. The allowed values of the energy are called *energy levels*. You are probably familiar with the idea of energy levels from a previous physics or chemistry course; for example, the spectral lines of atoms are due to the emission of light when an atom changes from one energy level to another. Because the energy levels are well defined, the energy difference, and hence the frequency or color of the light, is also well defined (see Chapter 14).

A particle in a box has a whole set of energy levels at energies determined by the size and shape of the box. Compared to macroscopic measurements of energy, these levels are very close together. The particle can be in any one of these levels; which energy the particle has is specified by a set of *quantum numbers*. If the particle moves in three dimensions, three quantum numbers are needed

to specify the energy level. If there are  $N$  particles, it will be necessary to specify three quantum numbers for each particle or  $3N$  numbers in all. (If there are  $M$  molecules, each made up of  $a$  atoms, then  $N = aM$ . The number of quantum numbers is less than  $3N$  because the atoms cannot all move independently. If the molecules were thought of as single particles, there would be  $3M$  quantum numbers. But the molecules can rotate and vibrate, so that the number of quantum numbers is greater than  $3M$  and less than  $3N$ .)

The total number of quantum numbers required to specify the state of all the particles in the system is called the number of *degrees of freedom* of the system,  $f$ .

*A microstate of a system is specified if all the quantum numbers for all the particles in the system are specified.*

In most of this chapter, it will not be necessary to consider the energy levels in detail. The important fact is that each particle in a system has discrete energy levels, and a microstate is specified if the energy level occupied by each particle is known.

### 3.3 The Energy of a System: The First Law of Thermodynamics

Figure 3.5 shows some energy levels in a system occupied by a few particles. The total energy of the system  $U$  is the sum of the energy of each particle. In making this drawing, we have assumed that all the particles are the same and that they do not interact with one another very much. Then each particle has the same set of energy levels, and the presence of other particles does not change them. In that case, we can say that there is a certain set of energy levels in the system and that each level can be occupied by any number of particles. The energy of the  $i$ th level, occupied or not, will be called  $u_i$ . For the example of Fig. 3.5, the total energy is

$$U = 2u_{23} + u_{25} + u_{26} + 3u_{28}.$$

Suppose that the system is isolated so that it does not gain or lose energy. It is still possible for particles within

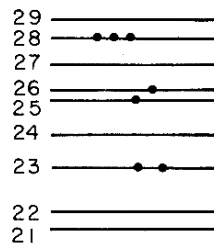


FIGURE 3.5. A few of the energy levels in a system. If a particle has a particular energy, a dot is drawn on the level. More than one particle in this system can have the same quantum numbers.

<sup>4</sup>A more detailed discussion of equilibrium states is found in Reif (1964).

the system to exchange energy and move to different energy levels, as long as the total energy does not change. (Classically, two particles could collide, so that one gained and one lost energy.) Therefore the number of particles occupying each energy level can change, as long as the total energy remains constant. For a system in equilibrium, the average number of particles in each level does not change with time.

There are two ways in which the total energy of a system can change. *Work* can be done on the system by the surroundings, or *heat* can flow from the surroundings to the system. The meaning of work and heat in terms of the energy levels of the system is quite specific and is discussed shortly. First, we define the sign conventions associated with them.

It is customary to define  $Q$  to be the heat flow *into* a system. If no work is done, the energy change in the system is

$$\Delta U = Q.$$

It is also customary to call  $W$  the work done *by* the system *on* the surroundings. When  $W$  is positive, energy flows from the system to the surroundings. If there is no accompanying heat flow, the energy change of the system is

$$\Delta U = -W.$$

The most general way the energy of a system can change is to have both work done by the system and heat flow into the system. The statement of the conservation of energy in that case is called the *first law of thermodynamics*:

$$\Delta U = Q - W. \quad (3.5)$$

The joule is the SI unit for energy, work and heat flow. The calorie (1 cal = 4.184 J) is sometimes used. The dietary calorie is 1000 cal.

The positions of the energy levels in a system are determined by some macroscopic properties of the system. For a gas of particles in a box, for example, the positions of the levels are determined by the size and shape of the box. For charged particles in an electric field, the positions of the levels are determined by the electric field. If the macroscopic parameters that determine the positions of the energy levels are not changed, the only way to change the total energy of a system is to change the average number of particles occupying each energy level, as in Fig. 3.6. This energy change is called *heat flow*.

Work is associated with the change in the macroscopic parameters (such as volume) that determine the posi-

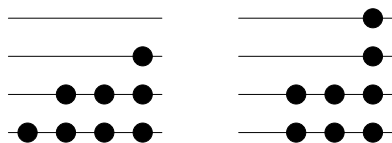


FIGURE 3.6. No work is done on the system, but heat is added. The positions of the levels do not change; their average population does change.

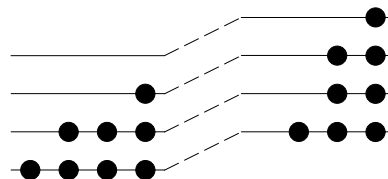


FIGURE 3.7. Work is done on the system, but no heat flows. Each level has been shifted to a higher energy.

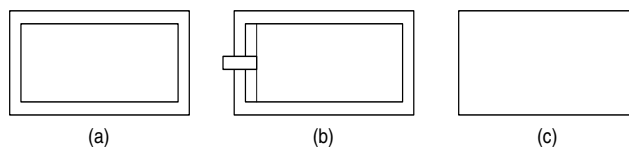


FIGURE 3.8. Symbols used to indicate various types of isolation in a system. (a) This system is completely isolated. (b) There is no heat flow through the double wall, but work can be done (symbolized by a piston). (c) No work can be done, but there can be heat flow through the single wall.

tions of the energy levels. If the energy levels are shifted by doing work without an accompanying heat flow, the change is called *adiabatic*. An adiabatic change is shown in Fig. 3.7. In general, there is also a shift of the populations of the levels in an adiabatic change; the average occupancy of each level can be calculated using the Boltzmann factor, described in Sec. 3.7. There is no heat flow, but work is done on or by the system, and its energy changes.

To summarize: Pure heat flow involves a change in the average number of particles in each level without a change in the positions of the levels. Work involves a change in the macroscopic parameters, which changes the positions of at least some of the energy levels. In general, this means that there is also a shift in the average population of each level. The most general energy change of a system involves both work and heat flow. In that case the total energy change is the sum of the changes due to work and to heat flow.

It is customary in drawing systems to use the symbols in Fig. 3.8 to describe how the system can interact with the surroundings. A double-walled box means that no heat flows, and any processes that occur are adiabatic. This is shown in Fig. 3.8(a). If work can be done on the system, a piston is shown as in Fig. 3.8(b). If heat can flow to or from the system, a single wall is used as in Fig. 3.8(c).

### 3.4 Ensembles and the Basic Postulates

In the next few sections we will develop some quite remarkable results from statistical mechanics. Making the

postulate that when a system is in equilibrium each microstate is equally probable, and arguing that as the energy, volume, or number of particles in the system is increased the number of microstates available to the system increases, we will obtain several well-known results from thermodynamics: heat flows from one system to another in thermal contact until their temperatures are the same; if their volumes can change they adjust themselves until the pressures are the same; and the systems exchange particles until their chemical potentials are the same. We will also obtain the concept of entropy; the Boltzmann factor; the theorem of equipartition of energy; and the Gibbs free energy, which is useful in chemical reactions in living systems where the temperature and pressure are constant.

The initial postulates are deceptively simple. Unfortunately, a fair amount of mathematics is required to get from them to the final results. We start with the basic postulates.

The microstate of a system is determined by specifying the quantum numbers of each particle in the system. The total number of quantum numbers is the number of degrees of freedom. The macrostate of a system is determined by specifying two things:

1. All of the external parameters, such as the volume of a box of gas or any external electric or magnetic field, on which the positions of the energy levels depend. (Classically, all the external parameters that affect the motion of the particles in the system.)
2. The total energy of the system,  $U$ .

The external parameters determine a set of energy levels for the particles in the system; the total energy determines which energy levels are accessible to the system.

Statistical physics deals with average quantities and probabilities. We imagine a whole set or ensemble of “identical” systems, as we did in Eq. 3.1. The systems are identical in that they all are in the same macrostate. Different systems within the ensemble will be in different microstates. Imagine that at some instant of time we “freeze” all the systems in the ensemble and examine which microstate each is in. From this we can determine the probability that a system in the ensemble is in microstate  $i$ :

$$P(\text{of being in microstate } i) = \frac{\text{number of systems in microstate } i}{\text{total number of systems in the ensemble}}.$$

Imagine that we now “unfreeze” all the systems in the ensemble and let the particles move however they want. At some later time we freeze them again and examine the probability that a system is in each microstate. These probabilities may have changed with time. For example, if the system is a group of particles in a box, and if the initial “freeze” was done just after a partition confining all

the particles to the left half of the box had been removed, we would have found many systems in the ensemble in microstates for which most of the particles are on the left-hand side. Later, this would not be true. We would find microstates corresponding to particles in both halves of the box.

We will make two basic *postulates* about the systems in the ensemble.<sup>5</sup>

1. If an isolated system (really, an ensemble of isolated systems) is found with equal probability in each one of its accessible microstates, it is in equilibrium.<sup>6</sup> Conversely, if it is in equilibrium, it is found with equal probability in each one of its accessible microstates.
2. If it is not in equilibrium, it tends to change with time until it is in equilibrium. Therefore the equilibrium state is the most random, most probable state.

For the rest of this chapter, we deal with equilibrium systems. According to our first postulate, each microstate that is accessible to the system (that is, consistent with the total energy that the system has) is equally probable. We will discover that this statement has some far-reaching consequences.

Suppose that we want to consider some variable  $x$ , which takes on various values. This variable might be the pressure of a gas, the number of gas molecules in some volume of the box, or the energy that one of the molecules has. For each value of  $x$ , there will be some number of microstates in which the system could be that are consistent with that value of  $x$ . There will also be some total number of microstates in which the system could be, consistent with its initial preparation. We will use the Greek letter  $\Omega$  to denote the number of microstates. The total number of accessible microstates (for all possible values of  $x$ ) is  $\Omega$ ; the number for which  $x$  has some particular value is  $\Omega_x$ . It is consistent with the first assumption to say that the probability that the variable has a value  $x$  when the system is in equilibrium is

$$P_x = \frac{\Omega_x}{\Omega}. \quad (3.6)$$

We have been considering ensemble averages. For example, the variable of interest might be the pressure, and we could find the ensemble average by calculating

<sup>5</sup>For a more detailed discussion of these assumptions, see Reif (1964), Ch. 3.

<sup>6</sup>In thermodynamics and statistical mechanics, *equilibrium* and *steady state* do not mean the same thing. Steady state means that some variable is not changing with time. The concentration of sodium in a salt solution flowing through a pipe could be in steady state as the solution flowed through, but the system would not be in equilibrium. Only a few microstates corresponding to bulk motion of the fluid are occupied. In other areas, such as feedback systems, the words equilibrium and steady state are used almost interchangeably.



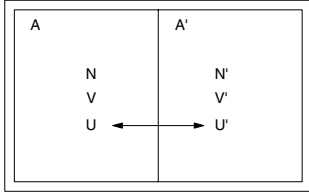


FIGURE 3.9. Two systems are in thermal contact with each other but are isolated from the rest of the universe. They can exchange energy only by heat flow.

$\bar{p} = \sum P_p p$ , where  $P_p$  is the probability of having pressure  $p$ . In equilibrium  $P_p$  is given by Eq. 3.6, and  $\bar{p}$  does not change with time. We could also consider a single system, measure  $p(t)$   $M$  times, and compute the time average,  $\langle p(t) \rangle = \sum_i p(t_i)/M$ . (The equivalence of the time average and the ensemble average for systems in equilibrium is called the *ergodic hypothesis*.)

### 3.5 Thermal Equilibrium

A system that never interacts with its surroundings is an idealization. The adiabatic walls of Fig. 3.8(a) can never be completely realized. However, much can be learned by considering two systems that can exchange heat, work, or particles, but that, taken together, are isolated from the rest of the universe. After we have learned how these two systems interact, the second system can be taken to be the rest of the universe. Eventually, we will allow all three exchanges—heat flow, work, and particles—to take place; for now, it will be convenient to consider only exchanges of energy by heat flow. Figure 3.9 shows the two systems,  $A$  and  $A'$ , isolated from the rest of the universe. The total system will be called  $A^*$ . The total number of particles is  $N^* = N + N'$ . For now  $N$  and  $N'$  are fixed. The total energy is  $U^* = U + U'$ . The two systems can exchange energy by heat flow, so that  $U$  and  $U'$  may change, as long as their sum remains constant.

The number of microstates accessible to the total system is  $\Omega^*$ . The combined system was originally given a total energy  $U^*$  before it was sealed off from the rest of the universe. The barrier between  $A$  and  $A'$  prevents exchange of particles or work. The total number of microstates depends on how much energy is in each system: when system  $A$  has energy  $U$ , the total number of microstates is  $\Omega^*(U)$ .<sup>7</sup>

There are many microstates accessible to the system, with  $U$  and  $U'$  having different values, subject always to  $U^* = U + U'$ . Let the total number of microstates, including all possible values of  $U$ , be  $\Omega_{\text{tot}}^*$ . Then, according to the postulate, the probability of finding system  $A$  with

<sup>7</sup>If  $\Omega$  is a continuous function of  $U$ , then  $\Omega(U)$  is actually the number of states with energy between  $U$  and  $U + dU$ . We ignore this distinction. For a discussion of it, see Chapter 3 of Reif (1964).

TABLE 3.3. An example of two systems that can exchange heat energy. The total energy is  $U^* = 10u$ . Each system contains two particles for which the energy levels are  $u, 2u, 3u$ , etc.

System $A$		System $A'$		System $A^*$
$U$	$\Omega$	$U'$	$\Omega'$	$\Omega^*$
$2u$	1	$8u$	7	7
$3u$	2	$7u$	6	12
$4u$	3	$6u$	5	15
$5u$	4	$5u$	4	16
$6u$	5	$4u$	3	15
$7u$	6	$3u$	2	12
$8u$	7	$2u$	1	7
				$\Omega_{\text{tot}}^* = 84$

energy  $U$  is

$$P(U) = \frac{\Omega^*(U)}{\Omega_{\text{tot}}^*} = C \Omega^*(U). \quad (3.7)$$

$C = 1/\Omega_{\text{tot}}^*$  is a constant (independent of  $U$ ).

If the meaning of Eq. 3.7 is obscure, consider the following example. Systems  $A$  and  $A'$  each consist of two particles, the energy levels for each particle being at  $u, 2u, 3u$ , and so forth. The total energy available to the combined system is  $U^* = 10u$ . The smallest possible energy for system  $A$  is  $U = 2u$ , both particles having energy  $u$ . If  $U = 3u$ , there are two states: in one, the first particle has energy  $u$  and the other  $2u$ ; in the second, the particles are reversed. Label these states  $(u, 2u)$  and  $(2u, u)$ . For  $U = 4u$ , there are three possibilities:  $(u, 3u)$ ,  $(2u, 2u)$ , and  $(3u, u)$ . In general, if  $U = nu$ , there are  $n - 1$  states, corresponding to the first particle having energy  $u, 2u, 3u, \dots, (n - 1)u$ . Table 3.3 shows values for  $U, U', \Omega$ , and  $\Omega'$ .

It is now necessary to consider  $\Omega^*$  in more detail. If there are two microstates available to system  $A$  and 6 available to system  $A^*$ , there are  $2 \times 6 = 12$  states available to the total system.  $\Omega^* = \Omega \Omega'$  is also given in Table 3.3. In a more general case, *the number of microstates for the total system is the product of the number for each subsystem*:

$$\Omega^*(U) = \Omega(U) \Omega'(U'). \quad (3.8)$$

For the specific example, there are a total of 84 microstates accessible to the system when  $U^* = 10u$ . Equation 3.7 says that since each microstate is postulated to be equally probable, the probability that the energy of system  $A$  is  $3u$  is  $12/84 = 0.14$ . The most probable state of the combined system is that for which  $A$  has energy  $5u$  and  $A'$  has energy  $5u$ .

The next question is how  $\Omega$  and  $\Omega'$  depend on energy in the general case. In the example,  $\Omega$  is proportional to  $U$ . For three particles, one can show that  $\Omega$  increases as  $U^2$  (see Problem 15). In general, the more particles there are in a system, the more rapidly  $\Omega$  increases with  $U$ .

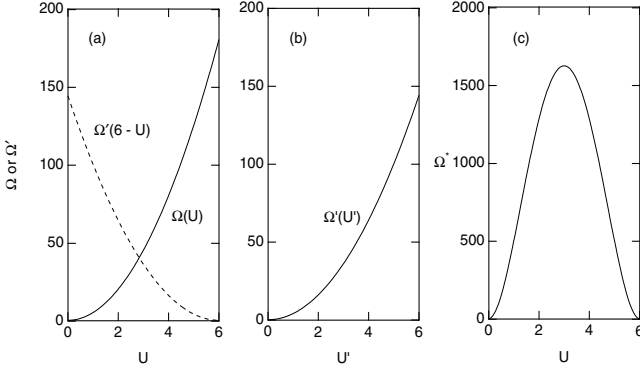


FIGURE 3.10. Example of the behavior of  $\Omega$ ,  $\Omega'$ , and  $\Omega^*$ . In this case, the values used are  $\Omega(U) = 5U^2$  and  $\Omega'(U') = 4(U')^2$ . (These functions give  $\Omega = 0$  when  $U = 0$ , which is not correct. But they are simple and behave properly at higher energies.) The total energy is 6, so only values of  $U$  between 0 and 6 are allowed. (a) Plot of  $\Omega(U)$ . The dashed line is  $\Omega'(6-U)$ . (b) Plot of  $\Omega'(U')$ . (c) Plot of  $\Omega^* = \Omega\Omega'$ .

For a system with a large number of particles, *increasing the energy drastically increases the number of microstates accessible to the system.*

As more energy is given to system  $A$  and  $\Omega(U)$  increases, there is less energy available for system  $A'$  and  $\Omega'(U')$  decreases. The product  $\Omega^* = \Omega\Omega'$  goes through a maximum at some value of  $U$ , and that value of  $U$  is therefore the most probable. These features are shown in Fig. 3.10, which assumes that  $U$  and  $\Omega$  are continuous variables. The continuous approximation becomes excellent when we deal with a large number of particles and very closely spaced energy levels. The solid line in Fig. 3.10(a) represents  $\Omega(U)$ ;  $\Omega'(U')$  is the solid line in Fig. 3.10(b). The function  $\Omega'$  is also plotted vs  $U$ , rather than  $U'$ , as the dashed line in Fig. 3.10(a). As more energy is given to  $A$ ,  $\Omega$  increases but  $\Omega'$  decreases. The product,  $\Omega^* = \Omega\Omega'$ , shown in Fig. 3.10(c), reaches a maximum at  $U = 3$ .

The most probable value of  $U$  is that for which  $P(U)$  is a maximum. Since  $P$  is proportional to  $\Omega^*$ ,  $\Omega^*(U)$  is also a maximum. Therefore,

$$\frac{d}{dU} [\Omega^*(U)] = 0 \quad (3.9)$$

at the most probable value of  $U$ . This derivative can be evaluated using Eq. 3.8. Since  $U + U' = U^*$ , Eq. 3.8 can be rewritten as

$$\Omega^*(U) = \Omega(U) \Omega'(U^* - U). \quad (3.10)$$

The derivative is

$$\frac{d\Omega^*}{dU} = \frac{d\Omega}{dU} \Omega' + \Omega \frac{d\Omega'}{dU}.$$

By the chain rule for taking derivatives,

$$\frac{d\Omega'}{dU} = \left( \frac{d\Omega'}{dU'} \right) \left( \frac{dU'}{dU} \right).$$

Since  $U' = U^* - U$ ,  $dU'/dU = -1$ . Therefore

$$\frac{d\Omega^*}{dU} = \Omega' \frac{d\Omega}{dU} - \Omega \frac{d\Omega'}{dU}. \quad (3.11)$$

Factoring out  $\Omega\Omega'$  gives

$$\frac{d\Omega^*}{dU} = \Omega\Omega' \left( \frac{1}{\Omega} \frac{d\Omega}{dU} - \frac{1}{\Omega'} \frac{d\Omega'}{dU} \right). \quad (3.12)$$

In equilibrium, this must be zero by Eq. 3.9. Since  $\Omega^* = \Omega\Omega'$  cannot be zero, the most probable state or the equilibrium state exists when

$$\frac{1}{\Omega} \frac{d\Omega}{dU} = \frac{1}{\Omega'} \frac{d\Omega'}{dU}. \quad (3.13)$$

It is convenient to define the quantity  $\tau$  by

$$\frac{1}{\tau} \equiv \frac{1}{\Omega} \frac{d\Omega}{dU}$$

for any system. We must remember that this derivative was taken when the number of particles and the parameters that determine the energy levels were held fixed. These parameters are such things as volume and electric and magnetic fields. To remind ourselves that everything *but*  $U$  is being held fixed, it is customary to use the notation for a *partial derivative*:  $\partial$  instead of  $d$  (Appendix N). Therefore, we write

$$\frac{1}{\tau} \equiv \frac{1}{\Omega} \left( \frac{\partial \Omega}{\partial U} \right)_{N, V, \text{etc}}. \quad (3.14)$$

Often we will be careless and just write  $\partial\Omega/\partial U$ .

The quantity  $\tau$  defined by Eq. 3.14 depends only on the variables of one system, system  $A$ . It is therefore a property of that system. Thermal equilibrium occurs when  $\tau = \tau'$ . Since  $\Omega$  is just a number, Eq. 3.14 shows that  $\tau$  has the dimensions of energy.

Systems  $A$  and  $A'$ , which are in thermal contact, will be in equilibrium (the state of greatest probability) when  $\tau = \tau'$ . This is reminiscent of something that is familiar to all of us: if a hot system is placed in contact with a cold one, the hotter one cools off and the cooler one gets warmer. The systems come to equilibrium when they are both at the same temperature. This suggests that  $\tau$  is in some way related to temperature, even though it has the dimensions of energy. We will not prove it, but many things work out right if the absolute temperature  $T$  is defined by the relationship

$$\tau = k_B T. \quad (3.15)$$

The proportionality constant is called *Boltzmann's constant*. If  $T$  is measured in kelvin (K),  $k_B$  has the value

$$\begin{aligned} k_B &= 1.380\,651 \times 10^{-23} \text{ J K}^{-1} \\ &= 0.861\,734 \times 10^{-4} \text{ eV K}^{-1}. \end{aligned} \quad (3.16)$$

[The *electron volt* (eV) is a unit of energy commonly used when considering atoms or molecules.  $1 \text{ eV} = 1.60218 \times$

$10^{-19}$  J.] The most convincing evidence in this book that Eq. 3.15 is reasonable is the derivation of the thermodynamic identity in Sec. 3.16.

The absolute temperature  $T$  is related to the temperature in degrees centigrade or Celsius by

$$T = (\text{temperature in } ^\circ\text{C}) + 273.15. \quad (3.17)$$

### 3.6 Entropy

The preceding section used the idea that the number of microstates accessible to a system increases as the energy of the system increases, to develop a condition for thermal equilibrium. There are two features of those arguments that suggest that there are advantages to working with the natural logarithm of the number of microstates. First, the total number of microstates is the product of the number in each subsystem:  $\Omega^* = \Omega\Omega'$ . Taking natural logarithms of this gives

$$\ln \Omega^* = \ln \Omega + \ln \Omega'. \quad (3.18)$$

The other feature is the appearance of  $(1/\Omega)(\partial\Omega/\partial U)$  in the equilibrium condition. For any non-negative, differentiable function  $y(x)$ ,

$$\frac{d}{dx}(\ln y) = \frac{1}{y} \frac{dy}{dx}.$$

Therefore, Eq. 3.14 can be written as

$$\frac{1}{\tau} = \frac{\partial}{\partial U}(\ln \Omega). \quad (3.19)$$

The *entropy*  $S$  is defined by

$$S = k_B \ln \Omega, \quad \Omega = e^{S/k_B}. \quad (3.20)$$

If both sides of Eq. 3.19 are multiplied by  $k_B$ , it is seen that

$$\left(\frac{\partial S}{\partial U}\right)_{N,V,\text{etc.}} = \frac{k_B}{\tau} = \frac{1}{T}. \quad (3.21)$$

This is a fundamental property of entropy that may be familiar to you from other thermodynamics textbooks; if so, it forms a justification for defining temperature as we did.

Another important property of the entropy is that the entropy of system  $A^*$  is the sum of the entropy of  $A$  and the entropy of  $A'$ :

$$S^* = S + S'. \quad (3.22)$$

This can be proved by multiplying Eq. 3.18 by  $k_B$ .

A third property of the entropy is that  $S^*$  is a maximum when systems  $A$  and  $A'$  are in thermal equilibrium. This result follows from the fact that  $\Omega^*$  is a maximum at equilibrium, since  $S^* = k_B \ln \Omega^*$  and the logarithm is a monotonic function.

Finally, the entropy change in the system can be related to the heat flow into it. Equation 3.21 shows that if there is an energy change in the system *when  $N$  and the parameters that govern the spacing of the energy levels are fixed*, then

$$dS = \left(\frac{\partial S}{\partial U}\right)_{N,V,\text{etc.}} dU = \left(\frac{dU}{T}\right)_{N,V,\text{etc.}}.$$

But the energy change when  $N, V$  and any other parameters are fixed is the heat flow  $dQ$ :

$$dS = \frac{dQ}{T}. \quad (3.23)$$

### 3.7 The Boltzmann Factor

Section 3.5 considered the equilibrium state of two systems that were in thermal contact. It is often useful to consider systems in thermal contact when one of the systems is a single particle. This leads to an expression for the total number of microstates as a function of the energy in the single-particle system, known as the *Boltzmann factor*. The Boltzmann factor is used in many situations, as is its alternate form, the *Nernst equation* (Sec. 3.8).

Let system  $A$  be a single particle in thermal contact with a large system or *reservoir*  $A'$ . Transferring energy from  $A'$  to  $A$  decreases the number of microstates in  $A'$ . The number of microstates in  $A$  may change by some factor  $G$  or remain the same. We will discuss  $G$  at the end of this section.

To make this argument quantitative, consider system  $A$  when it has two different energies,  $U_r$  and  $U_s$ . Reservoir  $A'$  is very large so that its temperature  $T'$  remains constant, and it has many energy levels almost continuously distributed. Let  $\Omega'(U')$  be the number of microstates in  $A'$  when it has energy  $U'$ . The relative probability that  $A$  has energy  $U_s$  compared to having energy  $U_r$  is given by the ratio of the total number of microstates accessible to the combined system:

$$\frac{P(U_s)}{P(U_r)} = \frac{\Omega^*(U = U_s)}{\Omega^*(U = U_r)} = \frac{\Omega(U_s)\Omega'(U^* - U_s)}{\Omega(U_r)\Omega'(U^* - U_r)}. \quad (3.24)$$

This probability is the product of two functions, one depending on system  $A$  and one on reservoir  $A'$ :

$$G = \frac{\Omega(U_s)}{\Omega(U_r)}, \quad R = \frac{\Omega'(U^* - U_s)}{\Omega'(U^* - U_r)}. \quad (3.25)$$

Ratio  $R$  is calculated most easily by using Eq. 3.14, remembering the definition  $\tau = k_B T$ . Since neither the volume nor number of particles is changed, we use an ordinary derivative. We write it in terms of the temperature

of the reservoir:

$$\frac{1}{\Omega'} \left( \frac{d\Omega'}{dU'} \right) = \frac{1}{k_B T'},$$

$$\frac{d\Omega'}{dU'} = \left( \frac{1}{k_B T'} \right) \Omega'. \quad (3.26)$$

Since  $T'$  is constant, this is easily integrated:

$$\Omega'(U') = \text{const} \times e^{U'/k_B T'}.$$

Therefore the ratio is

$$R = \frac{\text{const} \times e^{(U^* - U_s)/k_B T'}}{\text{const} \times e^{(U^* - U_r)/k_B T'}}$$

$$= e^{-(U_s - U_r)/k_B T}. \quad (3.27)$$

Although the temperature  $T'$  is a property of the reservoir, we drop the prime. This ratio is called the *Boltzmann factor*. It gives the factor by which the number of microstates in the reservoir decreases when the reservoir gives up energy  $U_s - U_r$  to the system  $A$ .

The relative probability of finding system  $A$  with energy  $U_r$  or  $U_s$  is then given by

$$\frac{P(U_s)}{P(U_r)} = G e^{-(U_s - U_r)/k_B T} = \left[ \frac{\Omega(U_s)}{\Omega(U_r)} \right] e^{-(U_s - U_r)/k_B T}. \quad (3.28)$$

The exponential Boltzmann factor is a property of the reservoir. The factor  $G$  is called the *density of states factor*. It is a property of the system. If system  $A$  is a single atom with discrete energy levels and we want to know the relative probability that the atom has a particular value of its allowed energy,  $G$  may be unity. In other cases, there may be two or more sets of quantum numbers corresponding to the same energy, a situation called *degeneracy*. In that case  $G$  may be a small number. We would have to know the details to calculate it.

## 3.8 The Nernst Equation

The Nernst equation is widely used in physiology to relate the concentration of ions on either side of a membrane to the electrical potential difference across the membrane. It is an example of the Boltzmann factor.

Suppose that certain ions can pass easily through a membrane. If the membrane has an electrical potential difference across it, the ions will have different energy on each side of the membrane. As a result, when equilibrium exists they will be at different concentrations. The ratio of the probability of finding an ion on either side of the membrane is the ratio of the concentrations on the two sides:

$$\frac{C_2}{C_1} = \frac{P(2)}{P(1)}.$$

The total energy of an ion is its kinetic energy plus its potential energy:  $U = E_k + E_p$ . Chapter 6 will show that

when the electrical potential is  $v$ , the potential energy is  $E_p = zev$ . In this equation  $z$  is the valence of the ion (+1, -1, +2, etc.) and  $e$  is the elementary charge ( $1.6 \times 10^{-19}$  C).

The concentration ratio is given by a Boltzmann factor, Eq. 3.28:

$$\frac{C_2}{C_1} = \left[ \frac{\Omega(2)}{\Omega(1)} \right] e^{-(U_2 - U_1)/k_B T}. \quad (3.29)$$

We must now evaluate the quantity in square brackets. It is the ratio of the number of microstates available to the ion on each side of the membrane. The concentration is the number of ions per unit volume and is proportional to the probability that an ion is in volume  $\Delta x \Delta y \Delta z$ . We will state without proof that for a particle which can undergo translational motion in three dimensions,  $\Omega(U)$  is  $\alpha \Delta x \Delta y \Delta z$ , where  $\alpha$  is a proportionality constant. Therefore

$$\frac{\Omega(2)}{\Omega(1)} = \frac{\alpha \Delta x \Delta y \Delta z}{\alpha \Delta x \Delta y \Delta z} = 1.$$

The energy difference is

$$U_2 - U_1 = E_k(2) - E_k(1) + ze(v_2 - v_1).$$

It will be shown in Sec. 3.10 that the average kinetic energy on both sides of the membrane is the same if the temperature is the same. Therefore,

$$\frac{C_2}{C_1} = e^{-ze(v_2 - v_1)/k_B T}. \quad (3.30)$$

If the potential difference is  $v_2 - v_1$  then the ions will be in equilibrium if the concentration ratio is as given by Eq. 3.30. If the ratio is not as given, then the ions, since they are free to move through the membrane, will do so until equilibrium is attained or the potential changes.

If the ions are positively charged and  $v_2 > v_1$ , then the exponent is negative and  $C_2 < C_1$ . If the ions are negatively charged, then  $C_2 > C_1$ .

The concentration difference is explained qualitatively by the electrical force within the membrane that causes the potential difference. If  $v_2 > v_1$ , the force within the membrane on a positive ion acts from region 2 toward region 1. It slows positive ions moving from 1 to 2 and accelerates those moving from 2 to 1. Thus it tends to increase  $C_1$ .

The Nernst equation is obtained by taking logarithms of both sides of Eq. 3.30:

$$\ln \left( \frac{C_2}{C_1} \right) = -\frac{ze}{k_B T} (v_2 - v_1).$$

From this,

$$v_2 - v_1 = \frac{k_B T}{ze} \ln \left( \frac{C_1}{C_2} \right).$$

Multiplying both numerator and denominator of  $k_B T/ze$  by Avogadro's number  $N_A = 6.022142 \times 10^{23}$  molecule

$\text{mol}^{-1}$  gives the quantities  $N_A k_B$  and  $N_A e$ . The former is the gas constant:

$$N_A k_B = R = 8.31451 \text{ J mol}^{-1} \text{ K}^{-1}. \quad (3.31)$$

The latter is the Faraday constant:

$$N_A e = F = 96485.31 \text{ C mol}^{-1}. \quad (3.32)$$

The coefficient is therefore

$$\frac{k_B T}{ze} = \frac{RT}{zF}. \quad (3.33)$$

At body temperature,  $T = 37^\circ\text{C} = 310 \text{ K}$ , the value of  $RT/F$  is  $0.0267 \text{ J C}^{-1} = 26.7 \text{ mV}$ .

In the form

$$v_2 - v_1 = \frac{RT}{zF} \ln\left(\frac{C_1}{C_2}\right), \quad (3.34)$$

the Boltzmann factor is called the *Nernst equation*.

### 3.9 The Pressure Variation in the Atmosphere

That atmospheric pressure decreases with altitude is well known. This truth has medical significance because of the effects of lower oxygen at high altitudes. We will derive an approximate, constant temperature model for the decrease using the Boltzmann factor, and then we will do it again using hydrostatic equilibrium.

The gravitational potential energy of an air molecule at height  $y$  is  $mgy$ , where  $m$  is the mass of the molecule and  $g$  is the gravitational acceleration. If the atmosphere has a constant temperature, there will be no change of kinetic energy with altitude. For a molecule to increase its potential energy, and therefore its total energy, by  $mgy$ , the energy of all the other molecules (the reservoir) must decrease, with a corresponding decrease in the number of accessible microstates. The number of particles per unit volume is given by a Boltzmann factor:

$$C(y) = C(0)e^{-mgy/k_B T}. \quad (3.35)$$

Since for an ideal gas  $p = Nk_B T/V = Ck_B T$ , the pressure also decreases exponentially with height.

The same result can be obtained without using statistical physics, by considering a small volume of the atmosphere that is in static equilibrium. Let the volume have thickness  $dy$  and horizontal cross-sectional area  $S$ , as shown in Fig. 3.11. The force exerted upward across the bottom face of the element is  $p(y)S$ . The force down on the top face is  $p(y + dy)S$ . The  $N$  molecules in the volume each experience the downward force of gravity. The total gravitational force is  $Nmg$ . In terms of the concentration,  $N = CSdy$ . Therefore, the condition for

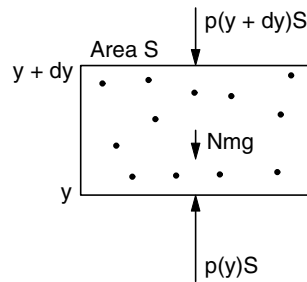


FIGURE 3.11. Forces on a small volume element of the atmosphere.

equilibrium is  $p(y)S - p(y + dy)S - CSmg dy = 0$ . Since  $p(y) - p(y + dy) = -(dp/dy) dy$ , this can be written as

$$\left[ -\left(\frac{dp}{dy}\right) - Cgm \right] S dy = 0.$$

The next step is to use the ideal gas law to write  $p = Ck_B T$ :

$$-k_B T \frac{dC}{dy} - Cgm = 0.$$

If this is written in the form

$$\frac{dC}{dy} = -\frac{mg}{k_B T} C \quad (3.36)$$

it will be recognized as the equation for exponential decay. The solution is Eq. 3.35.

### 3.10 Equipartition of Energy and Brownian Motion

A very important application of the Boltzmann factor is the proof that the average translational kinetic energy per degree of freedom of a particle in thermal contact with a reservoir at temperature  $T$  is  $k_B T/2$ . This result holds for any term in the total energy that depends on the square of one of the variables (such as a component of the position or the momentum).

The proof is done for the kinetic energy resulting from the  $x$  component of momentum. The same procedure can be used for the other components. When the  $x$  component of the momentum of a particle is between  $p_x$  and  $p_x + dp_x$ , the kinetic energy is  $p_x^2/2m$ . The relative probability that the particle has this energy is given by the Boltzmann factor,  $e^{-p_x^2/2mk_B T}$ . We assert that the probability that the particle has momentum in this interval is also proportional to  $dp_x$ .<sup>8</sup> The average kinetic energy associated with  $p_x$  is obtained by multiplying the energy

<sup>8</sup>A more detailed justification of this is found in earlier editions of this book, in texts on statistical mechanics, or on the website associated with this book.

by the Boltzmann factor and integrating over all values of  $p_x$ . We normalize the probability by dividing by the integral of the Boltzmann factor. (See the first equation in Appendix G.)

$$\overline{\left(\frac{p_x^2}{2m}\right)} = \frac{\int_{-\infty}^{\infty} (p_x^2/2m)e^{-p_x^2/2mk_B T} dp_x}{\int_{-\infty}^{\infty} e^{-p_x^2/2mk_B T} dp_x}. \quad (3.37)$$

The integral in the denominator is evaluated in Appendix K and is  $(2\pi mk_B T)^{1/2}$ . The integral in the numerator of Eq. 3.37 is

$$\left(\frac{1}{m}\right) \left(\frac{1}{4}\right) (2mk_B T)(2\pi mk_B T)^{1/2}.$$

Combining these gives

$$\overline{\left(\frac{p_x^2}{2m}\right)} = \frac{k_B T}{2}. \quad (3.38)$$

The average value of the kinetic energy corresponding to motion in the  $x$  direction is  $k_B T/2$ , independent of the mass of the particle. The only condition that went into this derivation was that the energy depended on the square of the variable. Any term in the total energy that is a *quadratic function of some variable* will carry through the same way, so that the average energy will be  $k_B T/2$  for that variable. This result is called the *equipartition of energy*.

The total translational kinetic energy is the sum of three terms  $(p_x^2 + p_y^2 + p_z^2)/2m$ , so the total translational kinetic energy has average value  $\frac{3}{2}k_B T$ .

This result is true for particles of *any* mass: atoms, molecules, pollen grains, and so forth. Heavier particles will have a smaller velocity but the same average kinetic energy. Even heavy particles are continually moving with this average kinetic energy. The random motion of pollen particles in water was first seen by a botanist, Robert Brown, in 1827. This *Brownian motion* is an important topic in the next chapter.

## 3.11 Heat Capacity

Consider a system into which a small amount of heat  $\Delta Q$  flows. In many cases the temperature of the system rises. (An exception is when there is a change of state such as the melting of ice.) The *heat capacity*  $C$  of the system is defined as

$$C = \frac{\Delta Q}{\Delta T}. \quad (3.39)$$

Heat capacity has units of  $\text{J K}^{-1}$ . It depends on the size of the object and the substance it is made of. The specific heat capacity,  $c$ , is the heat capacity per unit mass ( $\text{J K}^{-1} \text{kg}^{-1}$ ) or the heat capacity per mole ( $\text{J K}^{-1} \text{mol}^{-1}$ ).

The heat capacity also depends on any changes in the macroscopic parameters that take place during the heat

flow. Recall the first law of thermodynamics, Eq. 3.5:  $\Delta U = Q - W$ . Only part of the energy transferred to the system by the heat flow increases the internal energy. Some also goes to work done by the system. For example, if the volume changes, there will be pressure-volume work done by the system (Sec. 1.16).

One special case is the heat capacity at constant volume,  $C_V$ . In that case, no  $pdV$  work is done by the system and  $\Delta U = \Delta Q$ , so

$$C_V = \left(\frac{\partial U}{\partial T}\right)_V. \quad (3.40)$$

Many processes in the body occur at constant pressure, and the heat capacity at constant pressure,  $C_p$ , is not equal to  $C_V$ . If both the pressure and volume change during the process, the heat capacity depends on the details of the pressure and volume changes.

The simplest example is the heat capacity at constant volume of a monatomic ideal gas. The average kinetic energy of a gas molecule at temperature  $T$  moving in three dimensions is  $\frac{3}{2}k_B T$ , and the total energy of  $N$  molecules is  $U = \frac{3}{2}Nk_B T$ . Therefore at constant volume  $C_V = \frac{3}{2}Nk_B$ . For one mole of monatomic ideal gas the heat capacity is  $\frac{3}{2}N_A k_B = \frac{3}{2}R$ . Molecules with two or more atoms can also have rotational and vibrational energy, and the heat capacity is larger. The heat capacity can also depend on the temperature.

As a biological example, consider the energy loss from breathing [Denny (1993)]. In each breath we inhale about  $V = 0.51$  of air. Our body warms this air from the surrounding temperature to body temperature. (The body has a much higher heat capacity and does not significantly cool. See Problem 43.) The specific heat of air under these conditions is  $c \approx 1000 \text{ J K}^{-1} \text{kg}^{-1}$ , and the density of air is  $\rho = 1.3 \text{ kg m}^{-3}$ . Therefore the heat flow required to raise the air temperature in each breath is

$$\Delta Q = c\rho V (T_{\text{body}} - T_{\text{surroundings}}). \quad (3.41)$$

For a body temperature of  $37^\circ\text{C}$  and surroundings at  $20^\circ\text{C}$ , the temperature difference is  $17^\circ\text{C} = 17 \text{ K}$ . From Eq. 3.41,  $\Delta Q = 11 \text{ J}$ . We breathe about once every 5 seconds, so the average power lost to the air we breathe is  $2.2 \text{ W}$ . A typical basal metabolic rate is about  $100 \text{ W}$ , so this represents 2% of our energy consumption.

## 3.12 Equilibrium When Particles Can Be Exchanged: The Chemical Potential

Section 3.5 considered two systems that could exchange heat. The most probable or equilibrium state was that in which energy had been exchanged so that the total number of microstates or total entropy was a maximum.

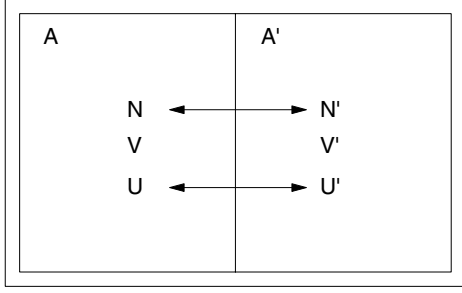


FIGURE 3.12. Two systems can exchange energy by heat flow and particles. The volume of each system remains fixed.

This occurred when (Eq. 3.13)

$$\frac{1}{\Omega} \left( \frac{\partial \Omega}{\partial U} \right)_{N,V} = \frac{1}{\Omega'} \left( \frac{\partial \Omega'}{\partial U'} \right)_{N',V'},$$

which is equivalent to  $T = T'$ . Since  $S = k_B \ln \Omega$  this is also equivalent to

$$\left( \frac{\partial S}{\partial U} \right)_{N,V} = \left( \frac{\partial S'}{\partial U'} \right)_{N',V'}.$$

This section considers the case in which the systems can exchange both energy by heat flow and particles; they are in thermal and diffusive contact (Fig. 3.12). The number of particles in each system is not fixed, but their sum is constant:

$$N + N' = N^*. \quad (3.42)$$

Equilibrium will exist for the most probable state, which means that there is heat flow until the two temperatures are the same and Eq. 3.13 is satisfied. The most probable state also requires a maximum in  $\Omega^*$  or  $S^*$  vs  $N$ . The arguments used in the earlier section for heat exchange can be applied to obtain the equilibrium condition

$$\frac{1}{\Omega} \left( \frac{\partial \Omega}{\partial N} \right)_{U,V} = \frac{1}{\Omega'} \left( \frac{\partial \Omega'}{\partial N'} \right)_{U',V'}. \quad (3.43)$$

The condition in terms of entropy is

$$\left( \frac{\partial S}{\partial N} \right)_{U,V} = \left( \frac{\partial S'}{\partial N'} \right)_{U',V'}. \quad (3.44)$$

For thermal contact, the temperature was defined in terms of the derivative of  $S$  with respect to  $U$ , so that equilibrium occurred when  $T = T'$ . An analogous quantity, the *chemical potential*, is defined by

$$\mu \equiv -T \left( \frac{\partial S}{\partial N} \right)_{U,V}. \quad (3.45)$$

(The reason  $T$  is included in the definition will become clear later.) Both thermal and diffusive equilibrium exist when

$$T = T', \quad \mu = \mu'. \quad (3.46)$$

Two systems are in thermal and diffusive equilibrium when they have the same temperature and the same chemical potential.

The units of the chemical potential are energy (J). Since the units of  $S$  are  $\text{J K}^{-1}$  and the units of  $N$  are dimensionless,<sup>9</sup> Eq. 3.45 shows that the units of  $\mu$  are J.

Consider next what happens to the entropy of the total system if particles are exchanged when the system is not in equilibrium. Let the number of particles in the unprimed system increase by  $\Delta N$  and the number in the primed system increase by  $\Delta N'$ . The change of total entropy is

$$\Delta S^* = \left( \frac{\partial S^*}{\partial N} \right) \Delta N = \left( \frac{\partial S}{\partial N} \right) \Delta N + \left( \frac{\partial S'}{\partial N'} \right) \Delta N'.$$

Using the definition of the chemical potential and the fact that  $\Delta N' = -\Delta N$ , we can rewrite this as

$$\Delta S^* = \left( -\frac{\mu}{T} \right) \Delta N - \left( -\frac{\mu'}{T'} \right) \Delta N.$$

If the two temperatures are the same, this is

$$\Delta S^* = \left( \frac{\mu' - \mu}{T} \right) \Delta N. \quad (3.47)$$

We see again that the entropy change will be zero for a small transfer of particles from one system to the other if  $\mu = \mu'$ . Suppose now that particles flow from  $A'$  to  $A$ , so that  $\Delta N$  is positive. If  $\mu' > \mu$ , that is, the chemical potential of  $A'$  is greater than that of  $A$ , this will cause an increase in entropy of the combined system. *If particles move from a system of higher chemical potential to one of lower chemical potential, the entropy of the total system increases.*

### 3.13 Concentration Dependence of the Chemical Potential

The change in chemical potential of an ideal gas (or a solute in an ideal solution)<sup>10</sup> when the concentration changes from  $C_0$  to  $C$  and there is also a change in its potential energy has the form

$$\Delta \mu = k_B T \ln \left( \frac{C}{C_0} \right) + \Delta(\text{potential energy per particle}). \quad (3.48)$$

We will derive this in Sec. 3.18; for now we show that it is plausible and consistent with the Boltzmann factor.

We know from experience that particles tend to move from a region of higher to lower potential energy, thus

<sup>9</sup>In this book,  $N$  represents the number of particles, and the chemical potential has units of energy per particle. In other books it may have units of energy per mole.

<sup>10</sup>An ideal solution is defined in Sec. 3.18.

increasing their kinetic energy, which can then be transferred as heat to other particles by collision. We also know that particles will spread out to reduce their concentration if they are allowed to. This latter process, called diffusion, is discussed in Chapter 4. Both processes, decreasing the potential energy and decreasing the concentration, cause a decrease in the chemical potential and therefore an increase in the entropy.

It is the combination of these two factors that causes the Boltzmann distribution of particles in the atmosphere. When the atmosphere is in equilibrium, the potential energy term increases with height and the concentration term decreases with height so that the chemical potential is the same at all heights.

To see the equivalence between Eq. 3.48 and the Boltzmann factor, suppose that particles can move freely from region 1 to region 2 and that the potential energy difference between the two regions is  $\Delta E_p$ . The particles will be in equilibrium when  $\mu_1 = \mu_2$ . From Eq. 3.48 this means that

$$k_B T \ln C_1 + E_{p1} = k_B T \ln C_2 + E_{p2}.$$

This equation can be rearranged to give

$$\ln C_2 - \ln C_1 = -\frac{E_{p2} - E_{p1}}{k_B T}.$$

If exponentials are taken of each side, the result is

$$\frac{C_2}{C_1} = e^{-\Delta E_p/k_B T}.$$

If the temperature of each region is the same, the average kinetic energy will be the same in each system, and  $\Delta E_p = \Delta U$ . This is then the same as the Boltzmann factor, Eq. 3.29.

There is still another way to look at the concentration dependence. In an ideal gas, the pressure, volume, temperature, and number of particles are related by the equation of state  $pV = Nk_B T$ . In terms of the particle concentration  $C = N/V$ , this is  $p = Ck_B T$ . The work necessary to concentrate the gas from volume  $V_1$  and concentration  $C_1$  to  $V_2$  and  $C_2$  is (see Eq. 1.56)

$$W_{\text{on gas}} = -\int_{V_1}^{V_2} p(V) dV. \quad (3.49)$$

The concentration work at a constant temperature is

$$W = -Nk_B T \int_{V_1}^{V_2} \frac{dV}{V} = -Nk_B T \ln \frac{V_2}{V_1}.$$

If the final volume is smaller than the initial volume, the logarithm is negative and the concentration work is positive. In terms of the particle concentration  $C = N/V$  or the molar concentration  $c = n/V$ , the concentration work is

$$W_{\text{conc}} = Nk_B T \ln \frac{C_2}{C_1} = nRT \ln \frac{c_2}{c_1}. \quad (3.50)$$

The last form was written by observing that  $Nk_B = nR$  where  $R$  is the gas constant per mole.

Comparing Eq. 3.50 with Eq. 3.48, we see that the concentration work at constant temperature is proportional to the change in chemical potential with concentration. It is, in fact, just the number of molecules  $N$  times the change in  $\mu$ :  $W_{\text{conc}} = N\Delta\mu$ .

The concentration work or change of chemical potential can be related to the Boltzmann factor in still another way. Particles are free to move between two regions of different potential energy at the same temperature. The work required to change the concentration is, by Eq. 3.50,

$$W_{\text{conc}} = N\Delta\mu = Nk_B T \ln \frac{C_2}{C_1}.$$

The concentration ratio is given by a Boltzmann factor:

$$C_2/C_1 = e^{-(E_{p2} - E_{p1})/k_B T},$$

so that  $\ln(C_2/C_1) = -(E_{p2} - E_{p1})/k_B T$ . Therefore, the concentration work is  $W_{\text{conc}} = -N(E_{p2} - E_{p1})$ .

If  $C_2 < C_1$ ,  $W$  is negative and is equal in magnitude to the increase in potential energy of the molecules. The concentration energy lost by the molecules is precisely that required for them to move to the region of higher potential energy. If  $C_2 > C_1$ , the loss of potential energy going from region 1 to region 2 provides the energy necessary to concentrate the gas. Alternatively, one may say that the sum of the concentration energy and the potential energy is the same in the two regions. This was, in fact, the statement about the chemical potential at equilibrium:  $\mu_2 = \mu_1$ .

The same form for the chemical potential is obtained for a dilute solute. (We will present one way of understanding why in Sec. 3.18.) Therefore, the concentration work calculated for an ideal gas is the same as for an ideal solute. The work required to concentrate 1 mol of substance by a factor of 10 at 310 K is  $(1 \text{ mol})(8.31 \text{ J mol}^{-1} \text{ K}^{-1})(310 \text{ K}) \ln(10)$  or  $5.93 \times 10^3 \text{ J}$ . One of the most concentrated substances in the human body is  $\text{H}^+$  ion in gastric juice, which has a pH of 1. Since it was concentrated from plasma with a pH of about 7, the concentration ratio is  $10^6$ . The work necessary to concentrate 1 mol is therefore  $RT \ln(10^6) = (8.31)(310)(13.82) = 3.56 \times 10^4 \text{ J}$ .

## 3.14 Systems That Can Exchange Volume

We have considered two systems that can exchange energy or particles. Now consider the systems shown in Fig. 3.13. They are isolated from the rest of the universe. The vertical line that separates them is a piston that can move and conduct heat, so that energy and volume can be exchanged between the two systems. The piston prevents particles from being exchanged. The constraints are



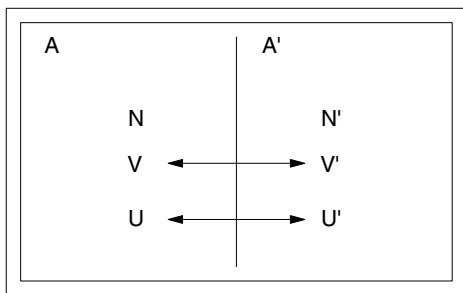


FIGURE 3.13. Two systems that can exchange volume are separated by a movable piston. Heat can also flow through the piston.

$V^* = V + V'$  and  $U^* = U + U'$  from which  $dV = -dV'$ ,  $dU = -dU'$ . As before, equilibrium exists when the total number of microstates or the total entropy is a maximum. The conditions for maximum entropy are

$$\left(\frac{\partial S^*}{\partial U}\right)_{N,V} = 0, \quad \left(\frac{\partial S^*}{\partial V}\right)_{N,U} = 0.$$

The derivation proceeds as before. For example,

$$\begin{aligned} \left(\frac{\partial S^*}{\partial V}\right)_{N,U} &= \left(\frac{\partial S}{\partial V}\right)_{N,U} + \left(\frac{\partial S'}{\partial V}\right)_{N,U} \\ &= \left(\frac{\partial S}{\partial V}\right)_{N,U} - \left(\frac{\partial S'}{\partial V'}\right)_{N',U'}. \end{aligned}$$

Equilibrium requires that  $T = T'$  so that there is no heat flow. The piston will stop moving and there will be no change of volume when

$$\left(\frac{\partial S}{\partial V}\right)_{N,U} = \left(\frac{\partial S'}{\partial V'}\right)_{N',U'}. \quad (3.51)$$

These derivatives can be evaluated in several ways. The method used here involves some manipulation of derivatives; a more detailed description, consistent with the microscopic picture of energy levels, is found in Reif (1964, pp. 267–273).

For a small exchange of heat and work, the first law can be written as  $dU = dQ - dW$ . In the present case the only form of work is that related to the change of volume, so  $dU = dQ - pdV$ . It was shown in Eq. 3.23 that  $dQ = TdS$ . Therefore  $dU = TdS - pdV$ . This equation can be solved for  $dS$ :

$$dS = \left(\frac{1}{T}\right) dU + \left(\frac{p}{T}\right) dV. \quad (3.52)$$

The entropy depends on  $U, V$  and  $N$ :  $S = S(U, V, N)$ . If  $N$  is not allowed to change, then

$$dS = \left(\frac{\partial S}{\partial U}\right)_{N,V} dU + \left(\frac{\partial S}{\partial V}\right)_{N,U} dV. \quad (3.53)$$

Comparison of this with Eq. 3.52 shows that

$$\left(\frac{\partial S}{\partial U}\right)_{N,V} = \frac{1}{T},$$

$$\left(\frac{\partial S}{\partial V}\right)_{N,U} = \frac{p}{T}. \quad (3.54)$$

The first of these equations was already seen as Eq. 3.21. The second gives the condition for equilibrium under volume change. Referring to Eq. 3.51 we see that at equilibrium

$$\frac{p}{T} = \frac{p'}{T'}.$$

Therefore, equilibrium requires both  $T = T'$  and

$$p = p'. \quad (3.55)$$

This agrees with common experience. The piston does not move when the pressure on each side is the same.

### 3.15 Extensive Variables and Generalized Forces

The number of microstates and the entropy of a system depend on the number of particles, the total energy, and the positions of the energy levels of the system. The positions of the energy levels depend on the volume and may also depend on other macroscopic parameters. For example, they may depend on the length of a stretched muscle fiber or a protein molecule. For charged particles in an electric field, they depend on the charge. For a thin film such as the fluid lining the alveoli of the lungs, the entropy depends on the surface area of the film. The number of particles, energy, volume, electric charge, surface area, and length are all *extensive variables*: if a homogeneous system is divided into two parts, the value of the variable for the total system (volume, charge, etc.) is the sum of the values for each part. A general extensive variable will be called  $x$ .

An adiabatic energy change is one in which no heat flows to or from the system. The energy change is due to work done on or by the system as a macroscopic parameter changes, shifting at least some of the energy levels. For each extensive variable  $x$  we can define a *generalized force*  $X$  such that the energy change in an adiabatic process is

$$dU = -dW = Xdx. \quad (3.56)$$

(Remember that  $dU$  is the increase in energy of the system and  $dW$  is the work done by the system on the surroundings.) Examples of extensive variables and their associated forces are given in Table 3.4.

### 3.16 The General Thermodynamic Relationship

Suppose that a system has  $N$  particles, total energy  $U$ , volume  $V$ , and another macroscopic parameter  $x$  on which the positions of the energy levels may depend. The

TABLE 3.4. Examples of extensive variables and the generalized force associated with them.

$x$	$X$	$dU = -dW$
Volume $V$	–pressure $-p$	$-p dV$
Length $L$	Force $F$	$F dL$
Area $a$	Surface tension $\sigma$	$\sigma da$
Charge $q$	Potential $v$	$v dq$

number of microstates, and therefore the entropy, will depend on these four variables:  $S = S(U, N, V, x)$ . If each variable is changed by a small amount, there is a change of entropy

$$dS = \left(\frac{\partial S}{\partial U}\right)_{N,V,x} dU + \left(\frac{\partial S}{\partial N}\right)_{U,V,x} dN + \left(\frac{\partial S}{\partial V}\right)_{U,N,x} dV + \left(\frac{\partial S}{\partial x}\right)_{U,N,V} dx. \quad (3.57)$$

Now consider the change of energy of the system. If only heat flow takes place, there is an increase of energy  $dQ = TdS$ . If an adiabatic process with a constant number of particles takes place, the energy change is  $-dW = Xdx - pdV$ . If particles flow into the system without an accompanying flow of heat or work, the energy change is  $dU_N$ . It seems reasonable that this energy change, due solely to the movement of the particles, is proportional to  $dN$ :  $dU_N = a dN$ . (It will turn out that the proportionality constant is the chemical potential.) For the total change of energy resulting from all these processes, we can write a statement of the conservation of energy:  $dU = TdS + Xdx - pdV + adN$ . This is an extension of Eq. 3.5 to the additional variables on which the energy can depend. It can be rearranged as

$$dS = \left(\frac{1}{T}\right) dU - \left(\frac{a}{T}\right) dN + \left(\frac{p}{T}\right) dV - \left(\frac{X}{T}\right) dx. \quad (3.58)$$

Comparison of Eqs. 3.57 and 3.58 shows that

$$\left(\frac{\partial S}{\partial U}\right)_{N,V,x} = \frac{1}{T}, \quad (3.59a)$$

$$\left(\frac{\partial S}{\partial N}\right)_{U,V,x} = -\frac{a}{T}, \quad (3.59b)$$

$$\left(\frac{\partial S}{\partial V}\right)_{U,N,x} = \frac{p}{T}, \quad (3.59c)$$

$$\left(\frac{\partial S}{\partial x}\right)_{U,N,V} = -\frac{X}{T}. \quad (3.59d)$$

Comparison of Eq. 3.59b with Eq. 3.45 shows that  $a = \mu$ . This is why the factor of  $T$  was introduced in Eq. 3.45.

Equation 3.58, with the correct value inserted for  $a$ , is

$$TdS = dU - \mu dN + p dV - X dx. \quad (3.60)$$

This is known as the *thermodynamic identity* or the *fundamental equation of thermodynamics*. It is a combination of the conservation of energy with the relationship

between entropy change and heat flow in a reversible process. (A reversible process is one that takes place so slowly that all parts of the system have the same temperature, pressure, etc.) This equation and derivative relations such as Eqs. 3.59 form the basis for the usual approach to thermodynamics.

Finally, let us consider the addition of a particle to a system when the volume is fixed. If we do this without changing the energy, it increases the number of ways the existing energy can be shared and hence the number of microstates. Therefore the entropy increases. If we want to restore the entropy to its original value, we must remove some energy. Exactly the same argument can be made mathematically. We have seen in Eqs. 3.45 and 3.59b that

$$\mu = -T \left(\frac{\partial S}{\partial N}\right)_{U,V}.$$

Since adding the particle at constant energy increases the entropy,  $(\partial S/\partial N)_{U,V}$  is positive and the chemical potential is negative. Next, we rearrange Eq. 3.60 as  $dU = TdS + \mu dN - pdV$  and by inspection see that

$$\mu = \left(\frac{\partial U}{\partial N}\right)_{S,V}.$$

Therefore adding a particle at constant volume while keeping the entropy constant requires that energy be removed from the system.

## 3.17 The Gibbs Free Energy

### 3.17.1 Gibbs Free Energy

A conventional course in thermodynamics develops several functions of the entropy, energy, and macroscopic parameters that are useful in certain special cases. One of these is the *Gibbs free energy*, which is particularly useful in describing changes that occur in a system while the temperature and pressure remain constant. Most changes in a biological system occur under such conditions.

Imagine a system  $A$  in contact with a much larger reservoir as in Fig. 3.14. The reservoir has temperature  $T'$  and

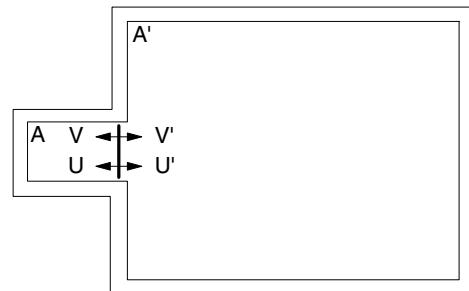


FIGURE 3.14. System  $A$  is in contact with reservoir  $A'$ . Heat can flow through the piston, which is also free to move. The reservoir is large enough to ensure that anything that happens to system  $A$  takes place at constant temperature and pressure.

pressure  $p'$ . A movable piston separates  $A$  and  $A'$ . (At equilibrium,  $T = T'$  and  $p = p'$ .) The reservoir is large enough so that a change of energy or volume of system  $A$  does not change  $T'$  or  $p'$ .

Consider the change of entropy of the total system that accompanies an exchange of energy or volume between  $A$  and  $A'$ . Above, this entropy change was set equal to zero to obtain the condition for equilibrium. In this case, however, we will express the total entropy change of system plus reservoir in terms of the changes in system  $A$  alone. The total entropy is  $S^* = S + S'$ , so the total entropy change is  $dS^* = dS + dS'$ .

If reservoir  $A'$  exchanges energy with system  $A$ , the energy change is

$$dU' = T' dS' - dW' = T' dS' - p' dV'.$$

This can be solved for  $dS'$ , and the result can be put in the expression for the total entropy change:

$$dS^* = dS + \frac{dU'}{T'} + \frac{p' dV'}{T'}.$$

We are trying to get  $dS^*$  in terms of changes in system  $A$  alone. Since  $A$  and  $A'$  together constitute an isolated system,  $dU = -dU'$  and  $dV = -dV'$ . Therefore,

$$dS^* = -\frac{-T' dS + dU + p' dV}{T'}. \quad (3.61)$$

(Note that a minus sign was introduced in front of this equation.) This expresses the total entropy change in terms of changes of  $S$ ,  $U$ , and  $V$  in system  $A$  and the pressure and temperature of the reservoir.

The Gibbs free energy is *defined* to be

$$G \equiv U - T'S + p'V. \quad (3.62)$$

If the reservoir is large enough so that interaction of the system and reservoir does not change  $T'$  and  $p'$ , then the change of  $G$  as system  $A$  changes is

$$dG = dU - T'dS + p'dV. \quad (3.63)$$

Comparison of Eqs. 3.61 and 3.63 shows that

$$dS^* = -\frac{dG}{T'}. \quad (3.64)$$

*The change in entropy of system plus reservoir is related to the change of  $G$ , which is a property of the system alone, as long as the pressure and temperature are maintained constant by the reservoir.*

To see why  $G$  is called a free energy, consider the conservation of energy in the following form:

(work done by the system) = (energy lost by the system)  
+ (heat added to the system),

$$dW = -dU + T dS.$$

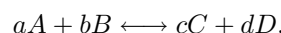
Subtracting  $p dV$  from both sides of this equation gives

$$dW - p dV = -dU + T dS - p dV = -dG.$$

The right-hand side is the decrease of Gibbs free energy of the system. The work done in any isothermal, isobaric (constant pressure) reversible process, *exclusive of  $p dV$  work*, is equal to the decrease of Gibbs free energy of the system. This non- $p dV$  work is sometimes called *useful work*. It may represent contraction of a muscle fiber, the transfer of particles from one region to another, the movement of charged particles in an electric field, or a change of concentration of particles. It differs from the change in energy of the system,  $dU$ , for two reasons. The volume of the system can change, resulting in  $p dV$  work, and there can be heat flow during the process. For example, let the system be a battery at constant temperature and pressure which decreases its internal (chemical) energy and supplies electrical energy. From a chemical energy change  $dU$  we subtract  $T dS$ , the heat flow to the surroundings, and  $-p dV$ , the work done on the atmosphere as the liquid in the battery changes volume. What is left is the energy available for electrical work.

### 3.17.2 An Example: Chemical Reactions

As an example of how the Gibbs free energy is used, consider a chemical reaction that takes place in the body at constant temperature and pressure. System  $A$ , the region in the body where the reaction takes place, is in contact with a reservoir  $A'$  that is large enough to maintain constant temperature and pressure. Suppose that there are four species of particles that interact. Capital letters represent the species and small letters represent the number of atoms or molecules of each that enter in the reaction:



An example is  $1 \text{ glucose} + 6\text{O}_2 \longleftrightarrow 6\text{CO}_2 + 6\text{H}_2\text{O}$ , where  $a = 1$ ,  $b = 6$ ,  $c = 6$ ,  $d = 6$ . The state of the system depends on  $U$ ,  $V$ ,  $N_A$ ,  $N_B$ ,  $N_C$ , and  $N_D$ .

We begin with the definition of  $G$ , Eq. 3.62, and we call the pressure and temperature of the system and reservoir  $p$  and  $T$ :

$$G = U - TS + pV.$$

Differentiating, we obtain

$$dG = dU - T dS - S dT + p dV + V dp.$$

Generalize Eq. 3.60 for the case of four chemical species:

$$T dS = dU - \mu_A dN_A - \mu_B dN_B - \mu_C dN_C - \mu_D dN_D + p dV.$$

Insert this in the equation for  $dG$  and remember that since the process takes place at constant temperature and pressure,  $dT$  and  $dp$  are both zero. The result is

$$dG = \mu_A dN_A + \mu_B dN_B + \mu_C dN_C + \mu_D dN_D.$$

In Sec. 3.13 we saw that the concentration dependence of the chemical potential is given by a logarithmic term. Equation 3.48 can be used to write

$$\mu_A = \mu_{A0} + k_B T \ln(C_A/C_0),$$

where  $\mu_{A0}$  is the chemical potential at a standard concentration (usually 1 mol) and depends on temperature, pH, etc. Note that  $C_0$  is the same reference concentration for all species. As the reaction takes place to the right, we can write the number of molecules gained or lost as  $dN_A = -adN$ ,  $dN_B = -bdN$ ,  $dN_C = cdN$ ,  $dN_D = ddN$ , so that we have

$$\begin{aligned} dG &= [\mu_{A0} + k_B T \ln(C_A/C_0)](-a dN) \\ &+ [\mu_{B0} + k_B T \ln(C_B/C_0)](-b dN) \\ &+ [\mu_{C0} + k_B T \ln(C_C/C_0)](c dN) \\ &+ [\mu_{D0} + k_B T \ln(C_D/C_0)](d dN). \end{aligned}$$

This can be rearranged as (letting  $C_A = [A]$ , etc.)

$$\begin{aligned} dG &= [c\mu_{C0} + d\mu_{D0} - a\mu_{A0} - b\mu_{B0} \\ &+ k_B T \ln \left( \frac{[C]^c [D]^d}{[A]^a [B]^b} \right) - k_B T \ln \left( \frac{[C_0]^c [C_0]^d}{[C_0]^a [C_0]^b} \right)] dN. \end{aligned}$$

The two logarithm terms together represent logs of concentration ratios. Therefore concentrations  $[A]$ ,  $[B]$ ,  $[C]$ ,  $[D]$ , and  $C_0$  must all be measured in the same units. The last term can be made to vanish if the units are such that  $C_0$  is unity (for example, 1 mol per liter). Then

$$\begin{aligned} dG &= [c\mu_{C0} + d\mu_{D0} - a\mu_{A0} - b\mu_{B0} \\ &+ k_B T \ln \left( \frac{[C]^c [D]^d}{[A]^a [B]^b} \right)] dN. \end{aligned}$$

Multiplying the expression in square brackets by Avogadro's number converts the chemical potential per molecule to the standard Gibbs free energy per mole, and  $k_B T$  to  $RT$ . To compensate, the change in number of molecules  $dN$  is changed to moles  $dn$  or  $\Delta n$ :

$$\begin{aligned} \Delta G &= [(cG_{C0} + dG_{D0} - aG_{A0} - bG_{B0}) \\ &+ RT \ln \left( \frac{[C]^c [D]^d}{[A]^a [B]^b} \right)] \Delta n. \end{aligned} \quad (3.65)$$

The term in small parentheses is the standard free energy change for this reaction,  $\Delta G^0$ , which can be found in tables. At equilibrium  $\Delta G = 0$ , so

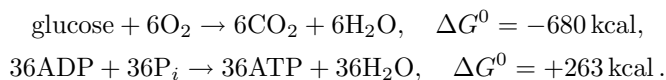
$$0 = \Delta G^0 + RT \ln \left( \frac{[C]^c [D]^d}{[A]^a [B]^b} \right) = \Delta G^0 + RT \ln K_{\text{eq}}.$$

The equilibrium constant  $K_{\text{eq}}$  is related to the standard (1 molar) free-energy change by

$$\Delta G^0 = -RT \ln K_{\text{eq}},$$

$$K_{\text{eq}} = \frac{[C]^c [D]^d}{[A]^a [B]^b}.$$

Many biochemical processes in the body receive free energy from the change of adenosine triphosphate (ATP) to adenosine diphosphate (ADP) plus inorganic phosphate ( $P_i$ ). This reaction involves a decrease of free energy. The energy is provided initially by forcing the reaction to go in the other direction to make an excess of ATP. One way this is done is through a very complicated series of chemical reactions known as the *respiration of glucose*. The net effect of these reactions is<sup>11</sup>



The decrease in free energy of the glucose more than compensates for the increase in free energy of the ATP. The creation of glucose or other sugars is the reverse of the respiration process and is called *photosynthesis*. The free energy required to run the reaction the other direction is supplied by light energy.

### 3.18 The Chemical Potential of a Solution

We now consider a binary solution of *solute* and *solvent* and how the chemical potential changes as these two substances are intermixed.<sup>12</sup> This is a very fundamental process that will lead us to the logarithmic dependence of the chemical potential on solute concentration that we saw in Sec. 3.13, as well as to an expression for the chemical potential of the solvent that we will need in Chapter 5.

To avoid having the subscript  $s$  stand for both solute and solvent, we call the solvent water. The distinction between solute and water is artificial; the distinction is usually that the concentration of solute is quite small. We need the entropy change in a solution when  $N_s$  solute molecules, which initially were segregated, are mixed with  $N_w$  water molecules. We make the calculation for an ideal solution—one in which the total volume of water molecules does not change on mixing and in which there is no heat evolved or absorbed on mixing. This is equivalent to saying that the solute and water molecules are the same size and shape, and that the force between a water molecule and its neighbors is the same as the force between a solute molecule and its neighbors.<sup>13</sup> The resulting entropy change is called the *entropy of mixing*.

To calculate the entropy of mixing, imagine a system with  $N$  sites, all occupied by particles. The number of microstates is the number of different ways that particles can be placed in the sites. The first particle can go in any

<sup>11</sup>There are multiple pathways in glucose respiration. The 36 is approximate.

<sup>12</sup>See also Hildebrand and Scott (1964), p. 17, and Chapter 6.

<sup>13</sup>Extensive work has been done on solutions for which these assumptions are not true. See Hildebrand and Scott (1964); Hildebrand *et al.* (1970).

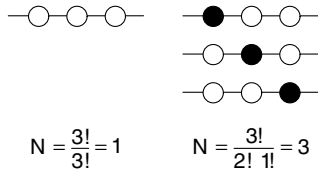


FIGURE 3.15. The system on the left contains three water molecules. Because they are indistinguishable there is only one way they can be arranged. The system on the right contains two water molecules and one solute molecule. Three different arrangements are possible. In each case the number of arrangements is given by  $(N_w + N_s)! / (N_w! N_s!)$ .

site. The second can go in any of  $N - 1$  sites, and so forth. The total number of different ways to arrange the particles is  $N!$  But if the particles are identical, these states cannot be distinguished, and there is actually only one microstate. The number of microstates is  $N! / N!$ , where the  $N!$  in the numerator gives the number of arrangements and the  $N!$  in the denominator divides by the number of indistinguishable states.<sup>14</sup>

Suppose now that we have two different kinds of particles. The total number is  $N = N_w + N_s$ , and the total number of ways to arrange them is  $(N_w + N_s)!$  The  $N_w$  water molecules are indistinguishable, so this number must be divided by  $N_w!$  Similarly it must be divided by  $N_s!$  Therefore, purely because of the ways of arranging the particles, the number of microstates  $\Omega$  in the mixture is  $(N_w + N_s)! / (N_w! N_s!)$ . An example of counting microstates is shown in Fig. 3.15.

There could also be dependence on volume and energy; in fact, the dependence on volume and energy may also contain factors of  $N_w$  and  $N_s$ . However, our assumption that the molecules of water and solute have the same size, shape, and forces of interaction ensures that these dependencies will not change as solute molecules are mixed with water molecules. The only entropy change will be the entropy of mixing.

The entropy change of the mixture relative to the entropy of  $N_w$  molecules of pure water and  $N_s$  molecules of pure solute is

$$S_{\text{solution}} - S_{\text{pure water, pure solute}} = k_B \ln \left( \frac{\Omega_{\text{solution}}}{\Omega_{\text{pure water, pure solute}}} \right). \quad (3.66)$$

Since with our assumptions  $\Omega$  is unity for the pure solute and the pure water, the entropy difference is

$$\begin{aligned} S_{\text{solution}} - S_{\text{pure water, pure solute}} &= k_B \ln \left( \frac{(N_w + N_s)!}{N_w! N_s!} \right) \\ &= k_B \{ \ln [(N_w + N_s)!] - \ln(N_w!) - \ln(N_s!) \}. \end{aligned} \quad (3.67)$$

<sup>14</sup>The fact that there is only one microstate because of the indistinguishability of the particles is called the Gibbs paradox. For an illuminating discussion of the Gibbs paradox, see Casper and Freier (1973).

This is symmetric in water and solute, and it is valid for any number of molecules.

Since we usually deal with large numbers of molecules and factorials are difficult to work with, let us use Stirling's approximation (Appendix I) to write

$$\begin{aligned} S_{\text{solution}} - S_{\text{pure water, pure solute}} &= k_B [(N_w + N_s) \ln(N_w + N_s) - N_w \ln N_w - N_s \ln N_s]. \end{aligned} \quad (3.68)$$

The next step is to relate the entropy of mixing to the chemical potential. This is done by recalling the definition of the Gibbs free energy, (Eq. 3.62):  $G = U + pV - TS$ . The sum of the first two terms,  $H = U + pV$ , is called the *enthalpy*. Any change of the enthalpy is the heat of mixing; in our case it is zero. (The present case is actually more restrictive:  $p$ ,  $V$ , and  $U$  are all constant.) Therefore, since  $T$  is also constant, the change in Gibbs free energy is due only to the entropy change:

$$\begin{aligned} \Delta G &= -T \Delta S = k_B T \left[ N_w \ln \left( \frac{N_w}{N_w + N_s} \right) \right. \\ &\quad \left. + N_s \ln \left( \frac{N_s}{N_w + N_s} \right) \right]. \end{aligned} \quad (3.69)$$

This is still symmetric with water and solute, but it diverges if either  $N_w$  or  $N_s$  is zero, because of our use of Stirling's approximation.

We now need an expression that relates the change in  $G$  to the chemical potential. This can be derived for the general case using the following thermodynamic arguments. We use Eq. 3.62 to write the most general change in  $G$ :

$$dG = dU + p dV + V dp - T dS - S dT.$$

The fundamental equation of thermodynamics, Eq. 3.60, generalized to two molecular species, is

$$T dS = dU - \mu_w dN_w - \mu_s dN_s + p dV,$$

so

$$dG = \mu_w dN_w + \mu_s dN_s + V dp - S dT. \quad (3.70)$$

This can be used to write down some partial derivatives by inspection that are valid in general:

$$\mu_w = \left( \frac{\partial G}{\partial N_w} \right)_{N_s, p, T}, \quad (3.71a)$$

$$\mu_s = \left( \frac{\partial G}{\partial N_s} \right)_{N_w, p, T}, \quad (3.71b)$$

$$V = \left( \frac{\partial G}{\partial p} \right)_{N_s, N_w, T}, \quad (3.71c)$$

$$S = - \left( \frac{\partial G}{\partial T} \right)_{N_s, N_w, p}. \quad (3.71d)$$

To find the chemical potential, we differentiate our expression for  $G$ , Eq. 3.69, with respect to  $N_w$  and  $N_s$  to obtain

$$\mu_w = k_B T \ln x_w, \quad \mu_s = k_B T \ln x_s. \quad (3.72)$$

These have been written in terms of the *mole fractions* or *molecular fractions*

$$x_w = \frac{N_w}{N_w + N_s}, \quad x_s = \frac{N_s}{N_w + N_s}. \quad (3.73)$$

Each chemical potential is zero when the mole fraction for that species is one (i.e., the pure substance). The expressions for  $\mu$  diverge for  $x_w$  or  $x_s$  close to zero because of the failure of Stirling's approximation for small values of  $x$ .

The last step is to write the chemical potential in terms of the more familiar concentrations instead of mole fractions. We can write the change in chemical potential of the *solute* as the concentration changes from a value  $C_1$  to  $C_2$  as

$$\Delta\mu_s = \mu_s(2) - \mu_s(1) = k_B T \ln(x_2/x_1).$$

As long as the solute is dilute,  $N_w + N_s \approx N_w$ , so  $x_2/x_1 = C_2/C_1$  and

$$\Delta\mu_s = k_B T \ln(C_2/C_1),$$

which agrees with Eq. 3.48.

The change in chemical potential of the *water* can be written in terms of the *solute* concentration. Since  $x_w + x_s = 1$ ,  $\mu_w = k_B T \ln(1 - x_s)$ . For small values of  $x_s$  the logarithm can be expanded in a Taylor's series (Appendix D):

$$\ln(1 - x_s) = -x_s - \frac{1}{2}x_s^2 - \dots$$

The final result is

$$\begin{aligned} \mu_w &= -k_B T x_s = -k_B T N_s/(N_s + N_w) \\ &\approx -k_B T (N_s/V)/(N_w/V), \end{aligned}$$

or

$$\mu_w \approx -k_B T \frac{C_s}{C_w}. \quad (3.74a)$$

To reiterate, this is the chemical potential of the water for small solute concentrations. The zero of chemical potential is pure water. The term is negative because the addition of solute decreases the chemical potential of the water, due to the entropy of mixing term. For a change of solute concentration, the chemical potential of the water changes by

$$\Delta\mu_w = -\frac{k_B T \Delta C_s}{C_w}. \quad (3.74b)$$

We now know the concentration dependence of the chemical potential. In Chapter 5 we will be concerned with the movement of solute and water, and we will need to know the dependence of the chemical potentials on pressure. To find this, we write

$$\Delta\mu_w = \left( \frac{\partial\mu_w}{\partial p} \right)_{T, N_w, C_s} \Delta p + \left( \frac{\partial\mu_w}{\partial C_s} \right)_{T, p, N_w} \Delta C_s.$$

The second term is just Eq. 3.74b. To obtain the derivative in the first term, we use the fact that when the

partial derivative of a function is taken with respect to two variables, the result is independent of the order of differentiation (Appendix N):

$$\left[ \frac{\partial}{\partial p} \left( \frac{\partial G}{\partial N_w} \right)_{T, p, N_s} \right]_{T, N_w} = \left[ \frac{\partial}{\partial N_w} \left( \frac{\partial G}{\partial p} \right)_{T, N_w, N_s} \right]_{T, p}$$

From Eqs. 3.71a and 3.71c, we get

$$\left( \frac{\partial\mu_w}{\partial p} \right)_{T, N_w} = \left( \frac{\partial V}{\partial N_w} \right)_{T, p}. \quad (3.75)$$

For a process at constant temperature, the rate of change of  $\mu_w$  with  $p$  for constant solute concentration is the same as the rate of change of  $V$  with  $N_w$  when  $p$  is fixed.

The quantity  $(\partial V/\partial N_w)_{T, p}$  is the rate at which the volume changes when more molecules are added at constant temperature and pressure. For an ideal incompressible liquid it is the molecular volume,  $\bar{V}_w$ . We can repeat this argument for the solute to obtain

$$\left( \frac{\partial\mu_w}{\partial p} \right)_{T, N_w} = \bar{V}_w, \quad \left( \frac{\partial\mu_s}{\partial p} \right)_{T, N_s} = \bar{V}_s. \quad (3.76)$$

In a solution, the total volume is  $V = N_w \bar{V}_w + N_s \bar{V}_s$  where  $\bar{V}_w$  and  $\bar{V}_s$  are the average volumes occupied by one molecule of water and solute. Dividing by  $V$  gives  $1 = C_w \bar{V}_w + C_s \bar{V}_s$ . If the solution is dilute,

$$\bar{V}_w \approx \frac{1}{C_w}. \quad (3.77)$$

In an ideal solution  $\bar{V}_w = \bar{V}_s$ . For an ideal dilute solution, we then have

$$\Delta\mu_w = \bar{V}_w (\Delta p - k_B T \Delta C_s) \approx \frac{\Delta p - k_B T \Delta C_s}{C_w}. \quad (3.78)$$

$$\begin{aligned} \Delta\mu_s &= k_B T \ln(C_{s2}/C_{s1}) + \bar{V}_s \Delta p \\ &\approx k_B T \ln(C_{s2}/C_{s1}) + \bar{V}_w \Delta p. \end{aligned} \quad (3.79)$$

We saw this concentration dependence earlier, in Sec. 3.13. If the concentration difference is small, we can write  $C_{s2} = C_{s1} + \Delta C_s$  and use the expansion  $\ln(1+x) \approx x$  to obtain

$$\Delta\mu_s \approx \frac{k_B T \Delta C_s}{C_s} + \frac{\Delta p}{C_w}. \quad (3.80)$$

### 3.19 Transformation of Randomness to Order

When two systems are in equilibrium, the total entropy is a maximum. Yet a living creature is a low-entropy, highly ordered system. Are these two observations in conflict? The answer is no; the living system is not in equilibrium, and it is this lack of equilibrium that allows the entropy to

be low. The conditions under which order can be brought to a system—its entropy can be reduced—are discussed briefly in this section.

A car travels with velocity  $\mathbf{v}$  and has kinetic energy  $\frac{1}{2}mv^2$ . In addition to the random thermal motions of the atoms making up the car, all the atoms have velocity  $\mathbf{v}$  in the same direction (except for those in rotating parts, which have an ordered velocity that is more complicated to describe). If the brake shoes are brought into contact with the brake drums, the car loses kinetic energy, and the shoes and drums become hot. Ordered energy has been converted into disordered, thermal energy; the entropy has increased. Is it possible to heat the drums and shoes with a torch, apply the brakes, and have the car move as the drums and shoes cool off? Energetically, this is possible, but there are only a few microstates in which all the molecules are moving in a manner that constitutes movement of the car. Their number is vanishingly small compared to the number of microstates in which the brake drums are hot. The probability that the car will begin to move is vanishingly small.

An animal is placed in an insulated, isolated container. The animal soon dies and decomposes. Energetically, the animal could form again, but the number of microstates corresponding to a live animal is extremely small compared to all microstates corresponding to the same total energy for all the atoms in the animal.

In some cases, thermal energy can be converted into work. When gas in a cylinder is heated, it expands against a piston that does work. Energy can be supplied to an organism and it lives. To what extent can these processes, which apparently contradict the normal increase of entropy, be made to take place? These questions can be stated in a more basic form.

1. To what extent is it possible to convert internal energy distributed randomly over many molecules into energy that involves a change of a macroscopic parameter of the system? (How much work can be captured from the gas as it expands the piston?)
2. To what extent is it possible to convert a random mixture of simple molecules into complex and highly organized macromolecules?

Both these questions can be reformulated: under what conditions can the entropy of a system be made to decrease?

The answer is that the entropy of a system can be made to decrease if, and only if, it is in contact with one or more auxiliary systems that experience at least a compensating increase in entropy. Then the total entropy remains the same or increases. This is one form of the *second law of thermodynamics*. For a fascinating discussion of the second law, see Atkins (1994).

One device that can accomplish this process is a *heat engine*. It operates between two thermal reservoirs at different temperatures, removing heat from the hotter one

and injecting heat into the cooler one. Even though less heat goes into the cooler reservoir than was removed from the hotter one (the difference being the mechanical work done by the engine), the overall entropy of the two reservoirs increases. The entropy change of the hot reservoir is a decrease,  $-\Delta Q/T$ , while the entropy change of the cooler reservoir is an increase,  $+\Delta Q'/T'$ . Since  $T' < T$ , the entropy increase more than balances the decrease, even though  $\Delta Q' < \Delta Q$ . The increase in the number of accessible microstates of the cooler reservoir is greater than the decrease in the number of accessible microstates of the hotter reservoir. The coupled chemical reactions that we saw in Sec. 3.17 are analogous.

## Symbols Used in Chapter 3

Symbol	Use	Units	First used on page
$\mathbf{a}$	Acceleration	$\text{m s}^{-2}$	49
$a$	Number of atoms in a molecule		53
$a, b, c, d$	Number of atoms of species $A, B, C$ , and $D$		66
$a$	Area	$\text{m}^2$	65
$c_j$	Concentration (molar)	$\text{mol m}^{-3}$ , $\text{mol l}^{-1}$	63
$c$	Specific heat capacity	$\text{J K}^{-1} \text{kg}^{-1}$	61
$e$	Base of natural logarithms		58
$e$	Elementary charge	C	59
$f$	Number of degrees of freedom		53
$g$	Gravitational acceleration	$\text{m s}^{-2}$	60
$k_B$	Boltzmann's constant	$\text{J K}^{-1}$	57
$m$	Mass	kg	49
$n$	Number of particles in a volume		50
$p$	Probability of "success"		51
$p$	Pressure	Pa	56
$p_x, p_y, p_z$	Momentum	$\text{kg m s}^{-1}$	60
$q$	Probability of "failure"		51
$q$	Electric charge	C	65
$t$	Time	s	49
$u_i$	Energy of the $i$ th energy level	J	53
$v, v'$	Volume	$\text{m}^3$	51
$v$	Electrical potential	V	59
$v, v_x, v_y, v_z$	Velocity	$\text{m s}^{-1}$	49
$x, y, z$	Position coordinate	m	49
$x$	General variable		55
$x$	Extensive variable		64
$x_s, x_w$	Mole fractions of solute and water		69
$y$	General variable		58

Symbol	Use	Units	First used on page	$X$ $\alpha$ $\rho$ $\sigma$ $\tau$ $\mu$ $\mu_w, \mu_s$ $\Omega, \Omega', \Omega^*$ — $\langle \rangle$	Generalized force General variable Density Surface tension $k_B T$ Chemical potential Chemical potential of water or solute Number of accessible microstates A bar over any quantity means that it is averaged over an ensemble of many identically prepared systems Angular brackets mean an average over time	64 59 61 65 57 62 68 55 52 52 52 52 58 66 68 67 53 56 50 67 59 66 50 54 58 59 60 58 57 53 51 69 54 63
$y$	Height	m	60			
$z$	Valence		59			
$A, A', A^*$	Thermodynamic systems		56			
$A, B, C, D$	Chemically reacting species		66			
$C_i, C$	Concentration (particles per volume)	$\text{m}^{-3}, \text{l}^{-1}$	59			
$C$	Heat capacity	$\text{J K}^{-1}$	61			
$E_k$	Kinetic energy	J	59			
$E_p$	Potential energy	J	59			
$\mathbf{F}, F_x, F_y, F_z$	Force	N	49			
$F$	Force	N	65			
$F$	Faraday constant	$\text{C mol}^{-1}$	59			
$G$	Ratio of accessible microstates in a small system		58			
$G$	Gibbs free energy	J	66			
$H$	Enthalpy	J	68			
$K_{\text{eq}}$	Equilibrium constant in a chemical reaction		67			
$M$	Number of molecules in a system		53			
$M$	Number of repeated measurements		56			
$N, N', N^*$	Number of particles		50			
$N_w, N_s$	Number of solvent (water) or solute molecules		67			
$N_A$	Avogadro's number	$\text{mol}^{-1}$	59			
$N_A, N_B, N_C, N_D$	Number of molecules of species $A, B, C,$ and $D$ consumed or produced in a chemical reaction		66			
$P$	Probability		50			
$Q$	Flow of heat to a system	J	54			
$R$	Ratio of accessible states in a reservoir (Boltzmann factor)		58			
$R$	Gas constant	$\text{J mol}^{-1} \text{K}^{-1}$	59			
$S$	Area	$\text{m}^2$	60			
$S, S', S^*$	Entropy	$\text{J K}^{-1}$	58			
$T$	Absolute temperature	K	57			
$U, U', U^*$	Total energy of a system	J	53			
$V$	Volume	$\text{m}^3$	51			
$\bar{V}_w, \bar{V}_s$	Volume of water or solute molecule	$\text{m}^3$	69			
$W$	Work done by a system on the surroundings	J	54			
$W_{\text{conc}}$	Work done on a system to increase the concentration	J	63			

## Problems

### Section 3.1

**Problem 1** Some systems are so small that only a few molecules of a particular type are present, and statistical arguments begin to break down. Estimate the number of hydrogen ions inside an *E. coli* bacterium with  $\text{pH} = 7$ . (When  $\text{pH} = 7$  the concentration of hydrogen ions is  $10^{-7} \text{ mol l}^{-1}$ .)

**Problem 2** Use the last column of Table 3.2 to calculate the average value of  $n$ , which is defined by  $\bar{n} = \sum nP(n)$ . Verify that  $\bar{n} = Np$  in this case.

**Problem 3** A loose statement is made that “if we throw a coin 1 million times, the number of heads will be very close to half a million.” What is the mean number of occurrences of heads in 1 million tries? What is the standard deviation? What does “very close” mean? (You may need to consult Appendices G and H.)

**Problem 4** Evaluate  $P(n; 4, 0.5)$  using Eq. 3.4. Check your results against the histogram of Fig. 3.2 and by listing all the possible arrangements of four particles in the left or right sides of the box.

**Problem 5** Write a computer program to simulate measurements of which half of a box a gas molecule is in. Make several measurements with different sets of random numbers, and plot a histogram of the number of times  $n$  molecules are found in the left half. Try this for  $N = 1, 10,$  and 100. In BASIC, use the function RND to obtain the random number. Since the numbers are not really random but form a well-defined sequence, a new experiment will require changing the seed of the sequence. This is done with the statement RANDOMIZE. Other languages have similar functions.

**Problem 6** Color blindness is a sex-linked defect. The defective gene is located in the X chromosome. Females



carry an  $XX$  chromosome pair, while males have an  $XY$  pair. The trait is recessive, which means that the patient exhibits color blindness only if there is no normal  $X$  gene present. Let  $X_d$  be a defective gene. Then for a female, the possible gene combinations are

$$XX, XX_d, X_dX_d.$$

For a male, they are

$$XY, X_dY.$$

In a large population about 8% of the males are color-blind. What percentage of the females would you expect to be color-blind?

**Problem 7** A patient with heart disease will sometimes go into ventricular fibrillation, in which different parts of the heart do not beat together, and the heart cannot pump. This is cardiac arrest. The following data show the fraction of patients failing to regain normal heart rhythm after attempts at ventricular defibrillation by electric shock [W. D. Weaver (1982). *New Engl. J. Med.* **307**: 1101–1106.]

Number of attempts	Fraction persisting in fibrillation
0	1.00
1	0.37
2	0.15
3	0.07
4	0.02

Assume that the probability  $p$  of defibrillation on one attempt is independent of other attempts. Obtain an equation for the probability that the patient remains in fibrillation after  $N$  attempts. Compare it to the data and estimate  $p$ .

**Problem 8** There are  $N$  people in a class ( $N = 25$ ). What is the probability that no one in the class has a birthday on a particular day? Ignore seasonal variations in birth rate and ignore leap years.

**Problem 9** The death rate for 75-year-old people is 0.089 per year (Commissioners 1941 Standard Ordinary Mortality Table).

(a) What is the probability that an individual aged 75 will die during a 12-hour period? Neglect the fact that some are sick, some are terminally ill, and so on, and assume that the probability is the same for everyone.

(b) Suppose that 10,000 people, all aged 75, are given the flu vaccine at  $t = 0$ . What is the probability that none will die during the next 12 hours? (This underestimates the probability, since sick people would not be given the vaccine, but they are included in the death rate.)

**Problem 10** This problem is intended to help you understand some of the nuances of the binomial probability distribution.

(a) In a macabre “game” of “roulette” the victim places one bullet in the cylinder of a revolver. (A less hazardous game could be done with dice.) There is room for six bullets in the cylinder. The victim spins the cylinder, so there is a probability of  $1/6$  that the bullet is in firing position. The victim then places the gun to the head and fires. If the victim survives, the cylinder is spun again and the process is repeated. We can look either at the cumulative probability of “success” (being killed), or the cumulative probability of “failure” (surviving). Make a table for 1000 victims who keep playing the game over and over. Plot the number surviving, the number killed on each try, and the cumulative number killed.

(b) Show that the number surviving can be expressed as  $1000e^{-bN}$ , where  $N$  is the number of tries, and find  $b$ .

(c) The data in the following table are from Fédération CECOS, D. Schwartz and M. J. Mayaux (1982). Female fecundity as a function of age, *N. Engl. J. Med.* **306**(7): 404–406. They show the cumulative success rates in different age groups for patients being treated for infertility by artificial insemination from a donor. That is, each month at the time of ovulation each patient who has not yet become pregnant is inseminated artificially. Plot these data. What do they suggest? Make whatever plots can confirm or rule out what you suspect.

Cycle	Fraction pregnant, age $\leq 25$	Fraction pregnant, age $\geq 35$
0	0	0
1	0.11	0.03
2	0.23	0.14
3	0.30	0.20
4	0.39	0.27
5	0.44	0.35
6	0.51	0.35
7	0.55	0.36
8	0.63	0.39
9	0.65	0.43
10	0.67	0.43
11	0.70	0.46
12	0.74	0.54

### Section 3.3

**Problem 11** A thermally insulated ideal gas of particles is confined within a container of volume  $V$ . The gas is initially at absolute temperature  $T$ . The volume of the container is very slowly reduced by moving a piston that constitutes one wall of the container. Give qualitative answers to the following questions.

(a) What happens to the energy levels of each particle?

(b) Is the work done on the gas as its volume decreases positive or negative?

(c) What happens to the energy of the gas?

## Section 3.5

**Problem 12** System  $A$  has  $10^{20}$  microstates, and system  $A'$  has  $10^{19}$  microstates. How many microstates does the combined system have?

**Problem 13** Calculate the Celsius and absolute temperatures corresponding to a room temperature of  $68^\circ\text{F}$ , a normal body temperature of  $98.6^\circ\text{F}$ , and a febrile body temperature of  $104^\circ\text{F}$ .

**Problem 14** Calculate and plot  $\Omega$ ,  $\Omega'$ , and  $\Omega^*$  for Fig. 3.10, thus reproducing the figure. Write down an analytic expression for  $\Omega^*$  and differentiate to find the value of  $U$  for which  $\Omega^*$  is a maximum.

**Problem 15** Systems  $A$  and  $A'$  each consist of three particles, whose energy levels are  $u$ ,  $2u$ ,  $3u$ , etc. The total energy available to the combined system is  $U^* = 12u$ .

(a) Make a table similar to Table 3.3. (If you have difficulty, see part (d) of this problem.)

(b) Find the most probable state. To what values of  $U$  and  $U'$  does it correspond?

(c) Plot  $\Omega^*$  vs.  $U$ . What is the probability that all three particles in system  $A$  have energy  $u$ ?

(d) Consider system  $A$ . If it has energy  $U$ , the maximum energy the first particle can have is  $U - 2u$ . How many microstates are there for which the first particle has energy  $U - 2u$ ?  $U - 3u$ ? Show that the total number of microstates for system  $A$  is given by

$$\sum_{i=1}^{U/u-2} \left( \frac{U}{u} - i - 1 \right) = \frac{1}{2} \left[ \left( \frac{U}{u} \right)^2 - 3 \left( \frac{U}{u} \right) + 2 \right].$$

This proves the assertion in the text that for 3 particles,  $\Omega$  increases as  $U^2$ .

**Problem 16** We have seen that in general with volume, number of particles, and other parameters that determine the positions of the energy levels held fixed,

$$\frac{1}{\Omega} \frac{d\Omega}{dU} = \frac{1}{k_B T}.$$

Suppose that  $U = CT$ , where  $C$  is the heat capacity of the system. Find  $\Omega(U)$ .

**Problem 17** Systems  $A$  and  $A'$  are in thermal contact. Show that if  $T < T'$ , energy flows from  $A'$  to  $A$  to increase  $\Omega^*$ , while if  $T > T'$ , energy flows from  $A$  to  $A'$ .

**Problem 18** A simple system has only two energy levels for each single entity in the system. (The system could, for example, be a collection of “gates” in a cell membrane, each with two states, open and closed.) One level has energy  $u_1$ , the other has energy  $u_2$ . There are  $N$  entities in the system. You can answer the following questions without doing any calculations.

(a) What is the minimum energy of the system? How many microstates are there for the minimum energy?

(b) What is the maximum energy of the system? How many microstates are there for which the system has maximum energy?

(c) Sketch what  $\Omega(U)$  must look like.

(d) Recall the definition of  $T$ , Eqs. 3.14 and 3.15. Are there any values of  $U$  for which the temperature is negative? Where?

## Section 3.6

**Problem 19** Consider the following arrangements of the 26 capital letters of the English alphabet: (a) TWO, (b) any three letters, in any order, that are all different, and (c) any three letters, in any order, which may repeat themselves. For (b) and (c), consider the same letters in a different order to be a different arrangement. If each arrangement is a “microstate,” find  $\Omega$  and  $S$  in each case.

**Problem 20** Ice and water coexist at  $273\text{K}$ . To melt 1 mol of ice at this temperature,  $6000\text{J}$  are needed. Calculate the entropy difference and the ratio of the number of microstates for 1 mol of ice and 1 mol of water at this temperature. (Do not worry about any volume changes of the ice and water.)

**Problem 21** If a system is maintained at constant volume, no work is done on it as the energy changes. In that case  $dU = C(T) dT$ , where  $U$  is the internal energy,  $C$  is the heat capacity, and  $T$  is the temperature. The specific heat in general depends on the temperature. Suppose that in some temperature region the specific heat varies linearly with temperature:  $C(T) = C_0 + DT$ .

(a) What is the entropy change of the system when it is heated from temperature  $T_1$  to temperature  $T_2$ , both of which are in the region where  $C(T) = C_0 + DT$ ?

(b) What is the ratio of the number of microstates at  $T_2$  to the number at  $T_1$ ?

**Problem 22** A substance melts at constant temperature. There are 7 times as many microstates accessible to each molecule of the liquid as there were to each molecule of the solid. Ignore volume changes.

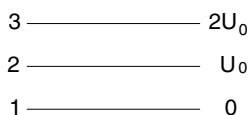
(a) What is the change in entropy of each molecule?

(b) How much heat is required to melt a mole of the substance if the melting temperature is  $50^\circ\text{C}$ ?

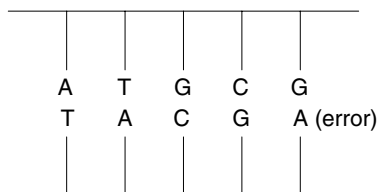
**Problem 23** The entropy of a monatomic ideal gas at constant energy depends on the volume as  $S = Nk_B \ln V + \text{const}$ . A gas of  $N$  molecules undergoes a process known as a free expansion. Initially it is confined to a volume  $V$  by a partition. The partition is ruptured and the gas expands to occupy a volume  $2V$ . No work is done and no heat flows, so the total energy is unchanged. Calculate the change of entropy and the ratio of the number of microstates after the volume change to the number before.

## Section 3.7

**Problem 24** A pore has three configurations with the energy levels shown. The pore is in thermal equilibrium with the surroundings at temperature  $T$ . Find the probabilities  $p_1$ ,  $p_2$ , and  $p_3$  of being in each level. Each level has only one microstate associated with it.



**Problem 25** The DNA molecule consists of two intertwined linear chains. Sticking out from each monomer (link in the chain) is one of four bases: adenine (A), guanine (G), thymine (T), or cytosine (C). In the double helix, each base from one strand bonds to a base in the other strand. The correct matches, A–T and G–C, are more tightly bound than are the improper matches. The chain looks something like this, where the last bond shown is an “error.”



The probability of an error at 300 K is about  $10^{-9}$  per base pair. Assume that this probability is determined by a Boltzmann factor  $e^{-U/k_B T}$ , where  $U$  is the additional energy required for a mismatch.

(a) Estimate this excess energy.

(b) If such mismatches are the sole cause of mutations in an organism, what would the mutation rate be if the temperature were raised  $20^\circ\text{C}$ ?

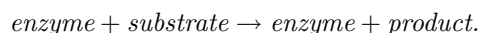
**Problem 26** In Chapter 18 we will study how the “spin” magnetic moment of an atomic nucleus interacts with a magnetic field  $\mathbf{B}$ , leading to “magnetic resonance imaging.” Assume a nucleus has a “magnetic dipole moment”  $\mu$ , which can point in only one of two directions: parallel to  $B$  (“spin up”) or antiparallel (“spin down”). The energy of a nucleus with spin up is  $-\mu B$ ; with spin down it is  $+\mu B$ . Use the Boltzmann factor to determine an expression for the ratio of the number of particles with spin up to the number with spin down. Evaluate this ratio for  $\mu = 1.4 \times 10^{-26} \text{ J T}^{-1}$ ,  $B = 2 \text{ T}$ , and  $T = 300 \text{ K}$ .

**Problem 27** The data of Problem 2.10 were used to obtain an empirical relationship between the charge integration time  $\tau$  and the temperature  $T$ . It might be that  $\tau$  is determined by a chemical reaction whose rate is given by a Boltzmann factor. Make a new plot based on that assumption and determine the appropriate constants.

**Problem 28** Oxygen and carbon monoxide compete for binding to hemoglobin. If enough CO binds to hemoglobin,

the ability of the blood to deliver oxygen is impaired, and carbon monoxide poisoning ensues. Consider the hemoglobin molecule to be a two-state system: the heme group is bound either to  $\text{O}_2$  or to CO. Calculate the probability of binding to CO. Let the  $G$  factor of Eq. 3.25 be equal to the ratio of the concentrations of CO and  $\text{O}_2$ . Assume CO is 100 times less abundant than  $\text{O}_2$ . CO is more tightly bound than  $\text{O}_2$  to the heme group by about 0.15 eV. Let  $T = 300 \text{ K}$ .

**Problem 29** The function of many enzymes is to act as a catalyst: they increase the speed of a chemical reaction. To get an idea of how a catalyst works, consider the reaction



In order for the reaction to proceed, some energy barrier  $\Delta E$  must be overcome. The probability of the substrate having an energy  $\Delta E$  or greater depends primarily on a Boltzmann factor,  $e^{-\Delta E/k_B T}$ . Determine by what factor this probability increases if the enzyme decreases the activation energy by (a) 0.1 eV, (b) 1 eV. Assume  $T = 310 \text{ K}$ .

**Problem 30** Chemists use  $Q_{10}$  to characterize a chemical reaction. It is defined by

$$Q_{10} = \frac{(\text{reaction rate at } T + 10)}{(\text{reaction rate at } T)},$$

where  $T$  is the absolute temperature. If the reaction rate is proportional to the fraction of reacting atoms that have an energy exceeding some threshold  $\Delta U$ , then to a first approximation

$$R \propto \int_{\Delta U}^{\infty} e^{-U/k_B T} dU.$$

(This neglects more slowly varying factors such as a  $U^{1/2}$  which are introduced in more accurate analyses.)

(a) Show that  $R \propto k_B T e^{-\Delta U/k_B T}$ .

(b) Show that

$$\frac{Q_{10} T}{T + 10} = \exp \left[ \frac{\Delta U}{k_B} \frac{10}{T(T + 10)} \right].$$

(c) Estimate  $\Delta U$  if  $Q_{10} = 2$  at  $T = 300 \text{ K}$ .

(d) To use  $Q_{10}$  to determine reaction rate as a function of temperature, one usually assumes exponential behavior:

$$R(T) = R(T_0) (Q_{10})^{\frac{T-T_0}{10}}.$$

Use values  $T_0 = 298 \text{ K}$ , and  $\Delta U = 0.6 \text{ eV}$ , to calculate  $R(T)/R(T_0)$  using the  $Q_{10}$  model, the approximation  $R(T)/R(T_0) = (T/T_0) (e^{-\Delta U/k_B T}/e^{-\Delta U/k_B T_0})$ , and the approximation  $R(T)/R(T_0) = (e^{-\Delta U/k_B T}/e^{-\Delta U/k_B T_0})$ . Temperature corrections for metabolic rate vs. mass have been used by Gillooly et al. (2001).

**Problem 31** The vapor pressure of a substance can be calculated using the following model. All molecules in the vapor that strike the surface of the liquid stick. (This number is proportional to the pressure.) Those molecules in the liquid that reach the surface and have enough energy escape. Equilibrium is established when the number sticking per unit area per unit time is equal to the number escaping.

(a) The number of molecules with energy  $U$  is proportional to  $e^{-U/k_B T}$ . What will be the number with energy greater than the escape energy,  $U_0$ ?

(b) Use the result of part (a) and look up values for the vapor pressure of water as a function of temperature, to make a plot on semilog paper. From this plot, estimate the escape energy  $U_0$ .

(c) The “heat of vaporization” of water is 540 calories per gram. Convert the energy per molecule you found in part (b) to calories per gram and compare it with this figure.

**Problem 32** A macromolecule of density  $\rho$  and mass  $m$  is immersed in an incompressible fluid of density  $\rho_w$  at temperature  $T$ . The volume  $v$  occupied by one macromolecule is known. A dilute solution of the macromolecules is placed in an ultracentrifuge rotating with high angular velocity  $\omega$ . In the frame of reference rotating with the centrifuge, a particle at rest is acted on by an outward force  $m\omega^2 r$ , where  $r$  is the distance of the particle from the axis.

(a) What is the net force acting on the particle in this frame? Include the effect of buoyancy of the surrounding fluid, of density  $\rho_w$ .

(b) Suppose that equilibrium has been reached. Use the Boltzmann factor to find the number of particles per unit volume at distance  $r$ .

**Problem 33** Suppose that particles in water are subjected to an external force  $F(y)$  that acts in the  $y$  direction. The force is related to the potential energy  $E_p(y)$  by  $F = -dE_p/dy$ . Neglect gravity and buoyancy effects.

(a) Apply Newton’s first law to a slice of the fluid in equilibrium to obtain an expression for  $p(y)$ .

(b) If the particles have a Boltzmann distribution, show that  $p(y) - p(0) = k_B T [C(y) - C(0)]$ .

### Section 3.8

**Problem 34** The concentrations of various ions are measured on the inside and outside of a nerve cell. The following values are obtained when the potential inside the cell is  $-70$  mV with respect to the outside.

Ion	Inside (mmol $l^{-1}$ )	Outside (mmol $l^{-1}$ )
$Na^+$	15	145
$K^+$	150	5
$Cl^-$	9	125

Comment on which species have concentrations that are consistent with being able to pass freely through the cell wall. Assume  $T = 300$  K.

**Problem 35** Calculate the volume of 1 mole of water. Pour yourself a mole of water and drink it.

### Section 3.9

**Problem 36** A virus has a mass of  $1.7 \times 10^{-14}$  g. If the virus particles are in thermal equilibrium in the atmosphere, their concentration will vary with height as  $C(y) = C(0)e^{-y/\lambda}$ . Evaluate  $\lambda$ . Do you think this answer is reasonable?

**Problem 37** Calculate the length constant  $\lambda$  for the exponential decay ( $e^{-y/\lambda}$ ) of atmospheric pressure. Assume the atmosphere is made up entirely of nitrogen,  $N_2$ . Nitrogen has an atomic weight of 14. Use your result to compare air pressure at sea level to air pressure at the top of Mt. Everest (8.8 km.) Assume the atmosphere is all at the same temperature; it is not.

### Section 3.10

**Problem 38** Calculate the average kinetic energy (in J and eV) of a particle moving in three dimensions at body temperature,  $37^\circ C$ .

**Problem 39** This is our first model for the important problem of detecting a “signal” in the presence of “noise.” We will discuss this in detail in Chapters 9 and 11. A sensitive balance consists of a weak spring hanging vertically in the earth’s gravitational field. The equilibrium position of the end of the spring is  $x = 0$ . When a mass  $m$  is added to the spring, it elongates to an average position  $x_0$ , around which it vibrates because of thermal energy. In terms of  $\Delta x = x - x_0$ , the momentum of the mass  $p_x$  and the spring constant  $K$ , the force that the spring exerts on the mass is  $Kx_0$ , and the total energy is  $U = p_x^2/2m + \frac{1}{2}K(\Delta x)^2$ .

(a) What is  $x_0$  in terms of  $m$ ,  $g$ , and  $K$ ?

(b) Find  $\overline{\Delta x^2} = \overline{(x - x_0)^2}$ .

(c) What is the smallest mass that can be measured taking a single “snapshot” of the system to find the position of the mass?

### Section 3.11

**Problem 40** The specific heat capacity of water is  $4184$  J  $K^{-1}$   $kg^{-1}$  [Denny (1993)]. Convert this to  $cal$   $g^{-1}$   $^\circ C^{-1}$ . Historically, the calorie was defined in terms of the specific heat capacity of water.

**Problem 41** The “calorie” we see listed on food labels is actually 1000 cal or 1 kilocalorie. How many kilocalories do you expend each day if your average metabolic rate is 100 W?

**Problem 42** Your body must dissipate energy from metabolism at a rate of about 100 W by various mechanisms to keep the body from overheating. Suppose these mechanisms stopped working (perhaps you are wrapped in a very good thermal blanket, so no heat can flow from or to your body). At what rate will your body temperature increase? How long will it take for your body temperature to increase by 5°C? Assume you have a mass of 70 kg, and the specific heat of your body tissue is the same as of water, 4200 J K<sup>-1</sup> kg<sup>-1</sup>.

**Problem 43** A person of mass 70 kg and body temperature 37°C breathes in 0.5 l of air at a temperature of 20°C. Assume that there are no other sources of heat (turn off metabolism for a moment), and the body as a whole is insulated so no heat is lost to the environment. Find the equilibrium temperature that the air and body will ultimately attain. Useful data:  $\rho_{\text{air}} = 1.3 \text{ kg m}^{-3}$ ,  $\rho_{\text{water}} = 1000 \text{ kg m}^{-3}$ ,  $c_{\text{air}} = 1000 \text{ J K}^{-1} \text{ kg}^{-1}$ ,  $c_{\text{water}} = 4200 \text{ J K}^{-1} \text{ kg}^{-1}$ . Assume that the person's body tissue has the same heat capacity and density as water.

**Problem 44** Fish are cold-blooded, and “breathe” water (in other words, they extract dissolved oxygen from the water around them using gills). Could a fish be warm-blooded and still breathe water? Assume a warm-blooded fish maintains a body temperature that is 20°C higher than the surrounding water. Furthermore, assume that the blood in the gills is cooled to the temperature of the surrounding water as the fish breathes water. Calculate the energy required to reheat 1 l of blood to the fish's body temperature. One liter of blood carries sufficient oxygen to produce about 4000 J of metabolic energy. Is the energy needed to reheat 1 l of blood to body temperature greater than or less than the metabolic energy produced by 1 l of blood? What does this imply about warm-blooded fish? Why must a warm-blooded aquatic mammal such as a dolphin breathe air, not water? Use  $c = 4200 \text{ J K}^{-1} \text{ kg}^{-1}$  and  $\rho = 10^3 \text{ kg m}^{-3}$  for both the body and the surrounding water. For more on this topic, see Denny (1993).

**Problem 45** Forensic scientists sometimes use “Newton's law of cooling” to determine how long ago a victim died. Assume that at the time of death ( $t_{\text{death}}$ ) the body had a temperature  $T_{\text{body}}$ , and after death it cools to the temperature of the surroundings,  $T_{\text{surround}}$ . Assume that the rate of heat loss by the body is proportional to the surface area of the body,  $S$ , and the temperature difference  $T - T_{\text{surround}}$ . The constant of proportionality is called the “convection coefficient.” As the corpse cools, the decrease in temperature is determined by the heat capacity.

(a) Relate the rate of heat loss to the rate of temperature change, and derive a differential equation for the body temperature  $T$ .

(b) Solve this differential equation (if you are having trouble, see Section 2.7). The solution is Newton's law of cooling.

(c) Write an expression for the time constant of cooling in terms of the specific heat capacity, density, volume, area, and the convection coefficient.

(d) For two bodies with the same shape but different sizes, which will cool faster: the large body or the small one?

**Problem 46** Determine whether the specific heat capacity of air,  $1000 \text{ J K}^{-1} \text{ kg}^{-1}$  is the same as the molar specific heat capacity of a monatomic ideal gas,  $3R/2$ . If not, why not? Assume air is all nitrogen,  $N_2$ .

### Section 3.12

**Problem 47** A small system  $A$  is in contact with a reservoir  $A'$  and can exchange both heat and particles with the reservoir. The number of microstates available to system  $A$  does not change. Show that the difference in total entropy when  $A$  is in two distinct states is

$$\Delta S^* = -(N_1 - N_2) \left( \frac{\partial S}{\partial N} \right)_U - (U_1 - U_2) \left( \frac{\partial S}{\partial U} \right)_N,$$

so that

$$\frac{P(N_1, U_1)}{P(N_2, U_2)} = \frac{e^{(N_1\mu - U_1)/k_B T}}{e^{(N_2\mu - U_2)/k_B T}},$$

where  $T$  and  $\mu$  are the temperature and chemical potential of the reservoir. This is called the Gibbs factor, and it reduces to the Boltzmann factor if  $N_1 = N_2$ . Chemists use the notation  $\lambda = e^{\mu/k_B T}$ , where  $\lambda$  is the absolute activity. Then

$$\frac{P(N_1, U_1)}{P(N_2, U_2)} = \frac{\lambda^{N_1} e^{-U_1/k_B T}}{\lambda^{N_2} e^{-U_2/k_B T}}.$$

**Problem 48** Specialize the results of the previous problem to a series of binding sites on a surface, such as a myoglobin molecule. The two states are

$$\begin{array}{ll} \text{No particle bound at the site} & N_1 = 0, \quad U_1 = 0 \\ \text{One particle bound at the site} & N_2 = 1, \quad U_2 = U_0 \end{array}$$

(a) Show that the fraction of sites occupied is

$$f = \frac{\lambda e^{-U_0/k_B T}}{1 + \lambda e^{-U_0/k_B T}}.$$

(b) If the sites are in equilibrium with a gas, then  $\mu_{\text{gas}} = \mu_{\text{sites}}$  or  $\lambda_{\text{gas}} = \lambda_{\text{sites}}$ . From the definition  $\mu = -T(\partial S/\partial N)_{U,V}$  and the expression for the entropy of a monatomic ideal gas,

$$S(U, V, N) = Nk_B \left( \ln V + \frac{3}{2} \ln U - \frac{5}{2} \ln N + \frac{5}{2} + \text{const} \right),$$

where  $\text{const} = \frac{3}{2} \ln(m/3\pi\hbar^2)$ , show that  $f = p/(p_0 + p)$ , where  $p$  is the gas pressure and

$$p_0 = \frac{(k_B T)^{5/2} m^{3/2} e^{U_0/k_B T}}{(2\pi\hbar^2)^{3/2}}.$$

This expression fits the data very well. See A. Rossi-Fanelli and E. Antonini (1958). *Archives Biochem. Biophys.* **77**: 478.

Section 3.13

**Problem 49** The entropy of a monatomic ideal gas is

$$S(U, V, N) = Nk_B \left( \ln V + \frac{3}{2} \ln U - \frac{5}{2} \ln N + \frac{5}{2} + \text{const} \right),$$

where  $\text{const} = \frac{3}{2} \ln(m/3\pi\hbar^2)$  depends only on the mass of the molecule. Consider two containers of gas at the same temperature and pressure that can exchange particles. Expand the total entropy in a Taylor's series, keep terms to second order, and use the result to find the variance in the fluctuating number of particles in one system. Assume  $N \ll N'$ . You should obtain the same result obtained from the binomial distribution ( $\sigma^2 = N$ ) if you take into account that it is the temperature of the gas in the container, and not its energy, that should be held fixed. (For a monatomic ideal gas  $U = 3Nk_B T/2$ . Use this result to rewrite the entropy in terms of  $T, V$ , and  $N$ .)

**Problem 50** Show that the chemical potential of an ideal gas is proportional to the logarithm of the concentration, a result that we have now seen several times for dilute ideal systems. To do so, use the expression for the entropy of a monatomic ideal gas given in the previous problems. Rewrite the thermodynamic identity as  $dU = TdS + \mu dN - p dV$ , from which we can identify the partial derivative

$$\mu = \left( \frac{\partial U}{\partial N} \right)_{S, V}.$$

The chemical potential is the increase in energy of the system if one particle is added while keeping the entropy and volume fixed. Use the expression for the entropy of the monatomic ideal gas, for the case of  $N$  particles with total energy  $U$  and  $N+1$  particles with total energy  $U+\mu$ , to show that the chemical potential of the ideal gas is

$$\mu = k_B T \left[ \ln \left( \frac{N}{V} \right) - \frac{3}{2} \ln(3k_B T/2) - \text{const} \right]$$

or

$$\mu = -k_B T \ln \left[ \frac{V}{N} \left( \frac{mk_B T}{2\pi\hbar^2} \right)^{3/2} \right].$$

[A more extensive discussion for other simple systems is given by Cook and Dickerson (1995).]

**Problem 51** Derive the Nernst equation (Eq. 3.34) by making the chemical potential the same on each side of a charged membrane. Use Eq. 3.48, with the potential energy per particle given as  $zev$ .

Section 3.15

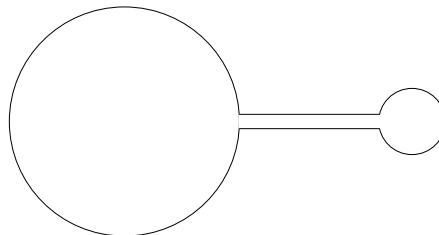
**Problem 52** Consider two systems that can exchange energy  $U$  and surface area  $a$ , but not volume  $V$  or number of particles  $N$ . The total energy is  $U^* = U + U'$  and the

total surface area is  $a^* = a + a'$ . Repeat the analysis of Sec. 3.5 and show that in equilibrium  $T = T'$  and  $\sigma = \sigma'$ , where the surface tension is defined as

$$\sigma = -T \left( \frac{\partial S}{\partial a} \right)_{U, V, N}.$$

**Problem 53** Consider a spherical air bubble in water.

(a) Equate the pressure-volume work to the surface work, and find a relationship between the pressure and the radius. This relationship is analogous to the Law of Laplace (Problem 1.19).



(b) Consider a small bubble attached to a large one. Use the relationship derived in (a) to determine which bubble has the larger internal pressure. Which bubble tends to shrink and which tends to expand?

(c) The bubbles in (b) are a model for two alveoli connected by a bronchiole in our lungs. Explain why a special fluid called a surfactant is needed to reduce the surface tension in the water on the surface of the alveolus. For more on the biological implications of surface tension, see Denny (1993).

Section 3.16

**Problem 54** Use the analysis presented in Sec. 3.16 to show that the surface tension is

$$\sigma = \left( \frac{\partial U}{\partial a} \right)_{S, V, N}.$$

Therefore, increasing the surface area when the entropy, volume and number of particles are fixed requires energy. For water, the surface tension is approximately  $0.07 \text{ J m}^{-2}$ , which is a large value [Denny (1993)].

Section 3.17

**Problem 55** The reaction  $1 \text{ glucose} + 6\text{O}_2 \longleftrightarrow 6\text{CO}_2 + 6\text{H}_2\text{O}$  must conserve the number of each type of atom. Determine the chemical formula of glucose.

Section 3.18

**Problem 56** System A consists of  $N$  particles that move from a region where the concentration is  $C_1$  to another where the concentration is  $C_2$ , each experiencing a change in chemical potential  $\Delta\mu = k_B T \ln(C_2/C_1)$ . The process

occurs at constant temperature and pressure. What is the ratio of the total number of microstates of system and surroundings after the move to the number before the move? Assume the concentrations do not change.

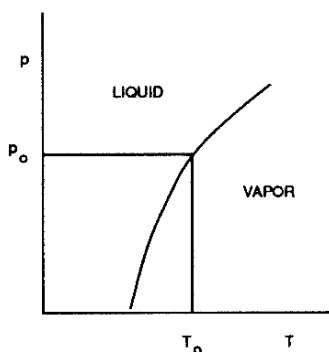
**Problem 57** If one increases the volume of a liquid at constant  $p$  and  $T$ , a portion of the liquid evaporates. The amount of liquid decreases as  $V$  increases until all the liquid is vaporized. The pressure at which the two phases coexist is called the vapor pressure. The vapor pressure depends on the temperature, as shown. When two phases are in equilibrium, they are in mechanical, thermal, and diffusive equilibrium:  $T_l = T_g$ ,  $p_l = p_g$ ,  $\mu_l = \mu_g$ . Thus, at any arbitrary point on the vapor-pressure curve,  $\mu_g(T_0, p_0) = \mu_l(T_0, p_0)$ . Consider some nearby point in the vapor-pressure curve, and expand both chemical potentials in a Taylor's series to show that

$$\frac{dp}{dT} = \frac{(\partial\mu_g/\partial T)_p - (\partial\mu_l/\partial T)_p}{(\partial\mu_l/\partial p)_T - (\partial\mu_g/\partial p)_T},$$

where  $dp/dT$  is the slope of the vapor-pressure curve. Use the fact that  $G = N\mu(p, T)$ , that  $(\partial G/\partial T)_{N,p} = -S$ , and that  $(\partial G/\partial p)_{N,T} = V$ , to show that

$$\frac{dp}{dT} = \frac{L}{T\Delta V},$$

where  $L$  is the latent heat of vaporization and  $\Delta V$  is the volume change on vaporization. (Since  $L$  and  $V$  are both extensive parameters, they can be expressed per mole or per molecule.) This is called the Clausius–Clapeyron equation.



**Problem 58** Use the definition of Gibbs free energy  $G = U - TS + pV$  and the thermodynamic identity  $TdS = dU - \mu dN + pdV$  to find the partial derivatives of  $G$  when  $N$ ,  $T$ , and  $p$  are the independent variables. Note that  $U$ ,  $S$ , and  $V$  are all extensive variables so that  $G$  is proportional to  $N$ :  $G = N\Phi$ . Thereby relate  $G$  to the chemical potential.

**Problem 59** (a) Find the change in Gibbs free energy  $G = U - TS + pV$  for an ideal gas that changes pressure reversibly from  $p_1$  to  $p_2$  at a constant temperature.

(b) Since  $\Delta G = N\Delta\mu$ , find  $\Delta\mu$ .

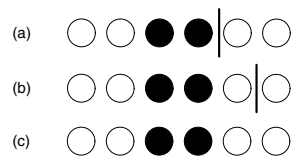
**Problem 60** Use the Clausius–Clapeyron equation for the vapor pressure as a function of temperature (see Problem 57),  $dp/dT = L/T\Delta V$ , and assume an ideal gas so that  $\Delta V \approx V_g = Nk_B T/p$  to find the vapor pressure  $p$  as a function of temperature.

**Problem 61** The argument leading to the change in  $G$  in a chemical reaction can be applied to a single particle moving from a region where the chemical potential is  $\mu_A$  to a region where the chemical potential is  $\mu_B$  by letting  $dN = -dN_A = dN_B$ , in which case  $dG = (\mu_B - \mu_A) dN$ . We saw in Sec. 3.13 that the chemical potential of a solute in an ideal solution had the form  $\Delta\mu = k_B T \ln(C/C_0) + \Delta(\text{potential energy per particle})$ . Sodium ions of charge  $+e$  ( $e = 1.6 \times 10^{-19}$  C) are found on one side of a membrane at concentration  $145 \text{ mmol l}^{-1}$ . The electrical potential is zero. On the other side of the membrane the concentration is  $15 \text{ mmol l}^{-1}$  and the potential is  $90 \text{ mV}$ . The change in electrical potential energy is  $e\Delta v$ . What is the change in Gibbs free energy if a single sodium ion goes from one side to the other? The temperature is  $310 \text{ K}$  and the pressure is atmospheric.

### Section 3.18

**Problem 62** Suppose that a potential energy term as well as a pressure must be added to the chemical potential, as was argued in Sec. 3.13. Consider a column of pure water. What is the difference in chemical potential between the top of the column and the bottom?

**Problem 63** The open circles in the drawing represent water molecules. The solid circles are solute molecules. The vertical line represents a membrane that is permeable to water but not solute. In case (a) there are two water molecules to the right of the membrane. In (b) there is one, and in (c) none. What is the total number of microstates of the combined system in each case?



**Problem 64** If we want to apply Eq. 3.80 when there is an appreciable difference in concentration, we can define an average concentration by

$$\Delta\mu_s = k_B T \ln(C_{s2}/C_{s1}) \equiv k_B T (\Delta C_s / \bar{C}_s),$$

$$\bar{C}_s \equiv \frac{\Delta C_s}{\ln(C_{s2}/C_{s1})} = \frac{\Delta C_s}{\ln(1 + \Delta C_s/C_{s1})}.$$

Use the Taylor's-series expansion  $y = x/\ln(1+x) \approx 1 + x/2 - x^2/12 + \dots$  to find an approximate expression for  $\bar{C}_s$ .

**Problem 65** Verify that differentiation of Eq. 3.69 with respect to  $N_w$  and  $N_s$  gives Eq. 3.72.

## References

- Atkins, P. W. (1994). *The 2nd Law: Energy, Chaos and Form*. New York, Scientific American.
- Casper, B. M., and S. Freier (1973). "Gibbs Paradox" paradox. *Am. J. Phys.* **41**: 509–511.
- Cook, G., and R. H. Dickerson (1995). Understanding the chemical potential. *Am. J. Phys* **63**(8): 737–742.
- Denny, M. W. (1993). *Air and Water: The Biology and Physics of Life's Media*. Princeton, Princeton University Press.
- Gillooly, J. F., J. H. Brown, G. B. West, V. M. Savage and E. L. Charnov (2001). Effects of size and temperature on metabolic rate. *Science*. **248**: 2248-2251. See also erratum posted in the on-line version on 16 Nov., 2001.
- Hildebrand, J. H., J. M. Prausnitz, and R. L. Scott (1970). *Regular and Related Solutions: the Solubility of Gases, Liquids, and Solids*. New York, Van Nostrand Reinhold.
- Hildebrand, J. H., and R. L. Scott (1964). *The Solubility of Nonelectrolytes*, 3rd ed. New York, Dover.
- Reif, F. (1964). *Statistical Physics*. Berkeley Physics Course, Vol. 5. New York, McGraw-Hill.
- Reif, F. (1965). *Fundamentals of Statistical and Thermal Physics*. New York, McGraw-Hill.
- Weaver W. (1963) *Lady Luck: The Theory of Probability*. Garden City, NY, Anchor.



# 4

## Transport in an Infinite Medium

Chapters 4 and 5 are devoted to one of the most fundamental problems in physiology: the transport of solvent (water) and uncharged solute particles. Chapter 4 develops some general ideas about the movement of solutes in a solution. Chapter 5 applies these ideas to movement of water and solute through a membrane.

Section 4.1 defines flux and fluence rate and derives the continuity equation. Section 4.2 shows how to calculate the solute fluence rate when the solute particles are drifting with a constant velocity, as when they are being dragged along by flowing solvent.

The next several sections are devoted to diffusion, the random motion of solute particles. Sections 4.3–4.5 describe random motion in a gas and a liquid. Section 4.6 states Fick’s first law, which relates the fluence rate of diffusing particles to the gradient of their concentration. Section 4.7 relates the proportionality constant in Fick’s first law to the viscous drag coefficient of the particle in the solution. Section 4.8 combines Fick’s first law and the equation of continuity to give Fick’s second law, the diffusion equation, that tells how the concentration  $C(x, y, z, t)$  evolves with time. Section 4.9 discusses various time-independent (steady-state) solutions to the diffusion equation. Section 4.10 analyzes steady-state diffusion to or from a cell, including both diffusion through the membrane and in the surrounding medium. Section 4.11 discusses a model of steady-state diffusion of a substance that is being produced at a constant rate inside a spherical cell. Section 4.12 develops a steady-state solution when both drift and diffusion are taking place in one dimension. One technique for solving the time-dependent diffusion equation is introduced in Sec. 4.13. Section 4.14 describes a simple random-walk model for diffusion.

### 4.1 Flux, Fluence, and Continuity

#### 4.1.1 Definitions

Flow was introduced in Sec. 1.15 of Chapter 1. The *flow rate*, *volume flux*, or *volume current*  $i$  is the total volume of material transported per unit time and has units of  $\text{m}^3 \text{s}^{-1}$ . One can also define the *mass flux* as the total mass transported per unit time or the *particle flux* as the total number of particles, and so on.

The *particle fluence* is the number of particles transported per unit area across an imaginary surface ( $\text{m}^{-2}$ ). The *volume fluence* is the total volume transported across the surface and has units  $\text{m}^3$  times  $\text{m}^{-2}$ , or  $\text{m}$ .

The *fluence rate* or *flux density* is the amount of “something” transported across an imaginary surface per unit area per unit time. It can be represented by a vector pointing in the direction the “something” moves and is denoted by  $\mathbf{j}$ . It has units of “something”  $\text{m}^{-2} \text{s}^{-1}$ . It is traditional to use a subscript to tell what is being transported:  $\mathbf{j}_s$  is solute particle fluence rate ( $\text{m}^{-2} \text{s}^{-1}$ ),  $\mathbf{j}_m$  is mass fluence rate ( $\text{kg m}^{-2} \text{s}^{-1}$ ), and  $\mathbf{j}_v$  is volume flux density ( $\text{m}^3 \text{m}^{-2} \text{s}^{-1}$  or  $\text{m s}^{-1}$ ). In a flowing fluid  $\mathbf{j}_v$  is the velocity with which the fluid moves.

Slightly different nomenclature is used in different fields. The words *flux* and *flux density* are often used interchangeably. Table 4.1 shows some of the names that are encountered. Do not spend much time studying it; it is provided to help you when you must deal with the notation in other books.

TABLE 4.1. Units and names for  $j$  and  $jS$  in various fields.

	$j$		$jS$	
	Units	Names	Units	Names
Particles	$m^{-2} s^{-1}$	Particle fluence rate Particle current density Particle flux density Particle flux	$s^{-1}$	Particle flux Particle current Particle flux
Electric charge	$C m^{-2} s^{-1}$ or $A m^{-2}$	Current density	$C s^{-1}$ or $A$	Current
Mass	$kg m^{-2} s^{-1}$	Mass fluence rate Mass flux density Mass flux	$kg s^{-1}$	Mass flux Mass flow
Energy	$J m^{-2} s^{-1}$ or $W m^{-2}$	Energy fluence rate Intensity Energy flux	$J s^{-1}$ or $W$	Energy flux Power

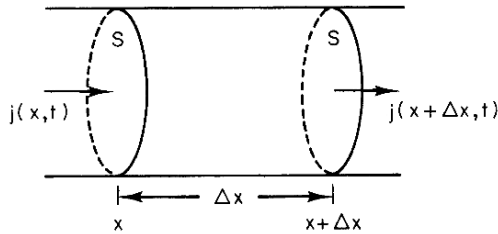


FIGURE 4.1. The fluence rates used to derive the continuity equation in one dimension.

#### 4.1.2 The Continuity Equation in One Dimension

As long as we are dealing with a substance that does not appear or disappear (as in a chemical reaction, radioactive decay, etc.), the number of particles or the mass, or in the case of an incompressible liquid, the volume, remains constant or is *conserved*. This conservation leads to a very useful equation called the *equation of continuity*. It will be derived here in terms of the number of particles.

We will first derive it in one dimension. Let the fluence rate of some species be  $j$  particles per unit area per unit time, passing a point. All motion takes place in the  $x$  direction along a tube of constant cross-sectional area  $S$ . The value of  $j$  may depend on position in the tube and on the time:  $j = j(x, t)$ . The number of particles in the volume shown in Fig. 4.1 between  $x$  and  $x + \Delta x$  is  $N(x, t)$ . At  $x$  there may be particles moving both to the right and to the left; the net number to the right in  $\Delta t$  is  $j(x, t)$  times the area  $S$  times the time  $\Delta t$ . A flux density in the  $+x$  direction is called positive. The net number of particles in at  $x$  is  $j(x, t)S\Delta t$ . Similarly, the net number out at  $x + \Delta x$  is  $j(x + \Delta x, t)S\Delta t$ . Combining these

gives the net increase in the number of particles in the volume  $S\Delta x$ :

$$\Delta N = [j(x, t) - j(x + \Delta x, t)] S \Delta t. \quad (4.1)$$

As  $\Delta x \rightarrow 0$ , the quantity involving  $j$  is, by definition, related to the partial derivative of  $j$  with respect to  $x$  (Appendix N):

$$j(x, t) - j(x + \Delta x, t) = -\frac{\partial j(x, t)}{\partial x} \Delta x.$$

Similarly, the increase in  $N(x, t)$  is

$$\Delta N(x, t) = N(x, t + \Delta t) - N(x, t) = \frac{\partial N}{\partial t} \Delta t.$$

These two expressions can be substituted in Eq. 4.1 to give

$$\frac{\partial}{\partial t} N(x, t) = -(S\Delta x) \frac{\partial}{\partial x} j(x, t).$$

This equation can be written in terms of the concentration  $C(x, t)$  by dividing both sides by the volume  $S\Delta x$ :

$$\frac{\partial C}{\partial t} = -\frac{\partial j}{\partial x}. \quad (4.2)$$

This is the *continuity equation in one dimension*.

#### 4.1.3 The Continuity Equation in Three Dimensions

In three dimensions,  $\mathbf{j}$  is a vector with components  $j_x$ ,  $j_y$ , and  $j_z$ . The flux across a surface  $dS$  oriented at some arbitrary direction with the  $x, y, z$  axes is equal to the component of  $\mathbf{j}$  perpendicular to the surface times  $dS$ . To see this, imagine that  $\mathbf{j}$  lies in the  $xy$  plane with components  $j_x$  and  $j_y$ . If  $\mathbf{j}$  makes an angle  $\phi$  with the vertical, then  $j_x = j \sin \phi$ ,  $j_y = j \cos \phi$ .

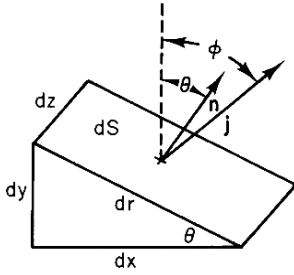


FIGURE 4.2. Volume element used to relate the fluence rate across the slant face to the components of the fluence rate parallel to the  $x$  and  $y$  axes.

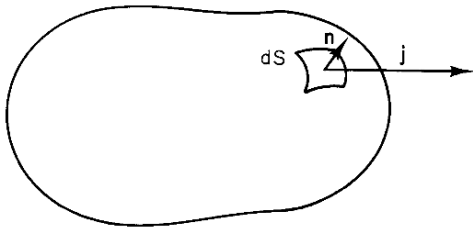


FIGURE 4.3. The total number of particles per second passing through the closed surface (flux) is the sum of the contributions  $j_n dS$  from all elements of the surface.

Consider the small volume shown in Fig. 4.2. If there is no buildup of particles within the volume, the flux in across the two faces parallel to the axes is equal to the flux across  $dS$ . The area  $dS$  of the slant surface is  $drdz$ , where  $dz$  is the thickness of the volume perpendicular to the paper. The number of particles per second across the face  $dydz$  is  $j_x dydz = (j \sin \phi)(dydz)$ . Since  $dy = dr \sin \theta$ , this may be written as  $j \sin \phi \sin \theta dzdr$ . Similarly, the number of particles per second in across the bottom face is  $j_y dx dz = j \cos \phi \cos \theta dzdr$ . The sum of these must be equal to the number leaving across the slant face:  $j dzdr(\sin \phi \sin \theta + \cos \phi \cos \theta) = j dzdr \cos(\phi - \theta) = j dS \cos(\phi - \theta)$ . The number of particles per unit area per second across the slant face is, therefore,  $j \cos(\phi - \theta)$ . Now  $\phi - \theta$  is the angle between  $\mathbf{j}$  and the unit vector  $\hat{\mathbf{n}}$  perpendicular to the surface. We can write the flux density across  $dS$  as  $j_n$  (the component of  $\mathbf{j}$  parallel to  $\hat{\mathbf{n}}$ ), or  $\mathbf{j} \cdot \hat{\mathbf{n}}$  (the dot product of  $\mathbf{j}$  and the normal). The flow per second is sometimes written as

$$(\mathbf{j} \cdot \hat{\mathbf{n}})dS, \quad j_n dS, \quad \text{or} \quad (\mathbf{j} \cdot d\mathbf{S}). \quad (4.3)$$

These are all equivalent: vector  $d\mathbf{S}$  is defined to have magnitude  $dS$  and to point along the normal to the surface that points outward from the enclosed volume. The same result is obtained (with more algebra) when  $\mathbf{j}$  is not in the  $xy$  plane.

#### 4.1.4 The Integral Form of the Continuity Equation

If we consider a closed volume as shown in Fig. 4.3, the total number of particles flowing out of the volume can be obtained by adding up the contribution from each element  $dS$ . It is

$$\begin{aligned} & \text{(total number of particles out in time } \Delta t) \\ &= \left( \iint_{\text{closed surface}} j_n dS \right) \Delta t. \end{aligned}$$

Since the total number of particles in the volume enclosed by the surface is

$$\iiint_{\text{enclosed volume}} C(x, y, z, t) dx dy dz,$$

we can write<sup>1</sup>

$$\frac{\partial}{\partial t} \iiint_{\text{enclosed volume}} C dV = - \iint_{\text{surface enclosing the volume}} j_n dS. \quad (4.4)$$

The outward flux density or fluence rate of the substance integrated over a closed surface (the net flux through the surface) is equal to the rate of decrease of the amount of substance within the volume enclosed by the surface.

How to evaluate the surface integral is best shown by two examples. First consider a volume defined by a sphere of radius  $r$ . Inside the sphere is a lamp radiating light uniformly in all directions. The light leaves through the surface of the sphere. The amount of light energy in the volume defined by the sphere is not changing, so the rate of energy production by the lamp  $P$  is equal to the energy flux through the surface of the outer sphere:

$$P = \iint j_n dS. \quad (4.5)$$

Because of the spherical symmetry,  $\mathbf{j}$  is perpendicular to the surface and is the same at all points on the sphere. Therefore,

$$P = j_n \iint dS.$$

Since the integral of  $dS$  over the surface of a sphere of radius  $r$  is  $4\pi r^2$ ,

$$j = j_n = \frac{P}{4\pi r^2}. \quad (4.6)$$

The amount of energy per unit area per unit time crossing the surface of the sphere is the energy fluence rate or the intensity.

The second example is slightly more complicated. Suppose that  $\mathbf{j}$  is parallel to the  $z$  axis and has the same value

<sup>1</sup>We can write  $dV$  as  $d^3\mathbf{r}$  or  $dx dy dz$ .

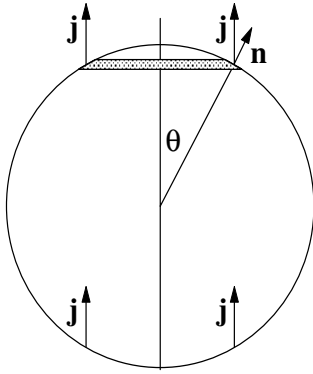


FIGURE 4.4. The fluence rate is the same everywhere. The flux is  $\int j_n dS$  over the entire sphere. When the normal component of the fluence rate is outward, the contribution is positive. When it is inward, the contribution is negative.

everywhere. The net flux through any closed surface will be zero in that case, and we will verify it to show how to evaluate a surface integral. Consider the situation shown in Fig. 4.4, where  $j_n$  is integrated over the surface of the sphere. At every point in the shaded strip,  $j_n = j \cos \theta$ . The strip has width  $r d\theta$  and circumference  $2\pi r \sin \theta$ , so its area is  $2\pi r^2 \sin \theta d\theta$ . Thus

$$\begin{aligned} \int j_n dS &= \int_0^\pi j \cos \theta 2\pi r^2 \sin \theta d\theta \\ &= 2\pi r^2 j \int_0^\pi \cos \theta \sin \theta d\theta = 0. \end{aligned}$$

#### 4.1.5 The Differential Form of the Continuity Equation

The continuity equation can be expressed in terms of derivatives instead of integrals. To derive this form, consider a small rectangular volume located at  $(x, y, z)$  and having sides  $(dx, dy, dz)$  as shown in Fig. 4.5. Apply Eq. 4.4 to each face of the volume. The rate the substance flows in through the face at  $x$  is  $j_x(x)(dydz)$ . At face  $x + dx$  it flows out at a rate  $j_x(x + dx)dydz$ . There is

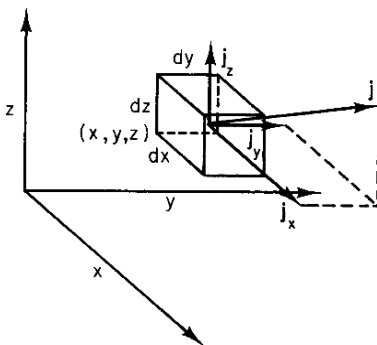


FIGURE 4.5. The small volume used to derive the differential form of the continuity equation.

no contribution to the flow through this face from  $j_y$  or  $j_z$ , since they are parallel to the face. The net increase in particles in the volume is

$$- [j_x(x + dx) - j_x(x)] dydz = - \frac{\partial j_x}{\partial x} dx dy dz.$$

Similar terms can be written for the faces perpendicular to the  $y$  and  $z$  axes. The total amount of the substance entering the volume per unit time is the rate of change of the amount within the volume, which is the rate of change of concentration times the volume  $dx dy dz$ . Therefore,

$$\frac{\partial C}{\partial t} (dx dy dz) = - \left( \frac{\partial j_x}{\partial x} + \frac{\partial j_y}{\partial y} + \frac{\partial j_z}{\partial z} \right) (dx dy dz)$$

or

$$- \frac{\partial C}{\partial t} = \frac{\partial j_x}{\partial x} + \frac{\partial j_y}{\partial y} + \frac{\partial j_z}{\partial z}. \tag{4.7}$$

This is the differential form of the continuity equation. Equation 4.2 was a special case of this when  $\mathbf{j}$  was parallel to the  $x$  axis.

The combination of derivatives on the right-hand side of Eq. 4.7 occurs frequently enough to warrant a special name. It is called the *divergence* of the vector  $\mathbf{j}$ :<sup>2</sup>

$$\text{div } \mathbf{j} = \nabla \cdot \mathbf{j} = \frac{\partial j_x}{\partial x} + \frac{\partial j_y}{\partial y} + \frac{\partial j_z}{\partial z}.$$

The continuity equation is therefore

$$\frac{\partial C}{\partial t} = -\text{div } \mathbf{j}. \tag{4.8}$$

This differential form of the continuity equation is completely equivalent to the integral form, Eq. 4.4. It is sometimes more convenient to use Eq. 4.4 and at other times more convenient to use Eq. 4.8.

The continuity equation says that the rate of decrease of the amount of a conserved substance in a certain region expressed as  $-\partial C/\partial t$  is equal to the rate at which it leaves the region expressed as the flow through the surface surrounding the region. The substance may be a certain kind of molecule, electric charge, heat, or mass. If it is electric charge,  $\mathbf{j}$  is the electric current per unit area and  $C$  is the charge per unit volume. If it is mass,  $C$  is the mass per unit volume or density  $\rho$ . The continuity equation is found in many contexts; in each it expresses the conservation of some quantity.

In the flow of a liquid, the density of the liquid  $\rho$ , the mass  $M$ , and volume  $V$  are related by  $M = \rho V$ . If the liquid is incompressible, a given mass always occupies the same volume, and the density does not change. Therefore,  $\partial \rho/\partial t = 0$ , and the equation of continuity gives

$$\text{div } \mathbf{j}_m = 0. \tag{4.9}$$

<sup>2</sup>The divergence is one of the concepts of vector calculus. A good review of vector calculus is Schey (1997).

### 4.1.6 The Continuity Equation with a Chemical Reaction

Our derivation of the continuity equation assumed that the substance was conserved—neither created nor destroyed. If a chemical reaction is creating the substance at a rate  $Q$  particles  $\text{m}^{-3} \text{s}^{-1}$  (which may depend on position) then the continuity equation becomes

$$\frac{\partial C}{\partial t} = Q - \text{div } \mathbf{j}, \quad (4.10a)$$

$$\begin{aligned} \frac{\partial}{\partial t} \iiint_{\text{volume}} C(x, y, z) dV \\ = \iiint_{\text{volume}} Q(x, y, z) dV - \iint_{\substack{\text{surface} \\ \text{enclosing} \\ \text{the volume}}} j_n dS. \end{aligned} \quad (4.10b)$$

If particles are being consumed in the chemical reaction, then  $Q$  is negative.

## 4.2 Drift or Solvent Drag

One simple way that solute particles can move is to drift with constant velocity. They can do this in a uniform electric or gravitational field if they are also subject to viscous drag, or they can be carried along by the solvent, a process called *drift* or *solvent drag*. (The solute particles are dragged by the solvent.) The solute fluence rate is  $\mathbf{j}_s$ , with units of particles  $\text{m}^{-2} \text{s}^{-1}$  or just  $\text{m}^{-2} \text{s}^{-1}$ . The number of solute particles passing through a surface is the volume of solution that moves through the surface times the concentration of solute particles. Therefore,

$$\mathbf{j}_s = C \mathbf{j}_v. \quad (4.11)$$

This effect will be explored in greater detail in Sec. 4.12.

## 4.3 Brownian Motion

There is also movement of solute molecules when the water is at rest. If the solution is dilute, the solute particles are far apart and hit one another only occasionally. They are struck by water molecules much more often. The result is that they are in continual helter-skelter motion. Each solute molecule is influenced by water molecules, but not by other solute molecules.

In Chapter 3, it was shown that the relative probability for a particle to have energy  $u$  when it is in thermal equilibrium with a reservoir at temperature  $T$  is given by a Boltzmann factor:<sup>3</sup>  $P \propto e^{-u/k_B T}$ . In Chapter 3, the

<sup>3</sup>The Boltzmann factor provided Jean Perrin with the first means to determine Avogadro's number. The density of particles

TABLE 4.2. Values of the rms velocity for various particles at body temperature.

Particle	Molecular weight	Mass (kg)	$v_{\text{rms}}$ ( $\text{m s}^{-1}$ )
H <sub>2</sub>	2	$3.4 \times 10^{-27}$	1940
H <sub>2</sub> O	18	$3 \times 10^{-26}$	652
O <sub>2</sub>	32	$5.4 \times 10^{-26}$	487
Glucose	180	$3 \times 10^{-25}$	200
Hemoglobin	65 000	$1 \times 10^{-22}$	11
Bacteriophage	$6.2 \times 10^6$	$1 \times 10^{-20}$	1.1
Tobacco mosaic virus	$40 \times 10^6$	$6.7 \times 10^{-20}$	0.4
<i>E. coli</i>		$2 \times 10^{-15}$	0.0025

Boltzmann factor was used to show that if any energy term depends on the square of some variable, then the average value of that term is  $k_B T/2$ . A particle with kinetic energy of translation  $m(v_x^2 + v_y^2 + v_z^2)/2$  has an average energy  $k_B T/2$  for each of the three terms, or a total translational kinetic energy of  $3k_B T/2$ . This is true regardless of the mass of the particle. Any particle in thermal equilibrium with a reservoir (which can be the surrounding fluid) will move with a mean square velocity given by<sup>4</sup>

$$\overline{v^2} = \frac{3k_B T}{m}. \quad (4.12)$$

The square root of  $\overline{v^2}$  is called the *root-mean-square*, or *rms*, velocity. It decreases with increasing mass of the particle. Table 4.2 shows values of  $v_{\text{rms}} = (\overline{v^2})^{1/2}$  for different particles at body temperature.

This movement of microscopic-sized particles, resulting from bombardment by much smaller invisible atoms, was first observed by the English botanist Robert Brown in 1827 and is called *Brownian motion*. Solute particles are also subject to this random motion. If the concentration of particles is not uniform, there will be more particles wandering from a region of high concentration to one of low concentration than vice versa. This motion is called *diffusion*.

In the next several sections, we study random motion and diffusion, first for a gas and then for a liquid.

## 4.4 Motion in a Gas: Mean Free Path and Collision Time

It is possible to define a *mean free path*, which is the average distance a particle travels between successive

in the atmosphere is proportional to  $\exp(-mgy/k_B T)$ , where  $mgy$  is the gravitational potential energy of the particles. Using particles for which  $m$  was known, Perrin was able to determine  $k_B$  for the first time. Since the gas constant  $R$  was already known, Avogadro's number was determined from the relationship  $R = N_A k_B$ .

<sup>4</sup>The average velocity is  $\overline{v_x} = 0$ , since a particle with a given speed moves with equal probability to the left or right.

collisions, and a *collision time*, the average length of time between collisions. Consider a collection of  $N_0$  molecules. The number that have moved distance  $x$  without suffering a collision is  $N(x)$ . For short distances  $dx$ , the probability that a molecule collides with another molecule is proportional to  $dx$ : call it  $(1/\lambda)dx$ . Then, on the average, the number of molecules having their first collision between  $x$  and  $x + dx$  is  $dN = -N(x)(1/\lambda)dx$ . This is the familiar equation for exponential decay. The number of molecules surviving without any collision is  $N(x) = N_0 e^{-x/\lambda}$ .

To compute the average distance traveled by a molecule between collisions, we multiply each possible value of  $x$  by the number of molecules that suffer their first collision between  $x$  and  $x + dx$ . Since  $N(x)$  is the number surviving at distance  $x$ , and  $dx/\lambda$  is the probability that one of those will have a collision between  $x$  and  $x + dx$ , the mean value of  $x$  is

$$\bar{x} = \frac{1}{N_0} \int_0^{\infty} x N(x) \frac{1}{\lambda} dx.$$

With the substitutions  $s = x/\lambda$  and  $N(x) = N_0 e^{-s}$ , this can be written as

$$\begin{aligned} \bar{x} &= \lambda \int_0^{\infty} e^{-s} s ds \\ &= -\lambda [e^{-s}(s+1)]_0^{\infty} = \lambda. \end{aligned} \quad (4.13)$$

Thus  $\lambda$  is the mean free path.

A similar argument can be made for the length of time that each molecule survives before being hit. The probability that a molecule is hit during a short time  $dt$  is proportional to  $dt$ : call it  $(1/t_c)dt$ . The number of molecules surviving a time  $t$  is given by  $N = N_0 e^{-t/t_c}$ , and the mean time between collisions can be calculated as above. It is  $t_c$ , which is called the *collision time*. The number of collisions per second is the *collision frequency*,  $1/t_c$ .

It is possible to estimate the mean free path and the collision frequency. Consider a particle of radius  $a_1$  moving through a dilute gas of other particles of radius  $a_2$ . For convenience, imagine that particle 1 is moving and that all the other particles are fixed in position. The path of the first particle is shown in Fig. 4.6. If the center of one of these other molecules lies within a distance  $a_1 + a_2$  of the

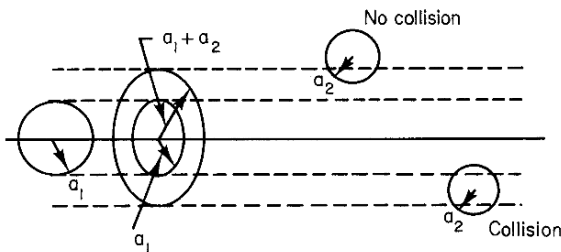


FIGURE 4.6. A particle of radius  $a_1$  moves through a gas of particles of radius  $a_2$ . A collision will occur if the center of another particle lies within a distance  $a_1 + a_2$  of the trajectory of the particle under consideration.

moving molecule, there will be a collision. The effect is the same as if the moving particle had radius  $a_1 + a_2$  and all the other particles were points. In moving a distance  $x$ , the particle sweeps out a volume  $V(x) = \pi(a_1 + a_2)^2 x$ . On average, when the particle has traveled a mean free path there is one collision. The average number of gas particles in the volume  $V(\lambda) = \pi(a_1 + a_2)^2 \lambda$  is therefore 1. The average number of particles per unit volume is  $C$ . Thus,  $1 = C\pi(a_1 + a_2)^2 \lambda$ , or

$$\lambda = \frac{1}{\pi(a_1 + a_2)^2 C}. \quad (4.14)$$

The quantity  $\pi(a_1 + a_2)^2$  is the area of a circle. It is called the *cross section* for the collision of these particles. The concept of cross section is used extensively in Chapter 15.

This estimation is somewhat crude in its assumption that only one molecule is moving. If all the molecules are of the same kind, then the factor 1 in the numerator is replaced by  $2^{-1/2} = 0.707$  [Reif (1965, p. 471)].

For a gas at standard temperature and pressure, the volume of 1 mol is 22.4 liter =  $22.4 \times 10^{-3} \text{ m}^3$ , so  $C = 2.7 \times 10^{25} \text{ m}^{-3}$ . If  $a_1 = a_2 = 0.15 \text{ nm}$ , then Eq. 4.14 can be used to calculate the mean free path:

$$\begin{aligned} \lambda &= \frac{1}{(3.14)(.3 \times 10^{-9})^2 \text{ m}^2 (2.7 \times 10^{25} \text{ m}^{-3})} \\ &= 0.13 \mu\text{m}. \end{aligned}$$

For a gas at standard temperature and pressure, the mean free path is about 1000 times the molecular diameter, and the assumption of infrequent collisions is justified.

The collision time can be estimated by saying that

$$t_c = \frac{\lambda}{\bar{v}},$$

where  $\bar{v}$  is the average speed of the molecules. Using the rms velocity for  $\bar{v}$ , we can use Eq. 4.12 to write

$$t_c \approx \lambda \left( \frac{m}{3k_B T} \right)^{1/2}. \quad (4.15)$$

The important feature of this is the dependence on  $m^{1/2}$  and on  $\lambda$ . For air at room temperature,  $t_c = 2 \times 10^{-10} \text{ s}$ .

## 4.5 Motion in a Liquid

The assumptions of the previous section do not hold in a liquid, in which the particle is being continually bombarded by neighbors. Blindly applying Eq. 4.14 to water, we can use the fact that 1 mol is 18 g and occupies 18  $\text{cm}^3$ , to obtain  $\lambda = 0.1 \text{ nm}$ , so that  $a/\lambda \approx 1$ , and the assumptions behind the derivation break down. Estimating the collision time with Eq. 4.15 gives a value that is a factor of 1000 less than for the gas, or  $10^{-13} \text{ s}$ .

Although these estimates of the mean free path and the collision time are undoubtedly wrong, the concepts

appear to be valid. Computer simulations of molecular collisions show that the distribution of free paths is exponential even though the mean free path is only a fraction of a molecular diameter. In Sec. 4.12 we will regard diffusion as a random walk of the diffusing particles and relate the diffusion constant to the mean free path and collision time. Equations 4.14 and 4.15 can then be used to show that the diffusion constant should be inversely proportional to the square of the particle radius. This has been verified experimentally for the diffusion of certain liquids. Evidence for the validity of this random-walk model for diffusion in liquids has been summarized by Hildebrand *et al.* (1970, pp. 36–39).

A particle in a liquid is subject to a fluctuating force  $\mathbf{F}(t)$ , which is random in magnitude and direction. The particle begins to move in response to this force. However, after it has begun to move, it suffers more collisions in front than behind, so the force slows it down. Because the particle can neither stay at rest nor continue to move in the same direction, it undergoes a random, zig-zag motion with average translational kinetic energy  $3k_B T/2$ . The mean square velocity is not zero, but the mean vector velocity is zero.

For each particle, Newton's second law is  $m(d\mathbf{v}/dt) = \mathbf{F}(t)$ . This is not very useful as it stands. To make it more tractable, consider a particle with average velocity  $\bar{\mathbf{v}}$ . (The average means that an ensemble of identically prepared particles is examined.) The particle has more collisions on the front that slow it down. We therefore break up  $\mathbf{F}(t)$  into two parts: an average drag force, which will be the same for all the particles in the ensemble, and a rapidly fluctuating part  $\mathbf{g}(t)$ , which will vary with time and from particle to particle. Newton's second law is then  $m(d\mathbf{v}/dt) = (\text{drag force}) + \mathbf{g}(t)$ , where  $\mathbf{g}(t)$  is random in direction. The drag force will be zero when  $\bar{\mathbf{v}}$  is zero. For average velocities that are not too large it can be approximated by a linear term:

$$(\text{drag force}) = -\beta\bar{\mathbf{v}}.$$

With this approximation, Newton's second law is known as the *Langevin equation*:

$$m\frac{d\mathbf{v}}{dt} = -\beta\bar{\mathbf{v}} + \mathbf{g}(t). \quad (4.16)$$

(If the liquid is moving, the drag force will be zero when the particle has the same average velocity as the liquid. So  $\bar{\mathbf{v}}$  can be interpreted as the relative velocity of the particle with respect to the liquid.) This equation often has another term in it, which does not average to zero and which represents some external force such as gravity that acts on all the particles. This approximate equation can be solved in some cases, though with difficulty, and has formed the basis for some treatments of the motion of large particles in fluids. With suitable interpretation, it can describe motion of the fluid molecules themselves.<sup>5</sup>

<sup>5</sup>See, for example, Pryde (1966, p. 161).

In particular, when dealing with molecular motion it is necessary to consider the fact that the molecules do not move independently of one another.

For a Newtonian fluid (Eq. 1.33) with viscosity  $\eta$ , one can show (although it requires some detailed calculation<sup>6</sup>) that the drag force on a spherical particle of radius  $a$  is given by

$$\mathbf{F}_{\text{drag}} = -\beta\bar{\mathbf{v}} = -6\pi\eta a\bar{\mathbf{v}}. \quad (4.17)$$

This equation is valid when the sphere is so large that there are many collisions of fluid molecules with it and when the velocity is low enough so that there is no turbulence. This result is called *Stokes' law*.

If the sphere is not moving in an infinite medium but is confined within a cylinder, then a correction must be applied.<sup>7</sup> In that case the viscous drag depends on the velocity of the spherical particle through the fluid, the average velocity of the fluid through the cylinder, and the distance of the particle from the axis of the cylinder.<sup>8</sup>

## 4.6 Diffusion: Fick's First Law

Diffusion is the random movement of particles from a region of higher concentration to a region of lower concentration. The diffusing particles move independently of one another; they may collide frequently with the molecules of the fluid in which they are immersed, but they rarely collide with one another. The surrounding fluid may be at rest, in which case diffusion is the only mechanism for transport of the solute, or it may be flowing, in which case it carries the solute along with it (solvent drag). Both effects can occur together.

We first consider diffusion from a macroscopic point of view and write down an approximate differential equation to describe it. We then obtain a second equation describing diffusion by combining this with the continuity equation. After discussing some solutions to these

<sup>6</sup>This is an approximate equation. See Barr (1931, p. 171).

<sup>7</sup>An early correction for particles on the axis of a cylinder is found in Barr (1931), p. 183. More recent work is by Levitt (1975), Bean (1972), and Paine and Scherr (1975).

<sup>8</sup>Stokes' law is valid for a particle in a gas if the mean free path is much less than the particle radius  $a$ , so that many collisions with neighboring molecules occur. At the other extreme, a mean free path much greater than the particle radius, the drag force turns out to be  $F_{\text{drag}} = \alpha\eta a(a/\lambda)\bar{\mathbf{v}}$ . Although this will not be directly useful to us in considering biological systems, it is mentioned here to show how important it is to understand the conditions under which an equation is valid. Although the dimensions of this new equation are unchanged (we have introduced a factor  $a/\lambda$ , which is dimensionless), the drag force depends on  $a^2$  instead of on  $a$ . The reason for the difference is that collisions are now infrequent and that the probability of a collision that imparts some average momentum change is proportional to the projected cross-sectional area of the sphere,  $\pi a^2$ . In the regime of interest to us, in which there are many collisions, we would not expect the force to depend on  $\lambda$ . We hope that this will convince you of the danger in using someone else's equation without understanding it.

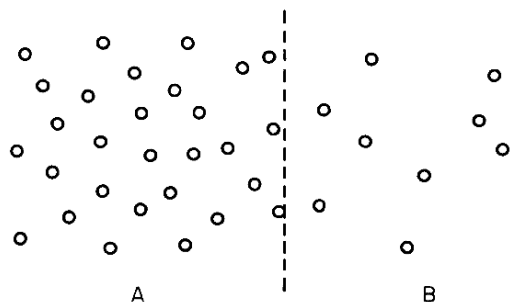


FIGURE 4.7. An example of diffusion. Each molecule at A or B can wander with equal probability to the left or right. There are more molecules at A to wander to the right than there are at B to wander to the left. There is a net flow of molecules from A to B.

equations, we look at the problem from a microscopic point of view, considering the random motion of the particles, and show that we get the same results.

Suppose that the surrounding solvent does not move. If the solute concentration is completely uniform, there is no net flow. As many particles wander to the left as to the right, and the concentration remains the same. There will be local fluctuations in concentration, analogous to those we saw in the preceding chapter for fluctuations in the concentration of a gas, but that is all.

However, if the concentration is higher in region A than in region B to the right of it, there are more particles to wander to the right from A to B than there are to wander to the left from B to A (Fig. 4.7). If the problem is one-dimensional, there is no net flow if  $\partial C/\partial x = 0$ , but there is flow if  $\partial C/\partial x \neq 0$ . If the concentration difference is small, then the flux density  $j$  is linearly proportional to the concentration gradient  $\partial C/\partial x$ . The equation is

$$j_x = -D \frac{\partial C}{\partial x}. \tag{4.18a}$$

Constant  $D$  is called the *diffusion constant*. The units of  $D$  are  $\text{m}^2 \text{s}^{-1}$ , as may be seen by noting that the units of  $j$  are (something)  $\text{m}^{-2} \text{s}^{-1}$  and the units of  $\partial C/\partial x$  are (something)  $\text{m}^{-4}$ . This relationship is called *Fick's first law of diffusion*, after Adolf Fick, a German physiologist in the last half of the nineteenth century. The minus sign shows that the flow is in the direction from higher concentration to lower concentration: if  $\partial C/\partial x$  is positive, the flow is in the  $-x$  direction.

If the actual process is not linear, this can be thought of as the first term of a Taylor's series expansion (Appendix D).

Fick's first law is one of many forms of the transport equation. Other forms are shown in Table 4.3. The units of the constant are different for the last three entries in the table because the quantity that appears on the right has different units than the quantity on the left. In each case, however, a fluence rate or flux density (of particles, mass, energy, electric charge, or momentum) is related

TABLE 4.3. Various forms of the transport equation.

Substance flowing	Equation	Units of $j$	Units of the constant
Particles	$j_s = -D \frac{\partial C}{\partial x}$	$\text{m}^{-2} \text{s}^{-1}$	$\text{m}^2 \text{s}^{-1}$
Mass	$j_m = -D \frac{\partial C}{\partial x}$	$\text{kg m}^{-2} \text{s}^{-1}$	$\text{m}^2 \text{s}^{-1}$
Heat	$j_H = -\kappa \frac{\partial T}{\partial x}$	$\text{J m}^{-2} \text{s}^{-1}$ or $\text{kg s}^{-3}$	$\text{J K}^{-1} \text{m}^{-1} \text{s}^{-1}$
Electric charge	$j_e = -\sigma \frac{\partial V}{\partial x}$	$\text{C m}^{-2} \text{s}^{-1}$	$\text{C m}^{-1} \text{s}^{-1} \text{V}^{-1}$ or $\Omega^{-1} \text{m}^{-1}$
Viscosity ( $y$ component of momentum transported in the $x$ direction)	$\frac{F}{S} = -\eta \frac{\partial v_y}{\partial x}$	$\text{N m}^{-2}$ or $\text{kg m}^{-1} \text{s}^{-2}$	$\text{kg m}^{-1} \text{s}^{-1}$ or $\text{Pa s}$

to a rate of change of some other quantity with position. This rate of change is called the *gradient* of the quantity. The gradient is often called the *driving force*. The concentration gradient or driving force causes the diffusion of particles; the temperature gradient “causes” the heat flow; the electric voltage gradient “causes” the current flow; the velocity gradient “causes” the momentum flow.

The diffusive fluence rate can be related to the gradient of the chemical potential of the solute. With the notation  $C_1 = C_s$  and  $C_2 - C_1 = \Delta C_s$ , equation 3.48 can be rewritten as

$$\begin{aligned} \Delta\mu_s &= k_B T \ln(C_2/C_1) = k_B T \ln(1 + \Delta C_s/C_s) \\ &\approx k_B T \Delta C_s/C_s, \end{aligned}$$

from which  $\Delta C_s \approx C_s \Delta\mu_s/k_B T$ , so

$$\frac{\partial C_s}{\partial x} = \frac{C_s}{k_B T} \frac{\partial \mu_s}{\partial x}$$

and

$$j_{sx} = -\frac{DC_s}{k_B T} \frac{\partial \mu_s}{\partial x}. \tag{4.18b}$$

The solute flux density is proportional to the diffusion constant, the solute concentration, and the gradient in the chemical potential per solute particle.

In three dimensions, the flow of particles can point in any direction and have components  $j_x$ ,  $j_y$ , and  $j_z$ . An equation can be written for each component that is analogous to Eq. 4.18a or 4.18b. We can write one vector equation instead of three equations for the three components by defining  $\hat{\mathbf{x}}$ ,  $\hat{\mathbf{y}}$ , and  $\hat{\mathbf{z}}$  to be unit vectors along the



axes. Then

$$j_x \hat{\mathbf{x}} + j_y \hat{\mathbf{y}} + j_z \hat{\mathbf{z}} = -D \left( \frac{\partial C}{\partial x} \hat{\mathbf{x}} + \frac{\partial C}{\partial y} \hat{\mathbf{y}} + \frac{\partial C}{\partial z} \hat{\mathbf{z}} \right).$$

We have created a vector that depends on  $C(x, y, z, t)$  by performing the indicated differentiations on  $C$  and multiplying the results by the appropriate unit vectors. This vector function is the *gradient* of  $C$  in three dimensions:

$$\text{grad } C = \nabla C = \frac{\partial C}{\partial x} \hat{\mathbf{x}} + \frac{\partial C}{\partial y} \hat{\mathbf{y}} + \frac{\partial C}{\partial z} \hat{\mathbf{z}}. \quad (4.19)$$

Fick's first law with this notation is

$$\mathbf{j} = -D \text{grad } C = -D \nabla C. \quad (4.20)$$

Remember that this is simply shorthand for three equations like Eq. 4.18a. If you feel a need to review vector calculus, which deals with the divergence and gradient, an excellent text is the one by Schey (1997).

### 4.7 The Einstein Relationship Between Diffusion and Viscosity

Before we can apply Fick's first law to real problems, we must determine the value of the diffusion constant  $D$ . The experimental determination of  $D$  is often based on Fick's second law of diffusion, which combines the first law with the equation of continuity and is discussed in the next section. It is closely related to the viscosity, as was first pointed out by Albert Einstein. This is not surprising, since diffusion is caused by the random motion of the particles under the bombardment of neighboring atoms, and viscous drag is also caused by the bombardment by neighboring atoms. What is remarkable is that a general relationship between them can be deduced quite easily by imagining just the right sort of experiment.

Consider a collection of particles uniformly suspended in a fluid at rest. Imagine that each particle is suddenly subjected to an external force  $\mathbf{F}_{\text{ext}}$  (such as gravity) that acts in the  $-y$  direction, as shown in Fig. 4.8. The particles will all begin to drift downward, speeding up until the upward viscous force on them balances the external force:  $\mathbf{F}_{\text{ext}} - \beta \bar{\mathbf{v}} = 0$ . In terms of magnitudes,  $F_{\text{ext}} = \beta v$ .

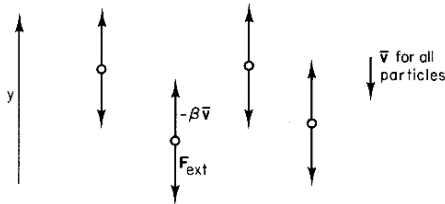


FIGURE 4.8. Particles drifting under the influence of a downward force  $\mathbf{F}_{\text{ext}}$ .

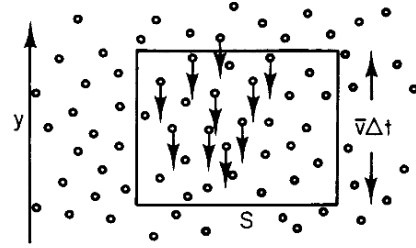


FIGURE 4.9. Calculating the fluence rate of particles drifting downward.

Because these particles are all moving downward, there is a downward flux density. With reference to Fig. 4.9, the number of particles crossing area  $S$  in time  $\Delta t$  will be those within the cylinder of height  $\bar{v} \Delta t$ . That number is the concentration times the volume ( $S \bar{v} \Delta t$ ). Dividing by  $S$  and  $\Delta t$  gives

$$\mathbf{j}_{\text{drift}} = -\bar{v} C(y) \hat{\mathbf{y}}.$$

As the particles move down, they deplete the upper region of the fluid and cause a concentration gradient. This concentration gradient causes an upward diffusion of particles, with a flux density given by

$$\mathbf{j}_{\text{diff}} = -D \frac{\partial C}{\partial y} \hat{\mathbf{y}}.$$

Equilibrium will be established when these two flux densities are equal in magnitude:  $|\mathbf{j}_{\text{drift}}| = |\mathbf{j}_{\text{diff}}|$ ,

$$|\bar{v} C(y)| = \left| D \frac{\partial C}{\partial y} \right|. \quad (4.21)$$

But equilibrium means that the particles have a Boltzmann distribution in  $y$ , because their potential energy increases with  $y$  (work is required to lift them in opposition to  $\mathbf{F}_{\text{ext}}$ ). For a constant  $\mathbf{F}_{\text{ext}}$  independent of  $y$ , the energy is  $u(y) = F_{\text{ext}} y$ , where  $F_{\text{ext}}$  is the magnitude of the force. The concentration is

$$C(y) = C(0) e^{-F_{\text{ext}} y / k_B T}.$$

Therefore

$$\frac{\partial C}{\partial y} = -\frac{F_{\text{ext}}}{k_B T} C(y).$$

Inserting this in Eq. 4.21 gives  $\bar{v} = D F_{\text{ext}} / k_B T$  or  $D = \bar{v} k_B T / F_{\text{ext}}$ . In equilibrium the magnitude of  $F_{\text{ext}}$  is equal to the magnitude of the viscous force  $\mathbf{f}$ . Therefore  $D = k_B T \bar{v} / f$ . Since the viscous force is proportional to the velocity,  $|f| = |\beta \bar{v}|$ ,

$$D = \frac{k_B T}{\beta}. \quad (4.22)$$

The derivation of this equation required only that the velocities be small enough so that the linear approximations for Fick's first law and the viscous force are valid.

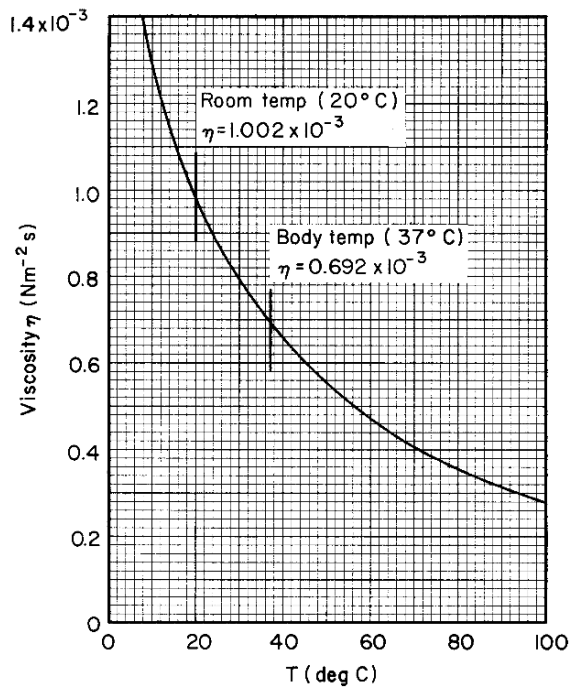


FIGURE 4.10. Viscosity of water at various temperatures. Data are from the *Handbook of Chemistry and Physics*, (1972), 53rd ed., Cleveland, Chemical Rubber, p. F-36.

It is independent of the nature of the particle or its size. If in addition the diffusing particles are large enough so that Stokes' law is valid, then  $\beta = 6\pi\eta a$  and<sup>9</sup>

$$D = \frac{k_B T}{6\pi\eta a}. \quad (4.23)$$

The diffusion constant is inversely proportional to the fluid viscosity and the radius of the particle.

Combining Eqs. 4.18b and 4.22 shows that in terms of the chemical potential,

$$j_{sx} = -\frac{C_s}{\beta} \frac{\partial \mu_s}{\partial x}.$$

Sometimes minus the gradient of the chemical potential is called the driving force. To see why, note that for solvent drag,  $j_s = C_s \bar{v}$ , so  $\beta \bar{v} = -\partial \mu_s / \partial x$  is the driving force.

The viscosity of water varies rapidly with temperature, as shown in Fig. 4.10. These values of viscosity and Eq. 4.23 have been used to calculate the solid lines for  $D$  vs  $a$  shown in Fig. 4.11. Various experimental values are also shown. The diffusion constant increases rapidly with temperature, so that care must be taken to specify the temperature at which the data are obtained. Since not all the molecules are spherical, there is some uncertainty in the value of the particle radius  $a$ .

<sup>9</sup>For self-diffusion (such as radioactively tagged water in water), a hydrodynamic calculation shows that  $\beta = 4\pi\eta a$  [R. B. Bird, W. E. Stewart, and E. N. Lightfoot (1960). *Transport Phenomena*, New York, Wiley, p. 514ff].

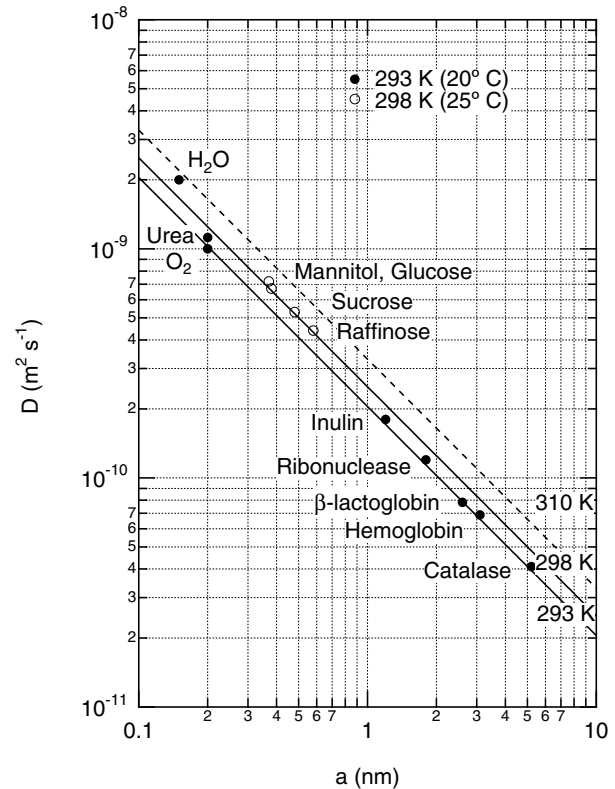


FIGURE 4.11. Diffusion constant versus sphere radius  $a$  for diffusion in water at three different temperatures. Experimental data at 20°C (293 K) are from Benedek and Villars (2000), Vol. 2, p. 122. Data at 25°C (298 K) are from *Handbook of Chemistry and Physics*, (1972), 53rd ed., Cleveland, Chemical Rubber, p. F-47.

Figure 4.12 is a plot of  $D$  for particles diffusing in water at 20°C (293 K) vs. molecular weight  $M$ . Although the solid line provides a rough estimate of  $D$  if  $M$  is known, scatter is considerable because of varying particle shape. DNA lies a factor of 10 below the curve, presumably because it is partially uncoiled and presents a larger size than other molecules of comparable molecular weight.

It is possible to measure the *self-diffusion* of water in water by using a few water molecules in which one hydrogen atom is radioactive and measuring how they diffuse. Water has an unusually large self-diffusion constant.

If all of the molecules shown had the same density, then their radius would depend on  $M^{1/3}$  and the line would have a slope of  $-\frac{1}{3}$ . The slope is steeper than this, suggesting that the molecules are larger for large  $M$  than constant density would predict. This increase in size may be partially attributable to water of hydration. The precise values of diffusion constants depend on many details of the particle structure; however, the lines in Fig. 4.12 provide an order-of-magnitude estimate.

The assumption that the flux depends linearly on the concentration gradient was an approximation. The diffusion constant is found, as a result, to be somewhat concentration dependent.

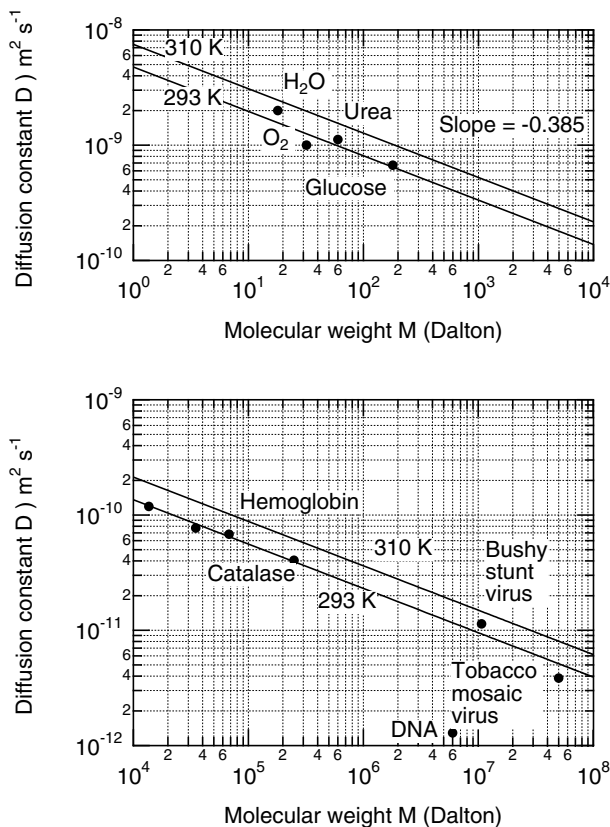


FIGURE 4.12. Diffusion constant versus molecular weight in daltons. (One dalton is the mass of one hydrogen atom.) Data at 293 K are from Benedek and Villars (2000), Vol. 2, p. 122. The 293-K solid line was drawn by eye through the data; the line at 310 K was drawn parallel to it using the temperature change in Eq. 4.23. Data scatter around the line by about 30%, with occasional larger departures.

## 4.8 Fick's Second Law of Diffusion

Fick's first law of diffusion, Eq. 4.18a, is the observation that for small concentration gradients, the diffusive flux density is proportional to the concentration gradient:  $j_x = -D \partial C / \partial x$ . If this is differentiated, one obtains  $\partial j_x / \partial x = -D \partial^2 C / \partial x^2$ . Similar equations hold for the  $y$  and  $z$  directions. The equation of continuity, Eq. 4.2, is

$$-\frac{\partial C}{\partial t} = \frac{\partial j_x}{\partial x} + \frac{\partial j_y}{\partial y} + \frac{\partial j_z}{\partial z}.$$

If we combine these two equations, we get *Fick's second law of diffusion*, also known as the *diffusion equation*:

$$\frac{\partial C}{\partial t} = D \left( \frac{\partial^2 C}{\partial x^2} + \frac{\partial^2 C}{\partial y^2} + \frac{\partial^2 C}{\partial z^2} \right). \quad (4.24)$$

The first law relates the flux of particles to the concentration gradient. The second law tells how the concentration at a point changes with time. It combines the first law and the equation of continuity. The function on the

right-hand side of Eq. 4.24,

$$\frac{\partial^2 C}{\partial x^2} + \frac{\partial^2 C}{\partial y^2} + \frac{\partial^2 C}{\partial z^2},$$

is called the *Laplacian* of  $C$ . It is often abbreviated as  $\nabla^2 C$  (read “del squared  $C$ ”) in American textbooks or  $\Delta C$  in European books. It is given in other coordinate systems in Appendix L.

In principle, if  $C(x, y, z)$  is known at  $t = 0$ , Eq. 4.24 can be solved for  $C(x, y, z, t)$  at all later times. (We develop a general, and sometimes useful, equation for doing this below.) We may also look at this equation as a local equation, telling how  $C$  changes with time at some point if we know how the concentration changes with position in the neighborhood of that point. The change of concentration with position determines the flux  $\mathbf{j}$ . The changes in flux with position determine how the concentration changes with time.

There is extensive literature on how to solve the diffusion equation (or the heat-flow equation, which is the same thing).<sup>10</sup> Instead of discussing a large number of techniques, we show by substitution that a Gaussian or normal distribution function, spreading in a certain way with time, is one solution to Eq. 4.24. In Sec. 4.14 we independently derive the same solution from a random-walk model of diffusion. An important feature of the Gaussian solution is that the center of the distribution of concentration does not move.

For simplicity, consider the one-dimensional case. Take the distribution to be centered at the origin and find those conditions under which<sup>11</sup>

$$C(x, t) = \frac{N}{\sqrt{2\pi\sigma(t)}} e^{-x^2/2\sigma^2(t)}. \quad (4.25)$$

We can view the one-dimensional case in either of two ways. If it represents diffusion along a pipe, then  $C(x, t)$  is the number of particles per unit length in a slice between  $x$  and  $x+dx$ , and  $N$  is the total number of particles. If it represents a three-dimensional problem with concentration changing only in the  $x$  direction, then  $C(x, t)$  is the number of particles per unit volume and  $N$  is the number of particles per unit area.

Equation 4.25 is a solution to the one-dimensional version of Eq. 4.24:

$$\frac{\partial C}{\partial t} = D \frac{\partial^2 C}{\partial x^2}. \quad (4.26)$$

<sup>10</sup>See, for example, Crank (1975) or Carslaw and Jaeger (1959).

<sup>11</sup>The properties of the Gaussian function, Eq. 4.25, are discussed in Appendix I.

To do this, we will need various derivatives of Eq. 4.25. They can be evaluated using the chain rule:

$$\begin{aligned}\frac{\partial C}{\partial t} &= \frac{N}{\sqrt{2\pi}} \left( -\frac{1}{\sigma^2} e^{-x^2/2\sigma^2} + \frac{x^2}{\sigma^4} e^{-x^2/2\sigma^2} \right) \frac{d\sigma}{dt}, \\ \frac{\partial C}{\partial x} &= -\frac{N}{\sqrt{2\pi}} e^{-x^2/2\sigma^2} \frac{x}{\sigma^3}, \\ \frac{\partial^2 C}{\partial x^2} &= \frac{N}{\sqrt{2\pi}} \left( -\frac{1}{\sigma^3} e^{-x^2/2\sigma^2} + \frac{x}{\sigma^3} e^{-x^2/2\sigma^2} \frac{x}{\sigma^2} \right).\end{aligned}$$

When these are substituted in Eq. 4.26, the result is

$$\begin{aligned}\frac{N}{\sqrt{2\pi}\sigma^2} e^{-x^2/2\sigma^2} \left( -1 + \frac{x^2}{\sigma^2} \right) \frac{d\sigma}{dt} \\ = D \frac{N}{\sqrt{2\pi}\sigma^3} e^{-x^2/2\sigma^2} \left( -1 + \frac{x^2}{\sigma^2} \right).\end{aligned}$$

We can divide both sides of this equation by

$$\frac{N}{\sqrt{2\pi}\sigma^2} e^{-x^2/2\sigma^2}$$

because this factor is never zero. The result is

$$\left( \frac{x^2}{\sigma^2} - 1 \right) \frac{d\sigma}{dt} = \frac{D}{\sigma} \left( \frac{x^2}{\sigma^2} - 1 \right).$$

We can divide by  $(x^2/\sigma^2 - 1)$  for all values of  $x$  except  $x = \pm\sigma$ . These values of  $x$  are where the second derivative of  $C$  vanishes; at these points,  $\partial C/\partial t = 0$  for any value of  $\sigma$ . At all other points, the solution will satisfy the equation only if

$$\sigma \frac{d\sigma}{dt} = D.$$

This can be integrated to give

$$\int \sigma d\sigma = \int D dt$$

or

$$\frac{1}{2}\sigma^2(t) = Dt + \text{const.}$$

Multiply through by 2 and observe that  $\sigma^2(0) = 2 \text{ const.}$ , so that

$$\sigma^2(t) = 2Dt + \sigma^2(0). \quad (4.27)$$

If the concentration is initially Gaussian with variance  $\sigma^2(0)$ , after time  $t$  it will still be Gaussian, centered on the same point, with a larger variance given by Eq. 4.27. Figure 4.13 shows this spreading in a typical case. At still earlier times the concentration would have been even more narrowly peaked. In the limit when  $\sigma(t)$  is zero, all the particles are at the origin, giving an infinite concentration. This is, of course, impossible. However, all the particles could be very close to the origin, giving a very tall, narrow curve for  $C(x)$ .

The width of the curve, determined by  $\sigma$ , increases as the square root of the time. A square root increase is

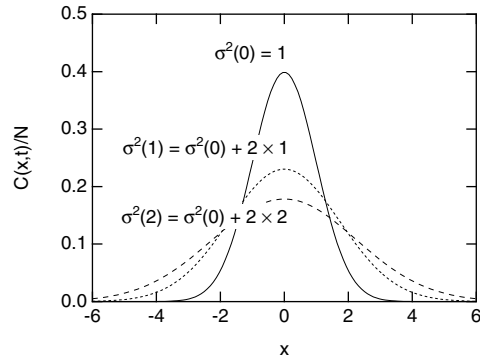


FIGURE 4.13. Spreading of particles by diffusion assuming  $D = 1$ .

less rapid than a linear increase, reflecting the fact that as the particles spread out the concentration does not change as rapidly with distance, so that the flux and the rate of spread decrease.

Note that the rate of change of concentration with time depends on the second derivative of the concentration with distance. This is because the rate of buildup is the flux into a region at some surface minus the flux out through a nearby surface; each flux is proportional to the gradient of the concentration, so the buildup is proportional to the difference in gradients or the second derivative.

In the Problems at the end of this chapter you will discover that diffusion of small particles through water for a distance of  $1 \mu\text{m}$  takes about 1 ms, and diffusion through  $100 \mu\text{m}$  takes  $100^2$  times as long, or 10 s. The times are even longer for larger particles. Thus, diffusion is an effective mode of transport for distances comparable to the size of a cell, but it is too slow for larger distances. This is why multicelled organisms evolve circulatory systems.

## 4.9 Time-Independent Solutions

In this section we develop general solutions for diffusion and solvent drag when particles are conserved and the concentration and fluence rate are not changing with time. The system is in the steady state. The continuity equation, Eq. 4.8, then becomes  $\text{div } \mathbf{j} = 0$ . We consider the solutions for  $C$  and  $\mathbf{j}$  in one, two, and three dimensions when the symmetry is such that  $\mathbf{j}$  depends on only one position coordinate,  $x$  or  $r$ . These solutions are sometimes appropriate models for limited regions of space. There is always some other region of space, serving as a source or sink for the particles that are diffusing, where the model does not apply.

The behavior of  $\mathbf{j}$  can be deduced from the continuity equation. In one dimension, such as flow in a pipe or between two infinite planes, the continuity equation is

$$\frac{dj_x}{dx} = 0, \quad (4.28)$$

which has a solution  $j_x = b_1$  where  $b_1$  is a constant. (The subscript denotes the constant for the one-dimensional case.) The total flux or current  $i$  is constant, so

$$j_x = \frac{i}{S}, \quad (4.29)$$

where  $S$  is the area perpendicular to the flow.

In two dimensions, we consider a problem with cylindrical symmetry and consider only flow radially away from or towards the  $z$  axis. In that case, the equation in Table L.1 for the divergence becomes

$$\frac{1}{r} \frac{d}{dr}(rj_r) = 0, \quad (4.30)$$

from which

$$\frac{d}{dr}(rj_r) = 0. \quad (4.31)$$

This means that  $(rj_r)$  is constant, or

$$j_r = \frac{b_2}{r}. \quad (4.32)$$

This is valid everywhere except along the  $z$  axis, where there is a source of particles and the divergence is not zero. The total current  $i$  leaving a region of length  $L$  parallel to the  $z$  axis is also constant,

$$j_r = \frac{i}{2\pi Lr}. \quad (4.33)$$

In three dimensions with spherical symmetry, the radial component of the divergence is

$$\frac{1}{r^2} \frac{d}{dr}(r^2 j_r) = 0,$$

from which

$$\frac{d}{dr}(r^2 j_r) = 0, \quad (4.34)$$

so that

$$j_r = \frac{b_3}{r^2} \quad (4.35)$$

or

$$j_r = \frac{i}{4\pi r^2}. \quad (4.36)$$

This is valid everywhere except at the origin, where there is a source of particles.

These results depend only on continuity, time independence, and the assumed symmetry. They are true for diffusion, solvent drag, or any other process. Note the progression in going to higher dimensions: in  $n$  dimensions  $r^{n-1}j_r$  is constant.

Now consider how the concentration varies in the two limiting cases of pure solvent drag and pure diffusion. (Section 4.12 discusses what happens when both transport modes are important.)

For solvent drag, the velocity of the solvent is the volume flux density  $\mathbf{j}_v$  which also satisfies the continuity equation. In one dimension  $j_v = i_v/S$ . In two dimensions

$j_v = i_v/2\pi Lr$ , and in three dimensions  $j_v = i_v/4\pi r^2$ . In each case

$$C_s = \frac{j_s}{j_v} = \frac{i_s}{i_v}. \quad (4.37)$$

Since  $C_s$  is constant, there is no diffusion.

For the case of diffusion,  $\mathbf{j} = -D\nabla C$ . In one dimension this becomes

$$\frac{dC}{dx} = -\frac{i}{SD},$$

which is integrated to give

$$C = -\frac{i}{SD}x + b_1,$$

where  $b_1$  is the constant of integration. The concentration varies linearly in the one-dimensional case. If  $i$  is positive (flow in the  $+x$  direction),  $C$  decreases as  $x$  increases. Often the concentration is known at  $x_1$  and  $x_2$ , and one wants to know the current. We can write

$$C_1 = -\frac{i}{SD}x_1 + b_1,$$

$$C_2 = -\frac{i}{SD}x_2 + b_1,$$

and solve for  $i$ :

$$i = \frac{C_1 - C_2}{x_2 - x_1} SD. \quad (4.38a)$$

In two dimensions

$$\frac{dC}{dr} = -\frac{i}{2\pi LD} \frac{1}{r},$$

and the solution is

$$C(r) = -\frac{i}{2\pi LD} \ln r + b_2.$$

We can again solve for the current when the concentrations are known at two different radii:

$$i = \frac{2\pi LD(C_1 - C_2)}{\ln(r_2/r_1)} = \frac{2\pi LD(C_2 - C_1)}{\ln(r_1/r_2)}. \quad (4.38b)$$

Diffusion in two dimensions with cylindrical symmetry has been used to model the concentration of substances in the region between two capillaries.

In three dimensions, the diffusion equation is

$$\frac{dC}{dr} = \frac{i}{4\pi Dr^2},$$

which has a solution

$$C(r) = \frac{i}{4\pi Dr} + b_3.$$

The current in terms of the concentration is

$$i = \frac{4\pi D [C(r_1) - C(r_2)]}{1/r_1 - 1/r_2}. \quad (4.38c)$$

The three-dimensional case is worth further discussion, because it can help us to understand the diffusion of nutrients to a single spherical cell or the diffusion of metabolic

waste products away from the cell. Consider the case in which the cell has radius  $r_1 = R$ , the concentration at the cell surface is  $C_0$ , and the concentration at infinity is zero. Then

$$i = 4\pi D C_0 R, \quad (4.39a)$$

$$C(r) = \frac{C_0 R}{r}, \quad (4.39b)$$

$$j_r = \frac{C_0 D R}{r^2}. \quad (4.39c)$$

The particle current depends on the radius of the cell,  $R$ , not on  $R^2$ . This very important result is not what we might naively expect. Diffusion-limited flow of solute in or out of the cell is proportional not to the cell surface area, but to the cell radius. The reason is that the particle movement is limited by diffusion in the region around the cell, and as the cell radius increases, the concentration gradient decreases. (It is possible for the rate of particle migration into the cell to be proportional to the surface area of the cell if some other process, such as transport through the cell membrane, is the rate-limiting step.)

If diffusion is toward the cell, the concentration is  $C_0$  infinitely far away. At the cell surface, every diffusing molecule that arrives is assumed to be captured, and the concentration is zero. The solutions are then

$$i = -4\pi D C_0 R, \quad (4.40a)$$

$$C(r) = C_0 (1 - R/r), \quad (4.40b)$$

$$j_r(r) = -\frac{C_0 D R}{r^2}. \quad (4.40c)$$

#### 4.10 Example: Steady-State Diffusion to a Spherical Cell and End Effects

In the preceding section we considered diffusion from infinitely far away to the surface of a spherical cell where the concentration was zero. We now add the effect of steady-state diffusion through a series of pores or channels in the cell membrane. This will lead to a very important result: it does not require very many pores per unit area in the cell membrane to “keep up with” the rate of diffusion of chemicals toward or away from the cell. The result is important for understanding how cells acquire nutrients, how bacteria move in response to chemical stimulation (chemotaxis), and how the leaves of plants function.

To develop the model we need one more result: the current due to diffusion from a disk of radius  $a$  where the concentration is  $C_1$  to a plane far away where the concentration is  $C_2$ . The disk is embedded in the surface of an impervious plane as shown in Fig 4.14, so particles cannot cross to the region behind the disk. The current is (Eq. 6.98)

$$i = 4Da (C_1 - C_2). \quad (4.41)$$

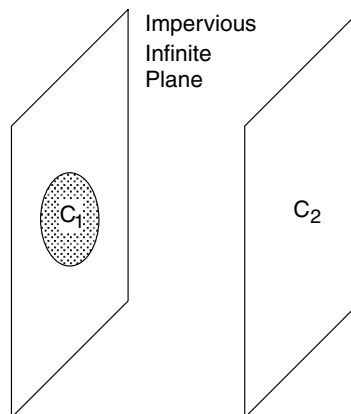


FIGURE 4.14. The diffusion flux from the disk of radius  $a$  and concentration  $C_1$  to the infinite sheet where the concentration is  $C_2$  is given by  $i = 4Da(C_1 - C_2)$ .

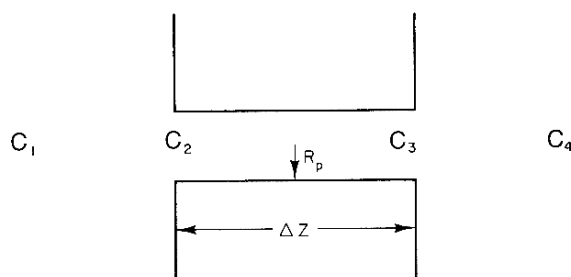


FIGURE 4.15. End effects in diffusion through a pore.

It is proportional to the radius of the disk, not its surface area. [Obtaining this result requires solving the diffusion equation in three dimensions. See Carslaw and Jaeger (1959), p. 215.]

Consider diffusion through a pore of radius  $R_p$  which pierces a membrane of thickness  $\Delta Z$ , including diffusion in the medium on either side of the membrane (Fig. 4.15). If the material on either side were well stirred, there would be a uniform concentration  $C_1$  on the left and  $C_4$  on the right. Because it is not stirred, there is diffusion in the exterior fluid. Let  $C_1$  and  $C_4$  be measured far away, and call the concentrations at the ends of the pore  $C_2$  on the left and  $C_3$  on the right.

Equation 4.38a gives the diffusion flux within the pore

$$i = \frac{\pi R_p^2 D (C_2 - C_3)}{\Delta Z}. \quad (4.42)$$

Diffusion from  $C_1$  to  $C_2$  is given by Eq. 4.41. It is

$$i = 4D R_p (C_1 - C_2), \quad (4.43)$$

while from  $C_3$  to  $C_4$ , it is

$$i = 4D R_p (C_3 - C_4). \quad (4.44)$$

In the steady state, there is no buildup of particles and  $i$  is the same in each region. We can solve Eqs. 4.42–4.44

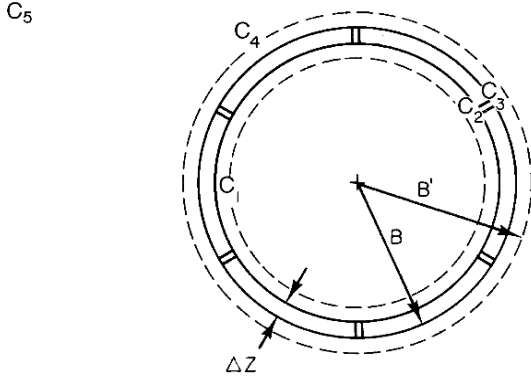


FIGURE 4.16. Diffusive end effects for a spherical cell pierced by pores.

simultaneously to relate  $i$  to concentrations  $C_1$  and  $C_4$ :

$$i = \frac{\pi R_p^2 D}{\Delta Z + 2\pi R_p/4} (C_1 - C_4). \quad (4.45)$$

This has the same form as Eq. 4.42, except that the membrane thickness has been replaced by an effective thickness

$$\Delta Z' = \Delta Z + 2\frac{\pi R_p}{4}. \quad (4.46)$$

An extra length  $\pi R_p/4$  has been added at each end to correct for diffusion in the unstirred layer on each side of the pore. This correction is important when the pore length is less than two or three times the pore radius.

Now consider diffusion in or out of the spherical cell shown in Fig. 4.16. The radius of the cell is  $B$ . The membrane has thickness  $\Delta Z$  and is pierced by a total of  $N$  pores, each of radius  $R_p$ . Within the cell we do not know the details of the concentration distribution, since they depend on what sort of chemical reactions are taking place and where. But we will assume that at the radius where diffusion to the pores becomes important, the concentration is  $C_1$ . At the inner face of each pore it is  $C_2$ , at the outer face it is  $C_3$ , and over an approximately spherical surface of radius  $B'$  it is  $C_4$ . Far away, the concentration is  $C_5$ . As a result, there are four separate regions in which we must consider diffusion. The first is from  $C_1$  to the opening of each pore; the second is through the pore; third, there is diffusion from the outer face of each pore to  $C_4$ ; and, finally, there is diffusion from the spherical object of radius  $B'$  to the surrounding medium.

#### 4.10.1 Diffusion Through a Collection of Pores, Corrected

The first three processes are taken into account by applying the end correction to each end of the pores. The flow through one pore is using Eq. 4.45

$$i_{\text{pore}} = \frac{\pi R_p^2 D}{\Delta Z'} (C_1 - C_4), \quad (4.47)$$

where  $\Delta Z'$  is given by Eq. 4.46. Since there are  $N$  pores in all, the total flow through the cell wall is

$$i_{\text{cell}} = N i_{\text{pore}} = \frac{N\pi R_p^2 D}{\Delta Z'} (C_1 - C_4). \quad (4.48)$$

The diffusion from  $C_4$  to infinity is given by Eq. 4.38c.

$$i_{\text{cell}} = 4\pi D B' (C_4 - C_5), \quad (4.49)$$

where  $B'$  is the effective radius for diffusion to the surrounding medium. It is slightly larger than  $B$ . If we equate Eqs. 4.48 and 4.49, solve for  $C_4$  and substitute this result back in Eq. 4.49, we get

$$i_{\text{cell}} = \frac{4\pi D B' N R_p^2}{N R_p^2 + 4B' \Delta Z'} (C_1 - C_5). \quad (4.50)$$

This can be rewritten as

$$i_{\text{cell}} = \frac{N\pi R_p^2 D}{\Delta Z_{\text{eff}}} (C_1 - C_5), \quad (4.51)$$

where

$$\Delta Z_{\text{eff}} = \Delta Z + 2\frac{\pi R_p}{4} + N\frac{R_p^2}{4B'}. \quad (4.52)$$

The first term in  $\Delta Z_{\text{eff}}$  is the membrane thickness. The second term corrects for diffusion from the end of each pore to the surrounding fluid; the last corrects for diffusion away from the cell into the surrounding medium. The third term can be expressed as

$$\frac{N R_p^2}{4B'} = \frac{B}{B'} B f,$$

where

$$f = \frac{N\pi R_p^2}{4\pi B^2} \quad (4.53)$$

is the fraction of the cell surface occupied by pores.

We now assume that  $B = B'$ . (Problem 28 shows that the difference is usually very small.) The effective pore length is then

$$\Delta Z_{\text{eff}} = \Delta Z + 2\left(\frac{\pi R_p}{4}\right) + B f. \quad (4.54)$$

Equations 4.51–4.54 treat the problem as diffusion through a collection of  $N$  pores, corrected for diffusion outside the pore by increasing the length of the pore.

#### 4.10.2 Diffusion from a Sphere, Corrected

It is also useful to write these results as the equation for diffusion to or from a sphere, Eqs. 4.39, corrected for the diffusion through the cell wall. Writing it in this form gives us insight into how much of the cell wall must be occupied by pores for efficient particle transfer. Solve

Eq. 4.53 for  $NR_p^2$  and substitute the result in Eq. 4.50. The result is

$$\begin{aligned} i_{\text{cell}} &= \frac{4\pi D B' B^2 f (C_1 - C_5)}{B^2 f + B' \Delta Z'} \\ &= 4\pi B D (C_1 - C_5) \left( \frac{B'}{B} \right) \frac{f}{f + (B'/B)(\Delta Z'/B)}. \end{aligned} \quad (4.55)$$

This has the form of diffusion to the sphere multiplied by a correction factor. With  $B'/B$  again approximated by unity, the correction factor is

$$\frac{f}{f + \Delta Z'/B}.$$

The correction factor is zero when  $f$  is zero and becomes nearly unity when the entire cell surface is covered by pores.

#### 4.10.3 How Many Pores Are Needed?

We now ask what fraction of the cell's surface area must be occupied by pores. The cell will receive half the maximum possible diffusive flow when the fraction  $f = \Delta Z'/B$ . For a typical cell with  $B = 5 \mu\text{m}$  and  $\Delta Z = 5 \text{ nm}$ ,  $f = 0.001$ . This is a surprisingly small number, but it means that there is plenty of room on the cell surface for different kinds of pores. There are two ways to understand why this number is so small. First, we can regard the ratio of concentration difference to flow as a resistance, analogous to electrical resistance. The total resistance from the inside of the cell to infinity is made up of the resistance from the outside of the cell to infinity plus the resistance of the parallel combination of  $N$  pores.

When the resistance of this parallel combination is equal to the resistance from the cell to infinity, adding more pores in parallel does not change the overall resistance very much. The second way to look at it is in terms of the random walks of the diffusing solute molecules. When a solute molecule has diffused into the neighborhood of the cell, it undergoes many random walks. When it strikes the cell wall, it wanders away again, to return shortly and strike the cell wall someplace else. If the first contact is not at a pore, there are more opportunities to strike a pore on a subsequent contact with the surface.

#### 4.10.4 Other Applications of the Model

The same sort of analysis that we have made here can be applied to a plane surface area, such as the underside of a leaf [Meidner and Mansfield (1968)] and to a cylindrical geometry, such as a capillary wall.

The analysis can also be applied to the problem of bacterial chemotaxis—the movement of bacteria along concentration gradients. This problem has been discussed in

detail by Berg and Purcell (1977).<sup>12</sup> The cell detects a chemical through some sort of chemical reaction between the chemical and the cell. Suppose that the reaction takes place between the chemical and a binding site of radius  $R_p$  on the surface of the cell. We want to know what fraction of the surface area of the cell must be covered by binding sites. This is similar to the diffusion problem of Eq. 4.55, except that if the binding site is on the surface of the cell, there is no diffusion through a pore of length  $\Delta Z$ . The effective pore length  $\Delta Z'$  is just the end correction for one end of the pore,  $\pi R_p/4$ . Half of the maximum possible flow to the binding site occurs when

$$f = \pi R_p/4B.$$

A typical bacterium might have a radius  $B = 1 \mu\text{m}$ ; the binding site might have a radius of a few atoms or 1 nm. With these values  $f = 7.9 \times 10^{-4}$ . The number of sites would be  $f 4\pi B^2/\pi R_p^2 = \pi B/R_p = 3000$ . There is plenty of room on the cell surface for many different binding sites, each specific for a particular chemical.

An *Escherichia coli* cell typically travels 10–20 body lengths per second. It detects concentration gradients as changes with time. Because of this, Berg and Purcell concluded that a uniform distribution of chemoreceptors over the surface of the cell would be optimum. It would give the highest probability of capture of a chemical molecule that wandered near the cell. However, recent studies of *E. coli* have shown that the receptors are located near the poles of the cell [Maddock and Shapiro (1993); see also the comment by Parkinson and Blair (1993), who point out that the reduced efficiency of sensors could make sense if “eating” or transport into the cell is more important than “smelling.”]

The Berg–Purcell model has been extended to provide a time-dependent solution and allow the receptors not to be perfectly absorbing [Zwanzig and Szabo (1991)] and also to have a process in which the molecules attach to the membrane and then diffuse in the two-dimensional membrane surface [Wang *et al.* (1992); Axelrod and Wang (1994).]

## 4.11 Example: A Spherical Cell Producing a Substance

Here is a simple model that extends the arguments of Sec. 4.9 to develop a steady-state solution for a spherical cell excreting metabolic products. The cell has radius  $R$ . The concentration of some substance inside the cell is  $C(r)$ , independent of time  $t$  and the spherical coordinate angles  $\theta$  and  $\phi$ . (Spherical coordinates are described in Appendix L.) The substance is produced at a constant rate  $Q$  particles per unit volume per second throughout the cell and

<sup>12</sup>See also Berg (1975, 1983) and Purcell (1977).



leaves through the walls of the cell at a constant fluence rate  $j(R)$ , independent of  $t$ ,  $\theta$ , and  $\phi$ . Assume that all transport is by pure diffusion and the diffusion constant for this substance is  $D$  everywhere inside and outside the cell. The material inside the cell is not well stirred. (For this model we assume that the cell membrane does not affect the transport process. We could make the model more complicated by introducing the features described in Sec. 4.10.) With these assumptions, the cell can be modeled as an infinite homogeneous medium with diffusion constant  $D$  that contains a spherical region producing material at rate  $Q$  per unit volume per second.

We first find the concentration  $C(r)$  inside and outside the cell by using a technique that only works because of the spherical symmetry. We use the continuity equation in the form Eq. 4.10b. Because the concentration is not changing with time, the total amount of material flowing through a spherical surface of radius  $r$  is equal to the amount produced within that sphere. For  $r < R$

$$\begin{aligned} 4\pi r^2 j(r) &= 4\pi r^3 Q/3, \\ j(r) &= Qr/3. \end{aligned}$$

For  $r > R$

$$\begin{aligned} 4\pi r^2 j(r) &= 4\pi R^3 Q/3, \\ j(r) &= QR^3/3r^2. \end{aligned}$$

Using the fact that  $j(r) = -DdC/dr$ , we obtain for  $r < R$

$$\begin{aligned} \frac{dC}{dr} &= -\frac{Q}{3D}r, \\ C(r) &= -\frac{Qr^2}{6D} + b_1, \end{aligned}$$

where  $b_1$  is the constant of integration. For  $r > R$ ,

$$\begin{aligned} \frac{dC}{dr} &= -\frac{QR^3}{3Dr^2}, \\ C(r) &= \frac{QR^3}{3Dr} + b_2. \end{aligned}$$

The fact that the concentration must be zero far from the cell means that  $b_2 = 0$ . Matching the two expressions at  $r = R$  gives

$$\begin{aligned} -QR^2/6D + b_1 &= QR^2/3D, \\ b_1 &= QR^2/2D, \end{aligned}$$

so that

$$C(r) = \begin{cases} \frac{Q}{6D}(3R^2 - r^2), & r \leq R \\ \frac{QR^3}{3Dr}, & r \geq R. \end{cases}$$

The other method is more general and can be extended to problems that do not have spherical symmetry. We

find solutions to Fick's second law, modified to include the production term  $Q$  and with the concentration not changing with time:

$$\begin{aligned} 0 &= \frac{\partial C}{\partial t} = D \nabla^2 C + Q, \\ \nabla^2 C &= -\frac{Q}{D}. \end{aligned}$$

In spherical coordinates [Appendix L; Schey (1997)] this is

$$\begin{aligned} \frac{1}{r^2} \frac{\partial}{\partial r} \left( r^2 \frac{\partial C}{\partial r} \right) + \frac{1}{r^2 \sin \theta} \frac{\partial}{\partial \theta} \left( \sin \theta \frac{\partial C}{\partial \theta} \right) \\ + \frac{1}{r^2 \sin^2 \theta} \left( \frac{\partial^2 C}{\partial \phi^2} \right) = -\frac{Q}{D}. \end{aligned}$$

Since there is no angular dependence, we have separate equations for each domain:

$$\frac{1}{r^2} \frac{d}{dr} \left( r^2 \frac{dC}{dr} \right) = \begin{cases} -\frac{Q}{D}, & r < R \\ 0, & r > R. \end{cases}$$

It is necessary to solve each equation in its domain, and then at the boundary require that  $C$  be continuous and also that  $j$  and therefore  $dC/dr$  be continuous. For  $r < R$  we get the following ( $b_1$  and  $b_2$  are constants of integration):

$$\begin{aligned} r^2 \frac{dC}{dr} &= -\frac{Qr^3}{3D} + b_1, \\ \frac{dC}{dr} &= -\frac{Qr}{3D} + \frac{b_1}{r^2}, \\ C(r) &= -\frac{Qr^2}{6D} - \frac{b_1}{r} + b_2. \end{aligned}$$

Since the concentration is finite at the origin,  $b_1 = 0$ :

$$C(r) = b_2 - \frac{Qr^2}{6D}, \quad r < R.$$

For  $r > R$  we can use the general solution with  $Q = 0$  and different constants:

$$C(r) = -\frac{b'_1}{r} + b'_2.$$

Far away the concentration is zero, so  $b'_2 = 0$ . Matching  $dC/dr$  at the boundary gives

$$-\frac{QR}{3D} = \frac{b'_1}{R^2}, \quad b'_1 = -Q \frac{R^3}{3D}.$$

Matching  $C(r)$  at the boundary gives

$$-\frac{QR^2}{6D} + b_2 = -\frac{b'_1}{R}.$$

Putting all of this together gives the same expression for the concentration we had earlier. This technique is a bit more cumbersome, but there are many mathematical tools to extend this technique to cases where there is not spherical symmetry and where  $Q$  is a function of position. These advanced techniques can also be used when  $C$  is changing with time.

## 4.12 Drift and Diffusion in One Dimension

The particle fluence rate due to diffusion in one dimension is  $j_{\text{diff}} = -D(\partial C/\partial x)$ . That of particles drifting with velocity  $v$  is  $j_{\text{drift}} = vC$ . The total flux density or fluence rate is the sum of both terms:

$$j_s = -D \frac{\partial C}{\partial x} + vC. \quad (4.56)$$

The homogeneous ( $j_s = 0$ ) solution was discussed in Sec. 4.7, where cancellation of these two terms in equilibrium was used to derive the relationship between the diffusion constant and viscosity. Using the techniques of Appendix F, we can write the homogeneous solution as

$$C(x) = Ae^{(v/D)x}. \quad (4.57)$$

This can be used to solve the problem of  $j_s = \text{const}$  when the concentration is  $C_0$  at  $x = 0$  and  $C'_0$  at  $x = x_1$ .  $C(x)$  must vary in such a way that the total flux density, the sum of the diffusive and drift terms, is constant. Suppose that both terms give flow from left to right. If the concentration is high, then the drift flux density is large and the concentration gradient must be small. If the concentration is small, the diffusive flux, and hence the gradient, must be large. To develop a formal solution, write Eq. 4.56 as

$$\frac{dC}{dx} - \frac{1}{\lambda}C = -\frac{j_s}{D}, \quad (4.58)$$

where  $\lambda = D/v$  has the dimensions of length and can be interpreted as the distance over which diffusion is important. If the velocity is zero, diffusion is important everywhere and  $\lambda = \infty$ . If the velocity is very large,  $\lambda \rightarrow 0$ . Since  $v$  can be either positive or negative, so can  $\lambda$ . A particular solution to Eq. 4.58 is

$$C(x) = \frac{\lambda j_s}{D} = \frac{j_s}{v}.$$

The general solution is the sum of the particular solution and the homogeneous solution, Eq. 4.57:

$$C(x) = Ae^{x/\lambda} + j_s/v. \quad (4.59)$$

The situation is slightly different than what we encountered in Chap. 2. We must determine two constants,  $A$  and  $j_s$ , given the two concentrations  $C_0$  and  $C'_0$ . Writing Eq. 4.59 for  $x = 0$  and for  $x = x_1$ , we obtain

$$\begin{aligned} C_0 &= A + \frac{j_s}{v}, \\ C'_0 &= Ae^{x_1/\lambda} + \frac{j_s}{v}. \end{aligned} \quad (4.60)$$

Subtracting these gives

$$\begin{aligned} C'_0 - C_0 &= A(e^{x_1/\lambda} - 1), \\ A &= (C'_0 - C_0)/(e^{x_1/\lambda} - 1). \end{aligned} \quad (4.61)$$

This can be combined with either of Eqs. 4.60 to give

$$j_s = \frac{C_0 e^{x_1/\lambda} - C'_0}{e^{x_1/\lambda} - 1} v. \quad (4.62)$$

We can also substitute Eqs. 4.61 and 4.62 in 4.59 to obtain an expression for  $C(x)$ . The result is

$$C(x) = \frac{C_0(e^{x_1/\lambda} - e^{x/\lambda}) + C'_0(e^{x/\lambda} - 1)}{e^{x_1/\lambda} - 1}. \quad (4.63)$$

We will discuss the implications of this equation below.

Let us first determine the average concentration between  $x = 0$  and  $x = x_1$ . The average concentration is defined by

$$\bar{C} = \frac{1}{x_1} \int_0^{x_1} C(x) dx. \quad (4.64)$$

While one could integrate this directly, it is much easier to integrate Eq. 4.56 from 0 to  $x_1$ :

$$-D \int_0^{x_1} \left( \frac{dC}{dx} \right) dx + v \int_0^{x_1} C(x) dx = +j_s \int_0^{x_1} dx.$$

The first term is  $-D(C'_0 - C_0)$ . The second is  $v x_1 \bar{C}$ . The third is  $j_s x_1$ . The equation can therefore be rewritten as

$$v \bar{C} = \frac{D(C'_0 - C_0)}{x_1} + j_s. \quad (4.65)$$

Substituting Eq. 4.62 for  $j_s$  gives the average concentration

$$\bar{C} = \frac{C_0 e^{x_1/\lambda} - C'_0}{e^{x_1/\lambda} - 1} - \frac{\lambda}{x_1} (C_0 - C'_0). \quad (4.66)$$

The exponentials can be expanded to give an approximate expression for small values of  $x_1/\lambda$ <sup>13</sup>

$$\bar{C} = \frac{(C_0 + C'_0)}{2} + \frac{x_1}{\lambda} \frac{1}{12} (C_0 - C'_0). \quad (4.67)$$

For larger values of  $x_1/\lambda$ , the mean can be written

$$\bar{C} = \frac{C_0 + C'_0}{2} + (C_0 - C'_0) G\left(\frac{x_1}{\lambda}\right). \quad (4.68)$$

The correction factor  $G(x_1/\lambda) = G(\xi)$ , given by

$$G(\xi) = \frac{1}{2} \frac{e^\xi + 1}{e^\xi - 1} - \frac{1}{\xi}, \quad (4.69)$$

is plotted in Fig. 4.17. The function is odd, and only values for  $\xi \geq 0$  are shown. For  $\xi = 0$  ( $\lambda = \infty$ , pure diffusion), the average concentration is  $(C_0 + C'_0)/2$ .

Figure 4.18 shows the concentration profile calculated from Eq. 4.63. The concentration is 5 times larger on the left, so diffusion is from left to right. When  $x_1/\lambda =$

<sup>13</sup>See Levitt (1975, p. 537). For  $x_1/\lambda = 1.5$ , this approximation is within 1%. For  $x_1/\lambda = 2.5$ , the error is about 6%.

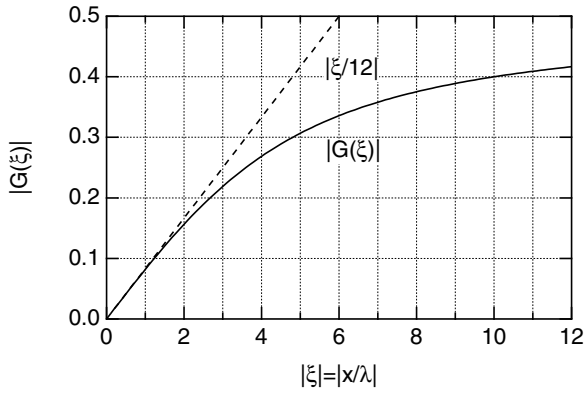


FIGURE 4.17. The correction factor  $G(\xi)$  used in Eq. 4.68. The dashed line is the approximation  $G(\xi) = \xi/12$ , which is valid for small  $\xi$  and is used in Eq. 4.67.

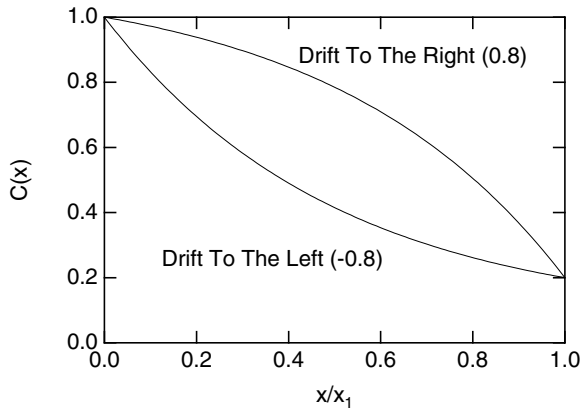


FIGURE 4.18. Concentration profile for combined drift and diffusion. The concentration is 1.0 on the left and 0.2 on the right. For  $x_1/\lambda = x_1v/D = 0.8$ , drift and diffusion are both to the right. As the concentration falls, the magnitude of the gradient increases. For  $x_1/\lambda = x_1v/D = -0.8$  drift opposes diffusion. As the concentration falls, so does the magnitude of the gradient.

$x_1v/D = 0.8$ , drift is also from left to right. As the concentration falls, the magnitude of the gradient rises, so that the sum of the diffusive and drift fluxes remains the same. When  $x_1/\lambda = -0.8$ , drift is opposite to diffusion. Therefore, both the concentration and the magnitude of the gradient must rise and fall together to keep total flux density constant.

Equation 4.65 can be rewritten as

$$j_s = \frac{-D(C'_0 - C_0)}{x_1} + v\bar{C}. \quad (4.70)$$

This can be interpreted as meaning that the fluence rate is given by the sum of a diffusion term with the average concentration gradient and a drift term with the average concentration. However, the discussion in the preceding paragraph showed that there is actually a continuous change of the relative size of the diffusion and drift terms for different values of  $x$ .

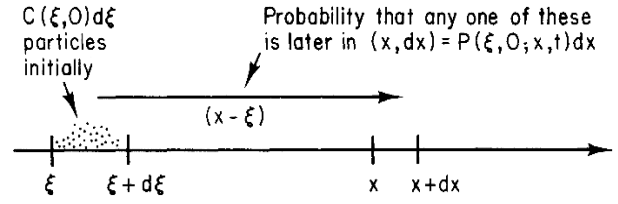


FIGURE 4.19. Diffusion from  $\xi$  to  $x$ .

### 4.13 A General Solution for the Particle Concentration as a Function of Time

If  $C(x, 0)$  is known for  $t = 0$ , it is possible to use the result of Sec. 4.8 to determine  $C(x, t)$  at any later time. The key to doing this is that if  $C(x, t) dx$  is the number of particles in the region between  $x$  and  $x + dx$  at time  $t$ , it may be interpreted as the probability of finding a particle in the interval  $(x, dx)$  multiplied by the total number of particles. (Recall the discussion on p. 91 about the interpretation of  $C(x, t)$ .) The spreading Gaussian then represents the spread of probability that a particle is between  $x$  and  $x + dx$ .

If a particle is definitely at  $x = \xi$  at  $t = 0$ , then  $\sigma^2(0) = 0$ . The particle cannot remain there because of equipartition of energy: collisions cause it to acquire a mean square velocity  $3k_B T/m$  and move. At some later time

$$\sigma(t) = (2Dt)^{1/2}. \quad (4.71)$$

Define  $P(\xi, 0; x, t) dx$  to be the probability that a particle has diffused to a location between  $x$  and  $x + dx$  at time  $t$ , if it was at  $x = \xi$  when  $t = 0$ . This probability is given by Eq. 4.25, except that the distance it has diffused is now  $x - \xi$  instead of  $x$ . The variance  $\sigma^2(t)$  is given by Eq. 4.71. The result is

$$P(\xi, 0; x, t) dx = \frac{1}{\sqrt{4\pi Dt}} e^{-(x-\xi)^2/4Dt} dx. \quad (4.72)$$

The number of particles initially between  $x = \xi$  and  $x = \xi + d\xi$  is the concentration per unit length times the length of the interval  $N = C(\xi, 0)d\xi$ , as shown in Fig. 4.19.

The particles can diffuse in either direction. At a later time  $t$ , the average number between  $x$  and  $x + dx$  that came originally from between  $x = \xi$  and  $x = \xi + d\xi$  is the original number in  $(\xi, d\xi)$  times the probability that each one got from there to  $x$ . This number is a differential of a differential,  $d[C(x, t)dx]$ , because it is only that portion of the particles in  $dx$  that came from the interval  $d\xi$ :

$$d[C(x, t) dx] = C(\xi, 0) d\xi \frac{1}{\sqrt{4\pi Dt}} e^{-(x-\xi)^2/4Dt} dx.$$

To get  $C(x, t)dx$ , it is necessary to integrate over all possible values of  $\xi$ :

$$C(x, t) dx = \frac{1}{\sqrt{4\pi Dt}} \left[ \int_{-\infty}^{\infty} C(\xi, 0) e^{-(x-\xi)^2/4Dt} d\xi \right] dx. \quad (4.73)$$

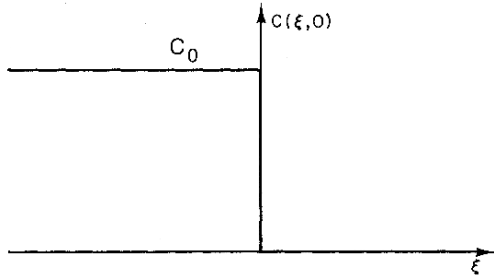


FIGURE 4.20. The initial concentration is constant to the left of the origin and zero to the right of the origin.

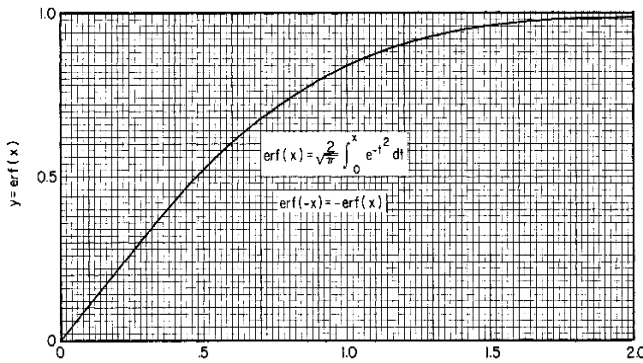


FIGURE 4.21. Plot of the error function erf(x).

This equation can be used to find  $C(x, t)$  at any time, provided that  $C(x, t)$  was known at some earlier time. The factor that multiplies  $C(\xi, 0)$  in the integrand is called the *influence function* or *Green's function* for the diffusion problem; it gives the relative weighting of  $C(\xi, 0)$  in contributing to the later value  $C(x, t)$ .

As an example of using this integral, consider a situation in which the initial concentration has a constant value  $C_0$  from  $\xi = -\infty$  to  $\xi = 0$  and zero for all positive  $\xi$ , as shown in Fig. 4.20. At  $t = 0$  the diffusion starts. The concentration at later times is given by

$$C(x, t) = \frac{C_0}{\sqrt{4\pi Dt}} \int_{-\infty}^0 e^{-(x-\xi)^2/4Dt} d\xi.$$

Such integrals are most easily evaluated by using the *error function* that is tabulated in many mathematical tables. It is defined by

$$\text{erf}(z) = \frac{2}{\sqrt{\pi}} \int_0^z e^{-t^2} dt. \tag{4.74}$$

The error function is plotted in Fig. 4.21. One must be careful in using tables, for other functions tabulated are related to the error function but differ in normalization constants and in the limits of integration.

To use the error function in evaluating the integral in Eq. 4.73, make the substitution  $s = (x - \xi)/(4Dt)^{1/2}$ .

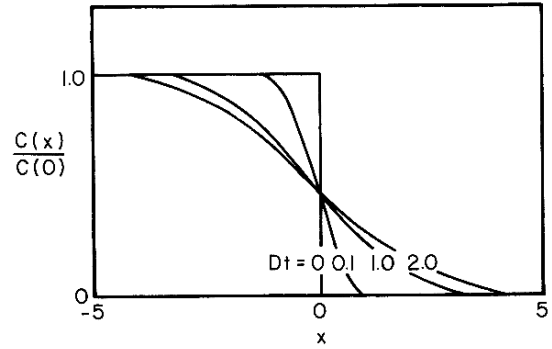


FIGURE 4.22. The spread of an initially sharp boundary due to diffusion.

The integral becomes

$$C(x, t) = \frac{-C_0}{\sqrt{4\pi Dt}} \int_{\infty}^{x/\sqrt{4Dt}} e^{-s^2} \sqrt{4Dt} ds.$$

Since  $\int_A^B f(x) dx = \int_0^B f(x) dx + \int_A^0 f(x) dx = \int_0^B f(x) dx - \int_0^A f(x) dx$ , this can be written as

$$C(x, t) = \frac{-C_0}{\sqrt{\pi}} \left( \int_0^{x/\sqrt{4Dt}} e^{-s^2} ds - \int_0^{\infty} e^{-s^2} ds \right) = \frac{C_0}{2} \left[ 1 - \text{erf}(x/\sqrt{4Dt}) \right]. \tag{4.75}$$

The plot in Fig. 4.22 shows how the initially sharp concentration step becomes more diffuse with passing time. Quantitative measurements of the concentration can be used to determine  $D$ . Benedek and Villars (2000, pp. 126–136) discuss some experiments to verify the solution we have obtained above and to determine  $D$ .

Many other solutions to the diffusion equation and techniques for solving it are known. See Crank (1975) or Carslaw and Jaeger (1959).

### 4.14 Diffusion as a Random Walk

The spreading solution to the one-dimensional diffusion equation that we verified can also be obtained by treating the motion of a molecule as a series of independent steps either to the right or to the left along the  $x$  axis. (The same treatment can be extended to three dimensions, but we will not do so.) The derivation gives us a somewhat simplified molecular picture of diffusion. The derivation also provides an opportunity to see how the Gaussian distribution approximates the binomial distribution. This section is not necessary to understand the rest of Chapters 4 and 5, and you should tackle it only if you are familiar with the binomial and Gaussian probability distributions (Appendices H and I). The model is more restrictive than the diffusion equation derived above, since the latter is the linear approximation to the transport problem.

We use a simplified model in which the diffusing particle always moves in steps of length  $\lambda$  (the mean free path), either in the  $+x$  or  $-x$  direction. Let the total number of steps taken by the particle be  $N$ , of which  $n$  are to the right and  $n'$  are to the left:  $N = n + n'$ . Also let  $m = n - n'$ . The particle's net displacement in the  $+x$  direction is then

$$n\lambda - n'\lambda = m\lambda.$$

Since the steps are independent and a step to the left or right is equally likely ( $p = 1/2$ ), the probability of having a displacement  $m\lambda$  is given by the binomial probability  $P(n; N)$ :

$$P(n; N) = \frac{N!}{(n!)(N-n)!} \left(\frac{1}{2}\right)^n \left(\frac{1}{2}\right)^{n'}. \quad (4.76)$$

Since this problem is analogous to throwing a coin, and we know that on the average we get the same number of heads (steps to the left) as tails (steps to the right), we know that the distribution is centered at  $n = n'$  or  $m = 0$ . We also know [Eq. G.4] that the variance in  $n$  is given by  $\overline{n^2} - \bar{n}^2 = Npq = N/4$ . Since  $\bar{n} = N/2$ , this says that  $\overline{n^2} = N/4 + N^2/4$ . However, we need the variance in  $m$ ,  $\overline{m^2} - \bar{m}^2$ . To obtain it, we write  $m = 2n - N$  and  $m^2 = 4n^2 + N^2 - 4nN$ . Therefore,

$$\overline{m^2} = 4\overline{n^2} + N^2 - 4N\bar{n} = N.$$

The variance of the distribution of displacement  $x$  is equal to the step length  $\lambda$  times the variance in the number of steps:

$$\sigma^2 = \overline{x^2} = \lambda^2 \overline{m^2} = \lambda^2 N.$$

The number of steps is the elapsed time divided by the collision time  $N = t/t_c$ . Therefore,

$$\sigma^2 = \frac{\lambda^2 t}{t_c}.$$

Comparing this with Eq. 4.70, we identify  $D = \lambda^2/2t_c$ , so that

$$\sigma^2 = 2Dt. \quad (4.77)$$

We have shown that this simple model gives a distribution with fixed mean which spreads with a variance proportional to  $t$ . We now must show that the shape is Gaussian. Appendix I shows that the Gaussian is an approximation to the binomial distribution in the limit of large  $N$ . Since  $\sigma_n^2 = N/4$  and  $\bar{n} = N/2$ , Eq. G.4 can be used to write

$$P(n) = \left(\frac{2\pi N}{4}\right)^{-1/2} e^{-(n-N/2)^2/(2N/4)}.$$

This can be rewritten in terms of the net number of steps to the right, since  $m = n - n' = 2n - N$ :

$$P(m) = \left(\frac{2}{\pi N}\right)^{1/2} e^{-m^2/2N}.$$

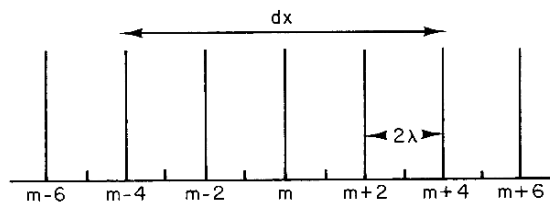


FIGURE 4.23. Relationship between the values of  $x$  and the allowed values of  $m$ . Every other value of  $m$  is missing.

Note that only every other value of  $m$  is allowed. Since  $m = 2n - N$ ,  $m$  goes in steps of 2 from  $-N$  to  $N$  as  $n$  goes from 0 to  $N$ .

To write the probability distribution in terms of  $x$  and  $t$ , refer to Fig. 4.23. The spacing between each allowed value of  $x$  is 2, so that the number of allowed values of  $m$  in interval  $(x, x + dx)$  is  $dx/2\lambda$ . Therefore,  $P(x) dx = P(m)(dx/2\lambda)$ ,

$$P(x) = \sqrt{\frac{2}{\pi N 4\lambda^2}} e^{-m^2/2N}.$$

With the substitutions  $m = x/\lambda$  and  $N = t/t_c$ , this becomes

$$P(x, t) = \sqrt{\frac{t_c}{2\pi\lambda^2 t}} e^{-x^2(t_c/2\lambda^2 t)}.$$

With the substitutions  $D = \lambda^2/2t_c$  and  $C(x, t) = C(0)P(x, t)$ , we obtain Eq. 4.25.

The result of Eq. 4.71 is easily extended to two dimensions. Imagine that a total of  $N$  steps are taken, half in the  $x$  direction and half in the  $y$  direction. Then  $\sigma_x^2 = \sigma_y^2 = \lambda^2(N/2)$ . If  $r^2 = x^2 + y^2$ ,  $\sigma_r^2 = \sigma_x^2 + \sigma_y^2 = \lambda^2 N$ . We still define  $D$  in any direction as  $\lambda^2/2t_c$ , where  $t_c$  is the time between steps in that direction. After a total time  $t$ ,  $N$  steps have been taken, but only half of them were in, say, the  $x$  direction. Therefore  $t_c = 2t/N$ . Therefore

$$\sigma_r^2 = \sigma_x^2 + \sigma_y^2 = 4Dt \quad (\text{two dimensions}). \quad (4.78)$$

A similar argument in three dimensions gives

$$\sigma_r^2 = \sigma_x^2 + \sigma_y^2 + \sigma_z^2 = 6Dt \quad (\text{three dimensions}). \quad (4.79)$$

Figure 4.24 shows the result of a computer simulation of a two-dimensional random walk. A random number is selected to determine whether to step one pixel to the left, up, right, or down—each with the same probability. The trail for 4000 steps is shown in Fig. 4.24(a). The results of continuing for 40,000 steps are shown in Fig. 4.24(b). Note how the particle wanders around one region of space and then takes a number of steps in the same direction to move someplace else. The particle trajectory is “thready.” It does not cover space uniformly. A uniform coverage would be very nonrandom. It is only when many particles are considered that a Gaussian distribution of particle concentration results.

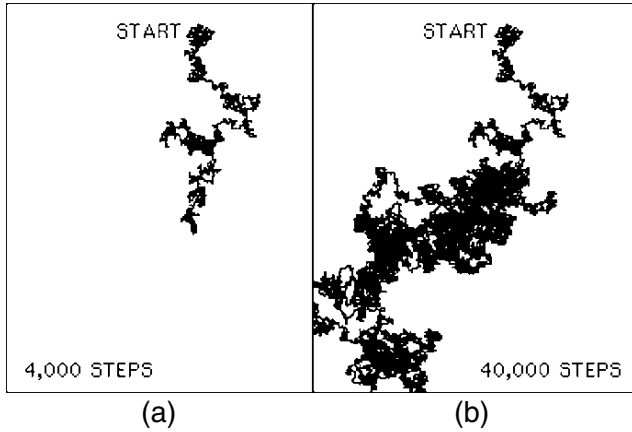


FIGURE 4.24. (a) Trail of a particle for 4000 steps. (b) Trail for additional steps to total 40,000.

Both results in Fig. 4.24 were for the same sequence of random numbers. A computer simulation with 328 runs of 10,000 steps each gave  $\bar{x} = -3.3$ ,  $\sigma_x^2 = 5142$ ,  $\bar{y} = 8.2$ ,  $\sigma_y^2 = 4773$ , and  $\overline{x^2 + y^2} = 10,027$ . The expected values are, respectively, 0, 5000, 0, 5000, and 10,000.

### Symbols Used in Chapter 4

Symbol	Use	Units	First used on page
$a, a_1, a_2$	Particle radius	m	86
$b_1, b_2, b_3$	Constants		93
$f$	Fraction of cell surface area		95
$g$	Gravitational acceleration	$\text{m s}^{-2}$	85
$\mathbf{g}$	Force	N	87
$i$	Particle current	$\text{s}^{-1}$	81
$j, \mathbf{j}, j_s$	Solute fluence rate	$\text{m}^{-2} \text{s}^{-1}$	81
$j_{\text{drift}}, j_{\text{diff}}$	Solute fluence rate due to drift velocity, diffusion	$\text{m}^{-2} \text{s}^{-1}$	89
$\mathbf{j}_m$	Mass fluence rate	$\text{kg m}^{-2} \text{s}^{-1}$	81
$j_n$	Component of $\mathbf{j}$ normal to a surface	$\text{m}^{-2} \text{s}^{-1}$	83
$\mathbf{j}_v$	Volume fluence rate	$\text{m s}^{-1}$	81
$j_x, j_y, j_z$	Components of $\mathbf{j}$	$\text{m}^{-2} \text{s}^{-1}$	83
$k_B$	Boltzmann's constant	$\text{J K}^{-1}$	85
$l$	Linear separation of pores on cell surface	m	106
$m$	Mass	kg	85
$\hat{n}$	Unit vector normal to a surface		101
$n, n'$	Number of steps to right, left		83
$p, q$	Probabilities		101
$r$	Distance, radius	m	83
$s$	Dummy variable		86
$t$	Time	s	81
$t_c$	Collision time	s	86
$u$	Energy of a particle	J	85
$v, \mathbf{v}$	Velocity	$\text{m s}^{-1}$	85
$x, y, z$	Cartesian coordinates	m	81
$A$	Constant		98
$B, B'$	Cell radius	m	95
$C, C_s$	Concentration	$\text{m}^{-3}$	81
$D$	Diffusion constant	$\text{m}^2 \text{s}^{-1}$	88
$F, \mathbf{F}, \mathbf{F}_{\text{ext}}$	Force	N	87
$G$	Correction factor for average concentration		98
$L$	Length	m	93

$M$	Mass	kg	84
$M$	Molecular weight		90
$N, N_0$	Number of molecules		82
$N$	Number of pores on cell surface		95
$N$	Number of steps in a random walk		101
$P$	Rate of energy production (power)	W	83
$P$	Probability		85
$Q$	Rate of creating a substance per unit volume	$\text{m}^{-3} \text{s}^{-1}$	85
$R$	Gas constant	$\text{J K}^{-1} \text{mol}^{-1}$	98
$R$	Radius of a sphere	m	94
$R_p$	Radius of a pore	m	94
$S$	Surface area	$\text{m}^2$	82
$d\mathbf{S}$	Vector surface element pointing in the direction of the normal	$\text{m}^2$	83
$T$	Absolute temperature	K	85
$V$	Volume	$\text{m}^3$	84
$\Delta Z$	Cell membrane thickness	m	94
$\alpha$	Proportionality constant		87
$\beta$	Proportionality constant between force and velocity	$\text{N s m}^{-1}$	87
$\kappa$	Thermal conductivity	$\text{J K}^{-1} \text{m}^{-1} \text{s}^{-1}$	88
$\lambda$	Mean free path	m	86
$\lambda$	Ratio of $D/v$	m	98
$\theta, \phi$	Angles		82
$\eta$	Coefficient of viscosity	Pa s	88
$\sigma$	Standard deviation		91
$\sigma$	Electrical conductivity	$\Omega^{-1} \text{m}^{-1}$	88
$\xi$	Position	m	99
$\xi$	Dimensionless variable		98
$\rho$	Mass density	$\text{kg m}^{-3}$	84
$\mu_s$	Chemical potential of solute	J molecule <sup>-1</sup>	88

### Problems

#### Section 4.1

**Problem 1** A cylindrical pipe with a cross-sectional area  $S = 1 \text{ cm}^2$  and length  $0.1 \text{ cm}$  has  $j_s(0)S = 200 \text{ s}^{-1}$  and  $j_s(0.1)S = 150 \text{ s}^{-1}$ .

(a) What is the total rate of buildup of particles in the pipe?

(b) What is the average rate of change of concentration in the section of pipe?

**Problem 2** Write the continuity equation in cylindrical coordinates if  $j_\phi = 0$  but  $j_r$  and  $j_z$  can be nonzero.

**Problem 3** Consider two concentric spheres of radii  $r$  and  $r + dr$ . If the particle fluence rate points radially and depends only on  $r$ , and the number of particles between  $r$  and  $r + dr$  is not changing, show that  $d(r^2 j)/dr = 0$ .

#### Section 4.2

**Problem 4** Suppose that the total blood flow through a region is  $F$  ( $\text{m}^3 \text{ s}^{-1}$ ). A chemically inert substance is carried into the region in the blood. The total number of molecules of the substance in the region is  $N$ . The amount of blood in the region is not changing. Show that  $dN/dt = (C_A - C_V)F$ , where  $C_A$  and  $C_V$  are the concentrations of substance in the arterial and venous blood. This is known

as the Fick principle or the Fick tracer method. It is often used with radioactive tracers.

### Section 4.3

**Problem 5** R. D. Allen et al. [(1982). *Science* **218**: 1127–1129] report seeing regular movement of particles in the axoplasm of a squid axon. At a temperature of 21 °C, the following mean drift speeds were observed:

Particle size ( $\mu\text{m}$ )	Typical speed ( $\mu\text{m s}^{-1}$ )
0.8 – 5.0	0.8
0.2 – 0.6	2

How do these values compare to thermal speeds? (Make a reasonable assumption about the density of particles and assume that they are spherical.)

### Section 4.4

**Problem 6** (a) Use the ideal gas law,  $pV = Nk_B T = nRT$  to compute the volume of 1 mole of gas at  $T = 30^\circ\text{C}$  and  $p = 1\text{ atm}$ . Express your answer in liters. Show that this is equivalent to a concentration of  $2.4 \times 10^{25}$  molecule  $\text{m}^{-3}$ .

(b) Find the concentration of liquid water molecules at room temperature.

**Problem 7** Using the information on the mean free path in the atmosphere and assuming that all molecules have a molecular weight of 30, find the height at which the mean free path is 1 cm. Assume the atmosphere has a constant temperature.

### Section 4.6

**Problem 8** Suppose  $C(x, t) = \left(N/\sqrt{4\pi Dt}\right)e^{-x^2/4Dt}$ . Find an expression for  $j_s(x, t)$ .

### Section 4.7

**Problem 9** If all macromolecules have the same density, derive the expression for  $D$  versus the molecular weight that was used to draw the line in Fig. 4.12.

**Problem 10** For diagnostic studies of the lung, it would be convenient to have radioactive particles that tag the air and that are small enough to penetrate all the way to the alveoli. It is possible to make the isotope  $^{99\text{m}}\text{Tc}$  into a “pseudogas” by burning a flammable aerosol containing it. The resulting particles have a radius of about 60 nm [W. M. Burch, I. J. Tetley, and J. L. Gras (1984). *Clin. Phys. Physiol. Meas* **5**: 79–85]. Estimate the mean free path for these particles. If it is small compared to the molecular diameter, then Stokes’ law applies, and you can use Eq. 4.23 to obtain the diffusion constant. (The viscosity of air at body temperature is about  $1.8 \times 10^{-5}$  Pa s.)

**Problem 11** Figure 4.12 shows that  $D$  for  $\text{O}_2$  in water at 298 K is  $1.2 \times 10^{-9} \text{ m}^2 \text{ s}^{-1}$  and that the molecular radius of  $\text{O}_2$  is 0.2 nm. The diffusion constant of a dilute gas (where the mean free path is larger than the molecular diameter) is  $D = \lambda^2/2t_c$ , where the collision time is given by Eq. 4.15.

(a) Find a numeric value for the diffusion constant for  $\text{O}_2$  in  $\text{O}_2$  at 1 atm and 298 K and its ratio to  $D$  for  $\text{O}_2$  in water. The molecular weight of oxygen is 32.

(b) Assuming that this equation for a dilute gas is valid in water, estimate the mean free path of an oxygen molecule in water.

### Section 4.8

**Problem 12** (a) The three-dimensional normalized analog of Eq. 4.25 is

$$C(x, y, z, t) = \frac{N}{[2\pi\sigma^2(t)]^{3/2}} \exp\left(-\frac{x^2 + y^2 + z^2}{2\sigma^2(t)}\right).$$

Find the three-dimensional analog of Eq. 4.27.

(b) Show that  $\sigma^2 = \overline{x^2} + \overline{y^2} + \overline{z^2} = 6Dt$ .

**Problem 13** A crude approximation to the Gaussian probability distribution is a rectangle of height  $P_0$  and width  $2L$ . It gives a constant probability for a distance  $L$  either side of the mean.

(a) Determine the value of  $P_0$  and  $L$  so that the distribution has the same value of  $\sigma$  as a Gaussian.

(b) Plot  $P(x, t)$  if  $\sigma$  is given by Eq. 4.27 and the mean remains centered at the origin for times of 1, 5, 50, 100, and 500 ms. Use  $D$  for oxygen diffusing in water at body temperature.

(c) How long does it take for the oxygen to have a reasonable probability of diffusing a distance of 8  $\mu\text{m}$ , the diameter of a capillary?

(d) For  $t = 100$  ms, plot both the accurate Gaussian and the rectangular approximation.

**Problem 14** Write an equation for Fick’s second law in three-dimensional Cartesian coordinates when the diffusion constant depends on position:  $D = D(x, y, z)$ .

**Problem 15** The heat flow equation in one dimension is

$$j_H = -\kappa \left(\frac{\partial T}{\partial x}\right),$$

where  $\kappa$  is the thermal conductivity in  $\text{W m}^{-1} \text{K}^{-1}$ . One often finds an equation for the “diffusion” of energy by heat flow:

$$\frac{\partial T}{\partial t} = D_H \left(\frac{\partial^2 T}{\partial x^2}\right).$$

The units of  $j_H$  are  $\text{J m}^{-2} \text{s}^{-1}$ . The internal energy per unit volume is given by  $u = \rho CT$ , where  $C$  is the heat capacity per unit mass and  $\rho$  is the density of the material. Derive the second equation from the first and show how  $D_H$  depends on  $\kappa$ ,  $C$ , and  $\rho$ .

**Problem 16** The dimensionless “Lewis number” is defined as the ratio of the diffusion constant for molecules and the diffusion constant for heat flow (see Problem 15.) If the Lewis number is large, molecular diffusion occurs much more rapidly than the diffusion of energy by heat flow. If the Lewis number is small, energy diffuses more rapidly than molecules. Use the following parameters:

	Air	Water
$D$ ( $m^2 s^{-1}$ )	$2 \times 10^{-5}$	$2 \times 10^{-9}$
$\kappa$ ( $W m^{-1} K^{-1}$ )	0.03	0.6
$C$ ( $J kg^{-1} K^{-1}$ )	1000	4000
$\rho$ ( $kg m^{-3}$ )	1.2	1000.

(a) Calculate the Lewis number for oxygen in air and in water.

(b) Is it possible using either air or water to design a system in which oxygen is transported by diffusion with almost no transfer of heat?

**Problem 17** A sheet of labeled water molecules starts at the origin in a one-dimensional problem and diffuses in the  $x$  direction.

(a) Plot  $\sigma$  vs  $t$  for diffusion of water in water.

(b) Deduce a “velocity” versus time.

(c) How long does it take for the water to have a reasonable chance of traveling  $1 \mu m$ ?  $10 \mu m$ ?  $100 \mu m$ ?  $1 mm$ ?  $1 cm$ ?  $10 cm$ ?

**Problem 18** In three dimensions the root-mean-square diffusion distance is  $\sigma = \sqrt{6Dt}$ , where  $t$  is the diffusion time. Consider the diffusion of oxygen from air to the blood in the lungs. The terminal air sacs in the lungs, the alveoli, have a radius of about  $100 \mu m$ . The radius of a capillary is about  $4 \mu m$ . Estimate the time for an oxygen molecule to diffuse from the center to the edge of an alveolus, and the time to diffuse from the edge to the center of a capillary. Which is greater? From the data in Table 1.4 estimate how long blood remains in a capillary. Is it long enough for diffusion of oxygen to occur? Assume the diffusion constant of oxygen in air is  $2 \times 10^{-5} m^2 s^{-1}$  and in water is  $2 \times 10^{-9} m^2 s^{-1}$ .

**Problem 19** Why breathe? Estimate the time required for oxygen to diffuse from our nose to our lungs. Assume the diffusion constant of oxygen in air is  $2 \times 10^{-5} m^2 s^{-1}$ .

**Problem 20** At a nerve-muscle junction, the signal from the nerve is transmitted to the muscle by a chemical junction or synapse. In order to activate a muscle, molecules of acetylcholine (ACh) must diffuse from the end of the nerve cell across an extracellular gap about  $20 nm$  wide to the muscle cell. Assuming one-dimensional diffusion, estimate the signal delay caused by the time needed for ACh to diffuse. The delay of the signal at the nerve-muscle junction is about  $0.5 ms$ . How does this compare to the diffusion time? Use a diffusion constant of  $5 \times 10^{-10} m^2 s^{-1}$ .

**Problem 21** A substance has diffusion constant  $D$ , and its concentration is distributed in space according to  $C(x, t) = A(t) \sin(2\pi x/L)$ , where  $L$  is the wavelength and  $A(t)$  is the amplitude of the distribution. Use the one-dimensional diffusion equation, Eq. 4.26, to show that the concentration decays exponentially with time,  $A(t) \propto e^{-t/\tau}$ . Determine an expression for the time constant  $\tau$  in terms of  $L$  and  $D$ . Which decays faster: a long-wavelength (diffuse) distribution, or a short-wavelength (localized) distribution? This result can be used with the Fourier methods developed in Chapter 11 to derive very general solutions to the diffusion equation.

**Problem 22** Some tissues, such as skeletal muscle, are anisotropic: the rate of diffusion depends on direction. In these tissues, Fick’s first law in two dimensions has the form

$$\begin{pmatrix} j_x \\ j_y \end{pmatrix} = - \begin{pmatrix} D_{xx} & D_{xy} \\ D_{yx} & D_{yy} \end{pmatrix} \begin{pmatrix} \partial C / \partial x \\ \partial C / \partial y \end{pmatrix}.$$

The  $2 \times 2$  matrix is called the “diffusion tensor.” It is always symmetric, so  $D_{xy} = D_{yx}$ .

(a) Derive the two-dimensional diffusion equation for anisotropic tissue. Assume the diffusion tensor depends on direction but not on position.

(b) If the coordinate system is rotated from  $(x, y)$  to  $(x', y')$  by

$$\begin{pmatrix} x' \\ y' \end{pmatrix} = \begin{pmatrix} \cos \theta & \sin \theta \\ -\sin \theta & \cos \theta \end{pmatrix} \begin{pmatrix} x \\ y \end{pmatrix},$$

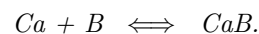
the diffusion tensor changes by

$$\begin{pmatrix} D_{x'x'} & D_{x'y'} \\ D_{x'y'} & D_{y'y'} \end{pmatrix} = \begin{pmatrix} \cos \theta & \sin \theta \\ -\sin \theta & \cos \theta \end{pmatrix} \begin{pmatrix} D_{xx} & D_{xy} \\ D_{xy} & D_{yy} \end{pmatrix} \begin{pmatrix} \cos \theta & -\sin \theta \\ \sin \theta & \cos \theta \end{pmatrix}.$$

Find the angle  $\theta$  such that the tensor is diagonal ( $D_{x'y'} = 0$ ). Typically, this direction is parallel to a special direction in the tissue, such as the direction of fibers in a muscle.

(c) Show that the trace of the diffusion tensor (the sum of the diagonal terms) is the same in any coordinate system ( $D_{xx} + D_{yy} = D_{x'x'} + D_{y'y'}$  for any  $\theta$ ). Basser et al. (1994) invented a way to measure the diffusion tensor using magnetic resonance imaging (Chapter 18). From the diffusion tensor they can image the direction of the fiber tracts. When they want images that are independent of the fiber direction, they use the trace.

**Problem 23** Calcium ions diffuse inside cells. Their concentration is also controlled by a buffer:



The concentrations of free calcium, unbound buffer, and bound buffer ( $[Ca]$ ,  $[B]$ , and  $[CaB]$ ) are governed, assum-



ing the buffer is immobile, by the differential equations

$$\begin{aligned} \frac{\partial [Ca]}{\partial t} &= D\nabla^2[Ca] - k^+[Ca][B] + k^-[CaB], \\ \frac{\partial [B]}{\partial t} &= -k^+[Ca][B] + k^-[CaB], \\ \frac{\partial [CaB]}{\partial t} &= k^+[Ca][B] - k^-[CaB]. \end{aligned}$$

(a) What are the dimensions (units) of  $k^+$  and  $k^-$  if the concentrations are measured in mole  $l^{-1}$  and time in s?

(b) Derive differential equations governing the total calcium and buffer concentrations,  $[Ca]_T = [Ca] + [CaB]$  and  $[B]_T = [B] + [CaB]$ . Show that  $[B]_T$  is independent of time.

(c) Assume the calcium and buffer interact so rapidly that they are always in equilibrium:

$$\frac{[Ca][B]}{[CaB]} = K,$$

where  $K = k^-/k^+$ . Write  $[Ca]_T$  in terms of  $[Ca]$ ,  $[B]_T$ , and  $K$  (eliminate  $[B]$  and  $[CaB]$ ).

(d) Differentiate your expression in (c) with respect to time and use it in the differential equation for  $[Ca]_T$  found in (b). Show that  $[Ca]$  obeys a diffusion equation with an “effective” diffusion constant that depends on  $[Ca]$ :

$$D_{\text{eff}} = \frac{D}{1 + \frac{K[B]_T}{K+[Ca]}}$$

(e) If  $[Ca] \ll K$  and  $[B]_T = 100K$  (typical for the endoplasmic reticulum), determine  $D_{\text{eff}}/D$ .

For more about diffusion with buffers, see Wagner and Keizer (1994).

**Problem 24** Inside cells, calcium is stored in compartments, such as the sarcoplasmic reticulum. In some cells, a rise in calcium concentration,  $C$ , triggers the release of this stored calcium. A model of such “calcium-induced calcium release” is

$$\frac{dC}{dt} = -\frac{k}{C_0^2}C(4C - C_0)(C - C_0) \quad (1)$$

(a) Plot the rate of calcium release (the right-hand side of Eq. 1) vs.  $C$ . Identify points for which the calcium release is zero (steady-state solutions to Eq. 1). By qualitative reasoning, determine which of these points are stable and which are unstable. (Will a small change in  $C$  from the steady-state value cause  $C$  to return to the steady-state value or move farther away from it?)

(b) If  $C \ll C_0/4$ , what does Eq. 1 become, and what is its solution?

(c) Eq. 1 is difficult to solve analytically. To find a numerical solution, approximate it as

$$\frac{C(t + \Delta t) - C(t)}{\Delta t} = -\frac{k}{C_0^2}C(t)[4C(t) - C_0][C(t) - C_0]. \quad (2)$$

Write a computer program to determine  $C(t)$  at times  $t = n\Delta t$ ,  $n = 1, 2, 3, \dots, 100$ , using  $\Delta t = 0.1$  s,  $k = 1$  s $^{-1}$ ,  $C_0 = 1$   $\mu$ M, and  $C(t = 0) = C'$ . Find the threshold value of  $C'$ , below which  $C(t)$  goes to zero, and above which  $C(t)$  goes to  $C_0$ .

(d) If we include diffusion of calcium in one dimension, Eq. 1 becomes

$$\frac{dC}{dt} = D\frac{\partial^2 C}{\partial x^2} - \frac{k}{C_0^2}C(4C - C_0)(C - C_0). \quad (3)$$

This is a type of “reaction-diffusion” equation. To solve Eq. 3 numerically, divide the distance along the cell into discrete points,  $x = m\Delta x$ ,  $m = 0, 1, 2, \dots, M$ . Approximate Eq. 3 as

$$\begin{aligned} \frac{C(x, t + \Delta t) - C(x, t)}{\Delta t} \\ = D\frac{C(x + \Delta x, t) - 2C(x, t) + C(x - \Delta x, t)}{(\Delta x)^2} \\ - \frac{k}{C_0^2}C(x, t)(4C(x, t) - C_0)(C(x, t) - C_0) \end{aligned} \quad (4)$$

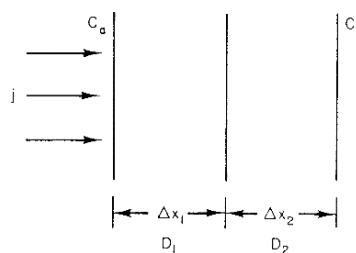
Assume the ends of the cell are sealed, so  $C(0, t) = C(\Delta x, t)$  at one end and  $C(M\Delta x, t) = C((M - 1)\Delta x, t)$  at the other. Start with the cell at  $C(x, 0) = 0$  for all points except at one end, where  $C(0, 0) = C_0$ . Calculate  $C(x, t)$  using  $\Delta x = 5$   $\mu$ m,  $\Delta t = 0.1$  s,  $D = 200$   $\mu$ m $^2$  s $^{-1}$ , and  $C_0 = 1$   $\mu$ M. You should get a wave of calcium propagating down the cell. What is its speed?

Calcium waves play an important role in many cells. This simple model does not include a mechanism to return the calcium concentration to its originally low value after the wave has passed (a process called recovery). For a more realistic model, see Tang and Othmer (1994). For more information about numerical methods, see Press et al. (1992).

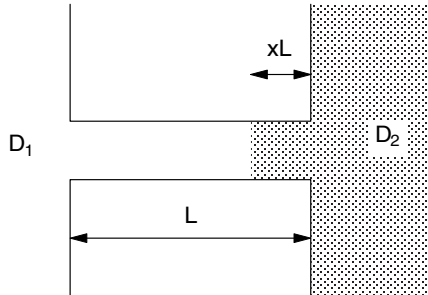
### Section 4.9

**Problem 25** Consider steady-state diffusion through two plane substances as shown in the figure. Show that the diffusion is the same as through a single membrane of thickness  $\Delta x_1 + \Delta x_2$ , with diffusion constant

$$D = \frac{D_1 D_2}{\frac{\Delta x_1}{\Delta x_1 + \Delta x_2} D_2 + \frac{\Delta x_2}{\Delta x_1 + \Delta x_2} D_1}$$



**Problem 26** A fluid on the right of a membrane has different properties than the fluid on the left. Let the diffusion constants on left and right be  $D_1$  and  $D_2$ , respectively, and let the pores in the membrane be filled by the fluid on the right a distance  $xL$ , where  $L$  is the thickness of the membrane.



(a) Use the results of Problem 25 to determine the effective diffusion constant  $D$  for a membrane of thickness  $L$  when  $D_2 = \gamma D_1$ ,  $\Delta x_1 = (1 - x)L$ , and  $\Delta x_2 = xL$ . Neglect end effects.

(b) In the case that oxygen is diffusing in air and water at 310 K, the diffusion constants are  $D_1 = 2.2 \times 10^{-5} \text{ m}^2 \text{ s}^{-1}$ ,  $D_2 = 1.6 \times 10^{-9} \text{ m}^2 \text{ s}^{-1}$ . Plot  $D/D_1$  vs  $x$ .

Section 4.10

**Problem 27** (a) Derive Eq. 4.45.

(b) Derive Eqs. 4.51 and 4.52 from Eqs. 4.48 and 4.49.

**Problem 28** We can estimate  $B/B'$  of Eqs. 4.49–4.55 by noting that  $B'$  must be larger than  $B$  because of two effects. First, it is larger by  $\pi R_p/4$  because of end effects. Second, the concentration varies near the pores and smooths out further away, so  $B'$  must also be larger by an amount roughly equal to  $l$ , the spacing of the pores. There are  $N/4\pi B^2$  pores per  $\text{m}^2$ , so  $l \approx R_p(\pi/f)^{1/2}$ . Use the example in the text:  $B = 5 \text{ }\mu\text{m}$ ,  $\Delta Z = 5 \text{ nm}$ ,  $f = 0.001$ , to estimate these two corrections. Assume that the pore radius,  $R_p$ , is smaller than  $\Delta Z$ . Are these corrections important?

**Problem 29** Consider an impervious plane at  $z = 0$  containing a circular disk of radius  $a$  having a concentration  $C_0$ . The concentration at large  $z$  goes to zero. Carslaw and Jaeger (1959) show that the steady-state solution to the diffusion equation is

$$C(r, z) = \frac{2C_0}{\pi} \sin^{-1} \left[ \frac{2a}{\sqrt{(r-a)^2 + z^2} + \sqrt{(r+a)^2 + z^2}} \right]$$

(a) (optional) Verify that  $C(r, z)$  satisfies  $\nabla^2 C = 0$ . The calculation is quite involved, and you may wish to use a computer algebra program such as Mathematica or Maple.

(b) Show that for  $z = 0$ ,  $C = C_0$  if  $r < a$ .

(c) Show that for  $z = 0$ ,  $dC/dz = 0$  if  $r > a$ .

(d) Integrate  $j_z$  over the disk ( $z = 0$ ,  $0 < r < a$ ) and show that  $i = 4DaC_0$ .

Section 4.11

**Problem 30** The processes of heat conduction and diffusion are similar: the concentration  $C$  and temperature  $T$  both obey the diffusion equation (Problem 15). Consider a spherical cow of radius  $R$  having a specific metabolic rate  $Q \text{ W kg}^{-1}$ . Assume the temperature of the outer surface of the cow is the same as the surroundings,  $T_{sur}$ . Assume that heat transfer within the cow is by heat conduction.

(a) Calculate the steady-state temperature distribution inside the animal and find the core temperature at the center of the sphere.

(b) Consider a smaller (but still spherical) animal such as a rabbit. What is its core temperature?

(c) Calculate the temperature distribution and core temperature in a rabbit covered with fur of thickness  $d$ .

Assume the bodies of the cow and rabbit have the thermal properties of water and that the fur has the thermal properties of air. Let  $d = 0.03 \text{ m}$  and  $T_{sur} = 20 \text{ }^\circ\text{C}$ .

	Water	Air
$\kappa \text{ (W m}^{-1} \text{ K}^{-1}\text{)}$	0.6	0.03
$C \text{ (J kg}^{-1} \text{ K}^{-1}\text{)}$	4000	1000
$\rho \text{ (kg m}^{-3}\text{)}$	1000	1.2
	Cow	Rabbit
$R \text{ (m)}$	0.3	0.05
$Q \text{ (W kg}^{-1}\text{)}$	0.6	1.6

**Problem 31** The goal of this problem is to estimate how large a cell living in an oxygenated medium can be before it is limited by oxygen transport. Assume the extracellular space is well-stirred with uniform oxygen concentration  $C_0$ . The cell is a sphere of radius  $R$ . Inside the cell oxygen is consumed at a rate  $Q \text{ molecule m}^{-3} \text{ s}^{-1}$ . The diffusion constant for oxygen in the cell is  $D$ .

(a) Calculate the concentration of oxygen in the cell in the steady state.

(b) Assume that if the cell is to survive the oxygen concentration at the center of the cell cannot become negative. Use this constraint to estimate the maximum size of the cell.

(c) Calculate the maximum size of a cell for  $C_0 = 8 \text{ mol m}^{-3}$ ,  $D = 2 \times 10^{-9} \text{ m}^2 \text{ s}^{-1}$ ,  $Q = 0.1 \text{ mol m}^{-3} \text{ s}^{-1}$ . (This value of  $Q$  is typical of protozoa; the value of  $C_0$  is for air and is roughly the same as the oxygen concentration in blood.)

**Problem 32** A diffusing substance is being consumed by a chemical reaction at a rate  $Q$  per unit volume per second. The reaction rate is limited by the concentration of some enzyme, so  $Q$  is independent of the concentration of the diffusing substance. For a slab of tissue of thickness  $b$  with concentration  $C_0$  at both  $x = 0$  and  $x = b$ , solve the equation to find  $C(x)$  in the steady state. This is known as the Warburg equation [Biochem Z. 142: 317–350 (1923)]. It is a one-dimensional model for the consumption of oxygen in tissue: points  $x = 0$  and  $x = b$  correspond to the walls of two capillaries side by side.

**Problem 33** Suppose that a diffusing substance disappears in a chemical reaction and that the rate at which it disappears is proportional to the concentration  $-kC$ . Write down the Fick's second law in this case. Show what the equation becomes if one makes the substitution  $C(x, y, z, t) = C'(x, y, z, t)e^{-kt}$ .

**Problem 34** A spherical cell has radius  $R$ . The flux density through the surface is given by  $j_s = -D \text{grad}C$ . Suppose that the substance in question has concentration  $C(t)$  inside the cell and zero outside. The material outside is removed fast enough so that the concentration remains zero. Using spherical coordinates, find a differential equation for  $C(t)$  inside the cell. The thickness of the cell wall is  $\Delta r \ll R$ .

**Problem 35** The cornea of the eye must be transparent, so it can contain no blood vessels. (Blood absorbs light.) Oxygen needed by the cornea must diffuse from the surface into the corneal tissue. Model the cornea as a plane sheet of thickness  $L = 500 \mu\text{m}$ . The oxygen concentration,  $C$ , is governed by a one-dimensional steady-state diffusion equation

$$D \frac{d^2C}{dx^2} = Q.$$

Assume the cornea is consuming oxygen at a rate  $Q = 4 \times 10^{22}$  molecule  $\text{m}^{-3} \text{s}^{-1}$  and has a diffusion constant  $D = 3 \times 10^{-9} \text{m}^2 \text{s}^{-1}$ . The rear surface of the cornea is in contact with the aqueous humor, which has a uniform oxygen concentration  $C_2 = 1.8 \times 10^{24}$  molecule  $\text{m}^{-3}$ . Consider three cases for the front surface:

(a) Solve the diffusion equation for  $C(x)$  when the front surface is in contact with air, which has an oxygen concentration  $C_1 = 5 \times 10^{24} \text{m}^{-3}$ .

(b) The eye is closed, but a layer of tears maintains the concentration at the front surface that is the same as the aqueous humor:  $C_1 = 1.8 \times 10^{24} \text{m}^{-3}$ . Plot  $C(x)$ .

(c) The eye is covered by an oxygen-impermeable contact lens, so that at the front surface  $dC/dx = 0$ . Solve the diffusion equation and plot  $C(x)$ .

Supplying oxygen to the cornea is a major concern for people who wear contact lenses. Often a tear layer between the contact and cornea, replenished by blinking, is sufficient to keep the cornea oxygenated. If you sleep wearing a contact, this tear layer may not be replenished, and the cornea will be deprived of oxygen. For a similar but somewhat more realistic model, see Fatt and Bieber (1968).

**Problem 36** The distance  $L$  that oxygen can diffuse in the steady state is approximately  $L = \sqrt{CD/Q}$ , where  $C$  is the oxygen concentration,  $D$  is the diffusion constant, and  $Q$  is the rate per unit volume that oxygen is used for metabolism.

(a) Show that  $L$  has dimensions of length.

(b) The diffusion of oxygen in air is about 10,000 times larger than the diffusion of oxygen in water [Denny (1993)]. By how much will the diffusion distance  $L$

change if oxygen diffuses through air instead of water, all other things being equal?

Insects deliver oxygen to their flight muscles by diffusion down air-filled tubes instead of by blood vessels, thereby taking advantage of the large diffusion constant of oxygen in air [Weiss-Fogh (1964)].

#### Section 4.12

**Problem 37** Dimensionless numbers, like the Reynolds number of Chapter 1, are often useful for understanding physical phenomena. The "Sherwood number" is the ratio of transport by drift to transport by diffusion. When the Sherwood number is large, drift dominates. The solute fluence rate from drift is  $Cv$ , where  $C$  is the concentration and  $v$  the solvent speed. The solute fluence rate from diffusion is  $D$  times the concentration gradient (roughly  $C/L$ , where  $L$  is some characteristic distance over which the concentration varies).

(a) Determine an expression for the Sherwood number in terms of  $C$ ,  $L$ ,  $v$ , and  $D$ .

(b) Verify that the Sherwood number is dimensionless.

(c) Which parameter in Section 4.12 is equivalent to the Sherwood number?

(d) Estimate the Sherwood number for oxygen for a person walking.

(e) Estimate the Sherwood number for a swimming bacterium. [For more about the Sherwood number, see Denny (1993) and Purcell (1977).]

**Problem 38** Extend Fick's second law in one dimension  $\partial C/\partial t = D(\partial^2 C/\partial x^2)$  to include solvent drag.

**Problem 39** Use Eqs. 4.63 and 4.64 to derive Eq. 4.66.

**Problem 40** Expand  $e^x = 1 + x + x^2/2! + x^3/3!$  to derive Eq. 4.67 from Eq. 4.66.

**Problem 41** Use a Taylor's series expansion to show that  $G(\xi)$  in Eq. 4.69 is equal to  $\xi/12$  for small  $\xi$ .

**Problem 42** Consider Eq. 4.63 with  $C_0 = 0$  and  $C'_0 = 1$ .

(a) If  $v > 0$ , write an equation for  $C(x)$ . Plot  $C(x)$  for  $0 < x/x_1 < 1$  for two cases:  $x_1 \ll \lambda$  and  $x_1 \gg \lambda$ . Interpret these results physically.

(b) Repeat the analysis for  $v < 0$ .

#### Section 4.14

**Problem 43** We can use the microscopic model of a random walk to derive important information about diffusion without ever using the binomial probability distribution. Let  $x_i(n)$  be the position of the  $i$ th particle after  $n$  steps of a random walk. Then

$$x_i(n) = x_i(n) \pm \lambda,$$

where half the time you take the + sign and half the time the – sign. Then  $\bar{x}(n)$ , the value of  $x$  averaged over  $N$  particles, is

$$\bar{x}(n) = \frac{1}{N} \sum_{i=1}^N x_i(n).$$

(a) Show that  $\bar{x}(n) = \bar{x}(n-1)$  so that on average the particles go nowhere.

(b) Show that  $\overline{x^2}(n) = \overline{x^2}(n-1) + \lambda^2$ . Use this result to show that  $\overline{x^2}(n) = n\lambda^2$ .

For a detailed discussion of this approach, see Denny (1993).

**Problem 44** We can write the diffusion constant,  $D$ , and the thermal speed  $v_{rms}$  in terms of the step size,  $\lambda$ , and the collision time,  $t_c$  as

$$D = \frac{\lambda^2}{2t_c},$$

$$v_{rms} = \frac{\lambda}{t_c}.$$

Solve for  $\lambda$  and  $t_c$  in terms of  $D$  and  $v_{rms}$ .

**Problem 45** Using the definitions in Problem 44, write the diffusion constant in terms of  $\lambda$  and  $v_{rms}$ . By how much do you expect the diffusion constant for “heavy water” (water in which the two hydrogen atoms are deuterium,  $^2H$ ) to differ from the diffusion constant for water? Assume the mean free path is independent of mass.

**Problem 46** Write a computer program to model a two-dimensional random walk. Make several repetitions of a random walk of 3600 steps and plot histograms of the displacements in the  $x$  and  $y$  directions and mean square displacement.

**Problem 47** Write a program to display the motion of 100 particles in two dimensions.

**Problem 48** Particles are released from a point between two perfectly absorbing plates located at  $x = 0$  and  $x = 1$ . The particles random walk in one dimension until they strike a plate. Find the probability of being captured by the right-hand plate as a function of the position of release,  $x$ . (Hint: The probability is related to the diffusive fluence rate to the right-hand plate if the concentration is  $C_0$  at  $x$  and is 0 at  $x = 0$  and  $x = 1$ .)

**Problem 49** The text considered a one-dimensional random-walk problem. Suppose that in two dimensions the walk can occur with equal probability along  $+x$ ,  $+y$ ,  $-x$ , or  $-y$ . The total number of steps is  $N = N_x + N_y$ , where the number of steps along each axis is not always equal to  $N/2$ .

(a) What is the probability that  $N_x$  of the  $N$  steps are parallel to the  $x$  axis?

(b) What is the probability that the net displacement along the  $x$  axis is  $m_x\lambda$ ?

(c) Show that the probability of a particle being at  $(m_x\lambda, m_y\lambda)$  after  $N$  steps is

$$P'(m_x, m_y) = \sum_{N_x} \left( \frac{N!}{N_x!(N-N_x)!} \right) \left( \frac{1}{2} \right)^N P(m_x, N_x) P(m_y, N-N_x),$$

where  $P(m, N)$  on the right-hand side of this equation is given by Eq. 4.76.

(d) The factor  $N!/N_x!(N-N_x)!$  is proportional to a binomial probability. What probability? Where does this factor peak when  $N$  is large?

(e) Using the above result, show that  $P'(m_x, m_y) = P(m_x, N/2) P(m_y, N/2)$ .

(f) Write a Gaussian approximation for two-dimensional diffusion.

## References

- Axelrod, D., and M. D. Wang (1994). Reduction-of-dimensionality kinetics at reaction-limited cell surface receptors. *Biophys. J.* **66**(3, Pt. 1): 588–600.
- Barr, G. (1931). *A Monograph of Viscometry*. London, Oxford University Press.
- Basser, P. J., J. Mattiello, and D. LeBihan (1994). MR diffusion tensor spectroscopy and imaging. *Biophys. J.* **66**: 259–267.
- Bean, C. P. (1972). The physics of neutral membranes—neutral pores, in G. Eisenman, ed., *Membranes—A Series of Advances*. New York, Dekker, Vol. 1, pp. 1–55.
- Benedek, G. B., and F. M. H. Villars (2000). *Physics with Illustrative Examples from Medicine and Biology. Vol. 2. Statistical Physics*. 2nd. ed. New York, NY, Springer.
- Berg, H. C. (1975). Chemotaxis in bacteria. *Ann. Rev. Biophys. Bioeng.* **4**: 119–136.
- Berg, H. C. (1983). *Random Walks in Biology*. Princeton, NJ, Princeton University Press.
- Berg, H. C., and E. M. Purcell (1977). Physics of chemoreception. *Biophys. J.* **20**: 193–219.
- Crank, J. (1975). *The Mathematics of Diffusion*. 2nd. ed. New York, Oxford University Press.
- Carslaw, H. S., and J. C. Jaeger (1959) *Conduction of Heat in Solids*. New York, Oxford University Press.
- Denny, M. W. (1993). *Air and Water: The Biology and Physics of Life’s Media*. Princeton, NJ, Princeton University Press.
- Fatt, I. and M. T. Bieber (1968). The steady-state distribution of oxygen and carbon dioxide in the in vivo cornea. *Exp. Eye Res.* **7**: 103–112.
- Hildebrand, J. H., J. M. Prausnitz, and R. L. Scott (1970). *Regular and Related Solutions: The Solubility of Gases, Liquids, and Solids*. New York, Van Nostrand Reinhold.

- Levitt, D. (1975). General continuum analysis of transport through pores. I. Proof of Onsager's reciprocity postulate for uniform pore. *Biophys. J.* **15**: 533–551.
- Maddock, J. R., and L. Shapiro (1993). Polar location of the chemoreceptor complex in the *Escherichia coli* cell. *Science* **259**: 1717–1723.
- Meidner, H., and T. A. Mansfield (1968). *Physiology of Stomata*. New York, McGraw-Hill.
- Paine, P. L., and P. Scherr (1975). Drag coefficients for the movement of rigid spheres through liquid-filled cylinders. *Biophys. J.* **15**: 1087–1091.
- Parkinson, J. S., and D. F. Blair (1993). Does *E. coli* have a nose? *Science* **259**: 1701–1702.
- Press, W. H., S. A. Teukolsky, W. T. Vetterling, and B. P. Flannery (1992). *Numerical Recipes in C: The Art of Scientific Computing*, 2nd ed., reprinted with corrections, 1995. New York, Cambridge University Press.
- Pryde, J. A. (1966). *The Liquid State*. London, Hutchinson University Library.
- Purcell, E. M. (1977). Life at low Reynolds number. *Am. J. Phys.* **45**: 3–11.
- Reif, F. (1965). *Fundamentals of Statistical and Thermal Physics*. New York, McGraw-Hill.
- Schey, H. M. (1997). *Div, Grad, Curl, and All That: An Informal Text on Vector Calculus*, 3rd. ed. New York, Norton.
- Tang, Y-h. and J. G. Othmer (1994). A model of calcium dynamics in cardiac myocytes based on the kinetics of ryanodine-sensitive calcium channels. *Biophys. J.* **67**: 2223–2235.
- Wagner, J., and J. Keizer (1994). Effects of rapid buffers on  $\text{Ca}^{++}$  diffusion and  $\text{Ca}^{++}$  oscillations. *Biophys. J.* **67**: 447–456.
- Wang, D., S-y. Gou, and D. Axelrod (1992). Reaction rate enhancement by surface diffusion of adsorbates. *Biophys. Chem.* **43**(2): 117–137.
- Weiss-Fogh, T. (1964). Diffusion in insect wing muscle, the most active tissue known. *J. Exp. Biol.* **41**: 229–256.
- Zwanzig, R., and A. Szabo (1991). Time-dependent rate of diffusion-influenced ligand binding to receptors on cell surfaces. *Biophys. J.* **60**(3): 671–678.

## Transport Through Neutral Membranes

The last chapter discussed some of the general features of solute movement in an infinite medium. Solute particles can be carried along with the flowing solution or they can diffuse. This chapter considers the movement of solute and solvent through membranes, ignoring any electrical forces on the particles.

The movement of electrically neutral particles through aqueous pores in membranes has many applications in physiology. They range from flow of nutrients through capillary walls, to regulation of the amount of fluid in the interstitial space between cells, to the initial stages of the operation of the kidney.

Sections 5.1 through 5.4 are a qualitative introduction to the flow of water through membranes as a result of hydrostatic pressure differences or osmotic pressure differences. The reader who is not interested in the more advanced material can read just this part of the chapter, culminating in the clinical examples of Sec. 5.4.

Sections 5.5 and 5.6 present phenomenological transport equations that are simple linear relationships between the flow of water and solute particles and the pressure and concentration differences that cause the flows. These relationships are valid for any type of membrane as long as a linear relationship adequately describes the flow and the proportionality constants are regarded as experimentally determined quantities. These equations are applied to the artificial kidney in Sec. 5.7.

Section 5.8 presents a simple model for countercurrent transport, which is important in artificial organs, the kidney, and in conserving heat loss from the extremities.

The last section, Sec. 5.9, provides a more advanced treatment of one particular membrane model: a membrane pierced by pores in which electrical forces can be neglected and in which Poiseuille flow takes place. The model leads to expressions for the phenomenological coefficients that can be compared to experimental data, though that is not done here. The last part of the section

uses this model to calculate the forces on a membrane when there are osmotic effects.

### 5.1 Membranes

All cells are surrounded by a membrane 7–10 nm thick. Furthermore, virtually all the physical substructures within the cell are also bounded by membranes. Membranes separate two regions of space; they allow some substances to pass through but not others. The membrane is said to be *permeable* to a substance that can pass through it; it is *semipermeable* when only certain substances can get through. A substance that can pass through is said to be *permeant*.

The simplest model that one can conceive for a semi-permeable membrane is shown in Fig. 5.1(a). A number of pores pierce the membrane. The pores could follow a longer path, as in Fig. 5.1(b). Another simple model is shown in 5.1(c): there are no pores, but small molecules actually “dissolve” in the membrane and diffuse through. Each example in Fig. 5.1 shows water molecules (open circles), solute molecules (small solid circles), and a large protein molecule that cannot pass through the membrane.

In Figs. 5.1(a) and 5.1(b) the motion of the water molecules is quite different from that of the small solute molecules. Each water molecule is in contact with neighboring water molecules so that when the water molecules move, they flow together. The result is the familiar bulk flow that occurs in a pipe. The solute molecules, on the other hand, are so dilute that they seldom collide with one another. Each one undergoes a random walk *independent of other solute molecules* due to collisions with water molecules.

The motion of each solute molecule is *not* independent of the motion of the surrounding water molecules. If the

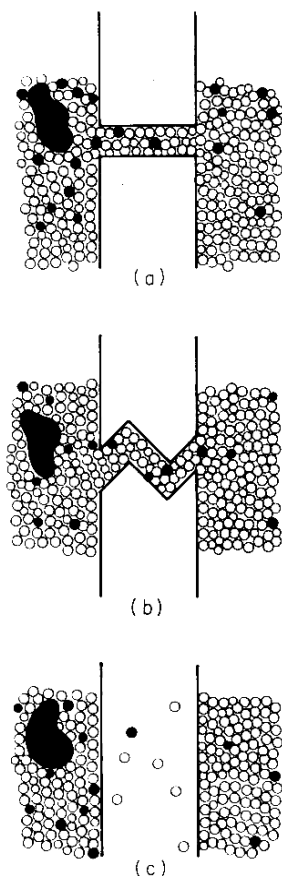


FIGURE 5.1. Simple models for a semipermeable membrane. (a) A straight pore. (b) A pore following a tortuous path. (c) Small molecules dissolve in the membrane and diffuse through.

water is at rest, the movement of the solute molecules is diffusion; if the water is moving, this diffusion is superimposed on a flow of the solute molecules with the moving fluid.

In Fig. 5.1(c), the water and solute molecules are very dilute within the membrane, so that both kinds of molecules diffuse. The water molecules are not in contact with each other, but are in some sort of interstices within the membrane structure, walking randomly in response to thermal agitation of the membrane.

## 5.2 Osmotic Pressure in an Ideal Gas

The selective permeability of a membrane gives rise to some striking effects. The flow of water that occurs because solutes are present that cannot get through the membrane is called *osmosis*. Although the phenomena seem strange when they are first encountered, they can be explained quite simply. They are important in a variety of clinical problems that are described in Sec. 5.4. We begin by finding the conditions under which no flow takes place and the direction of flow when it does occur.

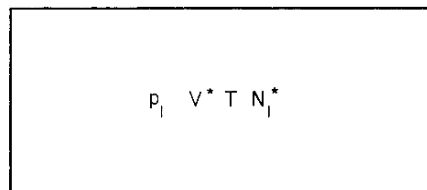


FIGURE 5.2. An ideal gas fills a box of volume  $V^*$ .

Later, in Sec. 5.5, we consider the rate of flow in response to a given pressure difference.

It is easiest to understand osmotic pressure by considering the special case of two ideal gases and a membrane that is permeable to one but not the other. This case is simple because the gas molecules do not interact with one another. Then, in Sec. 5.3, we will examine the phenomenon when the substances are liquids.

Suppose a box with total volume  $V^*$  contains  $N_1^*$  molecules of gas species 1. If the box is at temperature  $T$ , the ideal-gas law relates the pressure, temperature, and the number of molecules:

$$p_1 V^* = N_1^* k_B T. \quad (5.1)$$

This has been written the way physicists like to write it, in terms of the number of molecules  $N_1^*$ . Chemists write it in terms of the number of moles  $n_1^*$ :

$$p_1 V^* = n_1^* R T.$$

The only difference is that  $R$  is per mole instead of per molecule. Since 1 mole contains  $N_A$  molecules, where  $N_A$  is Avogadro's number,  $N_1^* = N_A n_1^*$  and  $R = N_A k_B$ . Numerical values are

$$\begin{aligned} N_A &= 6.022 \times 10^{23} \text{ mol}^{-1}, \\ k_B &= 1.3807 \times 10^{-23} \text{ J K}^{-1}, \\ R &= 8.3145 \text{ J mol}^{-1} \text{ K}^{-1}, \\ R &= 0.08206 \text{ l atm mol}^{-1} \text{ K}^{-1}. \end{aligned}$$

The concentration is the number of molecules or moles per unit volume. We denote *molecular* concentration by capital letter  $C$  and *molar* concentration by lowercase  $c$ :

$$\begin{aligned} C_1 &= \frac{N_1^*}{V^*} \text{ m}^{-3} \text{ or molecules m}^{-3}, \\ c_1 &= \frac{n_1^*}{V^*} \text{ m}^{-3} \text{ or mol m}^{-3}. \end{aligned}$$

If we were to imagine volume  $V^*$  divided into two subvolumes of volume  $V$  and  $V'$ , the average number of molecules in each subvolume would remain unchanged. The pressure in each subvolume would still be  $p_1$ , and the temperature would be  $T$ . We can write

$$p_1 V = N_1 k_B T, \quad p_1 V' = N_1' k_B T.$$

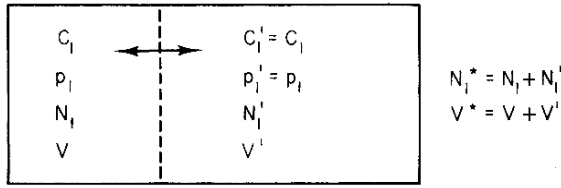


FIGURE 5.3. The introduction of a semipermeable membrane does not change the pressure or concentration of the gas.

Dividing both sides of each equation by the appropriate volume gives

$$p_1 = C_1 k_B T, \quad p_1 = p_1' = C_1' k_B T. \quad (5.2)$$

Now place a membrane along the surface separating the subvolumes, which has small holes so that the molecules can pass through, as shown in Fig. 5.3. This does nothing to change the fact that at equilibrium  $p_1 = p_1'$ . When the pressure is the same on both sides of the membrane, no molecules pass through on average. If the pressure is greater on one side than the other, molecules pass through to bring the pressures into equilibrium, as we saw in Chap. 3. Equations 5.2 say nothing about how frequently a molecule that strikes the membrane passes through. It could take hours or days for equilibrium to be attained if we started away from equilibrium and the molecules do not pass through very often.

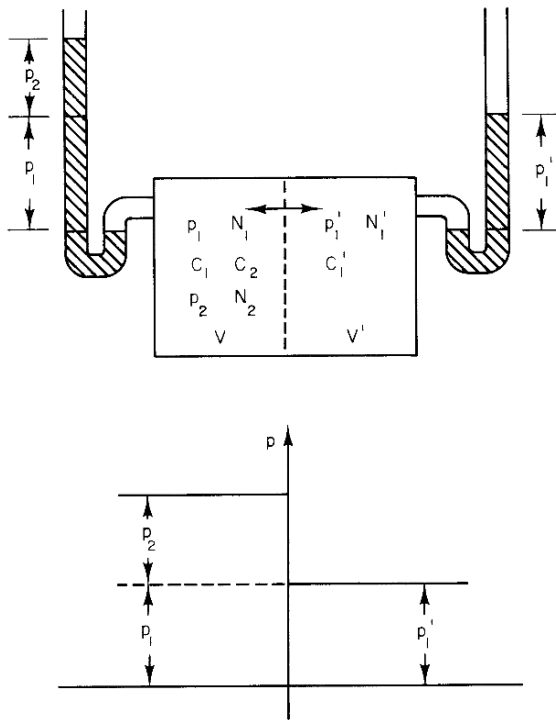


FIGURE 5.4. Species 2, which cannot pass through the membrane, has been introduced in  $V$ . The pressure in  $V$  is higher than in  $V'$  by the partial pressure  $p_2$ .

Now, keeping  $V$  fixed, introduce species 2 on the left as in Fig. 5.4. Suppose that species 2 cannot pass through the membrane. Bombardment of the membrane by the new molecules causes an additional force on the left side of the membrane. The total pressure in volume  $V$  is now the sum of the partial pressures  $p_1$  due to species 1 and  $p_2$  due to the second species:

$$\begin{aligned} p &= p_1 + p_2, \\ p_1 V &= N_1 k_B T, \\ p_2 V &= N_2 k_B T. \end{aligned} \quad (5.3)$$

The ideal-gas law is still obeyed in terms of the total number of molecules in  $V$ ,  $N = N_1 + N_2$ :  $pV = p_1 V + p_2 V = N_1 k_B T + N_2 k_B T = (N_1 + N_2) k_B T = N k_B T$ .

In an ideal gas the presence of the second species does not change the partial pressure  $p_1$ . The total pressure on the walls and the membrane is increased by  $p_2$  so the membrane is bowed towards the right, but the total pressure is simply the sum of the two partial pressures. The ratio  $p_1/p$  is the fraction of the pressure due to collisions of molecules of the first kind with the wall.

Suppose now that the pressure in  $V'$  is raised, either by compressing the gas or by introducing more molecules of type 1, so that instead of  $p_1' = p_1$ , we have  $p_1' = p$ . The partial pressure of species 1 is higher in  $V'$  than in  $V$ . Since these molecules can pass through the membrane, they will flow from  $V'$  to  $V$ . An identical flow could have been caused without having species 2, simply by raising the pressure in  $V'$ . Not every molecule striking the membrane will pass through, but some fraction of all collisions with the wall will result in a molecule passing through. The fraction will depend on the details of the membrane structure. The number going through will be proportional to the number of collisions on one side minus the number of collisions on the other and hence to the difference of partial pressures. If  $p_1 > p_1'$ , species 1 will flow from  $V$  to  $V'$ . If  $p_1 < p_1'$ , the flow will be in the other direction. The details of the membrane will determine how rapid this flow is. *The flow of any species of gas molecule that can pass through the membrane will be from the region of higher partial pressure to lower partial pressure.*

Suppose we start out with only species 1 on each side of the membrane and equal pressure on both sides so that  $p = p_1 = p_1' = p_1'$ . There are three ways to make  $p_1$  less than  $p_1'$ , thereby causing flow from right to left. One is simply to let the gas on the left expand into a larger volume, which lowers  $p = p_1$ . (Or we could have compressed the gas on the right, raising  $p_1' = p_1'$ .) The other two ways involve introducing on the left a species 2 that cannot pass through the membrane. The second way would be to keep the total pressure and volume on the left the same, but remove one molecule of species 1 for every molecule of species 2 that is introduced. The third way would be to increase the volume on the left as each molecule of species 2 is introduced, so that  $p = p_1 + p_2$  remains the same.



The total partial pressure of all species that cannot pass through the membrane is called the *osmotic pressure* in region  $V$  and is usually denoted by  $\pi$ . If the subscript 2 denotes all impermeant species,

$$\pi_2 = C_2 k_B T. \quad (5.4)$$

The flow through the membrane because of an increase in the osmotic pressure or a decrease in the total pressure is identical. In each case the flow is determined by the difference across the membrane of  $p_1$ , the total partial pressure of all the species that can pass through.

The description in the previous paragraphs of partial pressure is easy to visualize, and for the case given it is correct. It is more general, however, to express the condition for equilibrium in terms of the chemical potential. Recall that in Chapter 3 we derived the pressure in terms of volume changes of a system and the chemical potential in terms of the number of particles in the system.

Suppose that the membrane separating the two sides is actually a semipermeable piston that is free to move. Equality of the total pressure on both sides of the piston means that the piston will not move and the two systems will not exchange volume. Equality of the chemical potential of a species that can get through the membrane means that the two systems will not exchange particles. It is better, therefore, to say *the flow of any species that can pass through the membrane will be from the region of higher chemical potential to the region of lower chemical potential for that species. If the chemical potentials are the same, there will be no flow.*

The mixture of two ideal gases is a special case of the ideal solution that was described in Sec. 3.18. The chemical potential of species 1 that can pass through the membrane is given by Eq. 3.78:

$$\begin{aligned} \Delta\mu_1 &= \bar{V}_1(\Delta p - k_B T \Delta C_2), \\ \mu_1 - \mu'_1 &= \bar{V}_1[p - p' - k_B T(C_2 - 0)], \\ \mu_1 - \mu'_1 &= \bar{V}_1(p_1 + p_2 - p'_1 - k_B T C_2). \end{aligned}$$

Since  $p_2 = k_B T C_2$ , the chemical potential is the same on both sides of the membrane when  $p_1 = p'_1$ .

### 5.3 Osmotic Pressure in a Liquid

Imagine now that the two volumes are filled with a solvent, which we will call water. If the pressure of the water is the same in both regions there is no flow of water through the membrane, nor is there exchange of volume if the membrane piston is free to move. Increasing the pressure on one side of the fixed membrane causes water to flow through the membrane from the side with higher pressure to the side with lower pressure. The chemical potential contains a term proportional to the pressure. It

was shown in Sec. 3.18 that for an ideal solution<sup>1</sup>

$$\Delta\mu_w = \frac{\Delta p - k_B T \Delta C_s}{C_w}.$$

If there is a solute in the water that can pass freely through the membrane along with the water, the situation is unchanged.

Now let us add some solute on the left that cannot pass through the membrane. We will keep the volume on the left fixed. To add the solute in such a way that the pressure does not change, we must remove some water molecules as we add it.

We saw in Chapter 3 that replacing some water molecules with solute increases the entropy of the solution.<sup>2</sup> This means that the Gibbs free energy and the chemical potential are decreased. Water flows from the region on the right, where the chemical potential is higher, to the region on the left, where it is lower. The chemical potential of the water on the left can be increased by increasing the total pressure on the left. The osmotic pressure is the excess pressure that we must apply on the left to prevent the flow of water through the membrane. There is no flow of water when  $p = p' + \pi$ . It is more convenient to write all the unprimed quantities on the left:  $p - \pi = p'$ . The quantity  $p - \pi$  will occur so often in what follows that it is worth a special name. We will define the *driving pressure*

$$p_d \equiv p - \pi. \quad (5.5)$$

As far as we know, it has not been used by other authors. It is a monotonic function of the chemical potential. In an ideal solution it is  $C_w \mu_w$ . Except in an ideal gas, it is *not* the same as the partial pressure (a concept that is not normally used in a liquid). On the right there is no solute and  $p'_d = p'$ . *There is no flow when the driving pressure is the same on both sides,*

$$p_d = p'_d, \quad (5.6a)$$

or the chemical potential of the water is the same on both sides,

$$\mu_w = \mu'_w. \quad (5.6b)$$

*The water passes through the membrane in the direction from higher  $p_d$  to lower  $p_d$  (or from higher chemical potential to lower chemical potential). Either the total pressure or the osmotic pressure can be manipulated to change*

<sup>1</sup>An ideal solution can be defined in several equivalent ways. One is that it is a solution that obeys Eq. 3.78. Another is that when the separated components are mixed, there is no change of total volume and no heat is evolved or absorbed. See Hildebrand and Scott (1964), Chapter 2.

<sup>2</sup>This, recall, is because the water molecules are indistinguishable. A simple model shows why this happens. Suppose that four water molecules occupy four identical energy levels, and that these are the only four levels available. Because the molecules are indistinguishable, there is only one microstate and the entropy is zero. If one molecule is removed, there are then four separate microstates, corresponding to the empty level being any one of the four. The entropy is  $k_B \ln(4)$ .

$p_d$  (and  $\mu_w$ ). An increase of total pressure has the same effect as a decrease of osmotic pressure.

Increasing the concentration of the solute increases the osmotic pressure. The fact that  $p_d = p - \pi = C_w \mu_w$  means that for ideal solutions obeying Eq. 3.78,

$$\pi = Ck_B T = cRT. \tag{5.7}$$

In many cases this is confirmed by experiment, particularly in dilute solutions. This is known as the van't Hoff law for osmotic pressure.

An *osmole* is the equivalent of a mole of solute particles. The term *osmolality* is used to refer to the number of osmoles per kilogram of *solvent*, while *osmolarity* refers to the number of osmoles per liter of *solution*. The reason for introducing the osmole is that not all impermeant solutes are ideal; their osmotic effects are slightly less than  $Ck_B T$ . The osmole takes this correction into account.

### 5.4 Some Clinical Examples

As blood flows through capillaries, oxygen and nutrients leave the blood and get to the cells. Waste products leave the cells and enter the blood. Diffusion is the main process that accomplishes this transfer. The capillaries are about the diameter of a red cell; the red cells therefore squeeze through the capillary in single file. They move in plasma, which consists of water, electrolytes, small molecules such as glucose and dissolved oxygen or carbon dioxide, and large protein molecules. All but the large protein molecules can pass through the capillary wall.

Outside the capillaries is the interstitial fluid, which bathes the cells. The concentration of protein molecules in the interstitial fluid is much less than it is in the capillaries. Osmosis is an important factor determining the pressure in the interstitial fluid and therefore its volume. The following values (in units<sup>3</sup> of torr) are typical for the osmotic pressure inside and outside the capillary:<sup>4</sup>

Inside capillary	$\pi_i = 28$ torr
Outside capillary, interstitial fluid	$\pi_o = 5$ torr

Measurements of the total pressure in the interstitial fluid are difficult, but the value seems to be about  $-6$  torr. It is maintained below atmospheric pressure (taken here to be 0 torr) by the rigidity of the tissues. The driving pressure of water and small molecules outside is therefore

$$p_{wo} = p_o - \pi_o = -6 - 5 = -11 \text{ torr.}$$

The total pressure within the capillary drops from the arterial end to the venous end, causing blood to flow along

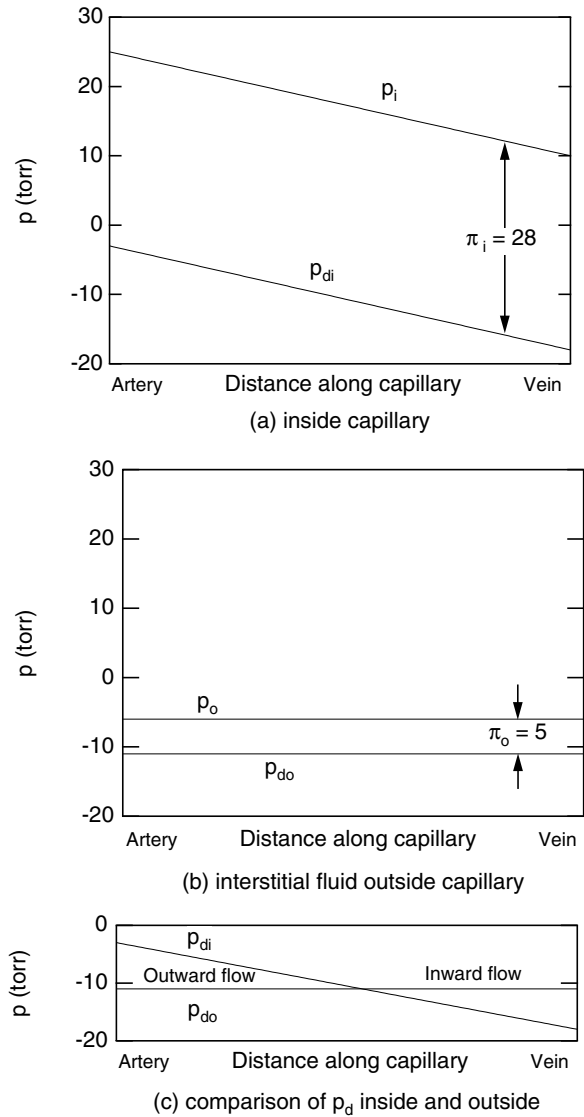


FIGURE 5.5. Pressures inside and outside the capillary. (a) Inside. (b) Outside. (c) Comparison of the water driving pressure inside and outside.

the capillary. A typical value at the arterial end is 25 torr; at the venous end, it is 10 torr. If the drop is linear along the capillary, the total pressures versus position is as plotted in Fig. 5.5(a).<sup>5</sup> Subtracting from this the osmotic pressure of the large molecules gives the curve for the driving pressure inside,  $p_{di}$ , which is also plotted in Fig. 5.5(a). Figure 5.5(b) shows the total and driving pressures in the interstitial fluid. Figure 5.5(c) compares the driving pressure inside and outside. The driving pressure is larger inside in the first half of the capillary and larger outside in the second half of the capillary. The result is an outward flow of plasma through the capillary

<sup>3</sup>1 torr = 1 mm Hg = 133.3 Pa = 0.019 34 lb in.<sup>-2</sup>.

<sup>4</sup>A short account of the pressures used here is found in Guyton (1991, Chapter 16). A more detailed discussion is in Guyton *et al.* (1975).

<sup>5</sup>This simple discussion uses pressures that compensate for the fact that the surface area of the capillary is larger at the venous end than at the arterial end.

wall in the first half and an inward flow in the second half. There is a very slight excess of outward flow. This fluid returns to the circulation via the lymphatic system.

There are three ways that the balance of Fig. 5.5 can be disturbed, each of which can give rise to *edema*, a collection of fluid in the tissue. The first is a higher average pressure along the capillary. The second is a reduction in osmotic pressure because of a lower protein concentration in the blood (hypoproteinemia). The third is an increased permeability of the capillary wall to large molecules, which effectively reduces the osmotic pressure. Each is discussed below.

#### 5.4.1 Edema Due to Heart Failure

A patient in right heart failure exhibits an abnormal collection of interstitial fluid in the lower part of the body (the legs for a walking patient; the back and buttocks for a patient in bed). This can be understood in terms of the mechanism discussed above. The right heart pumps blood from the veins through the lungs. If it can no longer handle this load, the venous blood is not removed rapidly enough, and the pressure in the veins and the venous end of the capillaries rises. There is a corresponding rise in  $p_d$  along the capillary. More fluid flows from the capillary to the interstitial space. The interstitial pressure rises until the net flow is again zero. When the interstitial pressure becomes positive, edema results.

The same process can occur in left heart failure in which the pressure in the pulmonary veins builds up. The patient then has pulmonary edema and may literally drown.

#### 5.4.2 Nephrotic Syndrome, Liver Disease, and Ascites

Patients can develop an abnormally low amount of protein in the blood serum, hypoproteinemia, which reduces the osmotic pressure of the blood. This can happen, for example, in *nephrotic syndrome*. The nephrons (the basic functioning units in the kidney) become permeable to protein, which is then lost in the urine. The lowering of the osmotic pressure in the blood means that the  $p_d$  rises. Therefore, there is a net movement of water into the interstitial fluid. Edema can result from hypoproteinemia from other causes, such as liver disease and malnutrition.

A patient with liver disease may suffer a collection of fluid in the abdomen. The veins of the abdomen flow through the liver before returning to the heart. This allows nutrients absorbed from the gut to be processed immediately and efficiently by the liver. Liver disease may not only decrease the plasma protein concentration, but the vessels going through the liver may become blocked, thereby raising the capillary pressure throughout the abdomen and especially in the liver. A migration of fluid out of the capillaries results. The surface of the liver “weeps”

fluid into the abdomen. The excess abdominal fluid is called *ascites*.

#### 5.4.3 Edema of Inflammatory Reaction

Whenever tissue is injured, whether it is a burn, an infection, an insect bite, or a laceration, a common sequence of events initially occurs that cause edema. They include the following.

1. *Vasodilation*. Capillaries and small blood vessels dilate, and the rate of blood flow is increased. This is responsible for the redness and warmth associated with the inflammatory process.
2. *Fluid exudation*. Plasma, including plasma proteins, leaks from the capillaries because of increased permeability of the capillary wall.
3. *Cellular migration*. The capillary walls become porous enough so that white cells move out of the capillaries at the site of injury.

#### 5.4.4 Headaches in Renal Dialysis

Dialysis is used to remove urea from the plasma of patients whose kidneys do not function. Urea is in the interstitial brain fluid and the cerebrospinal fluid in the same concentration as in the plasma; however, the permeability of the capillary–brain membrane is low, so equilibration takes several hours.<sup>6</sup> Water, oxygen, and nutrients cross from the capillary to the brain at a much faster rate than urea. As the plasma urea concentration drops, there is a temporary osmotic pressure difference resulting from the urea within the brain. The driving pressure of water is higher in the plasma, and water flows to the brain interstitial fluid. Cerebral edema results, which can cause severe headaches.

The converse of this effect is to inject into the blood urea or mannitol, another molecule that does not readily cross the blood–brain barrier. This lowers the driving pressure of water within the blood, and water flows from the brain into the blood. Although the effects do not last long, this technique is sometimes used as an emergency treatment for cerebral edema.<sup>7</sup>

#### 5.4.5 Osmotic Diuresis

The functional unit of the kidney is the *nephron*. Water and many solutes pass into the nephron from the blood at the glomerulus. As the urine flows through the rest of the nephron, a series of complicated processes cause a net reabsorption of most of the water and varying amounts of the solutes. Some medium-weight molecules such as

<sup>6</sup>Patton *et al.* (1989), Chapter 64.

<sup>7</sup>Fishman (1975); White and Likavek (1992).

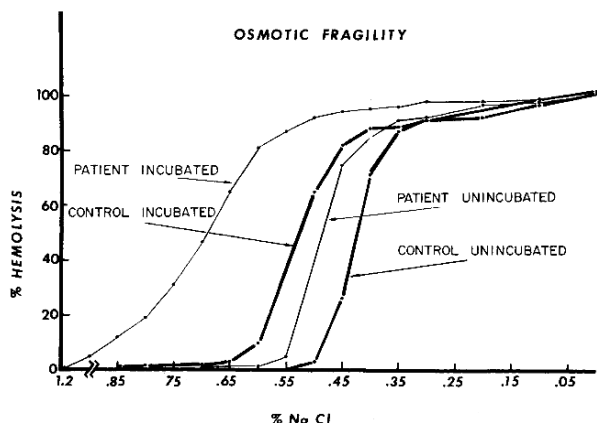


FIGURE 5.6. Osmotic fragility of red cells. The different curves are discussed in the text. From S. I. Rappoport (1971). *Introduction to Hematology*. New York, Harper & Row, p. 99. Reproduced by permission of Harper & Row.

mannitol are not reabsorbed at all. If they are present in the nephron, for example, from intravenous administration, the driving pressure of water is lowered and less water is reabsorbed than would be normally. The result is an increase in urine volume and a dehydration of the patient called osmotic diuresis.<sup>8</sup> Similar diuretic action takes place in a diabetic patient who “spills” glucose into the urine.

#### 5.4.6 Osmotic Fragility of Red Cells

Red cells (erythrocytes) are normally disk-shaped, with the center thinner than the rim. In the disease called *hereditary spherocytosis* the red cells are more rounded. If a red cell is placed in a solution that has a higher driving pressure than that inside the cell, water moves in and the cell swells until it bursts. Since cell membranes (as distinct from the lining of capillaries) are nearly impermeable to sodium, sodium is osmotically active for this purpose.

The osmotic fragility test consists of placing red cells in solutions with different sodium concentrations and determining what fraction of the cells burst. A typical plot of fraction vs. sodium concentration is shown in Fig. 5.6. Sodium concentration decreases and  $p_d$  increases to the right along the axis.

The patient with hereditary spherocytosis has cells that will be destroyed at a lower external  $p_d$  (higher sodium concentration) than normal, because the membrane is more permeable to the sodium.

If the red cells are incubated at body temperature in a sodium solution with the osmolality of plasma for 24 h, the fragility of hereditary spherocytosis cells is markedly increased. During this incubation period the concentration of sodium within the cell *increases*; the sodium can-

<sup>8</sup>Gennari and Kassirer (1974); Guyton (1991).

not escape rapidly when the external concentration is reduced, the driving pressure within the cell is lower than before incubation, and water flows into the cell even more rapidly.

## 5.5 Volume Transport Through a Membrane

In this section and the next we develop phenomenological equations to describe the flow of fluid and the flow of solute through a membrane. These are linear approximations to the dependence of the flows on pressure and solute concentration differences. Three parameters are introduced that are widely used in physiology: the filtration coefficient (or hydraulic permeability), the solute permeability, and the solute reflection coefficient.

The volume fluence rate or volume flow per unit area per second through a membrane is  $J_v$ .

$$J_v = \frac{\left( \begin{array}{c} \text{total volume per second} \\ \text{through membrane area } S \end{array} \right)}{S} = \frac{i_v}{S} \text{ m s}^{-1}. \quad (5.8)$$

Consider pure water. The fluence rate depends on the pressure difference across the membrane. When the pressure difference is zero, there is no flow. The direction of flow, and therefore the sign of the fluence rate, depends on which side of the membrane has the higher pressure. The simplest relationship that has this property is a linear one:<sup>9</sup>

$$J_v = L_p \Delta p. \quad (5.9)$$

The proportionality constant is called the *filtration coefficient* or *hydraulic permeability*. It depends on the details of the membrane structure, such as the properties of the pores. The SI units for  $L_p$  are  $\text{m s}^{-1} \text{ Pa}^{-1}$ ,  $\text{m}^3 \text{ N}^{-1} \text{ s}^{-1}$ , or  $\text{m}^2 \text{ s kg}^{-1}$ . Often in the literature, however, values of  $L_p$  are reported in units of  $(\text{cm/s})/\text{atm}$ . Since  $1 \text{ atm} = 1.01 \times 10^5 \text{ Pa}$ , the conversion is

$$1 \text{ cm s}^{-1} \text{ atm}^{-1} = 0.99 \times 10^{-7} \text{ m s}^{-1} \text{ Pa}^{-1}. \quad (5.10)$$

If a solute is present to which the membrane is completely impermeable, only water will flow, and the flow will depend on  $\Delta p_d$ :

$$\begin{aligned} \Delta p_d &= p_d - p'_d = p - \pi - (p' - \pi') \\ &= p - p' - (\pi - \pi') \\ &= \Delta p - \Delta \pi \end{aligned}$$

so

$$J_v = L_p (\Delta p - \Delta \pi). \quad (5.11)$$

<sup>9</sup>The traditional sign convention has been followed here. There would be a minus sign in the equation if  $\Delta p$  were defined to be  $p(x + \Delta x) - p(x)$ . However, it is usually defined as  $p - p'$ . The flow is from the region of higher pressure to the region of lower pressure.

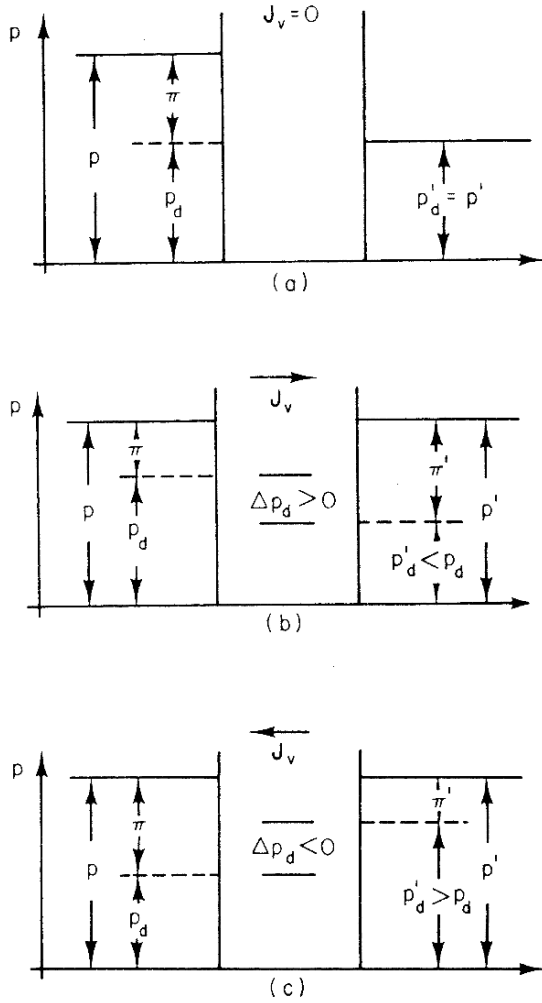


FIGURE 5.7. Different flow possibilities for a completely impermeant solute. (a)  $\Delta p_d = 0$ , so there is no flow even though  $p > p'$ . (b) Flow to the right even though  $p = p'$ . (c) Flow to the left even though  $p = p'$ .

Figure 5.7 shows the pressure relations on each side of the membrane for no flow and for flow in either direction.

When the solute is partially permeant, the volume flux rate in the linear approximation still depends on both  $\Delta p$  and  $\Delta \pi$ , but the proportionality constants may be different. Since the solute does not reduce the flow as much as in Eq. 5.11, it is customary to write the two constants as  $L_p$  and  $\sigma L_p$ :

$$J_v = L_p(\Delta p - \sigma \Delta \pi). \quad (5.12)$$

Parameter  $L_p$  is determined by measuring  $J_v$  and  $\Delta p$  when  $\Delta \pi = 0$ , while  $\sigma$  is determined from measurements of  $\Delta p$  and  $\Delta \pi$  when  $J_v = 0$ .

Parameter  $\sigma$  is called the *reflection coefficient*. It has different values for different solutes. When  $\sigma = 0$  there is no reflection, and the solute particles pass through like water. When  $\sigma = 1$  all the solute particles are reflected and Eq. 5.12 is the same as Eq. 5.11.

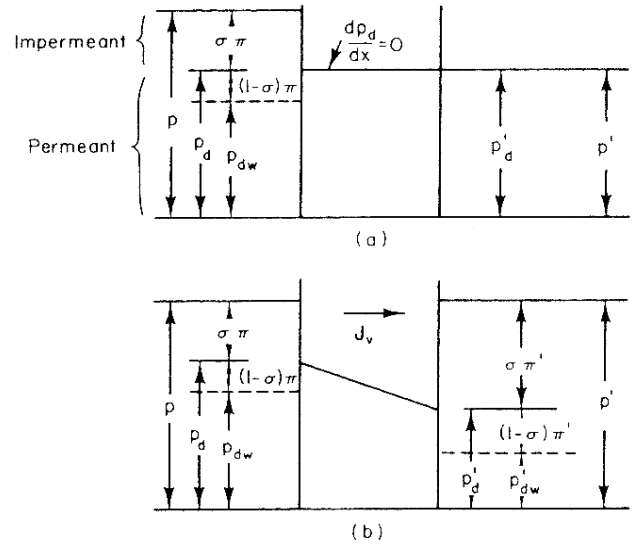


FIGURE 5.8. Pressure relationships on each side of the membrane when  $\sigma = \frac{2}{3}$ . (a) There is no bulk flow. (b) There is flow to the right.

We can imagine that part of the solute moves freely with the water and part is reflected. (Later, we will consider a model for partial reflection in which a solute particle of radius  $a < R_p$  can enter the pore, but its center cannot be closer to the wall than its radius.) We can write

$$p = p_d + \sigma \pi, \quad (5.13)$$

and we can further break this down to a driving pressure for the water  $p_{dw}$  and one for the permeant solute:

$$p = \underbrace{p_{dw}}_{\substack{\text{driving pressure} \\ \text{for permeant} \\ \text{molecules}}} + \underbrace{(1 - \sigma)\pi}_{\substack{\text{osmotic pressure} \\ \text{of all solute molecules}}} + \underbrace{\sigma \pi}_{\substack{\text{osmotic pressure} \\ \text{of impermeant} \\ \text{molecules}}} \quad (5.14)$$

With this substitution the flow equation becomes

$$J_v = L_p [\Delta p_{dw} + (1 - \sigma)\Delta \pi]. \quad (5.15)$$

Figure 5.8 shows the pressure relationships across the membrane.

In the approximation that van't Hoff's law holds,  $\pi = k_B T C = RT c$  and Eq. 5.12 can be written as

$$J_v = L_p(\Delta p - \sigma k_B T \Delta C), \quad (5.16)$$

$$J_v = L_p(\Delta p - \sigma RT \Delta c). \quad (5.17)$$

In Eq. 5.16 the concentration is in molecules  $\text{m}^{-3}$ ; in Eq. 5.17 it is mol  $\text{m}^{-3}$ . In both cases the units of  $k_B T \Delta C$  and  $RT \Delta c$  are pascals.

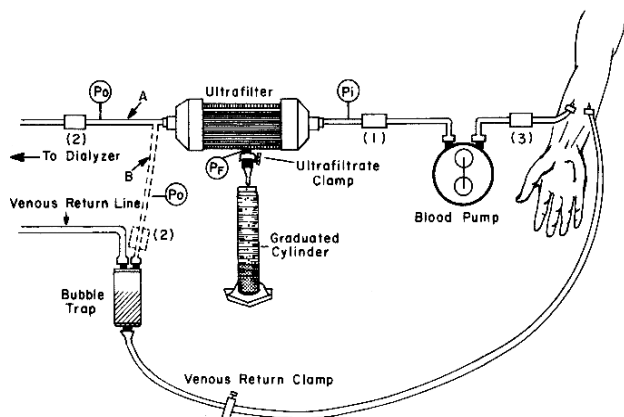


FIGURE 5.9. Apparatus used to treat fluid overload by ultrafiltration. Connection *A* is used for a patient connected to an artificial kidney. Connection *B* is used when the ultrafilter is used by itself. Pressure is monitored at  $P_i$  on the input side and  $P_o$  on the output side. The three numbered rectangles are (1) the anticoagulant infusion site, (2) the site for measuring clotting time in the filter, and (3) the site for measuring patient clotting time. From M. E. Silverstein, C. A. Ford, M. J. Lysaght, and L. W. Henderson. Treatment of severe fluid overload by ultrafiltration. Reproduced, by permission, from the *N. Engl. J. Med.* **291**: 747–751. Copyright © 1974 Massachusetts Medical Society. All rights reserved. Drawing courtesy of Prof. Henderson.

As an example of volume flow, consider ultrafiltration. *Ultrafiltration* is the process whereby water and small molecules are forced through a membrane by a hydrostatic pressure difference while larger constituents are left behind. An interesting clinical application of ultrafiltration has been proposed. A severely edematous patient (for any of the reasons mentioned in the previous section) must have the extra water removed from the body. This is usually accomplished with diuretics, drugs that increase the renal excretion of water. Some patients may not respond to these drugs, and in other cases, particularly pulmonary edema, the response may not be fast enough. In the latter case, phlebotomy (bloodletting) is sometimes used to reduce the body water rapidly. This has obvious disadvantages, for example, the removal of blood cells. Silverstein *et al.* (1974) have used ultrafiltration to remove water and sodium from the plasma while leaving the other constituents behind. The apparatus is shown in Fig. 5.9. The ultrafilter consists of a total area  $S = 0.2 \text{ m}^2$  of membrane, the permeability of which is  $1 \text{ ml min}^{-1} \text{ m}^{-2} \text{ torr}^{-1}$ . The pores are permeable to molecules of molecular weight less than 50,000. The filtration rate is set by clamping the ultrafiltrate line ( $P_F$  in Fig. 5.9), thereby increasing the pressure on the outside of the ultrafilter and decreasing the pressure drop across the membrane. The pressure was adjusted to give  $i_v$  of  $32 \text{ ml min}^{-1}$  or less, which is equal to that found in a normal kidney.

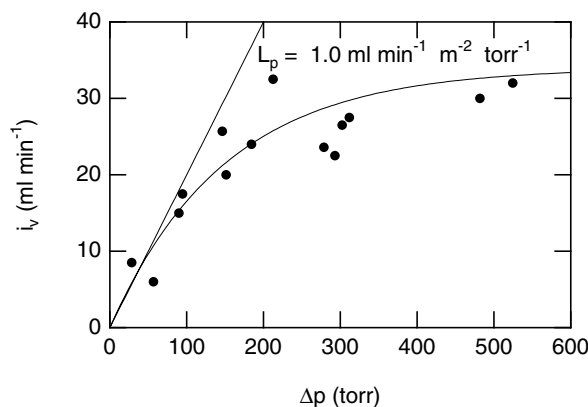


FIGURE 5.10. Filtration rate (flow)  $i_v$ , vs transmembrane pressure for a fixed blood flow of  $200 \text{ ml min}^{-1}$  through the apparatus in Fig. 5.9. The solid straight line shows a value of  $L_p$  of  $1 \text{ ml min}^{-1} \text{ m}^{-2} \text{ torr}^{-1}$  as reported by Silverstein *et al.* Modified, by permission, from the *N. Engl. J. Med.* **291**: 747–751. Copyright © 1974 Massachusetts Medical Society. All rights reserved.

Figure 5.10 shows the flow vs  $\Delta p$ . The initial slope of this curve determines  $L_p S$  and hence  $L_p$ . The curve is not linear but saturates at about  $32 \text{ ml min}^{-1}$  of filtration flow, possibly because of poor mixing within the blood.

Ultrafiltration is sometimes called reverse osmosis. The name is unfortunate, because it suggests some mysterious process unrelated to the principles of this section. Ultrafiltration is often used by campers for purifying water and has been suggested for desalinization of sea water.

## 5.6 Solute Transport Through a Membrane

Solute can pass through the membrane in two ways: it can be carried along with flowing water (solvent drag), and it can diffuse.

If there is no reflection ( $\sigma = 0$ ) and the solute concentration is the same on both sides of the membrane so there is no diffusion, the flux density or fluence rate is caused by solvent drag and is simply the solute concentration (particles per unit volume) times the volume fluence rate (Sec. 4.2):

$$J_s = C_s J_v.$$

If the solute particles are completely reflected ( $\sigma = 1$ ) then  $J_s = 0$ .

In the intermediate case with coefficient  $\sigma$ ,

$$J_s = (1 - \sigma)C_s J_v.$$

This is consistent with the idea expressed by Eq. 5.14 that a fraction  $(1 - \sigma)$  of the solute particles can enter the membrane. In that case,  $C_s$  is the solute concentration outside the membrane on both sides, and  $C_s(1 - \sigma)$  is

the solute concentration inside the membrane. We will develop a detailed model for transport in a right-cylindrical pore in Sec. 5.9. We anticipate that discussion and present a simple justification of the factor  $1 - \sigma$ . In bulk solution the concentration  $C_s$  is obtained by imagining a certain volume of solution, counting the number of solute particles whose centers lie within the volume, and taking the ratio. In a cylindrical pore of radius  $R_p$  and length  $\Delta Z$ , the volume of fluid is  $\pi R_p^2 \Delta Z$ . The centers of solute particles of radius  $a$  cannot be within distance  $a$  of the pore wall. The number of solute particles within the pore is therefore  $C_s \pi (R_p - a)^2 \Delta Z$ . The concentration in the pore is the number of particles divided by the pore volume:

$$\begin{aligned} C_{s, \text{ inside}} &= \frac{C_s \pi (R_p - a)^2 \Delta Z}{\pi R_p^2 \Delta Z} \\ &= C_s \left(1 - \frac{a}{R_p}\right)^2 = C_s (1 - \sigma). \end{aligned}$$

This correction is called the *steric factor*. Solvent flow within a distance  $a$  of the walls contributes to  $J_v$  but not to solvent drag. This model will be extended to a volume flow with a parabolic velocity profile in Sec. 5.9.4.

If  $J_v = 0$  there will be no solvent drag but there will be diffusion. The solute flux will be proportional to the concentration gradient and therefore to the concentration difference across the membrane:  $J_s \propto \Delta C_s$ . The proportionality constant depends on properties of the membrane. If the membrane is pierced by pores, for example, it depends on pore size, membrane thickness, number of pores per unit area, and the diffusion constant. The dependence will be derived later in this chapter. It is customary to write the proportionality constant as  $\omega RT$ :  $J_s = \omega RT \Delta C_s$ . The factor  $\omega$  is called the *membrane permeability* or *solute permeability*.

In the linear approximation the fluence rate resulting from both processes is the sum of these two terms:

$$J_s = (1 - \sigma) \bar{C}_s J_v + \omega RT \Delta C_s. \quad (5.18)$$

Here an average value  $\bar{C}_s$  has been written for the solvent drag term, because the concentration on each side of the membrane is not necessarily the same. The way that this average is taken will become clearer in the discussion of the pore model described in Section 5.9.

The solute equation has been written for both fluence rate and concentration in terms of particles. In terms of molar fluence rate and concentration, it is exactly the same:

$$J_s(\text{molar}) = (1 - \sigma) \bar{c}_s J_v + \omega RT \Delta c_s. \quad (5.19)$$

Either way, the diffusion proportionality constant is  $\omega RT$ . It does not change because  $C_s$  and  $J_s(\text{particles})$  are both written in terms of particles, and  $c_s$  and  $J_s(\text{molar})$  are both written in terms of moles. Referring to Eq. 5.18, the solvent drag term has units of (particles  $\text{m}^{-3}$ ) (m

$\text{s}^{-1}$ ) = particles  $\text{m}^{-2} \text{s}^{-1}$ . Therefore the factor  $\omega RT$  has units of  $\text{m} \text{s}^{-1}$ . Since the units of  $RT$  are joules or  $\text{N m}$  (per mole), the units of  $\omega$  are

$$\frac{\text{mol m s}^{-1}}{\text{N m}} = \text{mol N}^{-1} \text{s}^{-1}. \quad (5.20)$$

Further interpretation of  $\omega$  will be made for specific models.

We have used the same  $\sigma$  in both the solvent drag term and in the preceding section. Although this was made plausible by saying that  $1 - \sigma$  is the fraction of solute molecules that gets through the membrane, its rigorous proof is more subtle. It has been proved in general using thermodynamic arguments, which can be found in Katchalsky and Curran (1965). It can be proved in detail for specific membrane models.

## 5.7 Example: The Artificial Kidney

The artificial kidney provides an example of the use of the transport equations to solve an engineering problem. The problem has been extensively considered by chemical engineers, and we will give only a simple description here. Those interested in pursuing the problem further can begin with reviews by Galletti *et al.* (2000) or Lysaght and Moran (2000). The reader should also be aware that this “high-technology” solution to the problem of chronic renal disease is not an entirely satisfactory one. It is expensive and uncomfortable and leads to degenerative changes in the skeleton and severe atherosclerosis [Lindner *et al.* (1974)].

The alternative treatment, a transplant, has its own problems, related primarily to the immunosuppressive therapy. Anyone who is going to be involved in biomedical engineering or in the treatment of patients with chronic disease should read the account by Calland (1972), a physician with chronic renal failure who had both chronic dialysis and several transplants. The distinction between a high-technology treatment and a real conquest of a disease has been underscored by Thomas (1974, pp. 31–36).

The simplest model of dialysis is shown in Fig. 5.11. Two compartments, the body fluid and the dialysis fluid, are separated by a membrane that is porous to the

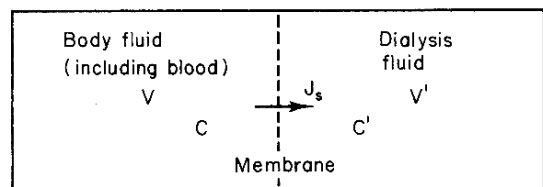


FIGURE 5.11. The simplest model of dialysis. All the body fluid is treated as one compartment; transport across the membrane is assumed to take longer than transport from various body compartments to the blood.

small molecules to be removed and impermeable to larger molecules. If such a configuration is maintained long enough, then the concentration of any solute that can pass through the membrane will become the same on both sides. The dialysis fluid is prepared with the desired composition of such small molecules as sodium, potassium, and glucose. Volume  $V'$  must be larger than  $V$  for effective dialysis to take place; otherwise, the concentration of solutes in the dialysis fluid builds up from the initially prepared values. In early work,  $V'$  was up to 100 l (since  $V$  is about 40 l). Although the fluid was replaced every 2 hours or so, it was an excellent medium in which to grow bacteria. Although the bacteria could not get through the membrane, they released exotoxins (or, if they died, endotoxins) which diffused back into the patient and caused fever. Now a continuous flow system has been used in which the solutes are continually metered into flowing dialysis fluid that is then discarded. Because of this, we will assume that there is no buildup of concentration in the dialysis fluid. (Effectively volume  $V'$  is infinite.) We will assume that  $\Delta p = 0$ . (Actually, proteins cause some osmotic pressure difference, which we will ignore.)

Without solvent drag, the solute transport is by diffusion,  $J_s = \omega RT(C - C')$ , where  $C$  is the concentration of solute in the blood and  $C'$  is the concentration in the dialysis fluid. If the surface area of the membrane is  $S$ , then the rate of change of the number of solute molecules  $N$  is

$$\frac{dN}{dt} = -S\omega RT(C - C').$$

If the solute is well mixed in the body fluid compartment, then  $N = CV$ , and this equation can be written as

$$\frac{dC}{dt} = -\frac{S\omega RT}{V}(C - C').$$

This is the equation for exponential decay. The steady-state solution is  $C = C'$ . The complete solution is (Appendix F)

$$C(t) = [C(0) - C']e^{-t/\tau} + C', \quad (5.21)$$

where the time constant is

$$\tau = \frac{V}{S\omega RT}. \quad (5.22)$$

The only variables that are adjustable in this equation are the membrane area  $S$  and its permeability  $\omega$ . The size of pores in the membrane is dictated by what solutes are to be retained in the blood. The number of pores per unit area and the thickness of the membrane can be controlled. Typical cellophane membranes have  $\omega RT = 5 \times 10^{-6} \text{ m s}^{-1}$  (with a thickness of 500  $\mu\text{m}$ ). The area may be 2  $\text{m}^2$ . With a fluid volume  $V = 40 \text{ l}$ , this gives a time constant

$$\tau = \frac{40 \times 10^{-3} \text{ m}^3}{(2 \text{ m}^2)(5 \times 10^{-6} \text{ m s}^{-1})} = 4 \times 10^3 \text{ s} = 1.1 \text{ h}.$$

Typically, dialysis requires several hours. This longer period is for two reasons. Some of the larger molecules

have smaller permeabilities and therefore longer time constants, and rapid dialysis causes cerebral edema and severe headaches.

The actual apparatus is quite complicated. First, it must be sterile, which requires a sterilized, disposable dialysis membrane. Second, the apparatus causes clots, so the blood must be treated with heparin as it enters the machine, and the heparin must be neutralized with protamine as it returns to the patient.

## 5.8 Countercurrent Transport

This section considers a problem that demonstrates the principle of *countercurrent* transport. An apparatus (perhaps a dialysis machine or an oxygenator) transports a single solute across a thin membrane of permeability  $\omega RT$ . On one side of the membrane (the “inside”) is a thin layer of solvent that flows along the membrane in the  $+x$  direction as shown in Fig. 5.12. On the “outside” is another thin layer of solvent that may be at rest or may flow in either the  $+x$  or the  $-x$  direction. When it flows in the opposite direction of the fluid inside we have the countercurrent situation.

Suppose that the concentration of solute in the two layers is  $C_{\text{in}}(x)$  inside and  $C_{\text{out}}(x)$  outside. Solute is transported in the  $x$  direction in each fluid layer by pure solvent drag. It diffuses through the membrane from the side with higher concentration to the other. We develop the model below and show that the steady-state concentration profiles are quite different depending on whether the solvent flows are in the same or opposite directions. The results are shown in Fig. 5.13 for the situation in which the value of  $C_{\text{in}}$  is 1 and the value of  $C_{\text{out}}$  is 0 where each solvent starts to flow across the membrane. In Fig. 5.13(a) both layers flow to the right; in Fig. 5.13(b) they flow in opposite directions. The countercurrent case is more effective in reducing  $C_{\text{in}}$ . The final value of  $C_{\text{in}}$  is 0.5 in the first case and 0.33 in the second.

To develop the model, we make the following assumptions. The concentration of solute in each fluid layer is independent of  $y$ ,  $z$ , and  $t$ . The thickness of the fluid layer inside is  $h_{\text{in}}$ . The fluid velocity  $j_v$  in is everywhere constant. The only important mechanism for solute transport within the fluid is solvent drag. Let the length of

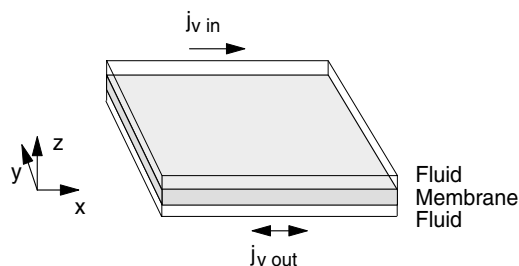
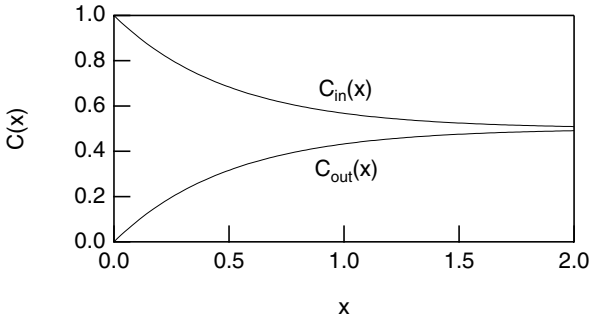
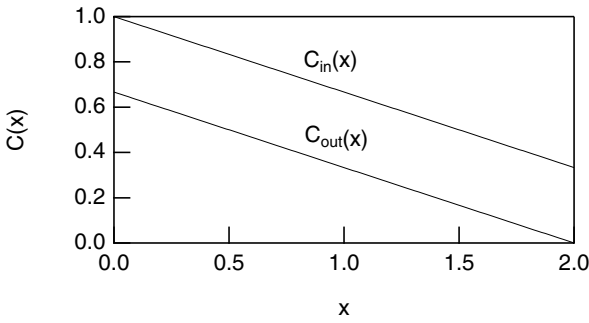


FIGURE 5.12. Layers of fluid containing a solute flow parallel to the  $x$  axis on either side of a membrane.





(a) Both flows are to the right.



(b) The flows are in opposite directions.

FIGURE 5.13. Solute concentration profiles for two different situations where solvent flows parallel to the membrane surface and solute moves through the membrane from inside to outside. (a) Both fluid layers flow to the right. The concentrations rise and falls exponentially, eventually becoming the same on both sides of the membrane. (b) The countercurrent case, in which the solvent flows are in opposite directions. The solvent outside flows from right to left. The concentrations vary linearly.

the slab in the  $y$  direction be  $Y$ . Inside, the number of particles per second in through the face of the rectangle of area  $Yh_{\text{in}}$  at  $x$  is  $C_{\text{in}}(x)j_v \text{ in } Yh_{\text{in}}$ . The number out through the face at  $x + dx$  is  $C_{\text{in}}(x + dx)j_v \text{ in } Yh_{\text{in}}$ . The number through the membrane into the exterior volume is  $[C_{\text{in}}(x) - C_{\text{out}}(x)]\omega RTY dx$ . Combining these we get

$$\frac{dC_{\text{in}}}{dx} = -\frac{\omega RT}{j_v \text{ in } h_{\text{in}}} [C_{\text{in}}(x) - C_{\text{out}}(x)]. \quad (5.23)$$

A similar expression can be derived for the exterior:

$$\frac{dC_{\text{out}}}{dx} = \frac{\omega RT}{j_v \text{ out } h_{\text{out}}} [C_{\text{in}}(x) - C_{\text{out}}(x)]. \quad (5.24)$$

Our notation allows  $j_v$  to have a different direction (sign). Defining  $a = \omega RT/j_v h$  we have the coupled differential equations

$$\begin{aligned} \frac{dC_{\text{in}}}{dx} &= -a_{\text{in}}(C_{\text{in}} - C_{\text{out}}), \\ \frac{dC_{\text{out}}}{dx} &= +a_{\text{out}}(C_{\text{in}} - C_{\text{out}}). \end{aligned} \quad (5.25)$$

We restrict ourselves to the case in which  $|a_{\text{in}}| = |a_{\text{out}}| = a$ . Changing the direction of  $j_v$  changes the sign of  $a$ . Assume  $a$  is the same on both sides. The equations show that the slope of  $C_{\text{in}}(x)$  is minus the slope of  $C_{\text{out}}(x)$  if both currents are in the same direction, and the two slopes are the same if the currents are in opposite directions. This can be seen in the solutions in Fig. 5.13.

You can verify that Eqs. 5.26 represent a solution of Eqs. 5.25:

$$\begin{aligned} C_{\text{in}}(x) &= \frac{c_1}{2} (1 + e^{-2ax}) + \frac{c_2}{2} (1 - e^{-2ax}), \\ C_{\text{out}}(x) &= \frac{c_1}{2} (1 - e^{-2ax}) + \frac{c_2}{2} (1 + e^{-2ax}), \end{aligned} \quad (5.26)$$

were  $c_1$  and  $c_2$  are the values of  $C_{\text{in}}$  and  $C_{\text{out}}$  at  $x = 0$ . Figure 5.13(a) shows the concentrations for  $c_1 = 1$  and  $c_2 = 0$  with  $a = 1$  and  $0 < x < 2$ . If the sign of  $a$  is changed in the second differential equation, then the fluid outside is flowing in the opposite direction to the fluid inside. Again you can verify that the most general solution is

$$\begin{aligned} C_{\text{in}}(x) &= c_1 + (c_2 - c_1)ax, \\ C_{\text{out}}(x) &= c_2 + (c_2 - c_1)ax. \end{aligned} \quad (5.27)$$

Figure 5.13(b) is a plot with the constants set so that the concentration inside on the left is 1 and on the outside on the right is zero ( $c_1 = 1, c_2 = 2/3, a = 1, 0 < x < 2$ ). This configuration is called *countercurrent* flow. We can see from the figure that the transport through the membrane is increased because the concentration difference across the membrane is, on average, greater.

The countercurrent principle is found in the renal tubules [Guyton (1991), p. 309; Patton *et al.* (1989), p. 1081], in the villi of the small intestine [Patton *et al.* (1989), p. 915], and in the lamellae of fish gills [Schmidt-Nielsen (1972), p. 45]. The principle is also used to conserve heat in the extremities—such as a person's arms and legs, whale flippers, or the leg of a duck. If a vein returning from an extremity runs closely parallel to the artery feeding the extremity, the blood in the artery will be cooled and the blood in the vein warmed. As a result, the temperature of the extremity will be lower and the heat loss to the surroundings will be reduced.

## 5.9 A Continuum Model for Volume and Solute Transport in a Pore

In this section we develop a model to predict the values of the phenomenological coefficients of Secs. 5.5 and 5.6. The success of the model depends on its ability to predict behavior, particularly as the size of solute particles is varied. This was an important problem in physiology in the 1960s and 1970s. Instead of comparing the model to experiment, we conclude the section by showing what the forces are on the membrane. This is important because

TABLE 5.1. Symbols used for porous membrane.

Quantity	On left	In pore	On right
Total pressure	$p$		$p'$
Solute concentration	$C_s$	$C(z)$	$C'_s$
Osmotic pressure	$\pi = k_B T C_s$		$\pi' = k_B T C'_s$
Effectively impermeant part of osmotic pressure	$\sigma\pi$		$\sigma\pi'$
Effectively permeant part of osmotic pressure plus water driving pressure	$(1 - \sigma)\pi + p_{dw}$	$p_d(z)$	$(1 - \sigma)\pi' + p'_{dw}$

there has been a fair amount of confusion in the literature about the forces on a semipermeable membrane. This section is fairly long. It stands alone; you can skip it if you wish.

The model assumes that the membrane has a particularly simple structure.

1. The membrane is pierced by  $n$  circular pores per unit area, all having radius  $R_p$  and all being right cylinders. The membrane thickness is  $\Delta Z$ .
2. The pore and the fluid are electrically neutral. No electrical forces are considered.
3. There is complete mixing on both sides of the pore, so that flow within the liquid on either side can be neglected.
4. The system is in the steady state. There is no variation in flux density (fluence rate) or concentration as a function of time.
5. The pores are large enough so that the bulk flow can be calculated by continuum hydrodynamics.

The quantities considered in this section are summarized in Table 5.1.

### 5.9.1 Volume Transport

The results of Chap. 1 can be used when the pore is filled with pure water or water and a solute for which  $\sigma = 0$ . From Eq. 1.40 the flux through a single pore is

$$i_v(\text{single pore}) = \frac{\pi R_p^4 \Delta p}{8\eta \Delta x}. \quad (5.28)$$

The fluence rate through the membrane is obtained by multiplying  $i_v$  by  $n$ , the number of pores per unit area. The result is

$$J_v = \frac{n\pi R_p^4 \Delta p}{8\eta \Delta Z}$$

so that

$$L_p = \frac{n\pi R_p^4}{8\eta \Delta Z}. \quad (5.29)$$

While  $L_p$  can be measured fairly easily using Eq. 5.12, it is much more difficult to measure the microscopic quantities needed to test Eq. 5.29. We will not compare the model to experiment here;<sup>10</sup> we will simply give an example of how calculations are done.

In discussing ultrafiltration we considered a filter (Fig. 5.10) for which  $L_p \approx 1 \text{ ml min}^{-1} \text{ m}^{-2} \text{ torr}^{-1}$ . Since  $760 \text{ torr} = 1 \times 10^5 \text{ Pa}$ , the hydraulic permeability in SI units is

$$\begin{aligned} L_p &= \frac{1 \text{ ml}}{1 \text{ torr min m}^2} \frac{1 \text{ min}}{60 \text{ s}} \frac{10^{-6} \text{ m}^3}{1 \text{ ml}} \frac{760 \text{ torr}}{1 \times 10^5 \text{ Pa}} \\ &= 1.27 \times 10^{-10} \text{ m s}^{-1} \text{ Pa}^{-1}. \end{aligned}$$

The manufacturer's literature<sup>11</sup> can be used to estimate

$$\begin{aligned} R_p &\approx 4.5 \text{ nm}, \\ \Delta Z &\approx 10 \text{ }\mu\text{m}. \end{aligned} \quad (5.30)$$

The viscosity of water is  $0.9 \times 10^{-3} \text{ Pa s}$  at  $25^\circ\text{C}$ . This gives us enough information to estimate  $n$  and the fraction of the filter surface that is pores. From Eq. 5.29

$$\begin{aligned} n &= \frac{8\eta \Delta Z L_p}{\pi R_p^4} = \left( \frac{(8)(0.9 \times 10^{-3} \text{ Pa s})(10 \times 10^{-6} \text{ m})}{\pi (4.5 \times 10^{-9})^4 \text{ m}^4} \right) \\ &\times (1.27 \times 10^{-10} \text{ m s}^{-1} \text{ Pa}^{-1}) \\ &= 7.1 \times 10^{15} \text{ m}^{-2}. \end{aligned}$$

Since the area of one pore is  $\pi R_p^2 = 6.36 \times 10^{-17} \text{ m}^2$ , the total pore area in  $1 \text{ m}^2$  is  $0.45 \text{ m}^2$ , a number that is not unreasonable.

Next consider the volume flow when the reflection coefficient is not zero. The position within the pore is specified by cylindrical coordinates  $(r, \phi, z)$ . The position along the axis of the pore is given by  $z$ . The position in a plane perpendicular to the axis of the pore is specified by polar coordinates  $r$  and  $\phi$ . Flow of the fluid is described by the vector volume fluence rate  $\mathbf{j}_v(r, \phi, z)$ . (We use  $J$  for fluence rate for the membrane as a whole and  $j$  for the fluence rate in bulk solution inside a pore.) It is possible to show rigorously that as long as the pore is a right circular cylinder,  $\mathbf{j}_v$  points only along  $z$  and is independent of  $\phi$  (the fluid does not flow in a spiral and does not flow into or out of the walls):

$$\mathbf{j}_v(r, \phi, z) = j_v(r, z)\hat{\mathbf{z}}. \quad (5.30)$$

The solution is in a steady state and the flow is not changing with time. Therefore, the flux density into a volume at  $z$  must be the same as the flux density out at  $z + dz$ :

$$\frac{\partial j_v}{\partial z} = 0 \quad (5.31)$$

<sup>10</sup>See earlier editions or, for example, Bean (1969, 1972).

<sup>11</sup>Amicon XM-50.

<sup>12</sup>This value may not be consistent with the value of  $L_p$  quoted. The pore length  $\Delta Z$  is not well known, and  $L_p$  is variable, depending on experimental conditions.

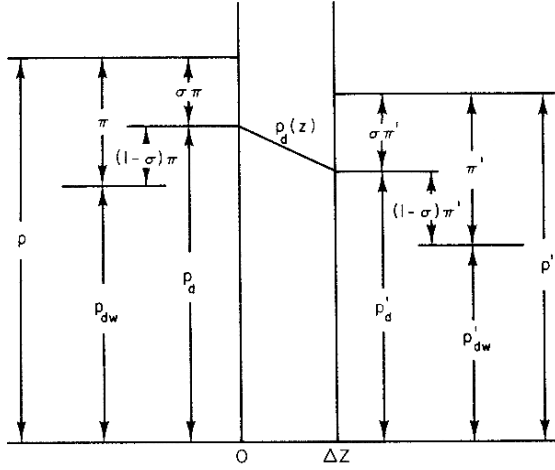


FIGURE 5.14. Pressure within a pore and at the boundaries in the steady state.

so that  $j_v$  is constant along the  $z$  axis (although it can be a function of  $r$ ). This is just what we saw in Chap. 1 for Poiseuille flow; the variation of  $j_v$  with  $r$  corresponds to the parabolic velocity profile. A value of  $j_v(r)$  that is constant in the  $z$  direction requires a constant value of  $\partial p/\partial z$  inside the pore.

In the pore, the driving pressure is  $p_d(z)$ . A typical pressure profile is shown in Fig. 5.14. The symbols are defined in Table 5.1. The pressure in the pore has been drawn with constant slope, since  $\partial p_d/\partial z$  is constant. Using Eqs. 5.16 and 5.29, we can write

$$J_v = L_p(\Delta p - \sigma k_B T \Delta C_s), \quad (5.32)$$

where  $L_p$  is given by Eq. 5.29. The value of  $\sigma$  is derived in the next section.

The average value of  $j_v(r)$  within the pore will be called  $\bar{j}_v$ . It is the total flux density through the pore divided by  $\pi R_p^2$ :

$$\begin{aligned} \bar{j}_v &= \frac{i(\text{single pore})}{\pi R_p^2} = \frac{1}{\pi R_p^2} \int_0^{R_p} j_v(r) 2\pi r dr \\ &= \frac{J_v}{n \pi R_p^2} = -\frac{R_p^2}{8\eta} \frac{\partial p_d}{\partial z}. \end{aligned} \quad (5.33)$$

### 5.9.2 Solute Transport

We now consider solute transport in our model pore. The arguments here are very similar to those for combined diffusion and solvent drag that were developed in Sec. 4.12. Those arguments are extended by averaging over the cross section of the pore.

Within the pore, the local solute flux is  $\mathbf{j}_s(r, \phi, z)$ . Arguments similar to those in the preceding section can be offered to show that  $\mathbf{j}_s$  points along the  $z$  axis and is independent of  $\phi$ :

$$\mathbf{j}_s(r, \phi, z) = j_s(r, z) \hat{\mathbf{z}}. \quad (5.34)$$

The solute concentration does not depend on  $\phi$ , or else there would be diffusion in the  $\phi$  direction and  $\mathbf{j}_s$  would have a  $\phi$  component. So  $C = C(r, z)$ . The  $r$  dependence must be kept because the center of a solute molecule of radius  $a$  cannot be within a distance  $a$  of the wall. (Recall the discussion of the steric correction on p. 120.) Thus  $C(r, z) = 0$  if  $r > R_p - a$ . We write<sup>13</sup>

$$C(r, z) = \begin{cases} 0, & R_p - a < r \\ C(z), & 0 \leq r \leq R_p - a. \end{cases} \quad (5.35)$$

The solute flux due to solvent drag is  $C_s j_v$ . For diffusion in one dimension the solute flux along the  $z$  axis is  $-D(\partial C/\partial z)$ . For the cylindrical pore we can combine these and write

$$j_s(r, z) = C(r, z) j_v(r, z) - D(r, a, R_p) \frac{\partial C(r, z)}{\partial z}. \quad (5.36)$$

The diffusion constant has been written as a function of  $r$ ,  $a$ , and  $R_p$  because in the pore, as distinct from an infinite medium, the constant depends on how close the particle is to the walls. (Remember the relation of  $D$  to the viscous drag and the fact that Stokes' law requires modification when the fluid is confined in a tube.)

The preceding section showed that for the steady state  $j_v$  is independent of  $z$ . A similar argument can be made using the continuity equation for solute particles, implying that  $j_s$  is independent of  $z$ . Therefore, Eq. 5.36 simplifies to

$$D(r, a, R_p) \frac{\partial C(r, z)}{\partial z} - j_v(r) C(r, z) = -j_s(r). \quad (5.37)$$

The easiest way to write  $C(r, z)$  in accordance with Eq. 5.35 is

$$C(r, z) = C(z) \Gamma(r),$$

where

$$\Gamma(r) = \begin{cases} 0, & R_p - a < r \\ 1, & 0 \leq r < R_p - a. \end{cases}$$

With this substitution Eq. 5.37 becomes

$$\Gamma(r) D(r, a, R_p) \frac{dC(z)}{dz} - C(z) \Gamma(r) j_v(r) = -j_s(r). \quad (5.38)$$

This equation can be multiplied by  $2\pi r dr$  and integrated from  $r = 0$  to  $r = R_p$ . The result is

$$\begin{aligned} &\left( \int_0^{R_p} \Gamma(r) D(r, a, R_p) 2\pi r dr \right) \frac{dC(z)}{dz} \\ &- \left( \int_0^{R_p} \Gamma(r) j_v 2\pi r dr \right) C(z) = - \int_0^{R_p} j_s(r) 2\pi r dr. \end{aligned} \quad (5.39)$$

The physical meaning of this integration can be understood with the aid of Fig. 5.15, which shows a slab of fluid

<sup>13</sup>It can be argued that this is the only possible form for  $C(r, z)$ . See Levitt (1975, p. 535ff.).

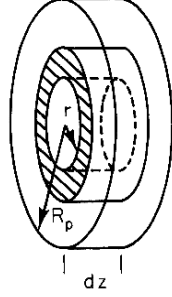


FIGURE 5.15. A slab of fluid in a pore between  $z$  and  $z + dz$ , showing how the integration over  $r$  is done.

in the pore between  $z$  and  $z + dz$ . Solute does not cross a surface of constant  $r$  but moves parallel to the  $z$  axis. Diffusion and solvent drag are considered in each shaded area  $2\pi r dr$ . The integration of Eq. 5.38 establishes an average solute fluence rate, since the right-hand side of the equation is the total flux or current of solute particles per second passing through the pore:

$$i_s = \int_0^{R_p} j_s(r) 2\pi r dr.$$

As with the volume fluence rate, it is convenient to call the average solute fluence rate  $\bar{j}_s$ :

$$\bar{j}_s = \frac{i_s}{\pi R_p^2} = \frac{1}{\pi R_p^2} \int_0^{R_p} j_s(r) 2\pi r dr. \quad (5.40)$$

The first term of Eq. 5.38 is the diffusive flux at  $z$  averaged over the entire cross section of the pore. Define an effective diffusion constant

$$D_{\text{eff}} = \frac{1}{\pi R_p^2} \int_0^{R_p} \Gamma(r) D(r, a, R_p) 2\pi r dr. \quad (5.41)$$

The second term on the left of Eq. 5.38 is the solvent drag flux averaged over the entire cross section of the pore. The integral is

$$\int_0^{R_p} j_v(r) \Gamma(r) 2\pi r dr = \int_0^{R_p-a} j_v(r) 2\pi r dr. \quad (5.42)$$

This integral can be evaluated because we know the velocity profile,  $j_v(r)$ , Eq. 1.39:<sup>14</sup>

$$j_v(r) = \frac{1}{4\eta} \frac{\Delta p}{\Delta z} (R_p^2 - r^2). \quad (5.43)$$

We have already defined the average volume fluence rate to be

$$\bar{j}_v = \frac{1}{\pi R_p^2} \int_0^{R_p} j_v(r) 2\pi r dr.$$

<sup>14</sup>This ignores the fact that since the walls affect the force on the solute particles, the solute must distort the velocity profile slightly. This point is discussed below.

The desired quantity differs only in the limits of integration. To calculate it, write

$$\int_0^{R_p-a} j_v(r) 2\pi r dr = \pi R_p^2 \bar{j}_v \frac{\int_0^{R_p-a} j_v(r) 2\pi r dr}{\int_0^{R_p} j_v(r) 2\pi r dr}.$$

The integrals are easily evaluated (see Problems). The result is

$$\int_0^{R_p} j_v(r) \Gamma(r) 2\pi r dr = \pi R_p^2 \bar{j}_v f(a/R_p), \quad (5.44a)$$

where the function  $f$  is

$$f(\xi) = 1 - 4\xi^2 + 4\xi^3 - \xi^4. \quad (5.44b)$$

When Eqs. 5.40, 5.41, and 5.44a are substituted into Eq. 5.38 and each term is divided by  $\pi R_p^2$ , the result is

$$D_{\text{eff}} \left( \frac{dC}{dz} \right) - j_v f \left( \frac{a}{R_p} \right) C(z) = -\bar{j}_s \quad (5.45a)$$

or

$$\frac{dC}{dz} - \frac{j_v f(a/R_p)}{D_{\text{eff}}} C(z) = -\frac{\bar{j}_s}{D_{\text{eff}}}. \quad (5.45b)$$

This is a differential equation for  $C(z)$ . The right-hand side is the total solute fluence rate, which is constant. On the left-hand side,  $C$  varies along the pore so that the diffusive and solvent-drag fluence rates add up to this constant value. If the constant in front of  $C(z)$  is written as

$$\frac{1}{\lambda} = \frac{j_v f(a/R_p)}{D_{\text{eff}}}, \quad (5.46)$$

this is recognized as Eq. 4.58 for drift plus solvent drag in an infinite medium. The results of Sec. 4.13 can be applied here. It is only necessary to determine values for  $C_0$  and  $C'_0$ . Recall that in the pore  $C(r, z) = C(z)\Gamma(r)$ . The function  $\Gamma(r)$  takes into account the reflection that occurs because solute particles cannot be closer to the pore wall than their radius. It was also assumed that the solution on either side of the membrane is well stirred. Therefore,  $C_0 = C_s$  and  $C'_0 = C'_s$ . Equation 4.70 becomes

$$\bar{j}_s = f \bar{j}_v \bar{C}_s + D_{\text{eff}} \frac{C_s - C'_s}{\Delta Z}. \quad (5.47)$$

This is an expression for  $\bar{j}_s$ , the average solute fluence rate in the pore. To get solute fluence rate in the membrane, it must be multiplied by  $\pi R_p^2$  and the number of pores per unit area. Since  $J_v = n\pi R_p^2 \bar{j}_v$ , we have

$$J_s = f \bar{C}_s J_v + \frac{n\pi R_p^2 D_{\text{eff}}}{\Delta Z} \Delta C_s. \quad (5.48)$$

Comparing this with the general phenomenological equation for solute flow, Eq. 5.18,

$$J_s = (1 - \sigma) \bar{C}_s J_v + \omega RT \Delta C_s$$

we see that

$$\begin{aligned}
 1 - \sigma &= f, \\
 \omega RT &= \frac{n \pi R_p^2 D_{\text{eff}}}{\Delta Z}, \\
 \lambda &= \frac{D_{\text{eff}}}{\bar{j}_v(1 - \sigma)} = \frac{\omega RT(\Delta Z)}{J_v(1 - \sigma)}.
 \end{aligned} \tag{5.49}$$

The average solute concentration  $\bar{C}$  is obtained from Eq. 4.66 with the substitution of  $\Delta Z$  for the pore length:

$$\bar{C}_s = \frac{C_s e^x - C'_s}{e^x - 1} - \frac{1}{x}(C_s - C'_s).$$

This can be rearranged as

$$\bar{C}_s = \frac{1}{2}(C_s + C'_s) + G(x)(C_s - C'_s) \tag{5.50a}$$

with

$$G(x) = \frac{1}{2} \left( \frac{e^x + 1}{e^x - 1} \right) - \frac{1}{x}, \tag{5.50b}$$

where  $x = \Delta Z/\lambda$ . This is the same function we saw in Fig. 4.17.

The solute concentration away from the sides of the pore is

$$C(z) = \frac{C_s(e^{\Delta Z/\lambda} - e^{z/\lambda}) + C'_s(e^{z/\lambda} - 1)}{e^{\Delta Z/\lambda} - 1}. \tag{5.51}$$

While the concentration profile is not usually measured experimentally, it is useful to plot it to help us visualize the interrelation of diffusion and solvent drag. Call  $\phi = C'_s/C_s$ . Equation 5.51 can be rearranged as

$$C(z) = C(0) \left( 1 - (1 - \phi) \frac{e^{z/\lambda} - 1}{e^{\Delta Z/\lambda} - 1} \right). \tag{5.52}$$

We can see several things from this equation. First, if the concentration is the same at each end of the pore,  $\phi = 1$ , the second term in large parentheses vanishes, and the concentration is uniform throughout the pore. If  $\phi \neq 1$ , then the concentration is that at  $z = 0$ , plus a factor which may be positive or negative, depending on whether  $\phi$  is less than or greater than 1. The ratio of exponentials occurring in that factor is plotted in Fig. 5.16 for different values of  $\Delta Z/\lambda$ , the ratio of the pore length to the effective diffusion distance.

These curves determine the shape of the concentration profile along the pore. If the flow is zero,  $\lambda = D_{\text{eff}}/\bar{j}_v(1 - \sigma)$  is infinite and  $\Delta Z/\lambda$  is zero. We then have pure diffusion, and the concentration changes uniformly along the pore, corresponding to the straight line in Fig. 5.16. The plots in Fig. 5.17 show what the concentration profiles are like for diffusion to the left and to the right when the flow is to the right. Compare the shape of the concentration profile on the left in Fig. 5.17 with the curve for  $\Delta Z/\lambda = 1$  in Fig. 5.16. When the concentration is higher on the left, we have to take the mirror

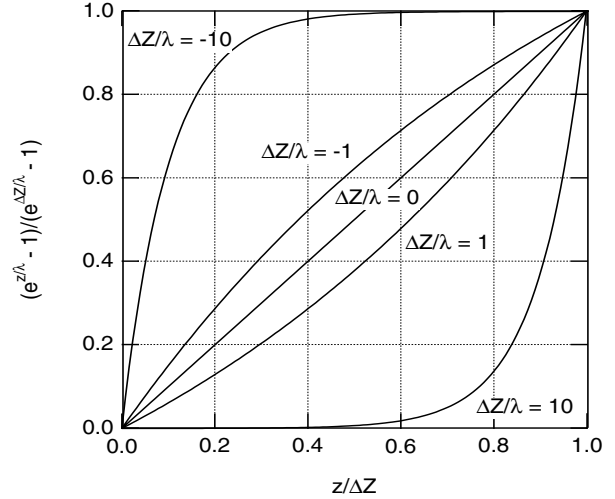


FIGURE 5.16. Plot of the factor  $(e^{z/\lambda} - 1)/(e^{\Delta Z/\lambda} - 1)$ , which appears in Eq. 5.52.

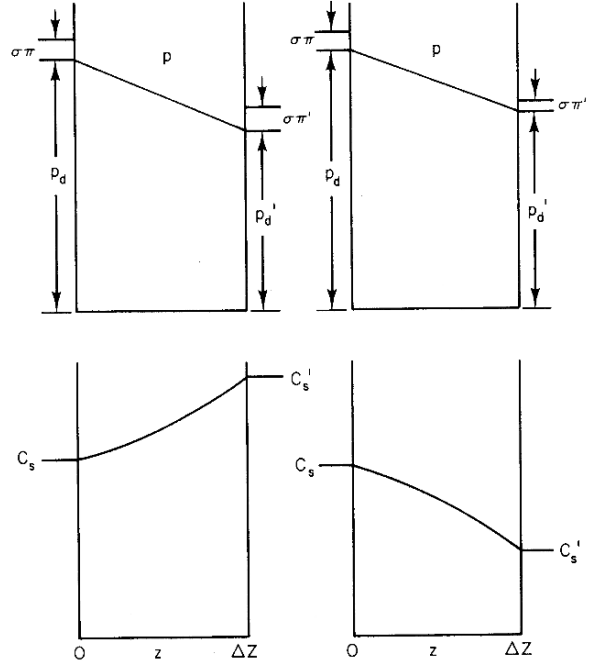


FIGURE 5.17. A possible set of values for  $p$ ,  $p_d$ , and  $C$  along a pore for diffusion to the left and diffusion to the right. The fluid on each side of the pore is well stirred and of sufficient volume so that concentrations do not change with time.

image of Fig. 5.16; the curve for  $\Delta Z/\lambda = -1$  gives the concentration profile in Fig. 5.17 on the right.

As the pore becomes very long compared to the diffusion length (for example,  $|\Delta Z/\lambda| = 10$  or more), the concentration along the pore is nearly that carried into the pore by bulk flow from the left until we get to the far end, where diffusion back up the pore gives a smooth transition to the final concentration on the right.

We can think of the pressure in the pore as being made up of driving pressures due to water and to the solute within the pore:

$$p_d(z) = p_{dw}(z) + p_{ds}(z).$$

Since the effective driving pressure for impermeant solute in the  $J_v$  equation is  $k_B T \Delta C$ , it would be nice to be able to write

$$p_d(z) = p_{dw}(z) + (1 - \sigma) k_B T C(z).$$

This is consistent with the solvent drag flux at position  $z$  in the pore, which was given in Eq. 5.45a by

$$\bar{j}_v f C(z) = \bar{j}_v (1 - \sigma) C(z).$$

The “effective” concentration for solvent drag is  $(1 - \sigma)C(z)$ .

### 5.9.3 Summary

To summarize, the combination of solvent and a solute with reflection coefficient has a volume flux

$$J_v = L_p(\Delta p - \sigma k_B T \Delta C_s) \quad (5.53)$$

and a solute flux

$$J_s = (1 - \sigma) \bar{C}_s J_v + \omega RT \Delta C_s. \quad (5.54)$$

The hydraulic permeability is

$$L_p = \frac{n \pi R_p^4}{8 \eta \Delta Z}. \quad (5.55)$$

The solute permeability is

$$\omega RT = \frac{n \pi R_p^2 D_{\text{eff}}}{\Delta Z}. \quad (5.56)$$

The characteristic length for diffusion is

$$\lambda = \frac{D_{\text{eff}}}{\bar{j}_v (1 - \sigma)} = \frac{\Delta Z \omega RT}{J_v (1 - \sigma)}. \quad (5.57)$$

The average concentration is

$$\bar{C}_s = \frac{1}{2}(C_s + C'_s) + G(x) \Delta C_s, \quad (5.58)$$

where  $G(x)$  is given by Eq. 5.50b. The parameter  $x$  is

$$x = \frac{J_v (1 - \sigma)}{\omega RT} = \frac{\Delta Z}{\lambda}. \quad (5.59)$$

Notice that the solvent drag term as well as the diffusion term depends on  $\Delta C_s$ , through the factor  $\bar{C}_s$ .

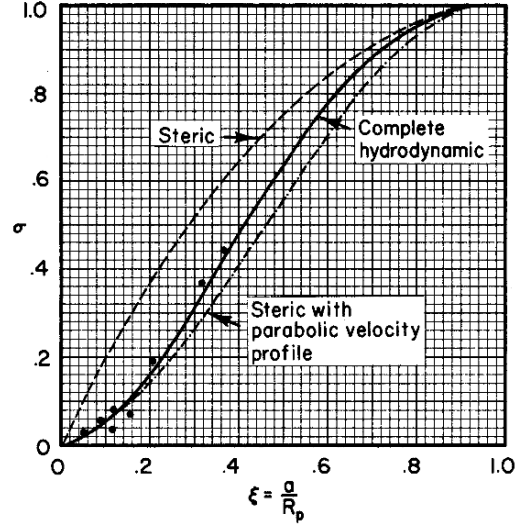


FIGURE 5.18. Calculated values of the reflection coefficient are indicated by the lines. Calculations are shown for the simple steric factor, the steric factor weighted by a parabolic velocity profile, Eq. 5.60, and a more detailed calculation, which takes account of the distortion of the velocity profile by the solute particles. The data points are from Durbin (1960) as reinterpreted by Bean (1972).

### 5.9.4 Reflection Coefficient

We have referred previously to the fact that the centers of solute particles can occupy only a fraction of the pore volume. A solute particle’s center cannot be further from the pore axis than  $R_p - a$ . The simplest correction is the steric factor, seen on p. 120. The ratio of effective area to total area approximates  $1 - \sigma$ . If  $\xi = a/R_p$ , then

$$1 - \sigma \approx \frac{\pi(R_p - a)^2}{\pi R_p^2} = 1 - \frac{2a}{R_p} + \frac{a^2}{R_p^2},$$

$$\sigma = 2\xi - \xi^2.$$

A better calculation was seen in the preceding subsection. Accept the fact (quoted from thermodynamic results) that the same  $\sigma$  occurs in the equations for  $J_v$  and  $J_s$ . We saw that the edges of the pore have less bulk flow than the center, so that the steric effect overestimates how many particles are reflected. From Eq. 5.44b,

$$\sigma = 1 - f = 4\xi^2 - 4\xi^3 + \xi^4. \quad (5.60)$$

These two approximations to  $\sigma$  are plotted in Fig. 5.18.

It was mentioned in a footnote that the calculation which resulted in Eq. 5.44a neglected the change in velocity profile caused by the solute particles. More rigorous calculations have been done by Levitt (1975) and by Bean (1972, pp. 29–35). Levitt’s result is

$$\sigma = \frac{16}{3}\xi^2 - \frac{20}{3}\xi^3 + \frac{7}{3}\xi^4 + 0.35\xi^5. \quad (5.61)$$

This is valid for  $\xi < 0.6$ . The three equations for  $\sigma$  are plotted in Fig. 5.18, along with some experimental data

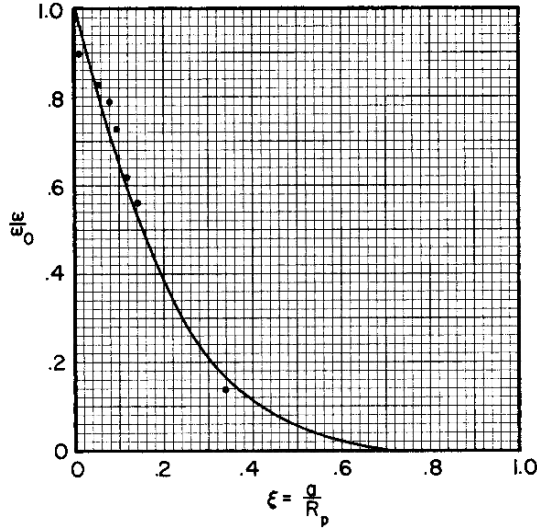


FIGURE 5.19. Plot of  $\omega/\omega_0$  for experimental data by Beck and Schultz (1970) and a calculation by Bean (1972).

from Durbin (1960) using the pore radius assigned by Bean.

### 5.9.5 The Effect of Pore Walls on Diffusion

The solute permeability is given by

$$\omega RT = \frac{n\pi R_p^2 D_{\text{eff}}}{\Delta Z}.$$

The effective diffusion coefficient takes into account the steric factor as well as the drag on the solute particles by the pore walls. If the pore had an infinitely large diameter, the unrestricted permeability would be

$$\omega_0 RT = \frac{n\pi R_p^2 D}{\Delta Z},$$

where  $D$  is the diffusion coefficient for an infinite medium. Figure 5.19 shows some data from Beck and Schultz (1970) and a curve for  $\omega/\omega_0$  calculated by Bean (1972).<sup>15</sup>

In Europe, filtration rather than dialysis is used to treat kidney patients. There is evidence that some as yet unidentified toxin of medium molecular weight accumulates in the blood. Comparison of  $1 - \sigma$  from Fig. 5.18 with  $\omega/\omega_0$  from Fig. 5.19 shows that solvent drag removes medium-sized molecules more effectively. The fluid and electrolytes lost by the patient must be replaced.

### 5.9.6 Net Force on the Membrane

We conclude the section by calculating the force of the fluid on the membrane. The results give some insight into the nature of osmotic pressure.

<sup>15</sup>The steric factor, which Bean includes separately, is built into  $D_{\text{eff}}$  through the function  $\Gamma(r)$ .

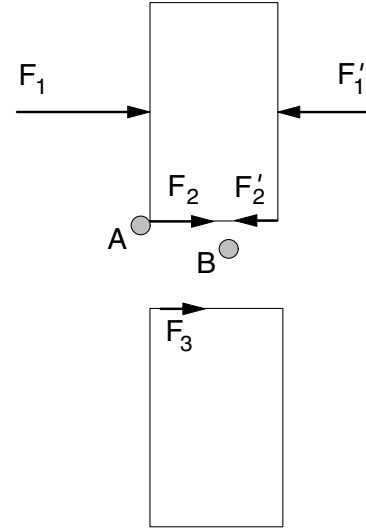


FIGURE 5.20. The forces on a membrane with pores. The fluid on the left exerts force  $\mathbf{F}_1$  due to the hydrostatic pressure  $p$ . A similar force  $\mathbf{F}'_1$  is exerted on the right. Solute molecules like  $A$  are reflected at the pore edge and exert force  $\mathbf{F}_2$ . Solute molecule  $B$  enters the pore. It contributes to the viscous force of the flowing fluid on the cylindrical walls of the pore,  $\mathbf{F}_3$ .  $\mathbf{F}_3$  is to the right if the fluid flows from left to right through the pore.

A membrane of total area  $S$  is pierced by  $n$  pores per unit area of radius  $R_p$ . The pressures in the fluid on each side of the membrane are  $p$  and  $p'$ . A solute with reflection coefficient  $\sigma$  has concentration  $C$  on the left and  $C'$  on the right. We want to calculate the total force exerted by the fluid on the membrane. There are three contributions to this force. These can be understood by referring to Fig. 5.20.

Forces  $F_1$  and  $F'_1$  are the forces exerted by the fluid on the walls of the membrane on each side. They are obtained by multiplying the total pressure on each side by the area of the membrane that is not occupied by pores. In a total area  $S$  there are  $nS$  pores, each of area  $\pi R_p^2$ .

$$F_1 = pS(1 - n\pi R_p^2)$$

$$F'_1 = p'S(1 - n\pi R_p^2).$$

The net force to the right is

$$F_1 - F'_1 = S(p - p')(1 - n\pi R_p^2). \quad (5.62)$$

Forces  $F_2$  and  $F'_2$  are exerted by solute molecules reflected from the pore region, such as molecule  $A$  in Fig. 5.20. These are the ones that contribute to the osmotic pressure. The net force to the right is therefore the total pore area  $Sn\pi R_p^2$  times the impermeant part of the osmotic pressure difference:

$$F_2 - F'_2 = Sn\pi R_p^2(\sigma\pi - \sigma'\pi). \quad (5.63)$$

Force  $F_3$  is the viscous drag exerted on the walls of the pores by the water and permeant solute molecules flowing

through them. To calculate it we recall that the viscous force per unit area is  $-\eta(\partial v/\partial r)$ . The velocity is  $v = j_v$ . Differentiating Eq. 5.43, we obtain

$$\frac{\partial j_v}{\partial r} = -\frac{1}{4\eta} \frac{\Delta(p - \sigma\pi)}{\Delta Z} 2r.$$

The total force is  $\eta$  times this quantity evaluated at  $r = R_p$ , times total area of the cylindrical walls of all the pores, which is  $(Sn)(2\pi R_p \Delta Z)$ :

$$F_3 = Sn2\pi R_p \Delta Z \eta \left( \frac{1}{4\eta} \frac{(p - p') - \sigma(\pi - \pi')}{\Delta Z} 2R_p \right) = Sn\pi R_p^2 [(p - p') - \sigma(\pi - \pi')]. \quad (5.64)$$

The net force on the membrane is the sum of these forces:

$$F_1 - F'_1 + F_2 - F'_2 + F_3 = S(p - p'). \quad (5.65)$$

We see that the net force on the membrane is the total pressure difference times the total area of the membrane, regardless of the differences in osmotic pressure on each side. Both solute and solvent exert a force on the non-pore area of the membrane. The solute molecules at the membrane surface whose centers are within the area of a pore may be reflected or may enter the pore. If they are reflected, they contribute to the force when they strike the membrane at the edge of a pore. If they are not reflected, they enter the pore and contribute to the viscous drag on the membrane due to flow through the pore.

## Symbols Used in Chapter 5

Symbol	Use	Units	First used on page
$a$	Solute particle radius	m	120
$a, a_{in}, a_{out}$	Parameters	$m^{-1}$	122
$c_1, c_2, c'_1, c'_2$	Solute concentration	(mole) $m^{-3}$	112
$f$	Temporary function		125
$h$	Thickness of fluid layer	m	121
$i$	Solute current through membrane	$s^{-1}$	131
$i_s$	Solute flow	$s^{-1}$	125
$i_v$	Volume flow	$m^3 s^{-1}$	117
$j_s, \mathbf{j}_s$	Solute fluence rate in pore	$m^{-2} s^{-1}$	124
$j_v, \mathbf{j}_v$	Volume fluence rate in pore	$m s^{-1}$	123
$k_B$	Boltzmann's constant	$J K^{-1}$	112
$n$	Number of moles		112
$n$	Number of pores per unit area	$m^{-2}$	120
$p_1, \text{etc.}$	Pressure	Pa	112
$p_d$	"Driving pressure"	Pa	114
$p$	Total pressure	Pa	114
$p_{dw}$	"Driving pressure" of water	Pa	114
$r$	Radius in cylindrical coordinates	m	123
$x, y, z$	Position	m	121

$x$	$\Delta Z/\lambda$		127
$z$	Distance along pore	m	123
$\hat{z}$	Unit vector in $z$ direction		123
$C, C_s, \text{etc.}$	Particle concentration of the species indicated by the subscript	(particle) $m^{-3}$	112
$D, D_{\text{eff}}$	Diffusion constant	$m^2 s^{-1}$	124
$F$	Force	N	128
$G$	Factor relating solvent drag and diffusion		126
$J_s$	Solute fluence rate through membrane	$m^{-2} s^{-1}$	119
$J_v$	Volume fluence rate through membrane	$m s^{-1}$	117
$L_p$	Hydraulic permeability	$m s^{-1} Pa^{-1}$	117
$N_1, \text{etc.}$	Number of molecules		112
$N_A$	Avogadro's number		112
$R$	Gas constant	$J mol^{-1} K^{-1}$	112
$R_p$	Pore radius	m	120
$S$	Surface area	$m^2$	117
$T$	Absolute temperature	K	112
$V, V', V^*$	Volume	$m^3$	112
$X, Y$	Distance	m	121
$\Delta Z$	Pore length	m	120
$\eta$	Viscosity	Pa s	123
$\lambda$	Effective diffusion distance	m	125
$\mu$	Chemical potential	$J molecule^{-1}$	114
$\xi$	$a/R_p$		127
$\pi$	Osmotic pressure	Pa	114
$\sigma$	Reflection coefficient		118
$\tau$	Time constant	s	121
$\omega$	Solute permeability	$mol N^{-1} s^{-1}$	120
$\omega_0$	Solute permeability in an infinite medium	$mol N^{-1} s^{-1}$	128
$\phi$	Angle in cylindrical coordinates		123
$\phi$	$C'_s/C_s$		126
$\Gamma$	Radial dependence of solute concentration		124

## Problems

### Section 5.3

**Problem 1** *The protein concentration in serum is made up of two main components: albumin (molecular weight 75,000) 4.5 g per 100 ml and globulin (molecular weight 170,000) 2.0 g per 100 ml. Calculate the osmotic pressure due to each constituent. (These results are inaccurate because of electrical effects.)*

**Problem 2** *If the osmotic pressure in human blood is 7.7 atm at 37°C, what is the solute concentration assuming that  $\sigma = 1$ ? What would be the osmotic pressure at 4°C?*

**Problem 3** *Sometimes after trauma the brain becomes very swollen and distended with fluid, a condition known as cerebral edema. To reduce swelling, mannitol may be injected into the bloodstream. This reduces the driving force of water in the blood, and fluid flows from the brain into the blood. If 0.01 mol  $l^{-1}$  of mannitol is used, what will be the approximate osmotic pressure?*



Section 5.4

**Problem 4** When a person is given an intravenous fluid, the solute concentration in the fluid must be matched to the solute concentration in the blood to avoid problems arising from a change in the blood's osmotic pressure. One such fluid, called "isotonic saline," can be made by adding salt (NaCl) to distilled water. The osmolarity of the blood is about 0.3 osmole.

(a) How many grams of NaCl must be added to a liter of water to make isotonic saline? What fraction of the solution's mass is NaCl? (Hint: Recall that NaCl dissolves into  $\text{Na}^+$  and  $\text{Cl}^-$ , and both contribute to the osmotic pressure.)

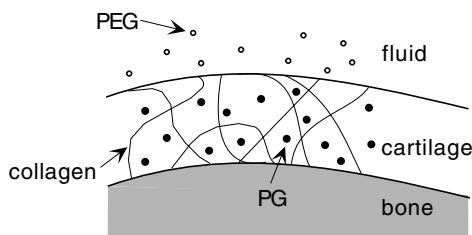
(b) Repeat for dextrose,  $\text{C}_6\text{H}_{12}\text{O}_6$ , which does not dissociate.

**Problem 5** An understanding of osmotic pressure is important in medicine. Consider the case reported by Steinmuller (1998) in the *New England Journal of Medicine*. A 5% solution of albumin was needed to infuse into a patient with kidney disease (renal insufficiency). No 5% solution was available, so the hospital pharmacy used 25% albumin diluted 1:4 with pure water. Injection of the solution into the patient caused renal failure. The albumin in a 25% albumin solution has an osmolarity of about 36 mosmol. Typically, such a solution also contains about 300 mosmol of other ions (see Problem 4).

(a) Calculate the osmolarity of the solution injected into the patient.

(b) Calculate the osmolarity of the solution if the pharmacy had properly used isotonic saline instead of pure water to perform the 1:4 dilution.

**Problem 6** Articular cartilage covers the ends of bones in joints and allows the bones to move smoothly against each other. It contains a network of collagen fibers that can exert a mechanical tensile stress to resist tissue swelling, resulting in a pressure  $P_c$  within the cartilage. The collagen fibers do not withstand compression. The cartilage also contains proteoglycan molecules that cause tissue swelling because of their osmotic pressure,  $\pi_{PG}$ . One can determine  $P_c$  by placing the cartilage in a polyethylene glycol solution with osmotic pressure  $\pi_{PEG}$ , measuring  $\pi_{PG}$  and  $\pi_{PEG}$ , and using the relationship  $P_c = \pi_{PG} - \pi_{PEG}$ .



Typical data are

$\pi_{PEG}$ (atm)	$\pi_{PG}$ (atm)
0.0	4.0
2.5	5.5
5.0	7.0
7.5	8.5
10.0	10.0

(a) What is the excess pressure  $P_c$  exerted by the collagen matrix under normal conditions ( $\pi_{PEG} = 0$ )?

(b) At what value of  $\pi_{PEG}$  does the collagen matrix exert no tensile stress (become "limp")?

(c) Plot  $P_c$  vs.  $\pi_{PEG}$ . Find a linear equation that fits the data.

(d) Osteoarthritis is thought to occur when the collagen matrix is weakened. If the collagen in an arthritic joint can only exert a pressure of 2 atm when  $\pi_{PEG} = 0$ , by how much will the tissue swell (by what percent will its volume change?)

In (b) and (d), assume that only the proteoglycans cause osmotic pressure and that their number does not change, but the tissue volume increases as the tissue swells with water. This problem is based on the work of Bassar et al. (1998), but the data have been modified.

Section 5.5

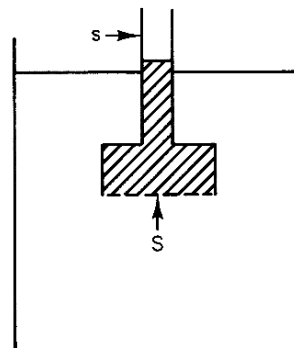
**Problem 7** Suppose that  $L_p$  is expressed in  $\text{m}^3 \text{N}^{-1} \text{s}^{-1}$  or  $\text{m s}^{-1} \text{Pa}^{-1}$ . Find conversion factors to express it in

(a)  $\text{ml min}^{-1} \text{cm}^{-2} \text{torr}^{-1}$ .

(b)  $\text{ml s}^{-1} \text{cm}^{-2} (\text{in. water})^{-1}$ .

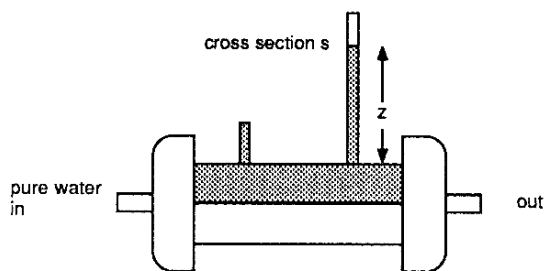
(c)  $\text{ml s}^{-1} \text{cm}^{-2} (\text{lb in.}^{-2})^{-1}$ .

**Problem 8** An ideal semipermeable membrane is set up as shown. The membrane surface area is  $S$ ; the cross-sectional area of the manometer tube is  $s$ . At  $t = 0$ , the height of fluid in the manometer is zero. The density of fluid is  $\rho$ . Show that the fluid height rises to a final value with an exponential behavior. Find the final value and the time constant. Ignore dilution of the solute.



**Problem 9** Consider the design of a lecture demonstration apparatus to show osmotic pressure that uses a commercially available filter as shown in the drawing. Assuming well-stirred fluid on both sides of the membrane

and neglecting the change of solute concentration in the manometer tube as water flows in, one finds that height  $z$  increases to the equilibrium value exponentially, with a time constant obtained in the previous problem. What would be the time constant if one used the membrane described in Fig. 5.10? For that membrane  $L_p = 1 \text{ ml min}^{-1} \text{ m}^{-2} \text{ torr}^{-1}$ , and the total membrane area is  $S = 0.2 \text{ m}^2$ . Suppose that the inner radius of the manometer tube is 1 mm. (One could not use sucrose as a solute, because this particular membrane is permeable to molecules of molecular weight less than 50,000.)



**Problem 10** A cell has variable volume  $V$  and fixed surface area  $S$ . The total hydrostatic pressure  $p$  is the same inside and outside the cell, and there is complete and instantaneous mixing. Initially the interior and exterior are both pure water. The initial volume of the cell is  $V_0$ . At  $t = 0$ , the exterior is bathed in a solution containing an impermeant solute of concentration  $C_0$ .

(a) Does the cell shrink to zero volume or expand to its maximum volume, which is a sphere of surface area  $S$ ?

(b) Derive a differential equation for the volume change and integrate it to find how long it takes for the cell to reach zero or maximum volume.

**Problem 11** A cell has variable volume  $V$  and fixed surface area  $S$ . The total hydrostatic pressure  $p$  is always the same both inside and outside the cell. There is complete and instantaneous mixing both inside and out. An impermeant solute has an initial concentration  $C(0)$  both inside and outside. The initial cell volume is  $V_0$ . At  $t = 0$  the exterior solute is removed.

(a) Does the cell shrink to zero volume or expand to its maximum volume, which is a sphere of surface area  $S$ ?

(b) Derive a differential equation for  $V(t)$  and find how long it takes for the cell to reach zero or maximum volume.

Section 5.6

**Problem 12** Two membranes have permeabilities  $\omega_1 RT$  and  $\omega_2 RT$ . Find the permeability of a two-layered membrane in terms of  $\omega_1$  and  $\omega_2$ .

**Problem 13** Solute is carried through a pipe by solvent drag. The radius of the pipe is  $b$ . The average flow along

the pipe is  $\bar{j}_v$  (independent of  $r$  because it has been averaged over  $r$ ). Assume that within the pipe the concentration of solute is independent of radius and can be written as  $C(z)$ . The solute is carried along purely by solvent drag. Solute concentration outside the pipe is zero. Solute diffuses through the wall of the pipe, which has solute permeability  $\omega RT$ . In terms of  $\bar{j}_v$ ,  $b$ , and  $\omega RT$ , obtain a differential equation for  $C(z)$  and show that  $C$  decays exponentially along the pipe. Find the decay constant.

Section 5.7

**Problem 14** A kidney machine has a membrane permeability  $\omega RT = 0.5 \times 10^{-3} \text{ cm s}^{-1}$ . If the membrane area is  $1 \text{ m}^2$ , the volume of body fluid is 40 l, and the volume of dialysant is effectively infinite, what is the time constant? How long will it take to reduce the BUN (blood urea nitrogen) concentration from 120 mg per 100 ml to 20 mg per 100 ml?

**Problem 15** Find the pair of coupled differential equations for  $C$  and  $C'$  for a dialysis machine in which  $V'$  is not infinite.

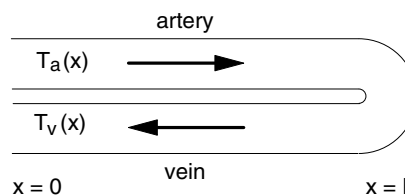
Section 5.8

**Problem 16** In the countercurrent model (Eq. 5.25) the total current  $i$  through the membrane when its length is  $X$  is

$$i = \omega RT Y \int_0^X [C_{in}(x) - C_{out}(x)] dx.$$

Solve this integral for the two cases given by Eqs. 5.26 and 5.27. Show that the current ratio in these two cases is 1.36 when  $a = 1$  and  $X = 2$ .

**Problem 17** The countercurrent model applies to the transport of heat as well as particles, with temperature taking the place of concentration. Consider a countercurrent heat exchanger, which represents the arrangement of blood vessels in the flipper of a whale [Schmidt-Nielsen (1972)].



The temperatures of the arterial and venous blood are governed by equations similar to Eqs. 5.27:

$$T_a = c_1 + (c_2 - c_1)ax,$$

$$T_v = c_2 + (c_2 - c_1)ax.$$

Assume that the arterial blood at  $x = 0$  is at the warm temperature of the whale's body,  $T_w$ . The arterial blood at  $x = L$  enters the capillaries at temperature  $T_a(L)$  and is

cooled to the temperature of the surrounding ocean water,  $T_c$ , by the time it enters the vein at  $x = L$ .

- (a) Determine  $c_1$  and  $c_2$  in terms of  $T_w$ ,  $T_c$ ,  $a$ , and  $L$ .
- (b) Plot  $T_a(x)$  and  $T_v(x)$  for  $T_w = 37^\circ\text{C}$ ,  $T_c = 7^\circ\text{C}$ ,  $a = 1\text{ mm}^{-1}$ , and  $L = 3\text{ mm}$ .
- (c) The loss of heat from the body to the surroundings is proportional to  $\Delta T = T_a(L) - T_c$ . Find an expression for  $\Delta T$ . What does  $\Delta T$  reduce to if  $aL \ll 1$ ? if  $aL \gg 1$ ? Interpret these results physically. To minimize heat loss to the ocean should  $aL$  be large or small?
- (d) The energy the body must supply to heat the returning venous blood is proportional to  $\Delta T' = T_w - T_v(0)$ . Find an expression for  $\Delta T'$ .

Section 5.9

**Problem 18** Derive Eqs. 5.44a and 5.44b.

**Problem 19** Show that Eq. 5.51 gives  $C(z) = \text{const}$  when  $\lambda = 0$  (pure solvent drag) and gives  $dC/dz = \text{const}$  when  $\lambda \rightarrow \infty$  (pure diffusion).

**Problem 20** Obtain expressions for  $J_s$  when  $\lambda = 0$  and  $\lambda \rightarrow \infty$ .

**Problem 21** Show that for very large pores when  $\sigma = 0$  the parameter  $x = \Delta Z/\lambda = J_v/\omega RT$  depends only on pore radius, solute particle radius, pressure difference and temperature, and not on viscosity, the number of pores per unit area, or the membrane thickness.

**Problem 22** When  $C'_s = 0$ , what are the limiting values of  $\bar{C}_s$  as  $x \rightarrow 0$ ? as  $x \rightarrow \infty$ ?

**Problem 23** (a) Write  $J_s$  in terms of  $C_s$ ,  $C'_s$ ,  $J_v$  and  $x$ .  
 (b) Specialize to the case  $C'_s = 0$ .

**Problem 24** (a) Find the ratio  $(1 - \sigma)\bar{C}_s J_v / [\omega RT(C_s - C'_s)]$  in terms of  $x$ ,  $C_s$ , and  $C'_s$ .  
 (b) Specialize to the case  $C'_s = 0$  and discuss limiting values for small and large  $x$ .

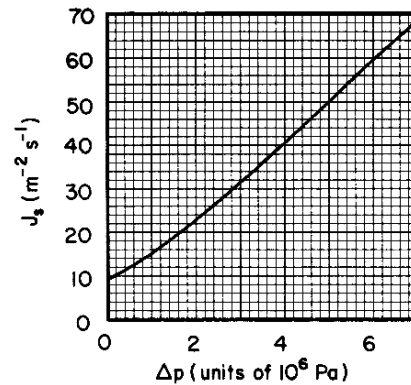
**Problem 25** (a) Show that

$$J_s = \omega RT \left( C_s \frac{x e^x}{e^x - 1} - C'_s \frac{x}{e^x - 1} \right)$$

where  $x = J_v(1 - \sigma)/\omega RT$ .

(b) Discuss the special case  $C'_s = 0$  in the limits  $x \rightarrow 0$  and  $x \rightarrow \infty$ .

(c) From the data shown, estimate  $L_p$  and  $\omega RT$ . The data are for the transport of radioactive water with a concentration of  $10^{15}$  molecules  $\text{m}^{-3}$  on one side of the membrane and zero on the other.



**Problem 26** Consider the following cases for transport of water through a membrane.

- (a) Water flows by bulk flow through the membrane with  $\Delta p = 0$ . There is an impermeant solute ( $\sigma = 1$ ) on the right with concentration  $C_{\text{big}}$  and zero concentration on the left. Find the particle fluence rate of water in terms of  $L_p$ .
- (b) There is no volume flow through the membrane ( $J_v = 0$ ). Some of the water molecules on the left are tagged with radioactive hydrogen (tritium). The concentration of tagged water molecules is  $C_s$  on the left and 0 on the right. Find the particle fluence rate of tagged water in terms of  $L_p$  and  $\omega RT$ .
- (c) There is volume flow, as in case (a), and there are also tagged water molecules on the left. Find the particle fluence rate of tagged water in terms of  $L_p$  and  $\omega RT$ .
- (d) Restate the answers in terms of the parameters of a collection of  $n$  pores per unit area of radius  $R_p$  and length  $\Delta Z$ .
- (e) Estimate the value of  $x$  for part (c) if  $R_p = 10^{-8}$  m and  $c_{\text{big}} = c_s = 0.1 \text{ mol l}^{-1}$ .

**Problem 27** Construct diagrams analogous to Fig. 5.17 (a) when the total pressure is the same on both sides and  $\pi' = 0$  and (b) when  $(p - \sigma\pi) < p'$  and  $\pi' = 0$ .

**Problem 28** Consider the case of water permeability shown in Fig. 5.1(c). Water and solute molecules move through the membrane in the same way. They “dissolve” from solution into the membrane. Assume that the concentration of water molecules just inside the membrane is proportional to the pressure just outside:  $C = \alpha p$ . The membrane has thickness  $\Delta Z$  and the diffusion constant for water in the membrane material is  $D$ . Under steady-state conditions, derive an expression for  $L_p$ .

**Problem 29** Consider the case in which solute moves along a tube by a combination of diffusion and solvent drag. Ignore radial diffusion within the tube, but assume that solute is moving out through the walls so that  $j_s$  is changing with position in the tube. In particular, the number of solute particles passing out through the wall in length  $dz$  in time  $dt$  is  $CA2\pi R_p dz dt$ , where  $A$  is related to the permeability of the wall. Consider a case in

which  $C$  does not change with time, but depends only on position along the tube.

(a) Write down the conservation equation for an element of the tube and show that

$$-\frac{\partial j}{\partial z} - \frac{2AC}{R_p} = 0.$$

(b) Combine the results of part (a) with Eq. 5.45a and show that  $C(z)$  must satisfy the differential equation

$$\frac{\partial^2 C}{\partial z^2} - \frac{\bar{j}_v f}{D} \frac{\partial C}{\partial z} - \frac{2A}{DR_p} C = 0.$$

Show that this equation will be satisfied if the concentration decreases exponentially along the tube as  $C(z) = C_0 e^{-\alpha z}$ , where

$$\alpha = \frac{\bar{j}_v f}{2D} \left[ -1 + \left( 1 + \frac{8AD}{R_p \bar{j}_v^2 f^2} \right)^{1/2} \right].$$

**Problem 30** The volume of a water molecule is  $V_w$  and the volume of a solute molecule is  $V_s$ . Define a new quantity  $J_w$  that is the number of water molecules per unit area per second passing through the membrane. What is  $J_w$  in terms of  $J_v$  and  $J_s$ ?

## References

- Basser, P. J., R. Schneidermann, R. A. Bank, E. Wachtel, and A. Maroudas (1998). Mechanical properties of the collagen network in human articular cartilage as measured by osmotic stress technique. *Arch. Biochem. Biophys.* **351**: 207–219.
- Bean, C. P. (1969). *Characterization of Cellulose Acetate Membranes and Ultrathin Films for Reverse Osmosis*. Research and Development Progress Report No. 465 to the U.S. Department of Interior, Office of Saline Water. Contract No. 14-01-001-1480. Washington, Superintendent of Documents, October 1969.
- Bean, C. P. (1972). The physics of porous membranes: Neutral pores, in G. Essenman, ed., *Membranes*. New York, Dekker, Vol. 1, pp. 1–55.
- Beck, R. E., and J. S. Schultz (1970). Hindered diffusion in microporous membranes with known pore geometry. *Science* **170**: 1302–1305.
- Calland, C. H. (1972). Iatrogenic problems in end-stage renal failure. *N. Engl. J. Med.* **287**: 334–336.
- Cokelet, G. R. (1972). The rheology of human blood, in Y. C. Fung *et al.*, eds. *Biomechanics: Its Foundations and Objectives*. Englewood Cliffs, NJ, Prentice Hall (especially p. 77, Fig. 4).
- Durbin, R. P. (1960). Osmotic flow of water across permeable cellulose membranes. *J. Gen. Physiol.* **44**: 315–326.
- Fishman, R. A. (1975). Brain edema. *N. Engl. J. Med.* **293**: 706–711.
- Galletti, P. M., C. K. Colton, and M. J. Lysaght (2000). Artificial kidney. In J. D. Bronzino, ed. *The Biomedical Engineering Handbook*, 2nd. ed., Vol. 2. Boca Raton, FL CRC Press.
- Gennari, F. J., and J. P. Kassirer (1974). Osmotic diuresis. *N. Engl. J. Med.* **291**: 714–720.
- Guyton, A. C. (1991). *Textbook of Medical Physiology*, 8th ed. Philadelphia, Saunders.
- Guyton, A. C., A. E. Taylor, and H. J. Granger (1975). *Circulatory Physiology II. Dynamics and Control of the Body Fluids*. Philadelphia, Saunders.
- Hildebrand, J. H., and R. L. Scott (1964). *The Solubility of Nonelectrolytes*. 3rd ed. New York, Dover.
- Katchalsky, A., and P. F. Curran (1965). *Nonequilibrium Thermodynamics in Biophysics*. Cambridge, Harvard University Press.
- Levitt, D. G. (1975). General continuum analysis of transport through pores. I. Proof of Onsager's reciprocity postulate for uniform pore. *Biophys. J.* **15**: 533–551.
- Lindner, A., B. Charra, D. J. Sherrard, and B. H. Scribner (1974). Accelerated atherosclerosis in prolonged maintenance hemodialysis. *N. Engl. J. Med.* **290**: 697–701.
- Lysaght, M. J., and J. Moran (2000). Peritoneal dialysis equipment. In J. D. Bronzino, ed. *The Biomedical Engineering Handbook*. 2nd ed., Vol. 2. Boca Raton, FL, CRC Press.
- Patton, H. D., A. F. Fuchs, B. Hille, A. M. Scher, and R. F. Steiner, eds. (1989). *Textbook of Physiology*, 21st ed. Philadelphia, Saunders.
- Schmidt-Nielsen, K. (1972). *How Animals Work*. Cambridge, Cambridge University Press.
- Silverstein, M. E., C. A. Ford, M. J. Lysaght, and L. W. Henderson (1974). Treatment of severe fluid overload by ultrafiltration. *N. Engl. J. Med.* **291**: 747–751.
- Steinmuller, D. R. (1998). A dangerous error in the dilution of 15 percent albumin. *N. Engl. J. Med.* **338**: 1226.
- Thomas, Lewis (1974). *Lives of a Cell*. New York, Viking.
- White, R. J., and M. J. Likavek (1992). Current concepts: The diagnosis and initial management of head injury. *N. Engl. J. Med.* **327**: 1502–1511.

# 6

## Impulses in Nerve and Muscle Cells

A nerve cell conducts an electrochemical impulse because of changes that take place in the cell membrane. These changes allow movement of ions through the membrane, setting up currents that flow through the membrane and along the cell. Similar impulses travel along muscle cells before they contract. This chapter reviews the basic properties of electric fields and currents that are needed to understand the propagation of the nerve- or muscle-cell impulse.

Section 6.1 introduces the physiology of nerve conduction. The next eight sections develop the electrostatics and the physics of current flow needed to understand how the action potential propagates along the cell.

The next sections deal with the charge distribution on a resting cell membrane (Sec. 6.10) and the cable model of the axon (Sec. 6.11). If the membrane properties do not change as the voltage across the membrane changes, this leads to electrotonus or passive spread (Sec. 6.12). If the membrane properties do change, a signal can propagate without change of shape. Section 6.13 tells how Hodgkin and Huxley developed equations to describe the membrane changes, and Secs. 6.14 and 6.15 apply their results to the propagation of a nerve impulse. The chapter to this point forms an integrated story of conduction in an unmyelinated axon.

Section 6.16 considers saltatory conduction: the “jumping” of an impulse from node to node in a myelinated fiber. Section 6.17 examines the capacitance of a bilayer membrane that has layers with different properties. Section 6.18 shows how minor alterations in the membrane properties can transform the Hodgkin–Huxley model to one that displays repetitive electrical activity.

Section 6.19 shows how tabulated solutions to the electrical capacitance of conductors in different geometries can be used to solve diffusion problems with similar geometric configurations.

### 6.1 Physiology of Nerve and Muscle Cells

A nerve<sup>1</sup> consists of many parallel, independent signal paths, each of which is a nerve cell or fiber. Each cell transmits signals in only one direction; separate cells carry signals to or from the brain. Each cell has an input end (dendrites), a cell body, a long conducting portion or *axon*, and an output end. It is the ends that give the cell its unidirectional character. The input end may be a transducer (stretch receptor, temperature receptor, etc.) or a junction (synapse) with another cell. A threshold mechanism is built into the input end; when an input signal exceeding a certain level is received, the nerve fires and an *impulse* or *action potential* of fixed size and duration travels down the axon. There may be several inputs that can either aid or inhibit each other, depending on the nature of the synapses.

Muscle cells are also long and cylindrical. An electrical impulse travels along a muscle cell to initiate its contraction. This chapter concentrates on the propagation of the action potential in a nerve cell, but the discussion can be regarded as a model for what happens in muscle cells as well.

The axon transmits the impulse without change of shape. The axon can be more than a meter in length, extending from the brain to a synapse low in the spinal cord or from the spinal cord to a finger or toe. Bundles of axons constitute a nerve. The output end branches out in fine nerve endings, which appear to be separated by a gap from the next nerve or muscle cell that they drive.

---

<sup>1</sup>A good discussion of the properties of nerves and the Hodgkin–Huxley experiments is found in Katz (1966). More modern descriptions of nerves and nerve conduction are found in many books, such as Patton *et al.* (1989).

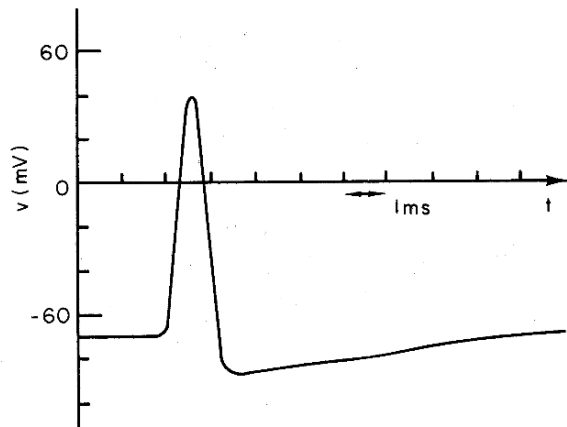


FIGURE 6.1. A typical nerve impulse or action potential, plotted as a function of time.

The long cylindrical axon has properties that are in some ways similar to those of an electric cable. Its diameter may range from less than one micrometer ( $1\ \mu\text{m}$ ) to as much as 1 mm for the giant axon of a squid; in humans the upper limit is about  $20\ \mu\text{m}$ . Pulses travel along it with speeds ranging from  $0.6$  to  $100\ \text{m s}^{-1}$ , depending, among other things, on the diameter of the axon. The axon core may be surrounded by either a membrane (for an *unmyelinated* fiber) or a much thicker sheath of fatty material (*myelin*) that is wound on like tape. A myelinated fiber has its sheath interrupted at intervals and replaced by a short segment of membrane similar to that on an unmyelinated fiber. These interruptions are called *nodes of Ranvier*. A typical human nerve might contain twice as many unmyelinated fibers as myelinated. We will see in Sec. 6.16 that the myelin gives a faster impulse conduction speed for a given axon radius. Myelinated fibers conduct motor information; unmyelinated fibers conduct information such as temperature, for which speed is not important. A typical unmyelinated axon might have a radius of  $0.7\ \mu\text{m}$  with a membrane thickness of  $5\text{--}10\ \text{nm}$ . Myelinated fibers have a radius of up to  $10\ \mu\text{m}$ , with nodes spaced every  $1\text{--}2\ \text{mm}$ . We will find later that the spacing of the nodes is about 140 times the inner radius of the fiber, a fact that is quite important in the relationship between conduction speed and fiber radius.

A microelectrode inserted inside a resting axon shows an electrical potential that is about  $70\ \text{mV}$  less than outside the cell. (We will define electrical potential difference in Sec. 6.4.) A typical nerve impulse or action potential or spike in an unmyelinated axon is shown as a function of time in Fig. 6.1. As the impulse passes by the electrode, the potential rises in a millisecond or less to about  $+40\ \text{mV}$ . The potential then falls to about  $-90\ \text{mV}$  and then recovers slowly to its resting value of  $-70\ \text{mV}$ . The membrane is said to *depolarize* and then *repolarize*.

The history of recording the action potential has been described by Geddes (2000). The action potential was first measured by Helmholtz around 1850. The measure-

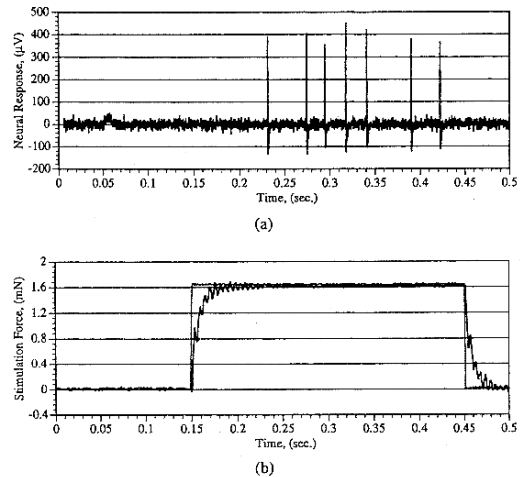


FIGURE 6.2. The response of a mechanical receptor in the cornea to an applied force. (a) The impulses recorded on the surface of the nerve bundle. (b) The applied force. Impulses occur while the force is applied. From B. J. Kane, C. W. Stormont, S. W. Crowder, D. L. Tanelian, and G. T. A. Kovacs. Force-sensing microprobe for precise stimulation of mechanoreceptive tissues. *IEEE Trans. Biomed. Eng.* **42**(8):745–750. © 1995 IEEE. Reprinted by permission.

ment technology steadily improved, culminating in the use of a microelectrode inserted by Hodgkin and Huxley (1939) into the cut end of the giant axon of the squid, to record the action potential directly.

The information sent along a nerve fiber is coded in the repetition rate of these pulses, all of which are the same shape. Figure 6.2 shows the response of a low-threshold mechanoreceptor in the cornea to a mechanical stimulus. The heavy curve in the bottom panel shows the applied force, and the upper panel shows the impulses.

Comparison of the *intracellular fluid* or *axoplasm* with the *extracellular fluid* surrounding each axon shows an excess of potassium and a deficit of sodium and chloride ions within the cell, as shown in Fig. 6.3. The regenerative action that produces the sudden changes of membrane potential is caused by changing permeability of the membrane to ions—primarily sodium and potassium. These changes are discussed in Secs. 6.13 and 6.14.

The axon can be removed from the rest of the cell and it will still conduct nerve impulses. The speed and shape of the action potential depend on the membrane and the concentration of ions inside and outside the cell. The axoplasm has been squeezed out of squid giant axons and replaced by an electrolyte solution without altering appreciably the propagation of the impulses—for a while, until the ion concentrations change appreciably. The axoplasm does contain chemicals essential to the long-term metabolic requirements of the cell and to maintaining the ion concentrations.

At the end of a nerve cell the signal passes to another nerve cell or to a muscle cell across a *synapse* or junction. A few synapses in mammals are electrical; most are

Inside of axon	Extracellular fluid	$c_o/c_i$
$[Na^+] = 15$	$[Na^+] = 145$	9.7
$[K^+] = 150$	$[K^+] = 5$	0.033
	$[Misc^+] = 5$	
$[Cl^-] = 9$	$[Cl^-] = 125$	13.9
$[Misc^-] = 156$	$[Misc^-] = 30$	0.19
$v = -70\text{mV}$	$v = 0$	

FIGURE 6.3. Ion concentrations in a typical mammalian nerve and in the extracellular fluid surrounding the nerve. Concentrations are in  $\text{mmol l}^{-1}$ ;  $c_o/c_i$  is the concentration ratio. The membrane thickness is  $b$ .

chemical [Nolte (2002), p. 193, Guyton and Hall (2000, Chapter 45)]. In electrical synapses, channels connect the interior of one cell with the next. In the chemical case a neurotransmitter chemical is secreted by the first cell. It crosses the synaptic cleft (about 50 nm) and enters the next cell.

At the neuromuscular junction the transmitter is *acetylcholine* (ACh). ACh increases the permeability of nearby muscle to sodium, which then enters and depolarizes the muscle membrane. The process is quantized.<sup>2</sup> Packets of acetylcholine of definite size are liberated [Katz (1966, Chapter 9); Patton *et al.* (1989, Chapter 6)].

There are a number of neurotransmitters in the central nervous system. *Glutamate* is a common excitatory neurotransmitter in the central nervous system. It increases the membrane permeability to sodium ions, which enhances depolarization. *Glycine*, on the other hand, is an inhibitory neurotransmitter. It causes the interior potential becomes more negative (hyperpolarized) and firing is inhibited. A number of other chemical mediators such as norepinephrine, epinephrine, dopamine, serotonin, histamine, aspartate, and gamma-aminobutyric acid, are also found in the nervous system [Guyton and Hall (2000, Chapter 45)].

If the potential becomes high enough (that is, more positive or less negative), the regenerative action of the membrane takes over, and the cell initiates an impulse. If the input end of the cell acts as a transducer, the interior potential rises when the cell is stimulated. If the input is from another nerve, the signal may cause the potential to increase by a subthreshold amount so that two or more stimuli must be received simultaneously to cause firing, or it may decrease the potential and inhibit stimulation by another nerve at the synapse. This makes possible the logic network that comprises the central nervous system.

<sup>2</sup>See Problem 3 in Appendix J.

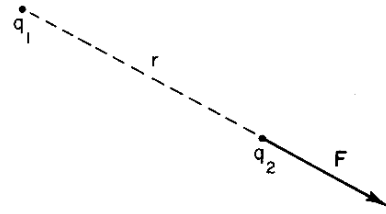


FIGURE 6.4. Force  $\mathbf{F}$  is exerted by charge  $q_1$  on charge  $q_2$ . It points along a line between them. An equal and opposite force  $-\mathbf{F}$  is exerted by  $q_2$  on  $q_1$ .

## 6.2 Coulomb's Law, Superposition, and the Electric Field

Coulomb's law relates the electrical force between two objects to their electrical charge and separation. For our purpose, Coulomb's law is a summary of many experiments. If two objects have electrical charge  $q_1$  and  $q_2$ , respectively, and are separated by a distance  $r$ , then there is a force between them, the magnitude of which is given by

$$|\mathbf{F}| = \left( \frac{1}{4\pi\epsilon_0} \right) \frac{q_1 q_2}{r^2}. \quad (6.1)$$

When the charge is measured in coulombs (C),  $F$  in newtons (N), and  $r$  in meters (m), the constant has the value

$$\frac{1}{4\pi\epsilon_0} \approx 9 \times 10^9 \text{ N m}^2 \text{ C}^{-2} \quad (6.2)$$

to an accuracy of 0.1%.<sup>3</sup> The direction of the force is along the line between the two charges as shown in Fig. 6.4. If the charges are both positive or both negative, the force is repulsive, which is consistent with assigning a positive sign to  $\mathbf{F}$ . If one is positive and the other negative, then the force is attractive, and  $\mathbf{F}$  has a negative value. Force  $\mathbf{F}$  is exerted by charge  $q_1$  on charge  $q_2$ . The force exerted by  $q_2$  on  $q_1$  has the same magnitude but points in the opposite direction. The forces on both charges act to separate them if they have the same sign and to attract them if the signs are opposite.

If two or more charges exert a force on the particular charge being considered, the total force is found by applying Coulomb's law to each charge (paired with the one on which we want to find the force) and adding the vector forces that are so calculated. An example of this is shown in Fig. 6.5. Charges  $q_1$ ,  $q_2$ , and  $q_3$  are  $+1.0 \times 10^{-6}$ ,  $-2.0 \times 10^{-6}$ , and  $+3.0 \times 10^{-6}$  C, respectively. The magnitude of the force that  $q_1$  exerts on  $q_3$  is

$$F_{1 \text{ on } 3} = \frac{(9 \times 10^9)(1 \times 10^{-6})(3 \times 10^{-6})}{(2 \times 10^{-2})^2} = 67.5 \text{ N}.$$

<sup>3</sup>The quantity  $1/4\pi\epsilon_0$  has been assigned the *exact* value  $8.9875517873681764 \times 10^9$ . This is because in 1983 the velocity of light,  $c$ , was defined to be exactly 299,792,458  $\text{m s}^{-1}$  and  $1/4\pi\epsilon_0 \equiv 10^{-7} c^2$ .

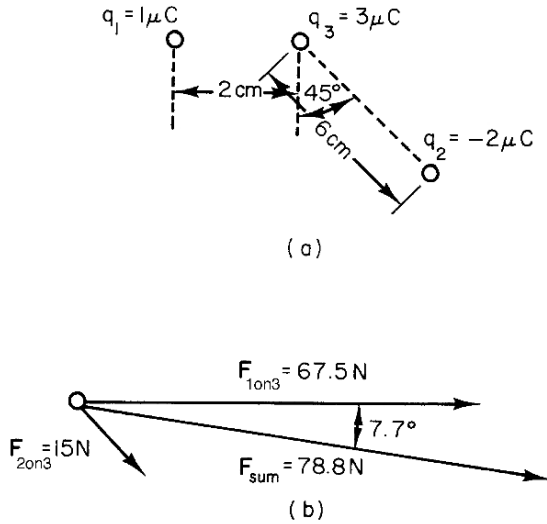


FIGURE 6.5. An example of applying Coulomb’s law and adding forces on  $q_3$  due to charges  $q_1$  and  $q_2$ . (a) The arrangement of charges. (b) The forces on  $q_3$ .

Similarly, the force exerted by  $q_2$  on  $q_3$  is

$$F_{2 \text{ on } 3} = \frac{(9 \times 10^9)(-2 \times 10^{-6})(3 \times 10^{-6})}{(6 \times 10^{-2})^2} = -15 \text{ N.}$$

The minus sign means that the force is attractive, that is, toward  $q_2$ . The two forces are shown in Fig. 6.5b, along with their vector sum. The sum can be found by components as in Chap. 1. The result is 78.8 N at an angle of  $7.7^\circ$  clockwise from the direction of  $\mathbf{F}_{1 \text{ on } 3}$ .

If a collection of charges causes a force to act on some other charge (a “test charge”) located somewhere in space, we say that the collection of charges produces an *electric field* at that point in space. One can think, for example, of charge  $q_1$  producing an electric field vector, of magnitude

$$|\mathbf{E}_1| = \frac{1}{4\pi\epsilon_0} \frac{q_1}{r^2} \tag{6.3}$$

pointing radially away from  $q_1$  (if  $q_1$  is positive) or radially toward  $q_1$  (if  $q_1$  is negative). The force on test charge  $q_2$  placed at the observing point is then

$$\mathbf{F} = q_2 \mathbf{E}_1. \tag{6.4}$$

### 6.3 Gauss’s Law

It is possible to derive a theorem about the electric field from a collection of charges, known as *Gauss’s law*. Rather than derive it from Coulomb’s law, we will state it and show that Coulomb’s law can be derived from it. Then we will consider some examples of its use.

Divide up *any* closed surface into elements of surface area, such as  $\Delta S$  in Fig. 6.6. For each element  $\Delta S$ , calculate the component of  $\mathbf{E}$  normal to the surface,  $E_n$ ,

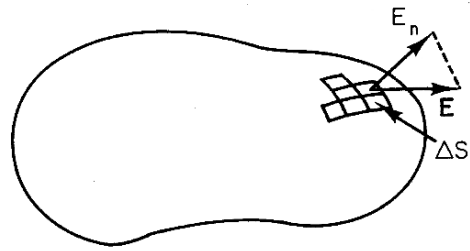


FIGURE 6.6. Calculating the integral of the normal component of  $\mathbf{E}$  through a surface.

and multiply it by the magnitude of the surface area  $\Delta S$ . Add these quantities for the entire closed surface, calling them positive if the normal component of  $\mathbf{E}$  points outward and negative if  $\mathbf{E}$  points inward. Gauss’s law says that the resulting sum is equal to the total charge inside the surface, divided by  $\epsilon_0$ . In symbols,<sup>4</sup>

$$\iint E_n dS = \frac{q}{\epsilon_0} = \frac{4\pi q}{4\pi\epsilon_0}. \tag{6.5}$$

This surface integral is exactly the same as the flux of the continuity equation, Eq. 4.4. It is in fact called the *electric field flux*.<sup>5</sup>

While Gauss’s law is always *true*, it is not always *useful*. It is helpful only in cases where  $\mathbf{E}$  is constant over the entire surface of integration, or when the surface can be divided into smaller surfaces, on each of which  $E_n$  can be argued to be constant or zero. One of the few cases in which Gauss’s law is useful to calculate  $\mathbf{E}$  is the case of a point charge, and another is related to the cell membrane. In each case, the symmetry of the problem allows the surface of integration to be specified so that  $E_n$  is either constant or zero.

The first example is a point charge in empty space. Since such a charge has no preferred orientation (it is a point), and since there is nothing else around to specify a preferred direction in space, the electric field must point radially toward or away from the charge and must depend only on distance from the charge. Therefore, if the surface of integration is a sphere centered on the charge,  $E_n$  is the same everywhere on the sphere. It can be taken outside the integral in Eq. 6.5 to give

$$\iint E_n dS = E \iint dS.$$

The integral of  $dS$  over the entire surface of the sphere is just the surface area of the sphere,  $4\pi r^2$  (see Appendix L). Gauss’s law gives

$$4\pi r^2 E = \frac{q}{\epsilon_0}$$

<sup>4</sup>Some books use one integral sign in this equation and others use two. Strictly speaking the integral over a surface is a two-dimensional integral.

<sup>5</sup>Additional discussion and examples can be found in Schey (1997).



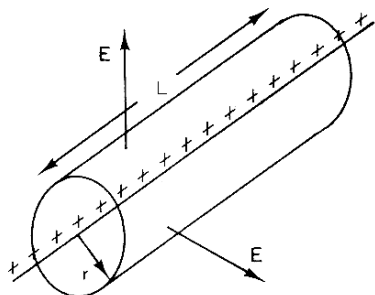


FIGURE 6.7. Gauss's law is used to calculate the electric field from an infinite line of charge. The Gaussian surface is a segment of a cylinder concentric with the line of charge.

or

$$E = \frac{q}{4\pi\epsilon_0 r^2}.$$

Gauss's law implies Coulomb's law for the case of a point charge.

If the charge in this problem is not a point charge, nothing changes in the argument as long as the charge distribution is spherically symmetric. The electric field at a distance  $r$  from the center of the distribution is the same as if all the charge within the sphere of radius  $r$  were located at the center of the sphere.

Next, consider a problem with cylindrical symmetry rather than spherical symmetry. An example is an infinitely long line of charge. For a segment of the line of charge of length  $L$ , the amount of charge is proportional to  $L$ ,  $q = \lambda L$ , where  $\lambda$  is the linear charge density in units  $\text{C m}^{-1}$ . Symmetry shows that  $\mathbf{E}$  must point radially outward (or inward) and be perpendicular to the line. Therefore if the Gaussian surface is a cylinder of length  $L$  and radius  $r$ , the axis of which is the line of charge, one can argue that on the end caps  $E_n = 0$ , while on the wrap-around surface of the cylinder  $E_n = |\mathbf{E}|$ . This is shown in Fig. 6.7. The total integral is therefore the integral for the wrap-around surface, which is  $E \iint dS$ . The surface area of the cylinder is its circumference ( $2\pi r$ ) times its length ( $L$ ). Therefore Gauss's law becomes  $2\pi r L E = \lambda L / \epsilon_0$ , or

$$E = \frac{\lambda}{2\pi\epsilon_0 r}. \quad (6.6)$$

Since the constant  $1/4\pi\epsilon_0$  is so easily remembered, it is convenient to write this as

$$E = \frac{1}{4\pi\epsilon_0} \frac{2\lambda}{r}. \quad (6.7)$$

Consider next an infinite sheet of charge, with charge per unit area  $\sigma \text{ C m}^{-2}$ . The symmetry of the situation requires that  $\mathbf{E}$  be perpendicular to the sheet. To see why, suppose that  $\mathbf{E}$  is not perpendicular to the sheet. I stand on the sheet looking in such a direction that  $\mathbf{E}$  points diagonally off to my left. If I turn around in place, I see  $\mathbf{E}$  pointing diagonally off to my right. Since the charge

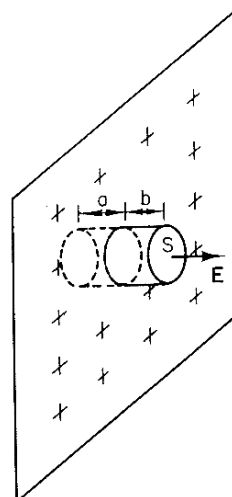


FIGURE 6.8. A portion of an infinite sheet of charge and the appropriate Gaussian surface.

per unit area is constant and extends an infinite distance in every direction, the charge distribution looks exactly the same as it did before I turned around. The only way to resolve this contradiction (that  $\mathbf{E}$  changed direction while the charge distribution did not change) is to have  $\mathbf{E}$  perpendicular to the sheet.

The Gaussian surface can be a cylinder with end caps of area  $S$  and sides perpendicular to the sheet. Let the end caps be a distance  $a$  from the charge sheet on one side and  $b$  from the charge sheet on the other, as in Fig. 6.8. Since there is no component of  $\mathbf{E}$  across the sides of the cylinder, changing  $b$  or  $a$  does not change the total flux through the surface. Since the charge inside the volume does not change,  $E$  must be independent of distance from the sheet of charge. (This is true only because the charge sheet is infinite.) By symmetry, the flux through each end cap is the same, as may be seen from the cross section of the surface in Fig. 6.9. The total flux is therefore  $2ES$ , while the charge within the volume is  $\sigma S$ . Therefore, Gauss's law gives

$$E = \frac{\sigma}{2\epsilon_0} = \frac{1}{4\pi\epsilon_0} 2\pi\sigma. \quad (6.8)$$

There is, of course, something quite unreal about a sheet of charge extending to infinity. However, it is a good approximation for an observation point close to a finite sheet of charge. If the sheet is limited in extent and the observation point is far away, the distance to all parts of the sheet from the observation point is nearly the same, and the charge sheet may be regarded as a point charge. If one considers a rectangular sheet of charge lying in the  $xy$  plane of width  $2c$  and length  $2b$ , as shown in Fig. 6.10, it is possible to calculate exactly the  $\mathbf{E}$  field along the  $z$  axis. By symmetry, the field points along the  $z$  axis. The surface charge density is  $\sigma$ . The distance is  $r = (x^2 + y^2 + z^2)^{1/2}$ . The component of  $\mathbf{E}$  parallel to the  $z$  axis is  $E \cos \theta = Ez/r$ . Therefore, if the charge in element

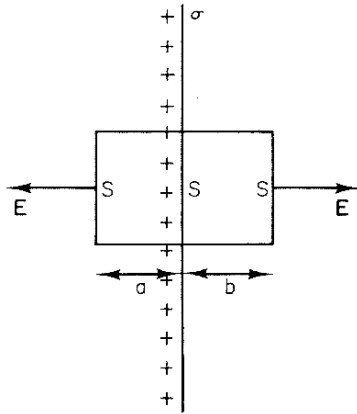


FIGURE 6.9. A side view of the Gaussian surface in Fig. 6.8.

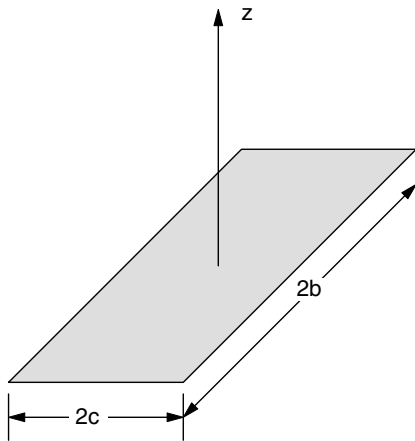


FIGURE 6.10. A rectangular sheet of charge. The electric field along the  $z$  axis is shown in Fig. 6.11 for  $2b = 200$  m and  $2c = 2$  m.

of area  $dx dy$  is  $\sigma dx dy$ , the field is

$$E = \frac{\sigma z}{4\pi\epsilon_0} \int_{-b}^b \int_{-c}^c (x^2 + y^2 + z^2)^{-3/2} dx dy. \quad (6.9)$$

This integral can be evaluated (see Problem 7). The result is

$$E = \frac{4\sigma}{4\pi\epsilon_0} \tan^{-1} \left( \frac{bc}{z\sqrt{c^2 + b^2 + z^2}} \right). \quad (6.10)$$

This is plotted in Fig. 6.11 for  $c = 1$  m,  $b = 100$  m. Close to the sheet ( $z \ll 1$ ) the field is constant, as it is for an infinite sheet of charge. Far away compared to 1 m but close compared to 100 m, the field is proportional to  $1/r$  as with a line charge. Far away compared to 100 m, the field is proportional to  $1/r^2$ , as from a point charge.

As a final example, consider two infinite sheets of charge, one with density  $-\sigma$  and the other with density  $+\sigma$ , as shown in Fig. 6.12. This can be solved by using the result for a single sheet of charge, Eq. 6.8, and the principle of superposition. Consider first the region I of Fig. 6.12. There, the negative charge will give an  $\mathbf{E}$  field

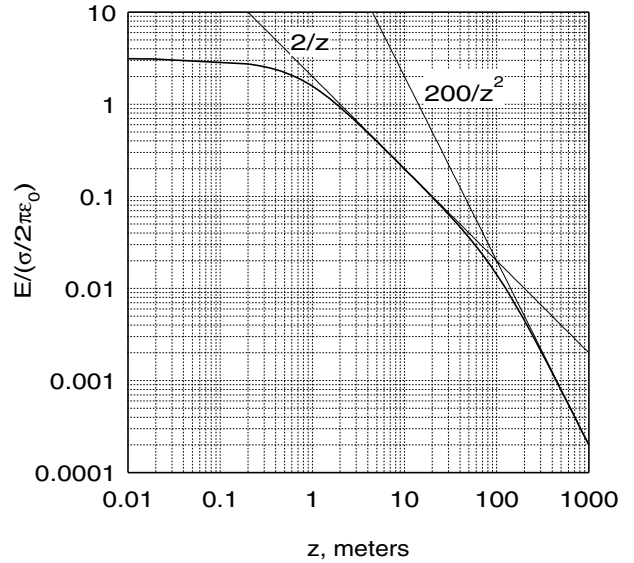


FIGURE 6.11. A log-log plot of the electric field from a sheet of charge of width 2 m and length 200 m, measured along the perpendicular bisector of the sheet (Fig. 6.10). Much closer than 1 m, the field is constant. Around 10 m the field is proportional to  $1/r$ , the field from a line charge. Farther away than 100 m the field is proportional to  $1/r^2$ , the field from a point charge.

that has magnitude  $\sigma/2\epsilon_0$  and points toward the right, while the positive sheet of charge will give an  $\mathbf{E}$  field of  $\sigma/2\epsilon_0$  pointing to the left. The total  $\mathbf{E}$  field in region I is zero. A similar argument can be made in region III with the field of the negative charge pointing left and that of the positive charge pointing to the right. Again the sum is zero. In region II, however, the two  $\mathbf{E}$  fields point in the same direction, and the total field is

$$E = \frac{\sigma}{\epsilon_0} = \frac{1}{4\pi\epsilon_0} 4\pi\sigma. \quad (6.11)$$

Notice the factor of 2 difference between Eqs. 6.8 and 6.11. Another way to explain the difference is that there is no  $\mathbf{E}$  in region III, so that a Gaussian surface can be constructed as shown in Fig. 6.13. Then the flux is zero through every surface except cap A. The charge within

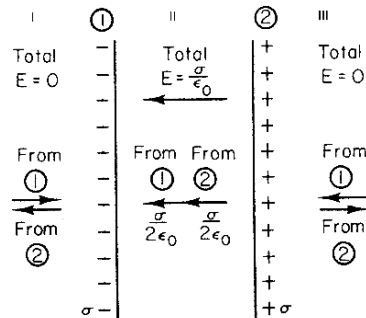


FIGURE 6.12. The electric field due to two infinite sheets of charge of opposite sign.

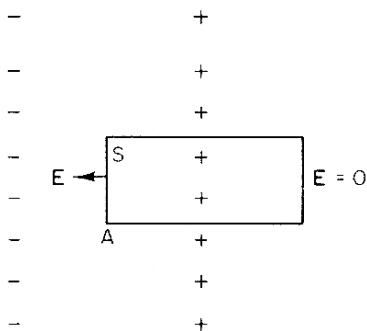


FIGURE 6.13. A Gaussian surface to determine the electric field between two sheets of charge.

the volume is  $\sigma S$ , while the flux through cap  $A$  is  $ES$ . Therefore,  $E = \sigma/\epsilon_0$ .

Within a cell membrane of 6 nm thickness surrounding a cell of radius 5  $\mu\text{m}$  or 5,000 nm, the electric field can be calculated by making the approximation that the sheets of charge are infinite. Suppose that the electric field within the membrane is  $1.17 \times 10^7 \text{ N C}^{-1}$ . (We will learn how to determine this value later.) From Eq. 6.11 the charge density is

$$\sigma = \frac{E}{4\pi(1/4\pi\epsilon_0)} = \frac{1.17 \times 10^7}{4\pi(9 \times 10^9)} = 1.03 \times 10^{-4} \text{ C m}^{-2}.$$

This tells us something about the makeup of the cell. The membrane is in contact with atoms, each of which has a diameter of about  $10^{-10}$  m. Therefore, there are approximately  $10^{20}$  atoms (in water molecules, as ions, etc.) in contact with one square meter of the membrane surface.

Suppose that the excess charge that causes the electric field in the membrane resides in these atoms and that each atom is either neutral or a monovalent ion. The number of atoms in the square meter which are charged is

$$\frac{1.03 \times 10^{-4} \text{ C m}^{-2}}{1.6 \times 10^{-19} \text{ C atom}^{-1}} = 6.4 \times 10^{14} \text{ atoms m}^{-2}.$$

The fraction of atoms that are charged is  $(6.4 \times 10^{14})/(10^{20}) = 6.4 \times 10^{-6}$ . Roughly 1 in every  $10^5$  atoms in contact with the membrane carries an unneutralized charge. (This result is modified by partial neutralization of this external charge by charge movement within the membrane. See Eq. 6.35.)

## 6.4 Potential Difference

It is often convenient to talk about the *electrical potential difference*, or *voltage difference* instead of the electric field. The potential is related to the difference in energy of a charge when it is at different points in space. Suppose

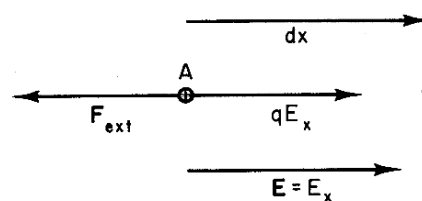


FIGURE 6.14. A charge  $q$  is moved from  $A$  to  $B$ , a distance  $dx$  in the  $x$  direction. External force  $\mathbf{F}_{\text{ext}}$  keeps the charge from being accelerated.

that an electric field  $\mathbf{E}$  of magnitude  $E_x$  points along the  $x$  axis. A positive charge is located at point  $A$ . A force  $\mathbf{F}_{\text{ext}}$  must be applied to the charge by something besides the electric field, or else the charge will be accelerated to the right by the force  $qE_x$ . The charge can be moved slowly to the right at a constant speed so that its kinetic energy remains fixed, if the external force is always to the left and its magnitude is adjusted so that  $F_{\text{ext}} = -qE_x$ .

This situation is shown in Fig. 6.14. The external force does work on the charge. One can either say that the total work done on the charge by both forces is equal to zero, or one can ignore the work done by the electric force and invent the idea of potential energy—energy of position—due to the electric field. The increase in potential energy<sup>6</sup> as the charge moves a distance  $dx$  is

$$dU = F_{\text{ext}} dx = -qE_x dx.$$

If  $E_x$  varies with position, the total change in potential energy when the particle is moved without acceleration from  $A$  to  $B$  is given by

$$\Delta U = U(B) - U(A) = -q \int_A^B E_x(x) dx. \quad (6.12)$$

For example, in a constant electric field of  $1.4 \times 10^7 \text{ N C}^{-1}$ , a particle with charge  $q = 1.6 \times 10^{-19} \text{ C}$  experiences an electric force equal to  $2.24 \times 10^{-12} \text{ N}$ . If it is moved 5 nm along the  $x$  axis, the electric force does  $1.12 \times 10^{-20} \text{ J}$  of work on it, increasing its kinetic energy. To prevent this increase in kinetic energy,  $F_{\text{ext}}$  must be applied. The external force does work  $-1.12 \times 10^{-20} \text{ J}$ . We can either say that the total work done by both forces is zero or we can ignore the electrical force and say that the external force changed the potential energy of the particle by  $-1.12 \times 10^{-20} \text{ J}$  as the particle moved from  $A$  to  $B$ .

If the displacement of the particle is perpendicular to the direction of the electric field, it is also perpendicular to the direction of  $\mathbf{F}_{\text{ext}}$ . Therefore neither force does work on the particle and the potential energy is unchanged.

<sup>6</sup>In earlier chapters the potential energy was called  $E_p$ , and the total energy was called  $U$ . For the next few pages  $U$  will be used for potential energy, to avoid confusion with a component of the electric field.

This fact can be used to prove [Halliday *et al.* (1992, p. 652)] that in three dimensions,

$$\begin{aligned} \Delta U &= U(B) - U(A) \\ &= -q \left( \int_A^B E_x dx + \int_A^B E_y dy + \int_A^B E_z dz \right). \end{aligned} \tag{6.13}$$

Using the notation of a “dot” or scalar product of two vectors (Sec. 1.8), this can also be written as a line integral along any path from  $A$  to  $B$ :

$$\Delta U = -q \int_A^B \mathbf{E} \cdot d\mathbf{r}. \tag{6.14}$$

It is easier to evaluate the integral along some paths than along others.

The potential energy difference is measured in joules. It is always proportional to the charge of the particle that is moved in the electric field. It is convenient to define the *potential difference* to be the potential energy difference per unit charge. When the energy difference is in joules and the charge is in coulombs, the ratio is  $\text{J C}^{-1}$ , which is called a *volt* (V):

$$\Delta v \text{ (V)} = \frac{\Delta U \text{ (J)}}{q \text{ (C)}}. \tag{6.15}$$

To move a charge of +3 C from point  $A$  to point  $B$  where the potential is 5 V higher requires that 15 J work be done on the charge. If the charge is then allowed to move back to point  $A$  under the influence of only the electric field, its kinetic energy increases by 15 J as the potential energy decreases by the same amount.

This definition of potential, when combined with the definition of potential energy, Eq. 6.12, gives

$$\Delta v = - \int_A^B E_x dx$$

or

$$E_x = - \frac{\partial v}{\partial x}. \tag{6.16a}$$

That is, the component of the electric field in any direction is the negative of the rate of change of potential in that direction. The units of  $\mathbf{E}$  were seen earlier to be  $\text{N C}^{-1}$  (from  $\mathbf{F} = q\mathbf{E}$ ). Equation 6.16 shows that the units of  $\mathbf{E}$  are also  $\text{V m}^{-1}$ . In three dimensions this relationship becomes

$$\mathbf{E} = - \text{grad } v = -\nabla v, \tag{6.16b}$$

where grad is the gradient operation defined in Eq. 4.19.

Notice that only differences in potential energy and differences in potential (or colloquially, differences in voltage) are meaningful. We can speak of the potential at a point only if we have previously agreed that the potential at some other point will be called zero. Then we are really speaking of the difference of potential between the reference point and the point in question.

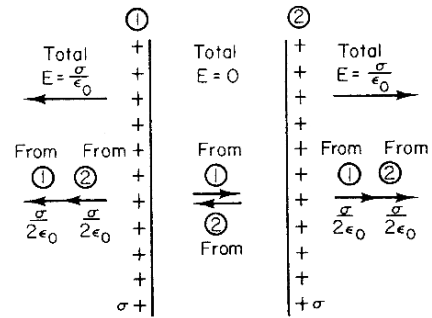


FIGURE 6.15. The electric field in and around an infinite plane conductor carrying a charge on each surface.

In many cases, it is customary to define the potential to be zero at infinity. Then the potential at point  $B$  is

$$v(B) = - \int_{\infty}^B E_x dx.$$

If you try to apply this equation to the infinite line and sheet of charge, you will discover that it does not work. The reason is that you cannot get infinitely far away from a charge distribution that extends to infinity.

## 6.5 Conductors

In some substances, such as metals or liquids containing ions, electric charges are free to move. When all motion of these charges has ceased and static equilibrium exists, there is no net charge within the conductor. To see why there is not, consider a small volume within the conductor. If there were an electric field within that region, the charges there would experience an electric force. Since they are free to move, this force would accelerate them. This force will vanish only when the electric field within the conductor is zero. Therefore, in the static case the electric field within a conductor is zero. Now apply Gauss’s law to a small volume within the conductor. Since the electric field in the conductor is zero everywhere, the flux through the Gaussian surface is zero, and the net charge within the volume is zero.

At the surface of the conductor, there may well be charge that gives rise to electric fields outside the conductor. Consider, for example, an infinite sheet of metal that has positive charge on it. The positive charge will distribute itself as shown in Fig. 6.15, and either superposition or Gauss’s law may be used to show that the electric field outside the conductor is  $\sigma/\epsilon_0$ .

Because the electric field is zero throughout a conductor in equilibrium, no work is required to move a charge from one point to another. All parts of the conductor are at the same potential. This statement is true only if the charges are not moving. We will see later that if they are (that is, if a current is flowing), then the electric field in

the conductor is not zero and the potential in the conductor is not the same everywhere.

## 6.6 Capacitance

Suppose that two conductors are fixed in space, with charge  $+Q$  on one and  $-Q$  on the other. The potential difference  $v$  between the conductors is proportional to  $Q$ . The proportionality constant depends on the geometrical arrangement of the conductors. When the proportionality is written as

$$Q = Cv \quad (6.17)$$

the proportionality constant  $C$  is called the *capacitance*. The units of capacitance are  $C\ V^{-1}$  or *farads* (F).

As an example of capacitance, consider two parallel conducting plates side by side. Let the area of each be  $S$  and the separation be  $b$ . The charge layers of Fig. 6.13 might be charge on the inner surface of each conductor. The total charge on each plate has magnitude  $\sigma S$ . The electric field between the plates is  $\sigma/\epsilon_0$  and the potential difference is  $v = Eb = \sigma b/\epsilon_0$ . (Note that the potential difference is proportional to the charge per unit area.) The capacitance is

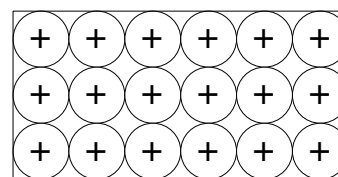
$$C = \frac{Q}{v} = \frac{\sigma S \epsilon_0}{\sigma b} = \frac{\epsilon_0 S}{b}. \quad (6.18)$$

If the plates are separated further with a fixed charge on them, the potential difference increases and the capacitance is decreased. Increasing the area and charge of the plates with fixed  $\sigma$  and fixed  $b$  increases  $Q$  and  $C$  but not  $v$ .

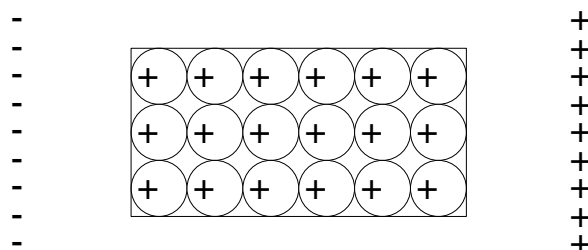
## 6.7 Dielectrics

Charges rearrange themselves so that there is no static electric field within a conductor. In a dielectric, charges are not free to move far enough to completely cancel the effect of any external electric field, but they can move far enough to cause a partial cancellation.<sup>7</sup>

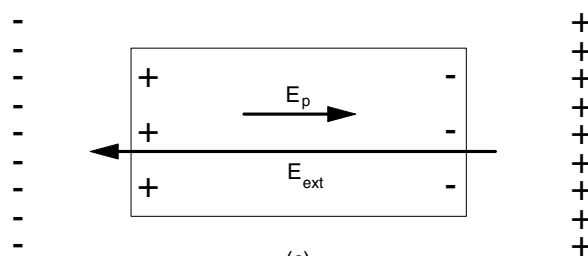
The partial neutralization of the external electric field can be understood from the following model. Consider a dielectric in the absence of external fields. The electron distribution of each atom is centered on the nucleus so that there is no electric field (at least when we average over a region containing many atoms). This is shown schematically in Fig. 6.16(a), in which each  $+$  sign represents a nucleus and each circle represents a distribution of negative charge in an atom.



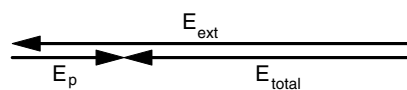
(a)



(b)



(c)



(d)

FIGURE 6.16. The polarization of a dielectric by an external electric field. (a) Atoms in the absence of an external field. (b) An external electric field causes a shift of each electron cloud relative to the positively charged nucleus. (c) There is a net buildup of positive charge at the left edge of the dielectric and of negative charge at the right edge. (d) The total electric field within the dielectric is the sum of the external electric field and the polarization electric field induced in the dielectric.

Figure 6.16(b) shows some external charges producing an electric field. If the dielectric is introduced in the space where this electric field exists, the negative electron clouds are shifted with respect to the nuclei, as shown in Fig. 6.16(b). The result is a polarization electric field  $\mathbf{E}_p$ , which is in the opposite direction to the external electric field. The total field within the dielectric is the vector sum of these two fields:<sup>8</sup>

$$\mathbf{E}_{\text{tot}} = \mathbf{E}_{\text{ext}} + \mathbf{E}_p. \quad (6.19)$$

<sup>7</sup>In some materials an electric field applied along one direction can cause charge displacement in a different direction. This book deals only with cases in which the induced electric field is parallel to the applied electric field.

<sup>8</sup>In most textbooks, it is customary to define the polarization by  $\mathbf{P} = -\mathbf{E}_p$  or  $\mathbf{P} = -\epsilon_0 \mathbf{E}_p$ . We have not done that in order to make the phenomenon easier to understand.

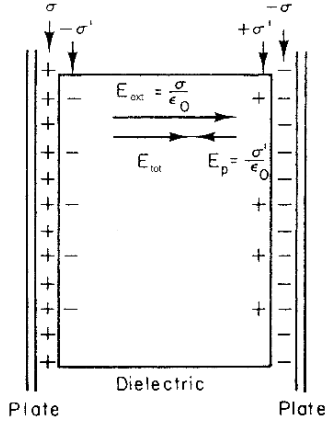


FIGURE 6.17. The polarization electric field reduces the electric field between the plates. The conducting plates could be extracellular and intracellular fluid, and the dielectric could be the cell membrane.

In simple materials all three vectors are parallel and  $E_p$  is proportional to  $E_{\text{tot}}$ . Then we can define the *electric susceptibility*  $\chi$  by the equation

$$E_p = -\chi E_{\text{tot}}.$$

This can be combined with the previous equation to get

$$E_p = -\frac{\chi}{1 + \chi} E_{\text{ext}}.$$

The polarization electric field is thus proportional to both the total electric field (proportionality constant  $-\chi$ ) and the external field [proportionality constant  $-\chi/(1 + \chi)$ ]. The former relationship is more fundamental, since the field displacing charges in one atom is the total field, due to both external charges and to the charges in neighboring atoms.

The total field within the dielectric is

$$E_{\text{tot}} = E_{\text{ext}} - \frac{\chi}{1 + \chi} E_{\text{ext}} = \frac{1}{1 + \chi} E_{\text{ext}} = \frac{1}{\kappa} E_{\text{ext}}. \quad (6.20)$$

The factor  $\kappa = 1 + \chi$  is called the *dielectric constant* of the dielectric. The electric field within the dielectric is reduced by the factor  $1/\kappa$  from that which would exist without the dielectric. The dielectric constant for typical nerve membranes<sup>9</sup> is about 7. The dielectric constant of water is quite high (around 80) because the water molecules can easily reorient their charged ends.

The relationship between the applied field, the polarization field, and the total field can be seen in the following example. The electric field between two parallel sheets of charge of density  $+\sigma$  and  $-\sigma$  per unit area has magnitude  $E_{\text{ext}} = \sigma/\epsilon_0$ . If there is dielectric between them (such as a cell membrane) and if the polarization in the

dielectric is uniform, then there is effectively a charge  $\pm\sigma'$  induced on the surface of the dielectric that partially neutralizes the external charges. This is shown in Fig. 6.17. The total electric field within the membrane is  $E_{\text{tot}} = |E_{\text{ext}} + E_p| = \sigma/\epsilon_0 - \sigma'/\epsilon_0 = \sigma_{\text{net}}/\epsilon_0 = E_{\text{ext}}/\kappa$ .

To recapitulate, in Fig. 6.17  $E_{\text{ext}}$  is  $\sigma/\epsilon_0$  and depends on the external charge distribution; the potential difference between the plates depends on the total field, and its magnitude is  $E_{\text{tot}}$  times the plate separation.

It is customary to refer to two different kinds of charge. The *free charge* is the charge that we bring into a region. We have some control over it. The *bound charge* is the charge induced in the dielectric by the movement or distortion of atoms and molecules in the dielectric in response to the free charge that has been introduced. Gauss's law can be written either in terms of the total charge (free plus bound)

$$\iint E_n dS = \frac{q_{\text{tot}}}{\epsilon_0} = \frac{q_{\text{free}} + q_{\text{bound}}}{\epsilon_0} \quad (6.21a)$$

or in terms only of the free charge

$$\iint \kappa E_n dS = \frac{q_{\text{free}}}{\epsilon_0}. \quad (6.21b)$$

The dielectric constant is placed inside the integral sign because the Gaussian surface could pass through materials with different values of the dielectric constant.

As another example of the effect of a dielectric, consider a spherical ion of radius  $a$  in which all the charge resides on the surface. In a vacuum, the potential at distance  $r$  is  $v = q/4\pi\epsilon_0 r$ , so on the surface of the ion, the potential is  $q/4\pi\epsilon_0 a$ . The work required to bring to the surface an additional charge  $dq$  is  $dW = vdq = qdq/4\pi\epsilon_0 a$ . The total work required to place charge  $Q$  on the ion is therefore

$$W = \int dW = \frac{1}{4\pi\epsilon_0 a} \int_0^Q q dq = \frac{\frac{1}{2}Q^2}{4\pi\epsilon_0 a}.$$

If the sphere is immersed in a uniform dielectric the total electric field and therefore the potential is reduced by a factor  $\kappa$ . The energy required to assemble the ion is then

$$W = \frac{\frac{1}{2}Q^2}{4\pi\epsilon_0 \kappa a}. \quad (6.22)$$

This is called the *Born charging energy*. For an ion of radius 0.2 nm (200 pm) and  $Q = 1.6 \times 10^{-19}$  C, the Born charging energy in a vacuum is  $5.8 \times 10^{-19}$  J ion<sup>-1</sup>. Multiplying by Avogadro's number gives  $3.5 \times 10^5$  J mol<sup>-1</sup>. Often in problems involving charges of a few times the electronic charge, it is convenient to use the energy unit electron volt: 1 eV =  $1.6 \times 10^{-19}$  J. For this problem, the Born charging energy is 3.6 eV ion<sup>-1</sup>.

If the ion is in a dielectric with  $\kappa = 2$  (a lipid, for example), the Born charging energy is reduced to 1.8 eV ion<sup>-1</sup>. Water has a very high dielectric constant (about 80) because the water molecules look roughly like that

<sup>9</sup>This value is high compared to the dielectric constant for a pure lipid, which is between 2 and 3. See the discussion in Sec. 6.17.

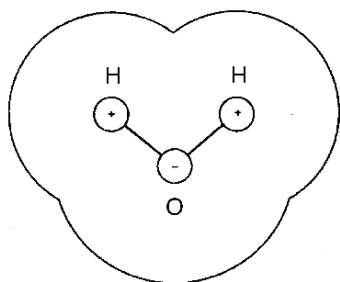


FIGURE 6.18. A schematic diagram of a water molecule. The hydrogen nuclei are 96.5 pm from the oxygen nucleus; the included angle is about  $104^\circ$ . The radius of each hydrogen atom is about 120 pm; the radius of the oxygen atom is about 140 pm. The water molecule has a permanent electric dipole moment.

in Fig. 6.18, and the molecules can easily align with an applied electric field. The same ion in water has a Born charging energy of 0.045 eV. At room temperature, the Boltzmann factor for the energy required to create the ion in vacuum is  $3.32 \times 10^{-61}$ . In a lipid, it is  $5.76 \times 10^{-31}$ , and in water, it is 0.175. This explains why it is easy to form ionic solutions in water but not in lipids.

## 6.8 Current and Ohm's Law

In the electrostatic case, there are no moving charges and no electric field within a conductor. When a current flows in a conductor, charges are moving and there is an electric field.

The electric current  $i$  in a wire is the amount of charge per unit time passing a point on the wire. If the amount of charge in time  $dt$  is  $dQ$ , the current is

$$i = \frac{dQ}{dt}. \quad (6.23)$$

The units of the current are  $\text{C s}^{-1}$  or amperes (A) (sometimes called amps). The current density  $j$  (or  $j_Q$  in the notation of Chapter 5) is the current per unit area,  $i/S$ . The units are  $\text{C m}^{-2} \text{ s}^{-1}$  or  $\text{A m}^{-2}$ . In an extended medium, the current density is a vector  $\mathbf{j}$  at each point in the medium. The direction of  $\mathbf{j}$  is the direction charge is moving at that point.

If there is no electric field in the conductor, there is no average motion of the charges. (There will be random thermal motion, but it will be equally likely in every direction. This random motion of charges is one cause of "noise" in electrical circuits.) To have a current there must be an electrical field in the conductor; this means that there will be a potential difference between two points in the conductor. If there is no potential difference between two points in the conductor, there is no current. For the simple conductor of Fig. 6.19, the current is found to be proportional to the voltage difference between the ends of the conductor. The current is shown

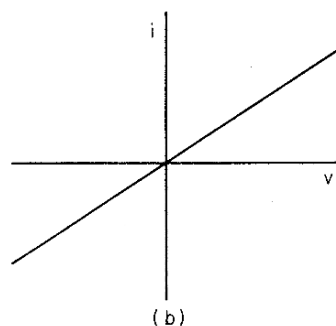
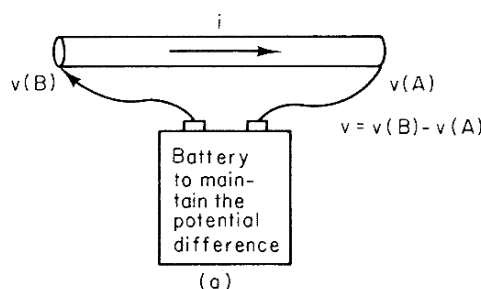


FIGURE 6.19. A current flows in the wire as long as the battery or some other device maintains a potential difference between two points on the wire. The potential difference means that there is an electric field within the wire. If the wire obeys Ohm's law, the current is proportional to the potential difference.

flowing from  $B$  to  $A$ . When  $v(B)$  is greater than  $v(A)$ ,  $v$  is positive and the current is positive. When  $v$  is negative, the current is in the other direction and is also negative.

For the wire of Fig. 6.19, the relationship between current and voltage difference is linear. In that case, we can write *Ohm's law*:

$$i = \frac{1}{R} v = Gv \quad (6.24a)$$

or

$$v = iR. \quad (6.24b)$$

$R$  is called the *resistance* of the conductor. Since the current is measured in amps and the voltage in volts, its units are  $\text{V A}^{-1}$  or ohms ( $\Omega$ ). The reciprocal of the resistance is the *conductance*  $G$ . Its units are  $\Omega^{-1}$  or siemens (S).

Ohm's law is not universal. It describes only certain types of conductors. Figure 6.20 shows the current-voltage characteristics of several devices that have non-linear behavior and that make modern electronic circuits possible. They are shown here not for their own sake, but to emphasize the limited validity of Ohm's law. The nerve cell membrane is not linear.

It is possible to write Ohm's law in another form. Placing two identical wires in parallel in the circuit of Fig. 6.19 would cause twice as much current to flow (assuming that the battery maintains the voltage difference at the original level). The current density  $j$  remains constant

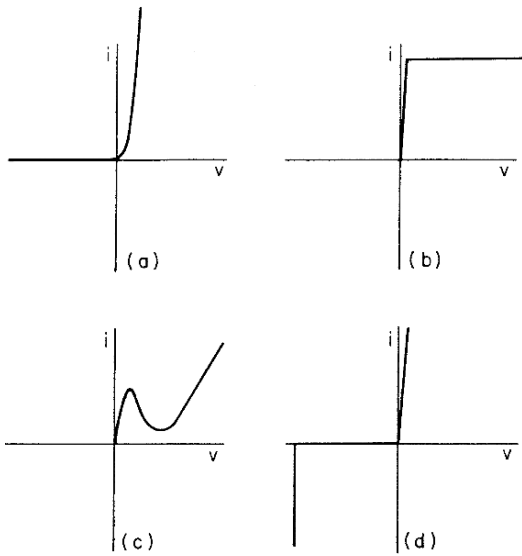


FIGURE 6.20. Current–voltage relationships for some nonlinear devices used in electronic circuits. (a) Diode. (b) Transistor. (c) Tunnel diode. (d) Zener diode.

as the cross-sectional area of the wire is changed, when the wire length and voltage difference are held fixed. Similarly, to maintain the same current through a single wire twice as long requires a voltage difference twice as great. Therefore, it is voltage per unit length that determines the current. In this spirit, Ohm’s law can be written as

$$j = \frac{i}{S} = \frac{v(B) - v(A)}{RS}$$

If  $L$  is the length of the wire and  $x$  the position along it, this can be written as

$$j_x = -\frac{L}{SR} \frac{v(x=L) - v(x=0)}{L} = -\frac{L}{SR} \frac{\partial v}{\partial x}, \tag{6.25a}$$

$$j_x = -\sigma \frac{\partial v}{\partial x}. \tag{6.25b}$$

In three dimensions this alternative statement of Ohm’s law becomes

$$\mathbf{j} = \sigma \mathbf{E}. \tag{6.26}$$

The  $\sigma$  in this equation<sup>10</sup> is the electrical conductivity, measured in  $(A\ m^{-2})/(V\ m^{-1})$  or  $S\ m^{-1}$ . Its reciprocal is the resistivity of the material,  $\rho$ . The units of resistivity are  $\Omega\ m$ . For a cylindrical conductor, the resistivity and the resistance are related by

$$\frac{1}{\rho} = \frac{L}{SR}$$

<sup>10</sup>Note that  $\sigma$  has now been used for two things in this chapter: surface charge per unit area and conductivity. This notation is standard in the literature. You can tell from the context which is meant. Similarly, the symbol  $\rho$  is used for charge per unit volume and for resistivity (and for mass density in other chapters). These double usages are found frequently in the literature.

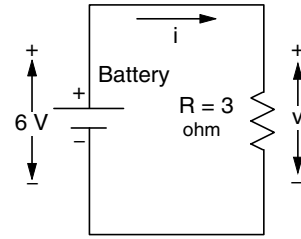


FIGURE 6.21. A resistor connected to a battery.

or

$$R = \rho \frac{L}{S}. \tag{6.27}$$

This shows that making the conductor longer increases its resistance, while increasing the cross-sectional area lowers the resistance.

Suppose that an electric field acts on a charge moving in a medium that obeys Ohm’s law. The electric field does work on the charge, but the energy is continually transferred to the medium by collisions between the charge and other particles in the medium. If a charge  $Q$  moves to a lower potential, all the energy it gained is transferred to heat. The rate of energy dissipation is the *power*

$$P = vi. \tag{6.28}$$

The units of power are  $J\ s^{-1}$  or watts (W). For a material that obeys Ohm’s law, Eq. 6.28 can be combined with Ohm’s law to give

$$P = i^2 R \tag{6.29}$$

or

$$P = \frac{v^2}{R}. \tag{6.30}$$

This type of energy loss has clinical significance. If a patient contacts a source of very high voltage such as an 11,000-V power line, the strong electric fields will cause current to flow throughout the patient’s body or limb, because  $\mathbf{j} = \sigma \mathbf{E}$ . The resistive heating can be enough to boil water within the tissues. If the limb is x rayed, the steam bubbles will look very much like the bubbles that appear in *clostridium* (gas gangrene) infections; if the x ray is deferred a few days, it will be impossible to tell from the x ray whether the bubbles are due to the electrical injury or subsequent infection.

## 6.9 The Application of Ohm’s Law to Simple Circuits

The ultimate goal of this chapter is to apply Ohm’s law to the axon. Before doing that, however, it is worthwhile to see how it can be applied to some simpler circuits in which the current and voltage are not changing with time.

The simplest circuit is a resistance  $R$  connected across a battery, as shown in Fig. 6.21. The battery voltage of



6 V is the potential difference across the resistor. If the resistance is  $3 \Omega$ , the current is  $i = v/R = 6/3 = 2 \text{ A}$ . The rate of heat production in the resistor is  $P = vi = (6)(2) = 12 \text{ W}$ . This could also have been calculated from  $P = v^2/R = 36/3$ , or  $P = i^2R = (4)(3)$ . A current of 2 A means that every second 2 C of charge leave the positive terminal of the battery and flow through the resistor. When the charge arrives at the other end of the resistor, it has lost 12 J of energy to heat. The 2 C then travel through the battery back to the positive terminal, gaining 12 J from a chemical reaction within the battery.

This example has been stated as though the positive charge moves. In a metallic conductor negative charges (electrons) move from the negative terminal of the battery through the resistor to the positive terminal. In salt water and most body fluids, both positive and negative ions move. From a macroscopic point of view, we cannot tell the difference between the transport of a charge  $-q$  from point  $A$  to point  $B$ , and the transport of a charge  $+q$  from point  $B$  to point  $A$ . Both processes make the total charge at  $B$  less positive and the total charge at  $A$  more positive by an amount  $q$ .

Two fundamental principles used in this discussion have not been stated explicitly. The first is the *conservation of electric charge*: all charge that leaves the battery passes through the resistor. The second is the *conservation of energy*: a charge that starts at some point in the circuit and comes back to its starting point has neither lost nor gained energy. (The energy gained by a charge in the battery is equal to the energy lost by it in passing through the resistor.) These principles become less obvious and more useful in a circuit that is more complicated than the one considered above. They are known as *Kirchhoff's laws*.

In a more complicated circuit, Kirchhoff's first law (conservation of charge) takes the following form. Any junction where the current can flow in different paths is called a *node*. The algebraic sum of all the currents into a node is zero. (By algebraic sum we mean that currents into the node are positive, while currents leaving the node are negative, or vice versa.) This ensures that no charge will accumulate at the node.<sup>11</sup>

As an example of Kirchhoff's first law, consider the node in Fig. 6.22. Conservation of charge requires that  $2 + 3 + i = 0$  or  $i = -5 \text{ A}$ . (In this case positive currents flow into the node; the negative current means that 5 A is flowing out of the node as current  $i$ .)

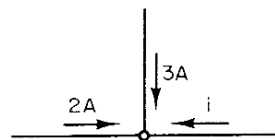


FIGURE 6.22. Conservation of charge means that current  $i$  is  $-5 \text{ A}$ .

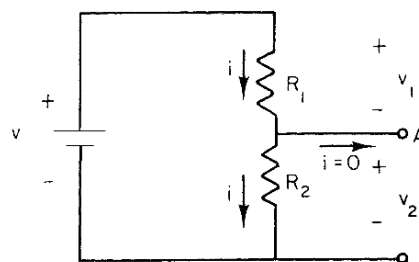


FIGURE 6.23. A more complicated circuit, sometimes called a voltage divider.

Kirchhoff's second law was used implicitly in the example above to say that the voltage across the resistor is 6 V. In general, Kirchhoff's second law says that if one goes around any closed path in a complicated circuit, the total voltage change is zero.

Kirchhoff's laws can be applied to show that the total resistance of a set of resistors in series is

$$R = R_1 + R_2 + R_3 + \cdots$$

This follows from the definition of resistance, the fact that the same current flows in each resistor, and the total potential difference across the set of resistors is the sum of the potential difference across each one. Kirchhoff's laws can also be used to show that for a collection of resistors in parallel, the total resistance is given by

$$\frac{1}{R} = \frac{1}{R_1} + \frac{1}{R_2} + \frac{1}{R_3} + \cdots,$$

(see Problem 23).

Consider a more complicated example in which two resistors are connected across a battery. The battery voltage is  $v$ , and the resistances are  $R_1$  and  $R_2$ , as shown in Fig. 6.23. If no current flows out lead  $A$ , then conservation of charge requires that the same current  $i$  flows in each resistor. The sum of the voltages  $v_1$  and  $v_2$  is  $v$ . Therefore,  $i = v_1/R_1 = v_2/R_2$  and  $v = v_1 + v_2 = iR_1 + iR_2 = i(R_1 + R_2)$ . The voltage across  $R_2$  is  $iR_2$  or

$$v_2 = \frac{R_2}{R_1 + R_2} v. \quad (6.31)$$

<sup>11</sup>More generally, the node could represent a conductor, such as the plate of a capacitor, on which charge can accumulate. In that case the charge  $Q$  changes with time:

$$\frac{dQ}{dt} = \sum (\text{all currents into the node}).$$

This statement is quite similar to the continuity equation of Sec. 4.1.

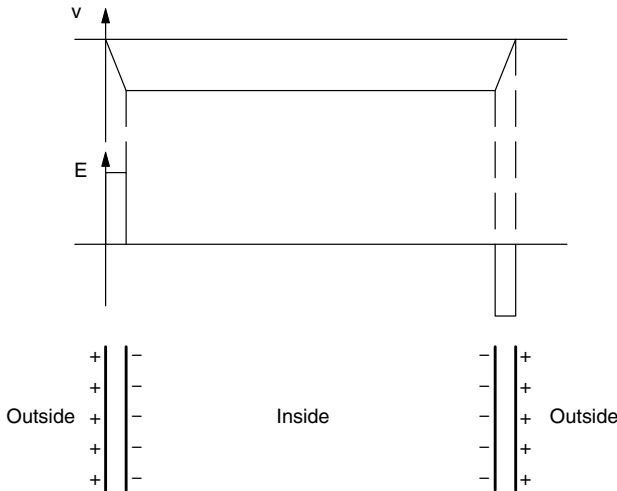


FIGURE 6.24. The potential, electric field, and charge at different points on the diameter of a resting nerve cell. Portions of the cell membrane on opposite sides of the cell are shown. Outside the cell on the left the potential and electric field are zero. As one moves to the right into the cell, the electric field in the membrane causes the potential to decrease to  $-70$  mV. Within the cell the field is zero and the potential is constant. Moving out through the right-hand wall the potential rises to zero because of the electric field within the membrane.

### 6.10 Charge Distribution in the Resting Nerve Cell

The axon consists of an ionic intracellular fluid and an ionic extracellular fluid, separated by a membrane. The intracellular and extracellular media are electrical conductors. When the cell is in equilibrium there is no current and no electric field in these regions. There will be a field and currents when an impulse is traveling along the axon.

Because the electric field in the resting cell is zero, there is no net charge in the fluid. Positive ions are neutralized by negative ions everywhere except at the membrane. A layer of charge on each surface generates an electric field within the membrane and a potential difference across it.

Measurements with a microelectrode show that the potential within the cell is about 70 mV less than outside. If the potential outside is taken to be zero, then the interior resting potential is  $-70$  mV. Figure 6.24 shows a slice across the cell, showing the membrane on opposite sides of the cell and the charges and electric field. If the potential drops 70 mV as one enters the cell on the left, if the membrane thickness is 6 nm, and if the electric field within the membrane is assumed to be constant, then

$$E = -\frac{dv}{dx} = -\frac{-70 \times 10^{-3} \text{ V}}{6 \times 10^{-9} \text{ m}} = 1.17 \times 10^7 \text{ V m}^{-1}. \tag{6.32}$$

This is how the value of  $E$  was determined for use on p. 141.

Except for the layers of charge on the inside and outside of the membrane, which are shown in Fig. 6.24 and which give rise to the electric field and potential difference, the extracellular and intracellular fluids are electrically neutral. However, the ion concentrations are quite different in each (Fig. 6.3). There is an excess of sodium ions outside and an excess of potassium ions inside.

It is possible to see which concentrations (if any) are consistent with the hypothesis that the ions can pass freely through the membrane. If a species is in equilibrium, the concentration ratio  $c_i/c_o$  across the membrane is given by a Boltzmann factor or the Nernst equation (see Chapter 3). The potential energy of the ion is  $zev$ , where  $z$  is the valence of the ion,  $e$  the electronic charge ( $1.6 \times 10^{-19}$  C), and  $v$  the potential in volts. Using subscripts  $i$  and  $o$  to represent inside and outside the cell, we have

$$\frac{c_i}{c_o} = \frac{e^{-zev_i/k_B T}}{e^{-zev_o/k_B T}} = e^{-ze(v_i-v_o)/k_B T}. \tag{6.33}$$

Here  $k_B$  is Boltzmann's constant,  $1.38 \times 10^{-23}$  J K $^{-1}$ . For a situation in which  $T = 310$  K and  $v_i - v_o = -70 \times 10^{-3}$  V,  $c_i/c_o$  is 13.7 for univalent positive ions and  $1/13.7 = 0.073$  for negative ions. The ratios in Fig. 6.3 are 0.103 for sodium, 30 for potassium, and 0.071 for chloride. The chloride concentration ratio is consistent with equilibrium, while the sodium concentration ratio is much too small (too few sodium ions inside) and the potassium concentration ratio is too large (too many potassium ions inside).

A potential of  $-90$  mV would bring the potassium concentration ratio into equilibrium, but then chloride would not be in equilibrium and sodium would be even farther from equilibrium. In fact, tracer studies show that potassium leaks out slowly and sodium leaks in slowly. The resting membrane is not completely impermeable to these ions [Hodgkin (1964, Chapter 6); Läuger (1991)]. To maintain the ion concentrations a membrane protein called the sodium-potassium pump uses metabolic energy to pump potassium into the cell and sodium out. The usual ratio of sodium to potassium ions in this active transport is 3 sodium to 2 potassium ions [Patton *et al.* (1989, Vol. 1, p. 27)].

The intracellular and extracellular fluids can be modeled as two conductors separated by a fairly good insulator. The conductors have a capacitance between them. We can estimate this capacitance in two ways. We can either regard the membrane as a plane insulator sandwiched between plane conducting plates (as if the membrane had been laid out flat as in Fig. 6.25), or we can treat it as a dielectric between concentric cylindrical conductors. The text will use the first approximation, while the second will be left to a problem. Suppose that two parallel plates have area  $S$  and charge  $\pm Q$ , respectively, then the charge density on each is  $\sigma = \pm Q/S$ . Equation 6.11 gives the electric field without a dielectric between the conductors:  $E_{\text{ext}} = \sigma/\epsilon_0 = Q/\epsilon_0 S$ .

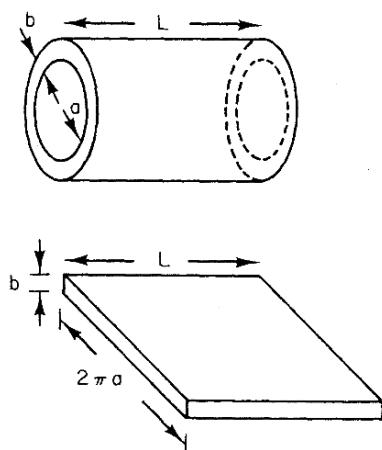


FIGURE 6.25. A portion of a cell membrane of length  $L$ , in its original configuration and laid out flat. The membrane thickness is  $b$  and the radius of the axon is  $a$ . The plane approximation is used to calculate both the capacitance and resistance of the membrane.

With the dielectric of dielectric constant  $\kappa$ , the field is reduced to  $E = E_{\text{ext}}/\kappa = \sigma/\kappa\epsilon_0 = Q/\kappa\epsilon_0 S$ , as was seen in Eq. 6.20. The magnitude of the potential difference is  $E$  times the plate separation  $b$ :  $v = Eb = Qb/\kappa\epsilon_0 S$ . The capacitance is  $C = Q/v$ :

$$C = \frac{Q\kappa\epsilon_0 S}{Qb} = \frac{\kappa\epsilon_0 S}{b}. \quad (6.34)$$

The charge density on the surface of the membrane is obtained from  $\sigma = Q/S = Cv/S = \kappa\epsilon_0 v/b$ .

Measurements of the dielectric constant  $\kappa$  for axon membrane show it to be about 7. Using values of  $-70$  mV for  $v$  and 6 nm for  $b$ , the capacitance per unit area of membrane can be calculated, as can  $\sigma$ :

$$\frac{C}{S} = \frac{(7)(8.85 \times 10^{-12})}{6 \times 10^{-9}} = 0.01 \text{ F m}^{-2} = 1 \mu\text{F cm}^{-2},$$

$$\sigma = (0.01)(70 \times 10^{-3}) = 7 \times 10^{-4} \text{ C m}^{-2}. \quad (6.35)$$

This value for the surface charge density is larger by a factor of 7 than that calculated in Sec. 6.3. The reduction of the electric field by polarization of the dielectric has been taken into account in the present calculation. A larger external charge is required to give the same field within the dielectric.

The value of  $b$  for myelinated fibers is much greater, typically 2000 nm instead of 6 nm. This reduces the capacitance per unit area by a factor of 300.

## 6.11 The Cable Model for an Axon

We now consider the rather complicated flow of charge in the interior of an axon, through the membrane, and

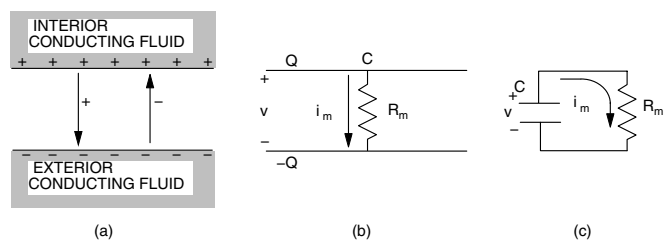


FIGURE 6.26. Leakage currents through the membrane. (a) The flow of positive and negative ions. (b) The membrane capacitance is represented by the parallel plates and the leakage resistance by a single resistor. (c) The capacitance and resistance are usually drawn like this.

in the conducting medium outside the cell during departures from rest. We will model the axon by electric conductors that obey Ohm's law inside and outside the cell and a membrane that has capacitance and also conducts current. We will apply Kirchhoff's laws—conservation of energy and charge—to a small segment of the axon. The result will be a differential equation that is independent of any particular model for the cell membrane. This is called the *cable model* for an axon. We will then apply the cable model in two cases. The first case is when the voltage change does not alter the properties of the membrane. The second case is a voltage change that changes the ionic permeability of the membrane, thereby generating a nerve impulse.

Consider the small segment of membrane shown in Fig. 6.26(a). For the moment we ignore the resting potential on the membrane. We will see later that accounting for the resting potential requires only a small change to the model. The upper capacitor plate, corresponding to the inside of the membrane, carries a charge  $Q$ . The lower capacitor plate (the outside of the membrane) has charge  $-Q$ . The charge on the membrane is related to the potential difference across the membrane by the membrane capacitance  $C_m$ :  $Q = C_m v$ . Figure 6.26(a) shows positive ions on the inside and negative ions on the outside of the membrane. (In a resting nerve cell, there is negative charge on the inside of the membrane,  $Q$  is positive,  $-Q$  is negative, and  $v < 0$ .)

If the resistance between the plates of a capacitor is infinite, no current flows, and the charge on the capacitor plates remains constant. However, a membrane is not a perfect insulator; if it were, there would be no nerve conduction. Some current flows through the membrane. We call this current  $i_m$  and define outward current to be positive, as in Fig. 6.26(b).

Imagine for now that there is no current along the axon. In that case  $i_m$  discharges the membrane capacitance, and the charge and potential difference fall to zero as charge flows through the resistor. When  $i_m$  is positive,  $Q$

and  $v$  decrease with time:

$$-i_m = \frac{dQ}{dt} = C_m \frac{dv}{dt}. \quad (6.36)$$

Let us explore the behavior of this isolated segment of axon a bit further. For now we think of the total leakage current as being through a single effective resistance  $R_m$ . This is shown in Fig. 6.26(b). It is customary to draw the resistance separately, as in Fig. 6.26(c). The current is then  $i_m = v/R_m$  and  $C_m(dv/dt) = -i_m = -v/R_m$ ,

$$\frac{dv}{dt} = -\frac{1}{R_m C_m} v. \quad (6.37)$$

This is the familiar equation for exponential decay of the voltage (see Chapter 2). If the initial voltage at  $t = 0$  is  $v_0$ , the solution is

$$v(t) = v_0 e^{-t/\tau}, \quad (6.38)$$

where the time constant  $\tau$  is given by

$$\tau = R_m C_m. \quad (6.39)$$

Referring to Fig. 6.25, we saw that if we have a section of membrane of area  $S$  and thickness  $b$  the capacitance is given by Eq. 6.34. For a conductor of the same dimensions we saw [Eq. 6.27] that the resistance is  $R_m = \rho_m b/S$ , so the time constant is

$$\tau = R_m C_m = \frac{\rho_m b}{S} \frac{\kappa \epsilon_0 S}{b} = \kappa \epsilon_0 \rho_m. \quad (6.40)$$

We have the remarkable result that the time constant is independent of both the area and thickness of the membrane. Doubling the area  $S$  doubles the amount of charge that must leak off, but it also doubles the membrane current. Doubling  $b$  doubles the resistance, but it also makes the membrane capacitance half as large. In each case the factors  $S$  and  $b$  cancel in the expression for the time constant.

If a very thin lipid membrane is produced artificially, it is found to have a very high resistivity—about  $10^{13} \Omega \text{ m}$  [Scott (1975, p. 493)]. Certain proteins added to the lipid material reduce the resistivity by several orders of magnitude. For natural nerve membrane the resistivity is about

$$\rho_m = 1.6 \times 10^7 \Omega \text{ m}. \quad (6.41)$$

This is the effective resistivity for resting membrane, taking into account all of the ion currents. If  $\rho_m$  had this constant value the time constant would be  $\tau = \kappa \epsilon_0 \rho_m = (7)(8.85 \times 10^{-12})(1.6 \times 10^7) = 1 \times 10^{-3} \text{ s}$ . (Actually, the resistivity changes drastically as the potential across the membrane changes during the propagation of a nerve impulse.) Since we observe a potential difference across the membrane, there must be a mechanism for renewing the charge on the membrane surface.

The resistance and capacitance of the portion of the axon membrane in Fig. 6.25 can be written in terms of

the axon radius  $a$  and the length  $L$  of the segment by noting that  $S = 2\pi aL$ . Then one has

$$C_m = \frac{\kappa \epsilon_0 2\pi aL}{b}, \quad R_m = \frac{\rho_m b}{2\pi aL}.$$

It is convenient to recall that  $v = iR$  can be written as  $i = Gv$  and introduce the conductance of the membrane segment

$$G_m = \frac{2\pi aL}{\rho_m b}. \quad (6.42)$$

Both the capacitance and the conductance are proportional to the area of the segment  $S$ . It is also convenient to introduce the lowercase symbols  $c_m$  and  $g_m$  to stand for the membrane capacitance and membrane conductance per unit area:

$$c_m = \frac{C_m}{S} = \frac{\kappa \epsilon_0}{b}, \quad (6.43)$$

$$g_m = \frac{G_m}{S} = \frac{1}{\rho_m b} = \frac{\sigma_m}{b}. \quad (6.44)$$

(Remember that  $\sigma_m = 1/\rho_m$  is the electrical conductivity, the reciprocal of the resistivity. It is *not* the charge per unit area.  $\sigma$  is frequently used for both quantities in the literature.)

Both  $c_m$  and  $g_m$  depend on the membrane thickness as well as the dielectric constant and resistivity of the membrane. The units of  $c_m$  and  $g_m$  are, respectively,  $\text{F m}^{-2}$  and  $\text{S m}^{-2}$ . Be careful: many sources give them per square centimeter instead of per square meter.

We can rewrite Eq. 6.36 in terms of the current density,  $j_m$ , which is proportional to the capacitance per unit area,  $c_m$ :

$$-j_m = c_m \frac{dv}{dt}. \quad (6.45)$$

Table 6.1 shows typical values for these quantities and some to be discussed later for an unmyelinated axon.<sup>12</sup> These values should not be associated with a particular species. Parameters such as the resistance and capacitance per unit length of the axon are measured directly. Others, such as  $\rho_m$ , require an estimate of membrane thickness and are less well known.

Now let us consider current that flows inside and outside the axon. Assume that the currents inside are longitudinal, that is, parallel to the axis of the axon. A discussion of departures from this assumption is found in Scott

<sup>12</sup>Some insight into the magnitude of the charge on the membrane can be obtained from these numbers. The excess charge on the surface of the membrane is  $7 \times 10^{-4} \text{ C m}^{-2}$  for the unmyelinated fiber. This corresponds to  $4.4 \times 10^{15}$  ions per square meter, if each ion has a charge of  $1.6 \times 10^{-19} \text{ C}$ . Each atom or ion in contact with the membrane surface occupies an area of about  $10^{-20} \text{ m}^2$ ; thus there are about  $10^{20}$  atoms or ions in contact with a square meter of membrane surface. These may be neutral or positively or negatively charged. If charged, most are neutralized by the presence of a neighbor of opposite charge. The excess charge density that is required can be obtained if  $4.4 \times 10^{15}/10^{20}$  or roughly one out of every 20,000 of the atoms in contact with the surface is ionized and not neutralized.

TABLE 6.1. Properties of a typical unmyelinated nerve.

$a$	Axon radius	$5 \times 10^{-6}$ m
$b$	Membrane thickness	$6 \times 10^{-9}$ m
$\rho_i$	Resistivity of axoplasm	$0.5 \Omega \text{ m}$
$r_i = \rho_i / \pi a^2$	Resistance per unit length inside axon	$6.4 \times 10^9 \Omega \text{ m}^{-1}$
$\kappa$	Dielectric constant of membrane	$7^a$
$\rho_m$	Resistivity of membrane	$1.6 \times 10^7 \Omega \text{ m}$
$\kappa \rho_m$		$112 \times 10^6 \Omega \text{ m}$
$c_m = \kappa \epsilon_0 / b$	Membrane capacitance per unit area	$10^{-2} \text{ F m}^{-2}$
$2\pi \kappa \epsilon_0 a / b$	Membrane capacitance per unit length of axon	$3 \times 10^{-7} \text{ F m}^{-1}$
$g_m = 1 / \rho_m b$	Conductance per unit area of membrane	$10 \text{ S m}^{-2}$
$1 / g_m$	Reciprocal of conductance per unit area	$0.1 \Omega \text{ m}^2$
$2\pi a / \rho_m b$	Membrane conductance per unit length of axon	$3.2 \times 10^{-4} \text{ S m}^{-1}$
$v_r$	Resting potential inside axon	$-70 \text{ mV}$
$E = v_r / b$	Electric field in membrane	$1.2 \times 10^7 \text{ V m}^{-1}$
$\kappa \epsilon_0 v_r / b$	Charge per unit area on membrane surface	$7 \times 10^{-4} \text{ C m}^{-2}$
	Net number of univalent ions per unit area	$4.4 \times 10^{15} \text{ m}^{-2}$
	Net number of univalent ions per unit length	$6.6 \times 10^7 \text{ m}^{-1}$

<sup>a</sup>See Sec. 6.17 for a discussion of the dielectric constant.

(1975, p. 492). With this assumption, the interior fluid can be regarded as a resistance of length  $L$  and radius  $a$  as shown in Fig. 6.27. The resistance of such a segment is  $R_i = \rho_i L / S = \rho_i L / \pi a^2$ . It is convenient to work with the resistance per unit length,  $r_i$ :

$$r_i = \frac{R_i}{L} = \frac{\rho_i}{\pi a^2} = \frac{1}{\pi a^2 \sigma_i}. \quad (6.46)$$

The question of resistance of the extracellular fluid for currents outside the axon is more complicated. If the extracellular fluid were infinite in extent, the longitudinal resistance outside the cell would be very small (see Chapter 7). On the other hand, in a nerve or a muscle the axons or muscle cells are packed closely together, there is not very much extracellular fluid, and the external resistance

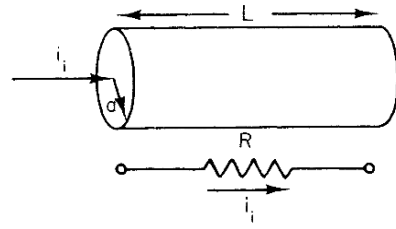


FIGURE 6.27. Axoplasm of length  $L$  and radius  $a$  can be treated like a simple resistor.

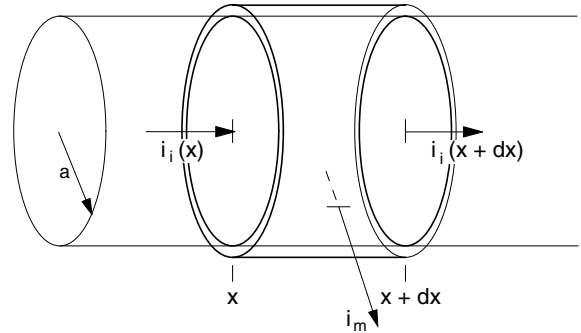


FIGURE 6.28. The membrane surrounding a small portion of an axon is shown, along with the longitudinal currents in and out of the segment.

per unit length can be significant. There are some important effects that occur because of this. We will discuss them in Chapter 7.

Now we can consider the effect of both membrane and longitudinal currents. Figure 6.28 shows a small region of the axon between  $x$  and  $x + dx$  and the surrounding membrane. Current  $i_i$  flows longitudinally along the axon on the inside. The current through the membrane is  $i_m$ . The potential difference across the membrane is  $v = v_i - v_o$ . In this section no attempt will be made to relate  $i_m$  or  $j_m$  to  $v$ . Charge  $Q$  resides on the inside surface of the membrane and can be either negative or positive. An equal and opposite charge  $-Q$  resides on the outer surface of the membrane.

Because the capacitance can charge or discharge, Kirchhoff's law (conservation of charge) does not say that the sum of the currents is zero. Rather, it says that the net current into the volume of axoplasm between  $x$  and  $x + dx$  changes the charge on the interior surface of the membrane:

$$i_i(x) - i_i(x + dx) - i_m = \frac{dQ}{dt} = C_m \frac{d(v_i - v_o)}{dt}. \quad (6.47a)$$

When  $i_i(x) = i_i(x + dx)$  this gives Eq. 6.36. The membrane current  $i_m$  represents an average value for the segment of membrane between  $x$  and  $x + dx$ . It is also a function of  $x$ .

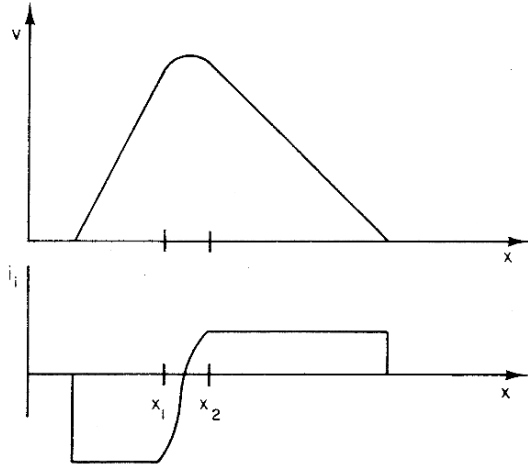


FIGURE 6.29. A hypothetical plot of  $v_i(x)$  and the longitudinal current  $i_i$  associated with it.

We can define  $di_i = i_i(x + dx) - i_i(x)$  as the increase in  $i_i$  along segment  $dx$ . Then we can rewrite Eq. 6.47a as

$$-di_i = C_m \frac{dv}{dt} + i_m. \quad (6.47b)$$

This is an important equation. It says that when the current flowing inside the axon decreases in a small distance  $dx$ , part of the current charges the capacitance of that segment of membrane, and the rest flows through the membrane.

Consider a small segment of axoplasm of length  $dx$ . The intracellular voltage at the left end is  $v_i(x)$ ; at the right end it is  $v_i(x + dx)$ . The current along the segment is the voltage difference between the ends divided by the resistance of the segment. The resistance is  $R_i = r_i dx$ . Therefore, the current is

$$i_i(x) = \frac{v_i(x) - v_i(x + dx)}{r_i dx} = -\frac{1}{r_i} \frac{dv_i}{dx}. \quad (6.48)$$

The voltage must change along the axon for a current to flow within it. The minus sign in Eq. 6.48 shows that a current flowing from left to right (in the  $+x$  direction) requires a voltage that decreases from left to right, and vice versa.

Figure 6.29 shows a hypothetical plot of  $v_i(x)$  and the current which would accompany it. Notice that the current is flowing from the region of higher voltage to lower voltage—towards both ends from the region between  $x_1$  and  $x_2$ . In that region either the charge on the membrane is changing or current is flowing through the membrane.

Consider again the cylindrical geometry shown in Fig. 6.28. The surface area of this portion of membrane is  $2\pi a dx$ . Dividing each term of Eq. 6.47a by the area and remembering the definitions of  $j_m$  and  $c_m$  we obtain

$$c_m \frac{\partial v}{\partial t} = -j_m + \frac{1}{2\pi a} \left[ \frac{i_i(x) - i_i(x + dx)}{dx} \right]. \quad (6.49)$$

It is necessary to use partial derivatives because the current and voltage depend on both  $x$  and  $t$  as an impulse travels down the nerve. As  $dx \rightarrow 0$

$$\frac{i_i(x + dx) - i_i(x)}{dx} \rightarrow \frac{\partial i_i}{\partial x}.$$

This can be evaluated using the expression for Ohm's law in the axoplasm, Eq. 6.48:

$$\frac{\partial i_i}{\partial x} = -\frac{1}{r_i} \frac{\partial^2 v_i}{\partial x^2}. \quad (6.50)$$

When this is inserted in Eq. 6.49 the result is

$$c_m \frac{\partial(v_i - v_o)}{\partial t} = -j_m + \frac{1}{2\pi a r_i} \frac{\partial^2 v_i}{\partial x^2}. \quad (6.51)$$

In many cases the extracellular potential is small. In that case the voltage across the membrane,  $v$ , is approximately the same as the intracellular voltage,  $v_i$ , so we can rewrite Eq. 6.51 as

$$c_m \frac{\partial v}{\partial t} = -j_m + \frac{1}{2\pi a r_i} \frac{\partial^2 v}{\partial x^2}. \quad (6.52)$$

This rather formidable looking equation is called the *cable equation* or *Telegrapher's equation*. It has the form of Fick's second law of diffusion, Eq. 4.26, with the addition of the  $j_m$  term.

It is worth recalling the origin of each term and verifying that the units are consistent. The term on the left is the rate at which the membrane capacitance is gaining charge per unit area. Therefore, all terms in the equation have the units of current per unit area. The first term on the right is the current per unit area through the membrane in the direction that discharges the membrane capacitance. The second term on the right gives the buildup of charge on this area of the membrane because of differences in current along the axon. If  $v(x)$  were constant, there would be no current along the inside of the axon. If function  $v(x)$  had constant slope, the current along the inside of the axon would be the same everywhere and there would be no charge buildup on the membrane. It is only because  $v(x)$  changes slope that  $i_i$  is different at two neighboring points in the axon and charge can collect on the membrane.

Now, for the units. Since  $i = C(dv/dt)$ , the units of  $c_m \partial v / \partial t$  are current per unit area. The  $j_m$  term is by definition current per unit area. Since  $r_i$  has the units of  $\Omega \text{ m}^{-1}$ , the term  $2\pi a r_i$ , has the units of  $\Omega$ . When this is combined with  $\partial^2 v / \partial x^2$ , which has units  $\text{V m}^{-2}$ , the result is  $\text{A m}^{-2}$  as required.

This is a very general equation stating Kirchhoff's laws for a segment of the axon. The only assumptions are that the currents depend only on time and position along the axon and that voltage changes on the outside of the axon can be neglected. Particular models for nerve conduction use different relations between  $j_m$  and  $v(x, t)$ .

## 6.12 Electrotonus or Passive Spread

The simplest membrane model is one that obeys Ohm's law. This approximation is valid if the voltage changes are small enough so that the membrane conductance does not change, or if something has been done to inactivate the normal changes of membrane conductance with voltage. It is also useful for myelinated nerves between the nodes of Ranvier. This is called *electrotonus* or *passive spread*.

In its quiescent state, the voltage all along the inside of the axon has the constant resting value  $v_r$ . Both  $\partial v/\partial t$  and  $\partial^2 v/\partial x^2$  are zero. Equation 6.52 can be satisfied only if  $j_m = 0$ . Although  $j_m$  is zero, it may be made up of several leakage components. In this section we simply assume that  $j_m$  is proportional to  $v - v_r$ :

$$j_m = g_m(v - v_r). \quad (6.53)$$

This simple model does predict that  $j_m = 0$  when  $v = v_r$ . It also predicts that the current will be positive (outward) if  $v > v_r$  and negative (inward) if  $v < v_r$ . It does not explain the propagation of an all-or-nothing nerve impulse. The conductance per unit area,  $g_m$ , is assumed to be independent of  $v$  and of the past history of the membrane. This is a good assumption only for very small voltage changes. With this assumption, Eq. 6.52 becomes

$$c_m \frac{\partial v}{\partial t} = -g_m(v - v_r) + \frac{1}{2\pi a r_i} \frac{\partial^2 v}{\partial x^2}. \quad (6.54)$$

This equation is usually written in a slightly different form by dividing through by  $g_m$ :

$$\frac{1}{2\pi a r_i g_m} \frac{\partial^2 v}{\partial x^2} - v - \frac{c_m}{g_m} \frac{\partial v}{\partial t} = -v_r.$$

It is also customary to make the assignments

$$\lambda^2 = \frac{1}{2\pi a r_i g_m},$$

$$\tau = \frac{c_m}{g_m},$$

so that the equation becomes

$$\lambda^2 \frac{\partial^2 v}{\partial x^2} - v - \tau \frac{\partial v}{\partial t} = -v_r. \quad (6.55)$$

In terms of the primary axon parameters, the parameters in Eq. 6.55 are

$$\lambda^2 = \frac{ab\rho_m}{2\rho_i}, \quad (6.56)$$

$$\tau = \kappa\epsilon_0\rho_m. \quad (6.57)$$

The time constant was seen before in Eq. 6.40. Equation 6.55 has a steady-state solution  $v = v_r$ . If a new variable  $v' = v - v_r$  is used, it becomes the homogeneous version of the same equation with a steady-state solution  $v' = 0$ . This homogeneous equation is known as the

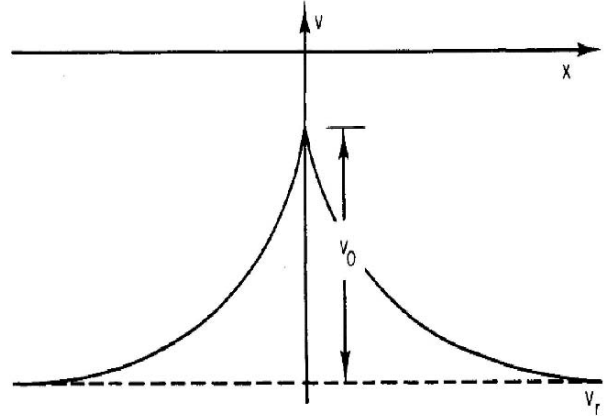


FIGURE 6.30. The voltage distribution along an axon in electrotonus when the membrane capacitance is charged and the voltage is not changing with time.

telegrapher's equation: it was once familiar to physicists and electrical engineers as the equation for a long cable, such as a submarine cable, with capacitance and leakage resistance but negligible inductance [Jeffreys and Jeffreys (1956, p. 602)].

For nerve conduction, the inhomogeneous equation with various exciting terms corresponding to physiological stimuli was discussed by Davis and Lorente de Nó (1947) and by Hodgkin and Rushton (1946). Their work is summarized by Plonsey (1969, p. 127).

Before considering general solutions to Eq. 6.55, consider some special cases. If  $c_m = 0$ , so that  $\tau = 0$ , or if enough time has elapsed so that the voltage is not changing with time and  $\partial v/\partial t = 0$ , the equation reduces to

$$\lambda^2 \frac{\partial^2 v}{\partial x^2} - v = -v_r.$$

You can verify by substitution that this has a solution

$$v - v_r = \begin{cases} v_0 e^{-x/\lambda}, & x > 0 \\ v_0 e^{x/\lambda}, & x < 0. \end{cases} \quad (6.58)$$

If the voltage is held at a constant value  $v = v_r + v_0$  at some point on the axon, the voltage will decay exponentially to  $v_r$  in both directions from that point. This is shown in Fig. 6.30.

Next, suppose that  $v(x, t)$  does not depend on  $x$ , so that there is no longitudinal current in the axon and  $\partial^2 v/\partial x^2 = 0$ . This can be accomplished experimentally by threading a wire axially along the axon, if the axon is fat enough. The equation reduces to

$$\tau \frac{\partial v}{\partial t} + v = v_r.$$

This is the familiar equation for exponential decay. If  $v$  were held at  $v_0 + v_r$  and then the constraint were removed at  $t = 0$ , the voltage would decay exponentially back to  $v_r$

$$v - v_r = v_0 e^{-t/\tau}.$$

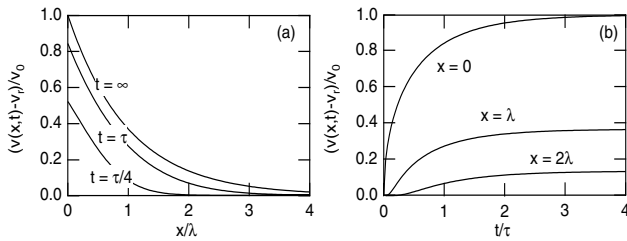


FIGURE 6.31. Some representative solutions to the problem of electrotonus after the application of a constant current at  $x = 0$ . (a) The voltage along the axon at different times (b) Voltage at a fixed point on the axon as a function of time.

This represents the discharge of the membrane capacitance through the membrane resistance.

The behavior of  $v(x, t) - v_r$  at various times after an excitation is applied is shown in Fig. 6.31. The excitation is a constant current injected at  $x = 0$  for all time  $t > 0$ . After a long time, the curve is identical to that in Fig. 6.30, as the membrane capacitance has fully charged. Only the membrane leakage current attenuates the signal. At earlier times the solution is not precisely exponential; the analytic solution involves error functions (Problem 34). The change of voltage with time at fixed positions along the cable is also shown. Both the finite propagation time and the attenuation of the signal are evident.

### 6.13 The Hodgkin–Huxley Model for Membrane Current

If the voltage at some point on the axon changes by a few millivolts from the resting value, the voltage at other points on the axon is described by electrotonus. However, if the inside voltage rises from the resting value by 20 mV or more, a completely different effect takes place. The potential rises rapidly to a positive value, then falls to about  $-80$  mV, and finally returns to the resting value (Fig. 6.1). This behavior is attributable to a very nonlinear dependence of membrane current on transmembrane voltage.

Considerable work was done on nerve conduction in the late 1940s, culminating in a model that relates the propagation of the action potential to the changes in membrane permeability that accompany a change in voltage. The model [Hodgkin and Huxley (1952)] does not explain why the membrane permeability changes; it relates the shape and conduction speed of the impulse to the observed changes in membrane permeability. Nor does it explain all the changes in current. (For example, the potassium current does fall eventually, and there are some properties of the sodium current that are not adequately described.) Nonetheless, the work was a triumph that led to the Nobel Prize for Alan Hodgkin and Andrew Huxley.

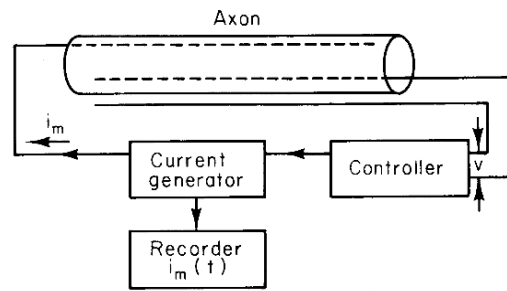


FIGURE 6.32. Apparatus for voltage-clamp measurements.

Most of the experiments that led to the Hodgkin–Huxley model were carried out using the giant axon of the squid. This is a single cell several centimeters long and up to 1 mm in diameter that can be dissected from the squid. The removal of axoplasm from the preparation and its replacement by electrolytes has shown that the critical phenomena all take place in the membrane. The important results are reviewed in many places [Katz (1966, Chapters 5 and 6); Plonsey (1969, p. 127); Plonsey and Barr (1988, Ch. 4); Scott (1975, pp. 495–507)].

#### 6.13.1 Voltage Clamp Experiments

Voltage-clamp experiments were particularly illuminating. Two long wire electrodes were inserted in the axon and connected to the apparatus shown in Fig. 6.32. The resistance of the wires was so low that the potential at all points along the axon was the same at any instant of time. The potential depended only on time, and not on position. This is called a *space-clamped* experiment. One electrode, paired with an electrode in the surrounding medium, measured the voltage difference across the membrane. The other electrode was used to inject or remove whatever current was necessary to keep this voltage difference constant. Measurement of this current allowed calculation of the membrane conductance. This technique is called *voltage clamping*. The experiment described here was both voltage- and space-clamped.

When the membrane potential was raised abruptly from the resting value to a new value and held there, the resulting current was found to have three components:

1. A current, lasting a few microseconds, that changed the surface charge on the membrane.
2. A current flowing inward which lasted for 1 or 2 ms. Various experiments, such as replacing the sodium ions in the extracellular fluid with some other monovalent ion, showed that this was due to the inward flow of sodium ions. (Had the potential not been voltage-clamped by the electronic apparatus, this inrush of positive charge would have raised the potential still further.)



3. An outward current that rose in about 4 ms and remained steady for as long as the potential was clamped at this value. Tracer studies showed that this current was due to potassium ions. (Over a time scale of several tens of milliseconds, the potassium current, like the sodium current, does fall back to zero.)

The first current is the  $c_m(\partial v/\partial t)$  term of Eq. 6.52; the second and third currents together constitute  $j_m$ . Because of the clamping wires, the  $\partial^2 v/\partial x^2$  term is zero.

The next step is to develop a model that describes the major ionic constituents of the current. The sodium and potassium contributions to the current will be considered separately; all other contributions will be combined in a “leakage” term:

$$j_m = j_{Na} + j_K + j_L. \quad (6.59)$$

The leakage includes charge movement due to chloride ions and any other ions that can pass through the membrane.

Consider movement of sodium through the membrane. Similar considerations apply to potassium. The concentrations of sodium inside and out are  $[Na_i]$  and  $[Na_o]$ . It will be seen later that the total number of ions moving through the membrane during a nerve pulse in a squid giant axon is too small to change the concentrations significantly. Therefore, the concentrations are fixed.

There would be no movement of sodium ions through the membrane, regardless of how permeable it is, when the concentrations and potential are related by the Boltzmann factor or Nernst equation (Eq. 6.33) with  $v = v_i - v_o$ :

$$\frac{[Na_i]}{[Na_o]} = e^{-ev/k_B T}.$$

For given concentrations, the sodium equilibrium or Nernst potential is

$$v_{Na} = \frac{k_B T}{e} \ln \left( \frac{[Na_o]}{[Na_i]} \right). \quad (6.60)$$

The sodium Nernst potential is usually about 50 mV. If  $v = v_{Na}$  there is no current of sodium ions, regardless of the membrane permeability to sodium. If  $v$  is greater than  $v_{Na}$  (more positive),  $j_{Na}$  flows outward. If  $v < v_{Na}$ , the sodium current is inward. These currents can be described by

$$j_{Na} = g_{Na}(v - v_{Na}). \quad (6.61)$$

The coefficient  $g_{Na}$  is the sodium conductance per unit area. It is not constant but depends on the value of  $v$  and, in fact, on the past history of  $v$ . Defining the conductance this way makes the functional form of  $g_{Na}$  less complex; in particular, it does not have to change sign as  $v$  moves through  $v_{Na}$  and the sodium current reverses direction.

This equation can be multiplied by the membrane area to give a current–voltage relationship. Many authors draw a circuit diagram to represent the current flow

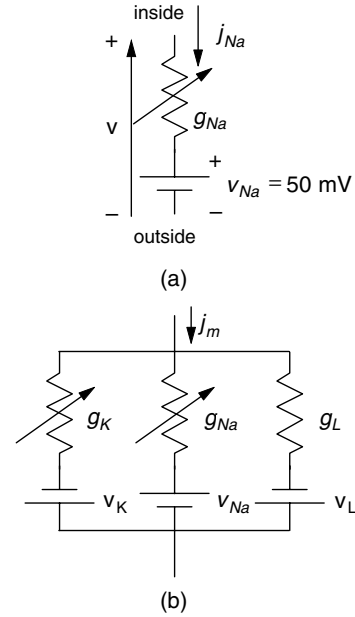


FIGURE 6.33. Equivalent circuits for the membrane current. (a) The sodium current–voltage relationship of Eq. 6.61 is the same as that for a variable resistance in series with a battery at the sodium Nernst potential. (b) The total membrane current can be modeled with three such equivalent circuits. See the discussion of the sign of the potassium and leakage Nernst potentials in the text.

through the membrane and along the axon. The sodium voltage–current relationship can be represented by a variable resistance corresponding to  $g_{Na}$  in series with a battery at the sodium Nernst potential, as shown in Fig. 6.33(a).

An expression similar to Eq. 6.61 can be written for the potassium current density:

$$j_K = g_K(v - v_K). \quad (6.62)$$

The potassium Nernst potential is negative—about  $-77$  mV—so the polarity of the potassium battery in Fig. 6.33(b) has been reversed. The leakage term will be considered later.

To summarize:  $v$  is the instantaneous voltage across the membrane. Both  $v_K$  and  $v_{Na}$  are constants depending on the relative ion concentrations inside and outside the cell and the temperature. The conductances per unit area depend on both the present value of  $v$  and its past history.

We can now describe the results of the voltage clamp experiments. The voltage in each experiment was changed from the resting value by an amount  $\Delta v$ . Therefore,  $v - v_{Na}$  and  $v - v_K$  had constant values after the change, and the changes in current density mirrored the changes in conductivity. Typical results for  $\Delta v = 25$  mV and  $T = 6^\circ\text{C}$  are shown in Figs. 6.34 and 6.35. [The method of distinguishing sodium from potassium current is described in the original papers, or in Hille (2001, p. 39).]

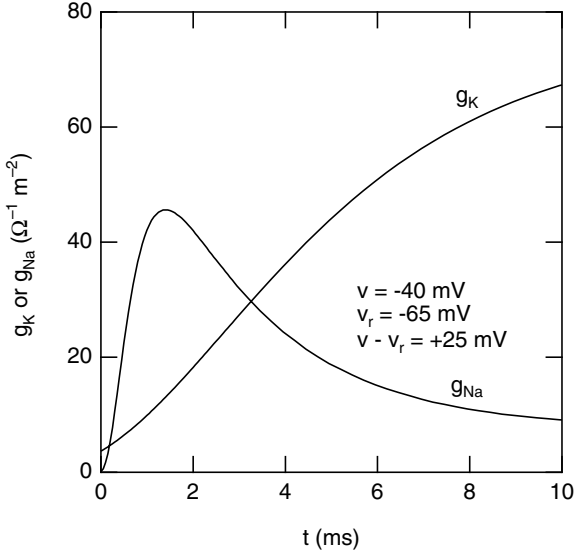


FIGURE 6.34. The behavior of the sodium and potassium conductivities with time in a voltage-clamp experiment. At  $t = 0$  the voltage was raised by 25 mV from the resting potential. The values are calculated from Eqs. 6.64–6.71 and are representative of the experimental data.

For a voltage clamp experiment the current and conductance have the same time variation. The sodium conductance rises from zero and then falls, while the potassium conductance rises more slowly from a small initial resting value. (The potassium current before the voltage clamp was applied was small, because the resting potential was close to the potassium Nernst potential.) Measurements for longer times show that the potassium conductivity rises to a constant value. Measurements for much longer times show that the potassium current falls after tens of milliseconds. For other values of  $\Delta v$  the conductance changes are different.

### 6.13.2 Potassium Conductance

Hodgkin and Huxley wanted a way to describe their extensive voltage-clamp data, similar to that in Figs. 6.34 and Fig. 6.35, with a small number of parameters. If we ignore the small nonzero value of the conductance before the clamp is applied, the potassium conductance curve of Fig. 6.34 is reminiscent of exponential behavior, such as  $g_K(v, t) = g_K(v)(1 - e^{-t/\tau(v)})$ , with both  $g_K(v)$  and  $\tau(v)$  depending on the value of the voltage. A simple exponential is not a good fit. Figure 6.36 shows why. The curve  $(1 - e^{-t/\tau})$  starts with a linear portion and is then concave downward. The potassium conductance in Figs. 6.34 and 6.35 is initially concave upward. The curve  $(1 - e^{-t/\tau})^4$  in Fig. 6.36 more nearly has the shape of the conductance data. This suggests that we try to describe the conductance by

$$g_K(v, t) = g_{K\infty} \left[ n_{\infty}(v)(1 - e^{-t/\tau(v)}) \right]^N. \quad (6.63)$$

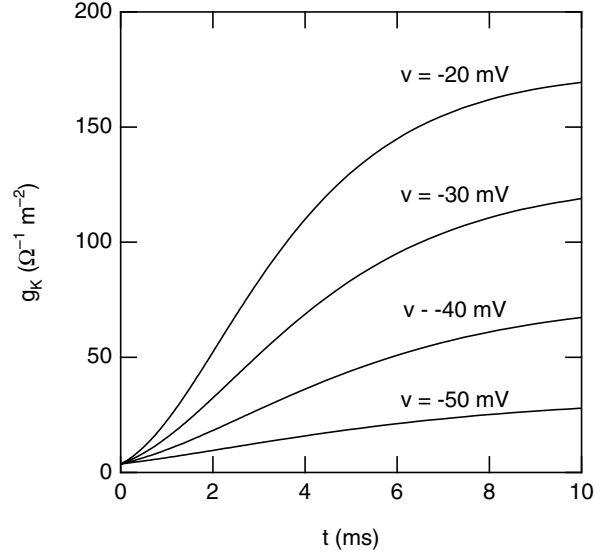


FIGURE 6.35. The behavior of the potassium conductance for different values of the clamping voltage. These are representative curves calculated from Eqs. 6.64–6.66.

In this expression,  $g_{K\infty}$  is the largest possible conductance per unit area. The value of  $n_{\infty}(v)$  varies between 0 and 1 and determines the asymptotic value of the conductance change for a particular value of the voltage step. Hodgkin and Huxley found a good fit to their data with  $N = 4$ . If the initial value of the conductance were zero, our empirical fit to the potassium conductance data would be

$$g_K(v, t) = g_{K\infty} n^4(v, t), \quad (6.64a)$$

$$n(v, t) = n_{\infty}(v)(1 - e^{-t/\tau(v)}). \quad (6.64b)$$

But the initial potassium conductance was not zero. How should this be handled? Hodgkin and Huxley assumed that  $n$  is a measure of some fundamental property of the potassium channels, and that the conductance is always described by Eq. 6.64a. When the clamp voltage changes, the subsequent change of  $n$  is described by an exponential decay with the appropriate values of  $n_{\infty}(v)$  and  $\tau(v)$ . If the initial value of  $n$  is  $n_0$ , the expression for  $n(v, t)$  after the voltage clamp change is

$$n(v, t) = n_{\infty}(v) \left[ 1 - \left( \frac{n_{\infty}(v) - n_0}{n_{\infty}(v)} \right) e^{-t/\tau(v)} \right]. \quad (6.64c)$$

The function  $n$  is a solution to the differential equation

$$\frac{dn}{dt} = -\frac{n}{\tau} + \frac{n_{\infty}}{\tau}. \quad (6.65a)$$

Hodgkin and Huxley wrote this instead in the form

$$\frac{dn}{dt} = \alpha_n(1 - n) - \beta_n n. \quad (6.65b)$$

The subscript  $n$  on  $\alpha_n$  and  $\beta_n$  distinguishes them from similar parameters for the sodium conductance.

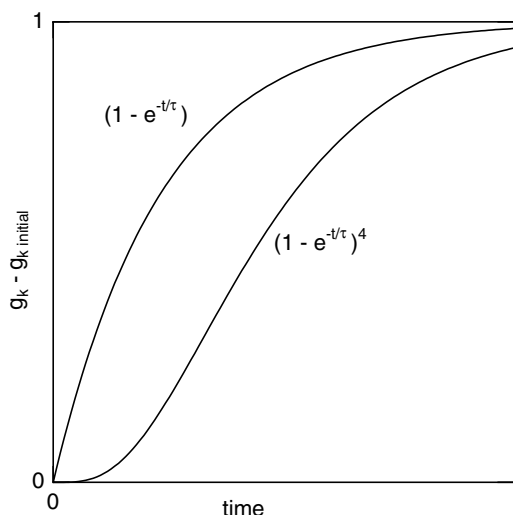


FIGURE 6.36. A comparison of  $(1 - e^{-t/\tau})$  with  $(1 - e^{-t/\tau})^4$ . The latter more closely approximates the shape of the potassium conductance in Fig. 6.34.

The dependence of  $\alpha_n$  and  $\beta_n$  on voltage is quite pronounced. With  $v$  in mV and  $\alpha_n$  and  $\beta_n$  in  $\text{ms}^{-1}$ , the equations used by Hodgkin and Huxley to describe their experimental values of  $\alpha_n$  and  $\beta_n$  are

$$\alpha_n(v) = \frac{0.01 [10 - (v - v_r)]}{\exp\left(\frac{10 - (v - v_r)}{10}\right) - 1}, \quad (6.66)$$

$$\beta_n(v) = 0.125 \exp\left(\frac{-(v - v_r)}{80}\right).$$

The quantities  $\alpha_n$  and  $\beta_n$  are rate constants in Eq. 6.65b. Like all chemical rate constants, they depend on temperature. The values above are correct when  $T = 279$  K ( $6.3^\circ\text{C}$ ). Hodgkin and Huxley assumed that the temperature dependence was described by a  $Q_{10}$  of 3. This means that the reaction rate increases by a factor of 3 for every  $10^\circ\text{C}$  temperature rise. The rate at temperature  $T$  is obtained by multiplying rates obtained from Eq. 6.66 by

$$3^{(T-6.3)/10}. \quad (6.67)$$

For example, if the temperature is  $18.5^\circ\text{C}$ , the rate must be multiplied by  $3^{1.22} = 3.82$ .

The variable  $n$  is often called the *potassium gate* or the *n gate*. It takes values between zero (a *closed gate*) and 1 (an *open gate*). The  $n$  gate is partially open at rest, making the resting membrane somewhat permeable to potassium. As  $v$  becomes more positive than the resting potential (“depolarizes”), the  $n$  gate opens further or “activates.”

The behavior of  $\alpha_n$  and  $\beta_n$  was determined from voltage-clamp experiments. In an actual nerve-conduction process,  $v$  is not clamped. Hodgkin and Huxley *assumed* that when  $v$  varies with time, the correct

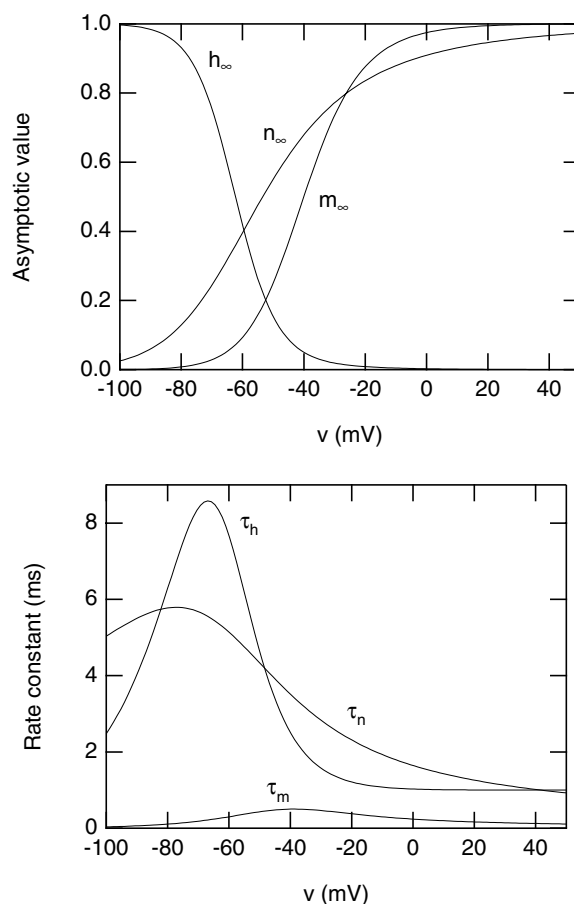


FIGURE 6.37. Plots of the sodium and potassium conductance parameters versus the transmembrane potential.

value of  $n$  can be obtained by integrating Eq. 6.65b. At each instant of time the values of  $\alpha_n$  and  $\beta_n$  are those obtained from Eq. 6.66 for the voltage at that instant. This was a big assumption—but it worked. The value of  $g_{K\infty}$  that they chose was  $360 \text{ S m}^{-2}$ .

### 6.13.3 Sodium Conductance

The sodium conductance was described by two parameters: one reproducing the rise and the other the decay of the conductance. The equation was

$$g_{Na} = g_{Na\infty} m^3 h. \quad (6.68)$$

The parameters  $m$  and  $h$  obeyed equations similar to that for  $n$ :

$$\frac{dm}{dt} = \alpha_m(1 - m) - \beta_m m, \quad (6.69)$$

$$\frac{dh}{dt} = \alpha_h(1 - h) - \beta_h h. \quad (6.70)$$

The  $v$  dependences were

$$\begin{aligned}\alpha_m &= \frac{0.1[25 - (v - v_r)]}{\exp\left(\frac{25 - (v - v_r)}{10}\right) - 1}, \\ \beta_m &= 4 \exp\left(\frac{-(v - v_r)}{18}\right), \\ \alpha_h &= 0.07 \exp\left(\frac{-(v - v_r)}{20}\right), \\ \beta_h &= \frac{1}{\exp\left(\frac{30 - (v - v_r)}{10}\right) + 1}.\end{aligned}\tag{6.71}$$

These values for  $\alpha$  and  $\beta$  are also for a temperature of 6.3 °C. The temperature scaling of Eq. 6.67 must be used for other temperatures. The value of  $g_{Na\infty}$  is 1200 S m<sup>-2</sup>. Figure 6.37 plots the time constants and asymptotic values as a function of membrane potential. These are the parameters for the equations in the form of Eq. 6.65a rather than Eq. 6.65b.

The variable  $m$  (called the *sodium activation gate* or *m gate*) is nearly closed at rest, preventing the resting membrane from being permeable to sodium. As  $v$  is depolarized  $m$  opens, allowing sodium to rush in. The sodium ions carry positive charge, so this inward current causes  $v$  to depolarize further, causing  $m$  to increase even more. This positive feedback (see Chapter 10) is responsible for the rapid upstroke of the action potential. The inward sodium current ends when  $v$  approaches the sodium Nernst potential, about 50 mV.

Variable  $h$  (the *sodium inactivation gate* or *h gate*) is different than the  $n$  and  $m$  gates because it is open at rest but closes upon depolarization. However, it is slow compared to the  $m$  gate (see Fig. 6.37), so during an action potential it does not fully close until after the  $m$  gate has opened completely. After the action potential is finished and  $v$  has returned to the resting value, the slow  $h$  gate takes a few milliseconds to completely re-open. During this time, the membrane cannot generate another action potential (it is “refractory”) because the closed  $h$  gate suppresses the sodium current.

#### 6.13.4 Leakage Current

All other contributions to the current (such as movement of chloride ions) were lumped in the leakage term  $j_L = g_L(v - v_L)$ . The empirical value for  $g_L$  is 3 S m<sup>-2</sup>. The parameter  $v_L$  was adjusted to make the total membrane current equal zero when  $v = v_r$ . For example, with the data given, zero current is obtained with  $v_r = -65$  mV and  $v_L = v_r + 10.6 = -54.4$  mV. The three contributions to the membrane current can be thought of as the circuit shown in Fig. 6.33b.

The Hodgkin–Huxley parameters have been used for a wide variety of nerve and muscle systems, even though they were obtained from measurements of the squid axon.

A number of other models have since been developed that incorporate the sodium–potassium pump, calcium, and so on. They have also been developed for various muscle and cardiac cells [Dennis *et al.* (1994); Luo and Rudy (1994); Wilders *et al.* (1991)].

## 6.14 Voltage Changes in a Space-Clamped Axon

A space-clamped axon has an interior potential  $v(t)$  that does not depend on  $x$ . If such an axon is stimulated, a voltage pulse is observed. The first test we can make of the Hodgkin–Huxley model is to see if the parameters from the voltage-clamp experiments can also explain this pulse. To do so, it is necessary to insert Eq. 6.59, with all the other equations that are necessary to use it, in Eq. 6.52. Life is made somewhat simpler by the fact that the spatial derivative in Eq. 6.52 vanishes when the wire is in the axon. The result is

$$c_m \frac{\partial v}{\partial t} = -g_{Na}(v - v_{Na}) - g_K(v - v_K) - g_L(v - v_L).\tag{6.72}$$

When  $v = v_r$  the right-hand side of this equation is zero and  $v$  does not change. It is necessary to introduce a stimulus to cause the pulse. This has been done in the computer program of Fig. 6.38, which solves Eq. 6.72. This program is not the most efficient that can be used; it has been written for ease of understanding. A stimulus of 10<sup>-4</sup> A cm<sup>-2</sup> = 1 A m<sup>-2</sup> is applied between 0.5 and 0.6 ms. This is an additional term in Eq. 6.72, so that in the program, Eq. 6.72 becomes

$$dvdt = (-jMemb + jStim)/Cmemb;$$

In this statement  $dvdt$  stands for  $\partial v/\partial t$ ,  $jMemb$  stands for  $j_m$ ,  $Cmemb$  for  $c_m$ , and  $jStim$  for the stimulus current. The equation is solved by repeated application of the approximation

$$v = v + dvdt * deltat;$$

which stands for

$$v(t + \Delta t) = v(t) + \left(\frac{\partial v}{\partial t}\right) \Delta t.$$

The program uses  $\Delta t = 10^{-6}$  s. The present value of  $v$  is used to calculate the rate constants in procedure `Calcab`. These are then used to calculate the present value of each conductivity. The membrane current is then calculated, and the entire process is repeated for the next time step. The results are tabulated in Fig. 6.39 and plotted in Fig. 6.40.

One can see from the plot that  $j_m$  is proportional to  $\partial v/\partial t$ . Note that although  $g_{Na}$  is a smooth curve,  $j_{Na}$  has an extra wiggle near  $t = 2$  ms, caused by the rapid

```

/program HodgkinHuxley
/Calculates Hodgkin-Huxley
/Space clamped axon at 6.3°C

#include <stdio.h>
#include <math.h>

const float
deltat = 1e-6 //deltat for integration
tPStep = 1e-4 //print line this often
vR = -65e-3, //Resting Potential
Cmemb = 1e-6, //Membrane capacitance
tMax = 5e-3, //Time to quit
vNa = 50e-3, //Sodium Nernst pot.
vK = -77e-3, //Potassium Nernst pot.

double
n, m, hh,
an, am, ah,
bn, bm, bh,
dndt, dmdt, dhdt, dvdt,
gK, gNa,
jK, jNa, jL, jMemb,
voltage, t,
jStim, //Stimulus current
tPrint; //Time interval to print

void CalcCab(void)
/* Calculates the alpha and betas for n,
l, h, using the Hodgkin-Huxley equations.
The original equations were in mV and ms;
these are in volts and seconds */
{
an = {10*(-1000*(voltage-vR)+10)}
//((exp(-1000*(voltage-vR)+10)/10)-1);
am = {100*(-1000*(voltage-vR)+25)}
//((exp(-1000*(voltage-vR)+25)/10)-1);
ah = 70*exp(-1000*(voltage-vR)/20);
bn = 125*exp(-1000*(voltage-vR)/80);
bm = 4000*exp(-1000*(voltage-vR)/18);
bh = 1000/(exp(-1000*(voltage-vR)+30)
/10)+1;
}

void Calc_Init_Values(void)
//Calculates initial values of n, m,
hh
{
CalcCab();
n = an/(an+bn);
m = am/(am+bm);
hh = ah/(ah+bh);
}

void Calc_Curr(void)
//Calculate conductances in siemens
//per sq cm and current densities
{
gK = 36e-3*pow(n, 4);
gNa = 120e-3*pow(m, 3)*hh;
jK = gK*(voltage-vK);
jNa = gNa*(voltage-vNa);
jL = 3e-4*(voltage-vR-10.6e-3);
jMemb = jK+jNa+jL;
}

main(void)
{
//Print Table Headings
printf("time v jMemb gNa gK jK jL\n");
t = 0;
voltage = vR;
tPrint = 0;
Calc_Init_Values();
while (t < tMax)
//Step through all the times
{
Calc_Curr(); //Calculate membrane
//current from conductances
if (t >= tPrint) //Print
at certain times
{
printf("%4.1f %1s %5.1f %1s ",
1000*t, "", 1000*voltage, "");
printf("%8.2e %1s %8.2e %1s
%8.2e", jMemb, "", gNa, "", jNa );
printf("%1s %8.2e %1s %8.2e %1s
%8.2e\n", "", gK, "", jK, "", jL);
tPrint = tPrint+tPStep;
} // end if

if ((t>=5e-4) && (t<=6e-4))
//Stimulus current at beginning
jStim = 1e-4;
else
jStim = 0; //No stimulus current
dvdt = (-jMemb+jStim)/Cmemb;
voltage = voltage+dvdt*deltat;
CalcCab(); //Calc alphas, betas
dndt = an*(1-n)-bn*n;
dmdt = am*(1-m)-bm*m;
dhdt = ah*(1-hh)-bh*hh;
n = n+dndt*deltat;
m = m+dmdt*deltat;
hh = hh+dhdt*deltat;
t = t+deltat;
} //end while
} //end main

```

FIGURE 6.38. The computer program used to calculate the response of a space-clamped axon to a stimulus. The results are shown in Figs. 6.39 and 6.40.

decrease in the magnitude of  $v - v_{Na}$  as the voltage approaches the sodium Nernst potential. The initial depolarization is due to an inrush of sodium ions. But there is still a considerable sodium current during the potassium current. The sodium and potassium currents are nearly balanced throughout most of the pulse. The pulse lasts about 2 ms.

If the temperature is raised, the pulse is much shorter. Figure 6.41 shows the impulse when the temperature is 18.5°C, calculated by multiplying each of the  $\alpha$  and  $\beta$  values by  $3^{(18.5-6.3)/10} = 3.82$ .

The potassium current is not actually needed to create a nerve impulse because of the leakage current (primarily chloride) and the fact that the sodium conductance decreases after the initial depolarization. The potassium current speeds up the repolarization process. It is easy to modify the program of Fig. 6.38 to show this.

## 6.15 Propagating Nerve Impulse

If the wire is not inserted along the axon, the voltage changes in the  $x$  direction. A strong enough stimulus at one point results in a pulse that travels along the axon

time	v	jMemb	gNa	jNa	gK	jK	jL
ms	mV	A/sq cm	S/sq cm	A/sq cm	S/sq cm	A/sq cm	A/sq cm
0.0	-65.0	-3.24e-06	1.36e-01	-1.22e-02	3.67e+00	4.40e-02	-3.18e-02
0.2	-65.0	-2.90e-06	1.36e-01	-1.22e-02	3.67e+00	4.40e-02	-3.18e-02
0.4	-65.0	-2.68e-06	1.36e-01	-1.22e-02	3.67e+00	4.40e-02	-3.18e-02
0.6	-55.3	5.75e-02	1.39e-01	-2.09e-02	3.74e+00	8.11e-02	-2.71e-03
0.8	-55.9	5.17e-03	7.38e-01	-7.50e-02	4.02e+00	8.48e-02	-4.59e-03
1.0	-55.6	-3.69e-02	1.19e-00	-1.25e-01	4.31e+00	9.22e-02	-3.58e-03
1.2	-54.5	-7.33e-02	1.59e-00	-1.77e-01	4.62e+00	1.04e-01	-2.79e-04
1.4	-52.6	-1.24e-01	2.45e-00	-2.52e-01	5.01e+00	1.22e-01	5.49e-03
1.6	-49.2	-2.30e-01	4.32e-00	-3.99e-01	5.52e+00	1.54e-01	1.56e-02
1.8	-42.2	-5.34e-01	8.59e-00	-7.92e-01	6.34e+00	2.21e-01	3.67e-02
2.0	-22.3	-1.73e+00	3.14e-01	-2.27e+00	8.15e+00	4.45e-01	9.62e-02
2.2	28.7	-2.08e+00	1.33e-02	-3.89e+00	1.48e+01	1.56e+00	2.49e-01
2.4	38.7	2.13e-01	3.17e-02	-3.60e+00	3.06e+01	3.53e+00	2.79e-01
2.6	32.0	4.18e-01	2.38e-02	-5.35e+00	5.05e+01	5.51e+00	2.59e-01
2.8	22.7	5.00e-01	2.50e-02	-6.81e+00	7.10e+01	7.08e+00	2.31e-01
3.0	12.5	5.19e-01	2.34e-02	-7.67e+00	8.53e+01	7.99e+00	2.01e-01
3.2	2.2	5.06e-01	1.55e-02	-7.91e+00	1.04e+02	8.25e+00	1.70e-01
3.4	-7.7	4.80e-01	1.32e-02	-7.63e+00	1.15e+02	7.97e+00	1.40e-01
3.6	-17.1	4.56e-01	1.34e-02	-6.97e+00	1.22e+02	7.31e+00	1.12e-01
3.8	-26.0	4.43e-01	7.93e-01	-6.03e+00	1.25e+02	6.39e+00	8.52e-02
4.0	-35.0	4.63e-01	5.71e-01	-4.85e+00	1.25e+02	5.26e+00	5.82e-02
4.2	-45.0	5.56e-01	3.55e-01	-3.38e+00	1.22e+02	3.90e+00	2.81e-02
4.4	-57.5	6.86e-01	1.45e-01	-1.56e+00	1.16e+02	2.25e+00	-9.43e-03
4.6	-70.0	4.64e-01	1.38e-00	-2.37e-01	1.07e+02	7.47e-01	-4.68e-02
4.8	-75.2	1.04e-01	8.39e-02	-1.01e-02	9.64e+01	1.76e-01	-6.23e-02

FIGURE 6.39. Results of the calculation for a space-clamped axon at 6.3°C.

without change of shape. The basic equation that describes it is again Eq. 6.52 with the spatial term and with the Hodgkin-Huxley model for the membrane current:

$$\frac{\partial v}{\partial t} = -\frac{j_m}{c_m} + \frac{1}{2\pi a r_i c_m} \frac{\partial^2 v}{\partial x^2},$$

$$j_m = g_{Na}(v - v_{Na}) + g_K(v - v_K) + g_L(v - v_L). \quad (6.73)$$

These can be solved numerically by setting up arrays for values of  $v$ ,  $n$ ,  $m$ , and  $h$  at closely spaced discrete values of  $x$ , then the discrete equation is

$$\begin{aligned} dvdt[i] = & -jMemb[i]/Cmemb \\ & + (1/(6.28 * a * r_i * Cmemb * dx * dx)) \\ & * (v[i + 1] - 2 * v[i] + v[i - 1]). \end{aligned}$$

Fig. 6.42 shows each term in Eq. 6.73 multiplied through by  $c_m$  to have the dimensions of current per unit area. The term

$$c_m \frac{\partial v}{\partial t}$$

is the rate at which charge per unit area on the membrane must to change the membrane potential at the rate  $\partial v/\partial t$ ,

$$-j_m = -g_{Na}(v - v_{Na}) - g_K(v - v_K) - g_L(v - v_L)$$

is the rate of charge buildup because of current through the membrane, and

$$\frac{1}{2\pi a r_i} \frac{\partial^2 v}{\partial x^2}$$

is the rate of charge buildup on the inner surface of the membrane because the longitudinal current is not uniform.

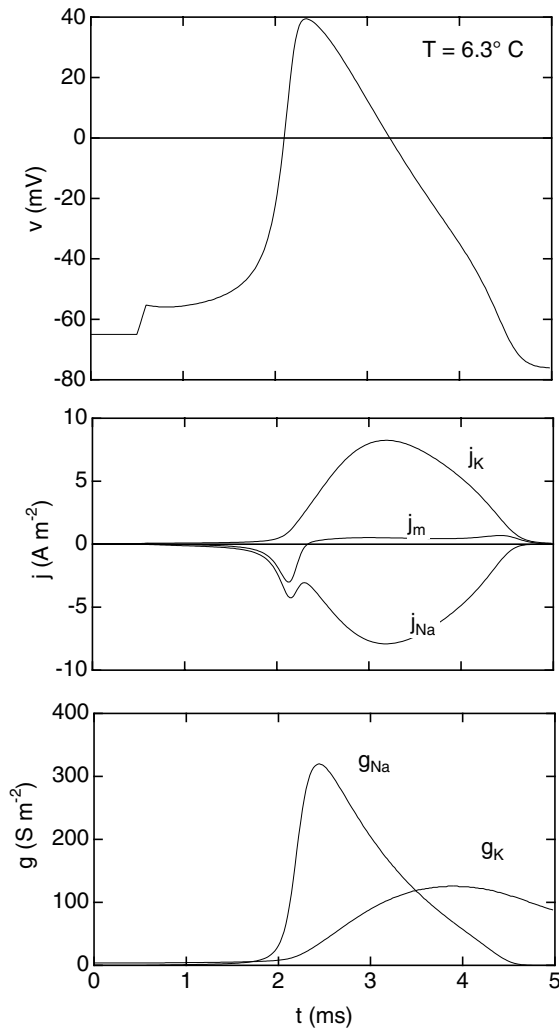


FIGURE 6.40. A plot of the computation presented in Fig. 6.38 for a pulse in a space-clamped squid axon at  $T = 6.3^\circ\text{C}$ . The axon was stimulated at  $t = 0.5$  ms for 0.1 ms.

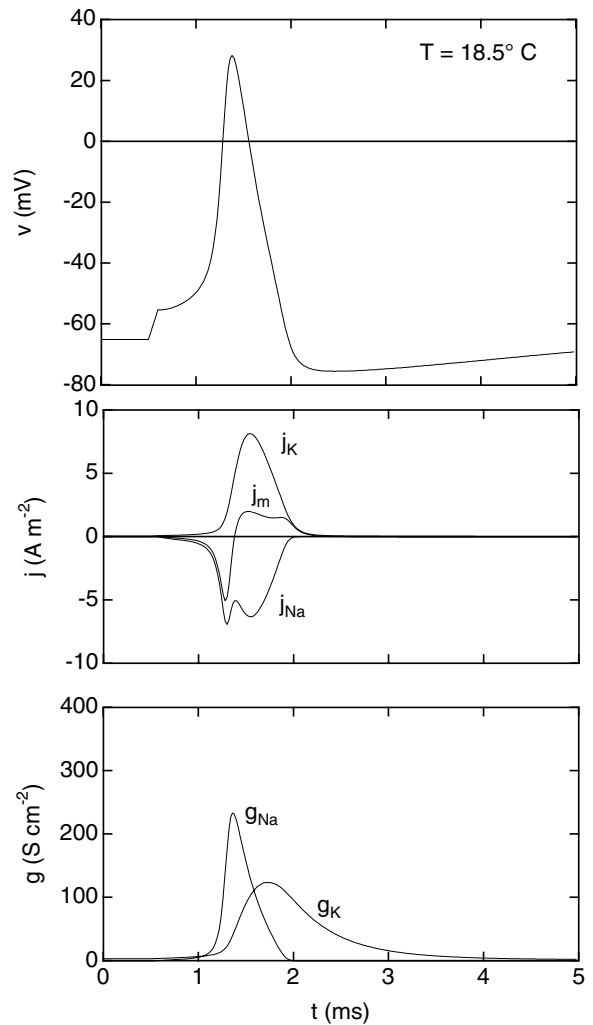


FIGURE 6.41. A pulse in a space-clamped axon at  $18.5^\circ\text{C}$ . The pulse lasts about 1 ms.

### 6.16 Myelinated Fibers and Saltatory Conduction

We have so far been discussing fibers without the thick myelin sheath. Unmyelinated fibers constitute about two-thirds of the fibers in the human body. They usually have radii of  $0.05\text{--}0.6\ \mu\text{m}$ . The conduction speed in  $\text{m s}^{-1}$  is given approximately by  $u \approx 1800\sqrt{a}$ , where  $a$  is the axon radius in meters.<sup>13</sup> (Strictly speaking, in this formula  $a$  should be replaced by the outer radius  $a + b$  including the membrane thickness, but for an unmyelinated fiber  $b \ll a$ .)

Myelinated fibers are relatively large, with outer radii of  $0.5\text{--}10\ \mu\text{m}$ . They are wrapped with many layers

of myelin between the nodes of Ranvier, as shown in Fig. 6.43. Typically, the outer radius is  $a + b \approx 1.67a$  and the spacing between nodes is proportional to the outer diameter  $D = 200(a + b) \approx 330a$  (See Problem 66). These empirical proportionalities between node spacing and radius and between myelin thickness and radius will be very important to our understanding of the conduction speed. The conduction speed in a myelinated fiber is given approximately by  $u \approx 12 \times 10^6(a + b) \approx 20 \times 10^6a$ . The conduction speeds of myelinated and unmyelinated fibers are compared in Fig. 6.44.

In the myelinated region the conduction of the nerve impulse can be modeled by electrotonus because the conductance of the myelin sheath is independent of voltage. At each node a regenerative Hodgkin–Huxley-type (HH-type) conductance change restores the shape of the pulse. Such conduction is called *saltatory conduction* because *saltare* is the Latin verb “to jump.”

<sup>13</sup>Values quoted in the literature range from  $u = 1000\sqrt{a}$  [Plonsey and Barr (1988)] to  $u = 3000\sqrt{a}$  [Rushton (1951)].

TABLE 6.2. Properties of unmyelinated and myelinated axons of the same radius.

Quantity	Unmyelinated	Myelinated
Axon inner radius, $a$	5 $\mu\text{m}$	5 $\mu\text{m}$
Membrane thickness, $b'$	6 nm	
Myelin thickness, $b$		3.4 $\mu\text{m}$
$\kappa\epsilon_0$	$6.20 \times 10^{-11} \text{ s}^{-1} \Omega^{-1} \text{ m}^{-1}$	$6.20 \times 10^{-11} \text{ s}^{-1} \Omega^{-1} \text{ m}^{-1}$
Axoplasm resistivity $\rho_i$	1.1 $\Omega \text{ m}$	1.1 $\Omega \text{ m}$
Membrane (resting) or myelin resistivity $\rho_m$	$10^7 \Omega \text{ m}$	$10^7 \Omega \text{ m}$
Time constant $\tau = \kappa\epsilon_0\rho_m$	$6.2 \times 10^{-4} \text{ s}$	$6.2 \times 10^{-4} \text{ s}$
Space constant $\lambda$	$\lambda = \sqrt{\frac{ab\rho_m}{2\rho_i}}$ $= 0.165\sqrt{a}$ $= 370 \mu\text{m}$	$\lambda = \sqrt{\frac{ab\rho_m}{2\rho_i}} = \sqrt{\frac{0.67a^2\rho_m}{2\rho_i}}$ $= a\sqrt{\frac{0.67\rho_m}{2\rho_i}}$ $= 1750a$ $= 8.8 \text{ mm}$
Node spacing $D$		$D = 340a = 1.7 \text{ mm}$
Conduction speed from model	$u_{\text{unmyelinated}} \propto \lambda/\tau \approx 270\sqrt{a}$	$u_{\text{myelinated}} \propto \lambda/\tau \approx 2.9 \times 10^6 a$ or $D/\tau = 0.55 \times 10^6 a$
Conduction speed, empirical	$u_{\text{unmyelinated}} \approx 1800\sqrt{a}$	$u_{\text{myelinated}} \approx 17 \times 10^6 a$
Ratio of empirical to model conduction speed	6.7	5.9 or 31
Space constant using thick membrane model		$\lambda = a\sqrt{\frac{\ln(1+b/a)\rho_m}{2\rho_i}}$ $= a\sqrt{\frac{\ln(1.67)\rho_m}{2\rho_i}}$ $= 1530a$ $= 7.6 \text{ mm}$

We saw that electrotonus is described by

$$\lambda^2 \frac{\partial^2 v}{\partial x^2} - v - \tau \frac{\partial v}{\partial t} = -v_r, \quad (6.74)$$

where the time constant is

$$\tau = \kappa\epsilon_0\rho_m \quad (6.75)$$

and the space constant is

$$\lambda = \sqrt{\frac{ab\rho_m}{2\rho_i}}. \quad (6.76a)$$

The results of Problem 65 can be used to show that when the myelin thickness is appreciable compared to the inner axon radius, the space constant should be modified:

$$\lambda_{\text{thick}} = \sqrt{\frac{\ln(1+b/a)\rho_m}{2\rho_i}} a. \quad (6.76b)$$

For a case in which  $a = 5 \mu\text{m}$  and  $b = 3.3 \mu\text{m}$ , the change is not very large. The thin membrane equation contains

the quantity  $ab = 17 \times 10^{-12} \text{ m}^2$  and the thick myelin equation contains  $a^2 \ln(1+b/a) = 12.8 \times 10^{-12} \text{ m}^2$ .

We now want to understand the different dependence on radius of the conduction speed in the two kinds of fibers. We could do computer modeling for the unmyelinated fiber using Eq. 6.73 with axons of different radii, but this would not provide an equation for  $u(a)$ . Rather than review the work that has been done (developing equations for the behavior of the foot of the action potential, for example), we will use a simple dimensional argument. This will not give an exact expression for  $u(a)$ , but it will indicate the functional form it must have.

In either the myelinated or the unmyelinated fiber the signal travels to neighboring regions by electrotonus, where it initiates HH-type membrane conductance changes. In the myelinated case the signal jumps from node to node; in the unmyelinated case the influence is on adjacent parts of the axon. When the neighboring region begins to depolarize, the HH change is much more rapid than that due to electrotonus. (Another way to say this is that during depolarization  $\rho_m$  and therefore  $\tau$

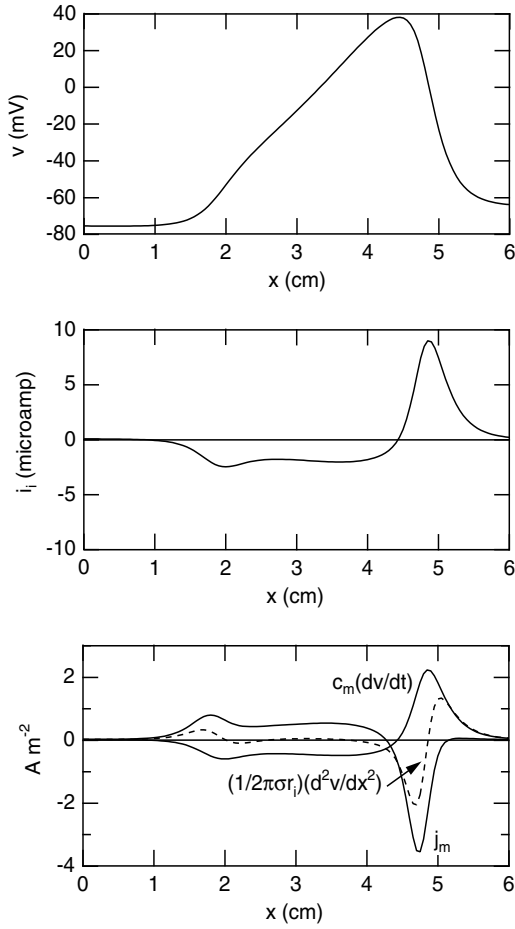


FIGURE 6.42. A propagating pulse plotted against position along the axon at an instant of time. The middle graph shows the longitudinal current inside the axon. The bottom curve shows the current charging or discharging the membrane and the two terms comprising the right-hand side of Eq. 6.73.

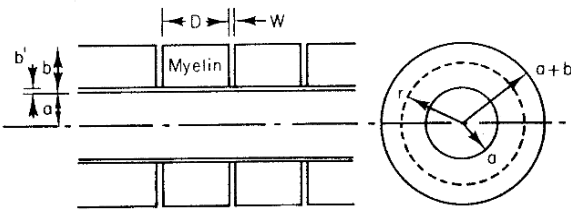


FIGURE 6.43. The idealized structure of a myelinated fiber in longitudinal section and in cross section. The internodal spacing  $D$  is actually about 100 times the outer diameter of the axon.

become much smaller.) Therefore the conduction speed is limited by electrotonus. Regardless of the details of the calculation, the speed is proportional to the characteristic length in the problem divided by the characteristic time. For the unmyelinated case it is plausible to assume that

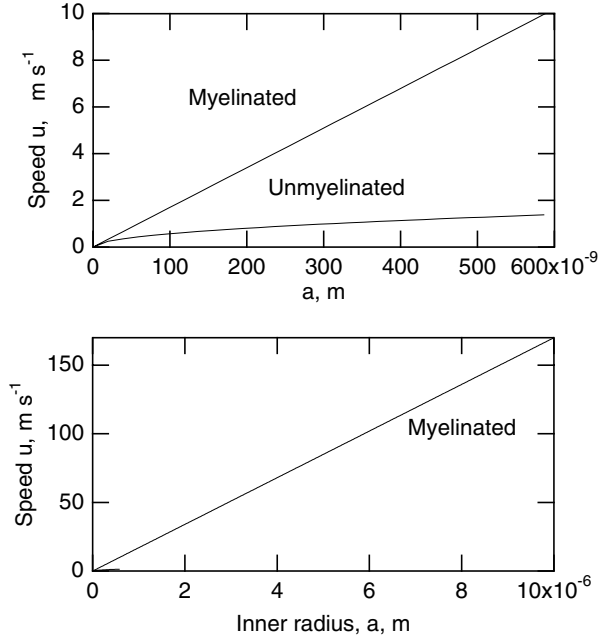


FIGURE 6.44. The conduction speed versus the inner axon radius  $a$  for myelinated and unmyelinated fibers. Unmyelinated fibers with  $a > 0.6 \mu\text{m}$  are not found in the body.

the only characteristic length and time are  $\lambda$  and  $\tau$ , so the speed is

$$u_{\text{unmyelinated}} \propto \frac{\lambda}{\tau} = \sqrt{\frac{b}{2\rho_i\rho_m}} \frac{1}{\kappa\epsilon_0} \sqrt{a}. \quad (6.77)$$

Since the membrane thickness for an unmyelinated fiber is always about 6 nm, this gives

$$u_{\text{unmyelinated}} \propto 270\sqrt{a} \quad (6.78)$$

as shown in Table 6.2.

For myelinated nerves the myelin thickness is  $b \approx 0.67a$ . This means that the space constant is proportional to  $a$ :

$$\lambda = \sqrt{\frac{ab\rho_m}{2\rho_i}} = \sqrt{\frac{0.67a^2\rho_m}{2\rho_i}} = a\sqrt{\frac{0.67\rho_m}{2\rho_i}} = 1750a. \quad (6.79)$$

The spacing between the nodes,  $D$ , is about  $340a$ . There are two characteristic lengths for the myelinated case, both proportional to  $a$  because of the way the myelin is arranged. If we assume that the speed is proportional to  $D/\tau$ , we obtain

$$u_{\text{myelinated}} \propto 0.55 \times 10^6 a. \quad (6.80)$$

If we assume that the speed is proportional to  $\lambda/\tau$ , we obtain

$$u_{\text{myelinated}} \propto 2.9 \times 10^6 a. \quad (6.81)$$

Table 6.2 compares the space constants, time constants and conduction speeds for myelinated and unmyelinated



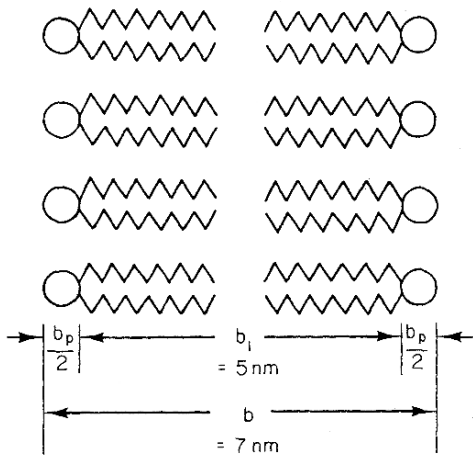


FIGURE 6.45. Structure of a bimolecular lipid membrane.

fibers. The empirical expressions for the conduction speed are seven or eight times greater than what we estimate based on  $\lambda/\tau$ . We might expect firing at the next node to occur when the signal has risen to about 10% of its final value. This would reduce the time by about a factor of 10.

The internodal spacing is about 20% of the space constant. Suppose that a constant current is injected at one node, as in Fig. 6.30. When the voltage has reached its full value at the next node it is given by

$$\frac{v}{v_0} = e^{-D/\lambda} = e^{-1.4/6.2} = 0.8.$$

If for some reason this node does not fire, the signal at the next node will be 0.64 of the original value, and so on. A local anesthetic such as procaine works by preventing permeability changes at the node. It is clear from this discussion that a nerve must be blocked over a distance of several nodes (a centimeter or more) in order for an anesthetic to be effective [Covino (1972)].

### 6.17 Membrane Capacitance

The value of 7 for the dielectric constant, which has been used throughout this chapter, is considerably higher than the value 2.2, which is known for lipids. The inconsistency arises because part of the membrane is very easily polarized and effectively belongs to the conductor rather than to the dielectric; if the thickness of the lipid alone is considered in calculating the capacitance, then a value of 2.2 for  $\kappa$  is reasonable; if the entire membrane thickness is used, then the much higher dielectric constant for water and the polar groups within the membrane contributes, and  $\kappa = 7$  is a reasonable value.

The easiest experiments to understand are those done with artificial bimolecular layers of lipid. The architec-

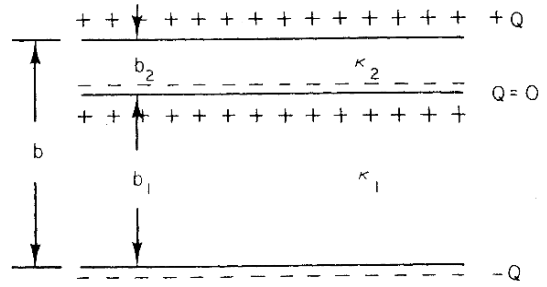


FIGURE 6.46. A membrane composed of two phases. The  $i$ th phase has thickness  $b_i$  and dielectric constant  $\kappa_i$ . The total thickness is  $b$  and the effective dielectric constant is  $\kappa$ . The charges shown are external charge; polarization of the dielectric is not shown but determines the value of  $\kappa$ .

ture of such a film is shown in Fig. 6.45. Each lipid molecule has a polar head and a hydrophobic tail. The molecules are arranged in a double layer with the heads in the aqueous solution. The dimensions in Fig. 6.45 are consistent with both measurements of the film thickness and with the known structure of the lipid molecules. Linear aliphatic hydrocarbons have a bulk dielectric constant of about 2. The polar heads have a much higher dielectric constant, probably about 50. Water has a dielectric constant of about 80.

The capacitance per unit area of bimolecular lipid films is about  $0.3 \times 10^{-2} \text{ F m}^{-2}$  ( $0.3 \mu\text{F cm}^{-2}$ ). The simplest way to explain this value is to assume that the polar heads are part of the surrounding conductor. The capacitance per unit area is then

$$\frac{C}{S} = \frac{\kappa\epsilon_0}{b_1} = \frac{(2.2)(8.85 \times 10^{-12})}{5 \times 10^{-9}} = 0.4 \times 10^{-2} \text{ F m}^{-2}.$$

A more sophisticated approach is to regard the membrane as made up of three layers: polar, lipid, polar. The same effect can be obtained by considering two layers with all the polar component lumped together, as in Fig. 6.46. Suppose that we put charge  $+Q$  on one surface and  $-Q$  on the other surface of the membrane. We put no charge on the interface between layers 1 and 2. The charge of zero on the interface can be thought of as a superposition of positive and negative charges as shown in Fig. 6.46. We are referring only to external charge which we place on the membrane; the charges induced by polarization of the dielectric are not shown. They are taken into account by the value of  $\kappa$ . The situation is that of two parallel-plate capacitors in series. Each layer has a capacitance  $C_i$ :  $Q = C_i v_i = \kappa_i \epsilon_0 S v_i / b_i$ . The total potential across the membrane is  $v = v_1 + v_2 = Q/C$ . The total capacitance is

$$C = \frac{Q}{v_1 + v_2} = \frac{Q}{\frac{Q b_1 / \kappa_1 \epsilon_0 S}{1} + \frac{Q b_2 / \kappa_2 \epsilon_0 S}{1}} = \frac{1}{\frac{b_1 / \kappa_1 \epsilon_0 S}{1} + \frac{b_2 / \kappa_2 \epsilon_0 S}{1}} \tag{6.82}$$

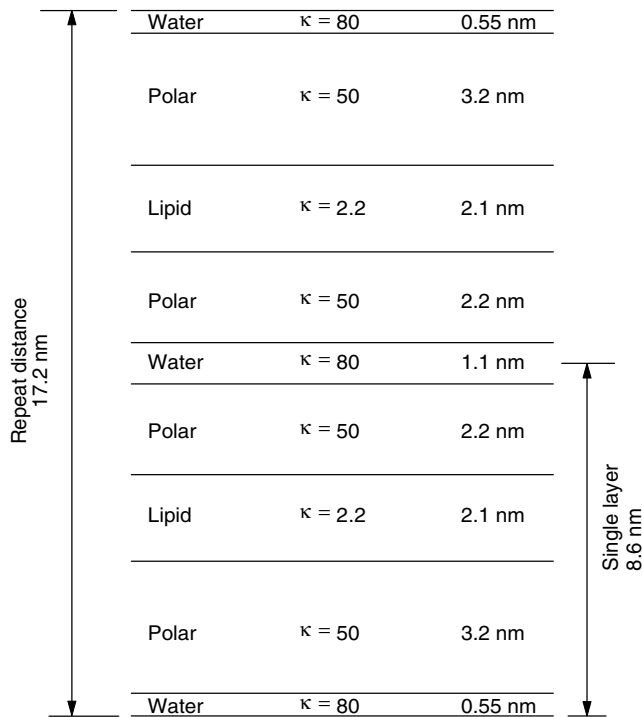


FIGURE 6.47. The results of x-ray diffraction measurements of the structure of myelin surrounding frog sciatic nerve. Data are adapted from Worthington (1971, p. 35).

The effective dielectric constant is obtained by equating the total capacitance to  $\kappa\epsilon_0 S/b$ :

$$\kappa = \frac{b}{b_1/\kappa_1 + b_2/\kappa_2}. \tag{6.83}$$

Application of these equations to the bimolecular lipid membrane (with  $\kappa_1 = 2.2$ ,  $\kappa_2 = 50$ ,  $b_1 = 5$  nm,  $b_2 = 2$  nm) gives

$$\kappa = 3.0, \tag{6.84}$$

$$\frac{C}{S} = 0.38 \times 10^{-2} \text{ F m}^{-2}.$$

The capacitance per unit area is nearly that obtained by assuming the polar groups are perfect conductors.

The myelin surrounding a nerve fiber consists of several layers wrapped tightly together. Each repeating layer is made up of two single layers back to back. The best data on the structure of these layers are from x-ray diffraction experiments. The layers repeat every 17 nm. One model for the structure within a repeat distance is shown in Fig. 6.47 [Worthington (1971, p. 35)]. A single layer of the myelin has a thickness of 8.55 nm. A surprising feature of this model is that the lipid layer is less than half the thickness of that in a bilayer lipid membrane. However, the measured capacitance of a nerve-cell membrane or myelin is greater than for the bilayer lipid membrane; if one is to keep the lipid value for  $\kappa$ , the membrane must be thinner. It is gratifying that the membrane thickness

as measured by x-ray diffraction is consistent with the observed membrane capacitance.

To check the consistency, note that Eqs. 6.82 and 6.83 are easily extended to more than two phases. Use the following data:

	$\kappa_i$	$b_i$ nm
Water	80	2.2
Lipid	2.2	4.2
Polar	50	10.8

With these values, the effective dielectric constant is

$$\kappa = \frac{17.2}{4.2/2.2 + 2.2/80 + 10.8/50} = 7.95.$$

If we assume that the membrane on an unmyelinated axon has the same structure as a half-unit of the myelin, then the thickness is 8.55 nm. With a dielectric constant of 7.95, the capacitance per unit area is calculated to be  $0.82 \times 10^{-2} \text{ F m}^{-2}$ . The measured value is  $1.0 \times 10^{-2} \text{ F m}^{-2}$ .

When one begins to look at the detailed structure of the membrane as we have done in this section, there is no justification for using the same membrane thickness  $b$  for the capacitance and the conductance of the membrane. The capacitance is determined primarily by the thickness of the lipid portion of the membrane; the conductance includes the effect of ions passing through the polar layers. The product,  $\kappa\rho$ , of the previous section is meaningful only for a membrane that is homogeneous and has the same thickness for both capacitive and conductive effects.

As long as the membrane structure is not being considered, it is safer to express such things as attenuation along the axon in terms of the directly measured parameters: length and time constants. Nonetheless, a preliminary formulation in terms of a homogeneous membrane model can be useful to start thinking about the problem.

## 6.18 Rhythmic Electrical Activity

Many cells exhibit rhythmic electrical activity. Various nerve transducers produce impulses with a rate of firing that depends on the input to which the transducer is sensitive. The beating of the heart is controlled by the *sinoatrial node* (SA node) that produces periodic pulses that travel throughout the heart muscle.

The mechanism for such repetitive activity is similar to what we have seen in the Hodgkin-Huxley model, though the details of the ionic conductance variations differ. The computer program of Fig. 6.38 can easily be modified to model rhythmic activity.

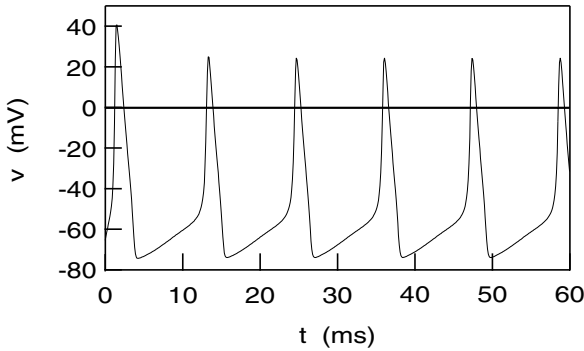


FIGURE 6.48. By changing the leakage current, it is possible to make the Hodgkin–Huxley model display periodic electrical activity.

Figure 6.48 shows a plot of the output of a modified program. The only modification was to make  $\mathbf{j}\text{stim}$  be a constant leakage current of  $0.2 \text{ A m}^{-2}$  ( $0.2 \times 10^{-4} \text{ A cm}^{-2}$ ). This provides the essential feature: a small inward current between beats that causes the potential inside the cell to increase slowly. When the voltage exceeds a certain threshold, the membrane channels open and the cell produces another impulse.

While this simple change produces repetitive firing, and in fact the shape of the curve in Fig. 6.48 is very similar to that measured in the SA node, the details of ionic conduction are actually very different. The SA node contains no sodium channels. The rapid depolarization is due to an inward calcium current. There are a number of contributions to the current in the SA node, and detailed ionic models of them have been described [Dennis *et al.* (1994); Noble (1995); Noble *et al.* (1989); Wilders *et al.* (1991).] The slow leakage is a complicated combination of currents, the details of which are still not completely understood [Anumonwo and Jalife (1995); DiFrancesco *et al.* (1995)].

## 6.19 The Relationship Between Capacitance, Resistance, and Diffusion

There is a fundamental relationship between the capacitance and resistance between two conductors in a homogeneous conducting dielectric. It is also possible to develop an analogy between capacitance and steady-state diffusion, so that known expressions for the capacitance of conductors in different geometries can be used to solve diffusion problems.

### 6.19.1 Capacitance and Resistance

Consider two conductors carrying equal and opposite charge and embedded in an insulating medium with di-

electric constant  $\kappa$ . The potential difference between the conductors is  $\Delta v$ , and the magnitude of the charge on each is  $Q = C\Delta v$ . The electric field is  $\mathbf{E}(x, y, z)$ . In a vacuum, Gauss's law applied to a surface surrounding the positively charged conductor gives  $\iint \mathbf{E} \cdot d\mathbf{S} = Q/\epsilon_0$ . Polarization in a dielectric surrounding the conductor reduces the electric field by a factor of  $\kappa$ . If  $\mathbf{E}$  refers to the electric field in the dielectric and  $Q$  to the charge on the conductor, Gauss's law becomes

$$\iint \mathbf{E} \cdot d\mathbf{S} = Q/\kappa\epsilon_0. \quad (6.85)$$

For a given charge on the conductor, the presence of the dielectric reduces  $\mathbf{E}$  and  $\Delta v$  by  $1/\kappa$  and, therefore, increases the capacitance by  $\kappa$ .

Suppose that the dielectric is not a perfect insulator but obeys Ohm's law and has conductivity  $\sigma$  ( $\mathbf{j} = \sigma\mathbf{E}$ ). If some process maintains the magnitude of the charge on each conductor at  $Q$ , the current leaving the positive conductor is

$$i = \iint \mathbf{j} \cdot d\mathbf{S} = \sigma \iint \mathbf{E} \cdot d\mathbf{S} = \sigma Q/\kappa\epsilon_0. \quad (6.86)$$

The resistance between the conductors is

$$R = \frac{\Delta v}{i} = \frac{Q/C}{\sigma Q/\kappa\epsilon_0} = \frac{\kappa\epsilon_0}{\sigma C}. \quad (6.87)$$

This inverse relationship between the resistance and capacitance is independent of the geometry of the conductors, as long as the dielectric constant and conductivity are uniform throughout the medium.

If the charge on the conductors is not replenished, it leaks off with a time constant  $\tau = RC = \kappa\epsilon_0/\sigma$ . We have seen this result earlier in several special cases; we now understand that it is quite general.

### 6.19.2 Capacitance and Diffusion

In Chapter 4, we saw that the transport equations for particles, heat, and electric charge all have the same form. We now develop an analogy between these transport equations and the equations for the electric field. The analogy is useful because it relates the diffusion of particles between different regions to the electrical capacitance between conductors with the same geometry; the electrical capacitance in many cases is worked out and available in tables.

Fick's first law of diffusion was developed in Chapter 4, Eq. 4.20:<sup>14</sup>

$$\mathbf{j}_s = -D\nabla c. \quad (6.88)$$

<sup>14</sup>In this section, we will use  $c$  for concentration of solute particles and  $C$  for the electrical capacitance.

The relationship between fluence rate (particle current density) and particle flux (current) is

$$\iint \mathbf{j}_s \cdot d\mathbf{S} = i_s, \quad (6.89)$$

where  $i_s$  is the current of particles out of the volume enclosed by the surface. This equation is very similar to Gauss's law,

$$\iint_{\text{surface}} \mathbf{E} \cdot d\mathbf{S} = \frac{q}{\kappa\epsilon_0}, \quad (6.90)$$

where  $q$  is the electric charge. The electric potential and the electric field are related by the three-dimensional version of Eq. 6.16:

$$\mathbf{E} = -\nabla v. \quad (6.91)$$

The similarity between Eqs. 6.91 and 4.20 and between 6.5 and 6.90 suggests that we make the substitutions

$$\begin{aligned} i_s &\longleftrightarrow \frac{q}{\kappa\epsilon_0}, \\ c &\longleftrightarrow \frac{v}{D}, \\ \mathbf{j}_s &\longleftrightarrow \mathbf{E}. \end{aligned} \quad (6.92)$$

For any electrostatic configuration in which there are two equipotential surfaces containing charge  $+q$  and  $-q$ , there is an analogous diffusion problem in which there is a flow of particles from one surface to another, each surface having a constant concentration on it. In the electrical case, the charge and potential are related by the capacitance, which is a geometric property of the two equipotential surfaces:  $q = C\Delta v$ . An analogous statement can be made for diffusion between two surfaces of fixed concentration:

$$i_s = -\frac{C\Delta v}{\kappa\epsilon_0} = -\frac{C}{\kappa\epsilon_0} D\Delta c. \quad (6.93)$$

We can find the rate of flow of particles if we know the diffusion constant, the concentration difference, and the capacitance for the electrical problem with the same geometry. To see the utility of this method, we will consider some cases of increasing geometrical complexity.

As a first example, suppose that two concentric spheres have radii  $a$  and  $b$ . You can show (from the work in Problem 16, for example) that the capacitance of this configuration is

$$\frac{C}{\kappa\epsilon_0} = \frac{4\pi}{1/a - 1/b}. \quad (6.94)$$

As  $b \rightarrow \infty$ , this becomes

$$\frac{C}{\kappa\epsilon_0} = 4\pi a. \quad (6.95)$$

This can be applied to diffusion to or from a spherical cell of radius  $a$ . If the diffusion is outward, as of waste products, imagine that the outward flow rate is  $i_s$  and

that the concentration difference between the cell surface and infinity is  $c_0$ . Then

$$i_s = -4\pi a D c_0. \quad (6.96)$$

If, on the other hand, the concentration infinitely far away is greater than that at the cell surface by an amount  $c_0$ , the number of particles in the cell will increase at a rate

$$i_s = +4\pi a D c_0. \quad (6.97)$$

These results were obtained directly in Chapter 4.

As another example, consider a circular disk of radius  $a$  with the other electrode infinitely far away. It is more difficult to calculate the capacitance in this case, but we can look it up [Smythe *et al.* (1957)]. It is  $C/\kappa\epsilon_0 = 8a$ . But this is the capacitance for the charge on *both sides* of the disk; the lines of  $\mathbf{E}$  and  $\mathbf{j}$  go off in both directions. We want only half of this, since we will use the result to calculate the end correction for a pore. (If we were concerned with diffusion to a disk-shaped cell, we would use the whole thing.) For the half-space

$$i_{s \text{ half}} = -4Da\Delta c \quad (6.98)$$

is proportional to the radius of the disk, not its area.

Still another geometrical situation that may be of interest is the diffusion of particles from one sphere of radius  $a$  to another sphere of radius  $a$ , when the centers of the spheres are separated by a distance  $b$ .

The capacitance between two such spherical electrodes is [Smythe *et al.* (1957, pp. 5–14)]

$$\frac{C}{\kappa\epsilon_0} = 2\pi a \sinh \beta \left( \frac{1}{\sinh \beta} + \frac{1}{\sinh 2\beta} + \frac{1}{\sinh 3\beta} + \dots \right),$$

where  $\cosh \beta = b/2a$ . This formula is written in terms of the "hyperbolic functions"

$$\begin{aligned} \sinh \beta &= \frac{1}{2}(e^\beta - e^{-\beta}), \\ \cosh \beta &= \frac{1}{2}(e^\beta + e^{-\beta}). \end{aligned} \quad (6.99)$$

When the spheres are far apart  $b/2a \rightarrow \infty$ , and  $\cosh \beta \approx \frac{1}{2}e^\beta$ ,  $\sinh \beta \approx \frac{1}{2}e^\beta$ . In that limit,

$$\begin{aligned} \frac{C}{\kappa\epsilon_0} &= 2\pi a \left(\frac{1}{2}e^\beta\right) \left( \frac{1}{\frac{1}{2}e^\beta} + \frac{1}{\frac{1}{2}e^{2\beta}} + \frac{1}{\frac{1}{2}e^{3\beta}} + \dots \right) \\ &= 2\pi a e^\beta (e^{-\beta} + e^{-2\beta} + e^{-3\beta} + \dots) \\ &= 2\pi a [1 + (a/b) + (a/b)^2 + \dots]. \end{aligned} \quad (6.100)$$

The diffusive flow between two spheres is therefore

$$i_s = -2\pi a D \Delta c \quad (6.101)$$

if they are sufficiently far apart. Note that this is just one-half of the flow from a sphere of radius  $a$  to a concentric sphere infinitely far away. The earlier results in this section show that the electrical resistance between two spherical electrodes sufficiently far apart is  $1/2\pi\sigma a$ .

## Symbols Used in Chapter 6

Symbol	Use	Units	First used on page				
				$v_r$	Resting membrane potential	V	153
				$x, y, z$	Distance	m	139
				$z$	Valence of ion		148
				$C$	Capacitance	F	143
$a$	Distance	m	139	$C_m$	Membrane capacitance	F	149
$a$	Axon inner radius	m	151	$D$	Length of myelinated segment	m	160
$a$	Radius of spherical ion or cell	m	166	$D$	Diffusion constant	$\text{m}^2 \text{s}^{-1}$	165
$a$	Radius of disk	m	166	$\mathbf{E}, E_x, E_y, E_z$	Electric field and components	$\text{V m}^{-1}$	138
$b, c$	Distance	m	139	$E_p$	Electric field due to polarization charge	$\text{V m}^{-1}$	143
$b$	Membrane thickness	m	137	$E_e, E_{\text{ext}}$	External electric field	$\text{V m}^{-1}$	143
$b$	Myelin thickness	m	160	$\mathbf{E}_{\text{tot}}$	Total electric field	$\text{V m}^{-1}$	143
$b'$	Membrane thickness at node of Ranvier	m	160	$\mathbf{F}$	Force	N	137
$b$	Sphere radius	m	166	$\mathbf{F}_{\text{ext}}$	External force	N	141
$c$	Concentration	$\text{m}^{-3}$	137	$G$	Conductance	$\Omega^{-1}$ or S	145
$c_i, c_o$	Ion concentrations	$\text{m}^{-3}$ ; $\text{mol l}^{-1}$	148	$G_m$	Conductance of a section of axon membrane	$\Omega^{-1}$ or S	150
$c_m$	Membrane capacitance per unit area	$\text{F m}^{-2}$	150				
$e$	Electronic charge	C	148	$L$	Length of cylinder or axon segment	m	139
$g_{Na}, g_K, g_m, g_L$	Membrane conductance per unit area	$\text{S m}^{-2}$	151	$[Na_i], [Na_o]$	Sodium concentrations inside and outside an axon	$\text{m}^{-3}$	155
$g_{Na\infty}, g_{K\infty}$	Asymptotic membrane conductance per unit area	$\text{S m}^{-2}$	156	$P$	Power	W	146
$h, h_\infty$	Parameters used to describe sodium conductance		157	$Q$	Electric charge	C	143
$i$	Electric current	A	145	$Q_{10}$	Factor by which the rate of a chemical reaction increases with a temperature rise of 10 K		157
$i_i$	Currents along inside of axon	A	151	$R$	Resistance	$\Omega$	145
$i_m$	Current through a section of membrane	A	149	$R_i$	Internal resistance along a segment of axon	$\Omega$	151
$i_s$	Solute current or flux	$\text{s}^{-1}$	165	$R_m$	Resistance across a segment of membrane	$\Omega$	150
$\mathbf{j}, \mathbf{j}$	Current per unit area	$\text{A m}^{-2}$	145	$S, \Delta S, dS$	Surface area	$\text{m}^2$	138
$\mathbf{j}_m$	Membrane current per unit area	$\text{A m}^{-2}$	150	$T$	Temperature	K	148
$\mathbf{j}_{Na}, \mathbf{j}_K, \mathbf{j}_L$	Membrane current per unit area for that species	$\text{A m}^{-2}$	155	$U$	Potential energy	J	141
$k_B$	Boltzmann's constant	$\text{J K}^{-1}$	148	$W$	Work	J	144
$m, m_\infty$	Parameter used to describe sodium conductance		157	$\alpha_m, \beta_m, \alpha_n, \beta_n, \alpha_h, \beta_h$	Rate parameters for Hodgkin-Huxley model	$\text{s}^{-1}$	156
$n, n_\infty$	Parameter used to describe potassium conductance		156	$\beta$	Dimensionless variable		166
				$\epsilon_0$	Electrical permittivity of empty space	$\text{N}^{-1} \text{m}^{-2}$ $\text{C}^2$	137
				$\kappa$	Dielectric constant		144
$\mathbf{p}, \mathbf{p}$	Dipole moment	C s	168	$\lambda$	Charge per unit length	$\text{C m}^{-1}$	139
$q$	Electric charge	C	137	$\lambda$	Electrotonus spatial decay constant	m	153
$q_{\text{bound}}, q_{\text{free}}$	Bound and free charge	C	144	$\rho$	Resistivity	$\Omega \text{m}$	146
$r, \mathbf{r}$	Distance	m	137	$\rho_i$	Resistivity of axoplasm	$\Omega \text{m}$	151
$r_i$	Resistance per unit length along inside of axon	$\Omega \text{m}^{-1}$	151	$\rho_m$	Resistivity of membrane	$\Omega \text{m}$	150
				$\theta$	Angle		139
$t$	Time	s	136	$\sigma$	Charge per unit area	$\text{C m}^{-2}$	139
$u$	Propagation velocity of a wave or signal	$\text{m s}^{-1}$	160	$\sigma$	Conductivity	$\text{S m}^{-1}$	146
$v$	Potential difference	V	136	$\chi$	Electrical susceptibility		144
$v$	$v_i - v_o$	V	151	$\tau$	Time constant	s	150
$v_K, v_{Na}$	Equilibrium (Nernst) potential for potassium, sodium	V	155	$\tau$	Electrotonus time constant	s	153
				$\tau_h, \tau_m, \tau_n$	Time constants in Hodgkin-Huxley model	s	157

## Problems

### Section 6.2

**Problem 1** Suppose that an action potential in a  $1\ \mu\text{m}$  diameter unmyelinated fiber has a speed of  $1.3\ \text{ms}^{-1}$ . Estimate how long it takes a signal to propagate from the brain to a finger. Repeat the calculation for a  $10\ \mu\text{m}$  diameter myelinated axon that has a conduction speed of  $85\ \text{ms}^{-1}$ . Speculate on the significance of these results for playing the piano.

**Problem 2** The median nerve in your arm has a diameter of about  $3\ \text{mm}$ . If the nerve consists only of  $1\ \mu\text{m}$ -diameter unmyelinated axons, how many axons are in the nerve? (Ignore the volume occupied by extracellular space.) Repeat the calculation for  $20\ \mu\text{m}$  outer diameter myelinated axons. Repeat the calculation for  $0.5\ \text{mm}$  diameter unmyelinated axons (about the size of a squid axon). Speculate on why higher animals have myelinated axons instead of larger unmyelinated axons.

### Section 6.2

**Problem 3** Two equal and opposite charges  $\pm q$  separated by a distance  $a$  form a dipole. The dipole moment  $\mathbf{p}$  is a vector pointing in the direction from the negative charge to the positive charge of magnitude  $p = qa$ . In electrochemistry the dipole moment is often expressed in debye:  $1\ \text{debye (D)} = 10^{-18}$  electrostatic units (statcoulomb cm) ( $1\ \text{statcoulomb} = 3.3356 \times 10^{-10}\ \text{C}$ ).

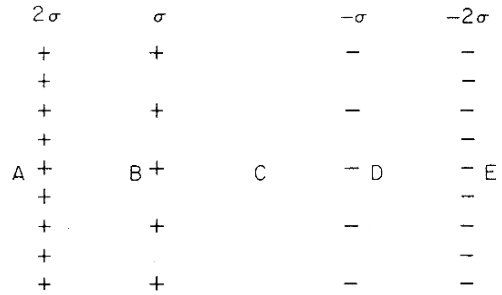
(a) Find the relationship between the debye and the SI unit for the dipole moment.

(b) Express the dipole moment of charges  $\pm 1.6 \times 10^{-19}\ \text{C}$  separated by  $2 \times 10^{-10}\ \text{m}$  in debye and in the appropriate SI unit.

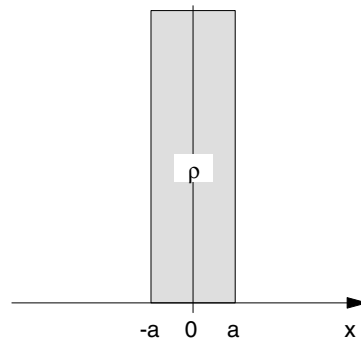
**Problem 4** The electric field of a dipole can be calculated by assuming the positive charge  $q$  is at  $z = a/2$  and the negative charge  $-q$  is at  $z = -a/2$  ( $x = y = 0$ ). The electric field along the  $z$  axis is found by vector addition of the electric field from the individual charges using Eq. 6.3. Find an expression for the electric field. (Hint:  $1/(1+x)^2$  is approximately equal to  $1 - 2x$  for small  $x$ .) By what power of  $z$  does the electric field fall off?

### Section 6.3

**Problem 5** Use the principle of superposition to calculate the electric field in regions A, B, C, D, and E in the figure.



**Problem 6** An infinite sheet of charge has a thickness  $2a$  as shown. The charge density is  $\rho\ \text{C m}^{-3}$ . Find the electric field for all values of  $x$ .



**Problem 7** Derive Eq. 6.10 from Eq. 6.9. At some point in your derivation you may need to use the substitution  $u = y/\sqrt{c^2 + y^2 + z^2}$  and the integrals

$$\int \frac{dx}{(x^2 + a^2)^{3/2}} = \frac{x}{a^2 \sqrt{x^2 + a^2}}$$

$$\int \frac{dx}{x^2 + a^2} = \frac{1}{a} \tan^{-1} \left( \frac{x}{a} \right).$$

**Problem 8** Show that Eq. 6.10 reduces to Eq. 6.8 when  $z \ll b, c$ . Show that Eq. 6.10 is consistent with Coulomb's law when  $z \gg b, c$ .

### Section 6.4

**Problem 9** Show that  $\text{N C}^{-1}$  is equivalent to  $\text{V m}^{-1}$ .

**Problem 10** Use Coulomb's law and  $v = -\int_{\infty}^x E_x dx$  to determine the potential along the  $x$  axis due to a point charge. Assume that  $v(x = \infty) = 0$ . Because there is no preferred direction in space, the potential in any radial direction from the charge has the same form.

**Problem 11** Try to apply the equation  $v(r) = -\int_{\infty}^r E_r dr$  to the equation for the electric field of a line of charge, Eq. 6.7. Why does it not work?

### Section 6.5

**Problem 12** A person stands near a high-voltage power line. Assume for this problem that its voltage is not changing with time. Since much of a person's body is an ionic solution, treat the body as a conductor and the surrounding air as an insulator. In a static situation, what is the electric field inside the person's body caused by the power line? (Hint: Think before you calculate.)

### Section 6.6

**Problem 13** Two plane parallel conducting plates each have area  $S$  and are separated by a distance  $b$ . One carries a charge  $+Q$ ; the other carries a charge  $-Q$ . Neglect edge effects.

(a) What is the charge per unit area on each plate? Where does it reside?

(b) What is the electric field between the plates?

(c) What is the capacitance?

(d) As the plate separation is increased, what happens to  $E$ ,  $v$ , and  $C$ ?

(e) If a dielectric is inserted between the plates, what happens to  $E$ ,  $v$ , and  $C$ ? (See Sec. 6.7.)

**Problem 14** It was shown in the text that the electric field from an infinitely long line of charge, of charge density  $\lambda$  C m<sup>-1</sup>, is  $E = \lambda/2\pi\epsilon_0 r$  at a distance  $r$  from the line.

(a) Show that if positive charge is distributed with density  $\sigma$  C m<sup>-2</sup> on the surface of a cylinder of radius  $a$ , the electric field is

$$\begin{aligned} 0, & \quad r < a \\ \sigma a/\epsilon_0 r, & \quad r > a. \end{aligned}$$

(b) Find the potential difference between a point a distance  $a$  from the center of the cylinder and a point a distance  $d$  from the center of the cylinder ( $d > a$ ).

(c) Is  $a$  or  $d$  at the higher potential?

(d) Suppose that another cylinder of radius  $d$  is placed concentric with the first. It has a charge  $-\sigma'$  per unit area. How will its presence affect the potential difference calculated in part (b)?

(e) Calculate the capacitance between the two cylinders and show that it is  $2\pi\epsilon_0 L/\ln(d/a)$ , where  $L$  is the length of the cylinder.

**Problem 15** Problem 14 showed that the capacitance of a pair of concentric cylinders, of radius  $a$  and  $d$  ( $d > a$ ) is  $2\pi\epsilon_0 L/\ln(d/a)$ . Suppose now that  $d = a + b$ , where  $b$  is the thickness of the region separating the two cylinders. (It might, for example, be the thickness of the axon membrane.) Use the fact that  $\ln(1+x) = x - x^2/2 + x^3/3 + \dots$  to show that, for small  $b$  (that is,  $b \ll a$ ), the formula for

the capacitance becomes the same as that for a parallel-plate capacitor.

**Problem 16** Find the capacitance of two concentric spherical conductors. The inner sphere has radius  $a$  and the outer sphere has radius  $b$ .

### Section 6.7

**Problem 17** A parallel-plate capacitor has area  $S$  and plate separation  $b$ . The region between the plates is filled with dielectric of dielectric constant  $\kappa$ . The potential difference between the plates is  $v$ .

(a) What is the total electric field in the dielectric?

(b) What is the magnitude of the charge per unit area on the inner surface of the capacitor plates?

(c) What is the magnitude of the polarization charge on the surface of the dielectric?

**Problem 18** For the unmyelinated axon of Table 6.1 and Fig. 6.3,

(a) How many sodium, potassium, and miscellaneous anions are there in a 1-mm segment?

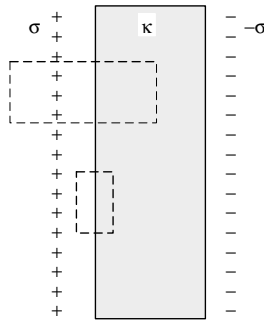
(b) How many water molecules are there in a 1-mm segment?

(c) What is the charge per unit area on the inside of the membrane?

(d) What fraction of all the atoms and ions inside the segment are charged and not neutralized by neighboring ions of the opposite charge?

**Problem 19** A nerve-cell membrane has a layer of positive charge on the outside and negative charge on the inside. These charged layers attract each other. The potential difference between them is  $v = 70$  mV. Assuming a dielectric constant  $\kappa = 5.7$  for the membrane, an axon radius of  $5 \mu\text{m}$ , and a membrane thickness  $b = 5$  nm, what is the force per unit area that the charges on one side of the membrane exert on the other? Express the answer in terms of  $b$ ,  $v$ , and  $\kappa$ . (Hint: The force is calculated by multiplying the charge in a given layer by the electric field due to the charge in the other layer. Think carefully about factors of 2.)

**Problem 20** The drawing represents two infinite plane sheets of charge with an infinite slab of dielectric filling part of the space between them. The dashed lines represent cross sections of two Gaussian surfaces. The sides are parallel to the electric field, and the ends are perpendicular to the electric field. Apply the second form of Gauss's law, Eq. 6.21b, to find the electric field within the dielectric using the upper Gaussian surface. Repeat using the lower Gaussian surface.



Section 6.8

**Problem 21** This problem will give you some insight into the resistance of electrodes used in neurophysiology. Consider two concentric spherical electrodes; the region between them is filled with material of conductivity  $\sigma$ . The inner radius is  $a$ , the outer radius is  $b$ .

(a) Imagine that there is a total charge  $Q$  on the inner sphere. Find the electric field between the spheres in terms of the potential difference between them and their radii.

(b) The current density in the conducting material is given by  $\mathbf{j} = \sigma \mathbf{E}$ . Find the total current.

(c) Find the effective resistance,  $R = v/i$ . What is the resistance as  $b \rightarrow \infty$ ? This is the resistance of a small spherical electrode in an infinite medium; infinite means the other electrode is "far away."

**Problem 22** Patients undergoing electrosurgery sometimes suffer burns around the perimeter of the electrode. Wiley and Webster (1982) analyzed the potential produced by a circular disk electrode of radius  $a$  and potential  $v_0$  in contact with a medium of conductivity  $\sigma$ . They found that the normal component of current density at the surface of the electrode is given by

$$j_n = \frac{2\sigma v_0}{\pi} \frac{1}{(a^2 - r^2)^{1/2}}, \quad 0 < r < a$$

(a) Calculate the total current  $I$  coming out of the electrode.

(b) Determine the resistance of the electrode.

(c) Plot  $j_n$  vs.  $r$ . Use the plot to explain why the patients suffer burns near the edge of the electrode.

Section 6.9

**Problem 23** Derive the equation for the resistance of a set of resistors connected (a) in series and (b) in parallel.

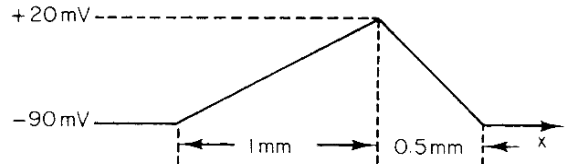
Section 6.10

**Problem 24** The resting concentration of calcium ions,  $Ca^{++}$ , is about  $1 \text{ mmol l}^{-1}$  in the extracellular space but is very low ( $10^{-4} \text{ mmol l}^{-1}$ ) inside muscle cells. Determine the Nernst potential for calcium. Is calcium in equilibrium at a resting potential of  $-70 \text{ mV}$ ?

Section 6.11

**Problem 25** The resistivity of the fluid within an axon is  $0.5 \Omega \text{ m}$ . Calculate the resistance along an axon  $5 \text{ mm}$  long with a radius of  $5 \mu\text{m}$ . Repeat for a radius of  $500 \mu\text{m}$ .

**Problem 26** The voltage along an axon is as shown at some instant of time. The axon radius is  $10 \mu\text{m}$ ; the resistivity of the axoplasm is  $0.5 \Omega \text{ m}$ . What is the longitudinal current in the axon as a function of position?

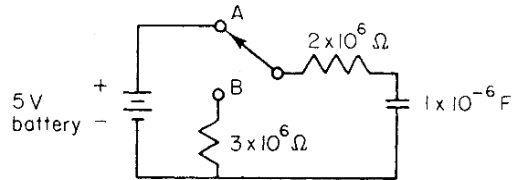


**Problem 27** This problem is designed to show you how a capacitance, such as the cell membrane, charges and discharges. To begin, the switch has been in position B for a long time, so that there is no charge on the capacitor. At  $t = 0$  the switch is put in position A. It is kept there for  $20 \text{ s}$ , then thrown back to position B.

(a) Write a differential equation for the voltage on the capacitor as a function of time when the switch is in position A and solve it.

(b) Repeat when the switch is in position B.

(c) Plot your results.



**Problem 28** Sometimes an organ is lined with a single layer of flat cells. (One example is the lining of the jejunum, the upper portion of the small intestine.) Experimenters can then apply a time-varying voltage across the sheet of cells and measure the resulting current. The cells are packed so tightly together that one model for them is two layers of insulating membrane of dielectric constant  $\kappa$  and thickness  $b$  that behave like a capacitor, separated by intracellular fluid of thickness  $a$  and resistivity  $\rho$ . Find a differential equation or integral equation that relates the total voltage difference across the layer of cells  $v(t)$  to the current per unit area through the layer,  $j(t)$ , in terms of  $\kappa$ ,  $\rho$ ,  $b$ ,  $a$ .

**Problem 29** The current that appears to go "into" a section of membrane is made up of two parts: that which charges the membrane capacitance and that which is a leakage current through the membrane:  $i = v/R + C(dv/dt)$ . Suppose that the total current is sinusoidal:  $i = I_0 \cos \omega t$ .



(a) Show that the voltage must be of the form  $v = I_0 R' \cos \omega t + I_0 X \sin \omega t$  and that the differential equation is satisfied only if

$$R' = \frac{R}{1 + \omega^2 (RC)^2},$$

$$X = R \frac{\omega (RC)}{1 + \omega^2 (RC)^2}.$$

(b) What happens to  $R'$  and  $X$  as  $\omega \rightarrow 0$ ?  $\omega \rightarrow \infty$ ? For what value of  $\omega$  is  $X$  a maximum? What is the corresponding value of  $R'$ ? Plot these points.

(c) Your plot in part b should suggest that the locus of  $X$  vs.  $R'$  is a semicircle, centered at  $X = 0$ ,  $R' = R/2$ . Prove that this is so. [Remember that the equation of a circle is  $(x - a)^2 + (y - b)^2 = r^2$ .]

### Section 6.12

**Problem 30** Consider the myelinated and unmyelinated axons of Tables 6.1 and 6.2. Compare the decay distance for electrotonus in both cases. Neglect attenuation due to the leakage at the node of Ranvier.

**Problem 31** Show by direct substitution that  $v(x) = v_0 e^{-x/\lambda} + v_r$  satisfies the equation

$$\frac{d^2 v}{dx^2} = 2\pi a g_m r_i (v - v_r)$$

if  $v_r$  is constant.

**Problem 32** In an electrotonus experiment a microelectrode is inserted in an axon at  $x = 0$ , and a constant current  $i_0$  is injected. After the membrane capacitance has charged, the voltage outside is zero everywhere and the voltage inside is given by Eq. 6.58:

$$v - v_r = \begin{cases} v_0 e^{-x/\lambda}, & x > 0 \\ v_0 e^{x/\lambda}, & x < 0. \end{cases}$$

- (a) Find  $i_i(x)$  in terms of  $v_0$ ,  $\lambda$ , and  $r_i$ .
- (b) Find  $j_m(x)$  in terms of  $g_m$ ,  $v_0$ , and  $\lambda$ .
- (c) Find the current  $i_0$  injected at  $x = 0$  in terms of  $v_0$ ,  $\lambda$ , and  $r_i$ .
- (d) Find the input resistance  $v_0/i_0$ .

**Problem 33** The cable equation is  $\lambda^2(\partial^2 v/\partial x^2) - v - \tau(\partial v/\partial t) = 0$ . Let  $v(x, t) = w(x, t) \exp(-t/\tau)$ . Substitute this expression into the cable equation and determine a new differential equation for  $w(x, t)$ . You should find that  $w(x, t)$  obeys the diffusion equation (Chapter 4). Find the diffusion constant in terms of the axon parameters and evaluate it for a typical case.

**Problem 34** The voltage along an axon when a constant current is injected at  $x = 0$  for all times  $t > 0$  is given by [Hodgkin and Rushton (1946)]

$$v(x, t) - v_r = \frac{v_0}{2} \left\{ e^{-|x|/\lambda} \left[ 1 - \operatorname{erf} \left( \frac{|x|}{2\lambda} \sqrt{\frac{\tau}{t}} - \sqrt{\frac{t}{\tau}} \right) \right] - e^{|x|/\lambda} \left[ 1 - \operatorname{erf} \left( \frac{|x|}{2\lambda} \sqrt{\frac{\tau}{t}} + \sqrt{\frac{t}{\tau}} \right) \right] \right\}$$

where the error function  $\operatorname{erf}(y)$  and its derivatives are

$$\operatorname{erf}(y) = \frac{2}{\sqrt{\pi}} \int_0^y e^{-z^2} dz$$

$$\frac{d}{dy} \operatorname{erf}(y) = \frac{2}{\sqrt{\pi}} e^{-y^2}.$$

(a) Show that the expression for  $v(x, t)$  obeys the cable equation, Eq. 6.55.

(b) Use  $\operatorname{erf}(0) = 0$ ,  $\operatorname{erf}(-\infty) = -1$ , and  $\operatorname{erf}(\infty) = 1$  to show that as  $t \rightarrow \infty$ , the expression for  $v(x, t)$  approaches the solution in Eq. 6.58 and Fig. 6.30.

(c) Find a simple expression for  $v(x, t)$  when  $x = 0$ . Use  $\operatorname{erf}(1) = 0.843$  and  $\operatorname{erf}(0.5) = 0.520$  to check that this expression is consistent with the plots in Fig. 6.31.

**Problem 35** Consider a space-clamped axon with a membrane time constant  $\tau$ . Initially ( $t \leq 0$ ),  $v' = 0$ . From  $t = 0$  until a time  $t = d$  a stimulus is applied to the membrane. Assume that when  $v' < V'$  the membrane behaves passively ( $V'$  is called the threshold potential), and when  $v' > V'$ , an action potential will fire.  $v'$  obeys the equation  $dv'/dt = -v'/\tau + s$ .

(a) Find  $v'$  for  $0 < t < d$  and for  $t > d$ . Note that  $v'$  is maximum for  $t = d$ .

(b) Find an expression for  $v(t = d)$ , and then solve it for  $s$ .

(c) Plot  $s$  as a function of the pulse duration  $d$ . This plot is called the “strength-duration curve.”

(d) Find the value of  $s$  that corresponds to threshold stimulation for very long durations, in terms of  $V'$  and  $\tau$ . This value of  $s$  is called the “rheobase” stimulus.

(e) Find the value of  $d$  corresponding to threshold stimulation using a stimulus strength of twice rheobase. This duration is called “chronaxie.”

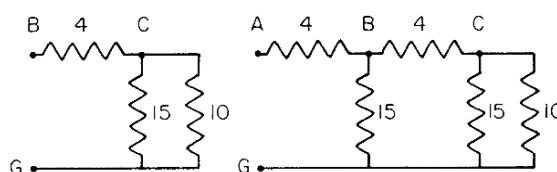
(f) Find an expression for  $\tau$  in terms of chronaxie. Measuring the strength-duration curve is one way to determine the membrane time constant.

**Problem 36** An alternative model to the cable equation is an attenuating network of resistors and capacitors. This problem is designed to show you how a “ladder” of resistances can attenuate a signal.

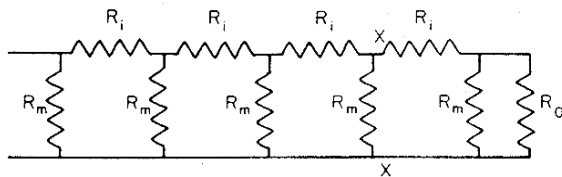
(a) Show that the resistance between points B and G in the circuit on the left is  $10 \Omega$ .

(b) Show that the resistance between points A and G in the circuit on the right is also  $10 \Omega$ . What will be the result if an infinite number of ladder elements are added to the left of AG?

(c) Assume that  $v_C$  (measured with respect to point G) is 6 V. Calculate  $v_B$  and  $v_A$ . Note that the ratios are the same:  $v_B/v_A = v_C/v_B$ .



**Problem 37** This is a more general version of the previous problem, which can be applied directly to electrotonus when capacitance is neglected. Consider the ladder shown, which represents an axon.  $R_0$  is the effective resistance between the inside and outside of the axon to the right of the section under consideration. The axon has been divided into small slices;  $R_i$  is the resistance along the inside of the axon in the small slice, and  $R_m$  is the resistance across the membrane in the slice. The resistance outside the axon is neglected. Note that the resistance looking into the axon to the right of points  $XX$  is also  $R_0$ .



(a) Show that  $R_0$  is given by a quadratic equation:  $R_0^2 - R_i R_0 - R_i R_m = 0$  and that the solution is

$$R_0 = \frac{1}{2} \left[ R_i + (R_i^2 + 4R_i R_m)^{1/2} \right].$$

(b) Show that the ratio of the voltage across one ladder rung to the voltage across the immediately preceding rung is

$$\frac{R_m R_0}{R_m R_0 + R_m R_i + R_i R_0}.$$

(c) Now assume that  $R_i = r_i dx$  and  $R_m = 1/(2\pi a g_m dx)$ . Calculate  $R_0$  and the voltage ratio. Show that the voltage ratio (as  $dx \rightarrow 0$ ) is

$$\frac{1}{1 + (2\pi a r_i g_m)^{1/2} dx}.$$

(d) The preceding expression is of the form  $1/(1+x)$ . For sufficiently small  $x$ , this is approximately  $1-x$ . Therefore, show that the voltage change from one rung to the next is  $dv = -[(2\pi a r_i g_m)^{1/2} dx] v$  so that  $v$  obeys the differential equation

$$\frac{dv}{dx} = -(2\pi a r_i g_m)^{1/2} v.$$

Section 6.13

**Problem 38** Use the Hodgkin-Huxley parameters to answer the following questions.

- (a) When  $v = v_r$ , what are  $\alpha_n$  and  $\beta_n$ ?
- (b) Show that  $dn/dt = 0$  when  $n = 0.318$ . What is the resting value of  $g_K$ ?
- (c) At  $t = 0$  the voltage is changed to  $-25$  mV and held constant. Find the new values of  $\alpha_n, \beta_n, n_\infty, \tau_n$  and the asymptotic value of  $g_K$ .
- (d) Find an analytic solution for  $n(t)$ . Plot  $n$  and  $n^4$  for  $0 < t < 10$  ms.

**Problem 39** Calculate the values of the gates  $m, n,$  and  $h$  for the resting membrane ( $v = -65$  mV), using the Hodgkin and Huxley model. Recall that at rest,  $m = m_\infty(v = -65$  mV), etc.

**Problem 40** If  $\alpha_n$  and  $\beta_n$  depend on temperature according to Eq. 6.67, how do  $n_\infty$  and  $\tau_n$  depend on temperature?

**Problem 41** Calculate the resting membrane conductance per unit area for the resting membrane, using the Hodgkin and Huxley model. Hint:  $j_m = 0$  at rest. Let  $v = v_r + dv$ , where  $dv$  is small. Determine the steady-state  $j_m$  as a function of  $dv$ . To keep things simple, ignore any changes to  $m, n,$  and  $h$  resulting from  $dv$ .

**Problem 42** In a voltage-clamp experiment, a wire of radius  $b$  is threaded along the interior of an axon of radius  $a$ . Assume the axoplasm displaced by the wire is pushed out the end so that the cross-sectional area of the axon containing the wire remains  $\pi a^2$ . The resistivities of wire and axoplasm are  $\rho_w$  and  $\rho_a$ . Find the wire radius needed so that voltage changes along the axon are reduced by a factor of 100 from what they would be without the wire. Ignore the electrode surface impedance.

**Problem 43** A wire of resistivity  $\rho_w = 1.6 \times 10^{-8} \Omega m$  and radius  $w = 0.1$  mm is threaded along the exact center of an axon segment of radius  $a = 1$  mm, length  $L = 1$  cm, and resistivity  $\rho_i = 0.5 \Omega m$ . The axon membrane has conductance  $g_m = 10 S m^{-2}$ . Find numerical values for

- (a) the resistance along the wire,
- (b) the resistance of the axoplasm from the wire to the membrane, and
- (c) the resistance of the membrane.

**Problem 44** If the voltage across an axon membrane is changed by 25 mV as in Fig. 6.34, how long will it take for all the potassium to leak out if it continues to move at the constant rate at which it first leaks out? Use the asymptotic value for the potassium conductance from Fig. 6.34. Use Table 6.1, and Fig. 6.3 for any other values you need.

Section 6.14

**Problem 45** Use the data of Fig. 6.40 to answer the following questions about a nerve impulse in a squid axon of radius  $a = 0.1$  mm.

- (a) Estimate the peak sodium ion flux (ions  $m^{-2} s^{-1}$ ) and the total number of sodium ions per unit area that pass through the membrane in one pulse.
- (b) By what fraction does the sodium concentration in the cell increase during one nerve pulse?
- (c) Estimate the peak potassium flux and total potassium transport.

**Problem 46** Show by direct substitution that Eq. 6.64c satisfies the equation  $dn/dt = \alpha_n(1-n) - \beta_n n$  if  $\alpha_n$  and  $\beta_n$  are functions of  $v$ , but not of time.

**Problem 47** The Hodgkin–Huxley equation for the potassium parameter  $n$  is  $dn/dt = \alpha_n(1-n) - \beta_n n$ . What is the asymptotic value of  $n$  when  $t \rightarrow \infty$ ?

**Problem 48** For  $t < 0$  a squid axon has a resting membrane potential of  $-65$  mV. The sodium Nernst potential is  $+50$  mV. The Hodgkin–Huxley parameters are  $m = 0.05$ ,  $h = 0.60$ , and  $g_{Na} = 1200$  S  $m^{-2}$ .

(a) What is  $j_{Na}$ ?

(b) For  $t > 0$  a voltage clamp is applied so that  $v = -30$  mV. Suppose that  $m = 0.72(1 - e^{-2.2t})$  and  $h = 0.6e^{-0.63t}$  (here  $t$  is in milliseconds). What is the total charge transported across unit area of the membrane by sodium ions?

**Problem 49** Consider a 1-mm long segment of a squid nerve axon, with a diameter of 1 mm.

(a) Let the intracellular sodium ion concentration be  $15$  mmol  $l^{-1}$ . Calculate the number of sodium ions in this segment of the axon.

(b) Use the plot of  $j_{Na}$  versus time in Fig. 6.41 to estimate the total number of sodium ions that enter the axon during the action potential (if you have to determine the area under the  $j_{Na}$  curve, just estimate it).

(c) Find the ratio of the number of sodium ions entering the axon in one action potential to the number present in the resting axon. Does a single action potential change the intracellular concentration of sodium ions significantly?

(d) What diameter axon is needed in order for the intracellular sodium ion concentration to change by 10% during one action potential?

**Problem 50** A stimulating current of  $1$  A  $m^{-2}$  is applied for  $100$   $\mu$ s. How much does it change the potential across the membrane?

**Problem 51** Using the resting value of  $j_K$  from Fig. 6.39, calculate how long it would take for the concentration of potassium inside an axon of radius  $100$   $\mu$ m to decrease by 1%.

**Problem 52** Modify the program in Fig. 6.38 to produce the values of  $m$ ,  $h$ , and  $n$  as functions of time during an action potential. Plot  $m(t)$ ,  $h(t)$ ,  $n(t)$ , and  $v(t)$ .

**Problem 53** Modify the program in Fig. 6.38 so it uses different stimulus strengths other than  $j_{stim} = 1$  A  $m^{-2}$ . Find the minimum value of  $j_{stim}$  that results in an action potential. This value is known as the “threshold stimulus strength.”

**Problem 54** Modify the program in Fig. 6.38 so it applies two stimulus pulses. The first is of strength  $j_1 = 1$  A  $m^{-2}$ , duration  $0.5$  ms, and starts at  $t_1 = 0$ . The second is of strength  $j_2$ , duration  $0.5$  ms, and starts at time

$t_2$ . For a given  $t_2$  value, determine the threshold stimulus strength  $j_2$ . Plot the threshold  $j_2$  as a function of the interval  $t_2 - t_1$ , for  $1$  ms  $< t_2 - t_1 < 10$  ms. This plot is called a “strength-interval curve.” The increase of threshold  $j_2$  for small intervals reflects the refractoriness of the membrane.

**Problem 55** When a squid nerve axon is “hyperpolarized” by a stimulus (the transmembrane potential is more negative than resting potential) for a long time and then released, the transmembrane potential drifts back toward resting potential, overshoots  $v_r$  and becomes more positive than  $v_r$ , and eventually reaches threshold and fires an action potential. This process is called “anode break” excitation: anode because the membrane is hyperpolarized, and break because the excitation doesn’t occur until after the stimulus ends. Modify the program in Figure 6.38, so that the stimulus lasts 3 ms, and the stimulus strength is  $-0.15$  A  $m^{-2}$ . Show that the program predicts anode break stimulation. Determine the mechanism responsible for anode break stimulation. Hint: Pay particular attention of the sodium inactivation gate (the  $h$  gate). You may want to plot  $h$  versus time to see how it behaves.

**Problem 56** Consider a space-clamped axon for which the resting potential is  $v_r$ . Assume that the membrane current density follows a very strange behavior:

$$j_m = \begin{cases} B(v - v_r)^2, & v > v_r \\ 0, & v < v_r. \end{cases}$$

(a) Write a differential equation for  $v(t)$ .

(b) What are the units of  $B$ ?

(c) What sign would  $B$  have for depolarization to take place after a small positive change of  $v$ ?

(d) Integrate the equation obtained in (a).

**Problem 57** A comment was made in the text that the potassium current is not required to generate an action potential. Modify the program of Fig. 6.38 to eliminate the potassium current. (First make sure that you have an unmodified program that reproduces Fig. 6.39 correctly.) Comment on the shape of the resulting pulse. After the pulse there is a new value of the resting potential. Why? Is it significant?

## Section 6.15

**Problem 58** A pulse that propagates along the axon with speed  $u$  is of the form  $v(x, t) = f(x - ut)$ .

(a) Use the chain rule to show that this means

$$\frac{\partial v}{\partial t} = -u \frac{\partial v}{\partial x}, \quad \frac{\partial^2 v}{\partial t^2} = u^2 \frac{\partial^2 v}{\partial x^2}.$$

(b) Find an expression for the membrane current per unit area in terms of  $c_m$ ,  $\rho_i$ ,  $\rho_m$ ,  $a$ , and the various partial derivatives of  $f$  with respect to  $x$ .

**Problem 59** Consider an action potential propagating along an axon. The “foot” of the action potential is that part of the initial rise of the transmembrane potential that occurs before the sodium channels open. Starting from Eq. 6.73, set the  $j_m$  equal to zero and assume that the action potential propagates with a uniform speed  $u$ . As in Problem 58, replace the spatial derivatives with temporal derivative and show that the transmembrane potential during the foot of the action potential rises exponentially. Find an expression for the time constant of this exponential rise in terms of  $r_i$ ,  $c_m$ ,  $a$ , and  $u$ .

**Problem 60** An unmyelinated axon has the following properties: radius of 0.25 mm, membrane capacitance of  $0.01 \text{ F m}^{-2}$ , resistance per unit length along the axon of  $2 \times 10^6 \text{ } \Omega \text{ m}^{-1}$ , and propagation velocity of  $20 \text{ m s}^{-1}$ . The propagating pulse passes an observer at  $x = 0$ . The peak of the pulse can be approximated by a parabola,  $v(t) = 20(1 - 10t^2)$ , where  $v$  is in millivolts and  $t$  is in milliseconds.

- (a) Find the current along the axon at  $x = 0$ ,  $t = 0$ .
- (b) Find the membrane current per unit area  $j_m$  at  $x = 0$ ,  $t = 0$ .

**Problem 61** A space-clamped axon ( $v$  independent of distance along axon) has a pulse of the form

$$v(t) - v_r = \begin{cases} 0, & t < -t_1 \\ v_0 [1 - (t/t_1)^2], & -t_1 < t < t_1 \\ 0, & t > t_1, \end{cases}$$

as shown in Problem 60. The axon has radius  $a$ , length  $L$ , resistivity  $\rho_i$ , and membrane capacitance  $c_m$  per unit area.

- (a) What is the total change in charge on the membrane from  $t = -t_1$  to  $t = 0$ ?
- (b) What is the total change in charge on the membrane from  $t = -t_1$  to  $t = +t_1$ ?
- (c) What is  $j_m(t)$ ?
- (d) If  $j_m$  is given by  $g_m(v - v_r)$ , what is  $g_m(t)$ ? Comment on its behavior.

**Problem 62** Modify the program in Fig. 6.38 to include  $x$ -dependence as outlined in the text. Reproduce Fig. 6.42 and determine the propagation speed. Use  $r_i = 19.89 \times 10^5 \text{ } \Omega \text{ m}^{-1}$  and  $a = 0.238 \text{ mm}$ .

### Section 6.16

**Problem 63** Consider a myelinated fiber in which the nodes of Ranvier are spaced every 2 mm. The resistance of the axoplasm per unit length is  $r_i = 1.4 \times 10^{10} \text{ } \Omega \text{ m}^{-1}$ . The nodal capacitance is about  $1.5 \times 10^{-12} \text{ F}$ .

- (a) If the voltage difference between nodes is 10 mV, what is the current along the axon? Assume that the voltages are not changing with time, so that the membrane charge does not change. Also neglect leakage current through the membrane.

- (b) If the nerve impulse rises from  $-70 \text{ mV}$  to  $+30 \text{ mV}$  in  $0.5 \text{ ms}$ , what is the average current required to charge the nodal capacitance?

**Problem 64** A myelinated cylindrical axon has inner radius  $a$  and outer radius  $b$ . The potential inside is  $v$ . Outside it is 0. The myelin is too thick to be treated as a plane sheet of dielectric. Express all answers in terms of  $a$ ,  $b$ , and  $v$ .

- (a) Give an expression for  $E$  for  $r < a$ .
- (b) Give an expression for  $E$  for  $a < r < b$ .
- (c) Give an expression for  $E$  for  $r > b$ .
- (d) Assuming  $\kappa = 1$ , what is the charge density on the inner surface? The outer surface?

**Problem 65** Develop equations for the resistance and capacitance of a cylindrical membrane whose thickness is appreciable compared to its inner radius. Use Gauss’s law for cylindrical symmetry, to determine the electric field. Consider total charge  $Q$  distributed uniformly over the inner surface of a section of the membrane of length  $D$  and inner radius  $a$ . The membrane has dielectric constant  $\kappa$ .

- (a) Any charge on the outer surface of the membrane has no effect on the calculation of the electric field between  $r = a$  and  $r = a + b$  as long as the charge is distributed uniformly on the outer cylindrical surface at  $r = a + b$ . Show that the electric field within the membrane is  $E = \left(\frac{1}{4\pi\epsilon_0\kappa}\right) 2Q/Dr$ .
- (b) Show that the potential difference is  $v = v(a) - v(a + b) = \frac{Q}{2\pi\epsilon_0\kappa D} \ln(1 + b/a)$ , and that the capacitance is

$$C = \frac{2\pi\kappa\epsilon_0 D}{\ln(1 + b/a)} \quad (\text{cylinder}).$$

- (c) Now place a conducting medium with resistivity  $\rho = 1/\sigma$  in the region of the membrane. Charge will move. It will be necessary to provide a battery to replenish it. Show that the resistance of the membrane segment of length  $D$  is given by  $R = \frac{\rho}{2\pi D} \ln(1 + b/a)$ , so that

$$\rho = \frac{2\pi R D}{\ln(1 + b/a)} \quad (\text{cylinder}).$$

- (d) Show that the resistivity of a plane resistor of cross sectional area  $2\pi a D$  and thickness  $b$  is

$$\rho = \frac{2\pi R D}{b/a} \quad (\text{plane}),$$

and that the capacitance of this plane section of membrane is

$$C = \frac{2\pi\kappa\epsilon_0 D}{b/a} \quad (\text{plane}).$$

- (e) How large is this correction for a myelinated axon in which  $b/a = 0.4$ ?

**Problem 66** Suppose that the outer radius of a myelinated axon,  $a + b$ , is fixed. Determine the value of  $b$  that maximizes the length constant of the axon (Eq. 6.76b). Ignore the Nodes of Ranvier. Your result should be expressed as  $b = \gamma a$ , where  $\gamma$  is a dimensionless constant.

**Problem 67** Use the empirical relationships between axon radius and conduction speed in Table 6.2 to determine the radius and speed at which the speed along a myelinated and unmyelinated fiber is equal. For radii less than this radius, is propagation faster in myelinated or unmyelinated fibers? For speeds greater than this speed, in what type of fibers is propagation fastest?

### Section 6.18

**Problem 68** Modify the computer program of Fig. 6.38 to have a constant value of  $jStim$  and run it.

## References

- Anumonwo, J. B., and J. Jalife (1995). Cellular and sub-cellular mechanisms of pacemaker activity initiation and synchronization in the heart. In D. P. Zipes and J. Jalife, eds. *Cardiac Electrophysiology: From Cell to Bedside*, 2nd. ed. Philadelphia, Saunders.
- Covino, B. G. (1972). Local anesthesia. *N. Engl. J. Med.* **286**: 975–983.
- Davis, Jr., L., and R. Lorente de Nó (1947). Contributions to the mathematical theory of electrotonus. *Stud. Rockefeller Inst. Med. Res.* **131**(Part 1): 442–496.
- Dennis, S. S., J. W. Clark, C. R. Murphy, and W. R. Giles (1994). A mathematical model of a rabbit sinoatrial node cell. *Am. J. Physiol.* **266**: C832–852.
- DiFrancesco, D., M. Mangoni, and G. Maccafferri (1995). The pacemaker current in cardiac cells. In D. P. Zipes and J. Jalife, eds. *Cardiac Electrophysiology: From Cell to Bedside*, 2nd ed. Philadelphia, Saunders.
- Geddes, L. A. (2000). Historical Perspectives 3: Recording of Action Potentials. In J. D. Bronzino, ed. *The Biomedical Engineering Handbook*, 2nd. ed., Vol. I. Boca Raton, FL, CRC Press, pp. HP3-1–HP3-11.
- Guyton, A. C. and J. E. Hall (2000). *Textbook of Medical Physiology*, 10th ed. Philadelphia, Saunders.
- Halliday, D., R. Resnick, and K. S. Krane (1992). *Physics*, 4th ed., extended version. New York, Wiley.
- Hille, B. (2001). *Ion Channels of Excitable Membranes*, 3rd. ed. Sunderland, MA, Sinauer Associates.
- Hodgkin, A. L. (1964). *The Conduction of the Nervous Impulse*. Springfield, IL, Thomas.
- Hodgkin, A. L. and P. Horowitz (1959). The influence of potassium and chloride ions on the membrane potential of single muscle fibers. *J. Physiol.* **148**: 127–160.
- Hodgkin, A. L., and A. F. Huxley (1939). Action potentials recorded from inside a nerve fiber. *Nature* **144**: 710.
- Hodgkin, A. L., and A. F. Huxley (1952). A quantitative description of membrane current and its application to conduction and excitation in nerve. *J. Physiol.* **117**: 500–544.
- Hodgkin, A. L., and W. A. Rushton (1946). The electrical constants of a crustacean nerve fiber. *Proc. R. Soc. B* **133**: 444–479.
- Jeffreys, H., and B. S. Jeffreys (1956). *Methods of Mathematical Physics*. London, Cambridge University Press, p. 602.
- Kane, B. J., C. W. Storment, S. W. Crowder, D. L. Tanelian, and G. T. A. Kovacs (1995). Force-sensing microprobe for precise stimulation of mechanoreceptive tissues. *IEEE Trans. Biomed. Eng.* **42**(8): 745–750.
- Katz, B. (1966). *Nerve, Muscle and Synapse*. New York, McGraw-Hill.
- Läuger, P. (1991). *Electrogenic Ion Pumps*. Sunderland, MA, Sinauer Associates.
- Luo, C. H., and Y. Rudy (1994). A dynamic model of the cardiac ventricular action potential. I. Simulations of ionic currents and concentration changes. *Circ. Res.* **74**(6): 1071–1096.
- Martin, A. R. (1966). Quantal nature of synaptic transmission. *Physiol. Rev.* **46**: 51–66.
- Noble, D., D. DiFrancesco, and J. C. Denyer (1989). Ionic mechanisms in normal and abnormal cardiac pacemaker activity. In Jacklet, J. W., ed. *Cellular and Neuronal Oscillators*. New York, Dekker, pp. 59–85.
- Noble, D. (1995). Ionic mechanisms in cardiac electrical activity. In D. P. Zipes and J. Jalife, eds. *Cardiac Electrophysiology: From Cell to Bedside*, 2nd ed. Philadelphia, Saunders.
- Nolte, J. (2002). *The Human Brain: An Introduction to Its Functional Anatomy*. 5th. ed. St. Louis, Mosby.
- Patton, H. D., A. F. Fuchs, B. Hille, A. M. Scher, and R. F. Steiner (1989). *Textbook of Physiology*. Philadelphia, Saunders.
- Plonsey, R. (1969). *Bioelectric Phenomena*. New York, McGraw-Hill.
- Plonsey, R. and R. C. Barr (1988). *Bioelectricity: A Quantitative Approach*. New York, Plenum.
- Rushton, W. A. H. (1951). A theory of the effects of fibre size in medullated nerve. *J. Physiol.*, **115**: 101–122.
- Schey, H. M. (1997). *Div, Grad, Curl and All That: An Informal Text on Vector Calculus*, 3rd. ed. New York, Norton.
- Scott, A. C. (1975). The electrophysics of a nerve fiber. *Rev. Mod. Phys.* **47**: 487–533.
- Smythe, W. R., S. Silver, J. R. Whinnery, and J. D. Angelakos (1957). Formulas. In D. E. Gray, ed. *American Institute of Physics Handbook*, New York, McGraw-Hill, Chapter 5b.
- Wilders, R., H. J. Jongasma, and A. C. G. van Ginnekin (1991). Pacemaker activity of the rabbit sinoatrial node: A comparison of models. *Biophys. J.* **60**: 1202–1216.

Wiley, J. D., and J. G. Webster (1982). Analysis and control of the current distribution under circular dispersive electrodes. *IEEE Trans. Biomed. Eng.* **29**: 381–385.

Worthington, C. R. (1971). X-ray analysis of nerve myelin, in J. W. Adelman, Jr., ed., *Biophysics and Physiology of Excitable Membranes*, New York, Van Nostrand Reinhold, pp. 1–46.

## The Exterior Potential and the Electrocardiogram

In Chapter 6 we assumed that the potential outside a nerve cell is zero. This is only approximately true. There is a small potential that can be measured and has clinical relevance. Before a muscle cell contracts, a wave of depolarization sweeps along the cell. This wave is quite similar to the wave along the axon. Measurement of these exterior signals gives us the electrocardiogram, the electromyogram, and the electroencephalogram.

In Sec. 7.1 we calculate the potential outside a long cylindrical axon bathed in a uniform conducting medium. Section 7.2 shows that the exterior potential is small compared to the potential inside the cell if there is enough extracellular fluid so that the outside resistance is low. Section 7.3 uses a model in which the action potential is approximated by a triangular pulse to calculate the potential far from the cell. Section 7.4 generalizes this calculation to the case of a pulse of arbitrary shape.

An unusual feature of heart muscle is that the myocardial cells remain depolarized for 100 ms or so, as described in Secs. 7.5 and 7.6. This means that the potential difference outside the cell is much larger than for other cells, giving rise to the electrocardiogram described in Sec. 7.7.

The next two sections discuss electrocardiography and some factors that contribute to the signal. They make no attempt to consider advanced techniques such as orthogonal leads that are used to reconstruct the electrical activity of the heart from potential difference measurements on the surface of the body. Rather, they are much closer to the way clinicians think about the electrocardiogram, and they can provide a basis from which to learn more complicated techniques.

Section 7.9 talks about improved models that take into account the interaction between the inside and outside of cells and the anisotropies that exist in tissue resistance. Section 7.10 discusses the problem of stimulation:

for measurement of evoked responses, for pacing, and for defibrillation.

Section 7.11 discusses the electroencephalogram.

### 7.1 The Potential Outside a Long Cylindrical Axon

When studying the action potential in Chapter 6 we assumed that the potential outside the axon is zero. Now we calculate the exterior potential distribution if the axon is in an infinite uniform conducting medium.<sup>1</sup> We will discover that for the case studied here the exterior potential changes are less than 0.1% of those inside. If the exterior medium is not infinite, the exterior potential changes are larger, as is discussed in Sec. 7.9. This model also applies to a muscle cell that is depolarizing before contraction. We will adapt these results to a group of heart (myocardial) cells that depolarize together, leading to a wave of depolarization propagating through the tissue.

Consider a single axon stretched along the  $x$  axis. Divide space into three regions as shown on the left in Fig. 7.1: the interior of the axon (the axoplasm), the axon membrane, and the surrounding medium. Imagine that the current inside the axon is constant to the left of a certain point and zero to the right of that point, as shown on the right in Fig. 7.1(b). Since the material inside the axon obeys Ohm's law, the interior potential decreases linearly with  $x$  as shown in Fig. 7.1(a). Where the current is zero, the interior potential does not change. At the point where the interior current falls to zero, conservation of charge requires that the current pass through the membrane and flow in the exterior conducting medium,

<sup>1</sup>Other textbooks examine this problem in greater detail [Gulrajani (1998), Malmivuo and Plonsey (1995)].

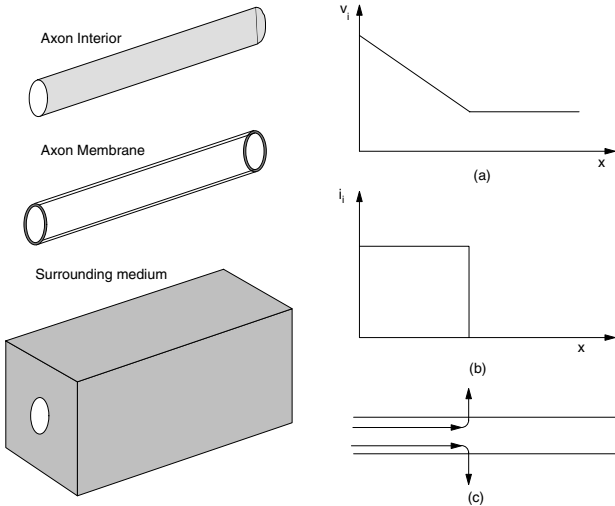


FIGURE 7.1. An axon is stretched along the  $x$  axis. (a) A plot of a portion of the interior action potential at one instant of time. (b) A plot of the interior current, proportional to the slope of the interior potential because of Ohm’s law. (c) Schematic representation of the axon, showing current flowing along the axon and into the exterior conducting medium at the point where the interior current falls to zero.

as stated in Eq. 6.47b. Figure 7.1(c) shows the axon with current flowing in the left part of the axon and then flowing into the surrounding medium.

Now consider how the current flows in the surrounding three-dimensional medium. Suppose that the surrounding or “outside” medium is infinite, homogeneous and isotropic and has conductivity  $\sigma_o$ . Suppose also that the axon stretched along the  $x$  axis is very thin and does not appreciably change the homogeneous and isotropic nature of the extracellular medium, except very close to the  $x$  axis. If a current  $i_o$  enters the surrounding medium at the origin, the current density  $\mathbf{j}$  is directed radially outward and has spherical symmetry. The current density at distance  $r$  has magnitude  $j = i_o/4\pi r^2$ . The magnitude of the electric field is  $E = j/\sigma_o = i_o/4\pi\sigma_o r^2$ . This has the same form as the electric field from a point charge, for which the electric field is  $E = q/4\pi\epsilon_0 r^2$ . We speak of  $i_o$  as a *point current source*.

We can use the expression for the electric field to calculate the exterior potential. The point current source is shown as the dot in the center of the sphere in Fig. 7.2. To calculate the potential difference between points  $A$  and  $B$ , it is easiest to integrate Eq. 6.16 along a path from  $A$  to  $B'$  parallel to the direction of  $\mathbf{E}$ , and then along  $B'B$  where the displacement is always perpendicular to  $\mathbf{E}$ . The potential change along  $B'B$  is zero. Therefore

$$v(B) - v(A) = - \int_{r_A}^{r_B} E_r dr = - \int_{r_A}^{r_B} \frac{i_o}{4\pi\sigma_o r^2} dr = \frac{i_o}{4\pi\sigma_o} \left( \frac{1}{r_B} - \frac{1}{r_A} \right).$$

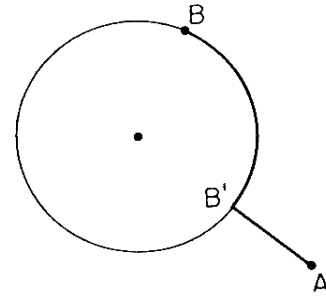


FIGURE 7.2. A point current source is at the center of a sphere. The path of integration to calculate the potential difference between points  $A$  and  $B$  goes first from  $A$  to  $B'$  and then from  $B'$  to  $B$ .

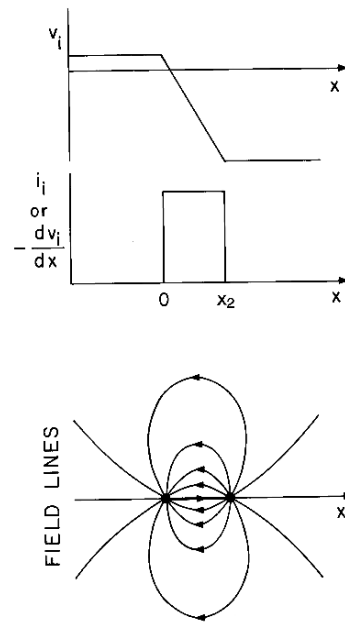


FIGURE 7.3. The potential of Fig. 7.1 is extended to the left in a region of constant (depolarized) potential. The interior current is plotted below the potential. The electric field or current-density lines are plotted at the bottom. The current to the right on the axis is current within the axon; the other lines represent current in the exterior conducting medium.

Only a difference of potential between two points has meaning. However, it is customary to define the potential to be 0 at  $r_A = \infty$  and speak of the potential as a function of position. Then the potential at distance  $r$  from a point current source  $i_o$  is

$$v(r) = \frac{i_o}{4\pi\sigma_o r}. \tag{7.1}$$

The analogous expression for the potential due to a point charge  $q$  is  $v(r) = q/4\pi\epsilon_0 r$ .

We do not yet have a useful model, because the potential cannot rise forever as we go along the axon to the left. Let us assume that the potential levels off at some point on the left, as shown in Fig. 7.3. (This will turn



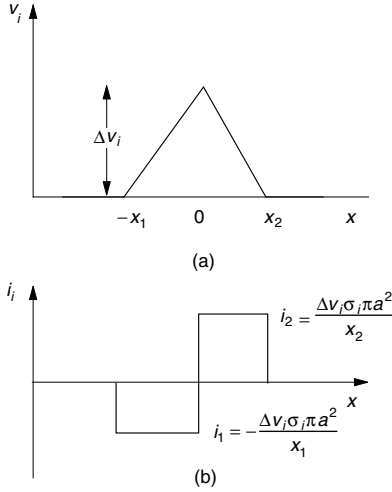


FIGURE 7.4. The action potential is approximated by a triangular wave form. In this piecewise-linear approximation the depolarization and repolarization are both linear. (a) The interior potential. (b) The interior current.

out to be a very good model for the electrocardiogram, because the repolarization of myocardial cells does not take place for about 100 ms, so the cells are completely depolarized before repolarization begins.) Define the location of the origin so that the depolarization takes place between  $x = 0$  and  $x = x_2$ . The potential change is shown at the top, and the current along the inside of the axon in the middle. The current exists only where there is a voltage gradient between  $x = 0$  and  $x = x_2$ . Its magnitude is  $i_i = \Delta v_i / R = \Delta v_i \sigma_i \pi a^2 / x_2$ . This current flows out into the surrounding medium at  $x = x_2$  and back into the axon at  $x = 0$ . Such a combination of source and sink of equal magnitude is called a *current dipole*. (A pair of equal and opposite electric charges is called an electric dipole.) The lowest part of the figure shows lines of  $\mathbf{j}$  or  $\mathbf{E}$ . The current is to the right inside the axon (along the axis) and returns outside the axon. The potential at any exterior point is due to two terms: one from the source  $i_i$  at  $x = x_2$  and the other from the sink  $-i_i$  at  $x = 0$ . If  $r_2$  is the distance from the observation point to  $x_2$  and  $r_0$  is the distance to the origin, then

$$v = \frac{\Delta v_i \sigma_i \pi a^2}{4\pi \sigma_o x_2} \left( \frac{1}{r_2} - \frac{1}{r_0} \right) = \frac{\Delta v_i \sigma_i a^2}{4\sigma_o x_2} \left( \frac{1}{r_2} - \frac{1}{r_0} \right). \quad (7.2)$$

To estimate the potential from a nerve impulse, we can approximate the action potential by a triangular potential as shown in Fig. 7.4(a). The potential is zero far to the left. It rises by an amount  $\Delta v_i$  between  $x = -x_1$  and  $x = 0$ . It falls linearly to zero at  $x = x_2$ . The current is plotted in Fig. 7.4(b). In the region just to the left of the origin it is

$$i_1 = -\frac{\Delta v_i \sigma_i \pi a^2}{x_1}. \quad (7.3a)$$

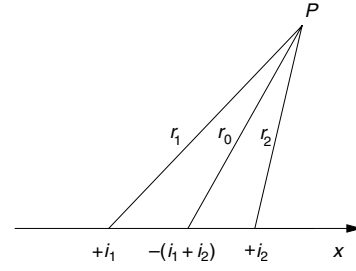


FIGURE 7.5. The axon of Fig. 7.4 is stretched along the  $x$  axis. There are current sources at  $x = -x_1$  and  $x = x_2$ , and a current sink at the origin. The distances from each source or sink to the observation point are shown.

(It is negative because it flows to the left.) To the right of the origin it is

$$i_2 = \frac{\Delta v_i \sigma_i \pi a^2}{x_2}. \quad (7.3b)$$

Figure 7.5 shows the surrounding medium. There is a source of current  $i_1$  at  $x = -x_1$ , a source  $i_2$  at  $x = x_2$ , and a sink  $-(i_1 + i_2)$  at the origin. The potential at observation point  $P$  is calculated by repeated application of Eq. 7.1:

$$v = \frac{1}{4\pi \sigma_o} \left( \frac{i_1}{r_1} - \frac{i_1 + i_2}{r_0} + \frac{i_2}{r_2} \right). \quad (7.3c)$$

Equations 7.3a–7.3c can be combined to give

$$v = \frac{\Delta v_i \sigma_i a^2}{4\sigma_o} \left( \frac{1/x_1}{r_1} - \frac{1/x_1 + 1/x_2}{r_0} + \frac{1/x_2}{r_2} \right). \quad (7.4)$$

Equations 7.3 and 7.4 are valid at any distance from the axon, as long as we can make the piecewise approximation of the action potential shown in Fig. 7.4.

## 7.2 The Exterior Potential is Small

Let us use Eq. 7.2 for the rising edge of the action potential to estimate the potential outside the axon when it is in an infinite conducting medium. We evaluate Eq. 7.2 close to the surface of the axon where the potential will be largest, say at  $x = 0$ . In that case  $r_2$  is approximately  $x_2$ . However,  $r_0$  is not zero. It can never become smaller than  $r_0 = a$ , the radius of the axon. (The potential would diverge if the model were extended to  $r = 0$ .) We will use an approximate value,  $r_0 = a$ , and call the height of the action potential  $\Delta v_i$ . Then

$$v(0) = \frac{\Delta v_i \sigma_i a^2}{4\sigma_o x_2} \left( \frac{1}{x_2} - \frac{1}{a} \right). \quad (7.5)$$

Since  $1/x_2 \ll 1/a$ , this becomes

$$v(0) \approx -\frac{\Delta v_i \sigma_i a}{4\sigma_o x_2}. \quad (7.6)$$

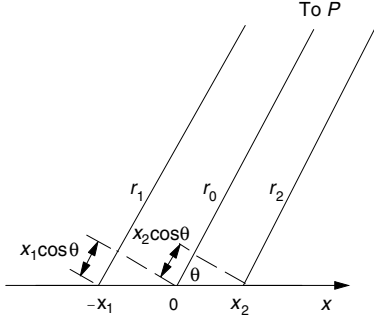


FIGURE 7.6. The observation point  $P$  is far away compared to distances  $x_1$  or  $x_2$ . The lines to  $P$  are nearly parallel.

Close to  $x = x_2$  the potential is

$$v(x_2) = \frac{\Delta v_i \sigma_i a^2}{4\sigma_o x_2} \left( \frac{1}{a} - \frac{1}{x_2} \right) \approx \frac{\Delta v_i \sigma_i a}{4\sigma_o x_2}. \quad (7.7)$$

The potential difference between these two exterior points is

$$\Delta v_o = v(x_2) - v(0) = \frac{\sigma_i a}{\sigma_o 2x_2} \Delta v_i. \quad (7.8)$$

If the conductivities were the same inside and outside, the ratio would be  $\Delta v_o / \Delta v_i = a / 2x_2$ .

The ratio of exterior to interior potential change is proportional to the ratio of the axon radius to the distance along the axon over which the potential changes. From Fig. 6.42 we see that the rising part of the squid action potential has a length  $x_2 \approx 1$  cm. If  $a = 0.5$  mm (a quite large axon), then the ratio is  $1/40$ . For a smaller axon, the ratio is even less.

The same result can be obtained by another argument. The resistance between two points is the ratio of the potential difference between the points to the current flowing between them. Inside the axon  $\mathbf{j}$  and  $\mathbf{E}$  are large because the current is confined to a small region of area  $\pi a^2$ . The resistance inside is  $R_i = x_2 / \pi a^2 \sigma_i$ . The same current flows outside, but it is spread out so that  $\mathbf{j}$  and  $\mathbf{E}$  are much less. The resistance between two electrodes in a conducting medium is related to their capacitance (Sec. 6.19). Equations 6.87 and 6.100 can be used to show that two spherical electrodes of radius  $a$  spaced distance  $x_2$  apart ( $x_2 \gg a$ ) have a resistance  $R_o = 1/2\pi\sigma_o a$ . The voltage ratio is

$$\frac{\Delta v_o}{\Delta v_i} = \frac{R_o}{R_i} = \frac{1}{2\pi\sigma_o a} \frac{\pi a^2 \sigma_i}{x_2} = \frac{\sigma_i a}{\sigma_o 2x_2},$$

the same result as Eq. 7.8.

### 7.3 The Potential Far From the Axon

In most cases measurements of the potential are made far from the axon—far compared to the distance the action potential spreads out along the axon. If point  $P$  is moved far away, Fig. 7.5 looks like Fig. 7.6. The lines  $r_1$ ,  $r_0$ , and

$r_2$  are nearly parallel. If point  $P$  is located a distance  $r_0$  from the origin at angle  $\theta$  with the  $x$  axis, then

$$r_2 \approx r_0 - x_2 \cos \theta, \quad r_1 \approx r_0 + x_1 \cos \theta. \quad (7.9)$$

Consider the potential in Eq. 7.2 due to the leading edge of the action potential. (We will argue later that this is a useful model for the electrocardiogram.) Substituting Eqs. 7.9 in Eq. 7.2 gives

$$v = \frac{\Delta v_i \sigma_i a^2}{4\sigma_o x_2} \left( \frac{1}{r_0 [1 - (x_2/r_0) \cos \theta]} - \frac{1}{r_0} \right).$$

You can verify by a Taylor's-series expansion or long division that

$$\frac{1}{1-x} = 1 + x + \dots, \quad (7.10)$$

so that

$$v = \frac{\Delta v_i \sigma_i a^2}{4\sigma_o r_0^2} \cos \theta. \quad (7.11)$$

This is a very important result that will form the basis for our model of the electrocardiogram:

1. The exterior potential  $v$  depends on  $\Delta v_i$  but not on  $x_2$ , the length of the depolarization region. This is because increasing  $x_2$  decreases the strength of the current at the same time that it increases  $v$  because the source and sink are further apart.
2. The potential falls off as  $1/r^2$  instead of  $1/r$  as it would from a point source.
3. The potential varies with angle, being positive to the right of the transition region and negative to the left.

It is convenient to define a vector  $\mathbf{p}$  that points along the axon in the direction of the advancing depolarization wave front (the region along the axon where the potential rises). It is called the *activity vector* or *current-dipole moment* for reasons discussed shortly. Its magnitude is

$$p = \pi a^2 \sigma_i \Delta v_i. \quad (7.12)$$

The exterior potential is then (dropping the subscript on  $\mathbf{r}$ )

$$v = \frac{\mathbf{p} \cdot \mathbf{r}}{4\pi\sigma_o r^3}. \quad (7.13)$$

Vector  $\mathbf{p}$  has units of A m. Its magnitude (apart from the conductivity) is the product of the cross-sectional area of the axon and the difference in potential along the axon between the resting and completely depolarized regions. It is called the current-dipole moment because it is the product of the current and the separation of the source and sink. (The electric-dipole moment is the product of the magnitude of the charges and their separation, with units C m.)

Equation 7.11 can also be written in the form

$$v(r) = \frac{\pi a^2 \cos \theta}{r^2} \frac{1}{4\pi} \frac{\sigma_i}{\sigma_o} \Delta v_i. \quad (7.14)$$

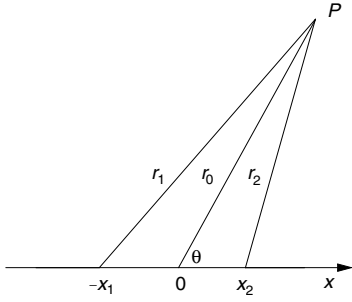


FIGURE 7.7. When the observation point is not so far away, or when a complete nerve impulse is being considered, the law of cosines must be used to relate  $r_1$  and  $r_2$  to  $r_0$ .

The quantity  $\pi a^2 \cos \theta / r^2$  is  $\Delta \Omega$ , the solid angle<sup>2</sup> subtended at the observation point by a cross section of the axon where the potential changes. The quantity  $4\pi$  is the maximum possible solid angle. In terms of the solid angle

$$v = \frac{\Delta \Omega}{4\pi} \frac{\sigma_i}{\sigma_o} \Delta v_i. \quad (7.15)$$

Now consider an entire pulse, one where the potential rises and then returns to the resting value. If the approximation of Eq. 7.10 is applied to Eq. 7.4, the result vanishes. It is necessary to make a more accurate approximation, one that takes into account the fact that the vectors  $\mathbf{r}_1$ ,  $\mathbf{r}_0$ , and  $\mathbf{r}_2$  are not exactly parallel. Figure 7.7 shows the geometry. We use the law of cosines to write [remember that  $\cos(\pi - \theta) = -\cos \theta$ ]

$$r_1 = r_0 \left[ 1 + (2x_1/r_0) \cos \theta + x_1^2/r_0^2 \right]^{1/2},$$

$$r_2 = r_0 \left[ 1 - (2x_2/r_0) \cos \theta + x_2^2/r_0^2 \right]^{1/2}.$$

When these are inserted in Eq. 7.4 and a Taylor's-series expansion is done to second order in both  $x_1/r_0$  and  $x_2/r_0$ , the result is

$$v = \frac{2\pi a^2}{4\pi r^3} \frac{\sigma_i}{\sigma_o} \frac{\Delta v_i (x_1 + x_2)}{2} \frac{3 \cos^2 \theta - 1}{2}. \quad (7.16)$$

The constants have been arranged to show that the term  $\Delta v_i (x_1 + x_2) / 2$  is the area under the impulse when  $v$  is plotted as a function of  $x$ . The angular factor as written with its factor of 2 in the denominator is tabulated in many places as the "Legendre polynomial  $P_2(\cos \theta)$ ".<sup>3</sup> The exterior potential now falls off more rapidly with distance, as  $1/r^3$ . The angular dependence, shown in Fig. 7.8, is symmetric about  $\pi/2$ . This shows the angular dependence as one moves around the impulse at a constant distance from it.

This is a very different situation and a very different curve from the potential measured at a fixed point outside the axon as an impulse travels past. In the latter

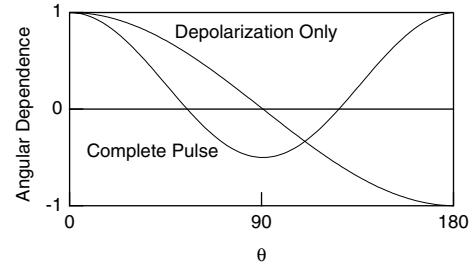


FIGURE 7.8. Plot of the angular dependence of the potential from the entire impulse, Eq. 7.16.

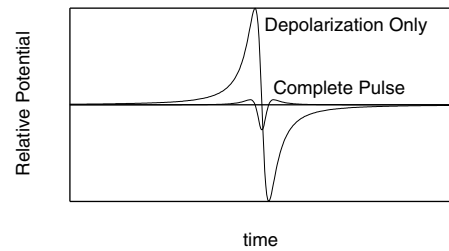


FIGURE 7.9. The potential far from the axon as a function of time as an impulse travels from left to right along the axis. The potential from the complete pulse has been multiplied by a factor of 10 in order to show it.

case  $r$  as well as  $\theta$  is changing. This behavior is discussed in Problems 8 and 9. The results are shown in Fig. 7.9. The potential from the depolarization is biphasic; that from the complete pulse is triphasic, being positive, then negative, then positive again.

For a single axon in an ionic solution the exterior conductivity is usually higher than in the axon, so  $\sigma_i/\sigma_o = 0.2$ . The conductivity of tissue is considerably less than the conductivity of an ionic solution, and the ratio becomes greater than one. For the electrocardiogram it will be more appropriate to use  $\sigma_o = 0.33 \text{ S m}^{-1}$  (muscle) or  $0.08 \text{ S m}^{-1}$  (lung), in which case  $\sigma_i/\sigma_o$  is 6 or 25. We will use an approximate value of 10.

## 7.4 The Exterior Potential for an Arbitrary Pulse

We have derived the results of the previous sections for an action potential that varies linearly during depolarization and repolarization, a piecewise-linear approximation. In general the action potential does not have sharp changes in slope. We will now consider the general case and find that the results are very similar. For depolarization alone, we will again have a potential depending on the dipole moment. For a complete pulse the potential will depend on the area under the pulse curve.

Again, the axon is stretched along the  $x$  axis in an infinite, homogeneous conducting medium. Consider a small

<sup>2</sup>The solid angle is defined in Appendix A.

<sup>3</sup>You can learn more about Legendre polynomials in texts on differential equations or, for example, in Harris and Stocker (1998).

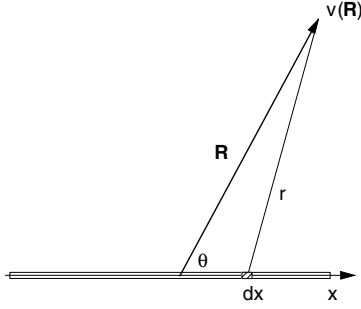


FIGURE 7.10. The potential  $v(\mathbf{R})$  is obtained by integrating the potential due to current  $di_o$  from each element  $dx$  of the cell.

segment of axon between  $x$  and  $x + dx$ . If the current entering this segment at  $x$  is greater than the current leaving at  $x + dx$ , the difference must flow into the exterior medium. From Eq. 6.47b,

$$di_o = -di_i = \frac{\partial i_i(x, t)}{\partial x} dx.$$

We can write Ohm's law for the axoplasm as

$$i_i(x, t) = -\pi a^2 \sigma_i \frac{\partial v_i}{\partial x}. \tag{7.17}$$

The current into the exterior medium from length  $dx$  of the axon is

$$di_o = \pi a^2 \sigma_i \frac{\partial^2 v_i}{\partial x^2} dx. \tag{7.18}$$

It is proportional to the derivative of the current along the axon with respect to  $x$  and therefore to the second derivative of the interior potential with respect to  $x$ . A small current source  $di_o$  generates a potential  $dv$  at some point in the exterior medium given by

$$dv = \frac{di_o}{4\pi\sigma_o r}. \tag{7.19}$$

If the radius of the axon stretched along the  $x$  axis is very small, the axon's influence can be replaced by a current distribution  $di_o(x)$  along the  $x$  axis. The potential at any point  $\mathbf{R}$  is obtained by integrating Eq. 7.19:

$$v(\mathbf{R}) = \int \frac{di_o}{4\pi\sigma_o r}. \tag{7.20}$$

Vector  $\mathbf{R}$  specifies the point at which the potential is measured, and  $r$  is the distance from the measuring point to the point on the  $x$  axis where  $di_o$  is injected, as shown in Fig. 7.10. Combining this with Eq. 7.18 gives

$$v(\mathbf{R}) = \int \frac{\pi a^2 \sigma_i}{4\pi\sigma_o} \frac{\partial^2 v_i}{\partial x^2} \frac{1}{r} dx. \tag{7.21}$$

Although it is difficult to integrate Eq. 7.21 analytically, the integration can be done numerically. Figure 7.11 shows a computer program to carry out this integration for a crayfish lateral giant axon immersed in sea

```
//program ClarkAndPlonsey;
/*This program integrates our approximate
equation for the extracellular potential.
Original calc. by J. Clark and R. Plonsey,
The extracellular potential field of the
single active nerve fiber in a volume
conductor. Biophys. J. 8:942-964 (1968)
The nerve pulse is a series of Gaussians
used by Clark and Plonsey to fit data of
Watanabe and Grundfest, J. Gen. Physiol.
45:267 (1961)
This program uses Romberg integration
function qromb, from Numerical Recipes
in C, 2nd ed.*/

#include<stdio.h>
#include<stdlib.h>
#include<math.h>
#include "nr.h" //N.R. in C header file

/*Global Variables*/
double x0,y0; //coordinates of obs point
float I;(float x)
{
/*Calculates integrand d2v/dx2 div by r
Uses common variables x0 , y0--
Observation point in meter*/
double xx, r, d2v, temp;
d2v = 0;
xx = (x-0.0054)/1.25e-3;
temp = (2*51/(1.25e-3*1.25e-3))
*exp(-xx*xx);
d2v = d2v+temp*(2*xx*xx-1);
xx = (x-0.0066)/1.876e-3;
temp = (2*72/(1.876e-3*1.876e-3))
*exp(-xx*xx);
d2v = d2v+temp*(2*xx*xx-1);
xx = (x-0.0085)/3.003e-3;
temp = (2*18/(3.003e-3*3.003e-3))
*exp(-xx*xx);
d2v = d2v+temp*(2*xx*xx-1);
r = sqrt((x0-x)*(x0-x)+y0*y0);
return d2v/r;
}

void main()
{
const
double SigRatio = 0.2, //interior/exterior
// conductivity ratio
a = 5.0e-5; //axon radius in m
float
xstart, xfinish, //limits of int.;
double
y[4], //Calculate at four distances
potential, xx //Exterior potential
Transmemb; //Transmembrane potential
int i;
FILE *oip; //Output file Pointer
if (!oip = fopen("Flonsey.out", "w"))
//Open output file
{
printf("cannot open output file\n");
exit(1);
}
xsuactl = 0.0;
xfinish = 0.02;
fprintf(oip, " x \t v ");
printf(" x v ");
for (i=0; i<4; i++)
{
y[i] = pow(2,i)*a;
fprintf(oip, "%9.3e", y[i]);
printf(" %9.3e ", y[i]);
}
fprintf(oip, "\n\n");
printf("\n\n");
for(x0 = 0.001; x0 < 0.012; x0 += 0.00025)
{
xx = (x0-0.0054)/1.25e-3;
Transmemb = 51*exp(-xx*xx);
xx = (x0-0.0066)/1.876e-3;
Transmemb = Transmemb+72*exp(-xx*xx);
xx = (x0-0.0085)/3.003e-3;
Transmemb = Transmemb+18*exp(-xx*xx);
fprintf(oip, "%9.3e\t%10.3e", x0, Transmemb);
printf("%9.3e %10.3e ", x0, Transmemb);
for (i=0; i<4; i++)
{
y0 = y[i];
Integral = qromb(f, xstart, xfinish);
//N.R. in C fen Call
potential=Integral*a*a*SigRatio/4.0;
fprintf(oip, "\t%10.3e", potential);
printf("%10.3e ", potential);
}
fprintf(oip, "\n");
printf("\n");
}
fclose(oip);
}
```

FIGURE 7.11. The computer program used to calculate the exterior potential by integrating Eq. 7.21 for the problem first solved by Clark and Plonsey (1968). The program uses Romberg integration procedure `qromb` from Press *et al.* (1992).

water. The axon radius is 60  $\mu\text{m}$ . The conductivity ratio is  $\sigma_i/\sigma_o = 0.2$ . The action potential was measured by Watanabe and Grundfest (1961). Clark and Plonsey (1968) showed that it could be well represented by a sum of three Gaussians, with  $v_i = 0$  taken to be the resting value. Since only  $\partial^2 v_i/\partial x^2$  enters into Eq. 7.21, the reference level does not matter. The representation (with  $v$  in mV and  $x$  in mm) is

$$v_i(x) = 51e^{-[(x-5.4)/1.25]^2} + 72e^{-[(x-6.6)/1.876]^2} + 18e^{-[(x-8.6)/3.003]^2}. \tag{7.22}$$

This function corresponds to an impulse traveling to the left. It can be differentiated to obtain an analytic expression for  $\partial^2 v_i/\partial x^2$ . If the potential is being measured at exterior point  $(x_0, y_0)$ , the value of  $r$  which is used in Eq. 7.21 is  $r = [(x - x_0)^2 + y_0^2]^{1/2}$ . The program allows four values of  $y_0$  to be used. The smallest is taken to be  $a$ , the radius of the axon.

The results of calculating the exterior potential at  $y_0 = a$  are shown in Fig. 7.12. The interior potential,

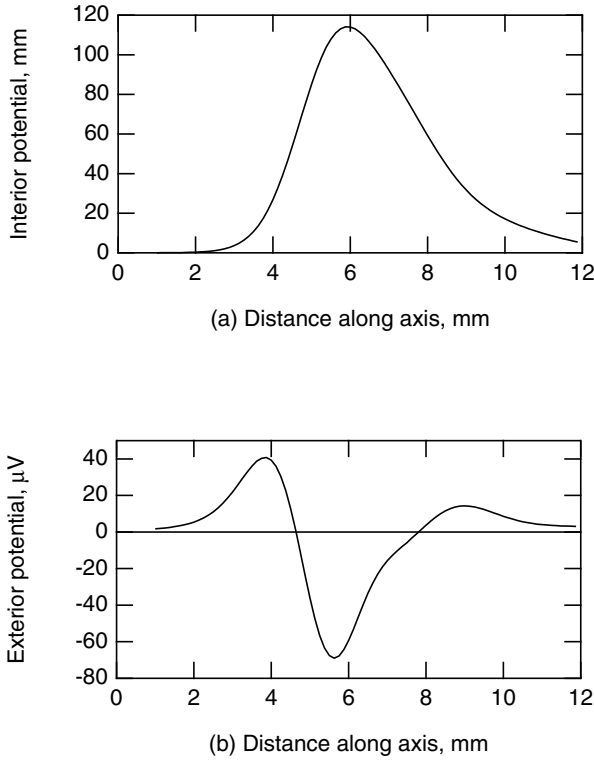


FIGURE 7.12. (a) The transmembrane potential used for the calculation in the program of Fig. 7.11. The impulse is traveling to the left. (b) The exterior potential along the axon calculated by the program for  $y_0 = a$ .

shown in (a), has a peak value of 114 mV. The potential on the surface of the axon (b) ranges from +0.04 to -0.07 mV. In general, the exterior potential is less than 0.1% of the interior potential. (This would be different if the extracellular fluid were not infinite.) The original calculation by Clark and Plonsey used much different mathematical techniques (see Problem 30); however, the results are very similar. The results of their more accurate calculation are plotted in Fig. 7.13.

The approximation that the observer is far from the axon can also be applied to the general case. The physics is exactly the same as in the previous section for the triangular pulse, except that now the pulse has an arbitrary shape so current passes through the membrane at all points along the axon where the second derivative is nonzero. The calculation requires making the same type of approximations in order to evaluate the integral (Eq. 7.21). Referring to Fig. 7.10, we again use the law of cosines to write

$$r(x) = R \left[ 1 - 2(x/R) \cos \theta + x^2/R^2 \right]^{1/2}.$$

We need to use this in Eq. 7.21. As in the previous section, we make a Taylor's-series expansion of  $1/r$ . To second order the result is

$$\frac{1}{r} \approx \frac{1}{R} \left( 1 + \frac{x}{R} \cos \theta + \frac{1}{2} \frac{x^2}{R^2} (3 \cos^2 \theta - 1) \right). \quad (7.23)$$

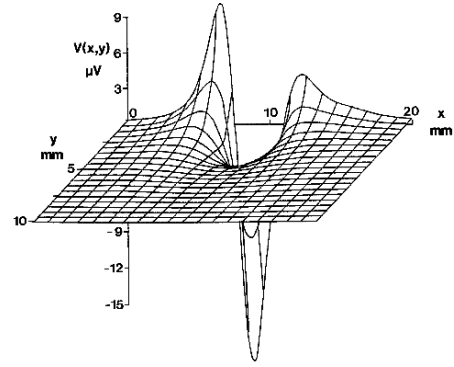


FIGURE 7.13. The exterior potential for the same problem calculated using the more accurate method of Clark and Plonsey (1968). The smallest distance from the axon is  $y = 0.5$  mm.

The expression for  $v(\mathbf{R})$  becomes

$$v(R) = \frac{\pi a^2 \sigma_i}{4\pi \sigma_o} \left[ \frac{1}{R} \int_{x_1}^{x_2} \frac{\partial^2 v_i}{\partial x^2} dx + \frac{\cos \theta}{R^2} \int_{x_1}^{x_2} \frac{\partial^2 v_i}{\partial x^2} x dx + \frac{3 \cos^2 \theta - 1}{2R^3} \int_{x_1}^{x_2} \frac{\partial^2 v_i}{\partial x^2} x^2 dx \right]. \quad (7.24)$$

There are three integrals that we must evaluate. Take limits of integration  $x_1$  and  $x_2$  to be points where  $\partial v_i / \partial x = 0$ . The first integral is  $\partial v_i / \partial x$  and vanishes. The second integral can be integrated by parts. Since  $\partial v_i / \partial x = 0$  at the end points the second integral is  $v_i(x_1) - v_i(x_2)$ . The third integral is integrated by parts twice and is

$$\int_{x_1}^{x_2} \frac{\partial^2 v_i}{\partial x^2} x^2 dx = \left[ x^2 \frac{\partial v_i}{\partial x} \right]_{x_1}^{x_2} - 2 [x v(x)]_{x_1}^{x_2} + 2 \int_{x_1}^{x_2} v_i(x) dx. \quad (7.25)$$

The first term of this vanishes because of the way the end points were chosen.

We now apply these results to Eq. 7.24 in two cases. The first is the case of depolarization only, which is useful in considering the electrocardiogram. Set up the coordinate system so the origin is some place in the impulse where  $\partial v_i / \partial x = 0$ . The total change in  $v_i$  is  $\Delta v_i$ . Then  $x_1 = 0$ ,  $v_i(x_1) = \Delta v_i$ ,  $v_i(x_2) = 0$ . The first nonvanishing term of Eq. 7.24 requires only the second integral:

$$v(\mathbf{R}) = \frac{\pi a^2 \sigma_i \cos \theta}{4\pi \sigma_o R^2} \Delta v_i. \quad (7.26)$$

We obtained this result in a special case as Eq. 7.11.

In the second case we consider the complete pulse, and we take  $x_1$  to the left of the pulse and  $x_2$  to the right. The first integral in Eq. 7.24 still vanishes. Now the second integral also vanishes because  $v_i(x_1) = v_i(x_2) = v_{\text{rest}}$  and  $\Delta v_i = 0$ . It is necessary to use the third integral, Eq. 7.25. The first term in Eq. 7.25 vanishes. The second and third terms must be considered together. Rewrite the potential in terms of departures from the resting potential:

$v_i(x) = v_{\text{rest}} + v_{\text{depol}}(x)$ . The second term in Eq. 7.25 is  $-2v_{\text{rest}}(x_2 - x_1)$ . The third term of Eq. 7.25 is

$$2 \int_{x_1}^{x_2} v_{\text{depol}}(x) dx + 2(x_2 - x_1)v_{\text{rest}}.$$

Adding these gives

$$v(\mathbf{R}) = \frac{2\pi a^2 \sigma_i}{4\pi \sigma_o} \frac{1}{R^3} \frac{3 \cos^2 \theta - 1}{2} \int_{x_1}^{x_2} [v_i(x) - v_{\text{rest}}] dx. \quad (7.27)$$

Again, we saw a special case of this as Eq. 7.16.

Note the progression in these results. When we are looking at one corner of a depolarization pulse, we have a current source or sink, and the potential is proportional to  $1/R$  [Eq. 7.1]. We do not find this situation in physiology, because the potential would have to keep rising forever. When we consider the entire depolarization portion of the wave form, the potential is proportional to  $1/R^2$ , as in Eqs. 7.11 or 7.26. (We will find that this is a good model for the electrocardiogram because the repolarization does not commence until the entire heart is depolarized.<sup>4</sup>) When the entire pulse is considered, the potential is proportional to  $1/R^3$  as in Eqs. 7.16 or 7.27. This is a good model for nerve conduction. The potential is considerably less in this case because of the  $1/R^3$  dependence.

This is an example of a technique called a *multipole expansion*. Generally, defining  $\xi = x/R$ , one can make the expansion

$$\frac{1}{(1 - 2\xi \cos \theta + \xi^2)^{1/2}} = P_0 + \xi P_1 + \xi^2 P_2 + \xi^3 P_3 + \dots, \quad (7.28)$$

where the  $P_n$  are functions of  $\cos \theta$  and are called *Legendre polynomials*.<sup>5</sup> The first few Legendre polynomials are

$$\begin{aligned} P_0 &= 1, \\ P_1 &= \cos \theta, \\ P_2 &= \frac{1}{2}(3 \cos^2 \theta - 1), \\ P_3 &= \frac{1}{2}(5 \cos^3 \theta - 3 \cos \theta). \end{aligned} \quad (7.29)$$

All of these calculations are based on a model in which the current flows parallel to the axis of the axon, passes through the membrane, and then returns in the extracellular conducting medium. This model is called the *line approximation*. It is, of course, impossible for current inside the axon to pass out through the membrane if it always flows parallel to the axis of the axon. It is possible to do an exact calculation in which  $\mathbf{j}$  has a radial component as well as one parallel to the axis of the axon. (See Sec. 7.9 for a description of how this is done.) Trayanova *et al.* (1990) have compared the exact solution with two approximations, one of which is the line approximation.

<sup>4</sup>This is not strictly true. Atrial repolarization begins before the ventricular depolarization is complete.

<sup>5</sup>Legendre polynomials are discussed in many books on differential equations or, for example, in Harris and Stocker (1998).

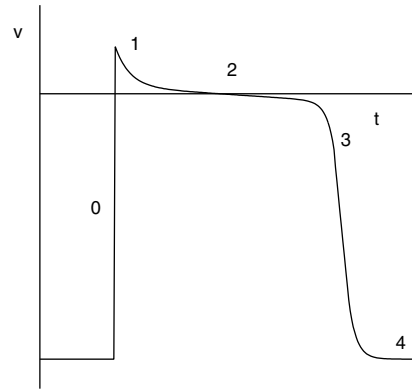


FIGURE 7.14. Depolarization and repolarization of a myocardial cell. The upstroke takes about 1 ms. The depolarization lasts 200–300 ms. The resting potential is about  $-90$  mV.

The line approximation is quite good if the radius of the axon is much smaller than the distance along the axon over which the depolarization takes place.

## 7.5 Electrical Properties of the Heart

There are many similarities between myocardial cells and nerve cells: a membrane separates extracellular and intracellular fluids; the concentrations of the principal ions are about the same; except for a small amount of charge on the membrane, the extracellular and intracellular fluids are electrically neutral; and selective ion channels are responsible for the initiation and propagation of the action potentials. There are also major differences: myocardial cells in mammals are about  $100 \mu\text{m}$  long and  $10 \mu\text{m}$  in diameter. The interiors of neighboring cells are connected through *gap junctions*, so current and ions flow directly from one cell to another [Delmar *et al.* (2004)]. This continuum of cells is called a *syncytium*. There are also important differences in the details of the ion currents. We continue for now to use the simple model of long, one-dimensional cells. Refinements to this model are discussed in Sec. 7.9.

In the resting state, the potential inside an atrial cell is at about  $-70$  mV, while that in a ventricular cell is at about  $-90$  mV. When a cell depolarizes, the action potential lasts for 100–300 ms, depending on the species. A “typical” action potential is shown in Fig. 7.14. There are variations in pulse shape between species and also in different parts of the heart. The initial rapid depolarization in heart muscle cells is caused by an inward sodium current (phase 0 on the curve) and takes about 1 ms. The fall at phase 1 is caused by a transient outward potassium current. This current is small in *endocardium* (near the inside of the heart) but is prominent enough in the *epicardium* (outer layers of the heart) so that there can

be a “spike and dome” shape to the potential [Campbell *et al.* (1995); Antzelevitch *et al.* (1995)]. This is followed by a  $\text{Ca}^{2+}$  influx that maintains the plateau (phase 2) of the action potential. The “slow” potassium channels finally open [Oudit (2004)], and potassium efflux causes repolarization (phase 3). During phase 4 the original ion concentrations are restored.

The heart can beat in isolation. If it is removed from an animal and bathed in nutrient solution, it continues to beat spontaneously. With each beat, a wave of depolarization sweeps over the heart, and it contracts. The wave is initiated by some specialized fibers located in the right atrium called the *sinoatrial node* (SA node). As was mentioned in Sec. 6.18, the SA node does not have the usual sodium channels, and the depolarization is due to calcium. The shape of the SA node potential is much more like Fig. 6.48 than Fig. 7.14. In humans the SA node fires about 60–100 times per minute; this rate is increased by the sympathetic nerves to the heart (which release norepinephrine) and decreased by the parasympathetic nerves (which release acetylcholine). Devices that produce such periodic firing are common in physics and engineering. They are called free-running relaxation oscillators.

Figure 7.15 shows how the depolarization progresses through the heart. Once the SA node has fired, the depolarization sweeps across both atria (a,b). When the atria are completely depolarized (c) there is no depolarization wavefront. The atria are separated from the ventricles by fibrous connective tissue that does not transmit the impulse. The only connection between the atria and the ventricles is some conduction tissue called the *atrioventricular node* (AV node). After passing through the AV node, the depolarization spreads rapidly over the ventricles on the *conduction system*—a set of specialized muscle cells on the inner walls of the ventricles—(d,e), and finally through the myocardium of each ventricle to the outer wall (e,f,g). The conduction system consists of the *common bundle* (or *bundle of His*), the *left and right bundles*, and the fine network of *Purkinje fibers*. The AV node will spontaneously depolarize at a rate of about 50 beats  $\text{min}^{-1}$ ; it usually does not because it is triggered by the more rapid beating of the atria. In well-trained athletes, the resting pulse rate can be so low that the AV node fires spontaneously, giving rise to what are called nodal escape beats. These are physiologic and are no cause for concern.

There is a difference between depolarization, which propagates as a wave, and repolarization, which is a local phenomenon. Sodium conductance increases as the transmembrane potential rises during depolarization. As the potential rises at some point on the advancing wave front, electrotonus increases the potential further along the cell. This causes the sodium conductance to rise at that point, enhancing the propagation of the signal. During repolarization, as the potential falls at one point, electrotonus tends to lower the potential at neighboring points. This

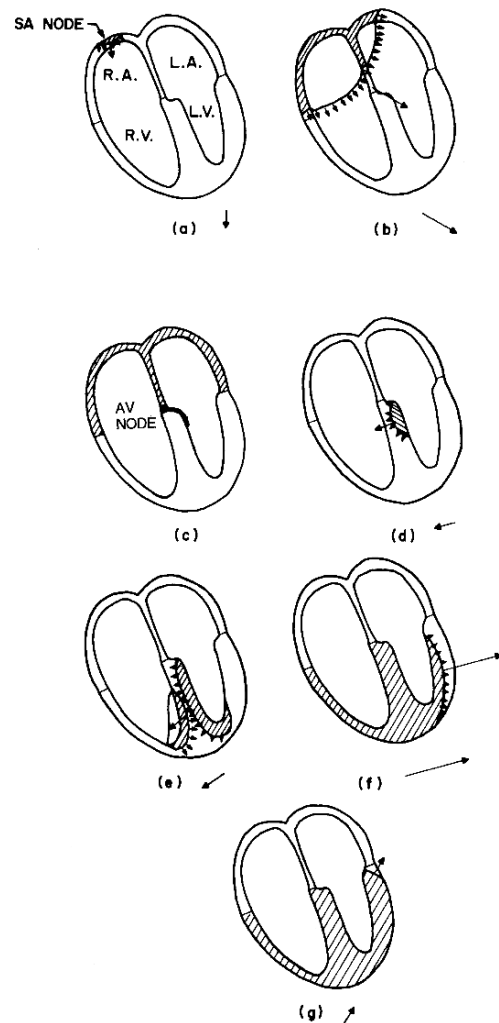


FIGURE 7.15. The wave of depolarization sweeping over the heart. Atrial and ventricular muscle are not connected except through the AV node. (a) Depolarization beginning at the SA node. (b) Atria nearly depolarized. (c) The AV node is conducting. (d) Beginning of depolarization of the left ventricle. (e, f) Continuing ventricular depolarization. (g) Ventricular depolarization nearly complete. Reprinted with permission from R. K. Hobbie. *The electrocardiogram as an example of electrostatics*. *Am. J. Phys.* **41**: 824–831. Copyright 1973, American Association of Physics Teachers.

means that the potassium conductance also falls, which tends to retard repolarization. Moreover, as the voltage falls during repolarization, the transmembrane potential is approaching the potassium Nernst potential, and the potassium current falls for this reason as well.<sup>6</sup> Therefore electrotonus does not assist in the propagation of the repolarization, which is a local phenomenon.

<sup>6</sup>This argument ignores the potassium “K1” channels, which do provide positive feedback late in the cardiac action potential.

Normally, depolarization progresses through the myocardium in an orderly fashion. It is followed by repolarization, and after a brief *refractory period* the heart is ready to beat again. During the refractory period the cells do not respond to a stimulus. It is possible in abnormal situations for a wave of depolarization to travel in a closed path through the myocardium. This closed path, called a *reentrant circuit*, can surround an obstacle such as scar tissue, the aorta, or the pulmonary artery. It can also surround an area that simply has different conduction properties.

If the time to travel around the reentrant circuit is greater than the refractory period, the wave can continue to travel on the closed path. Reentrant excitation is thought to be responsible for several kinds of heart disease, including most life-threatening ventricular tachycardias (rapid heart rate). Another type of reentrant excitation is spiral waves that occur because of the nonlinear nature of the myocardium [Davidenko (1995)]. (Such nonlinear behavior will be discussed in Chap. 10.) It is also possible for a reentrant wave to leave behind a refractory state that blocks normal conduction.

### 7.6 The Current-Dipole Vector of the Heart as a Function of Time

Each myocardial cell depolarizes and repolarizes during the cardiac cycle. These cells are short—about 100 μm in length—but are interconnected. We apply our axon model by noting that a current  $i_i$  flows within each cell during depolarization and a return current, which could be ignored in our axon model, flows in the surrounding tissue. We assume that each cell as it depolarizes has a current dipole moment, and that these can be summed.

The total current-dipole vector at any instant is then the sum of the vectors for all the cells in the heart. This section considers how the total current-dipole vector changes with time as the myocardium depolarizes and then repolarizes. Initially, all the cells are completely polarized (resting) and there is no net dipole moment. The cells begin to depolarize near the SA node, and a wave of depolarization sweeps across the atria. For each myocardial cell, the dipole vector points in the direction that the wave of depolarization is traveling<sup>7</sup> and moves along the cell with the depolarization wave. These vectors for all the cells that are depolarizing constitute an advancing wave that moves across the heart.

The potential at the point of observation can be calculated by applying Eq. 7.13 for each cell. Vector  $\mathbf{r}$  is the vector from the cell to the point of observation and is different for each cell. However, we will assume for now

<sup>7</sup>If one takes into account the anisotropies in the conductivities of myocardial tissue discussed in Sec. 7.9, the depolarization does not travel in the direction that  $\mathbf{p}$  points. We ignore this for now.

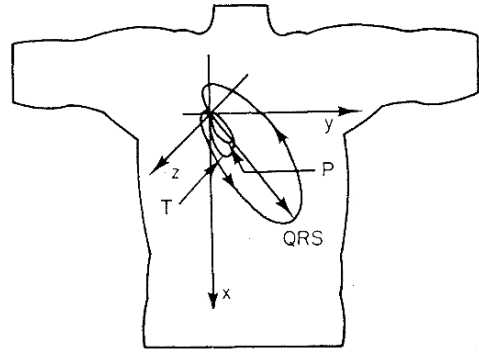


FIGURE 7.16. The locus of the tip of the total current-dipole vector during the cardiac cycle. The  $z$  axis is perpendicular to the  $x$  and  $y$  axes and the subject’s chest and comes out of the page.

that the observation point is so far from the heart that all points in the myocardium are nearly equidistant from it. This is a terrible assumption; later we will be more realistic. It allows us to speak of the *instantaneous total current-dipole moment*, which is the sum of the dipole moments of all depolarizing cells at that instant.

The locus of the tip of the total dipole moment during the cardiac cycle is shown in Fig. 7.16 for a typical case. The  $x$  axis points to the patient’s feet, the  $y$  axis to the patient’s left, and the  $z$  axis from back to front. The small loop labeled  $P$  occurs during atrial depolarization. The loop labeled  $QRS$  is the result of ventricular depolarization. Ventricular repolarization gives rise to the “ $T$  wave.” Atrial repolarization is masked by ventricular depolarization. A plot of the  $x$ ,  $y$ , and  $z$  components of  $\mathbf{p}$  is shown in Fig. 7.17. These components are typical; there can be considerable variation in the directions of the loops in Fig. 7.16.

### 7.7 The Electrocardiographic Leads

We turn next to how the electrocardiographic measurements are made. We model the torso as an infinite homogeneous conductor and continue to assume that every myocardial cell is the same distance from each electrode. Both assumptions are wrong, of course, and later we will improve upon them.

The potential at  $\mathbf{r}$  from a current dipole  $\mathbf{p}$  is given by Eq. 7.13. The potential difference between two points at positions  $\mathbf{r}_1$  and  $\mathbf{r}_2$ , each a distance  $r$  from the dipole, is therefore (see Fig. 7.18)

$$v(\mathbf{r}_2, \mathbf{r}_1) = \frac{\mathbf{p} \cdot (\mathbf{r}_2 - \mathbf{r}_1)}{4\pi\sigma_o r^3}.$$

Denoting  $\mathbf{r}_2 - \mathbf{r}_1$  by  $\mathbf{R}$ , we have

$$v = \frac{\mathbf{p} \cdot \mathbf{R}}{4\pi\sigma_o r^3}. \tag{7.30}$$



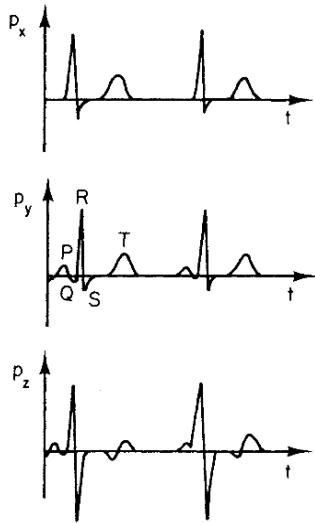


FIGURE 7.17. The three components of the total current-dipole vector  $\mathbf{p}$  as a function of time.

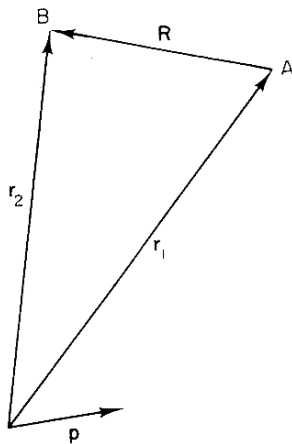


FIGURE 7.18. Geometry for calculating the potential difference due to  $\mathbf{p}$  between points  $A$  and  $B$ .

The potential difference between two electrodes separated by a displacement  $\mathbf{R}$  and equidistant from the current-dipole vector  $\mathbf{p}$  measures the instantaneous projection of vector  $\mathbf{p}$  on  $\mathbf{R}$ .

If the depolarization can be described by a single current-dipole vector, only three measurements are needed in principle, corresponding to the projections on three perpendicular axes. The standard electrocardiogram (ECG) records 12 potential differences using nine electrodes. There are many reasons for this. The body is not an infinite, homogeneous conductor, and the relationship between cellular dipole moments and the potential is more complicated than our model; to convert the three perpendicular components to the instantaneous values of  $\mathbf{p}$  would require a mathematical reconstruction; and the

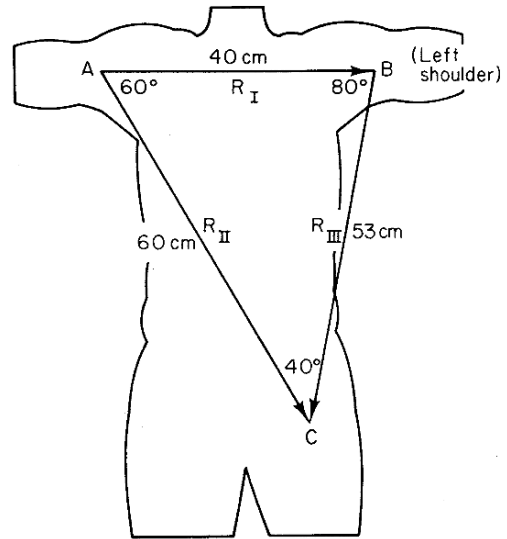


FIGURE 7.19. Vectors connecting the three electrodes for a typical patient. The limbs are extensions of the leads of the electrocardiograph machine.

electrodes are not far away compared to the size of the heart. With 12 recorded potential differences, it is fairly easy to interpret the electrocardiogram by inspection.

The first three electrodes are placed on each wrist and the left leg. The limbs serve as extensions of the wires, so that the potential is measured where the limbs join the body. This is a major correction to our crude model that the heart is in an infinite conducting medium. If the subject were immersed in a conducting medium such as sea water, movement of the arms would change the size of the ECG signal because it would change  $\mathbf{R}$ . In air, however, movement of the arms does not change the size of the signal. The simplest correction to explain this is to say that  $\mathbf{R}$  for the two arm electrodes goes from shoulder to shoulder. These three electrodes measure potential differences between three points located approximately as shown in Fig. 7.19. The dimensions are for a typical adult. The three potential differences are called *limb leads* I, II, and III:

$$\begin{aligned} \text{I} &= v_B - v_A, \\ \text{II} &= v_C - v_A, \\ \text{III} &= v_C - v_B. \end{aligned} \tag{7.31}$$

In the approximation used here, the voltage difference I is proportional to the projection of  $\mathbf{p}$  on  $\mathbf{R}_I$ , and so forth. These leads measure the projections of  $\mathbf{p}$  on the three vectors  $\mathbf{R}_I$ ,  $\mathbf{R}_{II}$ , and  $\mathbf{R}_{III}$  of Fig. 7.19.

It is customary also to combine these three potentials in a slightly different way to obtain projections of  $\mathbf{p}$  on three other directions. These combinations are called the *augmented limb leads*. They contain no information that was not already present in the limb leads, but the six

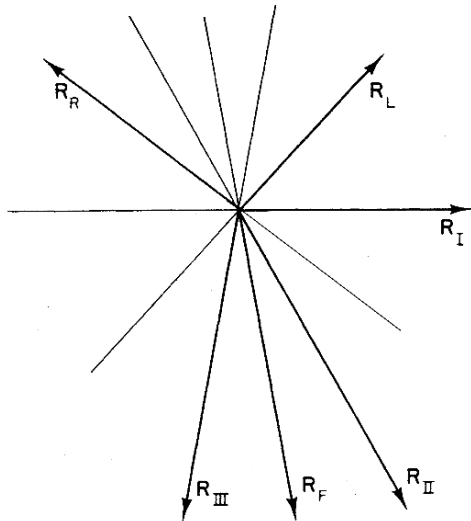


FIGURE 7.20. The six directions in the frontal plane defined by the limb leads and the augmented limb leads. The angles are for the same subject as in Fig. 7.19.

signals are easier to interpret by inspection. The combinations are

$$\begin{aligned}
 aVR &= v_A - \frac{1}{2}(v_B + v_C) = -\frac{1}{2}(I + II), \\
 aVL &= v_B - \frac{1}{2}(v_A + v_C) = \frac{1}{2}(I - III), \\
 aVF &= v_C - \frac{1}{2}(v_A + v_B) = \frac{1}{2}(II + III).
 \end{aligned}
 \tag{7.32}$$

These are proportional to the projections of  $\mathbf{p}$  on vectors  $\mathbf{R}_L$ ,  $\mathbf{R}_R$ , and  $\mathbf{R}_F$  of Fig. 7.20. The subscripts refer to the fact that the vectors point toward the left shoulder, right shoulder, and foot, respectively.

The six lines in Fig. 7.20 are spaced approximately every  $30^\circ$  in the frontal plane. Many texts argue that the leads are spaced exactly every  $30^\circ$  and that the triangle of Fig. 7.19 is an equilateral triangle (Einthoven's triangle). While the directions are not far from  $30^\circ$ , this assumption is not really necessary. Physicians often want to know the direction of  $\mathbf{p}$  at some point during the cardiac cycle, or the average direction of  $\mathbf{p}$  during the *QRS* wave (ventricular depolarization). With six directions measured, this can be determined by inspection.

These six leads measure projections in the frontal plane. It is also necessary to have at least one projection in a plane perpendicular to the frontal plane. It is customary to place six leads across the chest wall in front of the heart; they are called the *precordial leads*. Their locations are shown in Fig. 7.21. The potential difference is measured between each precordial electrode and the average of  $v_A$ ,  $v_B$ , and  $v_C$ . A lead therefore measures the projection of  $\mathbf{p}$  on a vector from the center of triangle  $ABC$  to the electrode for that lead. This fact is not obvious, and in fact is true only if differences in  $1/r^2$  are neglected. To

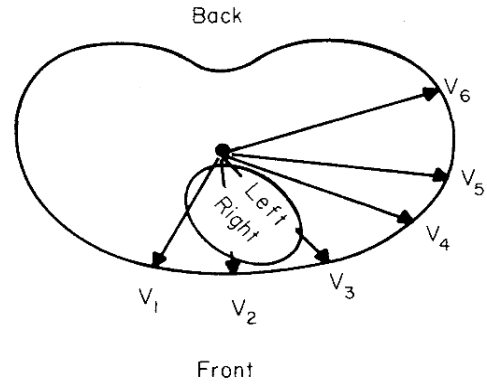


FIGURE 7.21. The location of the precordial leads and the directions of the components of  $\mathbf{p}$  which they measure. Reprinted with permission from R. K. Hobbie. The electrocardiogram as an example of electrostatics. *Am. J. Phys.* **41**: 824–831. Copyright 1973, American Association of Physics Teachers.

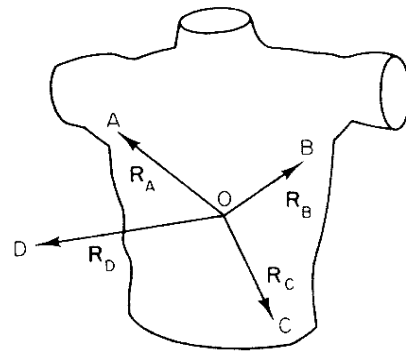


FIGURE 7.22. A perspective drawing of the vectors used to calculate the potential in a precordial lead. Reprinted with permission from R. K. Hobbie. The electrocardiogram as an example of electrostatics. *Am. J. Phys.* **41**: 824–831. Copyright 1973, American Association of Physics Teachers.

see that it is true with the appropriate approximation, pick an arbitrary point  $O$  and from it construct vectors  $\mathbf{R}_A$ ,  $\mathbf{R}_B$ ,  $\mathbf{R}_C$ , and  $\mathbf{R}_D$  to the points  $A$ ,  $B$ , and  $C$  of Fig. 7.22 and to the precordial electrode at  $D$ . The desired potential is

$$v = v_D - \frac{v_A + v_B + v_C}{3}.$$

It can be calculated using Eq. 7.30 for each term:

$$v = \frac{1}{4\pi\sigma_o} \left[ \frac{\mathbf{p} \cdot \mathbf{R}_D}{R_D^3} - \frac{1}{3} \left( \frac{\mathbf{p} \cdot \mathbf{R}_A}{R_A^3} + \frac{\mathbf{p} \cdot \mathbf{R}_B}{R_B^3} + \frac{\mathbf{p} \cdot \mathbf{R}_C}{R_C^3} \right) \right].$$

So far, the location of  $O$  is arbitrary. If it is picked to be at the center of the triangle, then  $\mathbf{R}_A + \mathbf{R}_B + \mathbf{R}_C = 0$ . (This is the definition of center.) Since  $R_A \approx R_B \approx R_C$ , the term in large parentheses vanishes. The desired potential difference is then

$$v = \frac{1}{4\pi\sigma_o} \frac{\mathbf{p} \cdot \mathbf{R}_D}{R_D^3}.$$

In this approximation, each precordial lead measures the projection of  $\mathbf{p}$  on a vector from the center of the triangle  $ABC$  to the electrode. The amplitude of the signal will be larger than for the limb leads, because  $R_D < R_A$ . Some of the precordial leads are quite close to the heart. The assumption that  $r$  is the same for all parts of the myocardium is not valid. Because of the factor  $1/r^2$ , the greatest contribution to the potential comes from the closest regions of myocardium. A lead is said to “look at” the myocardium closest to it.

## 7.8 Some Electrocardiograms

A normal electrocardiogram is shown in Fig. 7.23. When  $\mathbf{p}$  has its greatest magnitude during the  $QRS$  wave, it is nearly parallel to  $\mathbf{R}_{II}$ . There is almost no signal in  $aVL$ , which is perpendicular to  $\mathbf{R}_{II}$ .

Compare this to Fig. 7.24, which shows the electrocardiogram for a patient with *right ventricular hypertrophy*, an enlargement and thickening of the right ventricle. Because of the greater right ventricular muscle volume,  $\mathbf{p}$  points to the right during the  $QRS$  wave, so that the  $QRS$  signal is negative in lead I. Lead  $aVF$  shows that there is very little vertical component of  $\mathbf{p}$  during the  $QRS$  wave. The precordial leads  $V_1$  and  $V_2$  show the strongest signals, because the right ventricle faces the front of the body. In this case an extra lead  $V_4R$  has been used, which is symmetrical with  $V_4$  but on the right side of the body.

The electrocardiogram in Fig. 7.25 is from a patient with left ventricular hypertrophy. The thicker left ven-

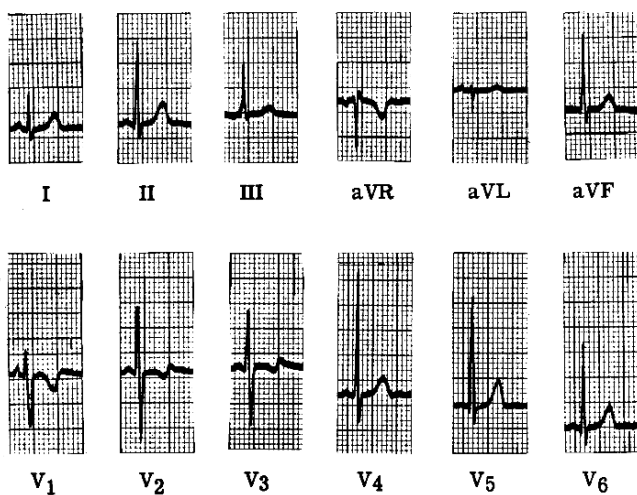


FIGURE 7.23. A normal electrocardiogram. The large divisions are 0.5 mV vertically and 0.2 s horizontally. Reprinted with permission from R. K. Hobbie. The electrocardiogram as an example of electrostatics. *Am. J. Phys.* 41: 824–831. Copyright 1973, American Association of Physics Teachers. The electrocardiogram was supplied by Prof. James H. Moller, M.D.

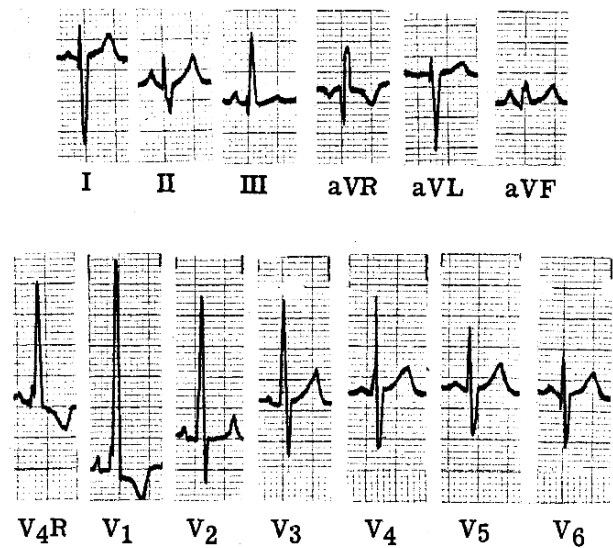


FIGURE 7.24. The electrocardiogram of a patient with right ventricular hypertrophy. Reprinted with permission from R. K. Hobbie. The electrocardiogram as an example of electrostatics. *Am. J. Phys.* 41: 824–831. Copyright 1973, American Association of Physics Teachers. The electrocardiogram was supplied by Prof. James H. Moller, M.D.

tricular wall causes the  $QRS$  dipole to point to the left. As a result, lead I has an abnormally high peak,  $aVL$  is large and positive,  $V_2$  is negative, and  $V_4$ ,  $V_5$ , and  $V_6$  have very large positive peaks. These last four leads are shown at half scale.

A fault in the conduction system known as a *bundle branch block* causes the depolarization wave to travel through the myocardium rather than over the conduction system. Since the speed of propagation in myocardium is slower than that in the conduction system, the depolarization takes longer than usual. An electrocardiogram for a patient with *right bundle branch block* (a block in the bundle for the right ventricle) is shown in Fig. 7.26. The effect is most striking in leads that are most sensitive to the right ventricle: precordial leads 1 and 2. In  $V_1$  the early part of the  $QRS$  wave has the usual biphasic, up-down pattern as the left ventricle depolarizes. This is followed by a large and prolonged vector pointing to the right, as the right ventricle slowly depolarizes. Lead  $V_2$  shows a strong and prolonged bipolar signal as the right ventricle depolarizes.

## 7.9 Refinements to the Model

Our model for the potential outside a nerve or muscle cell has been a long single conducting fiber in an infinite, homogeneous medium. We will consider four ways to extend and improve the model. The first is to recognize that current must also flow radially inside the cell. If it did not, it

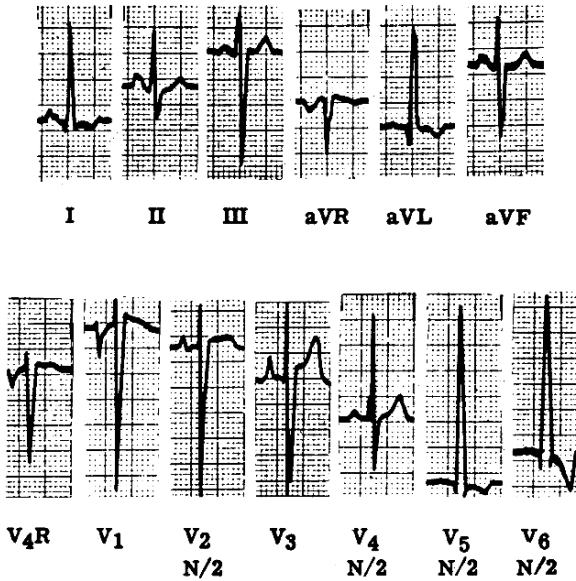


FIGURE 7.25. The electrocardiogram for a patient with left ventricular hypertrophy. Reprinted with permission from R. K. Hobbie. The electrocardiogram as an example of electrostatics. *Am. J. Phys.* 41: 824–831. Copyright 1973, American Association of Physics Teachers. The electrocardiogram was supplied by Prof. James H. Moller, M.D.

could never leave the cell. At the same time we will abandon the assumption that the presence of the cell along the  $x$  axis does not perturb the current outside the cell. The third improvement is to recognize that the conductivity may depend on position. This is particularly important outside the cell, where there are muscle, fat, lungs, etc. Finally, the conductivity at a given point may depend on which direction the current flows—for example, parallel or perpendicular to the cells.

In order to make these refinements to the model, we must develop a different formulation of the problem. Consider some region of space containing a conducting material described by Ohm’s law. The electric field is related to the potential by Eq. 6.16b:  $\mathbf{E} = -\text{grad } v = -\nabla v$ . If the material is isotropic and obeys Ohm’s law, then from Eq. 6.26

$$\mathbf{j} = \sigma \mathbf{E} = -\sigma \nabla v. \quad (7.33)$$

We now apply the equation of continuity or conservation of charge, casting Eq. 4.8 in terms of the electric current density  $\mathbf{j}$  and the electric charge per unit volume,  $\rho$ :

$$\frac{\partial \rho}{\partial t} = -\nabla \cdot \mathbf{j}. \quad (7.34)$$

Combining these two equations gives

$$\frac{\partial \rho}{\partial t} = \text{div}(\sigma \text{grad } v) = \nabla \cdot (\sigma \nabla v). \quad (7.35)$$

Leaving the conductivity inside the divergence term allows the conductivity to depend on position. If the conductivity is the same everywhere it can be taken outside

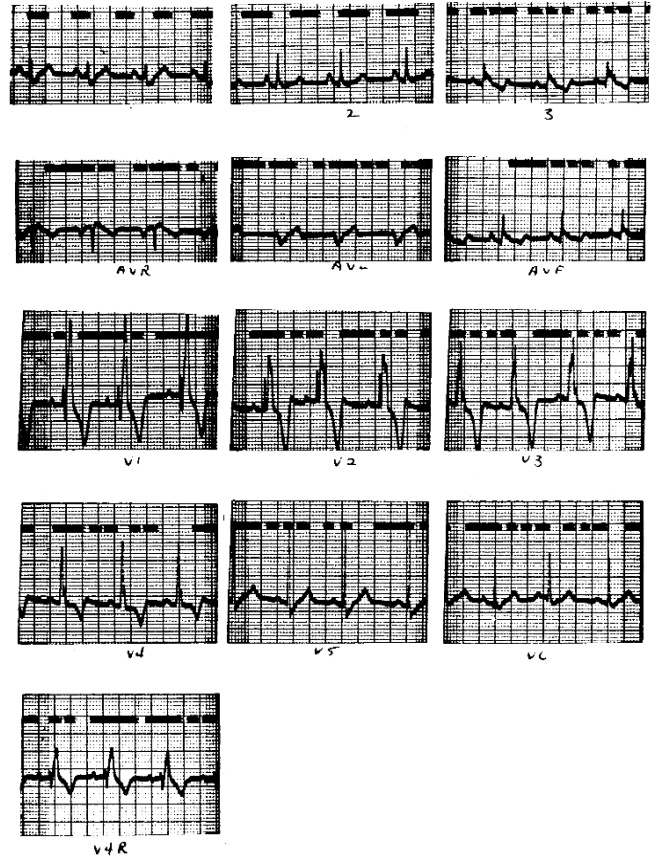


FIGURE 7.26. The electrocardiogram for a patient with right bundle branch block. The electrocardiogram was supplied by Prof. James H. Moller, M.D.

the divergence operator to give

$$\frac{\partial \rho}{\partial t} = \sigma \nabla^2 v = \sigma \left( \frac{\partial^2 v}{\partial x^2} + \frac{\partial^2 v}{\partial y^2} + \frac{\partial^2 v}{\partial z^2} \right). \quad (7.36a)$$

We can write this in cylindrical coordinates which are more useful for modeling a cylindrical cell stretched along the  $z$  axis. From Appendix L, assuming that the potential does not depend on the polar angle  $\phi$ , we have

$$\frac{\partial \rho}{\partial t} = \sigma \nabla^2 v = \sigma \left[ \frac{1}{r} \frac{\partial}{\partial r} \left( r \frac{\partial v}{\partial r} \right) + \frac{\partial^2 v}{\partial z^2} \right]. \quad (7.36b)$$

These are very general equations, applicable to any volume of space where the material is homogeneous and isotropic and obeys Ohm’s law. They were derived using Ohm’s law and the conservation of charge. Equation 7.36a is actually the same result we had in Eq. 6.51. This is demonstrated in Problem 29.

### 7.9.1 The Axon Has a Finite Radius

Now we can make the first two improvements: we relax the assumption that the axon radius is very small. Except

at the cell membrane, where charge on the membrane capacitance is changing as the membrane potential changes,  $\partial\rho/\partial t = 0$ . If we assume that the transmembrane potential  $v_m$  is known, then Eq. 7.36b can be applied separately to the extracellular and the intracellular fluid for a long straight axon to determine the potential everywhere outside (or inside). This was first done by Clark and Plonsey (1968). In the extracellular and intracellular fluids, Eq. 7.36b becomes

$$\begin{aligned} \frac{1}{r} \frac{\partial}{\partial r} \left( r \frac{\partial v_o(r, z)}{\partial r} \right) + \frac{\partial^2 v_o(r, z)}{\partial z^2} &= 0, \quad r > a \\ \frac{1}{r} \frac{\partial}{\partial r} \left( r \frac{\partial v_i(r, z)}{\partial r} \right) + \frac{\partial^2 v_i(r, z)}{\partial z^2} &= 0, \quad r < a \\ v_m(z) &= v_i(a, z) - v_o(a, z). \end{aligned} \quad (7.37)$$

With  $v_m$  known, these equations were solved for the potential distribution inside and outside the cell. This is the calculation that was done to obtain Fig. 7.13. The result of this type of calculation has been compared to the line-source model by Trayanova *et al.* (1990).

### 7.9.2 Nonuniform Exterior Conductivity

To make the next improvement, consider an extracellular region in which the conductivity is not uniform. In a region without sources, the potential obeys

$$\nabla \cdot (\sigma_o \nabla v_o) = 0. \quad (7.38)$$

Often, the conductivity is assumed to be “piecewise” homogenous, with a different value assigned to each kind of tissue. Within each tissue the potential then obeys Laplace’s equation,  $\nabla^2 v_o = 0$ . At the boundary between tissues, the potential and the normal component of the current are continuous.

When the different tissues have realistic and irregular boundaries, special techniques are needed to solve Laplace’s equation. One important technique is the “finite-element method” [Miller and Henriquez (1990)], and another is the “boundary-element method” [Gulrajani (1998)].

A typical application, which serves as the basis for “noninvasive electrocardiographic imaging,” is to measure the potential at the body surface and then calculate the potential on the epicardium (the outer surface of the heart) [Rudy and Burnes (1999); Stanley *et al.* (1986)]. One cannot calculate the potential inside the heart unless the sources are known, but finding the potential on the epicardial surface is possible.

### 7.9.3 Anisotropic Conductivity: The Bidomain Model

The final improvement recognizes that the cardiac tissue is generally not isotropic. If it is still described by Ohm’s

law, then we can write  $\mathbf{j} = \tilde{\sigma} \cdot \mathbf{E}$  where  $\tilde{\sigma}$  is a matrix or tensor. In Cartesian coordinates

$$\begin{pmatrix} j_x \\ j_y \\ j_z \end{pmatrix} = \begin{pmatrix} \sigma_{xx} & \sigma_{xy} & \sigma_{xz} \\ \sigma_{yx} & \sigma_{yy} & \sigma_{yz} \\ \sigma_{zx} & \sigma_{zy} & \sigma_{zz} \end{pmatrix} \begin{pmatrix} E_x \\ E_y \\ E_z \end{pmatrix}. \quad (7.39)$$

This is a compact notation for

$$j_x = \sigma_{xx} E_x + \sigma_{xy} E_y + \sigma_{xz} E_z,$$

with similar equations for  $j_y$  and  $j_z$ . It can be shown that the conductivity matrix must be symmetric, so there are actually six conductivity coefficients, not nine. It is often possible to make some of the matrix elements zero by suitable choice of a coordinate system and suitable orientation of the axes.

Problem 29 shows that for a small cylindrical region of isotropic axoplasm of length  $h$  and radius  $a$ , the cylindrical surface of which is surrounded by cell membrane, the total charge  $Q$  within the axoplasm changes according to

$$\frac{\partial Q}{\partial t} = \pi a^2 h \frac{\partial \rho_i}{\partial t} = C \frac{\partial v_m}{\partial t} + i_m = 2\pi a h \left( c_m \frac{\partial v_m}{\partial t} + j_m \right),$$

or

$$c_m \frac{\partial v_m}{\partial t} + j_m = \frac{\pi a^2 h}{2\pi a h} \sigma_i \frac{\partial^2 v_i}{\partial x^2} = \frac{\sigma_i a}{2} \frac{\partial^2 v_i}{\partial x^2}.$$

This can also be written as

$$\beta \left( c_m \frac{\partial v_m}{\partial t} + j_m \right) = \sigma_i \frac{\partial^2 v_i}{\partial x^2},$$

where  $\beta = 2\pi a h / \pi a^2 h = 2/a$  is the ratio of surface area to volume of the cell. Our cell was cylindrical. With other geometrical configurations, such as a cubic or a spherical cell,  $\beta$  would have a different value, but it always has the dimensions of (length)<sup>-1</sup>. In the general three-dimensional anisotropic case, the equivalent equation is

$$\begin{aligned} \beta \left( c_m \frac{\partial v_m}{\partial t} + j_m \right) &= \sigma_i \frac{\partial^2 v_i}{\partial x^2} \\ \text{zero, except at the cell membrane} & \\ = \operatorname{div}(\tilde{\sigma}_i \operatorname{grad} v_i) &= \nabla \cdot (\tilde{\sigma}_i \nabla v_i) \end{aligned} \quad (7.40)$$

Both  $\sigma_i$  and  $v_i$  are functions of position. The left-hand side is zero except at the cell membrane. The main theme of this chapter has been that current that stops flowing inside the cell must flow outside the cell. We can write an analogous equation for the region outside the cell:

$$\begin{aligned} -\beta \left( c_m \frac{\partial v_m}{\partial t} + j_m \right) &= \operatorname{div}(\tilde{\sigma}_o \operatorname{grad} v_o) \\ \text{zero, except at the cell membrane} & \\ &= \nabla \cdot (\tilde{\sigma}_o \nabla v_o) \end{aligned} \quad (7.41)$$

Myocardial cells are typically about 10  $\mu\text{m}$  in diameter and 100  $\mu\text{m}$  long. They have the added complication that they are connected to one another by gap junctions, as shown schematically in Fig. 7.27. This allows currents to

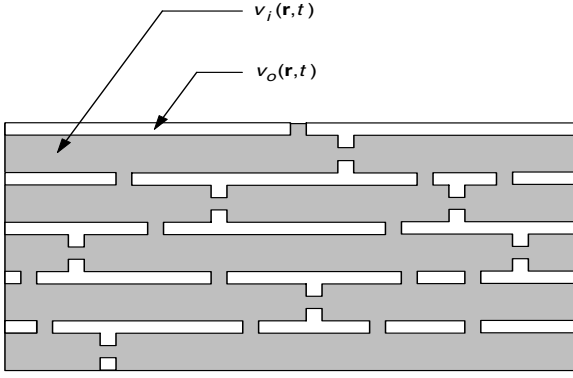


FIGURE 7.27. The interior of myocardial cells (shaded) is connected to adjoining cells by gap junctions. The bidomain model assumes that in a small region of space (large compared to a cell) there are two potentials: the interior potential and outside potential that are functions of position and time.

flow directly from one cell to another without flowing in the extracellular medium. The *bidomain* (two-domain) model is often used to model this situation [Henriquez (1993)]. It considers a region, small compared to the size of the heart, that contains many cells and their surrounding extracellular fluid. It simplifies the problem by assuming that each small volume element contains two domains, intracellular and extracellular.

Think of the volume element as the entire region shown in Fig. 7.27. There are two potentials in each small volume element:  $v_i(\mathbf{r}, t)$  and  $v_o(\mathbf{r}, t)$ . These potentials are averages over the intracellular and extracellular domains contained in the volume element. The transmembrane potential is the difference between these two potentials:  $v_m(\mathbf{r}, t) = v_i(\mathbf{r}, t) - v_o(\mathbf{r}, t)$ . Charge can pass freely between the two domains, but the total charge within a volume element is conserved. If the current densities in each domain are  $\mathbf{j}_i$  and  $\mathbf{j}_o$ , then the divergence of the sum is zero:  $\nabla \cdot (\mathbf{j}_i + \mathbf{j}_o) = 0$ . The divergence of each current individually passes through the membrane or charges the membrane capacitance. The anisotropic analogs of Eqs. 7.40 and 7.41 are now

$$\begin{aligned} \beta \left( c_m \frac{\partial v_m}{\partial t} + j_m \right) &= \text{div}(\tilde{\sigma}_i \cdot \text{grad } v_i) = \nabla \cdot (\tilde{\sigma}_i \cdot \nabla v_i), \\ -\beta \left( c_m \frac{\partial v_m}{\partial t} + j_m \right) &= \text{div}(\tilde{\sigma}_o \cdot \text{grad } v_o) \\ &= \nabla \cdot (\tilde{\sigma}_o \cdot \nabla v_o). \end{aligned} \quad (7.42)$$

The quantity  $\beta$  is the membrane surface area per unit volume of the entire bidomain—both intracellular and extracellular volumes. For example, if we consider that the cells are all cylindrical of length  $h$  and radius  $a$ , then the surface area of a cell is  $2\pi ah$ . If the fraction of the total volume occupied by cells is  $f$ , then the total volume associated with this cell is  $\pi a^2 h / f$ , so

$$\beta = \frac{2f}{a}. \quad (7.43)$$

The membrane current  $j_m$  can be modeled by either a passive membrane (Ohm's law—electrotonus) or with one of the models for an active membrane.

Anisotropy plays an important role in the bidomain model. To see why, consider a solution to Laplace's equation in a monodomain—a two-dimensional sheet of homogeneous, anisotropic tissue with straight fibers. If the  $x$  direction is chosen to be along the fiber direction (the direction of greatest conductivity), then Laplace's equation becomes

$$\sigma_{ox} \frac{\partial^2 v_o}{\partial x^2} + \sigma_{oy} \frac{\partial^2 v_o}{\partial y^2} = 0.$$

Now define a new set of coordinates  $x' = x$  and  $y' = \sqrt{\sigma_{ox}/\sigma_{oy}}y$ . You can show that in these new coordinates Laplace's equation becomes

$$\frac{\partial^2 v_o}{\partial x'^2} + \frac{\partial^2 v_o}{\partial y'^2} = 0.$$

We have removed the effect of anisotropy by rescaling distance in the direction perpendicular to the fibers. If you try a similar trick with the bidomain model

$$\sigma_{ix} \frac{\partial^2 v_i}{\partial x^2} + \sigma_{iy} \frac{\partial^2 v_i}{\partial y^2} = \beta \left( c_m \frac{\partial v_m}{\partial t} + j_m \right) \quad (7.44a)$$

$$\sigma_{ox} \frac{\partial^2 v_o}{\partial x^2} + \sigma_{oy} \frac{\partial^2 v_o}{\partial y^2} = -\beta \left( c_m \frac{\partial v_m}{\partial t} + j_m \right), \quad (7.44b)$$

you can find a new coordinate system that removes the effect of anisotropy in either the intracellular space or the extracellular space, but in general you cannot find a coordinate system that removes the anisotropy in both spaces simultaneously [Roth (1992)]. Only in the special case of equal anisotropy ratios ( $\sigma_{ix}/\sigma_{iy} = \sigma_{ox}/\sigma_{oy}$ ) will the equations simplify dramatically. But the anisotropy ratios in the heart are not equal. In the intracellular space the ratio of conductivities parallel and perpendicular to the fibers is about 10:1, while in the extracellular space this ratio is about 4:1 [Roth (1997)]. Anisotropy plays an essential role in the electrical behavior of the heart, especially during electrical stimulation.

## 7.10 Electrical Stimulation

The information that has been developed in this chapter can also be used to understand some of the features of stimulating electrodes. These may be used for electromyographic studies, for stimulating muscles to contract, for a cochlear implant to partially restore hearing, for cardiac pacing, and even for defibrillation. The electrodes may be inserted in cells, placed in or on a muscle, or placed on the skin.

In addition to the material in this section, see Problems 38–41.

A pulse of current is sent to the stimulating electrode. The current required to produce a response depends on

the shape and size of the electrode, its placement, the kind of cell being stimulated, and the duration of the pulse. For a given electrode geometry the shorter the pulse, the larger the current required for a tissue response. For very long pulses there is a minimum current required to stimulate that is called *rheobase*. The strength-duration curve was first discovered by G. Weiss in 1901. He expressed it in terms of total charge in the stimulating pulse. A description of the strength-duration curve and its history has been given by Geddes and Bourland (1985). They also describe some techniques for making accurate measurements. The strength-duration curve for current was first described by Lapicque (1909) as

$$i = i_R \left( 1 + \frac{t_C}{t} \right), \quad (7.45)$$

where  $i$  is the current required for stimulation,  $i_R$  is the rheobase,  $t$  is the duration of the pulse, and  $t_C$  is *chronaxie*, the duration of the pulse that requires twice the rheobase current.

Equation 7.45 provides an empirical fit to the experimental data. We can develop a model to explain it using information from Chapter 6. A nerve fires after a certain departure from the resting potential. Subthreshold behavior can be modeled by electrotonus. Suppose that we inject a stimulating current into a cell at the origin. Equation 6.58 gave the voltage along the axon for a current injected in the cell at the origin after an infinitely long time:  $v - v_r = v_0 e^{-|x|/\lambda}$ . The solution to Problem 32 shows that the current injected is

$$i_0 = 2v_0/\lambda r_i. \quad (7.46)$$

The quantities  $\lambda$  and  $r_i$  are defined in Chapter 6. The factor of 2 arises because current flows both ways along the cell. The rheobase current is

$$i_R = 2 \frac{v_{\text{threshold}}}{\lambda r_i}. \quad (7.47)$$

If we assume that the threshold voltage is independent of pulse duration, we can use the curve for  $x = 0$  in Fig. 6.31(c) to relate the minimum current to the pulse duration. As long as the pulse is applied, the voltage will rise along this curve. When the current is turned off, the voltage will start to fall. If the voltage had reached threshold, the cell will fire. This curve is the solution of Eq. 6.55. The solution is [Chapter 6, Problem 34; Plonsey (1969, p. 132)]

$$v(0, t) - v_r = v_0 \operatorname{erf} \left( \sqrt{\frac{t}{\tau}} \right), \quad (7.48)$$

where  $\tau$  is the membrane time constant,  $\kappa \epsilon_0 \rho_m$ . The error function is defined in Eq. 4.74 and is plotted in Fig. 4.21. The current required for stimulation with an intracellular electrode at the origin is therefore

$$i = \frac{2v_{\text{threshold}}}{\lambda r_i \operatorname{erf}(\sqrt{t/\tau})} = \frac{i_R}{\operatorname{erf}(\sqrt{t/\tau})}. \quad (7.49)$$

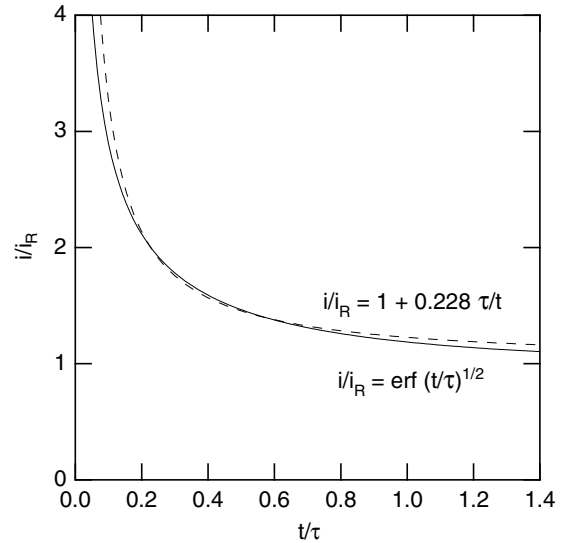


FIGURE 7.28. The stimulus strength-duration curve plotted for the chronaxie–rheobase model, Eq. 7.45 and for electrotonus, Eq. 7.49.

Chronaxie can be related to the time constant  $\tau$  by setting  $i = 2i_R$ :

$$2i_R = \frac{i_R}{\operatorname{erf}(\sqrt{t_C/\tau})}. \quad (7.50)$$

From a table of values of the error function, we find

$$t_C = 0.228\tau. \quad (7.51)$$

Figure 7.28 compares the standard empirical curve, Eq. 7.45, with this model. The curves are experimentally indistinguishable.

Equation 7.45 is also used for surface electrodes. Table 7.1 shows some experimental values for rheobase and chronaxie. The further the electrode from the tissue being stimulated, the greater the rheobase current that is required.

An electrode that is transferring positive charge to the medium is called an *anode*. One that is collecting positive

TABLE 7.1. Comparison of values for rheobase and chronaxie for different stimulations.

Stimulation	Rheobase (mA)	Chronaxie (ms)
Intracellular, from Table 6.1, $v_{\text{threshold}} = 15 \text{ mV}$	$6.7 \times 10^{-6}$	0.23
Myocardium, from good pacing electrodes	0.1	
Motor nerves for inspiration, from stimulation of chest wall [Voorhees <i>et al.</i> (1992)]	49	0.17
Myocardium, from stimulation of chest wall [Voorhees <i>et al.</i> (1992)]	204	1.82

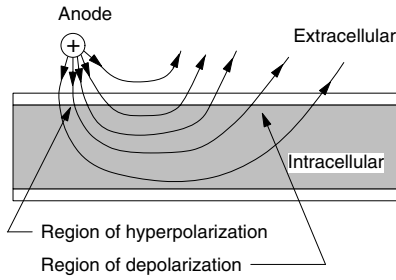


FIGURE 7.29. A schematic drawing showing why there is a region of hyperpolarization near a stimulating anode (positive electrode) with a region of weaker depolarization further away.

charge is called a *cathode*. If the stimulating electrode is inside the cell, a positive current leaving the electrode will increase the positive charge within the cell and depolarize it. Another way to say it is that current from the electrode flows out through the membrane, so the inside of the membrane will be made more positive than the outside. On the other hand, an anodic electrode just outside the cell will send positive current in through the membrane near the electrode, as shown in Fig. 7.29. This lowers the potential inside and hyperpolarizes the membrane near the electrode. Further away from the stimulation point will be a region where current flows out through the membrane, thus depolarizing the cell. However, the outward current is in general spread out over more membrane, so the current density and hence the depolarization is less than the hyperpolarization near the anode. The situation is, of course, reversed for a cathodic electrode. Figure 7.29 is conceptual; to draw the field lines accurately would require taking into account the conductivities of the extracellular and intracellular fluid as well as the membrane.

The electrotonus model also helps us understand another effect that is observed: the *virtual cathode*. The point of origin for a stimulus can be measured by placing sensing electrodes in or on the heart at different distances from the stimulating electrode and plotting the time required for the depolarization wave front to reach the electrode vs its position. Extrapolation to the time of stimulus gives the size of the region of initial depolarization. Imagine a stimulating electrode inside a one-dimensional cell. When the stimulus current is just above rheobase, the region of depolarization is very small and surrounds the electrode. As the stimulating current is increased, the size of the initial depolarized region grows. From Eqs. 6.58 and 7.50 we obtain

$$v_{\text{threshold}} = \frac{i_0 \lambda r_i}{2} e^{-x_{\text{vc}}/\lambda}$$

or

$$x_{\text{vc}} = \lambda \ln \left( \frac{i_0 \lambda r_i}{2v_{\text{threshold}}} \right) = \lambda \ln \left( \frac{i_0}{i_R} \right), \quad (7.52)$$

where  $x_{\text{vc}}$  is the size of the virtual cathode.

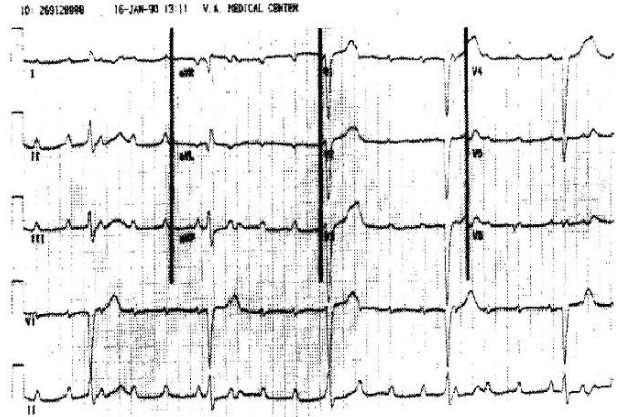


FIGURE 7.30. A patient with third-degree AV heart block. From Rardon, D. P., W. M. Miles, and D. P. Zipes (2000). Atrioventricular block and dissociation. In D. P. Zipes and J. Jalife, eds. *Cardiac Electrophysiology: From Cell to Bedside*, 3rd ed. Philadelphia, Saunders, pp. 451–459. Used by permission.

Cardiac pacemakers are a useful treatment for certain heart diseases [Jeffrey (2001), Moses *et al.* (2000); Barold (1985)]. The most frequent are an abnormally slow pulse rate (*bradycardia*) associated with symptoms such as dizziness, fainting (*syncope*), or heart failure. These may arise from a problem with the SA node (*sick sinus syndrome*) or with the conduction system (*heart block*). One of the first uses of pacemakers was to treat complete or “third degree” heart block. The SA node and the atria fire at a normal rate but the wave front cannot pass into the conduction system. The AV node or some other part of the conduction system then begins firing and driving the ventricles at its own, pathologically slower rate. Such behavior is evident in the ECG in Fig. 7.30, in which the timing of the QRS complex from the ventricles is unrelated to the P wave from the atria. A pacemaker stimulating the ventricles can be used to restore a normal ventricular rate.

A pacemaker can be used temporarily or permanently. The pacing electrode can be threaded through a vein from the shoulder to the right ventricle (transvenous pacing, Fig. 7.31) or placed directly in the myocardium during heart surgery. Sometimes two pacing electrodes are used, one in the atrium and one in the ventricle. The pacing electrode can be unipolar or bipolar. With a unipolar electrode, the stimulation current flows into the myocardium and returns to the case of the pacemaker, which is often placed in a pocket in the muscle of the chest wall near the shoulder. The return current in a bipolar electrode goes to a ring electrode a few centimeters back along the pacing lead from the electrode at the tip. The surface area of a typical tip is about 10 mm<sup>2</sup> (10<sup>-5</sup> m<sup>2</sup>). The current density required to initiate depolarization depends on the spatial distribution of the current and is approximately 100 A m<sup>-2</sup>. Thus, in this model the current is



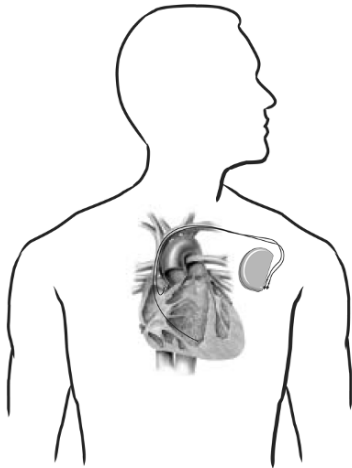


FIGURE 7.31. An implantable pacemaker. The battery and electronics are in a sealed container placed under the skin near the left shoulder. The electrode or “lead” is threaded through the subclavian vein into the right ventricle. Reprinted with permission from *Heart and Stroke Facts*, p. 29. ©1992–2003 by the American Heart Association.

about<sup>8</sup> 1 mA. The resistance of the tissue is typically 500  $\Omega$ , so the voltage is 0.5 V. After the pacing electrode is implanted, the size of the voltage pulse required to initiate ventricular activity rises because inflammatory tissue grows around the electrode. It is conducting, but the myocardium is further away, and the inflammatory tissue effectively increases the size of the electrode, thereby reducing the current density. After six months or so, the inflammation has been replaced by a small fibrous capsule, resulting in an effective electrode size larger than the bare electrode but smaller than the region of inflammation. Recently, electrodes that elute steroids have been used to reduce the inflammation.

Pacemakers can also be designed to detect an abnormal rhythm and apply an electrical stimulus to reverse it. Fig. 7.32 shows a patient with ventricular tachycardia due to a reentrant circuit (p. 186) which has been corrected by pacing very rapidly so that the refractory period prevents the propagation of the reentrant wave.

Ventricular fibrillation occurs when the ventricles contain many interacting reentrant wavefronts that propagate chaotically. Fibrillation is discussed in greater detail in Chapter 10. During fibrillation the ventricles no longer contract properly, blood is no longer pumped through the body, and the patient dies in a few minutes. Implantable defibrillators are similar to pacemakers, but are slightly larger. An implanted defibrillator continually measures the ECG. When a signal indicating fibrillation is sensed, it delivers a much stronger shock that can eliminate the

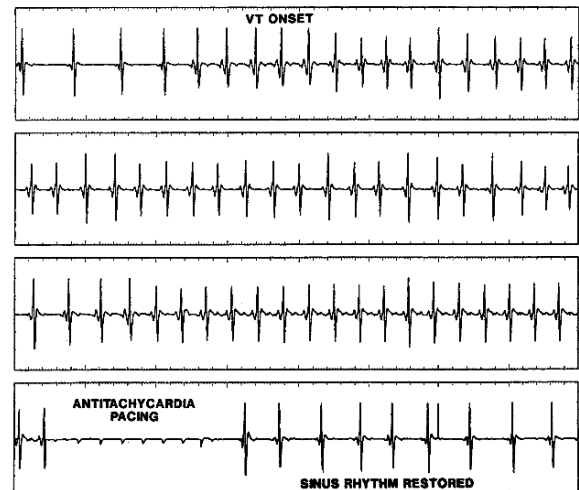


FIGURE 7.32. The top strip shows the onset of ventricular tachycardia, which persists in the next two strips. Very rapid pacing in the fourth strip restores a normal sinus rhythm. Mitrani, R. D., L. S. Klein, D. P. Rardon, D. P. Zipes and W. M. Miles (1995). Current trends in the implantable cardioverter–defibrillator. In D. P. Zipes and J. Jalife, eds. *Cardiac Electrophysiology: From Cell to Bedside*, 2nd ed. Philadelphia, Saunders, pp. 1393–1403. Used by permission.

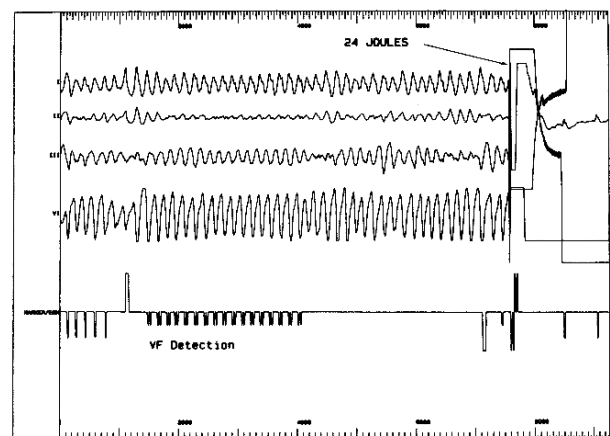


FIGURE 7.33. Ventricular fibrillation has been induced in the electrophysiology laboratory. A pacemaker cardioverter–defibrillator detects the ventricular fibrillation. A capacitor is then charged and applies a 24-joule defibrillation pulse that restores normal rhythm. Mitrani, R. D., L. S. Klein, D. P. Rardon, D. P. Zipes and W. M. Miles (1995). Current trends in the implantable cardioverter–defibrillator. In D. P. Zipes and J. Jalife, eds. *Cardiac Electrophysiology: From Cell to Bedside*, 2nd ed. Philadelphia, Saunders, pp. 1393–1403.

reentrant wavefronts and restore normal heart rhythm (Fig. 7.33).

The bidomain model has been used to understand the response of cardiac tissue to stimulation [Sepulveda *et al.* (1989); Roth and Wikswo (1994); Roth (1994); Wikswo (1995)]. The former simulation explains a remarkable

<sup>8</sup>Acute implants of smaller electrodes where the electrode resistance is low, as well as computer simulations have shown simulation with currents as small as 18  $\mu\text{A}$  [Lindemans and Denier van der Gon (1978)].

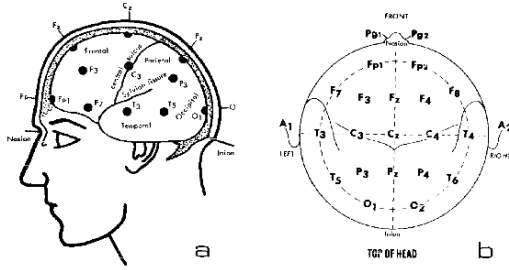


FIGURE 7.34. The standard “10–20” arrangement of electrodes on the scalp for the EEG. Courtesy of Grass, An Astro-Med, Inc., Product Group, West Warwick, RI.

experimental observation. Although the speed of the wave front is greater along the fibers than perpendicular to them, if the stimulation is well above threshold, the wave-front originates farther from the cathode in the direction perpendicular to the fibers—the direction in which the speed of propagation is slower. The simulations show that this is due to the anisotropy in conductivity. This is called the “dog-bone” shape of the virtual cathode. It can rotate with depth in the myocardium because the myocardial fibers change orientation. The difference in anisotropy accentuates the effect of a region of hyperpolarization surrounding the depolarization region produced by a cathodic electrode. Strong point stimulation can also produce reentry waves that can interfere with the desired pacing effect.

One of the fundamental problems with research in this area can be seen in equations like 7.42. The variable on the left is the transmembrane potential  $v_m$ . The variable on the right is the potential inside or outside the cell. Measurement of  $v_m$  requires measurement or calculation of the difference  $v_i - v_o$ . Experimental measurements of the transmembrane potential often rely on the use of a voltage-sensitive dye whose fluorescence changes with the transmembrane potential [Knisley *et al.* (1994); Neunlist and Tung (1995); Rosenbaum and Jalife (2001)].

### 7.11 The Electroencephalogram

Much can be learned about the brain by measuring the electric potential on the scalp surface. Such data are called the *electroencephalogram* (EEG). Nunez and Srinivasan (2005) have written an excellent book about the physics of the EEG. We briefly examine the topic here. The EEG is used to diagnose brain disorders, to localize the source of electrical activity in the brain in patients who have epilepsy, and as a research tool to learn more about how the brain responds to stimuli (“evoked responses”) and how it changes with time (“plasticity”). Typically, the EEG is measured from 21 electrodes attached to the scalp according to the “10–20” system (Fig.

7.34). A typical signal from an electroencephalographic electrode is shown in the top panel of Fig. 11.38. One difficulty in interpreting the EEG is the lack of a suitable reference electrode. None of the 21 electrodes in Fig. 7.34 qualifies as a distant ground against which all other potential recordings can be measured. One way around this difficulty is to subtract from each measured potential the average of all the measured potentials. In the problems, you are asked to prove that this “average reference recording” does not depend on the choice of reference electrode; it is a reference independent method.

### Symbols Used in Chapter 7

Symbol	Use	Units	First used on page
$a$	Axon radius	m	179
$c_m$	Membrane capacitance per unit area	F m <sup>-2</sup>	191
$f$	Intracellular volume fraction		192
$h$	Length of segment	m	191
$i$	Current	A	178
$i_i, i_o$	Current inside, outside axon	A	178
$i_R$	Rheobase current	A	193
$j, \mathbf{j}$	Current density	A m <sup>-2</sup>	178
$\mathbf{j}_m$	Current density through membrane	A m <sup>-2</sup>	191
$p, \mathbf{P}$	Activity vector or current dipole moment	A m	180
$q$	Charge	C	178
$r_i$	Resistance per unit length inside axon	$\Omega$ m <sup>-1</sup>	193
$r, \mathbf{r}$	Distance	m	178
$t$	Time	s	190
$t_C$	Chronaxie	s	193
$v$	Potential	V	178
$v_i, v_o$	Potential inside, outside axon	V	191
$v_m$	Potential across membrane	V	191
$x, y, z, x_0, x_1, x_2, y_0$	Distance or position	m	179
$x_{vc}$	Size of virtual cathode	m	194
$C$	Capacitance	F	191
$E, \mathbf{E}$	Electric field	V m <sup>-1</sup>	178
$P_n$	Legendre polynomial		181
$Q$	Electric charge	C	191
$R$	Resistance	$\Omega$	179
$R, \mathbf{R}$	Distance or position	m	182
$\beta$	Ratio of surface area to volume	m <sup>-1</sup>	191

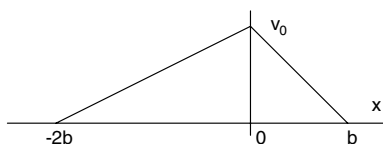
Symbol	Use	Units	First used on page
$\epsilon_0$	Permittivity of free space	$\text{N}^{-1} \text{m}^{-2} \text{C}^2$	178
$\lambda$	Space constant	m	193
$\sigma, \sigma_i, \sigma_o$	Electrical conductivity	$\text{S m}^{-1}$	178
$\rho$	Charge density	$\text{C m}^{-3}$	190
$\tau$	Time constant	s	193
$\theta$	Angle		180
$\xi$	Ratio of $x$ to $R$		184
$\Omega$	Solid angle		181

## Problems

### Section 7.1

**Problem 1** A single nerve or muscle cell is stretched along the  $x$  axis and embedded in an infinite homogeneous medium of conductivity  $\sigma_o$ . Current  $i_0$  leaves the cell at  $x = b$  and enters the cell again at  $x = -b$ . Find the current density  $\mathbf{j}$  at distance  $r$  from the axis in the  $x = 0$  plane.

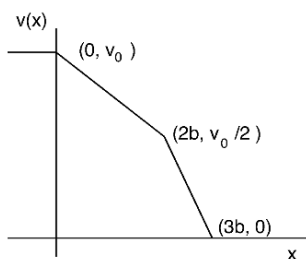
**Problem 2** An axon is stretched along the  $x$  axis. At one instant of time an impulse traveling along the axon has the form shown in the graph. The electrical conductivity inside the axon of radius  $a$  is  $\sigma_i$ . In the infinite external medium it is  $\sigma_o$ . Find an expression for the potential at point  $(x_0, y_0)$ .



**Problem 3** The interior potential of a cylindrical cell is plotted at one instant of time. Distances along the cell are given in terms of length  $b$ . The cell has radius  $a$  and electrical conductivity  $\sigma_i$ . The resting potential is 0 and the depolarized potential is  $v_0$ . The conductivity of the external medium is  $\sigma_o$ .

(a) Find expressions for, and plot, the current along the cell in the four regions ( $x < 0, 0 < x < 2b, 2b < x < 3b, 3b < x$ ).

(b) Find the potential at a point  $(x, y)$  outside the cell in terms of the parameters given in the problem. The point is not necessarily far from the cell.



### Section 7.2

**Problem 4** Modify the closing argument of Sec. 7.2 by considering electrodes that are disks rather than spheres. (Hint: The capacitance you will need is given in Sec. 6.19.)

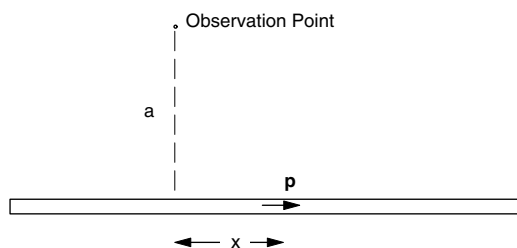
**Problem 5** Suppose an axon is surrounded by a thin layer of extracellular fluid of thickness  $d$ . Use arguments based on the intracellular resistance to estimate the ratio  $\Delta v_o / \Delta v_i$  in this case.

### Section 7.3

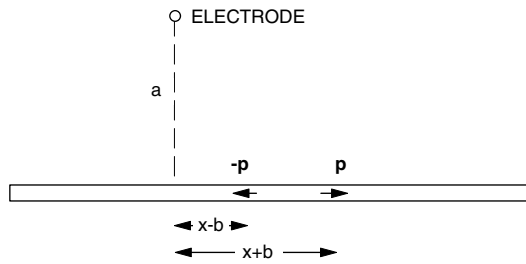
**Problem 6** Starting with Eq. 7.4, make the Taylor's series expansions described in the text, and use them to derive Eq. 7.16.

**Problem 7** What would be the current-dipole moment of a nerve cell of radius  $2 \mu\text{m}$  when it depolarizes? Would myelination make any difference? Does the result depend on the rise time of the depolarization? If the impulse lasts 1 ms and the conduction speed is  $5 \text{ m s}^{-1}$ , how far apart are the rising and falling edges of the pulse?

**Problem 8** An axon or muscle cell is stretched along the  $x$  axis on either side of the origin. As it depolarizes, a constant current dipole  $\mathbf{p}$  pointing to the right sweeps along the axis with velocity  $u$ . An electrode at  $(x = 0, y = a)$  measures the potential with respect to  $v = 0$  at infinity. Ignore repolarization. Find an expression for  $v$  at the electrode as a function of time and sketch it. Assume that at  $t = 0$ ,  $\mathbf{p}$  is directly under the electrode at  $x = 0$ .



**Problem 9** An electrode at  $(x = 0, y = a)$  measures the potential outside an axon with respect to  $v = 0$  at infinity. A nerve impulse is at point  $x$  along the axon, measured from the perpendicular from the electrode to the axon. At  $x + b$  a current dipole points to the right, representing the depolarization wave front. At  $x - b$  a vector of the same magnitude points to the left, representing repolarization. Obtain an expression for  $v$  as a function of  $x, b, p$ , and  $a$ . Plot it in the case  $a = 1, b = 0.05$ .



**Problem 10** A dipole  $\mathbf{p}$  located at the origin  $(0, 0, 0)$  is oriented in the  $x$  direction. The potential  $v_o(x)$  produced by this dipole is measured along the line  $y = 0, z = d$ .

(a) Find an equation for  $v_o(x)$  in terms of  $x, d, \sigma_o$  (the conductivity of the medium) and the dipole strength,  $p$ .

(b) Find an expression for the depth  $d$  of the dipole in terms of the distance  $\Delta x$ , defined as the distance between the minimum and maximum of  $v_o(x, y)$ . This is an example of an “inverse problem,” in which you try to learn about the source (in this case, the depth of  $\mathbf{p}$ ) from measurements of  $v_o$ .

**Problem 11** The “solid angle theorem” is often used to interpret electrocardiograms. The relationship between the exterior potential and the solid angle in Eq. 7.15 is a general result: the potential is proportional to the solid angle subtended by the wave front. Use this result to explain (a) why a closed wave front produces no exterior potential, and (b) why an open wave front produces a potential that depends only on the geometry of its opening or rim.

Section 7.4

**Problem 12** Run the program of Fig. 7.11 and plot the potential for different distances from the axon.

**Problem 13** Modify the program of Fig. 7.11 to calculate the potential from a single Gaussian action potential and plot the potential.

**Problem 14** Let the intracellular potential be zero except in the range  $-a < x < a$ , where it is given by

$$v_i = \begin{cases} 2 \left( \frac{a+x}{a} \right)^2, & -a < x < -a/2 \\ 1 - 2 \left( \frac{x}{a} \right)^2, & -a/2 < x < a/2 \\ 2 \left( \frac{a-x}{a} \right)^2, & a/2 < x < a. \end{cases}$$

Plot  $v_i$  vs  $x$ . Use Eq. 7.21 to calculate the exterior potential at  $(x_0, y_0)$ . You may need the integral

$$\int \frac{dx}{\sqrt{x^2 + b^2}} = \sinh^{-1} \left( \frac{x}{b} \right).$$

Section 7.5

**Problem 15** Suppose a wave front propagates at a speed of  $0.25 \text{ m s}^{-1}$  and its refractory period lasts 250 ms. Calculate the minimum path length of its reentrant circuit. Most reentrant wave fronts are somewhat slower and briefer than this, so their paths may be shorter.

Section 7.7

**Problem 16** Two electrodes are placed in a uniform conducting medium 10 cm from a cell of radius  $5 \mu\text{m}$  and 10 cm from each other, so that the two electrodes and the cell form an equilateral triangle. When the cell depolarizes the potential rises 90 mV. What will be the potential difference between the two electrodes when the cell orientation is optimum? How many cells would be needed to give a potential difference of 1 mV between the electrodes? Assume  $\sigma_i/\sigma_o = 10$ .

**Problem 17** Guess whatever parameters you need to predict the voltage at the peak of the QRS wave in lead II. Compare your results to the electrocardiogram of Fig. 7.23.

**Problem 18** At a particular instant of the cardiac cycle,  $\mathbf{p}$  is located at the midpoint of a line connecting two electrodes that are 50 cm apart, and  $\mathbf{p}$  is parallel to that line. At that instant the magnitude of the potential difference between the electrodes is 1.5 mV. Upon depolarization, the potential change within the cells has magnitude 90 mV.

- (a) What is the magnitude of  $\mathbf{p}$ ?
- (b) If  $\sigma_i/\sigma_o = 10$ , what is the cross-sectional area of the advancing region of depolarization?

**Problem 19** A semi-infinite slab of myocardium occupies the region  $z > 0$ . A hemispherical wave of depolarization moves radially away from the origin through the slab. At some instant of time the radius of the hemispherical depolarizing wavefront is  $R$ . Assume that  $\mathbf{p} = \int d\mathbf{p}$ , that  $d\mathbf{p}$  is everywhere perpendicular to the advancing wavefront, and that the magnitude of  $d\mathbf{p}$  is proportional to the local area of the wavefront. Find  $\mathbf{p}$ . Assume that the observation point is very far away compared to  $R$ .

**Problem 20** Make measurements on yourself and construct Fig. 7.19.

**Problem 21** Experiments have been done in which a dog heart was stimulated by an electrode deep within the myocardium. No exterior potential difference was detected until the spherical wave of depolarization grew large enough so that part of it intercepted one wall of the heart. Why?

**Problem 22** Prove directly from Eq. 7.31 that  $I - II + III = 0$ . (It is sometimes said that the equilateral nature of Einthoven’s triangle is necessary to prove this.)

**Problem 23** Derive Eqs. 7.32.

## Section 7.8

**Problem 24** Estimate the lower limit for the duration of the QRS complex by calculating the time required for a wave front to propagate across the heart wall. Assume the wall thickness is 10 mm and the propagation speed is  $0.2 \text{ m s}^{-1}$ .

**Problem 25** In an ECG recording, the width of one large square corresponds to 200 ms. A normal heart rate is between 60 and 100 beats  $\text{min}^{-1}$ . The heart rate is usually measured by counting the number of large squares between adjacent QRS complexes.

(a) How many large squares are there for a normal heart rate?

(b) In Fig. 7.30 determine the rate of the atria and of the ventricles.

**Problem 26** Consider Lead II of the normal ECG in Fig. 7.23. The QRS wave and the T wave are both positive. Use a one-dimensional model to convince yourself that the QRS complex and the T wave should have opposite polarities. Why then is the T wave inverted? Find a way to explain the inverted T wave by letting the action potential duration vary between epicardium (outside) and endocardium (inside). On which surface should the duration be longest?

## Section 7.9

**Problem 27** Ohm's law says that  $\mathbf{j} = \sigma \mathbf{E}$ . Draw what  $\mathbf{j}$  and  $\mathbf{E}$  look like (a) in a circuit consisting of a battery and a resistor; (b) for the current flowing when a nerve cell depolarizes.

**Problem 28** Obtain the values for  $\beta$  for a cube of length  $a$  on a side, for a cylinder of radius  $a$  and length  $h$ , and for a sphere of radius  $a$ .

**Problem 29** Show that Eq. 7.36a is the same as Eq. 6.51 by considering the interior of a single cell stretched along the  $x$  axis as in Fig. 6.28. Consider the charge in a small cylindrical region of axoplasm of length  $h$  and radius  $a$ , the cylindrical surface of which is surrounded by cell membrane. Show that the total charge  $Q$  within the axoplasm changes according to

$$\begin{aligned} \frac{\partial Q}{\partial t} &= \pi a^2 h \frac{\partial \rho_i}{\partial t} = C \frac{\partial v_m}{\partial t} + i_m \\ &= 2\pi a h \left( c_m \frac{\partial v_m}{\partial t} + j_m \right), \end{aligned}$$

and that this can be combined with Eq. 7.36a to give

$$\begin{aligned} c_m \frac{\partial v_m}{\partial t} + j_m &= \frac{\pi a^2 h}{2\pi a h} \sigma_i \frac{\partial^2 v_i}{\partial x^2} \\ &= \frac{\sigma_i a}{2} \frac{\partial^2 v_i}{\partial x^2}, \end{aligned}$$

which is the same as Eq. 6.51, except that it is written in terms of  $\sigma_i$ ,  $a$ , and  $h$  instead of  $a$  and  $r_i$ .

**Problem 30** Clark and Plonsey (1968) solved Eq. 7.37 for a cylindrical axon of radius  $a$  using the following method. Assume that the potentials all vary in the  $z$  direction sinusoidally, for instance  $v_m(z) = V \sin(kz)$ , where  $V$  is a constant.

(a) Show that the intracellular and extracellular potentials can be written as

$$\begin{aligned} v_i &= AI_0(kr) \sin(kz) \\ v_o &= BK_0(kr) \sin(kz), \end{aligned} \quad (7.53)$$

where  $I_n$  and  $K_n$  are "modified Bessel functions" obeying the equation

$$\frac{1}{r} \frac{\partial}{\partial r} \left( r \frac{\partial v}{\partial r} \right) - \left( k^2 + \frac{n^2}{r^2} \right) v = 0.$$

(b) Determine the constants  $A$  and  $B$  in terms of  $V$ , using the following two boundary conditions:  $v_m = v_i - v_o$ , and  $\sigma_i(\partial v_i / \partial r) = \sigma_o(\partial v_o / \partial r)$ , both evaluated at  $r = a$ . You will need to use the Bessel function identities  $dI_0(kr)/dr = kI_1(kr)$  and  $dK_0/dr = -kK_1(kr)$ . Clark and Plonsey used this result and Fourier analysis (Chapter 11) to determine  $v_i$  and  $v_o$  when they are not sinusoidal in  $z$ .

**Problem 31** Starting with the bidomain equations, divide Eq. 7.44a by  $\sigma_{ix}$  and 7.44b by  $\sigma_{ex}$ . Now subtract one equation from the other. Under what conditions do the equations contain  $v_m = v_i - v_o$  but not  $v_i$  and  $v_o$  individually?

## Section 7.10

**Problem 32** Verify Eq. 7.47.

**Problem 33** Verify the values given for rheobase and chronaxie in Table 7.1 that are based on Table 6.1.

**Problem 34** An approximation to the error function is given by Abramowitz and Stegun (1972)

$$\begin{aligned} \text{erf}(x) &\approx 1 - \left( 1 + 0.278393x + 0.230389x^2 \right. \\ &\quad \left. + 0.000972x^3 + 0.078108x^4 \right)^{-4}, \quad x > 0. \end{aligned}$$

Calculate  $\text{erf}(x)$  using this approximation for  $x = 0, 0.5, 1.0, 2.0$  and  $\infty$ . Using trial and error, determine the value of  $x$  for which  $\text{erf}(x) = 0.5$ . (See Eq. 7.50.)

**Problem 35** Find the equivalent of Eq. 7.45 in terms of the charge required for the stimulation.

**Problem 36** If the medium has a constant resistance, find the energy required for stimulation as a function of pulse duration.

**Problem 37** A typical pacemaker electrode has a surface area of  $10 \text{ mm}^2$ . What is its resistance into an infinite medium if it is modeled as a sphere? If it is modeled as a disk? (You will have to use results from Chapter 6 and assign a value for  $\sigma_o$ .)

**Problem 38** Equation 6.51 is the cable equation for a nerve axon. Assume that the axon membrane is passive [ $j_m = g_m(v_i - v_o)$ , where  $g_m$  is a constant].

(a) Express the equation in terms of  $v_m$  and  $v_o$  instead of  $v_i$  and  $v_o$ , where  $v_m = v_i - v_o$ .

(b) Divide the resulting equation by  $g_m$ , and then write the cable equation in terms of the time constant  $c_m/g_m$  and the length constant  $1/\sqrt{2\pi a r_i g_m}$ .

(c) Put all the terms containing  $v_m$  on the left side, and terms containing  $v_o$  on the right side. The resulting equation should look like Eq. 6.55, except for a new source term on the right side equal to  $-\lambda^2 \partial^2 v_o / \partial x^2$ . (Measure  $v_m$  with respect to resting potential so  $v_r = 0$  in Eq. 6.55). The negative of this new term has been called the “activating function” (Rattay, 1987). It is useful when studying electrical stimulation of nerves.

**Problem 39** For this problem, use the activating function derived in Problem 38. Assume that  $\lambda$  and  $\tau$  are negligibly small, so that  $v_m$  simply equals the activating function. Consider a point electrode in an infinite, homogeneous volume conductor at distance  $d$  from the axon. The extracellular potential  $v_o$  is  $v_o = (1/4\pi\sigma_o) I/r$ .

(a) Calculate  $v_m$  as a function of position  $x$  along the axon ( $x = 0$  is the closest position to the electrode).

(b) Assume that the axon will fire an action potential if  $v_m$  somewhere along the axon is greater than  $V_{\text{threshold}}$ . Calculate the ratio of the stimulation current  $I$  needed to excite the axon for a cathode (negative electrode) and an anode (positive electrode).

**Problem 40** For this problem, use the activating function derived in Problem 38. An action potential can be excited if a stimulus depolarizes an axon to a value greater than  $V_{\text{threshold}}$ , and a propagating action potential can be blocked if a stimulus hyperpolarizes to a value of  $v_m$  less than  $-V_{\text{block}}$  ( $V_{\text{block}} > V_{\text{threshold}}$ ).

(a) For a cathodal electrode [ $v_o = (1/4\pi\sigma_o) I/r$ ] calculate the ratio of the threshold current to the ratio of the current needed to block propagation.

(b) Use two electrodes (one cathodal and one anodal) to design a stimulator that will result in one-way propagation along the axon (say, propagation only in the positive  $x$  direction, but blocked in the negative  $x$  direction). For an application of such electrodes during functional electrical stimulation, see Ungar et al. (1986).

**Problem 41** For this problem, use the activating function derived in Problem 38, and block by hyperpolarization derived in Problem 40. The factor of  $\lambda^2$  in the activating function implies that larger diameter axons are easier to stimulate than smaller diameter axons. Sometimes you want to excite the smaller fibers without the larger fibers (“physiological recruitment”). Describe qualitatively how you can use a single electrode and block in the hyperpolarized region to obtain physiological recruitment. For a more complete discussion, see Tai and Jiang (1994).

**Problem 42** In “second degree” heart block, the wave front sometimes passes through the conduction system and sometimes does not. Qualitatively sketch the ECG for a heart with second degree block for at least five beats. Specifically include the case where every third wave is blocked. Include the P wave, the QRS wave, and the T wave.

**Problem 43** During “sinus exit block” the SA node functions normally but the wave front fails to propagate from the SA node to the atria. Sketch five beats of an ECG with all beats normal except the third, which undergoes sinus exit block.

**Problem 44** In “sick sinus syndrome” the SA node has a slow and erratic rate. The AV node and conduction system function properly. You plan to implant a pacemaker in the patient. Should it stimulate the atria or the ventricles? Why?

**Problem 45** A patient with “intermittent heart block” has an AV node which functions normally most of the time with occasional episodes of block, lasting perhaps several hours. Design a pacemaker to treat the patient. Ideally, your design will not stimulate the heart when it is functioning normally. Describe

(a) whether you will stimulate the atria or ventricles

(b) which chambers you will monitor with a recording electrode

(c) what logic your pacemaker will use to determine when to stimulate. Your design may be similar to a “demand pacemaker” described in Jeffrey (2001), p. 132.

**Problem 46** The Lapique strength-duration (SD) curve is

$$\frac{i}{i_R} = 1 + \frac{t_C}{t},$$

the SD curve in terms of the error function is

$$\frac{i}{i_R} = \frac{1}{\text{erf}\left(\sqrt{0.228t/t_C}\right)},$$

and the SD curve derived in Ch. 6 Prob. 35 is

$$\frac{i}{i_R} = \frac{1}{1 - e^{-0.693t/t_C}}.$$

(a) Plot all three curves for  $0 < t/t_C < 5$ . Use the equation in Problem 34 to evaluate the error function.

(b) Find approximations for each curve for  $t/t_C \ll 1$ . You may need the Taylor’s series expansions  $e^x \approx 1 + x$  and  $\text{erf}(x) \approx 2x/\sqrt{\pi}$ .

(c) Discuss the physical assumptions that were used to derive each curve.

**Problem 47** Consider a pacemaker delivering 2 mA, 1 V, 1 ms pulse every second. Pacemakers are often powered by a lithium-iodide battery that can deliver a total charge of 2 ampere hours.

- (a) What is the energy per pulse?  
 (b) What is the average power?  
 (c) How long will the battery last?  
 (d) Your answer to (c) is an overestimate of battery lifetime, in part because the battery voltage begins to decline before all its charge has been delivered, and in part because the pacemaker circuitry requires a small, constant current. For this pacemaker, add a constant current drain of  $5\ \mu\text{A}$  and assume that the useful lifetime of the battery is over when 75% of the total charge has been delivered. How long will the battery last in this case?

### Section 7.11

**Problem 48** When measuring the EEG with electrodes distributed according to the 10–20 system, you obtain measurements of the potential difference between the  $i$ th electrode ( $i = 1, \dots, 20$ ) and the reference electrode ( $i = 21$ ). Show that by computing the average reference  $v_i^* = (v_i - v_{20}) - (1/20) \sum_{j=1}^{20} (v_j - v_{20})$ , the resulting values of  $v_i^*$  are independent of the reference potential  $v_{21}$ .

**Problem 49** Consider a very simple model of the EEG: a dipole  $\mathbf{p}$  pointing in the  $z$  direction at the center of a spherical conductor of radius  $R$  and conductivity  $\sigma_o$ . The potential  $v_o$  can be written as the sum of two terms: the potential of a dipole in an unbounded medium plus a potential that obeys Laplace's equation

$$v_o = \frac{p \cos \theta}{4\pi\sigma_o r^2} + Ar \cos \theta$$

where  $r$  and  $\theta$  are in spherical coordinates, and  $A$  is an unknown constant.

(a) Use Appendix L to show that the second term in the expression for  $v_o$  obeys Laplace's equation.

(b) If the region outside the spherical conductor is air (an insulator), determine the value of  $A$  by using the boundary condition that the radial current at the surface of the sphere is zero.

(c) Calculate  $v_o$  as measured at the sphere surface ( $r = R$ ), and determine by what factor  $v_o$  differs from what it would be in the case of an unbounded volume conductor.

**Problem 50** Suppose you measure the EEG potential  $v_j$  at  $N$  locations  $\mathbf{r}_j = (x_j, y_j, z_j)$ ,  $j = 1, \dots, N$ . Assume  $v_j$  is produced by a dipole  $\mathbf{p} = (p_x, p_y, p_z)$  located at the origin. Define

$$R = \sum_{j=1}^N \left[ \frac{p_x x_j + p_y y_j + p_z z_j}{4\pi\sigma (x_j^2 + y_j^2 + z_j^2)^{3/2}} - v_j \right]^2,$$

which measures the least-squares difference between the data and the potential predicted by a single-dipole model. (Chapter 11 explores the least-squares method in greater detail.) The goal is to find the dipole components  $p_x, p_y, p_z$  that fit the data best (minimize  $R$ ).

(a) Minimize  $R$  with respect to  $p_x$  (set  $dR/dp_x = 0$ ) and find an equation relating  $p_x, p_y$ , and  $p_z$ .

(b) Repeat for  $p_y$  and  $p_z$ .

(c) Write the three equations in the form  $\mathbf{A}\mathbf{p} = \mathbf{b}$ , where  $\mathbf{A}$  is a  $3 \times 3$  matrix and  $\mathbf{b}$  is a  $3 \times 1$  vector. Find expressions for the components of  $\mathbf{A}$  and  $\mathbf{b}$ .

(d) If we had not assumed that we knew the location of the dipole, the problem would be much more difficult. Assume the dipole is at location  $\mathbf{r}_p = (x_p, y_p, z_p)$ . Modify  $R$  and then try to minimize it with respect to  $\mathbf{r}_p$ . Carry the calculation far enough to convince yourself that you must now solve nonlinear equations to determine  $\mathbf{r}_p$ . Press et al. (1992) discuss methods for making nonlinear least squares fits.

## References

Abramowitz, M., and I. A. Stegun. (1972). *Handbook of Mathematical Functions with Formulas, Graphs, and Mathematical Tables*. Washington, U.S. Government Printing Office.

Antzelevitch, C., S. Sicouri, A. Lukas, V. V. Nesterenko, D-W. Liu, and J. M. Di Diego (1995). Regional differences of electrophysiology in ventricular cells: physiological and clinical implications. In D. P. Zipes and J. Jalife, eds. *Cardiac Electrophysiology: From Cell to Bedside*, 2nd ed. Philadelphia, Saunders, pp. 228–245.

Barold, S. S. (1985). *Modern Cardiac Pacing*. Mount Kisco, NY, Futura.

Campbell, D. L., R. L. Rasmusson, M. B. Comer, and H. C. Strauss (1995). The cardiac calcium-independent transient outward potassium current: kinetics, molecular properties, and role in ventricular repolarization. In D. P. Zipes and J. Jalife, eds. *Cardiac Electrophysiology: From Cell to Bedside*, 2nd ed. Philadelphia, Saunders, pp. 83–96.

Clark, J. and R. Plonsey (1968). The extracellular potential field of a single active nerve fiber in a volume conductor. *Biophys. J.* **8**: 842–864.

Davidenko, J. M. (1995). Spiral waves in the heart: Experimental demonstration of a theory. In D. P. Zipes and J. Jalife, eds. *Cardiac Electrophysiology: From Cell to Bedside*, 2nd ed. Philadelphia, Saunders, pp. 478–488.

Delmar, M., H. S. Duffy, P. L. Sorgen, S. M. Taffet and D. C. Spray (2004). Molecular organization and regulation of the cardiac gap junction channel connexin43. In D. P. Zipes and J. Jalife, eds. *Cardiac Electrophysiology: From Cell to Bedside*, 4th ed. Philadelphia, Saunders, pp. 66–76.

Geddes, L. A., and J. D. Bourland (1985). The strength-duration curve. *IEEE Trans. Biomed. Eng.* **32**: 458–459.

Gulrajani, R. M. (1998) *Bioelectricity and Biomagnetism*. New York, Wiley.

- Harris, J. W., and H. Stocker (1998). *Handbook of Mathematics and Computational Science*. New York, Springer.
- Henriquez, C. S. (1993). Simulating the electrical behavior of cardiac tissue using the bidomain model. *Crit. Rev. Biomed. Eng.* **21**(1): 1–77.
- Jeffrey, K. (2001). *Machines in Our Hearts*. Baltimore, Johns Hopkins University Press.
- Knisley, S. B., B. C. Hill, and R. E. Ideker (1994). Virtual electrode effects in myocardial fibers. *Biophys. J.* **66**: 719–728.
- Lapicque, L. (1909). Definition experimentale de l'excitabilité. *Comptes Rendus Acad. Sci.* **67**(2): 280–283.
- Lindemans, F. W. and J. J. Denier van der Gon (1978). Current thresholds and liminal size in excitation of heart muscle. *Cardiovasc. Res.* **12**: 477–485.
- Malmivuo, J., and R. Plonsey (1995). *Bioelectromagnetism*. Oxford, Oxford University Press.
- Miller, C. E. and C. S. Henriquez. (1990). Finite element analysis of bioelectric phenomena. *Crit. Rev. Biomed. Eng.* **18**(3): 207–233.
- Mitrani, R. D., L. S. Klein, D. P. Rardon, D. P. Zipes and W. M. Miles (1995). Current trends in the implantable cardioverter–defibrillator. In D. P. Zipes and J. Jalife, eds. *Cardiac Electrophysiology: From Cell to Bedside*, 2nd ed. Philadelphia, Saunders, pp. 1393–1403.
- Moses, H. W., B. D. Miller, K. P. Moulton, and J. A. Schneider (2000). *A Practical Guide to Cardiac Pacing*. 5th ed. Philadelphia, Lippincott Williams and Wilkins.
- Neunlist, M. and L. Tung (1995). Spatial distribution of cardiac transmembrane potentials around an extracellular electrode: Dependence on fiber orientation. *Biophys. J.* **68**: 2310–2322.
- Nunez, P. L. and R. Srinivasan (2005). *Electric Fields of the Brain*. 2nd. ed. Oxford, Oxford University Press.
- Oudit, G. Y., R. J. Ramirez and P. H. Backx (2004). Voltage-regulated potassium channels. In D. P. Zipes and J. Jalife, eds. *Cardiac Electrophysiology: From Cell to Bedside*, 4th ed. Philadelphia, Saunders, pp. 19–32.
- Plonsey, R. (1969). *Bioelectric Phenomena*. New York, McGraw-Hill.
- Press, W. H., S. A. Teukolsky, W. T. Vetterling, and B. P. Flannery (1992). *Numerical Recipes in C: The Art of Scientific Computing*, 2nd ed., reprinted with corrections, 1995. New York, Cambridge University Press.
- Rardon, D. P., W. M. Miles, and D. P. Zipes (2000). Atrioventricular block and dissociation. In D. P. Zipes and J. Jalife, eds. *Cardiac Electrophysiology: From Cell to Bedside*, 3rd ed. Philadelphia, Saunders, pp. 451–459.
- Rattay, F. (1987) Ways to approximate current-distance relations for electrically stimulated fibers. *J. Theor. Biol.* **125**: 339–349.
- Rosenbaum, D. S. and J. Jalife (2001). *Optical Mapping of Cardiac Excitation and Arrhythmias*. Armonk, NY, Futura.
- Roth, B. J. (1992). How the anisotropy of the intracellular and extracellular conductivities influences stimulation of cardiac muscle. *J. Math. Biol.* **30**: 633–646.
- Roth, B. J. (1994). Mechanisms for electrical stimulation of excitable tissue. *Crit. Rev. Biomed. Eng.* **22**(3/4): 253–305.
- Roth, B. J. (1997). Electrical conductivity values used with the bidomain model of cardiac tissue. *IEEE Trans. Biomed. Eng.* **44**: 326–328.
- Roth, B. J. and J. P. Wikswo, Jr. (1994). Electrical stimulation of cardiac tissue: A bidomain model with active membrane properties. *IEEE Trans. Biomed. Eng.* **41**(3): 232–240.
- Rudy, Y. and J. E. Burnes (1999). Noninvasive electrocardiographic imaging. *Ann. Noninvasive Electrocardiol.* **4**(3): 340–359.
- Sepulveda, N. G., B. J. Roth, and J. P. Wikswo, Jr. (1989). Current injection into a two-dimensional anisotropic bidomain. *Biophys. J.* **55**: 987–999.
- Stanley, P. C., T. C. Pilkington, and M. N. Morrow (1986). The effects of thoracic inhomogeneities on the relationship between epicardial and torso potentials. *IEEE Trans. Biomed. Eng.* **33**(3): 273–284.
- Tai, C., and D. Jiang (1994). Selective stimulation of smaller fibers in a compound nerve trunk with single cathode by rectangular current pulses. *IEEE Trans. Biomed. Eng.* **41**: 286–291.
- Trayanova, N., C. S. Henriquez, and R. Plonsey (1990). Limitations of approximate solutions for computing extracellular potential of single fibers and bundle equivalents. *IEEE Trans. Biomed. Eng.* **37**(1): 22–35.
- Ungar, I. J., J. T. Mortimer, and J. D. Sweeney (1986). Generation of unidirectionally propagating action potentials using a monopolar electrode cuff. *Ann. Biomed. Eng.* **14**: 437–450.
- Voorhees, C. R., W. D. Voorhees III, L. A. Geddes, J. D. Bourland, and M. Hinds (1992). The chronaxie for myocardium and motor nerve in the dog with surface chest electrodes. *IEEE Trans. Biomed. Eng.* **39**(6): 624–628.
- Watanabe, A., and H. Grundfest (1961). Impulse propagation at the septal and commissural junctions of crayfish lateral giant axons. *J. Gen. Physiol.* **45**: 267–308.
- Wikswo, J. P., Jr. (1995). Tissue anisotropy, the cardiac bidomain, and the virtual cathode effect. In D. P. Zipes and J. Jalife, eds. *Cardiac Electrophysiology: From Cell to Bedside*, 2nd ed. Philadelphia, Saunders, pp. 348–361.



# 8

## Biomagnetism

The field of *biomagnetism* has exploded in recent decades. Magnetic signals have been detected from the heart, brain, skeletal muscles, and isolated nerve and muscle preparations. Measurements of the magnetic susceptibility of the lung show the effect of dust inhalation. Susceptibility measurements of the heart can determine blood volume, while the susceptibility of the liver can measure iron stores in the body. Bacteria and some animals contain aggregates of magnetic particles, often attached to neural tissue. Bacteria use these magnetic particles to determine which way is down. Magnetism is used for orientation by birds and other animals.

Sections 8.1 and 8.2 review the basics of magnetism. Section 8.3 calculates the magnetic field of an axon in an infinite conducting medium. This result, which shows that the field is due primarily to the current dipole in the interior of the axon, is approximately true for the magnetocardiogram and evoked responses from the brain, described in Secs. 8.4 and 8.5.

Section 8.6 reviews electromagnetic induction. Section 8.7 describes the use of varying magnetic fields to stimulate nerves or muscles. Section 8.8 introduces diamagnetic, paramagnetic, and ferromagnetic materials and describes biomagnetic effects that depend on magnetic materials. Section 8.9 reviews instrumentation for measuring these weak magnetic signals.

### 8.1 The Magnetic Force on a Moving Charge

Lodestone, compass needles, and other forms of magnetism have been known for centuries, but it was not until 1820 that Hans Christen Oersted showed that an electric current could deflect a compass needle. We now know that magnetism results from electric forces that moving

charges exert on other moving charges and that the appearance of the magnetic force is a consequence of special relativity. An excellent development of magnetism from this perspective is found in Purcell (1985). The development here is more traditional and is incomplete.

Suppose that a beam of electrons is accelerated in a cathode-ray tube (as in an oscilloscope, computer display, or television receiver) and causes a spot of light to be emitted where it strikes a fluorescent screen. The electron source is cathode  $C$  in Fig. 8.1. The accelerating electrode is  $E$ . The fact that the beam is accelerated toward a positively charged electrode confirms that the electrons are negatively charged. The beam normally strikes the screen at point  $X$ . Placing a battery between plates  $A$  and  $B$  creates an electric field that deflects the beam as it passes between the plates. If plate  $A$  is positively charged, the beam is deflected upward to point  $Y$ . If the battery is removed and the north pole of a bar magnet is brought to the position shown, the beam is deflected to point  $Z$ .

We say that a *magnetic field* exists in the space surrounding the bar magnet and that the direction of the magnetic field at any point is the direction a small compass needle located there would point. Experiment shows that the force is at right angles to both the direction of the magnetic field and the velocity of the charged particle. Detailed experiments show that the magnitude of the force  $\mathbf{F}$  is proportional to the charge, the magnitude of the velocity  $\mathbf{v}$ , and the strength of magnetic field  $\mathbf{B}$ . (In fact, modern definitions of the magnetic field are based on this proportionality.) The magnitude of the force is greatest when  $\mathbf{v}$  and  $\mathbf{B}$  are perpendicular. We have seen a relationship like this between three vectors before: the vector product or cross product, which was associated with torque and defined in Sec. 1.4. We write

$$\mathbf{F} = q(\mathbf{v} \times \mathbf{B}). \quad (8.1)$$

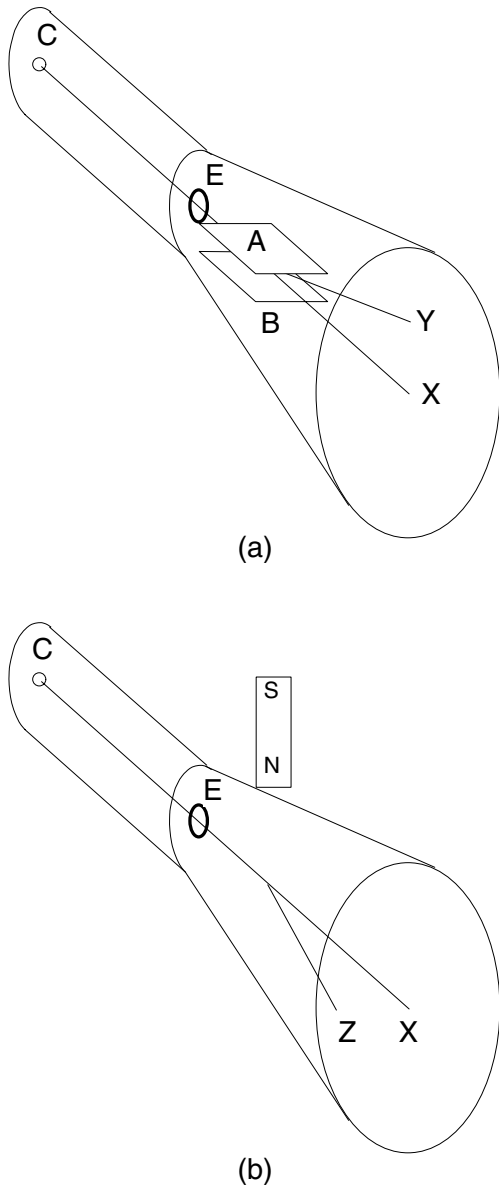


FIGURE 8.1. An electron beam generated at cathode  $C$  and accelerated through electrode  $E$  strikes the fluorescent screen on the right. (a) A positive charge on plate  $A$  and negative charge on plate  $B$  deflects the beam from  $X$  to  $Y$ . (b) A bar magnet brought close as shown deflects the beam to point  $Z$ .

The SI unit of  $\mathbf{B}$  is the tesla, T. An earlier name was the weber per square meter. The cgs unit is the gauss, G:  $1 \text{ T} = 10^4 \text{ G}$ . If a coordinate system is set up so that  $\mathbf{v}$  is along the  $x$  axis and  $\mathbf{B}$  is along the  $y$  axis, then  $\mathbf{v} \times \mathbf{B}$  and the force on a positive charge are along the  $+z$  axis. For negatively charged electrons  $\mathbf{F}$  is in the opposite direction. Combining Eq. 8.1 with the electric force gives the full expression for the electromagnetic force, often called the *Lorentz force*:

$$\mathbf{F} = q(\mathbf{E} + \mathbf{v} \times \mathbf{B}). \tag{8.2}$$

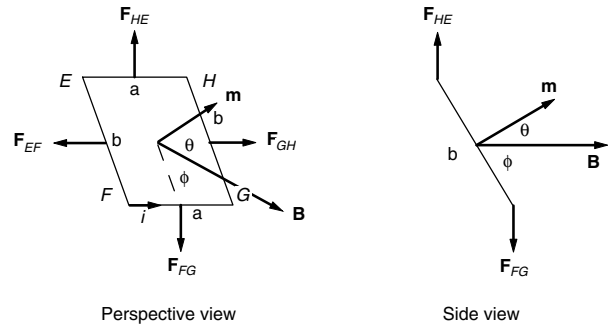


FIGURE 8.2. A current-carrying loop is in a uniform magnetic field. The dashed line from the center of the loop to the center of edge  $FG$ , vector  $\mathbf{B}$  and vector  $\mathbf{m}$  all lie in the same plane. The sum of angles  $\theta$  and  $\phi$  is  $\pi/2$ . The forces on opposite sides add to zero. There is a torque on the loop unless its plane is perpendicular to the field ( $\phi = \pi/2$ ). The magnetic moment  $\mathbf{m}$  is perpendicular to the plane of the loop.

Since current in a wire is the result of moving charges, there is a force on a segment of wire carrying a current. Suppose that there are  $C$  particles per unit volume, each with charge  $q$ , drifting with speed  $v$  along a segment of wire of length  $ds$  and cross-sectional area  $S$ . In time  $dt$  the total charge passing a given plane is  $CvqSdt$  [see Eq. 4.11] so that the current is  $i = CvqS$ . If there is a magnetic field perpendicular to the wire, the magnitude of the force on each particle is  $qvB$  and the total force is  $CS ds qvB = iB ds$ . If vector  $ds$  is defined along the wire in the direction of the positive current, then the contribution to the magnetic force from this segment of the wire is

$$d\mathbf{F} = i(ds \times \mathbf{B}). \tag{8.3}$$

If a small rectangular loop of wire is placed in a uniform magnetic field and a current is made to flow in the wire, there is a magnetic force on each arm of the loop. (The current can be led to and from the rectangle by two parallel closely spaced wires, in which the forces cancel because the currents are in opposite directions. Forces not considered here maintain the position of the loop.)

Figure 8.2 shows the orientation of the loop in the horizontal magnetic field. The magnetic moment  $\mathbf{m}$  is perpendicular to the loop and makes an angle  $\theta$  with the direction of  $\mathbf{B}$ . Sides  $HE$  and  $FG$  are of length  $a$  and perpendicular to the field. The other two sides have length  $b$ . The force on side  $EF$  has magnitude  $iBb \sin \phi$  and is directed as shown. Side  $GH$  has a force of equal magnitude in the opposite direction. On side  $FG$  the force is down and on side  $HE$  it is up, both with magnitude  $iBa$ . The vector sum of all the forces is zero. There is a torque, however. If the torque is taken about the center of the loop, the  $FG$  force and  $HE$  force each exert a torque of magnitude  $(iBa)(b/2) \cos \phi$ . The total torque is therefore  $iBab \cos \phi$ . The loop is said to have a magnetic moment  $\mathbf{m}$  of magnitude  $iS$ , where  $S = ab$  is the area of the loop. Vector  $\mathbf{m}$  is defined to point perpendicular to the loop in

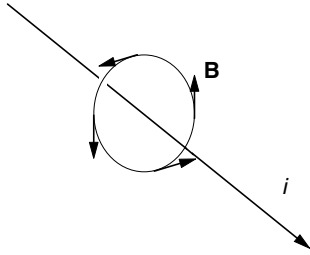


FIGURE 8.3. The magnetic field around a current-carrying wire is at right angles to the wire and the perpendicular from the observation point to the wire. The magnitude is inversely proportional to the distance from the wire.

the direction of the thumb of the right hand when the fingers curl in the direction of the current around the loop. The units of  $\mathbf{m}$  are  $\text{A m}^2$  or  $\text{J T}^{-1}$ . In terms of angle  $\theta$  between  $\mathbf{m}$  and  $\mathbf{B}$ , the torque  $\tau$  exerted by the magnetic field on the magnetic moment has magnitude  $iabB \sin \theta$ , so

$$\tau = \mathbf{m} \times \mathbf{B}. \tag{8.4}$$

The torque is zero when  $\mathbf{m}$  and  $\mathbf{B}$  are parallel or antiparallel. When they are parallel the equilibrium is stable: if there is a small rotation of  $\mathbf{m}$  the torque acts to return it to equilibrium. When they are antiparallel, the equilibrium is unstable.

A small current loop can be used to test for the presence of a magnetic field. At equilibrium  $\mathbf{m}$  points in the same direction that a small compass needle would point and gives the direction of  $\mathbf{B}$ . Measuring the torque for a known displacement of  $\mathbf{m}$  from this direction gives the magnitude of  $\mathbf{B}$ .

## 8.2 The Magnetic Field of a Moving Charge or a Current

### 8.2.1 The Divergence of the Magnetic Field Is Zero

With a compass needle or small sensing coil we can in principle map the magnetic field surrounding a bar magnet or a wire carrying a current. If we examine the field near a long straight wire carrying current  $i$ , we find that  $\mathbf{B}$  is always at right angles to the wire and at distance  $r$  has magnitude

$$B = \frac{\mu_0 i}{2\pi r}. \tag{8.5}$$

The constant  $\mu_0$  is analogous to  $\epsilon_0$  in electrostatics and is exactly  $4\pi \times 10^{-7} \text{ T m A}^{-1}$  (or  $\Omega \text{ s m}^{-1}$ ). Figure 8.3 shows the direction of  $\mathbf{B}$  at various locations around a wire. The direction of the force is consistent with Eq. 8.2 if the direction of  $\mathbf{B}$  is defined to be the direction in which the fingers of the right hand curl when the thumb points along the wire in the direction of the (positive) current.

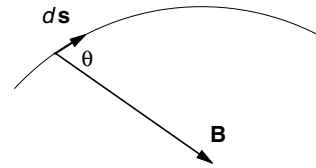


FIGURE 8.4. The line integral of  $\mathbf{B} \cdot d\mathbf{s}$  is calculated by multiplying  $d\mathbf{s}$  by the component of  $\mathbf{B}$  parallel to  $d\mathbf{s}$ , that is  $B \cos \theta$ .

Close to the wire  $\mathbf{B}$  is always at right angles to the wire, in contrast to the electric field, which close to a charge always points toward or away from it. In the electric case, the flux of  $\mathbf{E}$  through a closed surface is proportional to the charge within the volume enclosed by the surface (Gauss's law). In contrast, the flux of  $\mathbf{B}$  through a closed surface is always zero. In the notation of Sec. 4.1,

$$\iint_{\text{closed surface}} B_n dS = \iint_{\text{closed surface}} \mathbf{B} \cdot d\mathbf{S} = 0. \tag{8.6}$$

If single magnetic charges (magnetic monopoles) existed, the flux would be proportional to the magnetic charge within the volume. Magnetic monopoles have never been observed, in spite of considerable effort to find them.

As in the electric case, we can construct lines of  $\mathbf{B}$ . The tangent to the line always points in the direction of  $\mathbf{B}$ . For the long wire, the lines of  $\mathbf{B}$  are circles. One can show from Eq. 8.6 that lines of  $\mathbf{B}$  always close on themselves.

Equation 8.6 has the form of the continuity equation, Eq. 4.4, with  $\mathbf{B}$  substituted for  $\mathbf{j}$  and with  $C = 0$ . The differential version of Eq. 8.6 can therefore be obtained from Eq. 4.8. It is

$$\text{div } \mathbf{B} = \nabla \cdot \mathbf{B} = 0. \tag{8.7}$$

### 8.2.2 Ampere's Circuital Law

It is also interesting to consider the line integral of  $\mathbf{B}$  around a closed path. That is, for any element of the path  $d\mathbf{s}$  shown in Fig. 8.4 take the projection of  $\mathbf{B}$  in the direction of  $d\mathbf{s}$ ,  $B \cos \theta$ . Sum up all the contributions  $B \cos \theta ds$  along the entire closed path. For path  $ABCD$  in Fig. 8.5(a), the result is zero. The reason is that  $B \cos \theta ds$  is zero on segments  $AB$  and  $CD$ . On segment  $DA$  it is  $(\mu_0 i / 2\pi a)(a\phi) = \mu_0 i \phi / 2\pi$ , while on segment  $BC$  it is  $-(\mu_0 i / 2\pi b)(b\phi) = -\mu_0 i \phi / 2\pi$ . In Fig. 8.5(b) the path is circular with the wire at the center, and the line integral is  $B(2\pi a) = \mu_0 i$ . This result is general:

$$\oint B \cos \theta ds = \oint \mathbf{B} \cdot d\mathbf{s} = \mu_0 i. \tag{8.8}$$

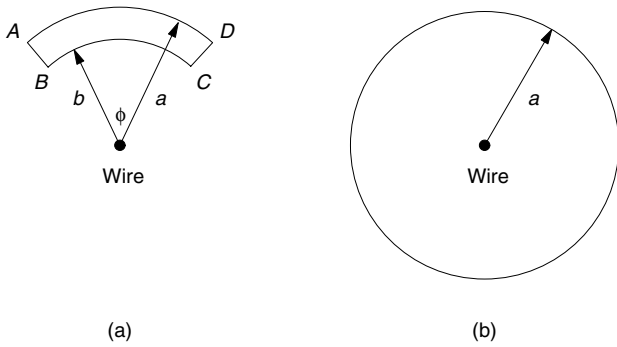


FIGURE 8.5. Two paths of integration. In (a) the path does not encircle the wire carrying the current, and  $\oint \mathbf{B} \cdot d\mathbf{s} = 0$ . In (b) the path encircles the wire and  $\oint \mathbf{B} \cdot d\mathbf{s} = \mu_0 i$ .

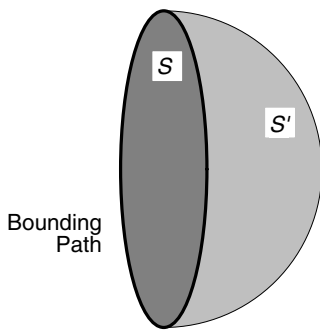


FIGURE 8.6. Since the total current or flux of  $\mathbf{j}$  through any closed surface is zero, the current through surface  $S$  is equal to the current through surface  $S'$ .

The circle on the integral sign means that the integral is taken around a closed path. The line integral of the magnetic field around a closed path is equal to  $\mu_0$  times the current through a circuit enclosed by that path. If two wires carrying equal and opposite currents are enclosed by the path of the line integral, the integral is zero. It does *not* mean that  $\mathbf{B}$  is zero everywhere on the path.

A more general statement is that for steady currents the line integral of  $\mathbf{B}$  around a closed path is equal to the integral of the current density  $\mathbf{j}$  through any surface enclosed by the path:

$$\oint \mathbf{B} \cdot d\mathbf{s} = \mu_0 \iint \mathbf{j} \cdot d\mathbf{S}. \quad (8.9)$$

This is known as *Ampere's circuital law*. Like Gauss's law, it is always true but not always useful. It is true for currents that do not vary with time, but it can be used to calculate the magnetic field only if symmetry can be used to argue that  $\mathbf{B}$  is always parallel to the path and has the same magnitude at all points on the path.

The surface used to calculate the right-hand side can be any surface bounded by the path used on the left. Since we are dealing with steady currents for which there is no charge accumulation, the continuity equation, Eq.

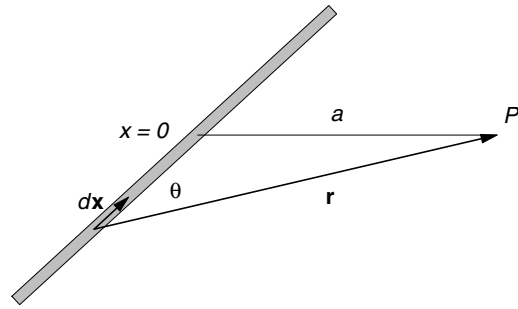


FIGURE 8.7. The Biot–Savart law is used to calculate the magnetic field at point  $P$  due to an infinite wire.

4.4, shows that the flux of  $\mathbf{j}$  (the total current) through any closed surface is zero. Two surfaces  $S$  and  $S'$ , both bounded by the path, form a closed surface as shown in Fig. 8.6. The total current through surface  $S$  is the same as the total current through  $S'$ .

### 8.2.3 The Biot-Savart Law

In situations where the symmetry of the problem does not allow the field to be calculated from Ampere's law, it is possible to find the field due to a steady current in a closed circuit using the *Biot–Savart* law. The contribution  $d\mathbf{B}$  to the magnetic field from current  $i$  flowing along a line element  $d\mathbf{s}$  is

$$d\mathbf{B} = \frac{\mu_0 i}{4\pi} \frac{d\mathbf{s} \times \mathbf{r}}{r^3}. \quad (8.10)$$

Vector  $\mathbf{r}$  is from the current element to the point where the field is to be calculated. The field is found by integrating over the *entire circuit*.

Figure 8.7 shows how this integration is done for an infinitely long straight wire along the  $x$  axis. The contribution at point  $P$  is obtained by dropping a perpendicular from  $P$  to the wire to define  $x = 0$ . The distance from  $P$  to the wire is  $a$ . The contribution from an element  $dx$  at point  $x$  is

$$dB = \frac{\mu_0 i}{4\pi} \frac{dx \sin \theta}{r^2} = \frac{\mu_0 i}{4\pi} \frac{a dx}{r^3}.$$

Since  $r^2 = a^2 + x^2$  the total field is

$$\begin{aligned} B &= \frac{\mu_0 i}{4\pi} \int_{-\infty}^{\infty} \frac{a dx}{(a^2 + x^2)^{3/2}} \\ &= \frac{\mu_0 i a}{4\pi} \left[ \frac{x}{a^2(x^2 + a^2)^{1/2}} \right]_{-\infty}^{\infty} = \frac{\mu_0 i}{2\pi a}. \end{aligned}$$

This agrees with Eq. 8.5 and the result obtained using Ampere's circuital law.

A steady current from a point source that spreads uniformly in all directions generates no magnetic field. To see why, consider Fig. 8.8. The source of current is at  $O$ . The magnetic field at  $P$  can be calculated using the Biot–Savart law. For any element  $d\mathbf{s}$  a symmetric element  $d\mathbf{s}'$

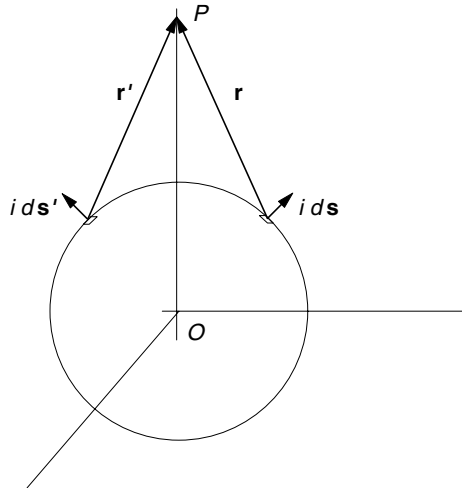


FIGURE 8.8. The magnetic field from a spherically symmetric radial distribution of current is zero. The source at  $O$  sends current uniformly in all directions.  $P$  is the observation point. For any element  $ds$  there is a corresponding  $ds'$  such that  $ds \times \mathbf{r} = -ds' \times \mathbf{r}'$ . The current through a small area  $dA$  around  $ds$  is  $i$ . The same current flows through a corresponding area around  $ds'$ . Can you obtain the same result by a symmetry argument?

can be selected, such that  $ds \times \mathbf{r} = -ds' \times \mathbf{r}'$ . Associated with each element is a small area  $dA$ , and the current along  $ds$  is  $i = j dA$ . We can set  $dA = dA'$  so  $i$  is the same in each case. Therefore,  $B = 0$ . (This can also be shown using Ampere's law; see Problem 10.)

#### 8.2.4 The Displacement Current

Derivation of Ampere's law requires that there be no charge buildup, so that the total current through a closed surface is zero. However, we will consider an action potential in which the membrane capacitance charges and discharges. To see how this affects Ampere's law, consider current  $i$  charging the two shaded capacitor plates in Fig. 8.9. The area of each capacitor plate is  $A$ . The region between the plates, of thickness  $b$ , is filled with dielectric of dielectric constant  $\kappa$ . The integral  $\iint \mathbf{j} \cdot d\mathbf{S}$  is  $i$  for surface  $S$  and zero for surface  $S'$ . Because of the current, the charge density  $\sigma$  on the left-hand plate is increasing at a rate given by  $i = Ad\sigma/dt$ , while on the right-hand plate the charge is decreasing because  $i = -Ad\sigma/dt$ . Since the electric field between the plates is  $E = \sigma/\kappa\epsilon_0$  we can say that  $i = Ad(\kappa\epsilon_0 E)/dt$ . The quantity  $D = \kappa\epsilon_0 E$  is called the *electric displacement*, and

$$j_d = \frac{\partial D}{\partial t}$$

is called the *displacement current density*. More careful consideration shows that Ampere's law is valid when

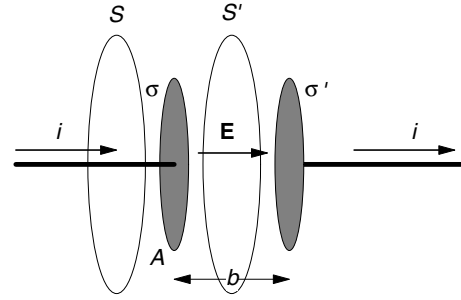


FIGURE 8.9. A wire and capacitor plates are shown. The integral of the current density through surface  $S$ , which is pierced by the wire, is  $i$ . Through surface  $S'$ , which is between the capacitor plates, the integral is zero. If the displacement current density is included, both surface integrals are the same. (If surfaces  $S$  and  $S'$  are not large enough, there is also a net displacement current through  $S$ , as can be seen from Fig. 8.10.)

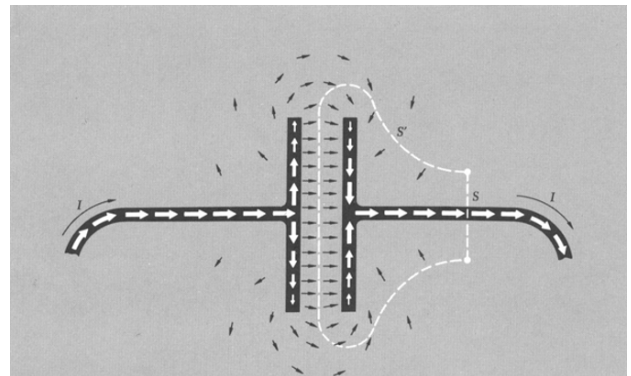


FIGURE 8.10. The conduction current (white arrows) and displacement current (black arrows) in a discharging capacitor are shown. The conduction current decreases with distance out the capacitor plates. The displacement current includes the fringing field. [From E. M. Purcell. *Electricity and Magnetism*, 2nd ed. Berkeley Physics Series, Vol. 2. New York, McGraw-Hill, 1985. Used by permission.]

there is charge buildup if we replace  $\mathbf{j}$  by  $\mathbf{j} + \mathbf{j}_d$ :

$$\oint \mathbf{B} \cdot d\mathbf{s} = \mu_0 \iint (\mathbf{j} + \mathbf{j}_d) \cdot d\mathbf{S}. \quad (8.11)$$

With this change, if  $S$  and  $S'$  are circles of radius  $a$ , Ampere's law gives  $B = \mu_0 i / 2\pi a$  for either one. (The radius of the circle must be very large; see the discussion in the next paragraph.)

What current should be used in the Biot-Savart law? A very surprising answer is that as long as the fields are relatively slowly varying (so that the emission of radio waves is not important), the displacement current contributes nothing. We are free to include it or ignore it. Purcell (1985, p. 328) and Shadowitz (1975, p. 416) discuss why this is so. It is not always easy to calculate the entire displacement current. For example, Fig. 8.10 shows how the conduction current and displacement current vary when

current charges a capacitor. Notice that some of the displacement current flows to and from the back sides of the capacitor plates. This is why we said in the previous paragraph that the radius of the curve defining surfaces  $S$  and  $S'$  must be very large in order that one surface have no net flux of displacement current and the other have all of it. Whatever their size, however, Eq. 8.11 is valid.

It was mentioned above that a steady current from a point source that spreads uniformly in all directions generates no magnetic field according to the Biot–Savart law. Yet any circular loop has current flowing through it, so Ampere’s law suggests that there is a field. The discrepancy is resolved by noting that the current comes from a charge  $q$  at the origin that is being drained off by  $i = -dq/dt$ . This gives rise to a displacement current  $\mathbf{j}_d$  that cancels  $\mathbf{j}$  (see Problem 10).

### 8.3 The Magnetic Field Around an Axon

We can use the Biot–Savart law to calculate the magnetic field due to an action potential propagating down an infinitely long axon stretched along the  $x$  axis and embedded in an infinite homogeneous conducting medium. Section 7.1 showed that there are three components to the current:  $i_i$  along the interior of the axon,  $di_o$  out through the membrane (including both displacement current and conduction current), and current in the surrounding medium.

The principle of superposition allows us to calculate the field due to the exterior current by finding the magnetic field  $d\mathbf{B}$  from current  $di_o$  into the surrounding medium from axon element  $dx$ , and then integrating along the axon.

We saw in Chapter 7 that the current in the *external* medium from a small element  $dx$  flows uniformly in all directions from a point source. We learned in the preceding section that the magnetic field generated by a spherically symmetric radial current is zero. Therefore, in the approximation that the axon is very thin, we can ignore the external current from each element  $dx$ . We can do this only because the medium is infinite, homogeneous, and isotropic. When the exterior conductor has boundaries or structure, the symmetry is broken and the external currents contribute to the magnetic field. Our calculation breaks down very close to the axon. Distortions from the field due to the external current because the axon is not infinitely thin are about 1% close to the axon. The current through the cell membrane gives a very small contribution to the magnetic field—roughly 1 part in  $10^6$ .

The major contribution is therefore from  $i_i$ . We use the law of Biot–Savart, Eq. 8.10. The observation point is in the  $xy$  plane at  $(x_0, y_0, 0)$  and the axon lies along the  $x$  axis so that  $d\mathbf{s} = \hat{\mathbf{x}} dx$ , as shown in Fig. 8.11. The

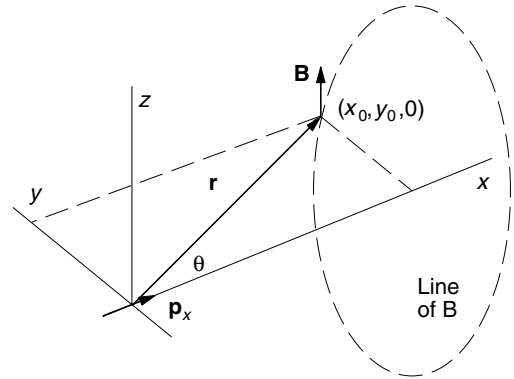


FIGURE 8.11. The geometry for calculation of the magnetic field due to a current element  $i dx$  or current dipole  $p_x$  stretched along the  $x$  axis.

product  $d\mathbf{s} \times \mathbf{r}$  can be evaluated using Eq. 1.8 or 1.9:

$$d\mathbf{s} \times \mathbf{r} = \begin{vmatrix} \hat{\mathbf{x}} & \hat{\mathbf{y}} & \hat{\mathbf{z}} \\ dx & 0 & 0 \\ x_0 - x & y_0 & 0 \end{vmatrix} = dx y_0 \hat{\mathbf{z}}.$$

The term in the denominator is  $r^3 = [(x_0 - x)^2 + y_0^2]^{3/2}$ . The magnetic field in the  $xy$  plane is in the  $z$  direction and has magnitude

$$B_z = \frac{\mu_0 y_0}{4\pi} \int \frac{i_i(x) dx}{[(x_0 - x)^2 + y_0^2]^{3/2}}.$$

It was shown in Eq. 7.17 that  $i_i = -\pi a^2 \sigma_i (dv_i/dx)$ . The final expression for  $B_z$  is

$$B_z = -\frac{\mu_0 a^2 \sigma_i y_0}{4} \int \frac{[dv_i(x)/dx] dx}{[(x_0 - x)^2 + y_0^2]^{3/2}}. \quad (8.12)$$

The computer program in Fig. 8.12 evaluates the field for the same crayfish axon whose external potential was studied in Sec. 7.4. The field at a distance  $2a$  from the axon is plotted in Fig. 8.13. Again, the results agree well with more sophisticated calculations [Swinney and Wikswo (1980); Woosley *et al.* (1985)]. The latter reference is particularly clear and should be accessible to those who have studied the convolution integral in Chapter 12. A three-dimensional plot of their results is shown in Fig. 8.14.

It is worth repeating that a calculation this simple succeeds only because the axon and the exterior medium are infinite. If there are boundaries, or if there are regions in the external medium where the conductivity changes, then current in the external medium does contribute to the magnetic field. For example, an isolated nerve preparation in air would have the external current flowing in a thin layer of ionic solution along the outside of the axon, where it would generate a field that almost completely cancels that from  $i_i$ .

An approximation valid at large distances can be obtained from Eq. 8.12 by expanding the denominator in

```

/*This program integrates to obtain the magnetic field for a problem which was first solved by K. R. Swinney and J. P. Wikswo, the extracellular magnetic field of the single active nerve fiber in a volume conductor. Biophys. J. 32:719-732 (1980). The nerve pulse is a series of Gaussians used by Clark and Plonsey to fit the data of Watanabe and Grandfest, J. Gen. Physiol. 45:267 (1961). Uses Romberg integration routine gromb from W. H. Press et al. Numerical Recipes in C.*/

#include <stdio.h>
#include <stdlib.h>
#include <math.h>
#include "nr.h"

/*Global Variables*/
const double pi = 3.14159265359;
double x0, y0, //coordinates of observation point
A[3], B[3], C[3]; //parameters for gaussian
float f(float x)
{
/*Calculates the integrand dv/dx divided by r^3*/
double xx, r, dv;
int i;
dv = 0;
for (i=0; i<3; i++)
{ xx = B[i] * (x - C[i]);
dv = dv - 2 * A[i] * B[i] * xx * exp(-xx * xx);}
r = sqrt((x0 - x) * (x0 - x) + y0 * y0);
return dv / (r * r * r);
}

void main()
{ FILE *ofp; //output file pointer
const double Mu0 = 4.0e-7 * pi; //permeability free space
axonradius = 6.0e-5;
xstart = 0.0;
xfinish = 0.020;
double integral, MagField, y[4];
//Calculate at four different distances //from axon
int i;

if (!(ofp = fopen("OutputFile", "w")))
{ printf("cannot open output file\n"); exit(1); }
A[0] = 0.051;
A[1] = 0.072;
A[2] = 0.018;
B[0] = 800;
B[1] = 533;
B[2] = 333;
C[0] = 0.0054;
C[1] = 0.0066;
C[2] = 0.0086;
y[0] = 2 * axonradius;
y[1] = 0.001;
y[2] = 0.003;
y[3] = 0.01;
printf("%12.5g %12.5g %12.5g %12.5g\n", y[0], y[1], y[2], y[3]);
fprint(ofp, "%12.5g %12.5g %12.5g %12.5g\n", y[0], y[1], y[2], y[3]);
for(x0 = xstart; x0<xfinish; x0+=0.00025)
{ printf("%12.5f", x0);
fprint(ofp, "%12.5f", x0);
for(i=0; i<4; i++)
{ y0 = y[i];
integral = gromb(f, xstart, xfinish);
MagField = -Mu0 * axonradius * axonradius * y0 * integral / 4.0;
printf("%12.5e", MagField);
fprint(ofp, "%12.5e", MagField);
printf("\n");
fprint(ofp, "\n");
}
fclose(ofp);
}
}

```

FIGURE 8.12. The program used to calculate the magnetic field outside an axon in an infinite homogeneous conductor using Eq. 8.12. It uses the Romberg integration routine `gromb` from Press *et al.* (1992).

much the same way we did to obtain Eqs. 7.26 and 7.27. The observation point is  $(R, \theta)$  in the  $xy$  plane. In this case we need the expansion of

$$\frac{1}{r^3} = \frac{1}{R^3} \left( 1 - 2\frac{x}{R} \cos \theta + \frac{x^2}{R^2} \right)^{-3/2} \approx \frac{1}{R^3} \left( 1 + \frac{3x \cos \theta}{R} + \dots \right).$$

The final result is

$$B_z = \frac{\mu_0 \pi a^2 \sigma_i \sin \theta}{4\pi R^2} (v_i(x_1) - v_i(x_2)) + \frac{\mu_0 \pi a^2 \sigma_i 3 \sin \theta \cos \theta}{4\pi R^3} \left[ xv_i(x) \Big|_{x_1}^{x_2} + \int_{x_1}^{x_2} v_i(x) dx \right]. \tag{8.13}$$

The first term is proportional to the current dipole,  $\mathbf{p}$  defined for the depolarization in the previous chapter. For a complete pulse the first term vanishes and the second term is used.

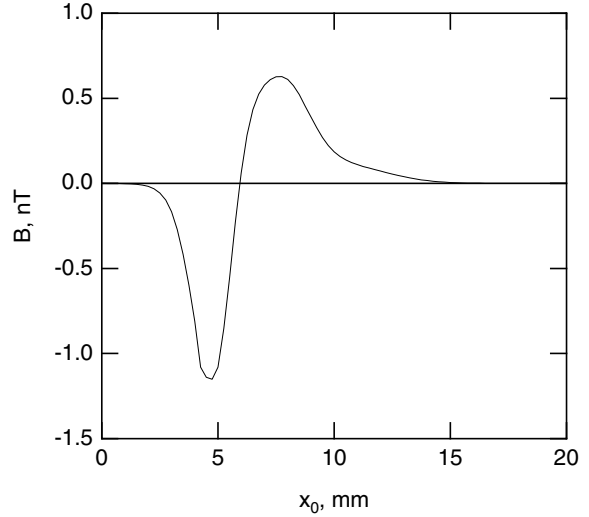


FIGURE 8.13. The magnetic field  $B_z$  0.12 mm from a crayfish axon in an infinite homogeneous conducting medium is shown. The field was calculated using the program of Fig. 8.12. The exterior potential for this configuration was calculated in Sec. 7.4.

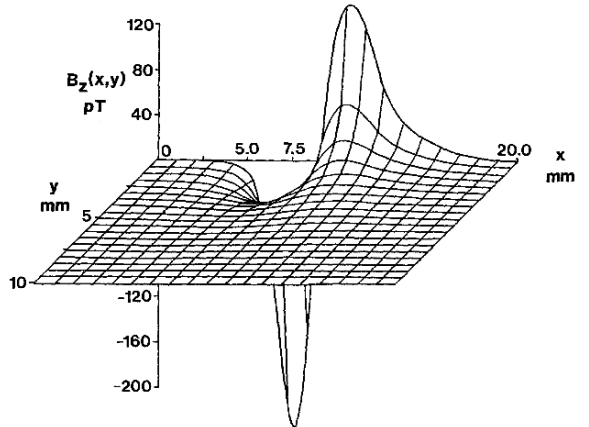


FIGURE 8.14. A three-dimensional plot of the magnetic field around the crayfish axon. The minimum distance from the axon is 0.5 mm.

## 8.4 The Magnetocardiogram

It is now feasible to measure magnetic fields arising from the electrical activity of the heart (the *magnetocardiogram* or *MCG*) and the brain (the *magnetoencephalogram* or *MEG*). The models developed in Sec. 8.3 and in Chapter 7 can be used to compare the electric and magnetic signals from a current dipole  $\mathbf{p}$ . The instrumentation for these measurements is described in Sec. 8.9.

For a single cell at the origin in a homogeneous conducting medium, the exterior potential at observation

point  $\mathbf{r}$  is given by Eq. 7.13:

$$v = \frac{\mathbf{p} \cdot \mathbf{r}}{4\pi\sigma_o r^3}.$$

The current dipole  $\mathbf{p}$  points along the cell in the direction of the advancing depolarization wave and has magnitude [Eq. 7.12]  $p = \pi a^2 \sigma_i \Delta v_i$ . An expression analogous to Eq. 7.13 describes the magnetic field of a depolarizing cell. We consider the field due to current along the  $x$  axis and then generalize the result. The derivation begins with Eq. 8.13 and uses the geometry of Fig. 8.11. The region of depolarization occupies only a millimeter or so along the cell. Since the measurements are made much farther away, the denominator can be removed from the integral, which is then just  $\int (dv/dx) dx$ . If the depolarization is at the origin, then the expression for  $B_z$  for  $z = 0$  is

$$B_z = -\frac{\mu_0 a^2 \sigma_i y_0 [v(x_2) - v(x_1)]}{4(x_0^2 + y_0^2)^{3/2}} = \frac{\mu_0}{4\pi} \frac{p y_0}{(x_0^2 + y_0^2)^{3/2}}. \quad (8.14)$$

Figure 8.11 shows that  $y_0 = r \sin \theta$ , so that  $p y_0 = p r \sin \theta = |\mathbf{p} \times \mathbf{r}|$ . The direction of  $\mathbf{B}$  is also consistent with the cross product. Generalizing, we have for a single cell,

$$\mathbf{B} = \mu_0 \frac{\mathbf{p} \times \mathbf{r}}{4\pi r^3}. \quad (8.15)$$

Note the remarkable similarity between Eqs. 7.13 and 8.15. One involves the dot product, and the other the cross product. For both, the field falls as  $1/r^2$ . If we are considering the cardiogram, either field from the entire heart is the superposition of the field from many cells. As with the electrocardiogram, the first approximation for the magnetocardiogram is to ignore changes in  $1/r^2$  and speak of the total current-dipole vector.

Measurements of either the potential or the magnetic field can be used to determine the location of  $\mathbf{p}$ . We will adopt the coordinate system usually used for the magnetocardiogram. The  $x$  axis points to the patient's left, the  $y$  axis points up, and the  $z$  axis points toward the front of the patient, roughly perpendicular to the chest wall. Assume that  $\mathbf{p}$  is at the origin and the anterior chest surface is the  $xy$  plane at some fixed value of  $z$ . We ignore distortions to the field which arise because no current can flow in the region beyond the body, and we assume that the conductivity of the body is homogeneous and isotropic. From Eq. 8.15, we obtain the three components of  $\mathbf{B}$  along the line  $(x, 0, z)$ :

$$\begin{aligned} B_x &= \frac{\mu_0 p_y z}{4\pi r^3}, \\ B_y &= \frac{\mu_0 (p_z x - z p_x)}{4\pi r^3}, \\ B_z &= -\frac{\mu_0 p_y x}{4\pi r^3}. \end{aligned} \quad (8.16)$$

Compare these results to the lines of  $\mathbf{B}$  in Fig. 8.15, which were drawn for the three components of  $\mathbf{p}$  using the right-hand rule. Along the line being considered

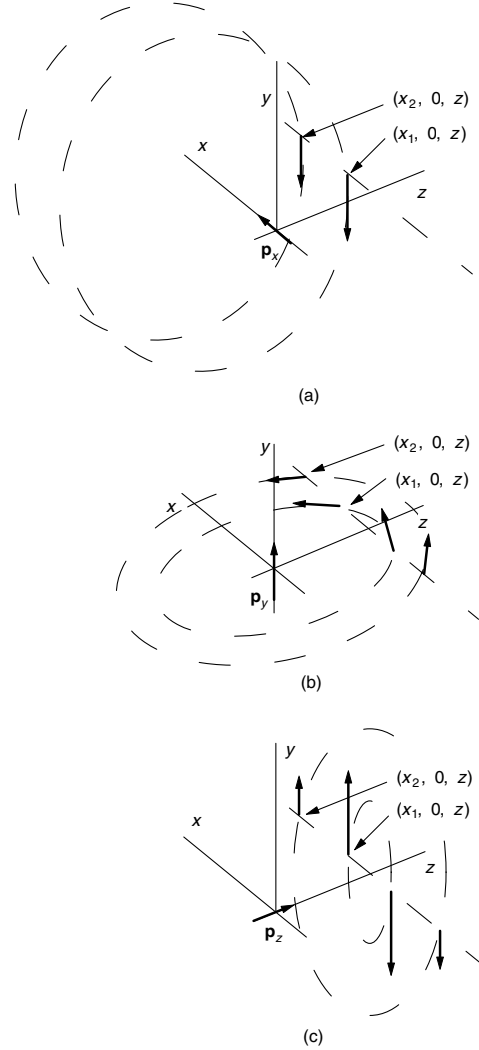


FIGURE 8.15. The magnetic field produced by the three components of a current dipole at the origin. The coordinate system is that customarily used for magnetocardiography. The  $x$  axis points toward the subject's left, the  $y$  axis is vertical, and the  $z$  axis points forward through the subject's chest. The coordinate system is viewed over the subject's right shoulder.

( $y = 0, z = \text{const}$ ),  $p_x$  contributes only to  $B_y$ , and  $B_y$  is always negative. Component  $p_y$  contributes to both  $B_x$  and  $B_z$ ; the latter changes sign while the former does not, as we change the value of  $x$ . Component  $p_z$  gives only a  $y$  component of  $\mathbf{B}$  that changes sign as  $x$  changes sign. The component normal to the body surface,  $B_z$  is given by

$$B_z(x, 0, z) = -\frac{\mu_0}{4\pi} \frac{p_y x}{(x^2 + z^2)^{3/2}}.$$

Figure 8.16 plots contours for the potential and the magnetic field component  $B_z$  perpendicular to the body surface when  $\mathbf{p}$  points along the  $y$  axis. Again, distortions because of changes in conductivity are ignored. The similarity of the two sets of contours is clear. The contours of constant potential are proportional to  $p_y y / r^3$ , while the contours for  $B_z$  are proportional to  $-p_y x / r^3$ . Either



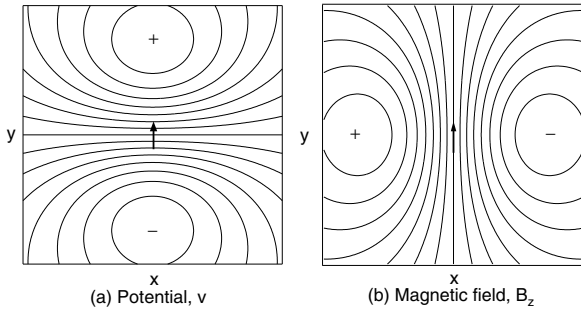


FIGURE 8.16. Contour plots in the  $xy$  plane for (a) the potential and (b) the  $z$  component of the magnetic field from a current dipole  $\mathbf{p}$  pointing along the  $y$  axis, calculated for an infinite, isotropic conducting medium.

contour map can be used to determine the location and depth of  $\mathbf{p}$ . To be specific, consider the contours for  $B_z$ . The field is proportional to the function  $x/(x^2 + z^2)^{3/2}$ , which changes sign right over the source and has a maximum and a minimum at  $x = \pm z/\sqrt{2}$ . The depth of the source  $z$  is related to the spacing  $\Delta x$  along the  $x$  axis between the maximum and minimum by

$$z = \frac{\Delta x}{\sqrt{2}}. \quad (8.17)$$

The source is located directly beneath the point on the axis where  $B_z = 0$ , and its strength is related to the maximum value of  $B_z$  by

$$B_z(\text{max}) = \frac{\mu_0 p_y}{6\pi\sqrt{3}z^2}. \quad (8.18)$$

Figure 8.17 shows real maps of the potential and the magnetic field on the surface of the chest. While the basic features are described by the simple current dipole model, the exact shape of the contours in Fig. 8.17 differs from the shape in Fig. 8.16. This is due to variations in conductivity of the body. The surface potential is distorted by conductivity differences throughout the thorax; the magnetic field is particularly susceptible to return currents flowing just below the surface of the body. Hosaka *et al.* (1976) did an early calculation of the effect of currents at the surface of the torso on the magnetocardiogram. They found that the return current modifies the component of  $\mathbf{B}$  perpendicular to the body surface by about 30%. Tangential components of  $\mathbf{B}$  are influenced more; this is why the normal component  $B_z$  is usually measured. Other calculations have been done by Purcell *et al.* (1988). Tan *et al.* (1992) show that using a model of the conductivities that matches the geometry of the patient's thorax allows accurate localization of the current dipole source from the surface measurements. Stroink (1993) reviews magnetic field maps; surface potential maps are reviewed by Taccardi and Punske (2004) and by Stroink *et al.* (1996).

The magnetic field close to the heart is affected by the anisotropy of the tissue conductivity. Figure 8.18 shows measurements made 1.5 mm from a 1-mm-thick

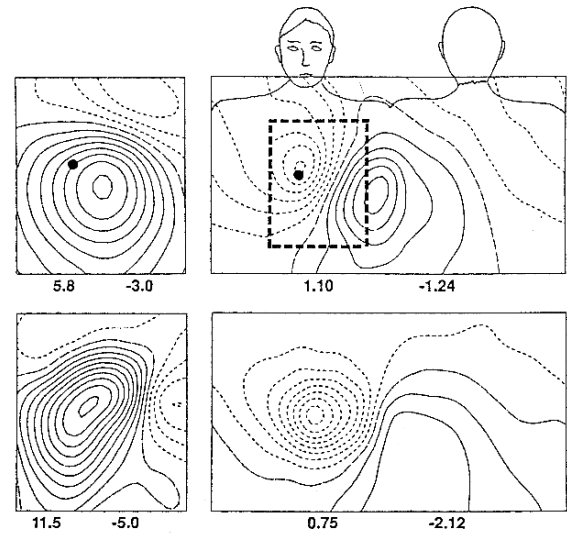


FIGURE 8.17. Maps of the magnetic field perpendicular to the body (left) and the body surface potential (right) in two patients. The upper row is for a normal patient, and the lower row for a patient with an anterior myocardial infarction. The dashed rectangle in the potential map corresponds to the area for which the magnetic field was measured. The dot in the upper row shows where the midline intersects the level of the fourth intercostal space. Note how the constant contours for the magnetic field are oriented at right angles to the isopotential lines, as in the previous figure. From G. Stroink, *Cardiomagnetic Imaging*. In R. A. Dunn and A. S. Berson, eds. *Frontiers in Cardiovascular Imaging*. Raven Press, 1992. pp. 161–177. Used by permission.

slice of canine myocardium by Staton *et al.* (1993). Panel A shows the time course of simultaneous recordings from three pickup coils 3 mm in diameter and separated by 4 mm. There are striking differences over 4 mm. Panel B shows a magnetic field contour map during stimulus from another experiment. Instead of having one peak and one valley as in Figs. 8.16 and 8.17, it shows a cloverleaf or *quatrefoil* pattern. Panels C and D show the field contours and the current flow in a third experiment, 6 ms after stimulation. This field and current pattern is predicted by bidomain calculations [Wikswó (1995b)].

## 8.5 The Magnetoencephalogram

The magnetic signals from a nerve action potential are weaker than those from the heart for two reasons. First, the current-dipole vector associated with the repolarization follows close behind the depolarization and reduces the field. (The largest unmyelinated axons in the body have a conduction speed of about  $1 \text{ m s}^{-1}$  and the pulse is about 1 mm long. Myelinated fibers have a pulse length up to 8–10 times longer.) Second, the cross-sectional area of the advancing wavefront is much smaller. However,

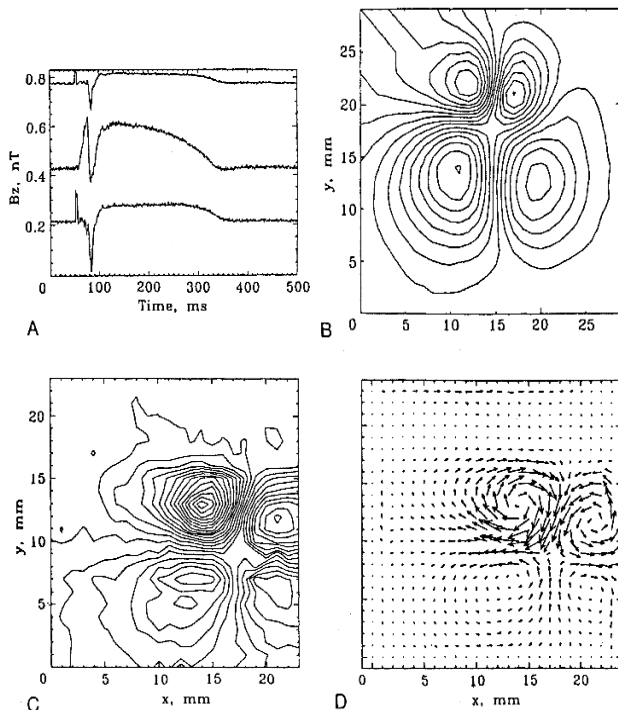


FIGURE 8.18. The results of magnetic field measurements very close to a slice of canine myocardium. The panels are described in the text. Part of the figure is reproduced from J. P. Wiksw, Jr. Tissue anisotropy, the cardiac bidomain, and the virtual cathode effect. In D. P. Zipes and J. Jalife, eds. *Cardiac Electrophysiology: From Cell to Bedside*, 2nd ed. pp. 348–361, ©1995 Elsevier, Inc., with permission of Elsevier. The rest is from D. J. Staton, R. N. Friedman, and J. P. Wiksw, Jr. (1993). High-resolution SQUID imaging of octupolar currents in anisotropic cardiac tissue. *IEEE Trans. Appl. Superconduct.* **3**(1):1934–1936. ©1993 IEEE.

the magnetic fields accompanying action potentials have been measured in nerve [Barach *et al.* (1985); Roth and Wiksw (1985)] and in muscle [Gielen *et al.* (1991)]. They have also been measured in green algae [Trontelj *et al.* (1994)].

We saw in Sec. 6.1 that nerve cells have an input end (dendrites), a cell body, and an axon. The signal that propagates from a synapse through the dendrites to the cell body and axon is much smaller (about 10 mV) and longer (10 ms) than an action potential that travels along the axon. The cells at the surface of the cerebral cortex have dendrites that are like the trunk of a tree perpendicular to the surface of the cortex, with branches from several directions coming to the trunk. The signal from the trunk is the primary contributor to the magnetoencephalogram (MEG) and electroencephalogram (EEG). The problems show that the magnetic field associated with the rise of the post-synaptic potential is more easily observed outside the brain than is the action potential.

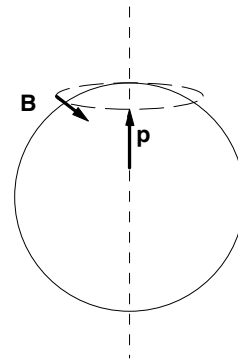


FIGURE 8.19. A current dipole  $\mathbf{p}$  is oriented radially inside a homogeneous conducting sphere. The return current is independent of the azimuthal angle,  $\phi$ . By symmetry the magnetic field, if any, must be in the  $\phi$  direction; the current in Ampere's circuital law, which is the sum of the current in  $p$  and the return current, is zero.

One can see from the symmetry argument in the caption of Fig. 8.19 that in a spherically symmetric conducting medium the radial component of  $\mathbf{p}$  and its return currents do not generate any magnetic field outside the sphere. Therefore the MEG is most sensitive to detecting activity in the fissures of the cortex, where the trunk of the post-synaptic dendrite is perpendicular to the surface of the fissure. A tangential component of  $\mathbf{p}$  does produce a magnetic field outside a spherically symmetric conductor. The extracellular current does not contribute to the radial component of the magnetic field [Hämäläinen *et al.* (1993)], so Eq. 8.15 gives  $B_r$  correctly. Extracellular current does influence the tangential components of the magnetic field. Since the skull is not a perfect sphere, there is some effect of the radial component of  $\mathbf{p}$  on the MEG. The EEG is sensitive to both radial and tangential components of  $\mathbf{p}$ . The information available from the EEG and MEG has been reviewed by Wiksw *et al.* (1993).

Measurements of the magnetoencephalogram are often based on evoked responses. A repetitive stimulus is presented to the subject—audible, visual, or tactile—or the subject is asked to perform a repetitive task such as flexing a finger. Signal-averaging techniques are used to identify the associated changes in magnetic field (see Chapter 11). Figure 8.20 shows averaged magnetic field contours measured over the scalp of a subject who heard a string of words presented in random order every 2.3 s. Sometimes the subject was asked to read something else and ignore the words. At other times the subject was asked to pay attention and count how many of the words were on a list. The first peak, 100 ms after presentation of the word, was the same in both cases. The sustained field peak, SF, was considerably stronger when the subject was paying attention to the list. Magnetic contours and the equivalent current dipole source are also shown.

Magnetic measurements have also been made of slower signals. Grimes *et al.* (1985) found ion currents in the

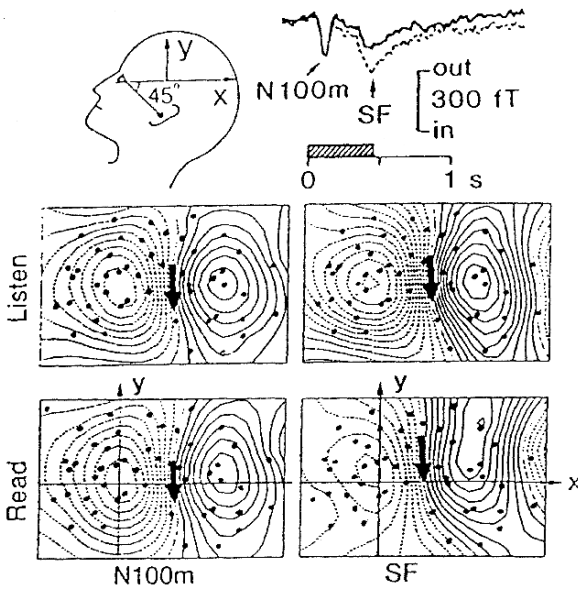


FIGURE 8.20. Magnetic field maps recorded over the scalp of a subject who heard a series of words and either ignored them by reading something else or listened carefully and counted how many of the words were in a predetermined list. The features are discussed in the text. Reprinted with permission from M. Hämäläinen, R. Harri, R. J. Ilmoniemi, J. Knuutila and O. V. Lounasmaa. *Magnetoencephalography—theory, instrumentation, and applications to noninvasive studies of the working human brain. Revs. Mod. Phys.* **65**(2): 413–497 1993. Copyright 1993 by the American Physical Society.

human leg that change over an hour or so. Thomas *et al.* (1993) found a quasistatic ionic current in the chick embryo, probably associated with active-transport pumps. Richards *et al.* (1995a) have measured a magnetic signal associated with slow currents in the small intestine of the rabbit and its supporting mesentery. The signal changes appreciably if the blood supply to the intestine is cut off. These measurements could be clinically useful, because mesenteric ischemia is difficult to diagnose early [Richards *et al.* (1995b), Petrie *et al.* (1996)].

## 8.6 Electromagnetic Induction

In 1831 Faraday discovered that a *changing* magnetic field causes an electric current to flow in a circuit. It does not matter whether the magnetic field is from a permanent magnet moving with respect to the circuit or from the changing current in another circuit. The results of many experiments can be summarized in the *Faraday induction law*:

$$\oint \mathbf{E} \cdot d\mathbf{s} = -\frac{d}{dt} \iint \mathbf{B} \cdot d\mathbf{S} = -\frac{d\Phi}{dt}. \quad (8.19)$$

It states that the line integral of  $\mathbf{E}$  around a closed path is equal to the negative of the rate of change of the magnetic flux through any surface bounded by the path. The relationship between the direction of  $\mathbf{S}$  and  $d\mathbf{s}$  is given by a right-hand rule: if the fingers of the right hand curl around the circuit in the direction of  $d\mathbf{s}$ , the thumb of the right hand points in the direction of a positive normal to  $\mathbf{S}$ . The units of magnetic flux  $\Phi = \iint \mathbf{B} \cdot d\mathbf{S}$  are  $\text{T m}^2$  or weber (Wb). Rapidly changing magnetic fields can induce currents large enough to trigger nerve impulses. This is discussed in Sec. 8.7.

The differential form of the Faraday induction law is (see Problem 20)

$$\text{curl } \mathbf{E} = \nabla \times \mathbf{E} = -\frac{\partial \mathbf{B}}{\partial t}. \quad (8.20)$$

The result of the vector operation curl is another vector. In Cartesian coordinates the components of  $\nabla \times \mathbf{E}$  are

$$\begin{aligned} (\nabla \times \mathbf{E})_x &= \frac{\partial E_z}{\partial y} - \frac{\partial E_y}{\partial z}, \\ (\nabla \times \mathbf{E})_y &= \frac{\partial E_x}{\partial z} - \frac{\partial E_z}{\partial x}, \\ (\nabla \times \mathbf{E})_z &= \frac{\partial E_y}{\partial x} - \frac{\partial E_x}{\partial y}. \end{aligned}$$

These can be abbreviated by using determinant notation as

$$(\nabla \times \mathbf{E}) = \begin{vmatrix} \hat{\mathbf{x}} & \hat{\mathbf{y}} & \hat{\mathbf{z}} \\ \frac{\partial}{\partial x} & \frac{\partial}{\partial y} & \frac{\partial}{\partial z} \\ E_x & E_y & E_z \end{vmatrix}. \quad (8.21)$$

Similarly (Problem 21) the differential form of Ampere's law is

$$\text{curl } \mathbf{B} = \nabla \times \mathbf{B} = \mu_0 \left( \mathbf{j} + \frac{\partial \mathbf{D}}{\partial t} \right). \quad (8.22)$$

The integral form of the Faraday induction law can be used to determine  $\mathbf{E}$  only if the symmetry is such that  $\mathbf{E}$  is always parallel to  $d\mathbf{s}$  and has the same magnitude all along the path. One situation where it can be used is a circular loop of wire in the  $xy$  plane centered at the origin. The radius of the loop is  $a$  and its normal is along the  $+z$  axis. Suppose that everywhere in the  $xy$  plane within the boundary of the circle the field points along  $z$  and depends only on time:  $\mathbf{B}(x, y, z, t) = B(t)\hat{\mathbf{z}}$ . Symmetry shows that  $\mathbf{E}$  has the same magnitude everywhere in the wire and is always tangent to the loop. Equation 8.19 gives

$$E = -\frac{a}{2} \frac{dB}{dt}. \quad (8.23)$$

If the loop is made of material that obeys Ohm's law, there is a current of density  $j = \sigma E = -(\sigma a/2)(dB/dt)$ . If the radius of the wire is  $b$  ( $b \ll a$ ), then  $i = -(\sigma \pi a b^2/2)(dB/dt)$ . Figure 8.21 shows the direction of the induced current if  $dB/dt$  is positive. The induced

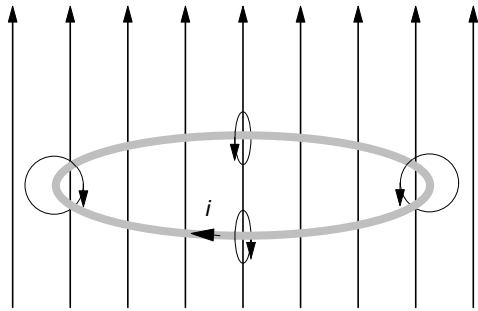


FIGURE 8.21. A magnetic field increasing in the direction shown induces a current in the loop. This current generates a magnetic field in the opposite direction, opposing the change in the magnetic field.

current sets up its own magnetic field which points in the  $-z$  direction within the loop, opposing the primary field increase within the loop. The induced current always opposes the *change* of magnetic field that produces it. This is called *Lenz's law*. If it were not true, the induced current, once started, would increase indefinitely.

This result does not require that the ring be hollow; it can be part of a much larger conductor. The larger the conductor, the greater the radius of the path along which the induced current can flow. The currents that changing magnetic fields induce in conductors are called *eddy currents* and cause heating losses in the conductor. Iron, which is a conductor, is often used as a core in transformer windings to increase the intensity of the magnetic field. To reduce the eddy-current losses, the cores are made of thin layers of iron insulated from one another by varnish. This limits the radius of the path in which the eddy currents can flow. Some coils and transformers are wound on cores of powdered iron dispersed in an insulating binder. Rooms with thick conducting walls (aluminum, about 2 cm thick) have been used to shield against 60 Hz magnetic fields from power wiring. The eddy currents induced in the aluminum attenuate the field by about a factor of 200 [Stroink *et al.* (1981)].

The quantity  $\int_a^b \mathbf{E} \cdot d\mathbf{s}$  is the work done per unit charge in moving from  $a$  to  $b$  and is called the *electromotive force along the path from  $a$  to  $b$* . Terminology is not always consistent; see the discussion by Page (1977). The details of how a changing magnetic field causes a current to flow were shown above for a circular conductor. The force on a moving charge due to the induced electric field is balanced by the drag force as the charge drifts through the conductor. Energy supplied by the changing magnetic field is dissipated as heat. If a voltmeter is attached to two points on the circle, the voltmeter reading may seem paradoxical, until one realizes that there may be changing flux in the voltmeter leads as well. An additional complication is that when there is any region of space in which  $\nabla \times \mathbf{E} \neq 0$ , then it is possible for  $\int_a^b \mathbf{E} \cdot d\mathbf{s}$  to depend on the path (rather than just the end points), even if the

magnetic field is zero at all points on the path. This is described clearly and in detail by Romer (1982).

## 8.7 Magnetic Stimulation

Since a changing magnetic field generates an induced electric field, it is possible to stimulate nerve or muscle cells without using electrodes. The advantage is that for a given induced current deep within the brain, the currents in the scalp that are induced by the magnetic field are far less than the currents that would be required for electrical stimulation. Therefore transcranial magnetic stimulation (TMS) is relatively painless. Magnetic stimulation can be used to diagnose central nervous system diseases that slow the conduction velocity in motor nerves without changing the conduction velocity in sensory nerves [Hallett and Cohen (1989)]. It could be used to monitor motor nerves during spinal cord surgery, and to map motor brain function. Because TMS is noninvasive and nearly painless, it can be used to study learning and plasticity (changes in brain organization over time). Recently, researchers have suggested that repetitive TMS might be useful for treating depression and other mood disorders.

One of the earliest investigations was reported by Barker *et al.* (1985) who used a solenoid in which the magnetic field changed by 2 T in 110  $\mu\text{s}$  to apply a stimulus to different points on a subject's arm and skull. The stimulus made a subject's finger twitch after the delay required for the nerve impulse to travel to the muscle. For a region of radius  $a = 10$  mm in material of conductivity  $1 \text{ S m}^{-1}$ , the induced current density for the field change in Barker's solenoid was  $90 \text{ A m}^{-2}$ . (This is for conducting material inside the solenoid; the field falls off outside the solenoid, so the induced current is less.) This current density is large compared to current densities in nerves (Chap. 6).

Magnetic stimulators are relatively high-power devices, requiring thousands of amps passed through coils for a few hundred microseconds. Most magnetic stimulators are capacitor discharge devices, in which a large capacitor is charged to a high voltage (several kV) and then discharged through the coil. Different coil geometries have been examined; the most common one is a figure-of-eight shape. Several theoretical analyses and models have been made, including those by Heller and van Hulsteyn (1992) and Esselle and Stuchly (1995). Magnetic stimulation is included in the review by Roth (1994) and is compared to other brain imaging methods by Ilmoniemi *et al.* (1999).

## 8.8 Magnetic Materials and Biological Systems

Just as the electric field can be altered by the polarization of a dielectric, the magnetic field can be altered by

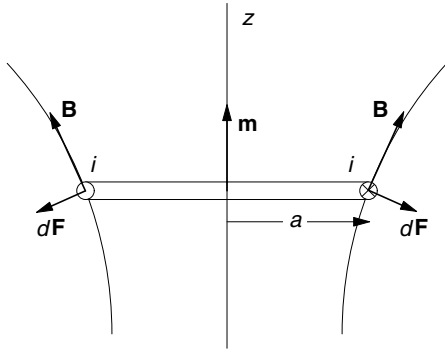


FIGURE 8.22. A current loop in an inhomogeneous magnetic field experiences a force toward the region of stronger magnetic field. The circular loop lies in a plane perpendicular to the  $z$  axis. Current flows into the page on the right and out of the page on the left.

matter. Biological measurements can be based on alterations of the field by an organ in the body. Some cells exhibit permanent magnetism, which is important for measuring direction in some bacteria, birds and other organisms.

### 8.8.1 Magnetic Materials

The effects of magnetic fields on material are more complicated than those of electric fields. Since there are no known magnetic charges (monopoles), we must consider the effect of magnetic fields on current loops or magnetic dipoles. Figure 8.22 shows a current loop in a magnetic field that decreases as  $z$  increases. As a result the lines of  $\mathbf{B}$  spread apart. The loop has radius  $a$ , carries current  $i$ , and has magnetic moment<sup>1</sup>  $\mathbf{m}$ . For the orientation shown, there is a force on the loop in the  $-z$  direction that is toward the region where the field is stronger. If the magnetic moment of the loop were not parallel to  $\mathbf{B}$ , there would also be a torque on the loop. For ease in calculation, imagine that the loop has been placed in the field in such a way that along the axis of the loop,  $\mathbf{B}$  points in the  $z$  direction. Then the spreading of the lines of  $\mathbf{B}$  means that  $\mathbf{B}$  has a component radially outward all around the loop. Because of the symmetry  $B_r$  has a constant magnitude everywhere around the loop, and the force on the loop is  $-2\pi a i B_r(a)$ .

Field  $B_r(a)$  is found by considering the fact that the total magnetic flux through all surfaces of the pillbox in Fig. 8.23 is zero (Eq. 8.6). The net outward flux is

$$[B_z(z + dz) - B_z(z)] \pi a^2 + B_r(a) 2\pi a dz = 0.$$

<sup>1</sup>Be careful. We are talking about two different kinds of dipoles in this chapter. The current dipole  $\mathbf{p}$  is a source and sink of current and has units A m. The magnetic dipole  $\mathbf{m}$ , equivalent to a small magnet with north and south poles, has units A m<sup>2</sup>. The magnetic field from a magnetic dipole falls off as  $1/r^3$ .

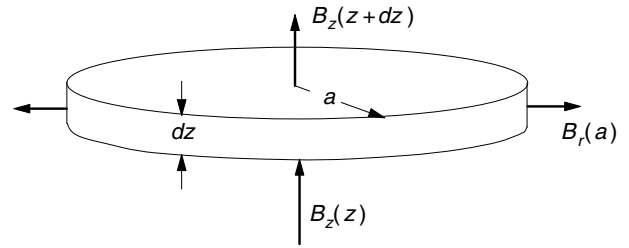


FIGURE 8.23. Gauss's law for  $\mathbf{B}$  is applied to a pillbox of radius  $a$  and thickness  $dz$ .

This can be rearranged to give

$$\left[ \frac{\partial B_z}{\partial z} + \frac{2}{a} B_r(a) \right] \pi a^2 dz = 0,$$

from which

$$B_r(a) = -\frac{a}{2} \frac{\partial B_z}{\partial z}.$$

The force on the loop is therefore

$$F_z = \pi a^2 i \frac{\partial B_z}{\partial z} = m_z \frac{\partial B_z}{\partial z}. \quad (8.24)$$

If  $\mathbf{m}$  is parallel to  $\mathbf{B}$  the force is toward the region of stronger field; if  $\mathbf{m}$  is antiparallel to  $\mathbf{B}$  the force is toward the region of weaker field.

An atom can have a magnetic moment because of two effects.<sup>2</sup> The motion of the electrons in orbit about the nucleus constitutes a current, as a result of which there may be an *orbital magnetic moment*. The intrinsic *spin* of each electron gives rise to a spin magnetic moment, independent of any orbital motion. In most atoms, the orbital magnetic moments average to zero, and most of the electrons are arranged in pairs whose spins cancel. The atom therefore usually has no net magnetic moment.

Most substances placed in an inhomogeneous field experience a weak force *away* from the region of strong field, and the force is roughly proportional to the square of the field strength, an effect called *diamagnetism*. It can be understood with a simple classical model. As the atom is moved into the magnetic field, the Faraday induction effect distorts the orbits of the electrons to induce a magnetic dipole moment proportional to  $\mathbf{B}$  and in the opposite direction, consistent with Lenz's law. The force is therefore proportional to  $B_z(\partial B_z/\partial z)$ . Purcell (1985) has a quantitative treatment of this model.

A few substances are *attracted* to the region of stronger field, again with a force that is often proportional to the square of the field. Each atom of these *paramagnetic* substances has a permanent magnetic moment associated with the spin of an unpaired electron. Thermal motion normally keeps the magnetic moments of different atoms

<sup>2</sup>Much weaker magnetic moments of the atomic nucleus are considered in Chapter 18.

oriented randomly. As the substance is brought into the magnetic field the spin magnetic moments of different atoms begin to align with the magnetic field. A magnetic dipole moment is induced in the substance, but this time it is in the direction of  $\mathbf{B}$ , and the substance is attracted to the magnet.

Some substances placed in an inhomogeneous magnetic field experience much stronger attraction than do paramagnetic substances. In these substances some of the atomic moments are aligned even in the absence of an external field. They are permanent magnets. Further alignment of the atomic moments may take place in an external field, but complete alignment often takes place in relatively weak external fields. These substances are called *ferromagnets*. The individual atoms have magnetic moments, and there are forces between atoms which cause the spins to align. Section 14-4 of Eisberg and Resnick (1985) provides a relatively simple explanation of the quantum-mechanical effects underlying this spin alignment. *Ferrimagnets* are similar to ferromagnets, but the crystals contain two different kinds of ions with different magnetic moments.

The *magnetization*  $\mathbf{M}$  is the average magnetic moment per unit volume. It is defined by considering volume  $\Delta V$  that has total magnetic moment  $\Delta \mathbf{m} = \sum \mathbf{m}_i$ , where the summation is taken over all atoms in the volume, and taking the ratio

$$\mathbf{M} = \frac{\Delta \mathbf{m}}{\Delta V}. \tag{8.25}$$

We have seen that a current loop possesses a magnetic moment of magnitude  $m = iS$ . One can imagine a current giving rise to any magnetic moment, even one associated with electron spin. Such currents are called *bound* currents and must be included in Ampere's law. The currents that flow due to conduction—that we can control by changing the conductivity of the material or throwing a switch—are called *free* currents. One can show that if we define the new vector

$$\mathbf{H} = \mathbf{B}/\mu_0 - \mathbf{M}, \tag{8.26}$$

it depends only on the free currents:

$$\oint \mathbf{H} \cdot d\mathbf{s} = \iint \mathbf{j}_{\text{free}} \cdot d\mathbf{S}. \tag{8.27}$$

Vector  $\mathbf{H}$  is called the *magnetic field intensity*. It has units  $\text{A m}^{-1}$ . It does not have the physical significance of  $\mathbf{B}$  (it does not appear in the Lorentz force or the Faraday induction law). However, it often simplifies computations, because we control free current in the laboratory.

In a vacuum,  $\mathbf{B} = \mu_0 \mathbf{H}$ . It has been traditional to define the *magnetic permeability* of a medium in which  $\mathbf{B}$ ,  $\mathbf{M}$ , and  $\mathbf{H}$  are all proportional to one another by the equation

$$\mathbf{B} = \mu \mathbf{H}, \tag{8.28}$$

in which case

$$\frac{\mu}{\mu_0} = 1 + \frac{M}{H} = 1 + \chi_m. \tag{8.29}$$

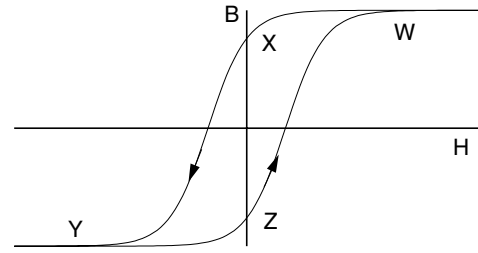


FIGURE 8.24. A typical curve of  $B$  vs  $H$  for a ferromagnetic material. The curve shows hysteresis, and the arrows show the direction of travel around the curve  $WXYZ$ . Points  $W$  and  $Y$  show where  $M$  saturates. Points  $X$  and  $Z$  show the remanent magnetic field when  $H = 0$ .

In diamagnetic materials the *magnetic susceptibility*  $\chi_m$  is negative and  $\mu < \mu_0$ . A typical diamagnetic susceptibility is  $\approx -1 \times 10^{-5}$ . In paramagnetic materials  $\chi_m$  is positive and  $\mu > \mu_0$ . A typical paramagnetic susceptibility is  $\approx 1 \times 10^{-4}$ .

The relationship between  $B$  and  $H$  in ferromagnetic substances is nonlinear and is characterized by a  $BH$  curve. A typical curve is shown in Fig. 8.24. The fact that the curves for increasing and decreasing  $H$  do not coincide is called *hysteresis*. The arrows show the direction in which  $H$  changes on each branch of the curve. *Saturation* takes place beyond points  $W$  and  $Y$ . The value of  $M$  saturates and  $B = \mu_0 (M_{\text{saturated}} + H)$ . When  $H = 0$  there is a *remanent* magnetic field (points  $X$  and  $Z$ ). If the temperature of the sample is raised above a critical temperature called the *Curie temperature*, the magnetism is destroyed.

### 8.8.2 Measuring Magnetic Properties in People

Several kinds of measurements can be based on magnetic effects in materials. A common component of dust inhaled by miners and industrial workers is magnetite,  $\text{Fe}_3\text{O}_4$ , which is ferrimagnetic. By placing the thorax in a fixed magnetic field for a few seconds, the particles can be aligned. The field is turned off and the remanent field measured. The use of *magnetopneumography* in occupational health is described by Stroink (1985). Cohen *et al.* (1984) have modeled the process by which the particles are magnetized, as well as the relaxation process by which the magnetization disappears after the external field is removed. Relaxation curves are used to estimate intracellular viscosity and the motility of macrophages (scavenger white cells) in the alveoli [Stahlhofen and Moller (1993)].

The magnetic susceptibility of blood and myocardium is different from the susceptibility of surrounding lung tissue. An externally applied magnetic field induces a field that changes as the volume of the heart changes. It can

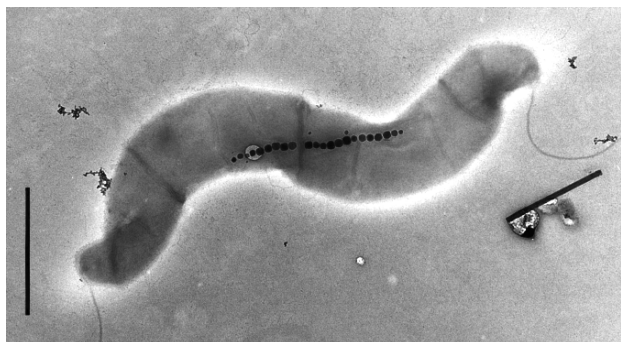


FIGURE 8.25. The small black dots are magnetosomes, small particles of magnetite in the magnetotactic bacterium *Aquaspirillum magnetotacticum*. The vertical bar is  $1\ \mu\text{m}$  long. The photograph was taken by Y. Gorby and was supplied by N. Blakemore and R. Blakemore, University of New Hampshire.

be measured externally. The theory and experiments have been described by Wikswo (1980).

Susceptibility measurements can also be used to measure the total iron stores in the body. Normally the body contains 3–4 g of iron. Approximately a quarter of it is stored in the liver. The amount of iron can be elevated from a large number of blood transfusions or in certain rare diseases such as hemochromatosis and hemosiderosis. The liver is an organ whose susceptibility can easily be measured. The susceptibility varies linearly with the amount of iron deposited. Magnetic susceptometry has been used to estimate body iron stores [Brittenham *et al.* (1983); Nielsen *et al.* (1995)].

### 8.8.3 Magnetic Orientation

Magnetism is used for orientation by several organisms. A history of studies in this area is provided in a very readable book by Mielczarek and McGrayne (2000). Several species of bacteria contain linear strings of up to 20 particles of magnetite, each about 50 nm on a side encased in a membrane [Frankel *et al.* (1979); Moskowitz (1995)]. Over a dozen different bacteria have been identified that synthesize these intracellular, membrane-bound particles or *magnetosomes* (Fig. 8.25). Bacteria in the northern hemisphere have been shown to seek the north pole. Because of the tilt of the earth's field, they burrow deeper into the environment in which they live. Similar bacteria in the southern hemisphere burrow down by seeking the south pole. In the laboratory the bacteria align themselves with the local field.

In the problems you will learn that there is sufficient magnetic material in each bacterium to align it with the earth's field just like a compass needle. Other bacteria that live in oxygen-poor, sulfide-rich environments contain magnetosomes composed of greigite, ( $\text{Fe}_3\text{S}_4$ ) rather than magnetite ( $\text{Fe}_3\text{O}_4$ ). In aquatic habitats, high concentrations of both kinds of magnetotactic bacteria

are usually found near the *oxic–anoxic transition zone* (OATZ). In freshwater environments the OATZ is usually at the sediment–water interface. In marine environments it is displaced up into the water column.

Since some bacteria prefer more oxygen and others prefer less, and they both have the same kind of propulsion and orientation mechanism, one wonders why one kind of bacterium is not swimming out of the environment favorable to it. Frankel and Bazylinski (1994) proposed that the magnetic field and the magnetosomes keep the organism aligned with the field, and that they change the direction in which their flagellum rotates to move in the direction that leads them to a more favorable concentration of some desired chemical.

Magnetosomes are found in other species and are likely also to be used for orientation. One species of algae contains about 3000 magnetic particles, each of which is about  $40 \times 40 \times 140\ \text{nm}$  [de Araujo *et al.* (1986)]. Bees, pigeons, and fish contain magnetic particles. It is more difficult to demonstrate their function, because of the variety of other sensory information available to these animals. For example, homing pigeons with magnets attached to their heads could orient well on sunny days but not on cloudy ones [Walcott *et al.* (1979)]. There is evidence that bees orient in a magnetic field [Frankel (1984)]. The net magnetic moment in the bees is oriented transversely in the body [Gould, Kirschvink and Deffeyes (1978)]. In pigeons the magnetic material is located in the dura (the outer covering of the brain) or skull. In all of these cases, the material has been identified as magnetite. In the yellowfin tuna, data are compatible with about  $8.5 \times 10^7$  magnetic particles, each of which is a single domain of magnetite in the shape of an approximately 50-nm cube [Walker *et al.* (1984)].

There is now evidence that birds may actually have three compasses. Since the magnetic and geographic poles are fairly far apart, migratory birds must correct their magnetic compasses as they fly. The Savannah sparrow is known to have a magnetic compass and a star compass and to take visual cues from the sky at sunset. Able and Able (1995) have shown that adult Savannah sparrows that are subjected to a field pointing in a different direction than the earth's field will at first trust their magnetic compasses, but over a few days they recalibrate their magnetic compasses with their star compasses. An accompanying editorial [Gould (1995)] places their work in context. More recently, Cochran *et al.* (2004) have shown that if migrating thrushes are placed in an eastward-pointing magnetic field at twilight and then released, they fly west instead of south. This strongly suggests that the birds recalibrate their magnetic compass at twilight each day.

The fact that the magnetite particles seem to be about 50 nm on a side is physically significant. Frankel (1984) summarizes arguments that if the particles are smaller than about 35 nm on a side, thermal effects can destroy the alignment of the individual particles. If they are larger

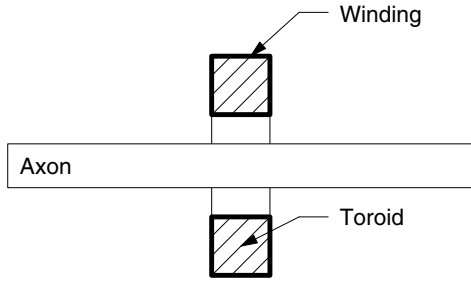


FIGURE 8.26. A nerve cell preparation is threaded through the magnetic toroid to measure the magnetic field. The changing magnetic flux in the toroid induces an electromotive force in the winding. Any external current that flows through the hole in the toroid diminishes the magnetic field.

than about 76 nm, multiple domains can form within a particle, decreasing the magnetic moment.

## 8.9 Detection of Weak Magnetic Fields

The detection of weak fields from the body is a technological triumph. The field strength from lung particles is about  $10^{-9}$  T; from the heart it is about  $10^{-10}$  T; from the brain it is  $10^{-12}$  T for spontaneous ( $\alpha$ -wave) activity and  $10^{-13}$  T for evoked responses. These signals must be compared to  $10^{-4}$  T for the earth's magnetic field. Noise due to spontaneous changes in the earth's field can be as high as  $10^{-7}$  T. Noise due to power lines, machinery, and the like can be  $10^{-5}$ – $10^{-4}$  T.

If the signal is strong enough, it can be detected with conventional coils and signal-averaging techniques that are described in Chapter 11. Barach *et al.* (1985) used a small detector through which a single axon was threaded. The detector consisted of a toroidal magnetic core wound with many turns of fine wire (Fig. 8.26). Current passing through the hole in the toroid generated a magnetic field that was concentrated in the ferromagnetic material of the toroid. When the field changed, a measurable voltage was induced in the surrounding coil.

The signals from the body are weaker, and their measurement requires higher sensitivity and often special techniques to reduce noise. Hämmäläinen *et al.* (1993) present a detailed discussion of the instrumentation problems. Sensitive detectors are constructed from *superconducting* materials. Some compounds, when cooled below a certain critical temperature, undergo a sudden transition and their electrical resistance falls to zero. A current in a loop of superconducting wire persists for as long as the wire is maintained in the superconducting state. The reason there is a superconducting state is a well-understood quantum-mechanical effect that we cannot go into here. It is due to the cooperative motion of many electrons in the superconductor [Eisberg and Resnick (1985), Sec. 14.1; Clarke (1994)].

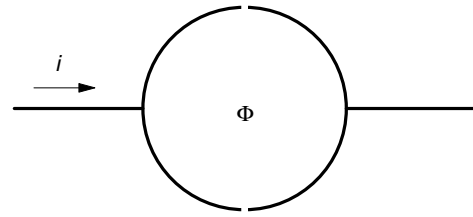


FIGURE 8.27. A dc SQUID is shown. The solid lines represent superconducting wires, broken by Josephson junctions at the top and bottom. The total current through both wires depends on  $\Phi$ , the magnetic flux through the circle.

The integral  $\oint \mathbf{E} \cdot d\mathbf{s}$  around a superconducting ring is zero, which means that  $d\Phi/dt$  is zero, and the magnetic flux through a superconducting loop cannot change. If one tries to change the magnetic field with some external source, the current in the superconducting circuit changes so that the flux remains the same.

The detector is called a *superconducting quantum interference device (SQUID)*. The operation of a SQUID and biological applications are described in the *Scientific American* article by Clarke (1994). Wikswo (1995a) surveys the use of SQUIDs for applications in biomagnetism and nondestructive testing. A technical discussion is also available [Hämmäläinen *et al.* (1993)]. The dc SQUID requires a superconducting circuit with two branches, each of which contains a very thin nonsuperconducting “weak link” known as a Josephson junction (Fig. 8.27). As the magnetic field is changed, these weak links allow the flux in the loop to change. The phase of the quantum-mechanical wave function of the collectively moving electrons differs in the two branches by an amount depending on the magnetic flux linked by the circuit. The total current depends on the interference of these two wave functions and is of the form  $I = 2I_0 \cos(\pi\Phi/\Phi_0)$ , where  $\Phi$  is the flux through the circuit. The quantity  $\Phi_0 = h/2e$ , where  $h$  is Planck's constant (see Chapter 14) and  $e$  is the electron charge, is the quantum-mechanical unit of flux and has a value equal to  $2.068 \times 10^{-15}$  T m<sup>2</sup>. Because interference changes corresponding to a small fraction of this can be measured, the SQUID is very sensitive. The SQUID must be operated at temperatures where it is superconducting. It used to be necessary to keep a SQUID in a liquid-helium bath, which is expensive to operate because of the high evaporation rate of liquid helium. With the advent of high-temperature superconductors, SQUIDS have the potential to operate at liquid-nitrogen temperatures, where the cooling problems are much less severe.

A typical magnetometer for biomagnetic research contains a *flux transporter*, a superconducting detector coil  $d$  a centimeter or so in radius, coupled to a very small multiturn output coil  $o$  that matches the size of the SQUID and is placed right next to it. This is shown schematically in Fig. 8.28. The wires between the two loops are close



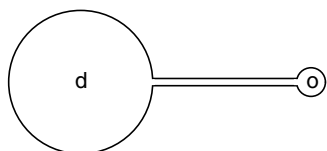


FIGURE 8.28. A superconducting loop shaped as shown becomes a flux transporter. Because the total flux in the loop is constant, a change of flux in the detecting loop  $d$  is accompanied by an equal and opposite flux change in the output loop  $o$ . The diameter of the output loop is matched to the size of the SQUID. Sensitivity is increased because the detecting loop has a larger area.

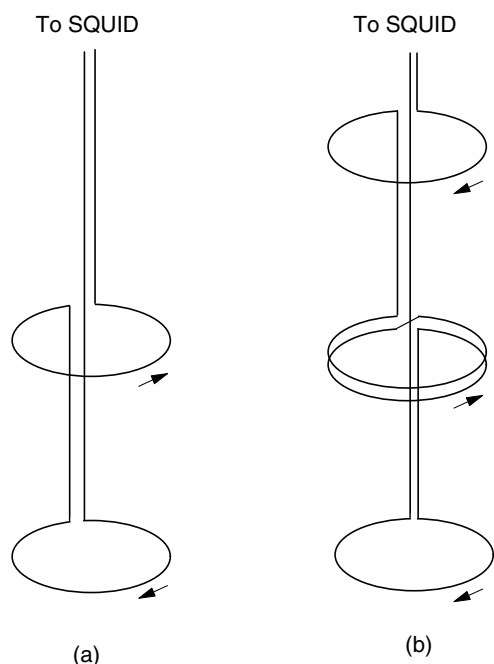


FIGURE 8.29. Gradiometers are sensitive to nearby sources of the magnetic field but are much less sensitive to distant sources. (a) A first-order gradiometer. (b) A second-order gradiometer.

together and have negligible area between them. The total flux, which is constant because the entire circuit is superconducting, is  $\Phi = \Phi_d + \Phi_o$ . The large area of the detecting coil increases its sensitivity. Any change in the magnetic field at the detector causes an opposite change in the flux and magnetic field at the output coil.

Because ambient natural and artificial background magnetic fields are so high, measurements are often made in special shielded rooms. These can be built of ferromagnetic materials, or of conductors to take advantage of eddy current attenuation, or they may have active circuits to cancel the background fields. It has proven possible in some cases to eliminate the need for these expensive rooms by using specially designed flux transporters that are less sensitive to distant sources but measure the nearby source with almost the same sensitivity as a single loop. If a distant background source can be represented

by a magnetic dipole, the field falls as  $1/r^3$ . The signal in a magnetometer (Fig. 8.28) would be proportional to this.

Problem 35 shows that the signal from a distant dipole detected by a first-order gradiometer [Fig. 8.29(a)] is proportional to  $1/r^4$  and that the signal in a second-order gradiometer [Fig. 8.29(b)] is proportional to  $1/r^5$ . Both gradiometers are insensitive to background that does not vary with position. Yet the loop closest to the nearby signal source detects a much stronger signal than the loops that are further away. With modern multichannel detector systems, one need not use gradiometer coils. Hundreds of coils are used at different locations, and the signals from them are combined to give the same suppression of background from distant sources.

### Symbols Used in Chapter 8

Symbol	Use	Units	First used on page
$a, b$	Distance	m	204
$e$	Elementary charge	C	218
$h$	Planck's constant	J s	218
$i$	Current	A	204
$j, \mathbf{j}$	Current density	A m <sup>-2</sup>	206
$j_d$	Displacement current density	A m <sup>-2</sup>	207
$m, \hat{m}$	Magnetic moment	A m <sup>2</sup>	204
$\mathbf{p}$	Current dipole moment	A m	209
$q$	Charge	C	203
$r, \mathbf{r}$	Distance	m	205
$s, \mathbf{s}$	Linear displacement	m	203
$t$	Time	s	207
$v, \mathbf{v}$	Velocity	m s <sup>-1</sup>	203
$v$	Electrical potential	V	208
$x, y, z$	Coordinates	m	206
$\hat{x}, \hat{y}, \hat{z}$	Unit vectors		208
$A$	Area	m <sup>2</sup>	207
$B, \mathbf{B}$	Magnetic field	T	203
$C$	Particle concentration	m <sup>-3</sup>	204
$D, \mathbf{D}$	Electric "displacement"	C m <sup>-2</sup>	207
$E, \mathbf{E}$	Electric field	V m <sup>-1</sup>	204
$F, \mathbf{F}$	Force	N	203
$H, \mathbf{H}$	Magnetic field intensity	A m <sup>-1</sup>	216
$I$	Current	A	218
$M, \mathbf{M}$	Magnetization	A m <sup>-1</sup>	216
$R$	Position	m	209
$S, \mathbf{S}$	Surface area	m <sup>2</sup>	204
$V$	Volume	m <sup>3</sup>	216
$\epsilon_0$	Electrical permittivity of free space	N <sup>-1</sup> m <sup>-2</sup> C <sup>2</sup>	205
$\theta$	Angle		204
$\kappa$	Dielectric constant		207

Symbol	Use	Units	First used on page
$\mu$	Magnetic permeability	$\Omega \text{ s m}^{-1}$	216
$\mu_0$	Magnetic permeability of free space	$\Omega \text{ s m}^{-1}$	205
$\sigma$	Charge per unit area	$\text{C m}^{-2}$	207
$\sigma_i, \sigma_o$	Electrical conductivity	$\text{S m}^{-1}$	208
$\tau, \tau$	Torque	$\text{N m}$	204
$\phi$	Angle		204
$\chi_m$	Magnetic susceptibility		216
$\Phi$	Magnetic flux	$\text{T m}^2$ or $\text{Wb}$	213
$\Phi_0$	Quantum of magnetic flux	$\text{T m}^2$ or $\text{Wb}$	218

## Problems

### Section 8.1

**Problem 1** An electric dipole consists of charges  $\pm q$  separated a distance  $b$ . Show that the torque  $\tau$  on an electric dipole  $\mathbf{p}$  in a steady electric field  $\mathbf{E}$  is given by  $\tau = \mathbf{p} \times \mathbf{E}$ , where  $\mathbf{p}$  has magnitude  $qb$ , pointing in the direction from  $-q$  to  $+q$ .

**Problem 2** Show that the units of  $\mathbf{m}$ ,  $\text{A m}^2$  or  $\text{J T}^{-1}$ , are equivalent.

**Problem 3** Show that the units of  $\mu_0$ ,  $\text{T m A}^{-1}$ , are equivalent to  $\Omega \text{ s m}^{-1}$ .

**Problem 4** It is possible that the Lorentz force law allows marine sharks, skates, and rays to orient in a magnetic field [Frankel (1984)]. If a shark can detect an electric field strength of  $0.5 \mu\text{V m}^{-1}$ , how fast would it have to swim through the earth's magnetic field to experience an equivalent force on a charged particle? The earth's field is about  $5 \times 10^{-5} \text{ T}$ .

**Problem 5** The introduction to this section says that magnetism is a consequence of special relativity. Consider the following thought experiment. (a) A line of positive charge lies along the  $x$  axis and moves in the positive  $x$  direction. Is there a magnetic field present? (b) Change to a frame of reference moving with the charge. In this frame, where the charge is stationary, is there a magnetic field present? So is there really a magnetic field present, or not?

**Problem 6** The speed of blood in an artery or vein can be measured using an electromagnetic blood flow meter. A blood vessel of radius  $R$  is oriented perpendicular to a magnetic field  $\mathbf{B}$ . Ions in the blood, which is moving with speed  $U$ , experience a Lorentz force. Positive ions

move to one side of the vessel and negative ions move to the other side, establishing an electric field  $E$  whose force just balances the magnetic force.

(a) Draw a diagram showing the vessel and the directions of  $\mathbf{U}$ ,  $\mathbf{E}$ , and  $\mathbf{B}$ .

(b) Find an expression for  $U$  in terms of  $E$  and  $B$ .

(c) The electric field can be approximated as a voltage  $v$  across the vessel divided by the width of the vessel. Find an expression for  $v$  in terms of  $U$ ,  $B$  and  $R$ .

(d) If  $B = 0.1 \text{ T}$ ,  $U = 0.01 \text{ m s}^{-1}$  and  $R = 1 \text{ mm}$ , what is  $v$ ?

### Section 8.2

**Problem 7** A very long solenoid of radius  $a$  has current  $i$  in the windings. The windings are closely spaced and there are  $N$  turns per meter. What is the magnetic field in the solenoid? (Hint: if the solenoid is very long, the field inside is uniform and the field outside is zero. Use Ampere's law.)

**Problem 8** Show that  $d\mathbf{D}/dt$  has the dimensions of current density.

**Problem 9** A circular loop of radius  $a$  and area  $S$  carries current  $i$ . The loop is at the origin and lies in the  $xy$  plane. Calculate the magnetic field at any point on the  $z$  axis using the Biot-Savart law. Show that it is proportional to the magnetic moment of the loop,  $|\mathbf{m}| = iS$ , and falls off as  $z^{-3}$  if  $z \gg a$ .

**Problem 10** Show that a point source of current in an infinite, homogeneous conducting medium discharges at such a rate that the displacement current density everywhere cancels the current density, so that Ampere's law also predicts that the magnetic field is zero.

### Section 8.3

**Problem 11** Derive Eq. 8.13 from Eq. 8.12.

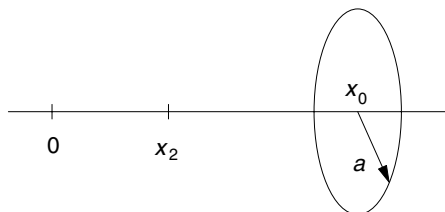
**Problem 12** The current along an axon is  $i_i(x) = i_0, 0 < x < x_1$  and is zero everywhere else. The axon is in an infinite homogeneous conducting medium.

(a) What is  $v_i(x)$ ?

(b) Find  $\mathbf{B}$  at a point  $(x_0, y_0)$ .

**Problem 13** One can obtain a very different physical picture of the source of a magnetic field using the Biot-Savart law than one gets using Ampere's law, even though the field is the same. A ring of radius  $a$  is perpendicular to the  $x$  axis and centered at  $x_0$ . Current flows along the  $x$  axis from  $x = 0$  to  $x = x_2$ . There is a spherically symmetric current in at  $x = 0$  and a spherically symmetric current out from  $x_2$ . Calculate the magnetic field at a point on the ring using Ampere's law and using the Biot-Savart law. Discuss the difference in interpretation; your expression for the field should be the same

as Prob. 12. A more extensive discussion of three different ways the source of the magnetic field can be viewed is given by Barach (1987).



**Problem 14** Suppose that  $i_i(t)$  is determined by measurement of the magnetic field around an axon. Numerical differentiation of the data gives derivatives of  $i_i$  also. Use the arguments of Sec. 6.11 and Problem 6.58 to show that for an action potential traveling without change of shape, one can determine the membrane current density from

$$j_m = \frac{1}{2\pi a u} \frac{\partial i_i}{\partial t} - c_m u r_i i_i.$$

For an application of this technique, see Barach et al. (1985).

### Section 8.4

**Problem 15** Use the same technique as in Chapter 7 to estimate the magnitude of the magnetocardiogram signal.

**Problem 16** (a) Derive Eqs. 8.17 and 8.18.

(b) What effect will  $y$  and  $z$  components of  $\mathbf{p}$  have for measurements taken along an axis with  $y = 0$ ?

**Problem 17** Consider a two-dimensional sheet of cardiac tissue represented using the bidomain model (Sec. 7.9.3). The intracellular and extracellular conductivity tensors are given by

$$\begin{aligned} \tilde{\sigma}_i &= \begin{pmatrix} \sigma_{ixx} & \sigma_{ixy} \\ \sigma_{ixy} & \sigma_{iyy} \end{pmatrix} \\ &= \begin{pmatrix} \sigma_{iL} \cos^2 \theta + \sigma_{iT} \sin^2 \theta & (\sigma_{iL} - \sigma_{iT}) \sin \theta \cos \theta \\ (\sigma_{iL} - \sigma_{iT}) \sin \theta \cos \theta & \sigma_{iL} \sin^2 \theta + \sigma_{iT} \cos^2 \theta \end{pmatrix} \\ \tilde{\sigma}_e &= \begin{pmatrix} \sigma_{exx} & \sigma_{exy} \\ \sigma_{exy} & \sigma_{eyy} \end{pmatrix} \\ &= \begin{pmatrix} \sigma_{eL} \cos^2 \theta + \sigma_{eT} \sin^2 \theta & (\sigma_{eL} - \sigma_{eT}) \sin \theta \cos \theta \\ (\sigma_{eL} - \sigma_{eT}) \sin \theta \cos \theta & \sigma_{eL} \sin^2 \theta + \sigma_{eT} \cos^2 \theta \end{pmatrix} \end{aligned}$$

where “L” means parallel to the fibers, “T” means perpendicular to the fibers, and  $\theta$  is the angle between the fiber direction and the  $x$  axis. The intracellular and extracellular current densities are given by  $\mathbf{j}_i = \tilde{\sigma}_i \cdot \mathbf{E} = -\tilde{\sigma}_i \cdot \nabla v_i$  and  $\mathbf{j}_e = -\tilde{\sigma}_e \cdot \nabla v_e$ . Assume that the intracellular and extracellular potentials are given by  $v_i = \sigma_{exx} v_m(x) / (\sigma_{ixx} + \sigma_{exx})$  and  $v_e = -\sigma_{ixx} v_m(x) / (\sigma_{ixx} + \sigma_{exx})$ , where  $v_m(x)$  is the transmembrane potential and is only a function of  $x$ , corresponding to a plane wave front propagating in the  $x$  direction.

(a) Draw a picture showing the 2-D sheet of tissue, the  $x$  and  $y$  axes, the fiber direction, and the direction of propagation.

(b) Show that  $j_x = j_{ix} + j_{ex}$  is identically zero.

(c) Derive an expression for  $j_y = j_{iy} + j_{ey}$  in terms of  $\sigma_{iL}$ ,  $\sigma_{iT}$ ,  $\sigma_{eL}$ ,  $\sigma_{eT}$ ,  $\theta$ , and  $v_m$ .

(d) Under what conditions is  $j_y$  identically zero?

(e) Describe qualitatively the magnetic field produced by a wave front in a sheet of cardiac tissue. For additional features of this model see Roth and Woods, IEEE Trans. Biomed. Eng. 46: 1288–1292 (1999).

### Section 8.5

**Problem 18** Consider two cylindrical cells of radius 1  $\mu\text{m}$ . One is an axon with an action potential lasting 1 ms and traveling at 1 m/s with a depolarization amplitude of 100 mV. The other is a dendrite with a post-synaptic potential depolarization of 10 mV. The conductivity within both cells is 1 S  $\text{m}^{-1}$ .

(a) Compare the magnetic field 5 cm away from the dendrite with depolarization only and the axon with a complete pulse.

(b) If the minimum magnetic field that can be detected is  $100 \times 10^{-15}$  T, how many dendrites must be simultaneously excited to detect the signal?

(c) Pyramidal cells in the cortex are aligned properly to generate this kind of signal. Assume the dendrite is 2 mm long. There are about 50,000 neurons/ $\text{mm}^3$  in the cortex, of which 70% are pyramidal cells. Find the volume of the smallest excited region that could be detected if all the pyramidal cells in the volume simultaneously had a post-synaptic depolarization of 10 mV.

**Problem 19** The magnetic field  $\mathbf{B}(\mathbf{r})$  produced by a current dipole  $\mathbf{p}$  located at  $\mathbf{r}_0$  in a spherical conductor is given by [Sarvas (1987)]

$$\mathbf{B}(\mathbf{r}) = \frac{\mu_0}{4\pi F^2} [F(\mathbf{p} \times \mathbf{r}_0) - (\mathbf{p} \times \mathbf{r}_0 \cdot \mathbf{r}) \nabla F],$$

where  $\mathbf{a} = \mathbf{r} - \mathbf{r}_0$ ,  $a = |\mathbf{a}|$ ,  $r = |\mathbf{r}|$ ,  $F = a(ra + r^2 - \mathbf{r}_0 \cdot \mathbf{r})$ ,

$$\nabla F = \left( \frac{a^2}{r} + \frac{\mathbf{a} \cdot \mathbf{r}}{a} + 2a + 2r \right) \mathbf{r} - \left( a + 2r + \frac{\mathbf{a} \cdot \mathbf{r}}{a} \right) \mathbf{r}_0,$$

and both  $r$  and  $r_0$  are measured from the center of the sphere.

(a) Show that if  $\mathbf{p}$  is radial,  $\mathbf{B} = 0$ .

(b) Show that the equation for the radial component of  $\mathbf{B}$  reduces to Eq. 8.15. Note that the radius of the sphere does not enter into these equations.

### Section 8.6

**Problem 20** Consider a rectangular current loop with one corner at  $(0, 0, 0)$  and the diagonally opposite corner at  $(dx, dy, 0)$ , in a changing magnetic field that has components  $(0, 0, dB/dt)$ . Show that for this configuration the

differential form of the Faraday induction law Eq. 8.20 follows from Eq. 8.19.

**Problem 21** Obtain the differential form of Ampere’s circuital law, Eq. 8.22 from Eq. 8.11.

**Problem 22** Write down in differential form (a) the Faraday induction law, (b) Ampere’s law including the displacement current term, (c) Gauss’s law, and (d) Eq. 8.7. (Ignore the effects of dielectrics or magnetic materials. That is, assume  $\mathbf{D} = \epsilon_0 \mathbf{E}$  and  $\mathbf{B} = \mu_0 \mathbf{H}$ .) These four equations together constitute “Maxwell’s equations.” Together with the Lorentz force law (Eq. 8.2), Maxwell’s equations summarize all of electricity and magnetism.

**Problem 23** Consider a square loop of wire in the  $xy$  plane that is moving in the positive  $x$  direction. There is a static magnetic field with a  $z$  component that increases linearly with  $x$ . Special relativity implies that the physics should be the same in any inertial frame of reference: that is, the physics should be the same in a reference frame moving with a constant velocity as it is in a frame at rest.

(a) Consider the frame described above, in which the loop moves and the magnetic field is static. Show qualitatively that the Lorentz force on the electrons in the wire induces a current.

(b) Now consider the situation from a frame of reference moving with the loop. Show qualitatively that Faraday induction will induce a current in the wire. Which “really” caused the current: the Lorentz force or Faraday induction?

**Problem 24** Suppose one is measuring the EEG when a time-dependent magnetic field is present (such as during magnetic stimulation). The EEG is measured using a disk electrode of radius  $a = 5$  mm and thickness  $d = 1$  mm, made of silver with conductivity  $\sigma = 63 \times 10^6$  S  $m^{-1}$ . The magnetic field is uniform in space, is in a direction perpendicular to the plane of the electrode, and changes from zero to 1 T in 200  $\mu$ s.

(a) Calculate the electric field and current density in the electrode due to Faraday induction.

(b) The rate of conversion of electrical energy to thermal energy per unit volume (Joule heating) is the product of the current density times the electric field. Calculate the rate of thermal energy production during the time the magnetic field is changing.

(c) Determine the total thermal energy change caused by the change of magnetic field.

(d) The specific heat of silver is 240 J  $kg^{-1} \text{ } ^\circ C^{-1}$ , and the density of silver is 10 500  $kg m^{-3}$ . Determine the temperature increase of the electrode due to Joule heating. The heating of metal electrodes can be a safety hazard during rapid (20 Hz) magnetic stimulation [Roth et al. (1992)].

**Problem 25** Suppose that during rapid-rate magnetic stimulation, each stimulus pulse causes the temperature

of a metal EEG electrode to increase by  $\Delta T$  (see Prob. 24). The hot electrode then cools exponentially with a time constant  $\tau$  (typically about 45 s). If  $N$  stimulation pulses are delivered starting at  $t = 0$  m with successive pulses separated by a time  $\Delta t$ , then the temperature at the end of the pulse train is  $T(N, \Delta t) = \Delta T \sum_{i=0}^{N-1} e^{-i\Delta t/\tau}$ . Find a closed-form expression for  $T(N, \Delta t)$  using the summation formula for the geometric series:  $1 + x + x^2 + \dots + x^{n-1} = (1 - x^n)/(1 - x)$ . Determine the limiting values of  $T(N, \Delta t)$  for  $N\Delta t \ll \tau$  and  $N\Delta t \gg \tau$ . [See Roth et al. (1992).]

Section 8.7

**Problem 26** Suppose that a magnetic stimulator consists of a single-turn coil of radius  $a = 2$  cm. It is desired to have a magnetic field of 2 T on the axis of the coil at a distance  $b = 2$  cm away.

(a) Calculate the current required, using symmetry and the Biot–Savart law. (Hint: Use the results of Problem 9.)

(b) Assume that the magnetic field rises from 0 to 2 T in 100  $\mu$ s. Assume also that the flux through the coil is equal to the field at the center of the coil multiplied by the area of the coil. Calculate the emf induced in the coil.

Section 8.8

**Problem 27** Magnetite,  $Fe_3O_4$ , has a density of 5.24  $g cm^{-3}$  and a magnetic moment of  $3.75 \times 10^{-23}$  A  $m^2$  per molecule. If a cubic sample 50 nm on a side is completely magnetized, what is the total magnetic moment? What is the magnitude of  $M$ ?

**Problem 28** The magnetic moment of a magnetosome, one of the small particles of magnetite in a bacterium, is about  $6.40 \times 10^{-17}$  A  $m^2$ . Assume that the magnetic activity in all the species listed is due to a collection of magnetosomes of this size. The table shows values given in the references cited in the text. The earth’s magnetic field is about  $5 \times 10^{-5}$  T. Fill in the remaining entries in the table.

Organism	Number of magnetosomes	Total magnetic moment (A $m^2$ )	$mB_{earth}/k_B T$
Bacterium	20		
Bee		$1.2 \times 10^{-9}$	
Pigeon		$5.0 \times 10^{-9}$	
Tuna	$8.5 \times 10^7$		

**Problem 29** In this problem you will work out the orientation of a bacterium if the entire organism simply aligns like a compass needle in the earth’s field of  $5 \times 10^{-5}$  T.

(a) Show that  $\tau = \mathbf{m} \times \mathbf{B}$  implies an orientation energy  $U = -mB \cos \theta$ .

(b) The bacterium has a single flagellum that causes it to swim in the direction of its long axis with speed  $v_0$ . The component of its velocity in the direction of the earth's field is  $v_x = v_0 \cos \theta$ . In the absence of the magnetic torque, the probability that a bacterium is at an angle between  $\theta$  and  $\theta + d\theta$  with the earth's field is  $d\Omega = 2\pi \sin \theta d\theta$ . With the torque, the probability that a bacterium is at angle with the earth's field is modified by a Boltzmann factor  $\exp(-U/k_B T)$ . Find the average velocity in the direction of the earth's field. Use  $m = 1.28 \times 10^{-15} \text{ A m}^2$ .

**Problem 30** Suppose that the bacterium of Problem 29 is swimming in a tank aligned with the earth's field. An external coil suddenly reverses the direction of the field but leaves the magnitude unchanged. Assume that the bacterium is a sphere of radius  $a$ . A torque on a small sphere of radius  $a$  in a medium of viscosity  $\eta$  causes the sphere to rotate at a rate  $d\theta/dt$ , such that  $\tau = 8\pi a^3 \eta (d\theta/dt)$ . For simplicity, assume that all motion takes place in a plane.

(a) Show that  $d\theta/dt = \sin \theta / t_0$ , where  $t_0 = 8\pi a^3 \eta / mB$ .

(b) Evaluate  $t_0$  for a bacterium of radius  $2 \mu\text{m}$  in the earth's magnetic field. Use  $m = 1.28 \times 10^{-15} \text{ A m}^2$ .

(c) The velocity component perpendicular to the field is  $v_y = v_0 \sin \theta$ . Show that when the bacterium rotates from angle  $\theta_1$  to  $\theta_2$  it has moved a distance  $y = v_0 t_0 (\theta_2 - \theta_1)$ .

(d) Show that the time required to change from angle  $\varepsilon$  to  $\pi - \varepsilon$  is  $t_0 \ln [(1 + \cos \varepsilon) / (1 - \cos \varepsilon)]$ .

**Problem 31** Magnetic cell sorting is a way to isolate cells of a particular type. Small superparamagnetic particles (about 50 nm diameter) are bound to an antibody that attaches specifically to the cell type of interest. ("Superparamagnetic" means that they behave linearly but have a magnetic susceptibility  $\chi_m \gg 1$ .) These cells are then placed in a magnetic field gradient, and the resulting force is used to manipulate the cell. What is the force if 100 spherical 50 nm diameter particles are attached to a cell that is in a magnetic field of 1 T with a magnetic field gradient of  $10 \text{ T m}^{-1}$ ?

## Section 8.9

**Problem 32** The spatial gradient in the earth's field is about  $10^{-11} \text{ T m}^{-1}$ . How much lateral movement can be tolerated in measuring a magnetoencephalogram of about  $10^{-13} \text{ T}$ ?

**Problem 33** Show that the units of  $h/2e$  are V s, and that this is also a unit of magnetic flux.

**Problem 34** Suppose that a SQUID of area  $0.1 \text{ cm}^2$  can resolve a magnetic flux change  $\Delta\Phi = 10^{-3}\Phi_0$ . What is the corresponding change in  $B$ ?

**Problem 35** The first difference of  $B$  is  $B(x+a) - B(x)$ . What is the second difference? Compare the first and

second differences to what is detected by a first-order and second-order gradiometer. Assume that  $B$  is constant over the area of each gradiometer loop. Use these results to determine the signal resulting from a distant but unwanted dipole source with a magnetic field that falls as  $1/r^3$ .

**Problem 36** A first-order gradiometer is used to measure the magnetic field at a point  $(x_0, 0, z_0)$  from a current dipole described by Eq. 8.16. The gradient is measured at position  $z = x_0/\sqrt{2}$ . The coils are at  $x_0$  and  $x_0 + a$  and are perpendicular to the  $z$  axis. Find the net flux in the gradiometer in terms of  $x_0$  and  $a$  and the radius  $b$  of the coils. Assume  $B$  is uniform across each coil.

**Problem 37** Figure 8.29(a) shows a gradiometer for measuring  $\partial B_z / \partial z$ . Sketch a gradient coil for measuring  $\partial B_z / \partial x$ .

**Problem 38** Consider a nerve threaded through the center of a toroid of magnetic permeability  $\mu$ , wound with  $N$  turns of wire, as shown in Fig. 8.26. The inner radius of the toroid is  $c$ , the outer radius is  $d$ , and the width is  $e$ . Assume a current  $I$  flows inside the axon and is uniform along its length.

(a) Calculate the magnetic flux  $\Phi = \int \mathbf{B} \cdot d\mathbf{S}$  through the toroid winding caused by the current in the axon.

(b) The magnetic flux divided by the current is called the mutual inductance,  $M$ , of the axon and coil. Show that the mutual inductance is  $M = \mu N e \ln(d/c) / 2\pi$ .

(c) By Faraday's induction law, the electromotive force (EMF) induced in the windings is  $EMF = -M(dI/dt)$ . Calculate the EMF when  $\mu = 10,000\mu_0$ ,  $N = 100$ ,  $c = 1 \text{ mm}$ ,  $d = 2 \text{ mm}$ ,  $e = 1 \text{ mm}$ , and  $I$  changes from zero to  $1 \mu\text{A}$  in  $1 \text{ ms}$ . For additional information about using a toroid to detect currents along an axon, see Gielen et al. (1986).

**Problem 39** A coil on a magnetic toroid as in Problem 38 is being used to measure the magnetic field of a nerve axon.

(a) If the axon is suspended in air, with only a thin layer of extracellular fluid clinging to its surface, use Ampere's law to determine the magnetic field,  $B$ , recorded by the toroid.

(b) If the axon is immersed in a large conductor such as a saline bath,  $B$  is proportional to the sum of the intracellular current plus that fraction of the extracellular current that passes through the toroid (see Problem 13). Suppose that during an experiment an air bubble is trapped between the axon and the inner radius of the toroid? How is the magnetic signal affected by the bubble? See Roth et al. (1985).

**Problem 40** When comparing calculated and measured magnetic fields, the calculated field should be integrated over the area of the detector coil to give the magnetic flux through the coil. Assume the detector coil is circular

with radius  $a$ . The flux can be approximated by

$$\iint \mathbf{B} \cdot d\mathbf{S} \approx \frac{\pi a^2}{3} \sum_{i=1}^3 B_n \left( r = \frac{a}{\sqrt{2}}, \theta = i \frac{2\pi}{3} \right),$$

where  $B_n$  is the component of  $\mathbf{B}$  normal to the coil, and  $r$  and  $\theta$  are polar coordinates with the origin at the coil center. Show that this equation is exact up to second order. In other words, show that this equation is exact for magnetic fields given by

$$B_n = c + dx + ey + fx^2 + gxy + hy^2,$$

where  $c, d, e, f, g,$  and  $h$  are constants,  $x = r \cos \theta$ , and  $y = r \sin \theta$ . Higher-order formulas for averaging the magnetic field can be found in Roth and Sato (1992).

## References

- Able, K. P., and M. A. Able (1995). Interactions in the flexible orientation system of a migratory bird. *Nature* **375**: 230–223.
- Barach, J. P. (1987). The effect of ohmic return current on biomagnetic fields. *J. Theor. Biol.* **125**: 187–191.
- Barach, J. P., B. J. Roth, and J. P. Wikswo (1985). Magnetic measurements of action currents in a single nerve axon: A core conductor model. *IEEE Trans. Biomed. Eng.* **32**: 136–140.
- Barker, A. T., R. Jalinous, and I. L. Freeston (1985). Non-invasive magnetic stimulation of the human cortex. *Lancet* **1**(8437): 1106–1107.
- Brittenham, G. M., D. E. Farrell, J. W. Harris, E. S. Feldman, E. H. Danish, W. A. Muir, J. H. Tripp, J. N. Brennan, and E. M. Bellon (1983). Diagnostic assessment of human iron stores by measurement of hepatic magnetic susceptibility. *Nuovo Cimento* **2D**: 567–581.
- Clarke, J. (1994). SQUIDS. *Sci. Am.* Aug. 1994: 46–53.
- Cochran, W. W., H. Mouritsen, and M. Wikelski (2004). Migrating songbirds recalibrate their magnetic compass daily from twilight cues. *Science*. **304**: 405–408.
- Cohen, D., I. Nemoto, L. Kaufman, and S. Arai (1984). Ferrimagnetic particles in the lung part II: The relaxation process. *IEEE Trans. Biomed. Eng.* **31**: 274–285.
- de Araujo, F. F., M. A. Pires, R. B. Frankel, and C. E. M. Bicudo (1986). Magnetite and magnetotaxis in algae. *Biophys. J.* **50**: 375–378.
- Eisberg, R., and R. Resnick (1985). *Quantum Physics of Atoms, Molecules, Solids, Nuclei and Particles*, 2nd ed. New York, Wiley.
- Esselle, K. P., and M. A. Stuchly (1995). Cylindrical tissue model for magnetic field stimulation of neurons: Effects of coil geometry. *IEEE Trans. Biomed. Eng.* **42**(9): 934–941.
- Frankel, R. B. (1984). Magnetic guidance of organisms. *Ann. Rev. Biophys. Bioeng.* **13**: 85–103.
- Frankel, R. B., R. P. Blakemore, and R. S. Wolfe (1979). Magnetite in freshwater magnetotactic bacteria. *Science* **203**: 1355–1356.
- Frankel, R. B., and D. A. Bazylinski (1994). Magnetotaxis and magnetic particles in bacteria. *Hyperfine Interactions* **90**: 135–142.
- Gielen, F. L. H., R. N. Friedman, and J. P. Wikswo, Jr. (1991). In vivo magnetic and electric recordings from nerve bundles and single motor units in mammalian skeletal muscle. Correlations with muscle force. *J. Gen. Physiol.* **98**(5): 1043–1061.
- Gielen, F. L. H., B. J. Roth and J. P. Wikswo, Jr. (1986). Capabilities of a toroid-amplifier system for magnetic measurements of current in biological tissue. *IEEE Trans. Biomed. Eng.* **33**: 910–921.
- Gould, J. L. (1995). Constant compass calibration. *Nature* **375**: 184.
- Gould, J. L., J. L. Kirschvink, and K. S. Deffeyes (1978). Bees have magnetic remanence. *Science* **201**: 1026–1028.
- Grimes, D. I. F., R. F. Lennard, and S. J. Swithenby (1985). Macroscopic ion currents within the human leg. *Phys. Med. Biol.* **30**: 1101–1112.
- Hallett, M., and L. G. Cohen (1989). Magnetism: A new method for stimulation of nerve and brain. *JAMA* **262**: 538–541.
- Hämäläinen, M., R. Harri, R. J. Ilmoniemi, J. Knuutila, and O. V. Lounasmaa (1993). Magnetoencephalography—theory, instrumentation, and applications to noninvasive studies of the working human brain. *Rev. Mod. Phys.* **65**(2): 413–497.
- Heller, L., and D. B. van Hulsteyn (1992). Brain stimulation using magnetic sources: Theoretical aspects. *Biophys. J.* **63**: 129–138.
- Hosaka, H., D. Cohen, B. N. Cuffin, and B. M. Horacek (1976). The effect of torso boundaries on the magnetocardiogram. *J. Electrocardiogr.* **9**: 418–425.
- Ilmoniemi, R. J., J. Ruohonen and J. Karhu (1999). Transcranial magnetic stimulation—A new tool for functional imaging of the brain. *Crit. Rev. Biomed. Eng.* **27**(3–5): 241–284.
- Mielczarek, E. V., and S. B. McGrayne. (2000). *Iron: Nature's Universal Element: Why People Need Iron and Animals Make Magnets*. New Brunswick, Rutgers U. Press.
- Moskowitz, B. M. (1995). Biomineralization of magnetic minerals. *Rev. Geophys. Suppl.* **33**(Part 1 Suppl. S): 123–128.
- Nielsen, P., R. Fischer, R. Englehardt, P. Tondury, E. E. Gabbe, and G. E. Janka (1995). Liver iron stores in patients with secondary haemosiderosis under iron chelation therapy with deferoxamine or deferiprone. *Brit. J. Hematology* **91**: 827–833.
- Page, C. H. (1977). Electromotive force, potential difference, and voltage. *Am. J. Phys.* **45**: 978–980.
- Petrie, R. J., P. van Leeuwen, B. Brandts, G. Turnbull, S. J. O. Veldhuyzen van Zanten, and G. Stroink (1996).

- Single and multichannel measurements of gastrointestinal activity in the fasted and fed states. In C. Aine, E. Flynn, Y. Okada, G. Stroink, S. Swithenby, and C. Woods, eds. *Biomag.96: Advances in Biomagnetism Research*. Berlin, Springer-Verlag.
- Press, W. H., S. A. Teukolsky, W. T. Vetterling, and B. P. Flannery (1992). *Numerical Recipes in C: The Art of Scientific Computing*, 2nd ed. reprinted with corrections, 1995. New York, Cambridge University Press.
- Purcell, E. M. (1985). *Electricity and Magnetism*, 2nd ed. Berkeley Physics Course. New York, McGraw-Hill, Vol. 2.
- Purcell, C. J., G. Stroink, and B. M. Horacek (1988). Effect of torso boundaries on electrical potential and magnetic field of a dipole. *IEEE Trans. Biomed. Eng.* **35**(9): 671–678.
- Richards, W. O., C. L. Garrard, S. H. Allos, L. A. Bradshaw, D. J. Staton, and J. P. Wikswo, Jr. (1995a). Non-invasive diagnosis of mesenteric ischemia using a squid magnetometer. *Ann. Surg.* **221**(6): 696–704.
- Richards, W. O., D. Staton, J. Golzarian, R. N. Friedman, and J. P. Wikswo, Jr. (1995b). Noninvasive SQUID magnetometer measurement of human gastric and small bowel electrical activity. In C. Baumgartner *et al.*, eds. *Biomagnetism: Fundamental Research and Clinical Applications*. Elsevier, IOS.
- Romer, R. H. (1982). What do voltmeters measure?: Faraday's law in a multiply connected region. *Am. J. Phys.* **50**: 1089–1093.
- Roth, B. J., J. K. Woosley, and J. P. Wikswo, Jr. (1985). An experimental and theoretical analysis of the magnetic field of a single axon. In H. Weinberg, G. Stroink and T. Katila, Eds. *Biomagnetism: Applications and Theory*. New York, Pergamon, pp. 78–82.
- Roth, B. J., A. Pascual-Leone, L. G. Cohen, and M. Hallett (1992). The heating of metal electrodes during rapid-rate magnetic stimulation: a possible safety hazard. *Electroenceph. Clin. Neurophysiol.* **85**: 116–123.
- Roth, B. J., and S. Sato (1992). Accurate and efficient formulas for averaging the magnetic field over a circular coil. In M. Hoke, S. N. Erne, T. C. Okada, and G. L. Romani, eds. *Biomagnetism: Clinical Aspects*. Amsterdam, Elsevier.
- Roth, B. J. (1994). Mechanisms for electrical stimulation of excitable tissue. *Crit. Rev. Biomed. Eng.* **22**(3/4): 253–305.
- Roth, B. J., and J. P. Wikswo, Jr. (1985). The magnetic field of a single axon: A comparison of theory and experiment. *Biophys. J.* **48**: 93–109.
- Sarvas, J. (1987). Basic mathematical and electromagnetic concepts of the biomagnetic inverse problem. *Phys. Med. Biol.* **32**: 11–22.
- Shadowitz, A. (1975). *The Electromagnetic Field*. New York, McGraw-Hill.
- Stahlhofen, W., and W. Moller (1993). Behaviour of magnetic micro-particles in the human lung. *Rad. Env. Biophys.* **32**(3): 221–238.
- Staton, D. J., R. N. Friedman, and J. P. Wikswo, Jr. (1993). High resolution SQUID imaging of octupolar currents in anisotropic cardiac tissue. *IEEE Trans. Appl. Superconduct.* **3**(1): 1934–1936.
- Stroink, G. (1985). Magnetic measurements to determine dust loads and clearance rates in industrial workers and miners. *Med. Biol. Eng. Computing* **23**: 44–49.
- Stroink, G. (1993). Cardiomagnetic imaging. In B. L. Zaret, L. Kaufman, A. S. Berson, and R. A. Dunn, eds. *Frontiers in Cardiovascular Imaging*. New York, Raven, pp. 161–177.
- Stroink, G., M. J. R. Lamothe, and M. J. Gardner (1996). Magnetocardiographic and electrocardiographic mapping studies. In H. Weinstock, ed. *SQUID Sensors: Fundamentals, Fabrication and Applications*. NATO ASI Series, Dordrecht, The Netherlands, Kluwer.
- Stroink, G., B. Blackford, B. Brown, and B. M. Horacek (1981). Aluminum shielded room for biomagnetic measurements. *Rev. Sci. Instrum.* **52**(3): 463–468.
- Swinney, K. R., and J. P. Wikswo, Jr. (1980). A calculation of the magnetic field of a nerve action potential. *Biophys. J.* **32**: 719–732.
- Taccardi, B., and B. B. Punske (2004). Body surface potential mapping. In D. P. Zipes and J. Jalife, eds. *Cardiac Electrophysiology: From Cell to Bedside*, 4th ed., Philadelphia, Saunders, pp. 1803–811.
- Tan, G. A., F. Brauer, G. Stroink, and C. J. Purcell (1992). The effect of measurement conditions on MCG inverse solutions. *IEEE Trans. Biomed. Eng.* **39**(9): 921–927.
- Thomas, I. M., M. Freake, S. J. Swithenby, and J. P. Wikswo, Jr. (1993). A distributed quasi-static ionic current in the 3–4 day old chick embryo. *Phys. Med. Biol.* **38**: 1311–1328.
- Trontelj, Z., R. Zorec, V. Jabinsek, and S. N. Erne (1994). Magnetic detection of a single action potential in *Chara corallina* internodal cells. *Biophys. J.* **66**: 1694–1696.
- Walcott, C., J. L. Gould, and J. L. Kirschvink (1979). Pigeons have magnets. *Science* **205**: 1027–1029.
- Walker, M. M., J. L. Kirschvink, S.-B. R. Chang, and A. E. Dizon (1984). A candidate magnetic sense organ in the yellowfin tuna. *Science* **224**: 751–753.
- Wikswo, J. P., Jr. (1980). Noninvasive magnetic detection of cardiac mechanical activity: Theory. *Med. Phys.* **7**: 297–306.
- Wikswo, J. P., Jr. (1995a). SQUID magnetometers for biomagnetism and nondestructive testing: Important questions and initial answers. *IEEE Trans. Appl. Superconduct.* **5**(2): 74–120.
- Wikswo, J. P., Jr. (1995b). Tissue anisotropy, the cardiac bidomain, and the virtual cathode effect. In D. P. Zipes and J. Jalife, eds. *Cardiac Electrophysiology: From Cell to Bedside*, 2nd ed., Philadelphia, Saunders, pp. 348–361.

Wiksw, J. P., Jr., A. Gevins, and S. J. Williamson (1993). The future of the EEG and MEG. *Electroencephalogr. Clin. Neurophysiol.* **87**: 1–9.

Woosley, J. K., B. J. Roth, and J. P. Wiksw, Jr. (1985). The magnetic field of a single axon; A volume conductor model. *Math. Biosci.* **76**: 1–36.



# Electricity and Magnetism at the Cellular Level

This chapter describes a number of topics related to charged membranes and the movement of ions through them. These range from the basics of how the presence of impermeant ions alters the concentration ratios of permeant ions, to the movement of ions under the combined influence of an electric field and diffusion, and to simple models for gating in ion channels in cell membranes. It also discusses mechanisms for the detection of weak electric and magnetic fields and the possible effects of weak low-frequency electric and magnetic fields on cells.

Section 9.1 discusses Donnan equilibrium in which the presence of an impermeant ion on one side of a membrane, along with other ions that can pass through, causes a potential difference to build up across the membrane. This potential difference exists even though the bulk solution on each side of the membrane is electrically neutral. Section 9.2 examines the Gouy–Chapman model for the charge buildup at each surface of the membrane that gives rise to this potential difference. This same model is extended in three dimensions to the cloud of counterions surrounding each ion in solution—the Debye–Hückel model of Sec. 9.3.

Since water molecules have a net dipole moment, they align themselves so as to nearly cancel the electric field of each ion. Very close to the ion the electric field is so strong that even complete alignment is insufficient to cancel the ion’s field. This saturation of the dielectric is described in Sec. 9.4.

Ions move in solution by *diffusion* if there is a concentration gradient and by *drift* if there is an applied electric field. The Nernst–Planck equation (Sec. 9.5) describes this motion. When several ion species are moving through a membrane, there can be zero total electric current, even though there is a flow of each species. A constant-field model for this situation leads to the Goldman equations of Sec. 9.6.

The next two sections describe channels in active cell membranes. Section 9.7 describes a simple model for gating—the opening and closing of channels—as well as limitations to the conductance of each channel imposed by diffusion to the mouth of the channel. Section 9.8 introduces noise—the fluctuations in channel current that limit measurement accuracy but also can be used to determine properties of the channels.

Section 9.9 describes how channels can detect very small mechanical motions, as in the ear, and how certain fish can detect very small electric fields in sea water. Both of these processes are working near the limit of sensitivity set by random thermal motion.

Section 9.10 introduces an area of great interest and controversy: whether weak, low-frequency electric and magnetic fields can have any effect on cells. We discuss some of the physical aspects of the problem and conclude that such effects are highly unlikely.

There are many similarities between the models for biological physics presented in this chapter and the models used in plasma physics [Uehara *et al.* (2000)].

## 9.1 Donnan Equilibrium

There is usually an electrical potential difference across the wall of a capillary. There is also a potential difference across the cell membrane, and the concentration of certain ion species is different in the intracellular and extracellular fluid. In Chapter 3 we saw that if the potential difference across the membrane is  $v' - v$ , an ion of valence  $z$  is in equilibrium when  $C'/C = e^{-ze(v' - v)/k_B T}$ . With this concentration ratio there is no current, even if the membrane is permeable to the species. This result is a special case of the Boltzmann factor, more familiar in

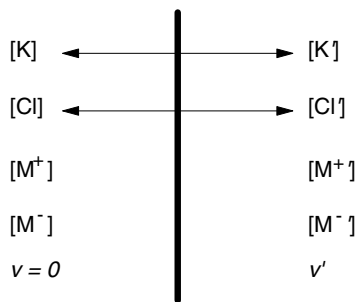


FIGURE 9.1. Ion concentrations on either side of a membrane. Species that can pass through the membrane are indicated by double-headed arrows.

physiology as the Nernst equation (Eq. 3.34):

$$v' - v = -\frac{k_B T}{ze} \ln\left(\frac{C'}{C}\right) = -\frac{RT}{zF} \ln\left(\frac{C'}{C}\right).$$

It is often said—incorrectly—that the Nernst equation shows how the concentration of an ion species causes the potential difference across the membrane. We saw in Chapter 6 that the potential difference across the membrane is caused by layers of charge on each side of the membrane that create an electric field in the membrane. The solutions on each side of the membrane are electrically neutral except at the boundary with the membrane. (If there were an electric field in the solution, ions would move until the field was zero; then Gauss's law could be used to show that any volume contains zero charge.) We will learn in Sec. 9.2 the typical distance from the membrane occupied by the charged layer, and in Sec. 9.3 we will find the distance scale over which there are microscopic departures from neutrality in a bulk ionic solution.

The concentration differences do not *directly* cause the potential difference. However, if the concentration of an ion species on one side of the membrane is varied, the potential often changes in a manner that is approximated by the Nernst equation over a wide range of concentrations. We will now explore one mechanism by which this can happen. This is particularly important for the walls of capillaries, where charged proteins in the blood are too large to pass through the gaps between cells in the capillary walls, but it is also applicable to the cell membrane.

In Donnan equilibrium, the potential difference arises because one ion species cannot pass through the membrane at all. Consider the hypothetical case of Fig. 9.1. Permeant potassium ions exist on either side of the membrane in concentrations  $[K]$  and  $[K']$ . In this case potassium is the only permeant cation; in a real situation there might be several permeant ions. The membrane is also permeable to chloride ions, which exist in concentrations  $[Cl]$  and  $[Cl']$ . Chloride is the only permeant anion. In addition, there are large charged molecules  $[M^+]$  and  $[M^-]$  that cannot pass through the membrane. Their concentrations are  $[M^+]$ ,  $[M^{+'}]$ ,  $[M^-]$ , and  $[M^{-'}]$ . For simplicity, we assume they are monovalent. The potential on the

left is 0; on the right it is  $v'$ . Assume that the concentrations of the large molecules are fixed. The potassium concentration on the left side of the membrane will be assumed known, and we must solve for four variables:  $[K']$ ,  $[Cl]$ ,  $[Cl']$ , and  $v'$ . Therefore, four equations are needed.

The first two equations state that the solutions on either side are electrically neutral:

$$[M^+] + [K] = [Cl] + [M^-], \quad (9.1)$$

$$[M^{+'}] + [K'] = [Cl'] + [M^{-'}]. \quad (9.2)$$

Equation 9.1 can be solved for  $[Cl]$ . It will be convenient to define  $[M] = [M^+] - [M^-]$  and  $[M'] = [M^{+'}] - [M^{-'}]$ :

$$[Cl] = [K] + ([M^+] - [M^-]) = [K] + [M]. \quad (9.3)$$

Note that adding any amount of KCl to the solution on the left automatically satisfies this equation, since any increase in  $[K]$  is accompanied by a like increase in  $[Cl]$ .

The other two equations state that the concentrations of potassium and chloride on the two sides of the membrane are related by a Boltzmann factor. Since the valence  $z = +1$  for  $[K]$  and  $-1$  for  $[Cl]$  we have

$$\frac{[K']}{[K]} = \frac{[Cl]}{[Cl']} = e^{-ev'/k_B T}. \quad (9.4)$$

The chloride concentration on the right is  $[Cl'] = [Cl]$  ( $[Cl'] / [Cl] = [K] / [K']$ ), so that from Eq. 9.2  $[K'] + [M'] = [Cl]$  ( $[K] / [K']$ ). This can be rewritten as a quadratic equation in  $[K']$ , since  $[K]$  and  $[M']$  are known and  $[Cl]$  is calculated from Eq. 9.3:

$$[K']^2 + [M'] [K'] - [K] [Cl] = 0.$$

The solution is

$$[K'] = \frac{-[M'] + \sqrt{[M']^2 + 4[K][Cl]}}{2}. \quad (9.5)$$

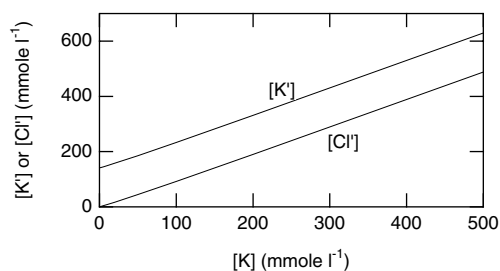
(The negative square root is discarded because it would give a negative potassium concentration.) Once we have solved for  $[K']$ ,  $[Cl']$  and  $v'$  are determined from Eq. 9.4. Solutions for different values of  $[K]$  are shown in Table 9.1 and Figs. 9.2 and 9.3 for the conditions

$$\begin{aligned} [M^+] &= 145 \text{ mmol l}^{-1}, & [M^{+'}] &= 15 \text{ mmol l}^{-1}, \\ [M^-] &= 30 \text{ mmol l}^{-1}, & [M^{-'}] &= 156 \text{ mmol l}^{-1}, \\ [M] &= 115 \text{ mmol l}^{-1}, & [M'] &= -141 \text{ mmol l}^{-1}. \end{aligned}$$

The temperature  $T = 310$  K, for which  $k_B T/e = 26.75$  mV.

TABLE 9.1. Variation of concentrations and voltage as  $[K]$  is varied.

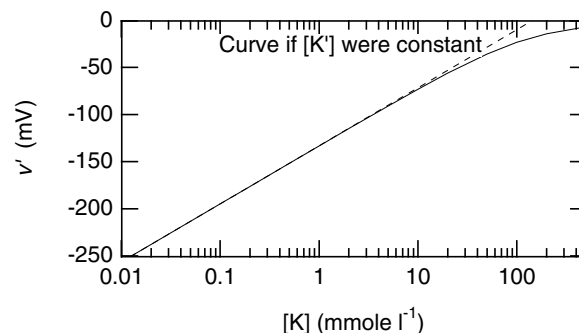
$[K]$	$[Cl]$	$[K']$	$[Cl']$	$\frac{[Cl]}{[Cl']} = \frac{[K']}{[K]}$	$v'$ (mV)
0.01	115.01	141.01	0.01	14101	-255.57
0.10	115.10	141.08	0.08	1410.8	-193.99
0.20	115.20	141.16	0.16	705.8	-175.46
0.50	115.50	141.41	0.41	282.8	-151.00
1.00	116.00	141.82	0.82	141.8	-132.53
2.00	117.00	142.64	1.64	71.32	-114.15
5.00	120.00	145.13	4.13	29.03	-90.10
10.00	125.00	149.37	8.37	14.94	-72.33
20.00	135.00	158.08	17.08	7.904	-55.30
50.00	165.00	185.48	44.48	3.710	-35.07
100.00	215.00	233.20	92.20	2.332	-22.65
200.00	315.00	331.21	190.21	1.656	-13.49
500.00	615.00	629.49	488.49	1.259	-6.16

FIGURE 9.2. Variation of  $[K']$  and  $[Cl']$  with  $[K]$  in the example of Donnan equilibrium.

Several features of this solution are worth noting. First, changing  $[K]$  does change the potential, but the mechanism is indirect. The Boltzmann factor still applies; minuscule changes in concentration are sufficient to provide layers of charge on the membrane surface that generate a potential difference such that these concentrations are at equilibrium. Table 9.1 shows that  $[K]$  can vary by three orders of magnitude—from 0.01 to 10, and  $[K']$  changes very little. Therefore, the curve of  $v'$  vs  $\ln [K]$  in Fig. 9.3 is nearly a straight line. The dashed line in Fig. 9.3 shows  $v'$  vs  $\ln [K]$  if  $[K']$  is held constant. We could equally well have regarded  $[Cl]$  as the independent variable.

The impermeable ions enter the equation only as their net charge,  $[M] = [M^+] - [M^-]$  and  $[M'] = [M'^+] - [M'^-]$ . As the concentrations  $[K]$  and  $[Cl]$  get larger, the impermeable ions become less important, the potential approaches zero, and the ratios  $[K']/[K]$  and  $[Cl']/[Cl]$  approach unity.

Donnan equilibrium may well explain the potential that exists across the capillary wall, which is impermeable to negatively charged proteins but is permeable to other ions. There is evidence that it does not adequately explain the potential across a cell membrane. For exam-

FIGURE 9.3. Membrane potential  $v'$  vs  $[K]$  for the example of Donnan equilibrium. For  $[K] < 10$  mM the curve is like the Nernst equation because  $[K']$  has a nearly constant value of 141 mM. The dashed line shows the relationship if  $[K']$  is constant.

ple, the membrane is known to be slightly permeable to sodium, although the sodium concentration is nowhere near what it would be if the sodium were in equilibrium.

## 9.2 Potential Change at an Interface: The Gouy–Chapman Model

In this section we study one model for how ions are distributed at the interface in Donnan equilibrium. The model was used independently by Gouy and by Chapman to study the interface between a metal electrode and an ionic solution. They investigated the potential changes along the  $x$  axis perpendicular to a large plane electrode. The same model is used to study the charge distribution in a semiconductor. Biological applications are described by Mauro (1962). We show the features of the model by examining the transition region for the Donnan equilibrium example described in the preceding section.

An infinitely thin membrane at  $x = 0$  is assumed to be permeable to potassium and chloride ions. Their concentrations are  $K(x)$  and  $Cl(x)$ . An impermeable positive cation has concentration  $M(x)$  for  $x > 0$ . For negative  $x$ ,  $M(x) = 0$ . There are no impermeable anions. Far to the left the potential is zero and the concentrations are  $[K]$  and  $[Cl]$ . Far to the right they are  $v'$ ,  $[K']$ ,  $[Cl']$ , and  $[M']$ .

The first step is to relate the charge distribution to the potential. If  $v$  and  $E$  change only in the  $x$  direction, then Gauss's law can be applied to a slab of cross-sectional area  $S$  between  $x$  and  $x + dx$  as shown in Fig. 9.4. The net flux out through the surface at  $x + dx$  is  $E_x(x + dx)S$ . The net outward flux at  $x$  is  $-E_x(x)S$ . There is no contribution to the flux through the other surfaces. The total ionic charge in the volume is  $\rho_{\text{ext}}(x)Sdx$ . We include the effect of water polarization by using the dielectric constant for water, which is about  $\kappa = 80$ . Applying Gauss's law in

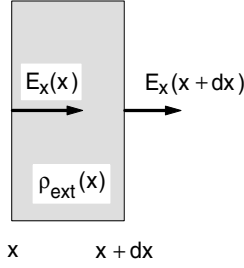


FIGURE 9.4. Gauss's law is applied to the shaded volume to derive Poisson's equation in one dimension.

the form Eq. 6.21b, we obtain<sup>1</sup>

$$E_x(x + dx) - E_x(x) = \frac{4\pi\rho_{\text{ext}}(x) dx}{4\pi\epsilon_0 \kappa},$$

$$\frac{dE_x}{dx} = \frac{4\pi\rho_{\text{ext}}(x)}{4\pi\epsilon_0 \kappa}.$$

Finally, since  $E_x = -\partial v/\partial x$ , we have the one-dimensional Poisson equation,

$$\frac{d^2v}{dx^2} = -\frac{4\pi\rho_{\text{ext}}(x)}{4\pi\epsilon_0 \kappa}. \quad (9.6)$$

This equation was derived in much the same way that the equation of continuity was combined with Fick's first law to derive Fick's second law (Sec. 4.8). The same procedure can be used in three dimensions to derive the general form of Poisson's equation:

$$\nabla^2 v = -\frac{4\pi\rho_{\text{ext}}(\mathbf{r})}{4\pi\epsilon_0 \kappa}. \quad (9.7)$$

For the model being considered the ions are all univalent, so the ionic charge density at  $x$  is related to the concentrations by

$$\rho_{\text{ext}}(x) = e[K(x) + M(x) - Cl(x)]. \quad (9.8a)$$

More generally, for a series of ion species each with concentration  $C_i$  and valence  $z_i$ ,

$$\rho_{\text{ext}}(\mathbf{r}) = e \sum_i z_i C_i(\mathbf{r}). \quad (9.8b)$$

The next step is to assume that the concentrations of all ions are given by Boltzmann factors and are therefore related to the potential by

$$K(x) = [K] e^{-ev(x)/k_B T} \quad \text{for all } x,$$

$$Cl(x) = [Cl] e^{ev(x)/k_B T} \quad \text{for all } x, \quad (9.9a)$$

$$M(x) = [M'] e^{-e(v(x)-v')/k_B T}, \quad x > 0.$$

<sup>1</sup>Throughout this section we keep  $4\pi$  in both numerator and denominator that could be canceled. We do this for two reasons. First, the quantity  $1/4\pi\epsilon_0$  has a numerical value of about  $9 \times 10^9$ , which is easy to remember; second, for those who do not use SI units, the factor  $1/4\pi\epsilon_0$  does not appear, but the other factor of  $4\pi$  remains.

(Remember that  $M(x) = 0$  to the left of the origin.) An equivalent general expression is

$$\rho_{\text{ext}}(\mathbf{r}) = e \sum_i z_i [C_i] \exp\left[\frac{-z_i ev(\mathbf{r})}{k_B T}\right], \quad (9.9b)$$

where  $C_i$  is the concentration in the region where  $v = 0$ .

Combining Eqs. 9.7 and 9.9b gives the *Poisson-Boltzmann equation* for a dielectric:

$$\nabla^2 v = -\frac{4\pi e}{4\pi\epsilon_0 \kappa} \sum_i z_i [C_i] \exp\left(\frac{-z_i ev(\mathbf{r})}{k_B T}\right). \quad (9.10)$$

For the specific problem at hand, the Poisson-Boltzmann equation takes the form

$$\frac{d^2v}{dx^2} = \frac{-4\pi e}{4\pi\epsilon_0 \kappa} \left( [K] e^{-ev(x)/k_B T} - [Cl] e^{ev(x)/k_B T} \right).$$

This applies for  $x < 0$  only. While it is possible to solve this using numerical techniques [see Mauro (1962)], we will confine ourselves to the case in which  $\xi = ev/k_B T \ll 1$  and we can make the approximation  $e^\xi \approx 1 + \xi$ . (This is accurate to 0.5% for  $\xi = 0.1$ , to 10% for  $\xi = 0.5$ , and to 25% for  $\xi = 0.8$ .) With this approximation

$$\rho_{\text{ext}} = e \sum [C_i] z_i \left( 1 - \frac{z_i ev}{k_B T} \right) = \quad (9.11)$$

$$e \sum [C_i] z_i - \frac{e^2}{k_B T} \sum [C_i] z_i^2 v. \quad (9.12)$$

Far from the membrane the solution is electrically neutral, so the first term vanishes. We are left with the *linear Poisson-Boltzmann equation*:

$$\nabla^2 v(\mathbf{r}) = \frac{4\pi e^2 \sum [C_i] z_i^2}{4\pi\epsilon_0 \kappa k_B T} v(\mathbf{r}). \quad (9.13)$$

The coefficient of  $v(\mathbf{r})$  on the right has the dimensions of  $1/(\text{length})^2$ . This length will also appear in other contexts. It is known as the *Debye length*,  $\lambda_D$ :

$$\frac{1}{\lambda_D^2} = \frac{4\pi e^2 \sum [C_i] z_i^2}{4\pi\epsilon_0 \kappa k_B T}. \quad (9.14)$$

The linearized Poisson-Boltzmann equation is

$$\nabla^2 v = \frac{v}{\lambda_D^2}. \quad (9.15)$$

For the one-dimensional problem and  $x < 0$ , it is

$$\frac{d^2v}{dx^2} = \frac{v}{\lambda_D^2}, \quad (9.16)$$

where

$$\frac{1}{\lambda_D^2} = \frac{4\pi e^2 ([K] + [Cl])}{4\pi\epsilon_0 \kappa k_B T}. \quad (9.17)$$

The methods of Appendix F can be applied to solve this equation.<sup>2</sup> The characteristic equation is  $s^2 = 1/\lambda_D^2$ , so

<sup>2</sup>We have seen this equation before in electrotonus when the membrane capacitance is fully charged (Sec. 6.12).

the solution for  $x < 0$  is  $v(x) = Ae^{-x/\lambda_D} + Be^{x/\lambda_D}$ . The potential is zero far to the left, so  $A = 0$ . Therefore, the solution is

$$v(x) = Be^{x/\lambda_D}, \quad x < 0. \quad (9.18)$$

It is most convenient to write the concentrations for  $x > 0$  in terms of the concentrations far to the right. It is now necessary to include the impermeant ions.

$$\begin{aligned} K(x) &= [K'] e^{-e[v(x)-v']/k_B T}, \\ Cl(x) &= [Cl'] e^{e[v(x)-v']/k_B T}, \\ M(x) &= [M'] e^{-e[v(x)-v']/k_B T}. \end{aligned} \quad (9.19)$$

The linearized Poisson–Boltzmann equation for  $x > 0$  is then

$$\begin{aligned} \frac{d^2 v}{dx^2} = & -\frac{4\pi e}{4\pi\epsilon_0\kappa} \left( [K'] - \frac{[K'] ev(x)}{k_B T} + \frac{[K'] ev'}{k_B T} - [Cl'] \right. \\ & - \frac{[Cl'] ev(x)}{k_B T} + \frac{[Cl'] ev'}{k_B T} + [M'] \\ & \left. - \frac{[M'] ev(x)}{k_B T} + \frac{[M'] ev'}{k_B T} \right). \end{aligned} \quad (9.20)$$

Neutrality requires that  $[K'] + [M'] - [Cl'] = 0$ . With the definition

$$\frac{1}{\lambda_D^2} = \frac{4\pi e^2([K'] + [Cl'] + [M'])}{4\pi\epsilon_0 \kappa k_B T}, \quad (9.21)$$

Eq. 9.20 can be written as

$$\frac{d^2 v}{dx^2} - \frac{v(x)}{\lambda_D^2} = -\frac{v'}{\lambda_D^2}. \quad (9.22)$$

This is an inhomogeneous linear differential equation with constant coefficients. As pointed out in Appendix F, the most general solution is the sum of the solution to the homogeneous equation (that is, with the right-hand side equal to 0) and any solution of the inhomogeneous equation, with the constants adjusted to satisfy whatever boundary conditions exist. In this case  $v(x) = v'$  satisfies the inhomogeneous equation, so the most general solution is  $v(x) = A'e^{-x/\lambda_D} + B'e^{x/\lambda_D} + v'$ . Far to the right  $v = v'$  so  $B' = 0$ . Therefore, the solution we need is

$$v(x) = A'e^{-x/\lambda_D} + v' \quad x > 0. \quad (9.23)$$

This solution for  $x > 0$  must be combined with the solution for  $x < 0$ , Eq. 9.18. At  $x = 0$  the potential must be continuous. Therefore  $B = A' + v'$ . Also at  $x = 0$  the electric field, and therefore  $dv/dx$ , is continuous. (If  $dv/dx$  were not continuous, the second derivative and  $\rho_{\text{ext}}$  would be infinite.) This requirement gives the equation  $B/\lambda_D = -A'/\lambda_D'$ . Solving these two equations, we obtain

$$A' = \frac{-v'\lambda_D'}{\lambda_D' + \lambda_D}, \quad B = \frac{v'\lambda_D}{\lambda_D' + \lambda_D}. \quad (9.24)$$

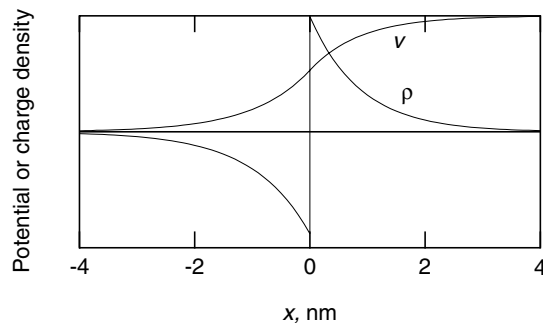


FIGURE 9.5. The potential and charge density in the vicinity of the Donnan membrane. There is a layer of negative charge on the left of the membrane and of positive charge on the right. Each decays with the Debye length given by the ion concentrations far from the membrane.

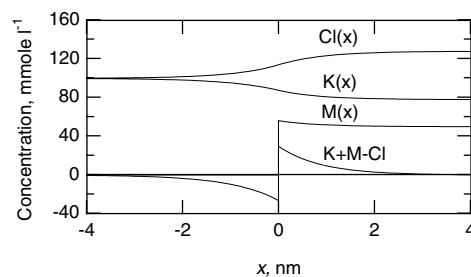


FIGURE 9.6. Concentration profiles across the Donnan membrane. The concentration  $K(x) + M(x) - Cl(x)$  is proportional to the charge density.

Figures 9.5 and 9.6 show the potential, concentration, and charge density for the case  $[K] = 100$  and  $[M'] = 50$  mmol  $l^{-1}$ . The other parameters are given in Table 9.2. The value of  $ev'/k_B T$  is 0.23.

Since the radii of ions are about 0.2 nm, the Debye length is several ionic diameters, and the continuous model we have used is reasonable.

The Poisson–Boltzmann equation is widely used to study charged molecules in solution [Honig and Nicholls (1995)]. However, in small-scale systems such as ion channels, which have a size similar to or smaller than the Debye length, continuous models may not be entirely reliable [Moy *et al.* (2000)].

## 9.3 Ions in Solution: The Debye–Hückel Model

In an ionic solution, ions of opposite charge attract one another. A model of this neutralization was developed by Debye and Hückel a few years after Gouy and Chapman developed the model in the previous section. The Debye–Hückel model singles out a particular ion and assumes that the average concentration of the counterions surrounding it is given by a Boltzmann factor. Screening

TABLE 9.2. Parameters for the Donnan interface when  $[K] = 100$ ,  $[M] = 0$ , and  $[M'] = 50 \text{ mmol l}^{-1}$  at  $T = 310 \text{ K}$ .

$[Cl]$	$100 \text{ mmol l}^{-1}$
$[K]$	$100 \text{ mmol l}^{-1}$
$[M]$	$0 \text{ mmol l}^{-1}$
$[K']$	$78.1 \text{ mmol l}^{-1}$
$[Cl']$	$128.1 \text{ mmol l}^{-1}$
$[M']$	$50 \text{ mmol l}^{-1}$
$v'$	$6.617 \text{ mV}$
$\lambda_D$	$0.991 \text{ nm}$
$\lambda'_D$	$0.875 \text{ nm}$

by the counterions causes the potential to fall much more rapidly than  $1/r$ . One major difficulty with this assumption is that each counterion is also a central ion; therefore, the notion of a continuous cloud of counterions represents some sort of average.

We consider a situation in which the electric field, potential, and charge distribution are spherically symmetric. We could begin with Eq. 9.7 and look up the Laplacian operator in spherical coordinates. However, it is instructive to derive Poisson's equation for the spherically symmetric case. Consider two concentric spheres of radius  $r$  and radius  $r + dr$ . Apply Gauss's law to the volume contained between the two surfaces. If  $\mathbf{E}$  is spherically symmetric, the flux through the inner sphere is  $4\pi r^2 E(r)$ . It points into the sphere and is therefore negative. The outward flux at  $r + dr$  is

$$\begin{aligned} & 4\pi(r + dr)^2 E(r + dr) \\ &= 4\pi [r^2 + 2rdr + (dr)^2] \left[ E(r) + \frac{dE}{dr} dr \right]. \end{aligned}$$

If we keep only terms of order  $dr$  or less, the outward flux through the outer sphere is

$$4\pi r^2 E(r) + 8\pi r E(r) dr + 4\pi r^2 \frac{dE}{dr} dr.$$

The net flux out of the volume is  $8\pi r E(r) dr + 4\pi r^2 (dE/dr) dr$ . The total charge in the shell is  $\rho_{\text{ext}}(r)$  times the volume of the shell,  $4\pi r^2 dr$ . Therefore, Gauss's law is

$$8\pi r E(r) dr + 4\pi r^2 \frac{dE}{dr} dr = \rho_{\text{ext}}(r) \frac{4\pi r^2}{\kappa \epsilon_0} dr$$

or

$$\frac{1}{r^2} \frac{d}{dr} (r^2 E(r)) = \frac{4\pi \rho_{\text{ext}}(r)}{4\pi \epsilon_0 \kappa}. \quad (9.25)$$

Since  $E(r) = -dv/dr$ , the final equation for the potential is

$$\frac{1}{r^2} \frac{d}{dr} \left( r^2 \frac{dv}{dr} \right) = -\frac{4\pi \rho_{\text{ext}}(r)}{4\pi \epsilon_0 \kappa}. \quad (9.26)$$

The Poisson–Boltzmann equation in spherical coordinates, the analog of Eq. 9.10, is

$$\frac{1}{r^2} \frac{d}{dr} \left( r^2 \frac{dv}{dr} \right) = -\frac{4\pi e}{4\pi \epsilon_0 \kappa} \sum z_i [C_i] \exp \left( \frac{-z_i e v(r)}{k_B T} \right). \quad (9.27)$$

We again make a linear approximation to the Boltzmann factor to obtain the linear Poisson–Boltzmann equation for spherical symmetry:

$$\frac{1}{r^2} \frac{d}{dr} \left( r^2 \frac{dv}{dr} \right) = \frac{1}{\lambda_D^2} v(r). \quad (9.28)$$

The Debye length  $\lambda_D$  is defined in Eq. 9.14. With the substitution  $v(r) = u(r)/r$ , the equation becomes

$$\frac{d^2 u}{dr^2} = \frac{1}{\lambda_D^2} u(r), \quad (9.29)$$

which is the same as Eq. 9.16. Therefore the solution is

$$v(r) = \frac{u(r)}{r} = \frac{Ae^{-r/\lambda_D} + Be^{r/\lambda_D}}{r}.$$

Requiring that  $v(r)$  approach 0 as  $r \rightarrow \infty$  means that  $B = 0$ . For small  $r$ , the electric field ( $dv/dr$ ) is that of an unshielded ion of charge  $ze$ . Therefore  $A = ze/4\pi \epsilon_0 \kappa$ , and the final solution is

$$v(r) = \left( \frac{ze}{4\pi \epsilon_0 \kappa} \right) \left( \frac{e^{-r/\lambda_D}}{r} \right). \quad (9.30)$$

This is the potential of a point charge  $ze$  in a dielectric, modified by an exponential decay over the Debye length. From Eq. 9.14 one sees that the greater the concentration of counterions, the shorter the Debye length.

Table 9.3 shows values of  $v(r)$ ,  $\xi = ev/k_B T$ , and the potential from an unscreened point charge in water of dielectric constant 80, when the ion concentrations are those given in Fig. 6.3. A typical ion radius is about 0.2 nm. We will discover in the next section that the dielectric constant saturates for  $r < 0.25 \text{ nm}$ . Therefore, values are given in Table 9.3 only for  $r > 0.3 \text{ nm}$ . The table shows that the assumption  $e^\xi \approx 1 + \xi$  is reasonable only for  $r > 0.5 \text{ nm}$ . The Debye length is  $\lambda_D = 0.77 \text{ nm}$ .

The charge density of the ion cloud can be obtained from Eqs. 9.26 and 9.30. The result is

$$\rho_{\text{ext}}(r) = \frac{-ze}{4\pi \lambda_D^2 r} e^{-r/\lambda_D}. \quad (9.31)$$

The total charge in the counterion cloud inside a sphere of radius  $a$  is

$$\int_0^a 4\pi r^2 \rho_{\text{ext}}(r) dr.$$

Adding to this a point charge  $ze$  at the origin gives the total charge due to both the ion and the counterion cloud inside radius  $a$ :

$$q(a) = ze \left( 1 + \frac{a}{\lambda_D} \right) e^{-a/\lambda_D}. \quad (9.32)$$

TABLE 9.3. The Debye-Hückel potential for a monovalent ion in a solution of ions at the concentration given in Fig. 6.2 for the interior of an axon. Also shown are the parameter  $zev/k_B T$ , the unscreened potential, and the charge inside a sphere of radius  $r$ .

$r$ (nm)	$v(r)$ (mV)	$e/(4\pi\epsilon_0\kappa r)$ (mV)	$zev/k_B T$	$q(r)/e$
0.3	40.6	59.9	1.52	0.94
0.4	26.8	44.9	1.00	0.90
0.5	18.8	36.0	0.70	0.86
0.6	13.8	30.0	0.51	0.82
0.7	10.4	25.7	0.39	0.77
0.8	8.0	22.5	0.30	0.72
0.9	6.2	20.0	0.23	0.67
1.0	4.9	18.0	0.18	0.63
1.2	3.2	15.0	0.12	0.54
1.4	2.1	12.8	0.08	0.46
1.6	1.4	11.2	0.05	0.39
1.8	1.0	10.0	0.04	0.32
2.0	0.7	8.99	0.03	0.27
2.2	0.5	8.17	0.02	0.22
2.4	0.3	7.49	0.01	0.18
2.6	0.2	6.91	0.01	0.15
2.8	0.2	6.42	0.01	0.12
3.0	0.1	5.99	0.00	0.10

This function approaches  $ze$ , the charge of the point ion, as  $a \rightarrow 0$ , and it approaches 0 as  $a \rightarrow \infty$ . Table 9.3 also shows the values of  $q(a)/e$ . Ninety percent of the counterion charge resides within 3 nm of the central ion. The charge on the central ion is half neutralized by charge in a sphere of radius 1.3 nm, about six ionic radii.

Figure 9.7 shows schematically an ion of radius 0.2 nm. Since a monovalent ion will be neutralized by a single counterion, it is clear that the assumption of a continuous charge distribution equal to the average is a bit strained. The shaded circle of radius 0.25 nm represents the region in which the water molecules are completely polarized and the dielectric constant is less than 80; this is discussed in the next section. (We have ignored the fact that close to the central ion the linear approximation is not valid.)

## 9.4 Saturation of the Dielectric

The electric field in a vacuum at distance  $r$  from a point charge  $q$  is  $E = q/(4\pi\epsilon_0 r^2)$ . If the charge is in a dielectric, the field is reduced by a factor  $1/\kappa$ , except at very small distances, where the electric field is so strong that the polarization of the dielectric is saturated.

A molecule of water appears schematically as shown in Fig. 6.18. The radius of each hydrogen atom is about 0.12 nm; the radius of the oxygen is about 0.14 nm. Each hydrogen nucleus is 96.5 pm from the oxygen; the angle between them is  $104^\circ$ . The hydrogen atoms share their electrons with the oxygen in such a way that each hydro-

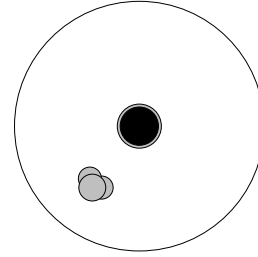


FIGURE 9.7. Schematic picture of the regions surrounding an ion. The solid circle in the center represents the ion of radius 0.2 nm. The shaded circle shows the region in which the polarization of the water is saturated. The outer circle of radius 1.3 nm represents the region within which the cloud of counterions has neutralized half of the charge on the ion, which means that on the average a counterion will be in this region half of the time. This radius depends on the ion concentrations that are those for the interior of a squid axon. A scale drawing of a water molecule is also shown.

gen atom has a net positive charge and the oxygen has a net negative charge. A pair of charges  $\pm q$  separated by distance  $b$  has an *electric dipole moment*  $\mathbf{p}_e$  of magnitude  $p_e = qb$ . The vector points from the negative to the positive charge. The magnitude of the dipole moment of a water molecule is  $6.237 \times 10^{-30}$  C m.

Each molecule of a dielectric in an applied electric field has an induced dipole moment that reduces the field. This dipole moment can be caused by a displacement of the electron cloud with respect to the nucleus, or it can represent (as for a polar molecule like water) an average molecular alignment against the tendency of thermal motion to orient the water molecules randomly.

The average induced dipole moment gives rise to the polarization field  $\mathbf{E}_{\text{pol}}$  [Eqs. 6.19–6.20]. To see the relationship, consider a small volume in the dielectric with  $N$  molecules per unit volume. Each molecule has a dipole moment  $p_e = qb$ . Far from this volume, the potential is due primarily to the dipole moment of each molecule. This can be shown by arguments like those in Secs. 7.3 and 7.4. The potential depends on the total dipole moment of the volume. The total number of dipoles in the volume is  $NSdx$ , so  $p_{\text{tot}} = p_e NSdx$ . This is equivalent to a charge  $q' = p_e NS$  on the ends of the volume element, or a surface of charge density

$$\sigma'_q = \frac{q'}{S} = p_e N. \quad (9.33)$$

Now consider a parallel-plate capacitor as shown in Fig. 9.8. Imagine a series of small volume elements in the dielectric. The induced charges  $\pm\sigma'_q$  on adjacent surfaces of each row of volume elements cancel except at the end of each row. The polarization field is therefore due entirely to the induced charge of surface density  $\pm\sigma'_q$  at each end of the dielectric. The magnitude of the field is

$$E_{\text{pol}} = \frac{\sigma'_q}{\epsilon_0} = \frac{Np_e}{\epsilon_0}. \quad (9.34)$$

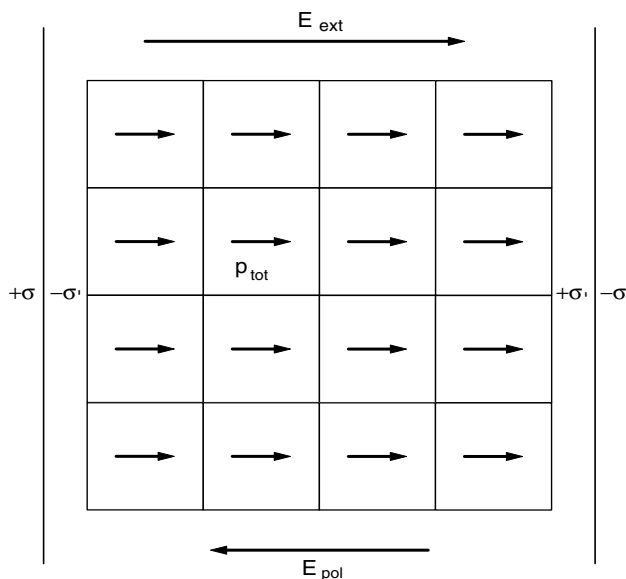


FIGURE 9.8. A dielectric is placed in a parallel-plate capacitor that has charge  $\pm\sigma$  on each plate. A dipole moment of magnitude  $p_{\text{tot}}$  is induced in each volume element of the dielectric. The total effect is the same as a charge density  $\pm\sigma'$  induced on the surfaces of the dielectric.

The quantity  $Np_e$  is the dipole moment per unit volume and is called the *polarization*  $P$ .

As the external electric field is increased,  $E_{\text{pol}}$ , which points in the opposite direction, also increases. This corresponds to the water molecules becoming more and more aligned. From the definition of susceptibility and the dielectric constant in Sec. 6.7, the magnitudes are related by

$$|E_{\text{pol}}| = \frac{\chi}{1 + \chi} |E_{\text{ext}}| = \left(1 - \frac{1}{\kappa}\right) |E_{\text{ext}}|.$$

For a monovalent ion in water,  $E_{\text{pol}} = (79/80)E_{\text{ext}} = (79/80)e/(4\pi\epsilon_0 r^2)$ . When the dipoles are completely aligned,  $E_{\text{pol}}$  saturates at its maximum value, given by Eq. 9.34 with the molecular dipole moment substituted for  $p_e$ . The number of water molecules per unit volume is obtained from the fact that 1 mol has a mass of 18 g, occupies  $1 \text{ cm}^3 \text{ g}^{-1}$ , and contains  $N_A$  molecules:

$$\begin{aligned} E_{\text{pol}}(\text{max}) &= \left[ \frac{(N_A \text{ molecule/mol})(1 \text{ g/cm}^3)(10^6 \text{ cm}^3/\text{m}^3)}{(18 \text{ g/mol})\epsilon_0 \text{ C V}^{-1} \text{ m}^{-1}} \right] \\ &\quad \times [6.237 \times 10^{-30} \text{ C m/molecule}] \\ &= 2.36 \times 10^{10} \text{ V m}^{-1}. \end{aligned}$$

Figure 9.9 shows the fields  $E_{\text{ext}}$  and  $E_{\text{pol}}$  around a monovalent ion. As  $E_{\text{pol}}$  saturates,  $E_{\text{tot}}$  rises toward the value it would have without a dielectric. The dielectric constant falls from 80 to 1 at about 0.23 nm. A more accurate model predicts similar behavior, but with a more

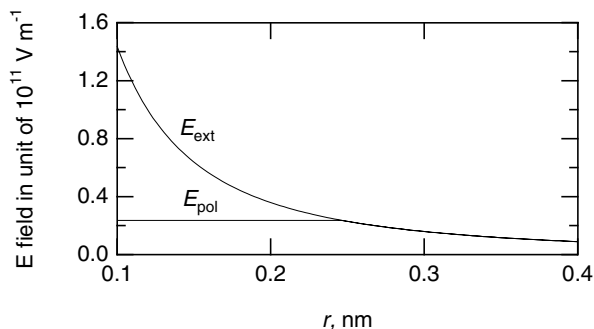


FIGURE 9.9. The electric field around a monovalent point charge and the polarization electric field due to the water. The polarization field saturates for  $r < 0.23$  nm.

gradual transition of the dielectric constant from 80 to 1.<sup>3</sup>

Close to an ion the potential is larger than  $q/(4\pi\epsilon_0 \kappa r)$ . This changes the Born charging energy [Eq. 6.22] and the free energy change as an ion dissolves in a solvent [Bockris and Reddy (1970), Chapter 2]. Also, close to an ion the continuum approximation breaks down.

## 9.5 Ion Movement in Solution: The Nernst–Planck Equation

Solute particles can move by diffusion. They can also move if they have an average velocity  $V_{\text{solute}}$ . There are two ways they can acquire an average velocity. The first is if they are at rest on average with respect to a moving solution. This is called *solvent drag*. The second is for the solute particles to be dragged through the solution by an external force that acts on them, such as gravity or an electric force, balanced by the viscous force on the particles. In both cases, the number per unit area per unit time crossing a plane is  $CV_{\text{solute}}$ . The solute particle fluence rate (particle current density) due to both diffusion and the solute velocity in the  $x$  direction is<sup>4</sup> (Sec. 4.12)

$$j_s = -D \frac{dC}{dx} + CV_{\text{solute}}. \quad (9.35)$$

Suppose that an external force  $\mathbf{F} = ze\mathbf{E}$  acts on the solute particles in the  $x$  direction. They will be accelerated until the viscous drag on them is equal to the magnitude of  $F$ . But we saw in Chapter 4 that the viscous drag is  $f = -\beta(V_{\text{solute}} - V_{\text{solvent}})$  where  $V_{\text{solute}} - V_{\text{solvent}}$  is the relative velocity of the solute through the solvent. Coefficient  $\beta$  is related to the diffusion constant by  $\beta = k_B T/D$ .

<sup>3</sup>A more sophisticated model for the alignment of the electric dipoles in the electric field is analogous to that for magnetic moments in Sec. 18.3.

<sup>4</sup>We use  $x$  for the distance in the direction parallel to  $\mathbf{E}$  because  $z$  is used for valence.



Therefore, the particles are no longer accelerated when

$$V_{\text{solute}} - V_{\text{solvent}} = zeE/\beta. \tag{9.36}$$

Equation 9.35 can be rewritten as

$$j_s = -D \frac{dC}{dx} + C [V_{\text{solvent}} + (V_{\text{solute}} - V_{\text{solvent}})].$$

Now  $V_{\text{solvent}}$  is the volume of solvent that flows per unit area per unit time and is just  $j_v$ . With this substitution and using Eq. 9.36, the particle current density is

$$j_s = -D \frac{dC}{dx} + C j_v + C zeE \frac{D}{k_B T}. \tag{9.37}$$

The first term represents solute motion due to diffusion, the second represents solute dragged along with the bulk flow of the solution (solvent drag), and the third represents drift due to the applied electric field.

We will consider only the case in which there is no bulk flow of solution, so  $j_v = 0$ . The equation then reduces to the *Nernst–Planck equation*:

$$j_s = -D \frac{dC}{dx} + \frac{zeE}{k_B T} DC. \tag{9.38}$$

Diffusion is always toward the region of lower concentration, while for positive charge the  $V_{\text{solute}}$  term is in the direction of  $\mathbf{E}$ . For negative charges it is in the opposite direction.

Consider the current density in bulk solution between planes at  $x = 0$  where  $v(x) = 0$  and  $x = L$  where  $v(x) = v$ . If there is no concentration gradient and the potential changes uniformly, then  $E = -dv/dx = -v/L$  points in the  $-x$  direction, and the particle current density is  $j_s = -zeDCv/k_B TL$ . The electrical current density  $j$  is obtained by multiplying  $j_s$  by the charge on each particle,  $ze$ :

$$j = -\frac{z^2 e^2 DC S v}{k_B T L} = -\frac{G(C)}{S} v. \tag{9.39}$$

If  $v(L) > v(0)$ , the current is to the left and is negative. Recalling that  $G = \sigma S/L = 1/R = S/\rho L$ , we obtain the conductivity in bulk solution

$$\sigma = \frac{1}{\rho} = \frac{z^2 e^2 DC}{k_B T}. \tag{9.40}$$

If several ion species carry current and can be assumed to move independently, then the total conductivity is the sum of the conductivities for each ion. Table 9.4 shows contributions to the conductivity for various species at typical concentrations.

This model is satisfactory for material such as the inside of an axon where the concentrations are constant and the material is electrically neutral, so that the ions themselves do not on average contribute to the electric field. We have assumed that the ions move independently, which will happen only if the electric field of other ions can be ignored.

TABLE 9.4. Conductivities of ions at various concentrations at 25°C, calculated using Eq. 9.40. Diffusion constants for each ion are from Hille (2001, p. 317). Concentrations are typical of mammalian nerve and are from Hille (2001, p. 17). The conductivities of each species add, and  $\rho = 1/\sigma$ . Larger ions with very small diffusion constants make the solutions electrically neutral.

	$D$ (m <sup>2</sup> s <sup>-1</sup> )	$C$ (mmol l <sup>-1</sup> )	$\sigma$ (S m <sup>-1</sup> )	$\rho$ (Ω m)
Extracellular squid axon				
Na	$1.33 \times 10^{-9}$	143	0.723	
K	$1.96 \times 10^{-9}$	4	0.029	
Cl	$2.03 \times 10^{-9}$	123	0.936	
			1.688	0.592
Intracellular squid axon				
Na	$1.33 \times 10^{-9}$	12	0.060	
K	$1.96 \times 10^{-9}$	155	1.139	
Cl	$2.03 \times 10^{-9}$	4.2	0.032	
			1.231	0.812

We can model ions flowing from a region of one concentration to another (such as crossing the axon membrane) with the Nernst–Planck equation. Writing it for the electric current density and using the fact that  $E(x) = -dv/dx$ , we have

$$j = -zeD \frac{dC}{dx} - \frac{z^2 e^2 D}{k_B T} \frac{dv}{dx} C. \tag{9.41}$$

It is simpler to use the dimensionless variable  $u(x) = ze v(x)/k_B T$ , which is the ratio of an ion’s energy to thermal energy:

$$j = -zeD \left( \frac{dC}{dx} + C \frac{du}{dx} \right). \tag{9.42}$$

If we assume that  $dv/dx$  is constant throughout the region,  $v(0) = 0$  and  $v(L) = v$ , then the gradient is  $dv/dx = v/L$ , and Eq. 9.41 becomes

$$\frac{dC}{dx} - \frac{1}{\lambda} C = -\frac{j}{zeD}, \tag{9.43}$$

where the characteristic length for this model (*not* the Debye length) is

$$\lambda = \frac{L}{u} = \frac{k_B T L}{ze v}. \tag{9.44}$$

Equation 9.43 is the same as Eq. 4.58, except for the denominator of the term involving  $j$ . Here the denominator is  $zeD$  because  $j$  is the electric current density instead of the particle current density. The solution analogous to Eq. 4.62 is

$$j = \frac{zeD}{\lambda} \frac{C_0 e^{L/\lambda} - C'_0}{e^{L/\lambda} - 1} = \frac{zeD}{\lambda} \frac{C_0 e^{-u} - C'_0}{e^{-u} - 1}, \tag{9.45}$$

where  $C_0$  is the ion concentration at  $x = 0$  and  $C'_0$  is the concentration at  $x = L$ .

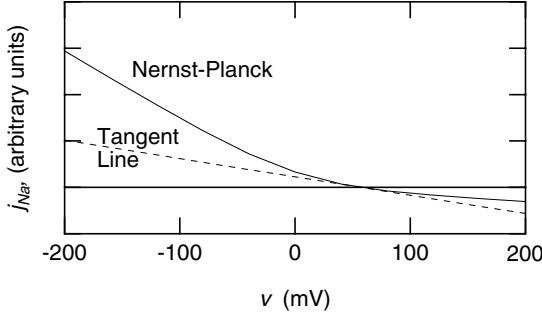


FIGURE 9.10. Sodium current versus applied potential for the constant field Nernst–Planck model when the sodium concentration is 145 mM on the left and 15 mM on the right. The calculation was done using Eq. 9.46 for  $T = 293$  K. The tangent line was calculated using Eq. 9.48. The nonlinearity or rectification occurs because of the different ion concentrations on each side.

The current vanishes if  $C_0 e^{L/\lambda} - C'_0 = 0$ , or  $C'_0/C_0 = e^{L/\lambda} = e^{-zev/k_B T} = e^{-u}$ . This is the Boltzmann factor.

Equation 9.45 can be written in terms of the original variables:

$$j = -\frac{z^2 e^2 D v C_0 e^{-zev/k_B T} - C'_0}{k_B T L} = -\frac{ze D u C_0 e^{-u} - C'_0}{L} \quad (9.46)$$

It is interesting to compare this to Eq. 9.39. Since  $G$  depends on concentration, it is useful to factor out a factor  $C_0$  and write

$$j = -\frac{z^2 e^2 D C_0}{k_B T L} \frac{e^{-zev/k_B T} - C'_0/C_0}{e^{-zev/k_B T} - 1} v = -\frac{G(C_0)}{S} \frac{e^{-zev/k_B T} - C'_0/C_0}{e^{-zev/k_B T} - 1} v. \quad (9.47)$$

If  $C_0 = C'_0$ , we recover Eq. 9.39. Figure 9.10 shows the current density in  $\text{A m}^{-2}$  for a situation where  $C_0 = 145 \text{ mmol l}^{-1}$  and  $C'_0 = 15$ . The diffusion constant for sodium from Table 9.4 has been used. Because  $C_0 > C'_0$ , equilibrium occurs when  $v = +57.3 \text{ mV}$  at  $20^\circ \text{C}$ .

Note the nonlinearity of the current–voltage relationship that arises because  $C_0 \neq C'_0$ . For very negative potentials the flow is almost entirely from left to right and the current density approaches  $G(C_0)v/S$  while for very positive potentials the flow is from right to left and the current density approaches  $G(C'_0)v/S$ . This asymmetry is fundamental. It occurs because there are different numbers of charge carriers on the left and right. When this behavior is seen in channels in cell membranes, they are often called *rectifier channels*. This same asymmetry in differences in the concentration of charge carriers is responsible for rectification in semiconductors.

Near the Nernst potential the current density has the form  $j = -(G/S)(v - v_{\text{Nernst}})$  if

$$\frac{G}{S} = \frac{G(C_0)(zev_{\text{Nernst}}/k_B T)}{S(e^{zev_{\text{Nernst}}/k_B T} - 1)}. \quad (9.48)$$

This equation was used to derive the tangent line shown in Fig. 9.10.

The constant-field model is an oversimplification. The field can be distorted by fixed charges near the channel through which the ions are flowing. Moreover, the model is internally inconsistent. There are electric fields generated by the flowing ions, which become important at high concentrations. The fact that  $j = 0$  when the potential is equal to the Nernst potential is fundamental and holds for any ion or model for conduction. It can be derived in the general case from Eq. 9.43 (see the Problems). A self-consistent analytic solution for the case of a single ion species has been known for 50 years. The solution has been extended by many workers and has been generalized by Leuchtag and Swihart (1977) to the case in which all the ions have the same charge.

## 9.6 Zero Total Current in a Constant-Field Membrane: The Goldman Equations

The Nernst-Planck equation can be used to calculate the current due to movement of ions through a membrane in which there is a constant electric field. We assume a constant field because it leads to an analytic solution and because we have no knowledge of internal structure or the behavior of counterions which could change the field. The resulting equations are called the *Goldman* or the *Goldman–Hodgkin–Katz* (GHK) equations.

The GHK equations can be derived by assuming either a homogeneous membrane, in which case the Nernst–Planck equation is simply applied to each species, or cylindrical pores of constant cross section. Since we know that the pores do not have a constant electric field (Sec. 9.7) and it is quite unlikely that they have constant cross section, the GHK equations are an approximation. Nevertheless, they have been used widely in the study of excitable membranes.

We will show the derivation for a cylindrical pore that has a constant circular cross section. We use cylindrical coordinates  $(r, \phi, x)$ , where  $x$  is the axis of the cylinder. (Again,  $z$  denotes the valence of the ions.) Let the outside of the membrane be at  $x = 0$  and the inside at  $x = L$ , where the potential is  $v$  and  $u = zev/k_B T$ . The arguments of Sec. 5.9 about the  $r$  and  $x$  dependence can be applied to Eq. 9.42. The analog of Eq. 5.37 is

$$j(r) = -zeD(r, a, R_p) \left( \frac{\partial C(r, x)}{\partial x} + \frac{u}{L} C(r, x) \right). \quad (9.49)$$

Again the concentration can be written as  $C(r, x) = C(x)\Gamma(r)$ . Equation 9.49 becomes

$$j(r) = -ze\Gamma(r)D(r, a, R_p) \left( \frac{\partial C(x)}{\partial x} + \frac{u}{L} C(x) \right). \quad (9.50)$$

This can be multiplied by  $2\pi r dr$  and integrated over the pore area. There are two integrals to consider. The first defines the average current density for a particular species:

$$\int_0^{R_p} j(r) 2\pi r dr = \pi R_p^2 \bar{j}. \quad (9.51)$$

The second defines an effective diffusion constant:

$$\int_0^{R_p} \Gamma(r) D(r, a, R_p) 2\pi r dr = \pi R_p^2 D_{\text{eff}}. \quad (9.52)$$

The integrated current density equation is

$$\bar{j} = -zeD_{\text{eff}} \left( \frac{dC(x)}{dx} + \frac{u}{L} C(x) \right). \quad (9.53)$$

Consideration of the  $r$  dependence in the pore has given an equation exactly like Eq. 9.42, but with  $D_{\text{eff}}$  instead of  $D$ . Equations 9.43 and 9.44 are still valid. The form of  $\lambda$  is unchanged:  $\lambda = -k_B T L / zev$ . Conversion from a single pore to unit area of the membrane requires multiplying  $\bar{j}$  by  $n\pi R_p^2$ . We define  $\omega_s RT = n\pi R_p^2 D_{\text{eff}} / L$  and call the concentration outside  $C_1$  and the concentration inside  $C_2$ . The electric current density per unit area of membrane is

$$\begin{aligned} J' &= \frac{z^2 e^2 \omega_s RT v}{k_B T} \frac{C_1 e^{-zev/k_B T} - C_2}{1 - e^{-zev/k_B T}} \\ &= z^2 e^2 v \omega_s N_A \frac{C_1 e^{-zev/k_B T} - C_2}{1 - e^{-zev/k_B T}}. \end{aligned} \quad (9.54)$$

Suppose that three species can pass through the membrane: sodium, potassium, and chloride. Equation 9.54 can be applied separately to each species to obtain the *GHK current equation* for each ion species:

$$J'_{\text{Na}} = e^2 v \omega_{\text{Na}} N_A \frac{[\text{Na}_1] e^{-ev/k_B T} - [\text{Na}_2]}{1 - e^{-ev/k_B T}}, \quad (9.55a)$$

$$J'_{\text{K}} = e^2 v \omega_{\text{K}} N_A \frac{[\text{K}_1] e^{-ev/k_B T} - [\text{K}_2]}{1 - e^{-ev/k_B T}}, \quad (9.55b)$$

$$J'_{\text{Cl}} = e^2 v \omega_{\text{Cl}} N_A \frac{[\text{Cl}_1] e^{+ev/k_B T} - [\text{Cl}_2]}{1 - e^{+ev/k_B T}}. \quad (9.55c)$$

The *reversal potential*,  $v_{\text{rev}}$ , is the potential for which the total membrane current or fluence rate, that is the sum of the three fluence rates, is zero. The amount of charge within the cell does not change with time, but the concentration of each species within the cell changes with time. This less stringent requirement becomes  $J'_{\text{Na}} + J'_{\text{K}} + J'_{\text{Cl}} = 0$ . Adding Eqs. 9.55 together and factoring out  $N_A e^2 v / (1 - e^{-ev/k_B T})$  gives

$$\begin{aligned} &(\omega_{\text{Na}} [\text{Na}_1] + \omega_{\text{K}} [\text{K}_1] + \omega_{\text{Cl}} [\text{Cl}_2]) e^{-ev/k_B T} \\ &= \omega_{\text{Na}} [\text{Na}_2] + \omega_{\text{K}} [\text{K}_2] + \omega_{\text{Cl}} [\text{Cl}_1], \end{aligned}$$

or the *GHK voltage equation*

$$v_{\text{rev}} = \frac{k_B T}{e} \ln \left( \frac{\omega_{\text{Na}} [\text{Na}_1] + \omega_{\text{K}} [\text{K}_1] + \omega_{\text{Cl}} [\text{Cl}_2]}{\omega_{\text{Na}} [\text{Na}_2] + \omega_{\text{K}} [\text{K}_2] + \omega_{\text{Cl}} [\text{Cl}_1]} \right). \quad (9.56)$$

As an example of the use of the GHK voltage equation, consider how the reversal potential depends on the concentration of some external ion. We will use the concentrations of Fig. 6.2, except for the ion whose concentration is being changed. The particle concentrations are in  $\text{mmol l}^{-1}$  (any units can be used since ratios are taken):

$$[\text{Na}_1] = 145, \quad [\text{Na}_2] = 15,$$

$$[\text{K}_1] = 5, \quad [\text{K}_2] = 150,$$

$$[\text{Cl}_1] = [\text{Na}_1] + [\text{K}_1] - 25, \quad [\text{Cl}_2] = [\text{Na}_2] + [\text{K}_2] - 156.$$

The permeabilities are not known. However, only the ratio to  $\omega_{\text{K}}$  matters. If we take the ratio  $\omega_{\text{K}} : \omega_{\text{Na}} : \omega_{\text{Cl}}$  to be 1.0 : 0.04 : 0.45 and use  $T = 300$  K, then Eq. 9.56 is (in mV)

$$v = 25.88 \ln \left( \frac{[\text{K}_1] + 0.04 [\text{Na}_1] + 0.45([\text{Na}_2] + [\text{K}_2] - 156)}{[\text{K}_2] + 0.04 [\text{Na}_2] + 0.45([\text{Na}_1] + [\text{K}_1] - 25)} \right).$$

This has been plotted in Fig. 9.11 for variations of  $[\text{K}_1]$  and  $[\text{Na}_1]$ . In each case Cl ions are also added to the external solution in an equal amount. There is a region of potassium concentration over which the behavior is nearly exponential, and one could be misled into thinking that the potential-concentration relation was given either by the Nernst equation alone or by Donnan equilibrium. The potential change with sodium concentration is much less because of the low permeability of the membrane to sodium.

The assumption that the total current through the membrane is zero guarantees that there will be no charge buildup inside the cell; however, the individual currents are not zero, so there may be concentration changes with time. We will next investigate the magnitude of this effect. Equation 9.54 can be converted to particle flux instead of charge flux by dividing by  $ze$ . The result for ion

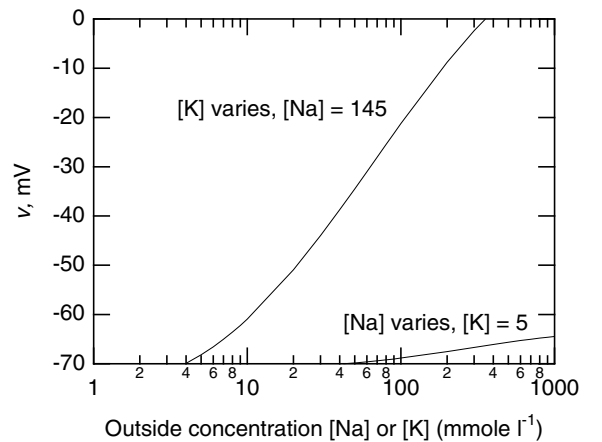


FIGURE 9.11. The potential difference across a cell membrane as a function of changes in the exterior concentration of KCl or NaCl, calculated using the Goldman equation.

s is

$$J_s = zev\omega_s \frac{C_1 e^{-zev/k_B T} - C_2}{1 - e^{-zev/k_B T}}.$$

The concentrations are converted from mmol l<sup>-1</sup> to particles m<sup>-3</sup> by multiplying by Avogadro's number. (The factors of 10<sup>3</sup> in the conversion happen to cancel out.) Consider the previous example at  $T = 300$  K,  $[K_1] = 5$ ,  $[Na_1] = 145$ , and  $v = -68.17$  mV. The exponential factor for the positive ions is  $e^{-ev/k_B T} = 13.929$ , while for the chloride ion it is the reciprocal, 0.0718. If we write  $\omega_{Na} = 0.04\omega_K$  and  $\omega_{Cl} = 0.45\omega_K$ , then the fluxes for the three ions are

$$J_K = +(6.55 \times 10^3)\omega_K(6.215),$$

$$J_{Na} = -(6.55 \times 10^3)\omega_K(6.202),$$

$$J_{Cl} = -(6.55 \times 10^3)\omega_K(0.013),$$

and the total current is zero.

Although the GHK equations are widely used because of their simplicity, some cautions are in order. Their derivation assumed independence of the moving ions. We know that this is an oversimplification for several reasons. Experiments show that the currents saturate for high concentrations. The distortion of the electric field by other ions was ignored. The permeability (diffusion constant) was assumed to be constant. The pore was assumed to have a constant cross section and constant electric field. A somewhat less restrictive model for the reversal potential (the potential at which the current density becomes zero and changes sign) can be derived for a pair of ions with the same valence if we assume that any variations in  $D(x)$  for the two ions are similar (Problem 18). With that assumption the reversal potential is

$$v_{\text{rev}} = \frac{k_B T}{ze} \ln \left( \frac{\omega_a C_{a1} + \omega_b C_{b1}}{\omega_a C_{a2} + \omega_b C_{b2}} \right). \quad (9.57)$$

When ions have different valences, the GHK equation becomes more complicated. Lewis (1979) has derived an analogous equation for transport of sodium, potassium and calcium.

## 9.7 Membrane Channels

In Chapter 6 we described some of the properties of the sodium and potassium channels in a squid axon. There are many other kinds of channels. Variations exist not only from one organism to another, but in different kinds of cells in the same organism. The classic monograph on ionic channels is the book by Hille (2001).

There are several different kinds of potassium channels. Most open after depolarization; a few open after hyperpolarization. Potassium channels in axons (such as the ones we encountered in Chapter 6) are called *delayed rectifiers* because of their delay in opening after a voltage step.

The properties of sodium channels are more uniform from one cell type to another.

Calcium channels pass much smaller currents than sodium or potassium channels because calcium concentrations are much smaller; the calcium current density is usually about  $\frac{1}{10}$  the current density for sodium or potassium. Calcium channels typically activate with depolarization. Since the concentration of calcium inside cells is usually very small, the interior calcium concentration can increase 20-fold in response to depolarization. This increase in concentration can initiate a chemical reaction, for example, to cause contraction of a muscle cell.

Chloride channels often have a large conductivity. The chloride concentration ratio in some muscle cells is such that the resting potential is close to the chloride Nernst potential. As a result, small changes in the potential cause relatively large chloride currents, which tend to stabilize the resting potential.

The earliest voltage-clamp measurements were difficult to sort out. Hodgkin and Huxley changed the concentration of extracellular sodium, substituting impermeant choline ions, to determine what part of the current was due to sodium and what was due to potassium. Figure 9.12(a) shows typical currents.

In the mid-1960s, various drugs were found that at very small concentrations selectively block conduction of a particular ion species. We now know that these drugs bind to the channels that conduct the ions. An example is tetrodotoxin (TTX), which binds to sodium channels and blocks them, making it a deadly poison.

The next big advance was patch-clamp recording [Neher and Sakmann (1976)]. Micropipettes were sealed against a cell membrane that had been cleaned of connective tissue by treatment with enzymes. A very-high-resistance seal resulted [(2–3) × 10<sup>7</sup> Ω] that allowed one to see the opening and closing of individual channels. For this work Erwin Neher and Bert Sakmann received the Nobel Prize in Physiology or Medicine in 1991. Around 1980, Neher's group found a way to make even higher-resistance (10<sup>10</sup>–10<sup>11</sup> Ω) seals that reduced the noise even further and allowed patches of membrane to be torn from the cell while adhering to the pipette [Hamill *et al.* (1981)]. The relationship of noise to resistance will be discussed below.

The patch-clamp studies revealed that the pores open and close randomly, as shown in Fig. 9.13. Thus, the Hodgkin–Huxley model describes the average behavior of many pores, not the kinetics of single pores. Note how the current through an open pore changes as a function of the applied potential. A single open pore can pass at least 1 pA of current or 6 × 10<sup>6</sup> monovalent ions per second. Most can pass much more. While no perfectly selective channel is known, most channels are quite selective: for example, some potassium channels show a 100:1 preference for potassium over sodium.

Gene splicing combined with patch-clamp recording provided a wealth of information. Regions of the DNA

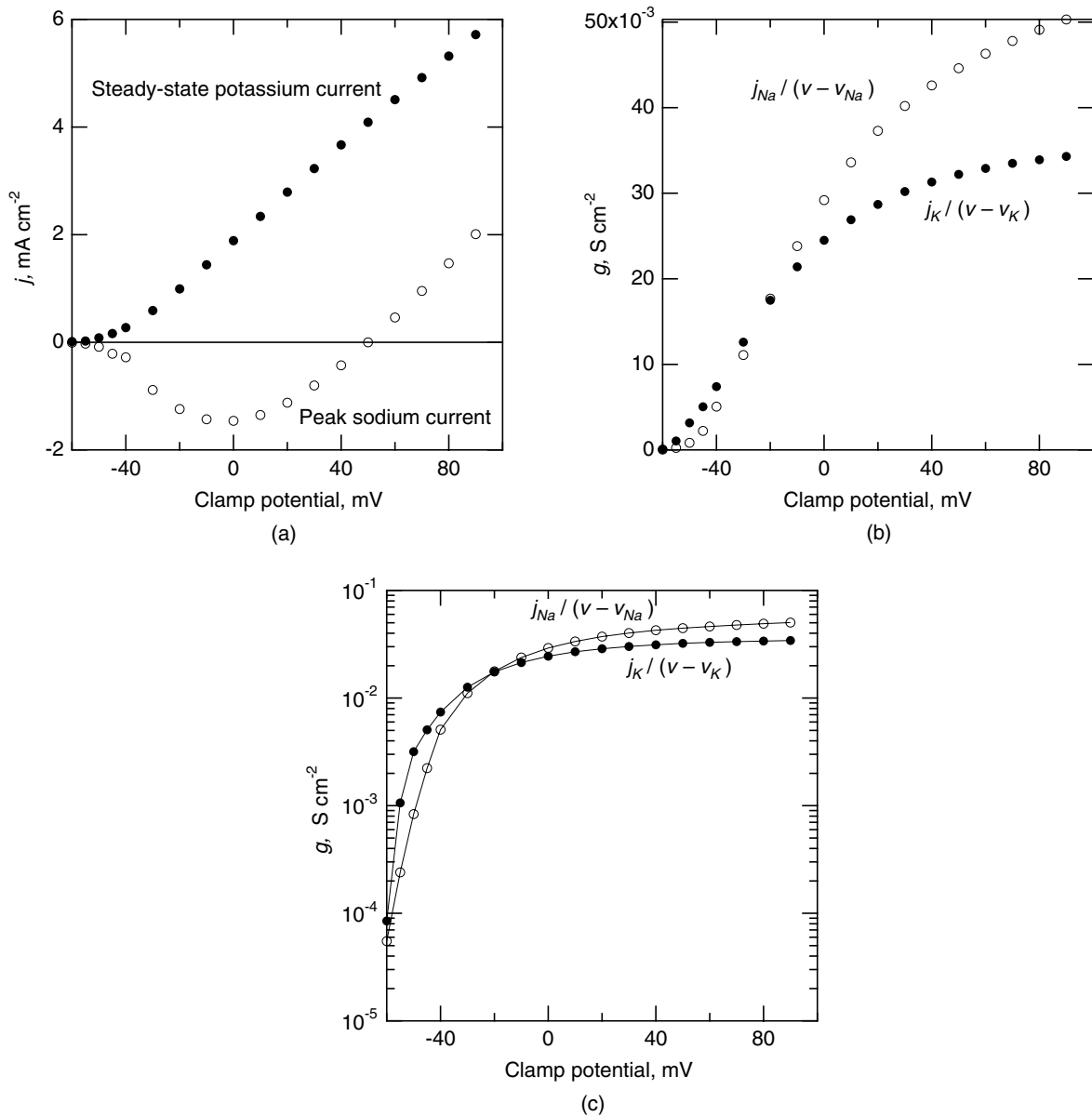


FIGURE 9.12. Steady-state potassium current and peak sodium current for a squid axon subject to a voltage clamp vs the transmembrane potential during the clamp. These are not real data, but were generated using the Hodgkin–Huxley model. (a) Current density. (b) Current density divided by the difference between the potential and the Nernst potential, to give the conductance per unit area [see Eq. 6.61.] (c) The same data as in (b) plotted on semi-log paper.

responsible for synthesizing the membrane channel have been identified. One example that has been extensively studied is a potassium channel from the fruit fly, *Drosophila melanogaster*. The *Shaker* fruit fly mutant shakes its legs under anesthesia. It was possible to identify exactly the portion of the fly's DNA responsible for the mutation. When *Shaker* DNA was placed in other cells that do not normally have potassium channels, they immediately made functioning channels.

The current view is that the *Shaker* potassium channel consists of four subunits that span the membrane. The pore presumably runs along the fourfold-symmetry

axis, as shown in end view in Fig. 9.14. Sodium and calcium channels are very similar. Voltage-gated channels are reviewed by Sigworth (1993) and by Keynes (1994).

Recently, MacKinnon and his colleagues determined the three-dimensional structure of a potassium channel using X-ray diffraction [Doyle *et al.* (1998); Jiang *et al.* (2003)]. The channel protein contains four identical subunits, arranged with fourfold symmetry around a central pore (Fig. 9.14). Each subunit has two alpha helices that cross the membrane and an inner pore region. One of the remarkable features of this channel is that potassium ions are 10,000 times more likely to pass through than sodium

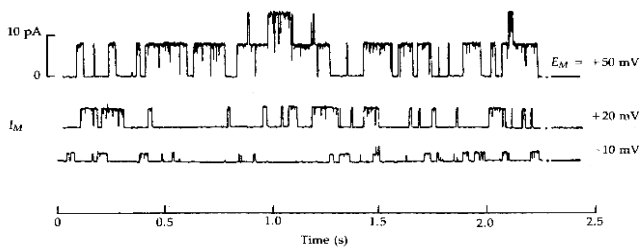


FIGURE 9.13. Opening of single K(Ca) channels. From B. S. Pallotta, K. L. Magleby, and J. N. Barrett (1981). Single channel recordings of  $\text{Ca}^{2+}$ -activated currents in rat muscle cell culture. *Nature* **293**: 471–474. Reprinted with permission from Nature (London).

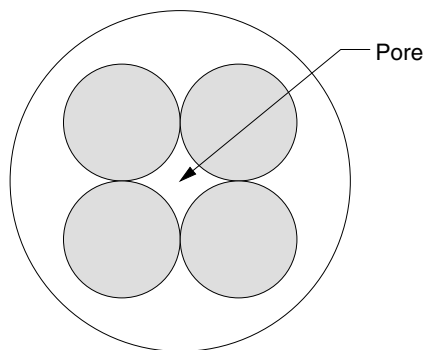


FIGURE 9.14. Current understanding of the structure of a *Shaker* potassium channel. There are four subunits that traverse the membrane and create a pore at their center.

ions. Yet, potassium and sodium have similar chemistry (they are in the same column of the Periodic Table), and their ions are identical except for size (0.133 nm radius for potassium, 0.095 nm for sodium).

The channel structure suggests that a narrow, 1.2 nm long region of the pore is responsible for selectivity. As the ion enters this region, there is not enough room for the polar water molecules that normally surround it and shield its charge. Instead, carbonyl oxygen atoms on the channel protein come in close contact with the potassium ion and provide the shielding. The size of the pore is such that potassium ions fit snugly with the surrounding carbonyl oxygen atoms, but sodium does not fit as well.

X-ray diffraction studies have also clarified the mechanism of voltage dependence in potassium channels. The pore is surrounded by charged structures on the channel's perimeter that sense the transmembrane voltage. These structures act somewhat like levers, opening and closing the pore in response to the voltage. The movement of these structures is responsible for gating currents in these channels. Roderick MacKinnon received the 2003 Nobel Prize in Chemistry for this work on the potassium channel.

Let us now explore some of the physics of channels. Combining the macroscopic current density with the current in a single channel shows that there are not many channels per unit area of the membrane (see Problems 19 and 20). It is illuminating to consider what effect currents of this magnitude and duration have on the transmembrane potential. The capacitance per unit area of biological membranes is about  $0.01 \text{ F m}^{-2}$  ( $1 \mu\text{F cm}^{-2}$ ). A channel conducting 1 pA for 1 ms allows  $10^{-15} \text{ C}$  to pass. This is enough charge to change the potential 100 mV on an area of  $10^{-12} \text{ m}^2$  or  $1 \mu\text{m}^2$ . This charge transfer corresponds to about 6,000 monovalent ions per  $\mu\text{m}^2$ .

Figure 9.12(a) shows the steady-state potassium and peak sodium current densities for a squid axon. The ion concentrations are known, and we saw in Chapter 6 that the Nernst potentials at  $6.3^\circ\text{C}$  were +50 mV for sodium and  $-77 \text{ mV}$  for potassium. Figure 9.12(b) shows the conductance per unit area, obtained by dividing the current by  $v - v_{\text{Nernst}}$ . Figure 9.12(c) shows a semilogarithmic plot of the conductance per unit area.

The sodium current density changes sign at the sodium Nernst potential. While a measured zero crossing is an accurate way to determine the Nernst potential, extrapolation to find the zero-crossing can be quite misleading. The potassium current density appears to be linear over a large region, and it is tempting to extrapolate to find  $v_K$ . The extrapolation shows zero current at about  $-40 \text{ mV}$ , which is far from  $v_K$ . The reason can be seen in Fig. 9.12(b), which shows that  $g_K$  is varying considerably over the region where  $j_K$  appears to be linear; this distorts the slope and changes the extrapolated intersection.

A simple two-state model can explain the shape of the curves in Fig. 9.12(c). The conductance per unit area of a membrane is the product of the conductance of an open pore and the average number of pores per unit area that are open. The model assumes that each channel has a gate that is either open or closed. When the gate is open, the channel has a conductance determined by the passive properties of the rest of the channel. The rapid increase of conductance between  $-60$  and  $-30 \text{ mV}$  corresponds to a rapidly increasing probability that the gate is open.

Suppose that each channel has a gate with two states: open and closed. When there is no average electric field in the membrane ( $v = 0$ ) the energy of the open state is  $w = u_o k_B T$  greater than the closed state. Suppose also that as the gate opens and closes, a charge  $q$  associated with the gate moves a small distance parallel to the axis of the pore. When there is a potential  $v$  across the membrane, the charge moves through a potential difference  $\alpha v$ , where  $\alpha < 1$ . The total energy change when the gate opens with potential  $v$  across the membrane is then  $w + q\alpha v$ . The quantity  $q\alpha$  is often written as  $ze$  and called the *equivalent gating charge*. In terms of  $k_B T$  the energy change when the pore opens is  $u = u_o + zev/k_B T$ .

Let  $p_o$  be the probability that a pore is open and  $p_c$  be the probability that it is closed. The probabilities are related by a Boltzmann factor:  $p_o = p_c e^{-u}$ . Since

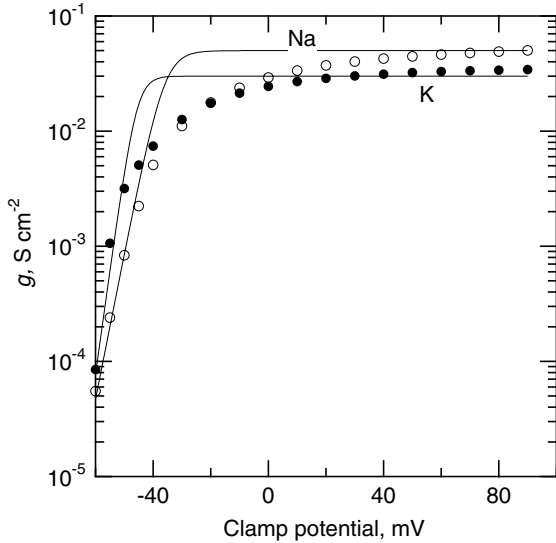


FIGURE 9.15. Plot of sodium and potassium conductivities from Fig. 9.12(c) with fits by Eq. 9.58. For sodium  $u_o = -10.5$  and  $z = -7$ ; for potassium  $u_o = -19$  and  $z = -10$ .

$$p_o + p_c = 1, p_o = e^{-u}/(1 + e^{-u}) = 1/(1 + e^u),$$

$$p_o = \frac{1}{1 + e^{u_o + zev/k_B T}}. \quad (9.58)$$

For very large values of  $u$  (small values of  $p_o$ ),

$$p_o \approx e^{-(u_o + zev/k_B T)}. \quad (9.59)$$

The conductance per unit area of the membrane is the conductance of an open pore times the number of pores per unit area (that is  $g_\infty$ ), times  $p_o$ .

Figure 9.15 shows plots of the “data” and lines generated from Eq. 9.58. The multiplicative constant has been adjusted to fit the flat region of the “data” at high  $v$ . Parameters  $u_o$  and  $z$  have been adjusted to provide good fits at the lowest conductances. For sodium  $u_o = -10.5$  and  $z = -7$ ; for potassium  $u_o = -19$  and  $z = -10$ . The fact that  $u_o$  is very negative means that when  $v = 0$ , the energy of an open gate is much less than the energy of a closed gate. Nearly all of the pores are open, as can be seen from the  $v = 0$  point in Fig. 9.15. The fact that  $z = -7$  or  $-10$  means that when the pore opens or closes, the equivalent of 7 (or 10) electron charges must move through the full transmembrane potential difference. Many more charges could be displaced a much smaller distance and experience a much smaller potential change. More sophisticated multilevel models are discussed by Sigworth (1993).

This charge movement constitutes a very small current called the *gating current*. It is different from the current to charge the membrane capacitance. We saw above that during a 1-pA pulse lasting 1 ms, about 6,000 monovalent ions flow through the membrane. The gating charge is about 10 monovalent charges, a ratio of about 600. The gating current is so small that it has not yet been

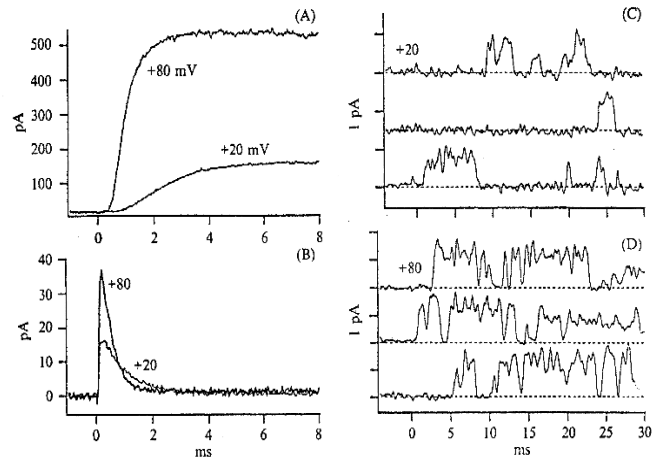


FIGURE 9.16. The results of a set of experiments with *Shaker* potassium channels. Panel A shows the macroscopic depolarizations to +20 and +80 mV for a patch with about 400 channels. Panel B shows the gating current recorded from another patch containing about 8,000 channels. Potassium was removed from the solution bathing the interior surface of the membrane. Panels C and D show recordings similar to panel A, but with many fewer channels in the patch. The results from three successive depolarizing pulses are shown in each case. From F. J. Sigworth (1993). Voltage gating of ion channels. *Quart. Rev. Biophys.* **27**: 1–40. Reprinted with permission of Cambridge University Press.

measured in a single channel, but it can be measured by manipulating the ions bathing the membrane in a patch-clamp experiment.

Figure 9.16 shows the results of a set of experiments with *Shaker* potassium channels. Panel A shows the macroscopic depolarizations to +20 and +80 mV for a patch with about 400 channels. The peak current at +80 mV is 1.25 pA per channel. Panel B shows the gating current recorded from another patch containing about 8,000 channels. Potassium was removed from the solution bathing the interior surface of the membrane. The gating current lasts slightly less than 1 ms and peaks at about  $4.5 \times 10^{-15}$  A per channel, about 300 times less than the channel current. The agreement with our first estimate of 600 times less is satisfactory, given the accuracy of the data. Panels C and D show recordings similar to panel A, but only a few channels in the patch. The results from three successive depolarizing pulses are shown in each case. The channel openings are similar to those in Fig. 9.13, but are recorded at a much shorter time scale. The increased current through an open channel and the higher probability of being open for a clamp of +80 mV are both apparent. The smooth macroscopic current shown in Fig. 9.16a is the sum of many discrete channel currents like those shown in Fig. 9.16c.

A very simple approximate calculation shows that there is not much ion-ion interaction in a channel. A

current of 1 pA is  $6.25 \times 10^6$  monovalent ions per second, so that the average time between the passage of successive ions through the channel is  $1.6 \times 10^{-7}$  s. In a uniform electric field giving 80 mV across the membrane, a monovalent ion would have a drift velocity of  $0.6 \text{ m s}^{-1}$  based on the bulk diffusion constant. [See the discussion surrounding Eq. 4.22.] Because ions in the pore are confined, let us use  $\frac{1}{10}$  of this, or  $0.06 \text{ m s}^{-1}$ . (The diffusion constant is proportional to the solute permeability; see Sec. 5.9. Ignoring electric forces, we see from Fig. 5.19 that  $\omega/\omega_0 = 0.1$  corresponds to  $a/R_p = 0.4$ . So this is probably still a high drift velocity.) Then the time it takes the ion to pass through the channel is its length (assume 6 nm) divided by the average speed, or  $10^{-7}$  s. The fraction of the time there is an ion in the channel is  $f = 0.625$ .

We can make some other estimates of channel parameters. Over some part of its length, the channel must be narrow enough so the wall can interact directly with the ion that is passing through, not shielded by water molecules. The pore must therefore narrow to a radius of 0.3 to 0.7 nm in some region. Let us assume a cylindrical pore of radius  $a = 0.7$  nm and length  $h = 6$  nm. The average number of water molecules in the channel is 308; the average concentration of ions is  $f/(\pi a^2 h) = 113 \text{ mmol l}^{-1}$ , which is about right. The resistance of a channel while it is open is  $R = v/i = 80 \text{ mV}/1 \text{ pA} = 8 \times 10^7 \Omega$ . (We should actually use  $v - v_{\text{Nernst}}$ , but this is a rough estimate. If we were going to be more accurate, we should also use the Nernst–Planck equation, recognizing that the ions move by diffusion as well as drift.)

## 9.8 Noise

The current fluctuates while a channel is open, as can be seen in Figs. 9.13 and 9.16. Some of the fluctuation is due to noise in the measurement apparatus. However, there are some fundamental physical lower limits to the fluctuations resulting from noise in the membrane patch itself. We discuss these briefly here, with a more extensive discussion in Chapter 11. DeFelice (1981) wrote an excellent book on noise in membranes.

### 9.8.1 Shot Noise

The first (and smallest) limitation is called *shot noise*. It is due to the fact that the charge is transported by ions that move randomly and independently through the channels. Imagine a single open conducting channel with an average current  $\bar{i}$  of monovalent ions. During time  $\Delta t$  (which can be any interval shorter than the time the channel is open) the average charge flow is  $\bar{i}\Delta t$  and the average number of ions is  $\bar{n} = \bar{i}\Delta t/e$ . Since there are a very large number of ions that might flow through the channel (occurrences) and the probability that any one ion moves through the channel during  $\Delta t$  is very small, we have the

Poisson limit of the binomial distribution (Appendix J). The variance in the number of ions is  $\sigma_n^2 = \bar{n} = \bar{i}\Delta t/e$ . Since the average charge transported is  $\bar{q} = \bar{n}e$ , the variance in the charge is  $\sigma_q^2 = e^2\sigma_n^2 = e\bar{i}\Delta t$ . When many samples of length  $\Delta t$  are measured, the variance in the current is  $\sigma_i^2 = \sigma_q^2/(\Delta t)^2$ . The standard deviations are

$$\begin{aligned}\sigma_n &= \left(\frac{\bar{i}\Delta t}{e}\right)^{1/2}, \\ \sigma_q &= (e\bar{i}\Delta t)^{1/2}, \\ \sigma_i &= \left(\frac{e\bar{i}}{\Delta t}\right)^{1/2},\end{aligned}\quad (9.60)$$

and the fractional standard deviations are

$$\frac{\sigma_n}{\bar{n}} = \frac{\sigma_q}{\bar{q}} = \frac{\sigma_i}{\bar{i}} = \left(\frac{e}{\bar{i}\Delta t}\right)^{1/2}. \quad (9.61)$$

For a current of 1 pA, the fractional standard deviation is 0.013 when the sampling time is 1 ms and 0.04 when the sampling time is 0.1 ms. These are much smaller than what is observed in the figures.

### 9.8.2 Johnson Noise

The next source of noise is called *Johnson noise*. It arises from thermal fluctuations or Brownian movement of the ions. It can be derived from a microscopic model of conduction (either in an ionic solution or a metal), but we will do it using the equipartition of energy.

First, we need an expression for the energy  $U$  contained in a charged capacitor. To obtain it, imagine that an amount of charge  $+dq$  is transferred from the negative to the positive conductor. This increases the amount of positive charge on the positive conductor and also increases the amount of negative charge on the negative conductor. The work required to transfer the charge when the potential difference between the conductors is  $v$  is  $vdq$ . The energy stored in the capacitor is the total work required to charge the conductor from 0 to  $q$ . Remembering that  $q = Cv$ , we have

$$U = \int_0^q v dq = \frac{1}{C} \int_0^q q dq = \frac{q^2}{2C} = \frac{Cv^2}{2}. \quad (9.62)$$

If the capacitor is completely isolated, there can be a constant charge on each conductor with no fluctuations. If the capacitor is in thermal contact with its surroundings and is in equilibrium, then the equipartition theorem applies. The capacitor can be brought into thermal equilibrium with its surroundings by connecting a resistance  $R$  between the conductors. This will discharge the capacitor so  $\bar{q} = \bar{v} = 0$ . There will be fluctuations around these zero values. Because the expression for the energy depends on the square of the variables, the mean square value is given by the equipartition of energy theorem,



Eq. 3.38. We will assume that when the capacitor is charged, thermal fluctuations give the same variances as when it is discharged:

$$\sigma_v^2 = (\overline{v^2} - \bar{v}^2) = \overline{v^2} = k_B T / C, \quad (9.63a)$$

$$\sigma_q^2 = (\overline{q^2} - \bar{q}^2) = \overline{q^2} = C k_B T. \quad (9.63b)$$

In a simple  $RC$  circuit,  $i = v/R$ , so

$$\sigma_i^2 = \sigma_v^2 / R^2 = k_B T / R^2 C. \quad (9.63c)$$

Since changes in current or voltage in an  $RC$  circuit occur with time constant  $\tau = RC$ , we can also write these as

$$\sigma_v^2 = R k_B T / \tau, \quad \sigma_i^2 = k_B T / R \tau. \quad (9.64)$$

These are special cases of a more general relationship that will be discussed in Chapter 11.

We can use these to determine some of the requirements for patch-clamp recording. In order to see the current from a single channel with some accuracy, let us require that the standard deviation of the current fluctuation be less than  $\frac{1}{8}$  of the signal we want to measure. (This signal-to-noise ratio, SNR, of 8 is arbitrary.) First consider the limitation due to Johnson noise. We want  $\sigma_i < \bar{i}/8$  or  $\sigma_i^2 < (\bar{i})^2 / 64$ . From this we obtain

$$R > \left( \frac{k_B T}{C} \right)^{1/2} \frac{8}{\bar{i}}. \quad (9.65)$$

The capacitance of a patch of membrane of  $1 \mu\text{m}$  radius is  $3.1 \times 10^{-14}$  F. At a temperature of 300 K and for an average current of 1 pA, this gives  $R > 3 \times 10^9 \Omega$ . Larger values of  $R$  will give an even higher SNR. There are several sources of thermal noise in a recording electrode, all discussed in the paper by Hamill *et al.* (1981). These are order-of-magnitude results; one must determine carefully which capacitances and resistances provide the dominant effects.

We can also see when shot noise is important. The ratio of Johnson noise to shot noise is

$$\frac{\sigma_i^2(\text{Johnson})}{\sigma_i^2(\text{shot})} = \frac{k_B T / R \tau}{e \bar{i} / \Delta t} = \frac{k_B T}{R e \bar{i}}. \quad (9.66)$$

This ratio is less than 1 and shot noise is important when  $R > k_B T / e \bar{i} = 2.6 \times 10^{10} \Omega$ . Shot noise has been detected in channel gating currents and subjected to very sophisticated analysis. See the paper by Crouzy and Sigworth (1993) and the references therein.

## 9.9 Sensory Transducers

Animals have very sensitive senses. We will see (Problem 13.19) that the ear can hear sounds at 1,000 Hz that are just greater than the pressure fluctuations due

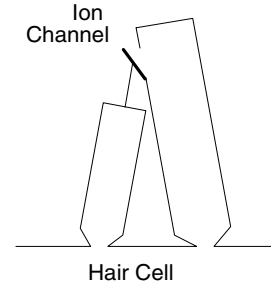


FIGURE 9.17. A schematic diagram of two stereocilia linked by a filament that opens a channel as the cilia move back and forth.

to molecular collisions on the ear drum. An eye that is adapted to the dark can detect flashes of light corresponding to a few photons (Chapter 14). Many animals can smell chemicals when only a few molecules strike their sensory organs. The electric skate can detect extremely small electric fields.

In each case a transducer converts the sensory stimulus into a series of nerve impulses. The transducer must have sufficient sensitivity to respond to the stimulus, and it must also absorb an amount of energy from the stimulus that is greater than what it receives from random thermal bombardment (Brownian movement).<sup>5</sup> We describe here two transducers: the mechanoreceptors (hair cells) of the inner ear and the electric organ of the skate.

Various transduction mechanisms are reviewed in Chapter 8 of Hille (2001). The mechanoreceptors of the bullfrog inner ear have been studied for many years. The hair-cell current rises from 0 to 100 pA with an  $0.5\text{-}\mu\text{m}$  displacement. Each hair cell is cylindrical. On its end face are found about 60 very small *stereocilia*, each  $1\text{--}50 \mu\text{m}$  long and with a  $100\text{--}500\text{-nm}$  radius. The tips of these stereocilia are linked by thin filaments. The hair cell and stereocilia that detect sound in the ear are attached to the basilar membrane in the cochlea of the ear and move in a very viscous fluid as the basilar membrane vibrates. Hair cells detecting accelerations of the entire animal are attached to a suspended dense body. It is believed that as the stereocilia move, these filaments pull open flaps at the end of ion channels, allowing ions to enter the cell and initiate the conduction process. This is shown schematically in Fig. 9.17. Denk and Webb (1989) have used a laser interferometer to measure the motion of the hair cells. They found that the spontaneous motion consists primarily of thermal excitation (Brownian motion). Fluctuations in the intracellular voltage were also measured. They often correlated with the motion of the hair cells.

Freshwater catfish respond to electric fields as low as  $10^{-4} \text{ V m}^{-1}$ . Saltwater sharks and rays can detect fields of  $5 \times 10^{-7} \text{ V m}^{-1}$ . A brief review has been given by Bastian (1994); Kalmijn (1988) provides a very complete

<sup>5</sup>For the detection of light, the amount of energy per photon is so much greater than  $k_B T$  that shot noise dominates.

review. The saltwater fish have a more complicated sensory apparatus than the freshwater fish, known as the *ampullae of Lorenzini*. Kalmijn and his colleagues discovered that the ocean flounder generates a current dipole of  $3 \times 10^{-7}$  A m. In sea water of resistivity  $0.23 \Omega \text{ m}$  this gives an electric field of  $2 \times 10^{-5} \text{ V m}^{-1}$  at a distance 10 cm in front of the flounder. They were able to show in a beautiful series of behavioral experiments that dogfish (a small shark) could detect the electric field 0.4 m from a current dipole of  $4 \times 10^{-7}$  A m, corresponding to an electric field of  $5 \times 10^{-7} \text{ V m}^{-1}$ . The fish would bite at the electrodes, ignoring a nearby odor source. A field of  $10^{-4} \text{ V m}^{-1}$  would elicit the startle response. A field  $\frac{1}{10}$  as large caused a physiologic response. The animals responded to a constant field or a sinusoidally alternating field up to 4 Hz. At 8 Hz the threshold increased by a factor of 2.

In a series of experiments, Lu and Fishman (1994) dissected out the ampulla of Lorenzini and measured its response in the laboratory. They found that the resting rate of firing of the organ is about 35 Hz (impulses per second) and that an applied electric potential increases or decreases the firing rate by about  $1 \text{ Hz } \mu\text{V}^{-1}$ , depending on its sign. The firing rate saturated for potential differences of  $100 \mu\text{V}$ .

The behavioral experiments showed sensitivity to an electric field of  $0.5 \mu\text{V m}^{-1}$ . The anatomy of the ampulla is such that the organ senses the potential difference between the surface of the fish and deep in its interior. Pickard (1988) shows that for a spherical fish of radius  $a$ , this gives a potential of  $3aE/2$ , where  $E$  is the external electric field. The amplitude of the potential difference oscillation of a fish of length  $\frac{1}{3}$  m is therefore  $0.25 \mu\text{V}$ . This is enough to cause a 1% change in firing rate, which could be detected by neuronal circuits [Adair *et al.* (1998)].

The Johnson noise is somewhat smaller than the signal detected. To estimate it, use Eq. 9.63a with the ampullary capacitance of  $0.15 \mu\text{F}$  measured by Lu and Fishman. The standard deviation of the noise is  $0.17 \mu\text{V}$ .

## 9.10 Possible Effects of Weak External Electric and Magnetic Fields

### 9.10.1 Introduction

There is a lingering controversy over whether radio-frequency and power-line-frequency (50–60 Hz) electric or magnetic fields can cause cancer. While the effect, if any, is quite small, the literature is extensive, involving both epidemiological and laboratory studies. Results are conflicting, and the mechanisms by which such an effect might occur are not yet understood. Mechanisms have been proposed, some of which are inconsistent with basic physical principles such as the Boltzmann factor, the mean free path of ions, and thermal fluctuations. It is be-

yond our scope to do more than provide pointers to the field and discuss some basic underlying physics.

A review in the physics-teaching literature was provided by Hafemeister (1996). An excellent discussion of the all aspects of the problem is available at a frequently updated website, *Powerlines and Cancer FAQ* [Moulder (Web)]. Similar websites for cell phones and for static fields can be reached through this one.

We have seen that electric charges give rise to electric fields, and moving electric charges (currents) generate magnetic fields. The electric field lines start and end on charges, and the magnetic field lines surround the currents. We will see in Chapter 14 that accelerated charges generate electromagnetic *radiation*, in which the electric and magnetic fields are interrelated and the field lines close on themselves far from the source charges. Energy is radiated: it leaves the source and never returns. This radiated energy is in the form of discrete packets or *photons*, whose energy is related to the frequency of oscillation of the fields. The energy of each photon is  $E = h\nu$ , where  $h$  is Planck's constant and  $\nu$  the frequency. At room temperature, the energy of random thermal motion is  $k_B T = 4 \times 10^{-21}$  J. At 60 Hz, the energy in each photon is much smaller:  $4 \times 10^{-32}$  J. At 100 MHz it is  $7 \times 10^{-26}$  J. For electromagnetic radiation in the ultraviolet and beyond, which certainly can harm cells, the photon energy is  $5 \times 10^{-19}$  J or greater, quite large compared to  $k_B T$ . At the very low frequencies we are considering, it is the strength of the electric or magnetic field that is important, not the energy of individual photons. A more detailed discussion of the distinction between these low-frequency “near fields” and “radiation fields” is found in Polk (1996).

### 9.10.2 Effects of Strong Fields

We have seen electrical burns, cardiac pacing, and nerve and muscle stimulation produced by electric or rapidly changing magnetic fields. Even stronger electric fields increase membrane permeability. This is believed to be due to the transient formation of pores (*electroporation*). Pores can be formed, for example, by microsecond-length pulses with a field strength in the membrane of about  $10^8 \text{ V m}^{-1}$  [Weaver (2000)]. Microwaves are used to heat tissue. Nerve stimulation requires a few millivolts across the cell membrane, or about  $10^5$ – $10^6 \text{ V m}^{-1}$ . Both electric and magnetic fields are used to promote bone healing, with field strengths in tissue in the fracture region of  $10^{-1} \text{ V m}^{-1}$  [Tenforde (1995)], though these results are still controversial [Adair (2000)].

### 9.10.3 Fields in Homes are Weak

Much weaker fields in homes are produced by power lines, house wiring, and electrical appliances. Barnes (1995) found average electric fields in air next to the body of about  $7 \text{ V m}^{-1}$ , with peak values of  $200 \text{ V m}^{-1}$ . (We will

find that since the body is a conductor, the fields within the body are much less.) Average residential magnetic fields are about  $0.1 \mu\text{T}$ , with peaks up to four times as large. Within the body they are about the same. Tenforde (1995) reviews both power-line- and radio-frequency field intensities.

#### 9.10.4 *Epidemiological Studies*

Epidemiological studies have been very valuable in tracing the cause of infectious outbreaks. They have also indicated that smoking increases the probability of developing lung cancer by 3,000%—a factor of 30. However, there are difficulties with epidemiological studies when the effect is small: there are inescapable statistical fluctuations unless the number of subjects is huge; associations do not prove causality; and there may be unrecognized variables that are confusing the picture. The problem is exacerbated when positive findings receive widespread publicity and negative findings are ignored by the press.

Epidemiological studies usually report “relative risk:” the incidence in an exposed group divided by the incidence in an unexposed group. A relative risk of one means no effect. Moulder (Web, question 20A) says,

A strong association is one with a relative risk (RR) of 5 or more. Tobacco smoking, for example, shows a strong association, with the risk of lung cancer in smokers being 10-30 times that of nonsmokers. A relative risk of less than about 3 indicates a weak association. A relative risk below about 1.5 is essentially meaningless unless it is supported by other data.

Most of the positive power-frequency studies have relative risks of 2 or less. The leukemia studies as a group have relative risks of 0.8-1.9, while the brain cancer studies as a group have relative risks of 0.8-1.6. This is a weak association. Interestingly, as the sophistication of the studies has increased, the relative risks have not increased.

One would also expect an increased response with increasing dose. Moulder continues,

No published power-frequency exposure study has shown a statistically significant dose-response relationship between measured fields and cancer rates, or between distances from transmission lines and cancer rates. However, there is some indication of a dose-response in some of the older childhood leukemia studies when wire codes or calculations of historic fields are used as exposure metrics. The lack of a clear relationship between exposure and increased cancer incidence is a major reason why most scientists are skeptical about the significance of much of the epidemiology.

#### 9.10.5 *Laboratory Studies*

The many laboratory studies are also reviewed by Moulder (Web). He concludes:

Power-frequency fields show little evidence of the type of effects on cells, tissues or animals that point towards their being a cause of cancer, or to their contributing to cancer. In fact, the existing laboratory data provides strong evidence that power-frequency fields of the magnitude to which people are exposed are not carcinogenic.<sup>6</sup>

#### 9.10.6 *Reviews and Panel Reports*

Moulder (Web) lists a number of review articles and reports by expert panels. We note only a few here. Reviews by Moulder and Foster (1995, 1999) find that the association between power-frequency fields and cancer is weak<sup>7</sup> for magnetic fields and even weaker for electric fields. Carstensen (1995) and Bren (1995) reach similar conclusions.

A report by a committee of the National Research Council concludes that

the current body of evidence does not show that exposure to these fields presents a human-health hazard.... The committee reviewed residential exposure levels to electric and magnetic fields, evaluated the available epidemiological studies, and examined laboratory investigations that used cells, isolated tissues, and animals.” [National Research Council (1997), p. 2]

There is no convincing evidence that exposure to 60-Hz electric and magnetic fields causes cancer in animals.... There is no evidence of any adverse effects on reproduction or development in animals, particularly mammals, from exposure to power-frequency 50- or 60-Hz electric or magnetic fields.” [National Research Council (1997), p. 7].

<sup>6</sup>Foster (1996) has reviewed many of the laboratory studies and describes cases where subtle cues meant the observers were not making truly “blind” observations. Though not directly relevant to the issue under discussion here, a classic study by Tucker and Schmitt (1978) at the University of Minnesota is worth noting. They were seeking to detect possible human perception of 60-Hz magnetic fields. There appeared to be an effect. For 5 years, they kept providing better and better isolation of the subject from subtle auditory clues. With their final isolation chamber, none of the 200 subjects could reliably perceive whether the field was on or off. Had they been less thorough and persistent, they would have reported a positive effect that does not exist.

<sup>7</sup>That is, the carcinogenic effects are in International Association for Research on Cancer group 2B (possibly carcinogenic), a group that includes coffee and pickled vegetables [Moulder (Web) Q. 27F].

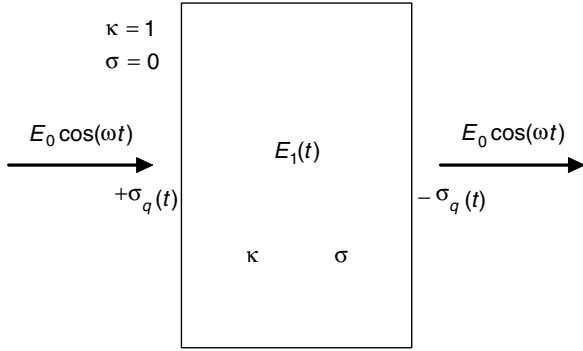


FIGURE 9.18. An infinite slab of tissue is immersed in an oscillating electric field of amplitude  $E_0$  in air.

### 9.10.7 Electric Fields in the Body

We now review some of the basic principles that govern the interaction of electric and magnetic fields with the body. One of the important principles is the relationship between the electric field in air and the field within the body, which is a conductor. A simple model that shows how this coupling takes place is the one-dimensional problem shown in Fig. 9.18.

An infinite slab of tissue has dielectric constant  $\kappa$  and conductivity  $\sigma$ . In the air perpendicular to the surface of the slab is an external oscillating electric field  $E(t) = E_0 \cos \omega t$ . We assume that the dielectric constant is independent of frequency and accounts for the polarization of the tissue. An ionic current flows and causes free charge per unit area  $\pm \sigma_q$  to accumulate on the surfaces of the slab. Within the slab the field is  $E_1(t)$  and the current density is  $j = \sigma E_1$ . Gauss's law (Eq. 6.21b) applied to either surface gives

$$-\epsilon_0 E_0 \cos \omega t + \kappa \epsilon_0 E_1(t) = \sigma_q(t). \quad (9.67)$$

Conservation of free charge at the surface requires that<sup>8</sup>

$$\sigma E_1 = j = -\frac{d\sigma_q}{dt}. \quad (9.68)$$

If we differentiate Eq. 9.67 and combine it with Eq. 9.68, we obtain

$$\frac{dE_1}{dt} + \frac{\sigma}{\kappa \epsilon_0} E_1 = \frac{\omega}{\kappa} E_0 \sin \omega t. \quad (9.69)$$

The factor  $\kappa \epsilon_0 / \sigma$  is characteristic of the tissue and has the dimensions of time. We will call it  $\tau_t$ .<sup>9</sup> Typical tissue conductivity is about  $0.1 \text{ S m}^{-1}$ . We must be careful

<sup>8</sup>Readers who are familiar with the concepts of reactance and complex impedance must be frustrated because we have not used them. The reason is pedagogic. Because many in our intended audience may have had only one year of calculus, we want to avoid the use of complex numbers. In Chapter 11 we introduce them as a parallel notation. They are widely used in the image reconstruction described in Chapter 12.

<sup>9</sup>Recall that the membrane time constant  $\tau$ , was used in Eq. 6.40. The values of conductivity or resistivity and dielectric constant are different in this case.

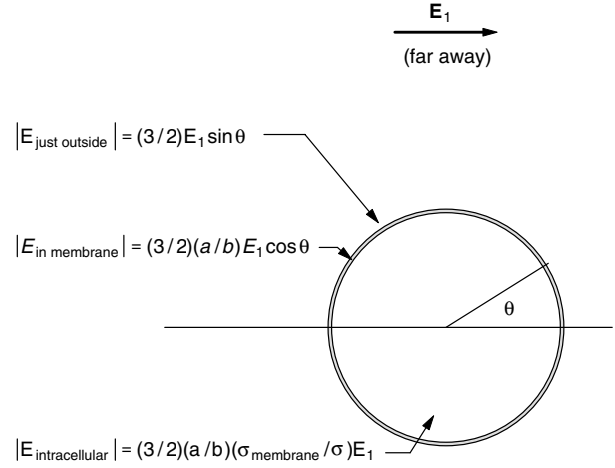


FIGURE 9.19. The electric fields in and around a spherical cell. The cell has radius  $a$  and membrane thickness  $b$ . The field far from the cell has amplitude  $E_1$ .

about the value of the dielectric constant. We have used a value of 80 for water. However, tissue is much more complex than pure water and there are several effects that alter the dielectric constant [Foster and Schwan (1996)]. It takes time for both the polarization charges and conducting ions to move. As a result, both the conductivity and the dielectric constant of tissue depend on the frequency of the applied electric field and in fact are not independent of one another [see Foster and Schwan (1996), especially pp. 31–41].

Several effects change the conductivity and dielectric constant as a function of frequency. At power-line frequencies the dominant effect is the slight movement of the counterions and charge in the double layer at a cell membrane in response to the applied electric field. As a result,  $\kappa \approx 10^6$  and  $\tau_t = 9.1 \times 10^{-5} \text{ s}$ .

We try a solution to Eq. 9.69 of the form  $E_1(t) = A \sin \omega t + B \cos \omega t$ . It satisfies the equation if

$$A = \frac{\omega \tau_t}{\kappa(1 + \omega^2 \tau_t^2)} E_0 \approx \frac{\omega \epsilon_0}{\sigma} E_0, \quad (9.70)$$

$$B = -\omega \tau_t A = -\frac{(\omega \tau_t)^2}{\kappa(1 + \omega^2 \tau_t^2)} E_0 \approx 0.$$

For 60 Hz and a dielectric constant of  $10^6$ ,  $A = 33 \times 10^{-9} E_0$ ,  $B = 1.1 \times 10^{-9} E_0$ . The amplitude of the field in tissue is  $E_1 \approx A$ . The field in air is reduced by a factor of about  $3 \times 10^{-8}$  in tissue because the tissue is a good conductor. The total reduction is nearly the same for a dielectric constant of 80, as can be seen from the fact that the approximate form for  $A$  does not depend on  $\kappa$ .

### 9.10.8 Electric Fields in a Spherical Cell

Another important factor is the electric fields that exist in and near a cell. Consider a spherical cell with inner radius  $a$  and membrane thickness  $b$  immersed in an infinite

conducting medium in which there is an electric field  $E_1$  far from the cell. The potential can be determined analytically by solving Poisson's equation (with zero charge density) in the three regions and matching boundary conditions much as we did to obtain Eq. 9.68. The results, valid for slowly varying applied fields such as a 50- or 60-Hz power line field, are shown in Fig. 9.19.<sup>10</sup>

Only the amplitude of the electric field is shown. Assume the conductivities of the extracellular and intracellular fluids are the same, that  $a = 10 \mu\text{m}$  and  $b = 6 \text{ nm}$ , and that  $\sigma_{\text{membrane}} = 2.4 \times 10^{-8} \sigma$ . The important features of this solution are that the field just outside the cell is roughly the same as the field far away, the field inside the membrane is magnified by a large factor ( $a/b$ ), and the field inside the cell is multiplied by a very small factor ( $a\sigma_{\text{membrane}}/b\sigma$ ). Thus, the cell membrane shields the intracellular space from extracellular electric fields, so these fields are not likely to directly affect cell organelles and important biomolecules such as DNA. This is reflected in the last line of Table 9.5.

### 9.10.9 Electrical Interactions and Noise

If an organism is affected in some way by an external field, then it can be regarded as a detector of that field. The external field can therefore be thought of as a signal. To be detected, the signal must be greater than the noise. The noise can be either thermal (Johnson) noise, shot noise, or noise from the electric currents that normally flow in the body due to nerve conduction and muscle contraction. To have a signal that is not masked by Johnson noise, we must have an electric field  $E$  such that

$$\frac{zev}{k_B T} = \frac{zeEd}{k_B T} > 1, \quad (9.71)$$

where  $z$  is the valence of an effective charge that moves a distance  $d$  in the electric field  $E$ . Table 9.5 shows the result of a calculation using a field in air of  $300 \text{ V m}^{-1}$ . We use a value  $z = 10e$ . For  $d$  we use the diameter of the cell,  $d = 10 \mu\text{m}$  (though for the membrane perhaps the much smaller thickness of the cell membrane should be used). The values of  $zeEd/k_B T$  are very small.

One proposal to overcome this signal-to-noise problem is that the biological effect is due to the averaging of the field over many cells or over time. This was first proposed by Weaver and Astumian (1990), and a specific model has been formulated by Astumian *et al.* (1995). The model applies the Nernst-Planck equation (Eq. 9.38) and shows that if the concentration of some substance outside the cell is much larger than inside, the response to an oscillating  $v$  is "rectification" or a net inward current. This would allow an accumulation of the substance within the cell. The averaging times in their model are 13 h. Weaver and Astumian (1995) review the entire causality problem,

TABLE 9.5. Comparison of the signal in a cell to thermal noise for an applied electric field in air of  $300 \text{ V m}^{-1}$ .  $T = 300 \text{ K}$ .  $z = 10e$ .  $d = 10^{-5} \text{ m}$ .

Model	Just outside the cell	In the cell membrane	Inside the cell
$E \text{ (V m}^{-1}\text{)}$	$1.01 \times 10^{-5}$	$1.62 \times 10^{-2}$	$5.40 \times 10^{-10}$
$k_B T/eE \text{ (m)}$	$2.57 \times 10^3$	1.59	$4.79 \times 10^7$
$zeEd/k_B T$	$3.9 \times 10^{-8}$	$6.3 \times 10^{-5}$	$2.1 \times 10^{-12}$

including the effects of shot noise. Adair (2000) reviews many other aspects of the problem.

### 9.10.10 Magnetic Interactions and Noise

The magnetic field is not attenuated at the body surface, as the electric field is. Kirschvink *et al.* (1992a) reported that the human brain contains several million magnetosomes per gram. Kobayashi *et al.* (1995) found that contamination with magnetic particles could affect laboratory experiments with cell cultures, even if the cells being studied do not normally contain magnetosomes. Commercial disposable, presterilized plastic laboratory ware used in tissue culture experiments were found to contain ferromagnetic particles smaller than  $100 \text{ nm}$  that are readily taken up by white blood cells.

What about the signal-to-noise ratio for magnetic effects? The situation is somewhat more favorable than for the electric case. We saw in Chapter 8 that a single magnetosome has appreciable alignment with the earth's magnetic field, even in the presence of thermal bombardment. The earth's field is about  $5 \times 10^{-5} \text{ T}$ . For a single magnetosome

$$\frac{mB_{\text{earth}}}{k_B T} = \frac{(6.4 \times 10^{-17})(5 \times 10^{-5})}{(1.38 \times 10^{-23})(300)} = 0.77. \quad (9.72)$$

For a larger magnetosome of radius  $100 \mu\text{m}$ ,  $m = 2 \times 10^{-15} \text{ A m}^2$  and the energy ratio in the earth's field is 24. The field due to a typical power line is about 100 times smaller: about  $2 \times 10^{-7} \text{ T}$ .

Kirschvink (1992) proposed a model whereby a magnetosome in a field of  $10^{-4}$ – $10^{-3} \text{ T}$  could rotate to open a membrane channel. As an example of the debate that continues in this area, Adair (1991, 1992, 1993, 1994) argued that a magnetic interaction cannot overcome thermal noise in a 60-Hz field of  $5 \times 10^{-6} \text{ T}$ . However, Polk (1994) argues that more biologically realistic parameters, including a large number of magnetosomes in a cell, could allow an interaction at  $2 \times 10^{-6} \text{ T}$ .

The essential features of all the models are like this. Imagine a particle with magnetic moment  $\mathbf{m}$  in the

<sup>10</sup>Calculated using equations in Polk (1995), p. 62.

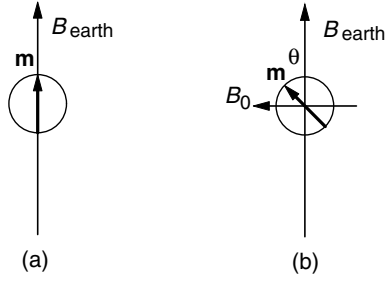


FIGURE 9.20. A particle with magnetic moment  $\mathbf{m}$  (a) aligned with the earth's magnetic field and (b) at an angle  $\theta$  with the earth's field because of an applied field  $B_0$ .

earth's field. It will tend to align with the field as shown in Fig. 9.20(a). The direction of the magnetic moment with the earth's field is  $\theta$ . Apply an alternating field  $B_0 \cos \omega t$  at right angles to the earth's field, as shown in Fig. 9.20(b). There are three torques on the particle. The first is viscous drag, which is proportional to the angular velocity of the particle  $d\theta/dt$  but in the opposite direction. The second is the torque tending to align  $\mathbf{m}$  with the earth's field,  $-mB_{\text{earth}} \sin \theta$ . The third tends to align  $\mathbf{m}$  with the alternating field,  $mB_0 \cos \omega t \cos \theta$ . Assume that the acceleration is so small that the particle is in rotational equilibrium. (This is not necessary, but it simplifies the math.) Then, from Eq. 1.14,

$$-\beta \frac{d\theta}{dt} + mB_{\text{earth}} \sin \theta - mB_0 \cos \omega t \cos \theta = 0. \quad (9.73)$$

In order to linearize the equation, assume that  $\theta$  is small enough so that  $\sin \theta \approx \theta$  and  $\cos \theta \approx 1$ . The linearized equation is

$$\beta \frac{d\theta}{dt} - mB_{\text{earth}} \theta = -mB_0 \cos \omega t. \quad (9.74)$$

This is a linear differential equation with constant coefficients that can be solved by the techniques of Appendix F. Consider only the particular solution and try a solution of the form

$$\theta = \theta_1 \cos \omega t + \theta_2 \sin \omega t. \quad (9.75)$$

Substitution of this in the equation shows that

$$\theta_1 = \frac{m^2 B_0 B_{\text{earth}}}{(\omega\beta)^2 + (mB_{\text{earth}})^2},$$

$$\theta_2 = -\frac{\omega\beta m B_0}{(\omega\beta)^2 + (mB_{\text{earth}})^2},$$

and

$$\theta_m = \frac{mB_0}{[(\omega\beta)^2 + (mB_{\text{earth}})^2]^{1/2}}, \quad (9.76)$$

where  $\theta_m$  is the maximum amplitude:  $\theta_m^2 = \theta_1^2 + \theta_2^2$ . We saw in Chap. 4 (Stokes' law) that the translational viscous drag on a spherical particle is  $6\pi\eta av$ . Similarly, the viscous torque on a rotating sphere is  $8\pi\eta a^3(d\theta/dt)$  [Lamb

(1932), pp. 588-589]. The measured values for viscosity inside a cell range from 0.003 to 0.015 N s m<sup>-2</sup> [Polk (1994)]. Using the average of these,  $\beta = 0.009a^3$ . The magnetic moment of a single-domain magnetosome is also proportional to volume:  $m = 2 \times 10^6 a^3$ . This leads to a maximum amplitude that is independent of  $a$ :

$$\theta_m = \frac{2 \times 10^6 a^3 B_0}{[(377)^2(0.23)^2 a^6 + (2 \times 10^6)^2 (5 \times 10^{-5})^2 a^6]^{1/2}} = 1.5 \times 10^4 B_0. \quad (9.77)$$

Kirschvink originally argued from data about hair-cell deformation that a deflection of 16° or 0.3 radian is needed. This would require  $B_0 = 5 \times 10^{-5}$  T. (He had a slightly different value because he used a different viscosity. He also included the torque due to the force on the channel gate.)

In the absence of the applied field, the thermal fluctuations in angle can be estimated as follows. In the linear approximation, the work required to displace the particle an amount  $\theta$  from the direction of the earth's field is

$$W = \int \tau d\theta = \int mB_{\text{earth}} \theta d\theta = mB_{\text{earth}} \frac{\theta^2}{2}. \quad (9.78)$$

Equipartition of energy again gives us

$$\overline{\theta^2}_{\text{thermal}} = \frac{k_B T}{mB_{\text{earth}}} = \frac{k_B T}{(2 \times 10^6)(5 \times 10^{-5})a^3} = \frac{k_B T}{100a^3}. \quad (9.79)$$

For a 50-nm magnetosome, this gives  $\theta_{\text{rms}} = 0.58$  radian. For a 100-nm magnetosome it is 0.2 radian, comparable to the maximum angles deduced from the model in the preceding paragraph.

## Symbols Used in Chapter 9

Symbol	Use	Units	First used on page
$a$	Radius	m	232
$b$	Spacing	m	233
$d$	Displacement of charge	m	247
$e$	Electron charge	C	227
$f$	Force	N	234
$f$	Fraction of time an ion is in a channel		242
$g_K$	Potassium conductance per unit area	S m <sup>-2</sup>	240
$h$	Length of cylindrical channel	m	242
$h$	Planck's constant	J s	244
$j, \bar{j}$	Electric current density	A m <sup>-2</sup>	235
$j_s$	Particle current density	m <sup>-2</sup> s <sup>-1</sup>	234
$j_v$	Volume current density	m s <sup>-1</sup>	235
$k_B$	Boltzmann constant	J K <sup>-1</sup>	227
$\mathbf{m}$	Magnetic moment	A m <sup>2</sup>	247
$n$	Number of ions		242
$p_e, \mathbf{p}_e, p_{\text{tot}}$	Electric dipole moment	C m	233

Symbol	Use	Units	First used on page					
				$\epsilon_0$	Electrical permittivity of vacuum	$C^2 m^{-2}$	$N^{-1}$	229
				$\kappa$	Dielectric constant			229
$p, p_c, p_o$	Probability		240	$\eta$	Coefficient of viscosity	Pa s		248
$q$	Charge	C	233	$\lambda_D$	Debye length	m		230
$r, \mathbf{r}$	Position	m	229	$\lambda$	Characteristic length	m		235
$r$	Radius in cylindrical coordinates	m	236	$\nu$	Frequency	Hz or $s^{-1}$		244
				$\rho, \rho_{ext}$	Charge density	$C m^{-3}$		229
$r$	Radius in spherical coordinates	m	232	$\rho$	Resistivity	$\Omega m$		235
				$\sigma_q, \sigma'_q$	Charge per unit area	$C m^{-2}$		233
$t$	Time	s	242	$\sigma$	Conductivity	$S m^{-1}$		235
$u$	$rv(r)$	V m	232	$\sigma_i$	Standard deviation of current	A		242
$u, u_o$	Energy (normalized to $k_B T$ )		235					
				$\sigma_n$	Standard deviation of number of ions			242
$v, v'$	Potential	V	227	$\sigma_q$	Standard deviation of charge	C		242
$v_{Nernst}$	Nernst potential	V	236					
$w$	Energy	J	240	$\sigma_q$	Charge per unit area	$C m^{-2}$		246
$x$	Position	m	229	$\sigma_v$	Standard deviation of voltage	V		242
$x$	Distance along cylindrical axis	m	236					
				$\tau$	Time constant	s		235
$z$	Valence		227	$\tau$	Torque	N m		248
$A, B, A', B'$	Constants	V	231	$\tau_t$	Tissue time constant	s		246
$B_{earth}$	Earth's magnetic field	T	247	$\theta$	Angle			248
$B_0$	Amplitude of applied oscillating magnetic field	T	248	$\phi$	Angle in cylindrical coordinates			236
$C, C'$	Concentration	$m^{-3}$	227	$\chi$	Susceptibility			234
$C_i$	Concentration of species $i$	$m^{-3}$	230	$\omega, \omega_s, \omega_0$	Solute permeability	$N^{-1} s^{-1}$		237
$[Cl], [Cl']$	Chloride concentration	$m^{-3}$	228	$\omega$	Angular frequency	$s^{-1}$		246
$C$	Capacitance	F	242	$\omega_t$	Characteristic angular frequency of tissue	$s^{-1}$		
$D, D_{eff}, D_0$	Diffusion constant	$m^2 s^{-1}$	234	$\xi$	Energy in units of $k_B T$			230
$E, E_x, E_0, E_1$	Electric field	$V m^{-1}$	229	$\Gamma$	Radial concentration factor			236
$E_{ext}$	External electric field	$V m^{-1}$	234					
$E_{pol}$	Polarization electric field	$V m^{-1}$	233					
$E$	Photon energy	J	244					
$F$	Faraday constant	$C mol^{-1}$	227					
$F, \mathbf{F}$	Force	N	234					
$G$	Conductance	S	235					
$J$	Current per unit area of membrane	$A m^{-2}$	237					
$[K], [K']$	Potassium concentration	$m^{-3}$	228					
$L$	Separation	m	235					
$[M^+], [M^{+'}]$	Concentration of impermeant cations	$m^{-3}$	228					
$[M^-], [M^{-'}]$	Concentration of impermeant anions	$m^{-3}$	228					
$[M], [M']$	Net concentration of impermeant ions	$m^{-3}$	228					
$N$	Number per unit volume	$m^{-3}$	233					
$N_A$	Avogadro's number	$mol^{-1}$	234					
$[Na], [Na']$	Sodium concentration	$m^{-3}$	228					
$P$	Polarization	$C m^{-2}$	234					
$R$	Gas constant	$J K^{-1} mol^{-1}$	227					
$R$	Resistance	$\Omega$	235					
$R_p$	Pore radius	m	236					
$S$	Area	$m^2$	229					
$T$	Temperature	K	227					
$U, W$	Energy	J	242					
$V$	Particle velocity	$m s^{-1}$	234					
$\alpha$	Proportionality constant		240					
$\beta$	Linear viscous drag coefficient	$N s m^{-1}$	234					
$\beta$	Rotational viscous drag coefficient	$N s m$	248					

## Problems

### Section 9.1

**Problem 1** The chloride ratio between plasma and interstitial fluid is 0.95. Plasma protein has a valence of about  $-18$ . In the interstitial fluid,  $[Na'] = [Cl'] = 155 \text{ mmol } l^{-1}$ . Find the sodium, chloride and protein concentrations in the plasma and the potential difference across the capillary wall, assuming Donnan equilibrium.

**Problem 2** Suppose that there are two compartments with equal volume  $V = 1 \text{ l}$ , separated by a membrane that is permeable to  $K$  and  $Cl$  ions. Impermeant positive ions have a concentration 0 on the left and  $[M'] = [M^{+'}] = 10 \text{ mmol } l^{-1}$  on the right. The initial concentration of potassium is  $[K_0] = 30 \text{ mmol } l^{-1}$  on the left.  $T = 310 \text{ K}$ .

(a) Find the initial concentrations of potassium and chloride on both sides and the potential difference.

(b) A fixed amount of potassium chloride (10 mmol) is added on the left. After things have come to equilibrium, find the new concentrations and potential difference.

**Problem 3** The extracellular space in cartilage contains large, immobile, negatively charged molecules called glycoaminoglycans (GAGs). An early sign of osteoarthritis is the loss of GAGs. The concentration of the GAGs is difficult to measure directly, but Shapiro et al. (2002)

measured the sodium ion concentration in cartilage using magnetic resonance imaging (see Chapter 18). Assume the interstitial fluid of the body consists of 150 mM of sodium ions and 150 mM of chloride ions, and that both of these ions can move freely between the body fluid and the extracellular space of cartilage. The cartilage sodium ion concentration is measured to be 250 mM. If Donnan equilibrium holds, what is the concentration of the GAGs? For simplicity, assume the GAGs are monovalent.

### Section 9.2

**Problem 4** Derive the Poisson equation from Gauss's law in Cartesian coordinates in three dimensions.

**Problem 5** Consider ions uniformly dispersed in a solution. Find the average linear separation of the ions for concentrations of 1, 10, 100, and 1,000 mmol  $l^{-1}$ .

**Problem 6** Verify Eq. 9.20.

**Problem 7** Verify the parameters presented in Table 9.2. How accurate is the approximation  $e^x \approx 1 + x$  in this case?

**Problem 8** Consider a solution consisting of an equal concentration,  $C$ , of monovalent cations and anions.

(a) Show that  $\rho_{ext} = -2Ce \sinh\left(\frac{ev}{k_B T}\right)$ .

(b) Let  $\xi = ev/k_B T$  and  $\mathbf{r}' = \mathbf{r}/\lambda_D$ , where  $\lambda_D$  is given by Eq. 9.14. Show that the nonlinear Poisson-Boltzmann equation (Eq. 9.13) becomes  $\nabla'^2 \xi = \sinh \xi$ .

**Problem 9** Analytical solutions to the nonlinear Poisson-Boltzmann equation are rare but not unknown. Consider the case when the potential varies in one dimension ( $x$ ), the potential goes to zero at large  $x$ , and there exists equal concentrations of monovalent cations and anions. Chandler et al. (1965) showed that the solution to the 1-d Poisson-Boltzmann equation,  $d^2 \xi/dx'^2 = \sinh \xi$  (see Prob. 8), is  $\xi(x') = 4 \tanh^{-1} \left[ \tanh(\xi_0/4) e^{-x'} \right]$ , where  $\xi_0$  is a constant and  $0 < x' < \infty$ .

(a) Verify that this expression for  $\xi$  satisfies  $d^2 \xi/dx'^2 = \sinh \xi$ . (You may need a math handbook with a collection of hyperbolic function identities).

(b) Linearize the Poisson-Boltzmann equation and show that its solution is  $\xi(x') = \xi_0 e^{-x'}$ .

(c) Show that both solutions are equal to  $\xi_0$  at  $x' = 0$  and equal to 0 at  $x' = \infty$ .

(d) Compare the solutions for the linear and nonlinear Poisson-Boltzmann equation at  $x' = 0.5$  for the cases  $\xi_0 = 0.1, 1, \text{ and } 10$ .

### Section 9.3

**Problem 10** The value of  $A$  used to obtain Eq. 9.30 was determined by saying that as  $r \rightarrow 0$ , the electric field must approach  $ze/\kappa 4\pi\epsilon_0 r^2$ . An elaboration of the model would

be to say that the central ion has radius  $a$  and that the electric field at  $r = a$  must be the same as the field at the surface of the ion,  $ze/\kappa 4\pi\epsilon_0 a^2$ . How does this change the expression for  $v(r)$ ?

**Problem 11** Using the method in Sec. 9.3, derive the Poisson-Boltzmann equation in cylindrical coordinates ( $r, \phi, z$ ; see Appendix L) assuming the electric field is radial and does not depend on  $\phi$  or  $z$ . Solutions to the linearized version of this equation are zeroth order modified Bessel functions [see Abramowitz and Stegun (1972)].

### Section 9.4

**Problem 12** A collection of molecular electric dipoles, each of moment  $\mathbf{p}$ , are in thermal equilibrium at temperature  $T$ . If the dipoles experience an electric field of strength  $E$ , then determine the average value of  $\cos \theta$ , where  $\theta$  is the angle between the dipole and the electric field. Hint: Assume the dipole orientations follow the Boltzmann distribution, which in this case is  $\exp(pE \cos \theta/k_B T)$ , and integrate over all solid angles  $d\Omega = 2\pi \sin \theta d\theta$ . Show that if  $pE \ll k_B T$  the average of  $\cos \theta$  is proportional to  $E$ , but if  $pE \gg k_B T$  the average of  $\cos \theta$  saturates at a value of one. Interpret this physically.

### Section 9.5

**Problem 13** Find an expression for the slope of the Nernst-Planck constant-field curve in Fig. 9.10 when  $v$  is equal to the Nernst potential,  $v_0$ . Hint: Expand the exponentials in Eq. 9.46 around  $v_0$ .

**Problem 14** Show that when  $j = 0$ , Eq. 9.41 gives  $C(x) = C_0 e^{-zev(x)/k_B T}$ , as we already know must be true in equilibrium. Hint: Solve for  $dv/dx$ .

**Problem 15** The discussion surrounding Eqs. 9.35–9.42 was for a model of ions in a pore with constant electric field. It is also possible to write an integral version of the Nernst-Planck equation. Consider a single channel in which the current is the same for all values of  $x$ , the distance along the channel. If the diffusion constant and cross-sectional area of the channel are allowed to vary, and with the usual substitution  $u(x) = zev(x)/k_B T$ , Eq. 9.42 becomes

$$i = j(x)S(x) = -zeD(x)S(x) \left( \frac{dC}{dx} + C(x) \frac{du}{dx} \right).$$

(a) Show that if each term is multiplied by  $e^u$ , this can be written as

$$\frac{ie^{u(x)}}{D(x)S(x)} = -ze \left( e^{u(x)} \frac{dC}{dx} + C(x) e^{u(x)} \frac{du}{dx} \right).$$



(b) Show that if the integration is carried from  $x_1$  to  $x_2$ , then the current in the channel is

$$i = -\frac{ze [C(x_2)e^{u(x_2)} - C(x_1)e^{u(x_1)}]}{I},$$

where the integral

$$I = \int_{x_1}^{x_2} \frac{e^{u(x)} dx}{S(x)D(x)},$$

contains all the information about the channel.

**Problem 16** Cardiac cells have a potassium channel, called “ $I_{K1}$ ,” which shows inward rectification (larger current for potentials more negative than the potassium Nernst potential,  $V_K$ , than for potentials more positive than  $V_K$ ). This channel sometimes is said to show “anomalous rectification.” Why is it anomalous? [The mechanism of anomalous rectification is described by Nichols et al. (1996)].

### Section 9.6

**Problem 17** Consider a channel that is 100 times more permeable to potassium than to sodium (ignore all other ions).

(a) Write an equation for the reversal potential as a function of the intracellular and extracellular sodium and potassium ion concentrations.

(b) Assume  $[K_i] = 150$ ,  $[Na_i] = 50$ , and  $[Na_e] = 150$  mM. Plot  $v_r$  versus  $[K_e]$  using semilog paper. On the same plot, draw the potassium Nernst potential as a function of  $[K_e]$ .

**Problem 18** Calculation of the permeability ratios from measurement of the reversal potential is difficult because the concentrations inside the axon are not known. One can overcome this by measuring how the reversal potential (Eq. 9.57) changes as outside concentrations are varied. Obtain an equation for the shift of reversal potential if two measurements are made: one in which the concentration  $C_{a1} = 0$ , the other with  $C_{b1} = 0$ .

### Section 9.7

**Problem 19** A patch-clamp experiment shows that the conductance of a single  $Ca^{2+}$  channel is  $G = 25$  pS. The membrane thickness is  $b = 6$  nm. Use  $v = 50$  mV.

(a) Assuming that the resistivity of the fluid in the channel is  $\rho = 0.5 \Omega m$ , find an expression and numerical value for the channel radius  $a$ .

(b) If the conductance per unit area is  $1,200 S m^{-2}$ , find the number of pores per unit area.

(c) The current is  $i = Gv$ , where  $v$  is the applied voltage. Find an expression for  $n$ , the number of calcium ions per second passing through the channel, in terms of whichever of parameters  $G$ ,  $v$ ,  $b$ , and  $a$  are necessary.

(d) How many calcium ions are in the channel at one time, if the calcium concentration is  $C$  mmol  $l^{-1}$ ?

**Problem 20** A potassium channel might have a radius of 0.2 nm and a length of 6 nm. If it contained potassium at a concentration of 150 mmol  $l^{-1}$ , how many potassium ions on average would be in the channel?

**Problem 21** How long does it take for a sodium ion to drift in the electric field (assumed constant) through a membrane of thickness  $L$  and applied potential  $v$ ? How long does it take to move by pure diffusion? Find numerical values when the membrane is 6 nm thick and potential difference is 70 mV.

**Problem 22** Suppose that a sodium pore when open passes 10 pA and  $j_{Na} = 0.2 A m^{-2}$ . Calculate the number of open pores per unit area and the average linear spacing between them.

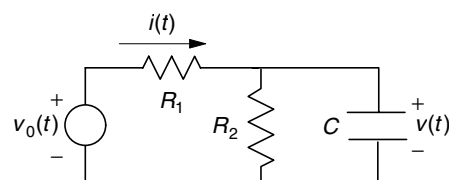
**Problem 23** Calculate the current density of sodium ions in a region of length 6 nm due to (a) pure diffusion when there is no potential difference and the concentrations are 145 and 15 mmol  $l^{-1}$ , (b) pure drift when the concentration is 145 mmol  $l^{-1}$  and the potential difference is 70 mV, and (c) both diffusion and drift if the electric field is constant.

**Problem 24** Patch-clamp recording is done with a micropipette of radius 1  $\mu m$ .

(a) If the pipette encircles a single channel with conductance 20 pS, what is the channel current when the channel is open and the voltage across the membrane is 20 mV away from the Nernst potential for the ion in question? Make a simple estimate using Ohm’s law.

(b) Assuming a capacitance of 0.01 F  $m^{-2}$ , what current charges the capacitance of the membrane patch under the micropipette if a 20-mV change occurs linearly in 5  $\mu s$ ?

**Problem 25** The following circuit illustrates the effects that must be considered when an electrode is used to measure the properties of a patch of membrane.  $R_1$  is the resistance of the electrode.  $R_2$  and  $C$  are properties of the membrane. The applied voltage  $v_0(t)$  is a step at  $t = 0$ . The electrode current is  $i(t)$ . The voltage across the membrane patch is  $v(t)$ .



(a) Show that

$$v_0(t) = R_1 C \frac{dv}{dt} + \frac{R_1 + R_2}{R_2} v(t).$$

(b) Show that the time constant is  $\tau = R_1 R_2 C / (R_1 + R_2)$  and that  $\tau \rightarrow R_1 C$  if  $R_1 \ll R_2$ ,  $\tau \rightarrow R_2 C$  if  $R_1 \gg R_2$ .

(c) If  $v_0(t)$  is a step of height  $v_0$  at  $t = 0$ , show that

$$v(t) = v_0 \frac{R_2}{R_1 + R_2} \left(1 - e^{-t/\tau}\right)$$

and

$$i(t) = \frac{v_0}{R_1 + R_2} \left(1 + \frac{R_2}{R_1} e^{-t/\tau}\right).$$

(d) Plot  $v(t)$  and  $i(t)$ .

(e) The case  $R_1 \ll R_2$  is called voltage-clamped. Find expressions for  $v(t)$  and  $i(t)$  in that case and plot them. Where does the transient current flow? For fixed  $R_2$ , what is the time constant?

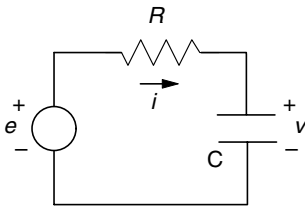
(f) In the current-clamped case,  $R_1 \gg R_2$  and  $i_0 = v_0/R_1$ . Find expressions for  $v(t)$  and  $i(t)$  and plot them. For fixed  $R_2$ , what is the time constant?

(g) Make numerical plots of  $v(t)$  and  $i(t)$  when  $v_0 = 150$  mV,  $R_1 = 10^6 \Omega$ ,  $C = 5$  pF, and  $R_2 = 10^{11} \Omega$ .

**Problem 26** A patch-clamp experiment is done with a micropipette having a resistance of  $10^6 \Omega$ . When 150 mV is applied across the membrane, the current is 0 when the pores are closed and 1 pA when one channel is open. The membrane capacitance is  $4 \times 10^{-3} \text{ F m}^{-2}$ . The microelectrode tip has an inner radius of 20  $\mu\text{m}$ . What is the time constant for voltage changes? Does it depend on whether the channel has opened or closed?

### Section 9.8

**Problem 27** Weaver and Astumian (1990) derived Eq. 9.63a for the thermal noise of the transmembrane potential using a different method than in Sec. 9.8. A resistor has a voltage noise spectral density,  $\sigma_e^2(f)$  (in units of  $\text{V}^2 \text{ Hz}^{-1}$ ), such that  $\sigma_e^2(f) = 4k_BTR$ , where  $f$  is the frequency. It corresponds to voltage  $e$  in the figure. Weaver and Astumian represented the membrane as a parallel combination of resistance  $R$  and capacitance  $C$ . The voltage across the capacitor,  $v$ , is the transmembrane potential.



(a) For a particular frequency  $f$ , derive a relationship between the spectral density of the voltage fluctuations of the transmembrane potential,  $\sigma_v^2(f)$ , and  $\sigma_e^2(f)$ . (Hint: Derive an equation governing the voltage in an RC circuit, and then solve it using the methods described in Appendix F.)

(b) Integrate  $\sigma_v^2(f)$  over all frequencies to get the voltage fluctuations  $\sigma_v^2$ .

(c) Estimate  $\sqrt{\sigma_v^2}$  for a spherical cell of radius 10 mm, having a membrane capacitance per unit area of  $0.01 \text{ F m}^{-2}$ .

### Section 9.9

**Problem 28** In some nerve membranes a region of “negative resistance” is found, in which the current decreases as the voltage is increased.

(a) Where have we seen this behavior before?

(b) To see why it happens, consider two cases. The current through the membrane is given by  $j = g(v)(v - v_0)$ , where  $g(v)$  is a property of the membrane, and the Nernst potential  $v_0$  depends on the ion concentration on either side of the membrane. For this problem let  $v_0 = +50$  mV. Calculate  $j$  as a function of  $v$  for two cases: (a)  $g(v) = 1$ ; (b) the conductance increases rapidly with voltage:  $g(v) = (5.6 \times 10^{-7})e^{0.288v}$  ( $v$  in mV).

(c) Negative resistance increases the sensitivity of the ampullae of Lorenzini, as measured by Lu and Fishman. To see why, calculate the output voltage in a two-resistance voltage divider network (as in Fig. 6.23) and discuss what happens if  $R_2$  is negative.

### Section 9.10

**Problem 29** Estimate the transmembrane potential that corresponds to the threshold for electroporation. Compare it to the normal cell resting potential.

**Problem 30** Here is one way that signal-to-noise ratio can be improved. Suppose that there are  $N$  receptors, connected in the nervous system in such a way that an output response requires a logical AND between all  $N$  receptors. Whether or not there is a response is sampled every  $T$  seconds. If the signal exists, all  $N$  receptors respond. If the signal does not exist, each receptor responds to thermal noise with a probability  $p$  (which might be  $p = e^{-U/k_B T}$ , where  $U$  is an activation energy). Assume that  $p$  is the same for each receptor, and that whether a receptor has responded to thermal noise is independent of the response of all other receptors and also independent of its response at any other time.

(a) What is the signal-to-noise ( $S/N$ ) ratio as a function of  $N$ ? Suppose that  $N = 8$ . Plot  $S/N$  as a function of  $p$ .

(b) Find  $U/k_B T$  vs  $N$  for  $S/N = 4$ .

**Problem 31** Here is another way to look at the signal-to-noise ratio.

(a) Show that the energy of a charged parallel-plate capacitor can be written as  $\kappa\epsilon_0 E^2 V/2$ , where  $V = Sd$  is the volume between the plates. This is a special case of a general relationship that the energy per unit volume associated with an electric field is  $\kappa\epsilon_0 E^2/2$ .

(b) Use the information about the magnitude of the electric field in the cell membrane from Fig. 9.19 to calculate the total electrostatic energy in the membrane.

(c) Compare the ratio of the total electrostatic energy to  $k_B T$  when the air field is  $300 \text{ V m}^{-1}$ . This overestimates the ratio, because the energy is spread over the entire membrane and is not available to interact in one place.

**Problem 32** Obtain Eq. 9.79 from the expression  $U = -mB \cos \theta$  that was derived in Problem 8.29, by making a suitable expansion for small angles.

**Problem 33** Electric fields in the body caused by exposure to power lines are produced by two mechanisms: direct coupling to the power line electric field, and Faraday induction from the power line magnetic field. Consider a high-voltage power line that produces an electric field of 10 kV/m and a magnetic field of 50 mT [Barnes, (1995)]. Estimate the electric field induced in the human body by these two mechanisms. Which is larger? Compare the strength of these powerline-induced electric fields to the strength of naturally occurring electric field produced in the body by the heart (estimate the strength of this endogenous field using the data in Fig. 7.23).

**Problem 34** Derive the equations for the electric field shown in Fig. 9.19. Use the following method. Let the potentials be  $v_{\text{outside}} = A \cos \theta / r^2 - E_1 r \cos \theta$  and  $v_{\text{intracellular}} = Br \cos \theta$ , where  $A$  and  $B$  are unknown constants. At the cell surface, the following boundary condition applies when the cell membrane is thin and obeys Ohm's law:

$$\begin{aligned} \sigma_{\text{outside}} \left( \frac{\partial v_{\text{outside}}}{\partial r} \right) \Big|_{r=a} &= \sigma_{\text{intracellular}} \left( \frac{\partial v_{\text{intracellular}}}{\partial r} \right) \Big|_{r=a} \\ &= (v_{\text{outside}} - v_{\text{intracellular}}) \frac{\sigma_{\text{membrane}}}{b} \Big|_{r=a} \end{aligned}$$

(a) Verify that the expressions for  $v_{\text{outside}}$  and  $v_{\text{intracellular}}$  obey Laplace's equation and behave properly at  $r = 0$  and  $r = \infty$ .

(b) Use the boundary condition to determine  $A$  and  $B$ .

(c) Use your expressions for the potential to determine the electric fields given in Fig. 9.19.

## References

- Abramowitz, M., and I. A. Stegun (1972). *Handbook of Mathematical Functions with Formulas, Graphs, and Mathematical Tables*. Washington, U. S. Government Printing Office.
- Adair, R. (1991). Constraints on biological effects of weak extremely-low-frequency electromagnetic fields. *Phys. Rev. A* **43**: 1039–1048.
- Adair, R. (1992). Reply to "Comment on 'Constraints on biological effects of weak extremely-low-frequency electromagnetic fields.'" *Phys. Rev. A* **46**: 2185–2187.
- Adair, R. (1993). Effects of ELF magnetic fields on biological magnetite. *Bioelectromagnetics* **14**: 1–4.
- Adair, R. (1994). Constraints of thermal noise on the effects of weak 60-Hz magnetic fields acting on biological magnetite. *Proc. Nat. Acad. Sci. USA* **91**: 2925–2929.
- Adair, R. K. (2000). Static and low-frequency magnetic field effects: Health risks and therapies. *Rep. Prog. Phys.* **63**: 415–454.
- Adair, R. K., R. D. Astumian, and J. C. Weaver (1998). Detection of weak electric fields by sharks, rays and skates. *Chaos* **8**: 576–587.
- Astumian, R. D., J. C. Weaver, and R. K. Adair (1995). Rectification and signal averaging of weak electric fields by biological cells. *Proc. Nat. Acad. Sci. USA* **92**: 3740–3743.
- Barnes, F. S. (1995). Typical electric and magnetic field exposures at power-line frequencies and their coupling to biological systems. In M. Blank, ed. *Electromagnetic Fields: Biological Interactions and Mechanisms*. Washington, American Chemical Society, pp. 37–55.
- Bastian, J. (1994). Electrosensory organisms. *Physics Today* **47**(2): 30–37.
- Bockris, J. O'M., and A. K. N. Reddy (1970). *Modern Electrochemistry*. New York, Plenum, Vol. 1.
- Bren, S. P. A. (1995). 60 Hz EMF health effects—a scientific uncertainty. *IEEE Eng. Med. Biol.* **14**: 370–374.
- Carstensen, E. L. (1995). Magnetic fields and cancer. *IEEE Eng. Med. Biol.* **14**: 362–369.
- Chandler, W. K., A. L. Hodgkin, and H. Meves (1965). The effect of changing the internal solution on sodium inactivation and related phenomena in giant axons. *J. Physiol.* **180**: 821–836.
- Crouzy, S. C., and F. J. Sigworth (1993). Fluctuations in ion channel gating currents: Analysis of nonstationary shot noise. *Biophys. J.* **64**: 68–76.
- DeFelice, L. J. (1981). *Introduction to Membrane Noise*. New York, Plenum.
- Denk, W., and W. W. Webb (1989). Thermal-noise-limited transduction observed in mechanosensory receptors of the inner ear. *Phys. Rev. Lett.* **63**(2): 207–210.
- Doyle, D. A., J. M. Cabral, R. A. Pfuetzner, A. Kuo, J. M. Gulbis, S. L. Cohen, B. T. Chait, and R. MacKinnon (1998). The structure of the potassium channel: Molecular basis of K<sup>+</sup> conduction and selectivity. *Science* **280**: 69–77.
- Foster, K. R. (1996). Electromagnetic field effects and mechanisms: In search of an anchor. *IEEE Eng. Med. Biol.* **15**(4): 50–56.
- Foster, K. R., and H. P. Schwan (1996). Dielectric properties of tissues. In C. Polk and E. Postow, eds. *Handbook of Biological Effects of Electromagnetic Fields*. Boca Raton, FL, CRC Press, pp. 25–102.
- Hafemeister, D. (1996). Resource Letter BELFEF-1: Biological effects of low-frequency electromagnetic fields. *Am. J. Phys.* **64**: 974–981.
- Hamill, O. P., A. Marty, E. Neher, B. Sakmann, and F. J. Sigworth (1981). Improved patch-clamp techniques for high-resolution current recording from cells and cell-free membrane patches. *Pflügers Arch.* **391**: 85–100.
- Hille, B. (2001). *Ion Channels of Excitable Membranes*, 3rd ed. Sunderland, MA, Sinauer Associates.

- Honig, B., and A. Nicholls (1995). Classical electrostatics in biology and chemistry. *Science* **268**: 1144–1149.
- Jiang, Y., A. Le, J. Chen, V. Ruta, M. Cadene, B. T. Chait, and R. MacKinnon (2003). X-ray structure of a voltage-dependent K<sup>+</sup> channel. *Nature* **423**: 33–41.
- Kalmijn, Ad. J. (1988). Detection of weak electric fields. In J. Aetma, *et al.*, eds. *Sensory Biology of Aquatic Animals*. New York, Springer, pp. 151–186.
- Keynes, R. D. (1994). The kinetics of voltage-gated ion channels. *Quart. Rev. Biophys.* **27**(4): 339–434.
- Kirschvink, J. L. (1992). Comment on “Constraints on biological effects of weak extremely-low-frequency electromagnetic fields.” *Phys. Rev. A* **46**: 2178–2184.
- Kirschvink, J. L., A. Kobayashi-Kirschvink and B. J. Woodford (1992a). Magnetite biomineralization in the human brain. *Proc. Natl. Acad. Sci. USA* **89**: 7683–7687.
- Kobayashi, A. K., J. L. Kirschvink, and M. H. Nesson (1995). Ferromagnetism and EMFs. *Nature* **374**: 123.
- Lamb, H. (1932) *Hydrodynamics*. Cambridge, Cambridge University Press.
- Leuchtag, H. R., and C. J. Swihart (1977). Steady-state electrodiffusion. Scaling, exact solutions for ions of one charge, and the phase plane. *Biophys. J.* **17**: 27–46.
- Lewis, C. A. (1979). Ion-concentration dependence of the reversal potential and the single channel conductance of ion channels at the frog neuromuscular junction. *J. Physiol.* **286**: 417–445.
- Lu, J., and H. M. Fishman (1994). Interaction of apical and basal membrane ion channels underlies electroreception in ampullary epithelia of skates. *Biophys. J.* **67**: 1525–1533.
- Mauro, A. (1962). Space charge regions in fixed charge membranes and the associated property of capacitance. *Biophys. J.* **2**: 179–198.
- Moulder, J. E. (Web). *Power Lines and Cancer: Frequently Asked Questions*, [www.mcw.edu/gcrc/cop/powerlines-cancer-FAQ/toc.html](http://www.mcw.edu/gcrc/cop/powerlines-cancer-FAQ/toc.html).
- Moulder, J. E., and K. R. Foster (1995). Biological effects of power-frequency fields as they relate to carcinogenesis. *Proc. Soc. Expt. Biol. Med.* **209**: 309–323.
- Moulder, J. E., and K. R. Foster (1999). Is there a link between power-frequency electric fields and cancer? *IEEE Engineering in Medicine and Biology* **18**(2): 109–116.
- Moy, G., B. Corry, S. Kuyucak, and S-H. Chung (2000). Tests of continuum theories as models of ion channels. I. Poisson-Boltzmann theory versus Brownian dynamics. *Biophys. J.* **78**: 2349–2362.
- National Research Council (1997). Committee on the Possible Effects of Electromagnetic fields on Biologic Systems. *Possible Health Effects of Exposure to Residential Electric and Magnetic Fields*. Washington, National Academy Press.
- Neher, E., and B. Sakmann (1976). Single-channel currents recorded from membrane of denervated frog muscle fibers. *Nature* **260**: 799–802.
- Nichols, C. G., E. N. Makhina, W. L. Pearson, Q. Sha, A. N. Lopatin (1996). Inward rectification and implications for cardiac excitability. *Circulation Research* **78**: 1–7.
- Pickard, W. F. (1988). A model for the acute electrosensitivity of cartilaginous fishes. *IEEE Trans. Biomed. Eng.* **35**(4): 243–249.
- Polk, C. (1994). Effects of extremely-low-frequency magnetic fields on biological magnetite. *Bioelectromagnetics* **15**: 261–270.
- Polk, C. (1995). Bioelectromagnetic dosimetry. In M. Blank, ed. *Electromagnetic Fields: Biological Interactions and Mechanisms*. Washington, American Chemical Society, pp. 57–78.
- Polk, C. (1996). Introduction. In C. Polk and E. Postow, eds. *Handbook of Biological Effects of Electromagnetic Fields*. Boca Raton, FL, CRC Press, pp. 1–23.
- Shapiro, E. M., A. Borthakur, A. Gougoutas, and R. Reddy (2002). <sup>23</sup>Na MRI accurately measures fixed charge density in articular cartilage. *Mag. Res. Med.* **47**: 284–291.
- Sigworth, F. J. (1993). Voltage gating of ion channels. *Quart. Rev. Biophys.* **27**(1): 1–40.
- Tenforde, T. S. (1995). Spectrum and intensity of environmental electromagnetic fields from natural and man-made sources. In M. Blank, ed. *Electromagnetic Fields: Biological Interactions and Mechanisms*. Washington, American Chemical Society, pp. 13–35.
- Tucker, R. D., and O. H. Schmitt (1978). Tests for human perception of 60 Hz moderate strength magnetic fields. *IEEE Trans. Biomed. Eng.* **25**: 509–518.
- Uehara, M., K. K. Sakane, H. S. Maciel, and W. I. Urruchi (2000). Physics and biology: Bio-plasma physics. *Amer. J. Phys.* **68**: 450–455.
- Weaver, J. C. (2000). Electroporation of cells and tissues. *IEEE Trans. Plasma Sci.* **28**: 24–33.
- Weaver, J. C., and R. D. Astumian (1990). The response of living cells to very weak electric fields: The thermal noise limit. *Science* **247**: 459–462.
- Weaver, J. C., and R. D. Astumian (1995). Issues relating to causality of bioelectromagnetic fields. In M. Blank, ed. *Electromagnetic Fields: Biological Interactions and Mechanisms*. Washington, American Chemical Society, pp. 79–96.

# 10

## Feedback and Control

We now turn to the way in which the body regulates such things as temperature, oxygen concentration in the blood, cardiac output, number of red or white blood cells, and blood concentrations of substances like calcium, sodium, potassium and glucose. Each of these is regulated by a feedback loop. A *feedback loop* exists if variable  $x$  determines the value of variable  $y$ , and variable  $y$  in turn determines the value of variable  $x$ .

Suppose that  $x$  is the deviation of a bullet from its desired path. A bullet has no feedback; after it has left the gun, its deviation from the desired path is determined by the initial aim of the gun, fall due to gravity, drift caused by the wind, and air turbulence. An accuracy of one part in  $10^4$  (about a tenth of an inch in 50 ft) is quite good. A car, on the other hand, is steered by the driver. If deviation from the center of the lane  $x$  becomes appreciable, the driver changes  $y$ , the position of the steering wheel. The value of  $y$  determines  $x$  through the steering mechanism and the tires. It is possible to have a car deviate less than 1 ft from the desired position within a lane after driving 3,000 miles, an accuracy of one part in  $10^7$ . This is an example of *negative feedback*. If  $x$  gets too large, the factors in the feedback loop tend to reduce it.

Negative-feedback systems can generate oscillations of their variables. We see oscillations in physiological systems on many different time scales, from the rhythmic activity of the heart, to changes in the rate of breathing, to daily variations in body temperature, blood pressure, and hormone levels, to monthly variations such as the menstrual cycle, to annual variations such as hibernation, coloring, fur growth, and reproduction.

It is also possible to have *positive feedback*. Two bickering children can goad each other to new heights of anger. Positive feedback initiates the action potential described in Chapter 6: depolarization of the axon leads to increased sodium permeability, which further speeds depolarization. Blood pressure is regulated in part by sen-

sors in the kidney. A patient with high blood pressure may suffer damage to the blood vessels, including those feeding the kidneys, which reduces the blood pressure at the sensors. The sensors then ask for still higher blood pressure, which accelerates the damage, which leads to still higher blood pressure, and so on.

The simplest feedback loop consists of two processes: one in which  $y$  depends on  $x$  and another in which  $x$  depends on  $y$ . The loop can have many more variables. Steering the car, in addition to the variables of lane position and steering wheel position, involves vision, neuromuscular processes, all of the variables in the automobile's steering mechanism, and the Newtonian mechanics of the car's motion—with external variables such as the behavior of other drivers continually bombarding the system.

Sections 10.1–10.3 deal with the relationships between the feedback variables when the system is in *equilibrium* or in the *steady state*, and none of the variables are changing with time. The techniques for determining the operating point—the steady-state values of the variables—are graphical and can be applied to any system if the relationship among the variables is known.

When the system is not at equilibrium, it returns to the equilibrium point if the system is stable. Although the equations describing this return to equilibrium are usually not linear, Secs. 10.4–10.6 discuss how linear systems behave when they are not at the operating point. A linear system may “decay” exponentially to the steady-state values, or it may exhibit oscillations.

Most systems are not linear. Section 10.7 discusses systems described by nonlinear equations in one or two dimensions, introducing some of the vocabulary and graphical techniques of nonlinear systems analysis. It closes with an example of resetting the phase of a biological oscillator. Section 10.8 introduces the ideas of *period doubling* and *chaotic behavior* through difference equations and

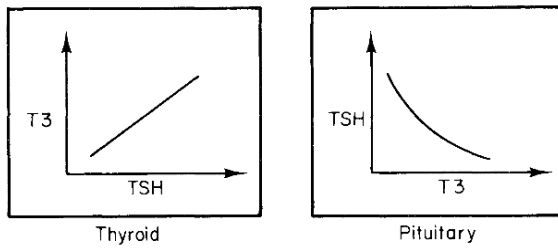


FIGURE 10.1. Schematic curves of the relationship between thyroid hormone (T3) and thyroid stimulating hormone (TSH) in the thyroid gland and in the pituitary.

the *logistic map*. It then describes a *linear map* that appears to be chaotic but is not. Section 10.9 shows how a linear differential equation that depends on a fixed delay in the variable can exhibit either damped or continuous oscillations. Section 10.10 summarizes the earlier sections, and Sec. 10.11 gives several biological examples.

A great deal of work was done on modeling physiological feedback systems between 1950 and 1975. Books from that era include Riggs (1970) and Stark (1968). A contemporary book that describes physiological models in detail, including computer modeling, is Khoo (2000).

## 10.1 Steady-State Relationships Among Variables

Any feedback loop can be broken down, conceptually at least, into separate processes that relate a dependent variable to an independent variable and possibly to some other parameters. Figure 10.1 shows an example. In the first process the thyroid gland, in response to thyroid-stimulating hormone (TSH) from the pituitary, produces the thyroid hormones thyroxine (T4) and triiodothyronine (T3). An increase of TSH increases production of T3 and T4. These processes depend on other parameters, such as the amount of iodine available in the body to incorporate into the T3 and T4. In the second process, the pituitary increases the production of TSH if the concentration of T3 in the blood falls. It may also respond to T4 and other variables as well. (This is an oversimplification. The pituitary actually responds to hormones secreted by the hypothalamus. The hypothalamus is responding to the levels of T3 and T4.)

For a quantitative example, consider a simple model relating the amount of carbon dioxide in the alveoli (air sacs of the lung) and the rate of breathing (ventilation rate). If the body is producing  $\text{CO}_2$  at a constant rate, a given ventilation rate corresponds to a definite value of  $P_{\text{CO}_2}$ , the partial pressure of carbon dioxide in the alveoli. In the steady state the amount of  $\text{CO}_2$  exhaled (the volume of gas leaving the lungs per minute times  $P_{\text{CO}_2}$ ) is just equal to the amount produced in the body.

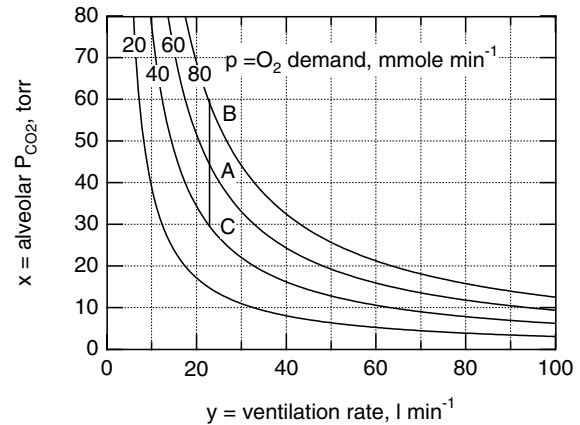


FIGURE 10.2. The pressure of  $\text{CO}_2$  in the alveoli of the lungs decreases as the ventilation rate is increased. The different curves correspond to different total metabolic rates.

Figure 10.2 shows this relationship when the pH and  $P_{\text{O}_2}$  of the blood are fixed. As ventilation rate rises,  $P_{\text{CO}_2}$  falls. We are ignoring several other feedback loops [Riggs (1970, pp. 401–418)]. If the metabolic rate rises,  $P_{\text{CO}_2}$  also rises. Experiments show that ventilation rate  $y$  and alveolar  $P_{\text{CO}_2}$  (which we will call  $x$ ) are related by (Riggs, op. cit.)

$$x = \frac{15.47p}{y - 2.07}. \quad (10.1)$$

In these equations  $y$  (the independent variable) is measured in  $\text{l min}^{-1}$ ,  $x$  (the dependent variable) is in torr, and parameter  $p$  is the body's oxygen consumption in  $\text{mmol min}^{-1}$ . A typical resting person requires  $p = 15 \text{ mmol min}^{-1}$ .

Equation 10.1 can be derived using a simple model for respiration. Let the metabolic rate of the body be described by  $o$ , the rate of oxygen consumption in  $\text{mol s}^{-1}$ . The respiratory quotient  $F$  relates  $o$  to the rate of  $\text{CO}_2$  production, so

$$\text{Rate of } \text{CO}_2 \text{ production} = Fo. \quad (10.2)$$

A typical value of  $F$  is 0.8.

Carbon dioxide is removed from the body by breathing. If the rate at which air flows through the alveoli is  $(dV/dt)_{\text{alveoli}}$  in  $\text{m}^3 \text{ s}^{-1}$ , then the rate of removal is obtained from the ideal-gas law:

$$\text{Rate of } \text{CO}_2 \text{ removal} = \frac{x(dV/dt)_{\text{alveoli}}}{RT}.$$

The rate  $(dV/dt)_{\text{alveoli}}$  is less than the ventilation rate  $y$  because air in the trachea and bronchi does not exchange

<sup>1</sup>Strictly speaking,  $(dV/dt)_{\text{alveoli}}$  is not the derivative of a function  $V$ . (It always has a positive value, and the lungs are not expanding without limit!) We use the notation to remind ourselves that it is the rate of air exchange in the alveoli.

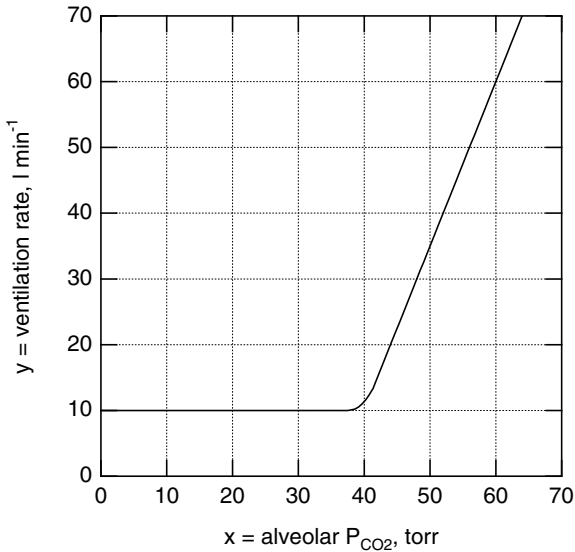


FIGURE 10.3. When  $P_{CO_2}$  in the blood rises above 40 torr, the breathing rate increases.

oxygen or carbon dioxide with the blood:  $(dV/dt)_{alveoli} = y - b$ . Therefore

$$\text{Rate of } CO_2 \text{ removal} = \frac{x(y - b)}{RT}. \quad (10.3)$$

In equilibrium the rate of production is equal to the rate of removal, so

$$F_o = \frac{x(y - b)}{RT}$$

or

$$x = \frac{RTF_o}{y - b}. \quad (10.4)$$

With the proper conversion of units from  $p$  to  $o$ , this is Eq. 10.1.

If the metabolic rate were to change without a change in breathing rate,  $x = P_{CO_2}$  would change drastically. Suppose that someone exercises moderately so that  $p = 60\ mmol\ min^{-1}$ ,  $y = 23\ l\ min^{-1}$ , and  $x = 44\ torr$  (point A in Fig. 10.2). If ventilation rate  $y$  remained constant while  $p$  rose to  $80\ mmol\ min^{-1}$ ,  $x = P_{CO_2}$  would soar to about 60; if  $p$  fell to 40,  $x$  would drop to 30. Feedback ensures that this does not happen. One of the feedback mechanisms consists of an area of the brain stem that senses the value of  $x = P_{CO_2}$  and causes  $y$  to change. Figure 10.3 shows a typical curve for a 70-kg male [Patton (1989, p. 1034)]. (The concentration of  $CO_2$  in blood is nearly the same as in the alveoli.)

## 10.2 Determining the Operating Point

We now have two processes relating the steady-state values of  $x$  and  $y$ . For alveolar gas exchange, we know  $x$  as a function of  $y$ :  $x = g(y, p)$ . For the regulatory mechanism, we know  $y = f(x)$ . Together, these constitute a

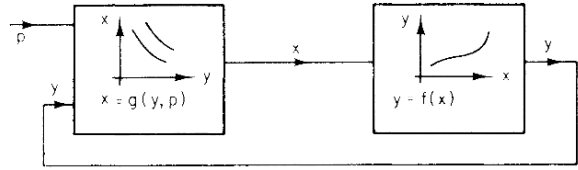


FIGURE 10.4. A general feedback loop. Either box may involve some parameters.

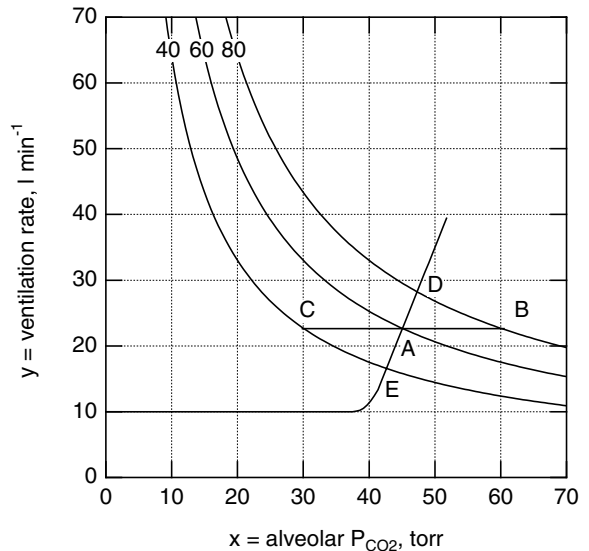


FIGURE 10.5. Regulation of the breathing rate. A change of metabolic rate (parameter  $p$ ) causes a change in ventilation rate  $y$ , so that  $x = P_{CO_2}$  does not change as much.

feedback loop, Fig. 10.4. To find the *operating point*, these two equations must be solved simultaneously. The easiest way to do this is to plot them on the same graph as in Fig. 10.5. When  $p = 60\ mmol\ min^{-1}$ , the operating point is at A. In a plot like this the horizontal axis represents the independent variable for one process and the dependent variable for the other.

If the feedback loop includes several variables, for example

$$x = f(w), \quad y = g(x), \quad z = h(y), \quad w = i(z),$$

we can combine three of these equations to get  $x = F(y)$  and plot it with  $y = g(x)$ .

## 10.3 Regulation of a Variable and Open-Loop Gain

We can also see from Fig. 10.5 how feedback causes  $y$  to change in response to a change in parameter  $p$  to reduce the change in  $x$ . If  $y$  does not change, a change of  $p$  from 60 to 80 causes the operating point to go from A to B.

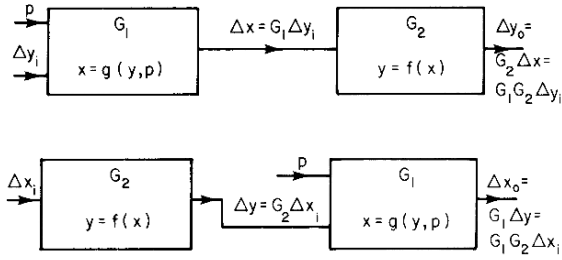


FIGURE 10.6. The open loop gain is calculated by opening the loop at any point. (a) Loop opened in  $y$ . (b) Loop opened in  $x$ .

In fact,  $y$  increases so that the new operating point is at  $D$ . The feedback loop is said to regulate the value of  $x$ .

The *gain* of a box is the ratio of the change in the output variable to the change in the input variable. For the first box in Fig. 10.4,

$$G_1 = \left( \frac{\Delta x}{\Delta y} \right)_{\text{box } g, p \text{ fixed}} = \left( \frac{\partial x}{\partial y} \right)_{\text{box } g, p \text{ fixed}} = \left( \frac{\partial g}{\partial y} \right)_p. \quad (10.5)$$

For the second box,

$$G_2 = \left( \frac{\Delta y}{\Delta x} \right)_{\text{box } f} = \left( \frac{\partial y}{\partial x} \right)_{\text{box } f} = \frac{\partial f}{\partial x}. \quad (10.6)$$

The product  $G_1G_2$  is called the *open-loop gain* (OLG). Its name comes from the fact that if the feedback loop is opened at any point and a small change is made in the input variable at the opening, the change in the output variable is the open-loop gain times the change in the input variable:

$$\text{OLG} = G_1G_2 = \left( \frac{\partial x}{\partial y} \right)_{\text{box } g} \left( \frac{\partial y}{\partial x} \right)_{\text{box } f} = \frac{\partial g}{\partial y} \frac{\partial f}{\partial x}. \quad (10.7)$$

The open-loop gain can be calculated by taking the derivatives in either order, which corresponds to breaking the loop after either box (Fig. 10.6).

If the relationships between the derivatives have been plotted as in Fig. 10.5, it may be easiest to evaluate the derivatives graphically. In that case, it is easiest to work with  $\partial y/\partial x$  for box  $g$ . But  $\partial y/\partial x = 1/(\partial x/\partial y)$ . Therefore,

$$\text{OLG} = G_1G_2 = \frac{(\partial y/\partial x)_{\text{box } f}}{(\partial y/\partial x)_{\text{box } g}}. \quad (10.8)$$

It is important to calculate the gain in the direction that causality operates. Going around the loop the wrong way gives the reciprocal of the open-loop gain.

We can now calculate how much feedback reduces the change in  $x$ , compared to the case in which there is no feedback and the value of  $y$  going into box  $g$  is held fixed. For box  $g$ , where  $x = g(y, p)$ , we can write for small

changes in  $p$  and  $y$

$$\begin{aligned} \Delta x &= \left( \frac{\partial x}{\partial p} \right)_{y, \text{ box } g} \Delta p + \left( \frac{\partial x}{\partial y} \right)_{p, \text{ box } g} \Delta y \\ &= \left( \frac{\partial x}{\partial p} \right)_{y, \text{ box } g} \Delta p + G_1 \Delta y. \end{aligned} \quad (10.9)$$

When there is no feedback,  $\Delta y$  is zero and

$$\Delta x = \left( \frac{\partial x}{\partial p} \right)_{y, \text{ box } g} \Delta p.$$

When there is feedback, there is a value of  $\Delta y$  to be included. If the change in  $x$  with feedback is  $\Delta x'$ , the change in  $y$  can be calculated from the second box:

$$\Delta y = \left( \frac{\partial f}{\partial x} \right) \Delta x' = G_2 \Delta x'. \quad (10.10)$$

This can be combined with Eq. 10.9:

$$\Delta x' = \left( \frac{\partial x}{\partial p} \right)_y \Delta p + G_1(G_2 \Delta x') = \Delta x + G_1G_2 \Delta x'$$

and solved for  $\Delta x'$ :

$$\Delta x' = \frac{\Delta x}{1 - G_1G_2} = \frac{\Delta x}{1 - \text{OLG}}. \quad (10.11)$$

The effect of feedback is to cause a change in  $y$  which reduces the change in  $x$  by the factor  $1 - \text{OLG}$ . When the feedback is negative, the open-loop gain is negative,  $1 - \text{OLG}$  is greater than one, and there is a reduction in  $\Delta x$ . If the feedback is positive and the open-loop gain is less than one,  $\Delta x'$  is larger than  $\Delta x$ .

For the respiration example, the equations for each box are

$$x = g(y, p) = \frac{15.47p}{y - 2.07}, \quad (10.12)$$

$$y = f(x) = \begin{cases} 10, & x \leq 40, \\ 10 + 2.5(x - 40), & x > 40. \end{cases}$$

The derivatives are

$$\begin{aligned} \left( \frac{\partial g}{\partial p} \right)_y &= \frac{15.47}{y - 2.07}, \\ G_1 = \left( \frac{\partial g}{\partial y} \right)_p &= -\frac{15.47p}{(y - 2.07)^2}, \\ G_2 = \left( \frac{\partial f}{\partial x} \right) &= 2.5. \end{aligned}$$

At operating point  $A$  in Fig. 10.5, the values are

$$x = 45.07, \quad p = 60, \quad y = 22.67,$$

$$\left( \frac{\partial g}{\partial p} \right)_y = 0.757, \quad (10.13)$$

$$G_1 = -2.19, \quad G_2 = 2.5, \quad \text{OLG} = -5.48.$$

If  $p$  changes from 60 to 62, then without feedback  $\Delta x = (0.757)(2) = 1.5$ . With feedback,  $\Delta x' = 1.5/(1 + 5.48) = 0.23$ .



## 10.4 Approach to Equilibrium without Feedback

The technique described in the preceding section allows us to determine the equilibrium state or operating point of a system if we can measure the functions  $f$  and  $g$ . It does not tell us how the system behaves when it is not at the equilibrium point, nor does it tell us how the system moves from one point to another when parameter  $p$  is changed. To learn that, we need an equation of motion for each process or box in the feedback loop. The equation of motion is usually a differential equation. In real systems the differential equation is often nonlinear and difficult to solve. We first consider models described by linear differential equations, and then we consider some of the behaviors of nonlinear systems.

The response of a system cannot be infinitely fast. At equilibrium the rate of exhaling carbon dioxide is the same as the rate of production throughout the body. If the rate of production rises in a certain muscle group, the extra carbon dioxide enters the blood and is distributed throughout the body, and the carbon dioxide concentrations in the blood and alveoli rise gradually.

To develop a quantitative model, assume that all the carbon dioxide in the body is stored in a single well-stirred compartment of volume  $V_c$ . This assumption of uniform concentration is certainly an oversimplification. The total number of moles is  $n$  and the concentration is  $n/V_c$ . The concentration in the blood is related to the partial pressure in the alveoli by a solubility constant  $\alpha$ :  $n/V_c = \alpha x$ . Therefore  $dn/dt = \alpha V_c dx/dt$ . Moreover,  $dn/dt$  is equal to the rate of production (Eq. 10.2) minus the rate of removal (Eq. 10.3):

$$\frac{dx}{dt} = \frac{Fo}{\alpha V_c} - \frac{x(y-b)}{\alpha V_c RT}.$$

We change the definition of  $F$  to take account of the fact that  $o$  and  $p$  are both the rate of oxygen consumption in slightly different units ( $o$  is in  $\text{mol s}^{-1}$  and  $p$  is in  $\text{mmol min}^{-1}$ ):

$$\frac{dx}{dt} = \frac{Fp}{\alpha V_c} - \frac{x(y-b)}{\alpha V_c RT}. \quad (10.14)$$

This differential equation depends on both  $x$  and  $y$  and in fact is nonlinear since the variables are multiplied together in the last term. At equilibrium  $dx/dt = 0$  and Eq. 10.14 gives Eq. 10.4.

If  $y$  is constant (a constant breathing rate, which could be accomplished by placing the subject on a respirator), then there is no feedback and Eq. 10.14 is a linear differential equation with constant coefficients:

$$\frac{dx}{dt} + \frac{y_0 - b}{\alpha V_c RT} x = \frac{Fp}{\alpha V_c}.$$

It can be solved using the techniques of Appendix F. Suppose that for  $t \leq 0$ ,  $p = p_0$ ,  $x = x_0$ , and  $y = y_0$ . For  $t > 0$

the subject exercises, so that  $p = p_0 + \Delta p$ ,  $x = x_0 + \xi$ , and  $y$  is unchanged. The equation then becomes

$$\frac{d\xi}{dt} + \frac{y_0 - b}{\alpha V_c RT} \xi = \frac{F\Delta p}{\alpha V_c}. \quad (10.15)$$

The homogeneous equation is

$$\frac{d\xi}{dt} + \frac{1}{\tau_1} \xi = 0, \quad (10.16)$$

where the time constant is

$$\tau_1 = \frac{RT\alpha V_c}{y_0 - b}. \quad (10.17)$$

The homogeneous solution is  $\xi = Ae^{-t/\tau_1}$ . The particular solution is

$$\xi = \frac{FRT}{y_0 - b} \Delta p = a \Delta p,$$

so the complete solution is  $\xi = a \Delta p + Ae^{-t/\tau_1}$ . We now use the initial condition to determine  $A$ . At  $t = 0$   $\xi = 0$ , so  $A = -a \Delta p$ . The complete solution without feedback that matches the initial condition is

$$x - x_0 = a \Delta p (1 - e^{-t/\tau_1}). \quad (10.18)$$

Figure 10.7 shows how  $x$  changes with time on a plot of  $x$  vs.  $t$  and a plot of  $y$  vs.  $x$ . The dots are spaced at equal times.

## 10.5 Approach to Equilibrium in a Feedback Loop with One Time Constant

Suppose now that  $y$  is allowed to change and that  $\eta = y - y_0$ . We can write the equation for the change in  $x$ , Eq. 10.14 as

$$\begin{aligned} \frac{d\xi}{dt} &= \frac{dx}{dt} = \frac{Fp_0}{\alpha V_c} + \frac{F\Delta p}{\alpha V_c} - \frac{(x_0 + \xi)(y_0 - b + \eta)}{\alpha V_c RT} \\ &= \underbrace{\frac{Fp_0}{\alpha V_c} - \frac{x_0(y_0 - b)}{\alpha V_c RT}}_{=0} + \frac{F\Delta p}{\alpha V_c} - \frac{\xi(y_0 - b)}{\alpha V_c RT} \\ &\quad - \frac{x_0\eta}{\alpha V_c RT} - \frac{\xi\eta}{\alpha V_c RT}. \end{aligned}$$

Multiplying all terms by  $\tau_1$  as defined in Eq. 10.17, and identifying

$$G_1 = \left( \frac{\partial g}{\partial y} \right)_p = -\frac{x_0}{y_0 - b},$$

we obtain

$$\tau_1 \frac{d\xi}{dt} = a \Delta p - \xi + G_1 \eta - \frac{\xi\eta}{y_0 - b}. \quad (10.19)$$

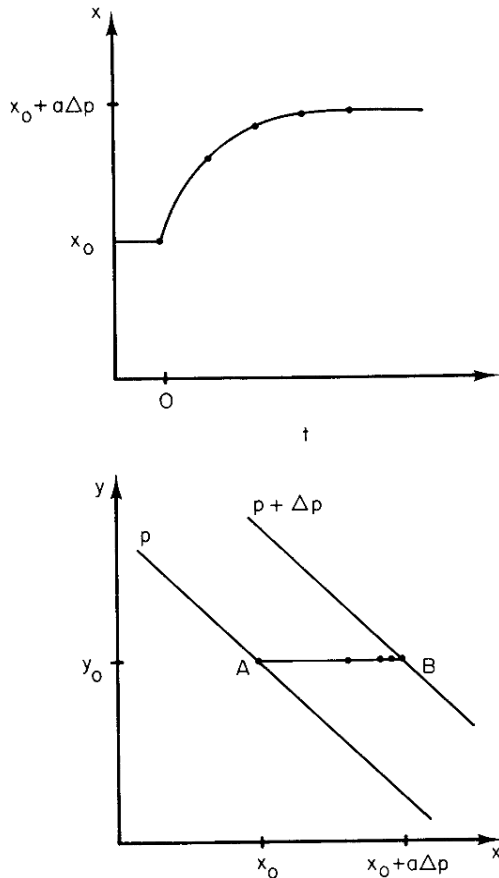


FIGURE 10.7. The change in  $x$  without feedback in response to a step change in parameter  $p$ . (a) Plot of  $x$  vs  $t$ . (b) Plot of  $y$  vs  $x$ .

The product  $\xi\eta$  in the last term makes the equation non-linear. If we assume that the last term can be neglected, we have a linear differential equation

$$\tau_1 \frac{d\xi}{dt} = a \Delta p - \xi + G_1 \eta. \quad (10.20)$$

Now assume that the response of the second box is linear and instantaneous, so that

$$\eta = G_2 \xi. \quad (10.21)$$

If this is substituted in the linearized equation, Eq. 10.20, the result is

$$\tau_1 \frac{d\xi}{dt} + (1 - G_1 G_2) \xi = a \Delta p. \quad (10.22)$$

The steady-state solution before  $t = 0$  is  $x_0 = a p_0 / (1 - G_1 G_2)$ . At  $t = 0$  the oxygen demand is changed to  $p_0 + \Delta p$ . The new steady-state (inhomogeneous) solution is  $\xi = a \Delta p / (1 - G_1 G_2)$  and the homogeneous solution is  $\xi = A e^{-t/\tau}$  where the time constant is

$$\tau = \frac{\tau_1}{1 - G_1 G_2}. \quad (10.23)$$

(You can show this by dividing each term in Eq. 10.22 by  $\tau_1$  and comparing it to the equation for exponential

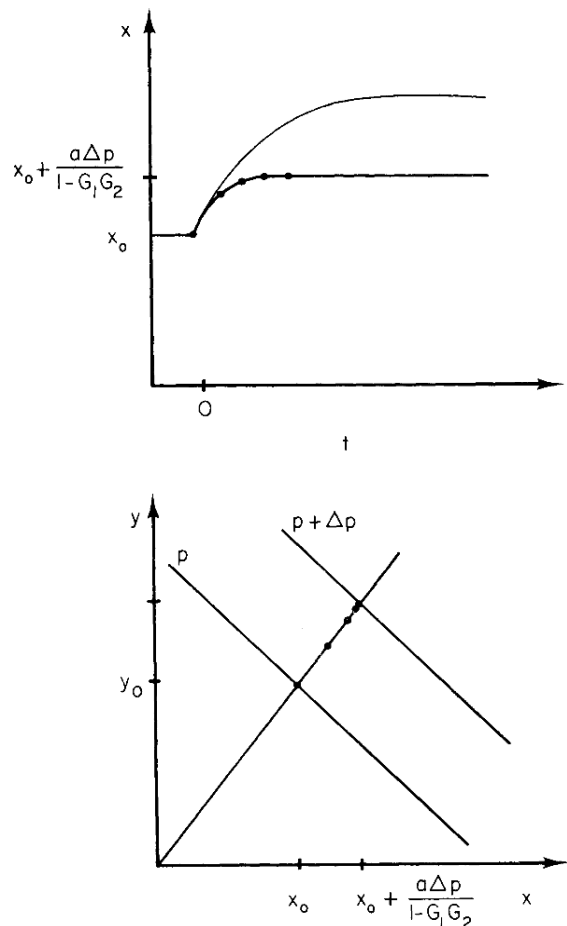


FIGURE 10.8. The change in  $x$  with feedback in response to a step change in parameter  $p$ . (a) Plot of  $x$  vs  $t$ . The change in  $x$  without feedback is shown for comparison. (b) Plot of  $y$  vs  $x$ .

decay.) After combining the homogeneous and inhomogeneous solutions and using the initial condition  $\xi(0) = 0$  to determine  $A$ , we obtain the final result:

$$\xi = x - x_0 = \frac{a \Delta p}{1 - G_1 G_2} (1 - e^{-t/\tau}). \quad (10.24)$$

This solution has the same form as Eq. 10.18. Both the total change in  $x$  and the time constant have been reduced by the factor  $1/(1 - G_1 G_2)$ . The change in  $y$  can be determined from  $\eta = G_2 \xi$ . The new solution is plotted along with the old solution in Fig. 10.8. This plot is for a system in which the open-loop gain is  $G_1 G_2 = -1.3$ . The time constant and the change in  $x$  are both reduced by  $1/2.3$ .

It is important to realize that although the feedback reduced the time constant, it has not made  $x$  change faster. The curve of  $x(t)$  with feedback has always changed less than the curve without feedback, and it has always changed more slowly. The reduction in time constant occurs because  $x$  does not change as much with feedback present, so it reaches its asymptotic value more quickly.

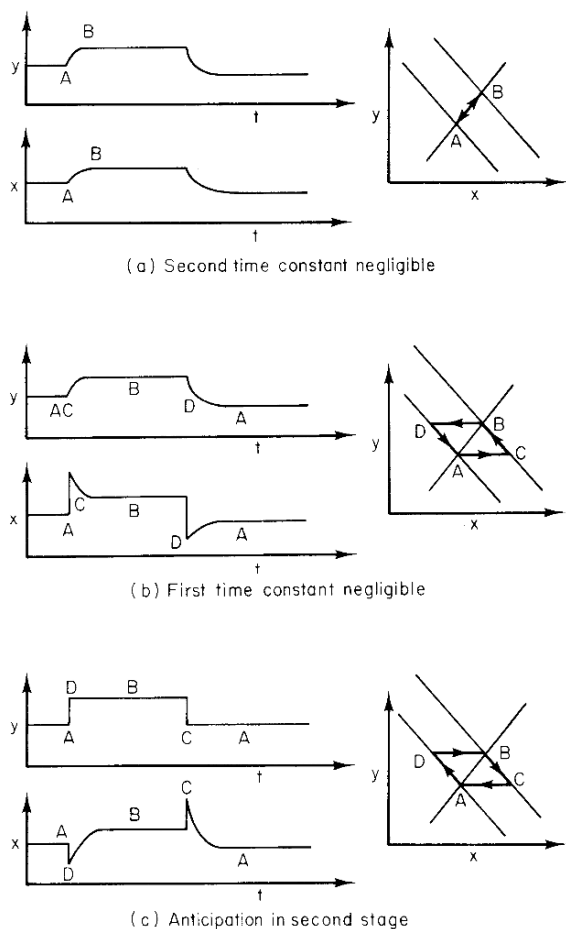


FIGURE 10.9. Changes in  $x$  and  $y$  after a step change in parameter  $p$ . (a) The second time constant is negligible compared to the first;  $x$  and  $y$  move exponentially to their new equilibrium values. (b) The first time constant is negligible; the slow change in  $y$  means that there is no feedback at first. (c) The second stage anticipates the change in  $y$  that will be required; there is too much feedback at first.

This result assumes that box  $f$  has a negligible time constant. Applied to the respiratory example, it means that the carbon dioxide-sensing system responds rapidly compared to the time it takes for carbon dioxide levels within the blood to change after a change in  $p$ . Figure 10.9(a) repeats Fig. 10.8 and shows the changes in  $x$  and  $y$  resulting from a step change in  $p$ . When the second time constant is negligible,  $y$  is always proportional to  $x$  and the system moves back and forth along line  $AB$ .

The  $\text{CO}_2$  sensors actually take a while to respond. To see what effect this might have, imagine the extreme case where the sensors are very slow compared to the change of carbon dioxide concentration in the blood. In that case, when  $p$  changes,  $y$  does not change right away. The system behaves at first as if there were no feedback, moving from point  $A$  to point  $C$  in Fig. 10.9(b). As the feedback slowly takes effect, the system moves from  $C$  to  $B$ . When the exercise ends, the system moves to point  $D$  because the

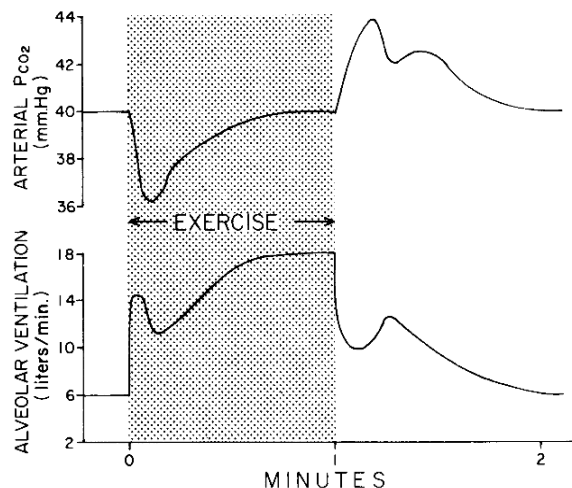


FIGURE 10.10. Change of arterial  $P_{\text{CO}_2}$  and alveolar ventilation in response to exercise. Note that  $x = P_{\text{CO}_2}$  is in the upper graph and the ventilation rate  $y$  is in the lower graph, the opposite of Fig. 10.9. Reprinted from A. C. Guyton. *Textbook of Medical Physiology*, 9th ed. p. 569, ©1995, Saunders-Elsevier, Inc. with permission of Elsevier. Data are extrapolated to humans from dogs. The dog experiments are described in C. R. Bainton (1972). *J. Appl. Physiol.* **33**: 778-787.

subject is breathing too hard. Then it finally moves from  $D$  back to  $A$ . The actual system behaves in a manner somewhere between these two extremes, as we will see in the next section.

Consider a third possibility, that a regulatory mechanism anticipates the increased metabolic demand. This might happen if we took deep breaths before we began to exercise, or if additional muscle movement signaled the respiratory control center before the carbon dioxide concentration had a chance to change. Suppose that such anticipation is the only feedback mechanism. With the initiation of exercise,  $y$  changes to its final value. The level of carbon dioxide has not yet built up, so the increased ventilation reduces  $x$  below its normal value. We can approximate this by point  $D$  in Fig. 10.9(c). As the increased activity drives  $x$  up, the system moves at constant  $y$  to point  $B$ . When the exercise stops,  $y$  drops immediately to the resting value, though carbon dioxide is still coming out of the muscles. The result is that  $x$  rises to point  $C$  before finally falling back to point  $A$ .

Figure 10.10 shows what actually happens in the control of respiration. There is a fast neurological control and a slower chemical control. The result is a combination of the processes in Figs. 10.9(a)-(c).

If we had not made the linear approximation we would not have been able to solve the equation, but the behavior would have been very similar. The nonlinear equation is obtained by substituting the equation for the second box, Eq. 10.21, in Eq. 10.19 instead of Eq. 10.20. The resulting

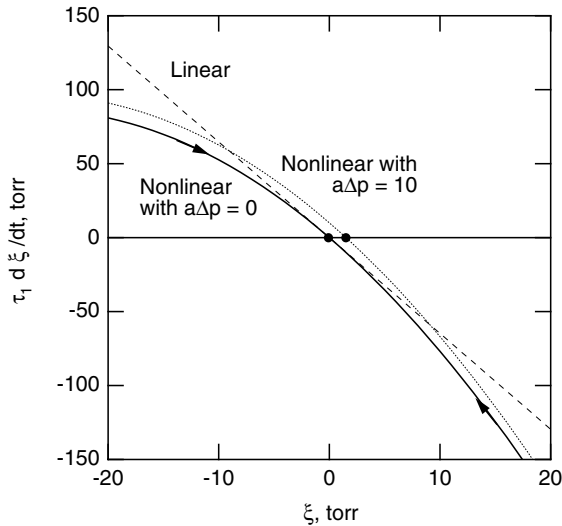


FIGURE 10.11. Plots of  $\tau_1(d\xi/dt)$  vs  $\xi$ . The straight dashed line is the linear approximation, Eq. 10.22. The parabolas are plots of the nonlinear equation, Eq. 10.25, for two different values of parameter  $a\Delta p$ . The closed circles show stable fixed points.

equation is

$$\tau_1 \frac{d\xi}{dt} = a \Delta p - (1 - G_1 G_2)\xi - \frac{G_2 \xi^2}{y_0 - b}. \quad (10.25)$$

Both this and the linear version are plotted in Fig. 10.11 for  $a \Delta p = 0$ . In each case  $d\xi/dt$  is positive when  $\xi < 0$  and negative when  $\xi > 0$ , so  $\xi$  approaches zero as time goes on. The direction of evolution of  $\xi$  is shown by the arrows on the nonlinear curve. This is often called a *one-dimensional flow*. The variable  $\xi$  “flows” to the origin, which is called a *stable fixed point* of the flow. If we change  $a \Delta p$  to 10, the curve shifts as indicated by the dotted line, and the fixed point moves to a slightly different value of  $\xi$ .

This is a particular case of a differential equation in one dependent variable of the form

$$\frac{dx}{dt} = f(x).$$

A great deal about the solution to the general equation can be learned by graphing it as we have done above. When the derivative is positive the function increases with time, and when it is negative it decreases. Figure 10.12(a) shows a more complicated function, with arrows showing the direction of the flow. The stable fixed point is indicated by a solid circle. There are two *unstable fixed points*, indicated by open circles. If  $x$  has precisely the value of an unstable fixed point, it remains there because  $dx/dt = 0$ . However, if it is displaced even a small amount, it flows away from the unstable point. Figure 10.12(b) shows just the  $x$  axis with the fixed points and the arrows. Stable fixed points are often called *attractors*

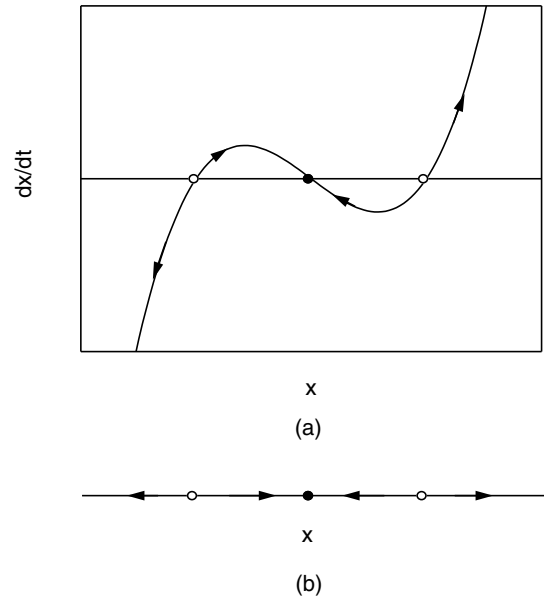


FIGURE 10.12. A more complicated flow on the line is shown. (a) Plot of  $dx/dt$  vs  $x$ . The arrows show the direction that  $x$  changes. The open circles show unstable fixed points, and the filled circle is a stable fixed point. (b) The fixed points and the direction of flow are shown on the  $x$  axis.

or *sinks*. The unstable fixed points are called *repellers* or *sources*. Chapter 2 of Strogatz (1994) has an excellent and detailed discussion of one-dimensional flows.

## 10.6 A Feedback Loop with Two Time Constants

In the preceding section we considered a feedback loop in which only one process had a significant time constant. The other process responded “instantaneously;” its time constant was much shorter. Here we consider the case in which both processes have comparable time constants. We will see that it is possible for such a (linear) system to exhibit damped sinusoidal behavior in response to an abrupt change in one of the parameters. Whether it does or not depends on the relative values of the two time constants and the open-loop gain. We consider both graphical and analytical techniques for solving this problem.

In earlier sections we discussed control of breathing. Equation 10.20 was the linear model for the departure of one variable from equilibrium:

$$\tau_1 \frac{d\xi}{dt} = -\xi + G_1 \eta + a \Delta p.$$

For the second process, instead of  $\eta = G_2 \xi$  we *assume* that the behavior is given by an analogous equation

$$\tau_2 \frac{d\eta}{dt} = G_2 \xi - \eta. \quad (10.26)$$

For negative feedback either  $G_1$  or  $G_2$  must be negative.

We have a special case of a pair of first-order differential equations

$$\begin{aligned} \frac{dx_1}{dt} &= f_1(x_1, x_2), \\ \frac{dx_2}{dt} &= f_2(x_1, x_2). \end{aligned} \tag{10.27}$$

(Here  $x_1$  and  $x_2$  are general variables and have no relationship to the breathing problem considered earlier.)

We first combine the two first-order equations to make a second-order equation which, because we are using linear equations, can be solved exactly. To do this, differentiate Eq. 10.20:

$$\tau_1 \frac{d^2\xi}{dt^2} + \frac{d\xi}{dt} = a \frac{dp}{dt} + G_1 \frac{d\eta}{dt}.$$

Substitute Eq. 10.26 in this and obtain

$$\tau_1 \frac{d^2\xi}{dt^2} + \frac{d\xi}{dt} = -\frac{G_1}{\tau_2} \eta + \frac{G_1 G_2}{\tau_2} \xi + a \frac{dp}{dt}.$$

To eliminate  $\eta$ , solve Eq. 10.20 for  $G_1 \eta$  and substitute it in this equation:

$$\tau_1 \frac{d^2\xi}{dt^2} + \frac{d\xi}{dt} = -\frac{\tau_1}{\tau_2} \frac{d\xi}{dt} - \frac{1}{\tau_2} \xi + \frac{a}{\tau_2} p + \frac{G_1 G_2}{\tau_2} \xi + a \frac{dp}{dt}.$$

After like terms are combined, the result is

$$\frac{d^2\xi}{dt^2} + \left( \frac{1}{\tau_1} + \frac{1}{\tau_2} \right) \frac{d\xi}{dt} + \frac{1 - G_1 G_2}{\tau_1 \tau_2} \xi = \frac{a}{\tau_1 \tau_2} p(t) + \frac{a}{\tau_1} \frac{dp}{dt}. \tag{10.28}$$

This is another linear differential equation with constant coefficients. The right-hand side is a known function of time, since  $p(t)$  is known. The homogeneous equation is very common in physics and is called the *harmonic oscillator equation*. It is usually written in the form

$$\frac{d^2\xi}{dt^2} + 2\alpha \frac{d\xi}{dt} + \omega_0^2 \xi = 0, \tag{10.29a}$$

with the identifications

$$2\alpha = \frac{1}{\tau_1} + \frac{1}{\tau_2} = \frac{\tau_1 + \tau_2}{\tau_1 \tau_2} \tag{10.29b}$$

and

$$\omega_0^2 = \frac{1 - G_1 G_2}{\tau_1 \tau_2}. \tag{10.29c}$$

Appendix F shows that as long as  $\alpha \geq \omega_0$ , the system is critically damped or overdamped and there will be no oscillation or “ringing.” This will be the case if

$$\frac{(\tau_1 + \tau_2)^2}{4\tau_1^2 \tau_2^2} \geq \frac{1 - G_1 G_2}{\tau_1 \tau_2}$$

or

$$\frac{(\tau_1 + \tau_2)^2}{4\tau_1 \tau_2} \geq 1 - G_1 G_2. \tag{10.30}$$

This equation is symmetric in  $\tau_1$  and  $\tau_2$ . The important parameter is  $x = \tau_1/\tau_2$ . There is no ringing when

$$\frac{(1+x)^2}{4x} \geq 1 - G_1 G_2.$$

Since the feedback is negative,  $G_1 G_2 = -|G_1 G_2|$ . Then there is no ringing if

$$|G_1 G_2| < \frac{x}{4} + \frac{1}{4x} - \frac{1}{2}, \quad G_1 G_2 < 0. \tag{10.31}$$

If the two time constants are equal ( $x = 1$ ), the right-hand side of Eq. 10.31 is zero. There will be ringing if the open-loop gain has a magnitude greater than zero. For large values of  $x$  (say  $x > 10$ ), the equation is approximately  $|G_1 G_2| < x/4$ . If the magnitude of the open-loop gain is larger than this, there will be ringing.

We can see the general behavior of Eqs. 10.20 and 10.26 by examining the behavior of the derivatives. Both derivatives are zero and there is a fixed point when

$$\xi = \frac{a \Delta p}{1 - G_1 G_2}, \quad \eta = \frac{G_2 a \Delta p}{1 - G_1 G_2}.$$

For  $\Delta p = 0$  the fixed point is at the origin. Figures 10.13 and 10.14 show plots of  $\xi$  and  $\eta$  for different values of the gain and damping. The plots of  $\eta$  vs  $\xi$  are called *state-space* plots or *phase-space* or *phase-plane* plots. The plots shown here spiral to the fixed point. Depending on the values of the gains and time constants (try positive feedback) there can also be exponentially growing solutions. An extensive literature exists analyzing stability for both Eqs. 10.27 and their linearized versions. See Chapters 5 and 6 of Strogatz (1994) or Chapter 3 of Hilborn (2000).

## 10.7 Models Using Nonlinear Differential Equations

We have used many models in this book. In Chapter 2 we introduced a linear differential equation that leads to exponential growth or decay. We used it to model tumor and bacterial growth and the movement of drugs through the body. We briefly examined some nonlinear extensions of this model. In Chapter 4, we modeled diffusion processes with linear equations—Fick’s first and second laws—and we used a linear model to describe solvent drag. In Chapter 5, we used the model of a right-cylindrical pore. In Chapter 6, we used both a linear model—electrotonus—and a nonlinear model—the Hodgkin–Huxley equations. In this chapter we introduced a linear model for feedback, and we saw how two linear processes in a feedback loop could lead to oscillations, the linear harmonic oscillator.

Linear models have one advantage: they can be solved exactly. But most processes in nature are not linear. Jules-Henri Poincaré realized around 1900 that systems described exactly by the completely deterministic equations of Newton’s laws could exhibit wild behavior.

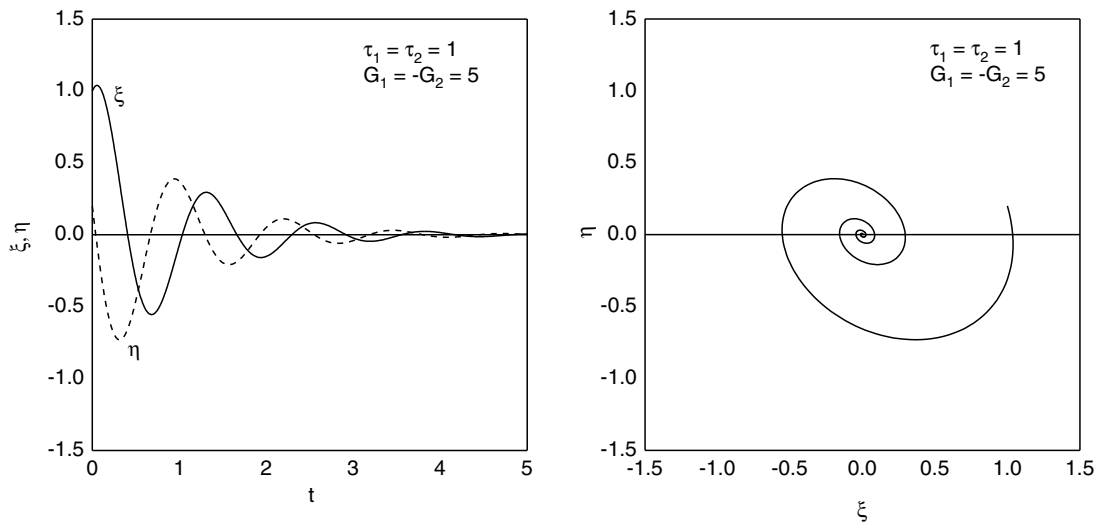


FIGURE 10.13. A solution to Eq. 10.28 is plotted that has a value 1 and time derivative zero when  $t = 0$ . The variable  $\eta$  is obtained from  $\xi$  by using Eq. 10.26. Plots of  $\xi$  and  $\eta$  vs  $t$  are shown on the left. A state-space plot of  $\eta$  vs  $\xi$  is shown on the right.

Poincaré was studying the three-body problem in astronomy (such as sun–earth–moon). While we are all familiar with the fact that the motion of the sun–earth–moon system is evolving smoothly with time and that eclipses can be predicted centuries in advance, this smooth behavior does not happen for all systems. For certain ranges of parameters (such as the masses of the objects) and initial positions and velocities, the solutions can exhibit behavior that is now termed *chaotic*. If we consider the motion that results from two sets of initial conditions that differ from each other only by an infinitesimal amount in one of the variables, we find that in chaotic behavior there can be solutions that diverge exponentially from each other as time goes on, even though the solutions remain bounded. Poincaré developed some geometrical techniques for studying the behavior of such systems. Thorough study of nonlinear systems requires the use of a digital computer. As a result, it has only been since the 1970s that we have realized how often chaotic behavior can occur in a system governed by deterministic equations. With computers we have gained more insight into the properties of chaotic behavior.

Just as the harmonic oscillator provides a model for behavior seen in many contexts from electric circuits to shock absorbers in automobiles to the endocrine system, certain features of nonlinear models have wide applicability. These include period doubling, the ability to reset the phase (timing) of a nonlinear oscillator, and deterministic chaos.

Some have said that Newtonian physics has been overthrown by chaos. This is not true. The same equations hold; predictable motions with which we have long been familiar still take place. Much of our current technology is based on them. We build television sets and send a spacecraft to explore several planets in succession. With chaos, we have come to understand a rich set of solutions

to these same equations that we were not equipped to study before.

Many books about nonlinear systems have been written. A particularly interesting one for this audience is by Kaplan and Glass (1995). It is written for biologists and has many clear and relevant examples. Others are by Glass and Mackey (1988), by Hilborn (2000), and by Strogatz (1994).

Space limitations prevent more than a brief hint at some of the features of nonlinear dynamics, here and in Chapter 11. In this section we will discuss some one- and two-dimensional nonlinear differential equations. These will not lead to chaos, but will allow us to describe a very simple model for *phase resetting*. In Sec. 10.8 we will discuss equations that exhibit chaotic behavior.

### 10.7.1 Describing a Nonlinear System

Suppose that a nonlinear system with  $N$  variables can be described by a set of first-order differential equations:

$$\begin{aligned} \frac{dx_1}{dt} &= f_1(x_1, x_2, \dots, x_N), \\ \frac{dx_2}{dt} &= f_2(x_1, x_2, \dots, x_N), \\ &\dots, \\ \frac{dx_N}{dt} &= f_N(x_1, x_2, \dots, x_N). \end{aligned} \quad (10.32)$$

(These are an extension of the pair of differential equations we saw as Eqs. 10.27. Our model of breathing had two variables. It would be more realistic to use a breathing model with more variables, since alveolar ventilation also depends on arterial pH, weakly on oxygen partial pressure, and on the nervous factors that were described earlier.)

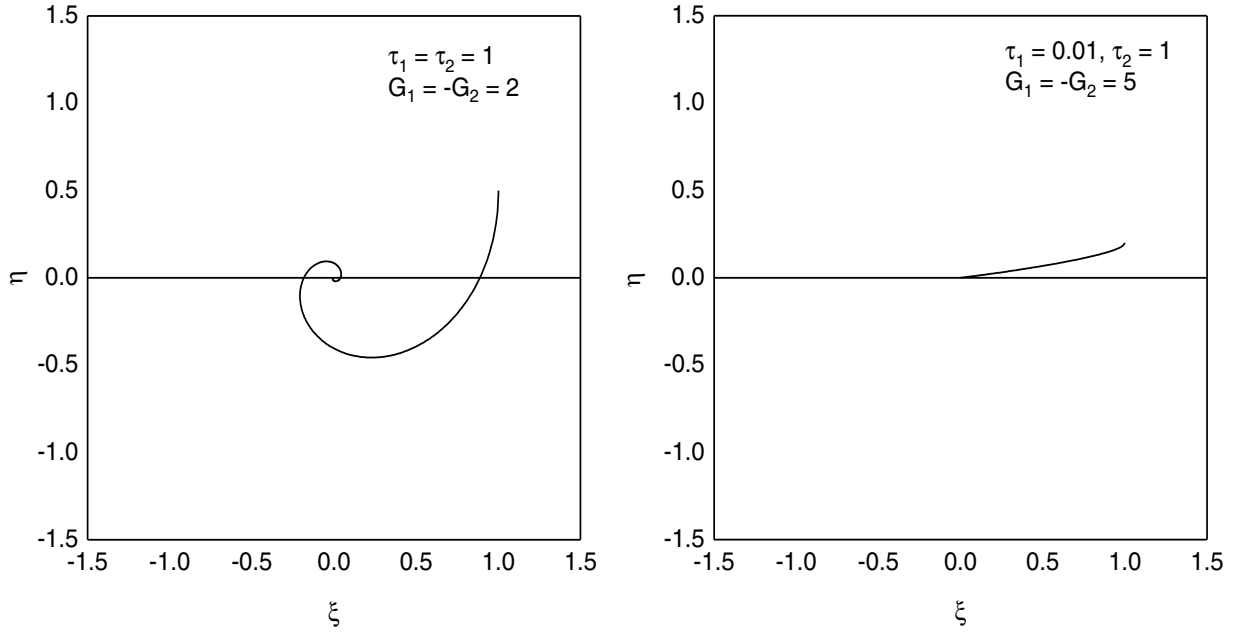


FIGURE 10.14. Additional state-space plots for the same initial conditions as in Fig. 10.13, but with different values of the parameters.

If the equations are cast in this form with  $N$  variables, then  $N$  initial conditions are required, corresponding to the constant of integration required for each equation. It is customary to say that there are  $N$  *degrees of freedom*. This is the language of *system dynamics*. This definition of degrees of freedom is different from what we used in Chap. 3, where each degree of freedom was represented by a second-order differential equation ( $d^2x/dt^2 = F_x/m$ , for example) and two initial conditions were required for each degree of freedom.

We can put Newton’s second law in this form by writing two first-order differential equations instead of one second-order equation. For motion in one dimension, instead of

$$m \frac{d^2x}{dt^2} = F(x, v),$$

we write a pair of first-order equations:

$$\frac{dv}{dt} = \frac{F(x, v)}{m}, \quad \frac{dx}{dt} = v.$$

This system has two degrees of freedom in our new terminology. In either description, two initial conditions are required.

In many situations the force (or more generally the function on the right-hand side of Eqs. 10.32) is time dependent. In standard form, the functions on the right do not depend on time. This is remedied by introducing one more variable,  $x_{N+1} = t$ . The additional differential equation is  $dx_{N+1}/dt = 1$ .

The evolution or “motion” of the system can be thought of as a trajectory in  $N$ -dimensional space, starting from the point that represents the initial conditions.

Time is a parameter. We have seen an example of this for two dimensions in Figs. 10.13 and 10.14. It is possible to prove that two distinct trajectories cannot intersect in a finite period of time and that a single trajectory cannot cross itself at a later time [see Hilborn (2000, p. 77) or Strogatz (1994, p. 149).] This is true in the full  $N$ -dimensional space; if we were to measure only two variables, we could see apparent intersections in the state plane that we were observing. This means that chaotic behavior, in which variables appear to change wildly and two-dimensional trajectories appear to cross, does not occur for a pair of differential equations of the form in Eqs. 10.32. At least three variables are required. A system with two degrees of freedom that is externally driven<sup>2</sup> can exhibit chaotic behavior because of the additional variable  $x_{N+1}$  that is introduced.

### 10.7.2 An Example of Phase Resetting: The Radial Isochron Clock

In Chapter 2 we studied the logistic differential equation

$$\frac{dy}{dt} = by \left( 1 - \frac{y}{y_\infty} \right).$$

It is convenient to rewrite the logistic equation in terms of the dimensionless variable  $x = y/y_\infty$ :

$$\frac{dx}{dt} = bx(1 - x). \tag{10.33}$$

<sup>2</sup>That is, one of the functions on the right-hand side of the set of equations depends on time.

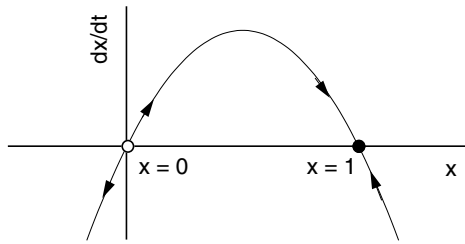


FIGURE 10.15. Plot of  $dx/dt$  vs  $x$  for the logistic differential equation.

This separates the scale factor  $y_\infty$  from the dynamic factor  $b$  that tells how rapidly  $y$  and  $x$  are changing.<sup>3</sup> A plot of  $dx/dt$  vs  $x$  is shown in Fig. 10.15. There is an unstable fixed point at  $x = 0$  and a stable fixed point at  $x = 1$ . The logistic equation is one of a whole class of nonlinear first-order differential equations for which  $dx/dt$  as a function of  $x$  has a maximum. It has been studied extensively because of its relative simplicity, and it has been used for population modeling. (Better models are available.<sup>4</sup> The logistic model assumes that the population is independent of the populations of other species, that the growth of the species does not affect the carrying capacity  $y_\infty$ , and that the population increases smoothly with time.)

Many of the important features of nonlinear systems do not occur with one degree of freedom. We can make a very simple model system that displays the properties of systems with two degrees of freedom by combining the logistic equation for variable  $r$  with an angle variable  $\theta$  that increases at a constant rate:

$$\frac{dr}{dt} = ar(1 - r), \quad \frac{d\theta}{dt} = 2\pi. \quad (10.34)$$

This has the form of Eqs. 10.32. We can interpret  $(r, \theta)$  as the polar coordinates of a point in the  $xy$  plane. When  $t$  has increased from 0 to 1 the angle has increased from 0 to  $2\pi$ , which is equivalent to starting again with  $\theta = 0$ . This system has been used by many authors. Glass and Mackey (1988) have proposed that it be called the *radial isochron clock*. Typical behavior is shown in Fig. 10.16(a). If  $r = 1$  there is a circular orbit corresponding to the stable fixed point of Eq. 10.33. Such a stable orbit is called a *stable limit cycle*.<sup>5</sup> There is an unstable limit cycle,  $r = 0$ , corresponding to the unstable fixed point of Eq. 10.33. Any initial conditions except  $r = 0$  give trajectories that move toward the stable circular limit cycle as time progresses. The set of points in the  $xy$  plane lying on orbits that move to the limit cycle as  $t \rightarrow \infty$

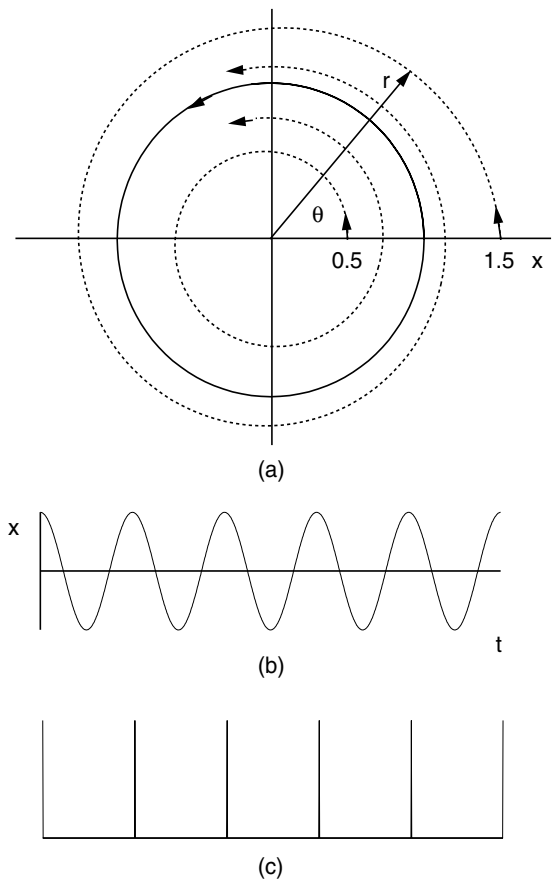


FIGURE 10.16. A system with two degrees of freedom. (a) The limit cycle is represented by the solid circle. Systems starting elsewhere in the plane have trajectories that approach the limit cycle as  $t \rightarrow \infty$ , as shown by the dashed lines. (b) The value of  $x = r \cos \theta$  is plotted as a function of time. (c) A timing pulse is generated every time  $\theta$  is a multiple of  $2\pi$ .

is called the *basin of attraction* for the limit cycle. In this case the basin of attraction includes all points except the origin. If we look at the time behavior, Fig. 10.16(b) shows the behavior of  $x = r \cos \theta$  on the limit cycle. The oscillator might provide timing information as the phase moves through some value. Figure 10.16(c) shows a series of pulses every time  $\theta$  is a multiple of  $2\pi$ .

In many cases the differential equations contain one or more parameters that can be varied, and the number and shape of the limit cycles change as the parameters are changed. A point in parameter space at which the number of limit cycles changes or their stability changes is called a *bifurcation*. We will see examples of bifurcations in the next section. See the references for a much more extensive discussion.

One important characteristic of nonlinear oscillators is that a single pulse can reset their phase. If they are subject to a series of periodic pulses they can be *entrained* to

<sup>3</sup>We could also, if we wish, define a new time scale,  $t' = bt$ , and deal with the completely dimensionless equation  $dx/dt' = x(1 - x)$ .

<sup>4</sup>See Begon *et al.* (1996).

<sup>5</sup>A *stable limit cycle* is an oscillation in the solutions to a set of differential equations that is always reestablished following any small perturbation.



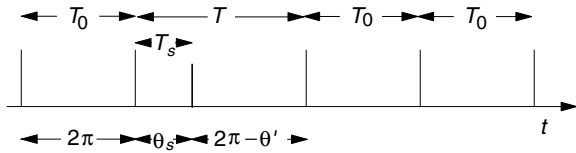


FIGURE 10.17. Resetting the phase of an oscillation. The oscillator fires regularly with period  $T_0$ . A stimulus a time  $T_s$  after it has fired causes a period of length  $T$ , after which the periods are again  $T_0$ .

oscillate at the driving frequency. (The nonlinear oscillators that sweep the electron beam across the screen of a television tube are entrained by synchronization pulses in the television signal.) Our simple two-dimensional model exhibits phase resetting that is very similar to that exhibited by cardiac tissue.<sup>6</sup>

Suppose that a cardiac pacemaker depolarizes every  $T_0$  seconds and that it can be modeled by our radial isochron clock. Assume that depolarization occurs when  $\theta = 0$  or a multiple of  $2\pi$ . A stimulus is applied at time  $T_s$  after the beginning of the cycle, as shown in Fig. 10.17. As a result the time from the previous depolarization to the next one is changed to  $T$ , after which the period reverts to  $T_0$ . (In a real experiment, it may be necessary to wait several cycles before measuring so that any transient behavior has time to decay, and then extrapolate back to find the value of  $T$ .) Often a stimulus early in the cycle is found to delay the next depolarization, while a stimulus late in the cycle advances it. Our model provides a simple geometric interpretation of this behavior, independent of any knowledge of the detailed dynamics.

A delayed depolarization is shown in Fig. 10.17. Pulses are occurring every  $T_0$  seconds when the phase is a multiple of  $2\pi$  (that is, 0). A stimulus is applied at a time  $T_s$  after the previous pulse, at which time the phase is  $\theta_s$ . Since the phase advances linearly, we have the proportion

$$\frac{T_s}{T_0} = \frac{\theta_s}{2\pi}.$$

Suppose the stimulus causes the system to move to a new state with a phase  $\theta'$ , which we do not yet know. Since  $d\theta/dt$  is constant in our model, the phase advances after the stimulus at the same rate as it would have without the stimulus. The next pulse occurs when the phase again reaches  $2\pi$ . This occurs at a time  $T$  after the previous pulse, or a time  $T - T_s$  after the stimulus, when the phase has increased from  $\theta'$  to  $2\pi$ . Therefore

$$\frac{T - T_s}{T_0} = \frac{2\pi - \theta'}{2\pi}$$

<sup>6</sup>This discussion is based on Glass and Mackey (1988), p. 104ff. See also the works by Winfree (1987, 1995, 2001). Strogatz (2003) discusses phase resetting and other nonlinear phenomena in an engaging and nonmathematical manner.

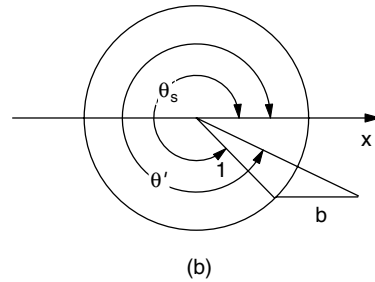
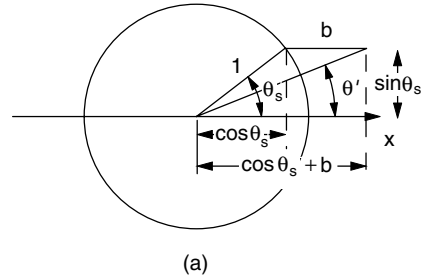


FIGURE 10.18. The limit-cycle oscillator model for resetting the phase of an oscillation. At phase  $\theta_s$  a stimulus changes the value of  $x$  by an amount  $+b$ . (a) For angles  $0 < \theta_s < \pi$ , this places the system on a trajectory with a smaller phase  $\theta'$ , delaying the next pulse. (b) For angles  $\pi < \theta_s < 2\pi$ , the stimulus results in a larger phase and the next pulse occurs earlier. The system returns to the limit cycle while  $\theta$  continues to increase at a constant rate.

and

$$\frac{T}{T_0} = \frac{2\pi + \theta_s - \theta'}{2\pi}. \quad (10.35)$$

We use our limit cycle model to relate  $\theta_s$  and  $\theta'$  as shown in Fig. 10.18. The system has been moving on a circle of unit radius representing the stable limit cycle. Assume that the only effect of the stimulus is to shift the value of  $x$  by a distance  $b$  along the  $+x$  axis. For the angles shown in Fig. 10.18(a) this results in a point with  $\theta' < \theta_s$ , a delay in the phase or  $T > T_0$ . For an initial angle in the lower half plane [Fig. 10.18(b)] it results in  $\theta' > \theta_s$  and  $T < T_0$ . The relation between the two angles can be obtained from the triangles:

$$\begin{aligned} \cos \theta' &= \frac{\cos \theta_s + b}{[(\cos \theta_s + b)^2 + \sin^2 \theta_s]^{1/2}} \\ &= \frac{\cos \theta_s + b}{(1 + b^2 + 2b \cos \theta_s)^{1/2}}. \end{aligned}$$

The stimulus changed both  $\theta$  and  $r$ . After the stimulus each evolves independently according to its own differential equation. The trajectory returns to the limit cycle as  $r$  returns to its attractor, but the phase is forever altered. Figure 10.19(a) is a plot of  $\theta'$  vs  $\theta_s$  for two values of  $b$ . When  $b < 1$ ,  $\theta'$  takes on all values, while for  $b > 1$ ,  $\theta'$  is restricted to values near 0 and  $2\pi$ . The first case is called a *type-1 phase resetting*, and the second is called a *type-0 phase resetting*. Figure 10.19(b) combines these results with Eq. 10.35 to determine  $T/T_0$  as a function of  $T_s/T_0$ .

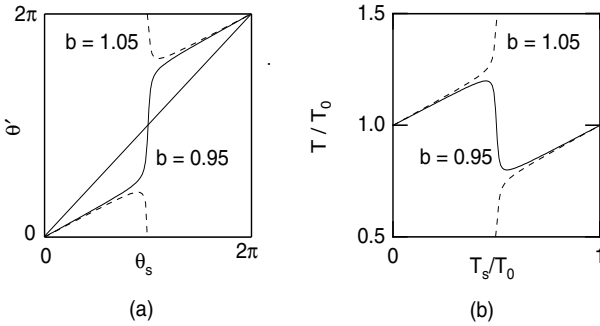


FIGURE 10.19. Plots of (a) the new phase vs the old phase and (b) the length of the period vs the time when the stimulus is applied.

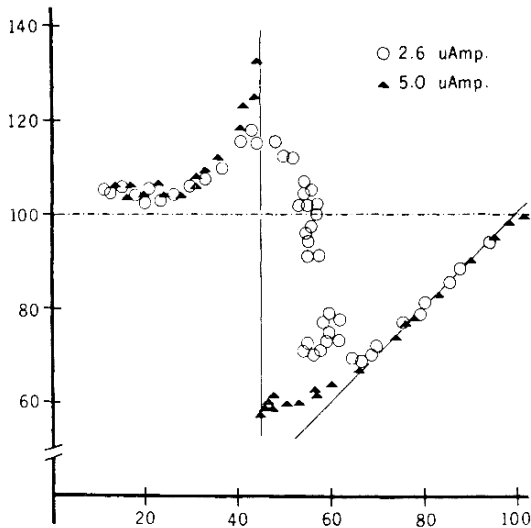


FIGURE 10.20. Phase resetting of a spontaneously oscillating Purkinje fiber by stimulation with an electrical impulse. The abscissa is  $T_s/T_0$  expressed as a percentage. The ordinate is  $T/T_0$  expressed as a percentage. Two different stimulus strengths were used. Compare the smaller stimulus (the open circles) to  $b = 0.95$  and the larger stimulus (solid triangles) to  $b = 1.05$  in Fig. 10.19(b). Reproduced with permission from J. Jalife and G. K. Moe (1976). Effect of electrotonic potential on pacemaker activity of canine Purkinje fibers in relation to parasystole. *Circ. Res.* **39**: 801–808. Copyright 1976 American Heart Association.

Figure 10.20 shows experimental data for electrotonically stimulated Purkinje fibers from the conduction system of a dog. The fibers were undergoing spontaneous oscillation with  $T_0 = 1.575$  s. Stimuli of two different amplitudes were applied at different parts of the cycle,  $T_s/T_0$ . Two different curves were obtained. The one with larger current looks like the curve with  $b = 1.05$  in Fig. 10.19(b), while the one with smaller current looks like the curve with  $b = 0.95$ .

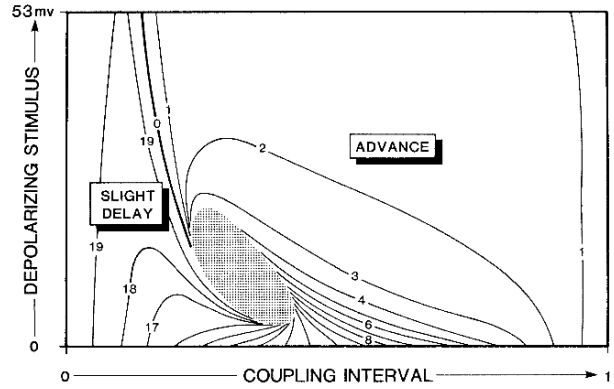


FIGURE 10.21. Phase resetting in a Hodgkin-Huxley model. The coupling interval is the delay from the previous pulse to the stimulation pulse in fractions of a period. The ordinate shows the size of the stimulus pulse in mV. The contours show the latency or time from the stimulus to the next pulse, measured in twentieths of a period. From A. T. Winfree (1987), *When Time Breaks Down*, Princeton, NJ, Princeton University Press. Copyright ©1987. Reproduced by permission of Prof. Arthur Winfree.

### 10.7.3 Stopping an Oscillator

It is theoretically possible to apply a stimulus that would put the system at the point  $r = 0$  in the state space. In that case it would not oscillate, though for this model  $r = 0$  is an unstable equilibrium point and any slight perturbation would lead the system back to the stable limit cycle. In more complicated models it is possible to have a region of state space corresponding to no oscillation and a basin of attraction that leads to it.

Figure 10.21 shows the results of a calculation by Winfree (1987) of the effect of stimuli on resetting the phase of the Hodgkin-Huxley equations adjusted to oscillate spontaneously. The abscissa is the coupling interval or the time after the previous pulse at which the stimulus is delivered. The ordinate is the height of the depolarizing pulse in mV. The contour lines show different values of the latency—the time in twentieths of a cycle period from the stimulus to the next pulse. Winfree calls the shaded region of state space where annihilation occurs a “black hole.”<sup>7</sup>

## 10.8 Difference Equations and Chaotic Behavior

We have alluded to the possibility of chaotic behavior, but we have not yet seen it. Chaotic behavior of nonlinear differential equations requires three degrees of freedom. It is possible to see chaotic behavior in difference equations with a single degree of freedom because the

<sup>7</sup>See Winfree (1987), especially Chapters 3 and 4, or Glass and Mackey (1988), pp. 93–97.

restriction that the trajectory cannot cross itself or another trajectory no longer applies. It arose from the continuous nature of the trajectories for a system of differential equations.

### 10.8.1 The Logistic Map: Period Doubling and Deterministic Chaos

We considered the logistic differential equation as a model for population growth. The differential equation assumes that the population changes continuously. For some species each generation is distinct, and a difference equation is a better model of the population than a differential equation. An example might be an insect population where one generation lays eggs and dies, and the next year a new generation emerges. A model that has been used for this case is the logistic difference equation or *logistic map*

$$y_{j+1} = ay_j \left( 1 - \frac{y_j}{y_\infty} \right)$$

with  $a > 0$  and  $j$  the generation number. It can again be cast in dimensionless form by defining  $x_j = y_j/y_\infty$ :

$$x_{j+1} = ax_j(1 - x_j). \tag{10.36}$$

While superficially this looks like the logistic differential equation, it leads to very different behavior. The stable points are not even the same. A plot of  $x_{j+1}$  vs  $x_j$  is a parabola, from which we can immediately see the following properties of the logistic map:

$$\begin{aligned} x_j < 0, & \quad x_{j+1} < 0, \\ x_j = 0, & \quad x_{j+1} = 0, \\ 0 < x_j < 1, & \quad x_{j+1} > 0, \\ x_j = 1, & \quad x_{j+1} = 0, \\ x_j > 1, & \quad x_{j+1} < 0. \end{aligned}$$

If we are to use this as a population model, we must restrict  $x$  to values between 0 and 1 so the values do not go to  $-\infty$ . In order to keep successive values of the map within the interval  $(0, 1)$  we also make the restriction  $a < 4$ .

For the logistic differential equation,  $x = 1$  was a point of stable equilibrium. However, for the logistic map, if  $x_j = 1$  the next value is  $x_{j+1} = 0$ . The equilibrium value  $x^*$  can be obtained by solving Eq. 10.36 with  $x_{j+1} = x_j = x^*$ :

$$x^* = ax^*(1 - x^*) = 1 - 1/a. \tag{10.37}$$

Point  $x^*$  can be interpreted graphically as the intersection of Eq. 10.36 with the equation  $x_{j+1} = x_j$  as shown in Fig. 10.22. You can see from either the graph or from Eq. 10.37 that there is no solution for positive  $x$  if  $a < 1$ .

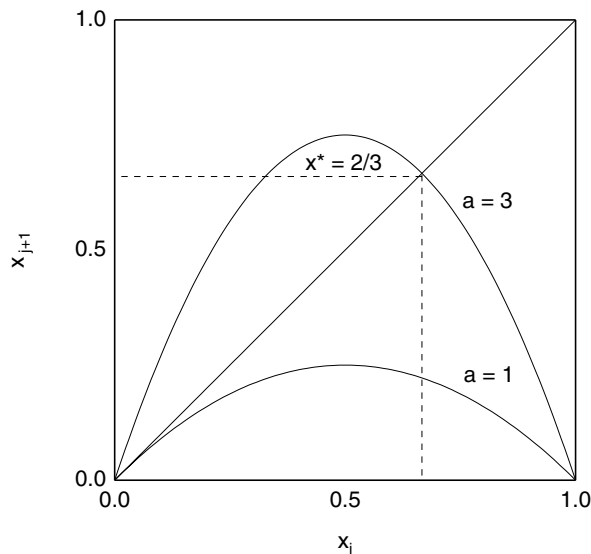


FIGURE 10.22. Plot of  $x_{j+1}$  vs  $x_j$  for the logistic difference equation or logistic map, for two values of parameter  $a$ .

For  $a = 1$  the solution occurs at  $x^* = 0$ . For  $a = 3$  the equilibrium solution is  $x = 2/3$ . Figure 10.23 shows how, for  $a = 2.9$  and an initial value  $x_0 = 0.2$ , the values of  $x_j$  approach the equilibrium value  $x^* = 0.655$ . This equilibrium point is called an *attractor*.

Figure 10.23 also shows the remarkable behavior that results when  $a$  is increased to 3.1. The values of  $x_j$  do not come to equilibrium. Rather, they oscillate about the former equilibrium value, taking on first a larger value and then a smaller value. This is called a *period-2 cycle*. The behavior of the map has undergone *period doubling*. What is different about this value of  $a$ ? Nothing looks strange about Fig. 10.22. But it turns out that if we consider the slope of the graph of  $x_{j+1}$  vs  $x_j$  at  $x^*$ , we find that for  $a > 3$  the slope of the curve at the intersection has a magnitude greater than 1. Many books explore the implications of this feature.

The period doubling continues with increasing  $a$ . For  $a > 3.449$  there is a cycle of period 4. A plot of the period-4 cycle for  $a = 3.5$  is also shown in Fig. 10.23. For  $a > 3.54409$  there is a cycle of period 8. The period doubling continues, with periods  $2^N$  occurring at more and more closely spaced values of  $a$ . When  $a > 3.569946$ , for many values of  $a$  the behavior is aperiodic, and the values of  $x_j$  never form a repeating sequence. Remarkably, there are ranges of  $a$  in this region for which a repeating sequence again occurs, but they are very narrow. The details of this behavior are found in many texts. In the context of ecology they are reviewed in a classic paper by May (1976).

For  $a < 3.569946$ , starting from different initial values  $x_0$  leads after a number of iterations to the same set of values for the  $x_j$ . For values of  $a$  larger than this, starting from slightly different values of  $x_0$  usually leads to very different values of  $x_j$ , and the differences become greater

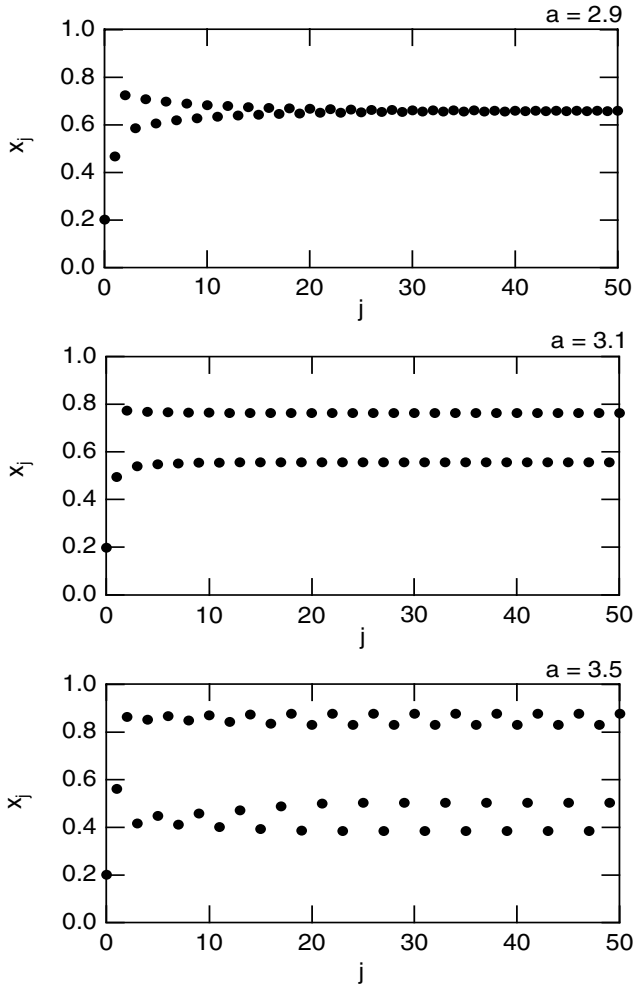


FIGURE 10.23. Plots of  $x_j$  vs  $j$  for different values of  $a$ , showing how the sequence of values converges to one, two, or four values of  $x$  called the *attractors*.

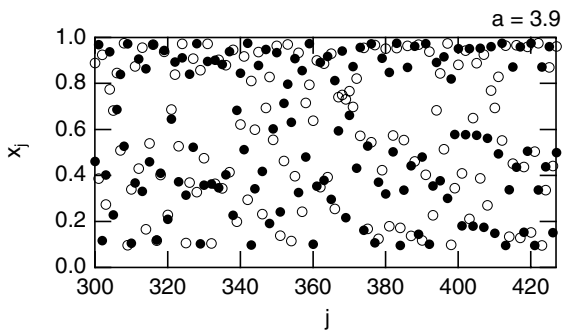


FIGURE 10.24. For this value of  $a$  the solution is aperiodic. There is no attractor.

and greater for larger values of  $j$ . This is shown in Fig. 10.24 for  $a = 3.9$ . The sequence is plotted from  $j = 301$  to  $j = 425$ . The solid circles represent the sequence starting with  $x_0 = 0.20$ ; the open circles represent the sequence for  $x_0 = 0.21$ .

This is an example of chaotic behavior or *deterministic chaos*. Deterministic chaos has four important characteristics:

1. The system is deterministic, governed by a set of equations that define the evolution of the system.
2. The behavior is bounded. It does not go off to infinity.
3. The behavior of the variables is aperiodic in the chaotic regime. The values never repeat.
4. The behavior depends very sensitively on the initial conditions.

### 10.8.2 The Bifurcation Diagram

Figure 10.25 shows the values of  $x_j$  that occur after any transients have died away for different values of parameter  $a$ . The diagram was made by picking a value of  $a$ . A value of  $x_0$  was selected and the iterations were made. After 50 iterations, the next 300 values of  $x_j$  were plotted. Then  $a$  was incremented slightly and the process was repeated. This is called a *bifurcation diagram*. The figure shows the range  $1 < a < 4$ . The asymptotic value of  $x_j$  rises according to  $x^* = 1 - 1/a$  until period doubling occurs at  $a = 3$ . A four-cycle appears for  $a > 3.449$ , and for  $a > 3.569946$  chaos sets in. Within the chaotic region are very narrow bands of finite periodicity.

Figure 10.26 shows a feature of many chaotic systems called *self-similarity*. The bifurcation diagram is plotted

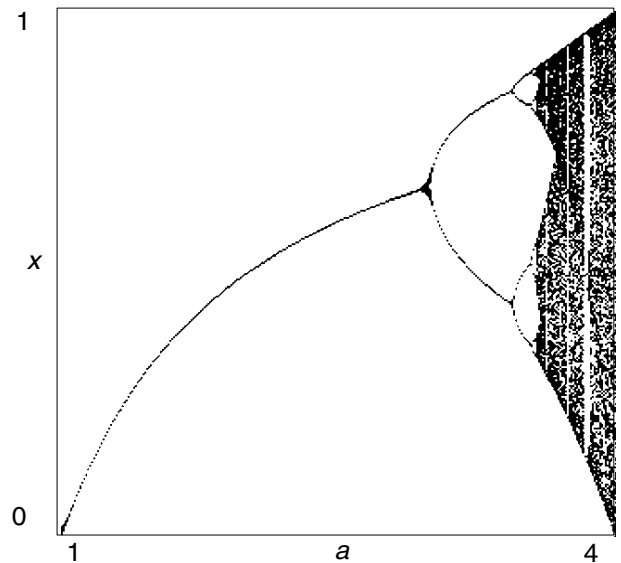


FIGURE 10.25. A bifurcation diagram for the logistic map, showing 300 values of  $x_j$  for values of  $a$  between 1 and 4. The plot was made using the Macintosh software *A Dimension of Chaos* by Matthew A. Hall.

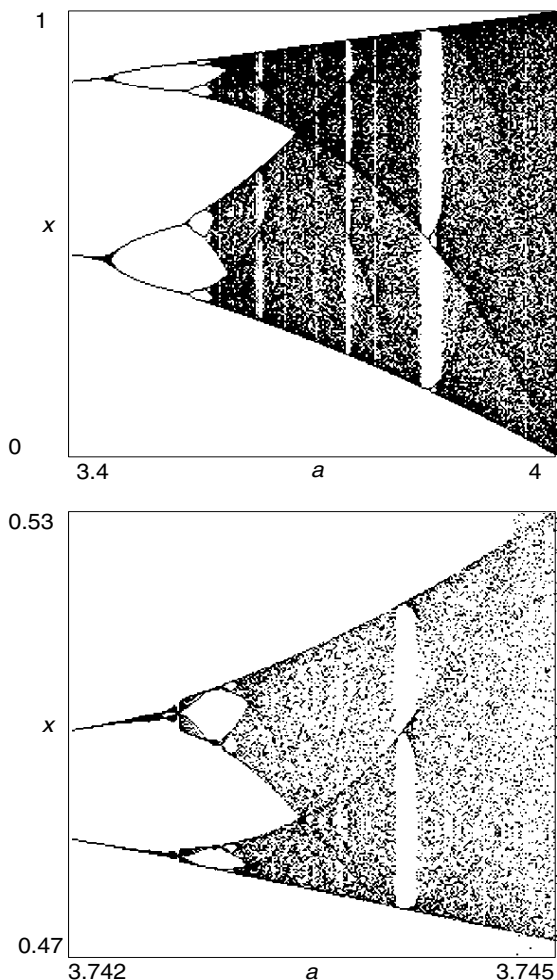


FIGURE 10.26. An example of self-similarity. The top curve shows  $3.4 < a < 4$ . The bottom curve shows  $3.742 < a < 3.745$ . Note its similarity to the top curve. The plot was made using the Macintosh software *A Dimension of Chaos* by Matthew A. Hall.

for two ranges of  $a$ :  $3.4\text{--}4.0$  and  $3.743\text{--}3.745$ . The  $x$  scale is expanded in the second diagram. Note the similarity of the two bifurcation diagrams.

Even though the plot of  $x_j$  vs.  $j$  in Fig. 10.24 has no obvious pattern, the values of  $x_j$  were obtained from the logistic map. When we plot  $x_j$  vs  $x_{j+1}$  the points fall on the map (Fig. 10.27).

The simplest systems in which chaotic behavior can be seen are first-order difference equations in which  $x_{j+1}$  is a function of  $x_j$ . The function is peaked and “tunable” by some parameter. Chaotic behavior occurs for some values of the parameter. In fact, it appears that the ratios of the parameter values involved in the period doubling and approach to chaos may be independent of the particular shape of the curve.<sup>8</sup>

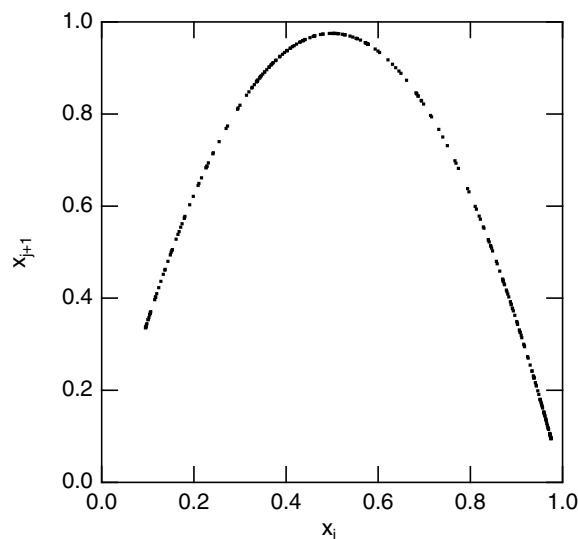


FIGURE 10.27. A plot of  $x_{j+1}$  vs  $x_j$  for the data of Fig. 10.24 recovers the logistic map.

### 10.8.3 Quasiperiodicity

Some systems exhibit *quasiperiodicity*. Consider the map  $x_{j+1} = x_j + b$  where  $b$  is a fixed parameter. Wrap the function back on itself so that  $x$  remains in the interval  $(0, 1)$ . This is done by using the modulo or remainder function.<sup>9</sup> The map is

$$x_{j+1} = x_j + b \pmod{1}. \tag{10.38}$$

The function is plotted in Fig. 10.28 for  $b = 0.3$ . The map is plotted in (a). The apparent discontinuities are due to the wrapping. A sequence of 50 points is plotted in Fig. 10.28(b). Because  $b = 3/10$  is a rational fraction, the points repeat themselves exactly every 10 steps. This can be seen in Fig. 10.28(c), which plots 128 consecutive points on a circle. The angle counterclockwise from the horizontal axis is  $\theta_j = 2\pi x_j$ . The 128 values all fall at 10 points on the circle. The plot of  $x_{j+1}$  vs  $x_j$  in Fig. 10.28(d) has 10 points that fall on the map.

Compare this with Fig. 10.29, which is a plot of the same map for an irrational value of the parameter,  $b = 1/\pi$ . The curve in (a) looks very similar. However, the values of  $x_j$  never repeat. This is difficult to see from Fig. 10.29(b), but can be seen in (c), where the 128 points are all at different values of  $\theta$ . If more points were plotted, the circle would be completely filled. All of the points plotted in (d) are also different, but of course they lie on the map function. If we were to make a bifurcation diagram the values of  $x_j$  would fill all points on the graph, unless  $b$  were a rational fraction, when there would be a finite number of points. This appears at first sight to be chaotic

<sup>8</sup>See Hilborn (1995), Chapter 2, Kaplan and Glass (1995), p. 30, or Strogatz (1994), p. 370.

<sup>9</sup>The function  $x \bmod n$  gives the number that remains after subtracting  $n$  from  $x$  enough times so that the result is less than 1. For example,  $1.5742 \bmod 1 = 0.5742$ ;  $7.5 \bmod 1 = 0.5$ .

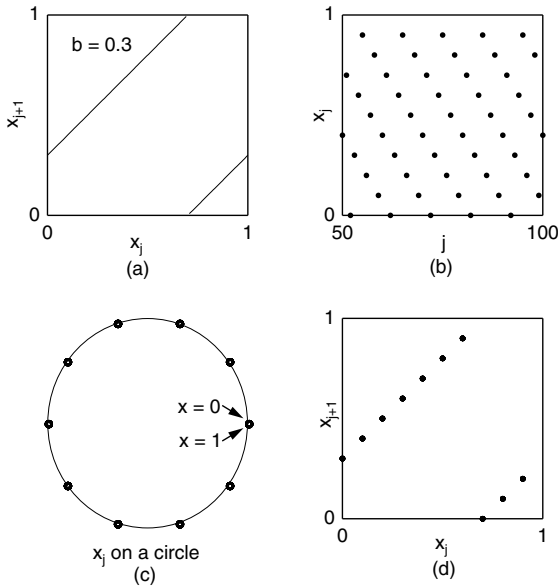


FIGURE 10.28. The linear map  $x_{j+1} = x_j + 0.3 \pmod{1}$ . (a) Plot of the map. (b) Plot of  $x_j$  vs  $j$  for 50 points. (c) The map plotted on a circle for 128 values of  $j$ , which lie on only 10 points. (d) A plot of 128 values of  $x_{j+1}$  vs  $x_j$  falls on 10 points on the map.

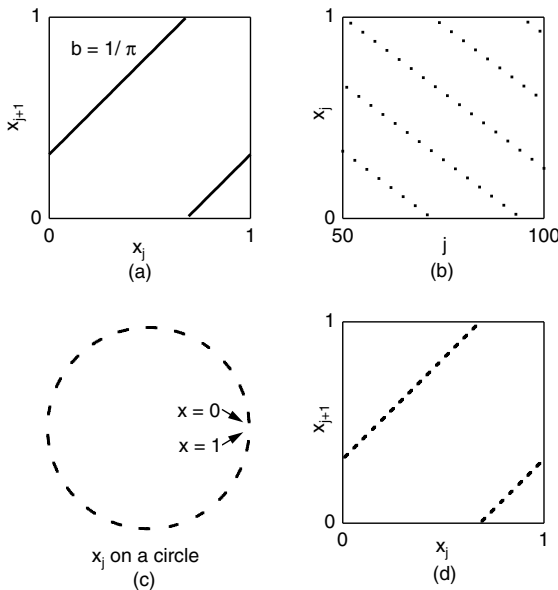


FIGURE 10.29. The linear map  $x_{j+1} = x_j + 1/\pi \pmod{1}$ . (a) Plot of the map. (b) Plot of  $x_j$  vs  $j$  for 50 points. (c) The map plotted on a circle for 128 points. (d) Plot of  $x_{j+1}$  vs  $x_j$  gives 128 points on the map.

behavior, but it is not. The function is deterministic, it is bounded, and the values of  $x$  never repeat. But it does not satisfy the last criterion: sensitive dependence on initial conditions. In chaotic behavior, two trajectories that start from initial points that are very close diverge in time. If a

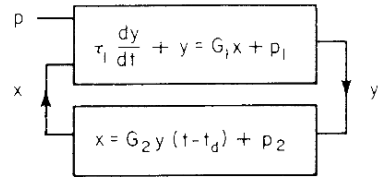


FIGURE 10.30. A two-stage feedback loop. The upper process is described by a single time constant; the lower one introduces a fixed time delay.

slightly different value of  $x_0$  is used for this map, all of the values in the new sequence are shifted from the original sequence by the same amount. There is no divergence of the two solutions. In quasiperiodicity, the trajectories for two points that are initially close remain close.

### 10.9 A Feedback Loop with a Time Constant and a Fixed Delay

In Sec. 10.6 we saw that if both processes in a two-stage feedback system had comparable time constants, there was the possibility for damped oscillations or “ringing.” Another possibility is that a portion of the system may respond to values of a state variable at some earlier time. The fixed time delay could be the time it takes a signal to travel along a nerve or the time it takes for a chemical to pass through a blood vessel.

We will consider a linear model for such a system, as shown in Fig. 10.30:

$$\begin{aligned} \tau_1 \frac{dy}{dt} + y &= G_1 x + p_1, \\ x &= G_2 y(t - t_d) + p_2. \end{aligned} \tag{10.39}$$

The first equation is like those in Sec. 10.6, except that the factor  $a$  multiplying  $p_1$  is set equal to unity. The second equation says that  $x(t)$  is proportional to the value of  $y$  at the earlier time  $t - t_d$ , plus some other parameter  $p_2$ . These can be combined to give a *delay-differential equation*:

$$\tau_1 \frac{dy}{dt} = -y + G_1 G_2 y(t - t_d) + p_1 + G_1 p_2$$

or, defining  $p = p_1 + G_1 p_2$  to eliminate clutter,

$$\tau_1 \frac{dy}{dt} = -y + G_1 G_2 y(t - t_d) + p. \tag{10.40}$$

This equation can give rise to sustained as well as damped oscillations. It is not hard to see why. Suppose that  $y$  is above some equilibrium value and that  $G_1 G_2 < 0$ . The first term on the right causes  $y$  to decrease toward equilibrium. But when it is nearly at equilibrium the second term, responding to an earlier positive value of  $y$ , continues to make  $y$  decrease so  $y$  goes negative. Now  $y$  is

below the equilibrium value and the same arguments can be applied as  $y$  increases. This paragraph could go on for a long time.

Why do we now have oscillations for a system with apparently only one degree of freedom? The reason is the delay term. In order to specify the initial state of the system at  $t = 0$ , we must specify the value of  $y$  for all times  $-t_d < t < 0$ . This is effectively an infinite number of values of  $y$ . Delay differential equations have an infinite number of degrees of freedom.

The mathematics for such a system become quite involved (even for the linear system we discuss here). The techniques for solving the equation were first described by Hayes (1950). The equation has been considered for biological examples by Glass and Mackey (1988).

The derivative is zero and the equation has a fixed point  $y_f$  when  $y_f = p/(1 - G_1G_2)$ . It is convenient to work with the new variable  $w = y - y_f$  and rewrite Eq. 10.40 as

$$\tau_1 \frac{dw}{dt} = -w + G_1G_2w(t - t_d).$$

We make another simplifying assumption; that the magnitude of the open-loop gain  $G_1G_2$  is so much greater than 1 that the  $-w$  term can be neglected.<sup>10</sup> Then the equation becomes

$$\frac{dw}{dt} = \frac{G_1G_2}{\tau_1}w(t - t_d).$$

Now recall that since  $G_1G_2 \ll -1$ , this coefficient is approximately the negative of the reciprocal of the time constant with no delay and *with* feedback [see Eq. 10.23]. Therefore the equation we will solve is

$$\frac{dw}{dt} = -\frac{1}{\tau}w(t - t_d). \quad (10.41)$$

If the delay time is zero, this is the familiar equation for exponential decay. As we argued above, a delay can allow oscillation. One can show by substitution that for certain values of the parameters one possible solution has the form  $w(t) = w_0e^{-\gamma t} \cos \omega t$ . We will find the conditions for a steady oscillation of the form  $w(t) = w_0 \cos \omega t$ . The left-hand side of Eq. 10.41 is  $dw/dt = -\omega w_0 \sin \omega t$ . The right-hand side is

$$\begin{aligned} -(1/\tau)w_0 \cos(\omega t - \omega t_d) &= -(1/\tau)w_0 \cos \omega t \cos \omega t_d \\ &\quad - (1/\tau)w_0 \sin \omega t \sin \omega t_d. \end{aligned}$$

Therefore the proposed solution will satisfy Eq. 10.41 only if

$$-\omega w_0 \sin \omega t = -(1/\tau)w_0 \sin \omega t_d \sin \omega t$$

and

$$0 = -(1/\tau)w_0 \cos \omega t_d \cos \omega t,$$

from which we get  $\omega = 1/\tau$  and  $\cos \omega t_d = 0$  or  $\omega t_d = \pi/2$ . Combining these gives  $t_d/\tau = \pi/2$ . From these we see exactly how the sustained oscillation occurs. The delay time and frequency are such that the shift is exactly one-quarter cycle. This is the same shift that would be obtained by taking the second time derivative of the undelayed function, which would lead to the undamped harmonic oscillator equation.

## 10.10 Negative Feedback Loops: A Summary

The last several sections have been mathematically complex. However, you do not need to memorize a large number of equations to carry away the heart of what is in them. The essential features are as follows:

1. If the equations relating the input and output variables of each process of a negative feedback loop are known, then their simultaneous solution gives the equilibrium or steady-state values of the variables. (In a biological system it may be very difficult to get these equations.) The solution is called the operating point or a fixed point of the system of equations.
2. If a single process in the negative feedback loop determines the time behavior, and the rate of return of a variable to equilibrium is proportional to the distance of that variable from equilibrium, then the return to equilibrium is an exponential decay and the system can be characterized by a time constant.
3. In a negative feedback system one variable changes to stabilize another variable. The amount of stabilization and the accompanying decrease in time constant depend on the open-loop gain.
4. It is possible to have oscillatory behavior with damped or constant amplitude if the two processes have comparable time constants and sufficient open-loop gain, or if one of the processes depends on the value of its input variable at an earlier time, or if the process has three or more degrees of freedom.
5. A nonlinear system oscillating on a limit cycle can have its phase reset by an external stimulus.
6. Nonlinear systems of difference equations with one or more degrees of freedom or nonlinear systems of differential equations with three or more degrees of freedom may exhibit bifurcations and chaotic behavior.

<sup>10</sup>If you are considering a problem where this is not a reasonable assumption, see the Appendix of Glass and Mackey (1988).

### 10.11 Additional Examples

This section provides some additional examples of the principles we have seen above. The details of the experiments and modeling are given in the references.

#### 10.11.1 Cheyne–Stokes Respiration

We have seen how the body responds to CO<sub>2</sub> levels in the blood by controlling the rate and amplitude of breathing to maintain the CO<sub>2</sub> concentration within a narrow range. The frequency and amplitude of breathing can also undergo oscillation. Some patients almost stop breathing for a minute or so and then breathe with much greater amplitude than normal. This is called *Cheyne–Stokes breathing*. Guyton *et al.* (1956) showed that diverting carotid artery blood in dogs through a long length of tubing increased the transit time between heart and brain and caused Cheyne–Stokes respirations. Cheyne–Stokes respirations have been modeled with a nonlinear delay-differential equation by Mackey and Glass (1977). Their results are shown in Fig. 10.31.

#### 10.11.2 Hot Tubs and Heat Stroke

Problems 10.10 and 10.11 discuss how the body perspires in order to prevent increases in body temperature. At the same time blood flows through vessels near the surface of the skin, giving the flushed appearance of an overheated person. The cooling comes from the evaporation of the perspiration from the skin. If the perspiration cannot evaporate or is wiped off, the feedback loop is broken and the cooling does not occur. If a subject in a hot tub overheats, the same blood flow pattern and perspiration occur, but now heat flows into the body from the hot water in the tub. The feedback has become positive instead of negative, and heat stroke and possibly death occurs. This has been described in the physics literature by Bartlett and Braun (1983).

#### 10.11.3 Pupil Size

The pupil changes diameter in response to the amount of light entering the eye. This is one of the most easily studied feedback systems in the body, because it is possible to break the loop and to change the gain of the system. Let the variables be as follows:  $x$  is the amount of light striking the retina,  $p$  is the light intensity, and  $y$  the pupil area. In the normal case,  $x$  is proportional to  $y$  and  $p$ :  $x = Apy$ . The body responds to increasing  $x$  by decreasing  $y$  so  $y = f(x)$ . These processes are shown in Fig. 10.32.

The reason this system can be studied so easily is that shining a very narrow beam of light into the pupil means that the change of pupil radius no longer affects  $x$ ; the loop is broken in the upper box of Fig. 10.32. Shining a light into the eye so that it is on the edge of the pupil

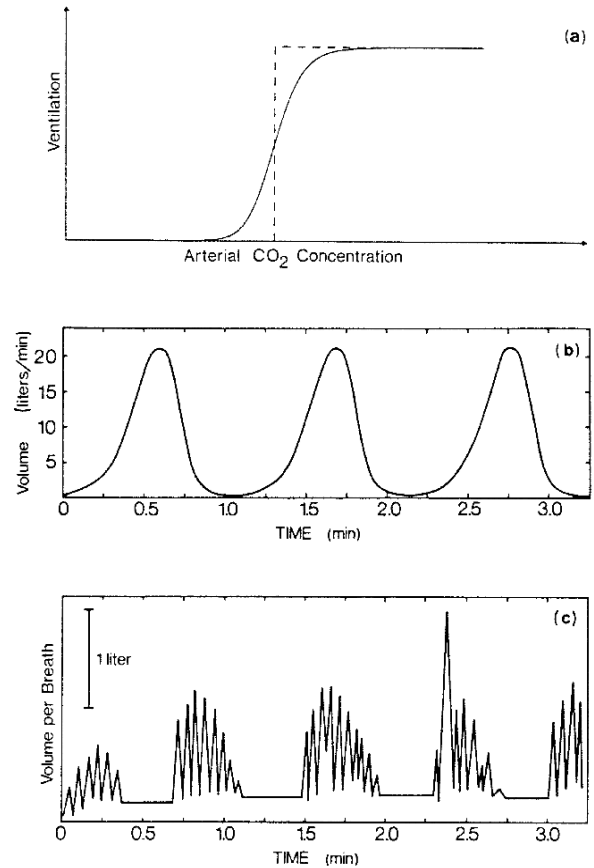


FIGURE 10.31. Cheyne–Stokes respirations. (a) The curve used to model  $y = g(x(t - t_d))$ . (b) The results of the model calculation. (c) Ventilation during Cheyne–Stokes respiration. Panel (a) from L. Glass and M. C. Mackey (1988). *From Clocks to Chaos*. Princeton, NJ, Princeton University Press. Copyright ©1988 by Princeton University Press. Reproduced by permission. Panels (b) and (c) reprinted with permission from M. C. Mackey and L. Glass (1977), *Oscillation and chaos in physiological control systems*. *Science* **197**: 287–289. Copyright 1977 AAAS.

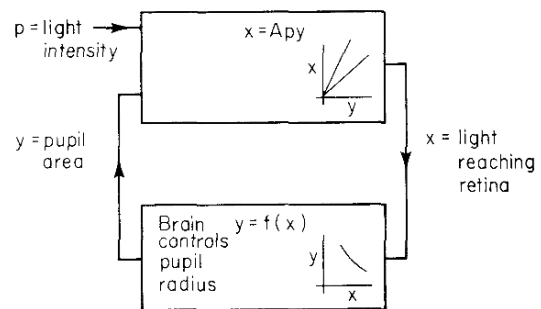


FIGURE 10.32. The feedback system for controlling the size of the pupil.

increases the gain in the upper box. These schemes are shown in Fig. 10.33. Furthermore, it has been discovered experimentally that the process in the lower box controls



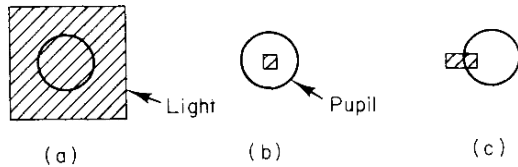


FIGURE 10.33. The feedback loop for pupil size can be changed by changing the way in which light strikes the eye. (a) In the normal situation  $x = Apy$ . (b) When the spot of light is smaller than the pupil, the feedback loop is broken. (c) When the spot of light strikes the edge of the pupil, the gain is increased.

the size of both pupils, even though light is directed at only one eye.

The properties of  $y = f(x)$  have been studied extensively by Stark [see Stark (1957, 1968, 1984)]. The results are consistent with a feedback loop having several time constants and also a fixed delay. Increasing the open loop gain as in Fig. 10.33(c) causes the pupil to oscillate at a frequency of about 1.3 Hz (cycles per second). Stark (1984) reviews this work, including the use of noise to analyze the system and nonlinearities.

#### 10.11.4 Oscillating White-Blood-Cell Counts

A delay-differential equation has been used to model the production of red and white blood cells. Figure 10.34 shows the actual white count for a patient with chronic granulocytic leukemia as well as the results of a model calculation. The striking feature of the model is the emergence of an aperiodic pattern when the delay time is increased from 6 to 20 days.

#### 10.11.5 Waves in Excitable Media

The propagation of an action potential is one example of the propagation of a wave in excitable media. We saw in Chapter 7 that waves of depolarization sweep through cardiac tissue. The circulation of a wave of contraction in a ring of cardiac tissue was demonstrated by Mines in 1914. It was first thought that such a wave had to circulate around an anatomic obstacle, but it is now recognized that no obstacle is needed.

Waves in thin slices of cardiac tissue often have the shape of spirals, very similar to simulations produced by a model similar to a two-dimensional Hodgkin–Huxley model [for example, see Pertsov and Jalife (1995)]. These waves turn out to occur in many contexts beside the heart. They have also been seen in the Belousov–Zhabotinsky chemical reaction,<sup>11</sup> in social amoebae, in the retina of the eye, and as calcium waves in

<sup>11</sup>There are many references. See Mielczarek *et al.* (1983); Epstein *et al.* (1983); and Winfree (1987).

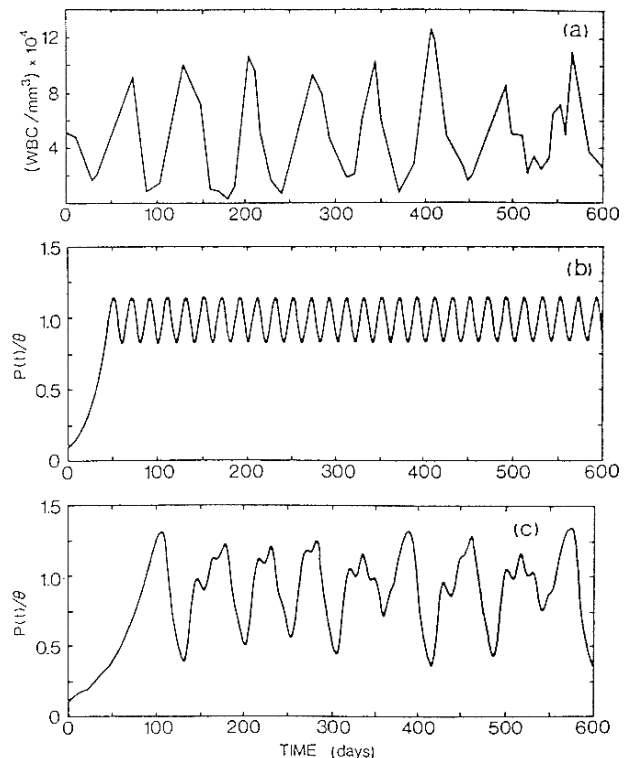


FIGURE 10.34. A nonlinear model for white-blood-cell production. (a) White-blood-cell count from a patient with chronic granulocytic leukemia. (b) The results of a nonlinear delay-differential equation model with a delay time of 6 days are an oscillation with a period of 20 days. (c) The results of using the same model with a delay time of 20 days are aperiodic. Reprinted with permission from M. C. Mackey and L. Glass (1977). Oscillation and chaos in physiological control systems. *Science* **197**: 287–289. Copyright 1977 AAAS.

oocytes. Beautiful photographs of all of these are found in Winfree (1987). A simple reaction-diffusion model that leads to a propagating chemical wave is found in Problem 4.24

These *spiral waves* seem to be another ubiquitous phenomenon (like period doubling) that depends primarily on the coarse features of the model. They can be generated with simple computer models called *cellular automata*. The rules for such an automaton and photographs of the resulting spiral waves are shown in Chapter 2 of Kaplan and Glass (1995).

The study of three-dimensional spiral waves in the heart is currently a very active field [Keener and Panfilov (1995); Mercader *et al.* (1995); Pertsov and Jalife (1995); Winfree (1994a, 1994b, 1995); Glass *et al.* (2002); Bub *et al.* (2002)]. They can lead to ventricular tachycardia, they can meander, much as a tornado does, and their breakup into a pattern resembling turbulence is a possible mechanism for the development of ventricular fibrillation (see the next example).

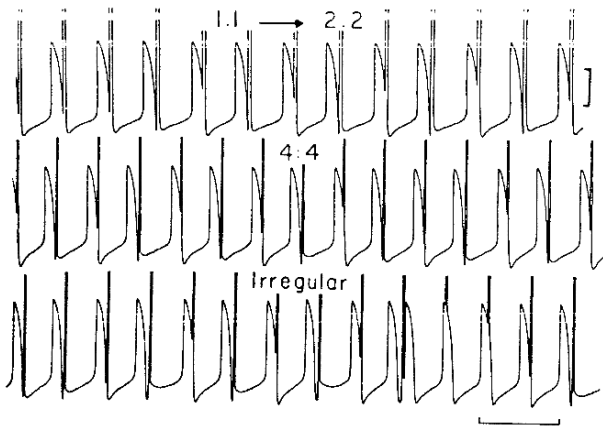


FIGURE 10.35. An aggregate of chick heart cells was periodically stimulated. Follow the bottom of the beginning of each sharp spike. The left part of the top strip shows phase locking. The right-hand portion of the top strip shows period doubling. The middle strip shows a period-4 behavior. The bottom strip shows irregular behavior consistent with deterministic chaos. Reprinted with permission from M. R. Guevara, L. Glass, and A. Shrier (1981). Phase locking, period-doubling bifurcations and irregular dynamics in periodically stimulated cardiac cells. *Science* **214**: 1350–1353. Copyright 1981 AAAS.

### 10.11.6 Period Doubling and Chaos in Heart Cells

Guevara *et al.* (1981) have subjected small aggregates of chick heart-cells to periodic stimulation. The stimulation frequency was slightly greater than the natural frequency of oscillation. The behavior of the preparation is shown in Fig. 10.35 and can best be seen by examining the *bottom* of the leading edge of the sharp positive pulse. The top strip on the left is phase locking. This is followed on the right in the top strip by an alternation characteristic of period doubling. The middle strip shows a variation of period 4. The bottom strip shows irregularity that is consistent with deterministic chaos.

Garfinkel *et al.* (1992) have also observed period doubling in a stimulated preparation of rabbit heart. Arrhythmias were induced by adding drugs to the solution perfusing the preparation. Figure 10.36 shows plots of the recorded action potentials and a plot of the map of  $I_n$  vs  $I_{n-1}$ , where  $I$  is the interval between beats. In panels A and B there is a constant interbeat interval and one point on the map. Panels C and D show period doubling. Panels E and F show a period-4 pattern. Panels G and H are completely aperiodic.

Ventricular fibrillation is “the rapid, disorganized, and asynchronous contraction of ventricular muscle. ... It represents the final common pathway for death in most patients who experience out-of-hospital cardiac arrest, and its rate of recurrence is on the order of 30% in the first year in successfully resuscitated patients.” [Epstein and Idris (1995)]. It appears to be due to meandering waves,

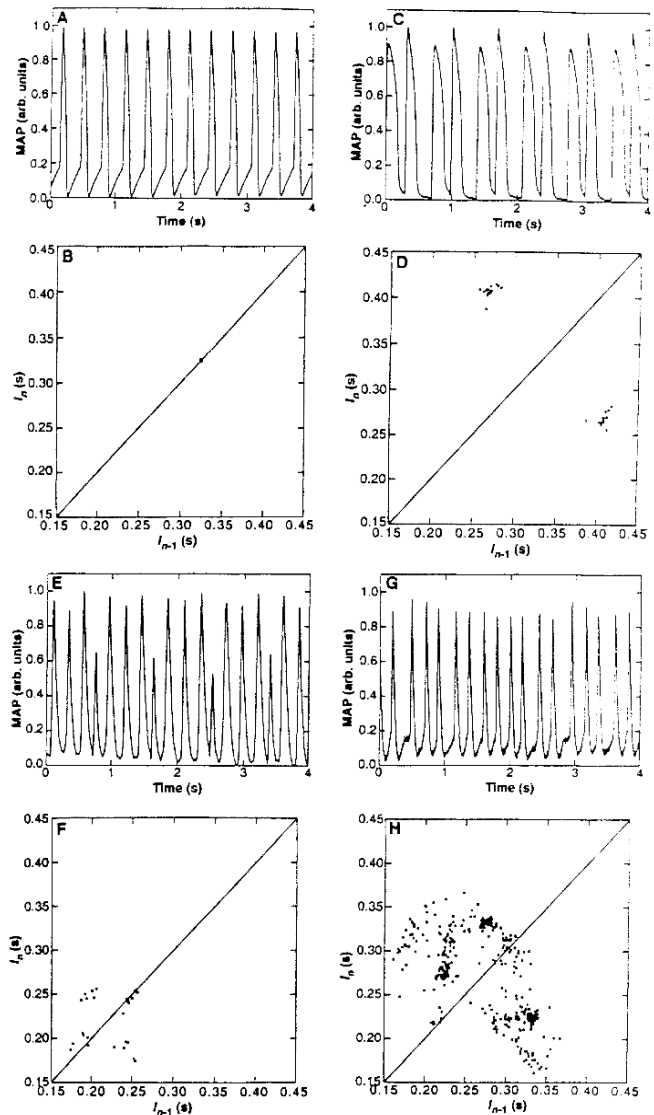


FIGURE 10.36. The results of experiments on a preparation consisting of intraventricular septum from a rabbit heart. Plots show the recorded action potentials and the map of  $I_n$  vs  $I_{n-1}$  where  $I$  is the interval between beats. In A and B there is a constant interbeat interval and one point on the map. Panels C and D show period doubling. Panels E and F show a period-4 pattern. Panels G and H are completely aperiodic. Reprinted with permission from A. Garfinkel, M. L. Spano, W. L. Ditto, and J. N. Weiss (1992). Controlling cardiac chaos. *Science* **257**: 1230–1235. Copyright 1992 AAAS.

and it does not occur unless the myocardium is sufficiently thick [Winfree (1994a, 1995)].

Witkowski *et al.* (1993, 1994) have made electrode arrays with a spacing of about  $200 \mu\text{m}$  that can be placed directly on the myocardium. The membrane current  $i_m$  can be estimated from the spatial derivatives of the extracellular (interstitial) potential. This technique has provided evidence that ventricular fibrillation has a component with simpler dynamics than had previously been thought

[Witkowski *et al.* (1995)]. More recent studies point toward more complex behavior [Hastings *et al.* (2000); Fox *et al.* (2002).]

## Symbols Used in Chapter 10

Symbol	Use	Units	First used on page
$a, b$	Arbitrary parameter		262
$a$	Parameter in logistic map		269
$a, b$	Constant in logistic equation		266
$b$	Reduction in ventilation rate because of dead space in lungs	$l \text{ min}^{-1}$	257
$b$	Amplitude of stimulus		267
$f, g, h, i$	Functions		257
$j$	Index for successive values in difference equation		269
$m$	Mass	kg	265
$n$	Number of moles of dissolved carbon dioxide		259
$o$	Rate of oxygen consumption	$\text{mol s}^{-1}$	256
$p$	Rate of oxygen consumption	$\text{mmol min}^{-1}$	256
$p$	Light intensity		274
$r$	Variable		266
$t$	Time	s	259
$t_d$	Delay time	s	272
$v$	Velocity	$\text{m s}^{-1}$	265
$w, x, y, z$	General variables		257
$x, y$	General variables in a feedback system		255
$x$	Partial pressure of carbon dioxide	torr	256
$x$	Amount of light striking the retina		274
$x^*$	Equilibrium value of $x$		269
$y$	Ventilation rate	$l \text{ min}^{-1}$	256
$y$	Pupil area	$\text{m}^2$	274
$y_\infty$	Constant (carrying capacity) in logistic equation		265
$A$	Proportionality constant		259
$A$	Pupil area	$\text{m}^2$	274
$F$	Respiratory quotient		256
$F$	General function		257
$F_x$	$x$ component of force	N	265
$G_1, G_2$	Gain		258
$I$	Interbeat interval	s	276
$N$	Number of variables		265
$P_{\text{CO}_2}$	Partial pressure of carbon dioxide	torr	256
$R$	Gas constant	$\text{J K}^{-1} \text{mol}^{-1}$	256
$T$	Temperature	K	256
$T, T_0, T_s$	Time	s	267

$V_c$	Compartment in which carbon dioxide is distributed throughout the body	$\text{m}^3$ or $l$	259
$\alpha$	Solubility constant	$\text{mol l}^{-1} \text{torr}^{-1}$	259
$\alpha$	Damping constant	$\text{s}^{-1}$	263
$\theta, \theta', \theta_s$	Angle		266
$\tau, \tau_1, \tau_2$	Time constant	s	259
$\omega, \omega_0$	Angular frequency	$\text{radian s}^{-1}$	263
$\xi, \eta$	Variables		259

## Problems

### Section 10.1

**Problem 1** Make the unit conversions to show that Eq. 10.4 is equivalent to Eq. 10.1.

### Section 10.2

**Problem 2** The level of the thyroid hormone thyroxine ( $T_4$ ) in the blood is regulated by a feedback system. Thyroid-stimulating hormone (TSH) is released by the pituitary. The thyroid responds to increased levels of TSH by producing more  $T_4$ . The  $T_4$  then acts through the hypothalamus and pituitary to reduce the amount of TSH.

(a) On a graph of  $T_4$  vs TSH, plot hypothetical curves showing these two processes and indicate the equilibrium or operating point.

(b)  $T_4$  contains four iodine atoms. If the body has an insufficient supply of dietary iodine, the thyroid cannot make enough  $T_4$ . What changes in the graphs will result? (This causes iodine deficiency goiter or thyroid hyperplasia. With the advent of iodized table salt and the use of iodine by bakers in bread dough to make their equipment easier to clean, the disease has almost disappeared.)

**Problem 3** For the feedback system  $x = [(y - p)/3]^{1/2}$ ,  $y = 4 - x^2$  assume that the variable on the right in each equation controls the variable on the left.

(a) Plot  $y$  vs  $x$  for each process.

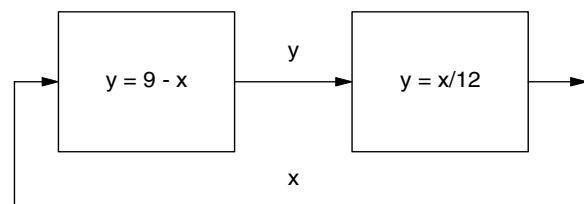
(b) Find the operating point when  $p = 0$ .

(c) Find the operating point when  $p = 1$ .

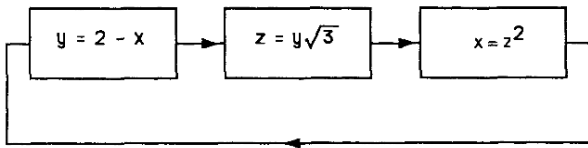
### Section 10.3

**Problem 4** Find the open-loop gain for the system described in Problem 10.3.

**Problem 5** Find the open-loop gain for the system shown.



**Problem 6** A feedback loop has the three stages shown. Find the operating point and the open-loop gain if these variables are all positive.



**Problem 7** Consider how thyroid hormone is removed from the body by the kidneys. The variables are  $V$ , the total plasma volume (l);  $C$ , the plasma concentration of thyroid hormone ( $\text{mol l}^{-1}$ );  $y$ , the total amount of hormone (mol); and  $R$ , the rate of hormone production ( $\text{mol s}^{-1}$ ). In the steady state, the rate of change is  $dy/dt = R - KC = 0$ . Then  $R = KC$  and  $y$  is not changing with time (see Chapter 2). The clearance  $K$  is a measure of the kidneys' ability to remove hormone, since the removal process depends on the concentration.

- (a) Plot  $K$  vs  $C$  for two different values of  $R$ . Show on your graph what happens if  $K$  remains fixed as  $R$  changes.
- (b) It has been found experimentally [D. S. Riggs (1952). *Pharmacol. Rev.* 4: 284-370] that  $K$  increases as  $C$  increases:  $K = aC$ . Plot this on your graph, too.
- (c) Draw a block diagram showing the proper cause and effect relationship between  $C$  and  $K$ .
- (d) Calculate the open-loop gain. Show how changes in  $C$  are altered by the feedback mechanism.

**Problem 8** A substance is produced in the body and removed at rate  $R$ . The concentration is  $C$ . The clearance is defined to be  $K$ . In the steady state  $0 = dy/dt = R - KC$ , or  $K = R/C$ . It is found experimentally that the clearance depends on the concentration as  $K = aC^n$ , where  $C$  is the independent variable. Find the open-loop gain, eliminating  $K$  and  $a$  from your answer.

**Problem 9** The kidney excretes phosphate in the following way. The total plasma volume  $V_p$  contains phosphate at concentration  $C_p$ :  $Q_p = C_p V_p$ . A volume of plasma  $(dV/dt)_f$  is filtered through the renal glomeruli into the nephrons each second. Within the nephron, phosphate is either reabsorbed into the plasma or excreted into the urine. Experiments show that virtually all phosphate is reabsorbed up to some rate  $(dQ/dt)_{max}$ :

$$\left(\frac{dQ}{dt}\right)_{reabs} = \begin{cases} C_p (dV/dt)_f, & C_p (dV/dt)_f < (dQ/dt)_{max} \\ (dQ/dt)_{max}, & C_p (dV/dt)_f \geq (dQ/dt)_{max} \end{cases}$$

As in Problem 7(a), at equilibrium the clearance of phosphate from the plasma is defined as

$$K = \frac{(dQ/dt)_{excreted\ into\ urine}}{C_p}$$

Suppose that exogenous phosphate is entering the plasma at a fixed rate  $R$  and that steady state has been reached so that  $R = (dQ/dt)_{excreted\ into\ urine}$ .

- (a) What value for reabsorption does this imply?
- (b) Determine two equations relating  $K$  and  $C_p$  and plot them.
- (c) Calculate the open-loop gain of the feedback loop.

**Problem 10** With considerable simplification, consider the body to have a constant temperature  $T$  throughout and a total heat capacity  $C$ . The total amount of thermal energy in the body is  $U$ . The heat capacity is defined so that  $dU = CdT$ . The source of the thermal energy is the body's metabolism:  $(dU/dt)_{in} = M$ . If sweating is ignored, the rate of loss of energy by convection and radiation is approximately proportional to the amount by which the body temperature exceeds the ambient or surrounding temperature:  $(dU/dt)_{loss} = K(T - T_a)$ .

- (a) What is the steady-state temperature as a function of  $M$  and  $T_a$ ?
- (b) Write a differential equation for  $T$  as a function of time. Suppose that  $M$  suddenly jumps by a fixed amount. What is the time constant?

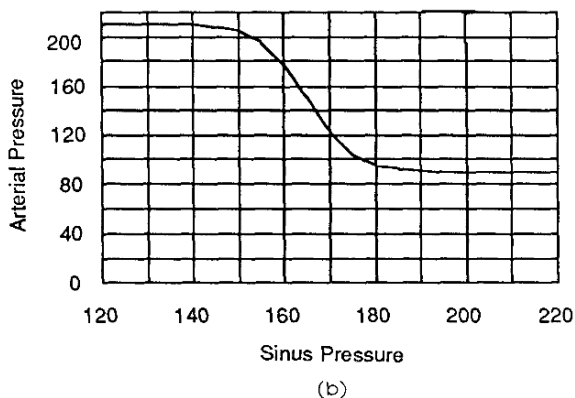
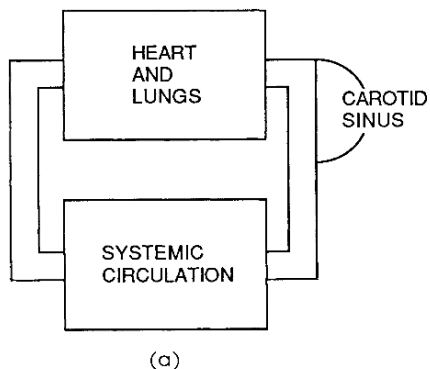
**Problem 11** When the body temperature is above  $37^\circ\text{C}$ , sweating becomes important. The rate of energy loss is proportional to the amount of water evaporated. If all the perspiration evaporates, sweating loss can be approximated by  $(dU/dt)_{sweat} = L(T - 37)$ .

(a) Modify the differential equation of the previous problem to include  $(dU/dt)_{sweat}$  as the input variable with  $T$  as the output variable. Combine it with this new equation to make a feedback loop. Determine the new equilibrium temperature and the time constant.

(b) Make numerical comparisons for the previous problem and this one when  $M = 71 \text{ kcal h}^{-1}$ ,  $C = 70 \text{ kcal }^\circ\text{C}^{-1}$ ,  $K = 25 \text{ kcal h}^{-1} \text{ }^\circ\text{C}^{-1}$ ,  $L = 750 \text{ kcal h}^{-1} \text{ }^\circ\text{C}^{-1}$ ,  $T_a = 38^\circ\text{C}$  (high enough to ensure sweating).

**Problem 12** A simplified model of the circulation is shown. Normally we know that the arterial pressure is the same as that in the carotid sinus:  $p_{art} = p_{sinus}$ . In experiments on dogs whose vagus nerves were cut, the carotid arteries were isolated and perfused by a separate pump. This broke the feedback loop and allowed the curve on the accompanying graph to be obtained. The empirical equation shown [based on the work of A. M. Scher and A. C. Young, (1963). *Serroanalysis of carotid sinus reflex effects on peripheral resistance. Circ. Res.* 12: 152-165, summarized in Riggs (1970)] is (with pressures in torr)

$$p_{art} = 90 + \frac{120}{1 + \exp[(p_{sinus} - 165)/5]}$$



- (a) Draw a block diagram of the complete feedback system. Label the blocks, show the functional relationship for each one, and indicate the proper cause-and-effect relationship.
- (b) Find the operating point.
- (c) Find the open-loop gain.

**Problem 13** Consider the following special case of linear feedback:  $\Delta x = G_1(\Delta p + \Delta y)$ ,  $\Delta y = G_2\Delta x$ . Find the ratio  $\Delta x/\Delta p$  when  $G_1 \ll -1$ ,  $G_2 < 1$ .

**Problem 14** Differentiate Eq. 10.4 and show that the expression for  $G_1$  is the same as in Eq. 10.19.

**Problem 15** For the thyroid problem, Problem 10.7, write a differential equation that can be solved to give  $C$  as a function of time. Suppose that at  $t = 0$ ,  $R$  suddenly becomes 0. What is the differential equation then? Solve the equation: note that it is not linear.

Section 10.5

**Problem 16** The following is a vastly oversimplified model of calcium regulation in dogs. Calcium is stored in body fluids and bones. Experiments show that the calcium concentration in the blood of a dog obeys approximately the equation [Riggs (1970, p. 491)]

$$3.9 \frac{dC}{dt} + 1.4C = 81.2 + \left(\frac{dQ}{dt}\right)_{iv} + \left(\frac{dQ}{dt}\right)_r(t),$$

where  $C$  is the plasma concentration in  $\text{mg l}^{-1}$ ,  $t$  is the time in  $\text{h}$ ,  $(dQ/dt)_{iv}$  is the rate of intravenous infusion of calcium in  $\text{mg h}^{-1}$ , and  $(dQ/dt)_r$  is the rate of reabsorption of calcium from bone into the blood in  $\text{mg h}^{-1}$ . (The numerical constants are consistent with these units.) The rate of reabsorption depends on the level of parathyroid hormone (PTH) concentration in the blood, which in turn depends on the calcium concentration. Instead of measuring the PTH concentration, experimenters found that  $(dQ/dt)_r$  and  $C$  are related empirically by  $(dQ/dt)_r = 188 - 1.34C$ , where  $C$  is the independent variable.

- (a) Draw a block diagram with variables  $(dQ/dt)_r$  and  $C$ .
- (b) Write equations to describe the steady state and find steady-state values of  $(dQ/dt)_r$  and  $C$  when  $(dQ/dt)_{iv} = 0$ .
- (c) Find the open-loop gain.
- (d) Find the time constant for the change of  $C$  when the parathyroid glands have been removed, in response to a step change in  $(dQ/dt)_{iv}$ .
- (e) Find the time constant for the change in  $C$  in response to a step change in calcium infusion when the parathyroid glands are intact, so that the feedback loop is closed.

**Problem 17** This problem is a simplification by the authors suggested by the data of Chick et al. [(1977). Artificial pancreas using living beta cells: Effects on glucose homeostasis in diabetic rats. *Science* **197**: 780–781]. Experimental data on diabetic rats show that the insulin level is 0 and the glucose level is 500. When an artificial pancreas is installed, a new operating point is reached for which  $i = 40$  and  $g = 100$ .

- (a) Make the simplest assumption possible: glucose level responds to insulin level according to  $g = A + G_1i$ , while insulin responds to glucose as  $i = G_2g$ . Find the open-loop gain.
- (b) The same series of experiments showed that when the feedback loop is closed, the time constant for glucose to fall is 1.67 h. When the artificial pancreas is removed, the glucose level rises with a time constant of 10.67 h. Estimate the open-loop gain, assuming that the insulin level changes instantaneously.

Section 10.6

**Problem 18** Multiply Eq. 10.28 by  $\tau_2$  and show that it reduces to Eq. 10.22 when  $\tau_2 \ll \tau_1$ .

**Problem 19** For the two-stage feedback loop with equal time constants  $\tau$ , show that oscillation results with a frequency  $\omega = (|OLG|)^{1/2}/\tau$ .

**Problem 20** Consider two substances in the plasma with concentrations  $X$  and  $Y$ . (They might be glucose and insulin.) Assume that experiment has established the following facts.

(i) The steady-state values of each concentration are  $X_0$  and  $Y_0$ . Departures from them are  $x = X - X_0$  and  $y = Y - Y_0$ .

(ii) When  $y = 0$ ,  $X$  is removed from the body at a rate proportional to  $x$ . This is true for both positive and negative values of  $x$ :  $dx/dt = -(1/\tau_1)x$ .

(iii) When  $x = 0$ ,  $Y$  influences the rate at which  $X$  changes in an approximately linear fashion. An increase of  $Y$  above  $Y_0$  ( $y > 0$ ) increases the rate of disappearance of  $x$ .

(iv) When  $x = 0$ ,  $y$  is cleared at a rate proportional to  $y$ :  $dy/dt = -(1/\tau_2)y$ .

(v) When  $y = 0$  and  $x$  is nonzero, a positive value of  $x$  stimulates the production of  $Y$ , while a negative value of  $x$  inhibits the production of  $Y$ .

Assume that the rate of production is a linear function of  $x$ . Write down two linear differential equations to model these observations. That is, add a term to each of the equations given that describes observations (iii) and (v).

**Problem 21** Combine the two equations obtained in the previous problem into a single differential equation in  $x$ . Show that it has the form

$$\frac{d^2x}{dt^2} + \left(\frac{1}{\tau_1} + \frac{1}{\tau_2}\right) \frac{dx}{dt} + \frac{1 - OLG}{\tau_1\tau_2}x = 0.$$

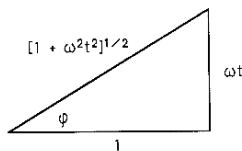
Use the result of Problem 17 to obtain  $1 - OLG$  and suppose that  $\tau_1 = 50$  min. For what value of  $\tau_2$  will critical damping occur? (If you find two values of  $\tau_2$ , which seems more reasonable?) If  $\tau_2$  is greater than the value you select, will the system be overdamped or underdamped? (Do not take these results too seriously.)

**Problem 22** This problem explores the response of a simple linear system from the point of view of the system's response to sinusoidal signals of various frequencies.

(a) The differential equation describing a system with time constant  $\tau$  and gain  $G$  is

$$\frac{dx}{dt} = -\frac{1}{\tau}x + \frac{G}{\tau}y.$$

Show by substitution that if  $y = Y \sin \omega t$ , then  $x = X \sin(\omega t + \phi)$ , where  $\tan \phi = \omega\tau$  and  $X(\omega\tau \sin \phi + \cos \phi) = GY$ .



(b) Use the relation  $\tan \phi = \omega\tau$  to establish the triangle shown, and use it to show that  $X = GY/(1 + \omega^2\tau^2)^{1/2}$ . These two relations give the response of the system in the frequency domain.

**Problem 23** The following model for the attrition of troops in battle was developed by F. W. Lanchester and

has been found to work reasonably well in several battles. The number of "friendly" troops is  $F(t)$  and the number of "enemy" troops is  $E(t)$ . The rates of change are given by  $dF/dt = -aE$ ,  $dE/dt = -bF$ , where  $a$  and  $b$  are the "effectiveness" of each side. The initial number of troops on each side is  $F_0$  and  $E_0$ .

- (a) What are the initial values of  $dF/dt$  and  $dE/dt$ ?
- (b) Obtain a differential equation for  $F$ .
- (c) Find the most general solution to this differential equation and determine the coefficients from the initial conditions.
- (d) Plot  $F$  and  $E$  for  $a = b = 0.05$  and  $E_0 = 2F_0$ .

**Problem 24** The equation  $dF/dt = -aE$  could also be thought of as describing a predator-prey situation if  $a$  represents the number of animals that the enemy eats per unit time. Ignoring latent periods such as gestation and infancy, what is the simplest way the equation could be modified to take account of reproduction and other ways of dying?

### Section 10.7

**Problem 25** Make a phase-space plot and discuss stability for  $dy/dt = by$ ,  $dy/dt = -by$ , and  $dy/dt = a - by$ .

**Problem 26** Make a drawing similar to Fig. 10.15 for the differential equation  $dx/dt = x(c - x^2)$  for different values of  $c$  (positive and negative) and describe the stability of the fixed points as a function of  $c$ .

**Problem 27** (a) Make drawings of the tip of the vector that defines  $\theta'$  in Fig. 10.18 to show that when  $b < 1$ ,  $\theta'$  takes on all values, while for  $b > 1$ ,  $\theta'$  is restricted to values near 0 and  $2\pi$ .

(b) Redraw Fig. 10.19(a) in the case that the angles are not reset to zero when they reach  $2\pi$ .

**Problem 28** Consider the undamped harmonic oscillator in the form  $dx/dt = v$ ,  $dv/dt = -\omega_0^2x$ .

- (a) Make a phase-plane plot.
- (b) Is the closed trajectory a limit cycle? Why or why not?
- (c) Add a damping force proportional to  $-v$  and redraw the phase-plane plot.

**Problem 29** In Fig. 10.19, the phase behavior changes dramatically between  $b = 0.95$  and  $b = 1.05$ . This change is most apparent for  $\theta_s = \pi$ , where  $\theta' = 0$  for  $b = 0.95$  and  $\theta' = \pi$  for  $b = 1.05$ . What happens for  $\theta_s = \pi$  and  $b = 1$  exactly?

**Problem 30** Reproduce qualitatively plots like Fig. 10.19 for  $b = -0.95$  and  $b = -1.05$ . This corresponds to a hyperpolarizing stimulus.

**Problem 31** Write a simple computer program to solve the two differential equations in Eq. 10.34 for  $r(t)$  and

$\theta(t)$ . (See Sec. 6.14 for some guidance on how to solve differential equations numerically.)

(a) Make plots of  $x(t) = r(t) \cos(\theta(t))$  as a function of time for different stimuli.

(b) Reproduce a few points in the plots of Fig. 10.19 using your program. In particular, examine stimuli given at or near  $\theta_s = \pi$  with  $b$  approximately equal to 1.

(c) Try varying the parameter  $a$ , and see how it affects the solution.

**Problem 32** Use the program written in Problem 31 to examine entrainment. Stimulate the radial isochron clock periodically, with a frequency near but not exactly equal to the natural frequency of oscillation. Find examples where the clock is entrained to the stimulus (the oscillation has the same frequency as the stimulus).

**Problem 33** A simple model for excitation of cardiac tissue is the FitzHugh–Nagumo model

$$\begin{aligned} \frac{dv}{dt} &= \frac{1}{\varepsilon} \left( v - \frac{v^3}{3} - u \right) \\ \frac{du}{dt} &= \varepsilon (v + \beta - \gamma u), \end{aligned}$$

where  $\varepsilon = 0.2, \gamma = 0.5$  and  $\beta = 0.8$ .

(a) Make a plot in phase space ( $v$  versus  $u$ ) of the “nullclines” (the curves obtained when  $dv/dt = 0$  and  $du/dt = 0$ ).

(b) Determine the steady-state solution (fixed point). You may have to do this numerically or graphically.

(c) Write a simple program to solve these equations on the computer. (See Sec. 6.14 for some guidance on how to solve differential equations numerically.) Plot  $v(t)$  and  $u(t)$  for the initial conditions  $v(0) = -0.70, u(0) = -0.65$ .

### Section 10.8

**Problem 34** Show that for the logistic difference equation, the slope  $dx_{n+1}/dx_n$  at  $x^*$  is given by  $2 - a$ , so that for  $a > 3$  the slope has magnitude  $> 1$ .

Use a spreadsheet to plot  $x_n$  for different values of  $a$  and explore the period doubling.

Plot  $x_{j+1}$  vs.  $x_j$ , and show why we restricted  $a$  to values less than four.

For the logistic map with  $a = 3.9$ , evaluate  $x_j$  using the two initial conditions  $x_1 = 0.2000$  and  $x_1 = 0.2001$ . Carry out the calculation for at least 20 iterations.

**Problem 35** Cyclic variations in the population of a species are often studied with a predator-prey model such as the Lotka-Volterra equations (Chapter 2 Problem 34). It is also possible to have cyclic variations of a single species. This problem explores one such model and is based on Appendix B of Ginzburg and Colyvan (2004).

Let  $N_t$  represent the population at generation  $t$ . Let  $X$  represent the quality of the resources available to that

species.  $R$  is the maximum growth rate, and  $f(X)$  is a monotonically increasing function that asymptotically approaches unity for large  $X$ . The population in the next generation is

$$N_{t+1} = N_t R f(X_t).$$

If  $f$  is constant, we have exponential growth or decay, depending on whether  $Rf$  is greater or less than 1. We will model  $f$  by  $f(X_t) = X_t/(k + X_t)$ , where parameter  $k$  determines how rapidly  $f$  approaches its asymptotic value.

Now assume the total amount of food,  $S$ , does not change with time and that  $X$  depends on the per capita food supply  $S/N$  through a monotonically increasing function  $g$ :

$$X_{t+1} = X_t g(S/N_{t+1}).$$

A crucial assumption is that the current quality depends on both the present per-capita food supply and the quality in the previous generation. When there is more food available to the mother, it increases the reproductive rate of the mother. Ginzburg and Colyvan call this the “maternal effect.”

Model functions  $f$  and  $g$  by

$$\begin{aligned} N_{t+1} &= N_t R \frac{X_t}{k + X_t} \\ X_{t+1} &= X_t M \frac{S/N_{t+1}}{p + S/N_{t+1}}. \end{aligned}$$

(a) Show that with the change of variables  $n = pN/S$  and  $x = X/k$  the equations reduce to

$$\begin{aligned} n_{t+1} &= n_t R \frac{x_t}{1 + x_t} \\ x_{t+1} &= x_t M \frac{1}{1 + n_{t+1}}. \end{aligned}$$

(b) Use a spread sheet to model the behavior for a range of values of  $R$  and  $M$ , starting with  $R = 20$  and  $M = 10$ . Use initial conditions  $n_0 = x_0 = 1$ . If  $M > 1$ , explore what values of  $R$  lead to oscillations.

(c) Use the spread sheet to construct phase-plane plots of  $\ln(n)$  vs.  $\ln(x)$ .

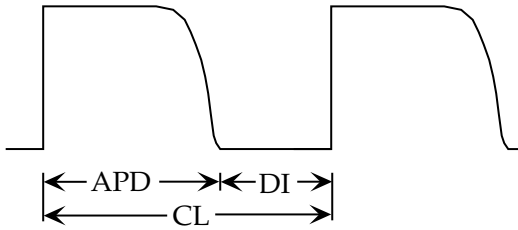
**Problem 36** Consider the two sets of data below, one produced by the logistic map and the other produced from a table of random numbers. Which is which?

Set 1	Set 2
0.9750	0.7464
0.0951	0.2349
0.3356	0.6017
0.8696	0.0213
0.4422	0.7935
0.9620	0.0336
0.1426	0.6476
0.4768	0.5630
0.9729	0.9116
0.1028	0.1748
0.3597	0.8706
0.8982	0.9058

**Problem 37** The onset of ventricular fibrillation in the heart can be understood in part as a property of cardiac “restitution.” The action potential duration (APD) depends on the previous diastolic interval (DI): the time from the end of the last action potential until the start of the next one. The relationship between APD and DI is called the “restitution curve.” In cardiac muscle, a typical restitution curve has the form

$$APD_{i+1} = 300 \left( 1 - e^{-DI_i/100} \right)$$

where all times are given in ms. Suppose we apply to the heart a series of stimuli, with period (or “cycle length”) CL.



Since  $APD + DI = CL$ , we have  $DI_{i+1} = CL - APD_{i+1}$ .

(a) Suppose we stimulate with a long cycle length ( $CL = 400$  ms). Using an initial value of  $DI_1 = 200$ , calculate  $APD_i$  and  $DI_i$  for ten iterations. What happens?

(b) Shorten the cycle length to  $CL = 300$  ms. Using the same  $DI_1$ , calculate  $APD_i$  and  $DI_i$  for ten iterations. What happens now? (In the jargon of cardiac electrophysiology, this behavior is often called “alternans”).

(c) Shorten the cycle length further to  $CL = 200$  ms. Using the same  $DI_1$ , calculate  $APD_i$  and  $DI_i$  for ten iterations. If  $DI_{i+1}$  is negative (corresponding to tissue so refractory that it fires no action potential), keep adding CL to it until it becomes positive before calculating the next APD. What happens now?

(d) Shorten the cycle length yet further to  $CL = 100$  ms. Using the same  $DI_1$ , calculate  $APD_i$  and  $DI_i$  for twenty iterations. What happens now?

Your results in part (d) should be chaotic, resembling ventricular fibrillation. We must not overinterpret this simple model, however, because fibrillation consists of propagating wave fronts, whereas this simple model does not include spatial effects. For a more detailed account of a model similar to this one, see Hastings et al. (2000).

**Problem 38** In Problem 37, the onset of alternans occurs when the slope of the restitution curve  $APD_{i+1} = 300(1 - e^{-DI_i/100})$  becomes greater than 1.

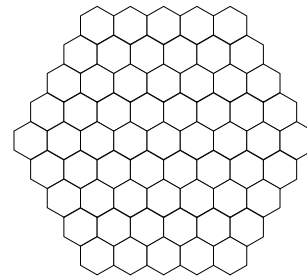
(a) Calculate the slope of the restitution curve  $d(APD)/d(DI)$  analytically.

(b) Set the slope equal to 1 and solve for the resulting value of DI. Use the restitution curve to determine the corresponding values of APD and CL.

(c) Calculate  $APD_i$  and  $DI_i$  for twenty iterations for CL 10% above and 10% below the value determined in part (b). What behaviors do you observe?

(d) Suppose you apply a drug to the heart that can change the restitution curve to  $APD_{i+1} = 300(1 - be^{-DI_i/100})$ . Plot APD as a function of DI for  $b = 0, 0.5, \text{ and } 1$ . What value of  $b$  ensures that the slope of the restitution curve is always less than 1? Garfinkel et al. (2000) have suggested that one way to prevent ventricular fibrillation is to use drugs that “flatten” the restitution curve.

**Problem 39** Elementary models of cellular excitable media (sometimes called “cellular automata”) provide valuable insight into the electrical behavior of the heart. Winfree (1987, pp. 106–107) describes one such model. A hexagonal array represents a sheet of cardiac tissue.



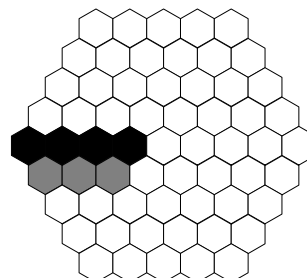
Each cell in the array can be in one of three states: excited (E), refractory (R), or quiescent (Q). A cell changes state by the following rules:

1. If in state E, then at the next time step it changes to state R,
2. If in state R, then at the next time step it changes to state Q,
3. If in state Q, then at the next time step it remains in state Q; unless one of its six nearest neighbors is in state E, in which case it changes to state E.

(a) Start with the central cell in state E, and the rest of the cells in state Q. What happens in subsequent time steps? You should get an outwardly propagating wave front. Let the simulation run long enough to see what happens when the wave front hits the edge of the array. Does it “reflect” off the edge? Does the tissue ever go to the state of all Q?

(b) Start with the top five and bottom five cells in state E, and the rest in state Q. What happens when the two resulting wave fronts collide? Does the tissue ever go to the state of all Q?

(c) Start with the four black cells in state E, the three gray cells in state R, and the rest in state Q.





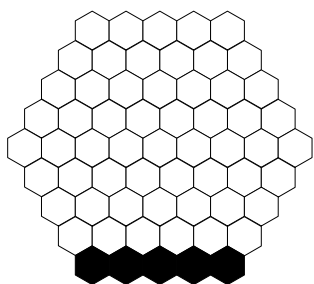
What happens? Does the tissue ever go to the state of all  $Q$ ? This result is called a “spiral wave,” and may be responsible for some heart arrhythmias, such as a “ventricular tachycardia.”

(d) In part (c), there is a special point called a “phase singularity” where cells in states  $E$ ,  $R$ , and  $Q$  all meet at one point. Find the phase singularities in the results of part (c). How many are there? Do they move?

**Problem 40** In the cellular excitable medium described in problem 39, what happens if you apply an electrical stimulus? The stimulus is described by a fourth rule:

4. A stimulus changes the state to  $E$ , regardless of the previous state.

Assume the stimulus is applied only to the central cell. Start with the initial condition



which will initiate a wave front propagating upwards. At a later time, apply the stimulus and see what happens. If the initial condition is  $t = 1$ , then try applying the stimulus at  $t = 4, 5$ , or  $6$ . Are there any situations in which you produce phase singularities? If so, how many? Is the timing of the stimulus important?

### Section 10.9

**Problem 41** By substitution show that  $w(t) = w_0 e^{-\gamma t} \cos \omega t$  can be a solution of the delay-differential equation, Eq. 10.41 if  $\gamma = (1/\tau) e^{\gamma t_d} \cos \omega t_d$ ,  $\omega = (1/\tau) e^{\gamma t_d} \sin \omega t_d$ . Introduce the dimensionless variables  $\alpha = t_d/\tau$ ,  $\xi = \omega t_d$ , and  $\eta = \gamma t_d$  and show that the result is the simultaneous equations

$$\xi = \alpha e^\eta \sin \xi, \quad \eta = \alpha e^\eta \cos \xi.$$

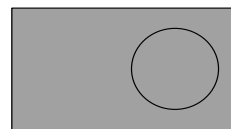
From these obtain the equivalent equations  $\eta = \xi \cot \xi$ . and  $\xi^2 = \alpha^2 e^{2\eta} - \eta^2$ . Show how these can be solved graphically if  $\alpha$  is known.

### Section 10.11

**Problem 42** Find an equation relating  $L$ , the total amount of light energy per second reaching the retina,  $I$ , the intensity of the light ( $W m^{-2}$ ), and  $R$ , the radius of the pupil. Calculate the gain  $G = \partial L / \partial R$  and the logarithmic gain  $g = (1/L)(\partial L / \partial R)$ . Consider the two cases shown in the figure.

(a) There is uniform illumination of the pupil.

(b) The rectangle of illumination partially overlaps the pupil so that the area within the pupil is  $a(R - b)$ .



### References

- Bartlett, A. A., and T. J. Braun (1983). Death in a hot tub: the physics of heat stroke. *Am. J. Phys.* **51**(2): 127–132.
- Begon, M., M. Mortimer, and D. J. Thompson (1996). *Population Ecology: A Unified Study of Animals and Plants*, 3rd ed. Cambridge, MA, Blackwell Science.
- Bub, G., A. Shrier, and L. Glass (2002). Spiral wave generation in heterogeneous excitable media. *Phys. Rev. Lett.* **88**.058101.
- Epstein, A. E., and R. E. Ideker (1995). Ventricular fibrillation. In D. P. Zipes and J. Jalife, eds. *Cardiac Electrophysiology: From Cell to Bedside*, 2nd ed. Philadelphia, Saunders, pp. 927–933.
- Epstein, I. R., K. Kustin, P. De Kepper, and M. Orban (1983). Oscillating chemical reactions. *Sci. Am.* March: 112–123.
- Fox, J. J., E. Bodenschatz, and R. F. Gilmour, Jr. (2002). Period-doubling instability and memory in cardiac tissue. *Phys. Rev. Lett.* **89**.138101.
- Garfinkel, A., M. L. Spano, W. L. Ditto, and J. N. Weiss (1992). Controlling cardiac chaos. *Science* **257**: 1230–1235.
- Garfinkel, A., Y.-H. Kim, O. Voroshilovsky, Z. Qu, J. R. Kil, M.-H. Lee, H. S. Karagueuzian, J. N. Weiss, and P.-S. Chen (2000). Preventing ventricular fibrillation by flattening cardiac restitution. *Proc. Natl. Acad. Sci. USA* **97**: 6061–6066
- Ginzburg, L., and M. Colyvan (2004). *Ecological Orbits: How Planets Move and Populations Grow*. Oxford. Oxford University Press.
- Glass, L., and M. C. Mackey (1988). *From Clocks to Chaos*. Princeton, NJ, Princeton University Press.
- Glass, L., Y. Nagai, K. Hall, M. Talajic, and S. Natel (2002). Predicting the entrainment of reentrant cardiac waves using phase resetting curves. *Phys. Rev. E*, **65**.021908.
- Guevara, M. R., L. Glass, and A. Shrier (1981). Phase-locking, period-doubling bifurcations and irregular dynamics in periodically stimulated cardiac cells. *Science* **214**: 1350–1353.

- Guyton, A. C., J. W. Crowell, and J. W. Moore (1956). Basic oscillating mechanism of Cheyne–Stokes breathing. *Am. J. Physiol.* **187**: 395–398.
- Hastings, H. M., F. H. Fenton, S. J. Evans, O. Homtomaroglu, J. Geetha, K. Gittelsohn, J. Nilson, and A. Garfinkel (2000). Alternans and the onset of ventricular fibrillation. *Phys. Rev. E* **62**: 4043–4048.
- Hayes, N. D. (1950). Roots of the transcendental equation associated with a certain difference-differential equation. *J. London Math. Soc.* **25**: 226–232.
- Hilborn, R. C. (2000). *Chaos and Nonlinear Dynamics*, 2nd ed. New York, Oxford University Press.
- Kaplan, D., and L. Glass (1995). *Understanding Nonlinear Dynamics*. New York, Springer-Verlag.
- Keener, J. P., and A. V. Panfilov (1995). Three-dimensional propagation in the heart: The effects of geometry and fiber orientation on propagation in the myocardium. In D. P. Zipes and J. Jalife, eds. *Cardiac Electrophysiology: From Cell to Bedside*, 2nd ed. Philadelphia, Saunders, pp. 335–348.
- Kho, M. C. K. (2000). *Physiological Control Systems: Analysis, Simulation and Estimation*. New York, IEEE.
- Mackey, M. C., and L. Glass (1977). Oscillation and chaos in physiological control systems. *Science* **197**: 287–289.
- May, R. M. (1976). Simple mathematical models with very complicated dynamics. *Nature (London)* **261**: 459–467.
- Mercader, M. A., D. C. Michaels, and J. Jalife (1995). Reentrant activity in the form of spiral waves in mathematical models of the sinoatrial node. In D. P. Zipes and J. Jalife, eds. *Cardiac Electrophysiology: From Cell to Bedside*, 2nd ed. Philadelphia, Saunders, pp. 389–403.
- Mielczarek, E. V., J. S. Turner, D. Leiter, and L. Davis (1983). Chemical clocks: Experimental and theoretical models of nonlinear behavior. *Am. J. Phys.* **51**(1): 32–42.
- Mines, G. R. (1914). On circulating excitation of heart muscles and their possible relation to tachycardia and fibrillation. *Trans. R. Soc. Can.* **4**: 43–53.
- Patton, H. D., A. F. Fuchs, B. Hille, A. M. Scher, and R. F. Steiner, eds. (1989). *Textbook of Physiology*, 21st ed. Philadelphia, Saunders.
- Pertsov, A. M., and J. Jalife (1995). Three-dimensional vortex-like reentry. In D. P. Zipes and J. Jalife, eds. *Cardiac Electrophysiology: From Cell to Bedside*, 2nd ed. Philadelphia, Saunders, pp. 403–410.
- Riggs, D. S. (1970). *Control Theory and Physiological Feedback Mechanisms*. Baltimore, Williams and Wilkins.
- Stark, L. (1957). A servoanalytic study of consensual pupil reflex to light. *J. Neurophys.* **20**: 17–26.
- Stark, L. (1968). *Neurological Control Systems: Studies in Bioengineering*. New York, Plenum, pp. 73–84.
- Stark, L. W. (1984). The pupil as a paradigm for neurological control systems. *IEEE Trans. Biomed. Eng.* **31**: 919–924.
- Strogatz, S. H. (1994). *Nonlinear Dynamics and Chaos*. Reading, MA, Addison-Wesley.
- Strogatz, S. (2003). *Sync: The Emerging Science of Spontaneous Order*. New York, Hyperion.
- Winfree, A. T. (1987). *When Time Breaks Down*. Princeton, NJ, Princeton University Press.
- Winfree, A. T. (1994a). Electrical turbulence in three-dimensional heart muscle. *Science* **266**: 1003–1006.
- Winfree, A. T. (1994b). Persistent tangled vortex rings in generic excitable media. *Nature* **371**: 233–236.
- Winfree, A. T. (1995). Theory of spirals. In D. P. Zipes and J. Jalife, eds. *Cardiac Electrophysiology: From Cell to Bedside*, 2nd ed., Philadelphia, Saunders, pp. 379–389.
- Winfree, A. T. (2001). *The Geometry of Biological Time*. 2nd ed. New York, Springer.
- Witkowski, F. X., K. M. Kavanagh, P. A. Penkoske, and R. Plonsey (1993). In vivo estimation of cardiac transmembrane current. *Circ. Res.* **72**(2): 424–439.
- Witkowski, F. X., R. Plonsey, P. A. Penkoske, and K. M. Kavanagh (1994). Significance of inwardly directed transmembrane current in determination of local myocardial electrical activation during ventricular fibrillation. *Circ. Res.* **74**(3): 507–524.
- Witkowski, F. X., K. M. Kavanagh, P. A. Penkoske, R. Plonsey, M. L. Spano, W. L. Ditto, and D. T. Kaplan (1995). Evidence for determinism in ventricular fibrillation. *Phys. Rev. Lett.* **75**(6): 1230–1233.

# The Method of Least Squares and Signal Analysis

This chapter deals with three common problems in experimental science. The first is fitting a discrete set of experimental data with a mathematical function. The function usually has some parameters that must be adjusted to give a “best” fit. The second is to detect a periodic change in some variable—a signal—which may be masked by random changes—noise—superimposed on the signal. The third is to determine whether sets of apparently un-systematic data are from a random process or a process governed by deterministic chaotic behavior.

These techniques are used in many fields, including physiology and biophysics. The fitting techniques lead naturally to Fourier series, which are used extensively in image reconstruction and image analysis. Using least squares or Fourier series normally requires extensive computation. Commercial packages for making these calculations are readily available. The problems at the end of the chapter are often artificially designed for simple computation, rather than being “real.” We hope that the chapter will help you develop some intuition for the techniques before you use the commercial packages.

This chapter is a self-contained discussion of signal analysis. It is a prerequisite to Chapter 12 on image reconstruction.

We will find that a periodic signal can be built up of sine waves of different frequencies, and that it is possible to speak of the *frequency spectrum* of a signal. The first five sections of the chapter show how to adjust the parameters in a polynomial or in a sum of sines and cosines to fit experimental data. Sections 11.5 and 11.6 discuss sine and cosine expansions for continuous periodic functions. Sections 11.7 and 11.8 introduce the cross-correlation and autocorrelation functions and their relation to the power spectrum. Sections 11.9 through 11.12 extend these techniques to pulses. Sections 11.13 and 11.14 introduce noise and the use of correlation functions to detect signals that are masked by noise.

Many linear feedback systems are most easily studied by how they respond to sinusoidal stimuli at various frequencies, and there are techniques using impulse or noise stimuli that provide the same information. Section 11.15 explains the frequency response of a linear system, and the next section describes the effect of a simple linear system on the power spectrum of Johnson noise. The next section introduces some of the concepts involved in testing data for chaotic behavior. Finally, Section 11.18 introduces a relatively new phenomenon, stochastic resonance, where introducing noise into a nonlinear system can enhance a desired effect.

## 11.1 The Method of Least Squares and Polynomial Regression

In this section we show how to approximate or “fit” a set of discrete data  $y_j$  with a polynomial function

$$y_j = y(x_j) = \sum_k a_k x_j^k.$$

Several criteria can be used to determine the “best” fit [Press *et al.* (1992), Sec. 15.7]; the one described in this chapter is called the *method of least squares*. Instead of immediately deriving the general polynomial result, we first consider the simple (and rather useless) fit  $y = x + b$  (the coefficient of  $x$  is unity), then the more useful linear fit  $y = ax + b$ .

### 11.1.1 The Simplest Example

Suppose that we wish to describe the data in Table 11.1 by a fitting function  $y(x)$ . A plot of the data suggests that a straight line will be a reasonable approximation to

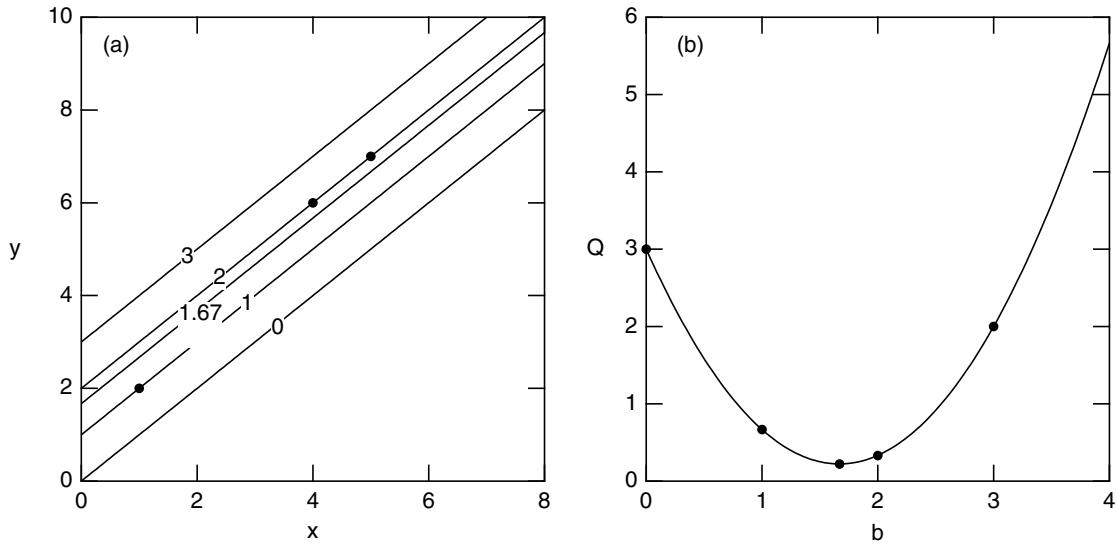


FIGURE 11.1. Fits to the data of Table 11.1 by a curve of the form  $y = x + b$ . (a) Plots of  $y$  vs.  $x$ . (b) Plot of  $Q$  vs  $b$ .  $Q$  is defined in Eq. 11.2.

TABLE 11.1. Sample data.

$x$	$y$
1	2
4	6
5	7

the data. For mathematical simplicity, we first try a line with unit slope but adjustable intercept:

$$y(x_j) = x_j + b. \tag{11.1}$$

Figure 11.1(a) plots  $y$  vs.  $x$  for different values of  $b$ . It is clear by inspection that the curves for  $b = 1$  and  $b = 2$  are closer to the points than those for  $b = 0$  or  $b = 3$ . For a quantitative measure of how good the fit is we will use the quantity

$$Q = \frac{1}{N} \sum_{j=1}^N [y_j - y(x_j)]^2, \tag{11.2}$$

which is called the *mean square error*. It is the square of the residuals [the differences between the measured values of  $y$  and the values of  $y$  calculated from the approximation to the data,  $y_j - y(x_j)$ ] summed over all  $N$  data points and divided by  $N$ . It is reminiscent of the variance, with the mean replaced by the fitting function  $y(x_j)$ . The least-squares technique adjusts the parameters in the function  $y(x_j)$  to make  $Q$  a minimum. Table 11.2 shows the steps in the calculation of  $Q$  for various values of  $b$ . Figure 11.1(b) shows how  $Q$  changes as  $b$  is changed.

It is tedious to calculate  $Q$  for many different values of  $b$ ; instead we can treat this as a maximum–minimum

problem in calculus. We write

$$\begin{aligned} Q &= \frac{1}{N} \sum_{j=1}^N (y_j - x_j - b)^2 \\ &= \frac{1}{N} [(y_1 - x_1 - b)^2 + (y_2 - x_2 - b)^2 + \dots]. \end{aligned}$$

The derivative is

$$\begin{aligned} \frac{dQ}{db} &= -\frac{1}{N} \sum_{j=1}^N 2(y_j - x_j - b) \\ &= \frac{1}{N} [-2(y_1 - x_1 - b) - 2(y_2 - x_2 - b) + \dots]. \end{aligned}$$

Setting this equal to zero to find the extremum gives

$$\sum_{j=1}^N y_j = \sum_{j=1}^N x_j + \sum_{j=1}^N b$$

or, not bothering to show explicitly that the index ranges over all the data points,

$$\sum_j y_j = \sum_j x_j + Nb.$$

Using this result for the example above gives  $15 = 10 + 3b$ , or  $b = 1.67$  for the smallest value of  $Q$ .

### 11.1.2 A Linear Fit

The previous example was rather artificial, because for simplicity we did not allow the slope of the line to vary. The maximum–minimum procedure is easily extended to

TABLE 11.2. Calculation of  $Q$  for the example of Eq. 11.1

Index				$b = 0$			$b = 1$			$b = 2$
$j$	$x_j$	$y_j$	$y(x_j)$	$[y_j - y(x_j)]^2$	$y(x_j)$	$[y_j - y(x_j)]^2$	$y(x_j)$	$[y_j - y(x_j)]^2$	$y(x_j)$	$[y_j - y(x_j)]^2$
1	1	2	1	1	2	0	3	1	3	1
2	4	6	4	4	5	1	6	0	6	0
3	5	7	5	4	6	1	7	0	7	0
Sum				9		2		1		
$Q$				3		0.67		0.33		

two or more parameters. If the fitting function is given by  $y = ax + b$ , then  $Q$  becomes

$$Q = \frac{1}{N} \sum_{j=1}^N (y_j - ax_j - b)^2.$$

At the minimum, both  $\partial Q/\partial a = 0$  and  $\partial Q/\partial b = 0$ . The former gives

$$\frac{\partial Q}{\partial a} = \frac{2}{N} \sum_{j=1}^N (y_j - ax_j - b)(-x_j) = 0$$

or

$$\sum_j x_j y_j - a \sum_j x_j^2 - b \sum_j x_j = 0. \tag{11.3}$$

The latter gives

$$\frac{\partial Q}{\partial b} = \frac{2}{N} \sum_{j=1}^N (y_j - ax_j - b)(-1) = 0$$

or

$$\sum_{j=1}^N y_j - a \sum_{j=1}^N x_j - Nb = 0. \tag{11.4}$$

For the example in Table 11.1  $\sum x_j = 10$ ,  $\sum y_j = 15$ ,  $\sum x_j^2 = 42$ , and  $\sum x_j y_j = 61$ . Therefore, Eqs. 11.3 and 11.4 become  $42a + 10b = 61$  and  $10a + 3b = 15$ . These can be easily solved to give  $a = 1.27$  and  $b = 0.77$ . The best straight-line fit to the data of Table 11.1 is  $y = 0.77 + 1.27x$ . The value of  $Q$ , calculated from Eq. 11.2, is 0.013. The best fit is plotted in Fig. 11.2. It is considerably better than the fit with the slope constrained to be one.

A general expression for the solution to Eqs. 11.3 and 11.4 is

$$a = \frac{N \left( \sum_{j=1}^N x_j y_j \right) - \left( \sum_{j=1}^N x_j \right) \left( \sum_{j=1}^N y_j \right)}{N \left( \sum_{j=1}^N x_j^2 \right) - \left( \sum_{j=1}^N x_j \right)^2}, \tag{11.5a}$$

$$b = \frac{\sum_{j=1}^N y_j}{N} - a \frac{\sum_{j=1}^N x_j}{N} \equiv \bar{y} - a\bar{x}. \tag{11.5b}$$

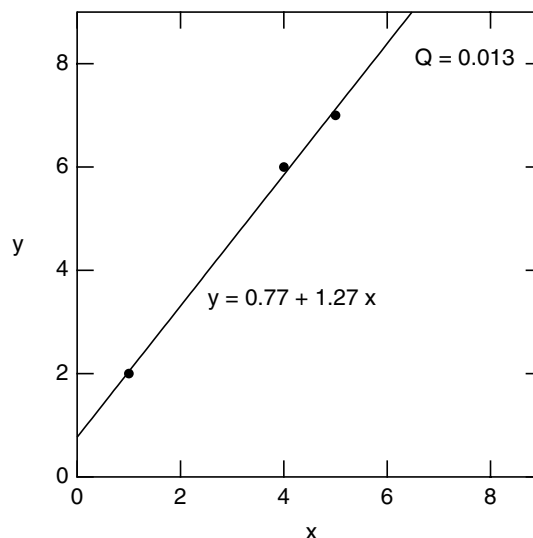


FIGURE 11.2. The best fit to the data of Table 11.1 with the function  $y = ax + b$ . Both the slope and the intercept have been chosen to minimize  $Q$ .

where  $\bar{x}$  and  $\bar{y}$  are the means. In doing computations where the range of data is small compared to the mean, better numerical accuracy can be obtained from

$$a = S_{xy}/S_{xx}, \tag{11.5c}$$

using the sums

$$S_{xx} = \sum_{j=1}^N (x_j - \bar{x})^2, \tag{11.5d}$$

and

$$S_{xy} = \sum_{j=1}^N (x_j - \bar{x})(y_j - \bar{y}). \tag{11.5e}$$

### 11.1.3 A Polynomial Fit

The method of least squares can be extended to a polynomial of arbitrary degree. The only requirement is that the number of adjustable parameters (which is one more

than the degree of the polynomial) be less than the number of data points. If this requirement is not met, the equations cannot be solved uniquely; see Problem 8. If the polynomial is written as

$$y(x_j) = a_0 + a_1x_j + a_2x_j^2 + \dots + a_nx_j^n = \sum_{k=0}^n a_kx_j^k, \quad (11.6)$$

then the expression for the mean square error is

$$Q = \frac{1}{N} \sum_{j=1}^N \left( y_j - \sum_{k=0}^n a_kx_j^k \right)^2. \quad (11.7)$$

Index  $j$  ranges over the data points; index  $k$  ranges over the terms in the polynomial. This expression for  $Q$  can be differentiated with respect to one of the  $n + 1$  parameters, say,  $a_m$ :

$$\frac{\partial Q}{\partial a_m} = \frac{2}{N} \sum_{j=1}^N \left[ \left( y_j - \sum_{k=0}^n a_kx_j^k \right) (-x_j^m) \right].$$

Setting this derivative equal to zero gives

$$\sum_{j=1}^N y_jx_j^m = \sum_{k=0}^n \sum_{j=1}^N a_kx_j^kx_j^m = \sum_{k=0}^n a_k \sum_{j=1}^N x_j^{k+m}.$$

This is one of the equations we need. Doing the same thing for all values of  $m$ ,  $m = 0, 1, 2, \dots, n$ , we get  $n + 1$  equations that must be solved simultaneously for the  $n + 1$  parameters  $a_0, a_1, \dots, a_n$ .

For  $m = 0$ :

$$\sum_{j=1}^N y_j = Na_0 + a_1 \sum_{j=1}^N x_j + a_2 \sum_{j=1}^N x_j^2 + \dots + a_n \sum_{j=1}^N x_j^n. \quad (11.8a)$$

For  $m = 1$ :

$$\begin{aligned} \sum_{j=1}^N x_jy_j &= a_0 \sum_{j=1}^N x_j + a_1 \sum_{j=1}^N x_j^2 + a_2 \sum_{j=1}^N x_j^3 \\ &+ \dots + a_n \sum_{j=1}^N x_j^{n+1}. \end{aligned} \quad (11.8b)$$

For  $m = n$ :

$$\begin{aligned} \sum_{j=1}^N x_j^n y_j &= a_0 \sum_{j=1}^N x_j^n + a_1 \sum_{j=1}^N x_j^{n+1} + a_2 \sum_{j=1}^N x_j^{n+2} \\ &+ \dots + a_n \sum_{j=1}^N x_j^{2n}. \end{aligned} \quad (11.8c)$$

Solving these equations is not as formidable a task as it seems. Given the data points  $(x_j, y_j)$ , the sums are all evaluated. When these numbers are inserted in Eqs. 11.8, the result is a set of  $n + 1$  simultaneous equations in the  $n + 1$  unknown coefficients  $a_k$ . This technique is called *linear least-squares fitting of a polynomial* or *polynomial regression*. Routines for solving the simultaneous equations or for carrying out the whole procedure are readily available.

### 11.1.4 Variable Weighting

The least-squares technique described here gives each data point the same weight. If some points are measured more accurately than others, they should be given more weight. This can be done in the following way. If there is an associated error  $\delta y_j$  for each data point, then one can weight each data point inversely as the square of the error and minimize

$$Q = \frac{1}{N} \sum_{j=1}^N \frac{[y_j - y(x_j)]^2}{(\delta y_j)^2}. \quad (11.9)$$

It is easy to show that the effect is to add a factor of  $(1/\delta y_j)^2$  to each term in the sums in Eqs. 11.8 [Gatland (1993)]. This assumes that errors exist only in the  $y$  values. If there are errors in the  $x$  values as well, it is possible to make an approximate correction based on an effective error in the  $y$  values [Orear (1982)] or to use an iterative but exact least-squares method [Lybanon (1984)]. The treatment of unequal errors has been discussed by Gatland (1993) and by Gatland and Thompson (1993).

## 11.2 Nonlinear Least Squares

The linear least-squares technique can be used to fit data with a single exponential  $y = ae^{-bx}$ , where  $a$  and  $b$  are to be determined. Take logarithms of each side of the equation:

$$\begin{aligned} \log y &= \log a - bx \log e, \\ v &= a' - b'x. \end{aligned}$$

This can be fit by the linear equation, determining constants  $a'$  and  $b'$  using Eqs. 11.5.

Things are not so simple if there is reason to believe that the function might be a sum of exponentials:

$$y = a_1e^{-b_1x} + a_2e^{-b_2x} + \dots$$

When the derivatives of this function are set equal to zero, the equations in  $a_1, a_2$ , etc., will be linear if we assume that the values of the  $b_k$  are known. However, the equations for determining the  $b$ 's will be transcendental equations that are quite difficult to solve. With a sum of two or more exponentials, taking logs does not avoid the problem.

The problem can be solved using the technique of *non-linear least squares*. In its simplest form, one makes an initial guess for each parameter<sup>1</sup>  $b_{10}, b_{20}, \dots, b_{k0}$  and says that the correct value of each  $b$  is given by  $b_k = b_{k0} + h_k$ . The calculated value of  $y$  is written as a Taylor's-series expansion with all the derivatives evaluated for  $b_{10}, b_{20}, \dots$ :

$$y(x_j; b_1, b_2, \dots) = y(x_j; b_{10}, b_{20}, \dots) + \frac{\partial y}{\partial b_1} h_1 + \frac{\partial y}{\partial b_2} h_2 + \dots$$

<sup>1</sup>The parameters  $a_k$  can either be included in the parameter list, or the values of  $a_k$  for each trial set  $b_k$  can be determined by linear least squares.

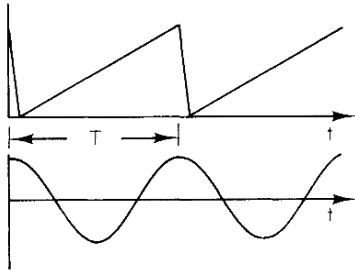


FIGURE 11.3. Two different periodic functions.

Since  $y$  and its derivatives can be evaluated using the current guess for each  $b$ , the expression is linear in the  $h_k$ , and the linear least-squares technique can be used to determine the values of the  $h_k$  that minimize  $Q$ . After each  $h_k$  has been determined, the revised values  $b_k = b_{k0} + h_k$  are used as the initial guesses, and the process is repeated until a minimum value of  $Q$  is found. The technique is not always stable; it can overshoot and give too large a value for  $h_k$ . There are many ways to improve the process to ensure more rapid convergence. The most common is called the Levenberg–Marquardt method [see Bevington and Robinson (1992) or Press *et al.* (1992)].

### 11.3 The Presence of Many Frequencies in a Periodic Function

A function  $y$  that repeats itself after a time<sup>2</sup>  $T$  is said to be *periodic* with period  $T$ . The mathematical description of this periodicity is

$$y(t + T) = y(t). \tag{11.10}$$

Two examples of functions with period  $T$  are shown in Fig. 11.3. One of these functions is a sine wave,  $y(t) = A \sin(\omega_0 t - \phi)$ , where  $A$  is the amplitude,  $\omega_0$  is the angular frequency, and  $\phi$  is the phase of the function. Changing the amplitude changes the height of the function. Changing the phase shifts the function along the time axis. The sine function repeats itself when the argument shifts by  $2\pi$  radians. It repeats itself after time  $T$ , where  $\omega_0 T = 2\pi$ . Therefore the angular frequency is related to the period by

$$\omega_0 = \frac{2\pi}{T}. \tag{11.11}$$

(The units of  $\omega_0$  are radian  $s^{-1}$ , but radians are dimensionless.) It is completely equivalent to write the function in terms of the frequency as  $y(t) = A \sin(2\pi f_0 t - \phi)$ . The

<sup>2</sup>Although we speak of  $t$  and time, the technique can be applied to any independent variable if the dependent variable repeats as in Eq. 11.10. Zebra stripes are (almost) periodic functions of position.

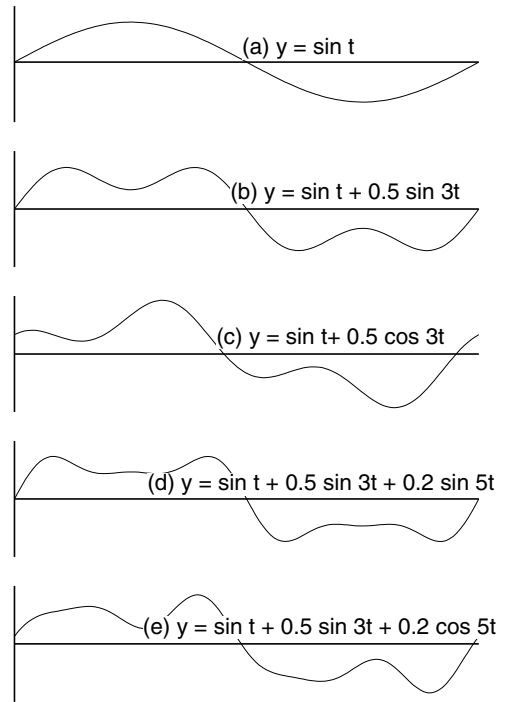


FIGURE 11.4. Various periodic signals made by adding sine waves that are harmonically related. Each signal has an angular frequency  $\omega_0 = 1$  and a period  $T = 2\pi$ .

frequency  $f_0$  is the number of cycles per second. Its units are  $s^{-1}$  or hertz (Hz) (hertz is not used for angular frequency):

$$f_0 = \frac{1}{T} = \frac{\omega_0}{2\pi}. \tag{11.12}$$

It is possible to write function  $y$  as a sum of a sine term and a cosine term instead of using phase  $\phi$ :

$$\begin{aligned} y(t) &= A \sin(\omega_0 t - \phi) = A(\sin \omega_0 t \cos \phi - \cos \omega_0 t \sin \phi) \\ &= (A \cos \phi) \sin \omega_0 t - (A \sin \phi) \cos \omega_0 t \\ &= S \sin \omega_0 t - C \cos \omega_0 t. \end{aligned} \tag{11.13}$$

The upper function graphed in Fig. 11.3 also has period  $T$ .

*Harmonics* are integer multiples of the fundamental frequency. They have the time dependence  $\cos(k\omega_0 t)$  or  $\sin(k\omega_0 t)$ , where  $k = 2, 3, 4, \dots$ . These also have period  $T$ . (They also have shorter periods, but they still satisfy the definition Eq. 11.10 for a function of period  $T$ .)

We can generate periodic functions of different shapes by combining various harmonics. Different combinations of the fundamental, third harmonic, and fifth harmonic are shown in Fig. 11.4. In this figure, (a) is a pure sine wave, (b) and (c) have some third harmonic added with a different phase in each case, and (d) and (e) show the addition of a fifth harmonic term to (b) with different phases.

An *even function* is one for which  $y(t) = y(-t)$ . For an *odd function*,  $y(t) = -y(-t)$ . The cosine is even, and the sine is odd. A sum of sine terms gives an odd function. A sum of cosine terms gives an even function.

## 11.4 Fourier Series for Discrete Data

### 11.4.1 Introducing the Fourier Series

The ability to adjust the amplitude of sines and cosines to approximate a specific shape suggests that discrete periodic data can be fitted by a function of the form

$$\begin{aligned}
 y(t_j) &= a_0 + \sum_{k=1}^n a_k \cos(k\omega_0 t_j) + \sum_{k=1}^n b_k \sin(k\omega_0 t_j) \\
 &= a_0 + \sum_{k=1}^n a_k \cos(k2\pi f_0 t_j) + \sum_{k=1}^n b_k \sin(k2\pi f_0 t_j).
 \end{aligned}
 \tag{11.14}$$

It is important to note that if we have a set of data to fit, in some cases we may not know the actual period of the data; we sample for some interval of length  $T$ . In that case the period  $T = 2\pi/\omega_0$  is a characteristic of the fitting function that we calculate, not of the data being fitted.

There are  $2n + 1$  parameters ( $a_0; a_1, \dots, a_n; b_1, \dots, b_n$ ). Since there are  $N$  independent data points, there can be at most  $N$  independent coefficients. Therefore,  $2n + 1 \leq N$ , or

$$n \leq \frac{N - 1}{2}.
 \tag{11.15}$$

This means that there must be at least two samples per period at the highest frequency present. This is known as the *Nyquist sampling criterion*.

If the least-squares criterion is used to determine the parameters, Eq. 11.14 is a *Fourier-series* representation of the data. Using the least-squares criterion to determine the coefficients to fit  $N$  data points requires minimizing the mean square residual

$$Q = \frac{1}{N} \sum_{j=1}^N \left[ y_j - a_0 - \sum_{k=1}^n a_k \cos(k\omega_0 t_j) - \sum_{k=1}^n b_k \sin(k\omega_0 t_j) \right]^2.
 \tag{11.16}$$

The derivatives that must be set to zero are

$$\begin{aligned}
 \frac{\partial Q}{\partial a_0} &= -\frac{2}{N} \sum_{j=1}^N \left[ \left( y_j - a_0 - \sum_{k=1}^n a_k \cos(k\omega_0 t_j) - \sum_{k=1}^n b_k \sin(k\omega_0 t_j) \right) (1) \right],
 \end{aligned}$$

$$\begin{aligned}
 \frac{\partial Q}{\partial a_m} &= -\frac{2}{N} \sum_{j=1}^N \left[ \left( y_j - a_0 - \sum_{k=1}^n a_k \cos(k\omega_0 t_j) - \sum_{k=1}^n b_k \sin(k\omega_0 t_j) \right) \cos(m\omega_0 t_j) \right],
 \end{aligned}$$

and

$$\begin{aligned}
 \frac{\partial Q}{\partial b_m} &= -\frac{2}{N} \sum_{j=1}^N \left[ \left( y_j - a_0 - \sum_{k=1}^n a_k \cos(k\omega_0 t_j) - \sum_{k=1}^n b_k \sin(k\omega_0 t_j) \right) \sin(m\omega_0 t_j) \right].
 \end{aligned}$$

Setting each derivative equal to zero and interchanging the order of the summations give  $2n + 1$  equations analogous to Eq. 11.8. The first is

$$\begin{aligned}
 \sum_{j=1}^N y_j &= Na_0 + \sum_{k=1}^n a_k \sum_{j=1}^N \cos(k\omega_0 t_j) \\
 &+ \sum_{k=1}^n b_k \sum_{j=1}^N \sin(k\omega_0 t_j).
 \end{aligned}
 \tag{11.17}$$

There are  $n$  equations of the form

$$\begin{aligned}
 \sum_{j=1}^N y_j \cos(m\omega_0 t_j) &= a_0 \sum_{j=1}^N \cos(m\omega_0 t_j) \\
 &+ \sum_{k=1}^n a_k \sum_{j=1}^N \cos(k\omega_0 t_j) \cos(m\omega_0 t_j) \\
 &+ \sum_{k=1}^n b_k \sum_{j=1}^N \sin(k\omega_0 t_j) \cos(m\omega_0 t_j)
 \end{aligned}
 \tag{11.18}$$

for  $m = 1, \dots, n$ , and  $n$  more of the form

$$\begin{aligned}
 \sum_{j=1}^N y_j \sin(m\omega_0 t_j) &= a_0 \sum_{j=1}^N \sin(m\omega_0 t_j) \\
 &+ \sum_{k=1}^n a_k \sum_{j=1}^N \cos(k\omega_0 t_j) \sin(m\omega_0 t_j) \\
 &+ \sum_{k=1}^n b_k \sum_{j=1}^N \sin(k\omega_0 t_j) \sin(m\omega_0 t_j).
 \end{aligned}
 \tag{11.19}$$

Since the  $t_j$  are known, each of the sums over the data points (index  $j$ ) on the right-hand side can be evaluated independent of the  $y_j$ .

### 11.4.2 Equally Spaced Data Points Simplify the Equations

If the data points are equally spaced, the equations become much simpler. There are  $N$  data points spread out



over an interval  $T$ :  $t_j = jT/N = 2\pi j/N\omega_0$ ,  $j = 1, \dots, N$ . The arguments of the sines and cosines are of the form  $(2\pi jk/N)$ . One can show that

$$\sum_{j=1}^N \cos\left(\frac{2\pi jk}{N}\right) = \begin{cases} N, & k = 0 \text{ or } k = N, \\ 0 & \text{otherwise} \end{cases} \quad (11.20)$$

$$\sum_{j=1}^N \sin\left(\frac{2\pi jk}{N}\right) = 0, \quad \text{for all } k, \quad (11.21)$$

$$\sum_{j=1}^N \cos\left(\frac{2\pi jk}{N}\right) \cos\left(\frac{2\pi jm}{N}\right) = \begin{cases} N/2, & k = m \text{ or } k = N - m, \\ 0 & \text{otherwise,} \end{cases} \quad (11.22)$$

$$\sum_{j=1}^N \sin\left(\frac{2\pi jk}{N}\right) \sin\left(\frac{2\pi jm}{N}\right) = \begin{cases} N/2, & k = m, \\ -N/2, & k = N - m, \\ 0 & \text{otherwise,} \end{cases} \quad (11.23)$$

$$\sum_{j=1}^N \sin\left(\frac{2\pi jk}{N}\right) \cos\left(\frac{2\pi jm}{N}\right) = 0 \text{ for all } k. \quad (11.24)$$

Because of these properties, Eqs. 11.17–11.19 become a set of independent equations when the data are equally spaced:

$$a_0 = \frac{1}{N} \sum_{j=1}^N y_j, \quad (11.25a)$$

$$a_m = \frac{2}{N} \sum_{j=1}^N y_j \cos\left(\frac{2\pi jm}{N}\right), \quad (11.25b)$$

$$b_m = \frac{2}{N} \sum_{j=1}^N y_j \sin\left(\frac{2\pi jm}{N}\right). \quad (11.25c)$$

### 11.4.3 The Standard Form for the Discrete Fourier Transform

It is customary to change the notation to make the equations more symmetric. Figure 11.5 shows the four different times corresponding to  $N = 4$  with  $j = 1, 2, 3, 4$ . Because of the periodicity of the sines and cosines,  $j = N$  gives exactly the same value of a sine or cosine as does  $j = 0$ . Therefore, if we reassign the data point corresponding to  $j = N$  to have the value  $j = 0$  and sum from 0 to  $N - 1$ , the sums will be unchanged:

$$a_0 = \frac{1}{N} \sum_{j=0}^{N-1} y_j, \quad (11.26a)$$

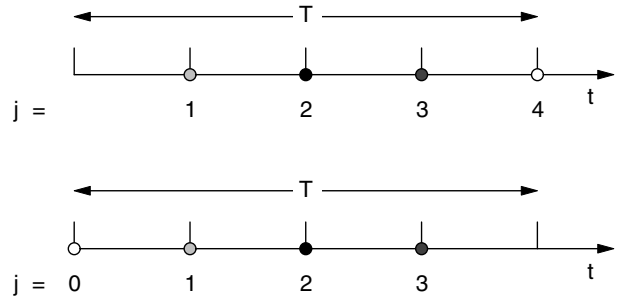


FIGURE 11.5. A case where  $N = 4$ . The values of time are spaced by  $T/N$  and distributed uniformly. In the top case the values of  $j$  range from 1 to  $N$ . In the lower case they range from 0 to  $N - 1$ . The values of all the trigonometric functions are the same for  $j = 0$  and for  $j = N$ .

$$a_m = \frac{2}{N} \sum_{j=0}^{N-1} y_j \cos\left(\frac{2\pi jm}{N}\right), \quad (11.26b)$$

$$b_m = \frac{2}{N} \sum_{j=0}^{N-1} y_j \sin\left(\frac{2\pi jm}{N}\right). \quad (11.26c)$$

For equally spaced data the function can be written as

$$y_j = y(t_j) = a_0 + \sum_{k=1}^n a_k \cos\left(\frac{2\pi jk}{N}\right) + \sum_{k=1}^n b_k \left(\frac{2\pi jk}{N}\right). \quad (11.26d)$$

You can show (see the problems at the end of this chapter) that the symmetry and antisymmetry in Eqs. 11.22 and 11.23 for  $k = N - m$  means that Eqs. 11.25 and 11.26 for  $k > N/2$  repeat those for  $k < N/2$ . We can use this fact to make the equations more symmetric by changing the factor in front of the summations in Eqs. 11.26b and 11.26c to be  $1/N$  instead of  $2/N$  and extending the summation in Eq. 11.26d all the way to  $n = N - 1$ . Since  $\cos(0) = 1$  and  $\sin(0) = 0$ , we can include the term  $a_0$  by including  $k = 0$  in the sum. We then have the set of equations

$$y_j = y(t_j) = \sum_{k=0}^{N-1} a_k \cos\left(\frac{2\pi jk}{N}\right) + \sum_{k=0}^{N-1} b_k \sin\left(\frac{2\pi jk}{N}\right), \quad (11.27a)$$

$$a_k = \frac{1}{N} \sum_{j=0}^{N-1} y_j \cos\left(\frac{2\pi jk}{N}\right), \quad (11.27b)$$

$$b_k = \frac{1}{N} \sum_{j=0}^{N-1} y_j \sin\left(\frac{2\pi jk}{N}\right). \quad (11.27c)$$

This set of equations is the usual form for the *discrete Fourier transform*. We will continue to use our earlier form, Eqs. 11.26, in the rest of this chapter.

### 11.4.4 Complex Exponential Notation

The Fourier transform is usually written in terms of complex exponentials. We have avoided using complex exponentials. They are not necessary for anything done in this

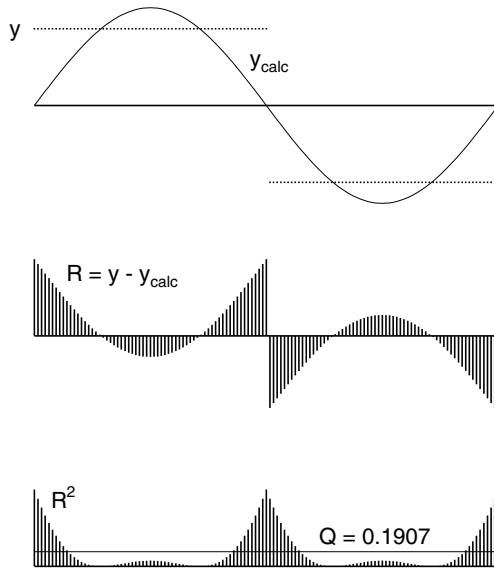


FIGURE 11.6. A square wave  $y(t_j)$  and the calculated function  $y(t) = b_1 \sin(\omega_0 t)$  are shown, along with the residuals and the squares of the residuals for each point. The value of  $b_1$  is  $4/\pi$ , which minimizes  $Q$  for that term.

book. The sole advantage of complex exponentials is to simplify the notation. The actual calculations must be done with real numbers. Since you will undoubtedly see complex notation in other books, the notation is included here for completeness.

The numbers that we have been using are called real numbers. The number  $i = \sqrt{-1}$  is called an *imaginary number*. A combination of a real and imaginary number is called a *complex number*. The remarkable property of imaginary numbers that make them useful in this context is that

$$e^{i\theta} = \cos \theta + i \sin \theta. \tag{11.28}$$

If we define the complex number  $Y_k = a_k - ib_k$ , we can write Eqs. 11.27 as

$$Y_k = \frac{1}{N} \sum_{j=0}^{N-1} y_j e^{-i2\pi jk/N} \tag{11.29a}$$

and

$$y_j = \sum_{k=0}^{N-1} Y_k e^{i2\pi jk/N}. \tag{11.29b}$$

Since our function  $y$  is assumed to be real, in the second equation we keep only the real part of the sum. To repeat: this gives only a more compact notation. It does not save in the actual calculations.

#### 11.4.5 Example: The Square Wave

Figures 11.6–11.9 show fits to a square wave with 128 data points. The function is  $y_j = 1, j = 0, \dots, 63$  and  $y_j = -1,$

TABLE 11.3. Fourier coefficients obtained for a square wave fit.

Term $k$	$a_k$	$b_k$
0	0.000	
1	-0.031	1.273
2	0.000	0.000
3	-0.031	0.424
4	0.000	0.000
5	-0.031	0.253
6	0.000	0.000
7	-0.031	0.181

$j = 64, \dots, 127$ . This is an odd function of  $t$ . Therefore, the series should contain only sine terms; all  $a_k$  should be zero. The calculated coefficients are shown in Table 11.3. Some of the  $a_k$  values are small but not exactly zero. This is due to the finite number of data points; the  $a_k$  become smaller as  $N$  is increased. The even values of the  $b_k$  vanish. We will see why below.

Figure 11.6 shows the square wave as dots and  $y(x)$  as a smooth curve when  $b_1 = 1.273$  and all the other coefficients are zero. This provides the minimum  $Q$  obtainable with a single term. Figure 11.7 shows why  $Q$  is larger for any other value of  $b_1$ . Figure 11.8 shows the terms for  $k = 1$  and  $k = 3$ . The value of  $Q$  is further reduced. Figure 11.9 shows why even terms do not reduce  $Q$ . In this case  $b_2 = 0.5$  has been added to  $b_1$ . The fit is improved for the regions  $0 < t < T/4$  and  $3T/4 < t < T$ , but between those regions the fit is made worse.

#### 11.4.6 Example: When the Sampling Time Is Not a Multiple of the Period of the Signal

The discussion just after Eq. 11.14 pointed out that in some cases we may not know the actual period and fundamental frequency  $\omega_0$  of the data. If we do know the actual period and the data points  $y_j$  are a sine or cosine with exact frequency  $\omega_0$  or a harmonic, and if no random errors are superimposed on the data, then only the coefficients corresponding to those frequencies will be nonzero. The reason is that if the function is exactly periodic, then by sampling for one period we have effectively sampled for an infinite time.

If the measuring duration  $T$  is not an integral multiple of the period of the signal—that is, the frequency of the signal  $y$  is not an exact harmonic of  $\omega_0$ —then the Fourier series contains terms at several frequencies. This is shown in Figs. 11.10 and 11.11 for the data  $y_j = \sin[3.3 \times 2\pi j/N]$ . Figure 11.10 shows the  $y_j$  for  $N = 20$  and  $N = 80$  samples during the period of the measurement. For 20 samples,  $n = 9$ ; for 80 samples,  $n = 39$ . Figure 11.11 shows  $(a_k^2 + b_k^2)^{1/2}$  for both sample sets for  $k = 0$  to 9, calculated using Eqs. 11.26. For

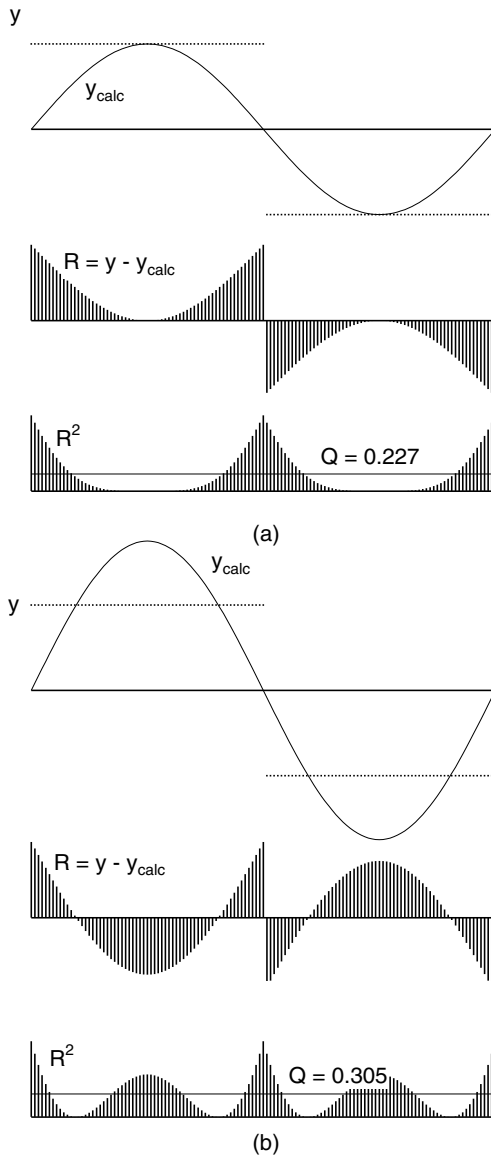


FIGURE 11.7. A single term is used to approximate the square wave. (a)  $b_1 = 1.00$ , which is too small a value. (b)  $b_1 = 1.75$ , which is too large. In both cases  $Q$  is larger than the minimum value for a single term, shown in Fig. 11.6.

80 samples, the value of  $(a_k^2 + b_k^2)^{1/2}$  is very small for  $k > 9$  and is not plotted. The frequency spectrum is virtually independent of the number of samples. There is a zero-frequency component because there is a net positive area under the curve. The largest amplitude occurs for  $k = 3$ . If one imagines a smooth curve drawn through the histogram, its peak would be slightly above  $k = 3$ . We will see later that the width of this curve depends on the duration of the measurement,  $T$ .

Figure 11.12 shows the fit to the data of Fig. 11.10a. Since the data points had no errors, the fitting function with 20 parameters passes through each of the 20 data points. However, it does not match  $y$  of Fig. 11.10a at

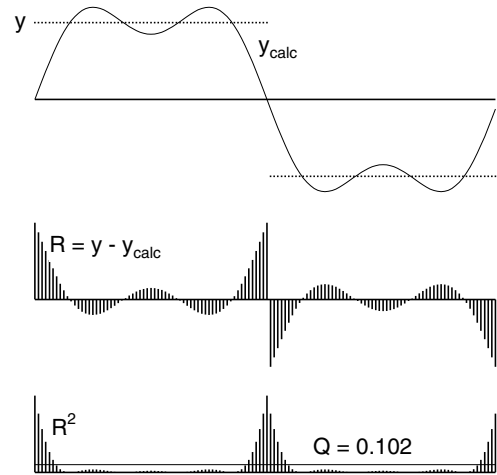


FIGURE 11.8. Terms  $b_1$  and  $b_3$  have their optimum values.  $Q$  is smaller than in Fig. 11.6.

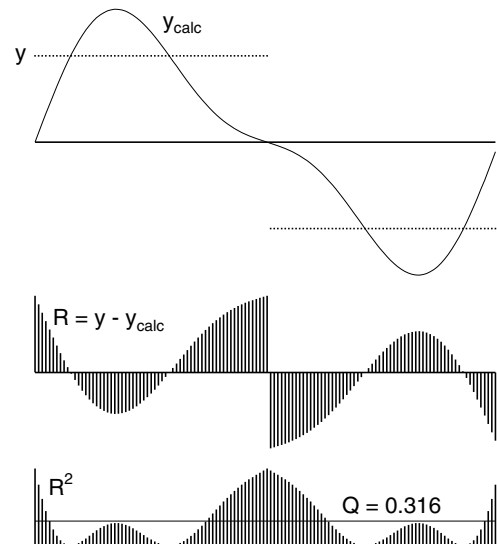


FIGURE 11.9. This figure shows why even terms do not contribute. A term  $b_2 = 0.5$  has been added to a term with the correct value of  $b_1$ . It improves the fit for  $t < T/4$  and  $t > 3T/4$  but makes it worse between  $T/4$  and  $3T/4$ .

other points. Note particularly the difference between the function near  $j = 1$  and near  $j = 19$ .

### 11.4.7 Example: Spontaneous Births

Figure 11.13 shows the number of spontaneous births per hour vs. local time of day for 600,000 live births in various parts of the world. The basic period is 24 hr; there is also a component with  $k = 3$  ( $T = 8$  hr). These data were reported by Kaiser and Halberg (1962). More recent data show peaks at different times [Anderka *et al.* (2000)]. Changes might be due to a difference in the duration of labor.

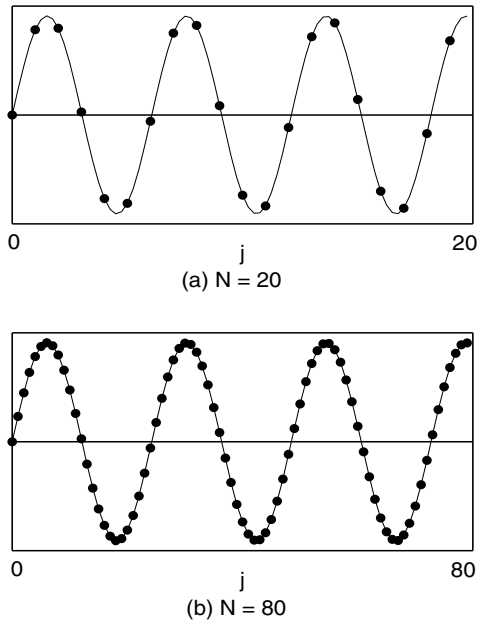


FIGURE 11.10. Sine wave  $y_j = \sin [3.3 \times 2\pi j/N]$  (a) with 20 data points and (b) with 80 data points. The sampling time is not an integral number of periods.

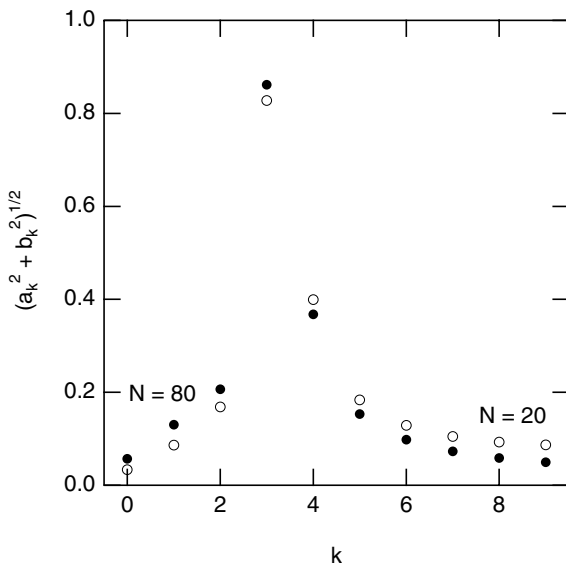


FIGURE 11.11. The amplitude of the mixed sine and cosine coefficients  $(a_k^2 + b_k^2)^{1/2}$  vs  $k$  for the function  $y_j = \sin 3.3 \times 2\pi j/N$ . The signal is sampled for 20 (open circles) or 80 (solid circles) data points. The amplitude spectrum is nearly independent of the number of samples.

#### 11.4.8 Example: Photosynthesis in Plants

Tobacco plant leaves were exposed to white light similar to sunlight, with the amplitude varying sinusoidally with a frequency  $\omega_0$  corresponding to a period of 60 or 80 s [Nedbal and Březina (2002)]. Fluorescence measurements showed an oscillation with predominant frequencies of  $\omega_0$ ,

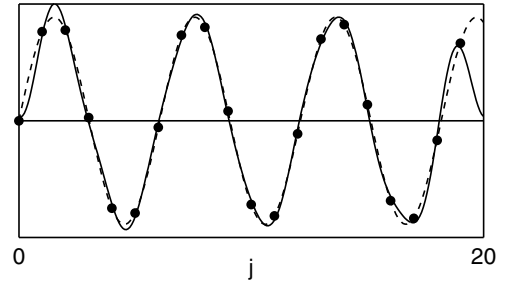


FIGURE 11.12. The solid line shows the calculated fit for the 20 data points in Fig. 11.10a. The dashed line is the same as the solid line in Fig. 11.10.

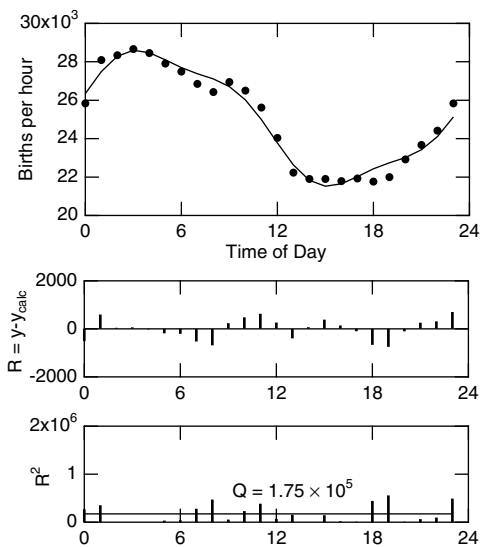


FIGURE 11.13. Data on the number of spontaneous births per hour, fit with terms having a period of 24 hr and 8 hr.

$2\omega_0$ , and  $3\omega_0$ . This is shown in Fig. 11.14. The authors present a feedback model, very similar to those in Sections 10.10.6 and 11.15. A nonlinearity in the model is responsible for generating the second and third harmonics.

#### 11.4.9 Pitfalls of Discrete Sampling: Aliasing

We saw in the preceding section that  $N$  samples in time  $T$  allow the determination of unique Fourier coefficients only for the terms from  $k = 0$  to  $n = (N - 1)/2$ . This means that for a sampling interval  $T/N$ , the maximum angular frequency is  $(N - 1)\omega_0/2$ . The period of the highest frequency that can be determined is  $T_{\min} = 2T/(N - 1)$ . This is approximately twice the spacing of the data points. One must sample at least twice per period to determine the coefficient at a particular frequency.

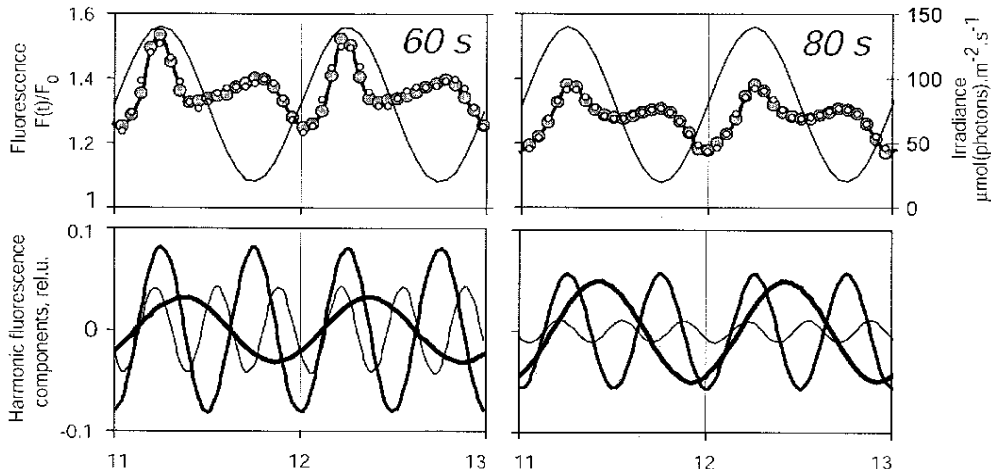


FIGURE 11.14. Tobacco leaves were exposed to sinusoidally varying light with a period of 60 s or 80 s (thin line, upper panels). The leaves were also interrogated with a measuring flash of orange light which stimulated fluorescence. The large circles show the resulting fluorescence. The lower panels show the frequencies in the fluorescence signal. From L. Nedbal and V. Březina. Complex metabolic oscillations in plants forced by harmonic irradiance. *Biophys. J.* **83**: 2180–2189 (2002). Used by permission.

If a component is present whose frequency is more than half the sampling frequency, it will appear in the analysis at a *lower* frequency. This is the familiar stroboscopic effect in which the wheels of the stagecoach appear to rotate backward because the samples (movie frames) are not made rapidly enough. In signal analysis, this is called *aliasing*. It can be seen in Fig. 11.15, which shows a sine wave sampled at regularly spaced intervals that are longer than half a period.

This phenomenon is inescapable if frequencies greater than  $(N - 1)\omega_0/2$  are present. They must be removed by analog or digital techniques *before* the sampling is done. For a more detailed discussion, see Blackman and Tukey (1958) or Press *et al.* (1992). An example of aliasing is found in a later section, in Fig. 11.41. Maughan *et al.* (1973) pointed out how researchers have been “stung” by this problem in hematology.

### 11.4.10 Fast Fourier Transform

The calculation of the Fourier coefficients using our equations involves  $N$  evaluations of the sine or cosine,  $N$  multiplications, and  $N$  additions for each coefficient. There are  $N$  coefficients, so that there must be  $N^2$  evaluations

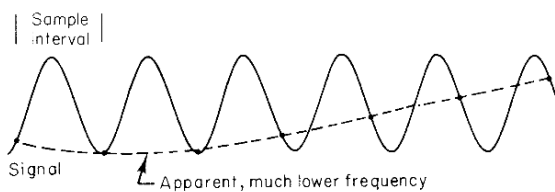


FIGURE 11.15. An example of aliasing. The data are sampled less often than twice per period and appear to be at a much lower frequency.

of the sines and cosines, which uses a lot of computer time. Cooley and Tukey (1965) showed that it is possible to group the data in such a way that the number of multiplications is about  $(N/2)\log_2 N$  instead of  $N^2$  and the sines and cosines need to be evaluated only once, a technique known as the *Fast Fourier Transform* (FFT). For example, for  $1024 = 2^{10}$  data points,  $N^2 = 1\,048\,576$ , while  $(N/2)\log_2 N = (512)(10) = 5120$ . This speeds up the calculation by a factor of 204. The techniques for the FFT are discussed by many authors [see Press *et al.* (1992) or Visscher (1996)]. Bracewell (1990) has written an interesting review of all the popular numerical transforms. He points out that the grouping used in the FFT dates back to Gauss in the early nineteenth century.

## 11.5 Fourier Series for a Periodic Function

It is possible to define the Fourier series for a continuous periodic function  $y(t)$  as well as for discrete data points  $y_j$ . In fact, the function need only be *piecewise continuous*, that is, with a finite number of discontinuities. The calculated function is given by the analog of Eq. 11.14:

$$y_{\text{calc}}(t) = a_0 + \sum_{k=1}^n a_k \cos(k\omega_0 t) + \sum_{k=1}^n b_k \sin(k\omega_0 t). \quad (11.30)$$

The quantity to be minimized is still the mean square error, in this case

$$Q = \frac{1}{T} \int_0^T [y(t) - y_{\text{calc}}(t)]^2 dt. \quad (11.31)$$

When  $Q$  is a minimum,  $\partial Q/\partial a_m$  and  $\partial Q/\partial b_m$  must be zero for each coefficient. For example,

$$\begin{aligned} \frac{\partial Q}{\partial a_m} &= \frac{1}{T} \frac{\partial}{\partial a_m} \int_0^T \left( y(t) - a_0 - \sum_{k=1}^n [a_k \cos(k\omega_0 t) + b_k \sin(k\omega_0 t)] \right)^2 dt \\ &= -\frac{2}{T} \int_0^T \left[ \left( y(t) - a_0 - \sum_{k=1}^n [a_k \cos(k\omega_0 t) + b_k \sin(k\omega_0 t)] \right) \times \cos(m\omega_0 t) \right] dt = 0. \end{aligned}$$

This integral must be zero for each value of  $m$  from 1 to  $n$ . If the order of integration and summation is interchanged, the result is

$$\begin{aligned} \int_0^T y(t) \cos(m\omega_0 t) dt - a_0 \int_0^T \cos(m\omega_0 t) dt \\ - \sum_{k=1}^n a_k \int_0^T \cos(k\omega_0 t) \cos(m\omega_0 t) dt \\ - \sum_{k=1}^n b_k \int_0^T \sin(k\omega_0 t) \cos(m\omega_0 t) dt = 0. \end{aligned}$$

The integral of  $\cos(m\omega_0 t)$  over a period vanishes. The last two integrals are of the form given in Appendix E, Eqs. E.4 and E.5:

$$\int_0^T \cos(k\omega_0 t) \cos(m\omega_0 t) dt = \begin{cases} 0, & k \neq m \\ T/2, & k = m, \end{cases} \quad (11.32)$$

$$\int_0^T \sin(k\omega_0 t) \cos(m\omega_0 t) dt = 0.$$

These results are the *orthogonality relations* for the trigonometric functions. Inserting these values, we find that only one term in the first summation over  $k$  remains, and we have

$$\int_0^T y(t) \cos(m\omega_0 t) dt - a_m \frac{T}{2} = 0,$$

or

$$a_m = \frac{2}{T} \int_0^T y(t) \cos(m\omega_0 t) dt. \quad (11.33a)$$

Minimizing with respect to  $b_m$  gives

$$b_m = \frac{2}{T} \int_0^T y(t) \sin(m\omega_0 t) dt, \quad (11.33b)$$

and minimizing with respect to  $a_0$  gives

$$a_0 = \frac{1}{T} \int_0^T y(t) dt. \quad (11.33c)$$

TABLE 11.4. Value of the  $k$ th coefficient and the value of  $Q$  when terms through the  $k$ th are included from Eq. 11.34.

$k$	$b_k$	$Q$
1	1.2732	0.19
3	0.4244	0.10
5	0.2546	0.07
7	0.1819	0.05
9	0.1415	0.04

These equations are completely general. Because of the orthogonality of the integrals, the coefficients are independent, just as they were in the discrete case for equally spaced data. This is not surprising, since the continuous case corresponds to an infinite set of uniformly spaced data.

Note the similarity of these equations to the discrete results, Eqs. 11.25. In each case  $a_0$  is the average of the function over the period. The other coefficients are twice the average of the signal multiplied by the sine or cosine whose coefficient is being calculated.

The integrals can be taken over any period. Sometimes it is convenient to make the interval  $-T/2$  to  $T/2$ . As we would expect, the integrals involving sines vanish when  $y$  is an even function, and those involving cosines vanish when  $y$  is an odd function.

For the square wave  $y(t) = 1, 0 < t < T/2; y(t) = -1, T/2 < t < T$ , we find

$$b_k = \begin{cases} a_k = 0, \\ 0, & k \text{ even,} \\ 4/\pi k, & k \text{ odd.} \end{cases} \quad (11.34)$$

Table 11.4 shows the first few coefficients for the Fourier series representing the square wave, obtained from Eq. 11.34. They are the same as those for the discrete data in Table 11.3. Figure 11.16 shows the fits for  $n = 3$  and  $n = 39$ . As the number of terms in the fit is increased, the value of  $Q$  decreases. However, spikes of constant height (about 18% of the amplitude of the square wave or 9% of the discontinuity in  $y$ ) remain. These are seen in Fig. 11.16. These spikes appear whenever there is a discontinuity in  $y$  and are called the *Gibbs phenomenon*.

Figure 11.17 shows the blood flow in the pulmonary artery of a dog as a function of time. It has been fitted by a mean and four terms of the form  $M_k \sin(k\omega_0 t - \phi_k)$ . The technique is useful because the elastic properties of the arterial wall can be described in terms of sinusoidal pressure variations at various frequencies [Milnor (1972)].

## 11.6 The Power Spectrum

Since the power dissipated in a resistor is  $v^2/R$  or  $i^2R$ , the square of any function (or signal) is often called the

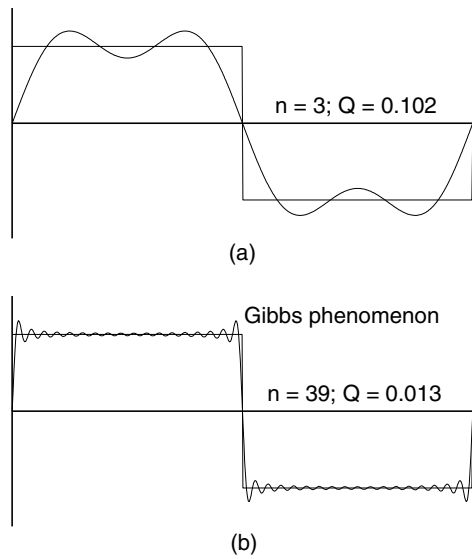


FIGURE 11.16. Fit to the square wave. (a) Fit with the terms for  $k = 1$  and  $k = 3$ . The value of  $Q$  is 0.102. (b) Fit with terms through  $k = 39$ .  $Q$  is very small, but the Gibbs phenomenon—spikes near the discontinuity—is apparent.

power. A periodic signal  $y(t)$  can be written as

$$y(t) = a_0 + \sum_{k=1}^n [a_k \cos(k\omega_0 t) + b_k \sin(k\omega_0 t)] + \epsilon_n(t), \quad (11.35)$$

where the error  $\epsilon_n(t)$  is the difference between the signal (represented by an infinite number of terms) and the sum over  $n$  terms. [This equation defines  $\epsilon_n(t)$ .  $\epsilon_n(t)$  does not represent “noise,” which is discussed in a later section.] The coefficients are given by Eqs. 11.33.

The average “power” in the signal is defined to be<sup>3</sup>

$$\langle y^2 \rangle = \lim_{T' \rightarrow \infty} \frac{1}{2T'} \int_{-T'}^{T'} y^2(t) dt. \quad (11.36)$$

For a periodic signal, the same result can be obtained by integrating over one period:

$$\langle y^2 \rangle = \frac{1}{T} \int_0^T y^2(t) dt. \quad (11.37)$$

To calculate this using Eq. 11.35 for  $y(t)$ , we have to write the sum twice and multiply both sums together:

$$\begin{aligned} \frac{1}{T} \int_0^T y^2(t) dt &= \frac{1}{T} \int_0^T \left( a_0 + \sum_{k=1}^n [a_k \cos(k\omega_0 t) + b_k \sin(k\omega_0 t)] + \epsilon_n(t) \right) \\ &\times \left( a_0 + \sum_{j=1}^n [a_j \cos(j\omega_0 t) + b_j \sin(j\omega_0 t)] + \epsilon_n(t) \right) dt. \end{aligned}$$

<sup>3</sup>The time average of a variable will be denoted by  $\langle \rangle$  brackets.

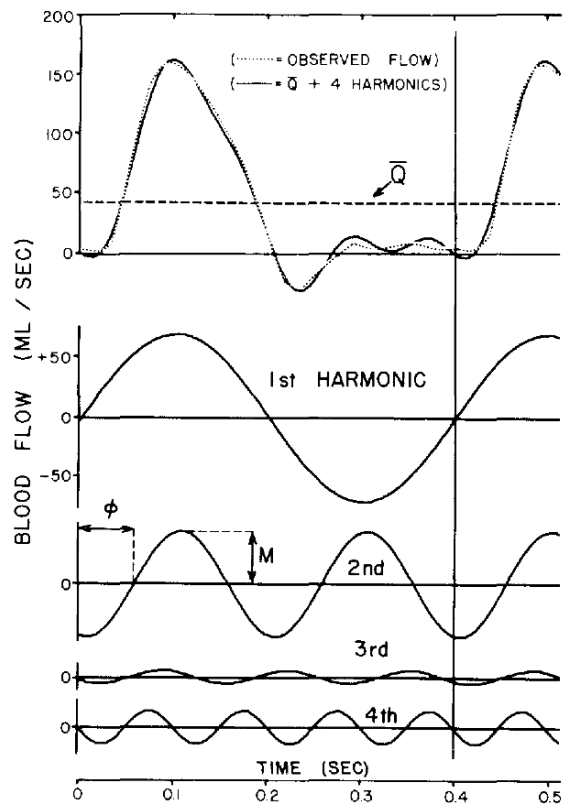


FIGURE 11.17. Analysis of the pulmonary arterial blood flow in a dog, in terms of a Fourier series. From W. R. Milnor, Pulsatile blood flow. *New Eng. J. Med.* **287**: 27–34. Copyright ©Massachusetts Medical Society. All rights reserved. Drawing courtesy of Professor Milnor.

When these terms are multiplied together and written out, we have

$$\begin{aligned} \langle y^2 \rangle &= \frac{1}{T} \int_0^T dt \left( a_0^2 + 2a_0 \sum_{k=1}^n [a_k \cos^{(ii)}(k\omega_0 t) + b_k \sin^{(iii)}(k\omega_0 t)] \right. \\ &+ 2a_0 \epsilon_n^{(iv)}(t) + \sum_{k=1}^n [a_k^2 \cos^{(v)}(k\omega_0 t) + b_k^2 \sin^{(vi)}(k\omega_0 t)] \\ &+ \sum_{k=1}^n \sum_{j \neq k}^{(vii)} a_k a_j \cos(k\omega_0 t) \cos(j\omega_0 t) \\ &+ \sum_{k=1}^n \sum_{j \neq k}^{(viii)} b_k b_j \sin(k\omega_0 t) \sin(j\omega_0 t) \\ &+ 2 \sum_{k=1}^n \sum_{j=1}^n a_k b_j \cos^{(ix)}(k\omega_0 t) \sin(j\omega_0 t) \\ &+ 2\epsilon_n^{(x)}(t) \sum_{k=1}^n [a_k \cos(k\omega_0 t) + b_k \sin(k\omega_0 t)] + \epsilon_n^{(xi)}(t) \left. \right). \end{aligned}$$

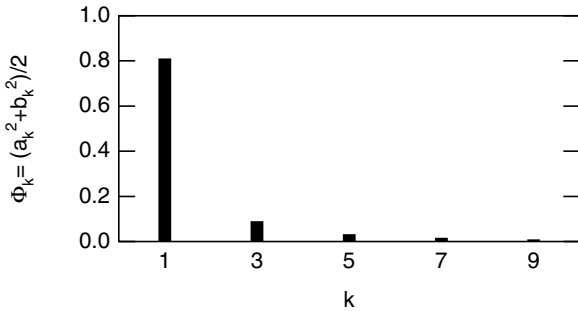


FIGURE 11.18. The power spectrum  $\Phi_k$  for the square wave of Fig. 11.6 or Fig. 11.17, calculated using the values of  $b_k$  from Table 11.4.

Each term has been labeled (i) through (xi). Assume that the function  $y$  is sufficiently well behaved so that the order of integration and summation can be interchanged. Term (i) gives  $a_0^2$ . Terms (ii) and (iii) are integrals of the cosine or sine over an integral number of cycles and vanish. Term (iv) gives<sup>4</sup>

$$2a_0 \frac{1}{T} \int_0^T \epsilon_n(t) dt = 0.$$

Terms (v) and (vi) give  $a_k^2/2$  and  $b_k^2/2$ . Terms (vii), (viii), and (ix) all vanish because of Eq. 11.32. Terms like (x) vanish because  $\epsilon_n(t)$  can be approximated by a sum of sine and cosine terms extending from  $k = n + 1$  to infinity that are orthogonal to terms for  $1 < k < n$ . Term (xi) is  $\langle \epsilon_n^2 \rangle$ . We finally have for the average power

$$\langle y^2(t) \rangle = a_0^2 + \frac{1}{2} \sum_{k=1}^n (a_k^2 + b_k^2) + \langle \epsilon_n^2 \rangle = \sum_{k=0}^n \Phi_k + \langle \epsilon_n^2 \rangle. \tag{11.38}$$

The coefficients are defined by Eqs. 11.33. We could have made a similar argument for the discrete Fourier series of Eqs. 11.25 or 11.26 and obtained the same result. In both cases the average power is a sum of terms  $\Phi_k$  that represent the average power at each frequency  $k\omega_0$ . The term  $\Phi_0 = a_0^2$  is the average of the square of the zero-frequency or dc (direct-current) term;  $\Phi_k = (a_k^2 + b_k^2)/2$  is the average of the squares of the terms  $a_k \cos(k\omega_0 t)$  and  $b_k \sin(k\omega_0 t)$ ; and  $\langle \epsilon_n^2 \rangle$  is the average of the square of the error term. Figure 11.18 shows the power spectrum of the square wave that was used in the example.

## 11.7 Correlation Functions

The correlation function is useful to test whether two functions of time are correlated, that is, whether a change

<sup>4</sup>The quantity  $y(t) - a_0$  has an average of zero. Since all the sine and cosine terms have an average of zero,  $\epsilon_n$  also has an average of zero.

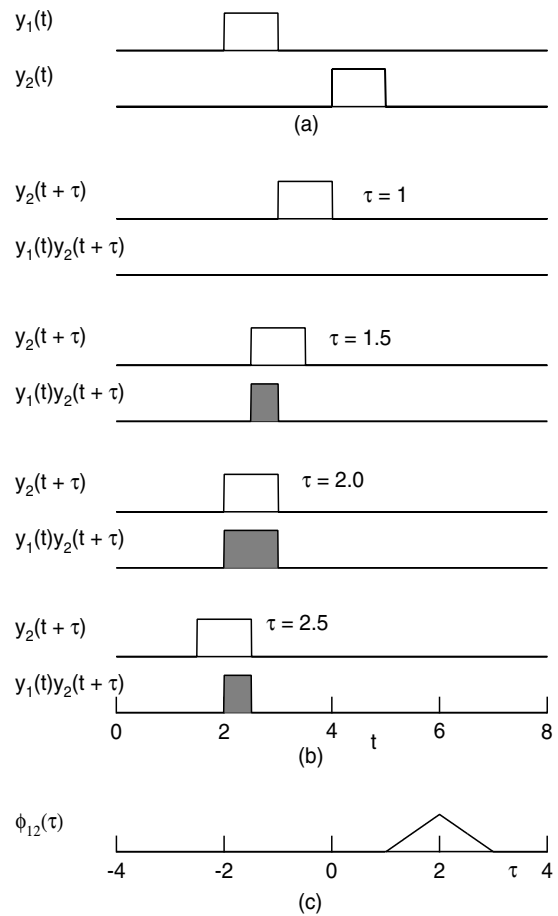


FIGURE 11.19. An example of the cross-correlation function. (a) The two signals to be correlated. (b) Plots of  $y_2(t + \tau)$  and the product  $y_1(t)y_2(t + \tau)$  for different values of  $\tau$ . (c) Plot of  $\phi_{12}(\tau)$ . The peak occurs when signal  $y_2$  has been advanced 2 s.

in one is accompanied by a change in the other. Let the two variables to be tested be  $y_1(t)$  and  $y_2(t)$ . The change in  $y_2$  may occur earlier or later than the change in  $y_1$ ; therefore the correlation must be examined as one of the variables is shifted in time. Examples of pairs of variables that may be correlated are wheat price and rainfall, urinary output and fluid intake, and the voltage changes at two different points along the nerve axon. The variables may or may not be periodic. Exhibiting a correlation does not establish a cause-and-effect relationship. (The height of a growing tree may correlate for several years with an increase in the stock market.)

### 11.7.1 Cross-Correlation of a Pulse

To calculate the cross-correlation function of  $y_1$  and  $y_2$ , advance  $y_2(t)$  by an amount  $\tau$ , multiply  $y_1$  by the shifted  $y_2$ , and integrate the product. Figure 11.19 shows the process for two pulses. The second pulse occurs 2 s later than the first. As the second pulse is advanced the pulses



begin to overlap. When the second pulse has been advanced by 2 s the overlap is greatest; as it is advanced more, the overlap falls to zero. The cross-correlation function depends on  $\tau$  and is plotted in Fig. 11.19(c). The mathematical statement of this procedure for a pulse is

$$\phi_{12}(\tau) = \int_{-\infty}^{\infty} y_1(t)y_2(t + \tau) dt. \quad (11.39)$$

The integrand makes a positive contribution to the integral if  $y_1(t)$  and  $y_2(t + \tau)$  are both positive at the same time or both negative at the same time. It makes a negative contribution if one function is positive while the other is negative.

### 11.7.2 Cross-Correlation of a Nonpulse Signal

If the signals are not pulses, then the cross-correlation integral is defined as

$$\phi_{12}(\tau) = \langle y_1(t)y_2(t + \tau) \rangle. \quad (11.40)$$

As before, the average is the integral over a long time divided by the time interval:

$$\phi_{12}(\tau) = \lim_{T \rightarrow \infty} \frac{1}{2T} \int_{-T}^T y_1(t)y_2(t + \tau) dt. \quad (11.41)$$

If the signals have period  $T$ , the average can be taken by integrating over a single period:

$$\phi_{12}(\tau) = \frac{1}{T} \int_{t'}^{t'+T} y_1(t)y_2(t + \tau) dt. \quad (11.42)$$

Note the difference in units between  $\phi_{12}$  as defined for pulses in Eq. 11.39 where the units of  $\phi$  are the units of  $y^2$  times time, and  $\phi_{12}$  defined in Eqs. 11.40–11.42 where the units are those of  $y^2$ .

The cross correlation depends only on the relative shift of the two signals. It does not matter whether  $y_2$  is advanced by an amount  $\tau$  or  $y_1$  is delayed by the same amount:

$$\phi_{21}(-\tau) = \phi_{12}(\tau). \quad (11.43)$$

### 11.7.3 Cross-Correlation Example

As an example of the cross correlation, consider a square wave that has value  $\pm 1$  and a sine wave with the same period (Fig. 11.20). When the square wave and sine wave are in phase, the product is always positive and the cross correlation has its maximum value. As the square wave is shifted the product is sometimes positive and sometimes negative. When they are a quarter-period out of phase, the average of the integrand is zero, as shown in Fig. 11.20(b). Still more shift results in the correlation function becoming negative, then positive again, with a shift of one full period giving the same result as no shift.

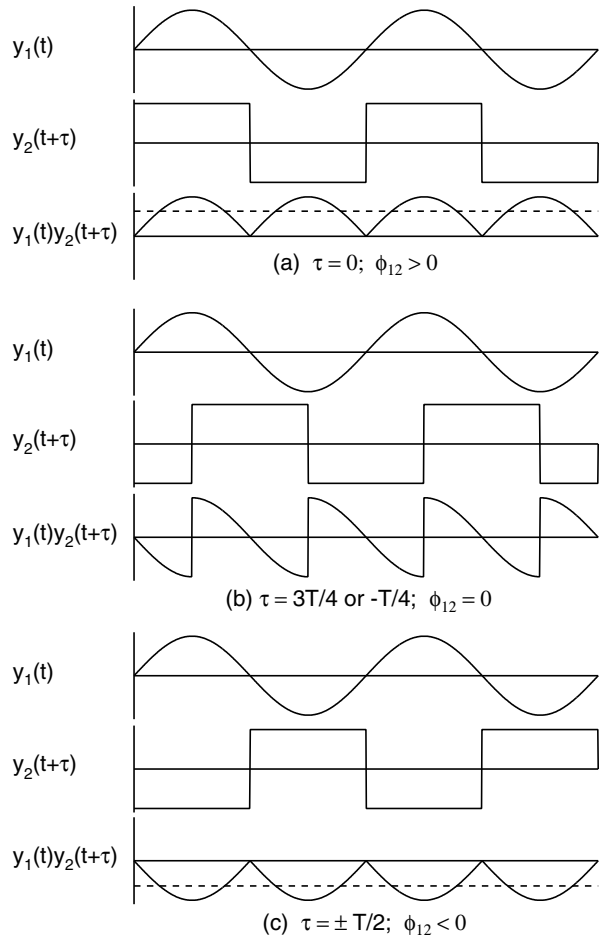


FIGURE 11.20. Cross correlation of a square wave and a sine wave of the same period.

### 11.7.4 Autocorrelation

The *autocorrelation* function is the correlation of the signal with itself:

$$\phi_{11}(\tau) = \int y_1(t)y_1(t + \tau) dt \quad (\text{pulse}), \quad (11.44)$$

$$\phi_{11}(\tau) = \langle y_1(t)y_1(t + \tau) \rangle \quad (\text{nonpulse}). \quad (11.45)$$

Since the signal is correlated with itself, advancing one copy of the signal is the same as delaying the other. The autocorrelation is an even function of  $\tau$ :

$$\phi_{11}(\tau) = \phi_{11}(-\tau). \quad (11.46)$$

### 11.7.5 Autocorrelation Examples

The autocorrelation function for a sine wave can be calculated analytically. If the amplitude of the sine wave is

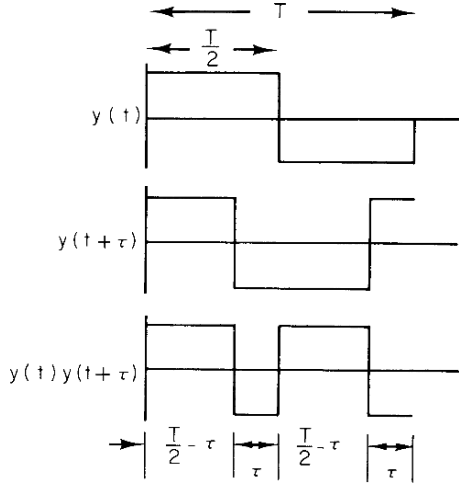


FIGURE 11.21. Plots of  $y(t)$ ,  $y(t + \tau)$ , and their product for a square wave.

$A$  and the frequency is  $\omega = 2\pi/T$ ,

$$\begin{aligned} \phi_{11}(\tau) &= \frac{A^2}{T} \int_0^T \sin(\omega t) \sin(\omega t + \omega\tau) dt \\ &= \frac{A^2}{T} \int_0^T \sin(\omega t) \\ &\quad \times [\sin(\omega t) \cos(\omega\tau) + \cos(\omega t) \sin(\omega\tau)] dt \\ &= A^2 \cos(\omega\tau) \left[ \frac{1}{T} \int_0^T \sin^2(\omega t) dt \right] \\ &\quad + A^2 \sin(\omega\tau) \left[ \frac{1}{T} \int_0^T \sin(\omega t) \cos(\omega t) dt \right]. \end{aligned}$$

It is shown in Appendix E that the first term in square brackets is  $\frac{1}{2}$  and the second is 0. Therefore the autocorrelation function of the sine wave is

$$\phi_{11}(\tau) = \frac{A^2}{2} \cos(\omega\tau). \tag{11.47}$$

As a final example, consider the autocorrelation of a square wave of unit amplitude. One period is drawn in Fig. 11.21 showing the wave, the advanced wave, and the product. The average is the net area divided by  $T$ . The area above the axis is  $(2)(T/2 - \tau)(1)$  since there are two rectangles of height 1 and width  $T/2 - \tau$ . From this must be subtracted the area of the two rectangles of height 1 and width  $\tau$  that are below the axis. The net area is  $T - 4\tau$ . The autocorrelation function is

$$\phi_{11}(\tau) = 1 - 4\tau/T, \quad 0 < \tau < T/2. \tag{11.48}$$

The plot of the integrand in Fig. 11.21 is only valid for  $0 < \tau < T/2$ . We can use the fact that the autocorrelation is an even function to draw  $\phi$  for  $-T/2 < \tau < 0$ . We then have  $\phi$  for the whole period. It is plotted in Fig. 11.22.

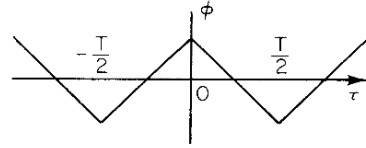


FIGURE 11.22. Plot of  $\phi_{11}(\tau)$  for the square wave.

## 11.8 The Autocorrelation Function and the Power Spectrum

We saw that the power spectrum of a periodic signal is related to the coefficients in its Fourier series (Eq. 11.38):

$$\langle y^2(t) \rangle = a_0^2 + \frac{1}{2} \sum_{k=1}^n (a_k^2 + b_k^2),$$

with the term for each value of  $k$  representing the amount of power carried in the signal component at that frequency. The Fourier series for the autocorrelation function carries the same information. To see this, calculate the autocorrelation function of

$$y_1(t) = a_0 + \sum_{k=1}^n [a_k \cos(k\omega_0 t) + b_k \sin(k\omega_0 t)].$$

We can write

$$\begin{aligned} \phi_{11}(\tau) &= \langle y_1(t)y_1(t + \tau) \rangle \\ &= \left\langle \left( a_0 + \sum_{k=1}^n [a_k \cos(k\omega_0 t) + b_k \sin(k\omega_0 t)] \right) \right. \\ &\quad \times \left( a_0 + \sum_{j=1}^n \left\{ a_j \cos[j\omega_0(t + \tau)] \right. \right. \\ &\quad \left. \left. + b_j \sin[j\omega_0(t + \tau)] \right\} \right) \right\rangle. \end{aligned}$$

The next step is to multiply out all the terms as we did when deriving Eq. 11.38. We then use the trigonometric identities<sup>5</sup>

$$\cos(x + y) = \cos x \cos y - \sin x \sin y,$$

$$\sin(x + y) = \cos x \sin y + \sin x \cos y.$$

For many of the terms, either the averages are zero or pairs of terms cancel. We finally obtain

$$\phi_{11}(\tau) = a_0^2 + \sum_{k=1}^n \frac{1}{2} (a_k^2 + b_k^2) \cos(k\omega_0\tau). \tag{11.49}$$

This has only cosine terms, since the autocorrelation function is even.

<sup>5</sup>One virtue of the complex notation is that these addition formulae become the standard rule for multiplying exponentials:  $e^{i(x+y)} = e^{ix} e^{iy}$ .

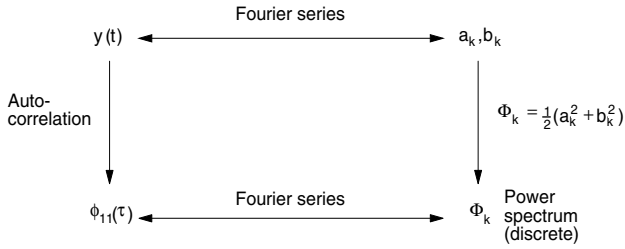


FIGURE 11.23. The power spectrum of a periodic signal can be obtained either from the squares of the Fourier coefficients of the signal or from the Fourier coefficients of the autocorrelation function.

For zero shift,

$$\phi_{11}(0) = a_0^2 + \sum_{k=1}^n \frac{1}{2}(a_k^2 + b_k^2).$$

Comparison with Eq. 11.38 shows that this is the power in the signal. We can get this result directly from Eq. 11.36. The integral is the same as the definition of the autocorrelation function when  $\tau = 0$ .

The Fourier series for the autocorrelation function is particularly easy to obtain. We need only pick out the coefficients in Eq. 11.49. Write the Fourier expansion of the autocorrelation function as

$$\phi_{11}(\tau) = \alpha_0 + \sum_{k=1}^n \alpha_k \cos(k\omega_0\tau). \tag{11.50}$$

Comparing terms in Eqs. 11.49 and 11.50 shows that  $\alpha_0 = a_0^2$  and  $\alpha_k = (a_k^2 + b_k^2)/2$ . We can also compare these with the definition of  $\Phi_k$  in Eq. 11.38 and say that

$$\begin{aligned} \Phi_0 &= \text{average dc (zero-frequency) power} &= \alpha_0 &= a_0^2, \\ \Phi_k &= \text{average power at frequency } k\omega_0 &= \alpha_k &= \frac{1}{2}(a_k^2 + b_k^2). \end{aligned} \tag{11.51}$$

The autocorrelation function contains no phase information about the signal. This is reflected in the fact that  $\alpha_k = (a_k^2 + b_k^2)/2$ ; the sine and cosine terms at a given frequency are completely mixed together.

There are two ways to find the power  $\Phi_k$  at frequency  $k\omega_0$ . Both are shown in Fig. 11.23. The function  $y(t)$  and its Fourier coefficients are completely equivalent, and one can go from one to the other. Squaring the coefficients and adding them gives the power spectrum. This is a one-way process; once they have been squared and added, there is no way to separate them again. The autocorrelation function also involves squaring and adding and is a one-way process. The autocorrelation function and the power spectrum are related by a Fourier series and can be calculated from each other.

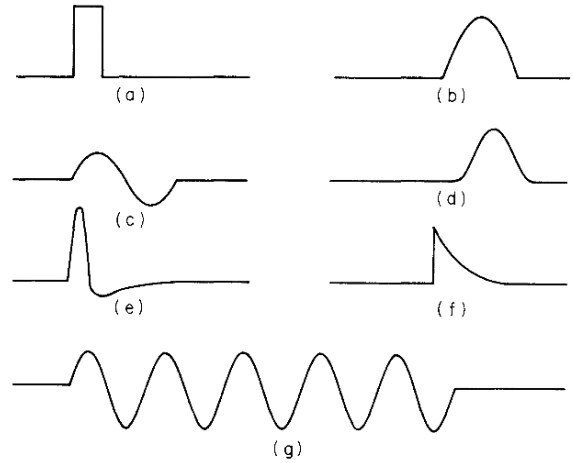


FIGURE 11.24. Various pulses. The common feature is that they occur once. (a) Square pulse. (b) Half cycle of a sine wave. (c) One cycle of a sine wave. (d) Gaussian. (e) Nerve pulse. (f) Exponentially decaying pulse. (g) Gated sine wave.

## 11.9 Nonperiodic Signals and Fourier Integrals

Sometimes we have to deal with a signal that is a pulse that occurs just once. Several pulses are shown in Fig. 11.24; they come in an infinite variety of shapes. Noise is another signal that never repeats itself and is therefore not periodic. The *Fourier integral* or *Fourier transform* is an extension of the Fourier series that allows us to deal with nonperiodic signals.

### 11.9.1 Introduce Negative Frequencies and Make the Coefficients Half as Large

The Fourier series expansion of a periodic function  $y(t)$  was seen in Eq. 11.30. If we let the number of terms be infinite, we have

$$y(t) = a_0 + \sum_{k=1}^{\infty} a_k \cos(k\omega_0 t) + \sum_{k=1}^{\infty} b_k \sin(k\omega_0 t),$$

with the coefficients given by Eqs. 11.33. Since  $y(t)$  has period  $T$ , the integrals in Eqs. 11.33 can be over any interval that is one period long. Let us therefore make the limits of integration  $-T/2$  to  $T/2$  and also remember that  $1/T = \omega_0/2\pi$ . With these substitutions, Eqs. 11.33 become

$$\begin{aligned} a_0 &= \frac{\omega_0}{2\pi} \int_{-T/2}^{T/2} y(t) dt, \\ a_k &= \frac{\omega_0}{\pi} \int_{-T/2}^{T/2} y(t) \cos(k\omega_0 t) dt, \\ b_k &= \frac{\omega_0}{\pi} \int_{-T/2}^{T/2} y(t) \sin(k\omega_0 t) dt. \end{aligned} \tag{11.52}$$

Now allow  $k$  to have negative as well as positive values. If the coefficients for negative  $k$  are also defined by Eqs. 11.52, they have the properties [since  $\cos(k\omega_0 t) = \cos(-k\omega_0 t)$  and  $\sin(k\omega_0 t) = -\sin(-k\omega_0 t)$ ],

$$a_{-k} = a_k, \quad b_{-k} = -b_k.$$

Therefore the terms  $a_k \cos(k\omega_0 t)$  and  $b_k \sin(k\omega_0 t)$  in Eq. 11.30 are the same function of  $t$  whether  $k$  is positive or negative. By introducing negative values of  $k$  we can make the coefficients in front of the integrals for  $a_k$  and  $b_k$  in Eqs. 11.52 become  $\omega_0/2\pi$ . This is the same trick used to obtain the discrete equations, Eqs. 11.27. With negative values of  $k$  allowed, we have

$$y(t) = a'_0 + \sum_{\substack{k=-\infty \\ k \neq 0}}^{\infty} [a'_k \cos(k\omega_0 t) + b'_k \sin(k\omega_0 t)],$$

$$a'_0 = \frac{\omega_0}{2\pi} \int_{-T/2}^{T/2} y(t) dt,$$

$$a'_k = \frac{\omega_0}{2\pi} \int_{-T/2}^{T/2} y(t) \cos(k\omega_0 t) dt,$$

$$b'_k = \frac{\omega_0}{2\pi} \int_{-T/2}^{T/2} y(t) \sin(k\omega_0 t) dt.$$

Since  $\cos(0\omega_0 t) = 1$  and  $\sin(0\omega_0 t) = 0$ , we can incorporate the definition of  $a'_0$  into the definition of  $a'_k$  and introduce  $b'_0$  which is always zero. The sum can then include  $k = 0$ :

$$y(t) = \sum_{k=-\infty}^{\infty} [a'_k \cos(k\omega_0 t) + b'_k \sin(k\omega_0 t)],$$

$$a'_k = \frac{\omega_0}{2\pi} \int_{-T/2}^{T/2} y(t) \cos(k\omega_0 t) dt, \quad (11.53)$$

$$b'_k = \frac{\omega_0}{2\pi} \int_{-T/2}^{T/2} y(t) \sin(k\omega_0 t) dt.$$

A final change of variables defines  $C_k = 2\pi a'_k/\omega_0$  and  $S_k = 2\pi b'_k/\omega_0$ . With these changes the Fourier series and its coefficients are

$$y(t) = \frac{\omega_0}{2\pi} \sum_{k=-\infty}^{\infty} [C_k \cos(k\omega_0 t) + S_k \sin(k\omega_0 t)],$$

$$C_k = \int_{-T/2}^{T/2} y(t) \cos(k\omega_0 t) dt, \quad (11.54)$$

$$S_k = \int_{-T/2}^{T/2} y(t) \sin(k\omega_0 t) dt.$$

To recapitulate, there is nothing fundamentally new in Eq. 11.54. Negative values of  $k$  were introduced so that the sum goes over each value of  $|k|$  twice (except for  $k = 0$ ). This allowed the coefficients to be made half as large.

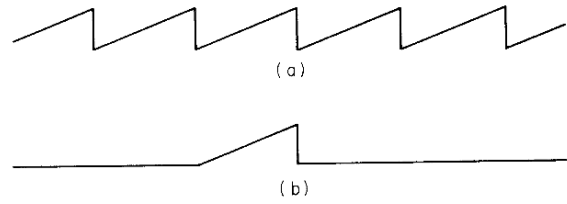


FIGURE 11.25. (a) A periodic signal. (b) A nonperiodic signal.

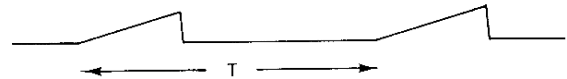


FIGURE 11.26. An approximation to the nonperiodic signal shown in Fig. 11.25(b).

### 11.9.2 Make the Period Infinite

These equations can be used to calculate the Fourier series for a periodic signal such as that shown in Fig. 11.25(a). Suppose that instead we want to find the coefficients for the nonperiodic signal shown in Fig. 11.25(b). This signal can be approximated by another periodic signal shown in Fig. 11.26. The approximation to Fig. 11.25(b) becomes better and better as  $T$  is made longer. As  $T$  becomes infinite, the fundamental angular frequency  $\omega_0$  approaches 0. Define  $\omega = k\omega_0$ . The frequencies  $\omega$  are discrete with spacing  $\omega_0$ . Consider a small frequency interval encompassing many values of  $k$ , as shown in Fig. 11.27. Since  $\omega_0$  is approaching zero, there can be many values of  $\omega$  and  $k$  between  $\omega$  and  $\omega + \Delta\omega$ . The frequencies will be nearly the same, so the values of  $C_k$  will be nearly the same. All of the terms in the sum in Eq. 11.54 can be replaced by an average value of  $C_k$  or  $S_k$  multiplied by the number of values of  $k$  in the interval, which is  $\Delta\omega/\omega_0$ . Finally, we set  $C_k=C(\omega)$  and  $\Delta\omega = d\omega$ . The sum becomes an integral with  $\Delta\omega = d\omega$ :

$$y(t) = \frac{\omega_0}{2\pi} \int_{-\infty}^{\infty} [C(\omega) \cos \omega t + S(\omega) \sin \omega t] \frac{d\omega}{\omega_0},$$

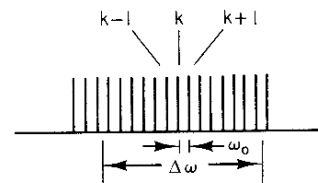


FIGURE 11.27. A histogram of  $C_k$  vs  $k$ .

or finally, since  $d\omega = 2\pi df$ ,

$$\begin{aligned}
 y(t) &= \frac{1}{2\pi} \int_{-\infty}^{\infty} [C(\omega) \cos \omega t + S(\omega) \sin \omega t] d\omega \\
 &= \int_{-\infty}^{\infty} [C(f) \cos(2\pi ft) + S(f) \sin(2\pi ft)] df, \\
 C(\omega) &= \int_{-\infty}^{\infty} y(t) \cos \omega t dt, \\
 S(\omega) &= \int_{-\infty}^{\infty} y(t) \sin \omega t dt.
 \end{aligned}
 \tag{11.55}$$

These equations constitute a *Fourier integral pair* or *Fourier transform pair*. They are completely symmetric in the variables  $f$  and  $t$  and symmetric apart from the factor  $2\pi$  in the variables  $\omega$  and  $t$ . One obtains  $C(\omega)$  or  $S(\omega)$  by multiplying the function  $y(t)$  by the appropriate trigonometric function and integrating over time. One obtains  $y(t)$  by multiplying  $C$  and  $S$  by the appropriate trigonometric function and integrating over frequency.

### 11.9.3 Complex Notation

Using complex notation, we define

$$Y(\omega) = C(\omega) - iS(\omega) \tag{11.56}$$

and write

$$\begin{aligned}
 y(t) &= \frac{1}{2\pi} \int_{-\infty}^{\infty} Y(\omega) e^{i\omega t} d\omega = \int_{-\infty}^{\infty} Y(\omega) e^{i\omega t} df, \\
 Y(\omega) &= \int_{-\infty}^{\infty} y(t) e^{-i\omega t} dt.
 \end{aligned}
 \tag{11.57}$$

### 11.9.4 Example: The Exponential Pulse

As an example, consider the function

$$y(t) = \begin{cases} 0, & t \leq 0 \\ Ae^{-at}, & t > 0. \end{cases} \tag{11.58}$$

The functions  $C$  and  $S$  are evaluated using Eqs. 11.55. Since  $y(t)$  is zero for negative times, the integrals extend from 0 to infinity. They are found in all standard integral tables:

$$\begin{aligned}
 C(\omega) &= A \int_0^{\infty} e^{-at} \cos \omega t dt = \frac{A/a}{1 + (\omega/a)^2}, \\
 S(\omega) &= A \int_0^{\infty} e^{-at} \sin \omega t dt = \frac{(A/a)(\omega/a)}{1 + (\omega/a)^2}.
 \end{aligned}
 \tag{11.59}$$

These are plotted in Fig. 11.28. Function  $C$  is even, while  $S$  is odd. The functions are plotted on log-log graph paper in Fig. 11.29. Remember that only positive values of  $\omega/a$  can be shown on a logarithmic scale, so the origin

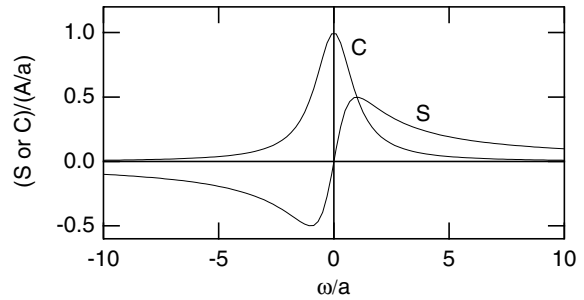


FIGURE 11.28. The sine and cosine coefficients in the Fourier transform of an exponentially decaying pulse.

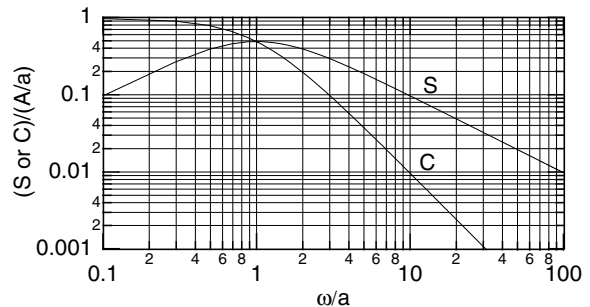


FIGURE 11.29. Log-log plot of the coefficients in Fig. 11.28.

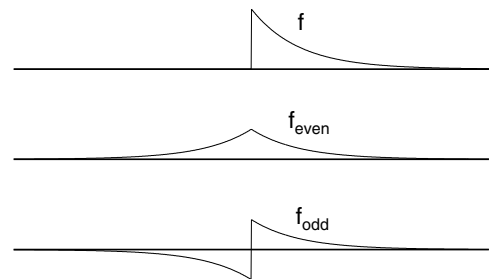


FIGURE 11.30. Function  $f(t)$  and its even and odd parts.

and negative frequencies cannot be shown. It is apparent from the slopes of the curves that  $C$  falls off as  $(\omega/a)^{-2}$  while  $S$  falls more slowly, as  $(\omega/a)^{-1}$ . One way of explaining this difference is to note that the function  $y(t)$  can be written as a sum of even and odd parts as shown in Fig. 11.30. The odd function, which is given by the sine terms in the integral, has a discontinuity, while the even function does not. A more detailed study of Fourier expansions shows that a function with a discontinuity has coefficients that decrease as  $1/\omega$  or  $1/k$ , while the coefficients of a function without a discontinuity decrease more rapidly. (Recall that the coefficients of the square wave were  $4/\pi k$ .)

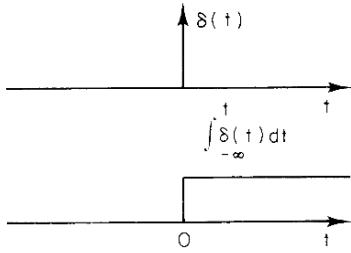


FIGURE 11.31. The  $\delta$  function and its integral.

### 11.10 The Delta Function

It will be useful in the next sections to introduce a pulse that is very narrow, very tall, and has unit area under its curve. Physicists call this function the *delta function*  $\delta(t)$ . Engineers call it the *impulse function*  $u_0(t)$ .

The  $\delta$  function is defined by the equations

$$\begin{aligned} \delta(t) &= 0, \quad t \neq 0 \\ \int_{-\epsilon}^{\epsilon} \delta(t) dt &= \int_{-\infty}^{\infty} \delta(t) dt = 1. \end{aligned} \tag{11.60}$$

The  $\delta$  function can be thought of as a rectangle of width  $a$  and height  $1/a$  in the limit  $a \rightarrow 0$ , or as a Gaussian function (Appendix I) as  $\sigma \rightarrow 0$ . Many other functions have the same limiting properties. The  $\delta$  function is not like the usual function in mathematics because of its infinite discontinuity at the origin. It is one of a class of “generalized functions” whose properties have been rigorously developed by mathematicians<sup>6</sup> since they were first used by the physicist P. A. M. Dirac.

Since integrating across the origin picks up this spike of unit area, the integral of the  $\delta$  function is a step of unit height at the origin. The  $\delta$  function and its integral are shown in Fig. 11.31. The  $\delta$  function can be positioned at  $t = a$  by writing  $\delta(t - a)$  because the argument vanishes at  $t = a$ .

Multiplying any function by the  $\delta$  function and integrating picks out the value of the function when the argument of the  $\delta$  function is zero:

$$\begin{aligned} \int_{-\infty}^{\infty} y(t)\delta(t) dt &= y(0) \int_{-\infty}^{\infty} \delta(t) dt = y(0), \\ \int_{-\infty}^{\infty} y(t)\delta(t - a) dt &= y(a) \int_{-\infty}^{\infty} \delta(t - a) dt = y(a). \end{aligned} \tag{11.61}$$

The second integral on each line is based on the fact that  $y(t)$  has a constant value when the  $\delta$  function is nonzero so it can be taken outside the integral.

<sup>6</sup>A rigorous but relatively elementary mathematical treatment is given by Lighthill (1958).

The  $\delta$  function has the following properties that are proved in Problem 28:

$$\begin{aligned} \delta(t) &= \delta(-t), \\ t\delta(t) &= 0 \\ \delta(at) &= \frac{1}{|a|}\delta(t). \end{aligned} \tag{11.62}$$

### 11.11 The Energy Spectrum of a Pulse and Parseval’s Theorem

For a signal with period  $T$ , the *average power* is  $\frac{1}{T} \int_0^T y^2(t) dt$ . We can also define the average power for a signal lasting a very long time as

$$\lim_{T' \rightarrow \infty} \frac{1}{2T'} \int_{-T'}^{T'} y^2(t) dt = a_0^2 + \frac{1}{2} \sum_k (a_k^2 + b_k^2).$$

In the limit of infinite duration, both the integral and the denominator are infinite, but the ratio is finite.

For a pulse the integral is finite and the average power vanishes. In that case we use the integral without dividing by  $T$ . It is called the *energy* in the pulse.

Since  $y(t)$  is given by a Fourier integral, the energy in the pulse can be written as

$$\begin{aligned} \int_{-\infty}^{\infty} y^2(t) dt &= \left(\frac{1}{2\pi}\right)^2 \int_{-\infty}^{\infty} dt \int_{-\infty}^{\infty} d\omega \int_{-\infty}^{\infty} d\omega' \\ &\quad [C(\omega) \cos \omega t + S(\omega) \sin \omega t] \\ &\quad \times [C(\omega') \cos \omega' t + S(\omega') \sin \omega' t]. \end{aligned} \tag{11.63}$$

If the terms are multiplied out, this becomes

$$\begin{aligned} \int_{-\infty}^{\infty} y^2(t) dt &= \left(\frac{1}{2\pi}\right)^2 \int_{-\infty}^{\infty} dt \int_{-\infty}^{\infty} d\omega \int_{-\infty}^{\infty} d\omega' \\ &\quad [C(\omega)C(\omega') \cos \omega t \cos \omega' t \\ &\quad + C(\omega)S(\omega') \cos \omega t \sin \omega' t \\ &\quad + S(\omega)C(\omega') \sin \omega t \cos \omega' t \\ &\quad + S(\omega)S(\omega') \sin \omega t \sin \omega' t]. \end{aligned} \tag{11.64}$$

To simplify this expression, we interchange the order of integration, carrying out the time integration first. We assume that the function  $y(t)$  is sufficiently well behaved so that this can be done.

Changing the order gives three integrals to consider:

$$\begin{aligned} &\int_{-\infty}^{\infty} \cos \omega t \cos \omega' t dt, \\ &\int_{-\infty}^{\infty} \cos \omega t \sin \omega' t dt, \\ &\int_{-\infty}^{\infty} \sin \omega t \sin \omega' t dt. \end{aligned}$$

These are analogous to the trigonometric integrals of Appendix E, except that they extend over all time instead of just one period. Therefore we might expect that an integral such as  $\int_{-\infty}^{\infty} \cos \omega t \sin \omega' t dt$  would vanish for all possible values of  $\omega$  and  $\omega'$ . We might expect that the integrals  $\int_{-\infty}^{\infty} \cos \omega t \cos \omega' t dt$  and  $\int_{-\infty}^{\infty} \sin \omega t \sin \omega' t dt$  would vanish when  $\omega \neq \omega'$  and be infinite when  $\omega = \omega'$ . Such is indeed the case. This is reminiscent of the  $\delta$  function, but it does not tell us the exact relationship of these integrals to it.

To find the exact values of the integrals we use the following trick. Let  $y(t)$  be the function for which  $C(\omega) = \delta(\omega - \omega')$ . Then, using Eqs. 11.55 and 11.61 we get

$$y(t) = \frac{1}{2\pi} \int_{-\infty}^{\infty} \delta(\omega - \omega') \cos \omega t d\omega = \frac{1}{2\pi} \cos \omega' t.$$

The inverse equation for  $C(\omega)$  is

$$C(\omega) = \int_{-\infty}^{\infty} y(t) \cos \omega t dt = \frac{1}{2\pi} \int_{-\infty}^{\infty} \cos \omega' t \cos \omega t dt.$$

But  $C(\omega) = \delta(\omega - \omega')$ . Therefore

$$\int_{-\infty}^{\infty} \cos \omega t \cos \omega' t dt = 2\pi \delta(\omega - \omega'). \quad (11.65a)$$

A similar argument shows that

$$\int_{-\infty}^{\infty} \sin(\omega t) \sin(\omega' t) dt = 2\pi \delta(\omega - \omega'). \quad (11.65b)$$

The fact that both the sine and cosine integrals are the same should not be surprising, since a sine curve is just a cosine curve shifted along the axis and we are integrating from  $-\infty$  to  $\infty$ .

### 11.11.1 Parseval's Theorem

The integrals in Eqs. 11.65 can be used to evaluate Eq. 11.64. The result is

$$\int_{-\infty}^{\infty} y^2(t) dt = \frac{1}{2\pi} \int_{-\infty}^{\infty} d\omega \int_{-\infty}^{\infty} d\omega' [C(\omega)C(\omega')\delta(\omega - \omega') + S(\omega)S(\omega')\delta(\omega - \omega')]$$

$$\int_{-\infty}^{\infty} y^2(t) dt = \frac{1}{2\pi} \int_{-\infty}^{\infty} d\omega [C^2(\omega) + S^2(\omega)]. \quad (11.66)$$

This result is known as *Parseval's theorem*. If we define the function

$$\Phi'(\omega) = C^2(\omega) + S^2(\omega), \quad (11.67a)$$

then Eq. 11.66 takes the form

$$\int_{-\infty}^{\infty} y^2(t) dt = \int_{-\infty}^{\infty} \Phi'(\omega) \frac{d\omega}{2\pi} = \int_{-\infty}^{\infty} \Phi'(f) df. \quad (11.67b)$$

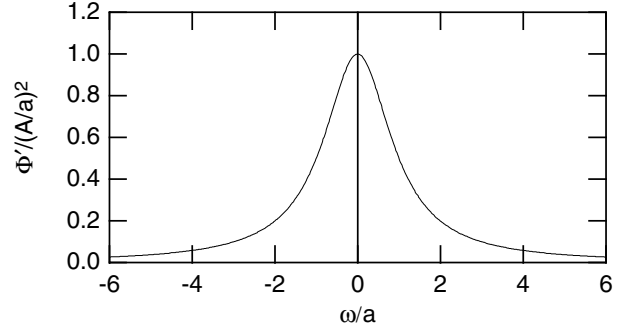


FIGURE 11.32. The energy spectrum  $\Phi'(\omega)$  for an exponential pulse.

The prime is to remind us that this is energy and not power. The left-hand side is the total energy in the signal, and  $y^2(t) dt$  is the amount of energy between  $t$  and  $t + dt$ . This suggests that we call  $\Phi'(\omega) d\omega/2\pi = \Phi'(f) df$  the amount of energy in the angular frequency interval between  $\omega$  and  $\omega + d\omega$  or the frequency interval between  $f$  and  $f + df$ .

### 11.11.2 Example: The Exponential Pulse

The energy spectrum of the exponential pulse that was used earlier as an example is

$$\Phi'(\omega) = C^2(\omega) + S^2(\omega) = \left(\frac{A}{a}\right)^2 \frac{1}{1 + (\omega/a)^2}. \quad (11.68)$$

It is plotted in Fig. 11.32.

## 11.12 The Autocorrelation of a Pulse and Its Relation to the Energy Spectrum

The correlation functions for pulses are defined as integrals instead of averages:

$$\begin{aligned} \phi_{12}(\tau) &= \int_{-\infty}^{\infty} y_1(t)y_2(t + \tau) dt, \\ \phi_{11}(\tau) &= \int_{-\infty}^{\infty} y_1(t)y_1(t + \tau) dt. \end{aligned} \quad (11.69)$$

Consider the autocorrelation function of the exponential pulse, Eq. 11.58. Figure 11.33 shows the functions involved in calculating the autocorrelation for a typical positive value of  $\tau$ . Since the autocorrelation function is even, negative values of  $\tau$  need not be considered. The product of the function and the shifted function is  $(Ae^{-at})(Ae^{-a(t+\tau)}) = A^2 e^{-a\tau} e^{-2at}$ . It can be seen from Fig. 11.33 that the limits of integration are from zero to infinity. Thus,

$$\phi_{11}(\tau) = A^2 e^{-a\tau} \int_0^{\infty} e^{-2at} dt = \frac{A^2 e^{-a\tau}}{2a}, \quad \tau > 0.$$

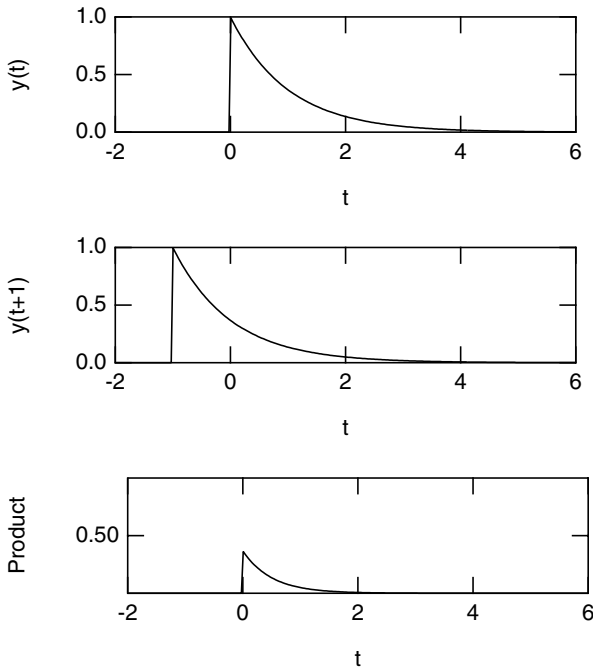


FIGURE 11.33. Calculation of the autocorrelation of the exponential pulse. The figure shows  $y(t)$ ,  $y(t + \tau)$ , and their product, for  $\tau = 1$ .

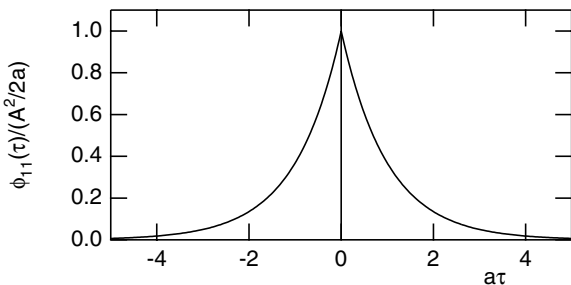


FIGURE 11.34. The autocorrelation function for an exponentially decaying pulse.

Because  $\phi_{11}$  is even, the full autocorrelation function is

$$\phi_{11}(\tau) = \frac{A^2}{2a} e^{-a|\tau|}. \tag{11.70}$$

This is plotted in Fig. 11.34.

The autocorrelation function has a Fourier transform  $\Phi'$ . Only the cosine term appears, since  $\phi_{11}$  is even:

$$\begin{aligned} \Phi'(\omega) &= \frac{A^2}{2a} \int_{-\infty}^{\infty} e^{-a|t|} \cos \omega t dt \\ &= \frac{A^2}{a} \int_0^{\infty} e^{-at} \cos \omega t dt. \end{aligned}$$

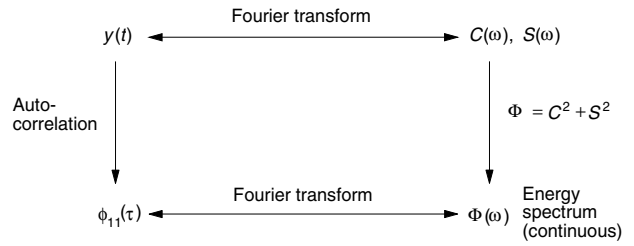


FIGURE 11.35. Two ways to obtain the energy spectrum of a pulse signal.

We have seen this integral before, in conjunction with Eq. 11.59. The result is

$$\Phi'(\omega) = \left(\frac{A}{a}\right)^2 \frac{1}{1 + (\omega/a)^2}.$$

Comparing this with Eq. 11.67, we again see that

$$\Phi'(\omega) = C^2(\omega) + S^2(\omega). \tag{11.71}$$

This relationship between the autocorrelation and  $\Phi'$  can be proved in general by representing each function in the definition of the autocorrelation function by its Fourier transform, using the trigonometric addition formulas, carrying out the time integration first, and using the  $\delta$ -function definitions. The result is

$$\begin{aligned} \phi_{11}(\tau) &= \frac{1}{2\pi} \int_{-\infty}^{\infty} [C^2(\omega) + S^2(\omega)] \cos \omega \tau d\omega \\ &= \frac{1}{2\pi} \int_{-\infty}^{\infty} \Phi'(\omega) \cos \omega \tau d\omega. \end{aligned} \tag{11.72}$$

As with the periodic signal, there are two ways to go from the signal to the energy spectrum. The Fourier transform is taken of either the original function or the autocorrelation function. Squaring and adding is done either in the time domain to  $y(t)$  to obtain the autocorrelation function, or in the frequency domain by squaring and adding the coefficients. The Fourier transforms can be taken in either direction. Squaring and adding is one-directional and makes it impossible to go from the energy spectrum back to the original function. These processes are illustrated in Fig. 11.35.

### 11.13 Noise

The function  $y(t)$  we wish to study is often the result of a measurement of some system: the electrocardiogram, the electroencephalogram, blood flow, etc., and is called a *signal*. Most signals are accompanied by *noise*. Random noise fluctuates in such a way that we cannot predict what its value will be at some future time. Instead we must talk about the probability that the noise has a certain value. A key problem is to learn as much as one can about a signal that is contaminated by noise. The techniques discussed in this chapter are often useful.



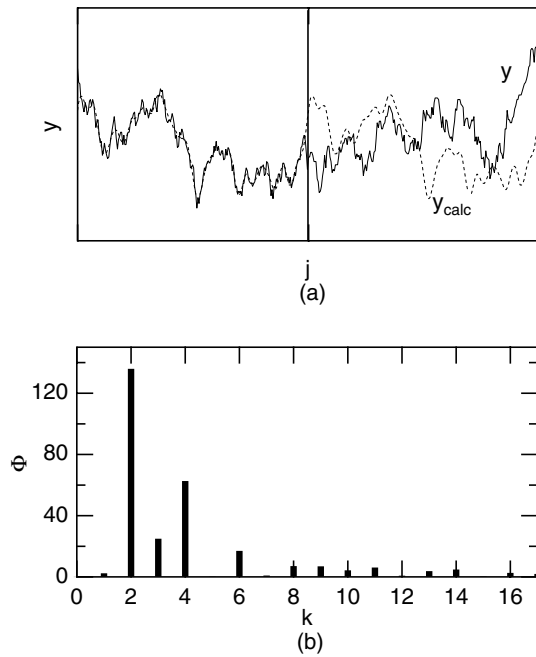


FIGURE 11.36. (a) The solid line shows function  $y_j$  that was calculated from a one-dimensional random walk with a Gaussian-distributed step length. The dashed line shows the function calculated from the Fourier coefficients of  $y_j$  based on the first half of the time interval. It does not fit the second half of the function. This is characteristic of random functions. (b) The power spectrum calculated from the first half of  $y_j$ . The zero-frequency component has been suppressed because it depends on the starting value of  $y$ .

A very important property of noise can be seen from the data shown in Fig. 11.36(a). The data consist of 460 discrete values that appear to have several similar peaks. A discrete Fourier transform of the first 230 values gives fairly large values for the first few coefficients  $a_k$  and  $b_k$ . Yet these values of  $a_k$  and  $b_k$  fail to describe subsequent values of  $y_j$ . The reason is that the  $y_j$  are actually random. In this case they are the net displacement after  $j$  steps in a random walk in which each step length is Gaussian distributed with standard deviation  $\sigma = 5$ . The Fourier transform of a random function does not exist. We can apply the recipe to the data and calculate the coefficients. But if we apply the same recipe to some other set of data points from the random function we get different values of the coefficients, although the sum of their squares,  $(a_k^2 + b_k^2)^{1/2}$ , would be nearly the same. The sum of the squares of the coefficients is plotted in Fig. 11.36(b). It is the phases that change randomly, while the amount of energy at a particular frequency remains constant or fluctuates slightly about some average value.

Noise is not periodic, but neither is it a pulse. It has finite power, but it will have infinite energy if the noise goes on “forever.” To describe noise we must use averages, cal-

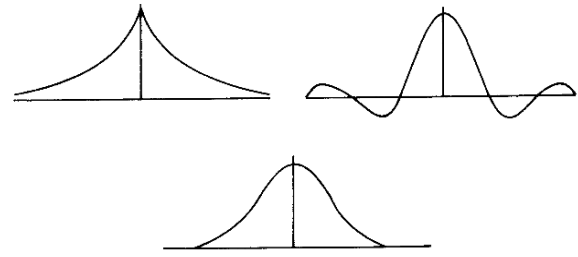


FIGURE 11.37. Some possible autocorrelation functions of noise.

culated over a time interval that is “long enough” so that the average does not change. Suppose that we are measuring the electrical potential between a pair of electrodes on the scalp. Assume that there is no obvious periodicity, and we think it is noise. If we measure the potential for only a few milliseconds, we will get one average value. If we measure for the same length of time a few minutes later, we may get a different average. But if we average for two or three minutes, then a repetition gives almost the same average.

In general, random signals may vary with time in such a way that this average changes. (If we repeat the measurements on the scalp in a few hours, the averages may be different.) We will *assume* that properties such as the mean and standard deviation and power spectrum do not change with time, so that if we average over a “long enough” interval and repeat the average at a later time, we get the same result. Processes that generate data with these properties are called *stationary*. We limit our discussion to stationary random processes.

The correlation functions are not particularly useful for well-defined periodic signals, but they are very useful to describe noise or a signal that is contaminated by noise. (In fact, they allow us to detect a periodic signal that is completely hidden by noise. The technique is described in the next section.)

Space limitations require us to state some properties of the autocorrelation function of noise without proof, though the results are plausible. Many discussions of noise are available. An excellent one with a biological focus is by DeFelice (1981).

The autocorrelation function is given by Eq. 11.45:

$$\phi_{11}(\tau) = \langle y_1(t)y_1(t+\tau) \rangle = \lim_{T \rightarrow \infty} \frac{1}{2T} \int_{-T}^T y_1(t)y_1(t+\tau) dt.$$

The properties of the autocorrelation function depend on the details of the noise. Some possible shapes for the autocorrelation function are shown in Fig. 11.37.

The following properties of the autocorrelation function can be proved:

1. The autocorrelation function is an even function of  $\tau$ . This follows from the definition.

2. The autocorrelation function for  $\tau = 0$ ,  $\phi_{11}(0)$ , measures the average power in the signal. This also follows from the definition.
3. For a random signal with no constant or periodic components, the autocorrelation function goes to zero as  $\tau \rightarrow \infty$ . This is plausible, since for large shifts, if the signal is completely random, there is no correlation.
4. The autocorrelation function has its peak value at  $\tau = 0$ . This is also plausible, since for any shift of a random signal there will be some loss of correlation.

## 11.14 Correlation Functions and Noisy Signals

### 11.14.1 Detecting Signals in Noise

The autocorrelation function is useful for detecting a periodic signal in the presence of noise. We assume that the system that measures these is linear: the response to two simultaneous signals is the sum of the responses to each individually. Section 11.18 will consider what happens when the response is non-linear. Suppose that the periodic signal is  $s(t)$ , the random noise is  $n(t)$ , and the average of both is zero. The combination of signal and noise is

$$y(t) = s(t) + n(t). \tag{11.73}$$

The autocorrelation of the combination is

$$\begin{aligned} \phi_{yy}(\tau) &= \langle [s(t) + n(t)][s(t + \tau) + n(t + \tau)] \rangle \\ &= \langle s(t)s(t + \tau) \rangle + \langle s(t)n(t + \tau) \rangle \\ &\quad + \langle n(t)s(t + \tau) \rangle + \langle n(t)n(t + \tau) \rangle. \end{aligned}$$

Each term in the average can be identified as a correlation function:

$$\phi_{yy}(\tau) = \phi_{ss}(\tau) + \phi_{sn}(\tau) + \phi_{ns}(\tau) + \phi_{nn}(\tau).$$

Since the noise is random, the cross correlations  $\phi_{ns}$  and  $\phi_{sn}$  should be zero if the averages were taken over a sufficiently long time. Therefore,

$$\phi_{yy}(\tau) = \phi_{ss}(\tau) + \phi_{nn}(\tau). \tag{11.74}$$

The autocorrelation of a periodic signal is periodic in  $\tau$ , while the autocorrelation of the noise approaches zero if  $\tau$  is long enough.

If we suspect that a periodic signal is masked by noise, we can calculate the autocorrelation function. If the autocorrelation function shows periodicity that persists for long shift times  $\tau$ , a periodic signal is present. The period of the correlation function is the same as that of the signal. Acquisition of the data and calculation of the correlation function are done with digital techniques. Press *et al.* (1992) have an excellent discussion of the techniques and pitfalls.

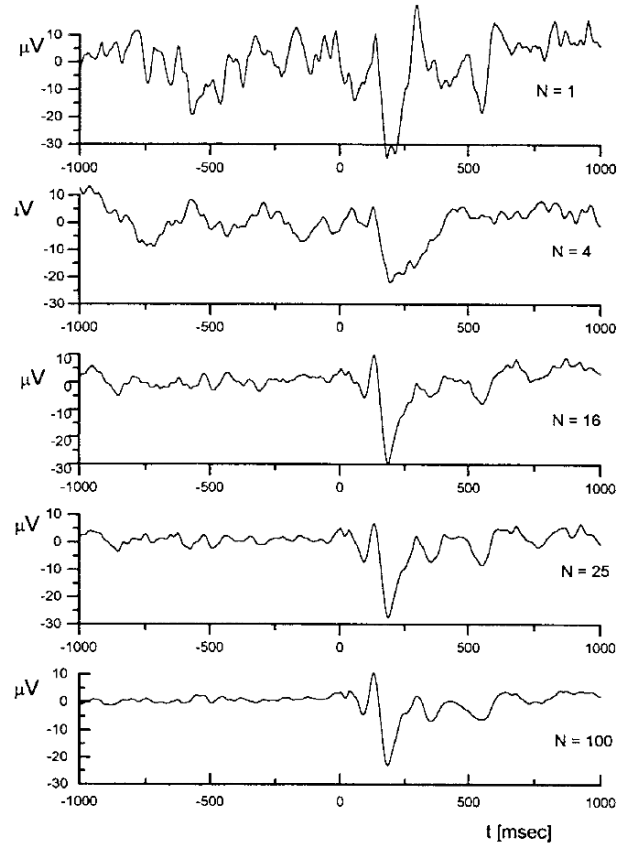


FIGURE 11.38. An example of signal averaging. An evoked response is recorded along with the EEG from a scalp electrode. As the number of repetitions  $N$  is increased, the EEG background decreases and the evoked response stands out. Copyright © 2000 from L. T. Mainardi, A. M. Bianchi, and S. Cerutti (2000). Digital biomedical signal acquisition and processing, in J. D. Bronzino, ed. *Biomedical Engineering Handbook. 2nd. ed.* Boca Raton, FL, CRC Press. Vol. 1, pp. 53-1–53-25. Reproduced by permission of Routledge/Taylor & Francis LLC.

### 11.14.2 Signal Averaging

If the period of a signal is known to be  $T$ , perhaps from the autocorrelation function or more likely because one is looking for the response evoked by a periodic stimulus, it is possible to take consecutive segments of the combined signal plus noise of length  $T$ , place them one on top of another, and average them. One can also do this for the response evoked by a stimulus. The signal will be the same in each segment, while the noise will be uncorrelated. After  $N$  sampling periods, the noise is reduced by  $1/\sqrt{N}$ .

Examples of this are the *visual* or *auditory evoked response*. The signal in the electroencephalogram (EEG) or magnetoencephalogram is measured in response to a flash of light or an audible click. (In other experiments the subject may perform a repetitive task.) The stimulus is repeated over and over while the signal plus noise is recorded and averaged. The average reproduces the shape

of the signal. Figure 11.38 shows an example of signal averaging for an evoked response in the EEG for increasing values of  $N$ .

The signal-averaging procedure can also be described in terms of a cross correlation with a series of  $\delta$  functions at the stimulus times. Suppose a local signal  $l(t)$  is produced in synchrony with the stimulus. The cross correlation of  $l(t)$  with  $y(t)$  is

$$\phi_{yl}(\tau) = \langle [s(t) + n(t)] l(t + \tau) \rangle = \phi_{sl} + \phi_{nl}.$$

Whatever the local signal is, its cross correlation with the noise approaches zero for long averaging times, so

$$\phi_{yl}(\tau) = \phi_{sl}(\tau). \tag{11.75}$$

If the local signal is a series of narrow spikes approximated by  $\delta$  functions, then

$$l(t) = \delta(t) + \delta(t - T) + \delta(t - 2T) + \dots$$

Since both  $s(t)$  and  $l(t)$  are periodic with the same period, the average can be taken over a single period. The integral then contains one  $\delta$  function:

$$\phi_{yl}(-\tau) = \phi_{sl}(-\tau) = \frac{1}{T} \int_0^T s(t) \delta(t - \tau) dt = \frac{s(\tau)}{T}.$$

### 11.14.3 Power Spectral Density

We have already seen that the Fourier transform of a random signal does not exist. Because the phases of a random signal are continually changing, we were unable to predict the future behavior of a time series in Fig. 11.36. If the signal is stationary, averages, including the average power, do not change with time and have meaning. The autocorrelation function of a random signal does exist, and so does the Fourier transform of the autocorrelation. If  $\Phi(\omega)$  is the Fourier transform of the autocorrelation function of a random signal, then

$$\lim_{T \rightarrow \infty} \frac{1}{2T} \int_{-T}^T y^2(t) dt = \int_{-\infty}^{\infty} \Phi(\omega) \frac{d\omega}{2\pi}, \tag{11.76}$$

and we can think of  $\Phi$  as giving the power between frequencies  $f$  and  $f + df$ . This is called the *Wiener theorem for random signals*. The quantity  $\Phi$  is often called the *power spectral density* or PSD. Figure 11.39 summarizes how the power or energy spectrum can be obtained for a periodic signal, a pulse, and a random signal.

In the digital realm there are several ways to calculate the power spectral density.<sup>7</sup> The Blackman–Tukey method makes a digital estimate of the correlation function and takes its discrete Fourier transform, as described in Fig. 11.39(c). The *periodogram* uses the discrete Fourier transform directly. Though the Fourier

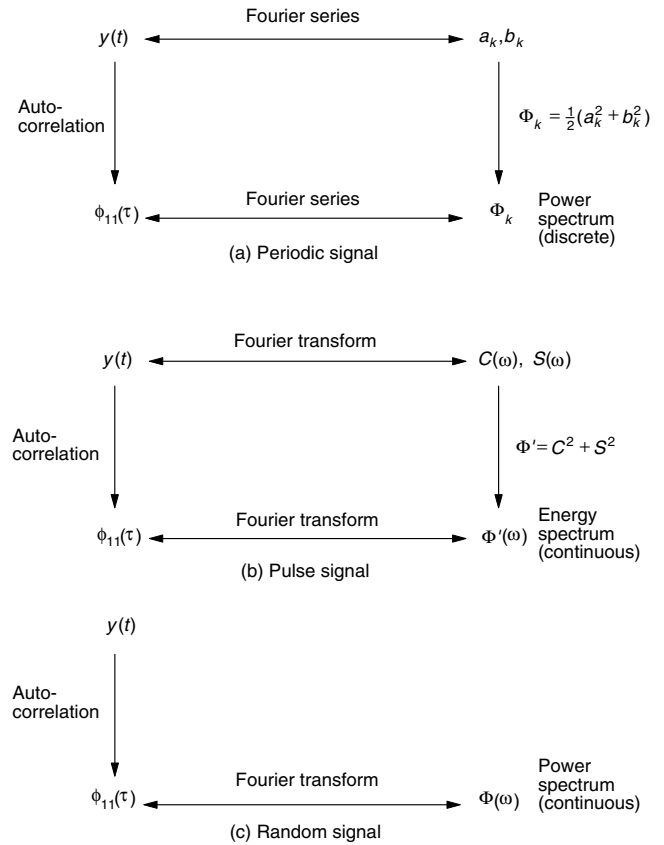


FIGURE 11.39. The relationships between the power spectrum or energy spectrum and (a) a periodic signal, (b) a pulse, (c) a random signal. The Fourier transform and series are bidirectional; the other processes are not.

transform of a random signal does not exist because of the randomly changing phases, the sum of the squares of the coefficients is stable. In fact, we plotted  $\Phi_k$  calculated from the discrete Fourier transform in Fig. 11.36(b). Figure 11.40 shows both ways of calculating  $\Phi(f)$  for a surface electromyogram—the signal from a muscle measured on the surface of the skin. Slight differences can be seen, but they are not significant.

Figure 11.41 shows the power spectrum of an EEG signal and also the effect of aliasing. The original signal has no frequency components above 40 Hz. Sampling was done at 80 Hz. A 50-Hz power frequency signal was added, and the Fourier transform shows a spurious response at 30 Hz. The second panel also shows the mirror-image power spectrum from 40 to 80 Hz that should be thought of as occurring at negative frequencies (the factor of 2 again).

### 11.14.4 Units

It is worth pausing to review the units of the various functions we have introduced. They become confusing because we have three different cases: a periodic signal that is infinite in extent, a pulse signal that is of finite duration, and a random-noise signal that is also infinite in extent

<sup>7</sup>See Press *et al.* (1992), Cohen (2000), or Mainardi *et al.* (2000).

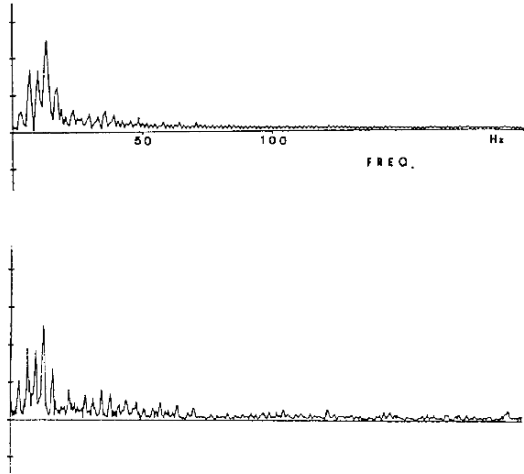


FIGURE 11.40. The power spectrum from a surface electromyogram calculated two different ways. The top panel shows the Blackman–Tukey method, which is a fast Fourier transform of a digital estimate of the autocorrelation function. The lower panel is the sum of the squares of the coefficients in a direct fast Fourier transform of the discrete data. Copyright © 2000 from A. Cohen (2000). *Biomedical signals: origin and dynamic characteristics; frequency-domain analysis*, in J. D. Bronzino, ed. *Biomedical Engineering Handbook*, 2nd. ed. Boca Raton, FL, CRC PPress. Vol. 1, pp. 52-1–52-24. Reproduced by permission of Routledge/Taylor & Francis Group, LLC.

TABLE 11.5. Units used in the various functions in this chapter, assuming that  $y$  is measured in [unit].

Type of function	Expansion coefficients	Correlation functions	Power or energy
<u>Discrete periodic</u> $y$ [unit]	$a_k, b_k$ [unit]	$\phi$ [unit <sup>2</sup> ]	Power [unit <sup>2</sup> ] $\Phi_k$ [unit <sup>2</sup> ]
<u>Pulse</u> $y$ [unit]	$C, S$ [unit s]	$\phi$ [unit <sup>2</sup> s]	Energy $\Phi'(\omega)$ [unit <sup>2</sup> s <sup>2</sup> ] $\Phi'(\omega) d\omega$ [unit <sup>2</sup> s]
<u>Random</u> $y$ [unit]		$\phi$ [unit <sup>2</sup> ]	Power [unit <sup>2</sup> ] $\Phi(\omega)$ [unit <sup>2</sup> s] $\Phi(\omega) d\omega$ [unit <sup>2</sup> ]

age, then the power dissipated in resistance  $R$  is  $v^2/R$  in watts. Our “power” defined from the equations above would be just  $v^2$ .

Suppose that the signal  $y$  is measured in “units.” Then the “power” is in (units)<sup>2</sup> and the “energy” for a pulse is in (units)<sup>2</sup> s. The correlation functions for the infinite signals are in (units)<sup>2</sup> while those for pulses are in (units)<sup>2</sup> s. Table 11.5 summarizes the situation.

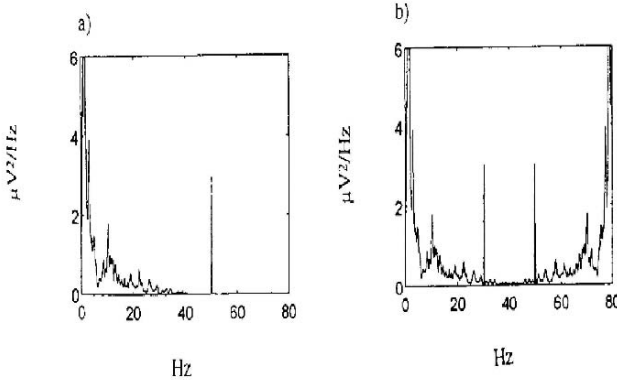


FIGURE 11.41. The power spectrum of an electroencephalogram signal showing the problem with aliasing, and also the presence of negative frequencies appearing as positive frequencies above the Nyquist frequency. Copyright © 2000 from L. T. Mainardi, A. M. Bianchi, and S. Cerutti. *Digital biomedical signal acquisition and processing*, in J. D. Bronzino, ed. *Biomedical Engineering Handbook*. 2nd. ed. Boca Raton, FL, CRC Press. Vol. 1, pp. 53-1–53-25. Reproduced by permission of Routledge/Taylor & Francis Group, LLC.

but not periodic. For both signals that are infinite in extent we must use the “power,” and for the pulse we must use “energy.”

Often in signal analysis the units of “power” and “energy” may not be watts or joules. If the signal is a volt-

### 11.15 Frequency Response of a Linear System

Chapter 10 discussed feedback in a linear system in terms of the solution of a differential equation that described the response of the system as a function of time. The simplest system treated there was described by Eq. 10.20:

$$\tau_1 \frac{dx}{dt} + x = ap(t) + G_1 y(t). \quad (11.77)$$

Function  $p(t)$  is the *input signal*. This equation was combined with Eq. 10.21 to obtain

$$\tau_1 \frac{dx}{dt} + (1 - G_1 G_2)x = ap(t). \quad (11.78)$$

It is often useful to characterize the behavior of a system by its response to sine waves of different frequencies instead of by its time response. The most familiar example is the audio amplifier: the output signal  $x(t)$  is some function of an input signal  $p(t)$  that is seldom a pure sinusoid. An equation analogous to Eq. 11.78 relates  $x$  and  $p$ . The amplifier is usually described as having “a frequency response of  $-0.5$  dB at 10 Hz and 30 kHz.” It is easy to feed a sinusoidal signal of different frequencies into the amplifier and measure the amplitude ratio of the

output sine wave to the input sine wave.<sup>8</sup> To describe the amplifier completely, it is also necessary to measure the phase delay or the time delay at each frequency. The combination of amplitude and phase response is called the *transfer function* of the amplifier.

In principle, once the properties of a linear system are known, either in terms of a differential equation or the transfer function, its response to any input can be calculated. In the time domain, one solves the differential equation with input  $p(t)$  on the right-hand side. In the frequency domain, one computes the Fourier transform of the input, makes the appropriate changes in amplitude and phase at every frequency according to the transfer function, and takes the inverse Fourier transform of the result. The inverse transform gives the output response as a function of time. Sometimes the differential equation may be impossible to solve analytically or the inverse Fourier transform cannot be obtained, and numerical solutions are all that can be obtained.

The frequency-response technique may be particularly useful if the system has several stages (a microphone, an amplifier, one or more loudspeakers); one can multiply the amplitudes and add the phases of each stage.

If the differential equation is known, the frequency response can be calculated. Conversely, if the frequency and phase responses are known, the differential equation can be deduced. We give an example of the former approach in this section. The latter technique requires more mathematics than we have developed.

### 11.15.1 Example of Calculating the Frequency Response

As an example of the frequency response method of describing the system, consider Eq. 11.78. With  $G_2 = 0$ , the results apply to the case without feedback, Eq. 11.77. Let  $p(t) = \cos \omega t$  and  $a = 1$ . We want a solution of the form

$$x(t) = G(\omega) \cos(\omega t - \theta), \quad (11.79)$$

where  $G(\omega)$  is the overall gain or amplitude ratio, and  $\theta(\omega)$  the phase shift, at frequency  $\omega$ . We can show by substitution that Eq. 11.79 is a solution of Eq. 11.78 if

$$G(\omega) = \frac{1}{1 - G_1 G_2} \left( \frac{1}{1 + \omega^2 \tau_1^2 / (1 - G_1 G_2)} \right)^{1/2},$$

$$\tan \theta = \frac{\omega \tau_1}{1 - G_1 G_2}. \quad (11.80)$$

The behavior of the gain is plotted in Fig. 11.42, both without feedback ( $1 - G_1 G_2 = 1$ ) and with feedback ( $1 - G_1 G_2 = 3$ ). At low frequencies the gain is constant. It falls at high frequencies ( $\omega \tau_1 \gg 1$ ) as  $\omega^{-1}$ . When  $\omega = 1/\tau_1$  (without feedback) or  $\omega = 3/\tau_1$  (with feedback),

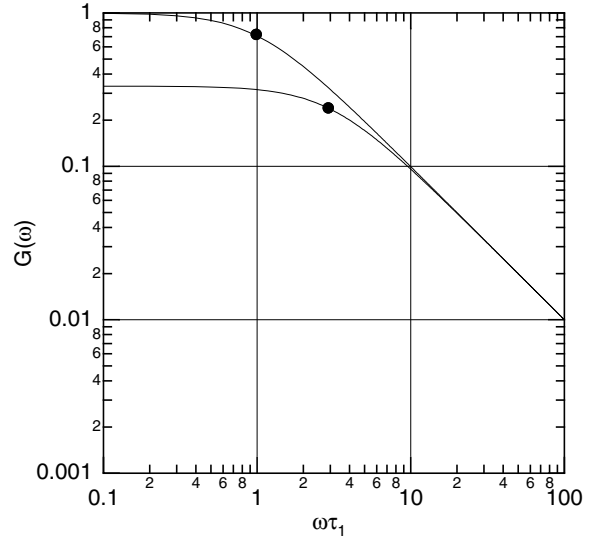


FIGURE 11.42. Plot of  $G(\omega)$  for a system described by Eq. 11.80. Two cases are shown: without feedback ( $1 - G_1 G_2 = 1$ ) and with feedback ( $1 - G_1 G_2 = 3$ ). The dots mark the half-power frequencies (see text).

the gain is  $1/\sqrt{2}$  times its value at zero frequency. This frequency is called the *half-power frequency* because the power is proportional to the square of the signal and its value at the half-power frequency is  $1/2$  times its value at zero frequency.

Negative feedback reduces the gain and also raises the half-power frequency from  $1/\tau_1$  to  $(1 - G_1 G_2)/\tau_1$ . The time constant is reduced by the feedback from  $\tau_1$  to  $\tau_1/(1 - G_1 G_2)$ . Recall Eq. 10.23.

### 11.15.2 The Decibel

The gain is often expressed in decibels<sup>9</sup> (dB):

$$\text{gain(dB)} = 20 \log_{10} G(\omega). \quad (11.81)$$

A gain ratio of unity is equivalent to 0 dB; a gain of 1,000 is  $20 \log_{10}(1,000) = 60$  dB. One advantage to expressing gain in decibels is that the gains in dB for several stages add. If the first process has a gain of 2 (6 dB) and the second has a gain of 100 (40 dB), the overall gain is 200 (46 dB). For the amplifier whose gain has fallen by 0.5 dB at 10 Hz and 30 kHz, the ratio  $G(\omega)/G_{\max}$  is given by solving

$$-0.5 = 20 \log_{10}(G/G_{\max}),$$

$$G/G_{\max} = 10^{-0.025} = 0.944.$$

The gain has fallen to 94.4% of its maximum value at 10 Hz and 30 kHz. If the maximum gain were 1,000 (60 dB),

<sup>8</sup>The technique works only for a linear system. If the system is not linear, the output will not be sinusoidal.

<sup>9</sup>The bel is the logarithm to the base 10 of the *power* ratio. The decibel is one-tenth as large as the bel. Since the power ratio is the square of the voltage ratio or gain, the factor in Eq. 11.81 is 20.

then the gain would have fallen to 944 (59.5 dB) at 10 Hz and 30 kHz.

The fall in gain is called the *roll-off*, in this case the high-frequency roll-off. At high frequencies the gain is proportional to  $1/\omega$ , so it drops by a factor of 2 (6 dB) when the frequency doubles (1 octave). Therefore the gain has a high-frequency roll-off of 6 dB per octave. A roll-off of 6 dB per octave is characteristic of systems with a single time constant, as in Eq. 11.78.

### 11.15.3 Example: Impulse Response

As an example we show that the response of the system to a  $\delta$  function calculated in the time domain is consistent with the frequency response. Let the input be  $p(t) = \delta(t)$ . The Fourier transform of the input is

$$C_{\text{in}}(\omega) = \int_{-\infty}^{\infty} \delta(t) \cos \omega t \, dt = 1,$$

$$S_{\text{in}}(\omega) = \int_{-\infty}^{\infty} \delta(t) \sin \omega t \, dt = 0.$$

The  $\delta$  function contains constant power at all frequencies. The sine coefficients are zero because a  $\delta$  function at  $t = 0$  is an even function. The gain and phase delay are applied to  $C(\omega)$  to get the Fourier transform of the output signal. Although we started with a purely even function (only cosine terms) the phase shift means that the output contains both sine and cosine terms. To calculate the output, we write Eq. 11.79 as

$$x(t) = \int [G(\omega) \cos \theta \cos \omega t + G(\omega) \sin \theta \sin \omega t] \, d\omega,$$

from which

$$C_{\text{out}}(\omega) = G(\omega) \cos \theta,$$

$$S_{\text{out}}(\omega) = G(\omega) \sin \theta.$$

From Eq. 11.80 we get (letting  $G_2 = 0$  and doing a fair amount of algebra)

$$C_{\text{out}}(\omega) = \frac{1}{1 + \omega^2 \tau_1^2},$$

$$S_{\text{out}}(\omega) = \frac{\omega \tau_1}{1 + \omega^2 \tau_1^2}. \tag{11.82}$$

It is easier to solve the differential equation, take the Fourier transform of the solution, and compare it to Eq. 11.82 than it is to find the inverse transform with the mathematical tools at our disposal. For  $G_2 = 0$  the equation to be solved is

$$\tau_1 \frac{dx}{dt} + x = \delta(t).$$

For all positive  $t$  a steady-state solution is  $x(t) = 0$ . The solution of the homogeneous equation is  $x(t) = Ae^{-t/\tau_1}$ .

The value  $A$  is obtained by integrating the equation from  $-\epsilon$  to  $\epsilon$  as  $\epsilon \rightarrow 0$ :

$$\tau_1 \int_{-\epsilon}^{\epsilon} \frac{dx}{dt} \, dt + \int_{-\epsilon}^{\epsilon} x \, dt = \int_{-\epsilon}^{\epsilon} \delta(t) \, dt.$$

The first term is  $x(\epsilon) - x(-\epsilon) \rightarrow x(0) - 0$ . The second term vanishes in the limit, since  $x$  is finite and the width goes to zero. From the definition of the  $\delta$  function the right-hand side of the equation is 1. Therefore

$$x = \begin{cases} 0, & t < 0 \\ (1/\tau_1)e^{-t/\tau_1}, & t > 0. \end{cases} \tag{11.83}$$

The Fourier coefficients of this function were calculated in Eqs. 11.59. They are

$$C(\omega) = \frac{1}{1 + \omega^2 \tau_1^2},$$

$$S(\omega) = \frac{\omega \tau_1}{1 + \omega^2 \tau_1^2}.$$

These agree with Eqs. 11.82. We have demonstrated that the response of this particular linear system to a  $\delta$  function is the Fourier transform of the transfer function of the system.

Although the system is not linear, one can see the frequency response of a physiological system in Figure 11.43. Glucose was administered intravenously to two subjects in a sinusoidal fashion with a period of 144 min, as shown in the top panel. The middle panel shows the resulting insulin secretion rate in a normal subject. Insulin secretion adjusts rapidly to the changing glucose level, and the normalized spectral power density has a peak at a period of 144 min. (Note that the spectrum is plotted vs. period, not frequency.) The bottom panel shows the results for a subject with impaired glucose tolerance (diabetes). There are oscillations in the insulin secretion rate, but they are irregular and at a shorter period, as can be seen in the normalized spectral power density.

## 11.16 The Frequency Spectrum of Noise

In Sec. 9.8 we introduced Johnson noise and shot noise. Both are inescapable. Johnson noise arises from the Brownian motion of charge carriers in a conductor; shot noise arises from fluctuations due to the discrete nature of the charge carriers.

### 11.16.1 Johnson Noise

When we introduced Johnson noise we said nothing about its frequency spectrum. We used the equipartition theorem to argue that since the energy on a capacitor depends on the square of the voltage, there would be fluctuations

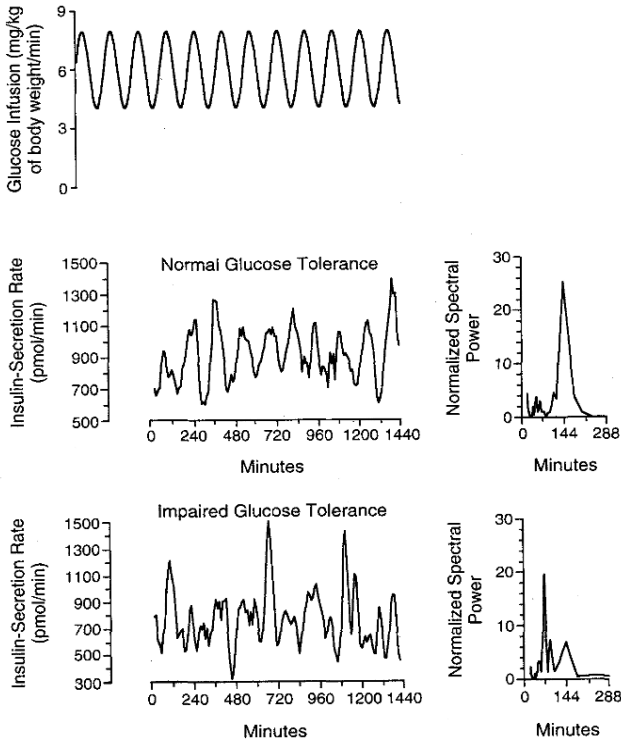


FIGURE 11.43. An example of the frequency response of a system. Glucose was administered intravenously to two subjects in a sinusoidal fashion with a period of 144 min, as shown in the top panel. The responses of the two subjects are discussed in the text. From K. S. Polonsky, J. Sturis, and G. I. Bell (1996). Non-insulin-dependent diabetes mellitus—A genetically programmed failure of the beta cell to compensate for insulin resistance. *New Engl. J. Med.* **334**(12): 777–783. Modified from N. M. O’Meara *et al.* (1993). Lack of control by glucose of ultradian insulin secretory oscillations in impaired glucose tolerance and in non-insulin-dependent diabetes mellitus. *J. Clin. Invest.* **92**: 262–271. Used by permission of the *New England Journal of Medicine* and the *Journal of Clinical Investigation*.

in a capacitor whose average voltage is zero given by (in the notation of this chapter)

$$\frac{1}{2}C \langle v^2 \rangle = \frac{1}{2}k_B T. \tag{11.84}$$

(In this section we will use  $T$  both for time and, when immediately following the Boltzmann constant, for temperature. We also have, briefly,  $C$  for capacitance as well as for the Fourier cosine coefficient. We will eliminate the use of  $C$  for capacitance as much as possible.)

If the capacitor is completely isolated the charge on its plates, and hence the voltage between them, cannot fluctuate. The equipartition theorem applies to the capacitor only when it is in thermal equilibrium with its surroundings. This thermal contact can be provided by a resistor  $R$  between the plates of the capacitor. It is actually the Brownian movement of the charge carriers in this resistor that cause the Johnson noise. In analyzing

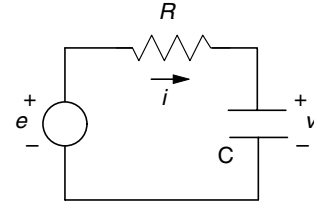


FIGURE 11.44. The circuit for analyzing the noise produced by a resistance  $R$  connected to capacitance  $C$ . The circuit assumes that the noise is generated in a voltage source  $e(t)$  in series with the resistance. The voltage across the capacitance is  $v$ .

the noise in electric circuits, it is customary to imagine that the noise arises in an *ideal voltage source*: a “battery” that maintains the voltage across its terminals—fluctuating randomly with time—regardless of how much current flows through it. It is placed in series with the resistor. This is not a real source. It is a fictitious source that gives the correct results in circuit analysis. We call the voltage across this noise source  $e(t)$  and we want to learn about its properties.

Imagine that we place the noise source and its associated resistor across the plates of a capacitor, as shown in Fig. 11.44. We want to relate the voltage across the capacitor,  $v$ , to the voltage across the noise source,  $e$ . We know that  $e(t) = v(t) + Ri(t)$ , and that  $i = Cdv/dt$ . (See the discussion surrounding Eqs. 6.36 and 6.37.) Therefore

$$e(t) = v(t) + RC \frac{dv}{dt} = \tau_1 \frac{dv}{dt} + v. \tag{11.85}$$

(By introducing  $\tau_1 = RC$  we eliminate the need to use  $C$  for capacitance until the very end of the argument. We use the subscript on  $\tau_1$  to distinguish it from the argument of the correlation function.)

Even though the voltage is random, let us assume we can write it as a Fourier integral. Our final results depend only on the power spectrum and not on the phases. We write

$$v(t) = \frac{1}{2\pi} \int_{-\infty}^{\infty} [C(\omega) \cos \omega t + S(\omega) \sin \omega t] d\omega. \tag{11.86}$$

Differentiating this gives an expression for  $dv/dt$ :

$$\frac{dv}{dt} = \frac{1}{2\pi} \int_{-\infty}^{\infty} [-\omega C(\omega) \sin \omega t + \omega S(\omega) \cos \omega t] d\omega. \tag{11.87}$$

Combining these with Eq. 11.85 gives us the Fourier transform of  $e(t)$ :

$$\begin{aligned} e(t) &= \frac{1}{2\pi} \int_{-\infty}^{\infty} \{ [C(\omega) + \omega\tau_1 S(\omega)] \cos \omega t \\ &\quad + [S(\omega) - \omega\tau_1 C(\omega)] \sin \omega t \} d\omega \\ &= \frac{1}{2\pi} \int_{-\infty}^{\infty} [\alpha(\omega) \cos \omega t + \beta(\omega) \sin \omega t] d\omega. \end{aligned}$$

We now need to calculate  $\langle v^2(t) \rangle$  and  $\langle e^2(t) \rangle$ . The calculation is exactly the same as what we did to derive Parseval's theorem, in Eqs. 11.63–11.66, except that we are dealing with random signals instead of pulses and we have to introduce

$$\lim_{T \rightarrow \infty} \frac{1}{2T}$$

on each side of the equation. When we do this, we find

$$\begin{aligned} \langle v^2(t) \rangle &= \frac{1}{2\pi} \int_{-\infty}^{\infty} [C^2(\omega) + S^2(\omega)] d\omega \\ &= \frac{1}{2\pi} \int_{-\infty}^{\infty} \Phi_v(\omega) d\omega, \\ \langle e^2(t) \rangle &= \frac{1}{2\pi} \int_{-\infty}^{\infty} [\alpha^2(\omega) + \beta^2(\omega)] d\omega \\ &= \frac{1}{2\pi} \int_{-\infty}^{\infty} \Phi_e(\omega) d\omega. \end{aligned} \tag{11.88}$$

If we expand  $\Phi_e$ , we find that

$$\begin{aligned} \Phi_e(\omega) &= \alpha^2(\omega) + \beta^2(\omega) \\ &= [C^2(\omega) + S^2(\omega)] (1 + \omega^2\tau_1^2) \\ &= \Phi_v(\omega)(1 + \omega^2\tau_1^2). \end{aligned} \tag{11.89}$$

Johnson noise was discovered experimentally by J. B. Johnson in 1926. The next year Nyquist explained its origin using thermodynamic arguments and showed that until one reaches frequencies high enough so that quantum-mechanical effects are important,  $\Phi_e$  is a constant independent of frequency [Nyquist (1928)]. We will not reproduce his argument; rather we will assume that  $\Phi_e$  is a constant and find the value of  $\Phi_e$  for which the mean square voltage across the capacitor satisfies the equipartition theorem, Eq. 11.84.

The expression for  $\Phi_v$  becomes

$$\Phi_v(\omega) = \frac{\Phi_e}{1 + \omega^2\tau_1^2}, \tag{11.90}$$

and from the first of Eqs. 11.88,

$$\begin{aligned} \langle v^2(t) \rangle &= \frac{1}{2\pi} \int_{-\infty}^{\infty} \Phi_v(\omega) d\omega = \frac{\Phi_e}{2\pi} \int_{-\infty}^{\infty} \frac{d\omega}{1 + \omega^2\tau_1^2} \\ &= \frac{\Phi_e}{2\pi\tau_1} \int_{-\infty}^{\infty} \frac{dx}{1 + x^2} \\ &= \frac{\Phi_e}{2\pi\tau_1} [\tan^{-1}(\infty) - \tan^{-1}(-\infty)] = \frac{\Phi_e}{2\tau_1}. \end{aligned} \tag{11.91}$$

Putting this expression in the equipartition statement, Eq. 11.84, and remembering that  $\tau_1 = RC$ , we obtain

$$\begin{aligned} \frac{C \langle v^2(t) \rangle}{2} &= \frac{1}{2} C \frac{\Phi_e}{2RC} = \frac{k_B T}{2}, \\ \Phi_e &= 2Rk_B T. \end{aligned} \tag{11.92}$$

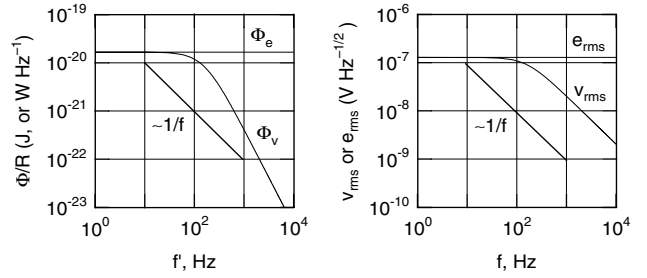


FIGURE 11.45. The power spectrum of the noise source  $e$  and the voltage across the capacitor  $v$ . The left panel plots  $\Phi/R$  vs  $f$ . The right panel plots  $v_{\text{rms}}$  in each frequency interval. The parameters are described in the text.

The units of  $\Phi_e$  are  $V^2 \text{ s}$  or  $V^2 \text{ Hz}^{-1}$ . This is for frequencies that extend from  $-\infty$  to  $\infty$ . If we were dealing with only positive frequencies, we would have

$$\Phi_e = 4Rk_B T \quad (\text{using positive frequencies only}). \tag{11.93}$$

Either way, this says that the power spectrum for the fictitious source  $e(t)$  is constant so there is equal power at all frequencies (up to the limits imposed by quantum mechanical effects). For this reason, Johnson noise is called *white noise*, in analogy with white light that contains all frequencies. The voltage fluctuations across the capacitor have the power spectrum

$$\Phi_v(\omega) = \begin{cases} \frac{2Rk_B T}{1 + \omega^2\tau_1^2}, & -\infty < \omega < \infty \\ \frac{4Rk_B T}{1 + \omega^2\tau_1^2}, & 0 < \omega < \infty. \end{cases} \tag{11.94}$$

Figure 11.45 shows the Johnson-noise power spectra and rms voltage spectra plotted vs frequency. These are based on  $T = 300 \text{ K}$ ,  $R = 10^6 \ \Omega$ ,  $C = 10^{-9} \text{ F}$ , and  $\tau_1 = RC = 10^{-3} \text{ s}$ . The labels on the ordinates are worth discussion. On the left we have  $\Phi/R$ , which from Eq. 11.94 is in joules, which is  $\text{W s}$  or  $\text{W Hz}^{-1}$ . The units for the graph on the right that are consistent with this are  $\text{W}^{1/2} \text{ s}^{1/2} = \text{W}^{1/2} \text{ Hz}^{-1/2} = \text{V } \Omega^{-1/2} \text{ Hz}^{-1/2}$ . The resistance has been included to make the units  $\text{V Hz}^{-1/2}$ . The  $1/f^2$  falloff at high frequencies is due to the frequency response of the RC circuit and is not characteristic of the noise.

Figure 11.46 shows an example: the spectral density of the magnetic field from an article on the magnetoencephalogram. The units are femtotesla  $\text{Hz}^{-1/2}$  (1 femtotesla =  $1 \text{ fT} = 10^{-15} \text{ T}$ ).

We can determine the autocorrelation functions  $\Phi_{ee}(\tau)$  and  $\Phi_{vv}(\tau)$ . Equation 11.72 gave the Fourier transform of the autocorrelation function for a pulse. For a random signal the autocorrelation is very similar but involves the



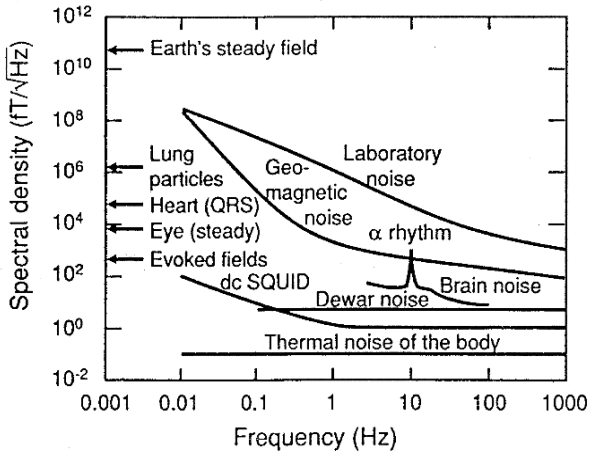


FIGURE 11.46. Spectral density of various sources of the magnetic field, expressed in terms of the magnetic field in femtoTesla ( $1 \text{ fT} = 10^{-15} \text{ T}$ ). Reprinted with permission from M. Hämäläinen, R. Harri, R. J. Ilmoniemi, J. Knuutila, and O. V. Lounasmaa. *Magnetoencephalography—theory, instrumentation, and applications to noninvasive studies of the working human brain. Rev. Mod. Phys.* **65**(2):413–497. 1993. Copyright 1993 by the American Physical Society.

power instead of the energy:

$$\begin{aligned}\phi_{ee}(\tau) &= \frac{1}{2\pi} \int_{-\infty}^{\infty} \Phi_e(\omega) \cos \omega \tau d\omega, \\ \phi_{vv}(\tau) &= \frac{1}{2\pi} \int_{-\infty}^{\infty} \Phi_v(\omega) \cos \omega \tau d\omega.\end{aligned}\quad (11.95)$$

For the voltage source the autocorrelation function is

$$\phi_{ee}(\tau) = \frac{2Rk_B T}{2\pi} \int_{-\infty}^{\infty} \cos \omega \tau d\omega. \quad (11.96)$$

To evaluate this, consider Eq. 11.65a, which shows the Fourier transform of the  $\delta$  function. The integral there is over time. Interchange the time and angular frequency variables to write

$$\int_{-\infty}^{\infty} \cos \omega \tau \cos \omega \tau' d\omega = 2\pi \delta(\tau - \tau'). \quad (11.97)$$

Let  $\tau' = 0$ :

$$\int_{-\infty}^{\infty} \cos \omega \tau d\omega = 2\pi \delta(\tau). \quad (11.98)$$

The final expression for the autocorrelation function of the noise source is

$$\Phi_{ee}(\tau) = 2Rk_B T \delta(\tau). \quad (11.99)$$

To find  $\phi_{vv}(\tau)$ , consider the discussion surrounding Eqs. 11.69 and 11.70. There we discussed the Fourier transform pair (letting  $a = 1/\tau_1$ )

$$\frac{A^2}{1 + \omega^2 \tau_1^2} \xrightarrow{\text{Fourier transform}} \frac{A^2}{2\tau_1} e^{-|\tau|/\tau_1}, \quad (11.100)$$

from which we obtain the autocorrelation function for the voltage across the capacitor:

$$\Phi_{vv}(\tau) = \frac{Rk_B T}{\tau_1} e^{-|\tau|/\tau_1}. \quad (11.101)$$

Let us compare these two results. The autocorrelation of the noise source is a  $\delta$  function. Any shift at all destroys the correlation. The noise equivalent voltage source and resistor, isolated from anything else, respond instantaneously to random noise changes, the correlation function is infinitely narrow, and all frequencies are present. When the source and resistor are connected to a capacitor, the voltage across the capacitor cannot change instantaneously. There is a high-frequency roll-off, and the voltage at one time is correlated with the voltage at surrounding times. As the time constant of the circuit becomes smaller,  $\phi_{vv}(\tau)$  becomes narrower and taller, approaching the  $\delta$  function.

The power spectrum across the capacitor has the same form as the square of the magnitude of the gain (transfer function) of Eq. 11.80. This is the transfer function for an RC circuit, as can be seen by comparing Eq. 11.78 with Eq. 11.85. This is a special case of a general result, that linear systems can be analyzed by measuring how they respond to white noise.

### 11.16.2 Shot Noise

Chapter 9 also mentioned shot noise, which occurs because the charge carriers have a finite charge, so the number of them passing a given point in a circuit in a given time fluctuates about an average value. One can show that shot noise is also white noise.

### 11.16.3 $1/f$ Noise

Johnson noise and shot noise are fundamental and independent of the details of the construction of the resistance. The former depends on the Brownian motion of the charge carriers, and the latter depends on the number of charge carriers required to transport a given amount of charge. They are irreducible lower limits on the noise (for a given resistance and temperature). If one measures the noise in a real resistor in a circuit, one finds additional or “excess” noise that can be reduced by changing the materials or construction of the resistor. This excess noise often has a  $1/f$  frequency dependence. For white noise the power in every frequency interval is proportional to the width of the interval, so there is 10 times as much power in the frequency decade from 10 to 100 Hz as in the decade from 1 to 10 Hz. For  $1/f$  noise, on the other hand, there is equal power in each frequency decade. This kind of noise is sometimes called “pink noise” in allusion to the fact that pink light has more power in the red (lower frequency) part of the spectrum than the rest.

Noise with a  $1/f$  spectrum had been discovered in many places: resistors, transistors, and the fluctuations

in the flow of sand in an hourglass, in traffic flow, in the heartbeat, and even in human cognition. It is thought that there might be some universal principle underlying  $1/f$  noise, possibly related to chaos, but this is still an area of active investigation.

## 11.17 Testing Data for Chaotic Behavior

A major problem in data analysis is to find the meaningful signal due to the physical or biological process in the presence of noise. We have introduced some of the analysis techniques in this chapter. A problem that has only become important in recent years is to determine whether a variable that is apparently random is due to truly random behavior in the underlying process or whether the process is displaying chaotic behavior. The techniques for determining this are still under development and are beyond the scope of this book. An excellent introduction is found in Chapter 6 of Kaplan and Glass (1995). We close by mentioning two of the tools used in this analysis: embedding and surrogate data.

One of the problems in analyzing data from complex systems is that we may not be able to measure all of the variables. For example, we may have the electrocardiogram or even an intracellular potential recording but have no information about the details of the ionic currents of several species through the membrane that change the potential. We may measure the level of thyroid hormones T3 and T4 but have no information about the other hormones in the thyroid–hypothalamus–pituitary feedback system. Fortunately, we do not need to measure all the variables. There is a data-reduction technique that can be applied to a few of the variables that shows the dynamics of the full system.

### 11.17.1 Embedding

To see how embedding works, consider a system with two degrees of freedom described by a set of nonlinear differential equations with the form of Eqs. 10.32. In order to make the subscript on  $x$  available to index measurements of the variable at different times, we write the variables as  $x$  and  $y$  instead of  $x_1$  and  $x_2$ :

$$\frac{dx}{dt} = f_1(x, y), \quad \frac{dy}{dt} = f_2(x, y).$$

A phase-space plot would be in the  $xy$  plane. Suppose we only measure variable  $x$ , and that we obtain a sequence of measurements  $x_j = x(t_j)$ . The time derivative is approximately

$$\frac{x_{j+h} - x_j}{t_{h+j} - t_j} \approx \frac{dx}{dt} = f_1(x, y).$$

A series of measurements at different times gives us information about how function  $f_1$  depends on  $x$ . A remarkable result that we state without proof is that it also gives information about the entire system. [See Kaplan and Glass (1995) for a more detailed discussion and references to the literature.] Figure 11.47 shows this in a specific case. It is a calculation using the van der Pol oscillator. This nonlinear oscillator has been used to model many systems since it was first proposed in the 1920s. It can be written as the pair of first-order equations

$$\frac{dx}{dt} = \frac{1}{a} \left( y - \frac{x^3}{3} + x \right), \quad \frac{dy}{dt} = -ax,$$

where  $a$  is a very small positive number. The top panel of Fig. 11.47 shows values of  $x_j$  vs  $j$  (labeled as  $D_t$  vs  $t$ ). The middle panel shows a phase-plane plot of  $y$  vs  $x$ . The bottom panel plots  $x_{j+10}$  vs  $x_j$ . Shading is used to identify some of the early data points in all three panels. The trajectory in the bottom panel has all the same characteristics as the phase-plane plot.

This is an example of a general technique called *time-lag embedding*. The set of differential equations with two degrees of freedom has been converted into a nonlinear map in one degree of freedom.

For a system with three degrees of freedom, we could make a three-dimensional plot by creating sets of three numbers from the  $n$  measured values, which we can think of and plot as the three components of a vector

$$\mathbf{x}_j = (x_j, x_{j-h}, x_{j-2h}), \quad j = 2h, 2h + 1, \dots, n - 1.$$

In general, we can construct a  $p$ -dimensional set of vectors

$$\mathbf{x}_j = (x_j, x_{j-h}, \dots, x_{j-ph}), \quad j = ph, \dots, n - 1.$$

We call  $p$  the *embedding dimension* and  $h$  the *embedding lag*. There are a number of further calculations that can be done to the embedded vector to help decide on the behavior of the underlying system. These are described in Kaplan and Glass (1995).

### 11.17.2 Surrogate Data

In general, a fully conclusive answer to the question of whether the data are due to a random process or a chaotic process cannot be obtained, though strong indications can be. The most rigorous way to test for the presence of chaotic behavior is to make the hypothesis—called the *null hypothesis*—that the data are explained by a linear process plus random noise. One then develops a test statistic (several standard tests are used) and compares the value of the test statistic for the real data to its value for sets of data that are consistent with the null hypothesis. These sets are called *surrogate data*. We examined one linear system with noise: the random walk of Fig. 11.36. The next value in the sequence was the previous value plus random noise. We saw that the power spectrum was defined, but the phases changed randomly. We

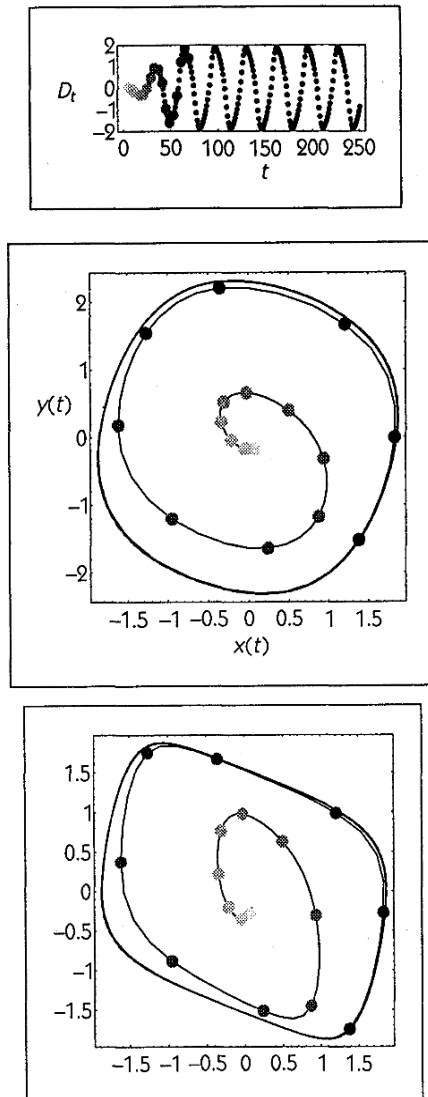


FIGURE 11.47. Plots of the solution to the van der Pol equation with a certain set of initial conditions. The top panel shows values of  $x_j$  vs  $j$  (labeled as  $D_t$  vs  $t$ ). The middle panel is a phase-plane plot of  $y$  vs  $x$ . The bottom panel plots  $x_{j+10}$  vs  $x_j$ . Shading is used to identify some of the early data points in all three panels. The trajectory in the bottom panel has the same characteristics as the phase-plane plot. Used by permission from D. Kaplan and L. Glass. *Understanding Nonlinear Dynamics*. New York, Springer-Verlag, 1995.

can think of any linear system driven by random noise as having a defined transfer function  $G(\omega)$  with random phases. Therefore, one can generate sets of surrogate data by taking the transform of the original data in the form of an amplitude and phase, related to  $C$  and  $S$  by Eq. 11.13. One then randomizes the phases and calculates the inverse Fourier transform of the randomized coefficients to generate the surrogate data sequence. The surrogate data have the same power spectrum and autocorrelation function as the original data. One then applies the various test statistics. If we were to do this to the data from Fig.

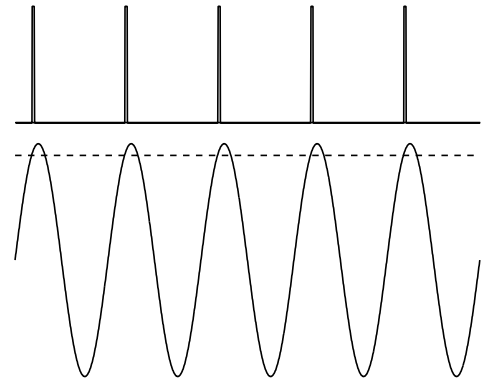


FIGURE 11.48. A sine wave of unit amplitude drives a threshold detector. A spike is generated every time the signal rises through 0.9.

11.36, we would find the tests the same for the original data and the sets of surrogate data, because the original data set is consistent with the null hypothesis.

## 11.18 Stochastic Resonance

A nonlinear phenomenon called *stochastic resonance* has been recognized in recent years. In stochastic resonance, random fluctuations increase the sensitivity to detect weak signals or allow some other desirable process to take place, such as ion transport. Stochastic resonance takes many forms. It was first invoked in 1981 to explain why the earth has periodic ice ages.<sup>10</sup> It has been proposed as a mechanism in biological processes, but the models are rather complicated.<sup>11</sup> We discuss two simple physical examples.

### 11.18.1 Threshold Detection

In a linear system, any amount of noise decreases the signal-to-noise ratio. In a non-linear system, weak noise can enhance signal detection. The simplest non-linear system that shows this is a threshold detector: an output signal is generated when the input (signal + noise) exceeds a fixed threshold.

Suppose that a sine-wave signal is sent to a threshold detector. Every time the signal rises above the threshold, a pulse is generated, as shown in Fig. 11.48. The output signal is a series of pulses spaced by  $T$ , the period of the sine wave. Problem 24 shows that for a series of

<sup>10</sup>References can be found in the articles by Wiesenfeld and Jaramillo (1998) and by Astumian and Moss (1998).

<sup>11</sup>See Astumian (1997); Astumian and Moss (1998); Wiesenfeld and Jaramillo (1998); Gammiatoni *et al.* (1998); Adair, Astumian and Weaver (1998); Glass (2001).

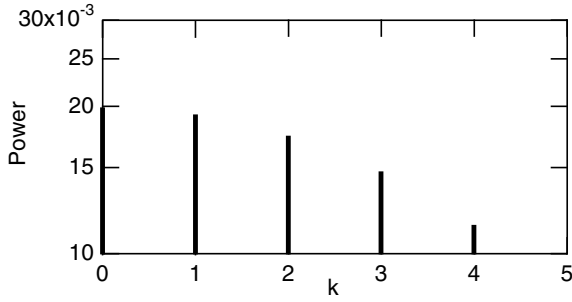


FIGURE 11.49. Power spectrum for a train of rectangular pulses of width  $2d$  when  $d/T = 1/20$ .

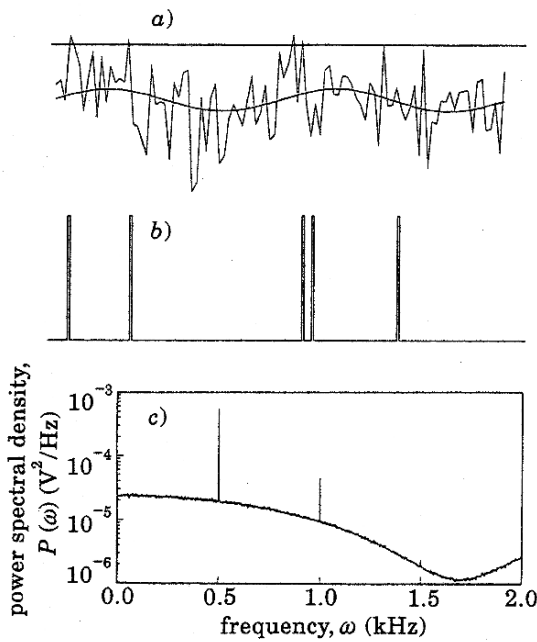


FIGURE 11.50. Stochastic resonance. (a) The two curves show the sinusoidal signal and the combination of Gaussian noise plus signal. The latter occasionally exceeds the threshold value shown by the straight line. (b) The pulses generated when the combination of signal plus noise rises above threshold. (c) The averaged power spectrum of the pulse train. From Z. Gingl, L. B. Kiss and F. Moss. Nondynamical stochastic resonance: Theory and experiments with white and arbitrarily coloured noise. *Europhys. Lett.* **29**(3): 191–196 (1995). Used by permission.

pulses of width  $2d$  separated by time  $T$ , the power at frequency  $k\omega_0 = 2\pi k/T$  is  $\Phi_k = (2/\pi^2 k^2) \sin^2(2\pi kd/T)$ . This power spectrum is plotted in Fig. 11.49.

If the amplitude of the sine wave in Fig. 11.49 is less than 0.9, the threshold will never be exceeded. However, if sufficient noise is added to a sine wave that is below threshold, the signal and noise combined will occasionally exceed the threshold. This will happen more frequently when the sine-wave signal is positive than when it is neg-

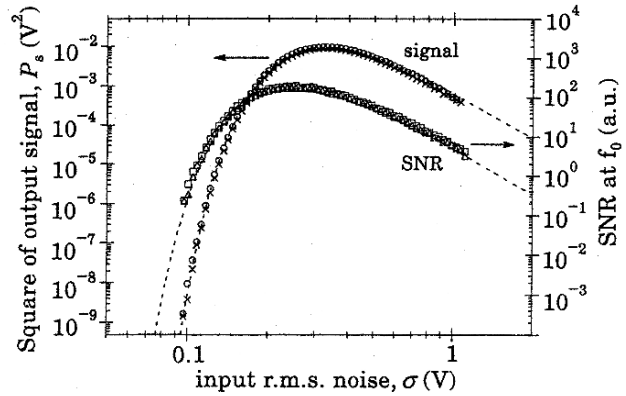


FIGURE 11.51. The results of an electronics experiment and a theoretical calculation of threshold detection. One curve shows the square of the output sinusoidal signal,  $P_s$ . The other shows the signal-to-noise ratio. From Z. Gingl, L. B. Kiss, and F. Moss. Non-dynamical stochastic resonance: Theory and experiments with white and arbitrarily coloured noise. *Europhys. Lett.* **29**(3): 191–196 (1995). Used by permission.

ative so output pulses will occur more frequently during peaks of the signal.

Experiments were done with an electronic circuit that behaves as we have described. The results are shown in Figures 11.50 and 11.51. Figure 11.50 shows the weak sinusoidal signal with and without the noise added to it, along with the resulting pulses and the power spectrum. Figure 11.51 shows the power in the pulse train at the signal frequency and the signal-to-noise ratio, as a function of noise level. The amplitude of the sine wave is 0.1 V. As the noise level increases, both the signal and the SNR increase, reach a maximum, and decrease. The signal-to-noise ratio peaks when the rms noise level is about 0.25 V; the power at the signal frequency peaks at about 0.3 V. As the noise increases above these values the SNR and signal decrease. The lines are theoretical fits; both the theory and the data are described by Gingl *et al.* (1995).

### 11.18.2 Feynman's Ratchet

Perpetual motion machines violate either the first or second law of thermodynamics (or both). In his *Lectures on Physics*, Richard Feynman (1963) analyzed a microscopic cog wheel (ratchet) and pawl as shown in Fig. 11.52. Feynman's analysis is elegant, full of insight, and well worth reading. The analysis here follows that in Astumian and Moss (1998). An amount of energy  $\Delta U$  is required to compress the spring enough to lift the pawl over the tooth. This energy can come either from an imbalance of the molecular bombardment of the paddle wheel at temperature  $T_1$ , or from molecular bombardment of the pawl spring, which is at temperature  $T_2$ . Clockwise rotation will result if the pawl rides up the ramped side of the ratchet and will occur with a probability proportional to  $e^{-\Delta U/k_B T_1}$ ; counterclockwise rotation requires energy

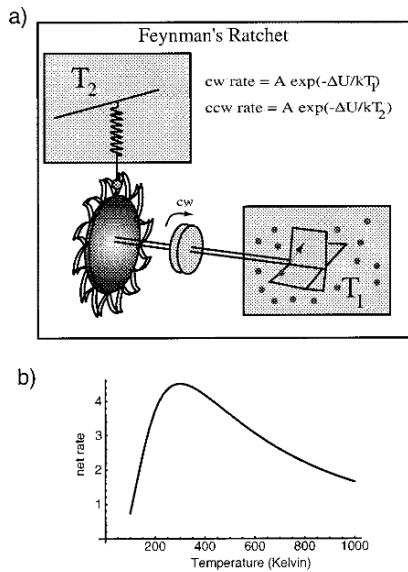


FIGURE 11.52. Feynman's ratchet. (a) A cog wheel is attached to a paddlewheel in a reservoir at temperature  $T_1$ . A pawl is attached to a spring located in a reservoir at temperature  $T_2$ . (b) The net rate of clockwise motion vs.  $T = (T_1 + T_2)/2$ . The details are discussed in the text. Reproduced by permission from Astumian, R. D. and F. Moss. Overview: The constructive role of noise in fluctuation driven transport and stochastic resonance. *Chaos*. 8(3): 533-538. (1998). Copyright 1998 American Institute of Physics.

transfer to the pawl spring, with a probability proportional to  $e^{-\Delta U/k_B T_2}$ . With  $T_1 = T + \Delta T$  and  $T_2 = T - \Delta T$ , one can show (see Problem 38), that the net rate is

$$\text{net rate} \propto \frac{2\Delta U \Delta T}{k_B T^2} e^{-\Delta U/k_B T}. \quad (11.102)$$

Fig. 11.52b plots the net rate for the parameters  $\Delta U = 0.05$  eV and  $\Delta T = 10$  K. While thermal gradients are not found in the body, Astumian and Moss show that particles in similar asymmetrically-shaped potentials can be driven by having the barrier height vary randomly with time.

### Symbols Used in Chapter 11

Symbol	Use	Units	First used on page
$a$	Coefficient in polynomial fit		285
$a$	Slope		285
$a$	Coefficient of even (cosine) term		290
$a$	Parameter in exponential		288
$a$	Arbitrary constant		304
$b$	Intercept		285
$b$	Parameter in exponential		288
$b$	Coefficient of odd (sine) term		290
$e$	Noise voltage source	V	313
$f, f_0$	Frequency	Hz	290
$f$	Function		316

$h$	Small quantity		288
$h$	Shift index		316
$i$	$\sqrt{-1}$		292
$i$	Current	A	296
$j$	Index, usually denoting a data point		285
$k$	Index denoting terms in a sum		285
$k_B$	Boltzmann constant	J K <sup>-1</sup>	313
$l, m$	Particular values of index $k$		290
$l$	Local signal		309
$n$	Maximum value of index $k$		290
$n$	Noise		308
$p$	Parameter or input signal		310
$p$	Dimension of a vector		316
$s$	Signal		308
$t$	Time	s	289
$v$	$\log y$		288
$v$	Voltage	V	296
$x$	Independent variable		285
$x$	Vector of data points		316
$y$	Dependent variable		285
$A$	Amplitude		289
$C, C_k$	Amplitude of cosine term		289
$C$	Capacitance	F	313
$G$	Gain		310
$N$	Number of data points		286
$Q$	Goodness of fit or mean square residual		286
$R$	Residual		292
$R$	Resistance	$\Omega$	296
$S, S_k$	Amplitude of sine term		289
$S_{xx}, S_{xy}$	Sums of residuals and their products		287
$T$	Period	s	289
$T$	Temperature	K	313
$U$	Energy	J	318
$Y, Y_k$	Complex Fourier transform or series of $y$		292
$\alpha$	Fourier coefficient in autocorrelation function		301
$\alpha, \beta$	Fourier coefficients	V Hz <sup>-1/2</sup>	313
$\delta y$	Uncertainty in $y$		288
$\delta$	Delta function		304
$\epsilon$	Error		297
$\epsilon$	Small number (limit of integration)		312
$\phi, \theta$	Phase		289
$\phi$	Correlation function		299
$\tau$	Shift time	s	299
$\tau_1$	Time constant	s	310
$\omega, \omega_0$	Angular frequency	s <sup>-1</sup>	289
$\Phi_k$	Power at frequency $k\omega_0$		298
$\Phi(\omega)$	Power in frequency interval		309
$\Phi'(\omega)$	Energy in frequency interval		305
$\langle \rangle$	Time average		297

### Problems

#### Section 11.1

**Problem 1** Find the least squares straight line fit to the following data:

$x$	$y$
0	2
1	5
2	8
3	11

**Problem 2** Suppose that you wish to pick one number to characterize a set of data  $x_1, x_2, \dots, x_N$ . Prove that the mean  $\bar{x}$ , defined by

$$\bar{x} = \frac{1}{N} \sum_{j=1}^N x_j,$$

minimizes the mean square error

$$Q = \frac{1}{N} \sum_{j=1}^N (x_j - \bar{x})^2.$$

**Problem 3** Derive Eqs. 11.5.

**Problem 4** Suppose that the experimental values  $y(x_j)$  are exactly equal to the calculated values plus random noise for each data point:  $y(x_j) = y_{\text{calc}}(x_j) + n_j$ . What is  $Q$ ?

**Problem 5** You wish to fit a set of data  $(x_j, y_j)$  with an expression of the form  $y = Bx^2$ . Differentiate the expression for  $Q$  to find an equation for  $B$ .

**Problem 6** Assume a dipole  $\mathbf{p}$  is located at the origin and is directed in the  $xy$  plane. The  $z$  component of the magnetic field,  $B_z$ , produced by this dipole is measured at nine points on the surface  $z = 50$  mm. The data are

$i$	$x_i$ (mm)	$y_i$ (mm)	$B_{zi}$ (fT)
1	-50	-50	-154
2	0	-50	-170
3	50	-50	-31
4	-50	0	-113
5	0	0	0
6	50	0	113
7	-50	50	31
8	0	50	170
9	50	50	154

The magnetic field of a dipole is given by Eq. 8.15, which in this case is

$$B_z = \frac{\mu_0}{4\pi} \left[ \frac{p_x y_i}{(x_i^2 + y_i^2 + z_i^2)^{3/2}} - \frac{p_y x_i}{(x_i^2 + y_i^2 + z_i^2)^{3/2}} \right].$$

Use the method of least squares to fit the data to the equation, and determine  $p_x$  and  $p_y$ .

**Problem 7** Consider the data

$x$	$y$
100	4004
101	4017
102	4039
103	4063

(a) Fit these data with a straight line  $y = ax + b$  using Eqs. 11.5a and 11.5b to find  $a$ .

(b) Use Eq. 11.5c to determine  $a$ . Your result should be the same as in part (a).

(c) Repeat parts (a) and (b) while rounding all the intermediate numbers to 4 significant figures. Do Eqs. 11.5a and 11.5b give the same result as Eq. 11.5c? If not, which is more accurate?

**Problem 8** This problem is designed to show you what happens when the number of parameters exceeds the number of data points. Suppose that you have two data points:

$x$	$y$
0	1
1	4

Find the best fits for one parameter (the mean) and two parameters ( $y = ax + b$ ). Then try to fit the data with three parameters (a quadratic). What happens when you try to solve the equations?

**Problem 9** The strength-duration curve for electrical stimulation of a nerve is described by Eq. 7.45:  $i = i_R(1 + t_C/t)$ , where  $i$  is the stimulus current,  $i_R$  is the rheobase, and  $t_C$  is the chronaxie. During an experiment you measure the following data:

$t$ (ms)	$i$ (mA)
0.5	2.004
1.0	1.248
1.5	0.997
2.0	0.879
2.5	0.802
3.0	0.749

Determine the rheobase and chronaxie by fitting these data with Eq. 7.45. Hint: let  $a = i_R$  and  $b = i_R t_C$ , so that the equation is linear in  $a$  and  $b$ :  $i = a + b/t$ . Use the linear least squares method to determine  $a$  and  $b$ . Plot  $i$  vs.  $t$ , showing both the theoretical expression and the measured data points.

### Section 11.2

**Problem 10** (a) Obtain equations for the linear least-squares fit of  $y = Bx^m$  to data by making a change of variables.

(b) Apply the results of (a) to the case of Problem 5. Why does it give slightly different results?

(c) Carry out a numerical comparison of Problems 5 and (b) with the data points

$x$	$y$
1	3
2	12
3	27

Repeat with

$x$	$y$
1	2.9
2	12.1
3	27.1

**Problem 11** Consider the data given in Problem 2.36 relating molecular weight  $M$  and molecular radius  $R$ . Assume the radius is determined from the molecular weight by a power law:  $R = BM^n$ . Fit the data to this expression to determine  $B$  and  $n$ . Hint: Take logarithms of both sides of the equation.

**Problem 12** In Prob. 6 the dipole strength and orientation were determined by fitting the equation for the magnetic field of a dipole to the data, using the linear least squares method. In that problem the location of the dipole was known. Now, suppose the location of the dipole  $(x_0, y_0, z_0)$  is not known. Derive an equation for  $B_z(p_x, p_y, x_0, y_0, z_0)$  in this more general case. Determine which parameters can be found using linear least squares, and which must be determined using nonlinear least squares.

Section 11.4

**Problem 13** Write a computer program to verify Eqs. 11.20–11.24.

**Problem 14** Consider Eqs. 11.17–11.19 when  $n = N$  and show that all equations for  $m > N/2$  reproduce the equations for  $m < N/2$ .

**Problem 15** The secretion of the hormone cortisol by the adrenal gland is subject to a 24-hour (circadian) rhythm [Guyton (1991)]. Suppose the concentration of cortisol in the blood,  $K$  (in  $\mu\text{g}$  per 100 ml) is measured as a function of time,  $t$  (in hours, with 0 being midnight and 12 being noon), resulting in the following data:

$t$	$K$
0	10.3
4	16.1
8	18.3
12	13.7
16	7.9
20	6.0

Fit these data to the function  $K = a + b \cos(2\pi t/24) + c \sin(2\pi t/24)$  using the method of least squares, and determine  $a$ ,  $b$ , and  $c$ .

**Problem 16** Verify that Eqs. 11.29 follow from Eqs. 11.27.

**Problem 17** This problem provides some insight into the Fast Fourier Transform. Start with the expression for an  $N$ -point Fourier transform in complex notation,  $Y_k$  in Eq. 11.29a. Show that  $Y_k$  can be written as the sum of two  $N/2$ -point Fourier transforms:  $Y_k = Y_k^e + W^k Y_k^o$ , where  $W = \exp(i2\pi/N)$ , superscript  $e$  stands for even values of  $j$ , and  $o$  stands for odd values.

Section 11.5

**Problem 18** Use Eqs. 11.33 to derive Eq. 11.34.

**Problem 19** The following data from Kaiser and Halberg (1962) show the number of spontaneous births vs. time of day. Note that the point for 2300 to 2400 is much higher than for 0000–0100. This is probably due to a bias: if a woman has been in labor for a long time and the baby is born a few minutes after midnight, the birth may be recorded in the previous day. Fit these data with a 24-hr period and again including an 8-hr period as well. Make a correction for the midnight bias.

Time	Births	Time	Births
0000-0100	23 847	1200-1300	24 038
0100-0200	28 088	1300-1400	22 234
0200-0300	28 338	1400-1500	21 900
0300-0400	28 664	1500-1600	21 903
0400-0500	28 452	1600-1700	21 789
0500-0600	27 912	1700-1800	21 927
0600-0700	27 489	1800-1900	21 761
0700-0800	26 852	1900-2000	21 995
0800-0900	26 421	2000-2100	22 913
0900-1000	26 947	2100-2200	23 671
1000-1100	26 498	2200-2300	24 149
1100-1200	25 615	2300-2400	27 819

Section 11.7

**Problem 20** Suppose that  $y(x, t) = y(x - vt)$ . Calculate the cross correlation between signals  $y(x_1)$  and  $y(x_2)$ .

**Problem 21** Calculate the cross-correlation,  $\phi_{12}$ , for the example in Fig. 11.20:

$$y_1(t) = \begin{cases} +1, & 0 < t < T/2 \\ -1, & T/2 < t < T \end{cases}$$

$$y_2(t) = \sin\left(\frac{2\pi t}{T}\right).$$

Both functions are periodic.

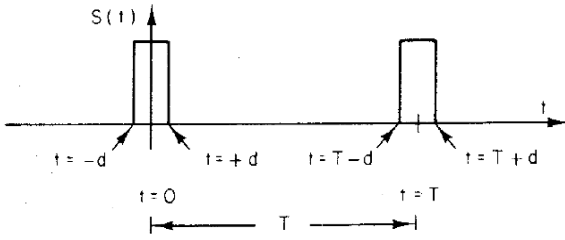
Section 11.8

**Problem 22** Fill in the missing steps to show that the autocorrelation of  $y_1(t)$  is given by Eq. 11.49.

**Problem 23** Consider a square wave of amplitude  $A$  and period  $T$ .

- (a) What are the coefficients in a Fourier-series expansion?
- (b) What is the power spectrum?
- (c) What is the autocorrelation of the square wave?
- (d) Find the Fourier-series expansion of the autocorrelation function and compare it to the power spectrum.

**Problem 24** The series of pulses shown are an approximation for the concentration of follicle-stimulating hormone (FSH) released during the menstrual cycle.



- (a) Determine  $a_0$ ,  $a_k$ , and  $b_k$  in terms of  $d$  and  $T$ .
- (b) Sketch the autocorrelation function.
- (c) What is the power spectrum?

**Problem 25** Consider the following simplified model for the periodic release of follicle-stimulating hormone (FSH). At  $t = 0$  a substance is released so the plasma concentration rises to value  $C_0$ . The substance is cleared so that  $C(t) = C_0 e^{-t/\tau}$ . Thereafter the substance is released in like amounts at times  $T, 2T$ , and so on. Furthermore,  $\tau \ll T$ .

- (a) Plot  $C(t)$  for two or three periods.
- (b) Find general expressions for  $a_0$ ,  $a_k$ , and  $b_k$ . Use the fact that integrals from 0 to  $T$  can be extended to infinity because  $\tau \ll T$ . Use the following integral table:

$$\int_0^\infty e^{-ax} dx = \frac{1}{a},$$

$$\int_0^\infty e^{-ax} \cos mx dx = \frac{a}{a^2 + m^2},$$

$$\int_0^\infty e^{-ax} \sin mx dx = \frac{m}{a^2 + m^2}.$$

- (c) What is the “power” at each frequency?
- (d) Plot the “power” for  $k = 1, 10, 100$  for two cases:  $\tau/T = 0.1$  and  $0.01$ . Compare the results to the results of Problem 24
- (e) Discuss qualitatively the effect that making the pulses narrower has on the power spectrum. Does the use of Fourier series seem reasonable in this case? Which description of the process is easier—the time domain or the frequency domain?
- (f) It has sometimes been said that if the transform for a given frequency is written as  $A_k \cos(k\omega_0 t - \phi_k)$  that  $\phi_k$  gives timing information. What is  $\phi_1$  in this case?  $\phi_2$ ? Do you agree with the statement?

**Problem 26** Calculate the autocorrelation function and the power spectrum for the previous problem.

Section 11.9

**Problem 27** Calculate the Fourier transform of  $\exp[-(at)^2]$  using complex notation (Eq. 11.57). Hint: complete the square.

Section 11.10

**Problem 28** Prove that

$$\delta(t) = \delta(-t),$$

$$t \delta(t) = 0,$$

$$\delta(at) = \frac{1}{|a|} \delta(t).$$

Section 11.11

**Problem 29** Rewrite Eqs. 11.59 in terms of an amplitude and a phase. Plot them.

**Problem 30** Find the Fourier transform of

$$f(t) = \begin{cases} 1, & -a \leq t \leq a, \\ 0, & \text{everywhere else.} \end{cases}$$

**Problem 31** Find the Fourier transform of

$$y = \begin{cases} e^{-at} \sin \omega_0 t, & t \geq 0, \\ 0, & t < 0. \end{cases}$$

Determine  $C(\omega)$ ,  $S(\omega)$ , and  $\Phi'(\omega)$  for  $\omega > 0$  if the term that peaks at negative frequencies can be ignored for positive frequencies.

Section 11.14

**Problem 32** Here are some data.

$t$	$y$	$t$	$y$	$t$	$y$
1	-1.18	13	1.84	25	0.43
2	1.39	14	5.01	26	0.91
3	0.67	15	0.75	27	1.32
4	-1.38	16	0.90	28	1.92
5	-0.76	17	-0.42	29	0.57
6	5.23	18	3.68	30	2.30
7	1.31	19	4.15	31	1.09
8	2.63	20	1.45	32	-0.71
9	1.03	21	-2.44	33	-1.72
10	4.62	22	4.44	34	4.22
11	1.98	23	-0.08	35	3.20
12	0.47	24	2.34	36	1.69

- (a) Plot them.
- (b) If you are told that there is a signal in these data with a period of 4 s, you can group them together and average them. This is equivalent to taking the cross correlation with a series of  $\delta$  functions. Estimate the signal shape.

Section 11.15

**Problem 33** Verify that Eqs. 11.79 and 11.80 are solutions of Eq. 11.78.



**Problem 34** Equation 11.80 is plotted on log-log graph paper in Fig. 11.42. Plot it on linear graph paper.

**Problem 35** If the frequency response of a system were proportional to  $1/[1 + (\omega/\omega_0)^3]$ , what would be the high frequency roll-off in decibels per octave for  $\omega \gg \omega_0$ ?

**Problem 36** Consider a signal  $y = A \cos \omega t$ . What is the time derivative? For a fixed value of  $A$ , how does the derivative compare to the original signal as the frequency is increased? Repeat these considerations for the integral of  $y(t)$ .

### Section 11.16

**Problem 37** Show that integration of Eq. 11.101 over all shift times is consistent with the integration of the  $\delta$  function that is obtained in the limit  $\tau_1 \rightarrow 0$ .

### Section 11.18

**Problem 38** Show that the net clockwise rate of rotation of the Feynman ratchet is given by Eq. 11.102.

## References

- Adair, R. K., R. D. Astumian, and J. C. Weaver (1998). Detection of weak electric fields by sharks, rays and skates. *Chaos*. **8**(3): 576–587.
- Anderka, M., E. R. Declercq, and W. Smith (2000). A time to be born. *Amer. J. Pub. Health* **90**(1): 124–126.
- Astumian, R. D. (1997). Thermodynamics and kinetics of a Brownian motor. *Science*. **276**: 917–922.
- Astumian, R. D., and F. Moss (1998). Overview: The constructive role of noise in fluctuation driven transport and stochastic resonance. *Chaos*. **8**(3): 533–538.
- Bevington, P. R., and D. K. Robinson (1992). *Data Reduction and Error Analysis for the Physical Sciences*, 2nd ed. New York, McGraw-Hill.
- Blackman, R. B., and J. W. Tukey (1958). *The Measurement of Power Spectra*. AT&T. New York, Dover, pp. 32–33.
- Bracewell, R. N. (1990). Numerical transforms. *Science* **248**: 697–704.
- Cohen, A. (2000). Biomedical signals: Origin and dynamic characteristics; frequency-domain analysis. In J. D. Bronzino, ed. *The Biomedical Engineering Handbook*, 2nd. ed. Vol. 1. Boca Raton, FL, CRC Press, pp. 52-1–52-4.
- Cooley, J. W., and J. W. Tukey (1965). An algorithm for the machine calculation of complex Fourier series. *Math. Comput.* **119**: 297–301.
- DeFelice, L. J. (1981). *Introduction to Membrane Noise*. New York, Plenum.
- Feynman, R. P., R. B. Leighton, and M. Sands (1963). *The Feynman Lectures on Physics*, Vol. 1, Chapter 46. Reading, MA, Addison-Wesley.
- Gammiatoni, L., P. Hänggi, P. Jung, and F. Marchesoni (1998). Stochastic resonance. *Rev. Mod. Phys.* **70**(1): 223–287.
- Gatland, I. R. (1993). A weight-watcher's guide to least-squares fitting. *Comput. Phys.* **7**(3): 280–285.
- Gatland, I. R., and W. J. Thompson (1993). Parameter bias estimation for log-transformed data with arbitrary error characteristics. *Am. J. Phys.* **61**(3): 269–272.
- Gingl, Z., L. B. Kiss, and F. Moss (1995). Non-dynamical stochastic resonance: Theory and experiments with white and arbitrarily coloured noise. *Europhys. Lett.* **29**(3): 191–196.
- Glass, L. (2001). Synchronization and rhythmic processes in physiology. *Nature*. **410**(825): 277–284.
- Guyton, A. C. (1991). *Textbook of Medical Physiology*, 8th ed. Philadelphia, Saunders.
- Kaiser, I. H., and F. Halberg (1962). Circadian periodic aspects of birth. *Ann. N. Y. Acad. Sci.* **98**: 1056–1068.
- Kaplan, D., and L. Glass (1995). *Understanding Non-linear Dynamics*. New York, Springer-Verlag.
- Lighthill, M. J. (1958). *An Introduction to Fourier Analysis and Generalized Functions*. Cambridge, England, Cambridge University Press.
- Lybanon, M. (1984). A better least-squares method when both variables have uncertainties. *Am. J. Phys.* **52**: 22–26.
- Mainardi, L. T., A. M. Bianchi, and S. Cerutti (2000). Digital biomedical signal acquisition and processing. In J. D. Bronzino, ed. *The Biomedical Engineering Handbook*, 2nd. ed. Vol. 1. Boca Raton, FL, CRC, pp. 53-1–53-25.
- Maughan, W. Z., C. R. Bishop, T. A. Pryor, and J. W. Athens (1973). The question of cycling of blood neutrophil concentrations and pitfalls in the analysis of sampled data. *Blood*. **41**: 85–91.
- Milnor, W. R. (1972). Pulsatile blood flow. *New Eng. J. Med.* **287**: 27–34.
- Nedbal, L. and V. Březnia (2002). Complex metabolic oscillations in plants forced by harmonic irradiance. *Biophys. J.* **83**: 2180–2189.
- Nyquist, H. (1928). Thermal agitation of electric charge in conductors. *Phys. Rev.* **32**: 110–113.
- Orear, J. (1982). Least squares when both variables have uncertainties. *Am. J. Phys.* **50**: 912–916.
- Press, W. H., S. A. Teukolsky, W. T. Vetterling, and B. P. Flannery (1992). *Numerical Recipes in C: The Art of Scientific Computing*, 2nd ed., reprinted with corrections, 1995. New York, Cambridge University Press.
- Visscher, P. B. (1996). The FFT: Fourier transforming one bit at a time. *Comput. Phys.* **10**(5): 438–443.
- Wiesenfeld, K., and F. Jaramillo (1998). Minireview of stochastic resonance. *Chaos* **8**(3): 539–548.

# 12

## Images

Images are very important in the remainder of this book. They may be formed by the eye, a camera, an x-ray machine, a nuclear medicine camera, magnetic resonance imaging, or ultrasound. The concepts developed in Chapter 11 can be used to understand and describe image quality. The same concepts are also used to reconstruct computed tomographic or magnetic resonance slice images of the body. A very complete, advanced mathematical treatment of all kinds of images is found in a 1500-page book by Barrett and Myers (2004).

The convolution integral of Sec. 12.1 shows how the response of a linear system can be related to the input to the system and the impulse ( $\delta$ -function) response of the system. It forms the basis for the rest of the chapter. The Fourier-transform properties of the convolution are also described in this section. Section 12.2 introduces quantitative ways to relate the image to the object, using the techniques developed in Chapter 11 to describe the blurring that occurs. Section 12.3 shows the importance of different spatial frequencies in an image and their effect on the quality of the image.

Sections 12.4 and 12.5 pose the fundamental problem of reconstructing slices from projections and introduce two techniques for solving it: the Fourier transform and filtered back projection. Section 12.6 provides a numerical example of filtered back projection for a circularly symmetric object.

This chapter is quite mathematical. The key understanding to take from it is the relationship between spatial frequencies and image quality in Sec. 12.3.

## 12.1 The Convolution Integral and its Fourier Transform

### 12.1.1 One Dimension

We now apply the techniques developed in Chapter 11 to describe the formation of images. An image is a function of position, usually in two dimensions at an *image plane*. We start with the simpler case of an image extending along a line. Functions of time are easier to think about, so let's imagine a one-dimensional example that is a function of time: a high-fidelity sound system. A hi-fi system is (one hopes) *linear*, which means that the relationship between the output response and a complicated input can be written as a superposition of responses to more elementary input functions. The output might be the instantaneous air pressure at some point in the room; the input might be the air pressure at a microphone or the magnetization on a strip of tape.

It takes a certain amount of time for the signal to propagate through the system. In the simplest case the response at the ear would exactly reproduce the response at the input a very short time earlier. In actual practice the response at time  $t$  may depend on the input at a number of earlier times, because of limitations in the electronic equipment or echoes in the room. If the entire system is linear, the output  $g(t)$  can be written as a superposition integral, summing the weighted response to inputs at other times. If  $f(t')$  is the input and  $h$  is the weighting, the output  $g(t)$  is

$$g(t) = \int_{-\infty}^{\infty} f(t')h(t, t') dt'. \quad (12.1)$$

Variable  $t'$  is a dummy variable. The integration is over all values of  $t'$  and it does not appear in the final result, which depends only on the functional forms of  $f$  and  $h$ . Note also that if  $f$  and  $g$  are expressed in the same units, then  $h$  has the dimensions of  $s^{-1}$ .

If input  $f$  is a  $\delta$  function at time  $t'_0$ , then

$$g(t) = \int_{-\infty}^{\infty} \delta(t' - t'_0)h(t, t') dt' = h(t, t'_0). \quad (12.2)$$

We see that  $h(t, t')$  is the *impulse response* of the system to an impulse at time  $t'$ . If the impulse response of a linear system is known, it is possible to calculate the response to any arbitrary input.

If, in addition to being linear, the system responds to an impulse the same way regardless of when it occurs, the system is said to be *stationary*. In the hi-fi example, this means that no one is adjusting the volume or tone controls. For a stationary system the impulse response depends only on the *time difference*  $t - t'$ :

$$h(t, t') = h(t - t'), \quad (12.3)$$

and the superposition integral takes the form

$$g(t) = \int_{-\infty}^{\infty} f(t')h(t - t') dt'. \quad (12.4a)$$

This is called the *convolution integral*. It is often abbreviated as

$$g(t) = f(t) \otimes h(t). \quad (12.4b)$$

For the hi-fi system the function  $h(t - t')$  is zero for all  $t'$  larger (later) than  $t$ ; the response does not depend on future inputs. For the images we will be considering shortly, where the variables represent positions in the object and image,  $h$  can exist for negative arguments.

We saw an example of the impulse response in Sec. 11.15, where we found that the solution of the differential equation for the system was a step exponential, Eq. 11.83. For that simple linear system we can write

$$h(t - t') = \begin{cases} 0, & t < t' \\ (1/\tau_1)e^{-(t-t')/\tau_1}, & t > t'. \end{cases} \quad (12.5)$$

We have seen superposition integrals before: for one-dimensional diffusion (Eq. 4.73) and for the potential (Eq. 7.21) and magnetic field (Eq. 8.12) outside a cell.

There is an important relationship between the Fourier transforms of the functions appearing in the convolution integral, which was hinted at in Sec. 11.15. If the sine and cosine transforms of function  $h$  are denoted by  $C_h(\omega)$  and  $S_h(\omega)$ , with similar notation for  $f$  and  $g$ , the relationships can be written

$$\begin{aligned} C_g(\omega) &= C_f(\omega)C_h(\omega) - S_f(\omega)S_h(\omega), \\ S_g(\omega) &= C_f(\omega)S_h(\omega) + S_f(\omega)C_h(\omega). \end{aligned} \quad (12.6a)$$

This is called the *convolution theorem*. If we were using complex exponential notation, the Fourier transforms would be related by

$$G(\omega) = F(\omega)H(\omega). \quad (12.6b)$$

The convolution of two functions in time is equivalent to multiplying their Fourier transforms.

Equations 12.6a are similar to the addition formulas for sines and cosines, which are of course used in the derivation. To derive them, we take the Fourier transforms of  $f$  and  $h$ :

$$f(t') = \frac{1}{2\pi} \int_{-\infty}^{\infty} [C_f(\omega) \cos \omega t' + S_f(\omega) \sin \omega t'] d\omega,$$

$$h(t - t') = \frac{1}{2\pi} \int_{-\infty}^{\infty} [C_h(\omega) \cos \omega(t - t') + S_h(\omega) \sin \omega(t - t')] d\omega.$$

Then

$$\begin{aligned} g(t) &= \int_{-\infty}^{\infty} f(t')h(t - t') dt' \\ &= \left(\frac{1}{2\pi}\right)^2 \int_{-\infty}^{\infty} dt' \left[ \int_{-\infty}^{\infty} d\omega [C_f(\omega) \cos \omega t' + S_f(\omega) \sin \omega t'] \right. \\ &\quad \left. \times \int_{-\infty}^{\infty} d\omega' [C_h(\omega') \cos \omega'(t - t') + S_h(\omega') \sin \omega'(t - t')] \right]. \end{aligned}$$

We can use the trigonometric addition formulas and the fact that  $\sin(-\omega't') = -\sin \omega't'$  to rewrite and expand this expression, much as we did in the last chapter. Carrying out the integration over  $t'$  first and using the properties of integrals of the  $\delta$  function gives

$$\begin{aligned} g(t) &= \frac{1}{2\pi} \int_{-\infty}^{\infty} d\omega [C_f(\omega)C_h(\omega) - S_f(\omega)S_h(\omega)] \cos \omega t \\ &\quad + \frac{1}{2\pi} \int_{-\infty}^{\infty} d\omega [C_f(\omega)S_h(\omega) + S_f(\omega)C_h(\omega)] \sin \omega t. \end{aligned}$$

Comparison of this with Eqs. 11.55 proves Eq. 12.6a.

Fourier techniques need not be restricted to frequency and time. The quality and resolution of the image on the retina, an x-ray film, or a photograph are best described in terms of *spatial frequency*. The distance across the image in some direction is  $x$ , and a sinusoidal variation in the image would have the form  $A(k) \sin(kx - \phi)$ . The *angular spatial frequency*  $k$  has units of radians per meter. It is  $k = 2\pi/\lambda$ , where  $\lambda$  is the wavelength, in analogy to  $\omega = 2\pi/T$ . Alternatively, we can use the *spatial frequency*  $1/\lambda$ , with units of cycles per meter or cycles per millimeter.

### 12.1.2 Two Dimensions

The convolution and Fourier transform in two dimensions are needed to analyze the response of a system that forms

a two-dimensional image of a two-dimensional object. The object can be represented by function  $f(x', y')$  in the *object plane*. The image is given by a function  $g(x, y)$  in the image plane:

$$g(x, y) = \int_{-\infty}^{\infty} \int_{-\infty}^{\infty} f(x', y') h(x, x'; y, y') dx' dy'. \quad (12.7)$$

If the contribution of object point  $(x', y')$  to the image at  $(x, y)$  depends only on the relative distances  $x - x'$  and  $y - y'$ , then the two-dimensional impulse response is  $h(x - x', y - y')$ , and the image is obtained by the two-dimensional convolution

$$g(x, y) = \int_{-\infty}^{\infty} \int_{-\infty}^{\infty} f(x', y') h(x - x', y - y') dx' dy' \quad (12.8a)$$

or

$$g(x, y) = f(x, y) \otimes \otimes h(x, y). \quad (12.8b)$$

The Fourier transform in two dimensions is defined by

$$f(x, y) = \left(\frac{1}{2\pi}\right)^2 \int_{-\infty}^{\infty} dk_x \int_{-\infty}^{\infty} dk_y [C(k_x, k_y) \cos(k_x x + k_y y) + S(k_x, k_y) \sin(k_x x + k_y y)]. \quad (12.9a)$$

The coefficients are given by

$$C(k_x, k_y) = \int_{-\infty}^{\infty} dx \int_{-\infty}^{\infty} dy f(x, y) \cos(k_x x + k_y y), \quad (12.9b)$$

$$S(k_x, k_y) = \int_{-\infty}^{\infty} dx \int_{-\infty}^{\infty} dy f(x, y) \sin(k_x x + k_y y). \quad (12.9c)$$

The Fourier transforms of the functions in the convolution are related by equations similar to those for the one-dimensional convolution.

$$\begin{aligned} C_g(k_x, k_y) &= C_f(k_x, k_y) C_h(k_x, k_y) \\ &\quad - S_f(k_x, k_y) S_h(k_x, k_y), \\ S_g(k_x, k_y) &= C_f(k_x, k_y) S_h(k_x, k_y) \\ &\quad + S_f(k_x, k_y) C_h(k_x, k_y). \end{aligned} \quad (12.10)$$

With complex notation we would define the two-dimensional Fourier transform pair by

$$\begin{aligned} F(k_x, k_y) &= \int_{-\infty}^{\infty} \int_{-\infty}^{\infty} f(x, y) e^{-i(k_x x + k_y y)} dx dy, \\ f(x, y) &= \left(\frac{1}{2\pi}\right)^2 \int_{-\infty}^{\infty} \int_{-\infty}^{\infty} F(k_x, k_y) e^{i(k_x x + k_y y)} dk_x dk_y, \end{aligned} \quad (12.11a)$$

and the convolution theorem would be

$$G(k_x, k_y) = F(k_x, k_y) H(k_x, k_y). \quad (12.11b)$$

## 12.2 The Relationship Between the Object and the Image

### 12.2.1 Point-Spread Function

Suppose that an object in the  $x'y'$  plane is described by a function  $L(x', y')$  that varies from place to place on the object. The image is

$$E_{\text{image}}(x, y) = \iint L(x', y') h(x, y; x', y') dx' dy'. \quad (12.12)$$

Function  $h$  is called the *point-spread function*. The point-spread function tells how information from a point source at  $(x', y')$  spreads out over the image plane. It receives its name from the following. If we imagine that the object is a point described by  $L(x', y') = L\delta(x' - x'_0)\delta(y' - y'_0)$ , then integration shows that

$$E_{\text{image}} = h(x, y; x'_0, y'_0).$$

The point-spread function has the same functional form as the image from a point source, just as did the impulse response in one dimension.

You can verify that the point-spread function for an ideal imaging system with magnification  $m$  is

$$h(x, y; x', y') = m^2 \delta(x - mx') \delta(y - my'). \quad (12.13)$$

The  $\delta$  functions pick out the values  $(x' = x/m, y' = y/m)$  in the object plane to contribute to the image at  $(x, y)$ . You can make the verification by substituting Eq. 12.13 in Eq. 12.12 and using the properties of the  $\delta$  function from Eq. 11.62.

This discussion assumes that *intensities* add. This is true when the oscillations of the radiant energy (such as the electric field for light waves) have random phases lasting for a time short compared to the measurement time. Such radiant energy is called *incoherent*.<sup>1</sup>

We have already seen that when the impulse response in a one-dimensional system depends on coordinate differences such as  $t - t'$  (or  $x - x'$  or  $x - mx'$ ), the system is stationary. In this case it is also said to be *space invariant*: changing the position of the object changes the position of the image but not its functional form. Stationarity is easier to obtain in a system such as a hi-fi system than in an imaging system, but we usually assume that it holds in an imaging system as well. For a space-invariant system

$$E_{\text{image}}(x, y) = \iint L(x', y') h(x - mx', y - my') dx' dy'. \quad (12.14)$$

<sup>1</sup>These arguments also work for coherent radiation, where the phases are important, but the point-spread function is for the amplitude of the wave instead of the square of the amplitude (intensity). The calculation then gives rise to interference and diffraction effects.

This is a two-dimensional convolution. The convolution theorem is

$$\begin{aligned}
 C_{\text{image}}(k_x, k_y) &= C_{\text{object}}(k_x, k_y)C_h(k_x, k_y) \\
 &\quad - S_{\text{object}}(k_x, k_y)S_h(k_x, k_y), \\
 S_{\text{image}}(k_x, k_y) &= C_{\text{object}}(k_x, k_y)S_h(k_x, k_y) \\
 &\quad + S_{\text{object}}(k_x, k_y)C_h(k_x, k_y).
 \end{aligned}
 \tag{12.15}$$

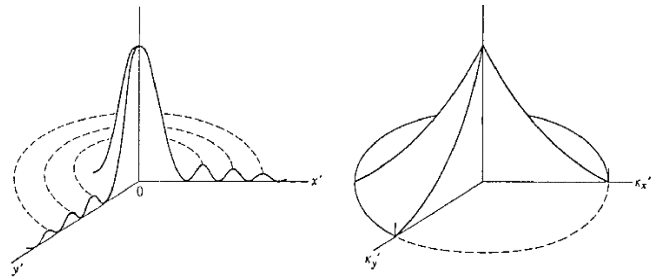


FIGURE 12.1. The point-spread function and modulation transfer function for a diffraction-limited circular aperture. From C. S. Williams and O. A. Becklund. *Optics: A Short Course for Engineers and Scientists*. New York, Wiley, 1972. Used by permission of the authors.

### 12.2.2 Optical-, Modulation-, and Phase-Transfer Functions

The *optical transfer function* (OTF) is the Fourier transform of the point-spread function,  $C_h(k_x, k_y)$  and  $S_h(k_x, k_y)$ . It is analogous to the transfer function for an amplifier (Sec. 11.15). The *modulation transfer function* (MTF) is the amplitude of the OTF:

$$\text{MTF}(k_x, k_y) = [C_h^2(k_x, k_y) + S_h^2(k_x, k_y)]^{1/2}. \tag{12.16}$$

The *phase transfer function* is

$$\text{PTF}(k_x, k_y) = \tan^{-1} \left( \frac{S_h(k_x, k_y)}{C_h(k_x, k_y)} \right). \tag{12.17}$$

Often the transfer functions are normalized by dividing them by their value at zero spatial frequency.

The modulation transfer function can be measured by using a set of objects for which  $L$  varies sinusoidally at different spatial frequencies. The property  $L$  cannot be negative and must be offset by a zero-frequency component:

$$L(x, y) = a + b \cos(k_x x + k_y y), \quad 0 < b < a. \tag{12.18}$$

The image is described by

$$\begin{aligned}
 E &= \text{MTF}(0, 0)a + \text{MTF}(k_x, k_y)b \cos \\
 &\quad \times [k_x x + k_y y + \phi(k_x, k_y)].
 \end{aligned}
 \tag{12.19}$$

The *modulation* of the object is defined to be

$$(\text{modulation}) = \frac{L_{\text{max}} - L_{\text{min}}}{L_{\text{max}} + L_{\text{min}}} = \frac{(a + b) - (a - b)}{(a + b) + (a - b)} = \frac{b}{a}. \tag{12.20}$$

A similar expression defines the modulation of the image. The modulation transfer function is the ratio of the modulation of the image divided by the modulation of the object. The phase of the optical transfer function describes shifts of the phase of the image at each angular frequency along the appropriate axis. It is fully as important as the amplitude, since it describes the evenness or oddness of the image about its stated origin.

The modulation transfer function of an ideal system would be flat for all spatial frequencies. However, there is an upper limit imposed by diffraction, if nothing else. Figure 12.1 shows the point-spread function and MTF for a diffraction-limited case. Figure 12.2 shows three possible modulation transfer functions for an imaging system.

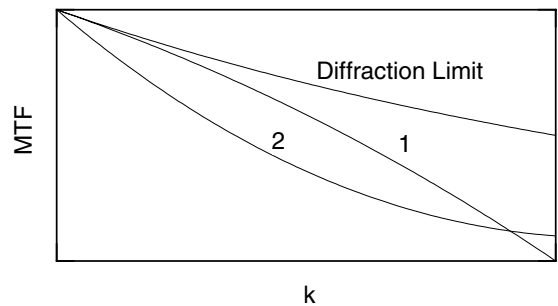


FIGURE 12.2. Three possible modulation transfer functions. The top one is the diffraction limit for monochromatic light. (Compare it with Fig. 12.1.) Curve 2 is higher than curve 1 at the highest value of  $k$  shown, but an image produced by system 2 would not have as much “punch.” It has less content at the middle spatial frequencies.

The upper one represents the diffraction limit. It has the same general shape as in Fig. 12.1. Curves 1 and 2 might be for real systems. While the second system transmits more of the highest spatial frequencies, it transmits less of the midrange frequencies, and its image would not have as much “punch” as the first system. Figure 12.3 shows the modulation transfer functions of several photographic films, with (a) being the most sensitive and (e) the least sensitive but with the highest resolution. Photographers are well aware of the trade-off between speed and resolution in film. Fast films are “more grainy” than slow films.

A complex imaging system may have several components, just as the hi-fi system did. If the system is linear, the modulation transfer function for the combined system is the product of the modulation transfer functions for each component. The optical transfer functions combine according to equations like Eq. 12.10.

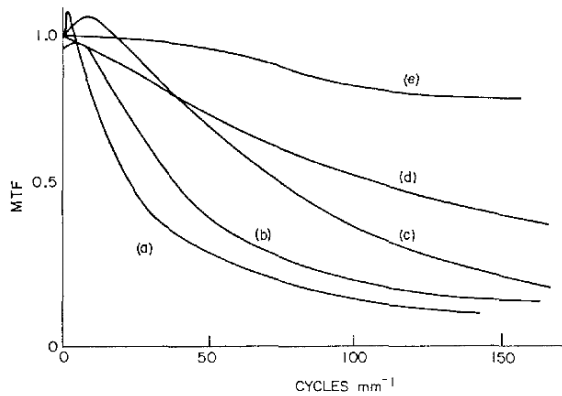


FIGURE 12.3. Some representative modulation transfer functions for various photographic films, showing how the resolution decreases as the film sensitivity increases. Film (a) has the greatest sensitivity and worst resolution. Film (e) is the least sensitive (“slowest”) and has the best resolution. With permission from R. Shaw. *Photographic Detectors*. Chapter 5 of *Applied Optics and Engineering*, New York, Academic, 1979. Vol. 7, pp. 121–154.

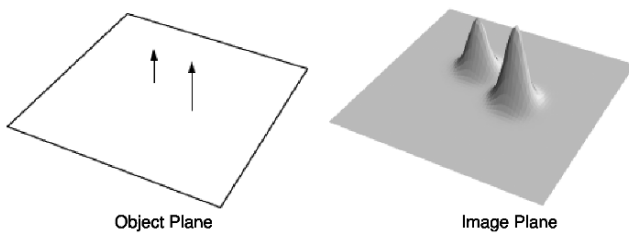


FIGURE 12.4. The point-spread function. Two impulse sources of different height are shown in the object plane. The response to them is shown in the image plane.

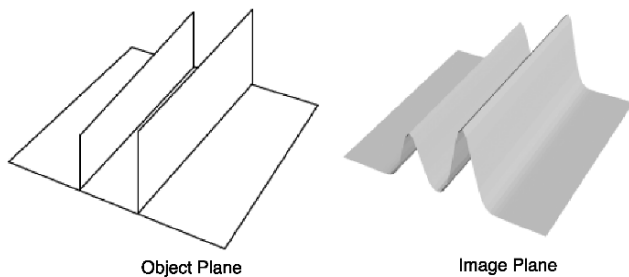


FIGURE 12.5. The line-spread function. Two line sources are shown in the object plane. The response to them is shown in the image plane.

### 12.2.3 Line- and Edge-Spread Functions

The *line-spread function* is the response of a system to a line object in a plane perpendicular to the axis of the lens. In general, the system is not isotropic and the line-spread function depends on the orientation of the line. The Fourier transform of the line-spread function along the  $y$  axis is  $C_h(k_x, 0)$  and  $S_h(k_x, 0)$ . Figure 12.4 shows a geometrical interpretation of the point-spread function.

Figure 12.5 shows the line-spread function. The *edge-spread function* is the response to an object that has a step in the radiance. All of these functions are interrelated. A discussion of how one can be obtained from another is found in many places, including Chapter 9 of Gaskill (1972).

## 12.3 Spatial Frequencies in an Image

There are some universal relationships between the spatial frequencies present in an image and the character of the image. These relationships hold whether the image is a photograph, an x-ray film, a computed tomographic scan, an ultrasound or nuclear medicine image, or a magnetic resonance image. In this section we describe these general relationships, which we will use throughout the rest of the book.

The first general relationship concerns the size of an image and the lowest spatial frequency present. For simplicity, consider the  $x$  direction and the corresponding spatial frequencies  $k$ . The *object* is nonperiodic. But its *image* is represented by a Fourier series which has period  $L$ . We saw in Chapter 11 that if the lowest angular frequency present is  $\omega_0$ , the period is  $T = 2\pi/\omega_0$ . The lowest spatial frequency present (other than zero) is  $k_0 = 2\pi/L$ . The series has harmonics with separation  $\Delta k = k_0$ . This leads to the fundamental relationship

$$L = \frac{2\pi}{k_0}. \quad (12.21)$$

*The lowest spatial frequency present (which equals the separation of the spatial frequencies) determines the size of the image  $L$  (the “field of view” or FOV).*

The second general relationship concerns the spatial resolution in an image and the highest spatial frequency present. If the image has  $N$  discrete samples, then the sampling interval or spatial resolution is  $\Delta x = L/N$ . This allows (or requires) the determination of  $N/2$  cosine coefficients and  $N/2$  sine coefficients. The highest spatial frequency present is  $k_{\max} = N\Delta k/2$ . We obtain

$$\Delta x = \frac{L}{2} \frac{\Delta k}{k_{\max}} = \frac{\pi}{k_{\max}}. \quad (12.22)$$

*The spatial resolution is inversely proportional to the highest spatial frequency present. As we saw for the Fourier series representing a square wave, the higher harmonics give fine detail and sharpness to the image.*

To reiterate: *The lowest spatial frequency in the image determines the field of view. The lower the minimum spatial frequency, the larger the field of view. The highest spatial frequency in the image determines the resolution. The higher the maximum spatial frequency, the finer the resolution.*

Here are a number of pictures that show how changing the coefficients in certain regions of  $k$  space affect an

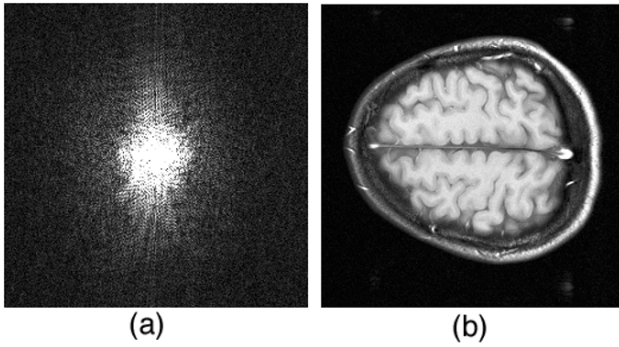


FIGURE 12.6. A magnetic resonance imaging head scan: (a) The squared amplitude  $C^2 + S^2$  in  $k$  space. (b) The image. This is a normal image to compare with the following figures. Prepared by Mr. Tuong Huu Le, Center for Magnetic Resonance Research, University of Minnesota. Thanks also to Professor Xiaoping Hu.

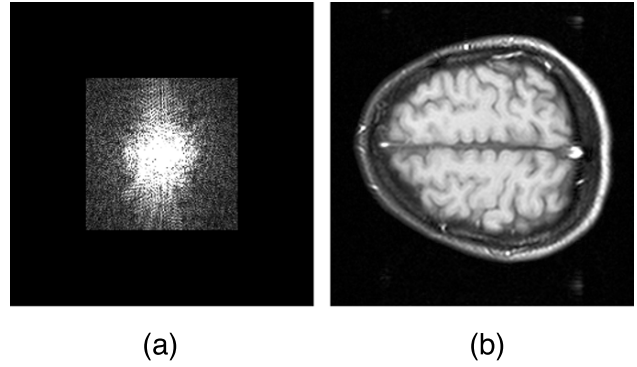


FIGURE 12.8. The image that results when the high-frequency Fourier components above  $k_{x \text{ max}}/2$  and  $k_{y \text{ max}}/2$  are removed. Note the blurring compared to Fig. 12.6. Prepared by Mr. Tuong Huu Le, Center for Magnetic Resonance Research, University of Minnesota. Thanks also to Professor Xiaoping Hu.

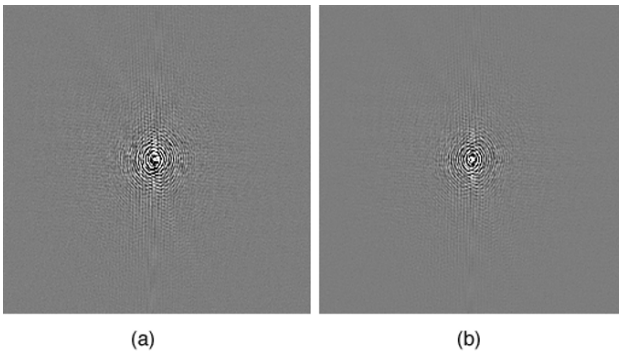


FIGURE 12.7. The sine and cosine coefficients for the image in Fig. 12.6. (a)  $C(k_x, k_y)$ . (b)  $S(k_x, k_y)$ . Prepared by Mr. Tuong Huu Le, Center for Magnetic Resonance Research, University of Minnesota. Thanks also to Professor Xiaoping Hu.

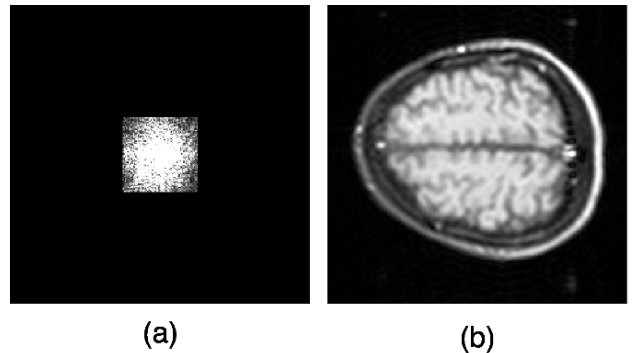


FIGURE 12.9. The image that results when the high-frequency Fourier components above  $k_{x \text{ max}}/4$  and  $k_{y \text{ max}}/4$  are removed. The blurring is even greater. Prepared by Mr. Tuong Huu Le, Center for Magnetic Resonance Research, University of Minnesota. Thanks also to Professor Xiaoping Hu.

image. Figure 12.6(b) shows a transverse scan of a head by magnetic resonance imaging. This is a normal image to compare with the following figures. It consists of 256 samples in each direction or  $256 \times 256$  pixels. The magnitude of its Fourier transform is shown in Fig. 12.6(a). Figure 12.7 shows the cosine and sine coefficients in the expansion.

Figures 12.8 and 12.9 show what happens when the high-frequency Fourier components are removed. In the first case they have been removed above  $k_{x \text{ max}}/2$  and  $k_{y \text{ max}}/2$ . In the second they are removed above  $k_{x \text{ max}}/4$  and  $k_{y \text{ max}}/4$ . Compare the blurring in these figures with the original image.

When the low-frequency coefficients are set to zero as in Fig. 12.10, only the high-frequency edges remain. In this case the Fourier components below  $k_{x \text{ max}}/4$  and  $k_{y \text{ max}}/4$  have been set to zero. (Keeping the same values of  $k_{x \text{ max}}$  and  $\Delta k$  and removing the information on those coefficients keeps the field of view the same.)

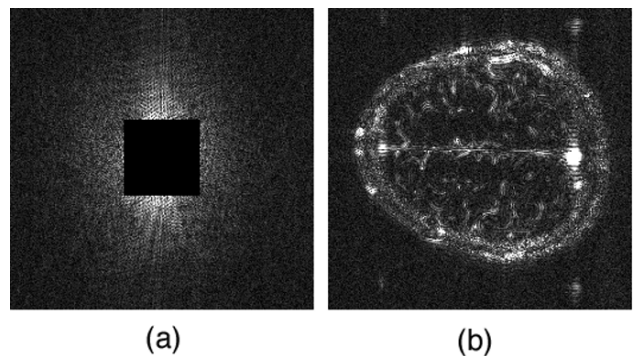


FIGURE 12.10. The image that results when the low-frequency Fourier components below  $k_{x \text{ max}}/4$  and  $k_{y \text{ max}}/4$  are removed. Prepared by Mr. Tuong Huu Le, Center for Magnetic Resonance Research, University of Minnesota. Thanks also to Professor Xiaoping Hu.

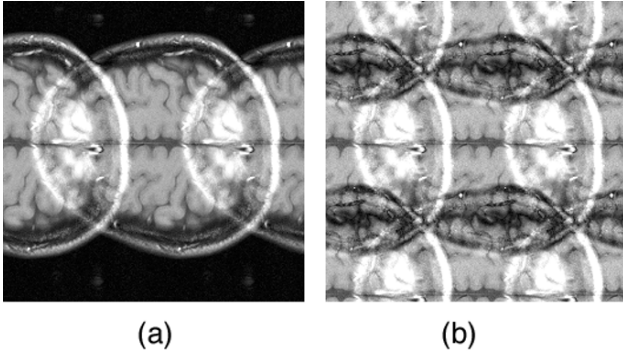


FIGURE 12.11. The Fourier coefficients for every other value of  $k$  have been set to zero. This has the effect of doubling  $\Delta k$  in Eq. 12.21. Since the width of the image has not been changed, this leads to aliasing, which shows up as the ghost images. (a) Every other value of  $k_x$  has been removed. (b) Every other value of both  $k_x$  and  $k_y$  has been removed. Prepared by Mr. Tuong Huu Le, Center for Magnetic Resonance Research, University of Minnesota. Thanks also to Professor Xiaoping Hu.

Figure 12.11 shows the aliasing that results from setting every other Fourier coefficient to zero. This has the effect of doubling  $\Delta k$  in Eq. 12.21. Since the width of the image has not been changed, this leads to aliasing, which shows up as the “ghost” images. In the first case alternate Fourier coefficients have been removed in  $k_x$  space; in the second they have been removed in both  $k_x$  and  $k_y$ .

### 12.3.1 Summary

In summary: *The lowest spatial frequency in the image determines the field of view. The lower the minimum spatial frequency, the larger the field of view. Low spatial frequencies provide shape, contrast, and brightness.*

*The highest spatial frequency in the image determines the resolution. The higher the maximum spatial frequency, the finer the resolution. High spatial frequencies provide resolution, edges, and sharp detail.*

## 12.4 Two-Dimensional Image Reconstruction from Projections by Fourier Transform

The reconstruction problem can be stated as follows. A function  $f(x, y)$  exists in two dimensions. Measurements are made that give *projections*: the integrals of  $f(x, y)$  along various lines as a function of displacement perpendicular to each line. For example, integration parallel to the  $y$  axis gives a function of  $x$ ,

$$F(x) = \int_{-\infty}^{\infty} f(x, y) dy, \tag{12.23}$$

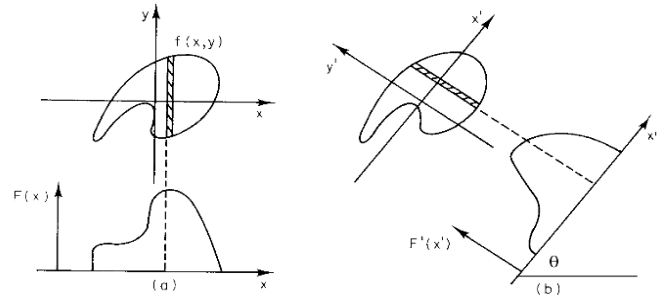


FIGURE 12.12. (a) Function  $F(x)$  is the integral of  $f(x, y)$  over all  $y$ . (b) The scan is repeated at angle with the  $x$  axis.

as shown in Fig. 12.12. The scan is repeated at many different angles  $\theta$  with the  $x$  axis, giving a set of functions  $F(\theta, x')$ , where  $x'$  is the distance along the axis at angle  $\theta$  with the  $x$  axis. The problem is to reconstruct  $f(x, y)$  from the set of functions  $F(\theta, x')$ . Several different techniques can be used. A detailed reference is the book by Cho *et al.* (1993).

We will consider two of these techniques: reconstruction by Fourier transform, where the Fourier coefficients are obtained from projections (in this section), and filtered back projection (Sec. 12.5).

The Fourier transform technique is easiest to understand. Consider Eqs. 12.9. If  $k_y = 0$  in Eq. 12.9b, the result is

$$\begin{aligned} C(k_x, 0) &= \int_{-\infty}^{\infty} \cos(k_x x) dx \int_{-\infty}^{\infty} f(x, y) dy \\ &= \int_{-\infty}^{\infty} \cos(k_x x) F(\theta = 0, x) dx. \end{aligned} \tag{12.24}$$

Similarly

$$S(k_x, 0) = \int_{-\infty}^{\infty} \sin(k_x x) F(0, x) dx. \tag{12.25}$$

To state this in words: the Fourier transform of  $F(0, x)$  determines the sine and cosine transforms of  $f(x, y)$  along the line  $k_y = 0$  (the  $k_x$  axis) in the spatial frequency plane. This is shown in Fig. 12.13.

A scan in another direction can be Fourier-transformed to give  $C$  and  $S$  at an angle  $\theta$  with the  $k_x$  axis. The Fourier transform of the projection at angle  $\theta$  is equal to the two-dimensional Fourier transform of the object, evaluated in the direction  $\theta$  in Fourier transform space. This result is known as the *projection theorem* or the *central slice theorem* (Problem 17). The transforms of a set of projections at many different angles provide values of  $C$  and  $S$  throughout the  $k_x k_y$  plane that can be used in Eq. 12.9a to calculate  $f(x, y)$ . In Chapter 18 we will find that the data from an MRI scan give the functions  $C(k_x, k_y)$  and  $S(k_x, k_y)$  directly.

In practice, the transforms are discrete. Using the notation that includes the redundant frequencies above  $N/2$  and makes the coefficients half as large (Eqs. 11.27), the



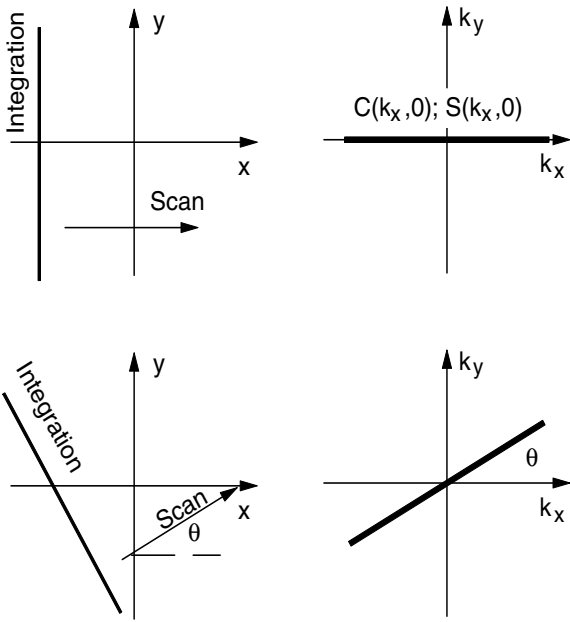


FIGURE 12.13. The Fourier transform of  $F(\theta = 0, x) = \int f(x, y)dy$  gives Fourier coefficients  $C$  and  $S$  along the  $k_x$  axis ( $k_y = 0$ ). The Fourier transform of scans at other angles  $\theta$  give  $C$  and  $S$  along corresponding lines in the  $k_x k_y$  plane.

two-dimensional discrete Fourier transform (DFT) is<sup>2</sup>

$$f_{jk} = \sum_{l=0}^{N-1} \sum_{m=0}^{N-1} C_{lm} \cos \left[ \frac{2\pi(jl + km)}{N} \right] + \sum_{l=0}^{N-1} \sum_{m=0}^{N-1} S_{lm} \sin \left[ \frac{2\pi(jl + km)}{N} \right]. \quad (12.26a)$$

The coefficients are given by

$$C_{lm} = \frac{1}{N^2} \sum_{j=0}^{N-1} \sum_{k=0}^{N-1} f_{jk} \cos \left[ \frac{2\pi(jl + km)}{N} \right], \quad (12.26b)$$

$$S_{lm} = \frac{1}{N^2} \sum_{j=0}^{N-1} \sum_{k=0}^{N-1} f_{jk} \sin \left[ \frac{2\pi(jl + km)}{N} \right]. \quad (12.26c)$$

Making a DFT of the projections gives values for  $C$  and  $S$  that lie on the circles in Fig. 12.14. But taking the inverse transform to calculate the reconstructed image requires values at the lattice points. They are obtained by interpolation. The details of how the interpolation is made are crucial when using the Fourier transform reconstruction technique.

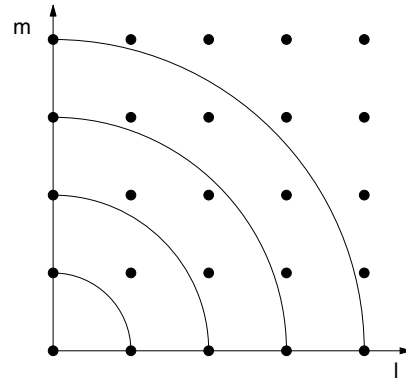


FIGURE 12.14. The two-dimensional Fourier reconstruction requires values of  $C$  and  $S$  at the lattice points shown. The Fourier transforms of the projections  $F(\theta, x)$  give the coefficients along the circular arcs. Interpolation is necessary to do the reconstruction.

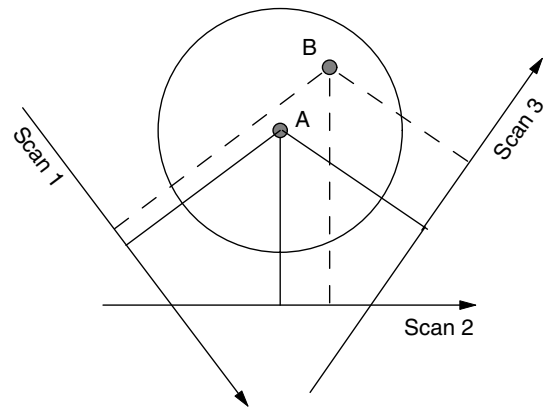


FIGURE 12.15. The principle of back projection. Each point in the image is generated by summing all values of  $F(\theta, x')$  that projected through that point. For point  $A$  at the center of rotation, the appropriate value of  $x'$  is the same at each angle. For other points such as  $B$ , the value of  $x'$  is different at each angle.

## 12.5 Reconstruction from Projections by Filtered Back Projection

Filtered back projection is more difficult to understand than the direct Fourier technique.<sup>3</sup> It is easy to see that every point in the object contributes to some point in each projection. The converse is also true. In a back projection every point in each projection contributes to some point in the reconstructed image. This can be seen from Figure 12.15, which shows two points  $A$  and  $B$  and three projections. For point  $A$ , which is at the center of rotation, the

<sup>2</sup>In this notation the low frequencies occur for low values of the indices  $l$  and  $m$ . Usually, as in Figs. 12.6–12.11, the indices are shifted so  $k = 0$  occurs in the middle of the sum.

<sup>3</sup>A simple experiment on back-projection using a laser pointer is described by Delaney and Rodriguez (2002).

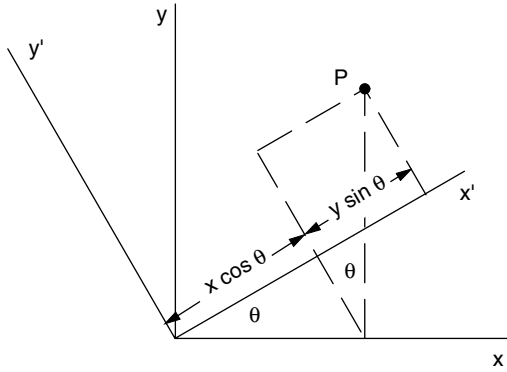


FIGURE 12.16. By considering components of the coordinates of point  $P$  in both coordinate systems, one can derive the transformation equations, Eqs. 12.27 and 12.28.

relevant value of  $x'$  is the same in each projection, while for point  $B$  the value of  $x'$  is different in each projection.

A very simple procedure would be to construct an image by back-projecting every projection. The back projection  $f_b(x, y)$  at point  $(x, y)$  is the sum of  $F(\theta, x')$  for every projection or scan, using the value of  $x'$  that corresponds to the original projection through that point. That is, for Fig. 12.15, the back projection at point  $A$  would be the sum of the three values for which the solid projection lines intersect the scans, while for point  $B$  it would be the sum of the values where the three dashed lines strike the scans. This gives a rather crude image, but we will see how to refine it.<sup>4</sup>

Figure 12.16 shows how to relate the values of  $x'$  and  $y'$  for a projection at angle  $\theta$  to the object or image coordinates  $x$  and  $y$ . The transformations are

$$\begin{aligned} x' &= x \cos \theta + y \sin \theta, \\ y' &= -x \sin \theta + y \cos \theta, \end{aligned} \tag{12.27}$$

and the inverse transformations are

$$\begin{aligned} x &= x' \cos \theta - y' \sin \theta, \\ y &= x' \sin \theta + y' \cos \theta. \end{aligned} \tag{12.28}$$

The projection at angle  $\theta$  is integrated along the line  $y'$ :

$$\begin{aligned} F(\theta, x') &= \int f(x, y) dy' \\ &= \int f(x' \cos \theta - y' \sin \theta, x' \sin \theta + y' \cos \theta) dy'. \end{aligned} \tag{12.29}$$

<sup>4</sup>To see why it is crude, suppose the original object is a disk at the origin. Every projection will be the same because of the symmetry in angle. Every back projection will lay down a contribution to the image along a stripe. Even though the reconstructed image will be largest where the original circle was, the image will have nonzero values throughout the image plane. We will see this example in Sec. 12.6.

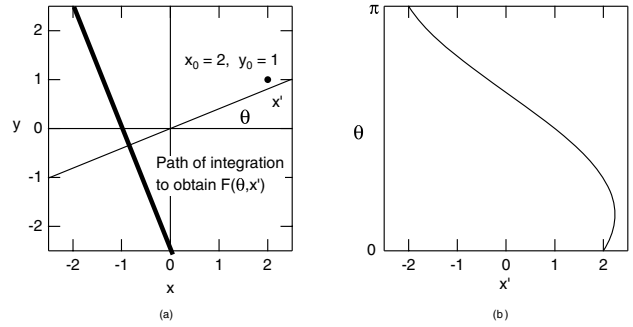


FIGURE 12.17. An object and its sinogram. The object is a  $\delta$  function at  $(x_0, y_0)$ . (a) The object and the path of a projection at angle  $\theta$ . (b) A sinogram of the object  $F(\theta, x')$ . The value of  $F$  would be plotted on an axis perpendicular to the  $x'\theta$  plane. The line shows the values of  $\theta$  and  $x'$  for which  $F$  is nonzero.

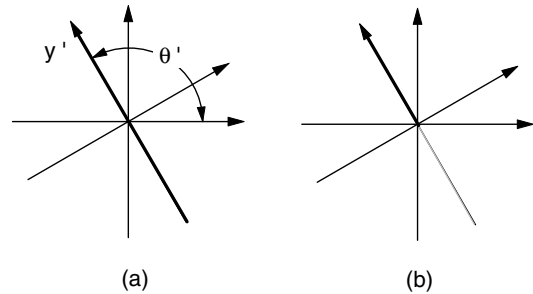


FIGURE 12.18. Integration for the back projection is over  $y'$  from  $-\infty$  to  $+\infty$ , as shown in (a). This can be converted to an integral from 0 to  $\pi$  if the angular integration is taken from 0 to  $2\pi$ , as shown in (b).

The process of calculating  $F(\theta, x')$  from  $f(x, y)$  is sometimes called the *Radon transformation*. When  $F(\theta, x')$  is plotted with  $x'$  on the horizontal axis,  $\theta$  on the vertical axis, and  $F$  as the brightness or height on a third perpendicular axis, the resulting picture is called a *sinogram*. For example, the projection of  $f(x, y) = \delta(x - x_0)\delta(y - y_0)$  is  $F(\theta, x') = \delta(x' - (x_0 \cos \theta + y_0 \sin \theta))$ . A plot of this object and its sinogram is shown in Fig. 12.17.

The definition of the back-projection is

$$f_b(x, y) = \int_0^\pi F(\theta, x') d\theta, \tag{12.30}$$

where  $x'$  is determined for each projection by using Eq. 12.27. The limits of integration are 0 and  $\pi$  since the projection for  $\theta + \pi$  repeats the projection for angle  $\theta$ .

We will now show that the image  $f_b(x, y)$  obtained by taking projections of the object  $F(\theta, x')$  and then back-projecting them is equivalent to taking the convolution of the object with the function  $h(x - x', y - y') = 1/r$ , where  $r$  is the distance in the  $xy$  plane from the object point to the image point. Function  $h$  depends only on the distance between the object and image points. This is discussed in greater detail by Barrett and Myers (2004, p. 280). To

simplify the algebra, we find the back projection at the origin. We want the set of projections for  $x' = 0$  as a function of scan angle  $\theta$ . They are, from Eq. 12.29,

$$F(\theta, 0) = \int_{-\infty}^{\infty} f(-y' \sin \theta, y' \cos \theta) dy'. \quad (12.31)$$

In terms of angle  $\theta' = \theta + \pi/2$  which is the angle from the  $x$  axis to the  $y'$  axis,

$$F(\theta', 0) = \int_{-\infty}^{\infty} f(y' \cos \theta', y' \sin \theta') dy'.$$

The arguments of  $f$  look very much like components of a vector, with magnitude  $r'$  and components  $r' \cos \theta'$  and  $r' \sin \theta'$ . This suggests expressing the integral in polar coordinates. Since  $y'$  is a dummy variable, call it  $r'$ . In terms of  $r'$  and  $\theta'$  the projection is

$$F(\theta', 0) = \int_{-\infty}^{\infty} f(r', \theta') dr'. \quad (12.32)$$

Inserting this expression in Eq. 12.30 gives for the back projection

$$f_b(0, 0) = \int_0^{\pi} F(\theta', 0) d\theta' = \int_{-\infty}^{\infty} \int_0^{\pi} f(r', \theta') dr' d\theta'. \quad (12.33)$$

Figure 12.18(a) shows how  $y'$  (that is,  $r'$ ) is integrated from  $-\infty$  to  $\infty$  while  $\theta'$  goes from 0 to  $\pi$ . For the purposes of Eq. 12.33 the limits of integration can be changed as in Fig. 12.18(b). Variable  $r'$  can range from 0 to  $\infty$  while  $\theta'$  goes from 0 to  $2\pi$ . Then the expression for  $f_b$  looks even more like an integration in polar coordinates:

$$f_b(0, 0) = \int_0^{\infty} \int_0^{2\pi} f(r', \theta') dr' d\theta'.$$

There is still one difference between this and polar coordinates. The element of area, which is  $dx' dy'$  in Cartesian coordinates, is  $r' dr' d\theta'$  in polar coordinates. Therefore, let us rewrite this as

$$f_b(0, 0) = \int_0^{\infty} \int_0^{2\pi} \left( \frac{f(r', \theta')}{r'} \right) r' dr' d\theta'. \quad (12.34)$$

We now change to the Cartesian variables  $x'$  and  $y'$ . The back-projected image at the origin is

$$f_b(0, 0) = \int_{-\infty}^{\infty} \int_{-\infty}^{\infty} \frac{f(x', y')}{(x'^2 + y'^2)^{1/2}} dx' dy'. \quad (12.35)$$

For an arbitrary point  $(x, y)$  the result is similar:

$$f_b(x, y) = \int_{-\infty}^{\infty} \int_{-\infty}^{\infty} \frac{f(x', y')}{[(x - x')^2 + (y - y')^2]^{1/2}} dx' dy'. \quad (12.36)$$

We have shown that the image obtained by taking projections of the object  $F(\theta, x')$  and then back projecting them is equivalent to taking the convolution of the object with the function  $h(x - x', y - y') = 1/r$ , where  $r$  is

the distance in the  $xy$  plane from the object point to the image point.

The back-projected image is not a faithful reproduction of the object. But it is possible to manipulate the projections  $F(\theta, x')$  to produce a function  $G(\theta, x')$  whose back projection is the desired  $f(x, y)$ . This is the process of *filtering* before making the back projection. To find the relationship between  $F$  and the desired function  $G$ , note that there is some function  $g(x, y)$  that we do not know, but which, when projected and then back projected, yields the desired function  $f(x, y)$ . That is,

$$f(x, y) = g_b(x, y) = \int_{-\infty}^{\infty} \int_{-\infty}^{\infty} \frac{g(x', y')}{[(x - x')^2 + (y - y')^2]^{1/2}} dx' dy'. \quad (12.37)$$

Equations 12.10 relate the Fourier coefficients of  $f, g$ , and  $h(r) = 1/r$ :

$$C_f(k_x, k_y) = C_g(k_x, k_y)C_h(k_x, k_y) - S_g(k_x, k_y)S_h(k_x, k_y),$$

$$S_f(k_x, k_y) = C_g(k_x, k_y)S_h(k_x, k_y) + S_g(k_x, k_y)C_h(k_x, k_y).$$

These can be solved for

$$S_g = \frac{C_h S_f - S_h C_f}{C_h^2 + S_h^2},$$

$$C_g = \frac{C_h C_f + S_h S_f}{C_h^2 + S_h^2}. \quad (12.38)$$

One can show by direct integration (see problem 28) that the Fourier transform of  $h(r) = 1/r$  is

$$C_h(k_x, k_y) = 2\pi(k_x^2 + k_y^2)^{-1/2},$$

$$S_h(k_x, k_y) = 0, \quad (12.39)$$

so that

$$C_g(k_x, k_y) = \frac{1}{2\pi}(k_x^2 + k_y^2)^{1/2}C_f(k_x, k_y),$$

$$S_g(k_x, k_y) = \frac{1}{2\pi}(k_x^2 + k_y^2)^{1/2}S_f(k_x, k_y). \quad (12.40)$$

If function  $g(x, y)$  were known and were projected to give  $G(\theta, x')$ , then back-projecting  $G$  would give the desired  $f(x, y)$ . The final step is to relate  $G(\theta, x')$  and  $F(\theta, x')$  so that we do not have to know  $g(x, y)$ . To establish this relationship, consider a projection on the  $x$  axis. Equations 12.24 and 12.25 show that

$$F(0, x) = \frac{1}{2\pi} \int_{-\infty}^{\infty} [C_f(k_x, 0) \cos(k_x x) + S_f(k_x, 0) \sin(k_x x)] dk_x,$$

while

$$G(0, x) = \frac{1}{2\pi} \int_{-\infty}^{\infty} [C_g(k_x, 0) \cos(k_x x) + S_g(k_x, 0) \sin(k_x x)] dk_x.$$

Equations 12.40 relate the Fourier coefficients for  $F$  and  $G$ . For  $k_y = 0$ ,  $(k_x^2 + k_y^2)^{1/2} = |k_x|$ . Therefore

$$G(0, x) = \left(\frac{1}{2\pi}\right)^2 \int_{-\infty}^{\infty} [C_f(k_x, 0) \cos(k_x x) + S_f(k_x, 0) \sin(k_x x)] |k_x| dk_x. \quad (12.41)$$

This result is independent of the choice of axis, so it must be true for any projection. There is a function  $h(x)$  which can be convolved with any  $F(\theta, x)$  to give the desired function  $G(\theta, x)$ . Equation 12.41 shows that

$$C_g(k_x, 0) = C_f(k_x, 0) |k_x|/2\pi, \\ S_g(k_x, 0) = S_f(k_x, 0) |k_x|/2\pi.$$

Comparison with Eqs. 12.9 shows that

$$C_h = |k_x|/2\pi, \quad S_h = 0.$$

Therefore

$$h(x) = \left(\frac{1}{2\pi}\right)^2 \int_{-\infty}^{\infty} |k_x| \cos(k_x x) dk_x.$$

Because the integrand is an even function, we can multiply by 2 and integrate from zero to infinity. The integral to infinity does not exist. However, there is some maximum spatial frequency, roughly the reciprocal of the resolution we want, which we call  $k_{x \max}$ . We can therefore cut the integral off at this maximum spatial frequency and obtain

$$h(x) = \frac{1}{2\pi^2} \int_0^{k_{x \max}} k_x \cos(k_x x) dk_x \\ = \frac{1}{2\pi^2} \left[ \frac{\cos(k_x x)}{x^2} + \frac{k_x \sin(k_x x)}{x} \right]_0^{k_{x \max}} \\ = \frac{k_{x \max}^2}{(2\pi)^2} [2 \operatorname{sinc}(\xi) - \operatorname{sinc}^2(\xi/2)], \quad (12.42)$$

where  $\xi = k_{x \max} x$  and  $\operatorname{sinc}(\xi) = \sin(\xi)/\xi$ . The function  $h(x)$  is plotted in Fig. 12.19. Using a sharp high-frequency cutoff introduces some problems, which are described below and which are easily overcome.

To summarize: *If each projection  $F$  is convolved with the function  $h$  of Eq. 12.42 and then back-projected, the back-projected image is equal to the desired image.*

Figure 12.20 summarizes the two methods of reconstructing an image from projections.

## 12.6 An Example of Filtered Back Projection

It is not difficult to write a computer program to perform filtered back projection if execution speed is not a concern. For our example we will use an object with circular symmetry, so that every projection is equivalent and only

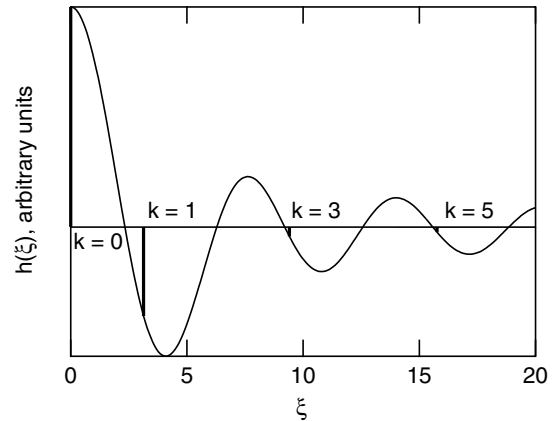


FIGURE 12.19. The weighting function  $h(x)$  of Eq. 12.42. The bars show the nonzero values for the example in Section 12.6.

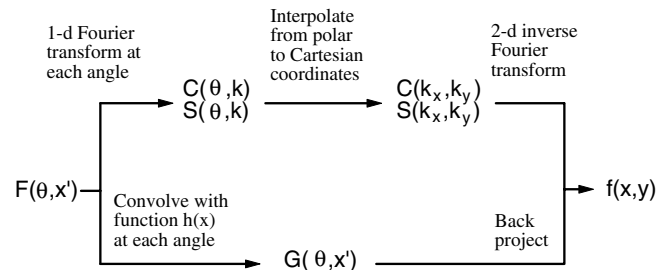


FIGURE 12.20. A summary of the two methods for reconstructing an image.

one projection needs to be convolved with the weighting function  $h$ . Because of the circular symmetry the back projection is needed only along one diameter. The program shown in Fig. 12.21 was used to reconstruct the image.

The “top-hat” function is used as the object:

$$f(x, y) = \begin{cases} 1, & x^2 + y^2 < a^2 \\ 0, & \text{otherwise.} \end{cases} \quad (12.43)$$

The projection is independent of  $\theta$ :  $F(x) = 2(a^2 - x^2)^{1/2}$  for  $x^2 < a^2$ . Procedure `CalcF` evaluates  $F(x)$  for 100 points. Variables  $x$  and  $i$  are related by  $x = 2i/N - 1$ , so that  $x$  ranges from  $-1$  to  $1$  as index  $i$  goes from 0 to 100. The value of  $a$  is 0.5.

The convolution is done by procedure `Convolve`, which uses convolving function  $h$  to operate on function  $F$  to produce  $G$ . The discrete form of  $h$  is obtained from Eq. 12.42 by the following argument, originally due to Ramachandran and Lakshminarayanan [see Cho *et al.*, (1993), p. 80]. Variable  $x$  is considered on the interval  $(-1, 1)$ , so the period is 2 and  $\omega_0 = \pi$ . The maximum spatial frequency is  $k_{x \max} = N\pi/2$ . The value of  $x$  in the weighting function  $h(x)$  depends on the value of index  $k = i - j$ :  $x_i - x_j = 2(i - j)/N = 2k/N$ . Therefore  $\xi = k_{x \max} x = (N\pi/2)(2/N)k = \pi k$ , where  $k$  is an

```
// Circular Back Projection
#include <stdio.h>
#include <stdlib.h>
#include <math.h>
#define N 180 //Number of data points
const int n = N;
const double pi = 3.141592654;
double F[N], Image[N],
//Projection of object and image
// along a line [i]
G[N]; //Convolved Projection
void CalcF(double *F)
/*Calculates the projection of a
circle of radius a centered at N/2.*/
{
    int i,i1,i2;
    double a = 0.5, x;
    i1 = (int)(50-a*((float)n)/2.0);
    i2 = (int)(50+a*((float)n)/2.0);
    for (i=0;i<n;i++)
    {
        x = 2*(i-1)/(float)n-1.0;
        F[i] = 0;
        if (i1 > i1 && i1 < i2)
            F[i] = F[i]*2*sqrt(pow(a,2)-pow(x,2));
    }
}
double E(int k)
{
    if (k==0)
        return pow((float)n,2)/16.0;
    else if(k%2 == 1 || (-k)%2 == 1)
        return -pow((float)n)/(
            pi*(float)k,2)/4.0;
    else
        return 0;
}
void Convolve(double*F, double*G)
{
    int i,j;
    double temp;
    for (i=0;i<n;i++)
    {
        temp = 0;
        for (j=0;j<n;j++)
            if (y[j] != 0)
                temp = temp+E(i-j)*y[j];
        G[i] = temp/(float)n;
    }
}
void BackProject(double*G,
double*Image)
{
    const int MaxProj = 180;
    int i,j,l;
    double x,xinterp,
        temp,c;
    for(i=0;i<n;i++)
        Image[i] = 0;
    for (j=0;j<MaxProj;j++)
    {
        c = cos(pi*((float)j)/180.0);
        for (i=0;i<n;i++)
        {
            x = ((float)n)/2.0+(i+1)
                -((float)n)/2.0*c;
            l = (int)x;
            xinterp = x-l;
            if (l<=1)
                temp = G[l];
            else if(l>=n)
                temp = G[n-1];
            else
                temp=G[l-1]-xinterp*(G[l]-G[l-1]);
            Image[i] = Image[i]+temp;
        }
    }
    for(i=0;i<n;i++)
        Image[i] = Image[i]*pi/
            ((float)MaxProj);
}
void PrintData(int n1, int n2,
double*x, FILE *fp, char *title)
{
    int i,j;
    fprintf(fp, "\n\n%s\n", title);
    j = 0;
    for (i = n1 - 1; i < n2; i++)
    {
        if (j%10 == 0)
            fprintf(fp, "\n%2i", i+1);
        fprintf(fp, "\t%.3f", x[i]);
        j++;
    }
    fprintf(fp, "\t%.3f", x[i]);
}
void main()
{
    FILE *ofp;
    if (!(ofp = fopen("OutputFile", "w")))
        printf("cannot open output file\n");
    exit(1);
}
fprintf(ofp, "\n");
CalcF(F);
PrintData(1,n,F,ofp,"Projected Object");
Convolve(F,G);
PrintData(1,n,G,ofp,"Convolved
Projection G");
BackProject(G,Image);
PrintData(1,n,Image,ofp,"Back Projected
Image");
fclose(ofp);
}
```

FIGURE 12.21. The program used to make a filtered back projection of a circularly symmetric function.

integer. From Eq. 12.42 we obtain

$$h(k) = \begin{cases} N^2/16, & k = 0 \\ 0, & k \text{ even} \\ -N^2/4k^2\pi^2 & k \text{ odd.} \end{cases} \quad (12.44)$$

Procedure `Convolve` replaces the integral of Eq. 12.4a by a sum. The factor  $dx$  in the integral becomes  $1/N$  in the sum.

Procedure `BackProject` forms the image from  $G$ . One hundred eighty projections are done in  $1^\circ$  increments from 0 to 179. The value of  $x$  is determined from  $x = i \cos \theta$ , but it is shifted so that the rotation takes place about  $i = 50$ . Unless  $x$  is at the end points, the value of  $G$  is obtained by linear interpolation. The value of  $\Delta\theta$  used to convert the integral to a sum is  $\pi/180$ .

Procedure `PrintData` writes the data for the plots shown in Fig. 12.22. One can see from inspection of Fig. 12.22 how the convolution converts the semicircular projection  $F$  into a function  $G$  that is flat-topped over the region of nonvanishing  $f$  and has a negative contribution in the wings. Figure 12.23 shows what the image looks

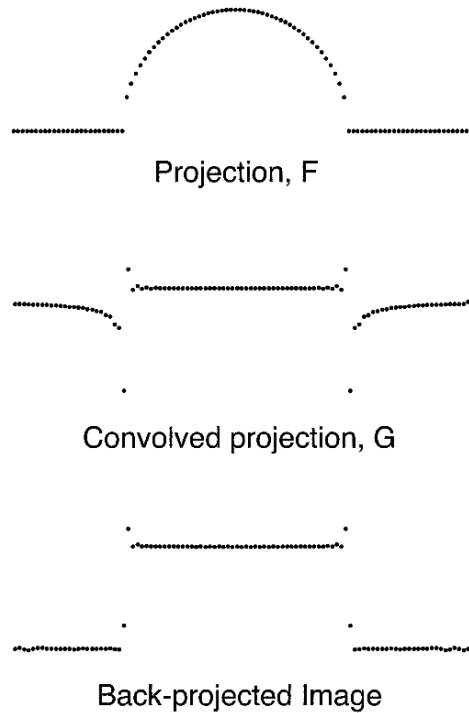


FIGURE 12.22. Reconstruction of a circularly symmetric image by filtered back projection. (a) The projection  $F(x)$ . (b) The convolved projection  $G(x)$ . (c) The image from back-projecting the convolved data.



FIGURE 12.23. Reconstruction by simple back projection without convolution. The object is the same as in Fig. 12.22.

like if the back projection is done without first performing the convolution.

One can also see from Fig. 12.22 that ringing is introduced at the sharp edges. This is characteristic of the sharp high-frequency cutoff at  $k_x$  (similar to the Fourier series representation of a square wave with only a finite number of terms). Early computer tomography (CT) scans created with the convolution function presented here showed a dark band just inside the skull where there was an abrupt change in  $f(x, y)$  upon going from bone to brain (Fig. 12.24). A gradual high-frequency cutoff changes the details of  $h(k)$  and eliminates this ringing (Fig. 12.25).

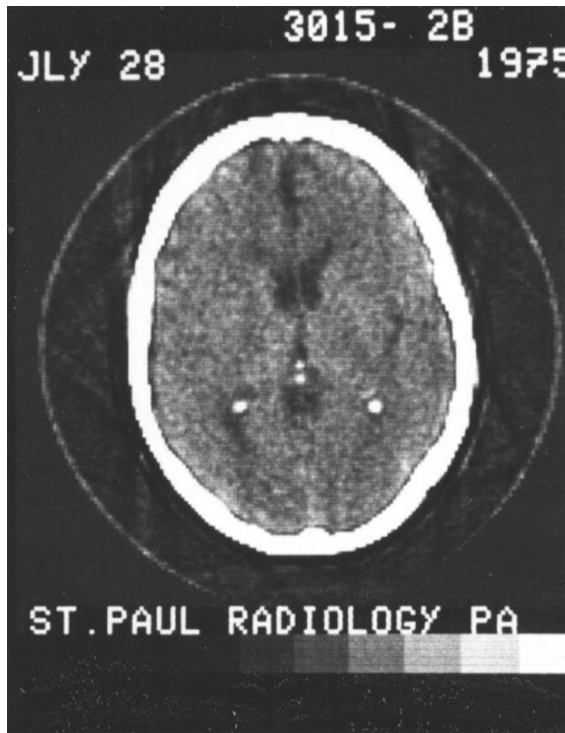


FIGURE 12.24. An early CT brain scan, showing ringing inside the skull. Photograph courtesy of St. Paul Radiology Associates, St. Paul, MN.

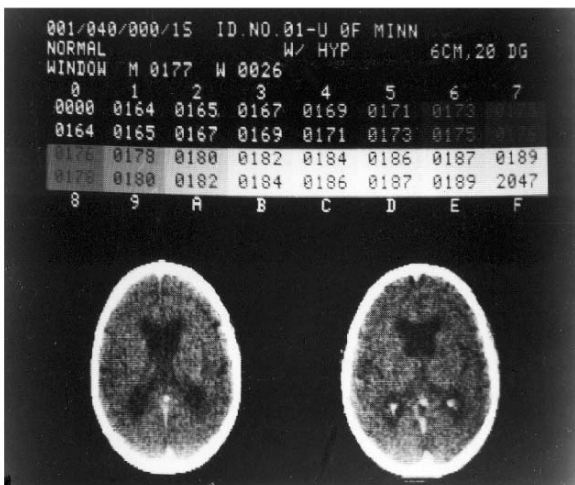


FIGURE 12.25. A set of brain scans using a gradual high-frequency cutoff to eliminate ringing. Photograph courtesy of Professor J. T. Payne, Department of Diagnostic Radiology, University of Minnesota.

$b'$	Length of object	m	326
$f, g$	Arbitrary functions		326
$f_b, g_b$	Back-projected images of $f, g$		333
$h$	Point-spread function; impulse response for convolution		326
$i$	$\sqrt{-1}$		327
$j, k$	Subscript indices for data		332
$k, k_x, k_y$	Spatial frequencies	$m^{-1}$	326
$l, m$	Subscript indices for Fourier coefficients		332
$m$	Magnification		327
$t, t'$	Time or arbitrary variable		326
$x, y, x', y'$	Distance; coordinates in image or object plane; rotated coordinate system for image reconstruction	m	327
$A$	Amplitude		326
$C_f$	Fourier cosine transform of function $f$		326
$D$	Length of image	m	329
$E$	Function describing an image		327
$F$	Projection of function $f$		331
$F, G, H$	Complex Fourier transforms of $f, g, h$		327
$L$	Property describing an object		327
$L$	Width of image or field of view (FOV)	m	329
$N$	Total number of data points; number of discrete values in one dimension of an image		329
$S_f$	Fourier sine transform of function $f$		326
$T$	Period	s	326
$\delta$	Dirac delta function		326
$\lambda$	Wavelength	m	326
$\phi$	Phase		326
$\theta, \theta'$	Angle		331
$\tau_1$	Time constant	s	326
$\omega, \omega_0$	Angular frequency	(radian) $s^{-1}$	326
$\xi$	Dummy variable		333

## Symbols Used in Chapter 12

Symbol	Use	Units	First used on page
$a, b$	Constants		328
$a$	Radius of "top-hat" function	m	335

## Problems

### Section 12.1

**Problem 1** Compare Eq. 12.4a to Eqs. 4.73 and 7.21 and deduce the impulse response for those two systems.

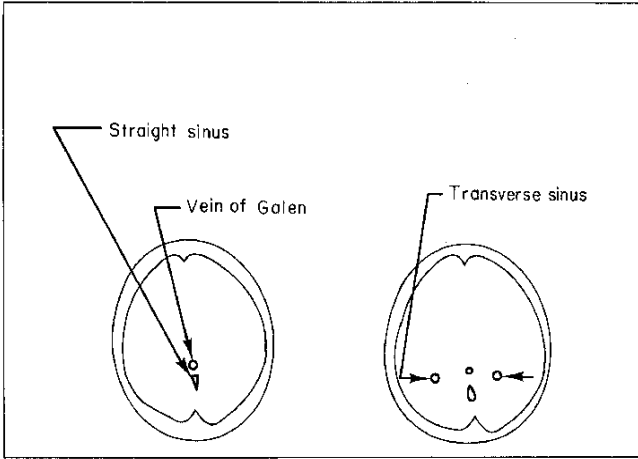


FIGURE 12.26. Anatomic features shown in Fig. 12.25

**Problem 2** Except for the minus sign, Eq. 12.4a is the same integral that defines the cross-correlation function. There are some important differences, however. Show that the convolution function is commutative—interchanging the order of variables gives the same result—but that the cross-correlation function is not.

**Problem 3** (a) Use the convolution integral, Eq. 12.4a, to calculate the convolution  $g(t)$  of the function  $h(t-t')$  in Eq. 12.5 with

$$f(t) = \begin{cases} 1, & 0 < t < T, \\ 0, & \text{otherwise} \end{cases}$$

Plot  $f(t)$  and  $g(t)$ .

(b) Calculate the Fourier transform of  $g(t)$ ,  $h(t-t')$ , and  $f(t)$  from part (a), and show that they obey Eq. 12.6a.

**Problem 4** Fill in the details in the derivation of Eq. 12.6a.

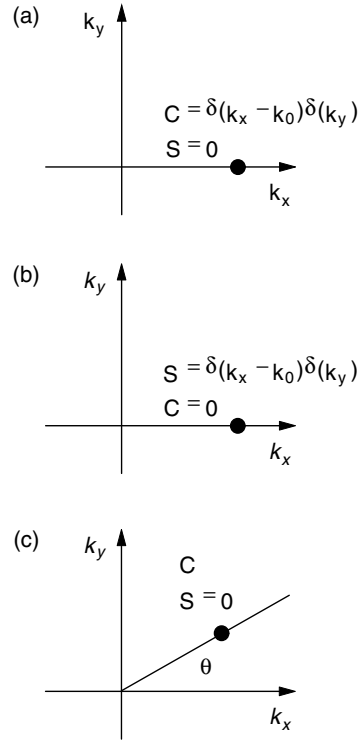
**Problem 5** Use the convolution integral to calculate  $g(x)$  from  $h(x-x') = a/[a^2 + (x-x')^2]$  and  $f(x) = \cos(kx)$ . Interpret this physically as a spatial frequency filter. Hint:

$$\int_{-\infty}^{\infty} \frac{\cos(ky)dy}{y^2 + b^2} = \frac{\pi}{b} e^{-kb},$$

$$\int_{-\infty}^{\infty} \frac{\sin(ky)dy}{y^2 + b^2} = 0.$$

**Problem 6** If you are familiar with complex variables, use the definition of the Fourier transform in Eq. 12.11a to prove the convolution theorem, Eq. 12.11b.

**Problem 7** What are the two-dimensional images whose Fourier transforms are shown?



**Problem 8** Calculate the two-dimensional Fourier transform of the function

$$f(x, y) = \begin{cases} 1, & -a/2 < x < a/2, \quad -b/2 < y < b/2, \\ 0, & \text{otherwise.} \end{cases}$$

Plot  $f(x, y)$  vs.  $x$  and  $y$  and  $C_f(k_x, k_y)$  vs.  $k_x$  and  $k_y$  for  $a = 2b$ .

**Problem 9** Calculate the two-dimensional Fourier transform of the function

$$f(x, y) = \operatorname{sech}\left(\frac{x}{a}\right) \operatorname{sech}\left(\frac{y}{b}\right).$$

You may need the relationship

$$\int_0^{\infty} \operatorname{sech}(uz) \cos(vz) dz = \frac{\pi}{2u} \operatorname{sech}\left(\frac{\pi v}{2u}\right).$$

**Problem 10** Calculate the two-dimensional Fourier transform of the function

$$f(x, y) = \begin{cases} 1, & \sqrt{x^2 + y^2} < a, \\ 0, & \sqrt{x^2 + y^2} > a. \end{cases}$$

Hint: convert to polar coordinates in both the  $xy$  and  $k_x k_y$  planes, and use the facts that

$$J_0(u) = \frac{1}{2\pi} \int_0^{2\pi} \cos(u \cos v) dv,$$

$$\int u J_0(u) du = J_1(u),$$

where  $J_0$  and  $J_1$  are Bessel functions of order zero and order one. Bessel functions are tabulated and have known properties, similar to trigonometric functions. See Abramowitz and Stegun (1972), p. 360.

Section 12.2

**Problem 11** Complete the verification of Eq. 12.13 suggested in the text.

**Problem 12** Find the Fourier transform of the point-spread function for the ideal imaging system, Eq. 12.13.

**Problem 13** Use Eq. 12.15 to show that the sum of the squares of the Fourier coefficients of the image is equal to the sum of the squares of the Fourier coefficients of the object times the square of the modulation transfer function, for a given set of spatial frequencies  $(k_x, k_y)$ .

**Problem 14** Write the modulation of the image in terms of the variables in Eq. 12.19.

**Problem 15** How does magnification  $m$  change the spatial frequencies in going from object to image? Since one is concerned about seeing detail in the object, resolution and spatial frequencies are usually converted to object coordinates in medical imaging, while they are left in terms of the detector coordinates in photography.

Section 12.3

**Problem 16** This problem shows how increasing the detail in an image introduces high-frequency components. Find the continuous Fourier transform of the two functions

$$f_1(x) = \begin{cases} 0, & x < 0, \\ 1, & 0 < x < 1, \\ 0, & x > 1 \end{cases}$$

$$f_2(x) = \begin{cases} 0, & x < 0, \\ \sqrt{3}/2, & 0 < x < 1/3, \\ 0, & 1/3 < x < 2/3, \\ \sqrt{3}/2, & 2/3 < x < 1, \\ 0, & x > 1. \end{cases}$$

Plot  $a(k_x) = [C^2(k_x) + S^2(k_x)]^{1/2}$  for each function using a spreadsheet or plotting package, for the range  $-45 < k_x < 45$ . Compare the features of each plot. Both functions have the same value of  $\int_{-\infty}^{\infty} f^2(x)dx$ .

Section 12.4

**Problem 17** Prove the central slice theorem analytically. Consider the cosine term of the two-dimensional Fourier transform  $C(k_x, k_y)$  in Eq. 12.9b. Rotate to the primed coordinates given by Eq. 12.28. Note that the area element  $dx dy$  transforms to  $dx' dy'$ . Express  $C$  as a function of polar coordinates in  $k$ -space,  $k_x = k \cos \theta$  and

$k_y = k \sin \theta$ . Show that

$$C(\theta, k) = \int_{-\infty}^{\infty} F(\theta, x') \cos(kx') dx',$$

$$S(\theta, k) = \int_{-\infty}^{\infty} F(\theta, x') \sin(kx') dx'.$$

**Problem 18** Suppose that  $f(x, y)$  is independent of  $y$ . Find expressions for  $C(k_x, k_y)$  and  $S(k_x, k_y)$  and insert them in the expression for  $f(x, y)$  to verify that  $f(x, y)$  is recovered. You will need Eqs. 11.65.

**Problem 19** Suppose that the object is a point at the origin, so that  $f(x, y) = \delta(x)\delta(y)$ . Find the projection  $F(x)$  and the transform functions  $C(k_x, 0)$  and  $S(k_x, 0)$ . Use these results to reconstruct the image using the Fourier technique.

**Problem 20** Figure 12.14 shows that taking the Fourier transform of the projection  $F(\theta, x')$  gives the Fourier coefficients  $C(k, \theta)$  at points along circular arcs in frequency space. In order to get these coefficients at equally spaced points in  $x$  and  $y$ , interpolation is necessary. One simple method is to use “bilinear” interpolation (Press et al., 1992). Suppose you know the Fourier coefficients at points  $r_i = i\Delta r$ ,  $\theta_j = j\Delta\theta$ , and you want to get the Fourier coefficients at points  $x_n = n\Delta x$ ,  $y_m = m\Delta y$ . For a given  $x_n, y_m$ , convert to polar coordinates to get  $r$  and  $\theta$ , then find the four known points that “surround” the desired point. The value of the coefficient is

$$C(x_n, y_m) = \frac{1}{\Delta r \Delta \theta} [C(r_i, \theta_j)(r_{i+1} - r)(\theta_{j+1} - \theta) + C(r_{i+1}, \theta_j)(r - r_i)(\theta_{j+1} - \theta) + C(r_i, \theta_{j+1})(r_{i+1} - r)(\theta - \theta_j) + C(r_{i+1}, \theta_{j+1})(r - r_i)(\theta - \theta_j)].$$

Suppose  $C(r, \theta) = \sin(r)/r$ , which is also called  $\text{sinc}(r)$ . If  $C$  is known at points with  $\Delta r = 0.5$  and  $\Delta\theta = \pi/8$ , evaluate  $C$  at point  $x = 2$ ,  $y = 3$  using bilinear interpolation. Compare this result to the exact value of  $C = \text{sinc}((x^2 + y^2)^{1/2})$ . Try this for other points  $(x_n, y_m)$ .

Section 12.5

**Problem 21** Derive Eqs. 12.27 and 12.28.

**Problem 22** An object is described by the function  $f(x, y) = e^{-(x^2 + y^2)/b^2}$ .

(a) Find the Fourier transform  $C(k_x, k_y)$  and  $S(k_x, k_y)$  directly from Eqs. 12.9 b and c.

(b) Find the projection  $F(\theta, x')$  using Eq. 12.29. Then take the one-dimensional Fourier transform of  $F(\theta, x')$  using the equations

$$C(\theta, k) = \int_{-\infty}^{\infty} F(\theta, x') \cos kx' dx'$$

$$S(\theta, k) = \int_{-\infty}^{\infty} F(\theta, x') \sin kx' dx'.$$



Use  $k = (k_x^2 + k_y^2)^{1/2}$  to express  $C$  and  $S$  in terms of  $k_x$  and  $k_y$ . Your answer should be the same as part (a).

Use the following integral table:

$$\int_{-\infty}^{\infty} e^{-az^2} dz = \sqrt{\frac{\pi}{a}}$$

$$\int_{-\infty}^{\infty} e^{-az^2} \cos bz dz = \sqrt{\frac{\pi}{a}} e^{-b^2/4a}$$

$$\int_{-\infty}^{\infty} e^{-az^2} \sin bz dz = 0.$$

**Problem 23** Assume you have just measured the projection function  $F(\theta, x') = \pi^{1/2} b e^{-(x'-a \cos \theta)^2/b^2}$ . (For this problem, ignore the fact that your measuring device would only give  $F$  at discrete values of  $\theta$  and  $x'$ .) Find  $f(x, y)$ . You may need the integrals from Problem 22.

**Problem 24** Repeat Prob. 23 using

$$F(\theta, x') = \frac{a\sqrt{\pi}}{2} e^{-x'^2/a^2} \left[ 1 + \cos^2 \theta \left( 2 \frac{x'^2}{a^2} - 1 \right) \right].$$

Look up any integrals you need.

**Problem 25** Suppose an object is a point at the origin,  $f(x, y) = \delta(x)\delta(y)$ . The projection is also a point:  $F(\theta, x') = \delta(x')$ . Calculate the back projection  $f_b(x, y)$  (without filtering) using Eq. 12.30. To solve the problem, use this property of  $\delta$  functions:

$$\delta(g(u)) = \sum_i \frac{\delta(u - u_i)}{|dg/du|_{u=u_i}},$$

where the  $u_i$  are the points such that  $g(u_i) = 0$ . Note that the back projection is not a point. Back projection without filtering does not recover the object.

**Problem 26** This problem is an extension of Prob. 25, but the object is no longer at the origin. Let  $f(x, y) = \delta(x - x_0)\delta(y - y_0)$ .

(a) Calculate  $F(\theta, x')$ . You may need the following properties of the  $\delta$  function:  $\int \delta(b-z)\delta(z-a)dz = \delta(b-a)$ ,  $\delta(az) = \delta(z)/|a|$ .

(b) Use the function  $F(\theta, x')$  you found in part (a) to calculate the back projection  $f_b(x, y)$  using Eq. 12.30. You will need the property of the  $\delta$  function given in Prob. 25.

(c) Show that  $f_b(x, y)$  is equivalent to the convolution of  $f(x, y)$  with the function  $1/\sqrt{(x-x')^2 + (y-y')^2}$ .

**Problem 27** Here is an easy way to show that the back projection  $f_b(x, y)$  cannot be equivalent to the object  $f(x, y)$ . If  $f(x, y)$  is dimensionless, determine the units of  $F(\theta, x')$  and  $f_b(x, y)$ . Do  $f(x, y)$  and  $f_b(x, y)$  have the same units?

**Problem 28** Consider the Fourier transform of  $1/r$ . The coefficients are given by

$$C(k_x, k_y) = \int_{-\infty}^{\infty} \int_{-\infty}^{\infty} \frac{dx dy \cos(k_x x + k_y y)}{(x^2 + y^2)^{1/2}},$$

$$S(k_x, k_y) = \int_{-\infty}^{\infty} \int_{-\infty}^{\infty} \frac{dx dy \sin(k_x x + k_y y)}{(x^2 + y^2)^{1/2}}.$$

Transform to polar coordinates ( $x = r \cos \theta, y = r \sin \theta$ ). Show from symmetry considerations of the angular integral that  $S = 0$ . Use the facts about the Bessel functions in Problem 10 and

$$\int_0^{\infty} J_0(kr) dr = 1/k$$

to derive Eqs. 12.39. The function  $J_0(x)$  is a Bessel function of order zero. It is tabulated and has known properties, similar to a trigonometric function. [See Abramowitz and Stegun (1972, p. 360).]

**Problem 29** An object consists of three  $\delta$  functions at  $(0, 2)$ ,  $(\sqrt{3}, -1)$ , and  $(-\sqrt{3}, -1)$ . Draw the sinogram of the object.

**Problem 30** Let  $f(x, y) = 1/[(x-a)^2 + y^2 + b^2]$ . Calculate  $F(\theta, x')$ .

**Problem 31** Let  $f(x, y) = x/(x^2 + y^2)^2$ . Calculate  $F(\theta, x')$ . Hint:

$$\int \frac{du}{(u^2 + v^2)^2} = \frac{u}{2v^2(u^2 + v^2)} + \frac{1}{2|v|^3} \tan^{-1} \left( \frac{u}{v} \right).$$

**Problem 32** Consider the object  $f(x, y) = a/\sqrt{a^2 - x^2 - y^2}$  for  $|x| < a$ , and 0 otherwise.

(a) Plot  $f(x, 0)$  vs.  $x$ .

(b) Calculate the projection  $F(\theta, x')$ . Plot  $F(0, x')$  vs.  $x'$ .

(c) Use the projection from part (b) to calculate the back projection  $f_b(x, y)$ . Plot  $f_b(x, 0)$  vs.  $x$ .

(d) Compare the object and the back projection. Explain qualitatively how they differ.

### Section 12.6

**Problem 33** Verify that

$$F(\theta, x) = \begin{cases} 2\sqrt{a^2 - x^2}, & |x| < a \\ 0, & |x| > a \end{cases}$$

is the projection of the function in Eq. 12.43.

**Problem 34** Verify Eqs. 12.44.

**Problem 35** Modify the program of Fig. 12.21 and run it without the convolution.

**Problem 36** Modify the program of Fig. 12.21 to reconstruct an annulus instead of a top-hat function.

## References

Abramowitz, M. and I. A. Stegun. (1972). *Handbook of Mathematical Functions with Formulas, Graphs and Mathematical Tables*. Washington, DC, U.S. Government Printing Office.

- Barrett, H. H., and K. J. Myers (2004). *Foundations of Image Science*. New York, Wiley-Interscience.
- Cho, Z.-h., J. P. Jones, and M. Singh (1993). *Foundations of Medical Imaging*. New York, Wiley.
- Delaney, C., and J. Rodriguez (2002). A simple medical physics experiment based on a laser pointer. *Amer. J. Phys.* **70**(10): 1068–1070.
- Gaskill, J. D. (1972). *Linear Systems, Fourier Transforms, and Optics*. 3rd. ed. New York, Wiley.
- Press, W. H., S. A. Teukolsky, W. T. Vetterling, and B. P. Flannery (1992). *Numerical Recipes in C: The Art of Scientific Computing*, 2nd ed., reprinted with corrections, 1995. New York, Cambridge University Press.
- Ramachandran, G. N., and A. V. Lakshminarayanan (1971). Three-dimensional reconstruction from radiographs and electron micrographs: Application of convolutions instead of Fourier transforms. *Proc. Nat. Acad. Sci. U.S.* **68**: 2236–2240.
- Shaw, R. (1979). Photographic detectors. Ch. 5 of *Applied Optics and Optical Engineering*, New York, Academic, Vol. **7**, pp. 121–154.
- Williams, C. S., and O. A. Becklund (1972). *Optics: A Short Course for Engineers and Scientists*. New York, Wiley.

# 13

## Sound and Ultrasound

Sound (or *acoustics*) plays two important roles in our study of physics in medicine and biology. First, animals hear sound and thereby sense what is happening in their environment. Second, physicians use high-frequency sound waves (*ultrasound*) to image structures inside the body. This chapter provides a brief introduction to the physics of sound and the medical uses of ultrasonic imaging. A classic textbook by Morse and Ingard (1968) provides a more thorough coverage of theoretical acoustics, and books such as Hendee and Ritenour (2002) describe the medical uses of ultrasound in more detail.

In Sec. 13.1 we derive the fundamental equation governing the propagation of sound: the wave equation. Section 13.2 discusses some properties of the wave equation, including the relationship between frequency, wavelength, and the speed of sound. The acoustic impedance and its relevance to the reflection of sound waves are introduced in Sec. 13.3. Section 13.4 describes the intensity of a sound wave and develops the decibel intensity scale. The ear and hearing are described in Sec. 13.5. Section 13.6 discusses attenuation of sound waves. Physicians use ultrasound imaging for medical diagnosis, as described in Section 13.7. Ultrasonic imaging can provide information about the flow of blood in the body by using the Doppler effect, as shown in Sec. 13.8.

### 13.1 The Wave Equation

In Chapter 1, we assumed that solids and liquids are incompressible. If a long rod were truly incompressible, a displacement of one end would instantly result in an identical displacement of the other end. In fact, the displacement does not propagate instantaneously. It travels at the speed of sound in the rod.

The propagation of sound involves small displacements of each volume element of the medium from its equilib-

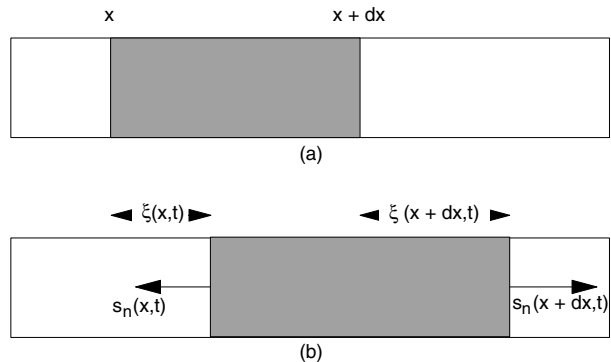


FIGURE 13.1. An elastic rod. (a) The rod in its equilibrium position. (b) Each point on the rod has been displaced from its equilibrium position by an amount  $\xi$  which depends on  $x$  and  $t$ . As a result there is a normal stress  $s_n$  which also depends on  $x$  and  $t$ .

rium position. In this section we consider sound waves propagating along the  $x$  axis. The results can be generalized to three dimensions [See Morse and Ingard (1968)]. We first consider an elastic rod, and then a fluid in which viscous effects are not important.

#### 13.1.1 Plane Waves in an Elastic Rod

The simplest case to consider is an elastic rod which is forced to move longitudinally at one end. This results in the propagation of a sound wave along the rod.<sup>1</sup> We set up a coordinate system where  $x$  measures distance along the rod from a fixed origin when no sound wave is traveling along the rod. We also assume that the disturbance of the rod depends only on the position along the rod,  $x$ ,

<sup>1</sup>This simple geometry assures that all motion is parallel to the  $x$  axis. In general, motion in an elastic solid involves both longitudinal waves and transverse waves.

and not on  $y$  or  $z$ , which are perpendicular to  $x$ . A wave in three dimensions that depends only on one dimension is called a *plane wave*.

When the sound travels along the rod, the material at point  $x$  is displaced from its undisturbed position by a small amount  $\xi(x, t)$ , as shown in Fig. 13.1. The material originally at  $x + dx$  is displaced by amount  $\xi(x + dx, t)$ . Since  $\xi(x + dx, t)$  is in general different from  $\xi(x, t)$ , there is a strain in the rod (Eq. 1.24)

$$\epsilon_n(x, t) = \frac{\Delta l}{l} = \frac{\xi(x + dx, t) - \xi(x, t)}{dx} = \frac{\partial \xi}{\partial x}. \quad (13.1)$$

Young's modulus,  $E$ , relates the stress in the rod,  $s_n$ , to the strain,  $\epsilon_n$  (Eq. 1.25):

$$s_n(x, t) = E\epsilon_n(x, t) = E \frac{d\xi}{dx}. \quad (13.2)$$

The difference between the stress at each end, multiplied by the cross-sectional area of the rod,  $S$ , provides a net force that accelerates the shaded volume element in Fig. 13.1. The net force on the volume element is

$$F_{\text{net}} = S[s_n(x + dx, t) - s_n(x, t)] = S \frac{\partial s_n}{\partial x} dx = SE \frac{\partial \epsilon_n}{\partial x} dx.$$

$$F_{\text{net}} = SE \frac{\partial^2 \xi}{\partial x^2} dx. \quad (13.3)$$

The mass of the shaded volume is  $\rho S dx$ , where  $\rho$  is the density, and the acceleration of the volume is  $\partial^2 \xi / \partial t^2$ . [Since we are not subtracting a value at one end from the value at the other, and since we are taking the limit as  $dx \rightarrow 0$ , we can ignore changes in  $\xi$  in the interval  $(x, x + dx)$ .] Therefore, Newton's second law becomes

$$\frac{\partial^2 \xi}{\partial x^2} = \frac{\rho}{E} \frac{\partial^2 \xi}{\partial t^2}. \quad (13.4)$$

This is the *wave equation*, and it is seen in many contexts, from the vibrations of a string to the propagation of electromagnetic waves. It is usually written as

$$\frac{\partial^2 \xi}{\partial x^2} = \frac{1}{c^2} \frac{\partial^2 \xi}{\partial t^2}, \quad (13.5)$$

where  $c$  is the speed of propagation of sound in the rod. In this case

$$c = \sqrt{\frac{E}{\rho}}. \quad (13.6)$$

As Young's modulus becomes very large or the density of the rod becomes very small, the speed with which a disturbance travels from one end of the rod to the other becomes larger and larger.

### 13.1.2 Plane Waves in a Fluid

Now we consider a sound wave propagating in a fluid, where shear can be neglected. We also neglect viscous

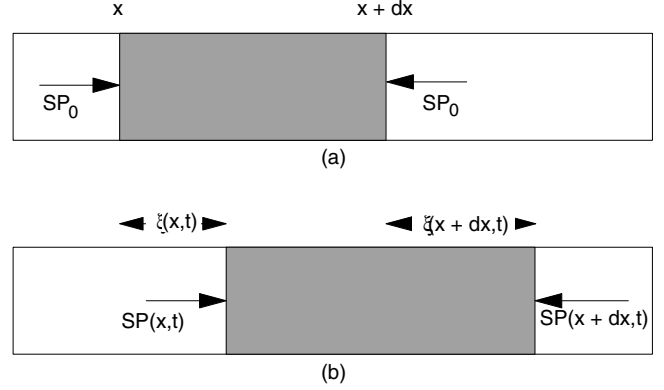


FIGURE 13.2. Sound propagates in one dimension in a fluid in a tube of cross-sectional area  $S$ . (a) In equilibrium the pressure is  $p_0$  and the force on the shaded volume of fluid has magnitude  $p_0 S$  on each end. (b) When the sound is propagating, the forces on each end are as shown.

effects. Changes in the fluid caused by the sound wave depend only on  $x$  and  $t$ .<sup>2</sup> To make it easier to imagine the situation, suppose the fluid is confined in a tube. Then we can construct a figure very similar to Fig. 13.1. A small volume of fluid at rest extends from position  $x$  to  $x + dx$ , with cross-sectional area  $S$  as shown in Fig. 13.2(a). The force pushing on the left side of the volume is  $SP_0$ , and the force on the right is  $-SP_0$ .<sup>3</sup> Here  $P_0$  is the pressure when the fluid is undisturbed by a sound wave. In equilibrium there is no net force on the volume element.

When the fluid element is displaced, as in Fig. 13.2(b), the net force to the right on the fluid element is

$$F_{\text{net}} = S[P(x, t) - P(x + dx, t)] = -S \frac{\partial P}{\partial x} dx. \quad (13.7)$$

The change of pressure from the equilibrium value  $P_0$  is related to the change of volume of the fluid by the compressibility,  $\kappa$  (Eq. 1.33):

$$P - P_0 = p = -\frac{1}{\kappa} \frac{dV}{V_0} = -\frac{1}{\kappa} \frac{d\xi}{dx}, \quad (13.8)$$

from which

$$F_{\text{net}} = \frac{S}{\kappa} \frac{\partial^2 \xi}{\partial x^2} dx. \quad (13.9)$$

To obtain the mass we use the volume  $S dx$  times the equilibrium density  $\rho_0$ . We multiply by the acceleration of the fluid element,  $\partial^2 \xi / \partial t^2$ , to obtain

$$\frac{\partial^2 \xi}{\partial x^2} = \rho_0 \kappa \frac{\partial^2 \xi}{\partial t^2}. \quad (13.10)$$

<sup>2</sup>We might be looking at a wave whose properties depend on all three coordinates,  $x$ ,  $y$ , and  $z$ , but where, in the region we are studying, the dependence on  $y$  and  $z$  is very slight. This is like the one-dimensional electrostatic approximations in Chapter 6.

<sup>3</sup>See Sec. 1.11; we ignore any forces arising from viscosity, gravity, or surface tension.

This is the wave equation, Eq. 13.5, with

$$c = \sqrt{\frac{1}{\kappa\rho_0}}. \quad (13.11)$$

In both of these cases, the wave equation has been written in terms of the displacement of elements of the rod or the fluid from their equilibrium positions. It is also possible to show that the pressure, fluid density, and velocity of the fluid element also satisfy the wave equation. The pressure is discussed in Problem 2. The velocity of the fluid due to the sound wave is

$$v = \frac{d\xi}{dt}. \quad (13.12)$$

Another important relationship is obtained by combining Eq. 13.12 with Eq. 13.8 and interchanging the order of differentiation (Appendix N):

$$\frac{\partial v}{\partial x} = -\kappa \frac{\partial p}{\partial t}. \quad (13.13)$$

Equations 13.8 and 13.10 can also be used to show that

$$\frac{\partial v}{\partial t} = -\frac{1}{\rho_0} \frac{\partial p}{\partial x}. \quad (13.14)$$

Finally, since the density is  $\rho = M/V$ , we can show that

$$\frac{d\rho}{\rho_0} = \kappa dp. \quad (13.15)$$

In this section we have considered Young's modulus  $E$  and compressibility  $\kappa$ . Remember from Chapter 3 that we can compress a gas at a constant temperature, and we can also do it adiabatically, when there is no heat flow and the temperature rises as the gas is compressed. The compressibility is different in these two cases. When static measurements of these parameters are made, there is usually time for the system being studied to remain isothermal. The pressure changes in a sound wave usually occur so rapidly that there is not time for heat to flow, and the adiabatic compressibility must be used. Values of Young's modulus are also different for isothermal and adiabatic stresses and strains.

## 13.2 Properties of the Wave Equation

The parameter  $c$  in the wave equation has units of speed. To appreciate its physical interpretation, consider the departure from the undisturbed pressure  $p(x, t) = P(x, t) - P_0 = f(x - ct)$ , where  $f$  is any function. This solution obeys the wave equation (see Prob. 5). It is called a *traveling wave*. A point on  $f(x - ct)$ , for instance its maximum value, corresponds to a particular value of the argument  $x - ct$ . To travel with the maximum value of  $f(x - ct)$ , as  $t$  increases  $x$  must also increase in such a way as to keep  $x - ct$  constant. This means that the pressure distribution propagates to the right with speed  $c$ , as shown

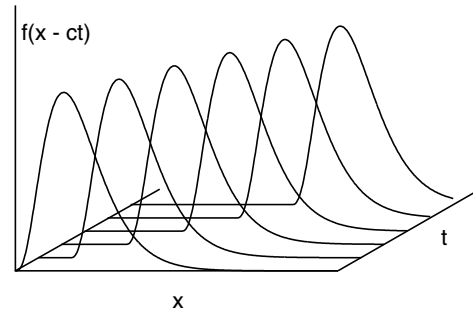


FIGURE 13.3. A wave  $f(x - ct)$  travels to the right with speed  $c$ .

in Fig. 13.3. Solutions  $p(x, t) = g(x + ct)$ , where  $g$  is any function, also are solutions to the wave equation, corresponding to a wave propagating to the left

The wave speed  $c$  is one of the most important parameters governing the propagation of sound waves. The density of water is about  $\rho_0 = 1,000 \text{ kg m}^{-3}$ , and the compressibility of water is approximately  $5 \times 10^{-10} \text{ Pa}^{-1}$ , so the speed of sound in water is about  $1,400 \text{ m s}^{-1}$ . The speed of sound in tissue is similar but slightly higher;  $1,540 \text{ m s}^{-1}$  is often taken as an average speed of sound in soft tissue. The speed of sound in air is about  $344 \text{ m s}^{-1}$ . See Denny (1993) for a more detailed comparison of the speed of sound in air and water.

One very useful traveling wave is  $p(x, t) = p_0 \sin\left[\frac{2\pi}{\lambda}(x - ct)\right] = p_0 \sin\left[2\pi\left(\frac{x}{\lambda} - \frac{t}{T}\right)\right] = p_0 \sin(kx - \omega t)$ . The pressure distribution oscillates sinusoidally with frequency

$$f = c/\lambda \quad (13.16)$$

cycles per second (Hz) or angular frequency  $\omega = 2\pi f$  (radians)  $\text{s}^{-1}$ . Equation 13.16 relates the frequency and wavelength. For instance, middle C has a frequency of  $261.63 \text{ Hz}$ . In air, the wavelength is  $(344 \text{ m s}^{-1})/(261.63 \text{ Hz}) = 1.315 \text{ m}$ . The *wave number* is

$$k = \frac{2\pi}{\lambda} = \frac{\omega}{c}. \quad (13.17)$$

*Standing waves* such as

$$p(x, t) = p \cos(\omega t) \sin(kx) \quad (13.18)$$

are also solutions to the wave equation. An example is shown in Fig. 13.4. The standing wave in Eq. 13.18 has nodes fixed in space where  $\sin(kx)$  is zero. Standing waves can occur, for example, in an organ pipe and in the ear canal (Problem 7).

A standing wave can also be written as the sum of two sinusoidal traveling waves, one to the left and one to the right. Conversely, two standing waves can be combined to give a traveling wave (Problem 8).

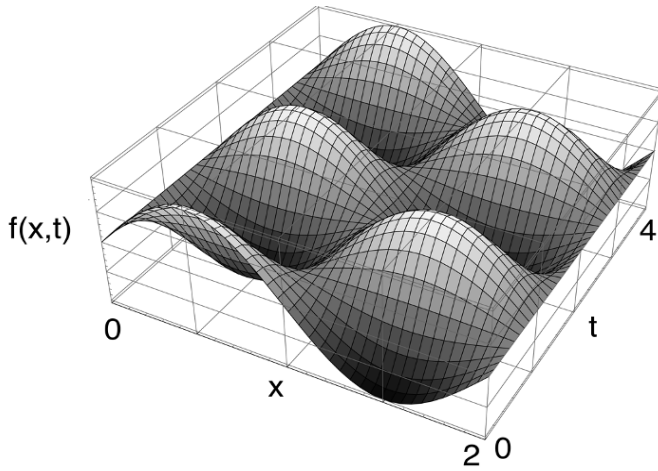


FIGURE 13.4. A standing wave  $f(x, t) = \sin \pi x \cos \pi t$ , plotted for  $0 < x < 2$  and  $0 < t < 4$ .

Since the fluid velocity  $v$  obeys the wave equation, it can also be represented as a sinusoidal wave. It is important to realize that the fluid oscillates back and forth. The fluid itself does not propagate with the wave. What propagates is the disturbance in the fluid. Sound in a fluid is a *longitudinal wave*, which means that the fluid oscillates along the same axis that the disturbance propagates (in this case, both move in the  $x$  direction). Other types of waves exist in nature, such as electromagnetic waves studied in Chapter 14. Electromagnetic waves are *transverse waves*, because the electric field oscillates in a direction perpendicular to the direction of wave propagation. Solids, such as bones, can support shear stresses and can propagate both longitudinal and transverse acoustic waves. But fluids and soft tissue cannot support significant shear stresses and only propagate longitudinal waves.

### 13.3 Acoustic Impedance

#### 13.3.1 Relationships Between Pressure, Displacement and Velocity in a Plane Wave

For a plane wave traveling to the right, the pressure, displacement and speed of the fluid have simple relationships. If the pressure change is

$$p(x, t) = p_0 \sin(kx - \omega t), \quad (13.19)$$

one can use Eqs. 13.8 and 13.12 to show that the fluid displacement is

$$\xi = \xi_0 \cos(kx - \omega t), \quad (13.20)$$

the fluid velocity is

$$v = v_0 \sin(kx - \omega t), \quad (13.21)$$

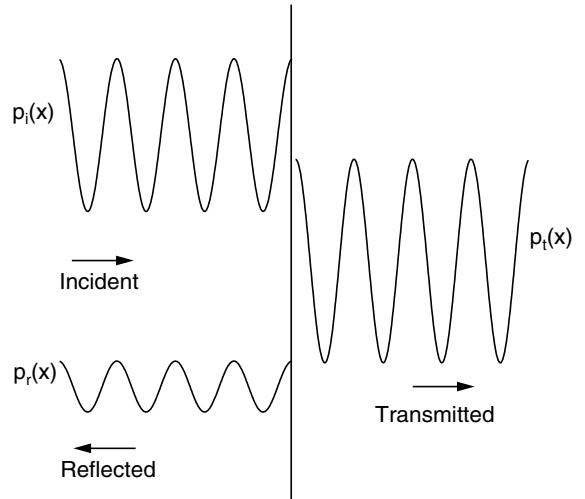


FIGURE 13.5. A sound wave with pressure amplitude  $p_i$  traveling to the right is incident on a boundary separating tissue 1 on the left from tissue 2 on the right. Each tissue has a different density  $\rho_0$  and compressibility  $\kappa$ . Part of the wave is transmitted to the right with amplitude  $p_t$ , and part is reflected to the left with amplitude  $p_r$ . The drawing shows one instant in time when  $Z_2 = 2Z_1$ .

and the amplitudes are related by

$$\xi_0 = p_0 \frac{\kappa}{k} = p_0 \frac{\kappa \lambda}{2\pi} = p_0 \frac{\kappa c}{\omega}, \quad (13.22)$$

$$v_0 = \frac{p_0}{\rho_0 c} = \frac{p_0}{Z}. \quad (13.23)$$

The quantity  $Z = \rho_0 c = \sqrt{\rho_0/\kappa}$  is called the *acoustic impedance* of the medium.<sup>4</sup> The acoustic impedance of water is about  $(10^3 \text{ kg m}^{-3})(1,400 \text{ m s}^{-1}) = 1.4 \times 10^6 \text{ Pa s m}^{-1}$ . The acoustic impedance of air is about  $400 \text{ Pa s m}^{-1}$ , so  $Z_{\text{air}} \ll Z_{\text{water}}$  (Denny, 1993).

#### 13.3.2 Reflection and Transmission of Sound at a Boundary

Consider next what happens at the boundary between two different media. Suppose a traveling wave is propagating to the right in a fluid with sound speed  $c_1$  and acoustic impedance  $Z_1$ . At  $x = 0$ , it encounters a second fluid, with speed  $c_2$  and impedance  $Z_2$ . In general, the interaction of the incoming wave with the boundary between the first and second fluids results in a reflected

<sup>4</sup>Strictly speaking, the acoustic impedance is the ratio  $Z = p_0/v_0$ , and carries information about both the amplitude ratio and the relative phase of the pressure and velocity. If the waves are in phase,  $Z$  is said to be “resistive;” if they are  $\pi/2$  out of phase,  $Z$  is said to be “reactive.” The *characteristic acoustic impedance* is a property of the medium:  $Z_0 = \rho_0 c$ . Both have units  $\text{Pa m s}^{-1}$  or  $\text{kg m}^{-2}\text{s}^{-1}$ . For a plane wave the impedance is resistive and  $Z = Z_0$ . For other waves, such as standing waves, there is a reactive component.

wave traveling to the left in fluid 1 and a transmitted (or refracted) wave traveling to the right in fluid 2 (Fig. 13.5). The acoustic impedances determine how much of the incoming wave is reflected and how much is transmitted. The waves must oscillate with the same frequency in both media. The pressure at the boundary must be the same in each medium, and the fluid velocity must also be continuous across the boundary. Let  $p_i(x, t) = p_i \sin \left[ \frac{\omega}{c_1}(x - c_1 t) \right]$ ,  $p_r(x, t) = p_r \sin \left[ \frac{\omega}{c_1}(x + c_1 t) \right]$ , and  $p_t(x, t) = p_t \sin \left[ \frac{\omega}{c_2}(x - c_2 t) \right]$  be the incoming, reflected, and transmitted pressures. The velocities are related to the pressures by the acoustic impedances. At the boundary, the pressure and the velocity must be continuous. In fluid 1 the amplitude of the pressure is  $p_i + p_r$ , and in fluid 2 it is  $p_t$ . In fluid 1 the amplitude of the velocity is  $(p_i - p_r)/Z_1$ , and in fluid 2 it is  $p_t/Z_2$ . (The minus sign arises because the reflected wave is traveling to the left.) Therefore

$$p_i + p_r = p_t \tag{13.24}$$

and

$$(p_i - p_r)/Z_1 = p_t/Z_2. \tag{13.25}$$

We can solve these two equations for  $p_r$  and  $p_t$  in terms of  $p_i$ :

$$p_r = \frac{Z_2 - Z_1}{Z_2 + Z_1} p_i, \tag{13.26}$$

$$p_t = \frac{2Z_2}{Z_2 + Z_1} p_i. \tag{13.27}$$

The *intensity*  $I$  of a sound wave is a measure of the power per unit area ( $\text{W m}^{-2}$ ). The instantaneous power per unit area transmitted by the wave in Eq. 13.19 at some point is

$$I(t) = p(t)v(t) = p_0 v_0 \sin^2 \omega t. \tag{13.28}$$

The average power per unit area is

$$I = \frac{1}{2} p_0 v_0 = \frac{1}{2} \frac{p_0^2}{Z}. \tag{13.29}$$

Problems 13–15 show that the *reflection* and *transmission coefficients* are

$$R = \frac{I_r}{I_i} = \left( \frac{Z_2 - Z_1}{Z_2 + Z_1} \right)^2, \tag{13.30}$$

and

$$T = \frac{I_t}{I_i} = \frac{4Z_1 Z_2}{(Z_1 + Z_2)^2}, \tag{13.31}$$

and that  $R + T = 1$ .

If the acoustic impedance of the two fluids is the same,  $Z_1 = Z_2$ , there is no reflected wave and the entire incoming wave is transmitted. If  $Z_1 \ll Z_2$  (for example, sound going from air to water), almost all of the sound is reflected.

## 13.4 Comparing Intensities: Decibels

### 13.4.1 The Decibel

When comparing two intensities, the range of differences is often so great that a logarithmic comparison scale is used. We first saw the decibel when discussing the frequency response of a linear system in Chapter 11. Intensity levels in decibels (dB) have meaning only in terms of ratios:

$$\text{Intensity difference (dB)} = 10 \log_{10} \left( \frac{I_2}{I_1} \right). \tag{13.32}$$

The intensity difference can also be written in terms of pressure (or displacement or velocity) ratios:

$$\begin{aligned} \text{Intensity difference (dB)} &= 10 \log_{10} \left( \frac{I_2}{I_1} \right) = 10 \log_{10} \left( \frac{p_2}{p_1} \right)^2 \\ &= 20 \log_{10} \left( \frac{p_2}{p_1} \right). \end{aligned} \tag{13.33}$$

This assumes that  $p_1$  and  $p_2$  are measured in the same medium, so the acoustic impedance does not change. If the intensity of a wave falls to 1% of its original value, the intensity difference is  $10 \log_{10}(0.01) = -20$  dB.

### 13.4.2 Hearing Response

In auditory acoustics, intensities are measured with respect to a reference intensity  $I_0 = 10^{-12} \text{ W m}^{-2}$ . This is the intensity of the faintest sound that a person can typically hear:

$$\text{Intensity level} = 10 \log_{10} \left( \frac{I}{I_0} \right). \tag{13.34}$$

A sound that is 10 times as intense as the threshold for hearing has an intensity level of 10 dB. A sound with an average intensity  $I = 1 \text{ W m}^{-2}$  is perceived as painful, so the threshold for pain has an intensity level of about 120 dB. Table 13.1 gives the intensity in decibels for some common sounds.

The sensitivity of the ear depends on frequency. A typical hearing response curve for a young person is shown in Fig. 13.6. The *minimum auditory field* (MAF) is measured with a loudspeaker; the slightly different *minimum auditory pressure* (MAP) is measured with headphones. The ear is most sensitive to sounds between about 100 and 5,000 Hz. A sound at 20 Hz will not be perceived to be as loud as one at 1,000 Hz with the same intensity. Commercial sound level meters typically have two “weightings.” The “C” weighting has almost the same sensitivity at all frequencies. The “A” weighting more nearly mimics the response of the normal ear. Sounds with the same level when the meter is on “A” weighting will be perceived as having the same loudness.

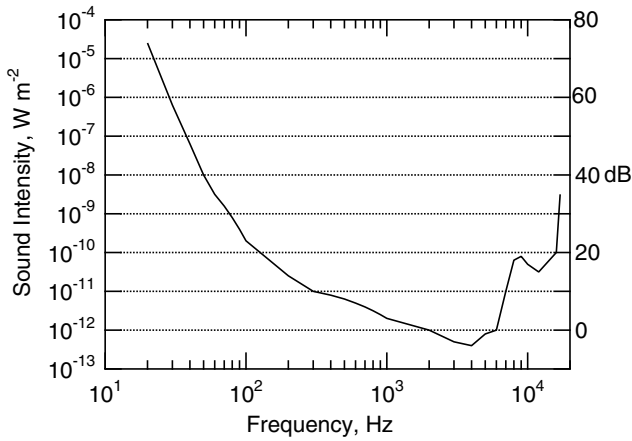


FIGURE 13.6. Hearing response (MAF) curve for a young adult.

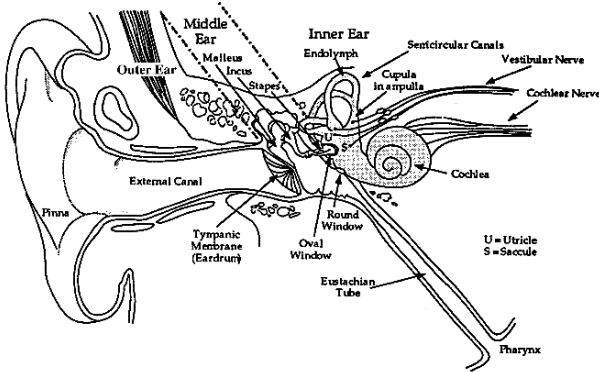


FIGURE 13.7. A cross section of the ear. From J. R. Cameron, J. G. Skofronick, and R. M. Grant. *Physics of the Body*. Madison, WI. Medical Physics Publishing. 1999. Used by permission.

### 13.5 The Ear and Hearing

A cross section of the ear is shown in Fig. 13.7. The ear can be thought of as having three different sections, each with a unique purpose: the *external ear* gathers sound, the *middle ear* transfers energy from the air (low acoustic impedance) to the liquid of the inner ear (high acoustic impedance); the *inner ear* transforms the signal into nerve impulses going to the brain.

The external ear consists of the *pinna*, the visible part of the ear, and an air-filled tube called the *ear canal*.

The middle ear is a small chamber filled with air that contains three small bones, or *ossicles* (Fig. 13.8). It is separated from the ear canal by the *ear drum*. The bone in contact with the ear drum is called the *malleus* (it is shaped a bit like a mallet or hammer). The next bone is the *incus* (from the Latin for anvil, which it resembles slightly). The third bone, in contact with the *oval window* to the inner ear, is the *stapes* (again from the Latin, for stirrup.) The *eustachian tube* leads from the middle

TABLE 13.1. Approximate intensity levels of various sounds.

Sound	Intensity (W m <sup>-2</sup> )	Level (dB, A weighting)
Rocket launch pad	10 <sup>5</sup>	170
F-84 jet at takeoff, 25 m from the tail; Large pneumatic riveting machine (1 m); boiler shop (maximum level); peak sound level at a rock concert	10 <sup>4</sup> 10 <sup>3</sup> 10 <sup>2</sup> 10	160 150 140 130
Sound that produces pain	1	120
Woodworking shop	10 <sup>-1</sup>	110
Near a pneumatic drill (“jack hammer”)	10 <sup>-2</sup>	100
Inside a motor bus	10 <sup>-3</sup>	90
Urban dwelling near heavy traffic	10 <sup>-4</sup>	80
Busy street	10 <sup>-5</sup>	70
Speech at 1 meter	10 <sup>-6</sup>	60
Office	10 <sup>-7</sup>	50
Average dwelling	10 <sup>-8</sup>	40
Maximum background sound level tolerable in a broadcast studio	10 <sup>-9</sup>	30
Whisper; maximum background sound level tolerable in a motion picture studio	10 <sup>-10</sup>	20
Minimum perceptible sound	10 <sup>-11</sup> 10 <sup>-12</sup>	10 0

ear to the mouth and throat (*nasopharynx*). Since the ear is sensitive to very small pressure changes, the eustachian tube serves the important function of keeping the pressure on both sides of the ear drum the same for slow changes, such as when we climb stairs or the weather changes. The walls of the eustachian tube are often collapsed together. Swallowing helps to open them up and equalize the pressure if necessary.

Sound arrives at the ear as a vibration in air. Sound energy must enter the inner ear in order to be converted into a nerve signal to the brain. Yet, the inner ear is filled with liquid. The acoustic impedance of the liquid in the inner ear is about 3,500 times larger than the acoustic impedance of air. This means that without the impedance transformation by middle ear, the intensity in the inner ear would be only about 1/1,000 of the pressure amplitude in air—a loss of about 30 dB (Problem 14).



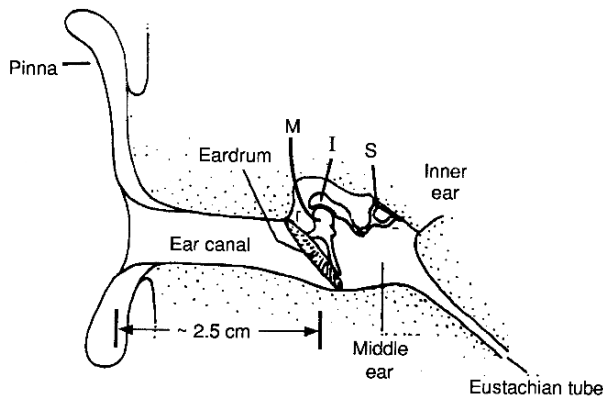


FIGURE 13.8. Details of the middle ear. From J. R. Cameron, J. G. Skofronick, and R. M. Grant. *Physics of the Body*. Madison, WI: Medical Physics Publishing, 1999. Used by permission.

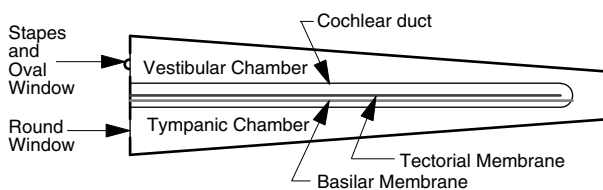


FIGURE 13.9. A schematic representation of the cochlea.

The middle ear transforms the impedance by two mechanisms. The first is a simple area change. The ear drum vibrates in response to the pressure changes in the sound wave. If a sound wave with pressure amplitude  $p_{\text{air}}$  impinges on the ear drum of area  $S_{\text{ear drum}}$ , the total excess force on the ear drum is  $F = p_{\text{air}} S_{\text{ear drum}}$ . For this simplest model, assume that the three bones behave like a single rigid rod and there are no effects of the boundary at the circumference of the ear drum. Then the bones transmit this force to the membrane at the oval window, which has area  $S_{\text{oval window}}$ . The pressure induced in the liquid in the inner ear is then  $p_{\text{inner ear}} = F/S_{\text{oval window}} = p_{\text{air}} S_{\text{ear drum}}/S_{\text{oval window}}$ . The area of the ear drum is about  $S_{\text{ear drum}} = 64 \text{ mm}^2$ , while the area of the area of the base of the stapes is  $3.2 \text{ mm}^2$  [Newman (1957)]. Therefore  $p_{\text{inner ear}} = 20p_{\text{air}}$ . Actually, the ear drum and the membrane at the oval window are not connected by a simple rigid rod. The malleus, incus, and stapes are pivoted in such a way that they serve as a set of levers multiplying the force at the oval window by an additional factor of 1.3. Therefore the total pressure amplification by the middle ear is 26. This corresponds to a 28 dB change in sound intensity, which almost compensates for the 30 dB loss going from air to the liquid of the inner ear. The bones of the middle ear have muscles that change their stiffness, so they can reduce the amount of pressure amplification to protect the inner ear from very loud, low-frequency noises.

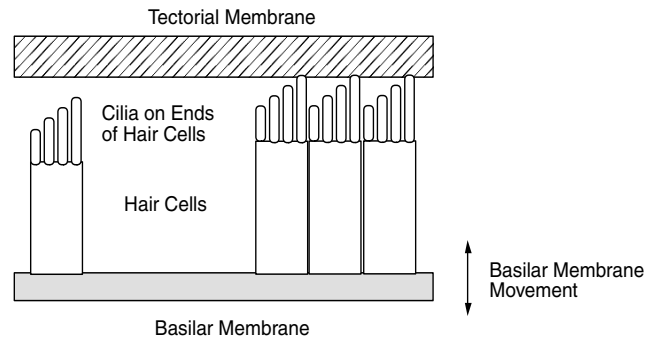


FIGURE 13.10. A cross section of the cochlea. The hair cells are deformed as the basilar membrane moves.

The inner ear contains three *semicircular canals*, which help control our sense of balance, and the *cochlea*, which changes the sound to nerve impulses. All are filled with liquid. The cochlea is a small spiral about the size of the tip of your little finger. If it is unwound, it is about 3 cm long. Figure 13.9 shows it schematically. There are three chambers. The *vestibular chamber* connects to the stapes in the middle ear through the oval window. At the other end of the cochlea the vestibular chamber connects to the *tympanic chamber*. The *round window* opens onto the middle ear and allows the pressure to be equalized at low frequencies. The third chamber is the *cochlear duct*.

When the stapes moves the oval window, it generates a sound wave that travels through the liquid in the cochlea. This produces a displacement of the *basilar membrane* in the third chamber, the cochlear duct. Two types of *hair cells* sit on the basilar membrane: one row of inner hair cells and three rows of outer hair cells. The hair cells in turn have very fine “hairs” on them, called *cilia*. The cilia of the outer hair cells touch another membrane, the *tectorial membrane*, but the cilia of the inner hair cells do not. A cross section of this is shown schematically in Figure 13.10. When the basilar and tectorial membranes are displaced by the sound wave, the cilia on the inner hair cells move in the liquid that fills the region between the membranes. It is just as if you submerged your head in a swimming pool and shook your head back and forth. Your hair would move in the water, but the motion of your hair would be altered as the water “dragged” it. As a result of this motion of the cilia in the liquid, the inner hair cells generate nerve impulses that then travel to the brain and provide our sensation of sound. The mechanism was discussed briefly in Sec. 9.9

## 13.6 Attenuation

A plane wave of sound propagating through a medium is *attenuated*: there is a decrease in intensity because of dissipative factors such as viscosity and heat conduction, which we did not include in Sec. 13.1. The attenuation

is exponential. The *amplitude attenuation coefficient*<sup>5</sup> is defined by

$$\alpha = -\frac{1}{p} \frac{dp}{dx}, \quad (13.35)$$

where  $x$  is the distance the wave travels in the medium. The sound pressure amplitude decays exponentially:

$$p(x) = p(0)e^{-\alpha x}. \quad (13.36)$$

Since the intensity is proportional to  $p^2$ ,

$$I(x) = I(0)e^{-2\alpha x}. \quad (13.37)$$

The *intensity attenuation coefficient* is  $\mu = 2\alpha$ . In acoustics, the attenuation is usually expressed in decibels per meter, which is then independent of whether  $\mu$  or  $\alpha$  is used.<sup>6</sup>

The wave equation for acoustics is an approximation, because the basic equations of fluid dynamics are non-linear. Therefore effects that we have ignored, such as waveform distortion, the generation of harmonics, and increased attenuation may occur, particularly at high sound intensities.

In air, the attenuation depends on the frequency of the sound and the temperature and humidity of the air [Lindsay and Beyer (1989); Denny (1993)]. Sound that we can hear (in the frequency range of 20 Hz to 20 kHz) is attenuated by about 0.1–10 dB km<sup>-1</sup>. Water transmits sound better than air, but its attenuation is an even stronger function of frequency. It also depends on the salt content. At 1,000 Hz, sound attenuates in fresh water by about  $4 \times 10^{-4}$  dB km<sup>-1</sup>. The attenuation in sea water is about a factor of ten higher [Lindsay and Beyer (1989)]. The low attenuation of sound in water (especially at low frequencies) allows aquatic animals to communicate over large distances [Denny (1993)].

The attenuation of sound depends strongly on frequency. Figure 13.11 shows some representative values. As a rule of thumb, at ultrasonic frequencies the attenuation is proportional to frequency, with the constant of proportionality being 100 dB m<sup>-1</sup> MHz<sup>-1</sup>. There are large variations in attenuation in tissue, depending on the age of the subject and other factors. Values can be found in Appendix A of ICRU 61 (1998).

There can also be scattering of the sound from some object, just as there is for light. The total scattering cross section for the object is defined by

$$\sigma_s = \frac{W_s}{I_0}, \quad (13.38)$$

where  $W_s$  is the total power scattered and  $I_0$  is the incident intensity. As in Chapter 14, the differential scattering cross section can also be defined.

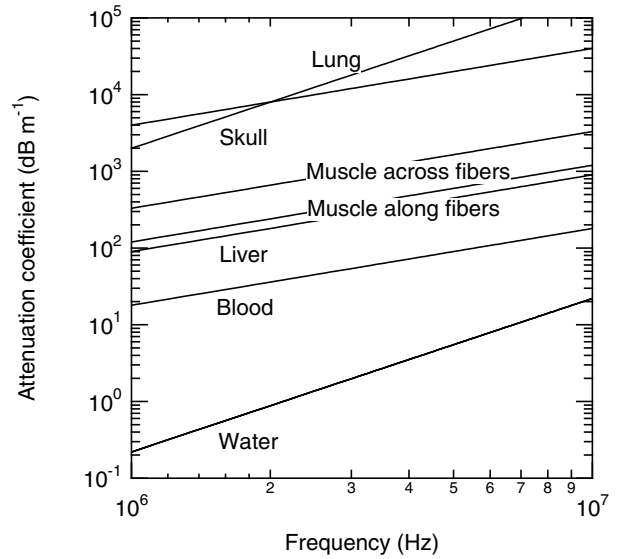


FIGURE 13.11. Representative values of the attenuation coefficient for ultrasound.

### 13.7 Medical Uses of Ultrasound

Ultrasound has several uses in medicine. The most common is to provide diagnostic images that complement those made with x-rays, nuclear medicine, and magnetic resonance. Another is to heat tissue (*diathermy*). It is also used to break up gall stones and kidney stones (*lithotripsy*), and, experimentally, to destroy tissue by intense heating.

The highest-frequency sounds that we can hear ( $\approx 15$  kHz) have a wavelength in water of 0.1 m. One property of waves is that diffraction limits our ability to produce an image. Only objects larger than or approximately equal to the wavelength can be imaged effectively. This property is what limits light microscopes (using electromagnetic waves to form an image) to resolutions equal to about the wavelength of visible light, 500 nm. If we used audible sound to form images, our resolution would be limited to about 0.07 m, which would be a poor image indeed. To overcome this difficulty, higher frequencies (ultrasound) are used to form images. Typically, diagnostic ultrasound uses frequencies on the order of 1 to 15 MHz, corresponding to wavelengths of 1.4 to 0.1 mm in tissue. Higher frequencies would result in even shorter wavelengths, but higher frequency sound has increased attenuation, which ultimately sets an upper bound to the useful frequency.

#### 13.7.1 Ultrasound Transducers

Ultrasound is typically produced using a *piezoelectric transducer*. A piezoelectric material converts a stress (or pressure) into an electric field, and vice versa. A high-frequency oscillating voltage applied across a piezoelectric material creates a sound wave at the same frequency.

<sup>5</sup>ICRU 61 (1998).

<sup>6</sup>Sometimes the attenuation coefficient is expressed in nepers m<sup>-1</sup>, in which case the natural logarithm of the intensity or pressure ratio is used.

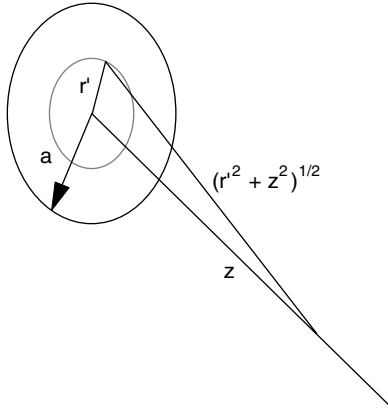


FIGURE 13.12. Coordinate system for calculating the intensity of sound radiated from a transducer of radius  $a$ . The  $z$  axis passes through the center of the transducer and is perpendicular to it.

Conversely, an oscillating pressure applied to a piezoelectric material creates an oscillating voltage across it. Measurement of this voltage provides a way to record ultrasonic waves. Thus, the same piezoelectric material can serve as both source and detector. One piezoelectric material often used in medical transducers is lead zirconate titanate (PZT). Its density is  $7.5 \times 10^3 \text{ kg m}^{-3}$ , the speed of sound in the material is  $4,065 \text{ m s}^{-1}$ , and the acoustic impedance is  $30 \times 10^6 \text{ Pa s m}^{-1}$ . About half of the electrical energy is converted to sound energy, and *vice versa*.

There are some important features of the radiation pattern from a transducer which we review next. Consider a circular transducer, the surface of which is oscillating back and forth in a fluid. Both faces set up disturbances in the fluid; however, we consider the radiation from only one face, since the transducer is placed in a holder that prevents radiation from the rear surface. We can easily calculate the intensity along the  $z$  axis, which we set up perpendicular to the piston and passing through its center, as shown in Fig. 13.12.

The displacement of the face of the transducer,  $\xi$ , is the same as the displacement of the fluid in contact with it. The entire face of the piston, and therefore the fluid immediately in front of it, vibrates with a fluid velocity  $d\xi/dt = v_0 \cos \omega t$ .<sup>7</sup> Each small element of the vibrating fluid creates a wave that travels radially outward, the points of constant phase being expanding hemispheres. The amplitude of each spherical wave decreases as  $1/r$ , the intensity falling as  $1/r^2$ . We want the pressure at a point  $z$  on the axis of the transducer. It is obtained by summing up the effect of all the spherical waves emanating from the face of the transducer. At time  $t$  the phase of the wave is the same as the phase of the wave leaving the annular ring  $r' dr'$  at the earlier time  $t - r/c$ :

$$p \propto \frac{d\xi(z, t)}{dt} \propto \int_0^a 2\pi r' dr' \frac{\cos[\omega(t - r/c)]}{r}$$

<sup>7</sup>We use  $d\xi/dt$  because it is in phase with the excess pressure.

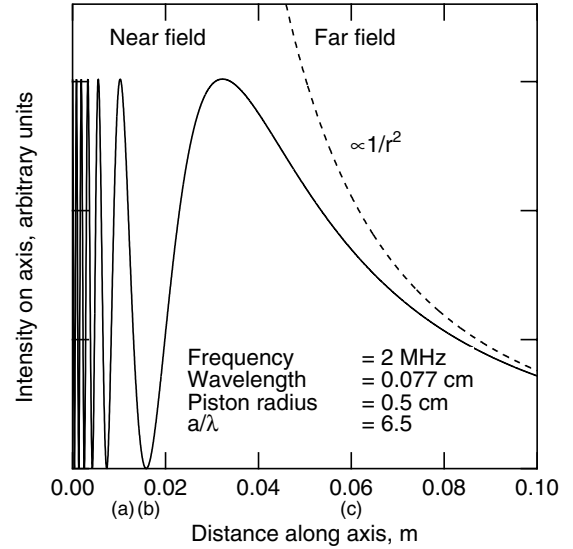


FIGURE 13.13. The sound intensity on the axis of a circular transducer. The sound frequency is 2 MHz, and the transducer radius is 0.5 cm. Both near- and far-field regions are shown. Labels (a), (b), and (c) show the positions of the transverse radial scans in Fig. 13.14.

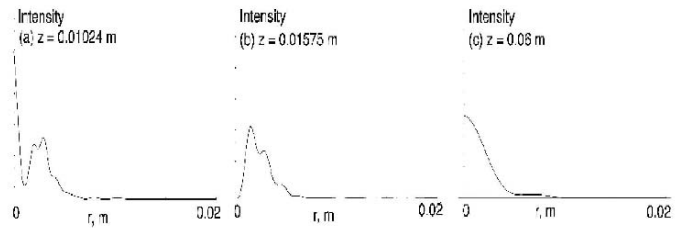


FIGURE 13.14. Scans across the beam from the transducer shown in Fig. 13.13. (a) In the near field at an on-axis maximum 0.01024 m from the transducer. (b) In the near field at an on-axis minimum 0.01575 m from the transducer. (c) In the far field 0.060 m from the transducer.

This is easily evaluated by changing variables. Since  $r^2 = r'^2 + z^2$ ,  $2r dr = 2r' dr'$ :

$$p \propto 2\pi \int_{r=z}^{r=\sqrt{a^2+z^2}} r dr \frac{\cos[\omega(t - r/c)]}{r} = \frac{2\pi}{k} \left[ \sin\left[\omega\left(t - \frac{1}{c}\sqrt{a^2 + z^2}\right)\right] - \sin[\omega(t - z/c)] \right]$$

To find the average intensity we square and average over one period. The result is

$$I \propto \sin^2 \left[ \frac{\omega}{2c} \left( z - \sqrt{a^2 + z^2} \right) \right] \tag{13.39}$$

The result is plotted in Fig. 13.13 for a fairly typical but small transducer ( $a = 0.5 \text{ cm}$ ,  $f = 2 \text{ MHz}$ ).

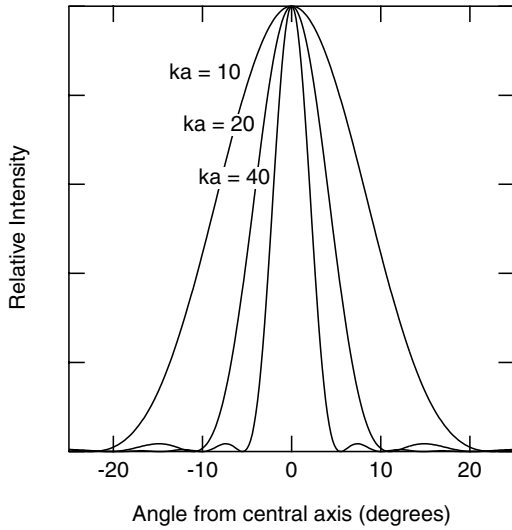


FIGURE 13.15. The far-field intensity as a function of angle, calculated from Eq. 13.40. The value  $ka = 10$  corresponds to 1 MHz and transducer radius  $a = 0.25$  cm. The value  $ka = 20$  corresponds to  $f = 2$  MHz and  $a = 0.25$  cm or  $f = 1$  MHz and  $a = 0.5$  cm. Value  $ka = 40$  corresponds to 4 MHz and  $a = 0.25$  cm or  $f = 2$  MHz and  $a = 0.5$  cm, the case examined in Fig. 13.13.

There are several important features of Fig. 13.13. Close to the transducer there are large oscillations in intensity along the axis; there are corresponding oscillations perpendicular to the axis, as shown in Fig. 13.14. The maxima and minima form circular rings. This is called the *near field* or *Fresnel zone*. Further away the intensity falls as  $1/r^2$ , in the *far field* or *Fraunhofer zone*. The depth of the Fresnel zone is approximately  $a^2/\lambda$ . For the example shown (2 MHz, transducer diameter 1 cm), the depth is about 3 cm; for a larger transducer or higher-frequency ultrasound, it would be greater.

In the far field, approximations can be made to simplify the calculation. The intensity is then given by

$$I \propto \frac{1}{r^2} \left( \frac{J_1(ka \sin \theta)}{ka \sin \theta} \right)^2. \quad (13.40)$$

Function  $J_1(x)$  is the *Bessel function of order 1*. It is found in math tables and is available in many spreadsheets. The angular dependence of the far-field intensity is plotted in Fig. 13.15.

By shaping the face of the transducer, it is possible to bring the beam to a focus at some particular depth. This improves the spatial resolution and increases the strength of the returning echo. Ultrasound imaging may be done in the near field, the far field, or the transition region. Modern transducers typically consist of an array of transducers which may lie on a straight or curved line. They can be driven in such a way as to produce waves that come to a focus, or that travel in an off-axis direction [see Hende and Ritenour (2002) or Fig. 13.17].

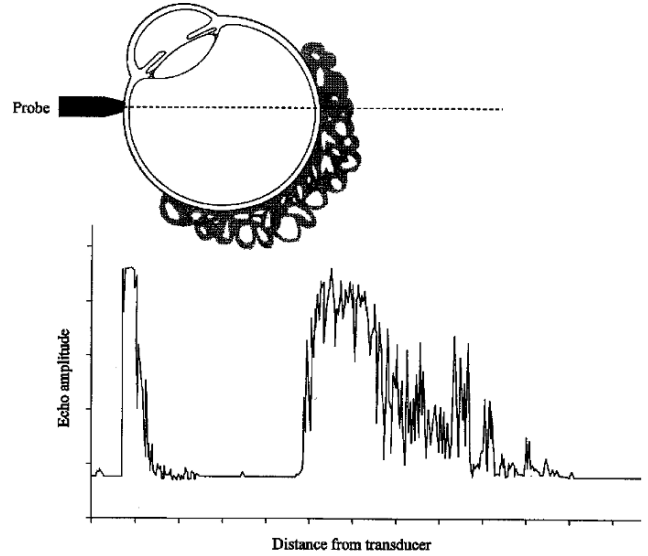


FIGURE 13.16. An A scan of the eye. From ICRU 61, p. 2. Used by permission.

The impedance of a typical transducer is about  $30 \times 10^6$  Pa s  $m^{-1}$ , so it is necessary to have an impedance-matching material between the transducer and the patient's skin. See Problem 16.

### 13.7.2 Pulse Echo Techniques

Most ultrasonic imaging is based on a pulse-echo technique. A short pulse (typically  $0.5 \mu s$  in duration with a central frequency of about 5 MHz) is applied to the tissue by a piezoelectric transducer. The pulse travels with a speed of about  $c = 1540$  m  $s^{-1}$  (or  $1.54$  mm  $\mu s^{-1}$ ). Whenever it approaches a boundary between two tissues having different acoustic impedances, part of the incident pulse is reflected as an echo, which can be detected by the same piezoelectric transducer. The longer the time  $\Delta t$  between the generation and detection of the pulse, the farther away the reflecting boundary. In general, the distance from the source to the boundary is  $\Delta x = c\Delta t/2$ , where  $c$  is the speed of sound in the tissue. Multiple boundaries produce multiple echoes, with each echo corresponding to a different distance from the source to boundary. A plot of echo intensity vs. time is called an *A scan*. An A scan of the eye is shown in Fig. 13.16. Because the attenuation is high, it is customary to increase the gain of the receiving amplifier as the echo time increases.

To form a two-dimensional image, it is necessary to scan in many different directions. In a *B scan* the brightness of the screen corresponds to the intensity of the echo, plotted vs. position in the body in the plane of the scan. The B-scan transducer sends a narrow beam into the body. The direction of the beam is rapidly changed to cover a fan-shaped region. This can be done with an oscillating or rotating transducer head (often containing three transducers), with an array of transducers that are

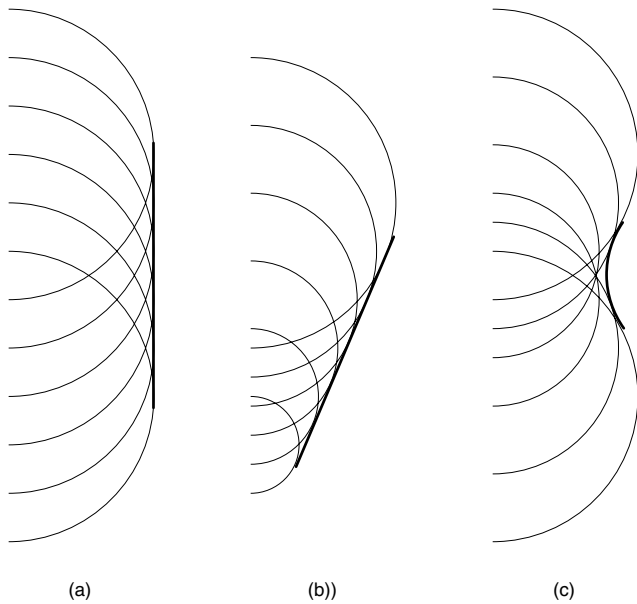


FIGURE 13.17. This shows how a phased array or delayed-pulse array works. Five transducers have been pulsed; the semi-circles show the propagating lines of constant phase from each one. The thick lines show the advancing wave front. In (a), all five transducers have been pulsed at the same time. The signals from each transducer add along the plane wave front traveling to the right. In (b), the top transducer was pulsed first. Each lower transducer was pulsed at successively later times, so the pulses have not traveled as far. This steers the beam downward. In (c), the outer transducers were pulsed first. As one goes inward, each transducer was pulsed later than the one before. This focuses the beam. The same technique can be used to steer or focus the scattered wave during detection.

pulsed sequentially, or with a *phased array* of transducers that are pulsed together. The operation of sequential pulsing or a phased array can be understood by referring to Fig. 13.17. The basic principle of using multiple one-dimensional ( $x$ ) echo scans along different lines through the body is explored in Problems 23 and 24.

Two-dimensional ultrasound is widely used in diagnostic medicine; for instance in monitoring the fetus during pregnancy. Figure 13.18 shows a typical ultrasound image of a fetus.

Other imaging methods include motion or *M mode* to observe the beating heart as a function of time, and detecting sound backscattered from structures in an organ that are smaller than a wavelength. Doppler-shift imaging is discussed below.

Because the tissue response to high-intensity ultrasound is nonlinear, harmonics of the original ultrasound pulse are generated in the tissue; the second-harmonic signals are used to form *harmonic images*. Several techniques are being developed to measure the elastic properties of tissue. For example, an A-mode signal is measured with and without a static force on the tissue; the slight changes in signal reflect changes in tissue density.



FIGURE 13.18. A B scan of a 16-week fetus.

The skin intensities used in diagnostic ultrasound range from  $0.1 \text{ W m}^{-2}$  for an obstetric examination to  $25,000 \text{ W m}^{-2}$  for some procedures that image the heart or blood vessels. These intensities occur over a small area of the body and for a limited period of time. Many studies have been done to see if any harm results from these sound intensities. No harmful effects have been found. The primary potential causes of harm are heating—direct warming of the tissue because of the energy deposited, and *cavitation*, a process in which very high intensity sound waves cause tiny bubbles of steam to form and then collapse violently. Cavitation requires intensities of  $3.5 \times 10^7 \text{ W m}^{-2}$  or more.

Another use of ultrasound is lithotripsy,<sup>8</sup> the destruction of kidney stones using sharply focused ultrasound. Lithotripsy uses extremely intense, pulsed ultrasound waves. The peak intensity is about  $3.8 \times 10^8 \text{ W m}^{-2}$ . The sound is intense enough so that bubbles of steam form and then collapse. When they collapse near the surface of the stone they “hammer” on the stone. With repeated blows, the stone shatters. These smaller pieces may pass in the urine, avoiding surgery.

## 13.8 The Doppler Effect

When the source of an ultrasound wave is moving, the frequency of the wave observed by a stationary receiver is different than the frequency of the source. This phenomenon is called the *Doppler effect*. When the source is moving toward the receiver, the frequency is higher, and when the source moves away from the receiver, the frequency is lower.

To see why this happens, consider the source moving to the right with speed  $v_s$  in a fluid for which the speed

<sup>8</sup> *Litho-* means stone.

of sound is  $c$ . At  $t = 0$ , the source emits the crest of a wave with period  $T$  (frequency  $f = 1/T$ ). The wave travels to the right. This crest takes a time  $t = L/c$  to reach a stationary receiver a distance  $L$  away. At  $t = T$ , one period later, another crest is emitted by the source. This crest takes less time to reach the receiver because the source has moved closer to the receiver. Specifically, the distance from source to receiver is now  $L - v_s T$ , so the crest reaches the receiver at  $t = T + (L - v_s T)/c$ . The time  $T'$  between crests reaching the receiver is  $T' = T + (L - v_s T)/c - L/c = T(1 - v_s/c)$ . The frequency observed by the receiver is

$$f' = 1/T' = \frac{f}{1 - v_s/c}. \tag{13.41}$$

If the source is moving toward the receiver with a speed equal to 10% of the speed of sound, then  $f'$  is about 11% higher than  $f$ . When the source is moving away from the receiver,  $f' = f/(1 + v_s/c)$  (see Problem 32). It is not difficult to include the effect of motion of the reflecting surface at an angle with the ultrasound beam.

In medical ultrasound applications, the detected wave is usually a reflection from moving tissue, such as red blood cells. In this case, the relationship between the frequency  $f$  produced by a stationary source and the frequency  $f'$  received by the stationary receiver after reflection from an object moving away from it at speed  $v_o$  is (see Problem 33)

$$f' = f \frac{1 - v_o/c}{1 + v_o/c}. \tag{13.42}$$

The difference in frequency between  $f$  and  $f'$  contains information about the speed of the object (Problem 35). Doppler ultrasound is often used in medicine to measure speed, such as the speed of moving blood cells. Often the Doppler shift is measured for a pulse of ultrasound, so that one can be sure of the depth at which the Doppler shift occurred. A distribution of red cell velocities can be measured by looking at the Doppler shift frequency spectrum.

### Symbols Used in Chapter 13

Symbol	Use	Units	First used on page
$a$	Transducer radius	m	351
$c$	Speed of sound	m s <sup>-1</sup>	344
$f, g$	Arbitrary functions		345
$f, f'$	Frequency	Hz	345
$h$	Arbitrary function		345
$k$	Wave number	m <sup>-1</sup>	345

$l$	Length	m	344
$p$	Excess pressure	Pa	344
$s_n$	Normal stress	Pa	344
$r, r'$	Position	m	351
$t$	Time	s	344
$v$	Fluid or particle velocity	m s <sup>-1</sup>	345
$v_s, v_o$	Velocity of source, observer	m s <sup>-1</sup>	354
$x, y, z$	Position	m	343
$E$	Young's modulus	Pa	344
$F$	Force	N	344
$I$	Intensity	W m <sup>-2</sup>	347
$J_1$	Bessel function of order 1		352
$L$	Distance	m	354
$M$	Mass	kg	345
$P$	Pressure	Pa	344
$R$	Reflection coefficient		347
$S$	Area	m <sup>2</sup>	344
$T$	Transmission coefficient		347
$T$	Period	s	354
$V$	Volume	m <sup>3</sup>	344
$W_s$	Power scattered	W	350
$Z$	Acoustic impedance	Pa s m <sup>-1</sup> or kg m <sup>-2</sup> s <sup>-1</sup>	346
$\alpha$	Amplitude attenuation coefficient	m <sup>-1</sup>	350
$\kappa$	Compressibility	Pa <sup>-1</sup>	344
$\epsilon_n$	Normal strain		344
$\lambda$	Wavelength	m	345
$\mu$	Intensity attenuation coefficient	m <sup>-1</sup>	350
$\rho$	Density	kg m <sup>-3</sup>	344
$\sigma$	Scattering cross section	m <sup>2</sup>	350
$\theta$	Angle		352
$\xi$	Displacement from equilibrium	m	344
$\omega$	Angular frequency	s <sup>-1</sup>	345

### Problems

#### Section 13.1

**Problem 1** Show that  $1/\sqrt{\rho_0 \kappa}$  has units of speed.

**Problem 2** Show that the pressure  $p$  satisfies the wave equation. Hint: Use Eqs. 13.13 and 13.14. Differentiate to obtain  $\partial^2 p/\partial x^2$  and  $\partial^2 p/\partial t^2$ . Also use the fact that when multiple partial derivatives are taken, the order of differentiation can be interchanged (Appendix N).

**Problem 3** Show that  $v$  and  $\rho$  also satisfy the wave equation.

**Problem 4** Derive Eq. 13.15.

Section 13.2

**Problem 5** Use the chain rule, with  $u = x - ct$ , to show that  $f(x - ct)$  obeys the wave equation for any function  $f$ . Show that  $g(x + ct)$  also obeys the wave equation.

**Problem 6** Calculate the wavelength in air for the lowest audible frequency (20 Hz for most people) and the highest audible frequency (20 kHz for most young people).

**Problem 7** The ear canal is about 2.5 cm long. It is open to the air at one end and closed by the ear drum at the other. This can cause a standing wave to form, which has a pressure node (zero amplitude) at the opening and pressure maximum at the ear drum. What is the longest wavelength of a standing wave that is set up? What frequency does this correspond to? Compare this to the most sensitive frequency of the ear (Fig. 13.6).

**Problem 8** . Use the trigonometric identity  $\sin(a \pm b) = \sin a \cos b \pm \cos a \sin b$  to show that a traveling wave can be written as the sum of two out-of phase standing waves, and that a standing wave can be written as the sum of two oppositely propagating traveling waves.

Section 13.3

**Problem 9** Derive the relationships between  $p_0$ ,  $\xi_0$  and  $v_0$  (Eqs. 13.22 and 13.23), where  $p_0$ ,  $\xi_0$  and  $v_0$  are the amplitudes of a sinusoidally varying plane wave.

**Problem 10** For the following five tissues, calculate the density and compressibility [data are from W. R. Hendeel and E. R. Ritenour (2002)]:

Tissue	$Z$ ( $\text{Pa s m}^{-1}$ )	$c$ ( $\text{m s}^{-1}$ )
Fat	$1.38 \times 10^6$	1475
Brain	$1.55 \times 10^6$	1560
Blood	$1.61 \times 10^6$	1570
Muscle	$1.65 \times 10^6$	1580
Bone	$6.10 \times 10^6$	3360

**Problem 11** Show that the intensity of a sound wave (Eq. 13.29) can be written as  $\frac{1}{2}ZV^2$ , as  $\frac{1}{2}PV$ , or as  $\frac{1}{2}\frac{P^2}{Z}$ .

**Problem 12** The threshold for audible sound is  $10^{-12} \text{ W m}^{-2}$ . Use Eq. 13.29 to convert this to the amplitude of the pressure oscillation in air, using  $Z_{\text{air}} = 400 \text{ Pa s m}^{-1}$ . Compare this to  $10^5 \text{ Pa}$  (atmospheric pressure), and to  $5 \times 10^{-6} \text{ Pa}$  (which is on the order of the amplitude of random pressure variations in the air due to thermal motion). Are the pressure oscillations small? Perform the same analysis for the threshold for pain,  $I = 10^{-4} \text{ W m}^{-2}$ .

**Problem 13** When an incident sound wave in fluid 1 encounters the boundary with fluid 2, the reflection coefficient,  $R$ , is defined as the fraction of the incident intensity that is reflected. Derive an expression for  $R$  in terms

of  $Z_1$  and  $Z_2$ . Use the data in Problem 10 to calculate what fraction of the incident intensity is reflected at the boundary going from muscle to fat. Do the same for the boundary going from fat to muscle.

**Problem 14** When an incident sound wave in fluid 1 encounters the boundary with fluid 2, the transmission coefficient,  $T$ , is defined as the fraction of the incident intensity that is transmitted. Derive an expression for  $T$  in terms of  $Z_1$  and  $Z_2$ . Hint: recall that fluids 1 and 2 are different, so that the value of  $Z$  in Eq. 13.29 is different for the incident and transmitted waves.

**Problem 15** Use the results of Problems 13 and 14 to show that  $R + T = 1$ .

**Problem 16** (a) Show that when sound goes from a transducer with  $Z_{\text{transducer}} = 30 \times 10^6 \text{ Pa s m}^{-1}$  to tissue with  $Z_{\text{tissue}} = 1.5 \times 10^3 \text{ Pa s m}^{-1}$ , the transmission coefficient is  $T = 2 \times 10^{-4}$ .

(b) Show that a coupling medium between the transducer and tissue will maximize the overall transmission if  $Z_{\text{coupling}} = \sqrt{Z_{\text{transducer}}Z_{\text{tissue}}}$ . Show that in that case the transmission is  $T = 8 \times 10^{-4}$ . Ignore interference effects ( $\lambda \gg$  the thickness of the coupling medium).

Section 13.4

**Problem 17** If the intensity of a sound wave falls to half its original value, what is the change in dB?

Section 13.5

**Problem 18** A sound wave with intensity of  $1 \times 10^{-12} \text{ W m}^{-2}$  is the threshold for hearing. Convert that to a pressure amplitude  $P$ . Convert the pressure amplitude to a displacement amplitude using Eq. 13.22, with  $f = 1 \text{ kHz}$ ,  $\kappa_{\text{air}} = 10^{-5} \text{ Pa}^{-1}$ , and  $c_{\text{air}} = 344 \text{ m s}^{-1}$ . Compare your result with the size of an atom, which is on the order of 0.1 nm. Surprised?

**Problem 19** The ear can just hear sound at about 1,000 Hz at a level that corresponds to a pressure change of  $2 \times 10^{-5} \text{ Pa}$ . Atmospheric pressure is  $10^5 \text{ Pa}$ . Since atmospheric pressure is due to collisions of molecules with the eardrum, there are pressure fluctuations because of fluctuations in the number of collisions in time  $\Delta t$ . We can expect that  $\Delta p/p$  is about  $1/(\text{number of collisions})^{1/2}$ . Suppose that the eardrum has area  $S$  and that when detecting a signal at 1,000 Hz it averages over a time interval of 0.5 ms. The number of collisions per unit area per unit time is given by  $nv/4$ , where  $n$  is the number of air molecules per unit volume and  $v$  is an average velocity of  $482 \text{ m s}^{-1}$ . The radius of the eardrum is 4.5 mm. Find  $\Delta p/p$ .

## Section 13.6

**Problem 20** Find the conversion between  $\alpha$  in  $\text{dB m}^{-1}$  and  $m^{-1}$  (as in  $I = I_0 e^{-\alpha x}$ ).

## Section 13.7

**Problem 21** An ultrasound pulse used in medical imaging has a frequency of 5 MHz and a pulse width of  $0.5 \mu\text{s}$ . Approximately how many oscillations of the sound wave occur in the pulse? The number of oscillations is sometimes called the quality,  $Q$ , of the pulse. A pulse with little damping has  $Q \gg 1$ , whereas a heavily damped pulse has  $Q \approx 1$ . Is the ultrasound pulse heavily damped?

**Problem 22** A heavily damped pulse does not represent a single frequency. Consider a pulse  $p(t)$  having the shape

$$p(t) = e^{-(t/\tau)^2} \cos \omega_0 t.$$

Using the techniques developed in Sec. 11.9, calculate the Fourier transform of this pulse. Determine the shape of the power spectrum. How is the parameter  $\tau$  related to the width of the power spectrum? What is the central frequency of the power spectrum?

**Problem 23** Suppose you send a short ultrasound pulse into the body at  $t = 0$ , and observe echoes at  $t = 31$ ,  $79$ , and  $95 \mu\text{s}$ . How far from the source are the three tissue boundaries? Assume  $c = 1540 \text{ m s}^{-1}$  in each tissue, and ignore attenuation. Draw a line corresponding to the  $x$  axis ( $x = 0$  is the source location), and draw a dot at the position corresponding to each boundary. You have just created a one-dimensional ultrasound image, using the B mode, where each dot (“bright” spot in the image, hence “B”) represents a boundary.

**Problem 24** Suppose you emit an ultrasound pulse in the  $x$  direction from a source at each of eight different positions  $y$ . Each pulse receives a series of echoes, as shown in the table below (Echo times are in  $\mu\text{s}$ ):

$y$ (mm):	0	10	20	30	40	50	60	70
Echo 1	35	37	39	40	45	47	48	49
Echo 2	97	98	58	56	57	96	91	90
Echo 3			71	73	71			
Echo 4			99	99	98			

Draw an  $x$ - $y$  coordinate system ( $x = 0$  is location of the source) and put a bright spot corresponding to each echo. Assume  $c = 1,540 \text{ m s}^{-1}$  in each tissue, and ignore attenuation. You have just created a two-dimensional ultrasound image.

**Problem 25** Assume the attenuation is proportional to frequency, and is given by  $100 \text{ dB m}^{-1} \text{ MHz}^{-1}$ . If you use a 5 MHz ultrasound wave to image a surface 30 mm below the surface of the skin, the measured echo is what fraction of the original intensity? Ignore impedance differences at

the surface of the skin and assume that 100% of the wave is reflected by the surface, so that the reduction of the echo intensity is caused entirely by attenuation. Remember that you must consider the round-trip distance traveled by the wave. Express your answer in decibels.

**Problem 26** The intensity of echoes depends on not only the nature of the boundary they reflect from, but also on the distance to the boundary. Consider a boundary that reflects 50% of the incident wave intensity. Compare the intensity of the echoes recorded by the detector for boundaries 10, 20, and 30 mm from the source. Assume an attenuation coefficient of  $500 \text{ dB m}^{-1}$ . Ignore any inverse-square fall-off. Clinical ultrasound imaging devices often use a technique called time gain compensation to selectively amplify later echoes, thereby correcting for the effect of attenuation that you just calculated.

**Problem 27** The depth resolution of an ultrasound image depends on the speed of sound and the width of the ultrasound pulse. A pulse having a width of  $0.5 \mu\text{s}$  has what spatial width (assume  $c = 1,540 \text{ m s}^{-1}$ )? Structures smaller than the spatial pulse width are difficult to resolve using ultrasound imaging.

**Problem 28** Ultrasound images are often generated using a series of ultrasound pulses, with echoes detected from each pulse. Images are obtained more quickly if the time between pulses is short. However, if this time is too short, echoes from consecutive pulses overlap, making the ultrasound signal difficult to interpret. Assume the deepest structure you wish to image is 80 mm from the source, and the speed of sound is  $1,540 \text{ m s}^{-1}$ . What is the minimum time between pulses you can use without overlapping echoes? How many pulses per second does this correspond to? If you need to use 256 pulses in order to build up a two-dimensional image, how many images can you generate per second?

**Problem 29** Suppose that an ultrasound wave is traveling to the right in muscle, which contains a 3 mm layer of fat (use the data in Problem 10 for the acoustic properties of these tissues). Part of the wave will reflect off the left surface of the fat, but part will be transmitted and then reflect off the right surface. This second echo is called a reverberation echo, and is one source of artifact in an ultrasound image. You can have more than one, since the wave can reflect back and forth between the left and right surfaces multiple times. Calculate the time between the first three reverberation echoes, and the relative intensities of each one (ignore attenuation).

**Problem 30** Assume there is a fat-muscle boundary 50 mm below the tissue surface. Calculate the intensity of the reflected wave, ignoring attenuation, using the data in Problem 10. Now, assume there is a bone that lies in the region from 20 to 30 mm below the surface, with the fat-muscle boundary still 50 mm below the surface. Calculate the intensity of the wave reflected from the fat-muscle



boundary, accounting for the front and back bone surfaces, ignoring attenuation. If the minimum measurable intensity is  $-25$  dB, will the fat-muscle boundary be observable in each case? In general, surfaces behind a bone do not appear in ultrasound images. The bone casts an acoustic shadow.

**Problem 31** Verify Eq. 13.39.

### Section 13.8

**Problem 32** Show that when a source of sound waves is moving away from the receiver, the frequency of the source,  $f$ , and the frequency measured by the receiver,  $f'$ , are related by  $f' = f/(1 + v_s/c)$ .

**Problem 33** Suppose a stationary source sends ultrasound waves to the right. They are reflected from an object moving to the right with speed  $v_o$ , and they are recorded by the stationary receiver (the receiver and source are at the same location). Derive the relationship in Eq. 13.42 between the frequency of the source,  $f$ , and the frequency recorded by the receiver,  $f'$ , using the following steps.

(a) Find the time  $t_1$  when the receiver records a signal that was emitted by the source at  $t = 0$ , traveled a distance  $L$ , was reflected, and then returned to the receiver.

(b) Find the time  $t_2$  when the receiver records a signal that was emitted by the source at  $t = T$ , traveled a distance  $L + \Delta L$ , was reflected, and then returned to the receiver.

(c) Relate the distance  $\Delta L$  to the speed of the speed of the object.

(d) Solve for  $T' = t_2 - t_1$ .

(e) Determine  $f'$  in terms of  $f$ .

**Problem 34** Show that if  $v_o \ll c$ , Eq. 13.42 reduces to  $f' = f(1 - 2v_o/c)$ .

**Problem 35** Solve Eq. 13.42 for  $v_o$  as a function of  $f'/f$ . This allows you to measure the emitted and received frequencies and determine the speed of the object.

## References

- Denny, M. W. (1993) *Air and Water*, Princeton, NJ, Princeton University Press.
- Hendee, W. R. and E. R. Ritenour (2002) *Medical Imaging Physics*, 4th. ed. New York, Wiley-Liss.
- ICRU (1998). *Tissue Substitutes, Phantoms and Computational Modeling in Medical Ultrasound*. International Commission on Radiation Units and Measurements Report 61. Bethesda, MD, ICRU.
- Lindsay, R. B., and R. T. Beyer (1989). Acoustics. Ch. 2 in H. L. Anderson, editor in chief, *A Physicist's Desk Reference*, New York, American Institute of Physics.
- Morse, P. M., and K. U. Ingard (1968) *Theoretical Acoustics*, New York, McGraw-Hill.
- Newman E. B. (1957). Speech and hearing. in D. E. Gray, coordinating editor, *American Institute of Physics Handbook*. New York, McGraw-Hill. p. 3-123.

# 14

## Atoms and Light

This chapter describes some of the biologically important properties of infrared, visible, and ultraviolet light. X rays are discussed in Chapters 15 and 16. A brief discussion of geometrical optics accompanies the description of image formation in the eye and errors of refraction.

This chapter considers light to be photons (Sec. 14.1). Photons can be emitted or absorbed when single atoms change energy levels, and they have certain frequencies characteristic of the atom, as described in Sec. 14.2. Molecules have additional energy levels shown in Sec. 14.3. Biological examples include spectrophotometry, photodissociation, immunofluorescence, infrared spectroscopy, and Raman scattering. There is such an extensive literature about these that the discussion here is quite brief.

Section 14.4 describes the scattering and absorption of radiation, processes that are important in the rest of this chapter and in Chapters 15–17. The probability of scattering or absorption is measured by the cross section, which is also introduced here. Photons may scatter many times in a substance without being absorbed. This leads to the concept of turbid media such as milk or clouds. In some cases the process can be modeled accurately with the diffusion approximation developed in Sec. 14.5. Biological examples of infrared scattering (including Raman scattering) are described in Sec. 14.6

Photons can be absorbed and emitted by some substances in a continuous range of frequencies or wavelengths. This happens when many atoms interact with one another and blur the energy levels, as in liquids and solids. This leads to the concept of thermal radiation described in Sec. 14.7. Examples of thermal radiation are infrared radiation by the skin and ultraviolet radiation by the sun. The former is discussed in Sec. 14.8.

Blue and ultraviolet light are used for therapy, as described in Sec. 14.9. They can also be harmful, particularly to skin and eyes.

Lasers are used to heat tissue, often rapidly enough to do surgery as water in the tissue suddenly boils. Models of this process include the bioheat equation that is developed in Sec. 14.10.

Section 14.11 describes the problem of radiometry: measuring radiation. All of the important quantities are defined, and the corresponding photometric and actinometric quantities are also introduced.

Section 14.12 describes how the eye focuses an image on the retina and the correction of simple errors of refraction. A final example of the photon nature of light is given in Sec. 14.13: the statistical limit to dark-adapted vision—shot noise—which is important when the eye is operating in its most sensitive mode.

### 14.1 The Nature of Light: Waves versus Photons

Light travels in a vacuum with a velocity  $c = 3 \times 10^8$  m  $s^{-1}$  (to an accuracy of 0.07%). When light travels through matter, its speed is less than this and is given by

$$c_n = \frac{c}{n}, \quad (14.1)$$

where  $n$  is the *index of refraction* of the substance. The value of the index of refraction depends on both the composition of the substance and the color of the light.

A controversy over the nature of light existed for centuries. In the seventeenth century, Sir Isaac Newton explained many properties of light with a particle model. In the early nineteenth century, Thomas Young performed some interference experiments that could be explained only by assuming that light is a wave. By the end of the nineteenth century, nearly all known properties of light, including many of its interactions with matter, could be

explained by assuming that light consists of an electromagnetic wave. By an electromagnetic wave, we mean that

1. Light can be produced by accelerating an electric charge.
2. Light has an electric and a magnetic field associated with it; the force that the light exerts on a charged particle is given by Eq. 8.2,  $\mathbf{F} = q(\mathbf{E} + \mathbf{v} \times \mathbf{B})$ . The force due to the magnetic field is usually very small.
3. The velocity of light traveling in a vacuum is given by electromagnetic theory as  $c = 1/\sqrt{\epsilon_0\mu_0}$ , where parameters  $\epsilon_0$  and  $\mu_0$  are measured in the laboratory for “ordinary” electric and magnetic fields.

In the early twentieth century, light was discovered to have *both* particle properties and electromagnetic wave properties at the same time. This rather disconcerting discovery was followed a few years later by the discovery that matter, which had been thought to consist of particles, also has wave properties.

A traveling wave of light can be described by a function of the form  $f(x - c_n t)$ , which represents a disturbance traveling along the  $x$  axis in the positive direction. (To keep a particular value for the argument of  $f$  constant,  $x$  must increase as time increases.) If the wave is sinusoidal, then the period,  $T$ , frequency,  $\nu$ ,<sup>1</sup> and wavelength,  $\lambda$ , are related by

$$\nu = \frac{1}{T}, \quad c_n = \lambda\nu. \quad (14.2)$$

As light moves from one medium into another where it travels with a different speed, the frequency remains the same. The wavelength changes as the speed changes.

Each particle of light or *photon* has energy  $E$ . The energy of each photon (a “particle” concept) is related to its frequency (a “wave” concept) by

$$E = h\nu = \frac{hc_n}{\lambda}. \quad (14.3)$$

The proportionality constant  $h$  is called *Planck’s constant*. It has the numerical value<sup>2</sup>

$$h = 6.63 \times 10^{-34} \text{ J s} = 4.14 \times 10^{-15} \text{ eV s}. \quad (14.4)$$

We use the number “ $h$  stroke” or “ $h$  bar”:

$$\hbar = \frac{h}{2\pi} = 1.05 \times 10^{-34} \text{ J s} = 0.66 \times 10^{-15} \text{ eV s}. \quad (14.5)$$

In terms of the angular frequency  $\omega = 2\pi\nu$ ,

$$E = \hbar\omega. \quad (14.6)$$

<sup>1</sup>We used  $f$  for frequency in earlier chapters because this is customary when discussing noise. Here we adopt  $\nu$  for frequency, the notation most often used in atomic physics.

<sup>2</sup>The electron volt (eV) is a unit of energy.  $1 \text{ eV} = 1.6 \times 10^{-19} \text{ J}$ . It is the energy acquired by an electron that moves through a potential difference of 1 V.

TABLE 14.1. The regions of the electromagnetic spectrum and their boundaries

Name	Wavelength	Frequency (Hz)	Energy (eV)
Radio waves	1 m	$300 \times 10^6$	$1.24 \times 10^{-6}$
Microwaves	1 mm	$300 \times 10^9$	$1.24 \times 10^{-3}$
Extreme infrared	15 $\mu\text{m}$	$20 \times 10^{12}$	0.083
Far infrared	6 $\mu\text{m}$	$50 \times 10^{12}$	0.207
Middle infrared	3 $\mu\text{m}$	$100 \times 10^{12}$	0.414
Near infrared	750 nm	$400 \times 10^{12}$	1.65
Visible	400 nm	$750 \times 10^{12}$	3.1
Ultraviolet	12 nm	$24 \times 10^{15}$	100
X rays, $\gamma$ rays			

TABLE 14.2. The visible electromagnetic spectrum

Color	Wavelength (nm)	Frequency ( $10^{12}$ Hz)	Energy (eV)
Red	750	400	1.65
Orange	610	490	2.03
Yellow	590	510	2.10
Green	570	530	2.17
Blue	500	600	2.48
Blue	450	670	2.76
Violet	400	750	3.11

The electromagnetic spectrum includes radio waves; microwaves, infrared, visible, and ultraviolet light; x rays; and gamma rays. Table 14.1 shows the wavelengths that separate these arbitrary regions, together with the frequencies and the energies of the photons. Visible-light photons have an energy of a few electron volts. X rays are  $10^4$ – $10^7$  times more energetic, while  $\gamma$  rays, which come from atomic nuclei, are often even more energetic but may have energies overlapping x-ray energies. The only difference between x rays and  $\gamma$  rays is their source.

The property of light that we associate with color is the frequency or the energy of each photon. Visible light covers a narrow range of frequencies, about an octave (a factor of 2). Table 14.2 shows the wavelengths and

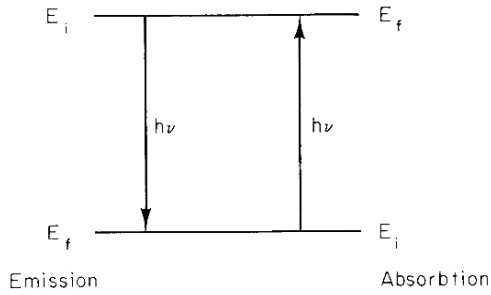


FIGURE 14.1. A system can change from one energy to another by emitting or absorbing a photon. The photon has an energy equal to the difference in energies of the two levels.

frequencies dividing the colors of the visible spectrum. The frequencies are in the 400–750 THz range.

Most of the effects discussed in this chapter can be explained by assuming that light is made up of photons.

## 14.2 Atomic Energy Levels and Atomic Spectra

The simplest system that can emit or absorb light is an isolated atom. An atom is isolated if it is in a monatomic gas. In addition to translational kinetic energy, isolated atoms have specific discrete internal energies, called *energy levels*. An atom can change from one energy level to another by emitting or absorbing a photon with an energy equal to the energy difference between the levels. Let the energy levels be labeled by  $i = 1, 2, 3, \dots$ , with the energy of the  $i$ th state being  $E_i$ . There is a lowest possible internal energy for the atom; when the atom is in this state, no further energy loss can take place. If  $E_i$  is greater than the lowest energy, then the atom can lose energy by emitting a photon of energy  $E_i - E_f$  and exist in a lower-energy state  $E_f$  (Fig. 14.1).

It is possible, using techniques of quantum mechanics, to calculate the energies of the levels with reasonable accuracy (and in some cases with spectacular accuracy). For our purposes, we need only recognize that energy levels exist and know their approximate values. You may be familiar with the hydrogen atom, in which the energy of the  $n$ th level is given by

$$E_n = - \left( \frac{1}{4\pi\epsilon_0} \right)^2 \frac{m_e e^4}{2\hbar^2 n^2}, \quad n = 1, 2, 3, \dots \quad (14.7)$$

The energy is in joules when the electron mass  $m_e$  is in kilograms, the electronic charge  $e$  is in coulombs, and  $\hbar$  is in J s. The Coulomb's law constant  $1/4\pi\epsilon_0$  is given in Eq. 6.2. Dividing the energy in joules by  $e$  gives the energy in electron volts:

$$E_n = - \frac{13.6}{n^2} \quad (\text{in eV}). \quad (14.8)$$

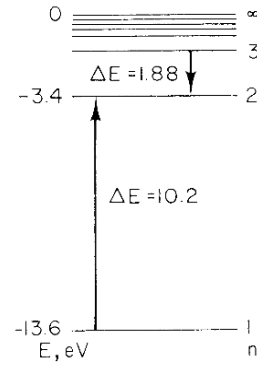


FIGURE 14.2. Energy levels in a hydrogen atom. Transitions are shown corresponding to the emission and absorption of light.

The energy-level diagram in Fig. 14.2 shows these energies and some transitions between them. In other cases, the energy depends not only on the integer  $n = 1, 2, 3, 4, \dots$ , but on other quantum numbers as well.

Figure 14.3 plots the spectrum for hydrogen vs wavelength, along with some of the energy levels of hydrogen. Letters  $a, b, c, \dots$  mark lines in the spectrum and the associated transitions.

In general, the internal energy of an atom depends on the values of five quantum numbers for each electron in the atom. The quantum numbers are

$n = 1, 2, 3, \dots$	the principal quantum number
$l = 0, 1, 2, \dots, n - 1$	the orbital angular momentum quantum number
$s = \frac{1}{2}$	the spin quantum number
$m_l = -l, -(l - 1), \dots, l - 1, l$	“z component” of the orbital angular momentum
$m_s = -\frac{1}{2}, \frac{1}{2}$	“z component” of the spin

Sometimes the last two quantum numbers,  $m_l$  and  $m_s$ , are replaced by two other quantum numbers,  $j$  and  $m_j$ . The allowed values of  $j$  and  $m_j$  are

$j = l - \frac{1}{2}$ or $l + \frac{1}{2}$ except that $j = \frac{1}{2}$ when $l = 0$	total angular momentum quantum number
$m_j = -j, -(j - 1), \dots, j - 1, j$	“z component” of total angular momentum

Whether one uses  $m_l$  and  $m_s$  or  $j$  and  $m_j$ , each electron is described by five quantum numbers, one of which is always  $\frac{1}{2}$ . There are four quantum numbers that can change, corresponding to the three space degrees of free-

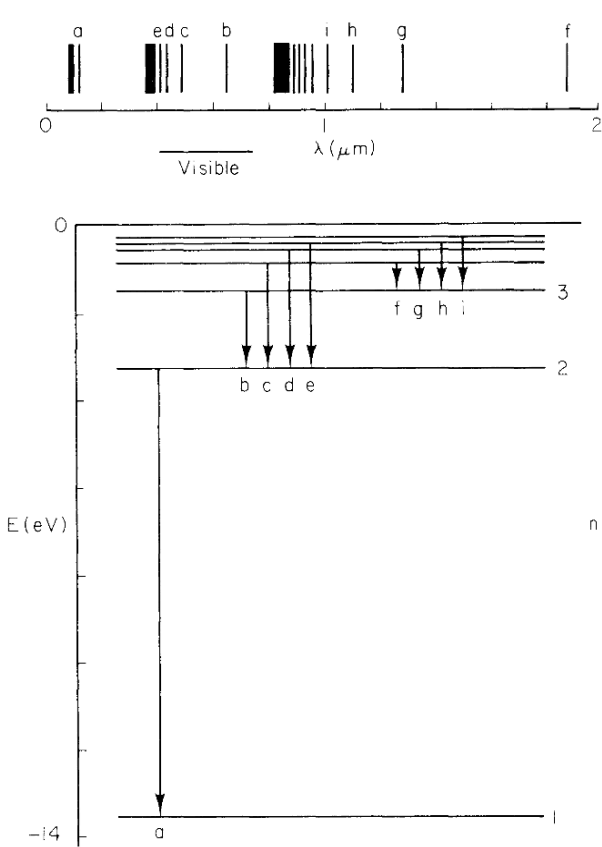


FIGURE 14.3. The spectrum for hydrogen plotted vs. wavelength and the energy levels for hydrogen. Some spectral lines and the corresponding transitions have been labeled.

dom and the spin associated with  $m_s$ . The internal energy of the atom is the sum of the kinetic and potential energies of each electron. The energy of each electron depends on the values of its quantum numbers. It is influenced by the electric field generated by the nucleus and all the other electrons. There are also magnetic interactions between electrons and between each electron and the nucleus, because the moving charges generate magnetic fields.

No two electrons in an atom can have the same values for all their quantum numbers, a fact known as the *Pauli exclusion principle*.

The *ionization energy* is the smallest amount of energy required to remove an electron from the atom when the atom is in its ground state. For hydrogen the ionization energy is 13.6 eV. In contrast, it takes only 5.1 eV to remove the least-tightly-bound electron from a sodium atom.

An atom can receive energy from an external source, such as a collision with another atom or some other particle. It can also absorb a photon of the proper energy. Absorbing just the right amount of energy allows one of its electrons to move to a higher energy level, as long as that level is not already occupied. The atom can then get

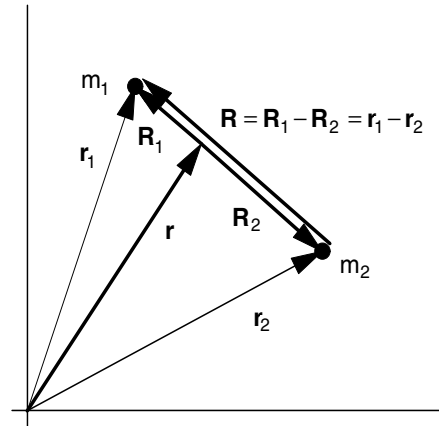


FIGURE 14.4. A diatomic molecule. Vectors  $\mathbf{r}_1$  and  $\mathbf{r}_2$  are the positions of the atoms measured in the laboratory. Vectors  $\mathbf{R}_1$  and  $\mathbf{R}_2$  are coordinates in the center-of-mass system. Vector  $\mathbf{r}$  is the position of the center of mass.

rid of this excess energy by radiating a photon, with the excited electron falling to an unoccupied state with lower energy. This change is usually consistent with the following *selection rules*, which can be derived using quantum mechanics:

$$\Delta l = 1, \quad \Delta j = 0, \pm 1. \quad (14.9)$$

### 14.3 Molecular Energy Levels

In addition to internal energy, an atom can have kinetic energy of translation with three degrees of freedom. The translational kinetic energy is also quantized, but as long as the atom is not confined to a very small volume, the levels are so closely spaced that the translational kinetic energy can be regarded as continuous.

Two atoms together have six degrees of translational freedom, because each can move in three-dimensional space. However, if the atoms are bound together, their motions are not independent. One can speak of the three degrees of freedom for translation of the molecule as a whole (center-of-mass motion) and also the vector displacement of one atom from the other. This is shown in Fig. 14.4. Vector  $\mathbf{r}$  locates the center of mass of the two atoms. It is located at a point such that  $m_1\mathbf{R}_1 = -m_2\mathbf{R}_2$ .

Consider two particles of mass  $m_1$  and  $m_2$ . Their positions with respect to some fixed origin are  $\mathbf{r}_1$  and  $\mathbf{r}_2$ . The velocity of each particle is  $\mathbf{v}_i = d\mathbf{r}_i/dt$ . The kinetic energy of the  $i$ th particle is  $T_i = m_i(\mathbf{v}_i \cdot \mathbf{v}_i)/2$ . Define the center of mass by

$$\mathbf{r} = \frac{m_1\mathbf{r}_1 + m_2\mathbf{r}_2}{m_1 + m_2}$$

and the vectors from the center of mass to each particle by

$$\mathbf{R}_1 = \mathbf{r}_1 - \mathbf{r} = \frac{m_2(\mathbf{r}_1 - \mathbf{r}_2)}{m_1 + m_2} = \frac{m_2\mathbf{R}}{m_1 + m_2},$$

$$\mathbf{R}_2 = \frac{-m_1\mathbf{R}}{m_1 + m_2}.$$

The total kinetic energy is  $T = m_1(\mathbf{v}_1 \cdot \mathbf{v}_1)/2 + m_2(\mathbf{v}_2 \cdot \mathbf{v}_2)/2$ . Since  $\mathbf{v}_i = \mathbf{v} + \mathbf{V}_i$ , we have

$$2T = (m_1 + m_2)(\mathbf{v} \cdot \mathbf{v}) + m_1(\mathbf{V}_1 \cdot \mathbf{V}_1) + m_2(\mathbf{V}_2 \cdot \mathbf{V}_2) + 2\mathbf{v} \cdot (m_1\mathbf{V}_1 + m_2\mathbf{V}_2).$$

The last term vanishes because  $m_1\mathbf{R}_1 + m_2\mathbf{R}_2 = 0$ . Consider the second term. Differentiating  $\mathbf{R}_1 = m_2\mathbf{R}/(m_1 + m_2)$  shows that

$$\mathbf{V}_1 \cdot \mathbf{V}_1 = \left(\frac{m_2}{m_1 + m_2}\right)^2 V^2,$$

$$\mathbf{V}_2 \cdot \mathbf{V}_2 = \left(\frac{m_1}{m_1 + m_2}\right)^2 V^2.$$

Therefore,

$$T = \frac{(m_1 + m_2)v^2}{2} + \frac{1}{2} \frac{m_1 m_2}{m_1 + m_2} V^2.$$

The first term is the kinetic energy of a point mass  $m_1 + m_2$  traveling at the speed of the center of mass. The second is the kinetic energy of a particle having the “reduced mass”  $m_1 m_2 / (m_1 + m_2)$  and the speed of relative motion of the two particles,  $V = |\mathbf{V}| = |d\mathbf{R}/dt|$ . If  $\mathbf{R}$  changes magnitude, the particles are *vibrating*. If  $\mathbf{R}$  has a fixed magnitude the molecule can *rotate*. If the molecule is rotating in some plane with angular velocity  $\omega$ , then

$$\frac{1}{2} \frac{m_1 m_2}{m_1 + m_2} V^2 = \frac{1}{2} \frac{m_1 m_2}{m_1 + m_2} R^2 \omega^2 = \frac{1}{2} I \omega^2.$$

The quantity  $I = [m_1 m_2 / (m_1 + m_2)] R^2 = m_1 R_1^2 + m_2 R_2^2$  is the *moment of inertia* of the two objects [Halliday, Resnick, and Krane (1992, p. 245ff)]. The angular momentum of a mass about some point is sometimes called the “moment of the momentum” about that point, in the same sense that the torque is the moment of a force about some point. In this case the angular momentum is

$$L = R_1(m_1 v_1) + R_2(m_2 v_2) = m_1 R_1^2 \omega + m_2 R_2^2 \omega = I \omega.$$

These two equations can be combined to give the rotational kinetic energy in terms of the angular momentum about the center of mass:

$$T = \frac{L^2}{2I}.$$

Quantum-mechanically, the angular momentum cannot take on any arbitrary value. The square of the angular momentum is restricted to the values

$$L^2 = r(r+1)\hbar^2, \quad r = 0, 1, 2, \dots$$

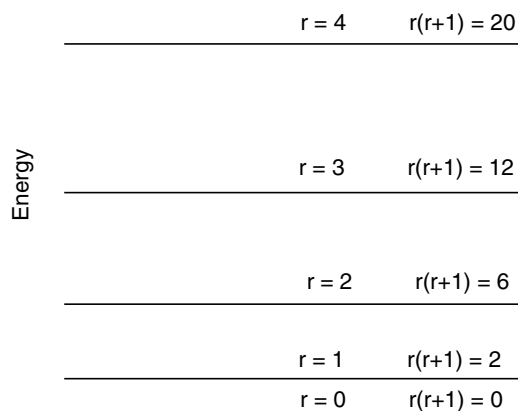


FIGURE 14.5. Energy levels of a rotating molecule.

Since there is no potential energy, the total energy of rotation of the molecule is

$$E_r = \frac{r(r+1)\hbar^2}{2I}, \quad r = 0, 1, 2, \dots \quad (14.10)$$

The spacing of the rotational levels is shown in Fig. 14.5. A detailed calculation using quantum mechanics shows that when a photon is emitted or absorbed,  $r$  must change by  $\pm 1$ . Therefore the photon energy is

$$\Delta E_r = E_r - E_{r-1} = \frac{\hbar^2}{I} r, \quad r = 1, 2, \dots \quad (14.11)$$

The problems at the end of the chapter show that these photons have low energies, so that rotational spectra lie in the far-infrared region (far meaning far from the visible region, that is, very long wavelengths).

The other possibility is that the atoms in the molecule vibrate back and forth along the line joining their centers. If two masses have an equilibrium position a certain distance apart, work must be done either to push them closer together or to pull them farther apart. In either case the potential energy is increased. At the equilibrium separation the potential energy is a minimum. Figure 14.6 shows the potential energy  $E_p$  of a sodium ion and a chloride ion as a function of their separation. The potential has a minimum at a separation of about 0.2 nm. The simplest function that has a minimum is a parabola. A parabola can be used to approximate the minimum in Fig. 14.6:  $E_p(R) = \frac{1}{2}k(R - R_0)^2$ .  $R_0$  is the equilibrium separation. Since (see Sec. 6.4)  $dE_p = -Fdr$ , the force between the ions is  $F = -dE_p/dR = -k(R - R_0)$ , which is the linear approximation to the force between the two ions. The force is attractive if  $R > R_0$  and repulsive if  $R < R_0$ .

A mass subject to a linear restoring force is called a *harmonic oscillator* (Appendix F). A mass  $m$  subject to a linear restoring force  $-kx$  oscillates with an angular frequency  $\omega^2 = k/m$ . Classically, the energy of the oscillating mass depends on the amplitude of the motion and can have any value. Quantum-mechanically, it is

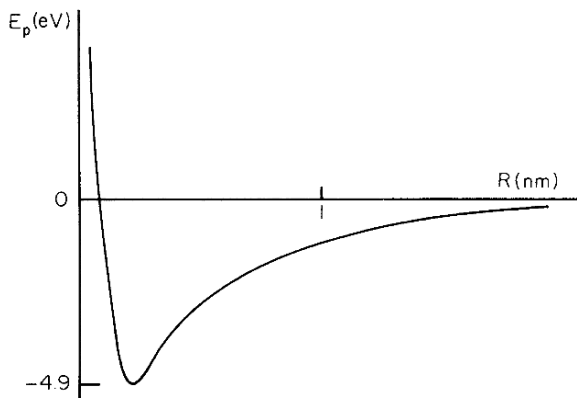


FIGURE 14.6. The potential energy of a sodium ion and a chloride ion as a function of their nuclear separation.

restricted to values

$$E_v = \hbar\omega \left( v + \frac{1}{2} \right), \quad v = 0, 1, 2, \dots \quad (14.12)$$

This is the total energy, including both kinetic and potential energy. The levels are spaced equally by an amount  $\hbar\omega$ . The spacing is usually greater than that for rotational levels, often in the infrared. The transitions that give rise to the emission or absorption of photons require a change in the rotational quantum numbers as well as the vibrational ones. The selection rules are

$$\Delta r = \pm 1, \quad \Delta v = \pm 1. \quad (14.13)$$

Some of these vibrational-rotational transitions are shown in Fig. 14.7.

Finally, there can be transitions involving  $v$ ,  $r$ , and the electronic quantum numbers as well. When the electronic quantum numbers change, the shape of the interatomic

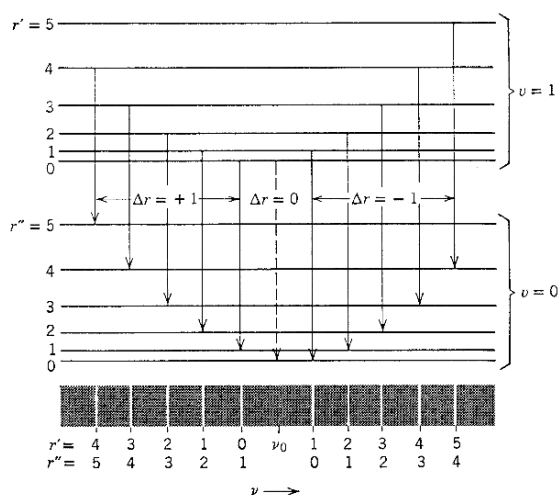


FIGURE 14.7. Transitions for vibrational-rotational spectra. From R. M. Eisberg and R. Resnick. *Quantum Physics of Atoms, Molecules, Solids, Nuclei and Particles*, 2nd ed. p. 428. Copyright ©1985 John Wiley & Sons. Reproduced by permission of John Wiley & Sons, Inc.

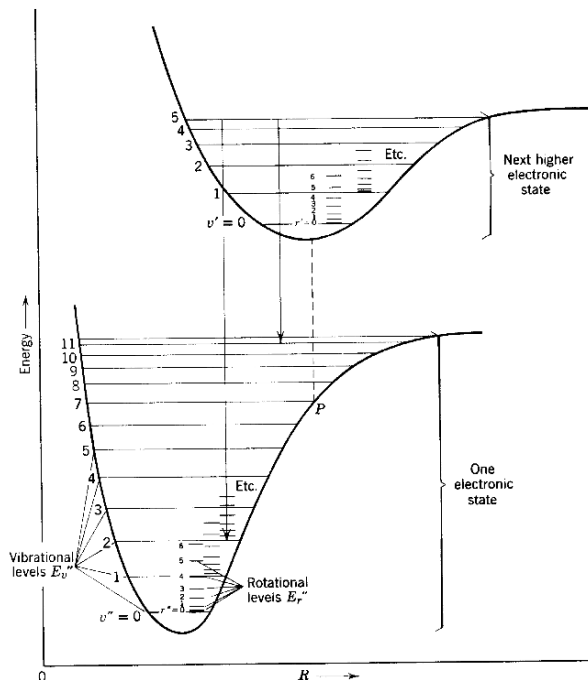


FIGURE 14.8. A combination of changes in electronic quantum numbers within an atom and of vibrational and rotational quantum numbers within the molecule. From R. Eisberg and R. Resnick. *Quantum Physics of Atoms, Molecules, Solids, Nuclei and Particles*, 2nd ed. p. 430. Copyright ©1985 John Wiley & Sons. Reproduced by permission of John Wiley & Sons, Inc.

potential changes, as shown in Fig. 14.8. The details of molecular spectra are fairly involved and are summarized in many texts. Transitions of biological importance are discussed in Grossweiner (1994, pp. 33–38). If the electron selection rules are satisfied, the transition is fairly rapid (typically  $10^{-8}$  s), a process called *fluorescence*. Sometimes the electron becomes trapped in a state where it cannot decay according to the electronic selection rules of Eq. 14.9. It may then have a lifetime up to several seconds before decaying, a phenomenon called *phosphorescence*.

### 14.4 Scattering and Absorption of Radiation; Cross Section

Photons in a vacuum travel in a straight line. When they travel through matter they are apparently<sup>3</sup> slowed down, leading to an index of refraction greater than unity; they may also be scattered or absorbed. Visible light does not

<sup>3</sup>Individual photons travel at speed  $c$ , yet the light wave travels at speed  $c/n$ . The slowing down of light in a medium is due to interference between the primary beam and scattered photons. This is discussed in Sherwood (1996), in Milonni (1996), and the references cited in these papers.

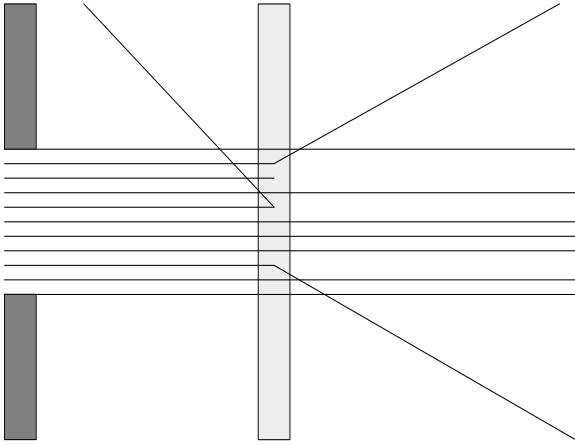


FIGURE 14.9. A collimated beam of photons passes from left to right through a thin slice of material. Some photons pass through, some are scattered, and some are absorbed.

pass through a building wall, but it does pass through a glass window. The absorption may depend on the frequency or wavelength of the light. The window can be made of colored glass. The light can also be scattered. This leads to the blue of the sky or to the white of clouds. If there is absorption as well as scattering, the clouds may appear gray instead of white. How light is scattered or absorbed in tissue has become very important in biophysics. Infrared light absorption can be used to measure chemical composition of the body. Light is also used for therapy and for laser surgery.

This section shows how to describe a single interaction of a photon with some substance. The photon can be scattered or absorbed. Section 14.5 develops one technique for calculating what happens when the photon undergoes many scattering events before being absorbed or emerging from the material.

Imagine that we have a distant source of photons that travel in straight lines, and that we collimate the beam (send it through an aperture) so that a nearly parallel beam of photons is available to us. Imagine also that we can see the tracks of the  $N$  photons in the beam, as in Fig. 14.9. When a thin sample of material of thickness  $dz$  is placed in the beam, a certain number of photons are scattered and a certain number are absorbed. If we repeat the experiment many times, we find that the number of photons scattered fluctuates about an average value that we call  $dN_s$  and the number absorbed fluctuates about an average value  $dN_a$ . When we vary the thickness of the absorber, we find that if it is sufficiently thin, the average number of photons scattered and absorbed is proportional to the thickness as well as the number of incident photons:

$$dN_s = \mu_s N dz, \quad dN_a = \mu_a N dz. \quad (14.14)$$

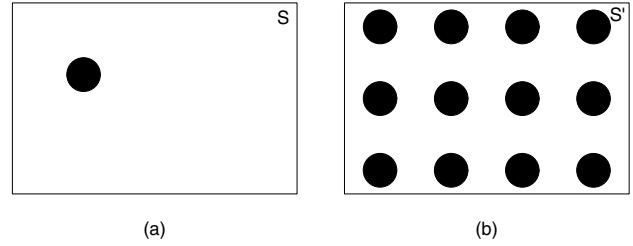


FIGURE 14.10. Each circle represents the cross section  $\sigma$  associated with a target entity such as an atom. (a) There is one atom in area  $S$ . (b) There are  $T$  target atoms per unit area in area  $S'$ .

The total number of unscattered photons  $N$  changes according to

$$dN = -(dN_s + dN_a) = -N(\mu_s + \mu_a)dz$$

with solution

$$N(z) = N_0 e^{-\mu z} = N_0 e^{-(\mu_s + \mu_a)z}. \quad (14.15)$$

The quantity  $\mu$  is the *total linear attenuation coefficient*. Quantities  $\mu_s$  and  $\mu_a$  are the linear scattering and absorption coefficients. Both depend on the material and the energy of the photons. This kind of exponential absorption is known as *Beer's law* or the *Beer-Lambert law*.

The interaction of photons with matter is statistical. The *cross section*  $\sigma$  is an effective area proportional to the probability that an interaction takes place. The interaction takes place with a “target entity.” It is sometimes convenient to define the target to be a single molecule, at other times an atom, and still other times one of the electrons within an atom. We can visualize the meaning of the cross section by considering either a single target entity interacting with a beam of photons or a single photon interacting with a thin foil of targets. Both are shown in Fig. 14.10. For the single target in Fig. 14.10(a), consider a beam of  $N$  photons passing through the area  $S$  with a uniform number per unit area  $N/S$ . Let the average number of interactions be  $\bar{n}$ . The cross section per target entity is defined by saying that the fraction of photons that interact is equal to the fraction of the area occupied by the cross section:

$$\frac{\bar{n}}{N} = \frac{\sigma}{S}. \quad (14.16)$$

We denote the number of photons per unit area by  $\Phi$  and write Eq. 14.16 as  $\bar{n} = \sigma\Phi$ . This is the average number of scatterings per target entity or the *probability of interaction per target entity when the beam has  $\Phi$  photons per unit area*:

$$p = \sigma\Phi. \quad (14.17)$$

Strictly speaking,  $\bar{n}$  is dimensionless,  $\sigma$  has the dimensions  $\text{m}^2$ , and  $\Phi$  has dimensions  $\text{m}^{-2}$ . However, it is often helpful to think of  $\bar{n}$  as being interactions per target entity and  $\sigma$  as being  $\text{m}^2$  per target entity.



Alternatively, imagine sending a beam of photons at the target of area  $S'$  shown in Fig. 14.10(b). There are  $N_T$  target entities per unit area in the path of the beam, each having an associated area  $\sigma$ . The fraction of the photons that interact is again the fraction of the area that is covered:

$$\frac{\bar{n}}{N} = \frac{\sigma S' N_T}{S'} = \sigma N_T. \tag{14.18}$$

This is the *probability that a single photon interacts when there are  $N_T$  target entities per unit area*. Note the symmetry with Eq. 14.17. In the first case there is one target entity and a certain number of photons per unit area. In the second case there is one photon and a certain number of target entities per unit area.

If a number of mutually exclusive interactions can take place (such as absorption and scattering), we can define a cross section for each kind of interaction. The probabilities and the cross sections add:

$$\sigma_{\text{tot}} = \sum_i \sigma_i. \tag{14.19}$$

The second interpretation we had above can be used to relate the cross section to the attenuation coefficient. The number of target entities per unit area is equal to the number per unit volume times the thickness of the target along the beam. To obtain the number of target atoms per unit volume, recall that 1 mol of atoms contains Avogadro's number  $N_A$  atoms. If  $A$  is the mass of a target containing 1 mol of atoms and the target has mass density  $\rho$ , then volume  $V$  has mass  $\rho V$  and contains  $\rho V/A$  mol and  $N_A \rho V/A$  atoms. Therefore, the number of atoms per unit volume is  $N_A \rho/A$ , and the number of atoms per unit area is

$$N_T = \frac{N_A \rho}{A} dz. \tag{14.20}$$

The linear coefficients are related to their corresponding cross sections by

$$\begin{aligned} \mu_s &= \frac{N_A \rho}{A} \sigma_s, \\ \mu_a &= \frac{N_A \rho}{A} \sigma_a, \\ \mu &= \frac{N_A \rho}{A} (\sigma_s + \sigma_a) = \frac{N_A \rho}{A} \sigma_{\text{tot}}. \end{aligned} \tag{14.21}$$

where  $\sigma_{\text{tot}}$  is the sum of all the interaction cross sections.

**Be careful with units!** Avogadro's number is defined to be  $6.022137 \times 10^{23}$  entities per mole, which is the number in a **gram** atomic weight. For carbon,  $A = 12.01 \times 10^{-3} \text{ kg mol}^{-1}$  and  $\rho = 2.0 \times 10^3 \text{ kg m}^{-3}$ . This is discussed further on p. 409.

We may wish to know the probability that particles (in this case photons) are scattered in a certain direction. We have to consider the probability that they are scattered into a small solid angle  $d\Omega$ . In this case  $\sigma$  is called the

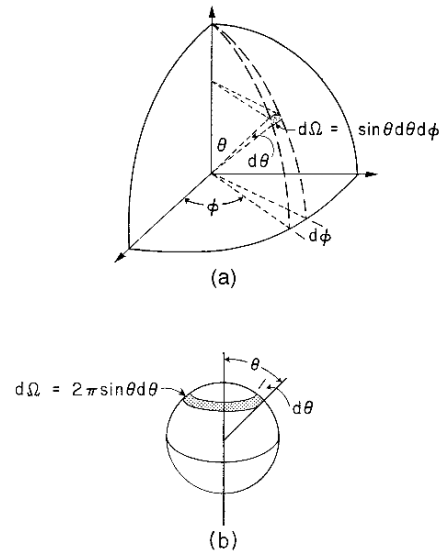


FIGURE 14.11. (a) A small solid angle  $d\Omega = \sin \theta d\theta d\phi$  surrounds the direction defined by angles  $\theta$  and  $\phi$ . (b) The solid angle  $d\Omega = 2\pi \sin \theta d\theta$  results from integrating over  $\phi$ .

*differential scattering cross section* and is often written as

$$\frac{d\sigma}{d\Omega} \quad \text{or} \quad \sigma(\theta) d\Omega. \tag{14.22}$$

The units of the differential scattering cross section are  $\text{m}^2 \text{sr}^{-1}$ . The differential cross section depends on  $\theta$ , the angle between the directions of travel of the incident and scattered particles. In a spherical coordinate system in which the incident particle moves along the  $z$  axis, the solid angle is  $d\Omega = \sin \theta d\theta d\phi$  (Appendix L). If the cross section has no  $\phi$  dependence, then the integration over  $\phi$  can be carried out and  $d\Omega = 2\pi \sin \theta d\theta$ . These solid angles are shown in Fig. 14.11.

There are three ways to interpret the exponential decay of the beam that has not undergone any interactions. First, the number of particles remaining in the beam that have undergone no interaction decreases as the target becomes thicker, so that the number of particles available to interact in the deeper layers is less. Second, the exponential can be regarded as taking into account the fact that in a thicker sample some of the target atoms are hidden behind others and are therefore less effective in causing new interactions. The third interpretation is in terms of the Poisson probability distribution (Appendix J). Each layer of thickness  $dz$  provides a separate chance for the beam particles to interact. The probability of interacting in any one layer  $dz$  is small,  $p = \sigma_{\text{tot}} N_A \rho dz/A$ , while the total number of “tries” is  $z/dz$ . The average number of interactions is  $m = p \times \text{number of tries}$ . The probability of no interaction is  $e^{-m} = \exp(-\sigma_{\text{tot}} N_A \rho z/A) = e^{-\mu z}$ .

When the cross section for scattering is large, things can become quite complicated. For example, photons may scatter many times and be traveling through the material in all directions. Various approximations have been used

to model photon transport in such a case. We will examine some of them shortly. One simple correction that is often made is to consider the average direction a scattered photon travels, for example, the average value of the cosine of the scattering angle,  $g = \cos \theta$ , where  $\theta$  is the angle of a single scattering. If the average angle of scattering is very small,  $g$  is nearly 1. If the photon is scattered backward,  $g = -1$ , and if the scattering is isotropic,  $g = 0$ . Formally,

$$g = \frac{\int_0^\pi \sigma(\theta) \cos \theta 2\pi \sin \theta d\theta}{\int_0^\pi \sigma(\theta) 2\pi \sin \theta d\theta}. \quad (14.23)$$

The *reduced scattering coefficient*

$$\mu'_s = (1 - g)\mu_s \quad (14.24)$$

is what is usually measured.

The values of the absorption and scattering coefficients vary widely. For infrared light at 780 nm, values are roughly<sup>4</sup>

$$\mu'_s = 1500 \text{ m}^{-1}, \quad \mu_a = 5 \text{ m}^{-1}.$$

## 14.5 The Diffusion Approximation to Photon Transport

### 14.5.1 General Theory

When photons enter a substance, they may scatter many times before being absorbed or emerging from the substance. This leads to *turbidity*, which we see, for example, in milk or clouds. The most accurate studies of multiple scattering are done with “Monte Carlo” computer simulations, in which probabilistic calculations are used to follow a large number of photons as they repeatedly interact in the tissue being simulated. However, Monte Carlo techniques use lots of computer time. Various approximate analytic solutions also exist. The field is reviewed in Chapter 5 of Grossweiner (1994). One of the approximations, the diffusion approximation, is described here. It is valid when many scattering events occur for each photon absorption. This is a valid approximation for most tissue, but not for cerebrospinal fluid or synovial (joint) fluid.

If the photons have undergone enough scattering in a medium, all memory of their original direction is lost. In that case the movement of the photons can be modeled by the diffusion equation. In Chapter 4 we wrote Fick’s second law as

$$\frac{\partial C}{\partial t} = D\nabla^2 C + Q.$$

<sup>4</sup>These are eyeballed from data for various tissues reported in the article by Yodh and Chance (1995). Values are up to ten times larger at other wavelengths. See Table 5.2 in Grossweiner (1994). Nickell *et al.* (2000) report values for skin that depend on both the direction of propagation and the degree of stretching of the skin. They are similar to the values reported here.

The left-hand side of the equation is the rate at which the concentration, the number of particles per unit volume, is increasing. The term  $D\nabla^2 C$  is the net diffusive flow into the small volume, the particle current being given by  $\mathbf{j} = -D\nabla C$ . The last term is the rate of production or loss of particles within the volume by other processes, depending on whether  $Q$  is positive or negative.

Let us suppose that we can apply this to photons. We will consider two contributions to  $Q$ . The concentration must be the number of *diffusing* photons per unit volume. Any in the incident beam are still traveling in the original direction and are not diffusing, but if they are scattered they become part of the diffusing photon pool. Therefore there may be a source term, which we will call  $s$ , due to the incident photons. But photons are also being absorbed. They are traveling with a speed  $c_n = c/n$ , where  $n$  is the index of refraction of the medium. In time  $dt$  they travel a distance  $dx = c_n dt$ , and the probability that they are absorbed is  $\mu_a dx = \mu_a c_n dt$ . Therefore, the diffusion equation for photons is

$$\frac{\partial C}{\partial t} = D\nabla^2 C + s - \mu_a c_n C. \quad (14.25)$$

Each term has the units of photons  $\text{m}^{-3} \text{s}^{-1}$ .

In photon transfer, it is customary to make two changes in this equation. The first is to divide all terms by the speed of the photons in the medium,<sup>5</sup>  $c_n$ . The result is

$$\frac{1}{c_n} \frac{\partial C}{\partial t} = D'\nabla^2 C - \mu_a C + \frac{s}{c_n},$$

where  $D' = D/c_n$  is referred to in the photon transfer literature as the *photon diffusion constant*. It has dimensions of length.

Two important quantities in radiation transfer are the *photon or particle fluence* and the *photon fluence rate*. The International Commission on Radiation Units and Measurements (ICRU) defines the particle fluence for any kind of particle, including photons as follows: At the point of interest construct a small sphere of radius  $a$ . Let the number of particles striking the surface of the sphere during some time interval have an *expectation value*  $N$ . (The expectation value is the mean of a set of measurements in the limit as the number of measurements becomes infinite.)

The particle fluence  $\Phi$  is the ratio  $N/\pi a^2$ , where  $\pi a^2$  is the area of a great circle of the sphere, that is, the area of a circle having the same radius as the sphere. This is shown in Fig. 14.12 and is a generalization of our earlier use of  $\Phi$  as the number of particles per unit area. It neatly avoids having to introduce obliquity factors, since for any direction the particles travel, one can construct a great circle on the sphere that is perpendicular to their path.

<sup>5</sup>Most papers in this field use  $c$  as the velocity of light in the medium. We prefer to reserve  $c$  for the fundamental constant, the velocity of light in vacuum.

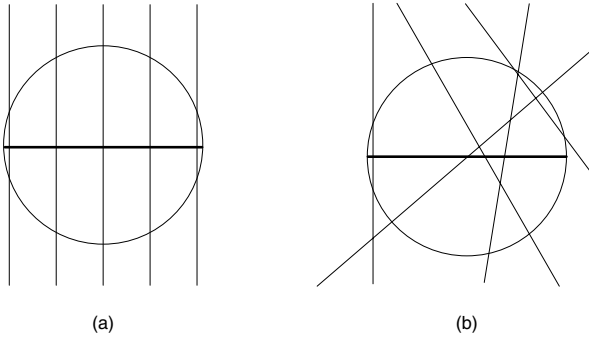


FIGURE 14.12. The particle fluence is the ratio of the expectation or average value of the number of particles passing through the sphere to the area of a great circle of the sphere,  $\pi a^2$ . It depends on the total number of particles passing through the sphere, regardless of the direction they travel. The fluence is the same in each case shown: five particles traverse each sphere.

The *particle fluence rate* is

$$\varphi = \frac{d\Phi}{dt}.$$

We saw in Chapter 4 that for a group of particles all traveling with the same speed, the number transported across a plane per unit area per unit time is equal to their concentration times their speed. The photon concentration is related to the photon fluence rate by  $C = \varphi/c_n$ , and the photon diffusion equation becomes

$$\frac{1}{c_n} \frac{\partial \varphi}{\partial t} = D' \nabla^2 \varphi - \mu_a \varphi + s. \quad (14.26)$$

This is the form that is usually found in the literature. The units of each term are photons  $\text{m}^{-3} \text{s}^{-1}$ . One can show that<sup>6</sup>

$$D' = \frac{1}{3[\mu_a + (1-g)\mu_s]} = \frac{1}{3(\mu_a + \mu'_s)}. \quad (14.27)$$

### 14.5.2 Continuous Measurements

If the tissue is continuously irradiated with photons at a constant rate, the term containing the time derivative vanishes. If in addition we use a broad beam of photons so that we have a one-dimensional problem and we are far enough into the tissue so that the source term can be ignored, the model is

$$D' \frac{d^2 \varphi}{dx^2} = \mu_a \varphi. \quad (14.28)$$

This has an exponential solution  $\varphi = \varphi_0 e^{-\mu_{\text{eff}} x}$ , where  $\mu_{\text{eff}} = \{3\mu_a [\mu_a + (1-g)\mu_s]\}^{1/2}$ . It is interesting to see

<sup>6</sup>See, for example, Duderstadt and Hamilton (1976, pp. 133–136).

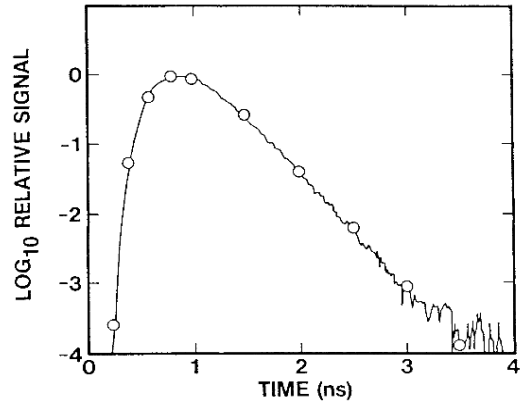


FIGURE 14.13. Time-resolved infrared spectroscopy. The line is a measurement of the reflected photons from the calf of a human volunteer at a distance of 4 cm from the pulsed source. The wavelength is 760 nm. The circles are calculated using Eq. 14.29 and normalized to the peak value. From M. S. Patterson, B. Chance, and B. C. Wilson (1989). Time resolved reflectance and transmittance for the noninvasive measurement of tissue optical properties. *Appl. Opt.* **28**(12): 2331–2336. Copyright by the Optical Society of America.

what these numbers mean. Using the “typical” values from Sec. 14.4, the number of photons that have not interacted (are not yet attenuated) falls exponentially with a characteristic length or mean depth

$$\lambda_{\text{unatten}} = \frac{1}{\mu} = \frac{1}{\mu_a + \mu'_s} = \frac{1}{1,505} = 0.66 \text{ mm}.$$

For the diffuse beam the mean depth is about 10 times this:

$$\lambda_{\text{diffuse}} = \frac{1}{\mu_{\text{eff}}} = \frac{1}{\sqrt{(3)(5)(1,505)}} = 6.7 \text{ mm}.$$

These values are for a wavelength where the tissue is fairly transparent. The diffusion equation can be solved for other geometries that model the light source being used.<sup>7</sup> One problem with these measurements is that they give only  $\mu_{\text{eff}}$ , which is a combination of  $\mu_a$  and  $\mu_s$ . Also, the path length may be ambiguous because the geometry cannot be modeled accurately.

### 14.5.3 Pulsed Measurements

A technique made possible by ultrashort light pulses from a laser is *time-dependent diffusion*. It allows determination of both  $\mu_s$  and  $\mu_a$ . A very short (150-ps) pulse of light strikes a small region on the surface of the tissue. A detector placed on the surface about 4 cm away records the multiply-scattered photons. A typical plot of the detected photon fluence rate is shown in Fig. 14.13.

<sup>7</sup>See, for example, Grossweiner (1994, p. 98).

Patterson *et al.* (1989) have shown that the reflected fluence rate after a pulse is approximately

$$R(r, t) = \frac{z_0}{(4D'c_n t)^{3/2}} e^{-\mu_a c_n t} e^{-(r^2+z_0^2)/4D'c_n t}. \quad (14.29)$$

Here  $r$  is the distance of the detector from the source along the surface of the skin,  $c_n t$  is the total distance the photon has traveled before detection, and  $z_0 = 1/[(1-g)\mu_s]$  is the depth at which all the incident photons are assumed to scatter and become part of the diffuse photon pool. This curve fits Fig. 14.13 well and can be used to determine  $\mu_a$  and  $(1-g)\mu_s$ . We can understand the various factors in Eq. 14.29. The last factor is a Gaussian spreading in the  $r$  direction away from the  $z$  axis where the photons were injected. This is a two-dimensional problem. Compare this with Eq. 4.77, which shows that in two dimensions  $\sigma_r^2 = 4Dt$ , and recall that  $D = D'c_n$ . The middle factor is the fraction of the photons in the pulse that have not been absorbed,  $\exp(-\mu_a x)$ , where  $x$  is the total distance the photons have traveled. The first factor is the normalization that reduces the amplitude of the Gaussian as it spreads.

A related technique is to apply a continuous laser beam, the amplitude for which is modulated at various frequencies between 50 and 800 MHz. The Fourier transform of Eq. 14.29 gives the change in amplitude and phase of the detected signal. Their variation with frequency can also be used to determine  $\mu_a$  and  $\mu_s$ .<sup>8</sup>

#### 14.5.4 Refinements to the Model

The diffusion equation, Eq. 14.26, is an approximation, and the solution given, Eq. 14.29, requires some unrealistic assumptions about the boundary conditions at the surface of the medium ( $z = 0$ ). Hielscher *et al.* (1995) compared experiment, Monte Carlo calculations, and solutions to the diffusion equation with three different boundary conditions. They found that Eq. 14.29 was the easiest to use but leads to errors in the estimates of the coefficients that become worse when the detector and source are close together. Their Monte Carlo calculations fit the data quite well. They also discuss the reflections that occur when light goes from one medium into another with a different index of refraction.

## 14.6 Biological Applications of Infrared Scattering

### 14.6.1 Near Infrared (NIR)

Near infrared light in the range 600–1000 nm is used to measure the oxygenation of the blood as a function of

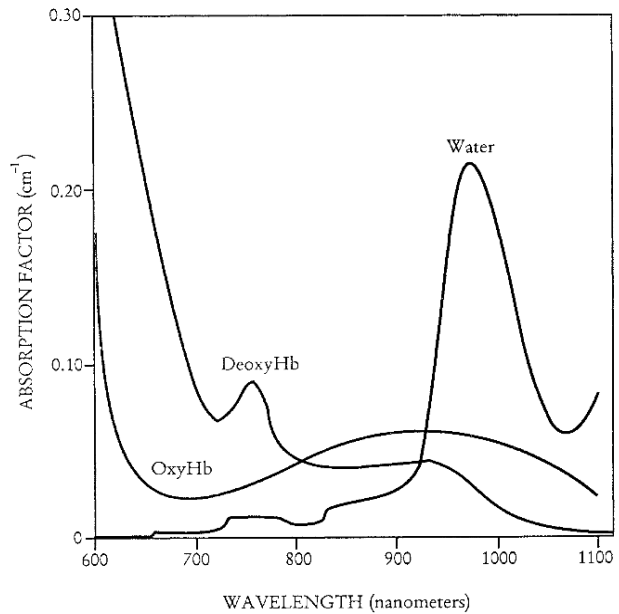


FIGURE 14.14. The absorption coefficient  $\mu_a$  for water, oxyhemoglobin, and deoxyhemoglobin. Reprinted with permission from A. Yodh and B. Chance. Spectroscopy and imaging with diffusing light. *Phys. Today*, March 1995: 34–40 Copyright ©1995, American Institute of Physics.

time by determining the absorption at two different wavelengths. Figure 14.14 shows the absorption coefficients for oxygenated and deoxygenated hemoglobin and water. The greater absorption of blue light in oxygenated hemoglobin makes oxygenated blood red. (The graph only shows wavelengths longer than 600 nm—red and infrared.) The wavelength 800 nm at which both forms of hemoglobin have the same absorption is called the *isosbestic point*. Measurements of oxygenation are made by comparing the absorption at two wavelengths on either side of this point.

One of the difficulties with these measurements is knowing the path length, since photons undergo many scatterings before being absorbed or reaching the detector. Scattering from many tissues besides hemoglobin distorts the signal. Nonetheless, *pulse oximeters* that fit over a finger are widely used. Webster (1997) provides a comprehensive discussion of the underlying physics, design, calibration and use of pulse oximeters. The basic feature is that arterial blood flow is pulsatile, not continuous. Therefore, measuring the time-varying (AC) signal selectively monitors arterial blood and eliminates the contribution from venous blood and tissue. Scattering corrections must still be made [Farmer (1997), Wieben (1997)].

Development of new applications for infrared scattering measurements continue as new detectors with different spectral sensitivities become available [Yamashita *et al.* (2001)]. Continuous sources are also used to determine blood oxygenation of tissue [Liu *et al.* (1995)].

<sup>8</sup>See, for example, Sevicik *et al.* (1991) or Pogue and Patterson (1994).

### 14.6.2 Optical Coherence Tomography (OCT)

Optical range measurements using the time delay of reflected or backscattered light from pulses of a few femtosecond ( $10^{-15}$  s) duration can be used to produce images similar to those of ultrasound A- and B-mode scans. The spatial extent of a 30 fs pulse in water is about  $7\ \mu\text{m}$ . Since it is difficult to measure time intervals that short, most measurements are done using interference properties of the light. *Optical coherence tomography* is conceptually similar to range measurements but uses interference measurements. It was first demonstrated by Huang *et al.* (1991) and has been developed extensively since then [see Schmitt (1999) or Bouma and Tearney (2002)].

This is one topic for which we must use the electromagnetic wave model for light, since it depends on interference effects. Light waves differ from sound waves because the electric field in the wave is a vector perpendicular to the direction of propagation of the wave. This gives rise to an important effect—polarization—that we ignore.

Suppose that a wave  $A \sin \frac{2\pi}{\lambda}(x - c_n t) = A \sin \omega(x/c_n - t)$  travels in a medium with index of refraction  $n$ . A detector responds to the energy fluence in the wave, which is proportional to the square of the amplitude averaged over time. The signal is  $y \propto A^2 \sin^2 \omega(x/c_n - t) = A^2/2$ . The wave is split, travels two paths of different lengths, and is recombined at a detector. The signal is proportional to the power averaged over many cycles of the wave. The power is proportional to the square of the electric field:

$$y \propto (A/2)^2 [\sin \omega(x_1/c_n - t) + \sin \omega(x_2/c_n - t)]^2 = \frac{A^2}{4} \left( 1 + \cos \frac{\omega}{c_n} (x_2 - x_1) \right). \quad (14.30)$$

The signal oscillates between 0 and  $A^2/2$  as the difference in path length is changed. When the path difference is zero,  $y \propto A^2/2$ , our original result. This dependence of the signal on path length forms the basis for *interferometry*, which can be used to measure changes in distance with high accuracy—counting maxima (fringes) as one path length is varied.

An important consideration is the *coherence* of the light beam: the number of cycles over which the phase of the wave does not change. When an atom emits light, the classical electromagnetic wave lasts for a finite time,  $\tau_{\text{coh}}$  (often around  $10^{-8}$  s). When another atom emits light, the phase is unrelated to the phase of light already emitted. This means that if  $(x_2 - x_1)/c_n > \tau_{\text{coh}}$ , the time average will go to zero.

Note that as long as light from a single source has been split and then recombined, the paths can be quite long. The interference fringes will be seen when the light is recombined and the path difference satisfies

$$x_2 - x_1 < c_n \tau_{\text{coh}}. \quad (14.31)$$

This provides a technique for determining the distance of a reflecting object from the light source, forming the basis

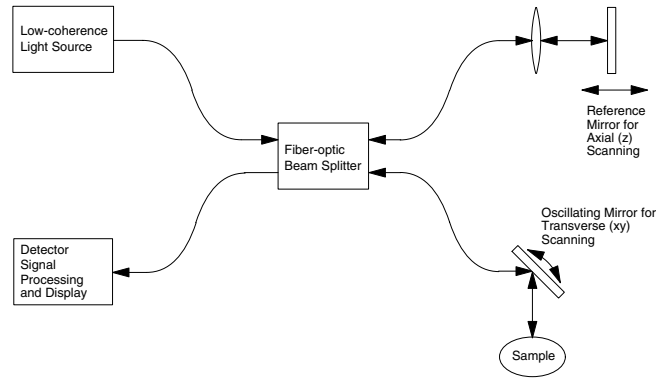


FIGURE 14.15. The basic apparatus for optical coherence tomography. The features are described in the text.

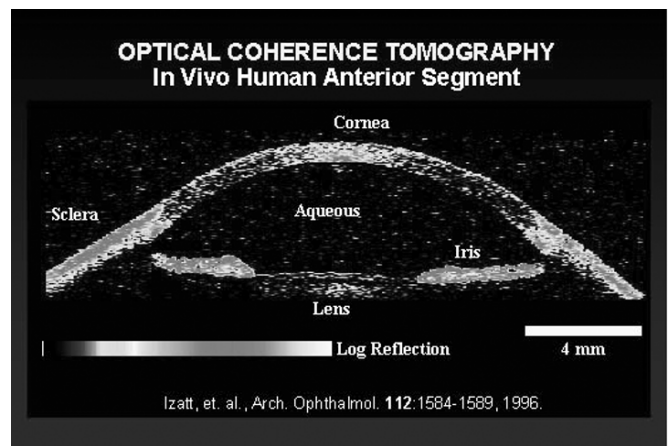


FIGURE 14.16. An optical coherence tomogram of the anterior eye. From J. A. Izatt, M. R. Hee, E. A. Swanson, C. P. Lin, D. Huang, J. S. Schuman, C. A. Puliafito, and J. G. Fujimoto. Micrometer-scale resolution imaging of the anterior eye with optical coherence tomography. *Archives of Ophthalmology* **112**: 1584–1589 (1994). Copyright ©1994 American Medical Association. All rights reserved.

for optical coherence tomography. A light source with a *short* coherence time is used for high resolution. The basic apparatus is shown in Fig. 14.15. Various light sources are used [Bouma and Tearney (2002)]. The light pulse travels over an optical fiber to a 50/50 beam splitter. Part travels to the sample, where it is reflected back to the 50/50 coupler and then to the detector. The other half of the light goes to the reference mirror, where it is also reflected back to the detector. Changing the position of the reference mirror changes the depth of the image plane in the sample. The lateral beam position is changed to scan the sample, as in an ultrasound B-mode scan. Figure 14.16 shows an image of the anterior eye.

It is possible to make many kinds of images. Fig. 14.17 shows the parabolic velocity profile of blood flowing in a blood vessel in the retina of  $176\ \mu\text{m}$  diameter. It was obtained by measuring the Doppler shift in light scattered from moving blood cells. It is also possible to image

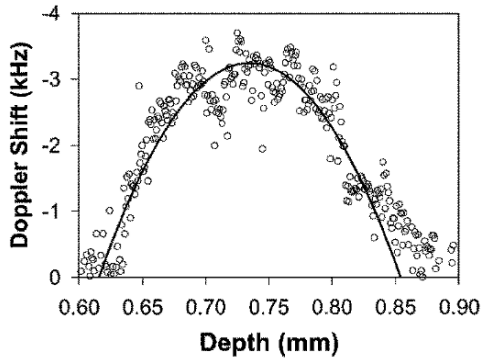


FIGURE 14.17. The parabolic velocity profile of blood flowing in a single retinal vessel of diameter  $176\ \mu\text{m}$ . From S. Yazdanfar, A.M. Rollins, and J. A. Izatt. Imaging and velocimetry of the human retinal circulation with color Doppler optical coherence tomography. *Optics Letters* **25**(19): 1448–1450 (2000). Used by permission.

glucose concentration, because glucose modifies the index of refraction and thereby the scattering coefficient [Esenaliev *et al.* (2001)]. Images are made of the surface layers of the skin, the eye, the walls of the mouth, teeth, larynx, esophagus, stomach, and intestine.

A number of tissues exhibit *birefringence*—the speed of light in the skin depends on the orientation of the electric field vector of the light wave with the cells in the tissue [De Boer *et al.* (2002)]. It is possible to make images with different orientations of the electric field vector to improve the resolution [Yasuno *et al.* (2002)].

There are a number of offshoots to OCT, such as optical coherence microscopy and full-field OCM [Saint-Jalmes *et al.* (2002)].

### 14.6.3 Raman Spectroscopy

Infrared and microwave probes are used extensively in the laboratory. Since the vibrational and rotational levels depend on the masses, separations, and forces between the various atoms bound in a molecule, it is not surprising that spectroscopy can be used to identify specific bonds. This is a useful technique in chemistry. Biological applications are difficult because the absorption coefficients are large; thin samples must be used, particularly in an aqueous environment.

One way around this is *Raman scattering*. Raman scattering is the scattering of light in which the scattered photon does not have its original energy, but has lost or gained energy corresponding to a rotational or vibrational transition. The effect was discovered by C. V. Raman in 1928. Raman scattering can be done with light of any wavelength, from infrared to ultraviolet. An idealized example is shown in Fig. 14.18. If the scattering molecule was originally in the vibrational ground state and returns to a vibrational excited state, the Raman-scattered photon has less energy than the original photon. This is called

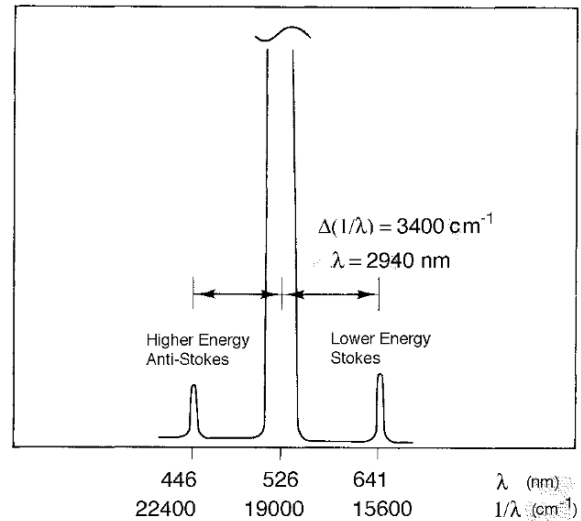


FIGURE 14.18. In Raman scattering, a photon gains or loses energy due to a change in the energy of the scattering molecule. An idealized example for water is shown. The very intense line has no energy change; the weak lines are Raman scattering. The abscissa is shown as wavelength  $\lambda$  and as reduced wave number  $k/2\pi = 1/\lambda$ . The Raman shift corresponds to  $\Delta(1/\lambda) = 3,400\ \text{cm}^{-1}$ . The wavelength of this infrared transition is  $\lambda = 2,940\ \text{nm}$ , but the measurement is made near  $500\ \text{nm}$ .

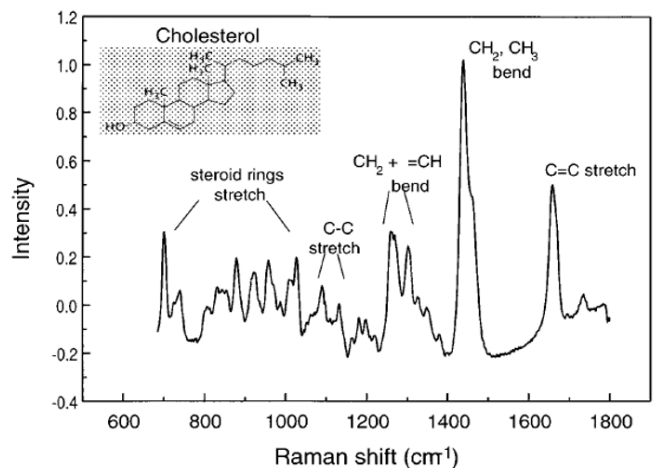


FIGURE 14.19. Vibrational Raman lines for cholesterol. A continuous background has been subtracted. The abscissa is  $1/\lambda = E/hc$ . From Hanlon, E. B., R. Manoharan, T-W. Koo, K. E. Shafer, J. T. Motz, M. Fitzmaurice, J. R. Kramer, I. Itzkan, R. R. Dasari, and M. S. Feld (2000). Prospects for *in vivo* Raman spectroscopy. *Phys. Med. Biol.* **45**: R1–R59. Used by permission.

*Stokes–Raman scattering*. If the scattering molecule was originally in a higher vibrational state and returns to the vibrational ground state, the Raman-scattered photon has higher energy than the original. The intensity of

this *Anti-Stokes–Raman* line will be less than the intensity of the Stokes–Raman line because populations of the original vibrational levels are governed by a Boltzmann factor. Fig. 14.19 shows the Stokes–Raman shift spectrum for cholesterol. Many discussions of Raman spectroscopy are available. A fairly theoretical one by Berne and Pecora (1976) relies heavily on autocorrelation functions and spectral analysis that we saw in Chapter 11. Diem (1993) is a detailed text on vibrational spectroscopy, including Raman spectroscopy.

Raman spectroscopy has been used extensively for laboratory studies; many groups are exploring its utility for *in vivo* measurements [Hanlon *et al.* (2000)]. Infrared light between 800 and 1000 nm is usually used.

#### 14.6.4 Far Infrared or Terahertz Radiation

For many years, there were no good sources or sensitive detectors for radiation between microwaves and the near infrared (0.1–100 THz; 1 THz =  $10^{12}$  Hz). Developments in optoelectronics have solved both problems, and many investigators are exploring possible medical uses of THz radiation (“T rays”). Classical electromagnetic wave theory is needed to describe the interactions, and polarization (the orientation of the  $\mathbf{E}$  vector of the propagating wave) is often important. The high attenuation of water in this frequency range means that studies are restricted to the skin or surface of organs such as the esophagus that can be examined endoscopically. Reviews are provided by Smye *et al.* (2001), Fitzgerald *et al.* (2002), and Zhang (2002).

## 14.7 Thermal Radiation

Any atomic gas emits light if it is heated to a few thousand kelvin. The light consists of a line spectrum. The famous yellow line of sodium has

$$\lambda = 589.2 \text{ nm},$$

$$\nu = c/\lambda = 5.092 \times 10^{14} \text{ Hz},$$

$$E = h\nu = hc/\lambda = 3.38 \times 10^{-19} \text{ J} = 2.11 \text{ eV}.$$

These photons are emitted when sodium atoms lose 2.11 eV and return to their ground state. If the sodium atoms are excited by thermal collisions, the probability that a sodium atom is in the excited state, relative to the probability that it is in the ground state, is given by the Boltzmann factor

$$\frac{P_{\text{excited}}}{P_{\text{ground}}} = e^{-E/k_B T}.$$

At room temperature  $k_B T = 4.14 \times 10^{-21}$  J, so  $e^{-E/k_B T} = e^{-81.5} = 3.8 \times 10^{-36}$ . The number of atoms in the excited state is utterly negligible. If the temperature is raised to 1500 K,  $e^{-E/k_B T}$  is  $8 \times 10^{-8}$ , and enough

TABLE 14.3. Approximate color temperatures. The range of values reflects differences between scales established by different observers.

Color	$T$ (K)
Red, just visible in daylight	750–800
“Cherry” red	975–1175
Yellow	1200–1505
White	1425–1800
Dazzling (bluish) white	1900

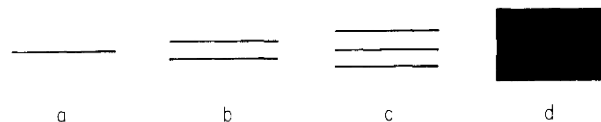


FIGURE 14.20. The splitting of energy levels as many atoms are brought together. (a) A single atom. (b) Two atoms. (c) Three atoms. (d) Many atoms.

atoms are excited to give off light as they fall back to the ground state.

If a piece of iron is heated to 1,500 K, it glows with a white–yellow color. Table 14.3 relates apparent color to temperature for a glowing metal. If the light is analyzed with a spectroscope, it is found to consist of a continuous range of colors rather than discrete lines.

The difference between the spectra of single atoms and the spectra of solids and liquids can be understood from the following argument. If we have  $N$  isolated identical atoms, each atom has an energy level at the energy shown in Fig. 14.20(a). There are a total of  $N$  levels, one for each atom. When two of these atoms are brought close together, the levels shift slightly and split into two closely spaced levels because of interaction between the atoms. The two levels for a pair of atoms are shown in Fig. 14.20(b). If three atoms are brought close together the level splits into three levels as shown in Fig. 14.20(c). If a large number of atoms are brought close together, the  $N$  level spreads out into a *band*, Fig. 14.20(d). Transitions from one band to another can have many different energies, and photons with a continuous range of energies can be emitted or absorbed.

The relative number of photons of different energies that will be emitted or absorbed depends on the nature of the substance. Glass and sodium chloride crystals are nearly transparent in the visible spectrum because the spacing of the levels is such that no photons of these energies are absorbed. When such substances are heated enough to populate the higher energy levels, no photons of these energies are emitted.

A substance that has so many closely spaced levels that it can absorb every photon that strikes it appears black. It is called a *blackbody*. It is difficult if not impossible to

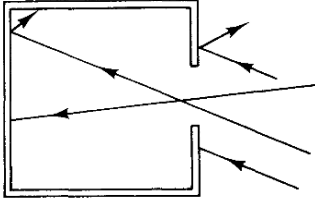


FIGURE 14.21. A small hole in the wall of a cavity is a better blackbody than the walls of the cavity are. Any light that enters the hole must be reflected several times before emerging. It can be absorbed by the wall at any reflection. If the walls appear black, the hole appears even blacker. (The walls are highly absorbing diffuse reflectors.)

make a surface that is completely absorbing; the absorption can be improved by making a cavity, as in Fig. 14.21. Photons entering the hole in the cavity bounce from the walls many times before chancing to pass out through the hole again, and they therefore have a greater chance of being absorbed. Such a hole in a cavity is a better approximation to a blackbody than is the absorbing material lining the cavity.

If the surface is not completely absorbing, we define the *emissivity*  $\epsilon(\lambda)$ , which is the fraction of light absorbed at wavelength  $\lambda$ . (Why emission and absorption are closely related is discussed below.) If the light all passes through some transparent material or is completely reflected, then  $\epsilon = 0$ ; if it is all absorbed,  $\epsilon = 1$ . A blackbody has  $\epsilon(\lambda) = 1$  for all wavelengths. An object for which  $\epsilon(\lambda)$  is constant but less than 1 is called a gray body.

When a blackbody is heated, the light given off has a continuous spectrum because the energy levels are so closely spaced. By imagining two different cavities in contact, one can argue<sup>9</sup> that the amount of energy coming out of a blackbody cavity depends only on the temperature of the walls and not on the nature of the surfaces.

The spectrum of power per unit area emitted by a completely black surface in the wavelength interval between  $\lambda$  and  $\lambda + d\lambda$  is

$$W_\lambda(\lambda, T)d\lambda,$$

a universal function called the *blackbody radiation function*. It has units of  $\text{W m}^{-3}$ , although it is often expressed as  $\text{W cm}^{-2} \mu\text{m}^{-1}$ . The value of  $W_\lambda$  is plotted for several different temperatures in Fig. 14.22. As the black surface or cavity walls become hotter, the spectrum shifts toward shorter wavelengths, which is consistent with the observations in Table 14.3. The visible region of the spectrum is marked on the abscissa in Fig. 14.22; even at 1,600 K when the radiating surface appears white, most of the energy is radiated in the infrared.

Figure 14.23 plots  $W_\lambda(\lambda, T)$  for two temperatures near body temperature ( $37^\circ\text{C} = 310\text{ K}$ ). Compare the scales

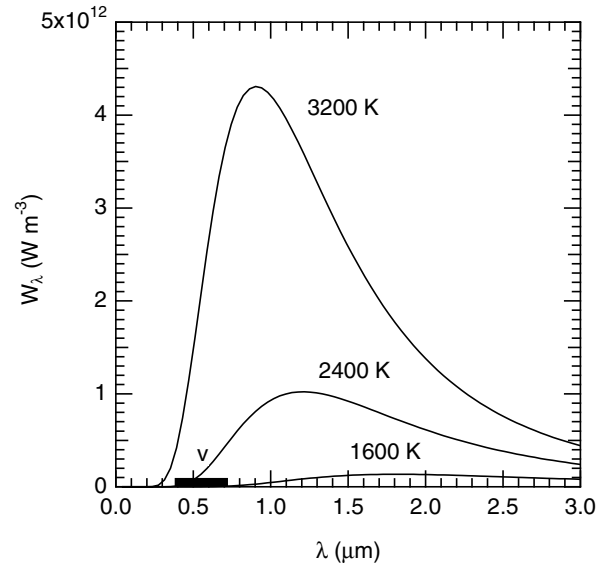


FIGURE 14.22. The blackbody radiation function for several temperatures. The visible spectrum is marked by  $v$ .

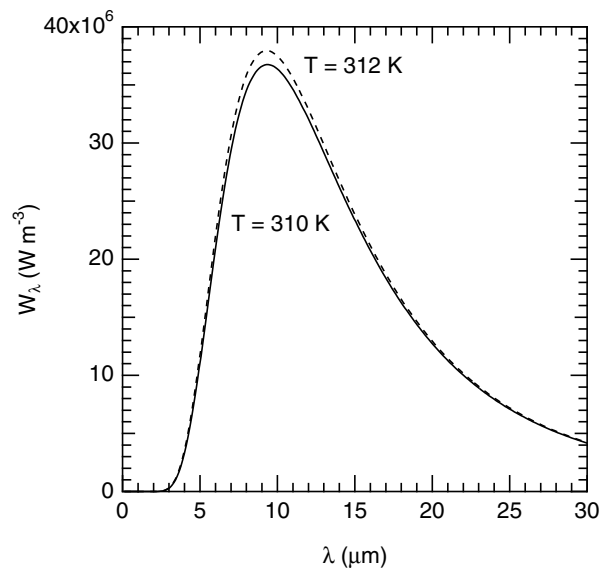


FIGURE 14.23. The blackbody radiation function  $W_\lambda(\lambda, T)$  for  $T = 310\text{ K}$  and  $T = 312\text{ K}$ .

of Figs. 14.22 and 14.23, and note how much more energy is emitted by a blackbody at the higher temperature and how it is shifted to shorter wavelengths.

Much work was done on the properties of blackbody or thermal or cavity radiation in the late 1800s and early 1900s. While some properties could be explained by classical physics, others could not. The description of the function  $W_\lambda(\lambda, T)$  by Planck is one of the foundations of quantum mechanics. We will not discuss the history of these developments, but will simply summarize the properties of the blackbody radiation function that are important to us.

<sup>9</sup>For a brief discussion see Halliday *et al.* (1992, p. 1021ff). A more detailed treatment is found in Bramson (1968, Chapter IV).



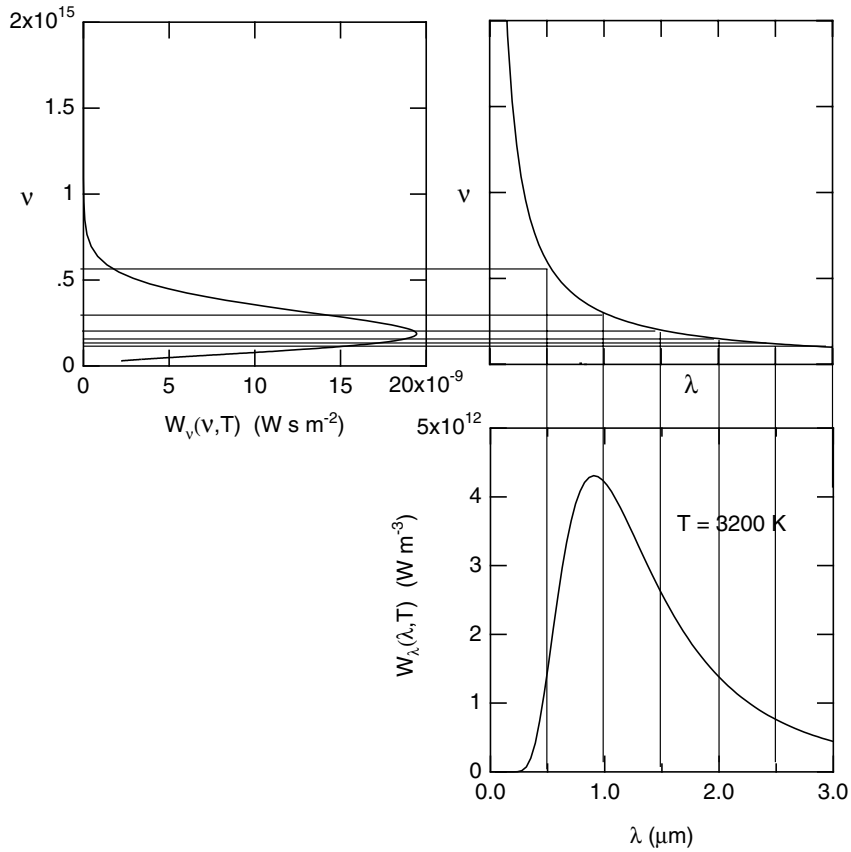


FIGURE 14.24. The transformation from  $W_\lambda(\lambda, T)$  to  $W_\nu(\nu, T)$  is such that the same amount of power per unit area is emitted in wavelength interval  $(\lambda, d\lambda)$  and the corresponding frequency interval  $(\nu, d\nu)$ . The spectrum shown is for a blackbody at 5,800 K, approximately the spectrum of sunlight.

The value of  $W_\lambda(\lambda, T)$  is given by

$$W_\lambda(\lambda, T) = \frac{2\pi c^2 h}{\lambda^5 (e^{hc/\lambda k_B T} - 1)}. \tag{14.32}$$

Consider the expression  $e^{hc/\lambda k_B T}$  in the denominator. Since light consists of photons of energy  $E = h\nu = hc/\lambda$ , the factor in parentheses in the denominator is  $e^{E/k_B T} - 1$ . For very large energies (short wavelengths) the 1 can be neglected and the effect of the denominator on Eq. 14.32 is like a Boltzmann factor.

We can find the total amount of power emitted per unit surface area by integrating<sup>10</sup> Eq. 14.32:

$$\begin{aligned} W_{\text{tot}}(T) &= \int_0^\infty W_\lambda(\lambda, T) d\lambda \\ &= \frac{2\pi^5 k_B^4}{15c^2 h^3} T^4 = \sigma_{SB} T^4. \end{aligned} \tag{14.33}$$

This is the *Stefan-Boltzmann law*. The Stefan-Boltzmann constant, which is traditionally denoted by  $\sigma_{SB}$  but which has no relationship to cross section, was

known empirically before Planck’s work. It has the numerical value

$$\sigma_{SB} = 5.67 \times 10^{-8} \text{ W m}^{-2} \text{ K}^{-4}. \tag{14.34}$$

Early measurements of the radiation function were done with equipment that made measurements vs. wavelength. It is also possible to measure vs. frequency. To rewrite the radiation function in terms of frequency, let  $\lambda_1$  and  $\lambda_2 = \lambda_1 + d\lambda$  be two slightly different wavelengths, with power  $W_\lambda(\lambda, T)d\lambda$  emitted per unit surface area at wavelengths between  $\lambda_1$  and  $\lambda_2$ . The same power must be emitted<sup>11</sup> between frequencies  $\nu_1 = c/\lambda_1$  and  $\nu_2 = c/\lambda_2$ :

$$W_\nu(\nu, T)d\nu = W_\lambda(\lambda, T)d\lambda. \tag{14.35}$$

Since  $\nu = c/\lambda$ ,  $d\nu/d\lambda = -c/\lambda^2$ , and

$$|d\nu| = +\frac{c}{\lambda^2} |d\lambda|. \tag{14.36}$$

<sup>11</sup> $W_\lambda(\lambda, T)$  and  $W_\nu(\nu, T)$  do not have the same functional form. In fact, they have different units. The units of  $W_\lambda(\lambda, T)$  are  $\text{W m}^{-3}$ , while those of  $W_\nu(\nu, T)$  are  $\text{W s m}^{-2}$ .

<sup>10</sup>This is not a simple integration. See Gasiorowicz (1974, p. 6).

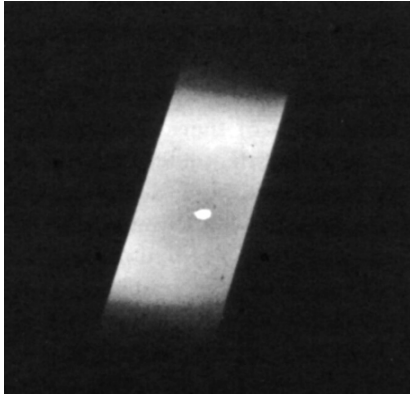


FIGURE 14.25. A photograph of an incandescent tungsten tube with a small hole drilled in it. The radiation emerging from the hole is brighter than that from the tungsten surface. From D. Halliday, R. Resnick, and K. S. Krane (1992). *Fundamentals of Physics*, 4th ed. extended edition. Vol. 2, p. 1022. Copyright ©1992 John Wiley & Sons. Reproduced by permission of John Wiley & Sons.

Equations 14.32–14.36 can be combined to give

$$W_\nu(\nu, T) = \frac{2\pi\nu^2(h\nu)}{c^2(e^{h\nu/k_B T} - 1)}. \quad (14.37)$$

This transformation is shown in Fig. 14.24. The amount of power per unit area radiated in the  $0.5 \mu\text{m}$  interval between two of the vertical lines in the graph on the lower right is the area under the curve of  $W_\lambda$  between these lines. The graph on the upper right transforms to the corresponding frequency interval. The radiated power, which is the area under the  $W_\nu$  curve between the corresponding frequency lines on the upper left, is the same. We will see this same transformation again when we deal with x rays. Note that the peaks of the two curves are at different frequencies or wavelengths.

We see in the figures above that at higher temperatures the peak occurs at shorter wavelengths. Eq. 14.32 can be differentiated to show that at temperature  $T$  the peak in  $W_\lambda$  occurs at wavelength

$$\lambda_{\text{max}}T = \frac{hc}{4.9651k_B} = 2.90 \times 10^{-3} \text{ m K}. \quad (14.38)$$

Similarly, we can differentiate Eq. 14.37 to show that

$$\frac{\nu_{\text{max}}}{T} = \frac{2.82144k_B}{h} = 5.88 \times 10^{10} \text{ K}^{-1} \text{ s}^{-1}.$$

The product  $\lambda_{\text{max}}\nu_{\text{max}} = 1.705 \times 10^8 \text{ m s}^{-1} = 0.57c$ .

All this is true for a blackbody. Thermodynamic arguments can be made to show that if a body does not completely absorb light at some wavelength, that is,  $\epsilon(\lambda) < 1$ , then the power emitted at that wavelength is

$$\epsilon(\lambda)W_\lambda(\lambda, T). \quad (14.39)$$

This is the same  $\epsilon(\lambda)$  that was introduced earlier in this section. It is called the *emissivity* of the surface. This

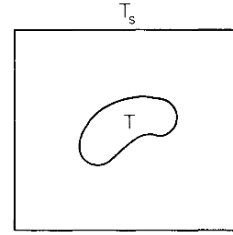


FIGURE 14.26. A blackbody at temperature  $T$  within a container with wall temperature  $T_s$ .

implies that a surface that appears blackest when it is absorbing radiation will be brightest when it is heated. Figure 14.25 shows a small hole in a piece of tungsten that has been heated. The hole forms the opening to a cavity and is therefore more absorbing than is the tungsten surface. When heated, the hole emits more light than the tungsten surface.

## 14.8 Infrared Radiation from the Body

The body radiates energy in the infrared, and this is a significant source of energy loss. Infrared radiation has been used for over 40 years to image the body, but the value of the technique is still a matter of debate. We saw earlier how the *scattering* of infrared radiation by the body can be used to learn information about tissue beneath the surface.

Measurements of the emissivity of human skin have shown that for  $1 \mu\text{m} < \lambda \leq 14 \mu\text{m}$ ,  $\epsilon(\lambda) = 0.98 \pm 0.01$ . This value was found for white, black, and burned skin [Steketee (1973)]. In the infrared region in which the human body radiates, the skin is very nearly a blackbody. Let us apply Eq. 14.33 to see what the blackbody radiation from the human body is. The total surface area of a typical adult male is about  $1.73 \text{ m}^2$ . The surface temperature is about  $33^\circ\text{C} = 306 \text{ K}$  (this is less than the core temperature of  $310 \text{ K}$ ). Therefore the total power radiated is  $w_{\text{tot}} = SW_{\text{tot}} = S\sigma_{SB}T^4 = 860 \text{ W}$ . This is a large number, nearly 9 times the basal metabolic rate of  $100 \text{ W}$ . The reason it is so large is that it assumes the surroundings are at absolute zero, or that the subject is radiating in empty space with no surroundings. When there are nearby surfaces, radiation from them is received by the subject, and the net radiation is considerably less than  $860 \text{ W}$ .

The easiest arrangement for which to calculate the net heat loss is a blackbody at temperature  $T$  surrounded by a similar surface at temperature  $T_s$  (Fig. 14.26). At equilibrium the temperature of both objects is the same,  $T = T_s$ . The power emitted by the body is equal to the power absorbed. Increasing  $T$  increases the power emitted according to  $W_{\text{tot}} = \sigma_{SB}T^4$ . The body then emits more power than it absorbs. Equilibrium is restored when the body has cooled or the surroundings have warmed so that

the temperatures are again the same. Thermodynamic arguments can be made to show that the net power radiated by the body is

$$w_{\text{tot}} = S\sigma_{SB}(T^4 - T_s^4). \quad (14.40)$$

If the object is not a blackbody or the wall temperature is not uniform, the net power loss is more complicated. However, this model represents a considerable improvement over our previous calculation. Suppose that the surroundings are at a temperature  $T_s = 293$  K ( $20^\circ\text{C}$ ). The net loss is

$$w_{\text{tot}} = (1.73)(5.67 \times 10^{-8})(306^4 - 293^4) = 137 \text{ W}.$$

This says that a nude subject surrounded by walls at  $20^\circ\text{C}$  would have to exercise to maintain body temperature, even if the air temperature were warm enough so that heat conduction and convection losses were zero.

If you have lived in a cold climate, you have probably felt cold in a room at night when the drapes are open, even though a thermometer records air temperatures that should be comfortable. This is because of radiation from you to the cold window. The glass is transparent only in the visible range; for infrared radiation it is opaque and has a high emissivity. The radiation of the cold window back to you is much less than your radiation to it, and you feel cold.

This same problem can occur with a premature infant in an incubator. If the incubator is placed near a window, one wall of the incubator can be cooled by radiation to the window. The infant can be cooled by radiation to the wall of the incubator, even though a shiny (low-emissivity) thermometer in the incubator records a reasonable air temperature. One solution is to be careful where an incubator is placed and insulate its walls; another is to redesign incubators with a feedback loop controlling the infant's temperature.

Infrared radiation can be used to image the body. Two types of infrared imaging are used. In infrared photography the subject is illuminated by an external source with wavelengths from 700 to 900 nm. The difference in absorption between oxygenated and nonoxygenated hemoglobin allows one to view veins lying within 2 or 3 mm of the skin. Either infrared film or a solid-state camera can detect the reflected radiation.

Thermal imaging detects thermal radiation from the skin surface. Significant emission from human skin occurs in the range 4–30  $\mu\text{m}$ , with a peak at 9  $\mu\text{m}$  (Fig. 14.23). The detectors typically respond to wavelengths below 6–12  $\mu\text{m}$ . Thermography began about 1957 with a report that skin temperature over a breast cancer was slightly elevated. There was great hope that thermography would provide an inexpensive way to screen for breast cancer, but there have been too many technical problems. Normal breasts have more variability in vascular patterns than was first realized, so that differences of temperature at corresponding points in each breast are not an

accurate diagnostic criterion. The thermal environment in which the examination is done is extremely important. The sensitivity (ability to detect breast cancer) is too low to use it as a screening device. Thermography has also been proposed to detect and to diagnose various circulatory problems. Thermography is generally not widely accepted [Cotton (1992); Blume (1993)], though it still has its proponents.

Infrared radiation from the tympanic membrane (eardrum) and ear canal is used to measure body temperature. One instrument is based on pyroelectric sensors, which were developed for use in motion detectors [Fraden (1991)]. The sensors have a permanent electric dipole moment whose magnitude changes with temperature.

### 14.8.1 Atherosclerotic Coronary Heart Disease

*Atherosclerotic coronary heart disease* (ACHD) has been or is being studied with every imaging technique described in this book. All of the techniques are invasive: a *catheter* is inserted into the artery in question. We arbitrarily mention them all here. In ACHD a fatty *plaque* forms in the *lumen* (interior passage way) of the artery.

The standard technique is coronary artery *angiography*: the heart is imaged by x-ray fluoroscopy (see Chapter 16) while a dye opaque to x rays is introduced in the vessel. This allows accurate determination of the degree of *stenosis* (blocking) of the vessel. It has been thought that when the artery is nearly blocked, the restricted blood flow leads to a *myocardial infarct* (heart attack). It has recently been realized that smaller plaques may become disrupted and lead to a myocardial infarct. Current research seeks to learn what makes these particular plaques *vulnerable*. There is an extensive literature, reviewed by MacNeill *et al.* (2003) and Verheye *et al.* (2002).

In *intravascular ultrasound* (IVUS), a 20–40 MHz transducer at the end of the catheter can detect calcium (which deposits in areas of tissue injury). IVUS *elastography* measures how the arterial wall changes during the pressure variations of the cardiac cycle, in the hope that changes in elasticity will indicate vulnerable plaques.

Optical coherence tomography can provide high-resolution (20  $\mu\text{m}$ ) structural details.

Coronary *angiography* attempts to directly view the arterial wall using a tiny fiber-optic endoscope. A serious problem here is blood getting between the tip of the endoscope and the arterial wall. This has been solved by temporarily *occluding* (blocking) the artery “upstream” with a balloon catheter or by flushing the area with saline solution.

Thermography has also been explored, first with a temperature-sensitive thermistor, and also with an infrared imaging mirror. Areas of inflammation have a somewhat higher temperature than surrounding areas.

Both Raman spectroscopy and near infrared spectroscopy have been used.

In intravascular magnetic resonance imaging (Magnetic resonance imaging is described in Chapter 18) the detector coil is made small enough to fit at the tip of the catheter.

All of these techniques are still experimental.

## 14.9 Blue and Ultraviolet Radiation

### 14.9.1 Treatment of Neonatal Jaundice

The energy of individual photons of blue and ultraviolet light is high enough to trigger chemical reactions in the body. These can be both harmful and beneficial. A beneficial effect is the use of blue light to treat neonatal jaundice. The most common harmful effect is the development of sunburn, skin cancer, and premature aging of the skin.

Neonatal jaundice occurs when *bilirubin* builds up in the blood. Bilirubin is a toxic waste product of the decomposition of the hemoglobin that is released when red blood cells die. It is insoluble in water and cannot be excreted through either the kidney or the gut. It is excreted only after being conjugated with glucuronic acid in the liver. Bilirubin monoglucuronate and bilirubin diglucuronate are both water soluble. They are excreted in the bile and leave via the gut. Some newborns have immature livers that cannot carry out the conjugation. In other cases there is an increased rate of red blood cell death (*hemolysis*) and the liver cannot keep up. The serum bilirubin level can become quite high, leading to a series of neurological symptoms known as *kernicterus*. The abnormal yellow color of the skin called *jaundice* is due to bilirubin in the capillaries under the skin.

It was discovered accidentally that when the skin of a newborn with jaundice was exposed to bright light, the jaundice color went away. Photons of blue light have sufficient energy to convert the bilirubin molecule into more soluble and apparently less harmful forms [McDonagh (1985)]. Photons of longer wavelength have less energy and are completely ineffective. The standard form of phototherapy used to be to place the baby "under the lights." Since the lights were bright and also emitted some ultraviolet, it was necessary to place patches over the baby's eyes. Also, since the baby's skin had to be exposed to the lights, it had to be placed in an incubator to keep it warm. A fiberoptic blanket has been developed that can be wrapped around the baby's torso under clothing or other blankets. The optical fibers conduct the light from the source directly to the skin. Eye patches are not needed, and the baby can be fed and handled. Typical energy fluence rates are  $(4-6) \times 10^{-2} \text{ W m}^{-2} \text{ nm}^{-1}$  in the range 425–475 nm. Acceptance by nursing staff and parents is very high [Murphy and Oellrich (1990)]. The blanket can even be used for home treatment, though this

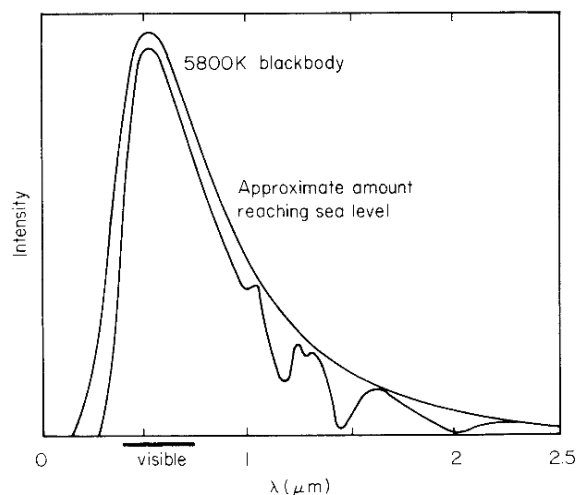


FIGURE 14.27. The solar spectrum and the approximate spectrum reaching the earth after atmospheric attenuation.

is still controversial. Volume 24, Issue 4 of *Health Devices* (August, 1995) is devoted to an assessment of fiberoptic phototherapy systems.

### 14.9.2 The Ultraviolet Spectrum

Ultraviolet light can come from the sun or from lamps. The maximum intensity of solar radiation is in the green, at about 500 nm. The sun emits approximately like a thermal radiator at a temperature of 5,800 K. Figure 14.27 shows a 5,800-K thermal radiation curve. The power per unit area from the sun at all wavelengths striking the earth's outer atmosphere, the *solar constant*, calculated by regarding the sun as a thermal radiator, is  $1,390 \text{ W m}^{-2}$  ( $2 \text{ cal cm}^{-2} \text{ min}^{-1}$ ).

Satellite measurements give  $1,372 \text{ W m}^{-2}$  [Madronich (1993)]. Because of reflection, scattering, atmospheric absorption, and so forth, the amount actually striking the earth's surface is about  $1,000 \text{ W m}^{-2}$ . Figure 14.27 also shows the effect of absorption of sunlight in the atmosphere. The sharp cutoff at 320 nm is due to atmospheric ozone ( $\text{O}_3$ ), which absorbs strongly from 200 to 320 nm. It absorbs more weakly at wavelengths as long as 360 nm. Molecular oxygen absorbs strongly below 180 nm.

The ultraviolet spectrum is qualitatively divided into the following regions:

UVA	315–400 nm
UVB	280–315 nm <sup>12</sup>
UVC or middle UV	200–280 nm
Vacuum UV	<240 nm
Far UV	120–200 nm
Extreme UV	10–120 nm

Only the first three are of biological significance, because the others are strongly absorbed in the atmosphere.

<sup>12</sup>In Europe the range of UVB radiation is 290–300 nm.

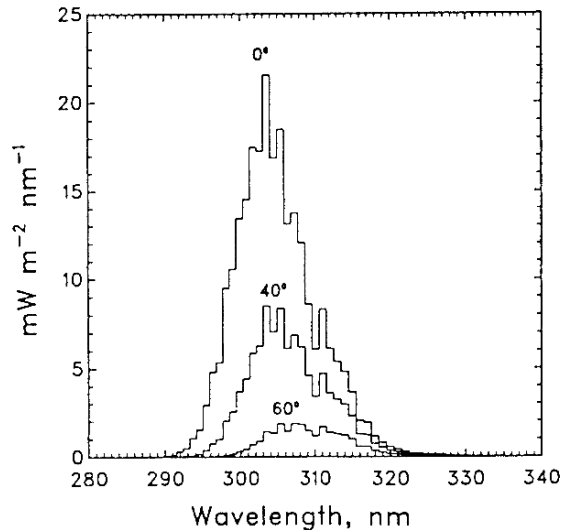


FIGURE 14.28. Spectral dose rates weighted for ability to damage DNA for three different angles of the sun from overhead. The calculation assumes clear skies and an ozone layer of 300 Dobson units ( $1 \text{ DU} = 2.69 \times 10^{20} \text{ molecule m}^{-2}$ ). From S. Madronich. The atmosphere and UV-B radiation at ground level. In A. R. Young *et al.*, eds. New York, Plenum, pp. 1–39 (1993). With kind permission of Springer Science and Business Media.

Madronich (1993) gives a detailed discussion of the various factors that reduce the ultraviolet energy reaching the earth's surface. The sensitivity of DNA decreases as the wavelength increases. Figure 14.28 shows the solar radiation reaching the ground when the sun is at different angles from the zenith (directly overhead), weighted for DNA sensitivity. Biological effects of ultraviolet light are reviewed by Diffey (1991). Computer programs are available that calculate the total dose during a day at different latitudes and altitudes.<sup>13</sup>

### 14.9.3 Response of the Skin to Ultraviolet Light

There are several responses of the skin to ultraviolet light. In order to understand them one must know something about the anatomy and physiology of skin. The outer layer of the skin, the *epidermis*, consists of three sublayers (Fig. 14.29). A single layer of *basal cells* is on the inside. Most of these cells produce keratin, a protein that gives the outer layers of skin its strength. About 10% of the cells are *melanocytes* that produce the pigment *melanin*. Next comes a sublayer of about seven cells, called the *prickle layer*. On top of this is a two- or three-cell layer called the *stratum granulosum* or granular layer. The surface is a layer of dead cells, primarily *keratin* but also cel-

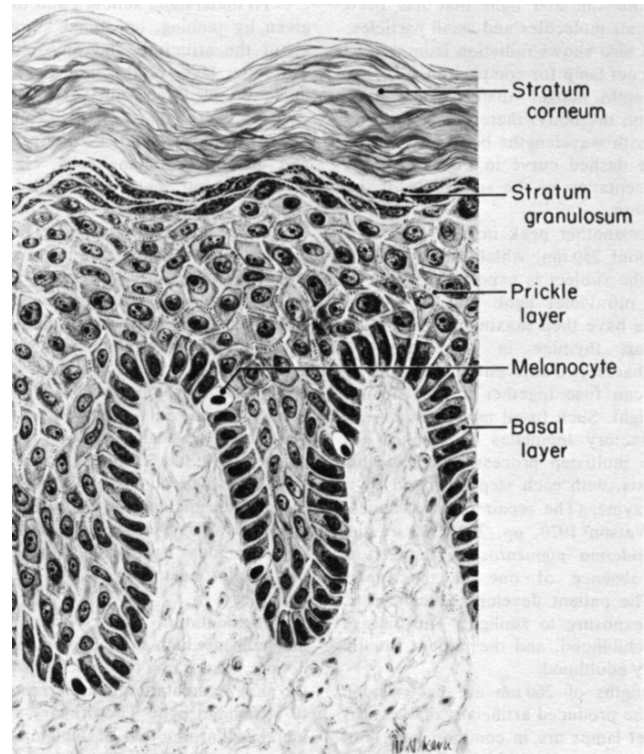


FIGURE 14.29. The epidermis. The basal layer contains the cells from which the other layers are derived. As the cells move toward the surface they become the prickle layer and the stratum granulosum (granular layer). The stratum corneum is dead cellular debris. The melanocytes, which produce melanin granules, are in the basal layer. Reprinted from D. M. Pillsbury and C. L. Heaton. *A Manual of Dermatology*. 2nd. ed. Philadelphia, Saunders, 1980, p. 5, with permission from Elsevier.

lular debris, called the *stratum corneum* or horny layer. Basal cells are constantly produced in the basal layer, migrate outward, become the stratum corneum, and are sloughed off.

In order to discuss injury to tissue, both here by ultraviolet light and in later chapters by x rays, we need to introduce some specialized terms. The body's immediate (*acute*) response to an injury, whether it is an infection, a bump, a cut or a burn, is the *inflammatory response* described on p. 116. Prolonged (*chronic*) irritation may result in abnormal cell growth. The abnormalities of cell growth that result in organs or tissues that are larger than normal are *hypertrophy*, an enlargement of existing cells, and *hyperplasia*, an enlargement due to the formation of new cells. The aberrations in cell growth patterns are shown in Table 14.4. They are *metaplasia*, *dysplasia*, and *anaplasia*. Metaplasia is reversible and goes away if the stimulus or irritant is removed. Dysplasia is sometimes reversible and sometimes progresses to become cancerous. Anaplastic changes are present in nearly all forms of cancer. Anaplasia may result from dysplasia, or it may arise directly from normal cells.

<sup>13</sup>A computer program for evaluating solar UV exposure has been provided, with a listing, by Schaefer (1993). See also Diffey and Cameron (1984).

TABLE 14.4. Abnormal changes in tissue

Metaplasia	A reversible change in which one cell type is replaced by another.	
Dysplasia	Variation in size, shape, and organization of the cells. Literally, “deranged development.”	
Anaplasia	A marked, irreversible, and regressive change from adult cells that are differentiated in form to more primitive, less differentiated cells.	
Differences between benign and malignant tumors		
Characteristic	Benign	Malignant
Histologic differentiation (microscopic appearance)	Often typical of the tissue of origin.	Not well differentiated; atypical cells.
Mode of growth	Expands inside a capsule.	Expansive; also infiltrative, with no capsule.
Rate of growth	Progressive; usually slow; few cells undergoing mitosis (division) at any one time.	May be rapid, with many cells undergoing mitosis.
Metastasis (distant spread)	Absent.	Frequently present.

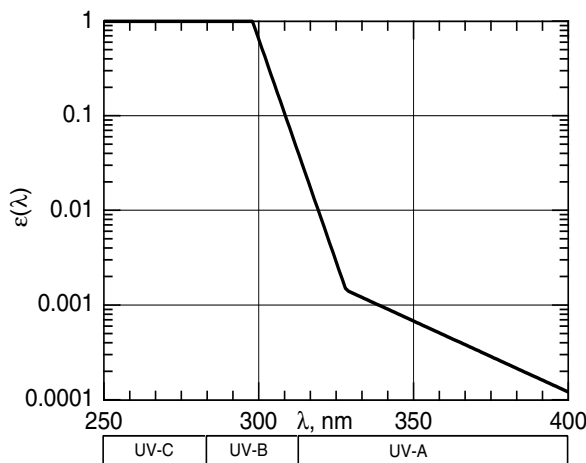


FIGURE 14.30. The erythema action spectrum  $\epsilon(\lambda)$  for ultraviolet light, as adopted by the CIE in 1987.

The acute effect of ultraviolet radiation is reddening of the skin or *erythema* due to increased blood flow in the *dermis*, the layer beneath the epidermis. This is part of the inflammatory reaction. The amount of energy that just produces detectable erythema is called the *minimum erythemal dose*. It is difficult to measure in an objective manner. New instrumentation allows quantitative measurements [Diffey and Farr (1991)]. The 1987 *reference*

*action spectrum* adopted by the CIE<sup>14</sup> shows the relative sensitivity of the skin versus wavelength for the production of erythema. It is

$$\epsilon(\lambda) = \begin{cases} 1.0, & 250 \leq \lambda \leq 298 \text{ nm} \\ 10^{0.094(298-\lambda)}, & 298 \leq \lambda \leq 328 \text{ nm} \\ 10^{0.015(139-\lambda)}, & 328 \leq \lambda \leq 400 \text{ nm} \end{cases} \quad (14.41)$$

This is plotted in Fig. 14.30. The minimum erythemal dose at 254 nm is about  $6 \times 10^7 \text{ J m}^{-2}$  [Diffey and Farr (1991, Table 2)]. There is considerable scatter from one experiment to another. When the degree of erythema is plotted vs energy per unit area, the slope of the curve depends on the wavelength. Early effects on skin include sunburn, tanning (now thought to be an injury response), and thickening. Daily exposure for 2 to 7 weeks causes a three- to fivefold thickening of the stratum corneum.

Some patients have an abnormally high sensitivity to ultraviolet exposure. They may exhibit abnormal photosensitivity because of various diseases or from taking drugs such as phenothiazines (one of the classes of major tranquilizers), sulfa drugs, dimethylchlortetracycline, the antidiabetic sulfonureas, and thiazide diuretics and even from drinking quinine water. Photocontact dermatitis is

<sup>14</sup> *Commission Internationale de l'Eclairage* or International Commission on Illumination.

caused by interaction of photons with substances placed on the skin, such as perfumes containing furocoumarins, lime peel, fungi, and fluorescein dye used in lipsticks.

Moseley (1994) reviews the safety issues involving ultraviolet light and lasers.

#### 14.9.4 Ultraviolet Light Causes Skin Cancer

Chronic exposure to ultraviolet radiation causes premature aging of the skin. The skin becomes leathery and wrinkled and loses elasticity. The characteristics of photo-aged skin are quite different from skin with normal aging [Kligman (1989)]. UVA radiation was once thought to be harmless. We now understand that UVA radiation contributes substantially to premature skin aging because it penetrates into the dermis. There has been at least one report of skin cancer associated with purely UVA radiation from a cosmetic tanning bed [Lever and Lawrence (1995)]. This can be understood in the context of studies showing that both UVA and UVB suppress the body's immune system, and that this immunosuppression plays a major role in cancer caused by ultraviolet light [Kripke (2003); Moyal and Fourtanier (2002)].

There are three types of skin cancer. *Basal-cell carcinoma* (BCC) is most common, followed by *squamous-cell carcinoma* (SCC). These are together called *non-melanoma or nonmelanocytic skin cancer* (NMSC). Basal-cell carcinomas can be quite invasive (Fig. 16.44) but rarely metastasize or spread to distant organs. Squamous-cell carcinomas are more prone to metastasis. *Melanomas* are much more aggressive and frequently metastasize.

Armstrong and Kricger (1995) review the epidemiology of skin cancer. This summary is based on their paper. There are geographic differences in *incidence*, the number of newly diagnosed cases per 100,000 population per year. Estimates of incidence for the three types of skin cancer for whites in the United States are given in Table 14.5. Melanoma incidence rates for whites in the United States are approximately 10 times higher than those for blacks living in the same geographic area, and 2–6 times higher than those for Hispanics living in the same area. An increase in melanoma incidence in professional or indoor occupations has been observed, probably related to an increase in recreational sun exposure. Also, the incidence is higher for people born in countries with lots of sunlight than for people who migrate to those countries, suggesting that the number of years of exposure or the age at exposure is important.

The incidence of melanoma increases with age until about age 50 and slows somewhat in older people. The incidence of NMSC increases steadily with age. The incidence of melanoma from the early 1960s to the late 1980s has increased at a rate of about 5% per year in populations of European origin, while increasing much less or not at all in other populations. Most of this increase has

been on the trunk, particularly in men. Similar increases in NMSC have been seen in the United States, primarily for BCC on the trunk. (It is much more difficult to obtain accurate figures for NMSC than for melanoma, because NMSC data are not typically kept since it has a much lower mortality.) The epidemiological data suggest an association between skin cancer and exposure to sunlight. There are also laboratory studies of the damage to cells caused by ultraviolet light. Armstrong and Kricger conclude that “the evidence leaves little room for doubt that sun exposure causes both melanoma and NMSC.” A pattern of infrequent, intense exposure to ultraviolet light is more likely to lead to melanoma than relatively continuous exposure; a plausible explanation has been proposed [Gilchrist *et al.* (1999)].

#### 14.9.5 Protection from Ultraviolet Light

Protection from the sun certainly reduces erythema and probably reduces skin cancer. Protection is most important in childhood years, both because children receive 3 times the annual sun exposure of adults and because the skin of children is more susceptible to cancer-causing changes. The simple sun protection factor (SPF) alone is not an adequate measure of effectiveness, because it is based on erythema, which is caused mainly by UVB. Some sunscreens do not adequately protect against UVA radiation. Buka (2004) reviews both sunscreens and insect repellents for children. He finds several products that adequately block both UVA and UVB. They are based on zinc oxide, titanium oxide, or avobenzone (Parsol 1789). An adequate amount must be used: for children he recommends 1 fluid ounce (30 ml) *per application*.

One study of the immunosuppressive protection factor (IPF) was done by exposing to UV light through various sunscreens the skin of volunteers who have a skin allergy to nickel. After exposure their skin is then coated with a nickel compound. If the irradiated skin showed less allergic response, the UV had caused immunosuppression [Poon *et al.* (2003)]. They showed that the IPF did not correlate strongly with the traditional SPF, but correlated strongly with the UVA protective factor. (The UVA-PF is determined by the degree of tanning.) While it is plausible that immunosuppression means that the body can less effectively reject tumors that begin to grow, direct evidence must wait for additional experiments [Kripke (2003)].

Because of the high reflectivity of sand and snow, beach umbrellas provide at most a factor of 2 protection. Hats need to have a brim that is at least 7.5 cm wide [Diffey and Cheeseman (1992)].

Automobile window glass provides protection against UVB; however, untinted glass transmits enough UVA to present a significant exposure over several hours of driving [Kimlin and Parisi (1999)].

TABLE 14.5. Estimates of skin cancer incidence rates per 100,000.<sup>a</sup>

Cancer type	Population	Males	Females
Melanoma	White, New Orleans, 1983–87	6.9	5.3
	White, Hawaii, 1983–1987	22.2	14.9
SCC	White, U.S., 1994 (rough est.)	100	45
BCC	White, U.S., 1994 (rough est.)	400	200

<sup>a</sup>Simplifications made by the authors from data in Armstrong and Kricger (1995).

### 14.9.6 Ultraviolet Light Damages the Eye

The effect of ultraviolet light on the eye has been reviewed by Bergmanson and Söderberg (1995). Acute effects include *keratitis* (inflammation of the cornea, the transparent portion of the eyeball) and *conjunctivitis* (inflammation of the conjunctiva, the mucous membrane covering the eye), also known as snow blindness or welder's flash. Laboratory studies show that ultraviolet-light exposure causes thickening of the cornea and disrupts corneal metabolism. UVC radiation is absorbed by the cornea. The crystalline lens absorbs UVB and, in older persons, UVA and visible light. Only a little UVA light reaches the retina. The retina is also susceptible to trauma from blue light. Low doses cause photochemical changes in tissues, while high doses also cause thermal damage.

Chronic low exposure to ultraviolet light causes permanent damage to the cornea, known as *droplet keratopathy* or *spheroid degeneration*. UVA radiation is a significant factor in the development of a *pterygium*, a hyperplasia of the conjunctiva that may grow over the cornea and impair sight. Rarely, it causes blindness.

Properly designed spectacles and contact lenses can protect the eye against ultraviolet light [Giasson *et al.* (2005)]. However, both must be designed to absorb ultraviolet. Soft contacts are larger and provide more protection than rigid gas-permeable contacts. Protection from high ultraviolet light-intensity requires sunglasses or welding goggles. Wide-brimmed hats also help protect the eye from ultraviolet light.

### 14.9.7 Ultraviolet Light Synthesizes Vitamin D

Ultraviolet light has one beneficial effect: it allows the body to synthesize vitamin D. Brief exposures are sufficient. Many foods are fortified with vitamin D, which has caused occasional overdoses [Haddad (1992)].

### 14.9.8 Ultraviolet Light Therapy

Ultraviolet light is used in therapy, primarily for the treatment of a skin disease called *psoriasis*. Psoriasis is an inflammatory disorder in which the basal cells move out to the stratum corneum in much less than the normal 28 days. The skin is red and has thick scaling. UVB radiation, often in conjunction with coal tar applied to

the skin, has been used as a treatment for psoriasis since the 1920s. In the 1960s a treatment was developed that uses UVA and a chemical either applied to the skin or administered systemically (photochemotherapy or PUVA—psoralen UVA). The chemical is a psoralen derivative. It affects DNA, and when the affected DNA is irradiated with ultraviolet light, cross-links form, preventing replication. There are well-defined guidelines for the use of PUVA [Studniberg and Weller (1993)]. Details of PUVA therapy are found in Grossweiner (1994, pp. 162–167). The treatment works, but it has also been found to increase the risk of NMSC [Nijsten and Stern (2003); Paul (2003)].

PUVA therapy is also useful in cutaneous T-cell lymphoma, a disease that first becomes apparent on the skin and then moves to internal organs. Another treatment, *extracorporeal photopheresis*, involves removing the patient's blood, extracting the red blood cells, irradiating the plasma and white blood cells with UVA light outside the body, and returning the red blood cells and the irradiated white blood cells and plasma to the patient [Grossweiner (1994, pp. 167f); Knobler *et al.* (2002)].

Recently it has been shown that children who are rejecting a transplant in spite of conventional immunosuppressive therapy can benefit from extracorporeal phototherapy [Messina *et al.* (2003)].

## 14.10 Heating Tissue with Light

Sometimes tissue is irradiated in order to heat it; in other cases tissue heating is an undesired side effect of irradiation. In either case, we need to understand how the temperature changes result from the irradiation. Examples of intentional heating are *hyperthermia* (heating of tissue as part of cancer therapy) or *laser surgery* (tissue ablation<sup>15</sup>). Tissue is ablated when sufficient energy is deposited to vaporize the tissue. Heating may be a side effect of phototherapy.

The temperature changes are often modeled by a heat-flow equation containing a source term for the deposition of photon energy and a term representing flow of energy away from the site in warmed blood. This is one form of

<sup>15</sup>In surgery, *ablation* means the excision or amputation of tissue.



the *bioheat equation*, which can include additional terms in more complicated models.

The linear equation for heat conduction was mentioned as one form of the transport equation in Table 4.3:

$$j_H = -K \frac{dT}{dx},$$

with the units of the thermal conductivity  $K$  being  $\text{J K}^{-1} \text{m}^{-1} \text{s}^{-1}$ . When extended to three dimensions and combined with the equation of continuity (conservation of energy), this gives a heat-conduction equation with the same form as Fick's second law for diffusion:

$$\rho_t C_t \frac{\partial T}{\partial t} = K \nabla^2 T. \quad (14.42)$$

Here  $\rho_t$  is the density of the tissue ( $\text{kg m}^{-3}$ ) and  $C_t$  the tissue specific heat capacity ( $\text{J K}^{-1} \text{kg}^{-1}$ ). The left-hand side of the equation is the rate of energy increase in the tissue per unit volume, and the right-hand side is the net rate of heat flow into that volume by conduction—energy flowing because warmer molecules with more kinetic energy transfer energy to cooler neighbors in a collision process analogous to a random walk. This model is for solids; in liquid one must also consider convection.

We now add a term for energy carried away by flowing blood. In the linear approximation it is proportional to the temperature difference between the tissue and the blood supply and also to the rate of blood flow. Units for this term can be quite confusing and need to be examined in detail. Blood flow is usually defined by physiologists as the *perfusion*  $P$ , which is the volume flow of blood per unit mass of tissue. The SI units for  $P$  are

$$P \frac{\text{m}^3 \text{ (blood)}}{[\text{kg (tissue)}] \text{ s}}.$$

Its product with the tissue density is the volume flow of blood per unit volume of tissue:

$$\rho_t P = \frac{[\text{kg (tissue)}] [\text{m}^3 \text{ (blood)}]}{[\text{m}^3 \text{ (tissue)}] [\text{kg (tissue)}] \text{ s}} = \frac{\text{m}^3 \text{ (blood)}}{\text{m}^3 \text{ (tissue)} \text{ s}} = \text{s}^{-1}.$$

The quantity is analogous to clearance (Chapter 2). Its inverse is the time it takes for a volume of blood equal to the tissue volume to flow through the tissue. Each term of our heat-flow equation has units of energy per unit volume of tissue per second. If we assume that the blood enters the tissue at temperature  $T_0$  and leaves at temperature  $T$ , the energy lost by the volume is the heat capacity of blood,  $C_b$ , times its mass per unit volume times the temperature rise. The new term in the heat-flow equation is

$$C_b \frac{\text{J}}{\text{K kg (blood)}} \times \rho_b \frac{\text{kg (blood)}}{\text{m}^3 \text{ (blood)}} \times \rho_t P \frac{\text{m}^3 \text{ (blood)}}{\text{m}^3 \text{ (tissue)} \text{ s}} \times [(T - T_0) \text{ K}]$$

or

$$C_b \rho_b \rho_t P (T - T_0) \frac{\text{J}}{\text{m}^3 \text{ (tissue)} \text{ s}},$$

so the heat-flow equation with blood flow added is

$$\rho_t C_t \frac{\partial T}{\partial t} = K \nabla^2 T - C_b \rho_b \rho_t P (T - T_0).$$

The last term we consider is the energy deposited by the photon beam. In Sec. 14.5 we defined the particle fluence and particle fluence rate for photons. The definition can be used for both collimated beams and diffuse radiation. In a similar way we define the *energy fluence*  $\Psi$  as the ratio of the expectation value of the amount of photon energy traversing a small sphere of radius  $a$  divided by the area of a great circle of the sphere,  $\pi a^2$ . The *energy fluence rate* is

$$\psi = \frac{d\Psi}{dt}. \quad (14.43)$$

The energy per unit volume lost by a beam with energy fluence rate  $\psi$  can be determined by the following argument. Consider only the fluence rate due to photons traveling in a certain direction. Orient the  $z$  axis in that direction and consider a small volume  $dS dz$ . The rate at which energy flows into the volume is  $\psi dS$ , and the rate at which it is absorbed is  $\psi dS \mu_a dz$ . Therefore, the rate of absorption per unit volume is  $\mu_a \psi$ , independent of the direction the photons travel. The final heat-flow equation is

$$\rho_t C_t \frac{\partial T}{\partial t} = K \nabla^2 T - C_b \rho_b \rho_t P (T - T_0) + \mu_a \psi. \quad (14.44)$$

For monoenergetic photons the photon energy fluence rate is related to the photon fluence rate by

$$\psi = h\nu\varphi. \quad (14.45)$$

In general, one must first solve Eq. 14.26 to determine  $\psi$  and then solve Eq. 14.44. We could add other terms, such as one for the thermal energy produced by metabolism within the tissue.

Sometimes Eq. 14.44 is written with all terms divided by  $\rho_t C_t$ , and sometimes with all terms divided by  $K$ . If we divide by  $\rho_t C_t$  the equation is similar in form to the diffusion equation in Chapter 4:

$$\frac{\partial T}{\partial t} = D \nabla^2 T - \frac{C_b}{C_t} \rho_b P (T - T_0) + \frac{\mu_a}{\rho_t C_t} \psi, \quad (14.46)$$

where

$$D = \frac{K}{\rho_t C_t}. \quad (14.47)$$

Values of  $D$  are in the range  $(0.5\text{--}2.5) \times 10^{-7} \text{ m}^2 \text{ s}^{-1}$  depending on the tissue type [Grossweiner (1994), pp. 127–129]. We saw in Chapter 4 that for a spreading Gaussian solution to the diffusion equation the variance is  $\sigma_x^2 = \sigma_y^2 = \sigma_z^2 = 2Dt$ . The thermal relaxation time, that is, the average time for the temperature rise to spread a

distance  $x$ , is therefore  $x^2/2D$  in one dimension,  $x^2/4D$  in two dimensions, and  $x^2/6D$  in three dimensions.

There is an interplay between the thermal conductivity term and the blood-flow term. The *thermal penetration depth*  $\delta_{\text{th}}$  is the distance at which the two terms are comparable. For larger distances blood flow is more important. To estimate the penetration depth, assume that  $T - T_0$  changes over this distance. Then the Laplacian is approximated by  $\nabla^2 T \approx (T - T_0)/\delta_{\text{th}}^2$ . Equating the diffusive and blood flow terms gives

$$D \frac{T - T_0}{\delta_{\text{th}}^2} = \frac{C_b}{C_t} \rho_b P (T - T_0)$$

so

$$\delta_{\text{th}}^2 = D \frac{C_t}{C_b} \frac{1}{\rho_b P} = \frac{K}{\rho_t C_b \rho_b P}. \quad (14.48)$$

Grossweiner (1994) discusses values for the various tissue parameters, their temperature dependence, and simple models for tissue heating and ablation.

## 14.11 Radiometry and Photometry

This section develops some of the concepts and vocabulary of *radiometry*, the measurement of radiant energy. We will be considering five types of radiant energy in the remaining chapters: infrared radiation, visible light, ultraviolet radiation, x rays, and charged particles. Concepts for the measurement of radiant energy were developed simultaneously in different disciplines and even in different wavelength regions, depending on the purpose and the measurement techniques that were originally available.

It is recommended that the term *photometry* be reserved for measurement of the ability of electromagnetic radiation to produce a human visual sensation, that *radiometry* be used to describe the measurement of radiant energy independent of its effect on a particular detector, and that *actinometry* be used to denote the measurement of photon flux or photon dose (total number of photons) independent of any subsequent photoactivated process [Zalewski (1995), p. 24.7].

This section reviews radiometric units and introduces a few of the related units from photometry and actinometry. Nomenclature is slightly different for x rays and charged particles.

Section 14.5 described two quantities, the photon fluence and the photon fluence rate. The energy fluence and energy fluence rate were introduced in Sec. 14.10. These are reviewed and compared here so that all the definitions are in one place. The definitions are summarized in Table 14.6. Symbols are shown for quantities used in this text. The third column shows symbols that have been recommended by the American Association of Physicists in Medicine [AAPM 57 (1996)]. They often differ from the usage in this book.

### 14.11.1 Radiometric Definitions

#### Radiant Energy and Power

The total amount of energy being considered is the *radiant energy*  $R$ , measured in joules. It can be the energy emitted by a source, transferred from one region to another, or received by a detector. We use subscripts  $s$  and  $d$  to refer to the source and detector. In optics the radiant energy is electromagnetic radiation. In radiological physics we will also consider energy transported by charged particles such as electrons, and protons, and by neutral particles such as photons and neutrons.

The rate at which the energy is radiated, transferred, or received is the *radiant power*  $P$  (watts).

#### Point Source: Radiant Intensity

The simplest source is a point that radiates uniformly in all directions. The *radiant intensity* or radiant power per unit solid angle (Appendix A) leaving a point source radiating uniformly in all directions is

$$\frac{dP}{d\Omega} = \frac{P}{4\pi} \quad (\text{W sr}^{-1}). \quad (14.49)$$

The power per unit area falls as  $1/r^2$ , while the power per unit solid angle is independent of  $r$ .<sup>16</sup> A point source need not radiate uniformly in all directions. For example, a searchlight 1 m in diameter viewed from a point several kilometers away appears to be a point. The light might be confined to a cone with a half-angle of  $1^\circ$ . Then a plot of  $dP/d\Omega$  might look like Fig. 14.31. The total power radiated by the point source is

$$P = \int \frac{dP}{d\Omega} d\Omega. \quad (14.50)$$

If the power per unit solid angle is symmetric about the axis of the beam and  $\theta$  is the angle with respect to the beam axis, then (see Appendix L)

$$P = \int_0^\pi \frac{dP}{d\Omega} 2\pi \sin \theta d\theta.$$

#### Extended Source: Radiance

The radiant energy leaving a source can travel in many different directions. The radiation striking a surface can come from many different directions. If we consider any small area in space there will generally be radiation passing through that area traveling in many different directions. In each case the radiant energy or the radiant power is proportional to the magnitude of the small area projected perpendicular to the direction the energy is traveling, and to the size of the solid angle—the range of directions—being considered.

<sup>16</sup>The lighting industry calls  $dP/d\Omega$  the intensity, while in physical optics intensity is used for power per unit area. We will try to avoid using the word intensity alone.

TABLE 14.6. A comparison of radiometric, photometric, and actinometric quantities. Symbols are given for those quantities used in this text. The column “Symbol sometimes used” gives an alternate symbol that is often found. See, for example, *AAPM57 (1996)*.

Radiometric quantity	Symbol used here	Symbol sometimes used	Units	Photometric quantity	Symbol	Units	Actinometric quantity	Symbol	Units
<u>General quantities</u>									
<i>Radiant energy</i> emitted, transferred, or received.	$R$	$Q$	J	<i>Luminous energy.</i>	$R_v$	lm s	<i>Number of photons</i> emitted, transferred, or received.	$N$	
<i>Radiant flux</i> or radiant power emitted, transferred, or received.	$P$	$P$ or $\Phi$ or $\dot{R}$	W	<i>Luminous flux</i>	$P_v$	lm	<i>Photon flux</i>		$s^{-1}$
<i>Radiance</i> : the radiant power per unit solid angle per unit area of surface projected perpendicular to the radiant energy. It can be defined on the surface of a source or detector or at any point on the path of a ray of radiation.	$L$	$r$	W $m^{-2}$ $sr^{-1}$	<i>Luminance</i>	$L_v$	candela $m^{-2}$ (cd $m^{-2}$ )	<i>Photon flux radiance</i>		$m^{-2} sr^{-1}$
<i>Energy fluence</i> : the ratio of the expectation value of the radiant energy striking a small sphere to the area of a great circle of the sphere.	$\Psi$	$H_0$	J $m^{-2}$				<i>Photon (or particle) fluence</i> : the ratio of the expectation value of the number of photons striking a small sphere to the area of a great circle of the sphere.	$\Phi$	$m^{-2}$
<i>Energy fluence rate</i> : the energy fluence per unit time.	$\psi$	$E_0$	W $m^{-2}$				<i>Photon fluence rate</i> : the photon fluence per unit time	$\phi$	$m^{-2} s^{-1}$
<u>Quantities emitted from a surface</u>									
<i>Radiant intensity</i> : radiant power or flux emitted by a <i>point source</i> in a given direction per unit solid angle.		$I$	W $sr^{-1}$	<i>Luminous intensity</i>		lm $sr^{-1}$ or candela (cd)	<i>Photon flux intensity.</i>		$sr^{-1}$
<i>Exitance</i> : radiant power or flux emitted or reflected per unit area.		$W_r$	W $m^{-2}$	<i>Luminous exitance</i>		lm $m^{-2}$	<i>Photon exitance</i>		$m^{-2}$
<u>Quantities incident on a surface</u>									
<i>Irradiance</i> : the power per unit area incident on a surface.	$E$	$E$	W $m^{-2}$	<i>Illuminance</i>		lm $m^{-2}$ or lux	<i>Photon flux irradiance</i>		$m^{-2} s^{-1}$
<i>Radiant exposure</i> : radiant energy arriving per unit area		$H$	J $m^{-2}$	<i>Luminous exposure</i>		lm s $m^{-2}$	<i>Photon flux exposure</i>		$m^{-2}$

The *radiance*  $L$  is the amount of radiant power per unit solid angle per unit surface area projected perpendicular to the direction of the radiant energy. The radiance of radiation traveling through a small area in space is sometimes difficult to visualize. Figures 14.32 and 14.33 may help. Figure 14.32 shows radiation leaving three points on a surface at the left. Some of it passes through the surface

represented by the vertical line on the right. The energy passing through that surface has components from each point on the radiating surface. Figure 14.33 shows radiation in a very narrow cone of solid angles passing through surface  $dS$  whose normal is at an angle  $\theta$  with the beam direction. The radiance is the power per unit solid angle divided by  $dS \cos \theta$ .

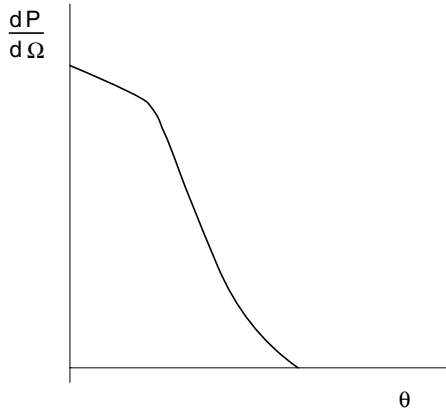


FIGURE 14.31. A plot of power per unit solid angle as a function of angle from the axis of a hypothetical searchlight.

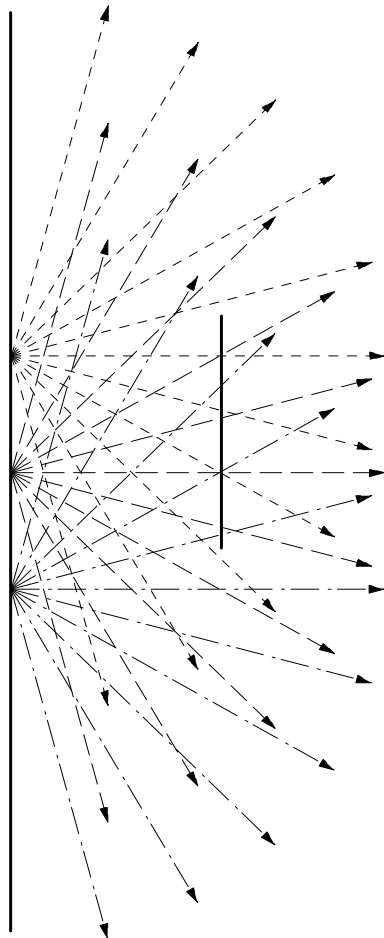


FIGURE 14.32. Radiation emitted from different points of the surface on the left strikes the surface on the right.

We have already seen the *energy fluence*  $\Psi$ , which is a measure of the total radiation entering or leaving a small volume of space. It is the total amount of energy striking a small sphere of radius  $a$  divided by the area of

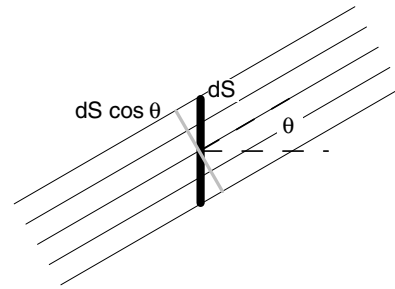


FIGURE 14.33. Surface area  $dS$ , projected perpendicular to the direction of the radiation, has projected area  $dS \cos \theta$ .

a great circle  $\pi a^2$  in the limit as the radius approaches zero. Strictly speaking, if we repeat the experiment many times, the amount of energy striking the sphere fluctuates. The energy fluence is defined in terms of the expectation value of this fluctuating quantity. Figure 14.12 shows two examples. In Fig. 14.12(a), a parallel beam with energy  $R$  passes through a circular area  $\pi a^2$  for a time  $\Delta t$ . In Fig. 14.12(b), a total amount of energy  $R$  strikes a sphere of radius  $a$  from many different directions. In both cases  $\Psi = R/\pi a^2$ . Notice that some of the energy passing through the sphere passes outside a great circle that is not perpendicular to the direction in which the radiation is traveling, but it does pass through a great circle constructed perpendicular to its direction of travel.

The *energy fluence rate* is the amount of energy fluence per unit time (which for the small sphere is  $P/\pi a^2$ ):

$$\psi = \frac{d\Psi}{dt}. \tag{14.51}$$

The *exitance*  $W_r$  is the radiant power or flux emitted per unit area of a surface.

Energy Striking a Surface: Irradiance

Now consider the energy striking a surface. The *irradiance*  $E$  is the power per unit area incident on a surface. The strict definition is the ratio of the power incident on an infinitesimal element of detector surface  $dS_d$  to the area projected perpendicular to the direction the radiant energy is traveling. If  $\theta_d$  is the angle between a normal to the surface and the direction of propagation, the irradiance is

$$E = \frac{dP}{\cos \theta_d dS_d}. \tag{14.52}$$

For a point source radiating uniformly in all directions, the power at distance  $r$  is spread uniformly over a sphere of area  $4\pi r^2$ , so the irradiance on a detecting surface perpendicular to a line back to the source is

$$E = \frac{P}{4\pi r^2} \quad (\text{isotropic point source}). \tag{14.53}$$

For an extended source the power emitted by the surface is proportional to both the size of the emitting area

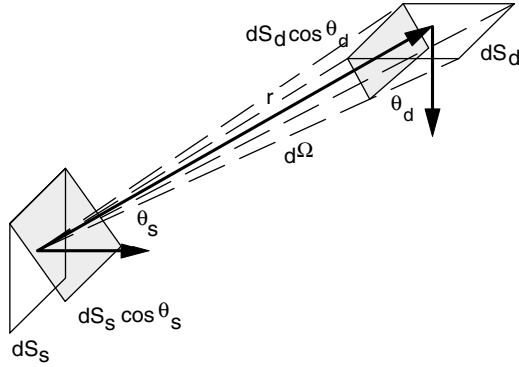


FIGURE 14.34. Radiant energy is emitted from a source of surface area  $dS_s$  into a cone of solid angle  $d\Omega$ . The direction of emission is at an angle  $\theta_s$  with the normal to the surface. A detecting surface has an element of area  $dS_d$  oriented at a direction  $\theta_d$  to the direction of travel of the radiation from source to detector. The shaded rectangles show the projections of  $dS_s$  and  $dS_d$  perpendicular to the line of length  $r$  from source to detector.

$dS_s$  and the solid angle of the cone  $d\Omega$  into which the energy is radiated, as shown in Fig. 14.34. The solid angle subtended by a small element of area on the detector is  $d\Omega$ , as shown by the dashed lines. The amount of power radiated into  $d\Omega$  from  $dS_s$  is

$$LdS_s d\Omega = \frac{d^2 P}{\cos \theta_s dS_s d\Omega} dS_s d\Omega, \quad (14.54)$$

where the radiance  $L$  depends on the direction of emission as well as the location on the surface. This equation is valid whether the energy is emitted directly from the source (as in a glowing object) or is scattered by the surface (as from this page). The total power emitted is

$$P = \iint L dS_s d\Omega. \quad (14.55)$$

The distinction between angles and areas for the source and the detector is shown in Fig. 14.34. Note that the solid angle subtended at the source by  $dS_d$  is  $d\Omega = dS_d \cos \theta_d / r^2$ . The power into an area  $dS_d$  of the detector from area  $dS_s$  of the source is therefore

$$d^2 P = \frac{L \cos \theta_s \cos \theta_d dS_s dS_d}{r^2}. \quad (14.56)$$

Plane-wave Relationships

We can derive some useful relationships for a beam of collimated radiation all traveling in one direction (a *plane wave*). Imagine that the collimated beam comes from a distant point source radiating power  $P$ . The energy fluence rate at distance  $r$  from the source is the power through a sphere of radius  $a$  divided by  $\pi a^2$ :

$$\psi = \frac{\pi a^2 P}{4\pi r^2} \frac{1}{\pi a^2} = \frac{P}{4\pi r^2}.$$

This is also the power per unit area incident on a circle of radius  $a$  oriented perpendicular to the beam. Therefore, for a collimated beam,

$$\psi = E \quad (\text{collimated beam}). \quad (14.57)$$

Isotropic Radiation: Lambert’s Law

In general,  $L$  may depend on the angle of emission. In some cases, such as reflection from a “perfectly diffuse” surface, the radiation is isotropic :  $L = L_0$ . This is called *Lambert’s law of illumination* or Lambert’s cosine law.<sup>17</sup>

A surface described by Lambert’s law will have equal power per unit area in the image regardless of the viewing angle. Look at surfaces around you. Do similar surfaces illuminated the same way appear to have the same brightness when they are oblique to your line of vision?

The power incident on a small element of surface area  $dS_d$  from angle  $d\Omega$  is  $L_0 dS_d \cos \theta_d d\Omega$ , where  $\theta_d$  is the angle that the incident radiation makes with the normal to the surface. The solid angle is  $2\pi \sin \theta_d d\theta_d$  [see Fig. 14.11(b)]. The irradiance is

$$E = \frac{dS_d 2\pi L_0 \int_0^{\pi/2} \cos \theta_d \sin \theta_d d\theta_d}{dS_d} = \pi L_0. \quad (14.58)$$

The same geometry is used with  $dS_s$  to show that for isotropic radiation the exitance is

$$W_r = \pi L_0. \quad (14.59)$$

To determine the energy fluence rate for isotropic radiation consider a small sphere of radius  $a$  and the radiation arriving in a small solid angle  $d\Omega$  about a line perpendicular to a great circle of the sphere. The power is  $L_0 \pi a^2 d\Omega$ . This argument applies for any direction of the radiation. Integrating over all directions gives the total power  $L_0 \pi a^2 4\pi$ . Therefore, for isotropic (Lambertian) radiation,

$$\psi = 4\pi L_0 = 4E \quad (\text{isotropic radiation}). \quad (14.60)$$

The Spectrum

When the energy is not monochromatic, we define the amount of energy per unit wavelength interval as  $R_\lambda$ , with units  $\text{J m}^{-1}$  or  $\text{J nm}^{-1}$ . The total energy between wavelengths  $\lambda_1$  and  $\lambda_2$  is

$$\int_{\lambda_1}^{\lambda_2} R_\lambda(\lambda) d\lambda \quad (14.61a)$$

and between frequencies  $\nu_1$  and  $\nu_2$  it is

$$\int_{\nu_1}^{\nu_2} R_\nu(\nu) d\nu. \quad (14.61b)$$

The relationship between  $R_\lambda$  and  $R_\nu$  is the same as in Eqs. 14.35 and 14.36.

<sup>17</sup>Sometimes Eq. 14.56 is defined without the factor  $\cos \theta_s$ , in which case Lambert’s law has the form  $L(\theta_s) = L_0 \cos \theta_s$ .

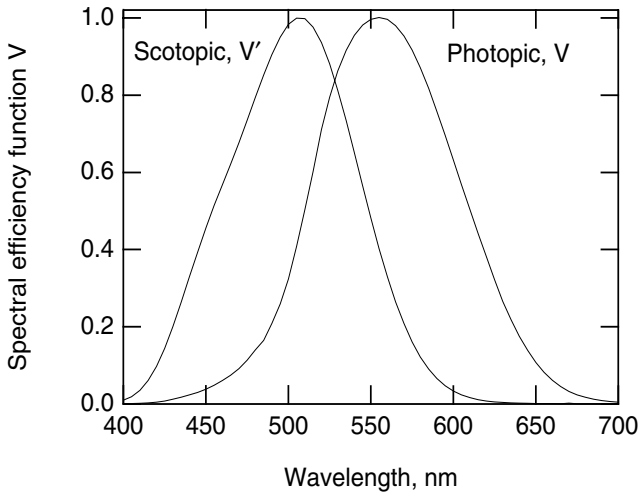


FIGURE 14.35. The spectral efficiency functions for the CIE standard eye. Plotted from data in Table 2 of Zalewski (1995).

### 14.11.2 Photometric Definitions

For the photometric units we also need to know the sensitivity of the eye. The eye contains two types of light receptors: *rods*, which have no color discrimination but are most sensitive, and *cones*, which are less sensitive and can discriminate color. *Photopic* vision is normal vision at high levels of illumination in which the eye can distinguish colors. *Scotopic* vision occurs at low light levels with a dark-adapted eye. The CIE has established the spectral efficiency function  $V$  for the eye of a standard observer for both photopic vision [ $V(\lambda)$ ] and scotopic vision [ $V'(\lambda)$ ]. Both are normalized to unity at their peak (Fig. 14.35).

The *luminous flux*  $P_v$  in lumens (lm) is the analog of the energy flux  $P$ . The peak sensitivity for photopic vision is for green light,  $\lambda = 555$  nm. At that wavelength the relationship between  $P$  and  $P_v$  is

$$\begin{aligned} P = 1 \text{ W} &\iff P_v = 683 \text{ lm}, \\ P_v = 1 \text{ lm} &\iff P = 1.464 \times 10^{-3} \text{ W}. \end{aligned} \quad (14.62a)$$

The ratio  $P_v/P$  at 555 nm is the *luminous efficacy* for photopic vision,  $K_m = 683 \text{ lm W}^{-1}$ . For a distribution of wavelengths,

$$P_v = K_m \int_{400 \text{ nm}}^{700 \text{ nm}} V(\lambda) P_\lambda(\lambda) d\lambda. \quad (14.62b)$$

An analogous relationship holds for scotopic vision, with  $K'_m \approx 1,700 \text{ lm W}^{-1}$ :

$$P_v(\text{scotopic}) = K'_m \int_{400 \text{ nm}}^{700 \text{ nm}} V'(\lambda) P_\lambda(\lambda) d\lambda. \quad (14.62c)$$

If  $P$  were spread uniformly over the visible spectrum, the overall conversion efficiency would be about  $200 \text{ lm W}^{-1}$ . A typical incandescent lamp has an efficiency of

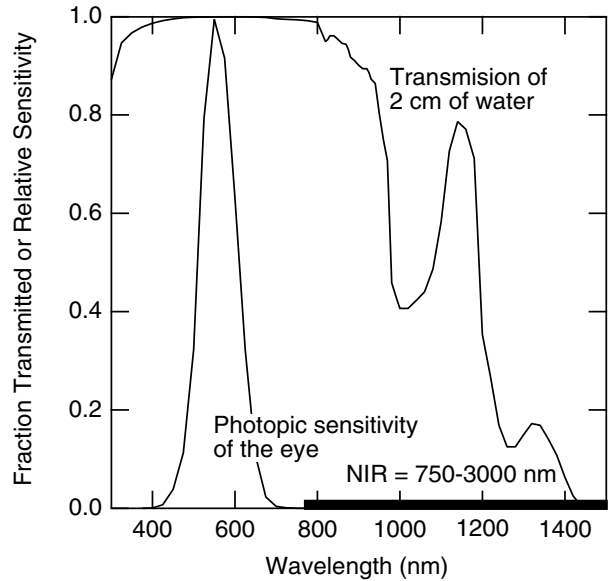


FIGURE 14.36. Transmission of light through 2 cm of water, compared to the spectral efficiency of the eye.

$10\text{--}20 \text{ lm W}^{-1}$ , while a fluorescent lamp has an efficiency of  $60\text{--}80 \text{ lm W}^{-1}$ . The number of lumens per steradian is the *luminous intensity*, in  $\text{lm sr}^{-1}$ . The lumen per steradian is also called the *candle*. Other units are shown in Table 14.6.

The peak of the eye's spectral efficiency function is at about the peak of the sun's blackbody spectrum when plotted as a function of wavelength (Eq. 14.32). Some authors have speculated that this is because we evolved in sunlight. There is a severe problem with this argument. The spectral efficiency function has the same value whether we consider a particular wavelength or its corresponding frequency. The blackbody spectrum is a distribution function—per wavelength interval (Eq. 14.32) or per frequency interval (Eq. 14.37).<sup>18</sup> The sun's blackbody spectrum plotted vs. frequency peaks at a frequency corresponding to a wavelength of 880 nm, far from the peak of the spectral efficiency function (See Fig. 14.24).

Soffer and Lynch (1999) have discussed this at length and describe several of the errors in the literature. The structures in the human eye, as in all vertebrate eyes, are mostly water. All vertebrate eyes are sensitive between 390 and 760 nm, with a peak at 500–550 nm. It is interesting to compare the spectral efficiency function with the transmission of light through 2 cm of water (Fig. 14.36). The eye's response is pretty well centered in this absorption window. Many insects, crustaceans, fish, birds and reptiles have ultraviolet-sensitive receptors [Kevan *et al.* (2001)]; their eyes do not contain water.

<sup>18</sup>Other distribution functions are also useful, for example, per logarithmic frequency or wavelength interval. See Soffer and Lynch (1999) or Heald (2003).

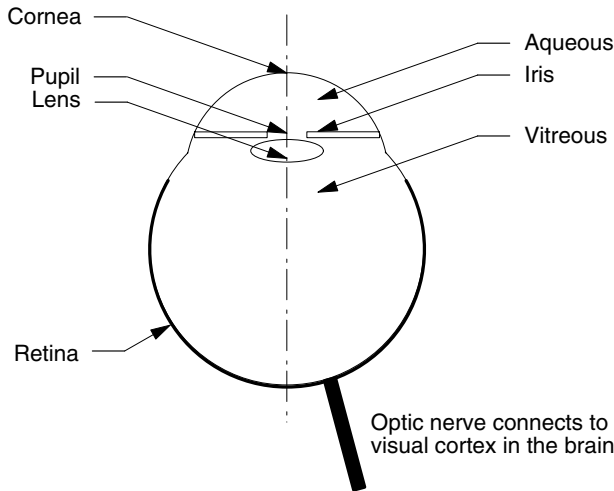


FIGURE 14.37. A simplified cross section of the left eye, viewed from above.

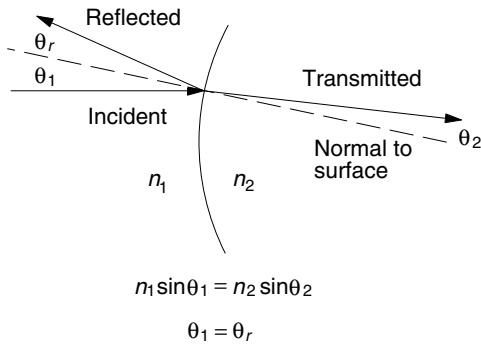


FIGURE 14.38. When light passes from one medium to another with a different index of refraction. All angles are measured with respect to the normal to the surface

### 14.11.3 Actinometric Definitions

The actinometric quantities count the number of photons. For monochromatic photons the energy is the number of photons times  $h\nu$ . Therefore, an actinometric quantity is easily obtained when the radiometric quantity is known. The units are shown in Table 14.6.

## 14.12 The Eye

This section presents a simple model for the eye, sufficient for us to understand how refractive errors are corrected and to see how photons strike the retina, so that the sensitivity of the eye can be determined in the next section.

A simplified cross section of the eye is shown in Fig. 14.37. The principal components through which the light passes are the curved, thin, transparent *cornea*, the *aqueous*, the *lens*, the *vitreous*, and the *retina*. The *iris* defines the area of the *pupil*, the opening in front of the lens through which light passes.

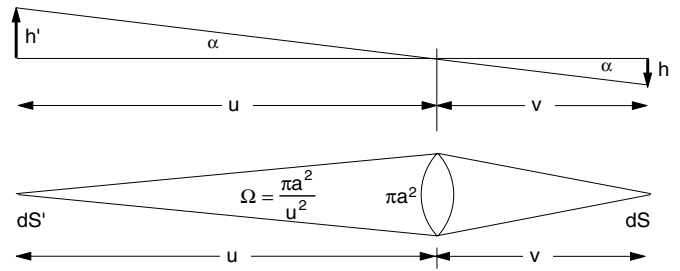


FIGURE 14.39. A source of height  $h'$  emits light in all directions. Some of this light is intercepted by a lens and focused in an image. (a) Relation between object and image distances and sizes. (b) Collection of light by the lens.

When light passes through a surface from one medium into another, part is reflected and part is transmitted. The transmitted light usually changes direction, a process called *refraction*. Figure 14.38 shows the angles involved, all measured with respect to the dashed line, which is normal to the surface at the point where the light ray strikes. The angle the reflected light makes with the normal is the same as the angle of incidence,  $\theta_r = \theta_1$ . The direction the refracted light travels is described by Snell's law,  $n_1 \sin \theta_1 = n_2 \sin \theta_2$ .

When light from an object strikes the eye, it must be refracted to form an image on the retina. Most of the refraction takes place at the surface between the air and the cornea. The cornea is very thin, and a light ray is deflected only a very small distance before it strikes the aqueous. Thus, most of the refraction occurs because of the difference between the index of refraction of the air ( $n = 1.00$ ) and the aqueous ( $n = 1.33$ ). The light then passes through the crystalline lens ( $n = 1.42$ ) and the vitreous ( $n = 1.33$ ). The lens changes shape to provide the adjustable part of the overall refraction.

A number of models at varying levels of sophistication are used to describe the formation of the image on the retina. The most detailed take into account the refraction at each surface where the index of refraction changes, including variations in different layers of the lens itself. Others treat only the refraction at the air–cornea, aqueous–lens, and lens–vitreous interfaces. The simplest model, and the one we will use, treats the eye as a thin lens of adjustable focal length  $f$ , with object distance  $u$  and fixed image distance  $v$ , as shown in Fig. 14.39. The object and image distances and focal length are related by the *thin-lens equation* found in any general physics book:

$$\frac{1}{u} + \frac{1}{v} = \frac{1}{f}. \tag{14.63}$$

When the object is infinitely far away the image distance is equal to the focal length of the lens,  $v = f$ . A typical value for  $v$  is 1.7 cm. As the object is brought closer to the eye  $v$  cannot change, but the lens changes to decrease the focal length.

TABLE 14.7. Convergence power of the eye in diopters.

Refracting structure	Relaxed normal eye	Most converging eye (age 25)
Air-cornea surface	45	45
Lens	14	24
Entire eye	59	69

In ophthalmology and optometry it is customary to describe the refraction of the eye in terms of the *vergence*. When light rays are emanating from a point they are diverging, and the vergence is negative. When they are coming toward a point the vergence is positive and they are converging. When they are parallel, the vergence is zero. Quantitatively, the vergences for the geometry shown in Fig. 14.39 are

$$\begin{aligned}
 U &= -\frac{1}{u} \quad (\text{diverging from the object}), \\
 V &= \frac{1}{v} \quad (\text{converging to the image}), \\
 F &= \frac{1}{f} \quad (\text{a converging lens}).
 \end{aligned}
 \tag{14.64}$$

The relationship between the vergences is

$$V = F + U. \tag{14.65}$$

When the distances are in meters, the vergences are in *diopters*.

A given eye requires a particular value of  $V$  to form the image. The converging power of all the refracting surfaces in the eye must be  $F = V$  in order to focus on an object infinitely far away. Closer objects require more convergence from the eye, which is provided by the lens. Table 14.7 shows typical values for the converging power of the eye. Most of the convergence is provided by the front surface. When the eye is relaxed,  $F = V = 59$  diopters,  $U = 0$ , and the eye is focused on an object infinitely far away. With  $F = 69$  diopters,  $U = 10$ , and the eye is focused on an object 0.1 m away. This ability of the lens to change shape and provide additional converging power is called *accommodation*.

In the normal or *emmetropic* eye, the length of the eye is such that when the lens is relaxed, rays with no vergence (parallel rays from a source infinitely far away) are focused on the retina ( $V = F$ ).

In nearsightedness or *myopia*, parallel rays come to a focus in front of the retina. The eye is slightly too long for the shape of the cornea ( $F > V$ ). The total converging power of the eye is too great, and the relaxed eye focuses at some closer distance, from which the rays are diverging. Accommodation can only increase the converging power of the eye, not decrease it, so the unassisted myopic eye cannot focus on distant objects. Myopia can be corrected by placing a diverging spectacle or contact

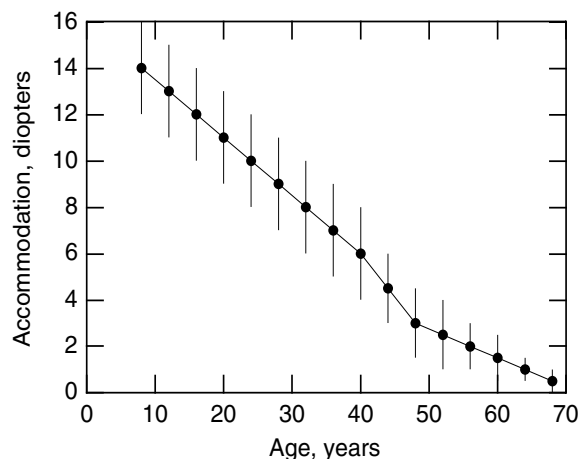


FIGURE 14.40. Accommodation vs age. There is considerable variation between individuals, shown by the error bars.

lens in front of the eye, so that incoming parallel rays are diverging when they strike the cornea.

The farsighted or *hypermetropic* eye does not have enough converging power ( $F < V$ ). The subject can focus on distant objects by providing some additional converging power from the lens, but then the lens cannot provide enough converging power to focus on nearby objects. The corrective lens provides additional convergence.

When the eye is not symmetric about an axis through the center of the lens, the images from objects oriented at different angles in the plane perpendicular to the axis form at different distances from the lens. This is called *astigmatism*, and it can be corrected with a spectacle lens that is not symmetric about the axis. The lack of symmetry usually occurs at the surface of the cornea, so a contact lens can restore the symmetry.

Surgery to change the radius of curvature of the cornea can also be used to correct errors of refraction.

As we age the accommodation of the eye decreases, as shown in Fig. 14.40. A normal viewing distance of 25 cm or less requires 4 diopters or more of accommodation. The graph shows that this limit is usually reached in the early 40s. Bifocals provide a portion of the spectacle lens that has increased converging power, usually in the bottom part of the lens. This can be done either by grinding the lower portion of the lens with a different radius of curvature or by fusing glass with a different index of refraction into the lens.

The sharpness of the image is reduced by two other effects: *chromatic aberration* and *spherical aberration*. Chromatic aberration occurs because the index of refraction varies with wavelength. There is nearly a 2-diopter change in overall refractive power from the red to the blue. Spherical aberration occurs because the refractive power changes with distance from the axis of the eye. This is different from astigmatism, which is a departure from symmetry at different angles about the axis.



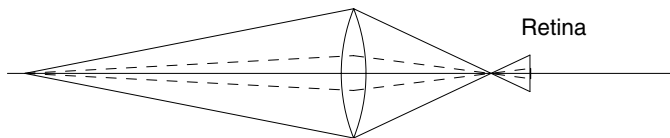


FIGURE 14.41. Depth of field is illustrated by this ray diagram. The retina is slightly behind the plane of focus. In dim light, the pupil of the eye is fully open and light from a point object is spread out over the larger circle on the retina. When the light is brighter and the pupil is smaller, light from the same point object is confined to the smaller circle defined by the dashed lines.

A concept important in both vision and photography is *depth of field*. The retina has a finite spatial resolution, so the image of a point still appears sharp, even if it is slightly out of focus. Consider Fig. 14.41. The retina is behind the plane in which the image is in focus. In dim light, the pupil of the eye is fully open and light from a point object is spread out over the larger circle on the retina defined by the solid rays. In brighter light the pupil is smaller, and light from the same point object is confined to the smaller circle defined by the dashed lines. As long as this circle is smaller than the spatial resolution, the image is sharp. This is why we can see better in brighter light. An older person whose accommodation is less and who is trying to avoid bifocals often finds that bright light makes it easier to see nearby objects.

Point-spread functions and modulation transfer functions can be used to describe the image. [See, for example, Charman (1995) or Grievenkamp *et al.* (1995).] A simpler model describes the image by a Gaussian with a certain standard deviation, equal to the square root of the sum of the variances due to various effects. The maximum photopic (bright-light) resolution of the eye is limited by four effects: diffraction of the light passing through the circular aperture of the pupil ( $5\text{--}8\ \mu\text{m}$ ), spacing of the receptors ( $\approx 3\ \mu\text{m}$ ), chromatic and spherical aberrations ( $10\text{--}20\ \mu\text{m}$ ) and noise in eyeball aim (a few micrometers) [Stark and Theodoris (1973)]. The total standard deviation is  $(6^2 + 3^2 + 15^2 + 5^2)^{1/2} = 17\ \mu\text{m}$  in the image on the retina. Since the diameter of the eyeball is about 2 cm, this corresponds to an angular size ( $\alpha$  in Fig. 14.39) of  $(17 \times 10^{-6}) / (2 \times 10^{-2}) = 8.5 \times 10^{-4}\ \text{rad} = 0.048^\circ = 2.9\ \text{minutes of arc}$ . [For further discussion, see Cornsweet (1970, Chapter 3).]

### 14.13 Quantum Effects in Dark-Adapted Vision

The visual process involves two steps. First, the eye creates an image of an external object on the retina as described above. Then the photon stimulus is transduced into neurological signals that are interpreted by the cen-

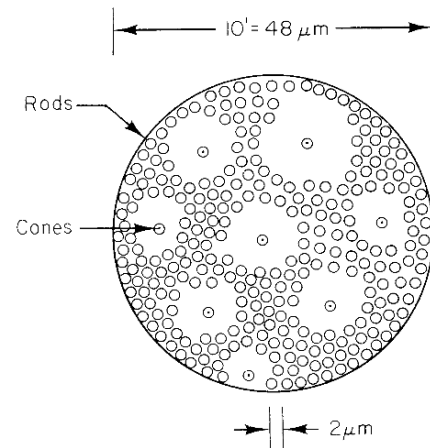


FIGURE 14.42. An example of a 10-minute-of-arc field superimposed on the rods and cones in the retina in the region of greatest sensitivity.

tral nervous system. The discussion here is limited to a classic experiment on scotopic vision that shows the importance of quantum effects (shot noise) in human vision in dim light.

The experiment was performed by Hecht *et al.* in 1942. It has been described in many places. A detailed non-mathematical description is that by Cornsweet (1970). A more mathematical review by Pirenne (1962) is also available.

The retina can be divided into two regions. The *fovea*, the area of greatest visual discrimination, is composed entirely of cones. The percentage of rods is highest a few millimeters away from the fovea, and this part of the retina is most sensitive to faint light. The dark-adapted eye increases sensitivity by a factor of about 5,000.

The experiment was done by having the subject look directly at a very dim red fixation point while a green light was flashed in such a place that its image fell on the most sensitive part of the retina. Experiments on the sensitivity of the dark-adapted eye to flashes of weak light have shown that if the flash duration is less than 100 ms and the light on the retina covers a *receptor field* less than 10 minutes of arc in size, the scotopic response of the eye depends on the total amount of energy or the total number of photons in the flash. Photons striking anywhere within the receptor field during this time have the same effect; the eye must combine the effects occurring in all receptors in the receptor field in a tenth of a second. A scotopic receptor field is shown in Fig. 14.42. This scotopic field size (10 minutes of arc) cannot be compared to the 2.9 minutes for maximum resolution, which is for photopic vision on a different part of the retina.

In the Hecht–Schlaer–Pirenne experiment the flashes were short enough and small enough so that only the total number of photons was important. The fraction of flashes that the subject recognized was measured as a function of the total flash energy. A typical response curve is shown

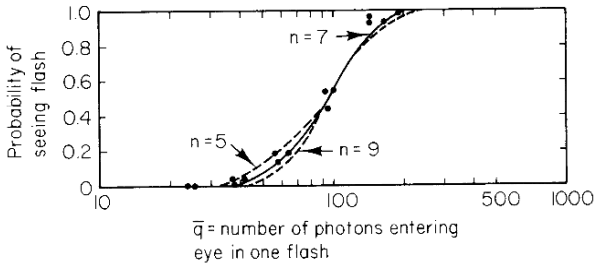


FIGURE 14.43. Typical response in the experiments of Hecht, Schlaer, and Pirenne. Curves are calculated using Eq. 14.68. Data are from S. Hecht, S. Schlaer, and M. H. Pirenne. *The Journal of General Physiology* **25**: 819–840 (1942) by copy-right permission of the Rockefeller University Press.

in Fig. 14.43. Let  $q$  be the number of photons striking the cornea in front of the pupil in each flash, which is the total energy in the flash divided by the energy of each photon. For the 510-nm green light used, the photon energy is  $hc/\lambda = 3.89 \times 10^{-19}$  J. The number of photons striking the cornea can be determined as follows. Let  $Lt$  be the radiance times the duration of the flash. Consider Eq. 14.56 with both  $\theta_s$  and  $\theta_d$  nearly zero. Refer also to the lower half of Fig. 14.39. The energy striking the cornea over the pupil area is

$$\frac{(Lt) dS_s dS_d}{r^2} = \frac{(Lt) dS' (\pi a^2)}{u^2}.$$

Because  $h = h'v/u$ , the area on the retina where photons from  $dS'$  fall is  $dS = dS'(v/u)^2$ . The number of photons striking the cornea that would be in  $dS$  if there were no losses is

$$q = \frac{(Lt)(\pi a^2)dS'}{h\nu u^2} = \frac{(Lt)(\pi a^2)dS}{h\nu v^2}. \quad (14.66)$$

The number of photons fluctuates from flash to flash. Therefore we should speak of  $\bar{q}$ , the average number of photons striking the cornea per flash. Of these, only some fraction  $f$  actually reach the retina and are absorbed by a visual pigment molecule. The average number absorbed is

$$m = f\bar{q}. \quad (14.67)$$

Let us next postulate that some minimum number of quanta  $n$  must be absorbed during the flash in order for the subject to see it. If the average number absorbed per flash is  $m$ , there will sometimes be more and sometimes less than  $n$  photons absorbed per flash. The probability of absorbing  $x$  photons per flash is given by the Poisson distribution  $P(x; m)$  (Appendix J). The probability of seeing the flash is the probability that  $x$  is greater than

or equal to  $n$  :

$$\begin{aligned} P(\text{seeing}) &= \sum_{x=n}^{\infty} P(x; m) = 1 - \sum_{x=0}^{n-1} P(x; m) \\ &= 1 - e^{-m} \left( 1 + m + \frac{m^2}{2!} + \cdots + \frac{m^{n-1}}{(n-1)!} \right). \end{aligned} \quad (14.68)$$

This function is plotted in Fig. 14.44 as a function of  $m$  for various values of  $n$ , with both a linear and a logarithmic scale for  $m$ .

Hecht *et al.* used an ingenious method to determine  $n$ . They plotted their data vs. the logarithm of  $\bar{q}$ . Since  $m = f\bar{q}$ ,  $\log m = \log f + \log \bar{q}$ ; different values of  $f$  correspond to shifting the curve along the axis. They then compared the experimental data to the various theoretical curves for the probability of seeing a flash, plotted against  $\log m$ . Sliding the paper containing the data along the  $\log m$  axis is equivalent to trying different values of  $f$ . The data in Fig. 14.43 are shown along with the curves for  $n = 5, 7,$  and  $9$ . For these data,  $n = 7$  gives the best fit. From Fig. 14.43, a 55% chance of detecting the flash corresponds to 100 photons for  $\bar{q}$  while being consistent with  $m = 7$ . Therefore,  $f = 0.07$ .

Hecht, Schlaer, and Pirenne deduced that about seven photons must be absorbed by the rods in the area of integration shown in Fig. 14.42 within 0.1 s in order for the brain to detect the flash of light. Their data were

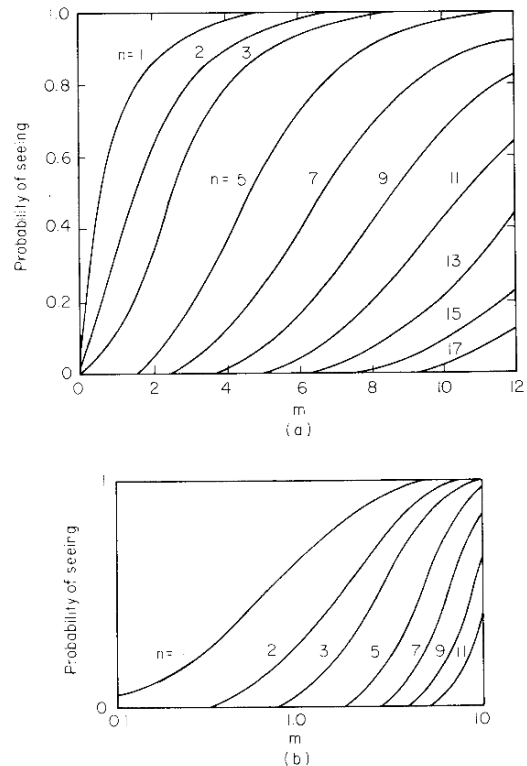


FIGURE 14.44. The probability of seeing a flash, plotted vs (a)  $m$ ; (b)  $\log m$ .

consistent with the hypothesis that the photons arrived at random, with the actual number in each flash obeying a Poisson distribution. Later work by Sakitt (1972) is consistent with the rods counting individual photons, with false positives produced by thermal noise within the retina [Barlow (1956)].

The phototransduction mechanism is quite complicated. Rieke and Baylor (1998) reviewed the detection of photons by rod cells. When stimulated with dim light pulses, the rod cell responds to each flash consistent with the absorption of 0, 1 or 2 photons. The rods have a dark current that is reduced when light falls on them. In other words, the light hyperpolarizes the cell. This lowers the rate of release of a neurotransmitter, cyclic GMP. The review discusses what is known about the chemical transduction process.

If the light intensity is increased,  $m$  increases. There will be shot-noise fluctuations with a standard deviation equal to  $m^{1/2}$ , and the eye should be unable to detect brightness changes smaller than this. Measurements by H. B. Barlow in 1957 showed that as long as short flashes spanning only one visual field are used, the minimum detectable intensity depends on the square root of the light intensity. This statistical limit to detecting intensity changes is a lower limit; for larger sources and longer exposure times the minimum detectable brightness change is larger and is more nearly proportional to the intensity than to the square root of the intensity [Rose (1973)].

### Symbols Used in Chapter 14

Symbol	Use	Units	First used on page
$a$	Radius	m	367
$c$	Speed of light in a vacuum	$m\ s^{-1}$	359
$c_n$	Speed of light in a medium	$m\ s^{-1}$	359
$e$	Charge on an electron	C	361
$f$	Focal length	m	388
$f$	Fraction of photons reaching retina		391
$g$	Scattering anisotropy factor		367
$h$	Planck's constant	J s	360
$h, h'$	Image height, object height	m	388
$\hbar$	Planck's constant divided by $2\pi$	J s	360
$i$	Label of energy level		361
$j$	Total angular momentum quantum number		361
$j_H$	Energy transport in heat flow	$W\ m^{-2}$	382
$k$	Spring constant	$N\ m^{-1}$	363
$k_B$	Boltzmann constant	$J\ K^{-1}$	372
$l$	Orbital angular momentum quantum number		361
$m$	Mass	kg	362
$m$	Average number		391
$m_e$	Mass of electron	kg	361
$m_i$	Mass of $i$ th particle	kg	363
$m_j, m_l, m_s$	$z$ quantum number for angular momentum		361

$n$	Index of refraction		359
$n$	Principal quantum number		361
$\bar{n}$	Average number of photons that interact		365
$n$	Minimum number of photons to trigger a response		391
$p$	Probability		366
$q$	Electric charge	C	360
$q$	Number of photons		391
$\bar{q}$	Average value of $q$		391
$r$	Rotational quantum number		363
$r, \mathbf{r}$	Coordinate	m	362
$s$	Spin quantum number		361
$s$	Source term in diffusion equation	$m^{-3}\ s^{-1}$	367
$t$	Time	s	360
$\mathbf{v}$	Velocity	$m\ s^{-1}$	360
$v$	Vibrational quantum number		364
$u, v$	Object and image distances	m	388
$w_{tot}$	Net power radiated	W	376
$x, z$	Distance	m	360
$z_0$	Depth of first scattering	m	369
$A$	Amplitude of wave		370
$A$	Molar mass	kg	366
$\mathbf{B}$	Magnetic field	T	360
$C$	Concentration	$m^{-3}$	367
$C_b, C_t$	Heat capacity of blood, tissue	$J\ kg^{-1}\ K^{-1}$	382
$D$	Diffusion constant	$m^2\ s^{-1}$	367
$D'$	Photon diffusion constant	m	367
$D$	Thermal diffusion constant	$m^2\ s^{-1}$	382
$\mathbf{E}$	Electric field	$V\ m^{-1}$	360
$E$	Energy	J	360
$E_p$	Potential energy	J	363
$E_r$	Rotational energy	J	363
$E_v$	Vibrational energy	J	364
$E$	Irradiance	$W\ m^{-2}$	386
$F, \mathbf{F}$	Force	N	360
$F$	Converging power of a lens	diopeter ( $m^{-1}$ )	389
$I$	Moment of inertia	$kg\ m^2$	363
$K$	Thermal conductivity	$W\ K^{-1}\ m^{-1}$	382
$K_m$	Luminous efficiency, photopic	$lm\ W^{-1}$	387
$K'_m$	Luminous efficiency, scotopic	$lm\ W^{-1}$	387
$L$	Angular momentum	$kg\ m^2\ s^{-1}$	363
$L$	Radiance	$W\ m^{-2}\ sr^{-1}$	386
$N$	Number of photons		365
$N_a$	Number absorbed		365
$N_s$	Number scattered		365
$N_A$	Avogadro's number		366
$N_T$	Number of target entities per unit area along beam	$m^{-2}$	365
$P$	Probability		372
$P$	Tissue perfusion	$m^3\ kg^{-1}\ s^{-1}$	382
$P$	Radiant power	W	383
$P_v$	Luminous flux	lm	387
$Q$	Rate of production	$m^{-3}\ s^{-1}$	367
$R, \mathbf{R}$	Coordinate of atom, distance	m	362
$R_\lambda$	Radiant energy per unit wavelength interval	$J\ m^{-1}$ or J $nm^{-1}$	386
$R$	Reflected fluence rate	$m^2\ s^{-1}$	369
$R$	Radiant energy	J	383
$S, S'$	Surface area	$m^2$	365
$T$	Period	s	360
$T$	Kinetic energy	J	363

Symbol	Use	Units	First used on page
$T, T_s, T_o$	Temperature	K	372
$U$	Object vergence	dioptr ( $m^{-1}$ )	389
$V, \mathbf{V}$	Velocity	$m\ s^{-1}$	363
$V$	Photopic spectral efficiency function		387
$V'$	Scotopic spectral efficiency function		387
$V$	Image vergence	dioptr ( $m^{-1}$ )	389
$W_\lambda$	Blackbody radiation function	$W\ m^{-3}$ or $W\ m^{-2}$ $nm^{-1}$	373
$W_\nu$	Blackbody radiation function	$W\ m^{-2}\ s$	374
$W_r$	Exitance	$W\ m^{-2}$	385
$\alpha$	Angle		388
$\delta_{th}$	Thermal penetration depth	m	383
$\epsilon_0$	Electrical permittivity of empty space	$N^{-1}\ C^2\ m^{-2}$	360
$\epsilon$	Emissivity		373
$\epsilon(\lambda)$	Reference action spectrum		379
$\theta, \phi$	Angles		366
$\varphi$	Particle fluence rate	$m^{-2}\ s^{-1}$	368
$\lambda$	Wavelength	m	360
$\mu$	Total linear attenuation coefficient	$m^{-1}$	365
$\mu_a$	Linear absorption coefficient	$m^{-1}$	365
$\mu_s$	Linear scattering coefficient	$m^{-1}$	365
$\mu'_s$	Reduced linear scattering coefficient	$m^{-1}$	367
$\mu_{eff}$	Effective linear attenuation coefficient	$m^{-1}$	368
$\mu_0$	Magnetic permeability of free space	$N\ s^2\ C^{-2}$	360
$\rho, \rho_b, \rho_t$	Density, density of blood, density of tissue	$kg\ m^{-3}$	366
$\sigma, \sigma_i, \sigma_a, \sigma_s, \sigma_{tot}$	Cross section	$m^2$	366
$\sigma(\theta), d\sigma/d\Omega$	Differential scattering cross section	$m^2\ sr^{-1}$	366
$\sigma_{SB}$	Stefan-Boltzmann constant	$W\ m^{-2}\ K^{-4}$	374
$\sigma_r^2, \sigma_x^2, \sigma_y^2, \sigma_z^2$	Variance for diffusion or heat flow	$m^2$	382
$\nu$	Frequency	$s^{-1}$	360
$\tau_{coh}$	Coherence time	s	370
$\omega$	Angular frequency	(radian) $s^{-1}$	360
$\psi$	Energy fluence rate	$W\ m^{-2}$	382
$\Psi$	Energy fluence	$J\ m^{-2}$	382
$\Phi$	Particle fluence	$m^{-2}$	365
$\Omega$	Solid angle	sr	366

## Problems

### Section 14.1

**Problem 1** The velocity of light  $c$  depends on the parameters  $\epsilon_0$  and  $\mu_0$ . Use dimensional analysis to find what the dependence must be. Insert numerical values to obtain  $c$ .

**Problem 2** An einstein is 1 mol of photons. Derive an expression for the energy in an einstein as a function

of wavelength. Express the answer in kilocalories and the wavelength  $\lambda$  in nanometers.

### Section 14.2

**Problem 3** Use Eq. 14.7 to derive Eq. 14.8.

**Problem 4** (a) Starting with Eq. 14.7, derive a formula for the hydrogen atom spectrum in the form

$$\frac{1}{\lambda} = R \left[ \frac{1}{n^2} - \frac{1}{m^2} \right],$$

where  $n$  and  $m$  are integers.  $R$  is called the Rydberg constant. Find an expression for  $R$  in terms of fundamental constants.

(b) Verify that the wavelengths of the spectral lines  $a$ – $d$  at the top of Fig. 14.3 are consistent with the energy transitions shown at the bottom of the figure.

### Section 14.3

**Problem 5** Estimate  $\hbar^2/2I$  for an HCl molecule. What would the spacing of rotational levels be?

**Problem 6** An inulin molecule has a molecular weight of 4,000 dalton (that is, 1 mol has a mass of 4000 g). Assume that it is spherical with a radius of 1.2 nm. What is the angular frequency  $\omega$  of a photon absorbed when its rotational quantum number changes from 10 to 11? The moment of inertia of a sphere rotating about an axis through its center is  $I = (2/5)mR^2$ .

**Problem 7** The rotational spectrum of HCl contains lines at 60.4, 69.0, 80.4, 96.4, and 120.4  $\mu m$ . What is the moment of inertia of an HCl molecule?

**Problem 8** Consider a combined rotational–vibrational transition for which  $r$  goes from 1 to 0 while  $v$  goes from  $v$  to  $(v-1)$ . Find the frequencies of the photons emitted in terms of the moment of inertia of the molecule  $I$ , the angular frequency of vibration of the atoms in the molecule  $\omega$ , and the quantum number  $v$ .

**Problem 9** A rotating molecule emits photons when the angular momentum changes by 1. Find the ratio of the angular frequency of the photons,  $\omega_{phot}$ , to the angular frequency of rotation of the molecule  $\omega_{rot}$ , as a function of the orbital angular momentum quantum number  $r$ .

### Section 14.4

**Problem 10** A beam with 200 particles per square centimeter passes by an atom. The particles are uniformly and randomly distributed in the area of the beam.

(a) Fifty particles are scattered. What is the total scattering cross section?

(b) Ten particles are scattered in a cone of 0.1 sr solid angle about a particular direction. What is the differential cross section in  $m^2\ sr^{-1}$ ?

**Problem 11** The differential scattering cross section for a beam of x-ray photons of a certain energy from carbon at an angle  $\theta$  is  $50 \times 10^{-30} \text{ m}^2 \text{ sr}^{-1}$ . A beam of  $10^5$  photons strikes a pure carbon target of thickness 0.3 cm. The density of carbon is  $2 \text{ g cm}^{-3}$ , and the atomic weight is 12. The detector is a circle of 1-cm radius located 20 cm from the target. How many scattered photons enter the detector?

**Problem 12** Photochemists often use the extinction coefficient  $e$ , defined by  $\mu_a = eC$ , where  $C$  is the concentration in moles per liter. This assumes the substance being measured is dissolved in a completely transparent solvent.

(a) What are the units of the extinction coefficient?

(b) What is the conversion between the extinction coefficient and the absorption cross section?

**Problem 13** Suppose that the absorption coefficient in some biological substance is  $5 \text{ m}^{-1}$ . Make the very crude assumption that the substance has the density of water and a molecular weight of 18. What is the absorption cross section?

**Problem 14** For blue light ( $\lambda = 470 \text{ nm}$ ), the attenuation coefficient in air is about  $2 \times 10^{-5} \text{ m}^{-1}$ , and the attenuation coefficient in pure water is about  $5 \times 10^{-3} \text{ m}^{-1}$ . Calculate the distance that blue light must pass through air and through water before the intensity is reduced to 1% of the original intensity. Compare these distances to the thickness of the atmosphere and the depth of the ocean. Do you think that aquatic plants can use photosynthesis effectively at the bottom of the ocean? [For more on the differences between the optical properties of air and water, see Denny (1993).]

### Section 14.5

**Problem 15** (a) Find the slope of the  $\log R$  vs.  $t$  in Eq. 14.29. What is its value for large times?

(b) What can be determined from the time when  $R$  has its maximum value? (Hint:  $R$  has a maximum when  $\log R$  has a maximum.)

**Problem 16** The result of one set of infrared measurements in human calf (leg) muscle gave a total scattering coefficient  $\mu_s = 8.3 \text{ cm}^{-1}$  and an absorption  $\mu_a = 0.176 \text{ cm}^{-1}$ .

(a) What fraction of the photons have not scattered in passing through a layer that is  $8 \mu\text{m}$  thick? (This corresponds roughly to the size of a cell.)

(b) On average, how many scattering events take place for each absorption event?

(c) What is the cross section for scattering per molecule? For this estimate, assume the muscle consists entirely of water, with molecular weight 18 and density  $10^3 \text{ kg m}^{-3}$ .

### Section 14.6

**Problem 17** Carry out the averages leading to Eq. 14.30.

**Problem 18** If yellow light from a source has a coherence time of  $10^{-8} \text{ s}$ , how many cycles are there in the wave?

**Problem 19** What coherence time is needed for a spatial resolution of  $1 \mu\text{m}$ ?

**Problem 20** An infrared transition involves an energy of 0.1 eV. What are the corresponding frequency and wavelength? If the Raman effect is observed with light at 550 nm, what will be the frequencies and wavelengths of each Raman line?

**Problem 21** A Raman spectrum has a line at 500 nm with subsidiary lines at 400 and 667 nm. What is the wavelength of the corresponding infrared line?

### Section 14.7

**Problem 22** Sodium is introduced into a flame at 2,500 K. What fraction of the atoms are in their first excited state? In their ground state? (Remember that the characteristic sodium line is yellow.) If the flame temperature changes by 10 K, what is the fractional change in the population of each state? Which method of measuring sodium concentration is more stable to changes in flame temperature: measuring the intensity of an emitted line or measuring the amount of absorption?

**Problem 23** (a) Show that the maximum of the thermal radiation function  $W_\lambda(\lambda, T)$  occurs at a wavelength such that  $e^x(5-x) = 5$ , where  $x = hc/(\lambda_{\max}k_B T)$ . Verify that  $x = 4.9651$  is a solution of this transcendental equation, so that

$$T\lambda_{\max} = \frac{hc}{4.9651k_B}.$$

(b) Similarly, show that

$$\frac{\nu_{\max}}{T} = \frac{2.82144k_B}{h}$$

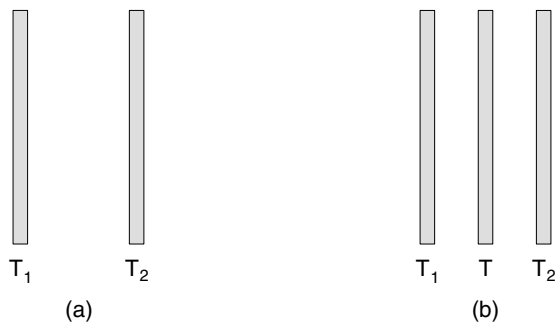
and that  $\lambda_{\max}\nu_{\max} = 0.57c$ .

**Problem 24** Integrate Eq. 14.32 over all wavelengths to obtain the Stephan-Boltzmann law, Eq. 14.33. You will need the integral

$$\int_0^\infty \frac{x^3 dx}{e^x - 1} = \frac{\pi^4}{15}.$$

**Problem 25** Two parallel surfaces of area  $S$  have unit emissivity and are at temperatures  $T_1$  and  $T_2$  [ $T_1 > T_2$ , panel (a)]. They are large compared to their separation, so that all radiation emitted by one surface strikes the other. Assume that radiation is emitted and absorbed only by the

two surfaces that face each other. Let  $P_0$  be the energy lost per unit time by body 1. A new sheet of perfectly absorbing material is introduced between bodies 1 and 2, as shown in panel (b). It comes to equilibrium temperature  $T$ . Let  $P$  be the net energy lost by surface 1 in this case. Find  $P/P_0$  in terms of  $T_1$  and  $T_2$ .



**Problem 26** The sun has a radius of  $6.9 \times 10^8$  m. The earth is  $149.5 \times 10^9$  m from the sun. Treat the sun as a thermal radiator at 5,800 K and calculate the energy from the sun per unit area per unit time striking the upper atmosphere of the earth (the solar constant). State the result in  $W m^{-2}$  and  $cal cm^{-2} min^{-1}$ .

**Problem 27** If all the energy received by the earth from the sun is lost as thermal radiation (a poor assumption because a significant amount is reflected from cloud cover), what is the equilibrium temperature of the earth?

#### Section 14.8

**Problem 28** Show that an approximation to Eq. 14.40 for small temperature differences is  $w_{tot} = SK_{rad}(T - T_s)$ . Deduce the value of  $K_{rad}$  at body temperature. Hint: Factor  $T^4 - T_s^4 = (T - T_s)(\dots)$ . You should get  $K_{rad} = 6.76 W m^{-2} K^{-1}$ .

**Problem 29** What fractional change in  $W_\lambda(\lambda, T)$  for thermal radiation from the human body results when there is a temperature change of 1 K at  $5 \mu m$ ?  $9 \mu m$ ?  $15 \mu m$ ?

#### Section 14.9

**Problem 30** (a) Suppose that the threshold for erythema caused by sunlight with  $\lambda = 300$  nm is  $30 J m^{-2}$ . Does this suggest that the result is thermal (an excessive temperature increase) or something else, like the photoelectric effect or photodissociation? Make some reasonable assumptions to estimate the temperature rise.

(b) The energy in sunlight at all wavelengths reaching the earth is  $2 cal cm^{-2} min^{-1}$ . Suppose that the total body area exposed is  $0.6 m^2$ . What would be the temperature rise per minute for a 60-kg person if there were no heat-loss mechanisms? Compare the rate of energy absorption to the basal metabolic rate, about 100 W.

**Problem 31** Suppose that the energy fluence rate of a parallel beam of ultraviolet light that has passed through

thickness  $x$  of solution is given by  $\psi = \psi_0 e^{-\mu_a x}$ . (Scattering is ignored.) The absorption coefficient  $\mu_a$  is related to the concentration  $C$  (molecules  $cm^{-3}$ ) of the absorbing molecules in the solution by  $\mu_a = aC$ . Biophysicists working with ultraviolet light define the dose rate to be the power absorbed per molecule of absorber. (This is a different definition of dose than is used in Chapter 15.) Calculate the dose rate for a thin layer ( $\mu_a x \ll 1$ ).

**Problem 32** A beam of photons passes through a monatomic gas of molecular weight  $A$  and absorption cross section  $\sigma$ . Ignore scattering. The gas obeys the ideal gas law,  $pV = Nk_B T$ .

(a) Find the attenuation coefficient in terms of  $\sigma$ ,  $p$ , and any other necessary variables.

(b) Generalize the result to a mixture of several gases, each with cross section  $\sigma_i$ , partial pressure  $p_i$ , and  $N_i$  molecules.

**Problem 33** The attenuation of a beam of photons in a gas of pressure  $p$  is given by  $d\Phi = -\Phi(\sigma p/k_B T) dx$ , where  $\sigma$  is the cross section,  $k_B$  the Boltzmann constant,  $T$  the absolute temperature, and  $x$  the path length. Suppose that the pressure is given as a function of altitude  $y$  by  $p = p_0 e^{-mgy/k_B T}$ . What is the total attenuation by the entire atmosphere?

**Problem 34** Consider a beam of photons incident on the atmosphere from directly overhead. The atmosphere contains several species of molecules, each with partial pressure  $p_i$ . The absorption coefficient is  $\mu_a = (1/k_B T) \sum_i \sigma_i p_i$ . If each constituent of the atmosphere varies with height  $y$  as  $p_i(y) = p_{0i} \exp(-m_i g y/k_B T)$ , show that the fluence rate striking the earth is given by an expression of the form  $e^{-\alpha}$  and find  $\alpha$ .

#### Section 14.10

**Problem 35** Consider a tissue with a heat capacity of  $3.6 J kg^{-1} K^{-1}$ , a density of  $1,000 kg m^{-3}$ , and a thermal conductivity of  $0.5 W m^{-1} K^{-1}$ . Assume the heat capacity of blood is the same, and that the tissue perfusion is  $4.17 \times 10^{-6} m^3 kg^{-1} s^{-1}$ . Find the thermal diffusivity, the time for the heat to flow 1 cm, and the thermal penetration depth.

#### Section 14.11

**Problem 36** Suppose that a sphere radiates uniformly from its surface according to Lambert's cosine law:  $L = L_0$ . By considering area  $dS = 2\pi r^2 \sin \theta d\theta$  on the surface of a sphere, find the power radiated per steradian in the direction of the  $z$  axis and the total power radiated.

**Problem 37** Show that the total power per unit area radiated from a surface obeying Lambert's cosine law is  $W_\tau = \pi L_0$ . This quantity is called the exitance.

**Problem 38** How many photons per second correspond to 1 lm at 555 nm for photopic vision? At 510 nm for scotopic vision?

Section 14.12

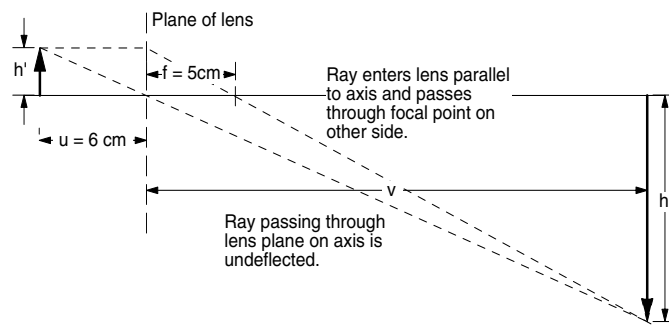
**Problem 39** A person is nearsighted, and the relaxed eye focuses at a distance of 50 cm. What is the strength of the desired corrective lens in diopters?

**Problem 40** What is the distance of closest vision for an average person with normal vision at age 20? Age 40? Age 60?

**Problem 41** A person of age 40 is fitted with bifocals with a +1 diopter strength bifocal lens. What are the closest and farthest distances of focus without the bifocal lens and with it? By the time the person is age 50, what are they with and without the same lens?

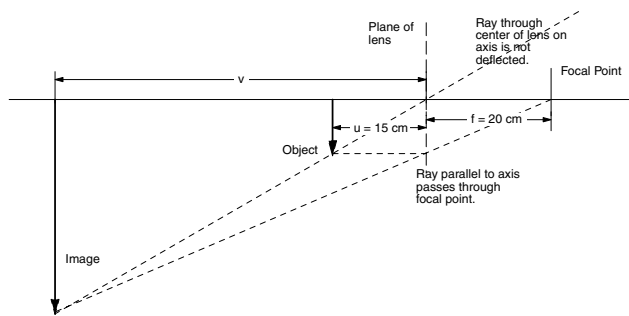
**Problem 42** You can make a rough measurement of your own eye's properties. Tape a piece of paper with some pattern on it on the wall. Cover one eye. Move away from the wall until the pattern starts to blur. Measure the distance to the wall in meters. Calculate the vergence of the object,  $U$ . Assume that the  $F$  of your relaxed eye is 59 diopters. Calculate  $V$  for your eye. Now find the closest distance at which you can see the paper. Calculate the accommodation of your eye.

**Problem 43** An object is placed 6 cm from a converging lens with a 5 cm focal length.



- (a) Use the thin-lens equation (Eq. 14.63) to calculate the image distance.
- (b) The magnification of the image is given by  $m = -u/v$ . (A negative magnification implies an inverted image.) What is the magnification for the image in part (a)? A value  $|m| > 1$  implies a “magnified” image. This is how a slide projector works.

**Problem 44** An object is placed 15 cm from a converging lens with a focal length of 20 cm.



- (a) Use the thin-lens equation (Eq. 14.63) to calculate the image distance. Your value should be negative, corresponding to a “virtual image.”
- (b) The magnification of the image is again given by  $m = -u/v$ . What is the magnification for the image in part (a)? This is how a magnifying glass works.

**Problem 45** Combine the results of Problems 43 and 44. Consider two lenses, the first with focal length 5 cm and the second with focal length 20 cm, separated by 45 cm. The object is 6 cm in front of the first lens. The image from the first lens is the object for the second.

- (a) Calculate the image distance and magnification of the image created by the first lens (called the objective).
- (b) Use the first image as the object for the second lens (called the eyepiece), and calculate the image distance and magnification of the second image.
- (c) The total magnification is the product of the magnifications of the objective and eyepiece. What is the total magnification? This is how the compound microscope works. The objective lens acts like a slide projector, and the eyepiece acts like a magnifying glass. Very large total magnifications can be obtained when the object is just to the left of the focal point of the objective, and the first image is just to the right of the focal point of the eyepiece.

**Problem 46** Snell's law,  $n_1 \sin \theta_1 = n_2 \sin \theta_2$ , gives an interesting result if light passes from a medium with a higher index of refraction to one with a lower index of refraction,  $n_1 > n_2$ . Assume light passes from glass ( $n_1 = 1.5$ ) to air ( $n_2 = 1.0$ ).

- (a) If  $\theta_1$  is  $30^\circ$ , what is  $\theta_2$ ?
- (b) If  $\theta_1$  is  $40^\circ$ , what is  $\theta_2$ ?
- (c) If  $\theta_1$  is  $50^\circ$ , what is  $\theta_2$ ?

This is really a trick question, because for  $\theta_1$  greater than some critical angle,  $\theta_c$ ,  $\theta_2$  exceeds  $90^\circ$ , and light cannot pass into the second medium. Instead all the light is reflected and remains within the first medium.

- (d) Calculate the critical angle for total internal reflection from glass to air.

Total internal reflection allows thin glass fibers to act as fiberoptic “light pipes,” which can be used to transmit signals. Bundles of such optical fibers are used in endoscopes to see inside the body.

**Problem 47** Table 14.7 shows that most of the converging power of the eye occurs at the air-cornea interface. When a person is under water, this must be supplied by

the water-cornea surface. The index of refraction of the cornea is closer to that of water than to that of air. What are the implications for seeing under water? What are the implications for the vision of aquatic animals? [For more information on the difference between the eyes of aquatic and terrestrial animals, see Denny (1993)].

### Section 14.13

**Problem 48** How many photons per 0.1 s enter the eye from a 100-W light bulb 1,000 ft away? Assume the pupil is 6 mm in diameter. How far away can a 100-W bulb be seen if there is no absorption in the atmosphere? Use a luminous efficiency of  $17 \text{ lm W}^{-1}$  and then assume an equivalent light source at 555 nm.

**Problem 49** The table below shows the radiance of some extended sources. Without worrying about obliquity factors (assume that all the light is at normal incidence), calculate the number of photons entering a receptive field of  $0.17^\circ$  diameter when the pupil diameter is 6 mm and the integration time is 0.1 s. Assume a conversion efficiency of  $100 \text{ lm W}^{-1}$  and then assume that all the photons are at 555 nm.

Source	Radiance ( $\text{lm m}^{-2} \text{ sr}^{-1}$ )
White paper in sunlight	25,000
Clear sky	3,200
Surface of the moon	2.900
White paper in moonlight	0.03

**Problem 50** A piece of paper is illuminated by dim light so that its radiance is  $0.01 \text{ lm m}^{-2} \text{ sr}^{-1}$  in the direction of a camera. A camera lens 1 cm in diameter is 0.6 m from the paper. The sheet of paper is  $10 \times 10$  cm. The shutter of the camera is open for 1 ms. Assume all the light is at 555 nm. How many photons from the paper enter the lens of the camera while the shutter is open?

**Problem 51** If three or more photons must be absorbed by a visual receptor field for the observer to see a flash, how often will the flash be seen if the average number of photons absorbed in a receptor field per flash is four?

**Problem 52** Assume that an average of  $d$  photons are detected and that the photons are Poisson distributed. What must  $d$  be to detect a signal that is a 1% change in  $d$ , if the signal-to-noise ratio must be at least 5?

**Problem 53** Suppose that the average number of photons striking a target during an exposure is  $m$ . The probability that  $x$  photons strike during a similar exposure is given by the Poisson distribution. What is the probability that an organism responds to an exposure of radiation in each of the following cases?

(a) The response of the organism requires that a single target within the organism be hit by two or more photons.

(b) The response of the organism requires that two targets within the organism each be struck by one or more photons during the exposure.

## References

- AAPM 57 (1996). *Recommended Nomenclature for Physical Quantities in Medical Applications of Light*. American Association of Physicists in Medicine (AAPM) Report No. 57. College Park, MD.
- Armstrong, B. K., and A. Kricger (1995). Skin cancer. *Dermatolog. Clinics* **13**(3): 583–594.
- Barlow, H. B. (1956). Retinal noise and absolute threshold. *J. Opt. Soc. Am.* **46**: 634–639.
- Barlow, H. B. (1957). Incremental thresholds at low intensities considered as signal/noise discriminations. *J. Physiol.* **136**: 469–488.
- Bergmanson, J. P. G., and P. G. Söderberg (1995). The significance of ultraviolet radiation for eye diseases. A review with comments on the efficacy of UV-blocking contact lenses. *Ophthalm. Physiol. Opt.* **15**(2): 83–91.
- Berne, B. J., and R. Pecora (1976). *Dynamic Light Scattering: With Applications to Chemistry, Biology, and Physics*. New York, Wiley.
- Blume, S. (1993). Social process and the assessment of a new imaging technique. *Intl. J. Technol. Assess. Health Care* **9**(3): 335–345.
- Bouma, B. E., and G. J. Tearney, eds. (2002). *Handbook of Optical Coherence Tomography*. New York, Marcel Dekker.
- Bramson, M. A. (1968). *Infrared Radiation*. New York, Plenum.
- Buka, R. L. (2004). Sunscreens and insect repellents. *Current Opinion in Pediatrics* **16**: 378–384.
- Charman, W. N. (1995). Optics of the eye, Chap. 24 in M. Bass, editor in chief, *Handbook of Optics*, 2nd ed. Sponsored by the Optical Society of America. New York, McGraw-Hill.
- Cornsweet, T. N. (1970). *Visual Perception*. New York, Academic.
- Cotton, P. (1992). AMA's council on scientific affairs to take a fresh look at thermography. *J. Am. Med. Assoc.* **267**(14): 1885–1887.
- De Boer, J. F., S. M. Srinivas, J. S. Nelson, T. E. Milner, and M. G. Ducros (2002). Polarization-sensitive optical coherence tomography. In Bouma, B. E. and G. J. Tearney, eds. *Handbook of Optical Coherence Tomography*. New York, Marcel Dekker, pp. 237–298.
- Denny, M. W. (1993). *Air and Water: The Biology and Physics of Life's Media*. Princeton, NJ, Princeton University Press.
- Diem, M. (1993). *Introduction to Modern Vibrational Spectroscopy*. New York, Wiley.
- Diffey, B. L. (1991). Solar ultraviolet radiation effects on biological systems. *Phys. Med. Biol.* **36**(3): 299–328.
- Diffey, B. L., and J. Cameron (1984). A microcomputer program to predict sunburn exposure. *Med. Phys.* **11**(6): 869–870.
- Diffey, B. L., and J. Cheeseman (1992). Sun protection with hats. *Brit. J. Dermatol.* **127**(1): 10–12.



- Diffey, B. L., and P. M. Farr (1991). Quantitative aspects of ultraviolet erythema. *Clin. Phys. Physiol. Meas.* **12**(4): 311–325.
- Duderstadt, J. J., and L. J. Hamilton (1976). *Nuclear Reactor Analysis*. New York, Wiley.
- Esenaliev, R. O., K. V. Larin, I. V. Larina, and M. Motamedi (2001). Noninvasive monitoring of glucose concentration with optical coherence tomography. *Optics Lett.* **26**(13): 992–994.
- Farmer, J. (1997). Blood oxygen measurement. Chap. 3 in J. Webster. *The Design of Pulse Oximeters*. Bristol, Institute of Physics Publishers.
- Fitzgerald, A. J., E. Berry, N. N. Zinonev, G. C. Walker, M. A. Smith and J. M. Chamberlain (2002). An introduction to medical imaging with coherent terahertz frequency radiation. *Phys. Med. Biol.* **47**: R67–R84.
- Fraden, J. (1991). Noncontact temperature measurements in medicine. In D. L. Wise, ed. *Bioinstrumentation and Biosensors*. New York, Dekker, pp. 511–549.
- Gasiorowicz, S. (1974). *Quantum Physics*. New York, Wiley.
- Giasson, C. J., N-M. Quesnel, and H. Boisjoly (2005). The ABCs of ultraviolet-blocking contact lenses: An ocular panacea for ozone loss? *International Ophthalmologic Clinics* **45**(1): 117–139.
- Gilchrist, B. A., M. S. Eller, A. C. Geller and M. Yaar (1999). The pathogenesis of melanoma induced by ultraviolet radiation. *New Engl. J. Med.* **340**(17): 1341–1348.
- Grievenkamp, J. E., J. Schwiegerling, J. M. Miller, and M. D. Mellinger (1995). Visual acuity modeling using optical raytracing of schematic eyes. *Am. J. Ophthalmol.* **120**(2): 227–240.
- Grossweiner, L. (1994). *The Science of Phototherapy*. Boca Raton, FL, CRC Press.
- Haddad, J. G. (1992). Vitamin D—Solar rays, the milky way, or both (Editorial). *New Engl. J. Med.* **326**(18): 1213–1215.
- Halliday, D., R. Resnick, and K. S. Krane (1992). *Fundamentals of Physics*, 4th ed. New York, Wiley.
- Hanlon, E. B., R. Manoharan, T-W. Koo, K. E. Shafer, J. T. Motz, M. Fitzmaurice, J. R. Kramer, I. Itzkan, R. R. Dasari, and M. S. Feld (2000). Prospects for *in vivo* Raman spectroscopy. *Phys. Med. Biol.* **45**: R1–R59.
- Heald, M. A. (2003). Where is the “Wien peak”? *Amer. J. Phys.* **71** (12): 1322–1323.
- Hecht, S., S. Schlaer, and M. H. Pirenne (1942). Energy, quanta, and vision. *J. Gen. Physiol.* **25**: 819–840.
- Hielscher, A., S. L. Jacques, L. Wang, and F. K. Titte (1995). The influence of boundary conditions on the accuracy of diffusion theory in time-resolved reflectance spectroscopy of biological tissues. *Phys. Med. Biol.* **40**: 1957–1975.
- Huang, D., E. A. Swanson, C. P. Lin, J. S. Schuman, W. G. Stinson, W. Chang, M. R. Hee, T. Flotte, K. Gregory, C. A. Puliafito, and J. G. Fujimoto (1991). Optical coherence tomography. *Science* **254**: 1178–1181.
- Kevan, P. G., L. Chittka, and A. G. Dyer (2001). Limits to the salience of ultraviolet: Lessons from colour vision in bees and birds. *J. Exp. Biol.* **204**: 2571–2580.
- Kimlin, M. G., and A. V. Parisi (1999). Radiation penetrating vehicle glass: a field-based comparative study. *Phys. Med. Biol.* **44**: 917–926.
- Kligman, L. H. (1989). Photoaging: manifestations, prevention, and treatment. *Clin. Geriatr. Med.* **5**: 235–251.
- Knobler, E., I. Warmuth, C. Cocco, B. Miller, and J. Mackay (2002). Extracorporeal immunotherapy: the Columbia-Presbyterian experience. *Photodermatology, Photoimmunology and Photomedicine* **18** (5): 232–237.
- Kripke, M. L. (2003). The ABCs of sunscreen protective factors [Comment]. *J. Invest. Dermatol.* **121**(1): vii–viii.
- Lever, L. R., and C. M. Lawrence (1995). Non-melanoma skin cancer associated with the use of a tanning bed. *New Engl. J. Med.* **332**(21): 1450–1451.
- Liu, H., D. A. Boas, Y. Zhang, A. G. Yodh, and B. Chance (1995). Determination of optical properties and blood oxygenation in tissue using continuous NIR light. *Phys. Med. Biol.* **40**: 1983–1993.
- MacNeill, B. D., H. C. Lowe, M. Takano, V. Fuster and I-K. Jang (2003). Intravascular modalities for detection of vulnerable plaque. *Arterioscler. Thromb. Vasc. Biol.* **23**: 1333–1342.
- Madronich, S. (1993). The atmosphere and UV-B radiation at ground level. In A. R. Young *et al.*, eds. *Environmental UV Photobiology*. New York, Plenum, pp. 1–39.
- McDonagh, A. F. (1985). Light effects on transport and excretion of bilirubin in newborns. In R. J. Wortman, M. J. Baum, and T. J. Potts, Jr., eds. *The Medical and Biological Effects of Light*. *Ann. N.Y. Acad. Sci.* **453**: 65–72.
- Messina, C., F. Locatelli, E. Lanino, C. Uderzo, G. Zaccarello, S. Cesaro, M. Pillon, C. Perotti, C. Del Fante, M. Faraci, L. Rivabella, E. Calore, P. De Stefano, M. Zecca, G. Giorgiani, A. Bruglio, A. Balduzzi, G. Dini, L. Zanesco and R. Dall’Amico (2003). Extracorporeal phototherapy for paediatric patients with graft-versus-host disease after haematopoietic stem cell transplantation. *Brit. J. Haematology.* **122** (1):118–127.
- Milonni, P. W. (1996). Answer to question on Snell’s law in quantum mechanics. *Am. J. Phys.* **64**(7): 842.
- Moseley, H. (1994). Ultraviolet and laser radiation safety. *Phys. Med. Biol.* **39**: 1765–1799.
- Moyal, D. D., and A. M. Fourtanier (2002). Effects of UVA radiation on an established immune response in humans and sunscreen efficacy. *Exp. Dermatol.* **11** (Suppl. 1): 28–32.
- Murphy, M. R., and R. G. Oellrich (1990). A new method of phototherapy: Nursing perspectives. *J. Perinatol.* **10**(3): 249–251.
- Nickell, S., M. Hermann, M. Essenpreis, T. J. Farrell, U. Krämer, and M. S. Patterson (2000). Anisotropy of

- light propagation in human skin. *Phys. Med. Biol.* **45**: 2873–2886.
- Nijsten, T. E. and R. S. Stern (2003). The increased risk of skin cancer is persistent after discontinuation of psoralen+ultraviolet A: a cohort study. *J. Invest. Dermatol.* **121** (2): 252–258.
- Patterson, M. S., B. Chance, and B. C. Wilson (1989). Time resolved reflectance and transmittance for the non-invasive measurement of tissue optical properties. *Appl. Opt.* **28**(12): 2331–2336.
- Paul, C. F. (2003). Treating severe psoriasis: How to navigate safely between Scylla and Charybdis? [Comment] *J. Invest. Dermatol.* **121** (2): ix–x.
- Pirenne, M. H. (1962). Chaps. 5 and 6 of H. Davidson, ed., *The Eye*. Vol. 2. *The Visual Process*. New York, Academic.
- Pogue, B. W., and M. S. Patterson (1994). Frequency-domain optical absorption spectroscopy of finite tissue volumes using diffusion theory. *Phys. Med. Biol.* **39**: 1157–1180.
- Poon, T. S. C., R. StC. Barneston and G. M. Halliday (2003). Prevention of immunosuppression by sunscreen in humans is unrelated to protection from erythema and dependent on protection from ultraviolet A in the face of constant ultraviolet B protection. *J. Invest. Dermatol.* **121**(1): 184–190.
- Rieke, F., and D. A. Baylor (1998). Single-photon detection by rod cells of the retina. *Revs. Mod. Phys.* **70**(3): 1027–1036.
- Rose, A. (1973). *Vision: Human and Electronic*. New York, Plenum.
- Saint-Jalmes, H., M. Lebec, E. Beaufrepaire, A. Dubois and A. C. Boccara (2002). Full-field optical coherence microscopy. In Bouma, B. E. and G. J. Tearney, eds. *Handbook of Optical Coherence Tomography*. New York, Marcel Dekker, pp. 299–333.
- Sakitt, B. (1972). Counting every quantum. *J. Physiol. (London)* **223**: 131–150.
- Schaefer, B. E. (1993). Suntan and the ozone layer. *Sky and Telescope* **86**(1): 83–86, July.
- Schmitt, J. M. (1999). Optical Coherence Tomography (OCT): A review. *IEEE J. Select. Topics Quantum Electron.* **5**: 1205–1215.
- Sevick, E. M., B. Chance, J. Leigh, S. Nioka, and M. Maris (1991). Quantitation of time- and frequency-resolved optical spectra for the determination of tissue oxygenation. *Analyt. Biochem.* **195**: 330–351.
- Sherwood, B. A. (1996). Answer to question on Snell's law in quantum mechanics. *Am. J. Phys.* **64**(7): 840–842.
- Smye, S. W., J. M. Chamberlain, A. J. Fitzgerald and E. Berry (2001). The interaction between terahertz radiation and biological tissue. *Phys. Med. Biol.* **46**: R101–R112.
- Soffer, B. H., and D. K. Lynch (1999). Some paradoxes, errors, and resolutions concerning spectral organization of human vision. *Amer. J. Phys.* **67** (11):946–953.
- Stark, L. C., and G. C. Theodoris (1973). Information theory in physiology, in J. H. U. Brown and D. S. Gans, eds. *Engineering Principles in Physiology*, New York, Academic, Vol. 1, pp. 13–31.
- Steketee, J. (1973). Spectral emissivity of skin and pericardium. *Phys. Med. Biol.* **18**: 686–694.
- Studniberg, H. M., and P. Weller (1993). PUVA, UVB, psoriasis, and nonmelanoma skin cancer. *J. Am. Acad. Dermatol.* **29**: 1013–1022.
- Verheye, S., L. Diamantopoulos, P. W. Serruys, and G. Van Langenhove (2002). Intravascular imaging of the atherosclerotic plaque: Spotlight on temperature measurement. *J. Cardiovasc. Risk* **9**: 247–254.
- Webster, J. (1997). *The Design of Pulse Oximeters*. Bristol, Institute of Physics Publishers.
- Wieben, O. (1997). Light absorbance in pulse oximetry. Chap. 4 in J. Webster. *The Design of Pulse Oximeters*. Bristol, Institute of Physics Publishers.
- Yamashita, Y., A. Maki, and H. Koizumi (2001). Wavelength dependence of the precision of noninvasive optical measurement of oxy-, deoxy-, and total hemoglobin concentration. *Med. Phys.* **28**(6): 1108–1114.
- Yasuno, Y., S. Makita, Y. Sutoh, M. Itoh, and T. Yatagai (2002). Birefringence imaging of human skin by polarization-sensitive spectral interferometric optical coherence tomography. *Optics Lett.* **27**(20): 1803–1805.
- Yazdanfar, S., A. M. Rollins and J. A. Izatt (2000). Imaging and velocimetry of the human retinal circulation with color Doppler optical coherence tomography. *Optics Lett.* **25**(19): 1448–1450.
- Yodh, A., and B. Chance (1995). Spectroscopy and imaging with diffusing light. *Phys. Today*. March: 34–40.
- Zalewski, E. F. (1995). Radiometry and photometry, Chap. 24 of M. Bass, editor in chief, *Handbook of Optics*, 2nd ed. Sponsored by the Optical Society of America. New York, McGraw-Hill.
- Zhang, X-C. (2002). Terahertz wave imaging: horizons and hurdles. *Phys. Med. Biol.* **47**: 3667–3677.

# Interaction of Photons and Charged Particles with Matter

An x-ray image records variations in the passage of x rays through the body because of scattering and absorption. A side effect of making the image is the absorption of some x-ray energy by the body. Radiation therapy depends on the absorption of large amounts of x-ray energy by a tumor. Diagnostic procedures in nuclear medicine (Chapter 17) introduce a small amount of radioactive substance in the body. Radiation from the radioactive nuclei is then detected. Some of the energy from the photons or charged particles emitted by the radioactive nucleus is absorbed in the body. To describe all of these effects requires that we understand the interaction of photons and charged particles with matter.

In Chapter 14 we discussed the transport of photons of ultraviolet and lower energy—a few electron volts or less. Now we will discuss the transport of photons of much higher energy—10 keV and above. We will also discuss the movement through matter of charged particles such as electrons, protons, and heavier ions. These high energy photons and charged particles are called *ionizing radiation*, because they produce ionization in the material through which they pass. The distinction is blurred, since ultraviolet light can also ionize.

A charged particle moving through matter loses energy by local ionization, disruption of chemical bonds, and increasing the energy of atoms it passes near. It is said to be *directly ionizing*. Photons passing through matter transfer energy to charged particles, which in turn affect the material. These photons are *indirectly ionizing*.

Photons and charged particles interact primarily with the electrons in atoms. Section 15.1 describes the energy levels of atomic electrons. Section 15.2 describes the various processes by which photons interact; these are elaborated in the next four sections, leading in Sec. 15.7 to the concept of a photon attenuation coefficient.

Attenuation is extended to compounds and mixtures in Sec. 15.8.

An atom is often left in an excited state by a photon interaction. The mechanisms by which it loses energy are covered in Sec. 15.9. The energy that is transferred to electrons can cause radiation damage. The transfer process is described in Secs. 15.10 and 15.15–15.17.

Section 15.11 introduces the charged-particle stopping power, which is the rate of energy loss by a charged particle as it passes through material. Extensions of this concept, which are important in radiation damage, are the linear energy transfer and the restricted collision stopping power, introduced in Sec. 15.12. A charged particle travels a certain distance through material as it loses its kinetic energy. This leads in Sec. 15.13 to the concept of range. Charged particles also lose energy by emitting photons. The radiation yield is also discussed in Sec. 15.13. Insight into the process of radiation damage is gained by examining track structure in Sec. 15.14.

The last three sections return to the movement of energy from a photon beam to matter. The discussion requires an understanding of both photon interactions and charged-particle stopping power and range.

## 15.1 Atomic Energy Levels and X-ray Absorption

A neutral atom has a nuclear charge  $+Ze$  surrounded by a cloud of  $Z$  electrons. As was described in Chapter 14, each electron has a definite energy, characterized by a set of five quantum numbers:  $n, l, s$  (which is always  $\frac{1}{2}$ ),  $j$ , and  $m_j$ . (Instead of  $j$  and  $m_j$ , the numbers  $m_l$  and  $m_s$

TABLE 15.1. Energy levels for electrons in a tungsten atom ( $Z = 74$ )

$n$	$l$	$j$	Number of electrons	X-ray label	Energy (eV)
1	0	$\frac{1}{2}$	2	$K$	-69,525
2	0	$\frac{1}{2}$	2	$L_I$	-12,100
	1	$\frac{1}{2}$	2	$L_{II}$	-11,544
	1	$\frac{3}{2}$	4	$L_{III}$	-10,207
3	0	$\frac{1}{2}$	2	$M_I$	-2,819
	1	$\frac{1}{2}$	2	$M_{II}$	-2,575
	1	$\frac{3}{2}$	4	$M_{III}$	-2,281
	2	$\frac{3}{2}$	4	$M_{IV}$	-1,872
	2	$\frac{5}{2}$	6	$M_V$	-1,809
4	0	$\frac{1}{2}$	2	$N_I$	-595
	1	$\frac{1}{2}$	2	$N_{II}$	-492
	1	$\frac{3}{2}$	4	$N_{III}$	-425
	2	$\frac{3}{2}$	4	$N_{IV}$	-259
	2	$\frac{5}{2}$	6	$N_V$	-245
	3	$\frac{5}{2}, \frac{7}{2}$	14	$N_{VI, VII}$	-35
5	0	$\frac{1}{2}$	2	$O_I$	-77
	1	$\frac{1}{2}$	2	$O_{II}$	-47
	1	$\frac{3}{2}$	4	$O_{III}$	-36
	2	$\frac{3}{2}, \frac{5}{2}$	4	$O_{IV, V}$	-6
6		2	$P_I$		

are sometimes used.) There are restrictions on the values of the numbers:

- $n = 1, 2, 3, \dots$  the principal quantum number
- $l = 0, 1, 2, \dots, n - 1$  the orbital angular momentum quantum number
- $s = \frac{1}{2}$  the spin quantum number
- $j = l - \frac{1}{2}$  or  $l + \frac{1}{2}$ , except that the total angular momentum quantum number
- $j = \frac{1}{2}$  when  $l = 0$
- $m_j = -j, -(j - 1), \dots, (j - 1), j$  "z component" of the total angular momentum

(15.1)

The dependence of the electron energy on  $m_j$  is very slight, unless the atom is in a magnetic field.

In each atom, only one electron can have a particular set of values of the quantum numbers. Since the atoms we are considering are not in a magnetic field, electrons with different values of  $m_j$  but the same values for  $n, l,$  and  $j$  will all be assumed to have the same energy. Electrons with different values of  $n$  are said to be in different shells. The shell for  $n = 1$  is called the  $K$  shell; those for  $n = 2, 3, 4, \dots$  are labeled  $L, M, N, \dots$ . Different values

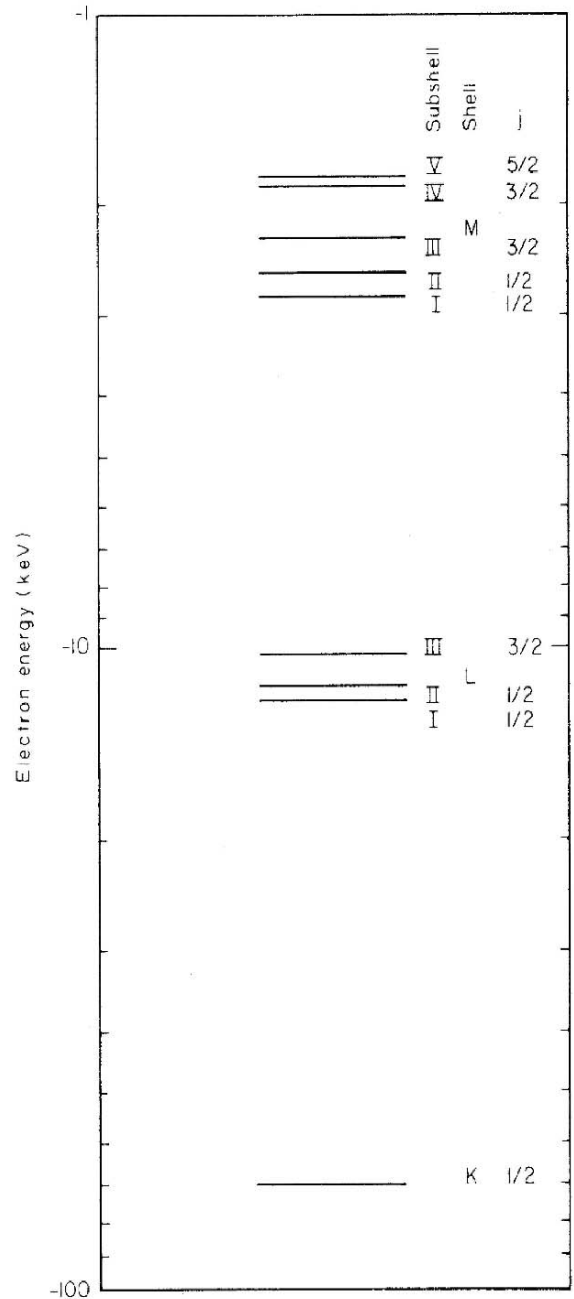


FIGURE 15.1. Energy levels for electrons in tungsten.

of  $l$  and  $j$  for a fixed value of  $n$  are called subshells, denoted by roman numeral subscripts on the shell labels. The maximum number of electrons that can be placed in a subshell is  $2(2l + 1)$ . Each electron bound to the atom has a certain negative energy, with zero energy defined when the electron is just unbound, that is, at rest infinitely far away from the atom. Table 15.1 lists the energy levels of electrons in tungsten. Some of the levels in Table 15.1 are shown in Fig. 15.1. The scale is logarithmic. Since the energies are negative, the magnitude increases in the downward direction. Tables of atomic energy levels can be

found many places, including [www.csrii.iit.edu/periodic-table.html](http://www.csrii.iit.edu/periodic-table.html).

The *ionization energy* is the energy required to remove the least-tightly-bound electron from the atom. For tungsten, it is about 6 eV. If one plots the ionization energy or the chemical valence of atoms as a function of  $Z$ , one finds abrupt changes when the last electron's value of  $n$  or  $l$  changes.

In contrast to this behavior of the outer electrons, the energy of an inner electron with fixed values of  $n$  and  $l$  varies smoothly with  $Z$ . To a first approximation, the two innermost  $K$  electrons are attracted to the nuclear charge  $Ze$ . The energy of the level can be estimated using Eq. 14.8 for hydrogen, with the nuclear charge  $e$  replaced by  $Ze$ :

$$E_K = -\frac{13.6Z^2}{1^2}. \quad (15.2)$$

The two electrons also repel each other and experience some repulsion by electrons in other shells. This effect is called *charge screening*. Experiment (measuring values of  $E_K$ ) shows that the effective charge seen by a  $K$  electron is approximately  $Z_{\text{eff}} \approx Z - 3$  for heavy elements, so that for  $K$  electrons ( $n = 1$ ),

$$E_K \approx -13.6(Z - 3)^2 \quad (\text{in eV}). \quad (15.3)$$

The screening is greater for electrons with larger values of  $n$ , which may be thought of as being in "orbits" of larger radius.

## 15.2 Photon Interactions

There are a number of different ways in which a photon can interact with an atom. The more important ones will be considered here. It is convenient to adopt a notation  $(\gamma, bc)$  where  $\gamma$  represents the incident photon and  $b$  and  $c$  are the results of the interaction. For example,  $(\gamma, \gamma)$  represents initial and final photons having the same energy; in a  $(\gamma, e)$  interaction the photon is absorbed and only an electron emerges. This section describes the common interactions and the energy balance for each case.

### 15.2.1 Photoelectric Effect

In the *photoelectric effect*,  $(\gamma, e)$ , the photon is absorbed by the atom and a single electron is ejected. The initial photon energy  $h\nu_0$  is equal to the final energy. The recoil kinetic energy of the atom is very small because its mass is large, so the final energy is the kinetic energy of the electron,  $T_{\text{el}}$ , plus the excitation energy of the atom. The excitation energy is equal to the binding energy of the ejected electron,  $B$ . The energy balance is therefore

$$h\nu_0 = T_{\text{el}} + B. \quad (15.4)$$

The atom subsequently loses its excitation energy. The deexcitation process described in Sec. 15.9 involves the

emission of additional photons or electrons. The photoelectric cross section is  $\tau$ .

### 15.2.2 Compton and Incoherent Scattering

In *Compton scattering*,  $(\gamma, \gamma'e)$ , the original photon disappears and a photon of lower energy and an electron emerge. The statement of energy conservation is

$$h\nu_0 = h\nu + T_{\text{el}} + B.$$

Usually the photon energy is high enough so that  $B$  can be neglected, and this is written as

$$h\nu_0 = h\nu + T_{\text{el}}. \quad (15.5)$$

The Compton cross section for scattering from a single electron is  $\sigma_C$ . *Incoherent scattering* is Compton scattering from all the electrons in the atom, with cross section  $\sigma_{\text{incoh}}$ .

### 15.2.3 Coherent Scattering

*Coherent scattering* is a  $(\gamma, \gamma)$  process in which the photon is elastically scattered from the entire atom. That is, the internal energy of the atom does not change. The recoil kinetic energy of the atom is very small (see Problem 6), and it is a good approximation to say that the energy of the incident photon equals the energy of the scattered photon:

$$h\nu_0 = h\nu. \quad (15.6)$$

The cross section for coherent scattering is  $\sigma_{\text{coh}}$ .

### 15.2.4 Inelastic Scattering

It is also possible for the final photon to have a different energy from the initial photon  $(\gamma, \gamma')$  without the emission of an electron. The internal energy of the target atom or molecule increases or decreases by a corresponding amount. Again, the recoil kinetic energy of the atom is negligible. Examples are fluorescence and Raman scattering. In fluorescence, if one waits long enough, additional photons are emitted, in which case the reaction could be denoted as  $(\gamma, \gamma'\gamma'')$ , or  $(\gamma, 2\gamma)$ , or even  $(\gamma, 3\gamma)$ .

### 15.2.5 Pair Production

*Pair production* takes place at high energies. This is a  $(\gamma, e^+e^-)$  reaction. Since it takes energy to create the (negative) electron and the positive electron or *positron*, their rest energies must be included in the energy balance equation:

$$h\nu_0 = T_+ + m_e c^2 + T_- + m_e c^2 = T_+ + T_- + 2m_e c^2. \quad (15.7)$$

The cross section for pair production is  $\kappa$ .

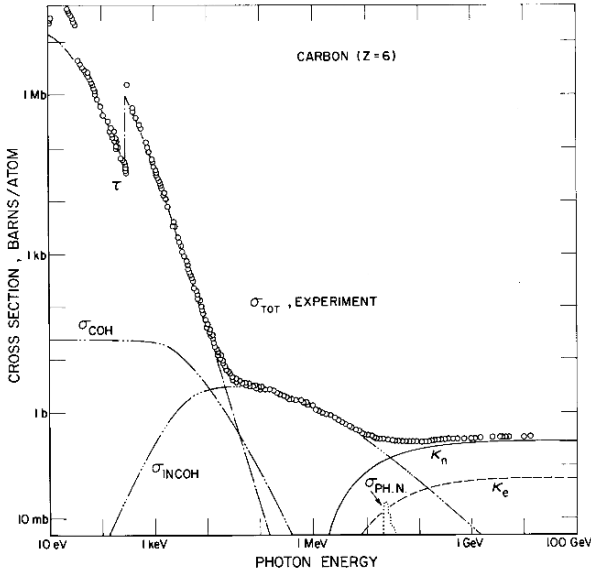


FIGURE 15.2. Total cross section for the interactions of photons with carbon vs. photon energy. The photoelectric cross section is  $\tau$ , the coherent scattering cross section  $\sigma_{\text{coh}}$ , the total Compton cross section  $\sigma_{\text{incoh}}$ , and the nuclear and electronic (triplet) pair production are  $\kappa_n$  and  $\kappa_e$ . The photonic nuclear scattering cross section PHN is also shown. The cross section is given in barns:  $1 \text{ b} = 10^{-28} \text{ m}^2$ . Reprinted with permission from J. H. Hubbell, H. A. Gimm, and I. Øverbø (1980). Pair, triplet and total atomic cross sections (and mass attenuation coefficients) for 1 MeV–100 GeV photons in elements  $Z = 1$  to 100. *J. Phys. Chem. Ref. Data* **9**: 1023–1147. Copyright 1980, American Institute of Physics. Figure courtesy of J. H. Hubbell.

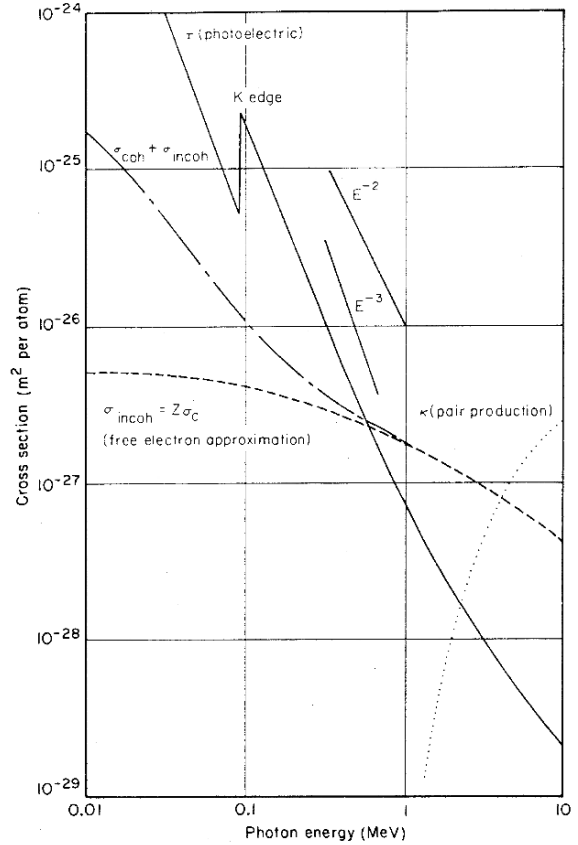


FIGURE 15.3. Cross sections for the photoelectric effect and incoherent and coherent scattering from lead. The binding energies of the  $K$  and  $L$  shells are 0.088 and 0.0152 MeV. Plotted from Table 3.22 of Hubbell (1969).

### 15.2.6 Energy Dependence

Figure 15.2 shows the cross section for interactions of photons with carbon for photon energies from 10 to  $10^{11}$  eV. At the lowest energies the photoelectric effect dominates. Between 10 keV and 10 MeV Compton scattering is most important. Above 10 MeV pair production takes over. There is a small bump at about 20 MeV due to nuclear effects, but its contribution to the cross section is only a few percent of that due to pair production. The four important effects are discussed in the next four sections.

## 15.3 The Photoelectric Effect

In the photoelectric effect a photon of energy  $h\nu_0$  is absorbed by an atom, and an electron of kinetic energy  $T_{\text{el}} = h\nu_0 - B$  is ejected.  $B$  is the magnitude of the binding energy of the electron and depends on which shell the electron was in. Therefore it is labeled  $B_K$ ,  $B_L$ , and so forth. The cross section for the photoelectric effect,  $\tau$ , is a sum of terms for each shell:

$$\tau = \tau_K + \tau_L + \tau_M + \dots \quad (15.8)$$

As the energy of a photon beam is decreased, the photoelectric cross section increases rapidly. For photon energies too small to remove an electron from the  $K$  shell, the cross section for the  $K$ -shell photoelectric effect is zero. Even though photons do not have enough energy to remove an electron from the  $K$  shell, they may have enough energy to remove  $L$ -shell electrons. The cross section for  $L$  electron photoelectric effect is much smaller than that for  $K$  electrons, but it increases with decreasing energy until its threshold energy is reached. This energy dependence is shown for lead in Fig. 15.3, which plots the cross section for the photoelectric effect, incoherent Compton scattering, and coherent scattering. The  $K$  absorption edge for the photoelectric effect is seen. The photoelectric effect below the  $K$  absorption edge is due to  $L, M, \dots$  electrons; above this energy the  $K$  electrons also participate. Above 0.8 MeV in lead Compton scattering becomes more important than the photoelectric effect.

The energy dependence of the photoelectric effect cross section is between  $E^{-2}$  and  $E^{-4}$ . An approximation to the  $Z$  and  $E$  dependence of the photoelectric cross section near 100 keV is

$$\tau \propto Z^4 E^{-3} \quad (15.9)$$



FIGURE 15.4. Momentum relationships in Compton scattering. (a) Before. (b) After. The photon emerges at angle  $\theta$ , the electron at angle  $\phi$ .

Once an atom has absorbed a photon and ejected a photoelectron, it is in an excited state. The atom will eventually lose this excitation energy by capturing an electron and returning to its ground state. The deexcitation processes are described in Sec. 15.9.

## 15.4 Compton Scattering

### 15.4.1 Kinematics

Compton scattering is a  $(\gamma, \gamma'e)$  process. The equations that are used to relate the energy and angle of the emerging photon and electron, as well as the equations that give the cross section for the scattering, are usually derived assuming that the electron is free and at rest. We turn first to the kinematics. A photon has energy  $E$  and momentum  $p$ , related by

$$E = h\nu = pc. \quad (15.10)$$

This is a special case of a more general relationship from special relativity:

$$E^2 = (pc)^2 + (m_0c^2)^2. \quad (15.11)$$

In these equations  $E$  is the total energy of the particle,  $p$  its momentum,  $m_0$  the “rest mass” of the particle (measured when it is not moving), and  $m_0c^2$  is the “rest energy.”<sup>1</sup> For a photon, which can never be at rest,  $m_0 = 0$ . Equation 15.10 can also be derived from the classical electromagnetic theory of light.

The conservation of energy and momentum can be used to derive the relationship between the angle at which the scattered photon emerges and its energy. A detailed knowledge of the forces involved is necessary to calculate the relative number of photons scattered at different angles; in fact, this calculation must be done using quantum mechanics. Figure 15.4 shows the geometry involved in the scattering. The electron emerges with momentum  $p$ , kinetic energy  $T$ , and total energy  $E = T + m_e c^2$ . It emerges at an angle  $\phi$  with the direction of the incident photon. The scattered photon emerges at angle  $\theta$  with a

reduced energy and a corresponding frequency  $\nu'$  which is lower than  $\nu_0$ , the frequency of the incident photon. Conservation of momentum in the direction of the incident photon gives

$$\frac{h\nu_0}{c} = \frac{h\nu'}{c} \cos \theta + p \cos \phi,$$

while conservation of momentum at right angles to that direction gives

$$\frac{h\nu'}{c} \sin \theta = p \sin \phi.$$

Conservation of energy gives

$$h\nu_0 = h\nu' + T.$$

The equation  $E = T + m_e c^2$  can be combined with Eq. 15.11 to give

$$(pc)^2 = T^2 + 2m_e c^2 T.$$

The last four equations can then be combined and solved for various unknowns.

The wavelength of the scattered photon is

$$\lambda' - \lambda_0 = \frac{c}{\nu'} - \frac{c}{\nu_0} = \frac{h}{m_e c} (1 - \cos \theta). \quad (15.12)$$

The wavelength shift (but not the frequency or energy shift) is independent of the incident wavelength. The quantity  $h/m_e c$  has the dimensions of length and is called the *Compton wavelength* of the electron. Its numerical value is

$$\lambda_C = \frac{h}{m_e c} = 2.427 \times 10^{-12} \text{ m} = 2.427 \text{ pm}. \quad (15.13)$$

If Eq. 15.12 is solved for the energy of the scattered photon, the result is

$$h\nu' = \frac{m_e c^2}{1 - \cos \theta + 1/x}, \quad (15.14)$$

where  $x$  is the energy of the incident photon in units of  $m_e c^2 = 511 \text{ keV}$ :

$$x = \frac{h\nu_0}{m_e c^2}. \quad (15.15)$$

The energy of the recoil electron is  $T = h\nu_0 - h\nu'$ :

$$T = \frac{h\nu_0(2x \cos^2 \phi)}{(1+x)^2 - x^2 \cos^2 \phi} = \frac{h\nu_0 x (1 - \cos \theta)}{1 + x(1 - \cos \theta)}. \quad (15.16)$$

Figure 15.5 shows the energy of the scattered photon and the recoil electron as a function of  $\theta$ , the angle of emergence of the photon. The sum of the two energies is 1 MeV, the energy of the incident photon.

<sup>1</sup>Since this is one of the few relativistic results we will need, it is not developed here. A discussion can be found in any book on special relativity.

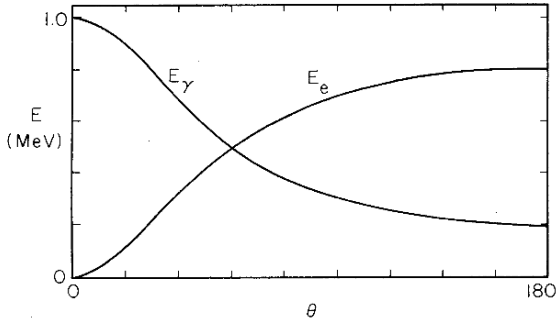


FIGURE 15.5. The energy of the emerging photon and recoil electron as a function of  $\theta$ , the angle of the emerging photon, for a 1-MeV incident photon.

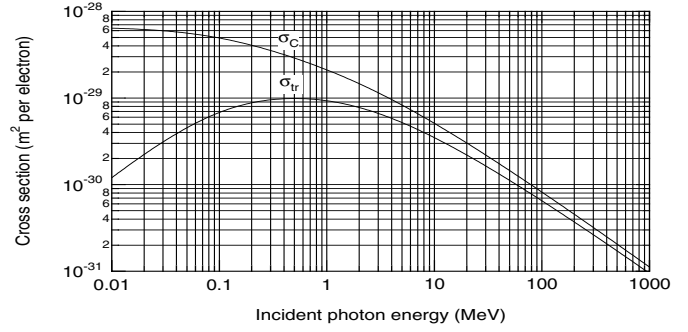


FIGURE 15.7. The total cross section  $\sigma_C$  for Compton scattering by a single electron and the cross section for energy transfer  $\sigma_{tr} = f_C \sigma_C$ .

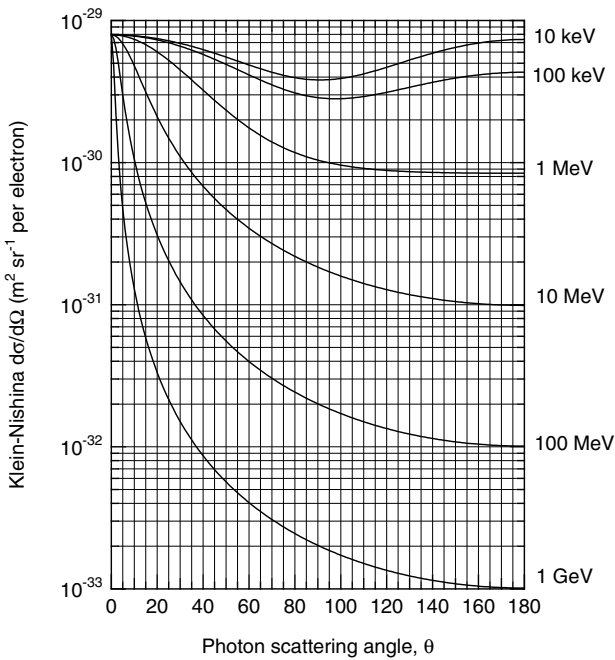


FIGURE 15.6. Differential cross section for Compton scattering of unpolarized photons from a free electron, calculated from Eq. 15.17. The incident photon energy for each curve is shown on the right.

### 15.4.2 Cross Section: Klein-Nishina Formula

The inclusion of dynamics, which allows us to determine the relative number of photons scattered at each angle, is fairly complicated. The quantum-mechanical result is known as the *Klein-Nishina* formula. The result depends on the polarization of the photons. For unpolarized photons, the cross section per unit solid angle for a photon to be scattered at angle  $\theta$  is

$$\frac{d\sigma_C}{d\Omega} = \frac{r_e^2}{2} \left[ \frac{1 + \cos^2 \theta + \frac{x^2(1 - \cos \theta)^2}{1 + x(1 - \cos \theta)}}{[1 + x(1 - \cos \theta)]^2} \right], \quad (15.17)$$

where

$$r_e = \frac{e^2}{4\pi\epsilon_0 m_e c^2} = 2.818 \times 10^{-15} \text{ m},$$

is the “classical radius” of the electron. The cross section is plotted in Fig. 15.6. It is peaked in the forward direction at high energies. As  $x \rightarrow 0$  (long wavelengths or low energy) it approaches

$$\frac{d\sigma_C}{d\Omega} = \frac{r_e^2(1 + \cos^2 \theta)}{2}, \quad (15.18)$$

which is symmetric about  $90^\circ$ .

Equation 15.17 can be integrated over all angles to obtain the total Compton cross section for a single electron:

$$\sigma_C = 2\pi r_e^2 \left[ \frac{1+x}{x^2} \left( \frac{2(1+x)}{1+2x} - \frac{\ln(1+2x)}{x} \right) + \frac{\ln(1+2x)}{2x} - \frac{1+3x}{(1+2x)^2} \right]. \quad (15.19)$$

As  $x \rightarrow 0$ , this approaches

$$\sigma_C \rightarrow \frac{8\pi r_e^2}{3} = 6.652 \times 10^{-29} \text{ m}^2. \quad (15.20)$$

Figure 15.7 shows  $\sigma_C$  as a function of energy.

The classical analog of Compton scattering is Thomson scattering of an electromagnetic wave by a free electron. The electron experiences the electric field  $\mathbf{E}$  of an incident plane electromagnetic wave and therefore has an acceleration  $-e\mathbf{E}/m$ . Accelerated charges radiate electromagnetic waves, and the energy radiated in different directions can be calculated, giving Eqs. 15.18 and 15.20. [See, for example, Rossi (1957, Chapter 8).] In the classical limit of low photon energies and momenta, the energy of the recoil electron is negligible.

### 15.4.3 Incoherent Scattering

The Compton cross section is for a single electron. For an atom containing  $Z$  electrons, the maximum value of



the incoherent cross section occurs if all  $Z$  electrons take part in the Compton scattering:

$$\sigma_{\text{incoh}} \leq Z\sigma_C.$$

For carbon  $Z\sigma_C = 4.0 \times 10^{-28} \text{ m}^2$ . This value is approached by  $\sigma_{\text{incoh}}$  near 10 keV. At low energies  $\sigma_{\text{incoh}}$  falls below this maximum value because the electrons are bound and not at rest. This falloff can be seen in Fig. 15.2. It is appreciable for energies as high as 7–8 keV, even though the  $K$ -shell binding energy in carbon is only 283 eV. The electron motion and binding in the target atom also cause a small spread in the energy of the scattered photons [Carlsson *et al.* (1982)].

Departures of the angular distribution and incoherent cross section from  $Z$  times the Klein–Nishina formula are discussed by Hubbell *et al.* (1975) and by Jackson and Hawkes (1981).

#### 15.4.4 Energy Transferred to the Electron

We will need to know the average energy transferred to an electron in a Compton scattering. Equation 15.16 gives the electron kinetic energy as a function of photon scattering angle. The transfer cross section is defined to be

$$\sigma_{\text{tr}} = \int_0^\pi \frac{d\sigma_C}{d\Omega} \frac{T(\theta)}{h\nu_0} 2\pi \sin\theta d\theta = f_C \sigma_C. \quad (15.21)$$

This can be integrated. The result is [see Attix (1986), p. 134]

$$\begin{aligned} \sigma_{\text{tr}} = 2\pi r_e^2 & \left[ \frac{2(1+x)^2}{x^2(1+2x)} - \frac{1+3x}{(1+2x)^2} \right. \\ & - \frac{(1+x)(2x^2-2x-1)}{x^2(1+2x)^2} - \frac{4x^2}{3(1+2x)^3} \\ & \left. - \left( \frac{1+x}{x^3} - \frac{1}{2x} + \frac{1}{2x^3} \right) \ln(1+2x) \right]. \quad (15.22) \end{aligned}$$

This quantity is also plotted in Fig. 15.7. Equation 15.22 is a rather nasty equation to evaluate, particularly at low energies, because many of the terms nearly cancel.

## 15.5 Coherent Scattering

A photon can also scatter elastically from an atom, with none of the electrons leaving their energy levels. This  $(\gamma, \gamma)$  process is called *coherent scattering* (sometimes called *Rayleigh scattering*), and its cross section is  $\sigma_{\text{coh}}$ . The entire atom recoils; if one substitutes the atomic mass in Eqs. 15.15 and 15.16, one finds that the atomic recoil kinetic energy is negligible.

The primary mechanism for coherent scattering is the oscillation of the electron cloud in the atom in response to the electric field of the incident photons. There are small contributions to the scattering from nuclear processes.

The cross section can be calculated classically as an extension of Thomson scattering, or it can be done using various degrees of quantum-mechanical sophistication [see Kissel *et al.* (1980) or Pratt (1982)].

The coherent cross section is peaked in the forward direction because of interference effects between electromagnetic waves scattered by various parts of the electron cloud. The peak is narrower for elements of lower atomic number and for higher energies. Coherent and incoherent scattering cross sections are shown in Fig. 15.8 for 100-keV photons scattering from carbon, calcium, and lead. Also shown for comparison is  $Z(d\sigma/d\Omega)_{KN}$ .

If the wavelength of the incident photon is large compared to the size of the atom, then all  $Z$  electrons behave like a single particle with charge  $-Ze$  and mass  $Zm_e$ . From Eqs. 15.18 and 15.20, one can see that the cross section in this limit is  $Z^2$  times the single-electron value:  $Z^2\sigma_C$ . The limiting value for carbon is  $2.39 \times 10^{-27} \text{ m}^2$ , which can be compared to the low energy limit for  $\sigma_{\text{coh}}$  in Fig. 15.2.

## 15.6 Pair Production

A photon with energy above 1.02 MeV can produce a particle–antiparticle pair: a negative electron and a positive electron or *positron*. Conservation of energy requires that

$$h\nu_0 = \underbrace{T_- + m_e c^2}_{\text{electron}} + \underbrace{T_+ + m_e c^2}_{\text{positron}} = T_+ + T_- + 2m_e c^2. \quad (15.23)$$

Since the rest energy ( $m_e c^2$ ) of an electron or positron is 0.51 MeV, pair production is energetically impossible for photons below  $2m_e c^2 = 1.02 \text{ MeV}$ .

One can show, using  $h\nu_0 = pc$  for the photon, that momentum is not conserved by the positron and electron if Eq. 15.23 is satisfied. However, pair production always takes place in the Coulomb field of another particle (usually a nucleus) that recoils to conserve momentum. The nucleus has a large mass, so its kinetic energy  $p^2/2m$  is small compared to the terms in Eq. 15.23. The cross section for this  $(\gamma, e^+e^-)$  reaction involving the nucleus is  $\kappa_n$ .

Pair production with excitation or ionization of the recoil atom can take place at energies that are only slightly higher than the threshold; however, the cross section does not become appreciable until the incident photon energy exceeds  $4m_e c^2 = 2.04 \text{ MeV}$ , the threshold for pair production in which a free electron (rather than a nucleus) recoils to conserve momentum. Because ionization and free-electron pair production are  $(\gamma, e^-e^-e^+)$  processes, this is usually called *triplet production*. Extensive data are given in Hubbell *et al.* (1980).

The cross section for both processes is  $\kappa = \kappa_n + \kappa_e$ . The energy dependence of  $\kappa$  can be seen in Figs. 15.2 and 15.3.

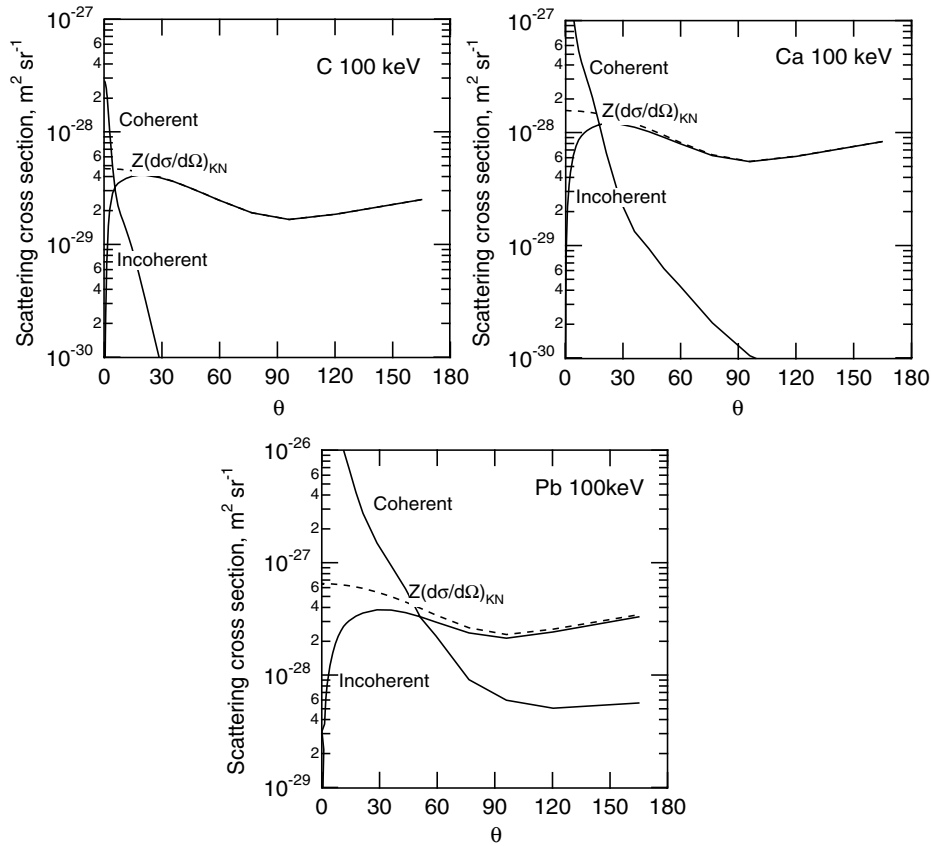


FIGURE 15.8. The coherent and incoherent differential cross sections as a function of angle for 100-keV photons scattering from carbon, calcium, and lead. Calculated from Hubbell (1975).

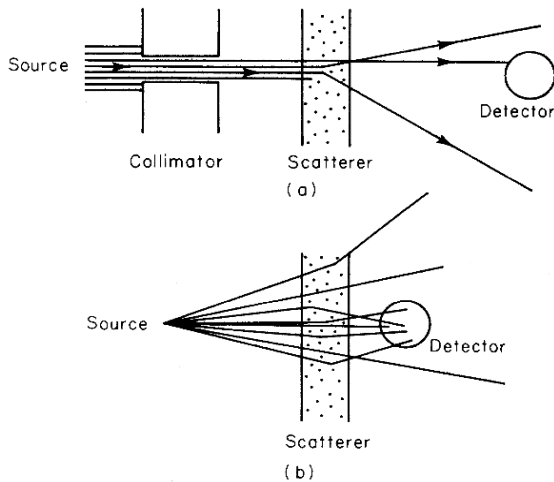


FIGURE 15.9. Measurements with (a) narrow-beam geometry and (b) broad-beam geometry.

### 15.7 The Photon Attenuation Coefficient

Consider the arrangement shown in Fig. 15.9(a), in which a beam of photons is collimated so that a narrow beam strikes a detector.

A scattering material is then introduced in the beam. Some of the photons pass through the material without interaction. Others are scattered. Still others disappear because of photoelectric effect or pair-production interactions. If we measure only photons that remain in the unscattered beam, the loss of photons is called *attenuation* of the beam. Attenuation includes both scattering and absorption. We record as still belonging to the beam only photons that did not interact; they still travel in the forward direction with the original energy. This is called a *narrow-beam geometry* measurement. It is an idealization, because photons that undergo Compton or coherent scattering through a small angle can still strike the detector. Figure 15.9(b) shows a source, scatterer, and detector geometry that is much more difficult to interpret. In this case photons that are initially traveling in a different direction are scattered into the detector. These are called *broad-beam geometry* experiments.

In narrow-beam geometry, the total cross section is related to the total number of particles that have interacted in the scatterer. Let  $N$  be the number of particles that have not undergone any interaction in passing through scattering material of thickness  $z$ . We saw in Sec. 14.4 that the number of particles that have not interacted decreases in thickness  $dz$  by

$$dN = -\frac{\sigma_{\text{tot}} N_A \rho}{A} N dz,$$

so that

$$\frac{dN}{dz} = -\mu_{\text{atten}}N,$$

where

$$\mu_{\text{atten}} = \frac{N_A \rho \sigma_{\text{tot}}}{A}. \quad (15.24)$$

In these equations  $\rho$  is the mass density of the target material and  $A$  is its atomic weight.<sup>2</sup> The number of particles that have undergone no interaction decays exponentially with distance:

$$N(z) = N_0 e^{-\mu_{\text{atten}} z}. \quad (15.25)$$

The quantity  $\mu_{\text{atten}}$  is called the *total linear attenuation coefficient*.

In a broad-beam geometry configuration the total number of photons reaching the detector includes secondary photons and is larger than the value given by Eq. 15.25.

The units in Eqs. 15.24 and 15.25 are worth discussing. Avogadro's number is  $6.022\,045 \times 10^{23}$  entities  $\text{mol}^{-1}$ . If the density  $\rho$  is in  $\text{kg m}^{-3}$  and  $\sigma_{\text{tot}}$  is in  $\text{m}^2$ , then  $A$  must be expressed in  $\text{kg mol}^{-1}$  and  $\mu_{\text{atten}}$  is in  $\text{m}^{-1}$ . On the other hand, it is possible to express  $\rho$  in  $\text{g cm}^{-3}$ ,  $\sigma_{\text{tot}}$  in  $\text{cm}^2$ , and  $A$  in  $\text{g mol}^{-1}$ , so that  $\mu_{\text{atten}}$  is in  $\text{cm}^{-1}$ . As an example, consider carbon, for which  $A = 12.011 \times 10^{-3} \text{ kg mol}^{-1} = 12.011 \text{ g mol}^{-1}$ . If  $\sigma_{\text{tot}} = 1.269 \times 10^{-28} \text{ m}^2 \text{ atom}^{-1} = 1.269 \times 10^{-24} \text{ cm}^2 \text{ atom}^{-1}$ , then either

$$\begin{aligned} \mu_{\text{atten}} &= \frac{(6.022 \times 10^{23} \text{ atom mol}^{-1})(2.000 \times 10^3 \text{ kg m}^{-3})}{12.011 \times 10^{-3} \text{ kg mol}^{-1}} \\ &\times (1.269 \times 10^{-28} \text{ m}^2 \text{ atom}^{-1}) = 12.7 \text{ m}^{-1} \end{aligned}$$

or

$$\begin{aligned} \mu_{\text{atten}} &= \left( \frac{(6.022 \times 10^{23} \text{ atom mol}^{-1})(2.000 \text{ g cm}^{-3})}{12.011 \text{ g mol}^{-1}} \right) \\ &\times (1.269 \times 10^{-24} \text{ cm}^2 \text{ atom}^{-1}) = 0.127 \text{ cm}^{-1}. \end{aligned}$$

The total cross section for photon interactions is

$$\sigma_{\text{tot}} = \sigma_{\text{coh}} + \sigma_{\text{incoh}} + \tau + \kappa. \quad (15.26a)$$

In many situations the coherently scattered photons cannot be distinguished from those unscattered, and  $\sigma_{\text{coh}}$  should not be included:

$$\sigma_{\text{tot}} = \sigma_{\text{incoh}} + \tau + \kappa. \quad (15.26b)$$

Tables usually include total cross sections and attenuation coefficients both with and without coherent scattering.

It is possible to regroup the terms in Eqs. 15.24 and 15.25 in a slightly different way:

$$dN = -N \frac{N_A \sigma_{\text{tot}}}{A} \rho dz.$$

<sup>2</sup>The atomic weight is potentially confusing. Sometimes  $A$  has no units (as in labeling an nuclear isotope), sometimes it is in grams per mole, and sometimes it is in kilograms per mole).

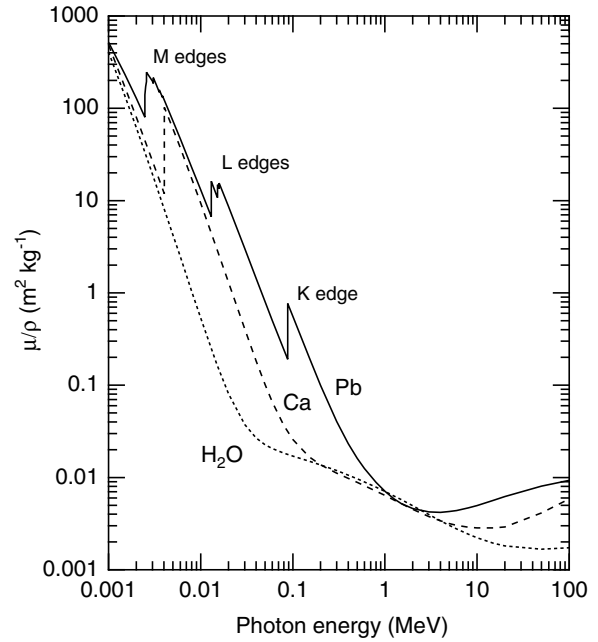


FIGURE 15.10. Mass attenuation coefficient vs. energy for lead, calcium, and water. Near 1 MeV the mass attenuation coefficient is nearly independent of  $Z$ . Plotted from data provided by NIST: <http://physics.nist.gov/PhysRefData/Xcom/Text/XCOM.html>.

The quantity  $N_A \sigma_{\text{tot}}/A$  is the *mass attenuation coefficient*,  $\mu_{\text{atten}}/\rho$  ( $\text{m}^2 \text{ kg}^{-1}$ ):

$$\frac{\mu_{\text{atten}}}{\rho} = \frac{N_A \sigma_{\text{tot}}}{A}. \quad (15.27)$$

The exponential attenuation is then

$$N(\rho z) = N_0 e^{-(\mu_{\text{atten}}/\rho)(\rho z)}. \quad (15.28)$$

The mass attenuation coefficient has the advantage of being independent of the density of the target material, which is particularly useful if the target is a gas. It has an additional advantage if Compton scattering is the dominant interaction. If  $\sigma_{\text{tot}} = Z\sigma_C$ , then

$$\frac{\mu_{\text{atten}}}{\rho} = \frac{Z\sigma_C N_A}{A}.$$

Since  $Z/A$  is nearly 1/2 for all elements except hydrogen, this quantity changes very little throughout the periodic table. This constancy is not true for the photoelectric effect or pair production. Figure 15.10 plots the mass attenuation coefficient vs energy for three elements spanning the Periodic Table. It is nearly independent of  $Z$  around 1 MeV where Compton scattering is dominant. The  $K$  and  $L$  absorption edges can be seen for lead; for the lighter elements they are below 10 keV.

Figure 15.11 shows the contributions to  $\mu_{\text{atten}}/\rho$  for air from the photoelectric effect, incoherent scattering, and pair production. Tables of mass attenuation coefficients

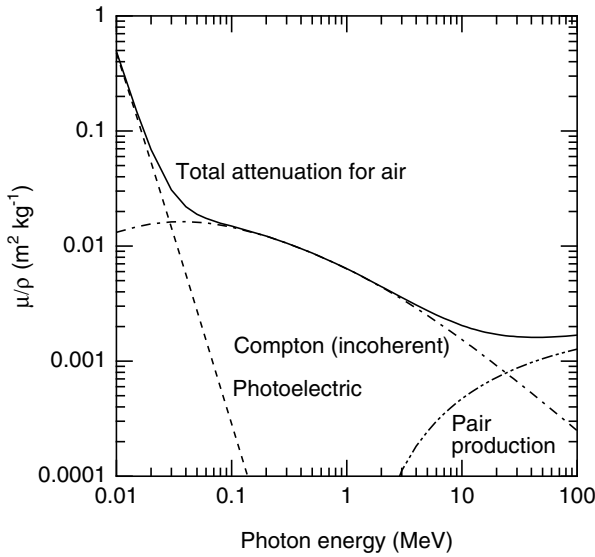


FIGURE 15.11. Mass attenuation coefficient vs energy for air. Plotted from data provided by NIST: <http://physics.nist.gov/PhysRefData/Xcom/Text/XCOM.html>.

are provided by the National Institute of Standards and Technology (NIST) at [physics.nist.gov/PhysRefData/](http://physics.nist.gov/PhysRefData/).

## 15.8 Compounds and Mixtures

The usual procedure for dealing with mixtures and compounds is to assume that each atom scatters independently. If the cross section for element  $i$  summed over all the interaction processes of interest is denoted by  $\sigma_i$ , then Eq. 14.18 is replaced by

$$\frac{\bar{n}}{N} = \sum_i \sigma_i(N_T)_i = \left( \sum_i \sigma_i(N_{TV})_i \right) dz, \quad (15.29)$$

where  $(N_T)_i$  is the number of target atoms of species  $i$  per unit projected area of the target and  $(N_{TV})_i$  is the number of target atoms per unit volume. The sum is taken over all elements in the compound or mixture.

It is possible to replace the sum by the product of the cross section per molecule multiplied by the number of molecules per unit volume. The cross section per molecule is the sum of the cross sections for all the atoms in the molecule. To see that this is so, note that a volume of scatterer  $V$  contains a total mass  $M = \rho V$ . The mass of each element is  $M_i$  and the mass fraction is  $w_i = M_i/M$ . The total number of atoms of species  $i$  in volume  $V$  is the number of moles times Avogadro's number:

$$(N_{TV})_i = \frac{M_i N_A}{A_i V} = \frac{w_i}{A_i} \rho N_A. \quad (15.30)$$

The mass fraction of element  $i$  in a compound containing  $a_i$  atoms per molecule with atomic mass  $A_i$  is

$$w_i = \frac{a_i A_i}{A_{\text{mol}}}, \quad (15.31)$$

where  $A_{\text{mol}}$  is the molecular weight. Therefore

$$\begin{aligned} \sum_i \sigma_i(N_{TV})_i &= \left( \sum_i \frac{a_i \sigma_i}{A_{\text{mol}}} \right) \rho N_A \\ &= \left( \sum_i a_i \sigma_i \right) \frac{\rho N_A}{A_{\text{mol}}} = \sigma_{\text{mol}}(N_{TV})_{\text{mol}}. \end{aligned} \quad (15.32)$$

The factor  $(N_{TV})_{\text{mol}} = \rho N_A / A_{\text{mol}}$  is the number of molecules per unit volume. When a target entity (molecule) consists of a collection of subentities (atoms), we can say that in this approximation (all subentities interacting independently), the cross section per entity is the sum of the cross sections for each subentity. For example, for the molecule  $\text{CH}_4$ , the total molecular cross section is  $\sigma_{\text{carbon}} + 4\sigma_{\text{hydrogen}}$  and the molecular weight is  $[(4 \times 1) + 12 = 16] \times 10^{-3} \text{ kg mol}^{-1}$ .

## 15.9 Deexcitation of Atoms

After the photoelectric effect, Compton scattering, or triplet production, an atom is left with a hole in some electron shell. An atom can be left in a similar state when an electron is knocked out by a passing charged particle or by certain transformations in the atomic nucleus that are discussed in Chapter 17.

The hole in the shell can be filled by two competing processes: a *radiative transition*, in which a photon is emitted as an electron falls into the hole from a higher level, or a *nonradiative* or *radiationless transition*, such as the emission of an *Auger electron* from a higher level as a second electron falls from a higher level to fill the hole. Both processes are shown in Fig. 15.12. In the radiative transition, the energy of the photon is equal to the difference in binding energies of the two levels. For the example of Fig. 15.12(b), the photon energy is  $B_K - B_L$ . The emission of an *L-shell Auger electron* is shown in Fig. 15.12(c): its energy is  $T = (B_K - B_L) - B_L = B_K - 2B_L$ . Table 15.2 shows the energy changes that occur after a hole is created in an atom by photoelectric excitation. It is worth understanding each table entry in detail. Two different paths for deexcitation are shown: one for photon emission and one for ejection of an Auger electron. The sum of the photon, electron, and atomic excitation energies does not change.

The photon that is emitted is called a *characteristic photon* or a *fluorescence photon*. Its energy is given by the difference of two electron energy levels in the atom. There is an historical nomenclature for these photons.

TABLE 15.2. Energy changes in the photoelectric effect and in subsequent deexcitation.

Process	Total photon energy	Total electron energy	Atom excitation energy	Sum
Before photon strikes atom	$h\nu$	0	0	$h\nu$
After photoelectron is ejected [Fig. 15.12(a)]	0	$h\nu - B_K$	$B_K$	$h\nu$
Case 1: Deexcitation by the emission of a $K$ and an $L$ photon				
Emission of $K$ fluorescence photon [Fig. 15.12(b)]	$B_K - B_L$	$h\nu - B_K$	$B_L$	$h\nu$
Emission of $L$ fluorescence photon	$B_K - B_L, B_L$	$h\nu - B_K$	0	$h\nu$
Case 2: Deexcitation by emission of an Auger electron from the $L$ shell				
Emission of Auger electron [Fig. 15.12(c)]	0	$h\nu - B_K, B_K - 2B_L$	$2B_L$	$h\nu$
First $L$ -shell hole filled by fluorescence	$B_L$	$h\nu - B_K, B_K - 2B_L$	$B_L$	$h\nu$
Second $L$ -shell hole filled by fluorescence	$B_L, B_L$	$h\nu - B_K, B_K - 2B_L$	0	$h\nu$

Because a hole moving to larger values of  $n$  corresponds to a decrease in the total energy of an atom, it is customary to draw the energy levels for holes instead of electrons, as in Fig. 15.13. Transitions in which the hole is initially in the  $n = 1$  state give rise to the  $K$  series of x rays, those in which the initial hole is in the  $n = 2$  state give rise to the  $L$  series, and so on. Greek letters (and their subscripts) are used to denote the shell (and subshell) of the final hole. The transitions shown in Fig. 15.13 are consistent with certain selection rules which can be derived using quantum theory:

$$\Delta l = \pm 1, \quad \Delta j = 0, \pm 1. \quad (15.33)$$

We saw in Eqs. 15.2 and 15.3 that the position of a level could be estimated by the Bohr formula corrected for screening. The energy of the  $K_\alpha$  line—which depends on screening for both the initial ( $n = 2$ ) and final ( $n = 1$ ) values of  $n$ —can be fitted empirically by

$$E_{K_\alpha} = \left(\frac{3}{4}\right) (13.6)(Z - 1)^2. \quad (15.34)$$

After creation of a hole in the  $K$  shell, it is random whether the atom deexcites by emitting a photon or an Auger electron. The probability of photon emission is called the *fluorescence yield*,  $W_K$ . The Auger yield is  $A_K = 1 - W_K$ . For a vacancy in the  $L$  or higher shells, one must consider the fluorescence yield for each subshell, defined as the number of photons emitted with an initial

state corresponding to a hole in a subshell, divided by the number of holes in that subshell. The situation is further complicated by the fact that radiationless transitions can take place within the subshell, thereby altering the number of vacancies in each subshell. These are called *Coster–Kronig transitions*, and they are also accompanied by the emission of an electron. For example, a hole in the  $L_I$  shell can be filled by an electron from the  $L_{III}$  shell with the ejection of an  $M$ -shell electron. A *super-Coster–Kronig transition* involves electrons all within the same shell, for example, a hole in the  $M_I$  shell filled by an electron from the  $M_{II}$  shell with the ejection of an electron from the  $M_{IV}$  shell.

One can define an average fluorescence yield  $\overline{W}_L, \overline{W}_M$ , etc. for each shell, but it is not a fundamental property of the atom, since it depends on the vacancy distribution in the subshells. Bambynek *et al.* (1972) review the physics of atomic deexcitations and present theoretical and experimental data for the fundamental parameters. They show that  $\overline{W}_L$  is less sensitive to the initial vacancy distribution than one might expect, because of the rapid changes in hole distribution caused by the Coster–Kronig transitions. Hubbell *et al.* (1994) provide a more recent review. Figure 15.14 shows values for  $W_K, \overline{W}_L$ , and  $\overline{W}_M$  as a function of  $Z$ . One can see from this figure that radiationless transitions are much more important (the fluorescent yield is much smaller) for the  $L$  shell than for the  $K$  shell. They are nearly the sole process for higher shells. The deexcitation is often called the *Auger cascade*.

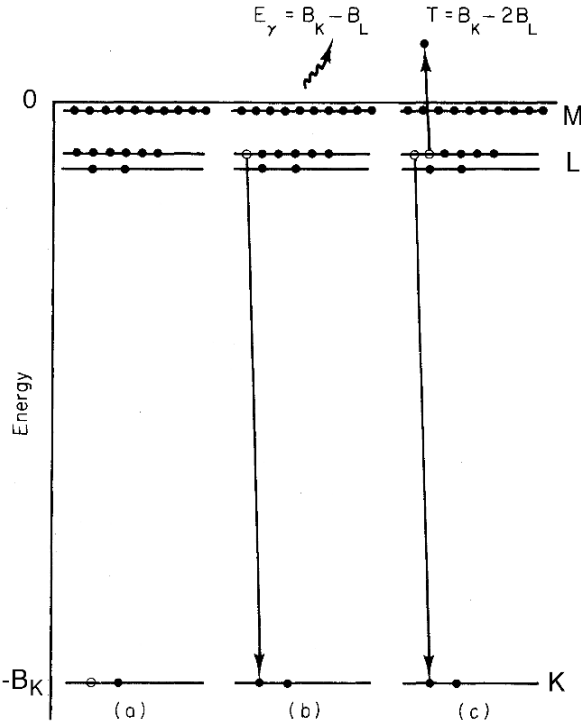


FIGURE 15.12. Two possible mechanisms for the deexcitation of an atom with a hole in the  $K$  shell. (a) The atom with the hole in the  $K$  shell. (b) An electron has moved from the  $L$  shell to the  $K$  shell with emission of a photon of energy  $B_K - B_L$ . (c) An electron has moved from the  $L$  shell to the  $K$  shell. The energy liberated is taken by another electron from the  $L$  shell, which emerges with energy  $B_K - 2B_L$ . This electron is called an Auger electron.

The Auger cascade produces many vacancies in the outer shells of the atom, and some of these may be filled by electrons from other atoms in the same molecule. This process can break molecular bonds. Moreover, the Auger and Coster–Kronig electrons from the higher shells can be quite numerous. They are of such low energy that they travel only a fraction of a cell diameter. This must be taken into consideration when estimating cell damage from radiation. The effect of radiationless transitions is quite important for certain radioactive isotopes that are administered to a patient, particularly when they are bound to the cellular DNA. We will discuss them further in Chapter 17.

### 15.10 Energy Transfer from Photons to Electrons

The attenuation coefficient gives the rate at which photons interact and leave the primary beam as they pass through material. If a beam of monoenergetic photons of energy  $E = h\nu$  and particle fluence  $\Phi$  passes through a thin layer  $dx$  of material, the number of particles

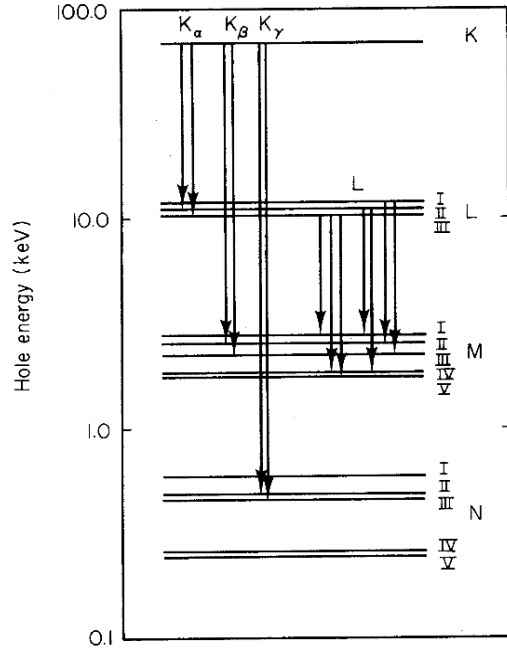


FIGURE 15.13. Energy-level diagram for holes in tungsten, and some of the x-ray transitions.

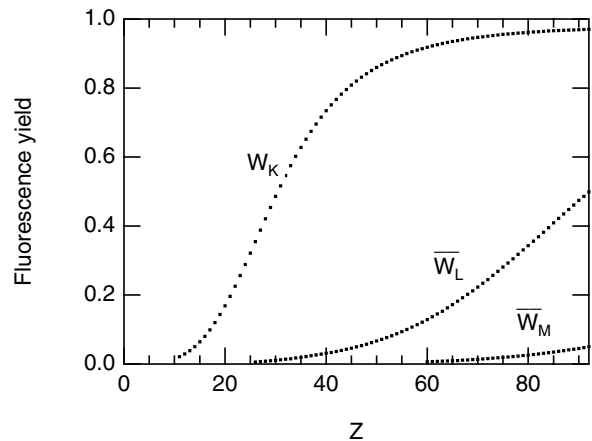


FIGURE 15.14. Fluorescence yields for  $K$ -,  $L$ -, and  $M$ -shell vacancies as a function of atomic number  $Z$ . Points are from Table 8 of Hubbell *et al.* (1994).

per unit area that interact in the layer,  $-d\Phi$ , is proportional to the fluence and the attenuation coefficient:  $-d\Phi = \Phi\mu_{\text{atten}} dx$ . The energy fluence is  $\Psi = h\nu\Phi$ . The reduction of energy fluence of unscattered photons is  $-d\Psi = -h\nu d\Phi$ . For a thick absorber we can say that the number of unscattered photons and the energy carried by unscattered photons decay as

$$\Phi_{\text{unscatt}} = \Phi_0 e^{-\mu_{\text{atten}} x}, \quad \Psi_{\text{unscatt}} = \Psi_0 e^{-\mu_{\text{atten}} x}. \tag{15.35}$$

The total energy flow is much more complicated. Every photon that interacts contributes to a pool of secondary

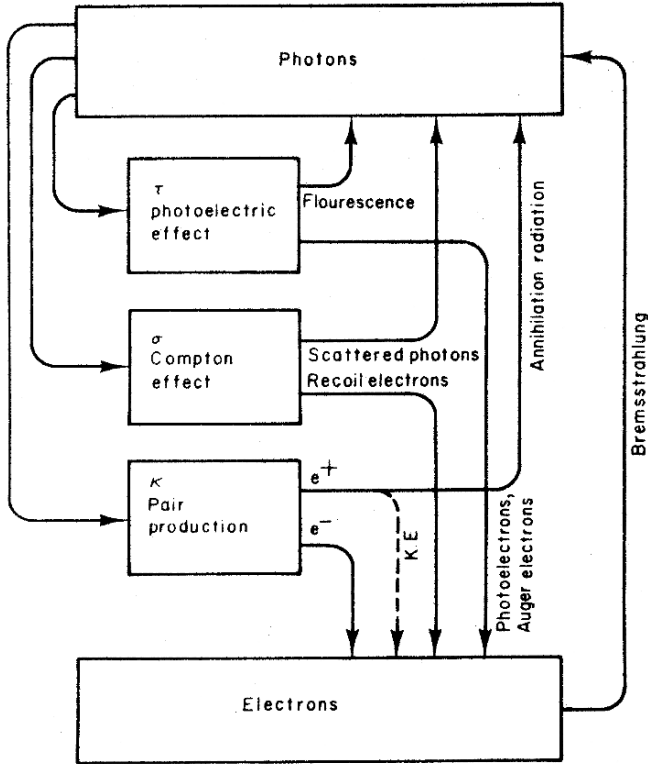


FIGURE 15.15. Routes for the transfer of energy between photons and electrons.

photons of lower energy and to a pool of electrons and positrons. Figure 15.15 shows the processes by which energy can move between the photon pool and the electron-positron pool. Energy that remains as secondary photons, such as those resulting from fluorescence or Compton scattering, can travel long distances from the site of the initial interaction. Ionizing particles (photoelectrons, Auger electrons, Compton recoil electrons, and electron-positron pairs) usually lose their energy relatively close to where they were produced. We will see in Sec. 15.13 that for primary photons below 10 MeV, the mean free path of the secondary electrons is usually short compared to that of the photons. Damage to cells is caused by local ionization or excitation of atoms and molecules. This damage is done much more efficiently by the electrons than by the photons.

The *mass energy transfer coefficient*  $\mu_{\text{tr}}/\rho$  is a measure of the energy transferred from primary photons to charged particles in the interaction. If  $N$  monoenergetic photons of energy  $E$  strike a thin absorber of thickness  $dx$ , the amount of energy transferred to charged particles is defined to be

$$\overline{dE_{\text{tr}}} = NE \mu_{\text{tr}} dx,$$

so that

$$\frac{\mu_{\text{tr}}}{\rho} = \frac{1}{\rho NE} \frac{dE_{\text{tr}}}{dx}. \quad (15.36)$$

We can relate  $\mu_{\text{tr}}$  to  $\mu_{\text{atten}}$ . Suppose the material contains a single atomic species and that  $f_i$  is the average fraction of the photon energy that is transferred to charged particles in process  $i$ . (Different values of  $i$  denote the photoelectric effect, incoherent scattering, coherent scattering, and pair production.) Multiplying the number of photons that interact by their energy  $E$  and by  $f_i$  gives the energy transferred. Comparison with Eq. 15.24 shows that

$$\frac{\mu_{\text{tr}}}{\rho} = \frac{N_A}{A} \sum_i f_i \sigma_i. \quad (15.37)$$

Coherent scattering produces no charged particles, so

$$\frac{\mu_{\text{tr}}}{\rho} = \frac{N_A}{A} (\tau f_\tau + \sigma_{\text{incoh}} f_C + \kappa f_\kappa). \quad (15.38)$$

Fraction  $f_\tau$  for the photoelectric effect can be written in terms of  $\delta$ , the average energy emitted as fluorescence radiation per photon absorbed. The quantity  $\delta$  is calculated taking into account all atomic energy levels and the fluorescence yield for each shell. The average electron energy is  $h\nu - \delta$ , so

$$f_\tau = \frac{h\nu - \delta}{h\nu} = 1 - \frac{\delta}{h\nu}. \quad (15.39)$$

We can estimate  $\delta$  by assuming that  $\tau_K$  is the dominant term in the photoelectric cross section, Eq. 15.8. The probability that the hole in the  $K$  shell is filled by fluorescence is  $W_K$ . The energy of the photon is  $B_K - B_L$  or  $B_K - B_M$ , and so on. A hole is left in a higher shell, which may decay by photon or Auger-electron emission. The latter is much more likely for the higher shells. Therefore nearly all of the photons emitted have energy  $B_K - B_L$ , so we have the approximate relationship

$$\delta \approx W_K (B_K - B_L). \quad (15.40)$$

For Compton scattering, the fraction of the energy transferred to electrons is implicit in Eqs. 15.21 and 15.22. The transfer cross section  $f_C \sigma_C$ , is plotted in Fig. 15.7.

For pair production, energy in excess of  $2m_e c^2$  becomes kinetic energy of the electron and positron. The fraction is

$$f_\kappa = 1 - \frac{2m_e c^2}{h\nu}. \quad (15.41)$$

All of these can be combined to estimate  $\mu_{\text{tr}}$ .

We will see in Sec. 15.11 that charged particles traveling through material can radiate photons through a process known as *bremsstrahlung*. The *mass energy-absorption coefficient*  $\mu_{\text{en}}$  takes this additional effect into account. It is defined as

$$\frac{\mu_{\text{en}}}{\rho} = \frac{\mu_{\text{tr}}}{\rho} (1 - g), \quad (15.42)$$

where  $g$  is the fraction of the energy of secondary electrons that is converted back into photons by

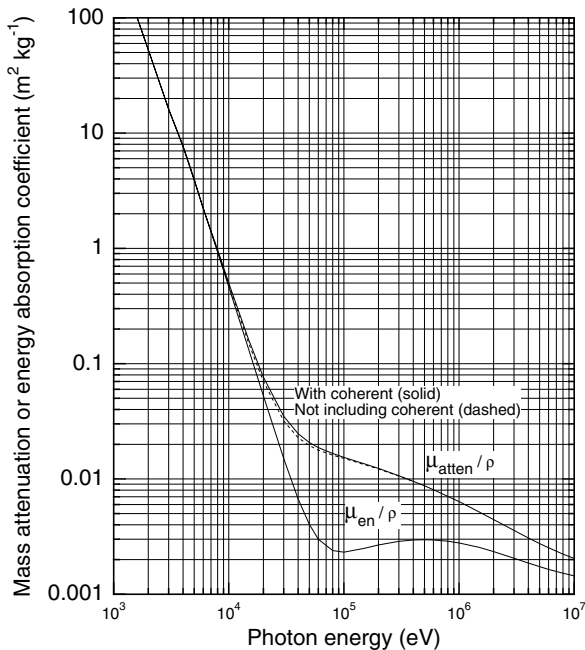


FIGURE 15.16. Coherent and incoherent attenuation coefficients and the mass energy absorption coefficient for water. Plotted from data in Hubbell (1982).

bremsstrahlung in the material. The fraction of the energy converted to photons depends on the energy of the electrons. Since the average electron energy is different in the three processes, we can write (again assuming noninteracting atoms in the target material)

$$\frac{\mu_{\text{en}}}{\rho} = \frac{N_A}{A} \sum_i f_i \sigma_i (1 - g_i). \quad (15.43)$$

In addition to bremsstrahlung, there is another process that converts charged-particle energy back into photon energy. Positrons usually come to rest and then combine with an electron to produce *annihilation radiation*. Occasionally, a positron annihilates while it is still in flight, thereby reducing the amount of positron kinetic energy that is available to excite atoms. While not mentioned in the International Commission on Radiation Units and Measurements (ICRU) Report 33 (1980) definition, this effect has been included in the tabulations of  $\mu_{\text{en}}/\rho$  by Hubbell (1982). Seltzer (1993) reviews the calculation of  $\mu_{\text{tr}}/\rho$  and  $\mu_{\text{en}}/\rho$ .

The energy-transfer and energy-absorption coefficients differ appreciably when the kinetic energies of the secondary charged particles are comparable to their rest energies, particularly in high- $Z$  materials. The ratio  $\mu_{\text{en}}/\mu_{\text{tr}}$  for carbon falls from 1.00 when  $h\nu = 0.5$  MeV to 0.96 when  $h\nu = 10$  MeV. For lead at the same energies it is 0.97 and 0.74. Tables are given by Attix (1986). The difference between the attenuation and the energy-absorption coefficients is greatest at energies where Compton scattering predominates, since the scat-

tered photon carries away a great deal of energy. Figure 15.16 compares  $\mu_{\text{atten}}/\rho$  and  $\mu_{\text{en}}/\rho$  for water.

Attenuation and energy-transfer coefficients are found in Hubbell and Seltzer (1996). These tables are also available on the web at [physics.nist.gov/PhysRefData/contents-xray.html](http://physics.nist.gov/PhysRefData/contents-xray.html). Another data source is a computer program provided by Boone and Chavez (1996).

We will return to these concepts in Sec. 15.15 to discuss the dose, or energy per unit mass deposited in tissue or a detector. First, we must discuss energy loss by charged particles.

## 15.11 Charged-Particle Stopping Power

The behavior of a particle with charge  $ze$  and mass  $M_1$  passing through material is very different from the behavior of a photon. When a photon interacts, it usually disappears: either being completely absorbed as in the photoelectric effect or pair production, or being replaced by a photon of different energy traveling in a different direction as in Compton scattering. The exception is coherent scattering, where a photon of the same energy travels in a different direction. A charged particle has a much larger interaction cross section than a photon—typically  $10^4$ – $10^5$  times as large. Therefore, the “unattenuated” charged-particle beam falls to zero almost immediately.

Each interaction usually causes only a slight decrease in the particle’s energy, and it is convenient to follow the charged particle along its path. Figure 15.27 shows the tracks of some  $\alpha$  particles (helium nuclei) in photographic emulsion. The spacing of the fiducial marks at the bottom is  $10 \mu\text{m}$ . Each particle entered at the bottom of the figure and stopped near the top. Figures 15.28 and 15.29 show the tracks of electrons. Figure 15.28 is in photographic emulsion, while Fig. 15.29 is in water. We will be discussing these tracks in detail in Sec. 15.14. For now, we need only note that the  $\alpha$  particle tracks are fairly straight, with some deviation near the end of the track. The electrons, being lighter, show considerably more scattering.<sup>3</sup>

It is convenient to speak of how much energy the charged particle loses per unit path length, the *stopping power*, and its *range*—roughly, the total distance it travels before losing all its energy. The stopping power is the expectation value of the amount of kinetic energy  $T$  lost by the projectile per unit path length. (The term *power* is historical. The units of stopping power are  $\text{J m}^{-1}$  not  $\text{J s}^{-1}$ .) The *mass stopping power* is the stopping power di-

<sup>3</sup>This distinction between photons and charged particles represents two extremes on a continuum, and we must be careful not to adhere to the distinction too rigidly. A photon may be coherently scattered through a small angle with no loss of energy, while a charged particle may occasionally lose so much energy that it can no longer be followed.



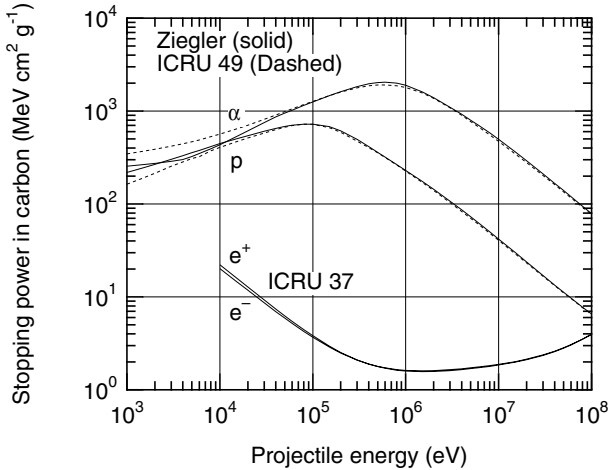


FIGURE 15.17. The mass stopping power for electrons ( $e^-$ ), positrons ( $e^+$ ), protons ( $p$ ), and  $\alpha$  particles in carbon vs. kinetic energy. Plotted from data in ICRU 37, ICRU 49, and the program SRIM (Stopping and Range of Ions in Matter), version 96.04 [see Ziegler *et al.* (1985)].

vided by the density of the stopping material and is analogous to the mass attenuation coefficient (often we will say stopping power when we actually mean mass stopping power):

$$S = -\frac{dT}{dx}, \quad \frac{S}{\rho} = -\frac{1}{\rho} \frac{dT}{dx}. \quad (15.44)$$

In the energy-loss process, the projectile interacts with the target atom. The projectile loses energy  $W$ , which becomes kinetic energy or internal excitation energy of the target atom. Internal excitation may include ionization of the atom. If the atoms in the material act independently, the cross section per atom for an interaction that results in an energy loss between  $W$  and  $W+dW$  is  $(d\sigma/dW)dW$ . The results of Sec. 14.4 can be used to write the probability that a projectile loses an amount of energy between  $W$  and  $W+dW$  while traversing a thickness  $dx$  of a substance of atomic mass number  $A$  and density  $\rho$ :

$$(\text{probability}) = \frac{\bar{n}}{N} = \frac{N_A \rho}{A} dx \frac{d\sigma}{dW} dW. \quad (15.45)$$

The average total energy loss is

$$dT = \frac{N_A \rho}{A} dx \int_0^{W_{\max}} W \frac{d\sigma}{dW} dW, \quad (15.46)$$

and the mass stopping power is

$$\frac{S}{\rho} = \frac{N_A}{A} \int_0^{W_{\max}} W \frac{d\sigma}{dW} dW. \quad (15.47)$$

The integral is sometimes called the *stopping cross section*  $\epsilon$ . Its units are  $\text{J m}^2$ .

Figure 15.17 shows the mass stopping power for protons,  $\alpha$  particles ( $z = 2$ ,  $M_\alpha = 4M_p$ ), and electrons and positrons ( $z = \pm 1$ ) in carbon as a function of energy. We see a number of features of these curves:

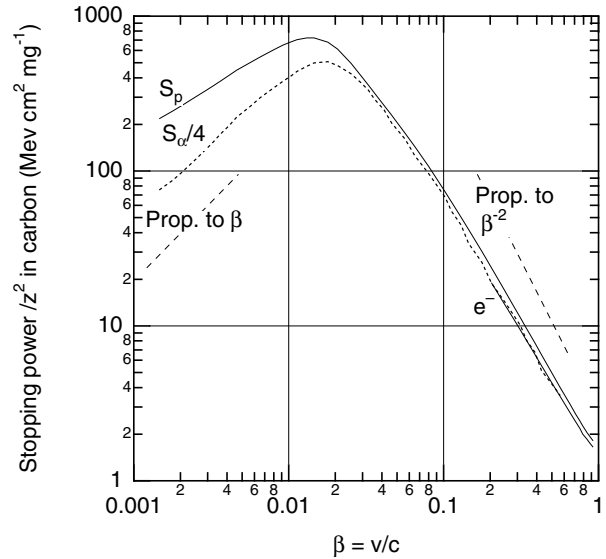


FIGURE 15.18. The scaled stopping power. The stopping power is plotted vs the speed  $\beta = v/c$  of the projectile for electrons, protons, and  $\alpha$  particles. The  $\alpha$ -particle stopping power has been divided by 4, the square of the particle charge  $z$ . Proton and  $\alpha$ -particle stopping powers are from the program SRIM (see caption for Fig. 15.17). The electron stopping power is from ICRU Report 37 (1984).

1. All of the stopping power curves have roughly the same shape, rising with increasing energy, reaching a peak, and then falling. (The electron and positron curves peak at a lower energy than is shown in the figure.)
2. There is a region where the stopping power falls approximately as  $1/T$ .
3. At still higher energies the curves rise again. This can be seen for the electron and positron curves above 1 MeV. Similar increases occur in the proton and  $\alpha$ -particle curves at higher energies than are plotted here.

The similarities suggest that the stopping power curves for different projectiles may be related. Figure 15.18 shows the similarities more clearly. The stopping powers are plotted vs particle speed in the form  $\beta = v/c$ . At low energies ( $\beta \ll 1$ )  $\beta$  is related to kinetic energy by

$$\beta = \left( \frac{2T}{Mc^2} \right)^{1/2}. \quad (15.48)$$

For larger values of  $\beta$ , the relativistically correct expression

$$\beta = \left[ 1 - \left( \frac{1}{T/Mc^2 + 1} \right)^2 \right]^{1/2}, \quad (15.49)$$

was used to convert Fig. 15.17 to Fig. 15.18. The  $\alpha$ -particle stopping power in Fig. 15.17 has been divided

by the square of the  $\alpha$ -particle charge number  $z^2 = 4$ . All three curves of  $(1/z^2)S/\rho$  vs  $\beta$  are described by very similar functions for  $\beta > 0.04$ , though the electron and  $\alpha$ -particle curves are about 10% below the proton curve.<sup>4</sup> At low speeds the scaled  $\alpha$ -particle curve falls significantly below the proton curve. The reason, the formation of an electron cloud on the  $\alpha$  particle, is discussed below.

It is not difficult to understand the basic shape of the stopping power curve. Most of the energy loss is from the projectile to the electrons of the target atom. Since the electrons are bound to the target nucleus, the speed with which the projectile passes the target is important. Imagine pushing slowly on a swing with a force that gradually increases and then decreases. The net force on the swing is the vector sum of the external force exerted  $\mathbf{F}_{\text{ext}}$ , the vertical pull of gravity, and the tension in the ropes and equals the swing's mass times acceleration. For small horizontal displacements  $x$  from equilibrium, the vector sum of the weight and the tension in the string is horizontal and nearly proportional to  $x$ . It points toward the equilibrium position, and for small displacements is approximately a linear restoring force. If the proportionality constant is  $k$ ,  $ma = F_{\text{ext}} - kx$ .

This is the equation of motion for an undamped harmonic oscillator (Chapter 10 and Appendix F). If the force builds up slowly, there is a very small acceleration, and the swing angle changes so that  $F_{\text{ext}} \approx kx$ . As the force decreases the swing returns to its resting position. All of the work that was done to displace the swing is now returned as work by the swing on the source of the external force. No net energy has been imparted to the swing. This is called an *adiabatic* process or approximation, a slightly different use of the term than in Chapter 3.

At the other extreme, the force could be applied for a very short time, building up to a peak and falling quickly. In this case, the swing does not have time to move and  $F_{\text{ext}} = ma$ . This can be integrated to give

$$\int F_{\text{ext}} dt = m \int a dt = m(v_{\text{final}} - v_{\text{initial}}). \quad (15.50)$$

The swing acquires a velocity and hence some kinetic energy. The integral of force with respect to time is called the *impulse*, and this limit is the *impulse approximation*.

The two limits depend on whether the duration of the force is long or short compared to the natural period of the swing. The atomic electrons are bound, and they have a natural period that is the circumference of their orbit divided by their speed  $v_{\text{electron}}$ . The length of time that a projectile exerts a force on the electrons is roughly the diameter of the atom divided by the projectile speed. Ignoring factors of  $2\pi$ , we see that the passage of the

projectile will be adiabatic if

$$\frac{d_{\text{atom}}}{v_{\text{projectile}}} \gg \frac{d_{\text{atom}}}{v_{\text{electron}}}$$

or  $v_{\text{projectile}} \ll v_{\text{electron}}$ . The impulse approximation will be valid if  $v_{\text{projectile}} \gg v_{\text{electron}}$ .

This is sufficient to explain the shape of the stopping-power curves in Fig. 15.18. When the projectile has very low energy it moves past the atom so slowly that the electrons have time to rearrange themselves<sup>5</sup> and then return to their original state as the projectile leaves, restoring to the projectile the energy that they received while rearranging. As the projectile speed increases, the process is no longer adiabatic, first for the more slowly moving outer electrons and then for more and more of the inner atomic electrons as the speed increases. At the other extreme, when the projectile speed becomes high enough, we can think of the process in terms of the impulse approximation. The faster the projectile moves by, the shorter the time the force is applied and the smaller the energy transfer. The energy transfer is most effective, and the peak of the stopping power occurs, when the speed of the projectile is about equal to the speed of the atomic electrons in the target.

The cross section  $d\sigma/dW$  in Eqs. 15.45–15.47 is the sum of cross sections for three possible processes. We have already described the stopping power due to interactions of the projectile with the target electrons,  $S_e$ . There is another contribution to the stopping power from interactions of the projectile with the target nucleus,  $S_n$ . It is also possible for the energy loss to involve the radiation of a photon, so we also have radiative stopping power,  $S_r$ . Because these are independent processes, the total stopping power and the cross section are each the sum of three terms:

$$\frac{S}{\rho} = \frac{S_e}{\rho} + \frac{S_n}{\rho} + \frac{S_r}{\rho}, \quad (15.51)$$

$$\frac{d\sigma}{dW} = \left( \frac{d\sigma}{dW} \right)_e + \left( \frac{d\sigma}{dW} \right)_n + \left( \frac{d\sigma}{dW} \right)_r.$$

To compare these processes, we need to consider the maximum energy that can be transferred, as well as the relative probability of each process. The maximum possible energy transfer  $W_{\text{max}}$  can be calculated using conservation of energy and momentum. For a collision of a projectile of mass  $M_1$  and kinetic energy  $T$  with a target particle of mass  $M_2$  which is initially at rest, a nonrelativistic calculation gives

$$W = \frac{4TM_1M_2}{(M_1 + M_2)^2}. \quad (15.52)$$

<sup>5</sup>Classically, if the electrons go around the nucleus many times while the projectile moves by, the shape of their orbits can change in response to the projectile. Quantum-mechanically, the shape of the wave function can change, but the quantum numbers do not change.

<sup>4</sup>A value  $\beta = 0.04$  corresponds to a kinetic energy of 400 eV for electrons, 800 keV for protons, and 3.2 MeV for  $\alpha$  particles.

TABLE 15.3. Maximum energy transfer and relative importance of nuclear and radiative interactions for various projectiles and targets.

Projectile	Target	Nuclear $W_{\max}$ (eV)	Electron $W_{\max}$ (eV)	$S_n/S$	$S_r/S$
Electron, 100 keV	Hydrogen	240	50,000		0.01%
	Carbon	20	50,000		0.09%
	Lead	1	50,000		2.2%
Electron, 1 MeV	Hydrogen	4,300	500,000		0.13%
	Carbon	360	500,000		0.65%
	Lead	20	500,000		11.5%
Proton, 10 keV	Hydrogen	5,000	20	1.7%	
	Carbon	2,800	20	1.6%	
	Lead	200	20	1.5%	
Proton, 100 keV	Hydrogen	50,000	220	0.17%	
	Carbon	28,400	220	0.15%	
	Lead	1,900	220	0.24%	
Proton, 1 MeV	Hydrogen	500,000	2,200	0.11%	
	Carbon	280,000	2,200	0.07%	
	Lead	19,000	2,200	0.09%	
$\alpha$ particle, 10 keV	Hydrogen	6,400	5	27%	
	Carbon	7,500	5	12%	
	Lead	700	5	10%	
$\alpha$ particle, 100 keV	Hydrogen	64,000	50	1.6%	
	Carbon	75,000	50	1.1%	
	Lead	7,400	50	1.8%	
$\alpha$ particle, 1 MeV	Hydrogen	640,000	500	0.13%	
	Carbon	750,000	500	0.12%	
	Lead	74,000	500	0.20%	

The analogous relativistic equation (needed, for example, when the projectile is an electron) is

$$W_{\max} = \frac{2(2 + T/M_1c^2)TM_1M_2}{M_1^2 + 2(1 + T/M_1c^2)M_1M_2 + M_2^2}. \quad (15.53)$$

The values of  $W_{\max}$  for representative projectiles and targets are shown in Table 15.3, along with the percentage of the stopping power due to nuclear collisions. For electrons, the table also shows the percentage of the stopping power due to radiative transitions. The percentages are calculated from ICRU Report 49 (1993). Electrons can scatter from nuclei, but the amount of recoil energy transferred to the nucleus is very small. Although electrons undergo a great deal of nuclear scattering, which results in a tortuous path through material, they lose very little energy in a nuclear scattering. The heavier projectiles can lose relatively more energy in each nuclear collision than in each electron collision. For a given kind of projectile, nuclear stopping is more important at lower energies, because less energy can be transferred to an electron. The heavier the projectile for a given energy, the more important the nuclear term becomes, for the same reason.

The collision of electrons with electrons is a special case. Equation 15.52 or 15.53 gives  $W_{\max} = T$ . Consider the collision of two billiard balls of the same mass. If the projectile misses the target, it continues straight ahead with its original energy and  $W = 0$ . If it hits the target head on, it comes to rest and the target travels in the same direction with the same energy that the projectile had—a situation indistinguishable from the complete miss. It is customary (but arbitrary) in the case of identical particles to say that the particle with higher energy is the projectile, so  $W_{\max} = T/2$ . This adjustment has been made in Table 15.3 for electrons on electrons and protons on protons.

Radiation is only important for electrons and occurs in a certain fraction of the elastic electron scatterings from the target nucleus. Nuclear scattering gives the electron a fairly large acceleration. Classically, an accelerated charged particle radiates electromagnetic waves. This process is called *bremstrahlung*—braking or deceleration radiation. The energy radiated is proportional to the square of the acceleration, so *bremstrahlung* is only important for light projectiles. There is also a contribution from electron–electron or positron–electron scattering.

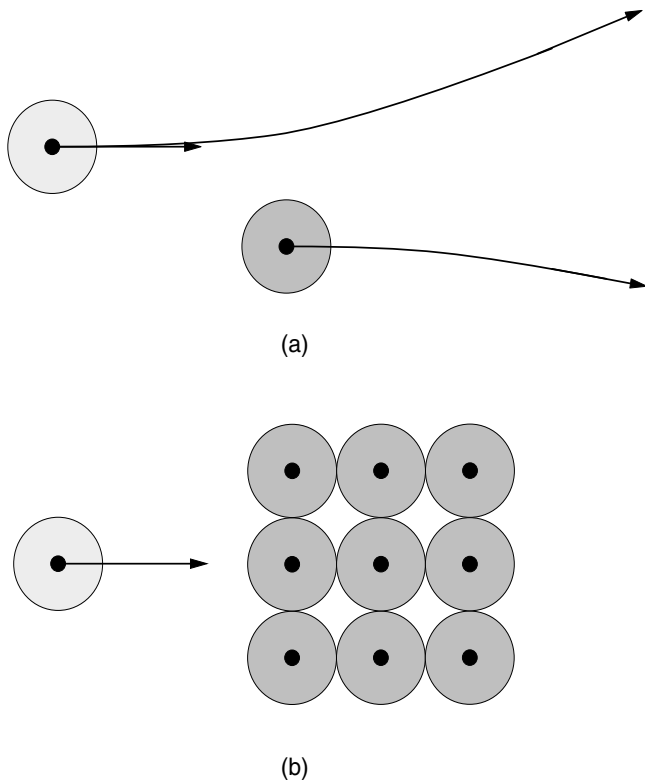


FIGURE 15.19. A projectile, which may or may not carry an electron cloud, moves past a target atom. (a) In a gas the projectile interacts with one atom at a time. (b) In a liquid or a solid, neighboring atoms may influence the interaction.

The electron–electron contribution vanishes at low energies, although the positron–electron bremsstrahlung does not.<sup>6</sup> We will see in Chapter 16 that bremsstrahlung is an important component of the x-ray spectrum produced when a beam of electrons strikes a target. Even so, the fraction of the electron energy that is converted to radiation is small.

An atom has a radius of a few times  $10^{-10}$  m. The nucleus of the atom is much smaller, about  $10^{-15}$  m, and contains most of the atom’s mass. The atom’s size is determined by the electron cloud around the nucleus. Figure 15.19(a) shows a projectile entering at the left and traveling to the right through a gas. It interacts with one target atom at a time. The solid black dots represent the nuclei of the projectile and the target atom. The shaded circles represent the electron clouds. The projectile may or may not have an electron cloud, which is shown with lighter shading. Figure 15.19(b) shows the interaction with a solid or liquid in which the target atoms

<sup>6</sup>This difference can be understood classically. In the first approximation, the radiation by a charge is proportional to the product of the charge times its acceleration,  $qa$ . For two interacting electrons,  $a_1 = -a_2$ ,  $q_1 = q_2$ , and the sum of these two terms vanishes. For an electron and a positron  $a_1 = -a_2$ ,  $q_1 = -q_2$ , and the two terms add.

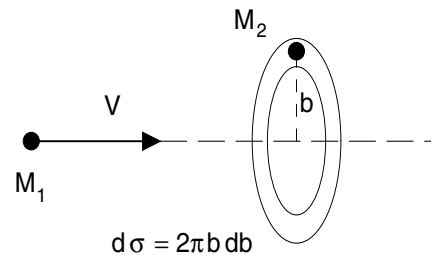


FIGURE 15.20. The impact parameter is the perpendicular distance from the target particle to a line extended from the projectile in the direction of its velocity before the interaction.

are tightly packed, and it may not be accurate to say that the projectile interacts with only one atom at a time.

Classically, the motion of a charged projectile past a charged target depends on the charges and masses of the particles, the initial velocity or kinetic energy of the projectile, and the *impact parameter*  $b$ , which is the perpendicular distance from a line through the initial velocity of the projectile to the target, as shown in Fig. 15.20. The classical cross section for having an impact parameter between  $b$  and  $b + db$  is the area of the ring,  $2\pi b db$ . If we could relate  $b$  to the energy loss  $W$ , we would have the cross section  $d\sigma/dW$  of Eq. 15.47.

The energy-loss process is quite complicated, and the cross section cannot be calculated exactly. A great deal of experimental and theoretical work on stopping powers has been done, extending from 1899 to the present time. Different models are used for the low energy regime and the high energy regime. The history is nicely reviewed by Ziegler *et al.* (1985). Much of the recent work on stopping powers has been motivated by the use of ion implantation to make semiconductors, the analysis of materials using ion beams, and medical applications. Currently stopping powers of low-energy heavy ions can be calculated with an accuracy of better than 10%. For high-speed light ions the accuracy is better than 2%. References are found in Ziegler *et al.* (1985).

### 15.11.1 Interaction with Target Electrons

We first consider the interaction of the projectile with a target electron, which leads to the *electronic stopping power*,  $S_e$ . Many authors call it the *collision stopping power*,  $S_{col}$ . There can be interactions in which a single electron is ejected from a target atom or interactions with the electron cloud as a whole (a “plasmon” excitation). The stopping power at higher energies, where it is nearly proportional to  $\beta^{-2}$ , has been modeled by Bohr, by Bethe, and by Bloch [see the review by Ahlen (1980)]. The Bethe–Bloch model is also valid for relativistic energies. A nonrelativistic model for high energies was developed by J. Lindhard and his colleagues [see references in

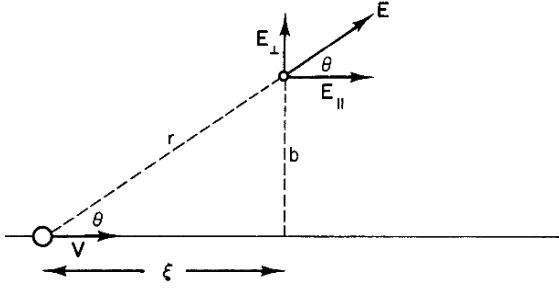


FIGURE 15.21. A heavy particle of charge  $ze$ , mass  $M$ , and velocity  $\mathbf{V}$  moves past a stationary electron.

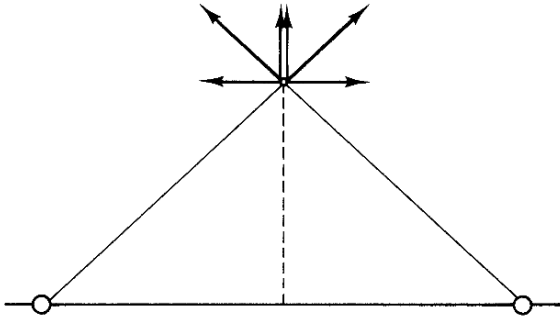


FIGURE 15.22. Why the parallel component of  $\mathbf{p}$  is zero. For every point where the projectile gives a particular  $\mathbf{E}_{\parallel}$ , there is a symmetric point where  $\mathbf{E}_{\parallel}$  is equal but opposite. The components  $\mathbf{E}_{\perp}$  are in the same direction in both places, so the perpendicular component of  $\mathbf{p}$  does not vanish.

Ziegler *et al.* (1985)]. It allows more accurate calculations of which electrons in the target receive energy from the projectile.

We can gain considerable insight into the high-energy loss process by making a classical calculation of the cross section for transferring energy to an electron using the impulse approximation. This is a simplification of the Bethe–Bloch model. In our model, a heavy projectile passes by a free electron that is at rest. Momentum is transferred from the projectile to the electron. Because of its large mass, the projectile's velocity does not change appreciably, but the lighter electron acquires an appreciable velocity and kinetic energy. If the momentum transferred to the electron is  $\mathbf{p}$ , its kinetic energy is  $p^2/2m_e$ . That kinetic energy must have been lost by the projectile.

Figure 15.21 shows a particle of mass  $M$ , charge  $ze$ , and velocity  $V = \beta c$  moving past a stationary electron. The impact parameter  $b$  is the perpendicular distance from the electron to the path of the projectile. The distance from the projectile to the electron is  $r$ , and the distance along the path to the point of closest approach is  $\xi$ . The momentum transferred to the electron is  $\mathbf{p} = \int \mathbf{F} dt = -e \int \mathbf{E} dt$ . By symmetry, there is no component of  $\mathbf{p}$  parallel to the path of the projectile. The reason is shown in Fig. 15.22. For each location of the projec-

tile that gives a parallel component of  $\mathbf{F}$  in one direction, there is a position an equal distance on the other side of the point of closest approach that gives a component of  $\mathbf{F}$  with the same magnitude but in the opposite direction. The perpendicular component of  $\mathbf{F}$  is the same for both locations, so there is a net perpendicular component of momentum transfer. The magnitude of the perpendicular component of  $\mathbf{E}$  is

$$E_{\perp} = E \sin \theta = \frac{ze \sin \theta}{4\pi\epsilon_0 r^2} = \frac{zeb}{4\pi\epsilon_0 r^3} = \frac{ze}{4\pi\epsilon_0} \frac{b}{(\xi^2 + b^2)^{3/2}}.$$

The perpendicular impulse is  $\int F_{\perp} dt = -e \int E_{\perp} (dt/d\xi) d\xi$ . If the fraction of energy lost by the projectile is small, then  $dt/d\xi = 1/\beta c$  does not change during the collision. The magnitude of the impulse is therefore

$$\begin{aligned} p &= -\frac{e}{V} \int E_{\perp} d\xi = -\frac{ze^2 b}{4\pi\epsilon_0 \beta c} \int_{-\infty}^{\infty} \frac{d\xi}{(\xi^2 + b^2)^{3/2}} \\ &= -\frac{ze^2 b}{4\pi\epsilon_0 \beta c} \lim_{x \rightarrow \infty} \left[ \frac{\xi}{b^2(\xi^2 + b^2)^{1/2}} \right]_{-x}^x \\ &= -\frac{2ze^2}{4\pi\epsilon_0 \beta cb}. \end{aligned}$$

The smaller the impact parameter, the greater the momentum transfer to the electron. The kinetic energy acquired by the electron is

$$W = \frac{p^2}{2m_e} = \frac{2z^2 e^4}{(4\pi\epsilon_0)^2 m_e c^2 \beta^2 b^2}.$$

The factor  $e^4/(4\pi\epsilon_0)^2 m_e c^2$  depends only on the charge and mass of the electron. It can be written as  $r_e^2 m_e c^2$ , where  $r_e$  is the classical radius of the electron [Eq. 15.18]. The factor has the numerical value

$$r_e^2 m_e c^2 = 6.50 \times 10^{-43} \text{ J m}^2 = 4.06 \times 10^{24} \text{ eV m}^2.$$

Using this notation the energy transfer per target electron is

$$W = \frac{2z^2 r_e^2 m_e c^2}{\beta^2 b^2}. \quad (15.54)$$

Here  $z$  is the charge on the projectile,  $\beta c$  is its speed, and  $b$  is the impact parameter. Note that  $W$  does not depend on the mass of the heavy projectile, but only on its speed. As the speed becomes less, the energy transfer becomes greater, because the projectile takes longer to move past the electron and the force is exerted for a longer time (as long as the time is still short enough so that the impulse approximation remains valid).

If the electrons are uniformly distributed, the cross section for each electron is  $d\sigma = (d\sigma/dW) dW = 2\pi b db$ . This can be written, with the help of Eq. 15.54, in terms of  $W$ :

$$\frac{d\sigma}{dW} dW = \frac{4\pi z^2 r_e^2 m_e c^2}{2\beta^2} \frac{dW}{W^2}. \quad (15.55)$$

This expression diverges as  $W$  approaches zero, corresponding to very large impact parameters. However, the assumption that the target electrons are free fails in this limit, so that there is some effective lower limit  $W_{\min}$ . Also, the greater the impact parameter, the longer the electron will experience the force exerted by the projectile (though it will be weaker). If the time is too long, the electron can move in response to the force and not absorb as much energy; the impulse approximation is no longer valid. We have already seen that there is a maximum energy transfer  $W_{\max}$ . Multiplying the cross section by  $W$ , integrating from  $W_{\min}$  to  $W_{\max}$ , and noting that there are  $Z$  electrons per target atom, we obtain

$$\frac{S_e}{\rho} = \frac{4\pi N_A r_e^2 m_e c^2}{\beta^2} \frac{Z}{A} z^2 \ln \left( \frac{W_{\max}}{W_{\min}} \right). \quad (15.56)$$

The factor  $4\pi N_A r_e^2 m_e c^2$  has the value  $30.707 \text{ eV m}^2 \text{ mol}^{-1} = 0.30707 \text{ MeV cm}^2 \text{ mol}^{-1}$ .

A quantum-mechanical calculation gives a result of essentially the same form as Eq. 15.56. The logarithmic term includes both ionization and plasmon excitation<sup>7</sup> and is called the *stopping number per atomic electron*  $L(\beta, z, Z)$ :

$$\frac{S_e}{\rho} = \frac{4\pi r_e^2 m_e c^2}{\beta^2} N_A \frac{Z}{A} z^2 L(\beta, z, Z). \quad (15.57)$$

For heavy charged particles  $L$  has the form

$$L(\beta, z, Z) = L_0 + zL_1 + z^2L_2, \\ L_0 = \ln \left( \frac{\beta^2}{1 - \beta^2} \right) + \ln \left( \frac{2m_e c^2}{I(z)} \right) - \beta^2 - \frac{C}{Z} - \frac{\delta}{2}. \quad (15.58)$$

Equation 15.57 with  $L = L_0$  is often called the *Bethe–Bloch formula*. The second term in  $L_0$  depends on  $I(Z)$ , the ionization potential of the atoms in the absorber, averaged over all the electrons in the atom. Values of  $I(Z)$  have been calculated theoretically and also derived from measurements of the stopping power. They range from 14.8 eV for hydrogen to 884 eV for uranium. The value 14.8 eV is greater than the ground-state energy of hydrogen, 13.6 eV, because the ejected electron has some average kinetic energy.

Published values of  $I$  can vary considerably, depending on whether the other correction terms are present. For example, values of  $I$  in the literature for hydrogen range from 11 to 20 eV. Discussions of values for  $I$  and the various terms in  $L$  can be found in ICRU Report 49 (1993), in Ahlen (1980), and in Attix (1986). The term  $\delta/2$  corrects for the *density effect*. The calculation above assumed that the electron experienced the full electric field of the projectile. However, other electrons in the absorber move slightly, polarizing the absorber and reducing the field. This effect becomes important at high

energies as the electric field is distorted by relativistic effects. It also depends on the density of the absorber. A small density effect persists in conductors even at low energies; however, it is usually incorporated into the value of  $I(Z)$ . For the projectile energies we are considering, the density effect is most important for electrons.

An alternative nonrelativistic treatment by Lindhard and colleagues allows the use of accurate atomic electron density distributions and also considers the effect of electrons in neighboring atoms.<sup>8</sup> In the Lindhard model the stopping power is

$$\frac{S_e}{\rho} = \frac{N_A}{A} \int z^2 I(V, \rho_e) \rho_e 4\pi r^2 dr, \quad (15.59)$$

where  $z$  is the projectile charge,  $I$  is the *stopping interaction strength* in  $\text{J m}^2$  (more often in  $\text{eV pm}^2$ ),<sup>9</sup>  $\rho_e$  is the electron density in the atom (in units of the electron charge), and  $4\pi r^2 dr$  is the volume element. Integration of  $\rho_e$  over all volume gives  $Z$ , the atomic number of the target. Comparison of Eqs. 15.59 and 15.47 shows that the integral in Eq. 15.59 is the stopping cross section per target atom.

Figure 15.23 shows how the Lindhard model explains why the stopping power falls below the  $1/\beta^2$  curve at lower projectile velocities. Each panel shows the electron density in copper,  $4\pi r^2 \rho_e$ , and the interaction strength  $I$ . Their product, the solid line, is the integrand in Eq. 15.59. The integral is taken from 0 to 0.14 nm (1.4 Å (angstrom)). The  $K$ ,  $L$ , and  $M$  shells of copper can be seen in the electron density curve. Figure 15.23(a) is for a 10-MeV proton or some other heavy ion with the same speed. The projectile is moving fast enough so that all electrons except those in the  $K$  shell interact with it. Contrast this with Fig. 15.23(b), which is for a 100-keV proton. The projectile speed is much less, and the interaction is almost exclusively with the outer electrons.<sup>10</sup>

Both the Bethe–Bloch and Lindhard models fail at low energy, because the electrons are not free and many of the interactions are adiabatic. Some models reviewed by Ziegler *et al.* (1985) predict a stopping power proportional to projectile velocity. This has been found to be true in general, though not for all elements. The experiments are quite difficult because of the thinness of the targets, contamination, and so on. Figure 15.24 shows the regions where the various models apply for protons. For electrons, relativistic effects are important above about

<sup>8</sup>The electron density functions are calculated using quantum mechanics. The problem is to find the electron distribution by solving Schrödinger's equation with the potential distribution due to the nucleus and the potential due to the electron charge distribution for which one is solving. This self-consistent computation is called the Hartree–Fock approximation.

<sup>9</sup> $I$  is not the same as the average ionization energy of Eq. 15.58.

<sup>10</sup>The solid line representing the integrand does not fall to zero at 0.12 nm = 1.2 Å because of the effect of electrons from neighboring atoms. In a solid there are no regions where the electron density is zero.

<sup>7</sup>A plasmon excitation is due to the interaction of the projectile with the entire electron cloud of the atom.

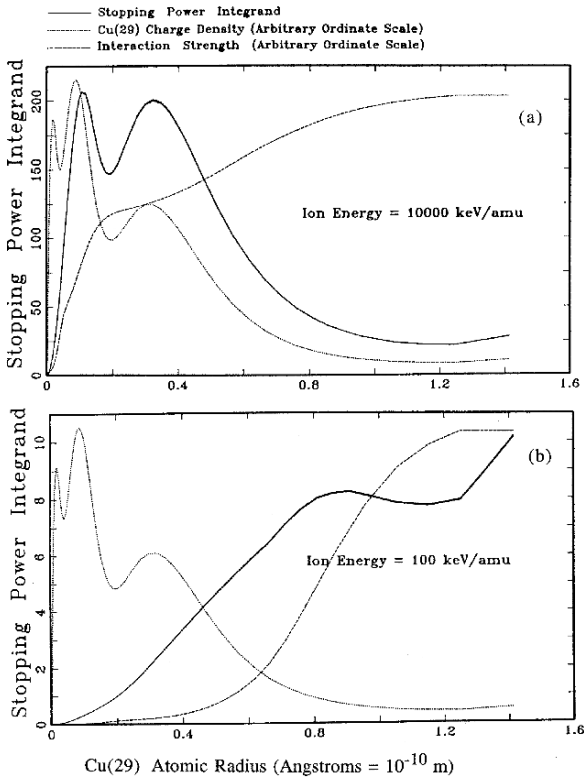


FIGURE 15.23. Calculation of the stopping power at low energies involves integrating the product of the electron charge distribution in the target atom and the interaction strength function, which depends on the projectile speed. The dotted line shows the electron charge density for copper. The solid line shows the integrand. (a) For 10-MeV protons, all electrons but those in the *K* shell contribute. (b) For 100-keV protons the interaction function has changed, and only the outermost electrons contribute. Note the much different ordinate scales in (a) and (b). Provided by J. F. Ziegler.

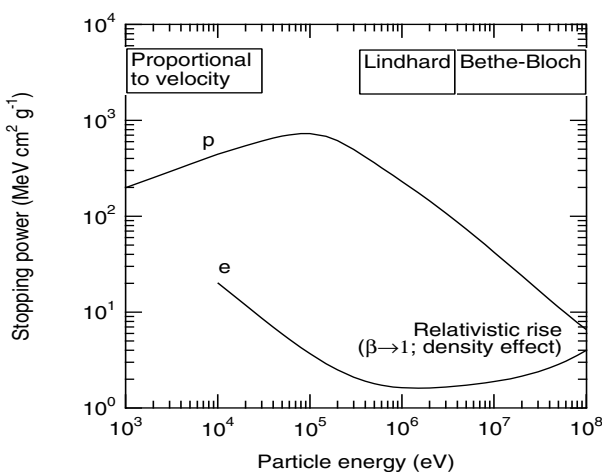


FIGURE 15.24. Proton and electron stopping power vs. energy in carbon, showing the regions in which various models are valid.

500 keV. The rise in stopping power at high energies is due to the density effect (polarization of the electrons).

Another important effect at low energies is that the slowly moving ion can capture electrons, decreasing the value of  $z^2$ . Ziegler *et al.* (1985) discuss the scaling of data for different projectiles and the appropriate effective charge values. The average projectile charge follows a universal curve when plotted as a function of the appropriate combination of the speeds of the projectile and target electrons. They, and the ICRU Report 49 (1993), assume that for protons the effective charge is always unity. The theoretical justification is that the radius of the electron orbit in hydrogen is larger than the interatomic separation in solids.

### 15.11.2 Scattering from the Nucleus

The projectile can also scatter from the target atom as a whole. The recoil kinetic energy of the atom is lost by the projectile. Since the nucleus contains most of the mass, the kinematics are those of the bare projectile and the target nucleus, and this process is called *nuclear scattering*, with stopping power  $S_n$ . (Sometimes it is called *elastic scattering*, with a subscript that can cause it to be confused with electron interactions.)

Just as with Compton scattering, knowing the angle through which the projectile is scattered defines the amount of energy transferred to the target. The angle depends on the impact parameter. The problem can be solved for a given impact parameter if the force between the projectile and target is a function only of their separation and one knows the potential energy of their separation. The details are found in Ziegler *et al.* (1985). We will simply comment on the contributions to the potential energy. They are

1. The Coulomb force between the projectile and the target nucleus.
2. The Coulomb force between the projectile and the electron cloud of the target atom.
3. The Coulomb attraction between the target nucleus and any electrons surrounding the projectile.
4. The Coulomb repulsion between the electron clouds of the target and the projectile.
5. A term due to the Pauli exclusion principle if the projectile is an ion with an electron cloud. To see how it arises, suppose that both the projectile and target have both of their possible *K*-shell electrons. If the nuclei get close enough, they effectively form a single nucleus that cannot have four *K*-shell electrons. Therefore, two of the electrons have to move to unfilled shells. This requires energy that comes from the kinetic energy of the projectile. This is called *Pauli promotion*. Even though the electrons have time to

return to their original orbits for a slow projectile, the effect changes the overall potential and hence the projectile orbit and the probability of a particular energy transfer.

6. An *exchange term* that also arises from the Pauli principle, related to whether the spins of the projectile and target electrons are parallel or antiparallel.

Because nuclear scattering is relatively unimportant for the charged particles we are considering and because it does not lead to ionization, we will not describe any details of the calculations.

### 15.11.3 Stopping of Electrons

Equations similar to Eq. 15.57 are obtained for electrons and positrons. Recall that energy loss in nuclear scattering is negligible for positrons and electrons because they are so light, and that bremsstrahlung transfers some of the electron kinetic energy to radiation. Electrons and positrons are assumed to collect no screening charge. Even at low energies, the electron velocities are high enough to that the Bethe–Bloch model is used. The collision stopping power for electrons is<sup>11</sup>

$$\frac{S_e}{\rho} = 4\pi N_A r_e^2 m_e c^2 \frac{1}{\beta^2} \frac{Z}{A} L_{\pm}. \quad (15.60)$$

The subscript  $\pm$  indicates that stopping number per electron is slightly different for electrons and for positrons. The exact forms can be found in Attix (1986) or in ICRU Report 37 (1984). In both cases,  $L$  depends on  $I(Z)$  and the density effect. An accurate calculation of the shell correction for electrons has not been made; therefore ICRU Report 37 omits the shell correction from the tables for electrons and positrons. This omission makes the use of Eq. 15.59 less accurate for electrons below 10 keV. The best values of  $S_e/\rho$  for electrons and positrons are obtained from theoretical calculations using Eq. 15.60 and values of  $I(Z)$  determined from proton data.

### 15.11.4 Compounds

In dealing with compounds, it is frequently assumed that each atom in the target interacts independently with the projectile, as we assumed for photons. The stopping power per molecule is then equal to the sum of the stopping powers for each atom in the molecule. This leads to a formula analogous to Eq. 15.32, known as the *Bragg rule*:

$$\frac{S}{\rho} = \sum_i w_i \left( \frac{S}{\rho} \right)_i. \quad (15.61)$$

This equation applies to the collision, radiative, nuclear, and total stopping powers. This approximation is quite

<sup>11</sup>The literature often replaces the  $4\pi$  by  $2\pi$  for electrons and makes  $L$  twice as large.

inaccurate near the peak of the stopping power curve, where the errors can be greater than a factor of 2. This is not surprising, given the behavior of the scattering function  $I$  in Fig. 15.23(b). Most of the energy loss is to outer electrons—the conduction electrons if the substance is a metal. In a semiconductor there are gaps in the energy levels, and this precludes the low-energy transfers. As a result, the stopping power is lower in semiconductors. In crystals, channeling can occur: the stopping power depends on the orientation of the trajectory with the crystal symmetry axis.

Carbon poses a particular problem. It is an important element in the body, and it has chemical bonds that range from metallic to insulating in nature. Various investigators have shown variations in stopping power of 30% for ions in pure carbon, depending on how it was fabricated. Graphite can be made with different electrical conductivities, and there are associated differences in stopping power. Ziegler and Manoyan (1988) have applied charge-scaling techniques to several organic carbon compounds by considering separately the stopping due to closed atomic shells (cores) and the remaining bonds between different pairs of atoms.

ICRU Reports 37 (1984) and 49 (1993) handle departures from the Bragg rule in the first approximation by using different values of  $I$  for electrons in compounds. The density effect is important for electrons and also does not follow the Bragg rule.

Stopping-power values are found in ICRU Report 37 for positrons and electrons. ICRU Report 49 has stopping powers for protons and  $\alpha$  particles. These data are also found on the web: [physics.nist.gov/PhysRefData/Star/Text/contents.html](http://physics.nist.gov/PhysRefData/Star/Text/contents.html). A computer program for protons and ions, SRIM (Stopping and Range of Ions in Matter) is described by Ziegler *et al.* (1985) and is available at [www.srim.org](http://www.srim.org).

## 15.12 Linear Energy Transfer and Restricted Collision Stopping Power

In modeling the effect of ionizing radiation on targets, whether they be radiation detectors, photographic emulsions, cells, or parts of cells, one often wants to know how much of a charged particle’s energy is absorbed “locally,” that is, within some region around a particle’s trajectory. An accurate calculation is difficult, since some of the electrons produced may leave the region of interest. Also, the energy absorbed in some region of interest around a particle track comes both from energy lost by the particle while traversing that track segment and also from photons and charged particles produced elsewhere by the projectile. [This is discussed in detail in ICRU Report 16 (1970).]



An approximation to the desired quantity is the *linear energy transfer* (LET) or the *restricted linear collision stopping power*  $L_\Delta$ . It is defined as the ratio  $dT/dx$ , where  $dx$  is the distance traveled by the particle and  $dT$  is the mean energy loss to electrons that results in energy transfers less than some specified  $\Delta$ . This use of the symbol  $L$  should not be confused with the stopping number of Eqs. 15.57–15.60. The quantity  $L_\Delta$  can be calculated by replacing  $W_{\max}$  by  $\Delta$  in the expression for the stopping power. The value of  $\Delta$  is usually specified in electron volts.

The electron stopping power  $S_e$  is numerically equal to  $L_\infty$ . However,  $S_e$  is defined in terms of the energy *lost by the particle*, while  $L_\infty$  is defined in terms of energy *imparted to the medium*.

Note that although the quantity actually of interest may be the energy imparted within some region around the trajectory, this definition is based on energy transfers less than  $\Delta$ . A quantity based on the region of interest would be easier to measure;  $L_\Delta$  is easier to calculate.

ICRU Report 37 calculates  $L_\Delta$  for positrons and electrons for values of  $\Delta$  down to 1 keV. The report points out that such calculations are inaccurate for smaller values of  $\Delta$ , even in light elements. ICRU Report 16 provides values of  $L_\Delta$  for protons and heavy ions.

### 15.13 Range, Straggling, and Radiation Yield

We can see in Fig. 15.27 that the  $\alpha$  particles, entering from the bottom with the same energy, all travel about the same distance before coming to rest. This distance is called the *range* of the  $\alpha$  particles. It will be defined more precisely below.

We can estimate the range in the following way. The stopping power represents an average energy loss per unit path length. The actual energy loss fluctuates about the mean values given by the stopping power. If these fluctuations are neglected and the projectiles are assumed to lose energy continuously along their tracks at a rate equal to the stopping power, then one is making the *continuous-slowing-down approximation* (CSDA). In this approximation one can calculate the range, the distance a particle with initial energy  $T_0$  travels before coming to rest or reaching some final kinetic energy  $T_f$ . A factor  $\rho$  is introduced to express the range in mass per unit area:

$$R_{\text{CSDA}}(T_0, T_f) = \rho \int_{T_f}^{T_0} dx = \rho \int_{T_f}^{T_0} \frac{dT}{S_e + S_n + S_r}. \quad (15.62)$$

ICRU Report 37 (1984) discusses the problem of carrying the integration to  $T_f = 0$ .

The CSDA range is not directly measurable. Measurements of the fraction  $F(R)$  of monoenergetic particles in a beam that passes through an absorber of thickness  $R$

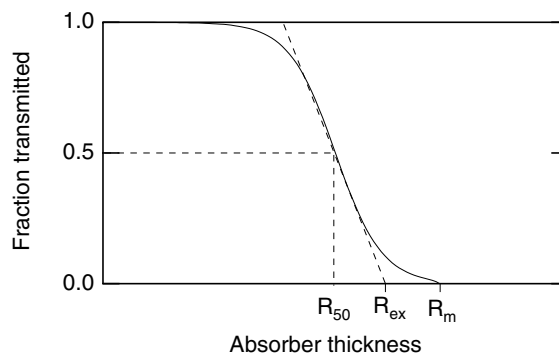


FIGURE 15.25. Plot of the number of particles passing through an absorber vs its thickness to show the definition of various ranges.  $R_{50}$  is the median range,  $R_{\text{ex}}$  is the extrapolated range, and  $R_m$  is the maximum range.

gives a curve like that of Fig. 15.25. Various ranges can be defined using this curve. The most easily measured is the median range  $R_{50}$ , corresponding to an absorber thickness that transmits 50% of the incident particles. The extrapolated range  $R_{\text{ex}}$  is obtained by extrapolating the linear portion of the curve to the abscissa. The maximum range  $R_m$  is the thickness that just stops all of the particles; it is, of course, very difficult to measure. If  $F(R)$  is known accurately one can define a *mean range*  $\bar{R} = \int R(-dF/dR)dR / \int (-dF/dR)dR$ . If the shape of the transmission curve is perfectly symmetrical about the mean, then  $R_{50}$  is equal to  $\bar{R}$ , even though they are conceptually quite different. For heavy projectiles  $\bar{R}$  (usually approximated by  $R_{50}$ ) provides the best estimate of  $R_{\text{CSDA}}$ .

The fluctuations in the range are called *straggling*. The straggling distribution has also been calculated. The track of a heavy projectile such as an  $\alpha$  particle is fairly straight, because the various scattering interactions result only in small angular deviations. The straggling results primarily from the fact that  $Sdx$  represents only an average energy loss in path length  $dx$ . The fluctuations can be integrated to give the spread in range; see Ahlen (1980) or ICRU Report 37 (1984) or ICRU Report 49 (1993) or the computer program SRIM [Ziegler *et al.* (1985)].

Electrons and positrons are so light that they undergo large-angle scattering (occasionally from an electron, more often from an atomic nucleus). The resulting electron trajectories are quite tortuous, as can be seen in Figs. 15.28 and 15.29. The median or mean range for an electron is considerably less than  $R_{\text{CSDA}}$ . For electrons and positrons the extrapolated range  $R_{\text{ex}}$  corresponds most closely to  $R_{\text{CSDA}}$ , at least in materials with atomic number up to silver [Tung *et al.* (1979)]. Figure 15.26 shows ranges in water. At medium energies the dependence on energy is approximately  $T^2$ .

Tables of ranges are found in the references cited above or at the NIST web site [physics.nist.gov/PhysRefData/Star/Text/contents.html](http://physics.nist.gov/PhysRefData/Star/Text/contents.html).

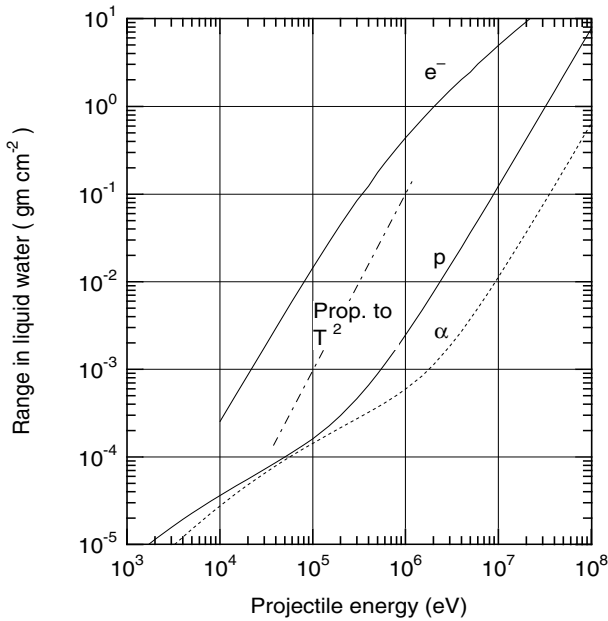


FIGURE 15.26. Range of electrons, protons, and  $\alpha$  particles in liquid water. Data are from ICRU Reports 37 (1984) and 49 (1993). Note that for water the range in  $\text{gm cm}^{-2}$  is the same as the range in cm.

The *radiation yield*,  $Y$ , is the fraction of the initial particle (usually electron) kinetic energy  $T_0$  that is converted to bremsstrahlung photons as the electron comes to rest in the medium in question. The yield is calculated using the continuous-slowing-down approximation as (neglecting  $S_n$ )

$$Y(T_0) = \frac{1}{T_0} \int_0^{T_0} \frac{S_r(T)dT}{S_e(T) + S_r(T)}. \quad (15.63)$$

### 15.14 Track Structure

We can gain insight into the interaction processes by examining tracks in photographic emulsions or in cloud chambers. Figures 15.27 and 15.28 are taken from a classic atlas of tracks in nuclear emulsions [Powell *et al.* (1959)]. They show the difference between the interaction of heavy and light particles in matter. Figure 15.27 shows the tracks of four cosmic-ray  $\alpha$  particles, each of which entered the bottom of the figure and stopped near the top. The fiduciary marks along the bottom are  $10 \mu\text{m}$  apart. Each track is about  $195 \mu\text{m}$  long, corresponding to an initial  $\alpha$ -particle energy of about 22 MeV. The emulsion has a density of  $3.6 \times 10^3 \text{ kg m}^{-3}$ . Each black dot is a sensitive silver halide grain about  $0.6 \mu\text{m}$  in diameter. At the beginning of the track,  $S$  is about  $70 \text{ keV } \mu\text{m}^{-1}$  or  $42 \text{ keV per grain}$ ;  $10 \mu\text{m}$  from the end of the track it is  $200 \text{ keV } \mu\text{m}^{-1}$  or  $120 \text{ keV per grain}$ . The energy that must be deposited in a grain to render it developable is about 2.8 keV. The amount of energy deposited in each

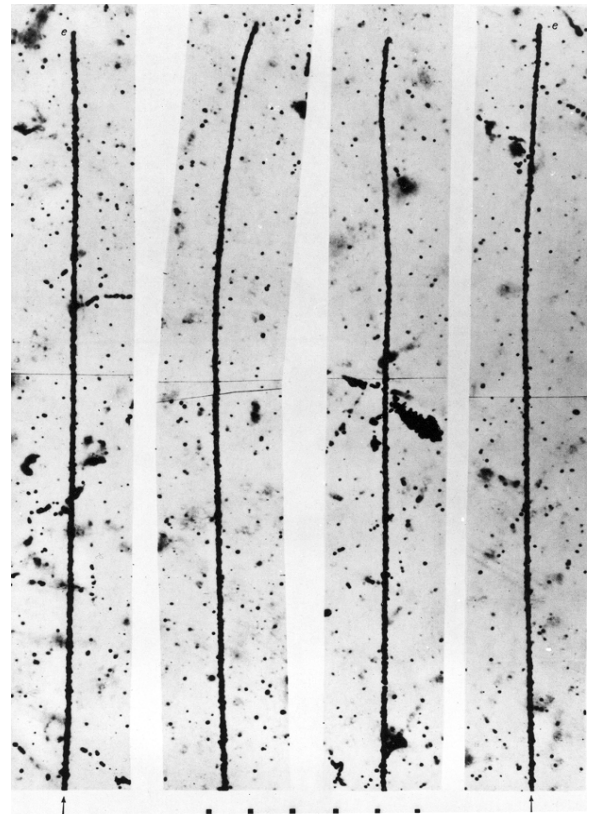


FIGURE 15.27. Tracks of 22-MeV  $\alpha$  particles in photographic emulsion. The  $\alpha$  particles enter at the bottom of the page and come to rest near the top. The small square fiducial marks at the bottom are  $10 \mu\text{m}$  apart. The features of the tracks are discussed in the text. From C. F. Powell, P. H. Fowler, and D. H. Perkins. *The Study of Elementary Particles by the Photographic Method*. Pergamon Press, 1959. Reproduced by permission of Professor D. H. Perkins.

grain is so much larger than this that the track density is uniform. Small bumps of 1–4 grains can be seen occasionally along each track. Some of these are due to  $\delta$  rays: electrons that have received enough energy to travel a few micrometers in the emulsion. Others are artifacts due to the general background fog. Multiple small-angle scattering causes small deviations in each track, which become greater as the  $\alpha$  particle slows down.

In Figure 15.28 an electron–positron pair has been produced in the lower left corner of the emulsion by a 1.5-MeV photon. Each particle has a kinetic energy of about 250 keV. One immediately notices the tortuous path of both particles due to large-angle scattering. The stopping power near the beginning of the track is about  $0.8 \text{ keV } \mu\text{m}^{-1}$ , so that about 0.5 keV is deposited in each grain. About  $30 \mu\text{m}$  from the end, the stopping power and the average amount of energy deposited in each grain are about 3 times larger. The upper track is considerably more dense near the end of its path. The failure of the other track to show this density increase could be due to annihilation of the positron in flight or to a large-angle scattering out of the emulsion.

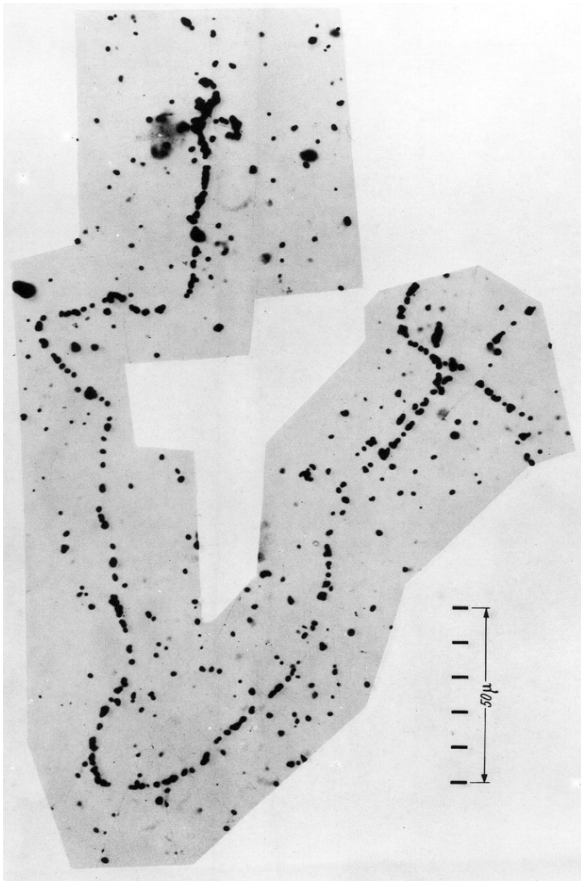


FIGURE 15.28. Tracks of electrons in emulsion. An electron—positron pair was produced in the lower left corner. Each particle has an energy of about 250 keV. The details are discussed in the text. From C. F. Powell, P. H. Fowler, and D. H. Perkins. *The Study of Elementary Particles by the Photographic Method*. Pergamon Press, 1959. Reproduced by permission of Professor D. H. Perkins.

Figure 15.29 shows the ionization produced by an electron at a much different scale. It was produced from a cloud chamber photograph of electron tracks in a low-density gas [Budd and Marshall (1983)]. The scale shows distances in liquid water or tissue that correspond to the same value of  $\rho x$ , corrected for phase effects. Note that the scale shows 10 *nanometers*. An atomic diameter is 0.2–0.6 nm. In each case a photoelectron of energy between 950 and 1480 eV has been ejected from a gas atom in the cloud chamber. Auger electrons are also seen.

## 15.15 Energy Transferred and Energy Imparted; Kerma and Absorbed Dose

The response of a substance to radiation, whether it is the darkening of a photographic film, an electrical pulse in an ionization chamber, or the response of a tumor to radiation therapy, is due, directly or indirectly, to the ioniza-

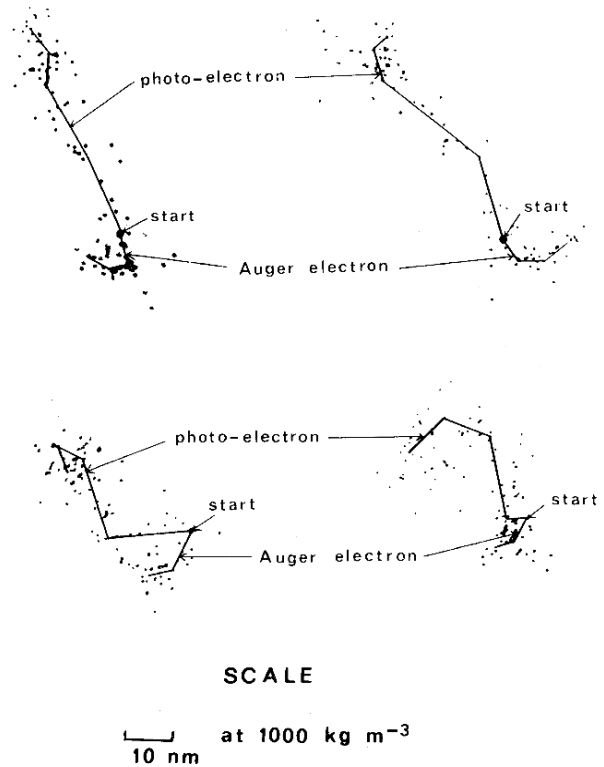


FIGURE 15.29. Tracks of  $\approx 1$  keV electrons in a cloud chamber. An equivalent scale in water or tissue has been added. Photoelectrons and Auger electrons can be seen. The lines were drawn to guide the eye. From T. Budd and M. Marshall. Microdosimetric properties of electron tracks measured in a low-pressure cloud chamber. *Radiation Research* **93**:19–32 (1983). Reproduced by permission of the Radiation Research Society.

tion produced by charged particles that lose their kinetic energy in the substance through the stopping mechanisms we have just discussed. We now define some quantities that are used to describe the transfer of energy from photons to charged particles and the energy lost by charged particles due to ionization.

### 15.15.1 An Example

Before discussing the formal definition of these quantities, let us consider some examples of energy transfer by photons. Figure 15.30 shows some schematic interactions of photons in a sample of water 10 cm thick. They are drawn to scale.<sup>12</sup>

In Fig. 15.30(a) five photons of energy 100 keV enter from the left. Photon tracks are dotted. One photon is absorbed by the photoelectric effect, and four are

<sup>12</sup>These examples were constructed with a pedagogical simulation program called MacDose [Hobbie (1992)]. The program is available at <http://www.oakland.edu/~roth/hobbie.html>. It runs on a Macintosh using OS-9 or earlier. A more realistic but easily understood Monte Carlo simulation is described by Arqueros and Montesinos (2003).

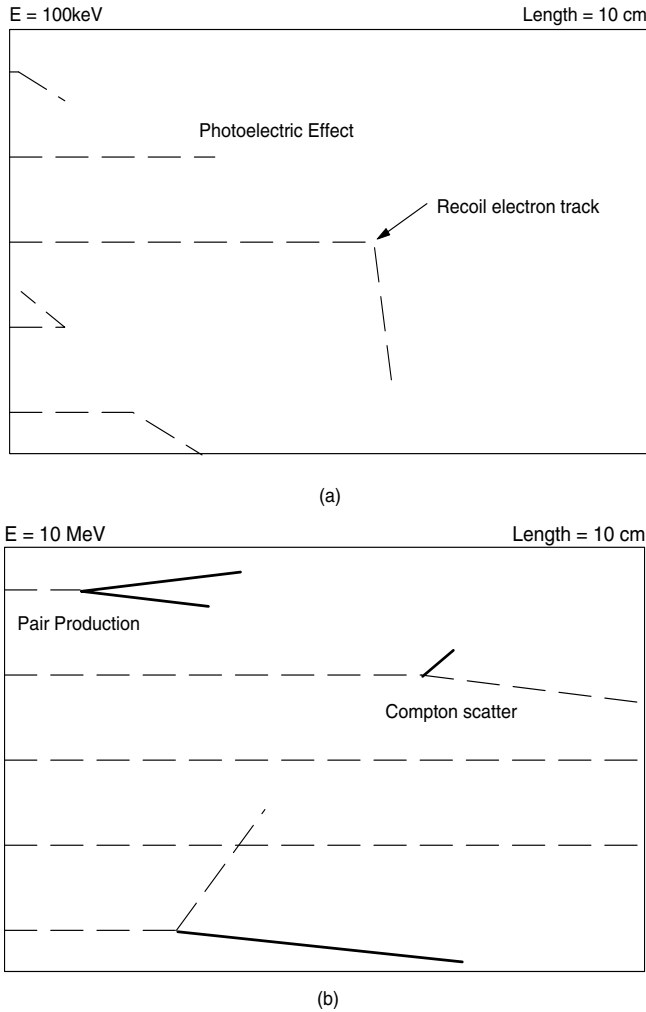


FIGURE 15.30. A simulation of photons passing through a layer of water 10 cm thick. (a) The photon energy is 100 keV. One photon has a photoelectric interaction. The other four are Compton scattered. (b) The photon energy is 10 MeV. Two photons do not interact, one produces an electron-positron pair, and two Compton scatter.

Compton scattered. The energy of the photoelectron and the Compton-scattered electrons is so low that the ranges are insignificant on this scale. In Fig. 15.30(b) the incident photons have 10 MeV energy. One has undergone pair production, two have Compton scattered, and two have passed through without interacting. The electron tracks are shown as thick solid lines. Their lengths are equal to the CSDA range of electrons or positrons of that energy. They are drawn as straight lines, even though the real tracks are tortuous.

One of the quantities of interest is the *energy transferred* to kinetic energy of charged particles in some mass of material. [We saw this briefly in the discussion surrounding Eq. 15.36.] Another is the *energy imparted* in some mass of material, which is the kinetic energy lost by charged particles as they come to rest. Figure 15.31 shows the distinction between the two quantities. It shows two

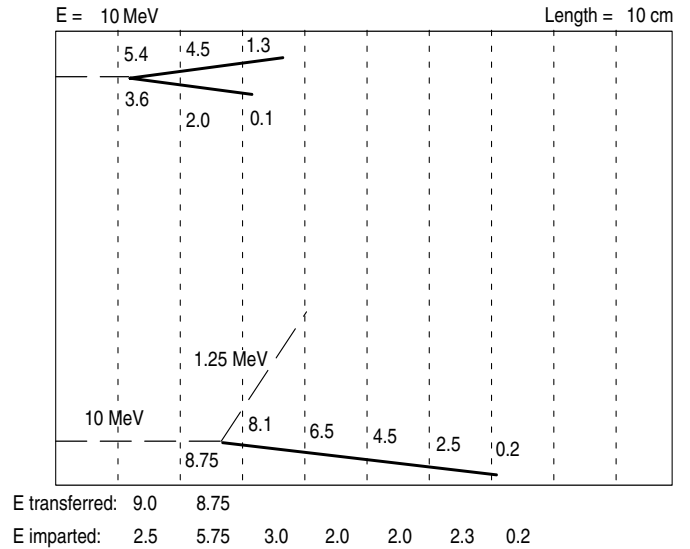


FIGURE 15.31. The difference between energy transferred and energy imparted. Two of the photons from Fig. 15.30(b) are shown. The water has been divided into ten 1-cm slices. The numbers on the drawing show the charged-particle energy at the entrance to each slice. The energy transferred and the energy imparted in each slice are shown at the bottom.

photons from Fig. 15.30(b): one that underwent pair production, and one that was Compton scattered. The water has been divided into ten slices, each 1 cm thick. No energy is transferred in the first slice. Energy is transferred by pair production in the second slice and by Compton scattering in the third slice. In each case the electron (or positron) produced loses kinetic energy in that slice and also in other slices. There is energy imparted in slices 2–8, even though the energy is transferred only in slices 2 and 3.

Consider now the actual numbers. In keeping with the literature,<sup>13</sup> we will call the energy transferred  $E_{tr}$ , even though we have been using  $T$  for kinetic energy. For pair production the energy transferred is

$$E_{tr} = T_+ + T_- = h\nu_0 - 2m_e c^2 = 10 - 2 \times 0.511 = 8.978 \approx 9.0 \text{ MeV.} \quad (15.64)$$

The partition of energy between the electron and positron is stochastic. We assume for this example that about 60% (5.4 MeV) goes to one member of the positron-electron pair and 40% (3.6 MeV) to the other. These numbers are shown at the vertex of Fig. 15.31. From these energies the ranges can be determined. Measuring the distance from the end of the track to the boundary between each slice allows us to determine the energy of each charged particle as it enters the slice. For the Compton scattering, 8.75 MeV is transferred to the recoil electron and the scattered photon has 1.25 MeV. The energy imparted by the 5.4-MeV particle is  $5.4 - 4.5 = 0.9$  MeV in slice 2,

<sup>13</sup>See ICRU Report 33 (1980) or Attix (1986).

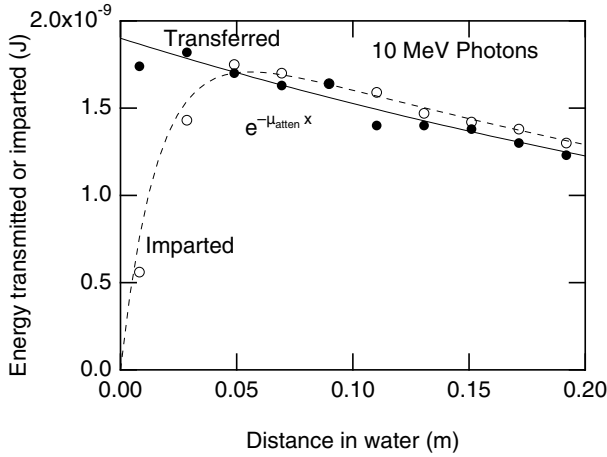


FIGURE 15.32. Plot of energy transferred and energy imparted for a simulation using 40,000 photons of energy 10 MeV. The filled circles are the energy transferred in each slice, and the open circles are the energy imparted in each slice.

4.5–1.3 = 3.2 MeV in slice 3, and 1.3 MeV in slice 4. Similar calculations can be done for the other charged particles. The energy transferred and the energy imparted in each slice are shown at the bottom of Fig. 15.31. This ignores any interaction of the 1.25-MeV Compton-scattered photon and assumes it leaves the volume of interest. Because for the 100-keV photons the range of the charged particles is small compared to 1 cm, the energy transferred and the energy imparted in each slice are the same in Fig. 15.30(a).

Figure 15.32 shows a plot of the transferred and imparted energy for a uniform beam of 10-MeV photons all traveling to the right and striking a slab of water 20 cm thick. Both the energy transferred and the energy imparted are stochastic quantities. This simulation was done for 40 000 photons, and you can see the scatter in the points. The energy transferred falls exponentially as  $\exp(-\mu_{\text{atten}}x)$ .

### 15.15.2 Energy Transferred and Kerma

We found the energy transferred by calculating the energy of each electron or positron produced. The standard definition uses slightly different bookkeeping. It subtracts the energy of the photons leaving the volume of interest from those entering, and adds a term  $Q$  for the energy going into the volume due to changes in rest mass. For example, this is the  $2m_e c^2$  of Eq. 15.64. The standard definition is

$$E_{\text{tr}} = (R_{\text{in}})_u - (R_{\text{out}})_u^{\text{nonr}} + Q. \quad (15.65)$$

The quantity  $R$  is radiant energy: the energy of particles (including photons) but not including rest energy. The subscript  $u$  means that it is the radiant energy of uncharged particles. The uncharged particles can be pho-

tons or neutrons.<sup>14</sup> Later we will use subscript  $c$  to denote the radiant energy of charged particles. The superscript “nonr” means that the quantity does not include radiant energy arising from bremsstrahlung or positron annihilation in flight from charged particles within the volume. The  $Q$  term is positive if mass is converted to energy (as in annihilation radiation) and negative if energy is converted to mass (as in pair production).

Using this method of calculating for Fig. 15.31 gives

$$\begin{aligned} E_{\text{tr}} &= (R_{\text{in}})_u - (R_{\text{out}})_u^{\text{nonr}} + \sum Q = 10 - 0 - 2 \times 0.511 \\ &= 9.0 \text{ MeV} \end{aligned}$$

for slice 2. For the third slice the equation gives

$$\begin{aligned} E_{\text{tr}} &= (R_{\text{in}})_u - (R_{\text{out}})_u^{\text{nonr}} + \sum Q = 10 - 1.25 + 0 \\ &= 8.75 \text{ MeV}. \end{aligned}$$

For the fourth slice, the uncharged radiant energy in is equal to the uncharged radiant energy out. In the fifth slice, if the 1.25-MeV photon actually interacts as it appears to, we would have to include its energy transfer. In all the other slices the energy transferred is zero.

The energy transferred is a stochastic quantity, and so is the energy transferred per unit mass,  $dE_{\text{tr}}/dm$ . Its expectation value is the *kerma* (kinetic energy released per unit mass):

$$K = \frac{d\overline{E}_{\text{tr}}}{dm}. \quad (15.66)$$

If we consider monoenergetic photons of energy  $h\nu$  and consider only the interaction of the primary photon beam (not any secondary photons, such as Compton-scattered photons or annihilation radiation), then the kerma is

$$K = \frac{\mu_{\text{tr}}}{\rho} \Psi, \quad (15.67)$$

where  $\Psi$  is the energy fluence. To see why this is true, note that if the  $N$  photons are spread over area  $S$ , then  $NE = \Psi S$  and  $dm = \rho S dx$ . The kerma is

$$K = \frac{d\overline{E}_{\text{tr}}}{dm} = \frac{\Psi S \mu_{\text{tr}} dx}{\rho S dx} = \frac{\mu_{\text{tr}}}{\rho} \Psi.$$

### 15.15.3 Energy Imparted and Absorbed Dose

The *energy imparted*,  $E$ , is the net energy into the volume from all sources: uncharged particles, charged particles, and changes of rest mass:

$$E = (R_{\text{in}})_u - (R_{\text{out}})_u + (R_{\text{in}})_c - (R_{\text{out}})_c + \sum Q. \quad (15.68)$$

The *absorbed dose* is the expectation value of the energy imparted per unit mass:

$$D = \frac{d\overline{E}}{dm}. \quad (15.69)$$

It is measured in joules per kilogram or *gray* (Gy).

<sup>14</sup>Neutrinos, which we will discuss in Chapter 17, travel such long distances without interacting that they are not considered in the calculations. Energy carried by neutrinos, which come from nuclear  $\beta$  decay, is assumed to have left the body.

### 15.15.4 Net Energy Transferred, Collision Kerma, and Radiative Kerma

Another quantity used in the literature is the *net energy transferred*. It subtracts from the energy transferred the energy that is reradiated (bremsstrahlung and radiation from positron annihilation in flight), even if the reradiation takes place outside the volume of interest. It is

$$E_{tr}^{net} = (R_{in})_u - (R_{out})_u^{nonr} - R_u^r + \sum Q. \quad (15.70)$$

The *collision kerma* and *radiative kerma* are defined as expectation values per unit mass:

$$K_C = \frac{dE_{tr}^{net}}{dm} = K - K_r, \quad (15.71)$$

$$K_r = \frac{dR_u^r}{dm}.$$

Considering only a primary beam of monoenergetic photons,

$$K_C = \frac{\mu_{en}}{\rho} \Psi. \quad (15.72)$$

## 15.16 Charged-Particle Equilibrium

There are three equilibrium conditions that sometimes exist or are assumed to exist, that make it possible to calculate the relationship between energy transferred and energy imparted.

### 15.16.1 Radiation Equilibrium

The first and most restrictive condition is *radiation equilibrium*. It is a useful model when considering an extended radioactive source that is distributed uniformly throughout some volume  $V$  (such as the body or a particular organ). The source is assumed to emit its radiation isotropically. The energy released to neutrinos is ignored. A point of interest within the large volume is surrounded by a smaller volume  $v$ . The volume  $v$  must be far enough from the edge of  $V$  so that any radiation emitted from  $v$  is absorbed before reaching the surface of  $V$ . The entire volume  $V$  is assumed to be of the same atomic composition and density. Because everything is isotropic, on average for every photon or neutron or charged particle entering volume  $v$ , another identical one leaves. This means that

$$(\overline{R}_{in})_c = (\overline{R}_{out})_c \quad (15.73a)$$

and

$$(\overline{R}_{in})_u = (\overline{R}_{out})_u. \quad (15.73b)$$

The average energy imparted is

$$\overline{E} = \sum \overline{Q}. \quad (15.74)$$

This means that when the conditions for radiation equilibrium are satisfied, the absorbed dose is the expectation

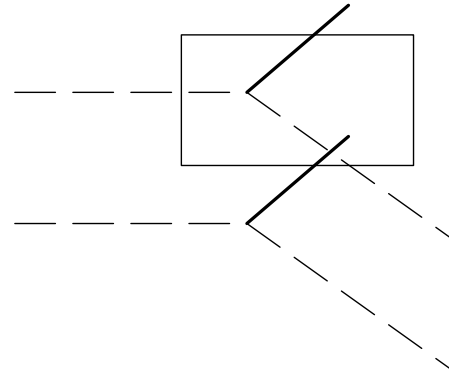


FIGURE 15.33. One of the conditions for charged-particle equilibrium is that on average, for every charged particle of a certain energy leaving volume  $v$  traveling in a certain direction, a corresponding particle enters the volume.

value of the energy released by the radioactive material per unit mass. If there is no radioactive source, there is no energy imparted in radiation equilibrium.

### 15.16.2 Charged-particle Equilibrium

A less restrictive assumption is *charged-particle equilibrium*, in which only Eq. 15.73a is satisfied: the average amount of charged-particle radiant energy entering the region is the same as the average amount leaving. The assumption of charged particle equilibrium is a useful model in several cases, but we will consider only the case of an external beam of photons striking volume  $V$ . Again we consider what happens in a smaller volume  $v$ , separated from the boundary of  $V$  by a distance larger than the maximum range of any secondary charged particles produced by the external radiation. We also assume that the medium is homogeneous and that only a small fraction of the primary radiation interacts within the volume so attenuation can be neglected. Then the average number of charged particles produced per unit volume and per unit solid angle in any given direction is the same everywhere in the volume. Though the charged particles need not be produced isotropically, on average for every particle that leaves volume  $v$ , a corresponding one will enter it, as shown in Fig. 15.33. For charged-particle equilibrium, the average energy imparted is

$$\overline{E} = (\overline{R}_{in})_u - (\overline{R}_{out})_u + \sum \overline{Q}.$$

Comparing this with the average of Eq. 15.70 shows that the average net energy transferred is

$$\overline{E}_{tr}^{net} = \overline{E} + (\overline{R}_{out})_u - (\overline{R}_{out})_u^{nonr} - \overline{R}_u^r.$$

Now recall that  $(\overline{R}_{out})_u$  is the average value of all the uncharged radiation leaving volume  $v$ ,  $(\overline{R}_{out})_u^{nonr}$  is the average value of all uncharged radiation leaving excluding bremsstrahlung and photons from annihilation

in flight that occur within the volume, and  $\overline{R}_u^r$  is the bremsstrahlung and annihilation-in-flight radiation from charged particles originating in  $v$  regardless of where it occurs. If there is charged-particle equilibrium, any radiative interaction by a charged particle after it leaves the volume will on average be replaced by an identical interaction inside  $v$ . If the volume is small enough so that all radiative loss photons escape from the volume before undergoing any subsequent interactions, then

$$(\overline{R}_{\text{out}})_u = (\overline{R}_{\text{out}})_u^{\text{nonr}} + \overline{R}_u^r.$$

Therefore, for charged-particle equilibrium,  $\overline{E} = \overline{E}_{\text{tr}}^{\text{net}}$ , and the dose is equal to the collision kerma:

$$D = K_C. \quad (15.75)$$

One situation where charged-particle equilibrium applies is for the thin slices in Fig. 15.30(a). The electron ranges are so short (10  $\mu\text{m}$  for a 25-keV electron) that a slice can be thin compared to  $1/\mu$  and yet all the electrons produced stay within the volume.

The conditions for charged-particle equilibrium fail if the source of photons is too close ( $\Psi$  is not uniform because of  $1/r^2$ ), close to a boundary (as between air and tissue or muscle and bone), for high-energy radiation (as in Fig. 15.32), or if there is an applied electric or magnetic field that alters the paths of the charged particles (as in some radiation detectors).

In Fig. 15.32, if we look at the situation far enough to the right, the energy imparted is proportional to the energy transferred. This situation is called *transient charged-particle equilibrium*.

The dose for a monoenergetic parallel beam of charged particles with particle fluence  $\Phi$  passing through a thin layer can be calculated by making three assumptions:

1. The volume of interest is thin enough so that  $S_e$  remains constant.
2. Scattering can be neglected, so every particle passes straight through the layer.
3. The net kinetic energy carried out of the layer by  $\delta$  rays is negligible, either because the layer is thick compared to the range of the  $\delta$  rays or because the layer is immersed in a material of the same atomic number so that charged-particle equilibrium exists.

Then the energy lost in collisions in a layer of thickness  $dz$  is  $E = \Phi(\text{area})(S_e/\rho)\rho dz$  and the mass is  $\rho(\text{area})dz$ , so the dose is

$$D = \frac{S_e}{\rho} \Phi. \quad (15.76)$$

Attix (1986, pp. 188–195) discusses corrections for situations where these assumptions are not valid.

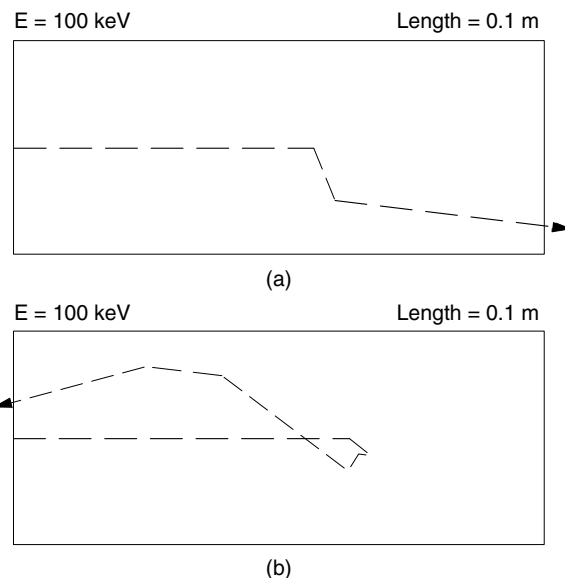


FIGURE 15.34. Secondary photons also interact in this simulation. One 100-keV photon enters from the left in each panel. (a) The primary photon undergoes a Compton scattering. The Compton-scattered photon also undergoes a Compton scattering. The third photon escapes from the water. (b) The primary photon is Compton scattered. Each Compton-scattered photon undergoes another Compton scattering, until the sixth scattered photon leaves through the upstream surface of the water, traveling nearly in the direction from which the incident photon came.

## 15.17 Buildup

We have been ignoring the interactions of secondary photons, primarily Compton-scattered photons and annihilation radiation. They can be quite significant. In fact, there can be a cascade of several generations of photons, though we will call them all “secondary photons.” Figure 15.34 compares two simulations in which the secondary photons are allowed to interact. In Fig. 15.34(a) there is one secondary interaction before the scattered photon escapes from the water. In Fig. 15.34(b) there are a total of six Compton scatterings before the secondary photon escapes.

All of these secondary photons produce electrons that contribute to the energy transferred and energy imparted. Figure 15.35 compares two cases where 25 photons of energy 100 keV enter the water from the left. The primary interactions are the same in both cases. In Fig. 15.35(a) the small dots represent the electrons produced by the interaction of the primary photons. In Fig. 15.35(b) the electrons produced by secondary and subsequent interactions are also shown. The energy transferred and energy imparted are much greater.

The *buildup factor* for any quantity is defined as the ratio of the quantity including secondary and scattered radiation to the quantity for primary radiation only. For example, if the primary beam has an energy fluence  $\Psi_0$  at the surface, the energy fluence at depth  $x$  in

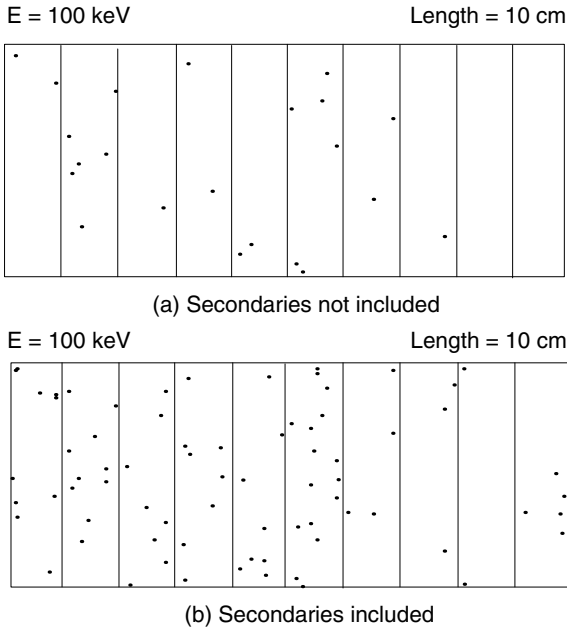


FIGURE 15.35. Twenty-five 100-keV photons entered the water from the left. The dots represent recoil electrons from Compton scattering or photoelectrons. (a) Only the first interaction of the primary photon is considered. (b) Subsequent interactions are also considered.

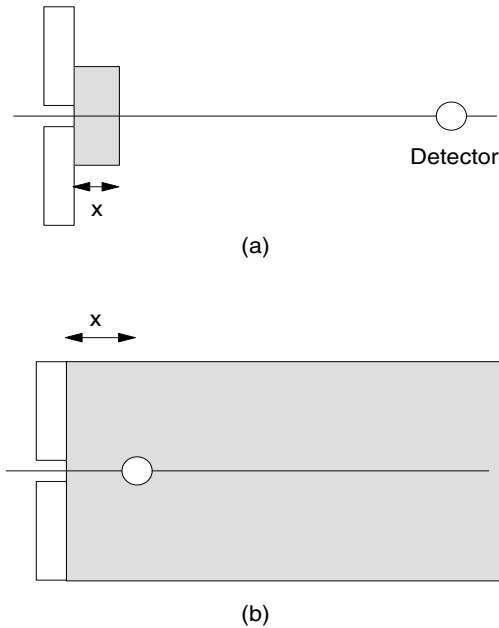


FIGURE 15.36. Two different detector geometries. (a) The detector is at a fixed location and the absorber thickness is increased. (b) The detector is at a varying distance from the source in a water bath.

the medium is

$$\Psi(x) = B(x)\Psi_0 e^{-\mu x}. \tag{15.77}$$

The buildup factor is quite sensitive to the geometry. Compare the two situations in Fig. 15.36. In Fig. 15.36(a) the detector is at a fixed location and the thickness of

the absorber is increased. As the absorber thickness  $x$  approaches zero, the buildup factor approaches unity. In Fig. 15.36(b) the detector is at depth  $x$  in a water bath. Because of the backscattered radiation seen in Fig. 15.34(b),  $B(x) > 1$  as  $x \rightarrow 0$ . In this case, it is sometimes called the *backscatter factor*. For further discussion, see Attix (1986).

### Symbols Used in Chapter 15

Symbol	Use	Units	First used on page
$a$	Acceleration	$\text{m s}^{-2}$	416
$a_i$	Number of atoms of constituent $i$		410
$b$	Impact parameter	m	418
$c$	Velocity of light	$\text{m s}^{-1}$	403
$d$	Diameter	m	416
$e$	Charge on electron	C	402
$f, f_C, f_i, f_\kappa, f_\tau$	Fraction of photon energy transferred to charged particles		407
$g$	Fraction of photon energy of secondary electrons converted back into photons by bremsstrahlung		413
$h$	Planck's constant	J s	403
$j$	Total angular momentum quantum number		402
$k$	Spring constant	$\text{N m}^{-1}$	416
$l$	Orbital angular momentum quantum number		402
$m$	Mass	kg	406
$m_e$	Electron rest mass	kg	403
$m_j$	Quantum number for the component of the total angular momentum along the $z$ axis		402
$m_0$	Rest mass	kg	405
$n$	Principal quantum number		402
$n$	Number		410
$p$	Momentum	$\text{kg m s}^{-1}$	405
$q$	Charge	C	418
$r$	Position	m	420
$r_e$	"Classical" electron radius	m	406
$s$	Spin quantum number		402
$t$	Time	s	416
$v$	Velocity	$\text{m s}^{-1}$	415
$w_i$	Mass fraction of constituent $i$		410
$x, y, z$	Coordinate axes	m	408
$x$	Dimensionless energy ratio		405
$z$	Charge of projectile in multiples of $e$		415
$A$	Atomic mass number		408



Symbol	Use	Units	First used on page	$\epsilon$ $\epsilon_0$	Stopping cross section of empty space	$J\ m^2$ $N^{-1}\ C^2\ m^{-2}$	415 406
$A_i, A_{mol}$	Atomic mass number of constituent $i$ or molecule	$(g\ mol)^{-1}$ or $(kg\ mol)^{-1}$	410	$\theta, \phi$ $\kappa$	Angles		405
$A_K$	Auger yield		411	$\lambda$	Wavelength	m	405
$B, B_K, etc.$	Binding energy	eV or J	403	$\mu, \mu_{atten}$	Attenuation coefficient	$m^{-1}$	408
$B$	Buildup factor or backscatter factor		430	$\mu_{en}$	Energy absorption coefficient	$m^{-1}$	413
$C$	Shell correction coefficient		420	$\mu_{tr}$	Energy transfer coefficient	$m^{-1}$	413
$D$	Absorbed dose	$J\ kg^{-1}$ or Gy (gray)	427	$\nu$ $\xi$	Frequency Position	Hz m	403 419
$E$	Energy	J	403	$\rho$	Density	$kg\ m^{-3}$	408
$E$	Electric field	$V\ m^{-1}$	406	$\sigma_C$	Total Compton cross section for one electron	$m^2$	403
$F$	Force	N	416				
$F$	Fraction of charged particles passing through an absorber		423	$\sigma_{coh}$	Coherent Compton cross section for one atom	$m^2$	403
$I$	Average ionization energy	eV or J	420	$\sigma_{incoh}$	Incoherent Compton cross section for one atom	$m^2$	403
$I$	Stopping interaction strength	$J\ m^2$	420				
$K, K_C$	Kerma, collision kerma	J	427	$\sigma_{tr}$ $\sigma_{tot}$	Transfer cross section Total cross section	$m^2$ $m^2$	407 409
$L$	Stopping number per atomic electron		420	$\tau$	Photoelectric cross section	$m^2$	404
$L_\Delta$	Restricted linear stopping power	$J\ m^{-1}$	423	$\Delta$ $\Phi$	Energy transfer Particle fluence	J $m^{-2}$	423 412
$M$	Mass	kg	410	$\Psi$	Energy fluence	$J\ m^{-2}$	412
$N$	Number of particles		408	$\Omega$	Solid angle	sr	406
$N_A$	Avogadro's number	$mol^{-1}$	408				
$N_T$	Number of target atoms per unit projected area	$m^{-2}$	410				
$N_{TV}$	Number of target atoms per unit volume	$m^{-3}$	410				
$Q$	Energy released from rest mass	J	427				
$R$	Range	m	423				
$R_u, R_c$	Radiant energy in the form of uncharged or charged particles	J	427				
$S$	Area	$m^2$	427				
$S$	Stopping power	$J\ m^{-1}$	415				
$S_e$	Electron (collision) stopping power	$J\ m^{-1}$	416				
$S_n$	Nuclear stopping power	$J\ m^{-1}$	416				
$S_r$	Radiative stopping power	$J\ m^{-1}$	416				
$T$	Kinetic energy	J	403				
$V$	Volume	$m^3$	410				
$V$	Velocity	$m\ s^{-1}$	419				
$W_{K,L,M}$	Probability that a hole in the $K, L,$ or $M$ shell is filled by fluorescence		411				
$W$	Energy lost in a single interaction	J	415				
$Y$	Radiation yield		424				
$Z$	Atomic number of target atom		402				
$\beta$	$v/c$		415				
$\delta$	Average energy emitted as fluorescence radiation per photon absorbed	J	413				
$\delta$	Density-effect correction		420				

## Problems

### Section 15.1

**Problem 1** The quantum numbers  $m_s = \pm\frac{1}{2}$  and  $m_l = l, l-1, l-2, \dots, -l$  are sometimes used instead of  $j$  and  $m_j$  to describe an electron energy level. Show that the total number of states for given values of  $n$  and  $l$  is the same when either set is used.

**Problem 2** Use Eq. 15.3 to estimate the  $K$ -shell energies for the following elements and compare them to the measured values of  $E_K$ .

$Z$	Element	Measured $E_K$ (keV)
6	Carbon	0.284
20	Calcium	4.04
53	Iodine	33.2
82	Lead	88.0

### Section 15.3

**Problem 3** The  $K$ -shell photoelectric cross section for 100-keV photons on lead ( $Z = 82$ ) is  $\tau = 1.76 \times 10^{-25}\ m^2\ atom^{-1}$ . Estimate the photoelectric cross section for 60-keV photons on calcium ( $Z = 20$ ).

**Problem 4** Describe how you could use different materials to determine the energy of monoenergetic  $x$  rays of energy about 50 keV by using changes in the attenuation coefficient. What materials would you use?

Section 15.4

**Problem 5** Derive Eq. 15.12 from the preceding four equations.

**Problem 6** Derive an equation for the direction of the recoil electron,  $\phi$ , in terms of  $\theta$  and  $\lambda_0$ .

**Problem 7** Show that the sum of the energies of the scattered photon (Eq. 15.14) and the recoil electron (Eq. 15.16) equals the energy of the incident photon.

**Problem 8** A 1-MeV photon undergoes Compton scattering from a carbon target. The scattered photon emerges at an angle of  $30^\circ$ .

(a) What is the energy of the scattered photon? What is the energy of the recoil electron?

(b) What is the differential scattering cross section for scattering at an angle of  $30^\circ$  from one electron? From the entire carbon atom ( $Z = 6$ ,  $A = 12$ )?

**Problem 9** What is the energy of a Compton-scattered photon at  $180^\circ$  when  $h\nu_0 \gg m_e c^2$ ? At  $90^\circ$ ?

**Problem 10** Integrate Eq. 15.18 over all possible scattering angles to obtain Eq. 15.20. Use the solid angle in spherical coordinates (Appendix L).

**Problem 11** Find the limit of Eq. 15.17 as  $x \rightarrow \infty$ .

**Problem 12** Write Eq. 15.17 in the form

$$\frac{d\sigma_C}{d\Omega} = \frac{r_e^2}{2} (1 + \cos^2 \theta) F_{KN},$$

where  $F_{KN}$  is the Klein–Nishina factor. Find an expression for  $F_{KN}$  in terms of  $\theta$  and  $x$ . Show that as  $x \rightarrow 0$ ,  $F_{KN} \rightarrow 1$ . Show that when  $\theta = 0$ ,  $F_{KN} = 1$ .

**Problem 13** Use the expansion  $\ln(1+x) = x - x^2/2 + x^3/3$  to show that Eq. 15.19 approaches Eq. 15.20 as  $x \rightarrow 0$ .

**Problem 14** Eq. 15.12 shows that the wavelength shift is independent of the wavelength of the incident photon. Calculate the fractional wavelength shift  $(\lambda - \lambda_0)/\lambda_0$  for an infrared photon ( $\lambda_0 = 10 \mu\text{m}$ ), an ultraviolet photon ( $\lambda_0 = 100 \text{ nm}$ ), a low-energy (“soft”) x ray ( $\lambda_0 = 1 \text{ nm}$ ), and a high-energy x ray ( $\lambda_0 = 0.01 \text{ nm}$ ).

**Problem 15** Suppose that attenuation is measured for 60-keV photons passing through water in such a way that photons scattered less than  $5^\circ$  still enter the detector. Estimate the incoherent Compton scattering cross section per electron for photons scattered through more than  $5^\circ$ .

Section 15.5

**Problem 16** A beam of 59.5-keV photons from  $^{241}\text{Am}$  scatters at  $90^\circ$  from some calcium atoms ( $A = 40$ ).

(a) What is the energy of a Compton-scattered photon?

(b) What is the energy of a coherently scattered photon?  
 (c) What is the recoil energy of the atom in coherent scattering?

Section 15.6

**Problem 17** Show that a single photon cannot produce an electron-positron pair in free space because energy and momentum cannot be simultaneously conserved.

Section 15.7

**Problem 18** Most diagnostic x rays use photon energies in the range 20–100 keV. For carbon (Fig. 15.2), which mechanism is most important in this range: photoelectric effect, Compton scattering, coherent scattering, or pair production?

**Problem 19** Use Fig. 15.7 to make the following estimates for 1-MeV photons. What is the mass attenuation coefficient for water? For aluminum? For lead? What is the linear attenuation coefficient in each case?

**Problem 20** Use Fig. 15.7 to estimate the attenuation coefficient for 0.1-MeV photons on carbon and lead. Compare your results to values you obtain from the internet or the literature. Repeat for 1-MeV photons.

**Problem 21** Consider photons of three energies: 0.01, 0.02, and 0.03 MeV. What fraction of the photons at each energy will be unattenuated after they pass through 0.1 mm of lead ( $\rho = 11.35 \text{ g cm}^{-3}$ )? Comment on the differences in your results.

Section 15.8

**Problem 22** Use Fig. 15.7 to find the mass attenuation coefficient for 0.2-MeV photons in a polyethylene absorber. The Compton effect predominates. Polyethylene has the formula  $(\text{CH}_2)_n$ .

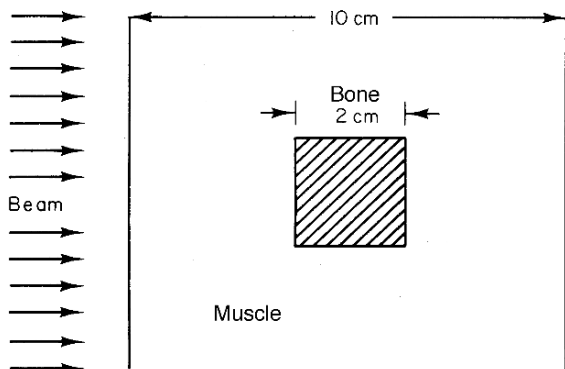
**Problem 23** What will be the attenuation of 40-keV photons in muscle 10 cm thick? Repeat for 200-keV photons.

**Problem 24** Assume that a patient can be modeled by a slab of muscle 20 cm thick of density  $1 \text{ g cm}^{-3}$ . What fraction of an incident photon beam will emerge without any interaction if the photons have an energy of 10 keV? 100 keV? 1 MeV? 10 MeV?

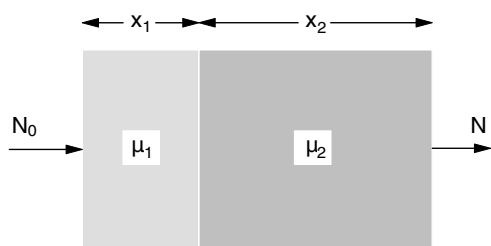
**Problem 25** Muscle and bone are arranged as shown. Assume the density of muscle is  $1.0 \text{ g cm}^{-3}$  and the density of bone is  $1.8 \text{ g cm}^{-3}$ . The attenuation coefficients are

$E$	$(\mu/\rho)_{\text{muscle}} (\text{cm}^2 \text{ g}^{-1})$	$(\mu/\rho)_{\text{bone}} (\text{cm}^2 \text{ g}^{-1})$
60 keV	0.200	0.274
1 MeV	0.070	0.068

Compare the intensity of the emerging beam that has passed through bone and muscle and just muscle at the two energies.



**Problem 26** A beam of monoenergetic photons travels through a sample made up of two different materials of unknown thickness  $x_1$  and  $x_2$ , as shown below. The attenuation coefficients at two different energies,  $E_a$  and  $E_b$ , are accurately known. They are  $\mu_1(a)$ ,  $\mu_2(a)$ ,  $\mu_1(b)$ , and  $\mu_2(b)$ . One measures accurately the log of the ratio of the number of photons emerging from the sample to the number entering,  $R = \ln(N_0/N)$ , at each energy so that  $R_a$  and  $R_b$  are known. Find an expression for  $x_2$  in terms of  $R_a$ ,  $R_b$ , and the attenuation coefficients.



**Problem 27** You wish to use x-ray fluorescence to detect lead that has been deposited in a patient's bone. You shine 100-keV photons on the patient's bone and want to detect the 73-keV fluorescence photons which are produced. The incident photon fluence is  $\Phi_0 = 10^{12}$  photons  $m^{-2}$ . There are  $10^{14}$  lead atoms (1 nanomole) in the region illuminated by the incident beam. The photoelectric cross section is  $1.76 \times 10^{-25} m^2 atom^{-1}$ . The fluorescence yield is  $W = 0.94$ . Assume for simplicity that the fluorescence photons are emitted uniformly in all directions. The detector has a sensitive area  $1 \times 2$  cm and is located 10 cm from the lead atoms. How many fluorescence photons are detected?

Section 15.10

**Problem 28** A 5-keV photon strikes a calcium atom. The following events take place:

1. A K-shell photoelectron is ejected.
2. A  $K_\alpha$  photon is emitted. This corresponds to the movement of a hole from the K shell to the L shell.

3. An electron in the M shell goes to the L shell and an M-shell photoelectron is emitted.

Give the excitation energy of the atom, the total energy in the form of photons, and the total energy in the form of electron kinetic energy at each stage. Use the following data for calcium:  $Z = 20$ ,  $A = 40$ ,  $B_K = 4,000$  eV,  $B_L = 300$  eV (ignore differences in subshells),  $B_M = 40$  eV.

**Problem 29** The following are the binding energies for

	H	O
hydrogen and oxygen.	$B_K = 13.6$ eV	$532$ eV
	$B_L$	$24$ eV

- (a) Determine  $f_\tau$  for hydrogen from first principles.
- (b) Use Eqs. 15.39 and 15.40 to estimate  $f_\tau$  (K shell) for oxygen.

**Problem 30** Use the Thomson scattering cross section,  $d\sigma/d\Omega = (r_e^2/2)(1 + \cos^2\theta)$ , the total cross section  $\sigma_C = 8\pi r_e^2/3$ , and the expression for the total energy of the recoil electron Eq. 15.16 to find an expression for  $f_C$  as  $x \rightarrow 0$ . Plot  $f_C \sigma_C$  incoh on Fig. 15.7.

- (a) For 50-keV photons on calcium, estimate  $f_\tau$ .
- (b) For 100-keV photons on calcium, the photoelectric cross section is  $\tau = 5.89 \times 10^{-28} m^2 atom^{-1}$ . Use  $f_\tau = 1.0$ . Estimate  $\mu_{tr}/\rho$ . Use the following data for calcium if you need them:  $Z = 20$ ,  $A = 40$ ,  $B_K = 4000$  eV,  $B_L = 300$  eV,  $B_M = 40$  eV.

Section 15.11

**Problem 31** Prove that if a particle of mass  $M_1$  and kinetic energy  $T$  collides head on with a particle of mass  $M_2$  which is at rest, the energy transferred to the second particle is  $4TM_2/M_1$  or  $2M_2V^2$  in the limit  $M_2 \ll M_1$ . The maximum energy is transferred when the particles move apart along the line of motion of the incident particle.

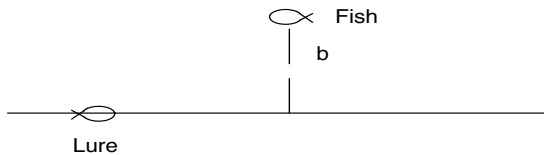
**Problem 32** The expression for  $S_e = dT/dx$  has the SI units  $J m^{-1}$ . Therefore  $S_e/\rho$  in Eq. 15.57 has units  $J m^2 kg^{-1}$ .

- (a) How must the coefficient in front of Eq. 15.57 be changed if  $T$  is in MeV? If  $x$  is in cm instead of m?
- (b) What numerical factors must be introduced if  $N_A$  is in atoms per g mol and  $\rho$  is in  $g cm^{-3}$ ?
- (c) What is the average force on a 10-MeV proton in carbon? On a 100-keV proton? Use  $I = 78$  eV.
- (d) What are the units of the stopping cross section [defined just below Eq. 15.47]?

**Problem 33** The peak in the stopping power occurs roughly where the projectile velocity equals the velocity of the atomic electrons in the target. Find an expression for the velocity of an electron in the  $n = 1$  Bohr orbit. Use Eq. 14.7, and the fact that the total energy is the sum of the kinetic and potential energies. Use the classical arguments and the fact that the electron is in a circular orbit

to relate the kinetic and potential energies. The acceleration in a circular orbit is  $v^2/r$ .

**Problem 34** A fishing lure is trolled behind a boat for a total distance  $D$ . Suppose that fish are distributed uniformly throughout the water at a concentration  $C$  fish  $m^{-3}$ , and that the probability of a fish striking the lure depends on  $b$ , the perpendicular distance from the path of the lure to the fish:  $p = \exp(-b/b_0)$ . Calculate the average number of fish caught.



### Section 15.13

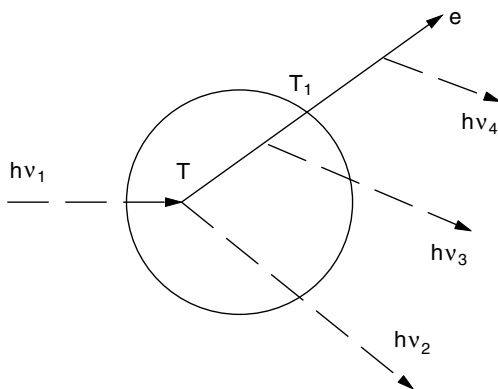
**Problem 35** What is the range–energy relationship for high-speed nonrelativistic particles if the variation of  $L$  with  $T$  is neglected and Eq. 15.57 is the dominant term?

**Problem 36** Estimate the maximum electron range, and hence the radius of the  $\delta$ -ray cloud surrounding the track of a 5-MeV  $\alpha$  particle. (The rest energy  $Mc^2$  of an  $\alpha$  particle is about four times 938 MeV.) The range of a low energy electron in cm is about  $10^{-2}\beta^2$ .

### Section 15.15

**Problem 37** Suppose that a photon of energy  $h\nu$  enters a volume of material and produces an electron–positron pair. Both particles come to rest in the volume, and the positron annihilates with an electron that was already in the volume. Both annihilation photons leave the volume. Show that the formal definition of energy transfer agrees with the common-sense answer that it is the kinetic energy of the electron and positron, which is  $h\nu - 2m_e c^2$ . What is the energy imparted?

**Problem 38** What are the energy transferred, the net energy transferred and the energy imparted in the volume shown?



## References

- Ahlen, S. P. (1980). Theoretical and experimental aspects of the energy loss of relativistic heavily ionizing particles. *Rev. Mod. Phys.* **52**: 121–173.
- Arqueros, F., and G. D. Montesinos (2003). A simple algorithm for the transport of gamma rays in a medium. *Amer. J. Phys.* **71**(1): 38–45.
- Attix, F. H. (1986). *Introduction to Radiological Physics and Radiation Dosimetry*. New York, Wiley.
- Bambynek, W., B. Crasemann, R. W. Fink, H. U. Freund, H. Mark, C. D. Swift, R. E. Price, and P. Y. Rao (1972). X-ray fluorescence yields, Auger, and Coster–Kronig transition probabilities. *Rev. Mod. Phys.* **44**: 716–717.
- Boone, J. M., and A. E. Chavez (1996). Comparison of x-ray cross sections for diagnostic and therapeutic medical physics. *Med. Phys.* **23**(12): 1997–2005.
- Budd, T., and M. Marshall (1983). Microdosimetric properties of electron tracks measured in a low-pressure chamber. *Radiat. Res.* **93**: 19–32.
- Carlsson, G. A., C. A. Carlsson, K-F. Berggren, and R. Ribberfors (1982). Calculation of scattering cross sections for increased accuracy in diagnostic radiology. 1. Energy broadening of Compton-scattered photons. *Med. Phys.* **9**(6): 868–879.
- Hobbie, R. K. (1992). MacDose: A simulation for understanding radiological physics. *Comput. Phys.* **6**(4): 355–359. MacDose is available at the Web site of this book: [www.oakland.edu/~roth/hobbie.htm](http://www.oakland.edu/~roth/hobbie.htm). It runs on a Macintosh computer using OS-9 or earlier.
- Hubbell, J. H. (1969). *Photon Cross Section, Attenuation Coefficients, and Energy Absorption Coefficients from 10 keV to 100 GeV*. NBS 29. Washington, D.C. U.S. Government Printing Office.
- Hubbell J. H. (1982). Photon mass attenuation and energy absorption coefficients from 1 keV to 20 MeV *Int. J. Appl. Radiat. Inst.* **33**: 1269–1290.
- Hubbell, J. H., and S. M. Seltzer (1996). *Tables of X-Ray Mass Attenuation Coefficients and Mass Energy-Absorption Coefficients 1 keV to 20 MeV for Elements Z = 1 to 92 and 48 Additional Substances of Dosimetric Interest*. National Institute of Standards and Technology. Report No. NISTIR 5632 Web Version. Available at [physics.nist.gov/PhysRefData/contents-xray.html](http://physics.nist.gov/PhysRefData/contents-xray.html).
- Hubbell, J. H., W. J. Veigele, E. A. Briggs R. T. Brown, D. T. Cromer and R. J. Howerton (1975). Atomic form factors, incoherent scattering functions and photon scattering cross sections. *J. Phys. Chem. Ref. Data* **4**: 471–538. errata *ibid.* **6**: 615–616 (1977).
- Hubbell, J. H., H. A. Gimm, and I. Øverbø (1980). Pair, triplet and total atomic cross sections (and mass attenuation coefficients) for 1 MeV–100 GeV photons in elements  $Z = 1$  to 100. *J. Phys. Chem. Ref. Data* **9**: 1023–1147.

- Hubbell, J. H., P. N. Trehan, N. Singh, B. Chand, D. Mehta, M. L. Garg, R. R. Garg, S. Singh, and S. Puri (1994). A review, bibliography, and tabulation of  $K$ ,  $L$ , and higher atomic shell x-ray fluorescence yields. *J. Phys. Chem. Ref. Data* **23**(2): 339–364.
- ICRU Report 16 (1970). *Linear Energy Transfer*. Bethesda, MD, International Commission on Radiation Units and Measurements.
- ICRU Report 33 (1980). *Radiation Quantities and Units*. Bethesda, MD, International Commission on Radiation Units and Measurements.
- ICRU Report 37 (1984). *Stopping Powers for Electrons and Positrons*. Bethesda, MD, International Commission on Radiation Units and Measurements. Information also available at [physics.nist.gov/PhysRefData/Star/Text/contents.html](http://physics.nist.gov/PhysRefData/Star/Text/contents.html).
- ICRU Report 49 (1993). *Stopping Powers and Ranges for Protons and Alpha Particles*. Bethesda, MD, International Commission on Radiation Units and Measurements. Information also available at [physics.nist.gov/PhysRefData/Star/Text/contents.html](http://physics.nist.gov/PhysRefData/Star/Text/contents.html).
- Jackson, D. F., and D. J. Hawkes (1981). X-ray attenuation coefficients of elements and mixtures. *Phys. Reports* **70**: 169–233.
- Kissel, L. H., R. H. Pratt, and S. C. Roy (1980). Rayleigh scattering by neutral atoms, 100 eV to 10 MeV. *Phys. Rev. A* **22**: 1970–2004.
- Powell, C. F., P. H. Fowler, and D. H. Perkins (1959). *The Study of Elementary Particles by the Photographic Method*. New York, Pergamon.
- Pratt, R. H. (1982). Theories of coherent scattering of x rays and  $\gamma$  rays by atoms, in *Proceedings of the Second Annual Conference of International Society of Radiation Physicists, Penang, Malaysia*.
- Rossi, B. (1957). *Optics*. Reading, MA, Addison-Wesley, Chapter 8.
- Seltzer, S. M. (1993). Calculation of photon mass energy-transfer and mass energy-absorption coefficients. *Radiat. Res.* **136**: 147–170.
- Tung, C. J., J. C. Ashley, and R. H. Ritchie (1979). Range of low-energy electrons in solids. *IEEE Trans. Nucl. Sci.* **NS-26**: 4874–4878.
- Ziegler, J. F., and J. M. Manoyan (1988). The stopping of ions in compounds. *Nucl. Instrum. Methods in Phys. Res.* **B35**: 215–228.
- Ziegler, J. F., J. P. Biersack, and U. Littmark (1985). *The Stopping and Range of Ions in Solids*. New York, Pergamon.

# 16

## Medical Use of X Rays

X rays are used to obtain diagnostic information and for cancer therapy. They are photons of electromagnetic radiation with higher energy than photons of visible light. Gamma rays are photons emitted by radioactive nuclei; except for their origin, they are identical to x-ray photons of the same energy. Section 16.1 describes the production of x rays. Section 16.2 introduces some new quantities that are important for measuring how the absorbed photon energy relates to the response of a detector—which might be a film, an ionization chamber, or a chemical detector. Several detectors are introduced in Section 16.3: film, fluorescent screens, scintillation detectors, semiconductor detectors, thermoluminescent dosimeters, and digital detectors. Section 16.4 describes the diagnostic radiograph, and the following section discusses image quality, particularly the importance of noise in determining image quality. Section 16.6 provides a brief mention of angiography, Sec. 16.7 discusses some of the special problems of mammography, and fluoroscopy is described in Sec. 16.8. Computed tomography with x rays is discussed in Sec. 16.9. The final sections deal with the biological effects of x rays, cancer therapy, dose, and the risk of radiation.

### 16.1 Production of X Rays

When a beam of energetic electrons stops in a target, photons called x rays are emitted. *Characteristic x rays* have discrete photon energies and are produced after excitation of an atom by the electron beam. *Bremsstrahlung* (Sec. 15.11) is the continuous spectrum of photon energies produced when an electron is scattered by an atomic nucleus. Bremsstrahlung is responsible for most of the photons emitted by most x-ray tubes. The total bremsstrahlung radiation yield as a function of electron energy for various materials is shown in Fig. 16.1. High- $Z$

materials are most efficient for producing x rays. Tungsten ( $Z = 74$ ) is often used as a target in x-ray tubes because it has a high radiation yield and can withstand high temperatures. For 100-keV electrons on tungsten, the radiation yield is about 1%: most of the electron energy heats the target. We now consider these two processes in greater detail.

#### 16.1.1 Characteristic X Rays

Atomic energy levels are described in Sec. 14.2. The levels for tungsten are shown in Table 15.1 and Fig. 15.1. An

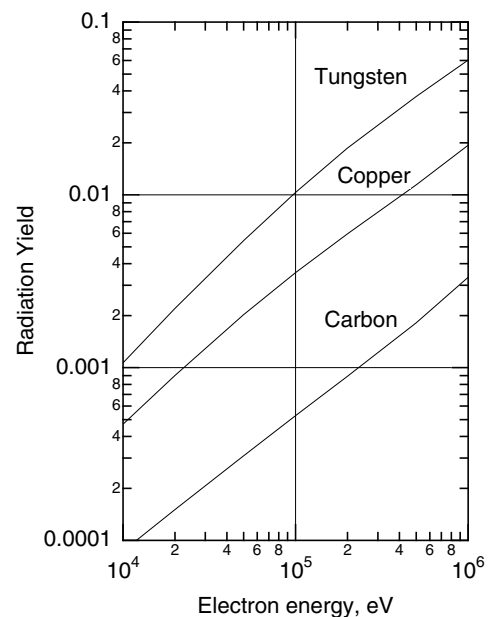


FIGURE 16.1. Radiation yield vs electron energy for carbon, copper, and tungsten. Plotted from data in ICRU Report 37 (1984). The radiation yield is the fraction of the electron's energy that is converted to photon energy; see Sec. 15.13.

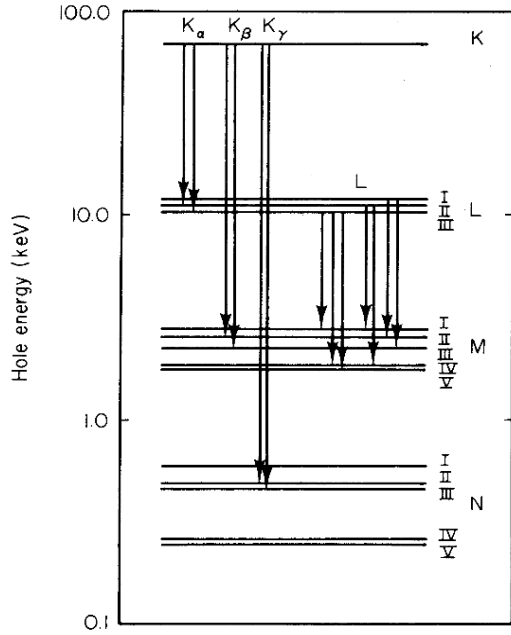


FIGURE 16.2. Energy-level diagram for holes in tungsten and some of the x-ray transitions.

electron bombarding a target can impart sufficient energy to a target electron to remove it from the atom, leaving an unoccupied energy level or *hole*. The deexcitation of the atom is described in Sec. 15.9. For a high- $Z$  material with a hole in the  $K$  shell, the fluorescence yield is large (see Fig. 15.14). The hole is usually filled when an electron in a higher energy level drops down to the unoccupied level. As it does so, the atom emits a characteristic x ray—a photon with energy equal to the difference in energies of the two levels. This leaves a new hole, which is then filled by an electron from a still higher level with the emission of another x ray, or by an Auger cascade.

Because a hole moving to larger values of  $n$  corresponds to a decrease of the total energy of the atom, it is customary to draw the energy-level diagram for holes instead of electrons, which turns the graph upside down, as in Fig. 16.2. The zero of energy is the neutral atom in its ground state. Because this is a logarithmic scale, zero cannot be shown. Creation of the hole requires energy to remove an electron. That energy is released when the hole is filled. Various possible transitions are indicated in Fig. 16.2. These transitions are consistent with these selection rules, which can be derived using quantum theory:

$$\Delta l = \pm 1, \quad \Delta j = 0, \pm 1. \quad (16.1)$$

The transitions are labeled by the letters  $K$ ,  $L$ ,  $M$  and so forth, depending on which shell the hole is in initially. Greek-letter subscripts distinguish the x rays from transitions to different final states.

Analogous to the approximate formula of Eq. 15.3 is the following estimate of the energy of the  $K_\alpha$  line (which

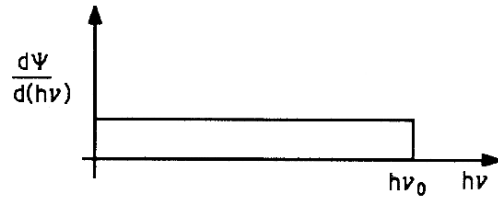


FIGURE 16.3. The energy fluence spectrum of bremsstrahlung x rays emitted when monoenergetic electrons strike a thin target.

depends on the screening for two values of  $n$ ), which we have seen before as Eq. 15.34:

$$E_{K_\alpha} = \frac{3}{4}(13.6 \text{ eV})(Z - 1)^2. \quad (16.2)$$

The factor  $3/4$  is what one would have for hydrogen if  $n_i = 2$  and  $n_f = 1$  are substituted in the Bohr formula, Eq. 14.8. The screening also depends strongly on  $l$ .

### 16.1.2 Bremsstrahlung

The other mechanism for x-ray production is the acceleration of electrons in the Coulomb field of the nucleus, described in Sec. 15.11. Classically, a charged particle at rest creates an electric field which is inversely proportional to the square of the distance from the charge. When in motion with a constant velocity it creates both an electric field and a magnetic field. When accelerated, additional electric and magnetic fields appear that fall off less rapidly—inversely with the first power of distance from the charge. This is classical electromagnetic radiation. Quantum-mechanically, when a charged particle undergoes acceleration or deceleration, it emits photons. The radiation is called deceleration radiation, braking radiation, or bremsstrahlung. It has a continuous distribution of frequencies up to some maximum value.

The photon *energy* fluence spectrum of bremsstrahlung radiation from monoenergetic electrons passing through a thin target is constant from a maximum energy  $h\nu_0$  down to zero, as shown in Fig. 16.3 [Evans (1955), p. 605]. The maximum frequency is related to the kinetic energy of the electrons by  $T = h\nu_0$ , as one would expect from conservation of energy. (A photon of energy  $h\nu_0$  is emitted when an electron loses all of its energy in a single collision.)

For a thick target, we assume that all electrons at the same depth have the same energy (that is, we ignore straggling), and we ignore attenuation of photons coming out of the target. The spectrum is then the integral of a number of spectra like that in Fig. 16.3. The thick-target spectrum is shown in Fig. 16.4. The spectral form is

$$\frac{d\Psi}{d(h\nu)} \equiv \frac{d\Psi}{dE} = CZ(h\nu_0 - h\nu) = CZ(T - E), \quad (16.3a)$$

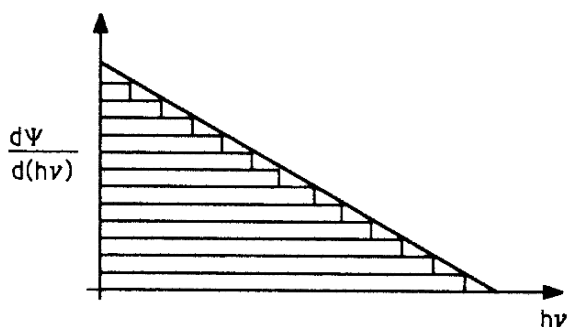


FIGURE 16.4. The energy fluence spectrum of bremsstrahlung x rays from a thick target, ignoring absorption of the photons in the target. The form is  $d\Psi/d(h\nu) = CZ(h\nu_0 - h\nu)$ .

where constant  $C$  depends on the target material and electron kinetic energy. The photon particle fluence spectrum is

$$\frac{d\Phi}{dE} = \frac{1}{h\nu} \frac{d\Psi}{dE} = CZ \left( \frac{h\nu_0}{h\nu} - 1 \right). \quad (16.3b)$$

More of the low-energy photons that are generated within the target are attenuated as they escape, because of the much larger values of the attenuation coefficient at low energies (recall Figs. 15.10 and 15.11). This cuts off the low-energy end of the spectrum. If the electron energy is high enough, the discrete spectrum due to characteristic fluorescence is superimposed on the continuous bremsstrahlung spectrum. Both of these effects are shown in Fig. 16.5, which compares calculations and measurements of the particle fluence spectrum  $d\Phi/dE$ .

## 16.2 Quantities to Describe Radiation Interactions: Radiation Chemical Yield, Mean Energy Per Ion Pair, and Exposure

Section 15.15 introduced the quantities energy transferred, energy imparted, kerma, and absorbed dose, which are used to describe radiation and its effects. This section introduces some additional quantities [ICRU Report 33 (1980, 1992)] that are used to describe the interaction of the radiation with the detectors discussed in Sec. 16.3.

### 16.2.1 Radiation Chemical Yield

The *radiation chemical yield*  $G$  of a substance is the mean number of moles  $\bar{n}$  of the substance produced, destroyed, or changed in some volume of matter, divided by the mean energy imparted to the matter:

$$G = \frac{\bar{n}}{\bar{E}}. \quad (16.4)$$

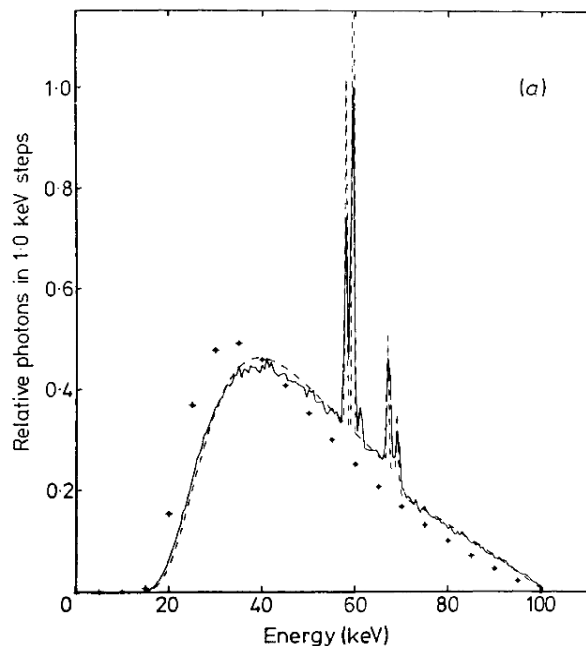


FIGURE 16.5. Plots of theoretical and measured photon particle spectra,  $d\Phi/d(h\nu)$  for 100-keV electrons striking a thick tungsten target. The solid line represents measurements with a high-resolution semiconductor detector. The dashed line is the theory of Birch and Marshall (1979), which takes photon absorption into account. The crosses show an earlier theoretical model. From R. Birch and M. Marshall. Computation of bremsstrahlung X-ray spectra and comparison with spectra measured with a Ge(Li) detector. *Phys. Med. Biol.* **24**:505–517 (1979). Used by permission of the Institute of Physics.

Its units are  $\text{mol J}^{-1}$ . (A related quantity expressed in non-SI units is the  $G$  value, expressed in molecules or moles per 100 eV of energy imparted.) The radiation chemical yield is particularly useful for describing chemical dosimeters. These are usually dilute aqueous solutions, so the radiation chemical yield of water is the important parameter.

### 16.2.2 Mean Energy per Ion Pair

Other detectors measure ionization produced in a gas by the radiation. The *mean energy expended in a gas per ion pair formed*,  $W$ , is

$$W = \frac{T_0}{\bar{N}_i}, \quad (16.5)$$

where  $T_0$  is the initial kinetic energy of a charged particle and  $\bar{N}_i$  is the mean number of ion pairs formed when  $T_0$  is completely dissipated in the gas. The units are joules or electron volts per ion pair. The mean energy expended per ion pair is not equal to the ionization energy. To see why, consider three processes that can take place. The first is ionization, with  $\bar{E}_i$  being the average energy of an ionized atom. Second, the collision may promote an atomic electron to an excited state without ionization.



TABLE 16.1. Some representative values of the average energy per ion pair,  $W$ .

Gas	$W$ (eV per ion pair for electrons <sup>a</sup> )
He	41.3
Ar	26.4
Xe	22.1
Air	33.97 <sup>b</sup>
Semiconductors	$W$ (eV per electron-hole pair)
Si	3.68
Ge	2.97

<sup>a</sup>From ICRU Report 31 (1979).

<sup>b</sup>ICRU Report 39 (1979) recommends 33.85 J C<sup>-1</sup>. Attix (1986) uses 33.97 J C<sup>-1</sup>. Note that 1 J C<sup>-1</sup> is equivalent to 1 eV per singly charged ion pair.

The average excitation energy is  $\bar{E}_{ex}$ . Finally, the charged particle may lose energy to impurities without producing ionization, a process called “subexcitation.” The average subexcitation energy is defined to be the energy lost by this process,  $E_{se}$ , divided by  $\bar{N}_i$ . Conservation of energy for this model leads to

$$T_0 = \bar{N}_i \bar{E}_i + \bar{N}_{ex} \bar{E}_{ex} + \bar{N}_i \bar{E}_{se},$$

where  $T_0$  is the initial projectile kinetic energy,  $\bar{N}_i$  is the mean number of ion pairs produced, and  $\bar{N}_{ex}$  is the mean number of atoms raised to an excited state but not ionized.

Dividing each term by  $\bar{N}_i$  leads to an expression for  $W$ . In general,  $W$  is determined experimentally, because the terms in this equation are quite difficult to calculate. However, they have been calculated for helium.<sup>1</sup> The mean energy of an ionized helium atom is only 62% of the value of  $W$ :

$$\underbrace{W}_{41.8 \text{ eV}} = \underbrace{\bar{E}_i}_{\substack{25.9 \text{ eV} \\ 62\%}} + \underbrace{(\bar{N}_{ex}/\bar{N}_i) \bar{E}_{ex}}_{\substack{0.4 \times 20.8 = 8.3 \text{ eV} \\ 20\%}} + \underbrace{\bar{E}_{se}}_{\substack{7.6 \text{ eV} \\ 18\%}}$$

Values of  $W$  are tabulated in ICRU Report 31 (1979). There are variations of a few percent depending on whether the charged particle is an electron or an  $\alpha$  particle. Table 16.1 provides a few representative values. Though defined for a gas,  $W$  is also applied to semiconductors as the average energy per electron-hole pair produced. Values of  $W$  for semiconductors are much smaller than for a gas.

### 16.2.3 Exposure

The *exposure*  $X$  is defined only for photons and measures the energy fluence of the photon beam. It is the amount of ionization (total charge of one sign) produced per unit

mass of dry air when all of the electrons and positrons liberated in a small mass of air are completely stopped in air:

$$X = \frac{dq}{dm}. \tag{16.6}$$

The units are coulomb per kilogram. Since the average amount of energy required to produce an ion pair is well defined, exposure is closely related to collision kerma in air. The definition of  $X$  does not include ionization arising from the absorption of bremsstrahlung emitted by the electrons, so there is a slight difference at high energies.<sup>2</sup> The relationship is

$$X = (K_c)_{air} \left( \frac{e}{W_{air}} \right) = \Psi \left( \frac{\mu_{en}}{\rho} \right)_{air} \left( \frac{e}{W_{air}} \right). \tag{16.7}$$

If charged-particle equilibrium exists, the dose in air is related to the beam energy fluence by Eqs. 15.72 and 15.75:

$$D_{air} = \left( \frac{\mu_{en}}{\rho} \right)_{air} \Psi.$$

The dose for the same energy fluence in some other medium is

$$D_{med} = \left( \frac{\mu_{en}}{\rho} \right)_{med} \Psi = \frac{(\mu_{en}/\rho)_{med}}{(\mu_{en}/\rho)_{air}} D_{air}. \tag{16.8}$$

The *roentgen* (R) is an old unit of exposure equivalent to the production of  $2.58 \times 10^{-4}$  C kg<sup>-1</sup> in dry air; this corresponds to a dose of  $8.69 \times 10^{-3}$  Gy. (The relationship is developed in Problem 8.)

## 16.3 Detectors

Detectors are used for recording an image and also for measuring the amount of radiation to which a patient is exposed. This section describes the most common kinds of detectors.

### 16.3.1 Film and Screens

Film is the original x-ray detector, and it is still widely used. A typical x-ray film has a transparent base about 200  $\mu\text{m}$  thick, coated on one or both sides with a sensitive emulsion containing a silver halide (usually silver bromide). We will not discuss the rather complicated sequence of steps by which the absorption of photons or energy loss by charged particles leads to a latent or developable image in the film. When the film is developed, the emulsion grains that have absorbed energy are reduced to black specks of metallic silver. The film is then

<sup>2</sup>There is also a problem at high energies because the range of the electrons is large. If they are to come to rest within the chamber, the size of the chamber becomes comparable to the photon attenuation coefficient.

<sup>1</sup>See Platzman (1961); also Attix (1986, pp. 339–343).

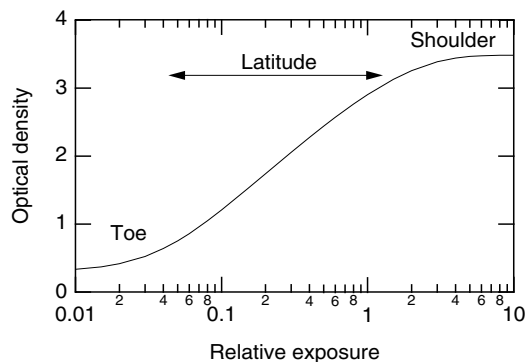


FIGURE 16.6. A plot of optical density vs the logarithm of the relative exposure for a hypothetical x-ray film.

fixed, a process in which the silver halide that was not reduced is removed from the emulsion. The result is a film that absorbs visible light where it was struck by ionizing radiation.

The fraction of incident light passing through the film after development is called the *transmittance*,  $T$ . The *optical density* or *density* is defined to be

$$\text{OD} = \log_{10}(1/T). \quad (16.9)$$

A film that transmits 1% of the incident viewing light has an optical density of 2.

The response of a film is described by plotting the optical density vs the log of the exposure in air immediately in front of the film (or equivalently, the absorbed dose in the film emulsion). Since the optical density is the logarithm of the transmittance, this is a log-log plot of the reciprocal of the fraction of the visible light transmitted when viewing the processed film vs the x-ray exposure before processing. A typical plot of film response is shown in Fig. 16.6. If the curve is linear, the transmittance is proportional to the exposure raised to some power:

$$T \propto X^{-\gamma}.$$

At very small exposures (the *toe*) the transmission is that of the base and “clear” emulsion. At very high exposures (the *shoulder*) all of the silver halide has been reduced to metallic silver, and the film has its maximum optical density. In between is a region which is almost linear (on a log-log scale). The ratio of maximum to minimum usable exposure is called the *latitude* of the film. The largest value of the exponent occurs at the inflection point and is called the *gamma* or *contrast* of the film. Both the exponent and the position of the curve along the log exposure axis depend on the development time, the temperature of the developing solution, and the energy of the x-ray beam. The *film speed* is the reciprocal of the exposure required for an optical density that is 1 greater than the base density.

A typical film has an emulsion containing AgBr. It requires a dose of  $1.74 \times 10^{-4}$  Gy ( $\text{J kg}^{-1}$ ) in air just in

front of the film to produce an optical density of 1. This might be where the body is not blocking the beam. The smaller dose to the film where there has been significant attenuation in the body gives a lighter region, as in the heart and bone shadows of Fig. 16.18.

The dose to the part of the body just in front of the film (the *exit dose* to the patient) can be written in several ways. For simplicity we assume monoenergetic photons. In terms of the energy fluence of the photon beam, the exit dose is

$$D_{\text{body}} = \left( \frac{\mu_{\text{en}}}{\rho} \right)_{\text{body}} \Psi. \quad (16.10a)$$

In terms of the dose in air just in front of the film it is

$$D_{\text{body}} = \frac{(\mu_{\text{en}}/\rho)_{\text{body}}}{(\mu_{\text{en}}/\rho)_{\text{air}}} D_{\text{air}}, \quad (16.10b)$$

and in terms of the dose in the film it is

$$D_{\text{body}} = \frac{(\mu_{\text{en}}/\rho)_{\text{body}}}{(\mu_{\text{en}}/\rho)_{\text{film}}} D_{\text{film}}. \quad (16.10c)$$

For 50-keV photons we find from the tables at [physics.nist.gov/PhysRefData/XrayMassCoef/tab4.html](http://physics.nist.gov/PhysRefData/XrayMassCoef/tab4.html)

that  $(\mu_{\text{en}}/\rho)_{\text{muscle}}/(\mu_{\text{en}}/\rho)_{\text{air}} = 0.004349/0.004098 = 1.061$ . Therefore the exit dose would be  $(1.74 \times 10^{-4})(1.061) = 1.85 \times 10^{-4}$  Gy. Because of attenuation, the entrance dose can be much larger.

The dose can be reduced by a factor of 50 or more if the film is sandwiched between two fluorescent *intensifying screens*. The x-ray photons have a low probability of interacting in the film. The screens have a greater probability of absorbing the x-ray photons and converting them to visible light, to which the film is more sensitive. For 50-keV photons on typical emulsion, the value of  $\mu_{\text{en}}/\rho$  is about  $0.261 \text{ m}^2 \text{ kg}^{-1}$ . A typical value of  $\rho\Delta x$  for the film might be  $0.02 \text{ kg m}^{-2}$ . Therefore,  $\mu_{\text{en}}\Delta x = 0.0052$ . The fraction of incident energy absorbed in the emulsion is  $1 - e^{-0.0052} = 0.0052$ .

A typical screen might consist of particles of terbium-doped gadolinium oxysulfide ( $\text{Gd}_2\text{O}_2\text{S:Tb}$ ) suspended in a carrier about  $150 \mu\text{m}$  thick ( $0.5\text{--}1.5 \text{ kg m}^{-2}$ ). This layer is backed by a thin reflective layer. Two such screens (one on each side of the film) with a total thickness of  $1.2 \text{ kg m}^{-2}$  absorb 28% of the 50-keV photons that pass through them (see Problem 12). The overall effect is to produce the same optical density when the energy fluence in the x-ray beam is reduced by a factor of 54—the ratio of the incident radiation absorbed in the screen and in the film in each case.<sup>3</sup> Typically, a sheet of film is placed in a light-

<sup>3</sup>The fluorescent radiation has a wavelength of about 545 nm (green), and each absorbed high-energy photon has sufficient energy to produce about 14,000 fluorescence photons. However, the efficiency of production is only about 5% so 700 photons are produced. Some of these escape or are absorbed. Each x-ray photon produces about 150 photons of visible and ultraviolet light that strike the emulsion—more than enough to blacken the film in the region where the x-ray photon was absorbed by the screen.

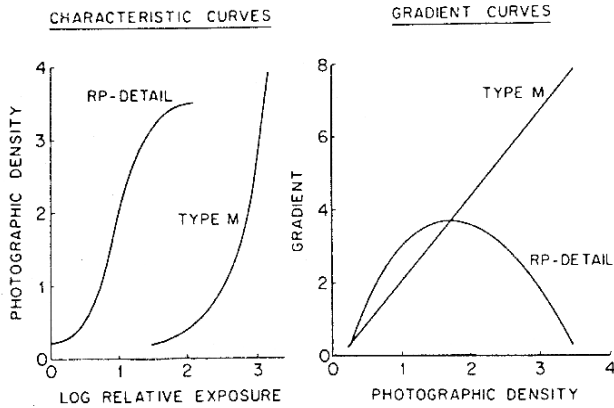


FIGURE 16.7. Plots of optical density vs logarithm exposure for a screen-film combination (RP) and a film (M). From K. Doi, H. K. Genant, and K. Rossman. Comparison of image quality obtained with optical and radiographic magnification techniques in fine-detail skeletal radiography: Effect of object thickness. *Radiology* **118**: 189-195 (1976). Reproduced by permission of the Radiological Society of North America.

tight “cassette” whose front and back walls are made of screen material.

Figure 16.7 shows a plot of optical density vs the log of the exposure  $X$  for two typical radiographic systems. “RP-detail” is a screen-film combination. Type M is a film without a screen. At an optical density of 1 or 2, the difference in  $\log_{10} X$  is about 1.9, corresponding to a factor of 80 in exposure, somewhat greater than the example given above. The curves are not linear. The slope at any point on the curve is<sup>4</sup>

$$\begin{aligned} \gamma &= \frac{d \log_{10}(1/T)}{d \log_{10} X} = \frac{d \ln(1/T)}{d \ln X} = -\frac{dT/T}{dX/X} \\ &= -\frac{X}{T} \frac{dT}{dX} = -\frac{1}{G} g, \end{aligned} \tag{16.11}$$

where  $G = T/X$  is the *large-signal transfer factor* and  $g = dT/dX$  is the *incremental-signal transfer factor*. This will be used in our discussion of detecting signals in noise in the next section.

### 16.3.2 Scintillation Detectors

When x-ray photons interact with matter, some of their energy is transferred to electrons. These electrons interact in turn, and some of their energy can become ultraviolet or visible photons. A *scintillator* is a substance that produces these photons with high efficiency, yet is transparent to them. The photons are then transferred by an optical fiber or a lens system to a light detector such as a photomultiplier tube or a solid-state photodetector. Each x-ray photon produces an electrical current pulse

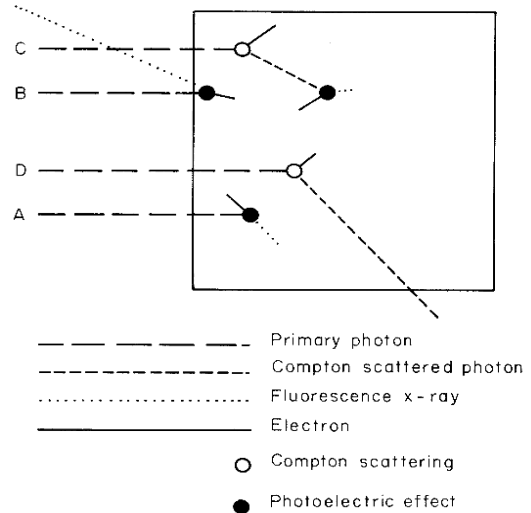


FIGURE 16.8. Mechanisms by which some of the energy of a primary photon can escape from a detector. Photons A and B undergo photoelectric absorption. All of the energy from A is absorbed in the detector, while the fluorescence x-ray from B escapes. Photons C and D are Compton scattered. The scattered photon from C undergoes subsequent absorption, while that from D escapes.

at the detector output, called a *count*. When the number of counts is recorded vs the pulse height (total charge in the pulse, which is proportional to the energy deposited in the scintillator), the result is a *pulse-height spectrum*. For monoenergetic photons, the ideal pulse height spectrum would consist of a single peak: all pulses would have the same height. This is not realized in practice for two reasons: statistical variations in the scintillation process cause the line to be broadened, and the entire energy of the incident photon is not converted into electrons.

An atom that has been excited by photoelectric absorption can decay by the emission of a fluorescence photon. If this photon is subsequently absorbed in the scintillator, all of the original photon energy is converted to electron energy so rapidly that the visible light is all part of one pulse. The pulse height then corresponds to the full energy of the original photon. However, if the initial photoelectric absorption takes place close to the edge of the detector, the fluorescence photon can escape, and the pulse has a lower height than those in the primary peak. This can be seen in Fig. 16.8. Photons A and B interact by photoelectric effect. All the energy for photon A is deposited in the scintillator, while the  $K$  fluorescence photon from B escapes. The effect on a pulse height spectrum is shown in Fig. 16.9 for a scintillator of sodium iodide.

In Compton scattering, the energy of the recoil electron is transferred to the scintillator (unless the electron escapes). The scattered photon may escape from the detector, as in D of Fig. 16.8. (If it is subsequently absorbed, as in mechanism C of Fig. 16.8, the pulse height will have the peak value.) The energy of the recoil electron is given

<sup>4</sup>An argument based on Eq. 2.14 can be used to show that  $\log_{10} x = (1/2.303) \ln x = 0.43 \ln x$ .

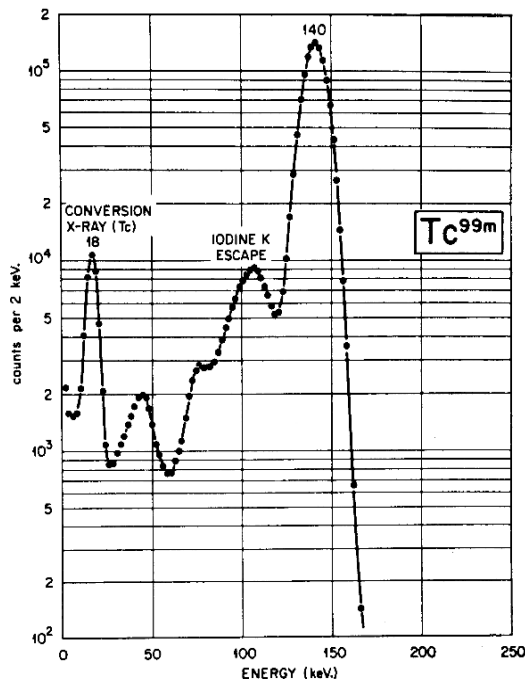


FIGURE 16.9. Spectrum of pulse heights for 140-keV photons from isotope  $^{99m}\text{Tc}$  incident on a sodium iodide scintillator. The 140-keV total energy peak is prominent, as is the peak at 110 keV corresponding to the escape of the K fluorescence x ray from iodine. The Compton scatter continuum runs from 49 keV down to zero energy. The peak at 18 keV is from additional radiation from  $^{99m}\text{Tc}$  (see Chapter 17). Reproduced from H. N. Wagner, Jr., ed. *Principles of Nuclear Medicine*, p. 162. Copyright 1968 by W. B. Saunders, by permission of Elsevier.

by Eq. 15.16. The maximum electron energy occurs when the photon is scattered through  $\theta = 180^\circ$ . Then

$$T_{\max} = \frac{2h\nu_0x}{1+2x} = \frac{(h\nu_0)^2}{h\nu_0 + m_e c^2/2}$$

If the photon energy is in keV, this is

$$T_{\max} = \frac{(h\nu_0)^2}{h\nu_0 + 256} \tag{16.12}$$

A pulse-height spectrum for “pure” Compton scattering of 662-keV photons (as emitted by  $^{137}\text{Cs}$ ) is shown in Fig. 16.10. The peak of the Compton continuum is at  $T_{\max} = (662)^2/(662 + 256) = 477$  keV. The cases of perfect resolution with complete absorption and real resolution with complete absorption are shown, along with the theoretical Compton continuum with perfect resolution, and a real spectrum.

When the energy of the primary photons is so large that pair production is important, an additional escape mechanism must be considered. We know (Eq. 15.23) that

$$h\nu_0 = T_+ + T_- + (m_e c^2)_{e^-} + (m_e c^2)_{e^+}$$

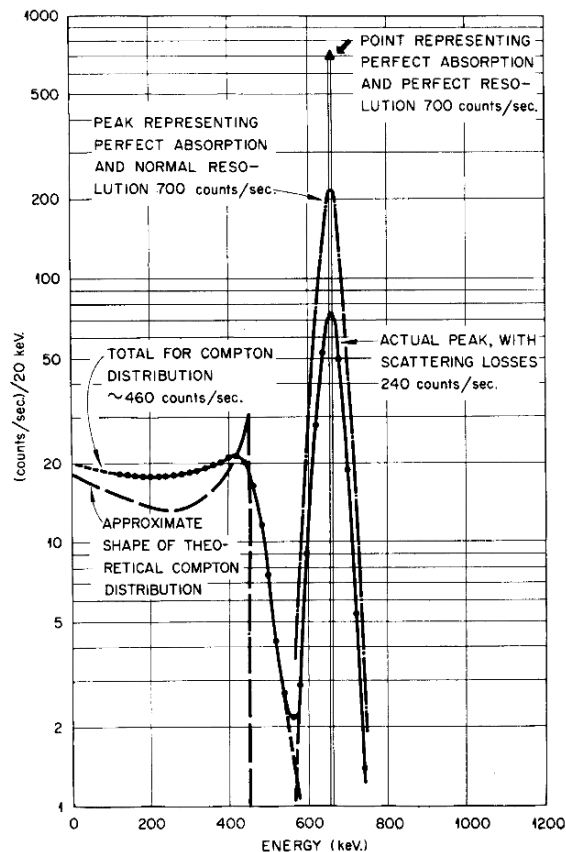


FIGURE 16.10. The response of a sodium iodide detector to 662-keV photons from  $^{137}\text{Cs}$ . Theoretical responses are shown for a detector that absorbs the energy of all photons and has perfect resolution, for a detector with perfect absorption and finite resolution, and for a detector in which Compton-scattered photons can escape. Experimental data are for a  $1\frac{1}{2}$ -in. by 1-in. NaI crystal. Redrawn from C. C. Harris, D. P. Hamblen, and J. E. Francis, Jr. (1969). *Basic Principles of Scintillation Counting for Medical Investigators*. ORNL-2808. Springfield, VA, Clearing House for Federal Scientific and Technical Information, National Bureau of Standards. Reproduced from H. N. Wagner, Jr., ed. *Principles of Nuclear Medicine*, Philadelphia, Saunders, p. 153. Copyright 1968 W. B. Saunders, by permission of Elsevier.

The positron will eventually combine with another electron to produce two annihilation radiation photons:

$$(m_e c^2)_{e^+} + (m_e c^2)_{\text{another } e^-} = 2E_\gamma$$

The energy of each annihilation photon is 511 keV. The initial photon energy is finally distributed as

$$h\nu_0 = T_+ + T_- + \gamma(511) + \gamma(511)$$

If all this energy is absorbed in the detector, the pulse height corresponds to the full energy of the incident photon. One or both of the annihilation photons can escape, giving the one-photon escape peak and the two-photon escape peak.

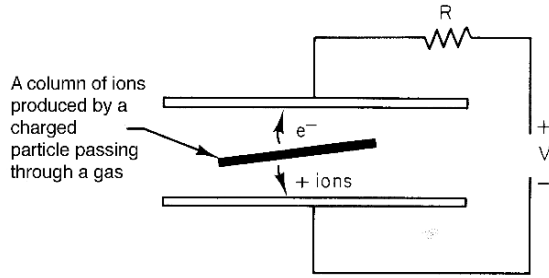


FIGURE 16.11. Schematic of an ionization chamber or proportional counter. The ions discharge the capacitor, which is recharged between counts through resistor  $R$ .

Scintillation detectors vary greatly in size. Large ones may be tens of centimeters in diameter; others can be less than a millimeter. A large number of materials are used [van Eijk (2002)].

### 16.3.3 Gas Detectors

Ionization in gas is the basis for three kinds of x-ray detectors: ionization chambers, proportional counters, and Geiger counters. A photon passing through a gas can produce photoelectric, Compton, or pair-production electrons. These then lose energy by electron collisions. Ion pairs are produced in the gas, the average number being proportional to the amount of energy lost in the gas. The average amount of energy required to produce an ion pair is  $W$ , as we saw in Sec. 16.2. Imagine that the ions are produced between the plates of a charged capacitor as shown in Fig. 16.11. The electrons are attracted to the positive plate and the positive ions travel to the negative plate. If all the electrons and ions are captured, the total charge collected on each plate has magnitude  $q = Ne$ , where  $e$  is the charge on the electron or ion and  $N$  is the number of ion pairs formed. If the capacitance is  $C$ , the change in voltage is  $\delta v = q/C = Ne/C$ . Such a device is called an *ionization chamber*. The cumulative discharge of the capacitor is measured in some pocket dosimeters; in other cases, the capacitor is slowly recharged through a large resistance  $R$  so that each photon detected generates a voltage pulse of height  $\delta v$ .

A certain minimum voltage between the two plates is necessary to ensure that all the ions produced are collected, corresponding to the ion chamber region of Fig. 16.12. The ionization chamber is the “workhorse” detector for accurately measuring radiation dose.

If the potential on the plates is raised further, the number of ions collected increases. Between collisions the electrons and ions are accelerated by the electric field, and they acquire enough kinetic energy to produce further ionizations when they collide with molecules of the gas, a process called *gas multiplication*. At moderate potentials, the multiplication factor is independent of the initial ionization, so the number of ions collected is larger than that

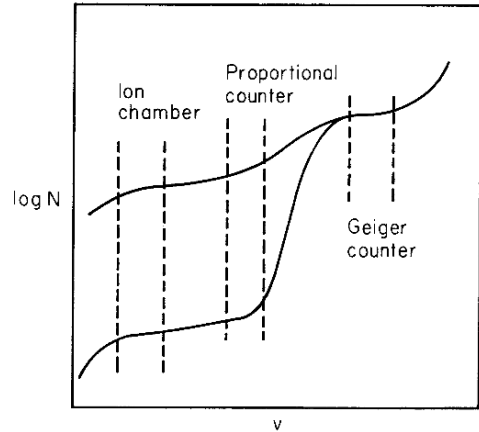


FIGURE 16.12. The number of ions collected vs collecting potential for two particles that deposit different amounts of energy in a gas detector. The voltage regions are indicated where the device operates as an ionization chamber, a proportional counter, and a Geiger counter.

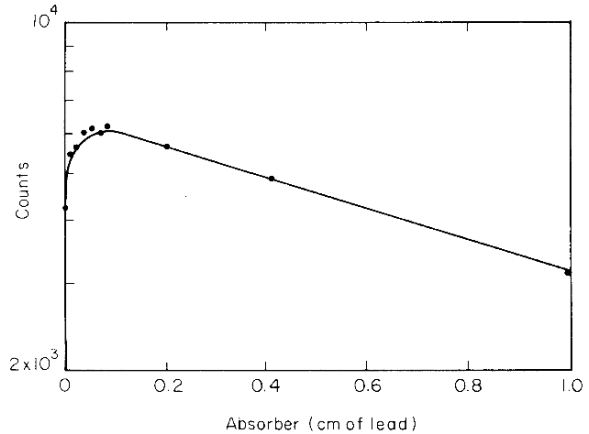


FIGURE 16.13. Counting rate of a Geiger counter vs. the thickness of a lead absorber in front of the detector, showing the buildup of counting rate due to the conversion of photons to electrons in the lead by Compton scattering. These electrons pass through the thin wall of the counter and ionize the gas. The photons were from  $^{60}\text{Co}$  and had an energy of 1.1 MeV.

in an ionization chamber but still is proportional to the initial number of ions. In this region of operation the device is called a *proportional counter*. Parallel-plate geometry is not used in a proportional counter. One electrode is a wire, and the other is a concentric cylinder.

At still higher values of the applied voltage, pulse size is independent of the initial number of ion pairs. In this mode of operation, the device is called a *Geiger counter*.

Any gas detector used to detect high-energy photons suffers from the fact that the gas is not very dense. At low energies the photoelectric cross section is high and most photons interact. At higher energies, many photons pass through the gas and detector walls without interacting. A thin sheet of absorber in front of the gas detector can actually increase the counting rate. An example is

shown in Fig. 16.13. The detector had an aluminum wall of thickness  $0.3 \text{ kg m}^{-2}$ . Electrons of 125 keV or more pass completely through the detector wall. The maximum energy of Compton electrons from the 1.1-MeV photons is 890 keV. Compton electrons produced in a thin layer of lead can pass through the aluminum and ionize the gas in the detector. Once the total thickness of lead and aluminum is sufficient to stop all the Compton electrons, the addition of more lead upstream does not increase the detector efficiency, and exponential attenuation is seen.

#### 16.3.4 Semiconductor Detectors

A semiconductor detector is very much like an ionization chamber, except that a solid is used as the detecting medium. The “ion pair” is an electron that has received sufficient energy to be able to leave its atom and move freely within the semiconductor (but not enough energy to leave the semiconductor entirely) and the “hole” that the electron left behind. Electrons from neighboring atoms can fall into the hole, so the hole can move from atom to atom just like a positive charge. Details of the operation of semiconductor detectors can be found in Lutz (1999).

A semiconductor detector has two principal advantages over a gas ionization chamber. First, the amount of energy required to create an electron–hole pair is only about 3 eV, one-tenth the value for a typical gas. This means that many more pairs are produced and the statistical accuracy is better. Second, the density of a solid is much greater than the density of a gas, so the probability that a photon interacts is larger. The cross section for interaction increases with high  $Z$ , so detectors made of germanium ( $Z = 32$ ) are better for photon detection than those made of silicon ( $Z = 14$ ). There have been technical problems making semiconductor detectors of large volume. Some of these have been overcome by using lithium-drifted germanium (Ge-Li) or silicon detectors. Their main drawback is that they have to be kept at liquid-nitrogen temperature to keep the lithium from drifting out once it has been implanted. Room-temperature detectors have been developed and are now fabricated as detector arrays [Lutz (1999), Schlesinger and James (1995)].

Diode detectors are used for real-time dose measurement in patients receiving radiation therapy [AAPM Report 87 (2005)].

#### 16.3.5 Thermoluminescent Dosimeters

Thermoluminescent phosphors consist of a small amount of dielectric material (0.1 g or less) that has been doped with impurities or has missing atoms in the crystal lattice to form metastable energy levels or traps. These impurities or defects are far from one another and are isolated in the lattice, so that electrons cannot move freely from one trap to another. When the phosphor is irradiated with ionizing radiation, some of the electrons are

trapped in these metastable states. There are levels associated with the material at an energy  $E$  above the trap energy (the conduction band) which allow electrons to move throughout the phosphor. The probability that an electron escapes from the trap is proportional to a Boltzmann factor,  $\exp(-E/k_B T)$ . If  $E$  is large enough, the lifetime in the trapped state can be quite large—up to hundreds of years. Heating allows the electrons to escape to the higher levels, where they then fall back to the normal state with the emission of visible photons. Ordinary table salt (NaCl) exhibits this behavior. If it is irradiated and then sprinkled on an electric hot plate in a darkened room, one can see the flashes of light. The light emitted on heating is called *thermoluminescence*. In a thermoluminescent dosimeter (TLD), the light emitted is measured with a photomultiplier tube as the temperature is gradually increased. The total amount of light released is proportional to the energy imparted to the phosphor by the ionizing radiation.

Thermoluminescent dosimeters can measure an integrated dose from  $10^{-5}$  to  $10^3$  Gy. Great care must be taken both in the preparation and reading of the phosphor. TLD chips are widely used to measure radiation doses because they are small and have the approximate atomic number and atomic weight of tissue. They are often made of LiF. Detailed descriptions are found in Chapter 14 of Attix (1986), Shani (1991) and Shani (2001). (The two editions of Shani complement one another.)

#### 16.3.6 Chemical Dosimetry

When radiation interacts with water, *free radicals* are produced. A free radical, such as H or OH, is electrically neutral but has an unpaired electron. Free radicals promote other chemical reactions. Typically, a dilute indicator of some sort is added to the water. A common dosimeter is the Fricke ferrous sulfate dosimeter. A 1 mM  $\text{FeSO}_4$  solution is irradiated. The radiation changes the iron from the ferrous ( $\text{Fe}^{2+}$ ) to the ferric ( $\text{Fe}^{3+}$ ) state with a  $G$  of about  $1.6 \times 10^{-6} \text{ mol J}^{-1}$ . The concentration of ferric ion can be measured by absorption spectroscopy. Details are found in Chapter 14 of Attix (1986) and in Shani (1991) and Shani (2001). Magnetic resonance imaging (Chapter 18) is also used to measure the amount of ferric ion in the Fricke dosimeter since the relaxation times depend on the ion concentration. This has led to the gel dosimeter which allows a three-dimensional measurement of the dose distribution—useful for planning radiation treatments [Shani (2001), Chapter 9].

Another form of chemical dosimeter is *radiochromic film*. It consists of a thin layer of radiosensitive dye bonded to a mylar base. The dye darkens with radiation. Radiochromic films are sensitive for doses of 1–500 Gy, making them useful for measuring doses in radiation therapy [Shani (2001), Chapter 5].

### 16.3.7 Digital Detectors

Digital x-ray detectors are replacing film in clinical radiography. A digitally recorded image generally has a greater dynamic range (latitude) than film. A factor-of-2 difference in exposure,<sup>5</sup> which renders a conventional radiographic image almost useless, is easily tolerated by digital recording.<sup>6</sup> A digitally stored image allows easier retrieval, transmission, and creation of multiple copies.

A number of techniques are used. The storage phosphor technology forms an image on a plate of phosphor crystals such as barium fluorobromide. Absorption of x-ray photons leaves the BaFBr crystals in a metastable state, like a TLD phosphor. Scanning by a thin laser beam in a horizontal and vertical raster pattern like a television image causes visible light to be emitted by the trapped electrons. The dynamic range of a storage phosphor can be as high as  $10^4$ , compared to about  $10^2$  for radiographic film [Rowlands (2002)].

The thin-film transistor arrays used in flat-panel computer screens are also used to make large detector arrays. The TFT arrays provide the spatial readout. They are combined either with an amorphous selenium photoconductor that converts the x-ray energy to charge, or with a structured scintillator such as a large array of CsI crystals [Seibert (2003)]. Each CsI crystal may be as small as  $6\ \mu\text{m}$  diameter by  $500\ \mu\text{m}$  long [Winsor (2003)].

## 16.4 The Diagnostic Radiograph

Figure 16.14 shows the typical elements for making a diagnostic x ray. An image recorded on film is called a *radiograph*. The x-ray tube ideally serves as a point source of photons. The photons are filtered and collimated to illuminate only the portion of the patient of interest. Typically, about 10% pass through the patient and strike the film–screen sandwich in a chest radiograph. In the abdomen the fraction is about 1%. There may be an optional collimator, as discussed below. We discuss each element below, and then discuss the quality of the image.

### 16.4.1 X-ray Tube and Filter

Most routine radiography is done with photons in the range from 35 to 85 keV. (Mammography uses lower energy, and computed tomography is somewhat higher.) Figure 16.15 shows the loss of radiographic contrast as the energy of the incident photons increases and Compton scattering becomes more important.

<sup>5</sup>Even though the film may have a linear response over a larger range, doubling the exposure usually makes the film too dense to read.

<sup>6</sup>Although a digital detector has greater dynamic range, proper exposure is still important. Too low an exposure introduces noise; an excessive exposure generates more scattered photons that strike the detector and reduce the contrast.

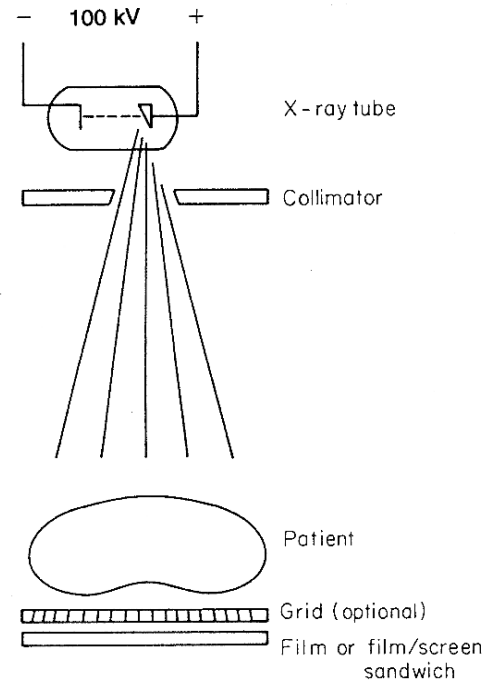


FIGURE 16.14. Overall scheme for making a radiograph. Photons are produced when electrons strike the tungsten anode. The beam is collimated to prevent unnecessary dose to the patient. The patient is placed directly in front of the grid (if any), and the film or a sandwich of film and intensifying screen.

The photons are typically produced by an x-ray tube running with a voltage between cathode and anode of about 100 kilovolts peak<sup>7</sup> (100 kVp). The anode is usually made of tungsten (which has a high radiation yield and withstands high temperatures) with a copper backing to conduct thermal energy away. The number of x rays produced for a given voltage difference depends on the total number of electrons striking the anode, which is proportional to the product of the current and the duration of the exposure (mA s). The anode rotates to help keep it cool. Additional filtration removes low-energy photons that would not get through the body and would not contribute to the image. Figure 16.16 shows the effects of different thicknesses of aluminum on the particle fluence ( $d\Phi/dE$ ) from a tube operating at 100 kVp. The average photon energy depends upon the filtration as well as the kVp, and is about 45 keV for 100 kVp and 2 mm of aluminum filtration (see Problem 19).

<sup>7</sup>The word *peak* is included because the voltage from power supplies in older machines had considerable “ripple” caused by the alternating voltage from the power lines. Even in modern machines, the voltage pulse applied to the tube may not have a purely rectangular waveform, and kVp may not uniquely determine the x-ray spectrum during the pulse. Modern kilovolt power supplies are described by Sobol (2002).

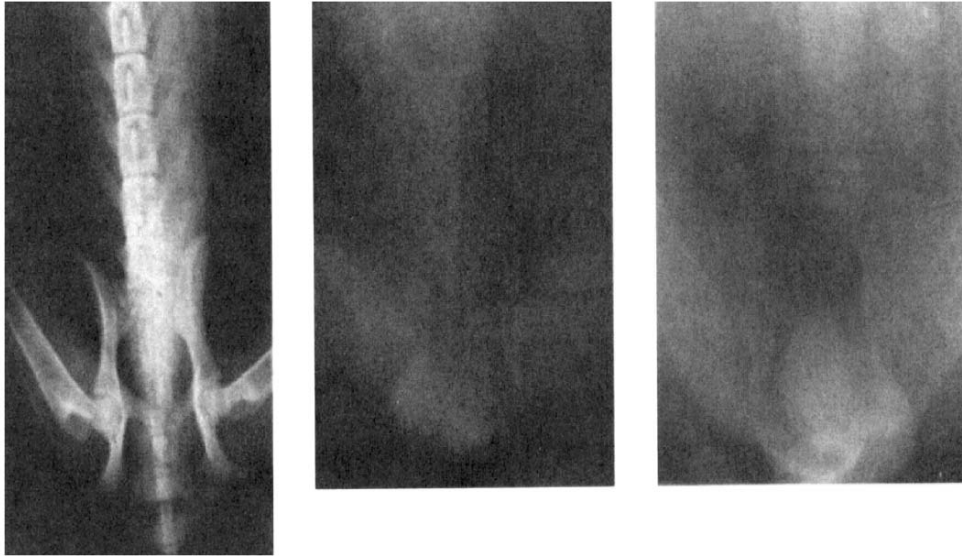


FIGURE 16.15. Radiographs taken at 70 kVp, 250 kVp, and 1.25 MeV ( $^{60}\text{Co}$ ), illustrating the loss of contrast for higher-energy photons. From W. R. Hendee and E. R. Ritenour (2002). *Medical Imaging Physics*, 4th. ed. New York, Wiley-Liss. Used by permission.

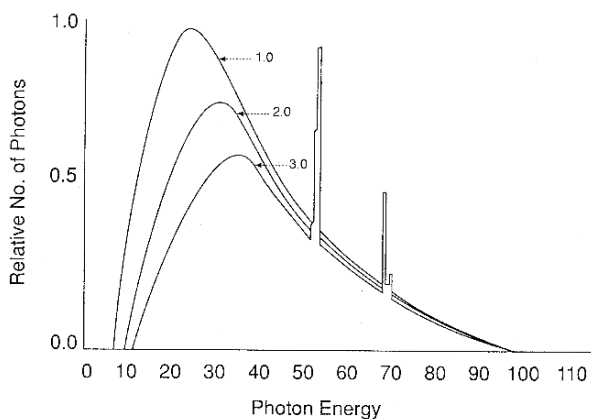


FIGURE 16.16. The particle energy spectrum  $d\Phi/dE$  from a tube operating at 100 kVp with 1, 2, and 3 mm of aluminum filtration. From W. R. Hendee and E. R. Ritenour (2002). *Medical Imaging Physics*, 4th ed. New York, Wiley-Liss. Used by permission.

### 16.4.2 Collimation

The collimator is placed just after the x-ray tube. It has adjustable jaws, usually of lead, that limit the size of the beam striking the patient. Making the beam as small as possible reduces the total energy absorbed by the patient. It also reduces the amount of tissue producing Compton-scattered photons that strike the film. Since the radiograph is based on shadows that assume the photons traveled in a straight line from the tube to the detector, scattered photons reduce the image quality.

### 16.4.3 Attenuation in the Patient: Contrast Material

The purpose of a radiograph is to measure features of the internal anatomy of a patient through differences in the attenuation of rays passing through different parts of the body. The photon fluence falls with distance from the x-ray tube as  $1/r^2$ . It also falls because of attenuation along the path. (We ignore the fact that scattered photons may also strike the film.) We saw in Sec. 15.8 that the mass attenuation coefficient of a compound can be calculated as a weighted average of the elements in the compound:

$$\frac{\mu}{\rho} = \sum_i \left( \frac{\mu}{\rho} \right)_i w_i.$$

Table 16.2 lists various elements, their mass attenuation coefficients at 50 keV, and their composition in water, fat, muscle, and bone. Water and muscle are quite similar, fat has a somewhat smaller attenuation coefficient, and the attenuation of bone is significantly greater.

Figure 16.17 shows attenuation vs.  $\rho x$  for the beam in Fig. 16.16 with 2 mm of Al filtration in water and in bone. Bone contains calcium, which has a relatively high atomic number, and the attenuation coefficient rises rapidly as the energy decreases. Also shown as dashed lines are the corresponding values of  $\exp(-\mu_{\text{atten}}x)$  for the average photon energy in the incident beam, which is 50 keV. In each case the transmitted fraction initially falls more steeply than the dashed line because there is more attenuation of the low-energy photons. For thicker bone the slope of the curve is less than the dashed line because only the high-energy photons remain. This shift of the



TABLE 16.2. Relative composition of various tissues and the attenuation coefficient for 50-keV photons.

Element	$\mu_{\text{atten}}/\rho^b$ ( $\text{m}^2$ $\text{kg}^{-1}$ )	Fractional mass composition <sup>a</sup>			
		Adipose tissue, adult #1	Water	Skeletal muscle	Cortical bone, adult
H	0.0336	0.112	0.112	0.102	0.034
C	0.0187	0.517		0.143	0.155
N	0.0198	0.013		0.034	0.042
O	0.0213	0.355	0.888	0.710	0.435
Na	0.0280	0.001		0.001	0.001
Mg	0.0329				0.002
P	0.0492			0.002	0.103
S	0.0585	0.001		0.003	0.003
Cl	0.0648	0.001		0.001	
K	0.0868			0.004	
Ca	0.1020				0.225
$\mu_{\text{atten}}/\rho$ ( $\text{m}^2 \text{ kg}^{-1}$ )		0.0214	0.0227	0.0227	0.0424
$\rho$ ( $\text{kg m}^{-3}$ )		970	1,000	1,050	1920
$\mu_{\text{atten}}$ ( $\text{m}^{-1}$ )		20.8	22.7	23.8	81.5

<sup>a</sup>Fractional mass compositions are available at <http://physics.nist.gov/PhysRefData/XrayMassCoef/tab2.html>.  
<sup>b</sup>Values are from Hubbell and Seltzer (1996).

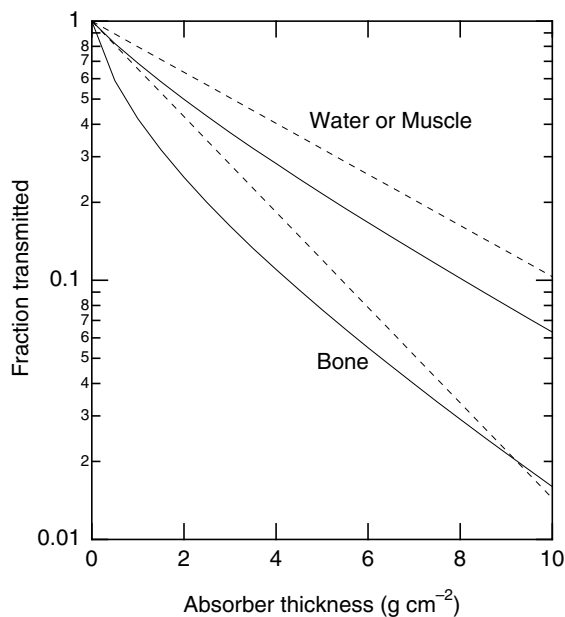


FIGURE 16.17. Attenuation of photons in water or muscle and in bone for the spectrum of Fig. 16.16 (100 kVp, 2 mm aluminum filtration). The dashed lines are for the attenuation coefficients at 50 keV.

beam energy and curvature of the attenuation curves is called *beam hardening*.

These differences in attenuation make it easy to distinguish bone from soft tissue. It is also easy to dis-

tinguish lungs from other tissues because they contain air and have much lower density. Air-filled lung has a density of 180–320  $\text{kg m}^{-3}$ , compared to about 1,000  $\text{kg m}^{-3}$  for water, muscle, or a solid tumor. Figure 16.18 shows a normal anterior–posterior (A–P) chest radiograph. You can see the exponential decay through layers of bone, the outline of the heart, the arch of the aorta, and the lacy network of blood vessels in the lungs. The patient in Fig. 16.20 has *pneumothorax*. Air has leaked into the pleural cavity and partially collapsed the lungs. You can see this collapse in the upper portion of each lung. Spontaneous pneumothorax can occur in any pulmonary disease that causes an alveolus (air sac) on the surface of the lung to rupture: most commonly emphysema, asthma, or tuberculosis. Pneumothorax can also be caused by perforating trauma to the chest wall. Spontaneous idiopathic (meaning cause unknown) pneumothorax occasionally occurs in relatively young people.

Abdominal structures are more difficult to visualize because except for gas in the intestine, everything has about the same density and atomic number. *Contrast agents* are introduced through the mouth, rectum, urethra, or bloodstream. One might think that the highest- $Z$  materials would be best. However the energy of the  $K$  edge rises with increasing  $Z$ . If the  $K$  edge is above the energy of the x rays in the beam, then only  $L$  absorption with a much lower cross section takes place. The  $K$  edge for iodine is at 33 keV, while that for lead is at 88 keV. Between these two limits (and therefore in the range of x-ray energies

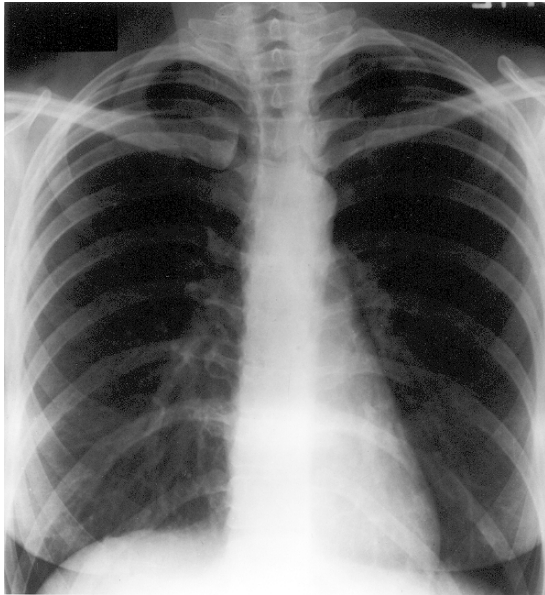


FIGURE 16.18. Radiograph of a normal chest. Some of the features are identified in Fig. 16.19 and are described in the text. Radiograph courtesy of D. Ketcham, M.D., Department of Diagnostic Radiology, University of Minnesota Medical School.

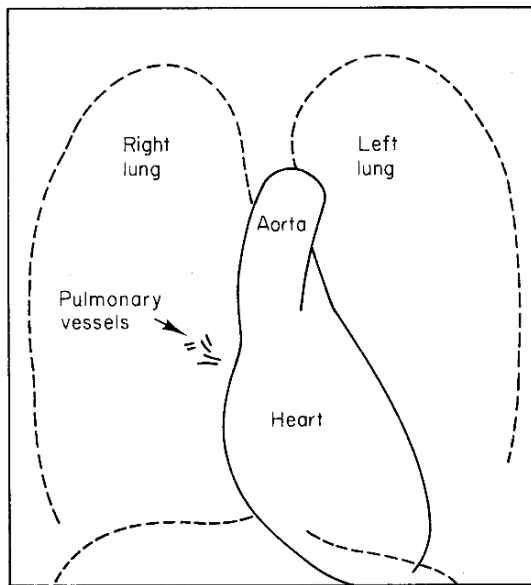


FIGURE 16.19. Some of the features in the radiograph of a normal chest, Fig. 16.18.

usually used for diagnostic purposes), the mass attenuation coefficient of iodine is about twice that of lead. The two most popular contrast agents are barium ( $Z = 56$ ,  $K$  edge at 37.4 keV) and iodine ( $Z = 53$ ). Barium is swallowed or introduced into the colon. Iodine forms the basis for contrast agents used to study the cardiovascular system (angiography), gall bladder, brain, kidney, and urinary tract.

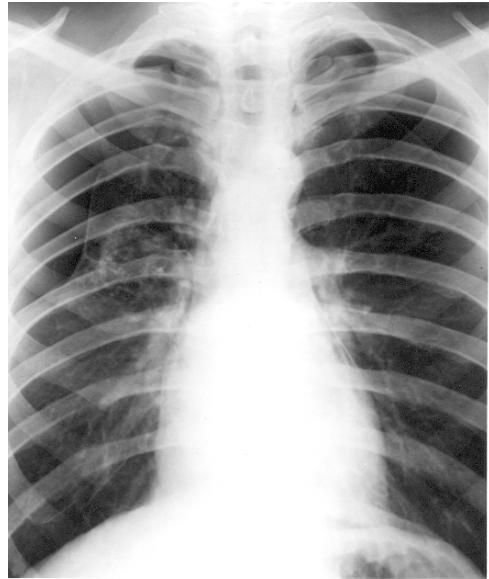


FIGURE 16.20. Radiograph of a patient with pneumothorax. Air has escaped from the lungs and caused them to collapse partially. The features are indicated in Fig. 16.21. Radiograph courtesy of D. Ketcham, M. D., Department of Diagnostic Radiology, University of Minnesota Medical School.

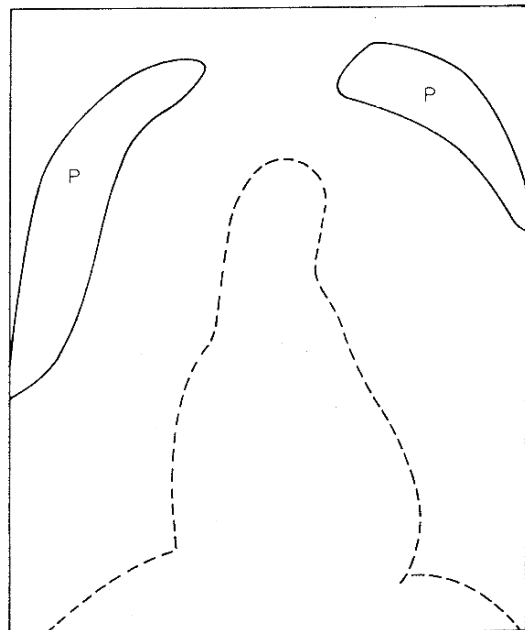


FIGURE 16.21. Key to features in Fig. 16.20. The areas of pneumothorax are indicated by (P). The one on the patient's left (the viewer's right) is difficult to see in the printed version; a radiographic film viewed by transmitted light has a much greater dynamic range.

Some pathologic conditions can be identified by the deposition of calcium salts. Such "dystrophic" (defective) calcification occurs in any form of tissue injury, particularly if there has been tissue necrosis (cell death). It

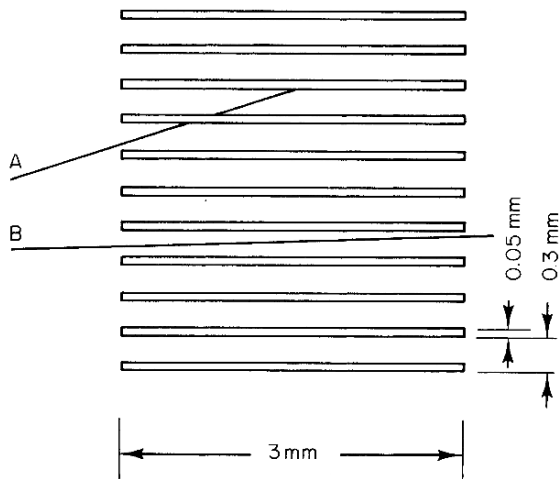


FIGURE 16.22. Scale drawing of the elements of a typical grid. The thin lead strips absorb photons that have been scattered through more than a few degrees. As a result background fog due to scattering is reduced and the contrast is increased. Since the x rays come from a point source, the elements of the grid are usually tilted toward the source and are not parallel over the entire film surface.

is found in necrotizing tumors (particularly carcinomas), atherosclerotic blood vessels, areas of old abscess formation, tuberculous foci, and damaged heart valves, among others.

#### 16.4.4 Antiscatter Grid

Since the radiograph assumes that photons either travel in a straight line from the point source in the x-ray tube to the film or are absorbed, Compton-scattered photons that strike the film reduce the contrast and contribute an overall background darkening. This effect can be reduced by placing an *antiscatter grid* (or radiographic grid, or “bucky” after its inventor, Gustav Bucky) just in front of the film.

Figure 16.22 shows how a grid works. The grid stops x rays that are not traveling parallel to the sides of the grid strips. A typical grid might have 10–50 strips of lead per centimeter that are 3 mm high and 0.05 mm thick, embedded in plastic or aluminum. The strips can be either parallel or “focused,” that is, slanted to aim at the point source on the anode of the x-ray tube. The grid can be either linear or crossed, with strips of lead running in both directions. A grid with a ratio of height to spacing of 12 improves the contrast by a factor of about 3.75, while increasing the exposure to the patient by a factor of about 4.25 to keep the film dose about the same [Hendee and Ritenour (2002), p. 227].] Sometimes the grid is moved during the exposure if the strips in the grid are thick enough to show up on the film.

#### 16.4.5 Film–Screen Combination

The film–screen combination was described in Sec. 16.3. The fluorescent screens, by absorbing more of the photons, reduce the dose to the patient for the same optical density of the developed film. They also degrade the spatial resolution of the image, because fluorescence photons from the point where the x-ray photon interacts start out in various directions and then scatter until they strike the film.<sup>8</sup>

#### 16.4.6 Computed and Direct Radiography

The term *computed radiography* (CR) is used to describe systems where a photophosphor or photostimulable phosphor replaces the film–screen combination. The latent image on this phosphor is “read” by a scanning laser beam in a process called photostimulated luminescence. The resulting image is digitized [Rowlands (2002)]. The term *direct radiography* is applied to the use of a TFT detector array (p. 446) which directly produces a digitized image.

### 16.5 Image Quality

The quality of a radiographic image depends on three things: *resolution*, *contrast*, and *noise*. The resolution and contrast can be described by concepts introduced in Chapter 12 for a linear, shift-invariant system: the point-spread function and its Fourier transform, the optical transfer function, whose magnitude is the modulation transfer function. The noise arises primarily from the fluctuations in the number of photons striking a given area of film—quantum noise—though granularity of the film is also important.

The transfer function for the entire system depends on many factors: the tube and spot size, filter, source–screen and source–patient distances, grid, film–screen combination, and scatter. If each of these subsystems operates in series, as in an audio system, one can successively convolve the point-spread functions or multiply together the (complex) optical transfer functions. It is also possible to have parallel<sup>9</sup> subsystems, each contributing to the final image, in which case the analysis is more complicated. An excellent review of the use of transfer-function analysis in radiographic imaging is the article by Metz and

<sup>8</sup>The point-spread function of a film or a screen–film system is easily measured. A point source is created by passing the x rays through a pinhole in a piece of lead placed directly on the screen. The resulting image in the film is the point-spread function. We saw in Chapter 12 how this is related to the modulation transfer function. Standard techniques have been developed for measuring the modulation transfer function (MTF) of the film–screen combination [ICRU Report 41 (1986); ICRU Report 54 (1996)].

<sup>9</sup>Examples of parallel subsystems are the two emulsion layers on double-coated film, and the effect of primary and scattered radiation on the formation of the image.

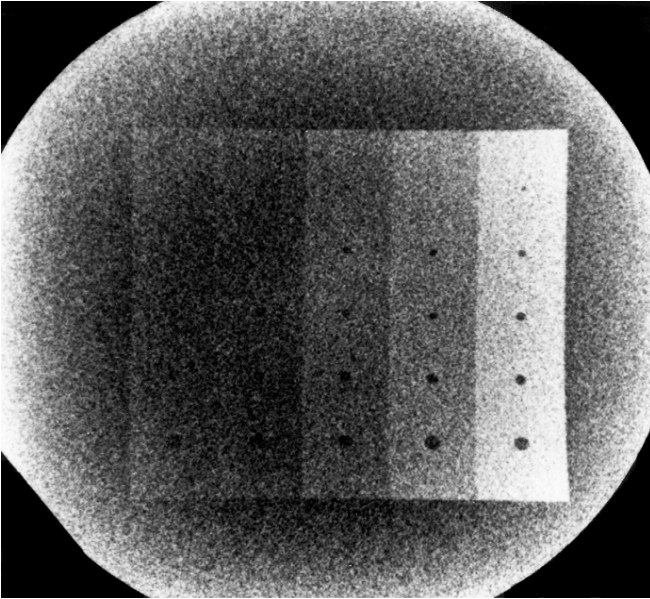


FIGURE 16.23. An example of the relationship among exposure, image size, and detectability. A type 1100 aluminum phantom was imaged with digital fluorography. It was exposed to an 80-kVp x-ray beam with 4.5-mm Al filter. As the image becomes lighter, the thickness of the aluminum phantom increases in steps: 0.85, 1.3, 2.1, 3.2, and 5.2 mm. The holes are 1, 1.5, 2, 2.5, and 3 mm in diameter. As the attenuation in the aluminum increases, so does the signal, and the easier it is to detect the smaller holes. Photograph courtesy of Richard Geise, Ph.D., Department of Radiology, University of Minnesota.

Doi (1979). The text by Macovski (1983) is at about the level of this book and presents many details of noise and convolution for radiographic, fluoroscopic, tomographic, nuclear medicine, and ultrasound images. The size of the spot where the electrons strike the anode of the x-ray tube is critical in determining the resolution of the final image, as discussed in detail by Wagner *et al.* (1974).

The *exposure contrast* is the change in exposure between two (usually adjacent) parts of the image divided by the average:

$$C_{\text{in}} = \frac{\Delta X}{X}. \quad (16.13)$$

This is similar to the modulation defined in Eq. 12.20. The *brightness contrast* is the analogous quantity for the light transmitted through the processed film when viewing the image:

$$C_{\text{out}} = \frac{\Delta T}{T}. \quad (16.14)$$

The exposure contrast and brightness contrast are proportional (Eq. 16.11):

$$C_{\text{out}} = \gamma C_{\text{in}}. \quad (16.15)$$

The *radiographic signal* is a small change in optical transmission in adjacent areas of the image. Changes in transmission below a certain value are not detectable by

the viewer. This is apparent in Fig. 16.23, which shows signals with different contrasts and different sizes on a uniform background. The smaller the diameter of the signal region, the more difficult the signal is to detect. We will develop a simple model to explain why.

Suppose first that there is no signal, but that the film (or screen–film combination) is illuminated with a uniform beam of x rays with a constant fluence. We make an exposure for a certain time and count the number of photons striking a “sampling area” of the film,  $S$ . Though the average fluence is constant across the film, the photons are randomly distributed. A somewhat different number of photons strike a nearby sampling area of the same size. This is a situation where the average number striking a sampling area of a given size is constant, the total number of photons is very large, and the probability that any one photon is absorbed in a given sampling area is small, so the situation is described by Poisson statistics (Appendix J). The mean number of photons striking a sampling area is  $\Phi S$  and the standard deviation is  $(\Phi S)^{1/2}$ . Suppose that some fraction  $f \leq 1$  of these photons actually interact with the silver halide grains in the emulsion. Then the mean number interacting is  $f\Phi S$  and the standard deviation is<sup>10</sup>  $(f\Phi S)^{1/2}$ . Thus there are fluctuations in the brightness of the transmitted image across the uniformly exposed viewing region, just because of the Poisson statistics—quantum noise or shot noise—of the x-ray photons striking the film.

The fluctuations in the number of photons striking area  $S$  can be related to fluctuations in the exposure of that area of the film, and hence to the transmission of visible light through the developed film. Since the exposure (measured in air just in front of the film) is proportional to the photon fluence,  $X = A\Phi$ ,  $\overline{(X - \bar{X})^2} = A^2(\overline{\Phi - \bar{\Phi}})^2$  and  $(\Delta X)_{\text{rms}} = A(\Delta\Phi)_{\text{rms}}$ . We define the *noise exposure contrast* to be the standard deviation of the number of photons affecting grains in area  $S$  divided by the average number affecting grains in an area that size:<sup>11</sup>

$$C_{\text{noise in}} \equiv \frac{(f\Phi S)^{1/2}}{f\Phi S} = (f\Phi S)^{-1/2}. \quad (16.16)$$

The *noise brightness contrast* is then

$$C_{\text{noise out}} = \gamma(f\Phi S)^{-1/2}. \quad (16.17)$$

The fluctuations in the noise, measured by noise contrast, are inversely proportional to the square root of the

<sup>10</sup>This is very similar to the arguments about the fraction of photons absorbed by a visual pigment molecule in Eq. 14.67. Changes in the value of  $f$  in Fig. 14.43 shift the response curve along the axis. They also shift the film response curves in Fig. 16.7.

<sup>11</sup>It is sometimes useful to write it as

$$\begin{aligned} C_{\text{noise in}} &\equiv \frac{(f\Phi S)^{1/2}}{f\Phi S} = \frac{1}{f^{1/2}S^{1/2}} \frac{(\Delta\Phi)_{\text{rms}}}{\Phi} = \frac{1}{f^{1/2}S^{1/2}} \frac{A(\Delta X)_{\text{rms}}}{AX} \\ &= \frac{1}{f^{1/2}S^{1/2}} \frac{(\Delta X)_{\text{rms}}}{X}. \end{aligned}$$

area of the lesion to be detected.<sup>12</sup> This is seen in Fig. 16.23. The noise in a screen–film system is measured by using a microdensitometer to measure the optical density across film that has received a uniform exposure. Variations with position can be described either in terms of its two-dimensional autocorrelation function or its Fourier transform, the *Wiener spectrum*. The radiographic noise consists of three components: *quantum mottle*, the statistical fluctuations in the number of photons absorbed in a small area (shot noise); *structure mottle* due to nonuniformities in the screen; and *film graininess*, variation in the size and distribution of the silver bromide grains in the emulsion. Here we discuss only quantum mottle.

Now introduce a signal, which is a small increase in the exposure or photon fluence:  $\Delta X_{\text{signal}} = A\Delta\Phi_{\text{signal}}$ . This gives a brightness contrast

$$C_{\text{signal out}} = \gamma \frac{\Delta X_{\text{signal}}}{X} = \gamma \frac{\Delta\Phi_{\text{signal}}}{\Phi}. \quad (16.18)$$

The ratio of the signal contrast to the noise contrast is called the *signal-to-noise ratio*:

$$\text{SNR} = \frac{C_{\text{signal out}}}{C_{\text{noise out}}} = \frac{\gamma (\Delta\Phi_{\text{signal}}/\Phi)}{\gamma (f\Phi S)^{-1/2}} = (fS)^{1/2} \frac{\Delta\Phi_{\text{signal}}}{\Phi^{1/2}}. \quad (16.19)$$

The signal will be detectable only if the signal brightness contrast exceeds the noise brightness contrast by a certain amount:<sup>13</sup>

$$\text{SNR} > k, \quad (fS)^{1/2} \frac{\Delta\Phi_{\text{signal}}}{\Phi^{1/2}} > k. \quad (16.20)$$

The larger the value of the signal-to-noise ratio, the greater the probability of detecting the signal. Many experiments on perception have been done; they will not be discussed here.<sup>14</sup> Values of  $k$  that are used range from 2 to 5.

Let us apply the result in Eq. 16.20 to a simple model: a monoenergetic x-ray beam passing through a patient. The total thickness of the patient is  $L$ . The attenuation coefficient is  $\mu$ . If an x-ray beam with fluence  $\Phi_0$  strikes the patient, the fluence of x-ray photons emerging is  $\Phi_1 = \Phi_0 e^{-\mu L}$ . Imagine a nearby region where for a distance  $x$

the attenuation coefficient is  $\mu - \Delta\mu$ . The x-ray fluence emerging along a line passing through this region is

$$\begin{aligned} \Phi_2 &= \Phi_0 e^{-\mu(L-x) - (\mu - \Delta\mu)x} = \Phi_0 e^{-\mu L} e^{\Delta\mu x} \\ &= \Phi_1 e^{\Delta\mu x} \\ &\approx \Phi_1 (1 + \Delta\mu x). \end{aligned} \quad (16.21)$$

The exposure contrast is therefore  $C_{\text{in}} = (\Delta\Phi)_{\text{signal}}/\Phi_1 \approx \Delta\mu x$ . We combine this with Eq. 16.20 to obtain

$$(fS\Phi_1)^{1/2} (\Delta\mu x) > k, \quad (16.22)$$

where  $\Phi_1$  is the fluence leaving the patient or striking the film. (These are the same if variations in  $1/r^2$  can be neglected, where  $r$  is the distance from the tube to the patient or the tube to the film.) The signal-to-noise ratio increases as the square root of the photon fluence or exposure, the square root of the area to be detected, and the square root of  $f$ , the fraction of the photons striking the film that are actually effective in rendering grains developable.

The fraction  $f$  in this Poisson model is equal to the *detective quantum efficiency* (DQE). It is easily visualized as the fraction of the photons striking the detector that actually affect it. The number of *noise equivalent quanta* (NEQ) in our model is  $f\Phi_1$ .<sup>15</sup>

We can apply Eq. 16.22 to determine the number of photons that must be transmitted through the patient for a given image size and given signal-to-noise ratio. We assume that  $f = 1$ . The required photon fluence emerging from the patient is (dropping the subscript on  $\Phi_1$ )

$$\Phi S > \left( \frac{k}{\Delta\mu x} \right)^2. \quad (16.23)$$

If the lesion thickness is  $x = 1$  cm and  $\Delta\mu = 0.01\mu_{\text{water}} = (0.01)(22.7) \text{ m}^{-1}$ , then  $\Delta\mu x = 0.00227$ . For  $k = 4$ , the number of photons in the image area must be greater than  $3 \times 10^6$ . The exit dose to the patient is (assuming monoenergetic photons)

$$\begin{aligned} D_{\text{body}} &= \Psi \left( \frac{\mu_{\text{en}}}{\rho} \right)_{\text{body}} = (h\nu)\Phi \left( \frac{\mu_{\text{en}}}{\rho} \right)_{\text{body}} \\ &= \frac{(h\nu)(3 \times 10^6)}{S} \left( \frac{\mu_{\text{en}}}{\rho} \right)_{\text{body}}. \end{aligned} \quad (16.24)$$

The dose increases as the area to be detected decreases. In order to detect an image 1 mm square using 50-keV photons, the exit dose in water would have to be at least  $9.8 \times 10^{-5}$  Gy.

<sup>12</sup>An analogous phenomenon is seen when counting individual photons with a radiation detector at a fixed average rate. The number counted in a given time interval fluctuates, with the fractional fluctuation inversely proportional to the square root of the counting time.

<sup>13</sup>There are statistical fluctuations in the signal as well as the noise. The variance of the difference between signal and noise will be the sum of the variances in the signal and in the noise. This has the effect of increasing the noise by a factor of  $\sqrt{2}$ , which can be absorbed in the value of  $k$  that is chosen. See Problem 23.

<sup>14</sup>The ability to detect the signal accurately is greater when the observer knows the nature of the signal and is only asked whether it is or is not present. That is, the ability of an observer to detect a signal is less in the more realistic situation where the observer does not know what the signal is or where it might be in the radiograph.

<sup>15</sup>This simple equality exists only because we are using a model with Poisson statistics. The DQE is defined more generally as the square of the of the signal-to-noise ratio of the detector output divided by the square of the signal-to-noise ratio of the detector input. The more general definitions of DQE and NEQ are discussed in Wagner (1983), Wagner (1977), and Dainty and Shaw (1974).

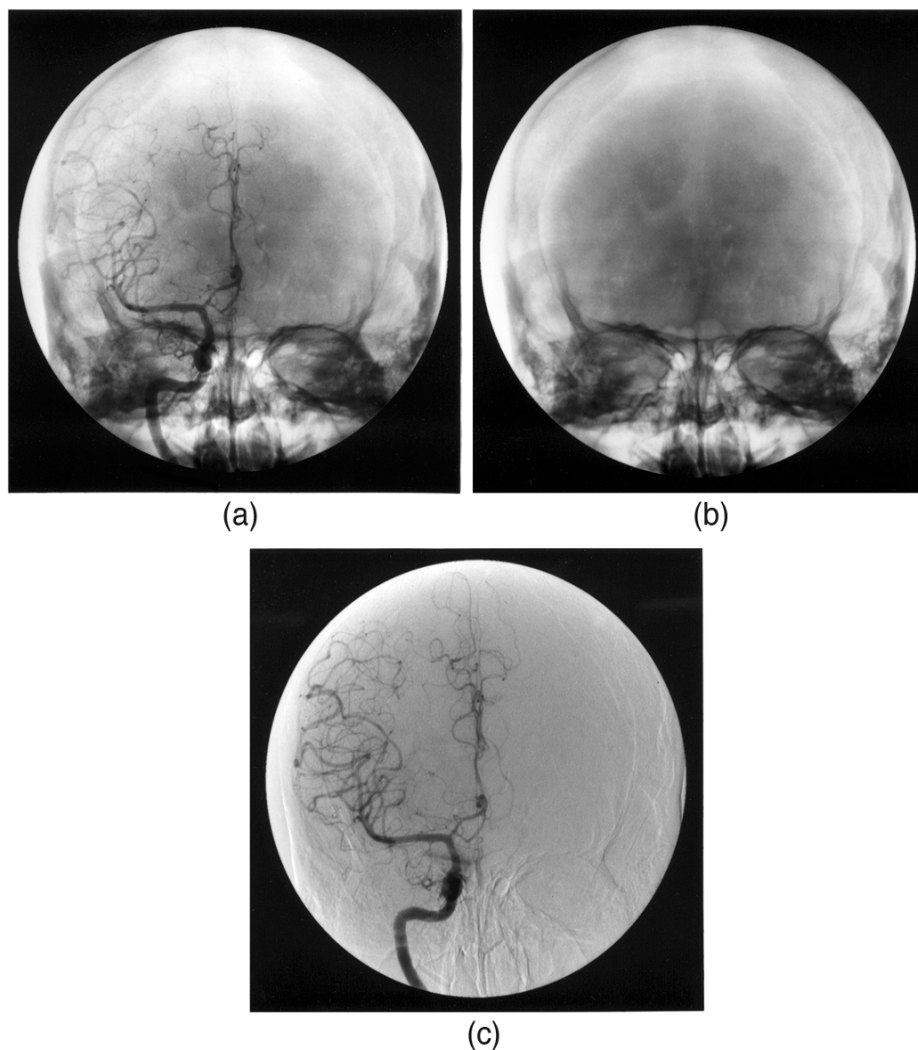


FIGURE 16.24. Digital subtraction angiography. (a) Image with contrast material. (b) Image without contrast material. (c) The difference image. Photograph courtesy of Richard Geise, Ph.D., Department of Radiology, University of Minnesota.

## 16.6 Angiography and Digital Subtraction Angiography

One important problem in diagnostic radiology is to image portions of the vascular tree. *Angiography* can confirm the existence of and locate narrowing (stenosis), weakening and bulging of the vessel wall (aneurysm), congenital malformations of vessels, and the like. This is done by injecting a contrast material containing iodine into an artery. If the images are recorded digitally, it is possible to subtract one without the contrast medium from one with contrast and see the vessels more clearly (Fig. 16.24).

In a typical angiographic study, 30–50 ml of contrast material is injected into an artery. For a vessel with a diameter of 8 mm,  $\rho x$  of the contrast material is about  $4 \text{ mg cm}^{-2}$ .

## 16.7 Mammography

*Mammography* poses particular challenges for medical physicists. The resolution needed is extremely high (about 15 line pairs (lp)  $\text{mm}^{-1}$  compared to 5 lp  $\text{mm}^{-1}$  for a chest radiograph).<sup>16</sup> The radiologist may use a magnifying glass to inspect the image. The contrast in a breast image is inherently low. Fat and glandular tissue must be distinguished by the slight differences in their attenuation coefficients (see Problem 25). The dose must be made as small as possible.

These challenges have been met. Spatial frequencies of 14–16 lp  $\text{mm}^{-1}$  are routinely obtained. Noise limits the minimum size of a detectable object to  $> 0.3 \text{ mm}$  for microcalcifications or a few millimeters for soft tissue.

<sup>16</sup>Line pairs (abbreviated lp) are analogous to the period of a square wave.

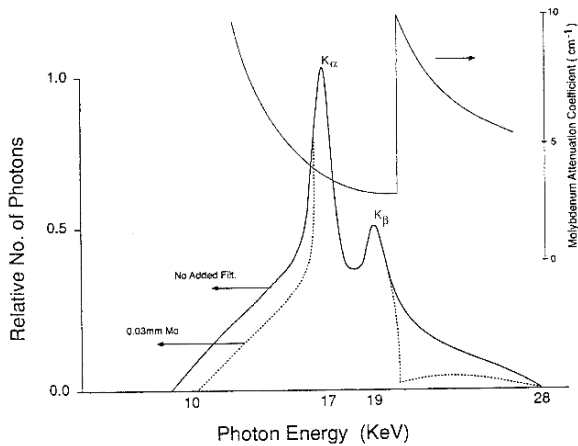


FIGURE 16.25. The x-ray spectrum from a molybdenum anode tube used for mammography, with and without filtration by a molybdenum foil. From W. R. Hendee and E. R. Ritenour (2002). *Medical Imaging Physics*, 4th ed. New York, Wiley-Liss. Used by permission.

Digital mammography is providing even higher resolution. The typical mammographic dose per view has been reduced from about 50 mGy in the 1960s and 4.1 mGy in the 1970s to 1.5 mGy in 1996.<sup>17</sup> One technique that has helped make these improvements is the molybdenum target x-ray tube, operating at 25–28 kVp. Figure 16.25 shows the photon fluence from such a tube, with the 17-keV  $K_{\alpha}$  and 19-keV  $K_{\beta}$  lines being quite prominent. Filtration of the beam with the same material, molybdenum, further sharpens the spectrum. The dashed lines show the spectrum when a molybdenum filter is used. These photons interact primarily by the photoelectric effect, so attenuation depends strongly on atomic number. There are few Compton-scattered photons to degrade the image. Meticulous attention to detail is required to obtain useful images.

## 16.8 Fluoroscopy

If a fluorescent screen replaces the screen–film cassette, one can observe an image that changes with time, as when the patient swallows a contrast agent. Although the x-ray tube current for fluoroscopy is several hundred times less than that for a radiograph, the dose absorbed by the patient would be quite high if the viewing time were very long. In order to reduce the dose, early fluoroscopic units were viewed by a radiologist using dark-adapted (scotopic) vision, which allows one to perceive a dimmer image but does not allow one to resolve great detail.

Currently, fluoroscopy is done using an *image intensifier tube*. Image intensifier tubes do not reduce the expo-

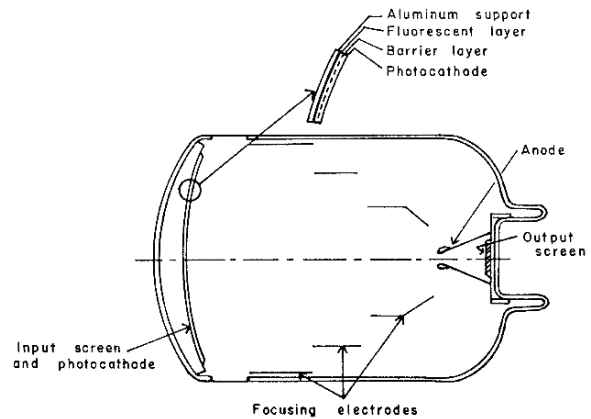


FIGURE 16.26. A schematic diagram of an image intensifier tube. From W. R. Hendee and E. R. Ritenour (2002). *Medical Imaging Physics*, 4th ed. New York, Wiley-Liss, p. 237. Used by permission.

sure very much, but they provide much brighter images so the radiologist can use photopic rather than scotopic vision and see more detail. A cross section of a typical image intensifier tube is shown in Fig. 16.26. A fluorescent screen, the input phosphor, is sandwiched to a photocathode, similar to the one in a photomultiplier tube. An aluminum support reflects light from the fluorescent screen back into the tube. An accelerating voltage difference of about 30 kV exists between the photocathode and the anode. Electrons are focused by a series of electrodes to pass through a hole in the anode and strike another fluorescent screen, the output phosphor. The energy added to each electron by the accelerating field increases the brightness of the image, though some spatial resolution is lost. The brightness is also enhanced because the output phosphor is smaller than the input phosphor. The output phosphor is viewed with a television camera.

Large detector arrays are replacing this traditional method of fluoroscopy. The measurement of the basic properties of one such detector—amorphous silicon—are described by Hunt *et al.* (2002).

## 16.9 Computed Tomography

Radiographs provide only an integrated value of the attenuation coefficient. That is, if  $N_0(y, z)$  monoenergetic x-ray photons traverse the body along a line in the  $x$  direction after entering the body at coordinates  $(y, z)$ , the number emerging without interaction is  $N(y, z) = N_0(y, z)e^{-\alpha(y, z)}$ , where

$$\alpha(y, z) = \int \mu(x, y, z) dx.$$

The radiograph measures  $N(y, z)$  or  $\alpha(y, z)$ . The desired information is  $\mu(x, y, z)$ . The radiographic image is often difficult to interpret because of this integration along  $x$ .

<sup>17</sup>See NCRP Report 100 (1989) for early data; R. Geise, private communication for 1996 data.

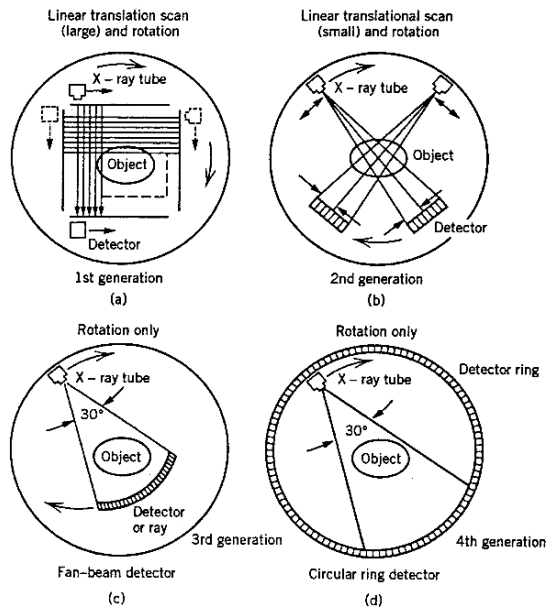


FIGURE 16.27. The scanning techniques used in the first four generations of CT scanners. From Z.-H. Cho, J. P. Jones, and M. Singh (1993). *Foundations of Medical Imaging*. Copyright ©1993 John Wiley–Interscience. Reprinted by permission of John Wiley & Sons, Inc.

For example, it may be difficult to visualize the kidneys because of the overlying intestines.

Several types of computed tomography (*tomos* means slice) have been developed in the last few decades. They include *transmission computed tomography* (CT), *single-photon emission computed tomography* (SPECT), and *positron emission tomography* (PET). They all involve reconstructing, for fixed  $z$ , a map of some function  $f(x, y)$  from a set of projections  $F(\theta, x)$ , as described in Secs. 12.4 and 12.5. For CT the function  $f$  is the attenuation coefficient  $\mu(x, y)$ . For SPECT and PET it is the concentration of a radioactive tracer within the body, as will be described in Chapter 17.

The history of the development of computed tomography is quite interesting [DiChiro and Brooks (1979)]. The Nobel Prize in Physiology or Medicine was shared in 1979 by a physicist, Allan Cormack, and an engineer, Godfrey Hounsfield. Cormack had developed a theory for reconstruction and had performed experiments with a cylindrically symmetric object that were described in two papers in the *Journal of Applied Physics* in 1963 and 1964. Hounsfield, working independently, built the first clinical machine, which was installed in 1971. It was described in 1973 in the *British Journal of Radiology*. The Nobel Prize acceptance speeches [Cormack (1980); Hounsfield (1980)] are interesting to read. A neurologist, William Oldendorf, had been working independently on the problem but did not share in the Nobel Prize [See DiChiro and Brooks (1979), and Broad (1980)].

Early machines had an x-ray tube and detector that moved in precise alignment on opposite sides of the pa-

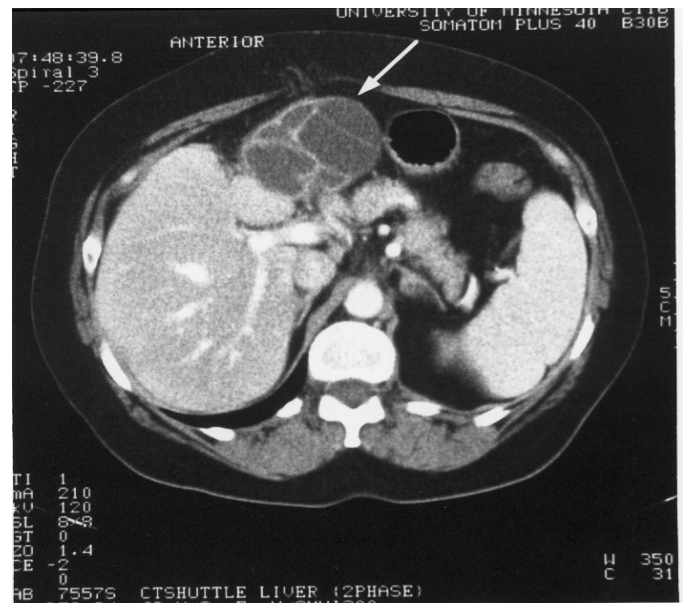


FIGURE 16.28. A spiral CT scan of the abdomen. The arrow points to a biliary cystadenoma, a benign tumor of the liver. Scan courtesy of E. Russell Ritenour, Ph.D., Department of Radiology, University of Minnesota Medical School.

tient to make each pass. The size of these machines allowed only heads to be scanned. After one pass, the gantry containing the tube and detector was rotated  $1^\circ$  and the next pass was taken. After data for 180 passes were recorded, the image was reconstructed. A complete scan took about 4 minutes. Modern CT units use an array of detectors and a fan-shaped beam that covers the whole width of the patient. The scan time is reduced to a few seconds. Figure 16.27 shows the early evolution of the scanning techniques.

On modern machines all of the electrical connections are made through slip rings. This allows continuous rotation of the gantry and scanning in a spiral as the patient moves through the machine. Interpolation in the direction of the axis of rotation (the  $z$  axis) is used to perform the reconstruction for a particular value of  $z$ . This is called *spiral CT* or *helical CT*. Kalender (2000) discusses the physical performance of CT machines, particularly the various forms of spiral machines. Array detectors are now used to fill in the space between the spirals. Table 16.3 shows how scanners have improved since they were first introduced. Spiral CT provides  $\mu(x, y, z)$ , and the images can be displayed in three dimensions.

Figure 16.28 is an abdominal scan showing a benign tumor in the liver. Computer analysis of  $\mu(x, y, z)$  data can be used to display 3-dimensional images of an organ (Fig. 16.29). The surface of an organ is defined by a change in  $\mu$ .

It is often desirable to measure the attenuation coefficient with an accuracy of  $\pm 0.5\%$ . For water at 60 keV,  $\mu = 20 \text{ m}^{-1}$ , so  $\mu$  must be measured with an accuracy of  $\delta\mu = 0.1 \text{ m}^{-1}$ . (A beam of 120 kVp with 2–3 mm of



TABLE 16.3. The evolution of typical values for high-performance CT machines. Adapted from Kalender (2000), p. 39.

Feature	1972	1980	1990	2000
Minimum scan time	300 s	5–10 s	1–2 s	0.3–1 s
Data per 360° scan	57.6 kB	1 MB	2 MB	42 MB
Data per spiral scan			24–48 MB	200–500 MB
Image matrix	80 × 80	256 × 256	512 × 512	512 × 512
Power (kW)	2	10	40	60
Slice thickness (mm)	13	2–10	1–10	0.5–5
Spatial resolution (Line pair cm <sup>-1</sup> )	3	8–12	10–15	12–25

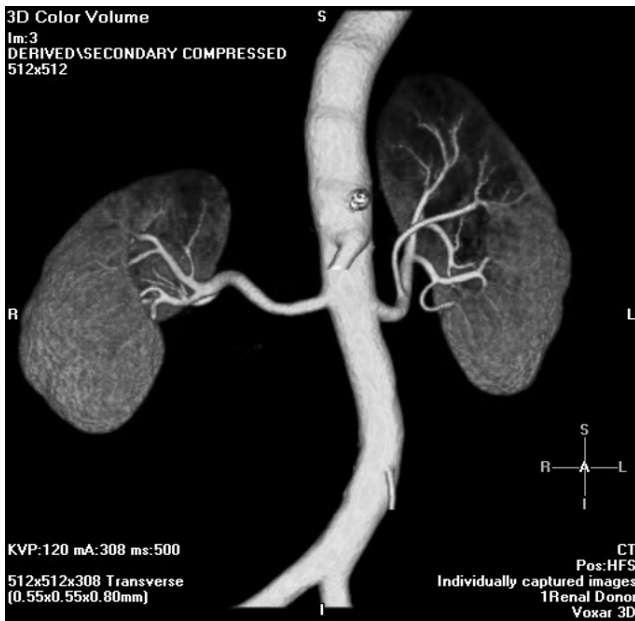


FIGURE 16.29. A 3-dimensional rendering of the aorta, renal arteries and kidneys. Scan courtesy of E. Russell Rite-nour, Ph.D., Department of Radiology, University of Minnesota Medical School.

aluminum filtration has about this average photon energy.) It is customary to report the fractional difference between  $\mu$  and  $\mu_{\text{water}}$ . The *Hounsfield unit* is

$$H = 1000 \frac{\mu_{\text{tissue}} - \mu_{\text{water}}}{\mu_{\text{water}}}. \tag{16.25}$$

The desired accuracy is  $\pm 5$  Hounsfield units.

There is a relationship between the dose to the patient and the resolution. Suppose we are reconstructing an object with a circular cross section as shown in Fig. 16.30. The object is to be resolved into volume elements or cells of length  $w$  on each side parallel to the  $x$  and  $y$  axes. The thickness of each cell along the  $z$  axis (perpendicular to the scan) is the slice thickness,  $b$ . The diameter of the object is  $L$ . For simplicity, we make the analysis assuming a first-generation machine, with rectilinear passes repeated at  $m$  different angles between  $0^\circ$  and  $180^\circ$ . The width of each sample in a pass is  $w$ . The number of samples in

each pass is

$$n = \frac{L}{w}, \tag{16.26}$$

and the number of cells in the object is approximately the area of the circular object divided by the area of a cell:  $\pi L^2/4w^2$  or  $\pi n^2/4$ . To determine  $\pi n^2/4$  independent values of  $\mu$  requires at least that many independent measurements. Since  $n$  measurements are made in each pass, we need  $m$  passes where  $mn = \pi n^2/4$  or

$$m = \frac{\pi n}{4}. \tag{16.27}$$

With more passes the situation is overdetermined; with fewer it is underdetermined. If the values of  $\mu$  are overdetermined, convolved back projection (Chapter 12) or a similar procedure can be used to assign the values of  $\mu$ .

Now consider the attenuation of photons in one sample along a diameter. In Sec. 16.5 we developed a relationship between the photon fluence in the beam needed to measure the attenuation with some desired accuracy [Eq. 16.21]. The same arguments can be applied in this case:

$$\delta\Phi = \Phi_1 \delta\mu w = \Phi_0 e^{-\mu L} \delta\mu w.$$

The photons arrive at the detector, which we assume for simplicity to have 100% efficiency, at a constant average

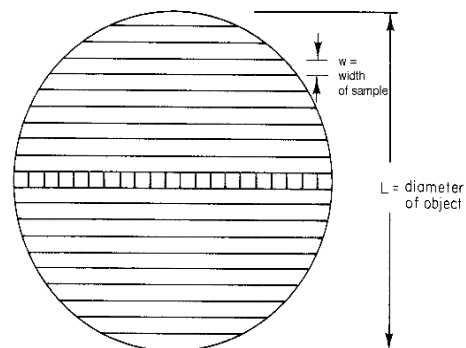


FIGURE 16.30. A circular object that is to be analyzed. The diameter of the object is  $L$ ; the width of each sample in the scan is  $w$ . It is desired to resolve cells in each sample which have a length  $w$ , as shown for the center diameter.

rate, so they are Poisson distributed. The standard deviation in the number of counts is  $(\Phi_1 S)^{1/2} = (\Phi_1 w b)^{1/2}$ . To detect the difference between the two samples,  $w^2 \delta \Phi$  must exceed this by the minimum signal-to-noise ratio,  $k$ . This gives the minimum number of photons that must be detected:

$$N = \Phi_1 w b > \frac{k^2}{w^2 (\delta \mu)^2}. \quad (16.28)$$

If  $w = 0.8$  mm and  $k = 4$ , then  $N > 2.5 \times 10^9$  photons must pass through the small region we are trying to measure. It can be shown [Brooks and DiChiro (1976)] that these counts can be divided among all  $m$  passes. Let  $N'$  be the number of photons detected in the sample at one angle:

$$N' = \frac{k^2}{m w^2 (\delta \mu)^2} = \frac{k^2}{(\pi/4) L w (\delta \mu)^2}. \quad (16.29)$$

The exit dose from one pass is

$$D' = \frac{\mu_{\text{en}}}{\rho} \Psi'_1 = \frac{\mu_{\text{en}}}{\rho} h \nu \Phi'_1,$$

where  $\Phi'_1 = \phi_1/m$ . The entrance dose is  $e^{\mu L}$  times this. We multiply by  $m$  to get the total dose. With the help of Eq. 16.28 we obtain an expression for the total entrance dose for the entire scan from all  $m$  passes:

$$D = \frac{\mu_{\text{en}}}{\rho} h \nu e^{\mu L} \Phi_1 = \frac{\mu_{\text{en}}}{\rho} \frac{h \nu e^{\mu L} k^2}{w^3 b (\delta \mu)^2}.$$

Three additional factors must be added to this equation. A more careful analysis of the statistics gives a factor  $\pi^2/12 = 0.82$ . The second factor  $\beta$  is introduced for photons that miss the detector and a detector efficiency that is less than unity.

Finally, the actual dose to the patient is less than the entrance dose. It must be averaged over all scans and must account for the attenuation of the beam as it goes through the patient. The result above is multiplied by the third factor  $\gamma$  (no relation to the film  $\gamma$ ). The values of  $\gamma$  depend on the machine configuration and the photon energy. A typical value for an early machine described by Brooks and DiChiro (1976) is  $\gamma = 0.34$  for 60-keV photons. Fig. 16.31 compares the dose to the head from projection radiography (equivalent to a single CT projection) and computed tomography.

With these added factors, the entrance dose is

$$D = \frac{(\pi^2/12) \beta \gamma h \nu e^{\mu L} (\mu_{\text{en}}/\rho) k^2}{w^3 b (\delta \mu)^2}. \quad (16.30)$$

This equation shows a fundamental relationship between dose and resolution. Decreasing both  $w$  and  $b$  by a factor of 2 requires a 16-fold increase in dose, while improving  $\delta \mu$  by a factor of 2 requires a dose that is 4 times as large.

We can insert typical numbers in Eq. 16.30 to calculate a minimum dose. Using  $\beta = 2$ ,  $\gamma = 0.34$ ,  $k = 2$ ,  $e^{\mu L} = 40$ ,

$h \nu = 60$  keV,  $\mu_{\text{en}}/\rho = 3.152 \times 10^{-3}$  m<sup>2</sup> kg<sup>-1</sup> (for water),  $\delta \mu = 0.1$  m<sup>-1</sup>,  $w = 1.0$  mm, and  $b = 1.0$  cm, we obtain

$$\begin{aligned} D &= \frac{(0.822)(2)(0.34)(40)(60 \times 10^3 \times 1.6 \times 10^{-19} \text{ J})(3.152 \times 10^{-3} \text{ m}^2 \text{ kg}^{-1})(2^2)}{(1.0 \times 10^{-3} \text{ m})^3 (1.0 \times 10^{-2} \text{ m})(0.1 \text{ m}^{-1})^2} \\ &= 27 \times 10^{-3} \text{ Gy}. \end{aligned}$$

Patient examinations usually involve several scans for different values of the distance along the  $z$  axis. Scattering from neighboring layers can more than double the dose. Spiral CT can reduce the dose if the pitch—the distance traversed in one revolution divided by the beam thickness  $b$ —is greater than one. Often, however, the pitch is less than one and the dose is increased. In some multidetector machines it is as low as 0.25. Pediatric doses are somewhat larger because there is less attenuation through the smaller patient.

The entrance skin dose is misleading, however. Figure 16.31 compares the dose distribution from a posterior-anterior head film with that from a head CT. The average dose within the slice for a given skin dose is higher for the CT because the beam enters from all sides. In addition, the entrance skin dose for the CT scan is about 20 times that of the PA radiograph: 40 mGy vs. 2 mGy [Huda (2002)]. On average, the dose from a single CT exam is about 4.5 times the annual background radiation received by the average person [Goodsitt *et al.* (2002)]. We will discuss this more in Sec. 16.13. Doses can be larger in small children, and children are more sensitive to radiation than adults [Hall (2002)].

Several steps are now taken to reduce the dose due to CT procedures. The cross section of the body is elliptical; the x-ray tube current can be reduced when the path through the body is shorter. The overall tube current can be reduced as long as the photon-noise-limited resolution is good enough to identify the anatomy of interest. Reducing the x-ray tube voltage (kVp) often increases the contrast for a given dose [Huda (2002)].

A disturbing recent trend is the use of annual full-body CT scans for screening. We discuss this in Sec. 16.13.

## 16.10 Biological Effects of Radiation

Radiation at sufficiently high doses can kill cells, tumors, organs, or entire animals. Radiation, along with surgery and chemotherapy, is a mainstay of cancer treatment. Radiation can also cause mutations. *Radiobiology*, the study of how radiation affects cells and organs, has provided major improvements in our understanding of cell death and damage in recent years. This understanding has modified and improved our approach to radiation therapy. This section provides a brief introduction to radiobiology, but it ignores many important details, such as our current understanding of specific proteins that cause some of

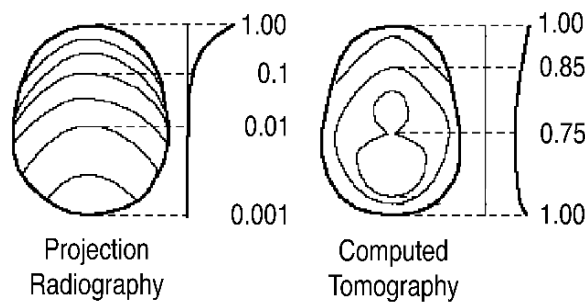


FIGURE 16.31. Contours of constant dose to the head for a conventional projection radiograph and a CT scan. The dose is normalized to the entrance dose. From Nagel *et al.* (2000). Used by permission.

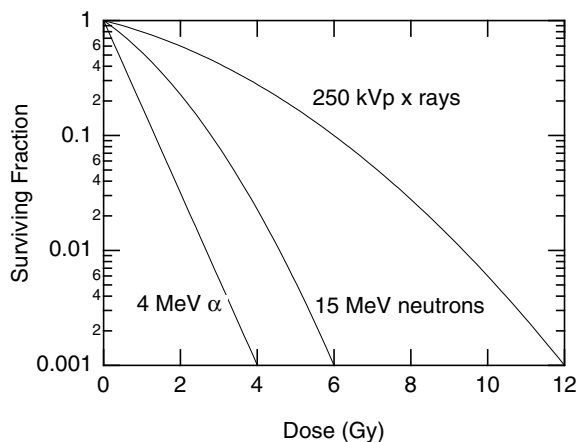


FIGURE 16.32. Typical survival curves for cell culture experiments, for 4 MeV  $\alpha$  particles, 15-MeV neutrons, and 250-kVp x rays. These are representations of typical experimental data.

the cellular responses.<sup>18</sup> The discussion starts with some cell-culture (*in vitro*) results, presents the most frequently used model for radiation damage, and then moves to *in vivo* tissue irradiation and the eradication of tumors.

### 16.10.1 Cell-Culture Experiments

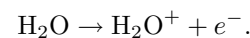
Cell-culture studies are the simplest conceptually. A known number of cells are harvested from a stock culture and placed on nutrient medium in plastic dishes. The dishes are then irradiated with a variety of doses including zero as a control. After a fixed incubation period the cells that survived have grown into visible colonies that are stained and counted. Measurements for many absorbed doses give *survival curves* such as those in Fig. 16.32. These curves are difficult to measure for very small surviving fractions, because of the small number of colonies that remain.

Failure to survive means either that the cell was killed or that it could no longer reproduce. If the cells die at-

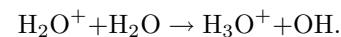
tempting the next or a later cell division (*mitosis*) it is called *mitotic death*. Some cells die by *apoptosis*: a mechanism whereby the cell initiates its own programmed death, going through a well-defined series of morphologic events that culminate in fragmentation of the DNA [Hall (2000)]. Recent experiments with microscopic beams of radiation and short-range particles aimed at different parts of the cell have demonstrated that damage to the cell's DNA is only one factor in the cell's response to the radiation. See, for example, Kassis (2004). Nonetheless, the differences in survival curve shapes that we discuss here are still important.

The shape of the survival curve depends on the linear energy transfer (LET) of the charged particles. For the  $\alpha$  particles in Fig. 16.32 the LET is about  $160 \text{ keV } \mu\text{m}^{-1}$ , for neutrons it is about  $12 \text{ keV } \mu\text{m}^{-1}$ , and for the electrons from the 250-kVp x rays it is about  $2 \text{ keV } \mu\text{m}^{-1}$ . The  $\alpha$  particles and neutrons are called high-LET radiation; the electrons are low-LET radiation.

High-LET radiation produces so many ion pairs along its path that it exerts a direct action on the cellular DNA. Low-LET radiation can also ionize, but it usually acts indirectly. It ionizes water (primarily) according to the chemical reaction



The  $\text{H}_2\text{O}^+$  ion decays with a lifetime of about  $10^{-10} \text{ s}$  to the hydroxyl free radical:



This then produces hydrogen peroxide and other free radicals that cause the damage by disrupting chemical bonds in the DNA. [Shabashon (1996), esp. pp. 64–69.]

### 16.10.2 Chromosome Damage

Cellular DNA is organized into *chromosomes*. In order to understand radiation damage to DNA, we must recognize that there are four *phases* in the cycle of cell division:

<sup>18</sup>For more information see the references by Hall (2000), and Moulder and Shadley (1996), by Orton (1997), and Steel (1996).

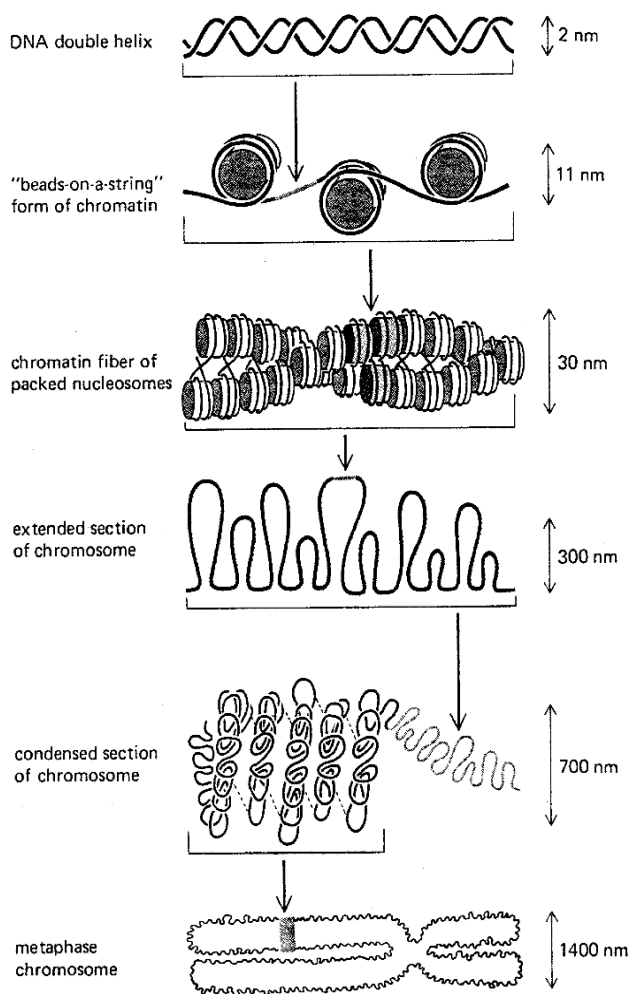


FIGURE 16.33. A schematic diagram of how the DNA is packed to give a chromosome, shown at metaphase of the cell cycle. From B. Alberts *et al.* *Molecular Biology of the Cell*, 4th. ed. New York, Garland (2002). p. 230. Used by permission of Taylor & Francis Group.

**M** Cell division. This stage includes both division of the nucleus (*mitosis*) and of the cytoplasm (*cytokinesis*). This phase may last one or two hours.

**G<sub>1</sub>** The first “gap” phase. The cell is synthesizing many proteins. The duration of G<sub>1</sub> determines how frequently the cells divide. It varies widely by kind of tissue, from a few hours to 200 hours.

**S** Synthesis. A new copy of all the DNA is being made. This lasts about 8 hours.

**G<sub>2</sub>** The second “gap” phase, lasting about 4 hours.

Figure 16.33 shows, at different magnifications, a strand of DNA, various intermediate structures which we will not discuss, and a chromosome as seen during the M phase of the cell cycle. The size goes from 2 nm for

the DNA double helix to 1400 nm for the chromosome. In addition to cell survival curves one can directly measure chromosome damage. There is strong evidence that radiation, directly or indirectly, breaks a DNA strand. If only one strand is broken, there are efficient mechanisms that repair it over the course of a few hours using the other strand as a template. If both strands are broken, permanent damage results, and the next cell division produces an abnormal chromosome.<sup>19</sup> Several forms of abnormal chromosomes are known, depending on where along the strand the damage occurred and how the damaged pieces connected or failed to connect to other chromosome fragments. Many of these chromosomal abnormalities are lethal: the cell either fails to complete its next mitosis, or it fails within the next few divisions. Other abnormalities allow the cell to continue to divide, but they may contribute to a multistep process that sometimes leads to cancer many cell generations later.

Even though radiation damage can occur at any time in the cell cycle (albeit with different sensitivity),<sup>20</sup> one looks for chromosome damage during the next M phase, when the DNA is in the form of visible chromosomes as in the bottom example in Fig. 16.33. If the broken fragments have rejoined in the original configuration, no abnormality is seen when the chromosomes are examined. If the fragments fail to join, the chromosome has a “deletion.” If the broken ends rejoin other broken ends, the chromosome appears grossly distorted.

A sequence of processes leads to cellular inactivation. Ionization is followed by initial DNA damage. Most of this is repaired, but it can be repaired incorrectly. No repair or misrepair results in DNA lesions that are then manifest as chromosome aberrations, which may be non-lethal, may cause mutations, or may lead to cell death. The numbers quoted here are from the review by Steel (1996). A cell dose of 1 Gy leads to the production of about  $2 \times 10^5$  ion pairs per cell nucleus, of which about 2000 are produced in the cell’s DNA. It has been estimated that the amount of DNA damage immediately after radiation can be quite large: 1000 single-strand breaks and 40 double-strand breaks per Gy. Yet survival curves for different cell types show between 0.3 and 10 lethal lesions per gray of absorbed dose. Thus the amount of repair that takes place is quite large, and the model that is introduced below is an oversimplification.

A number of chemicals enhance or inhibit the radiation damage. Some chemical reactions can “fix” (render permanent) the DNA damage, making it irreparable; others can scavenge and deactivate free radicals. One of the most important chemicals is oxygen, which promotes the formation of free radicals and hence cell damage. Cells with a poor oxygen supply are more resistant to radiation than those with a normal supply.

<sup>19</sup>This is a simplification. It is possible for a double strand break to repair properly. See Hall (2000), p. 19.

<sup>20</sup>In general, cells exhibit the greatest sensitivity in M and G<sub>2</sub>.

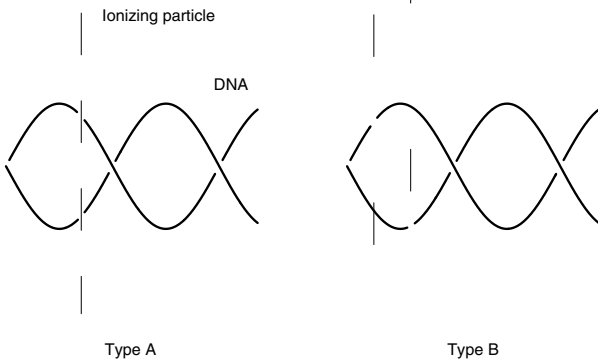


FIGURE 16.34. The two postulated types of DNA damage from ionizing radiation for our simple model to explain the linear-quadratic cell culture survival curve. In type-A damage a single ionizing particle breaks both strands. Two ionizing particles are required for type-B damage, one breaking each strand.

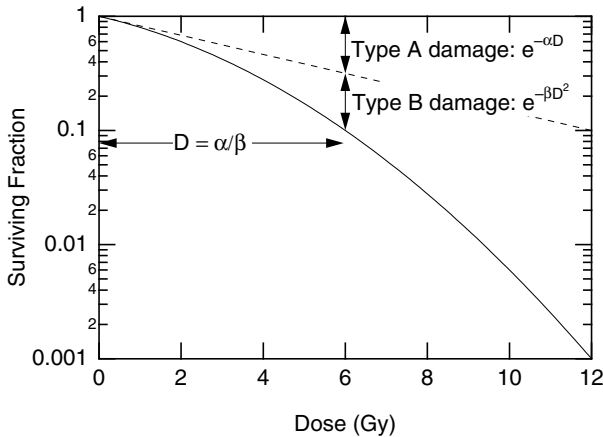


FIGURE 16.35. A survival curve, showing the linear exponent for type-A damage and the quadratic exponent for type-B damage.

### 16.10.3 The Linear-quadratic Model

The *linear-quadratic model* is usually used to fit cell survival curves. We introduce it in terms of a simplified model for DNA damage from ionizing radiation that recognizes two types of damage, shown in Fig. 16.34. In type-A damage a single ionizing particle breaks both strands of the DNA, and the chromosome is broken into fragments. In type-B damage, a single particle breaks only one strand. If another particle breaks the other strand “close enough” to the first break before repair has taken place, then the chromosome suffers a complete break.

The probability of type-A damage is proportional to the dose. The average number of cells with type-A damage after dose  $D$  is  $m = \alpha D = D/D_0$ , and the probability of no damage is the Poisson probability  $P(0; m) = e^{-m} =$

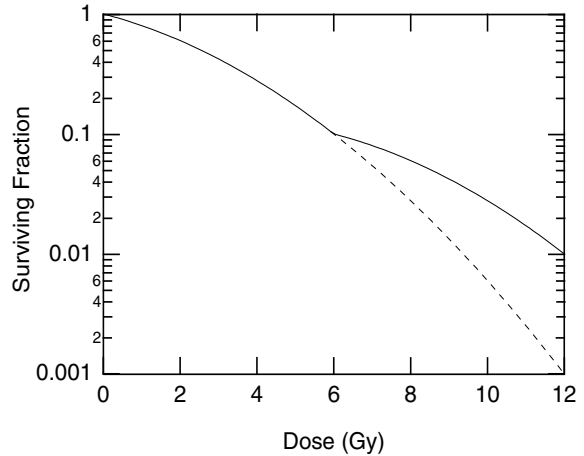


FIGURE 16.36. If the dose for low-LET radiations is divided into fractions, with a few hours between fractions, all of the single-strand breaks have been repaired, and survival follows the same curve as for the original fraction.

$e^{-\alpha D}$ . This is the dashed line in Fig. 16.35, which is redrawn from Fig. 16.32. For radiations with higher LET the proportionality constant is greater, as seen in Fig. 16.32.

In type-B damage one strand is damaged by one ionizing particle and the other by another ionizing particle. The probability of fragmenting the DNA molecule is therefore proportional to the square of the dose. The average number of molecules with type-B damage is  $\beta D^2$ , and the survival curve for type-B damage alone is  $e^{-\beta D^2}$ . This is also shown in Fig. 16.35. This leads to the linear-quadratic model for cell survival:

$$P_{\text{survival}} = e^{-\alpha D - \beta D^2}. \quad (16.31)$$

The dose at which mortality from each mechanism is the same is  $\alpha/\beta$ , as shown in Fig. 16.35.

An extension of the cell survival experiments is the *fractionation curve* shown in Fig. 16.36. After a given dose, cells from the culture were harvested and used to inoculate new cultures. After a few hours they were irradiated again. The survival curve plotted against total dose starts anew from the point corresponding to the first irradiation. The initial dose of 6 Gy caused both type-A and type-B damage. Before the second dose, the cells with single-strand damage had been repaired, and when the second dose was given, it acted on undamaged cells, so that only type-A damage occurred for small additional doses.

### 16.10.4 The Bystander Effect

Chromosome damage is not the entire story. The *bystander effect* in radiobiology refers to the “induction of biological effects in cells that are not directly traversed by a charged particle, but are in close proximity to cells that are” [Hall (2003)].

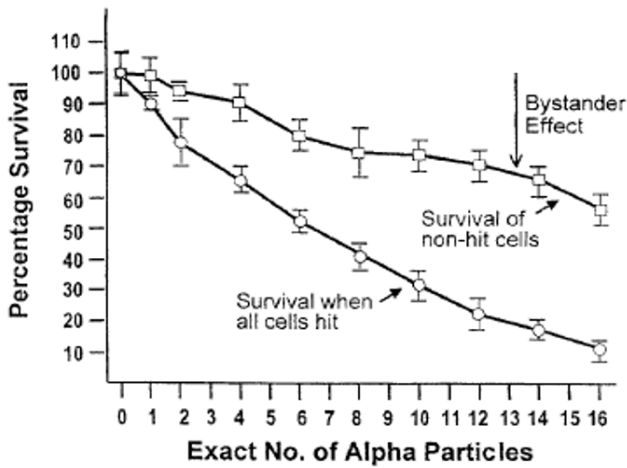


FIGURE 16.37. The bystander effect is seen in survival curves. Ten percent of the cells were stained with a low concentration of a dye. Each dyed cell was irradiated with a microbeam of 1 to 16  $\alpha$  particles. The dyed and undyed cells were then separated and cultured for survival. Survival of both the hit and non-hit cells showed a response to the irradiation. From E. J. Hall (2003). The bystander effect. *Health Physics* 85(1): 31–35 Used by permission.

One experiment showing the bystander effect involves irradiating cells in culture and transferring some of the culture medium to unirradiated cells, which then respond as if they had been irradiated. The effect is absent if the irradiated medium contains no cells. The irradiated cells secreted some chemical into the medium that affected the unirradiated cells. In one such experiment, apoptosis was induced in the nonirradiated culture by quite low doses to the irradiated cells. The dose response curve was nearly flat.

Another type of experiment used microbeams of  $\alpha$  particles to irradiate specific cells in a culture, and then measured the response of neighboring cells which had not been irradiated. Survival curves for both irradiated and unirradiated cells, vs. the number of  $\alpha$  particles traversing each irradiated cell are shown in Fig. 16.37. The survival of cells not irradiated decreased as their neighbors were hit with more  $\alpha$  particles. It is thought that some chemical produced in the irradiated cells migrated into the nonirradiated cells through gap junctions connecting the cytoplasm of neighboring cells. Similar experiments are done with radioactive nuclides that emit very-short range Auger electrons (see Chapter 17). The nuclides are attached to molecules that are selectively taken up by the cell nucleus or cytoplasm or that bond to the cell's DNA [Kassis (2004)].

### 16.10.5 Tissue Irradiation

There is considerable variation in the shape of the survival curves for human cells (Fig. 16.38). The shaded area labeled "human A-T cells" is for cells from patients with a

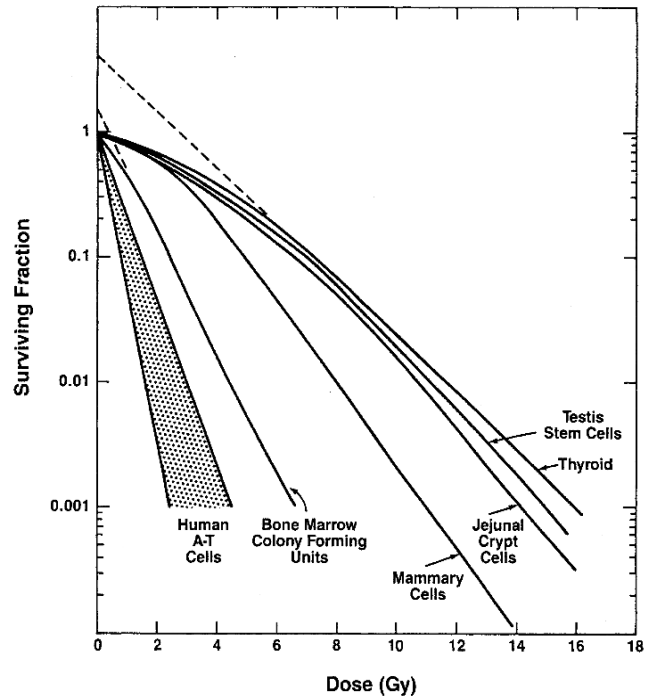


FIGURE 16.38. Survival curves for assays of human cells. There is a wide range in initial sensitivity, but not too much difference in final slope. The shaded area labeled "human A-T cells" is for cells from a disease, ataxia-tangliectasia, where repair mechanisms are lacking. Reproduced with permission from E. J. Hall. *Radiobiology for the Radiologist*, 5th ed. Philadelphia, Lippincott Williams & Wilkins, 2000, p. 328.

genetic disease, *ataxia-tangliectasia*, where repair mechanisms are lacking and breakage of a single strand of DNA leads to cell death.

The radiation damage to the DNA is not apparent until the cell tries to divide. At that point, the chromosomes are either so badly damaged that the cell fails to divide or the damage survives in later generations as a mutation. Some tissues respond to radiation quite quickly; others show no effect for a long time. This is due almost entirely to the duration of the G<sub>1</sub> phase or the overall time between cells divisions. Tissues are divided roughly into two groups: *early-responding* and *late-responding*. Early-responding tissues include most cancers, skin, the small and large intestine, and the testes. Late-responding tissues include spinal cord, the kidney, lung, and urinary bladder.

The central problem of radiation oncology is how much dose to give a patient, over what length of time, in order to have the greatest probability of killing the tumor while doing the least possible damage to surrounding normal tissue. While the dose is sometimes given all at once (over several minutes), it is usually given in *fractions* five days a week for four to six weeks. Some recent treatment plans, primarily for brachytherapy (see Sec. 17.15), use fractions given every few hours.

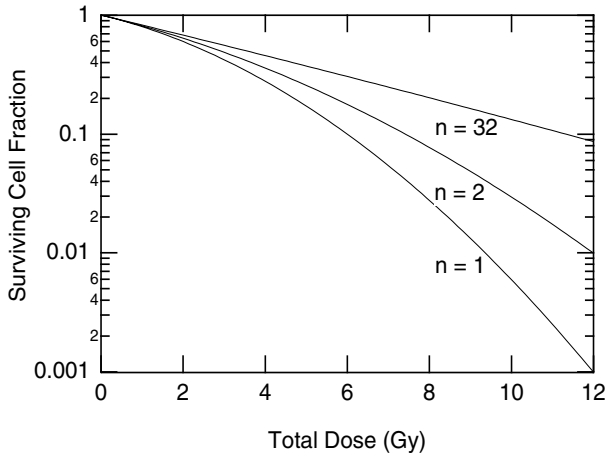


FIGURE 16.39. The fraction of cells surviving a total radiation dose when the dose is divided into 1, 2, and 32 fractions, showing how the curve approaches  $e^{-\alpha D}$  as the number of fractions becomes large.

What total dose (or dose per fraction) should be given in how many fractions, with what time between fractions? We can answer these questions using the linear-quadratic model. Let the dose per fraction be  $D_f$ , the number of fractions be  $n$ , and the total dose be  $D = nD_f$ . We now need to plot survival vs total dose for different numbers of fractions. We assume that the time between fractions allows for full repair of sublethal damage (single-strand breaks). The probability of a cell surviving after  $n$  fractions have been delivered is

$$P_s = P_{\text{survival}} = S = \left( e^{-\alpha D_f - \beta D_f^2} \right)^n = e^{-\alpha D - \beta D^2/n}. \tag{16.32}$$

As the number of fractions becomes very large for a given total dose, the survival curve approaches  $e^{-\alpha D}$ . This can be seen in Fig. 16.39, which plots survival vs total dose delivered in different numbers of fractions. With many fractions the dose per fraction is very small, all the single-strand breaks are repaired, and almost no type-B cell deaths take place.

Early-responding tissue and tumors have been found to have an  $\alpha/\beta$  ratio of about 10 Gy. The survival curve is primarily due to type-A damage. Late-responding tissues have an  $\alpha/\beta$  ratio of 2–3 Gy. There is considerable variation in these numbers.

Some of the problems of radiation therapy and the benefits of fractionation can be seen if we consider a strictly hypothetical example in which  $\alpha = 0.1 \text{ Gy}^{-1}$  for both the tumor and the surrounding tissue. The tumor is early responding with  $\alpha/\beta = 10 \text{ Gy}$ , and the surrounding tissue is late responding with  $\alpha/\beta = 2 \text{ Gy}$ . The surrounding tissue is actually more sensitive to the radiation than the tumor and has a lower survival curve. Figure 16.40 shows the cell-survival curves for 1 and 35 fractions. The tumor survival in each case is shown as a dashed line. The thicker curves correspond to delivering the dose in 35 fractions. (In this example, both tissues have the same value

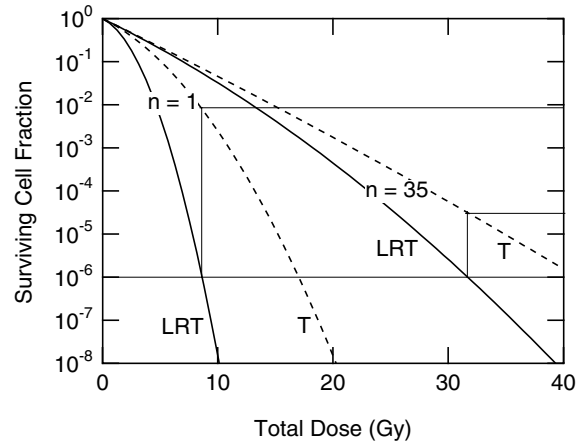


FIGURE 16.40. Cell survival curves for late-responding normal tissue (LRT) and for a hypothetical tumor (T), showing the improvement obtained by dividing the dose into fractions. With a single fraction, the tumor survives much better than the normal tissue. With 35 fractions, this discrepancy has been reduced. The details are discussed in the text.

of  $\alpha$  and the surrounding tissue receives the same dose. In real life,  $\alpha$  for the tumor may be greater than that for the normal tissue, and the treatment will be more effective.)

To see the benefit of fractionation, suppose that the patient can tolerate a dose at which only  $10^{-6}$  of the cells of the surrounding tissue survive, represented by the horizontal line on the graph. (This is not realistic!) For a single fraction, this corresponds to a total dose of about 9 Gy, which, applied to the dashed line, shows that the surviving fraction of tumor cells is about  $10^{-2}$ . For 35 fractions the normal tissue can tolerate about 32 Gy, yielding  $3 \times 10^{-5}$  as the fraction of tumor cells surviving.

Suppose next that it is possible to confine the radiation beam so that the dose to normal tissue is only about 0.6 times that to the tumor. This means that the tissue dose in Eq. 16.32 is multiplied by 0.6. The result is shown in Fig. 16.41 for 35 fractions. The dose can now be as high as 53 Gy for the same effect on surrounding tissues, leading to a tumor survival of only  $10^{-8}$ . We will see how beam shaping is accomplished in the next section.

These calculations are solely to illustrate the basic principles. Clinically useful calculations must take several additional factors into account: the actual values of  $\alpha$  for the tissue and tumor under consideration, the effect of cell growth after irradiation, the effect of the first dose on synchronizing the cycles of the remaining cells, and the oxygen level in the tumor cells. (The greater the oxygen concentration the more sensitive the cells are, particularly for low-LET radiation. Rapidly growing tumors often outstrip their blood supply, receive less oxygen, and are less radio-sensitive.) Fractionation is reviewed in Orton (1997) and in Hall (2000). It is also necessary to take into account the fact that neither the tumor nor the surrounding normal tissue receives a uniform dose of radiation.

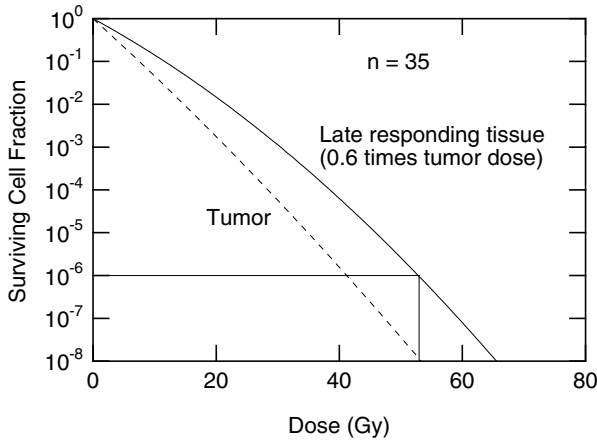


FIGURE 16.41. Survival curves for the same cells as in the previous figure, with the dose to the surrounding tissue reduced to 0.6 times that to the tumor. Now the probability of tumor survival at high doses is about 0.01 times that for the surrounding normal tissue. This shows the importance of confining the radiation to the tumor as much as possible.

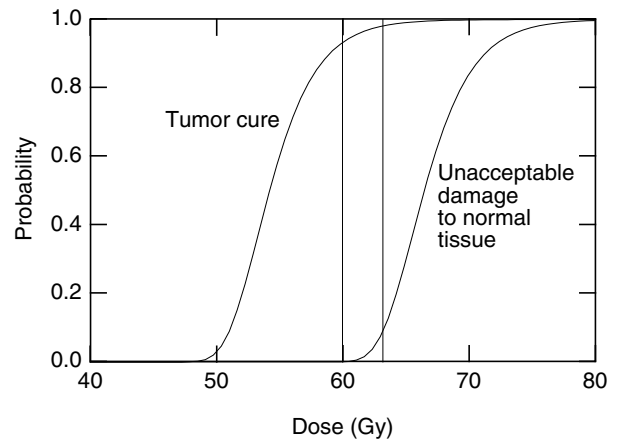


FIGURE 16.43. The probability of curing the tumor and the probability of unacceptable damage to normal tissue vs dose. Both the tumor and the normal tissue contain  $10^8$  cells. The 35-fraction doses shown in Fig. 16.41 have been used.

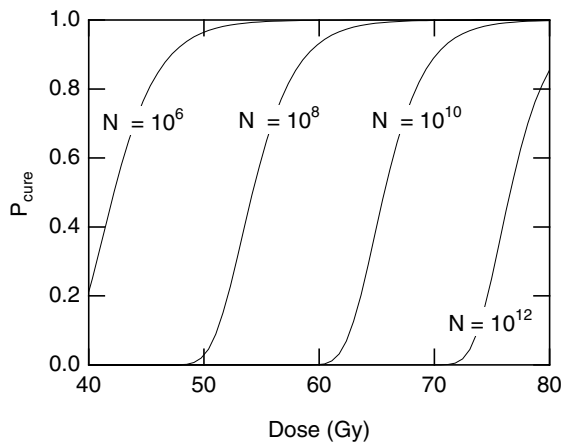


FIGURE 16.42. The probability of eradicating the tumor (no surviving tumor cells) as a function of dose for tumors containing different numbers of cells.

### 16.10.6 A Model for Tumor Eradication

The target theory model can be applied to a collection of cells to give us insight into the central problem of radiation therapy: eradication of the tumor or *tumor eradication*. Suppose that a tumor consists of  $N$  cells with identical properties. The cells are uniformly irradiated with dose  $D$ . If a collection of identical tumors were irradiated, the number of cells surviving in each tumor would fluctuate. The probability that a single cell survives is  $p_s(D)$ , which might be given by Eq. 16.32. If this number is small and  $N$  is large, the number surviving follows a Poisson distribution. The average number surviving is  $m = Np_s(D)$ . The probability of a cure is the probability that no tumor cells survive:

$$P_{\text{cure}} = e^{-m} = e^{-Np_s(D)}. \quad (16.33)$$

This can be evaluated using your cell-survival model of choice.

Figure 16.42 shows a tumor eradication curve based on the 35-fraction curve in Fig. 16.40. The larger the tumor, the greater the dose required for cure. Figure 16.43 shows a plot of the probability of tumor cure and the probability of unacceptable damage to the surrounding tissue, both based on  $10^8$  cells and the cell-survival curves in Fig. 16.41 (with the normal tissue receiving 0.6 times the dose received by the tumor). For this model, at least 60 Gy are required in order to have a good probability of cure; once the dose is higher than 63 Gy, the damage to normal tissue is unacceptable.

## 16.11 Radiation Therapy

The treatment of cancer must deal with two issues: eradication of the primary tumor (local control), and eradication of *metastases*, which may be in nearby tissue or may be at distant sites within the body. In many cases radiation therapy, either alone or combined with surgery, is the best technique for local control. Two oncologists have provided a review of the benefits and problems of radiation therapy, addressed specifically to the medical physics community [Schulz and Kagan (2002)]. They point out that many cancer deaths are due to metastatic disease, so improved local control does not necessarily provide a corresponding improvement in survival.

Which method of treatment is best can change dramatically as new treatments are developed. For example, a combination of radiation therapy and chemotherapy was once used to treat Hodgkin's disease; chemotherapy has been improved to the point where radiation is no longer necessary [DeVita (2003)].





FIGURE 16.44. X-ray therapy was used to treat a carcinoma of the nose. *A* shows the original lesion; *B* is the result one year later. The patient remained asymptomatic five years after treatment. Reprinted from William T. Moss and James D. Cox. *Radiation Oncology*, 6th ed. (1989) St. Louis, Mosby, with permission from Elsevier.

### 16.11.1 Classical Radiation Therapy

Doses for diagnostic radiology vary from about  $10^{-4}$  to  $10^{-2}$  Gy. Doses of 20–80 Gy are required to treat cancer. A great deal of physics is involved in planning the treatment for each patient. [See Khan (2003).] There is a choice of radiation beams: photons of various energies, electrons, neutrons, protons, or  $\alpha$  particles. Photons and electrons are routinely available; the other sources require special facilities. Only a few of the beam issues will be raised here. Some of the dose measurement issues are discussed in the next section.

An example of the effectiveness of radiation therapy is shown in Fig. 16.44. The patient developed a carcinoma of the nose and refused surgery. Radiation with a total dose of 50 Gy was used, and the results one year later are shown. It is ironic that the carcinoma probably developed because the patient was treated with x rays for acne many years earlier.

We have already seen the importance of reducing dose to tissue surrounding the tumor. Optimizing the dose determines the kind of radiation to be used and its energy, as well as the details of beam filtration and collimation and how it is aimed at the patient's body. For now, we discuss a photon beam. Attenuation and the  $1/r^2$  decrease of photon fluence help spare tissue downstream from the beam. Since  $\mu_{\text{atten}}$  decreases with increasing photon energy up to a few MeV, higher-energy photons penetrate more deeply and must be used for treating deeper lesions. There is also dose buildup with depth over distances comparable to the range of the Compton-scattered electrons. Both of these effects are shown in Fig. 16.45.

The beam is *collimated* to spare normal tissue. Originally, the collimator consisted of four lead jaws that provided a rectangular opening with adjustable length and

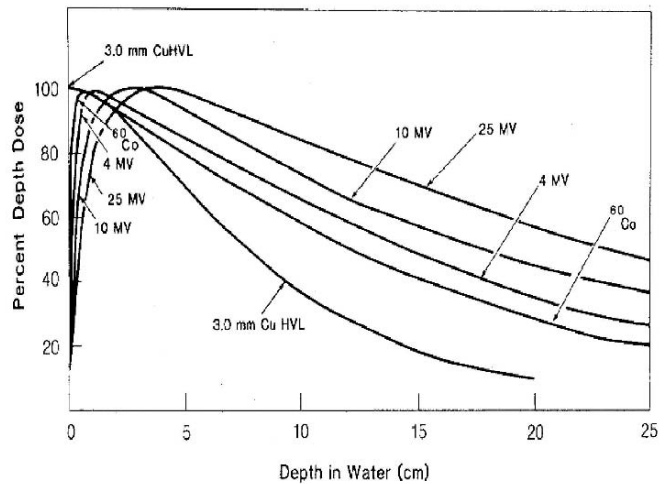


FIGURE 16.45. The dose vs depth for x-ray beams of different quality (energy) on the central axis of the beam. The source—surface distance (SSD) is 100 cm and the field size is 10 cm  $\times$  10 cm. The curve “3.0 mm Cu HVL” is for a photon beam that is reduced to half intensity by a copper filter 3.0 mm thick. The labels 4, 10 and 25 MV refer to the energy of the electron beam striking the target. From F. M. Khan (2003). *The Physics of Radiation Therapy*, 3rd. ed. Philadelphia, Lippincott Williams & Wilkins, p.163. ©2003 Lippincott Williams and Wilkins.

width. Later, masks of a special lead alloy were custom-made for each patient. A wedge was sometimes placed in the beam to vary the intensity across the collimated radiation field.

Figure 16.46 shows *isodose contours* for various beams. In addition to the differences with depth seen in Fig. 16.45, there are significant differences in the sharpness of the dose distribution across the beam. The extent of the lesion to be radiated must be carefully determined with radiographs or CT scans.

If the tumor is not near the surface, the ratio of tumor dose to normal tissue dose can be increased by irradiating the patient from several directions. Figure 16.47 shows how the relative dose to a deep tumor can be increased by irradiating with two “fields” on opposite sides of the patient. In Fig. 16.48 three and four fields are used. The angles of the fields can be changed by rotating the patient couch as well as the gantry holding the photon source and collimator.

Rectangular fields do not match the shape of the tumor. Two techniques can overcome this problem. A lead-alloy that melts at low temperature can be used to make a collimator that is customized for each patient to match the tumor. Or, a *multi-leaf collimator* can replace the original jaws on the therapy machine. A typical multileaf collimator has 40 pairs of tungsten alloy leaves, each  $\leq 1$  cm wide, which can be independently adjusted to provide a pattern like that in Fig. 16.49. This might be used for up to nine fields from different directions.

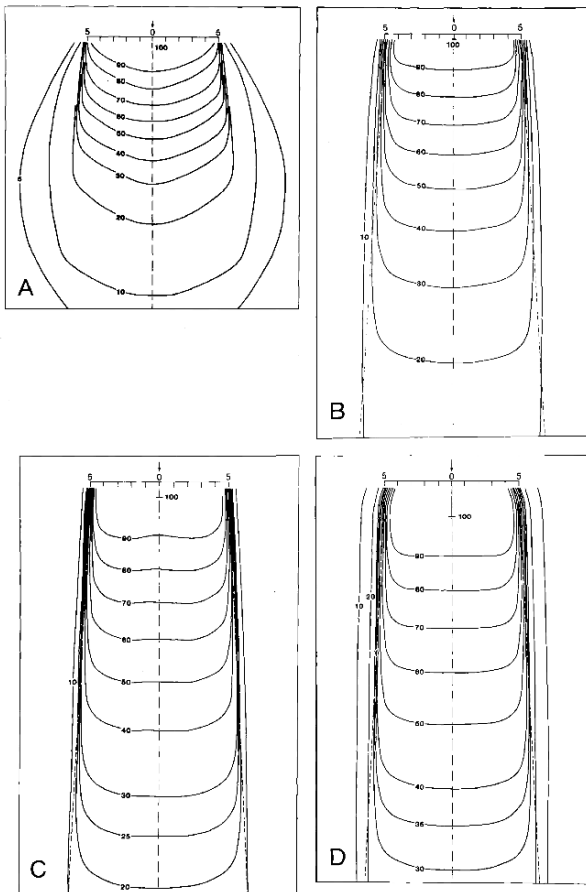


FIGURE 16.46. Isodose distributions for radiation under different conditions, all collimated to 10 cm×10 cm. (A) Radiation from an x-ray tube with 200 kVp, 0.5 m from the surface. (B) Photons from the radioactive isotope  $^{60}\text{Co}$ , 0.8 m from the surface. (C) 4-MV photons, 1 m from the surface. (D) 10-MV photons, 1 m from the surface. From F. M. Khan, *The Physics of Radiation Therapy*, 3rd. ed. p. 204. Philadelphia, Lippincott Williams & Wilkins. ©2003 Lippincott Williams & Wilkins.

### 16.11.2 Modern X-ray Therapy

The goal of radiation therapy is to provide as large a dose as possible to the tumor while sparing adjacent normal tissue. The normal tissue may be quite close to the tumor. *Three-dimensional conformal radiation therapy* uses 3-dimensional information about the target volume. This is difficult, because even with 3-D display of CT, MRI or ultrasound images, it may be impossible to see the edges of the tumor. Nevertheless, the *beam's-eye view* that can be computed from 3-D image data can be very useful in planning the treatment. For a discussion of conformal radiation therapy, see Khan (2003), Chapter 19.

In classical radiotherapy, the beam was either of uniform fluence across the field, or it was shaped by an attenuating wedge placed in the field. *Intensity-modulated radiation therapy* (IMRT) is achieved by stepping the collimator leaves during exposure so that the fluence varies

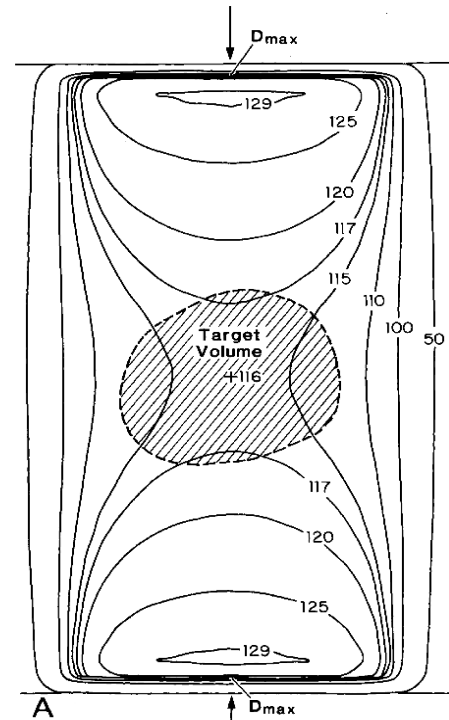


FIGURE 16.47. Isodose distribution when the patient is irradiated equally from opposite sides. From F. M. Khan, *The Physics of Radiation Therapy*, 3rd. ed. Philadelphia, Lippincott Williams & Wilkins. ©2003 Lippincott Williams & Wilkins.

from square to square in Fig. 16.49 [Webb (2001); Khan (2003), Ch. 20]. One form of IMRT is *helical tomotherapy* (slice therapy), which uses filtered back-projection techniques with a multileaf collimator to shape the radiation field as the patient moves axially through the beam—the analog of a spiral CT study [Holmes *et al.* (1995)]. It is, of course, impossible to make the filtered radiation field negative. This means that the dose outside the tumor is not strictly zero, but it can be made small. These techniques provide much better sparing of adjacent sensitive tissue and sometimes allow a boost in dose to the tumor. One drawback to IMRT is that although the dose to the tumor is about the same, the total number of x rays produced is a factor of 2–10 greater than in conventional therapy. This requires better-shielded radiation treatment rooms.

### 16.11.3 Charged Particles and Neutrons

Electrons, typically between 6 and 20 MeV, are also used for therapy. Because of the range–energy relationship, the field falls nearly to zero in a centimeter or two. Electrons are used primarily for skin and lip cancer, head and neck cancer, and irradiation of lymph nodes near the surface. Figure 16.50 shows the dose vs. depth as a percent of the maximum dose for electron beams of several different energies.

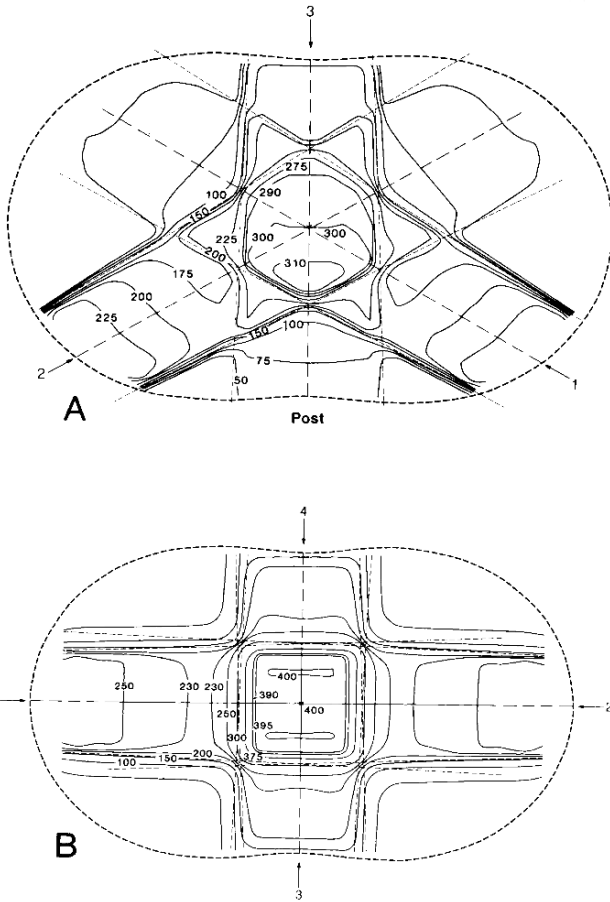


FIGURE 16.48. Isodose distribution for (A) three and (B) four radiation fields, each designed to give a relative dose of 100 at the center of the tumor. From F. M. Khan, *The Physics of Radiation Therapy*, 3rd. ed. Philadelphia, Lippincott Williams & Wilkins. ©2003 Lippincott Williams & Wilkins.

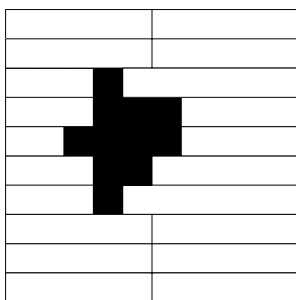


FIGURE 16.49. A multileaf collimator (MLC). The tungsten leaves are shown in white; the opening is black.

Protons are also used to treat tumors. Their advantage is the increase of stopping power at low energies. It is possible to make them come to rest in the tissue to be destroyed, with an enhanced dose relative to intervening tissue and almost no dose distally (“downstream”) as shown by the *Bragg peak* in Fig. 16.51. Placing an ab-

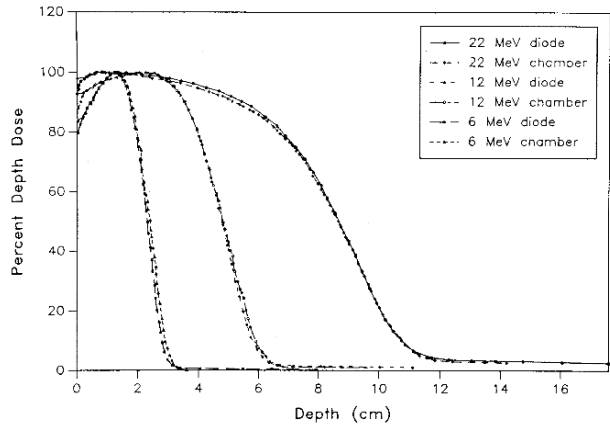


FIGURE 16.50. Depth-dose curves for electrons of different energies, measured with a solid-state detector (diode) and an ionization chamber. Both the range and the straggling increase with increasing energy. From F. M. Khan (1986). Clinical electron beam dosimetry. In J. G. Keriakes, H. R. Elson, and C. G. Born, eds. *Radiation Oncology Physics—1986*. College Park, MD, American Association of Physicists in Medicine. AAPM Monograph 15.

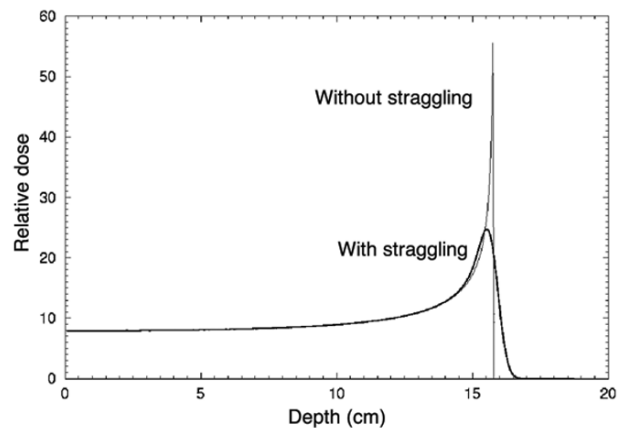


FIGURE 16.51. Energy loss vs depth for a 150 MeV proton beam in water, with and without straggling. The Bragg peak enhances the energy deposition at the end of the proton range. Courtesy of W. D. Newhauser, M. D. Anderson Cancer Center.

sorber in the proton beam before it strikes the patient moves the Bragg peak closer to the surface. Various techniques, such as rotating a variable-thickness absorber in the beam, are used to shape the field by spreading out the Bragg peak (Fig. 16.52). The edges of proton fields are much sharper than for x rays and electrons. This can provide better tissue sparing, but it also means that alignments must be much more precise [Moyers (2003)]. Sparing tissue reduces side effects immediately after treatment. It also reduces the incidence of radiation-induced second cancers many years later. These are particularly important in pediatric patients as the initial treatment

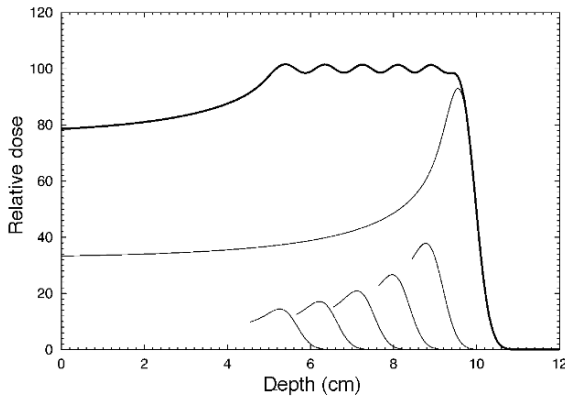


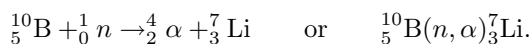
FIGURE 16.52. irradiating the patient through a number of absorbers of different thickness spreads out the region of maximum dose. Provided by W. D. Newhauser, M. D. Anderson Cancer Center.

proves more successful and the patients survive longer. Miralbell *et al.* (2002) estimated the incidence rate for secondary cancers in certain pediatric cancers and found a reduced incidence for proton therapy compared to both conventional x ray and IMRT. Intensity-modulated proton therapy could provide even more improvement.

Proton therapy is used in a number of diseases, such as prostate cancer [Slater *et al.* (2004)], retinal tumors such as choroidal melanoma, pituitary adenoma, arteriovenous malformations in the brain, and wet macular degeneration [Habrand *et al.* (1995), Suit and Urie (1992), Moyers (2003)]. Some institutions are experimenting with intensity-modulated proton therapy (IMPT).

Fast neutrons are used for therapy [Duncan (1994)]. The dose is due to charged particles: protons,  $\alpha$  particles ( ${}^4\text{He}$  nuclei), or recoil nuclei of oxygen and carbon that result from interactions of the neutrons with the target tissue. All of these have high LET, and the oxygen effect is less than for low-LET radiation. Fast neutron therapy shows promise in some salivary gland cancers [Douglas *et al.* (2003)].

Boron neutron capture therapy (BNCT) is based on a nuclear reaction which occurs when the stable isotope  ${}^{10}\text{B}$  is irradiated with neutrons, leading to the nuclear reaction (in the notation of Chapter 17)



Both the alpha particle and lithium are heavily ionizing and travel only about one cell diameter. BNCT has been tried since the 1950s; success requires boron-containing drugs that accumulate in the tumor. The field has recently been reviewed by Barth (2003).

*Brachytherapy* (brachy means short) involves the implantation of radioactive isotopes in a tumor and will be discussed in Chapter 17.

## 16.12 Dose Measurement

It is important to measure radiation doses accurately for radiation therapy in order to compare the effectiveness of different treatment protocols and to ensure that the desired protocol is indeed being followed. Accuracies of 2% are expected. An extensive literature about relating the dose in the measuring instrument to the dose in surrounding tissue exists.<sup>21</sup> Here we describe one of the techniques that is used.

A basic problem in dosimetry is that the measuring instrument has different properties than the medium in which it is immersed. Imagine, for example, that a gas-filled ionization chamber is placed in water. If the radiation field were very large and uniform, one could in principle use an ionization chamber whose dimensions are large compared to the range of secondary electrons, and the interaction of the radiation field with the chamber gas would be the dominant effect. This is not practical. At the other extreme, we imagine an ionization chamber that is so small that it does not alter the radiation field of the water. That is, its dimensions must be small compared to the range of the charged particles created in the water and passing through it.

We saw in Sec. 15.16 that the absorbed dose in a parallel beam of charged particles with particle fluence  $\Phi$  is (Eq. 15.76)

$$D = \frac{S_e}{\rho} \Phi.$$

Usually the beam consists of particles with different kinetic energies  $T$ . Let  $\Phi_T$  be the energy spectrum:

$$\Phi = \int_0^{T_{\max}} \Phi_T dT.$$

Then the dose is the integral of the number of particles with energy  $T$  times the mass stopping power for particles of that energy:

$$D = \int_0^{T_{\max}} \Phi_T \frac{S_e}{\rho} dT. \quad (16.34)$$

We can define an average mass collision stopping power:

$$\frac{\bar{S}_e}{\rho} = \frac{1}{\Phi} \int_0^{T_{\max}} \Phi_T \frac{S_e}{\rho} dT \quad (16.35)$$

so that

$$D = \Phi \frac{\bar{S}_e}{\rho}. \quad (16.36)$$

Let us apply this to the situation where a small detector (“gas”) is introduced in a medium (“water”) in which we want to know the dose. The charged particle fluence is not altered by the detector because it is small compared

<sup>21</sup>See Attix (1986), Chap. 10ff or Khan (2003), Chapter 8.

to the range of the charged particles. Applying Eq. 16.36 in both media, we obtain

$$\frac{D_w}{D_g} = \frac{(\bar{S}_e/\rho)_w}{(\bar{S}_e/\rho)_g} \equiv (\bar{S}_e/\rho)_g^w. \quad (16.37)$$

This is the *Bragg-Gray relationship* for the absorbed dose in the cavity. It is standard in the literature to denote the dimensionless ratio of the stopping powers in the two media by  $(\bar{S}_e/\rho)_g^w$  [or, in some books,  $(\bar{S}_c/\rho)_g^w$ ].

This equation is often used with ionization chambers. The charge created in an ionization chamber of mass  $m$  is the charge per ion pair  $e$  times the number of ion pairs formed in mass  $m$ . The number of ion pairs is the energy deposited,  $mD_g$ , divided by the average energy required to produce an ion pair,  $W$ :

$$q = e \frac{mD_g}{W}. \quad (16.38)$$

Combining this with Eq. 16.37 gives the dose in the medium in terms of the charge created:

$$D_w = \frac{q}{m} \left( \frac{W}{e} \right)_g (\bar{S}_e/\rho)_g^w. \quad (16.39)$$

The charge  $q$  created is usually greater than the charge collected in the ion chamber because of recombination of ions and electrons before collection. The collection efficiency and the chamber mass are deduced from calibration of the chamber. Once the chamber has been calibrated, the factor  $(\bar{S}_e/\rho)_g^w$  accounts for placing the chamber in different media.

## 16.13 The Risk of Radiation

Exposure to radiation may or may not cause a noticeable effect. Effects can include a change, which may not be harmful; damage to cells, which may not necessarily be deleterious to the individual; or harm, which is clinically observable in the subject or possibly a descendant (though current data suggest that genetic changes are rare). It may take years before the harm is observed. The International Commission on Radiological Protection in ICRP (1991) defines the *detriment* to an individual who receives a dose of radiation. It is a rather complex combination of the probability of harm, the severity of the harm, and the time of onset after exposure. It will be discussed more below.

In this section we focus on the increased probability of induction of cancer from an exposure to radiation. We have considerably more information about human exposure to ionizing radiation than we have for any other known or suspected carcinogen [Boice (1996)]. Several studies at moderate doses show that radiation is a relatively weak carcinogen, though this is not the public view.

We have already seen that the biological effect of radiation depends on the absorbed dose, the LET, the nature of the tissue that is irradiated, and the dose rate. It also depends on the age of the subject. This makes it very difficult to estimate the detriment. Ideally, we would multiply the dose to each organ or target in the body by the probability of a detriment to that target from that kind of radiation now and in the future, and sum over all the organs in the body. This is impossible: we do not know enough. We must simplify the problem while taking some of these differences into account.<sup>22</sup>

### 16.13.1 Equivalent and Effective Dose

#### Equivalent Dose

Our first simplification assumes that the LET dependence is the same for all target organs. ICRP defines the *radiation weighting factor*  $W_R$  for each radiation type  $R$  striking the body. It depends on the radiation type and energy and is independent of organ or tissue type. The radiation weighting factor for x rays is 1.  $W_R$  is determined “with guidance” from an earlier quantity, the *relative biological effectiveness* of the radiation (RBE). The weighting factor for each radiation  $W_R$  is multiplied by the average dose to the target organ or tissue  $D_{R,T}$  and summed to give the *equivalent dose*<sup>23</sup> to the target organ,  $H_T$ :

$$H_T = \sum_R W_R D_{R,T}. \quad (16.40)$$

The unit of  $H_T$  is the *sievert* (Sv).<sup>24</sup>

#### Detriment and Effective Dose

The *detriment* is a measure of the harm from an exposure to radiation. It might be a genetic effect (relatively rare) or the development of cancer some years later. If cancer, it might be fatal, shortening life span, or it might cause discomfort and inconvenience but not death. We want to estimate the detriment when a certain equivalent dose has been delivered to some target organs. We assume that

<sup>22</sup>RKH wishes to thank Cynthia McCullough, PhD, for a very helpful discussion of this section

<sup>23</sup>The nomenclature here is quite confusing. ICRP used to define the *dose equivalent*, also denoted by  $H$ , as  $QD$ , where  $Q$  was called the *quality factor* of the radiation. The radiation weighting factor is very similar, and essentially numerically equivalent, to the earlier quality factor,  $Q$ . Values of  $Q$  recommended by Nuclear Regulatory Commission (NRC) are 1 for photons and electrons, 10 for neutrons of unknown energy and high-energy protons, and 20 for  $\alpha$  particles, multiply charged ions, fission fragments, and heavy particles of unknown charge. The ICRP has its own recommendations, that differ slightly for protons and neutrons. See McCullough and Schueler (2000).

<sup>24</sup>Both the sievert and the gray are  $\text{J kg}^{-1}$ . Different names are used to emphasize the fact that they are quite different quantities. One is physical, and the other includes biological effects. An older unit for  $H$  is the rem.  $100 \text{ rem} = 1 \text{ Sv}$ .

TABLE 16.4. Contribution of some organs to the whole-body radiation detriment. From ICRP (1991) Table B-20.

Organ ( $T$ )	Cancer probability, per Sv	Severe genetic probability, per Sv	Corrected for life lost and nonfatal cancers, per Sv	Tissue weighting factor ( $W_T$ )
Bladder	$30 \times 10^{-4}$		$29.4 \times 10^{-4}$	0.04
Breast	$20 \times 10^{-4}$		$36.4 \times 10^{-4}$	0.05
Stomach	$110 \times 10^{-4}$		$100 \times 10^{-4}$	0.14
Gonads		$100 \times 10^{-4}$	$133 \times 10^{-4}$	0.18
Total	$500 \times 10^{-4}$		$752 \times 10^{-4}$	1.00

the probability of developing cancer in a target organ depends on the dose to that organ and not on the dose to any other part of the body. We also assume that the probabilities are small, so that if several organs have received a radiation dose, the probability of developing cancer is the sum of the probabilities for each organ.

Most of our information about the detriment comes from extensive studies of atomic-bomb survivors, for whom the entire body received a fairly uniform equivalent dose. These survivors have now been followed for over 50 years. Other studies include patients who have been followed for decades after receiving radiation therapy. ICRP (1991) estimates the radiation detriment using these data and taking into account the probability of a fatal cancer attributable to the radiation, the weighted probability of an attributable non-fatal cancer, the weighted probability of severe hereditary effects, and the relative decrease in lifespan. Table 16.4 shows four of the 14 entries in Table B-20 of ICRP (1991). The details of the various corrections are not shown; the point is to show how each organ contributes to the total detriment.<sup>25</sup>

The *effective dose*<sup>26</sup>  $E$  is a sum over all irradiated organs:

$$E = \sum_T W_T H_T = \sum_{R,T} W_T W_R D_{R,T}. \quad (16.41)$$

The *tissue weighting factor*  $W_T$  is the radiation detriment for organ  $T$  from a whole body irradiation as a fraction of the total radiation detriment. By definition, the sum of  $W_T$  over all organs equals unity. The last column of Table 16.4 shows the  $W_T$  assigned to each target organ in ICRP (1991). See also the review by McCollough and Schueler (2000).

As an example, consider a typical CT head scan, which provides a significant equivalent dose to the brain, bone marrow, thyroid, and bone surface, as shown in Table 16.5.<sup>27</sup> The effective dose is 1.8 mSv. The probability of developing a radiation-induced cancer is  $500 \times 10^{-4} \times 1.8 \times$

TABLE 16.5. Major contributions to the effective dose from a typical CT head scan.

Organ	$W_T$	$H_T$ (mSv)	$W_T H_T$ (mSv)
Brain	0.025	36	0.90
Bone marrow (red)	0.12	3	0.36
Thyroid	0.05	5.5	0.28
Bone surface	0.01	14	0.14
All other organs			0.10
Effective dose			1.8

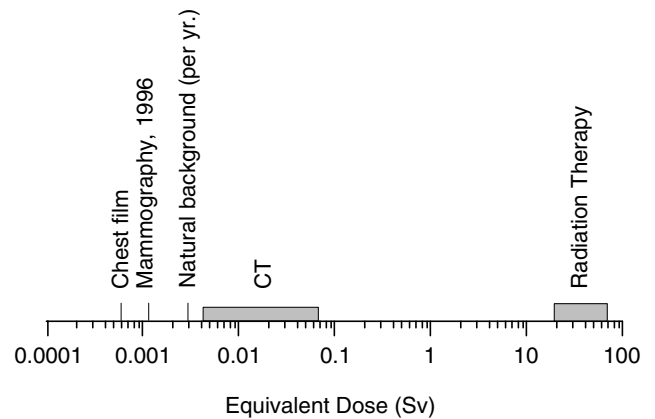


FIGURE 16.53. Various doses on a logarithmic scale. Natural background is per year; other doses are per exposure.

$10^{-3} = 9 \times 10^{-5}$ . If the whole body were to receive an equivalent dose of 36 mSv, the probability of a radiation-induced cancer would be  $500 \times 10^{-4} \times 36 \times 10^{-3} = 1.8 \times 10^{-3}$ .

### 16.13.2 Comparison with Natural Background

One way to express risk is to compare medical doses to the natural background. We are continuously exposed to radiation from natural sources. These include cosmic radiation, which varies with altitude and latitude; rock, sand, brick, and concrete containing varying amounts of radioactive minerals; the naturally occurring radionuclides in our bodies such as  $^{14}\text{C}$  and  $^{40}\text{K}$ ; and radioactive progeny from radon gas from the earth.<sup>28</sup> In a typical adult, there are about  $4 \times 10^7$  radioactive disintegrations per hour from all internal sources. Table 16.6 and Fig. 16.53 summarize the various sources of

<sup>25</sup>ICRP is expected to issue revised values of  $W_T$ , probably in 2007.

<sup>26</sup>An older, related quantity is the effective dose equivalent,  $H_E = W_T QD$ .

<sup>27</sup>Values of  $H_T$  were provided by C. McCollough.

<sup>28</sup>Radon is chemically inert gas that escapes from the earth. Since it is chemically inert, we breathe it in and out. When it decays in the air (the decay scheme is described in Sec. 17.16), the decay products attach themselves to dust particles in the air. When we breathe these dust particles, some become attached to the lining of the lungs, irradiating adjacent cells as they undergo further decay.

TABLE 16.6. Typical radiation doses from natural sources.

Radiation source	Detail	Effective dose rate to target organ (mSv yr <sup>-1</sup> )	U.S. population, average effective dose rate (mSv yr <sup>-1</sup> ) <sup>a</sup>
Cosmic radiation	New York City	0.30	0.27
	Denver (1.6 km)	0.50	
	La Paz, Bolivia (3.65 km)	1.8	
	Flying at 40,000 ft	7 × 10 <sup>-3</sup> mSv hr <sup>-1</sup>	
Terrestrial (radioactive minerals)			0.28
	Over fresh water	0	
	Over sea water	0.2	
	Sandy soil	0.1–0.25	
	Granite	1.3–1.6	
In the body			0.4
Inhalation of radon			2.0
Total			3.0

<sup>a</sup>NCRP Report 94 (1987) Table 9.7

TABLE 16.7. Typical radiation equivalent doses for the population of the United States. From NCRP 93.

Procedure	Equivalent dose (mSv)
Chest X ray (AP)	0.06
Skull X ray	0.2
Mammogram	0.3–0.6
CT	1–10
Barium enema	4.0
Coronary CT angiogram	5–12
Nuclear medicine—cardiovascular	7.1

radiation exposure. The radon entry in Table 16.6 is based on a  $W_R$  of 20 for  $\alpha$  particles from radon progeny, the value used by NCRP.<sup>29</sup> There is considerable uncertainty in this determination:  $W_R$  could be as low as 3, in which case radon would contribute much less to the natural background.

Diagnostic procedures give doses that are in general comparable to the average annual background dose, as can be seen in Table 16.7. The higher CT doses correspond to pediatric CT; see Fig. 16.56. One can explain

<sup>29</sup>The dose to the lungs from radon progeny is about 1 mGy yr<sup>-1</sup>. This is multiplied by  $W_r = 20$  and  $W_T = 0.12$  (lungs) to arrive at an effective dose of 2.4 mSv yr<sup>-1</sup>.

to a patient that a chest x ray is equivalent to about one week of natural background, and a mammogram is equivalent to a month or two. A conventional fluoroscopic study of the lower digestive system is equivalent to about a year of natural background.

### 16.13.3 Calculating Risk

Assessing the risk of radiation is complicated, since a radiation-induced cancer, for example, may not appear for many years. It is therefore necessary to specify how many years one watches a population after exposure, age at exposure, and current age. One also has to specify whether the risk is of acquiring the disease or of dying from it. Whatever criteria we use, we can define a risk  $r(H)$  that depends on the equivalent dose. We then define the *excess absolute risk*

$$EAR = r(H) - r(0) \tag{16.42}$$

and the *excess relative risk* as

$$ERR = \frac{r(H) - r(0)}{r(0)} = \frac{r(H)}{r(0)} - 1 = \frac{EAR}{r(0)}. \tag{16.43}$$

The units of  $r$  and excess absolute risk can vary. The risk might be per person per year, or it might be for a certain number of years or for a lifetime exposure. The excess relative risk has the advantage of being dimensionless. It is frequently reported, even though it can

be difficult to understand intuitively. (Plots of  $EAR$  vs. dose for breast cancer in Japanese women and women in the United States have nearly the same slope. However,  $r(0)$  is smaller for Japanese women, leading to a higher  $ERR$ .)

Consider a rare disease, and suppose that the probability of acquiring the disease over a lifetime is  $2 \times 10^{-3}$ , while in a population that has received a particular dose of something (which might be radiation, or a chemical, or a particular behavior) the probability is  $5 \times 10^{-3}$ . Then the excess absolute risk is  $3 \times 10^{-3}$ , while the excess relative risk is 150%. A person hearing that the relative risk has increased by 1.5 times might be unduly alarmed, not realizing that there are only three additional cases in 1,000 people.

Statistical fluctuations can make it quite difficult to measure excess risk. Suppose that we want to determine whether  $r$  increases linearly with dose. Measurements at lower doses to determine if the response is linear are difficult to make, requiring large numbers of subjects, as the following simplified example shows. Suppose that we have two measurements of the probability of acquiring cancer: one at zero dose, which gives  $r(0)$ , the “spontaneous” probability due to nonradiation causes, and one at a fairly large dose (say 0.25 Sv, represented by the vertical dashed line on the right in Fig. 16.54). At some lower dose we want to make a measurement to distinguish between a linear increase of probability with dose and a probability that remains at the “spontaneous” value because we are below some threshold dose for carcinogenicity. The probability  $p = r(H)$  of acquiring cancer is small, and the total population  $N$  is large. This means that if the experiment could be repeated several times on identical populations, the number of persons acquiring cancer,  $n$ , would be Poisson distributed with mean number  $m = Np = Nr(H)$  and standard deviation  $\sigma = \sqrt{m}$ . Figure 16.54 plots  $m$  vs dose for some value of  $N$ , with dotted lines to indicate  $m \pm \sigma$ . A measurement at the lower dose indicated by the vertical dashed line on the left will not distinguish between the two curves. The only way to reduce the width between the dotted lines at  $m \pm \sigma$  would be to use a larger population  $N$ .

To be quantitative, suppose that  $r(H) = e + \alpha H$ , with  $e = 0.044$  and  $\alpha = 0.013 \text{ Sv}^{-1}$ . At a dose of 0.25 Sv,  $r = 0.047$ . For  $10^5$  persons, the constant curve (expected in the absence of radiation or below threshold) gives  $m = 4,400 \pm 66$ , while the linear curve gives  $m = 4,730 \pm 69$ . The two curves are distinguishable. At a dose of 0.01 Sv,  $m$  for the constant curve is still  $4,400 \pm 66$ , while for the linear case it is  $4,410 \pm 66$ . It is impossible to distinguish between the linear and constant curves.

#### The Linear Nonthreshold Model and Collective Dose

In dealing with radiation to the population at large, or to populations of radiation workers, the policy of the various regulatory agencies has been to adopt the *linear-*

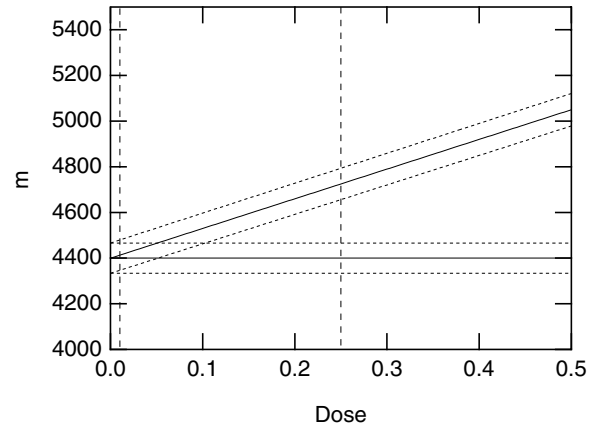


FIGURE 16.54. Plot of the average number of cases from a population  $N$  for a linear–no–threshold and a constant model. The dashed lines represent the mean  $\pm 1$  standard deviation.

*nonthreshold* (LNT) model to extrapolate from what is known about the excess risk of cancer at moderately high doses and high dose rates, to low doses, including those below natural background.

If the excess probability of acquiring a particular disease is  $\alpha H$  in a population  $N$ , the average number of extra persons with the disease is

$$m = \alpha NH. \quad (16.44)$$

The product  $NH$ , expressed in person-Sv, is called the *collective dose*. It is widely used in radiation protection, but it is meaningful only if the LNT assumption is correct. Small doses to very large populations can give fairly large values of  $m$ , assuming that the value of  $\alpha$  determined at large doses is valid at small doses.

It has been suggested that there may in some cases be a threshold for radiation-induced damage. If there is a threshold, then the LNT model gives an overestimate. The latest reports of expert panels continue to recommend the LNT model [NCRP Report 136 (2001), Upton (2003), BEIR Report VII (2005)], but their recommendation is still questioned [Higson (2004)].

To help put the risk in perspective, consider the following example from BEIR (2005), p. 15. Among 100 people, about 42 will be diagnosed with cancer during their lifetime in the absence of any excess radiation. If they had all received a dose of 0.1 Gy (100 mSv for low-LET radiation), there could be one additional cancer in the group.

Even if the LNT model is correct, it can lead to regulatory decisions which are not reasonable. For example, Brooks (2003) cites a study in which the process of cleaning up several Department of Energy sites resulted in more fatal worker accidents than the number of lives that were calculated to have been saved, based on the LNT model.



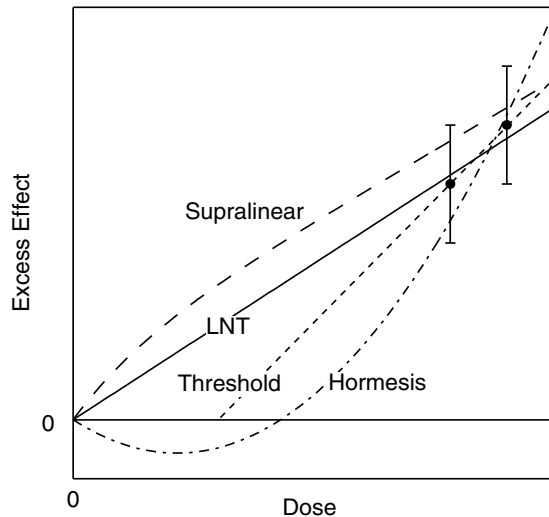


FIGURE 16.55. Possible responses to various doses. The two lowest-dose measurements are shown. With zero dose there is no excess effect. The curves are discussed in the text.

Other Models

Figure 16.55 plots the excess effect vs. dose, showing four possibilities for how some effect might depend on dose. By definition, there is no excess effect when the dose is zero. The two data points represent the lowest doses at which the effect has been measured. The LNT line is a linear interpolation to zero from these points. Lines are also shown for three other possibilities: (1) a *threshold* below which there is no excess effect, (2) a *supralinear* response, which is higher than predicted by the LNT model, and (3) *hormesis*. In hormesis there is a limited range in which the excess effect is negative—a reduction in the effect. Hormesis has been seen in the response of some organisms to chemicals and in some cases to radiation. Two issues of *Critical Reviews in Toxicology*, Vol. 31 No. 4–5 and Vol. 33, No. 3–4, have been devoted to reviews of hormetic effects in all fields.

Some investigators feel that there is evidence for a threshold dose, and that the LNT model overestimates the risk [Kathren (1996); Kondo (1993); Cohen (2002)]. Mossman (2001) argues against hormesis but agrees that the LNT model has led to “enormous problems in radiation protection practice” and unwarranted fears about radiation.

On the other hand, annual screening CTs [Brenner and Elliston (2004)] and CTs to children [Hall (2002)], lead to doses that are large enough so that there is a measured excess risk of developing cancer in an individual; no LNT extrapolation to lower doses is needed. This is shown in Fig. 16.56. A pediatric CT study can lead to a dose in the range of 5–100 mSv. This can be compared with data from the extensive study of 35,000 atomic bomb survivors who have been followed for 55 years. There is a

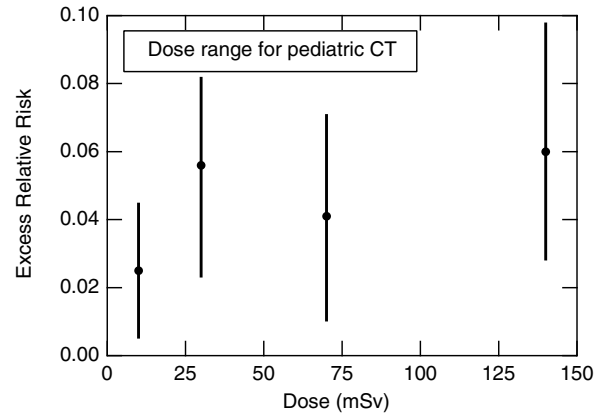


FIGURE 16.56. Excess relative risk for atomic bomb survivors who were exposed to a dose of 150 mSv or less and followed for 55 years show a small, but statistically significant increase in cancer incidence. The range of doses from pediatric CT is also shown. Redrawn from Hall, E. J. Helical CT and cancer risk: Introduction to session I. *Pediatr. Radiol.* **32**: 225–227 (2002). With kind permission of Springer Science and Business Media.

small but statistically significant excess risk of developing cancer.

16.13.4 Radon

The question of a hormetic effect or a threshold effect has received a great deal of attention for the case of radon, where remediation at fairly low radon levels has been proposed. Radon is produced naturally in many types of rock. It is a noble gas, but its radioactive decay products can become lodged in the lung. An excess of lung cancer has been well documented in uranium miners, who have been exposed to fairly high radon concentrations as well as high dust levels and tobacco smoke. Radon at lower concentrations seeps from the soil into buildings and contributes up to 55% of the exposure to the general population. Radon concentrations in the air are measured in the number of radioactive decays per second per cubic meter of air. One *becquerel* (Bq) is one decay per second.

Figure 16.57 shows a study by B. L. Cohen (1995) that plots annual age-adjusted lung-cancer mortality rates in 1601 counties in the United States vs the average radon concentration measured in that county. The radon concentration is expressed as  $r/r_0$ , where  $r_0$  is  $37 \text{ Bq m}^{-3}$  ( $1.0 \text{ pCi l}^{-1}$  in old units, which will be discussed in the next chapter). The upper two panels are for males, and the lower two are for females. The two panels on the right are corrected for the effects of smoking, using the radon-and-smoking model from BEIR Report V (1990). The dashed lines labeled *Theory* are based on the LNT model. The mortality rate falls with increasing radon concentration, though other studies have shown that it rises at radon concentrations higher than shown here.

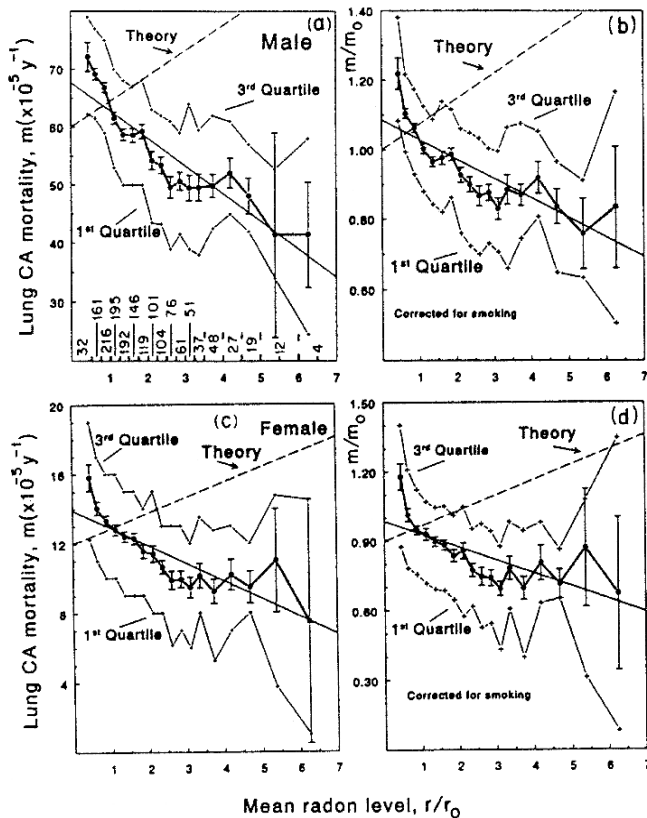


FIGURE 16.57. Lung cancer mortality rates vs mean radon level in 1601 U.S. counties. Graphs (a) and (b) are for males; (c) and (d) are for females. Graphs (b) and (d) have been corrected for smoking levels. Error bars show the standard deviation of the mean. The meaning of radon level is discussed in the text. From B. L. Cohen. Test of the linear-no threshold theory of radiation carcinogenesis for inhaled radon decay products. *Health Physics* **68**(2): 157–174, 1995. Used by permission of the Health Physics Society.

Epidemiological studies are difficult and can only be suggestive. A number of authors have criticized Cohen’s study for dealing with county-wide averages, and Cohen has defended his results.<sup>30</sup> Cohen argues that his data are valid below about 150 Bq m<sup>-3</sup>. Lubin (1999) compares an LNT fit and Cohen’s model to several other radon studies, shown in Fig. 16.58. The error bars are much larger than in Cohen’s figure because the populations are smaller. Lubin argues that this is irrelevant because Cohen has systematic errors. Cohen’s data points are not inconsistent with those shown by Lubin. Recall from Table 16.6 that the average annual dose from radon is about 2 mSv, and note where this lies on Fig. 16.56.

Even if the LNT model for radon is correct, some of our remediation efforts are misdirected. Ayotte *et al.* (1998) used the LNT model to assess the lung cancer risk from

<sup>30</sup>For example, see Lubin (1998); Cohen (1998); Lubin (1998b); Cohen (1999); Lubin (1999) and BEIR VI (1999).

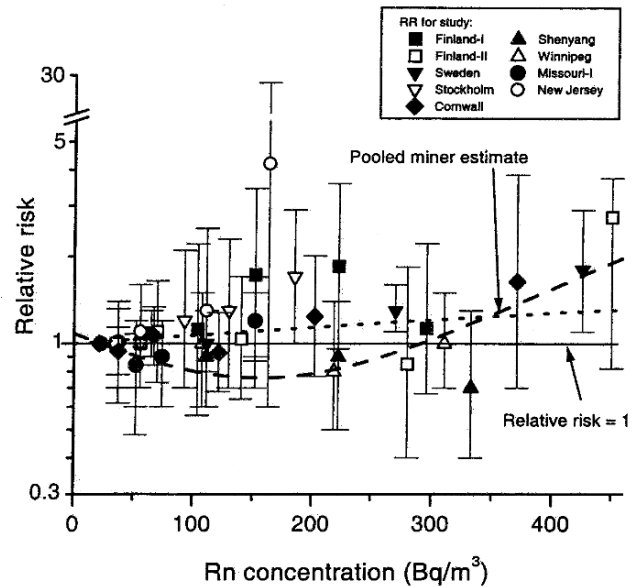


FIGURE 16.58. Relative risk (on a log scale) vs. radon concentration. The data points are for several studies, not including Cohen’s. The horizontal line shows a relative risk of 1. The dotted line is a linear extrapolation from the miner study. The dashed quadratic line is Cohen’s model. From Lubin, J. H. (1999). Response to Cohen’s comments on the Lubin rejoinder. *Health Phys.* **77**(3): 330–332. Used by permission.

radon in Québec. They predicted a total of 109 deaths from lung cancer in a population of 60,000. Mitigating radon in all residences with concentrations of 200 Bq m<sup>-3</sup> or more would reduce this number from 109 to 105. The same number of lives would be saved by reducing smoking by 0.04%.

## Symbols Used in Chapter 16

Symbol	Use	Units	First used on page
<i>b</i>	Thickness of slice being scanned	m	456
<i>c</i>	Velocity of light	m s <sup>-1</sup>	443
<i>e</i>	Electron charge	C	440
<i>f</i>	Fraction of photons that interact or detective quantum efficiency		451
<i>f</i>	General function to be represented		455
<i>g</i>	Incremental signal transfer function	kg C <sup>-1</sup>	442
<i>h</i>	Planck’s constant	J s	438
<i>j</i>	Total angular momentum quantum number		438

Symbol	Use	Units	First used on page	$Q$	Quality factor		
				$R$	Resistance	Ohm ( $\Omega$ )	444
				$S$	Area	$m^2$	452
$k$	Minimum signal-to-noise ratio		452	$S$	Surviving fraction		462
$k_B$	Boltzmann factor	$J K^{-1}$	445	$S_e$ (or $S_c$ )	Collision stopping power	$J m^{-1}$	467
$l$	Orbital angular momentum quantum number		438	$T$	Kinetic energy	J	438
$m$	Mass	kg	440	$T_0$	Initial kinetic energy	J	439
$m_e$	Mass of electron	kg	443	$T$	Optical transmission		441
$m$	Mean number		451	$T$	Temperature	K	445
$m$	Number of scans		457	$W$	Mean energy expended per ion pair formed	J or eV	439
$n$	Principal quantum number		438	$W_R$	Radiation weight factor		468
$n$	Number of slices in a scan		456	$W_T$	Tissue weighting factor		469
$n$	Number of moles of a substance	mol	439	$X$	Exposure	$C kg^{-1}$	440
$n$	Number of fractions		462	$Z$	Atomic number		437
$p$	Probability		463	$\alpha$	Integral of attenuation		454
$q$	Charge	C	440	$\alpha$	Dose proportionality constant	$Gy^{-1}$	460
$r$	Distance	m	447	$\alpha$	Excess risk proportionality constant	$Gy^{-1}$	471
$r$	Risk or probability	varies	470	$\beta$	Coefficient		457
$r, r_0$	Radon concentrations	$Bq m^{-3}$	472	$\beta$	Squared dose proportionality constant	$Gy^{-2}$	460
$v$	Voltage difference	V	444	$\gamma$	Fraction		457
$w$	Width of picture element	m	456	$\gamma$	Film contrast		441
$w_i$	Mass fraction of $i$ th constituent		447	$\mu, \mu_{atten}$	Attenuation coefficient	$m^{-1}$	447
$x$	Photon energy/electron rest mass energy		443	$\mu_{en}$	Energy absorption coefficient	$m^{-1}$	440
$x, y, z$	Coordinates	m	441	$\nu, \nu_0$	Frequency	Hz	438
$A$	Proportionality constant	$C m^2 kg^{-1}$	451	$\rho$	Density	$kg m^{-3}$	440
$C$	Constant	$J^{-1} m^{-2}$	438	$\sigma$	Standard deviation		471
$C$	Capacitance	F	444	$\Phi$	Particle fluence	$m^{-2}$	438
$C_{in}$	Exposure contrast		451	$\Phi_T$	Particle fluence per unit energy interval	$m^{-2} J^{-1}$ or $m^{-2} eV^{-1}$	467
$C_{out}$	Brightness contrast		451	$\Psi$	Energy fluence	$J m^{-2}$	438
$D$	Absorbed dose	$Gy (J kg^{-1})$	440				
$D'$	Absorbed dose in one scan	Gy	457				
$D_0$	Reciprocal of proportionality constant $\alpha$	Gy	460				
$D_{R,T}$	Absorbed dose of radiation type $R$ to target organ $T$	Gy	468				
$E$	Energy	J or eV	438				
$E$	Effective dose to an organ	$Sv (J kg^{-1})$	468				
$F$	Projection (integral) of $f$ along some direction		455				
$G$	Radiation chemical yield	$mol J^{-1}$	439				
$G$	Large signal transfer factor	$kg C^{-1}$	442				
$H$	Hounsfield CT unit		456				
$H$	Dose equivalent	$Sv (J kg^{-1})$	468				
$H_E$	Effective dose equivalent	Sv	469				
$H_T$	Equivalent dose	$Sv (J kg^{-1})$	468				
$K_c$	Collision kerma	$J kg^{-1}$	440				
$L$	Length of object	m	452				
$N$	Number		439				
OD	Optical density		441				
$P$	Probability		462				

## Problems

### Section 16.1

**Problem 1** Use Eqs. 15.3 and 16.2 to answer the following questions. Then compare your answers to values given in tables, such as those in the *Handbook of Chemistry and Physics*. What is the minimum energy of electrons striking a copper target that will cause the  $K$  x-ray lines to appear? What is the approximate energy of the  $K_\alpha$  line? Repeat for iodine, molybdenum, and tungsten.

**Problem 2** When tungsten is used for the anode of an x-ray tube, the characteristic tungsten  $K_\alpha$  line has a wavelength of  $2.1 \times 10^{-11} m$ . Yet a voltage of 69,525 V must be applied to the tube before the line appears. Explain the discrepancy in terms of an energy-level diagram for tungsten.

**Problem 3** Henry Moseley first assigned atomic numbers to elements by discovering that the square root of the frequency of the  $K_\alpha$  photon is linearly related to  $Z$ . Solve Eq. 16.2 for  $Z$  and show that this is true. Plot  $Z$  vs the square root of the frequency and compare it to data you look up.

**Problem 4** Compare the shapes of the curves of Eqs. 16.3a and 16.3b for  $h\nu_0 = 100$  keV, over the range 40–100 keV. Are the characteristics of Eq. 16.3b reflected in the theoretical points of Fig. 16.5?

**Problem 5** Express the formula for the thick-target x-ray energy fluence rate [Eq. 16.3a] as  $d\Psi/d\lambda$  and plot it.

**Problem 6** Starting from Eq. 16.3b, written as  $d\Phi/dE = (1/h\nu)d\Psi/d(h\nu)$ , use the chain rule to verify that  $d\Psi/d\lambda = (h^2c^2/\lambda^3)d\Phi/dE$ . (Recall that  $\lambda\nu = c$ .)

Section 16.2

**Problem 7** A beam of 0.08-MeV photons passes through a body of thickness  $L$ . Assume that the body is all muscle with  $\rho = 1.0 \times 10^3$  kg  $m^{-3}$ . The energy fluence of the beam is  $\Psi$  J  $m^{-2}$ .

(a) What is the skin dose where the beam enters the body?

(b) Assume the beam is attenuated by an amount  $e^{-\mu L}$  as it passes through the body. Calculate the average dose as a function of the fluence, the body thickness, and  $\mu$ .

(c) What is the limiting value of the average dose as  $\mu L \rightarrow 0$ ?

(d) What is the limiting value of the average dose as  $\mu L \rightarrow \infty$ ? Does the result make sense? Is it useful?

**Problem 8** The obsolete unit, the roentgen ( $R$ ), is defined as  $2.08 \times 10^9$  ion pairs produced in 0.001293 g of dry air. (This is 1  $cm^3$  of dry air at standard temperature and pressure.) Show that if the average energy required to produce an ion pair in air is 33.7 eV (an old value), then 1  $R$  corresponds to an absorbed dose of  $8.69 \times 10^{-3}$  Gy and that 1  $R$  is equivalent to  $2.58 \times 10^{-4}$  C  $kg^{-1}$ .

**Problem 9** During the 1930s and 1940s it was popular to have an x-ray fluoroscope unit in shoe stores to show children and their parents that shoes were properly fit. These marvellous units were operated by people who had no concept of radiation safety and aimed a beam of x rays upward through the feet and right at the reproductive organs of the children! A typical unit had an x-ray tube operating at 50 kVp with a current of 5 mA.

(a) What is the radiation yield for 50-keV electrons on tungsten? How much photon energy is produced with a 5-mA beam in a 30-s exposure?

(b) Assume that the x rays are radiated uniformly in all directions (this is not a good assumption) and that the x rays are all at an energy of 30 keV. (This is a very poor assumption.) Use the appropriate values for striated muscle to estimate the dose to the gonads if they are at a distance of 50 cm from the x-ray tube. Your answer will be an overestimate. Actual doses to the feet were typically 0.014–0.16 Gy. Doses to the gonads would be less because of  $1/r^2$ . Two of the early articles pointing out the danger are Hempelmann, L. H. (1949), Potential dangers in the uncontrolled use of shoe fitting fluoroscopes, *New Engl. J.*

*Med.* **241**: 335–337, and Williams, C. R. (1949), Radiation exposures from the use of shoe-fitting fluoroscopes, *New Engl. J. Med.* **241**: 333–335.

Section 16.3

**Problem 10** Rewrite Eq. 16.9 in terms of exponential decay of the viewing light and relate the optical density to the attenuation coefficient and thickness of the emulsion.

**Problem 11** Derive the useful rule of thumb  $\Delta(OD) = 0.43\gamma \Delta X/X$ .

**Problem 12** The atomic cross sections for the materials in a gadolinium oxysulfide screen for 50-keV photons are

Element	Cross section per atom ( $m^2$ )	A
Gd	$1.00 \times 10^{-25}$	157
S	$3.11 \times 10^{-27}$	32
O	$5.66 \times 10^{-28}$	16

(a) What is the cross section per target molecule of  $GdO_2S$ ?

(b) How many target molecules per unit area are there in a thickness  $px$  of material?

(c) What is the probability that a photon interacts in traversing 1.2 kg  $m^{-2}$  of  $GdO_2S$ ?

**Problem 13** The film speed is often defined as the reciprocal of the exposure (in roentgens) required to give an optical density that is 1 greater than the base density. Assume that in Fig. 16.6 a relative exposure of 1 corresponds to  $10^{-5}$  C  $kg^{-1}$ . Calculate the film speed.

**Problem 14** A dose of  $1.74 \times 10^{-4}$  Gy was estimated for part of the body just in front of an unscreened x-ray film. Suppose that a screen permits the dose to be reduced by a factor of 20. Calculate the skin dose on the other side of the body (the entrance skin dose) assuming 50-keV photons and a body thickness of 0.2 m. Ignore buildup, and assume that only unattenuated photons are detected.

**Problem 15** Find an expression for photon fluence per unit absorbed dose in a beam of monoenergetic photons. Then find the photon fluence for 50-keV photons that causes a dose of  $10^{-5}$  Gy in muscle.

**Problem 16** A dose of 100 Gy might cause noticeable radiation damage in a sodium iodide crystal. How long would a beam of 100-keV photons have to continuously and uniformly strike a crystal of 1- $cm^2$  area at the rate of  $10^4$  photon  $s^{-1}$ , in order to produce this absorbed dose? For  $NaI \mu_{en}/\rho = 0.1158$   $m^2$   $kg^{-1}$ .

**Problem 17** Another method to measure the absorbed dose is by calorimetry. Show that if all the energy imparted warms the sample, the temperature rise is  $2.39 \times 10^{-4}$  °C per Gy.

Section 16.4

**Problem 18** Plot  $\mu$  for lead, iodine, and barium from 10 to 200 keV.

**Problem 19** Use a spreadsheet to make the following calculations. Consider a photon beam with 100 kVp.

(a) Use Eq. 16.3b to calculate the photon fluence from a thick target at 1, 10, 20, 30, 40, 50, 60, 70, 80, 90, and 100 keV.

(b) The specific gravity of aluminum is 2.7. Make a table of the photon fluence at these energies emerging from 2 and 3 mm of aluminum. Compare the features of this table to Fig. 16.16.

(c) Use trapezoidal integration to show that the average photon energy is 44 keV after 2-mm filtration and 47 keV after 3-mm filtration.

(d) Repeat for 120 kVp and show that the average energies after the same filtrations are 52 and 55 keV.

**Problem 20** X-ray beams have a spectrum of photon energies. It would be very laborious to measure the spectrum every time we want to check the quality of the beam. In addition to kVp, one simple measurement that is used to check beam quality (related to the energy spectrum) is the “half-value layer” HVL—the thickness of a specified absorber (often Cu or Al) that reduces the intensity of the beam to one-half.

(a) For a monoenergetic beam, relate HVL to the attenuation coefficient. What is the HVL if the attenuation coefficient is  $0.46 \text{ mm}^{-1}$ ?

(b) For a monoenergetic beam, how does the quarter-value layer QVL relate to HVL?

(c) Suppose a beam has equal numbers of photons at two different energies. The attenuation coefficients at these energies are  $0.46 \text{ mm}^{-1}$  and  $0.6 \text{ mm}^{-1}$ . Find the HVL and QVL for this beam. You may need to plot a graph or use a computer algebra program.

**Problem 21** The “half-value layer” (HVL) is often used to characterize an x-ray beam. It is the thickness of a specified absorber that attenuates the beam to one-half the original value. Figure 16.45 refers to a beam with a 3.0 mm Cu HVL. What is the value of the attenuation coefficient? What monoenergetic x-ray beam does this correspond to?

**Problem 22** Assume an antiscatter grid is made of lead sheets 3 mm long with a spacing between sheets of 0.3 mm. Ignore the thickness of the sheets. If all photons hitting the sheets are absorbed, what is the largest angle from the incident beam direction that a photon can be scattered and still emerge?

Section 16.5

**Problem 23** Suppose that two measurements are made: one of the combination of signal and noise,  $y = s + n$ ,

and one of just the noise  $n$ . One wishes to determine  $s = y - n$ .

(a) Find  $s - \bar{s}$  in terms of  $y, \bar{y}, n,$  and  $\bar{n}$ .

(b) Show that if  $y$  and  $n$  are “uncorrelated,”  $\overline{(s - \bar{s})^2} = \overline{(y - \bar{y})^2} + \overline{(n - \bar{n})^2}$  and state the mathematical condition for being “uncorrelated.”

(c) If  $y$  and  $n$  are Poisson distributed, under what conditions is the  $\sqrt{2}$  factor of Footnote 13 needed?

Section 16.7

**Problem 24** A molybdenum target is used in special x-ray tubes for mammography. The electron energy levels in Mo are as follows:

K	20,000 eV	$L_I$	2886 eV	$M_I$	505 eV
		$L_{II}$	2625 eV	$M_{II}$	410 eV
		$L_{III}$	2520 eV	$M_{III}$	392 eV
				$M_{IV}$	230 eV
				$M_V$	227 eV

What is the energy of the  $K_\alpha$  line(s)? The  $K_\beta$  line(s) (defined in Fig. 16.2)?

**Problem 25** As a simple model for mammography, consider two different tissues: a mixture of 2/3 fat and 1/3 water, with a composition by weight of 12% hydrogen, 52% carbon and 36% oxygen; and glandular tissue, composed of 11% hydrogen, 33% carbon, and 56% oxygen. The density of the fat and water combination is  $940 \text{ kg m}^{-3}$ , and the density of glandular tissue is  $1020 \text{ kg m}^{-3}$ . What is the attenuation in 1 mm of fat and in 1 mm of glandular tissue for 50-keV photons? For 30-keV photons?

Section 16.9

**Problem 26** For a first-generation CT scanner with  $\mu = 18 \text{ m}^{-1}$ ,  $\Delta\mu/\mu = 0.005$ ,  $L = 30 \text{ cm}$ ,  $w = 0.1 \text{ cm}$ , and  $b = 1 \text{ cm}$ , calculate, for a scan time of 15 s,

- (a)  $N$ ,
- (b)  $m$ ,
- (c)  $N'$ , and
- (d) The dose.

**Problem 27** It is often said that the number of photons that must be detected in order to measure a difference in fluence with a certain resolution can be calculated from  $N = (\Delta\Phi/\Phi)^{-2}$ . (For example, if we want to detect a change in  $\Phi$  of 1% we would need to count  $10^4$  photons.) Use Eq. 16.20 to make this statement more quantitative. Discuss the accuracy of the statement.

**Problem 28** Spiral CT uses interpolation to calculate the projections at a fixed value of  $z$  before reconstruction. This has an effect on the noise. Let  $\sigma_0$  be the noise standard deviation in the raw projection data and  $\sigma$  be the noise in the interpolated data. The interpolated signal,  $\alpha$ , is the weighted sum of two values:  $\alpha = w\alpha_1 + (1 - w)\alpha_2$ .

(a) Show that the variance in  $\alpha$  is  $\sigma^2 = w^2\sigma_0^2 + (1-w)^2\sigma_0^2$ . Plot  $\sigma/\sigma_0$  vs  $w$ .

(b) Averaging over a  $360^\circ$  scan involves integrating uniformly over all weights:

$$\sigma^2 = \int_0^1 [w^2\sigma_0^2 + (1-w)^2\sigma_0^2] dw.$$

Find the ratio  $\sigma/\sigma_0$ .

**Problem 29** An experimental technique to measure cerebral blood perfusion is to have the patient inhale xenon, a noble gas with  $Z = 54$ ,  $A = 131$  [Suess et al. (1995)]. The solubility of xenon is different in red cells than in plasma. The equation used is

$$\text{Arterial enhancement} = \frac{5.15\theta_{Xe}}{(\mu/\rho)_w/(\mu/\rho)_{Xe}} C_{Xe}(t),$$

where the arterial enhancement is in Hounsfield units,  $C_{Xe}$  is the concentration of xenon in the lungs (end tidal volume), and

$$\theta_{Xe} = (0.011)(Hct) + 0.10.$$

*Hct* is the hematocrit: the fraction of the blood volume occupied by red cells. Discuss why the equation has this form.

### Section 16.10

**Problem 30** Use Equations 16.32 and 16.33 to obtain expressions for dose vs number of tumor cells for a probability of cure of 50%.

### Section 16.11

**Problem 31** Geiger's rule is an approximation to the range-energy relationship:

$$R = AE^p.$$

For protons in water  $A = 0.0022$  when  $R$  is in cm and  $E$  is in MeV. The exponent  $p = 1.77$ . This is a good approximation for  $E < 200$  MeV. Use Geiger's approximation to find  $dE/dx$  as a function of  $R$  for 100 MeV protons. Make a plot to show the Bragg peak when straggling is ignored.

### Section 16.12

**Problem 32** Calculate  $(\bar{S}_e/\rho)_g^w$  in argon for 0.1-, 1.0- and 10-MeV electrons. The values of  $S_e/\rho$  for argon at these energies are 2.918, 1.376, and 1.678  $\text{cm}^2 \text{g}^{-1}$ .

**Problem 33** An ion chamber contains  $10 \text{ cm}^3$  of air at standard temperature and pressure. Find  $q$  vs  $D$  for 0.5-MeV electrons.

### Section 16.13

**Problem 34** Suppose that the probability  $p$  per year of some event (death, mutations, cancer, etc.) consists of a spontaneous component  $S$  and a component proportional to the dose of something else,  $D$ :  $p = S + AD$ . The dose may be radiation, chemicals, sunlight, etc. Investigations of women given mammograms showed that if  $p$  is the probability of acquiring breast cancer,  $S = 1.91 \times 10^{-3}$  and  $A = 4 \times 10^{-4} \text{ Gy}^{-1}$ . How many women had to be studied to distinguish between  $A = 0$  and the value above if  $D = 2 \text{ Gy}$ ? If  $D = 10^{-2} \text{ Gy}$ ?

## References

AAPM Report 87 (2005). *Diode in Vivo Dosimetry for Patients Receiving External Beam Radiation Therapy*. College Park, MD. American Association of Physicists in Medicine. Report of Task Group 62 of the Radiation Therapy Committee.

Attix, F. H. (1986). *Introduction to Radiological Physics and Radiation Dosimetry*. New York, Wiley.

Ayotte, P., B. Lévesque, D. Gauvin, R. G. McGregor, R. Martel, S. Gingras, W. B. Walker, and E. G. Létourneau (1998). Indoor exposure to  $^{222}\text{Rn}$ : A public health perspective. *Health Phys.* **75**(3): 297–302.

Barth, R. F. (2003). A critical assessment of boron neutron capture therapy: an overview. *J. Neuro-Oncol.* **62**: 1–5. The entire issue of the journal is devoted to a review of BNCT.

BEIR Report V (1990). *Health Effects of Exposure to Low Levels of Ionizing Radiation*. Washington, DC, National Academy Press. Committee on the Biological Effects of Ionizing Radiation.

BEIR VI (1999). Committee on Health Risks of Exposure to Radon. *Health Effects of Exposure to Radon*. Washington, D.C., National Academy Press.

BEIR Report VII (2005). *Health Risks from Exposure to Low Levels of Ionizing Radiation*. Washington, DC, National Academy Press. Committee to Assess Health Risks from Exposure to Low Levels of Ionizing Radiation.

Birch, R., and M. Marshall (1979). Computation of bremsstrahlung x-ray spectra and comparison with spectra measured with a Ge(Li) detector. *Phys. Med. Biol.* **24**: 505–517.

Boice, J. D., Jr. (1996). Risk estimates for radiation exposures. In W. R. Hendee and F. M. Edwards, eds. *Health Effects of Exposure to Low-Level Ionizing Radiation*. Bristol, Institute of Physics.

Brenner, D. J., and C. D. Elliston (2004). Estimated radiation risks potentially associated with full-body CT screening. *Radiology* **232**: 735–738.

Broad, W. J. (1980). Riddle of the Nobel debate. *Science* **207**: 37–38.

- Brooks, A. L. (2003). Developing a scientific basis for radiation risk estimates: Goal of the DOE low dose research program. *Health Phys.* **85**(1): 85–93.
- Brooks, R. A., and G. DiChiro (1976). Principles of computer-assisted tomography in radiographic and radioisotope imaging. *Phys. Med. Biol.* **21**: 689–732; Statistical limitations in x-ray reconstructive tomography. *Med. Phys.* **3**: 237–240.
- Cho, Z.-H., J. P. Jones, and M. Singh (1993). *Foundations of Medical Imaging*. New York, Wiley-Interscience.
- Cohen, B. L. (1995). Test of the linear-no threshold theory of radiation carcinogenesis for inhaled radon decay products. *Health Phys.* **68**(2): 157–174.
- Cohen, B. L. (1998). Response to Lubin's proposed explanations of the discrepancy. *Health Phys.* **75**(1): 18–22.
- Cohen, B. L. (1999). Response to the Lubin rejoinder. *Health Phys.* **76**(4): 437–439.
- Cohen, B. L. (2002). Cancer risk from low-level radiation.[see comment]. *AJR. Amer. J. Roentgenology.* **179**(5):1137–43.
- Cohen, L. (1993). History and future of empirical and cell kinetic models for risk assessment in radiation oncology. In B. Paliwal, *et al.*, eds. *Prediction of Response in Radiation Therapy: Radiosensitivity and Repopulation*. Woodbury, NY, AIP for the American Association of Physicists in Medicine.
- Cormack, A. M. (1980). Nobel award address: Early two-dimensional reconstruction and recent topics stemming from it. *Med. Phys.* **7**(4): 277–282.
- Dainty, J. C., and R. Shaw (1974). *Image Science*. New York, Academic.
- DeVita, V. T. (2003). Hodgkin's disease—Clinical trials and travails. *New Engl. J. Med.* **348** (24): 2375–2376.
- DiChiro, G., and R. A. Brooks (1979). The 1979 Nobel prize in physiology or medicine. *Science.* **206**: 1060–1062.
- Doi, K., H. K. Genant, and K. Rossman (1976). Comparison of image quality obtained with optical and radiographic magnification techniques in fine-detail skeletal radiography: Effect of object thickness. *Radiology.* **118**: 189–195.
- Douglas, J. G., W. J. Koh, M. Austin-Seymour, and G. E. Laramore (2003). Treatment of salivary gland neoplasms with fast neutron radiotherapy. *Arch. Otolaryngol.-Head & Neck Surg.* **129**(9): 944–948.
- Duncan, W. (1994). An evaluation of the results of neutron therapy trials. *Acta Oncolog.* **33**(3): 299–306. This issue of the journal is devoted to fast-neutron therapy.
- Evans, R. D. (1955). *The Atomic Nucleus*. New York, McGraw-Hill.
- Goodsitt, M., E. Christodoulou, P. Strouse, A. Chien, J. Platt and E. Kazerooni (2002). Radiation doses for corresponding CT and radiographic/fluoroscopic exams. *Med. Phys.* **29**(6): 1298. (Meeting abstract)
- Habrand, J. L., P. Schlienger, L. Schwartz, D. Pontvert, C. Lenir-Cohen-Solal, S. Helfre, C. Haie, A. Mazal, and J. M. Cosset (1995). Clinical applications of proton therapy. Experiences and ongoing studies. *Radiat. Environment. Biophys.* **34**(1): 41–44.
- Hall, E. J. (2000). *Radiobiology for the Radiologist*. 5th ed. Philadelphia, Lippincott Williams & Wilkins.
- Hall, E. J. (2002). Helical CT and cancer risk: Introduction to session I. *Pediatr. Radiol.* **32**: 225–227.
- Hall, E. J. (2003). The bystander effect. *Health Phys.* **85**(1): 31–35.
- Hendee, W. R., and R. Ritenour (2002). *Medical Imaging Physics*, 4th. ed. New York, Wiley-Liss.
- Higson, D. J. (2004). The bell tolls for LNT. *Health Phys.* **87**(Supplement 2): S47–S50.
- Holmes, T. W., T. R. Mackie, and P. Reckwerdt (1995). An iterative filtered backprojection inverse treatment planning algorithm for tomotherapy. *Int. J. Radiation Oncolog. Biol. Phys.* **32**(4): 1215–1225.
- Hounsfield, G. N. (1980). Nobel award address: Computed medical imaging. *Med. Phys.* **7**(4): 283–290.
- Hubbell, J. H., and S. M. Seltzer (1996). *Tables of X-Ray Mass Attenuation Coefficients and Mass Energy-Absorption Coefficients 1 keV to 20 MeV for Elements Z=1 to 92 and 48 Additional Substances of Dosimetric Interest*. National Institute of Standards and Technology Report NISTIR 5632. [physics.nist.gov/PhysRefData/XrayMassCoef/cover.html](http://physics.nist.gov/PhysRefData/XrayMassCoef/cover.html)
- Huda, W. (2002). Adult and pediatric dose in CT. *Med. Phys.* **29**(6): 1363. Meeting abstract.
- Hunt, D. C., S. S. Kirby, and J. A. Rowlands (2002). X-ray imaging with amorphous selenium: X-ray to charge conversion gain and avalanche multiplication gain. *Med. Phys.* **29**(11): 2464–2471.
- ICRP (1991). 1990 Recommendations of the International Commission on Radiological Protection. *Annals of the ICRP.* **21** no. 1–3.
- ICRU Report 31 (1979). *Average Energy to Produce an Ion Pair*. Bethesda, MD, International Commission on Radiation Units and Measurements.
- ICRU Report 33 (1980, Reprinted 1992). *Radiation Quantities and Units*. Bethesda, MD, International Commission on Radiation Units and Measurements.
- ICRU Report 37 (1984). *Stopping Powers for Electrons and Positrons*. Bethesda, MD, International Commission on Radiation Units and Measurements.
- ICRU Report 39 (1985). *Determination of Dose Equivalents Resulting from External Radiation Sources*. Bethesda, MD, International Commission on Radiation Units and Measurements.
- ICRU Report 41 (1986). *Modulation Transfer Function of Screen-Film Systems*. Bethesda, MD, International Commission on Radiation Units and Measurements.
- ICRU Report 54 (1996). *Medical Imaging—The Assessment of Image Quality*. Bethesda, MD, International Commission on Radiation Units and Measurements.
- Kalender, W. A. (2000). *Computed Tomography: Fundamentals, System Technology, Image Quality and Applications*. Munich, Publicis MCD.

- Kassis, A. I. (2004). The amazing world of Auger electrons. *Int. J. Rad. Biol.*, **80**(11-12): 789–803.
- Kathren, R. L. (1996). Pathway to a paradigm: The linear nonthreshold dose-response model in historical context: The American Academy of Health Physics 1995 Radiology Centennial Hartman Oration. *Health Phys.* **70**(5): 621–635.
- Khan, F. M. (2003). *The Physics of Radiation Therapy*. 3rd ed. Philadelphia, Lippincott Williams & Wilkins.
- Kondo, S. (1993). *Health Effects of Low-Level Radiation*. Osaka, Japan, Kinki University Press. English translation: Madison, WI, Medical Physics.
- Lubin, J. H. (1998). On the discrepancy between epidemiologic studies in individuals of lung cancer and residential radon and Cohen's ecologic regression. *Health Phys.* **75**(1): 4–10.
- Lubin, J. H. (1998b). Rejoinder: Cohen's response to "On the discrepancy between epidemiologic studies in individuals of lung cancer and residential radon and Cohen's ecologic regression." *Health Phys.* **85**(1): 29–30.
- Lubin, J. H. (1999). Response to Cohen's comments on the Lubin rejoinder. *Health Phys.* **77**(3): 330–332.
- Lutz, G. (1999). *Semiconductor Radiation Detectors*. New York, Springer.
- Macovski, A. (1983). *Medical Imaging Systems*. Englewood Cliffs, NJ, Prentice-Hall.
- McCollough, C. H. and B. A. Schueler (2000). Educational Treatise: Calculation of effective dose. *Med. Phys.* **27**(5): 828–837.
- Metz, C. E., and K. Doi (1979). Transfer function analysis of radiographic imaging systems. *Phys. Med. Biol.* **24**(6): 1079–1106.
- Miralbell, R., A. Lomax, L. Cella, and U. Schneider (2002). Potential reduction of the incidence of radiation-induced second cancers by using proton beams in the treatment of pediatric tumors. *Int. J. Radiation Oncology Biol. Phys.* **54**(3): 824–829.
- Mossman, K. L. (2001). Deconstructing radiation hormesis. *Health Phys.* **80**(3): 263–269.
- Moulder, J. E., and J. D. Shadley (1996). Radiation interactions at the cellular and tissue levels. In W. R. Hendee and F. M. Edwards, eds. *Health Effects of Exposure to Low-Level Ionizing Radiation*. Bristol, Institute of Physics.
- Moyers, M. (2003). Proton therapy refresher course, Part II. Practical challenges and opportunities for proton therapy. *Med. Phys.* **30**(6): 1445–1446.
- Nagel, H. D., M. Galanski, N. Hidajat, W. Maer and T. Schmidt (2000). *Radiation Exposure in Computed Tomography: Fundamentals, Influencing Parameters, Dose Assessment, Optimisation, Scanner Data, Terminology*. COCIR, European Coordination Committee of the Radiological and Electromedical Industries. Hamburg, CTB Publications (ctb-publications@gmx.de)
- NCRP Report 93 (1987). *Ionizing Radiation Exposure of the Population of the United States*. Bethesda, MD, National Council on Radiation Protection and Measurements.
- NCRP Report 94 (1987). *Exposure of the Population in the United States and Canada from Natural Background Radiation*. Bethesda, MD, National Council of Radiation Protection and Measurements.
- NCRP Report 100 (1989). *Exposure of the U.S. Population from Diagnostic Medical Radiation*. Bethesda, MD, National Council of Radiation Protection and Measurements.
- NCRP Report 136 (2001). *Evaluation of the Linear-Nonthreshold Dose-Response Model for Ionizing Radiation*. Bethesda, MD, National Council of Radiation Protection and Measurements.
- Orton, C. (1997). Fractionation: Radiobiological principles and clinical practice. Chapter 11 in F. M. Khan and R. A. Potish, eds. *Treatment Planning in Radiation Oncology*. Baltimore, MD, Williams and Wilkins.
- Platzman, R. L. (1961). Total ionization in gases by high-energy particles: An appraisal of our understanding. *Intl. J. Appl. Rad. Isotopes* **10**: 116–127.
- Rowlands, J. A. (2002). The physics of computed radiography. *Phys. Med. Biol.* **47**: R123–R126.
- Schlesinger, T. E. and R. B. James, eds. (1995). *Semiconductors for Room Temperature Nuclear Applications*. New York, Academic Press.
- Schulz, R. J., and A. R. Kagan (2002). On the role of intensity-modulated radiation therapy in radiation oncology. *Med. Phys.* **29**(7): 1473–1482.
- Seibert, J. A. (2003). Digital fluoroscopic imaging: Acquisition, processing and display. *Med. Phys.* **30**(6): 1413.
- Shabashon, L. (1996). Radiation interactions: Physical and chemical effects. In W. R. Hendee and F. M. Edwards, eds. *Health Effects of Exposure to Low-Level Ionizing Radiation*. Bristol, Institute of Physics.
- Shani, G. (1991). *Radiation Dosimetry: Instrumentation and Methods*. Boca Raton, FL, CRC Press.
- Shani, G. (2001). *Radiation Dosimetry: Instrumentation and Methods*. 2nd. ed. Boca Raton, FL, CRC Press.
- Slater, J. D., C. J. Rossi, Jr., L. T. Yonemoto, D. A. Bush, B. R. Jabola, R. P. Levy, R. I. Grove, W. Preston, and J. M. Slater (2004). Proton therapy for prostate cancer: The initial Loma Linda University experience. *Int. J. Radiat. Oncol. Biol. Phys.* **59**(2): 348–352.
- Sobol, W. T. (2002). High frequency x-ray generator basics. *Med. Phys.* **29**(2): 132–144.
- Steel, G. G. (1996). From targets to genes: a brief history of radiosensitivity. *Phys. Med. Biol.* **41**(2): 205–222.
- Suess, C., A. Polacin, and W. A. Kalender (1995). Theory of xenon/computed tomography cerebral blood flow methodology. In M. Tomanaga, A. Tanaka, and H. Yonas, eds. *Quantitative Cerebral Blood Flow Measurements Using Stable Xenon/CT: Clinical Applications*. Armonk, NY, Futura.
- Suit, H., and M. Urie (1992). Proton beams in radiation therapy. *J. Natl. Cancer Inst.* **84**(3): 155–164.



- Upton, A. C. (2003). The state of the art in the 1990's: NCRP Report No. 136 on the scientific bases for linearity in the dose-response relationship for ionizing radiation. *Health Phys.* **85**(1): 15–22.
- van Eijk, C. W. E. (2002). Inorganic scintillators in medical imaging. *Phys. Med. Biol.* **47**: R85–R106
- Wagner, R. F. (1977). Toward a unified view of radiological imaging systems. Part II: Noisy images. *Med. Phys.* **4**(4): 279–296.
- Wagner, R. F. (1983). Low-contrast sensitivity of radiologic, CT, nuclear medicine, and ultrasound medical imaging systems. *IEEE Trans. Med. Imaging* **MI-12**(3): 105–121.
- Wagner, R. F., K. E. Weaver, E. W. Denny, and R. G. Bostrom (1974). Toward a unified view of radiological imaging systems. Part I: Noiseless images. *Med. Phys.* **1**(1): 11–24.
- Webb, S. (2001). *Intensity-Modulated Radiation Therapy*. Bristol and Philadelphia. Institute of Physics Publishing.
- Winsor, R. (2003). CCD digital detectors. *Med. Phys.* **30**(6): 1433. Meeting abstract.

## Nuclear Physics and Nuclear Medicine

Each atom contains a nucleus about 100,000 times smaller than the atom. The nuclear charge determines the number of electrons in the neutral atom and hence its chemical properties. The nuclear mass determines the mass of the atom. For a given nuclear charge there can be a number of nuclei with different masses or *isotopes*. If an isotope is unstable, it transforms into another nucleus through *radioactive decay*.

In this chapter we will consider some of the properties of radioactive nuclei and their use for medical imaging and for treatment, primarily of cancer.

Four kinds of radioactivity measurements have proven useful in medicine. The first involves no administration of a radioactive substance to the patient. Rather, a sample from the patient (usually blood) is mixed with a radioactive substance in the laboratory, and the resulting chemical compounds are separated and counted. This is the basis of various *competitive binding assays*, such as those for measuring thyroid hormone and the availability of iron-binding sites. The most common competitive binding technique is called *radioimmunoassay*. A wide range of proteins are measured in this manner.

In the second kind of measurement, radioactive tracers are administered to the patient in a way that allows the volume of a compartment within the body to be measured. Examples of such compartments are total body water, plasma volume, and exchangeable sodium. Time-dependent measurements include red-blood-cell survival and iron and calcium kinetics. Counting is of the whole body or of blood or urine samples drawn at different times after administration of the isotope.

For the third class of measurements, a *gamma camera* generates an image of an organ from radioactive decay of a drug that has been administered and taken up by the organ. These images are often made as a function of time.

The fourth class is an extension of these in which tomographic reconstructions of body slices are made. These include *single-photon emission computed tomography* and *positron emission tomography*.

Radioactive isotopes are also used for therapy. The patient is given a radiopharmaceutical that is selectively absorbed by a particular organ (for example, radioactive iodine for certain thyroid diseases). The isotope emits charged particles that lose their energy within a short distance, thereby giving a high dose to the target organ. Isotopes are also used in self-contained implants for *brachytherapy*.

The first four sections introduce some of the nuclear properties that are important: size, mass, and the modes of radioactive decay and the amount of energy released.

It is important to know the dose to the patient from a nuclear medicine procedure, and a standard technique for calculating it has been developed by the Medical Internal Radiation Dose (MIRD) Committee of the Society of Nuclear Medicine. Sections 17.5–17.8 show the steps in making these calculations. Section 17.9 describes some of the pharmacological considerations in selecting a suitable isotope, and Sec. 17.10 provides a sample dose calculation using this technique. Section 17.11 extends the dose discussion to the special considerations when an isotope emits Auger electrons and is bound to the DNA in the cell nucleus.

The next few sections describe various ways of forming images. Section 17.12 describes the gamma camera, and Sec. 17.13 extends this to single-photon emission tomography. Section 17.14 describes positron emission tomography, which can be done with special equipment when positron sources are available in the hospital.

Radiotherapy is described in Sec. 17.15, including both the relatively common brachytherapy and the less common injection of isotopes that target particular organs.

TABLE 17.1. Properties of nucleons, the electron, and the neutral hydrogen atom.

Property	Neutron	Proton	Electron	H atom
Mass <sup>a</sup>	1.008 664 916	1.007 276 47	0.000 548 579 9	1.007 825 035
Charge <sup>b</sup>	0	+e	-e	0
Rest energy $m_0c^2$ (MeV)	939.565	938.272	0.5110	938.783
Half-life	≈ 12 min	Stable	Stable	Stable
Spin	$\frac{1}{2}$	$\frac{1}{2}$	$\frac{1}{2}$	...

<sup>a</sup>1 u is the mass unit; the mass of <sup>12</sup>C is 12.000 u by definition;  
 1 u = 1.660 539 × 10<sup>-27</sup> kg.  
<sup>b</sup>e = 1.602 177 × 10<sup>-19</sup> C.

The final section describes the nuclear decay of radon and some of the considerations in calculating the dose and the risk to the general population. It supplements the material that was introduced in Sec. 16.13.

### 17.1 Nuclear Systematics

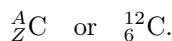
An atomic nucleus is composed of  $Z$  protons and  $N = A - Z$  neutrons. We call  $Z$  the *atomic number* and  $A$  the *mass number*. Neutrons and protons have very similar properties, as can be seen from Table 17.1. Therefore, they are classed as two different charge states of one particle, the *nucleon*.

Table 17.1 lists the *rest mass* and the *rest energy*, the rest mass times the square of the speed of light. One can show using special relativity that the total energy  $E$  of an object with rest mass  $m_0$  is related to its speed  $v$  and kinetic energy  $T$  by

$$E = \frac{m_0c^2}{(1 - v^2/c^2)^{1/2}} = m_0c^2 + T. \tag{17.1}$$

In this equation  $c$  is the velocity of light. The energy and mass of both the proton and neutral hydrogen atom are given; the distinction will be important later.

It is customary to specify a nucleus by a symbol such as the following for carbon ( $Z = 6, N = 6, A = 12$ ):



The mass number used to be written as a superscript on the right; however, this becomes confusing if the ionization state must also be specified. It is now customary to leave the right side of the symbol for atomic properties. Since the element symbol corresponds to a specific atomic number,  $Z$  is often omitted.

Different nuclei of the same element with different numbers of neutrons are called *isotopes*. Another isotope of carbon is <sup>11</sup>C, which has five neutrons.

The sizes of atoms are roughly constant as one goes through the Periodic Table, with exceptions as shells are filled. On the other hand, the size of nuclei grows steadily

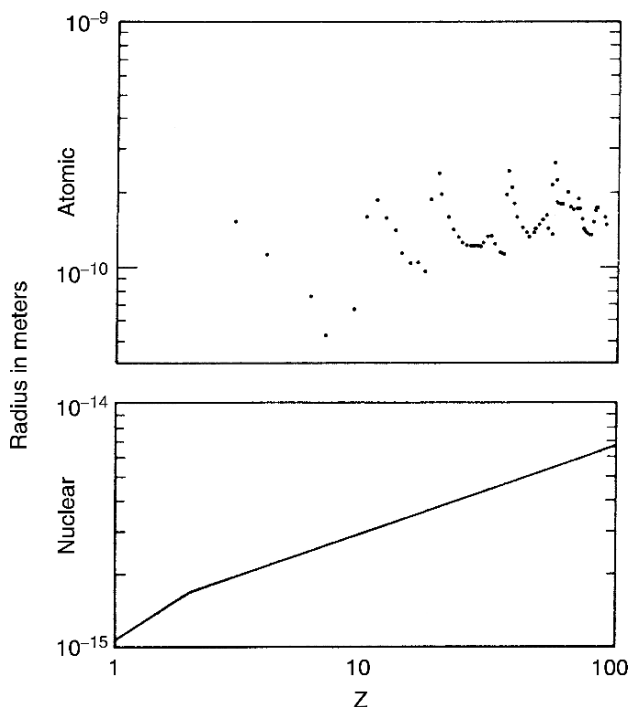


FIGURE 17.1. Plot of atomic radius and nuclear radius vs. atomic number, showing the relative constancy of the atomic radius and the systematic increase of nuclear radius. Shell effects in atomic radii are quite pronounced; slight shell effects in the nuclear radii are not shown. Atomic data are from Table 7b-3 of *The American Institute of Physics Handbook*, New York, McGraw-Hill, 1957. Nuclear radii are from Eq. 17.2, using the average atomic mass to estimate  $A$  from  $Z$ .

through the periodic table. The nuclear radius  $R$  and atomic mass number are related by

$$R = R_0A^{1/3}. \tag{17.2}$$

The precise value for  $R_0$  depends on how the nuclear radius is measured. If it is measured from the charge distribution, then

$$R_0 = 1.07 \times 10^{-15} \text{ m}. \tag{17.3}$$

Figure 17.1 shows how nuclear radii grow systematically, while atomic radii do not change appreciably with  $A$  (although they do change dramatically as shells close). The constancy of atomic size results from two competing effects: as  $Z$  increases the outer electrons have a larger value of the principal quantum number  $n$ . On the other hand, the greater charge means that Coulomb attraction makes the orbit radius smaller for a given  $n$ .

The  $A^{1/3}$  dependence in the nuclear case means that the nuclear density is independent of  $A$ . To see this, note that the volume of a spherical nucleus is  $4\pi R^3/3 = 4\pi R_0^3A/3$ . Since the mass and volume are both proportional to  $A$ , the density is constant. This implies that nucleons can get only so close to one another, and that as more are added, the nuclear volume increases. This constant density is the same effect we see in the aggregation of atoms in a crystal or a drop of water.

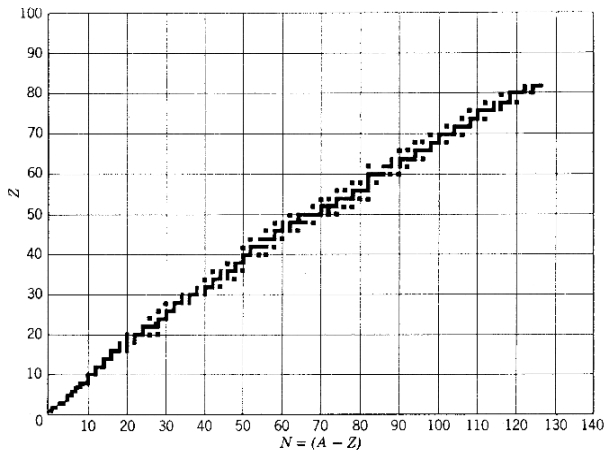


FIGURE 17.2. Stable nuclei. Solid squares represent nuclei which are stable and are found in nature. From Robert Eisberg and Robert Resnick, *Quantum Physics of Atoms, Molecules, Solids, Nuclei and Particles*, 2nd ed., New York, John Wiley & Sons, 1985, p. 524. Reprinted with permission of John Wiley & Sons.

Scattering experiments measure the force between two nucleons. At large distances, there is no force between two neutrons or between a neutron and a proton. (Between two protons, of course, there is Coulomb repulsion.) As two nucleons are brought close together, a strong attractive “nuclear” force exists; at still closer distances, the nuclear force becomes repulsive.

If we look at the nuclei that are stable against radioactive decay and are therefore found in nature, we find that for light elements,  $Z = N$ . As  $Z$  increases, the number of neutrons becomes greater than  $Z$ ; this can be seen in Fig. 17.2.

Eq. 17.1 shows that when an object is at rest, its total energy (which is its internal energy) is related to its rest mass by

$$E = m_0 c^2. \quad (17.4)$$

The measurement of nuclear masses has provided one way to determine nuclear energies. It is necessary to supply energy to a stable nucleus to break it up into its constituent nucleons (or else it would not be stable). The *binding energy* (BE) of the nucleus is the total energy of the constituent nucleons minus the energy of the nucleus:

$$\text{BE} = Zm_p c^2 + (A - Z)m_n c^2 - m_{\text{nuc}} c^2. \quad (17.5)$$

It represents the amount of energy that must be added to the nucleus to separate it into its constituent neutrons and protons.

Suppose we add  $Zm_e c^2$  to the first term. Then we have the energy of  $Z$  protons plus the energy of  $Z$  electrons. Except for the binding energy of each electron, this is the same as the mass of  $Z$  neutral hydrogen atoms, which we call  $M_p c^2$ . Similarly, we can add the mass of  $Z$  electrons to  $m_{\text{nuc}} c^2$  and neglect the electron binding energy to obtain  $M_{\text{atom}} c^2$ . Capital  $M$  represents the mass of a

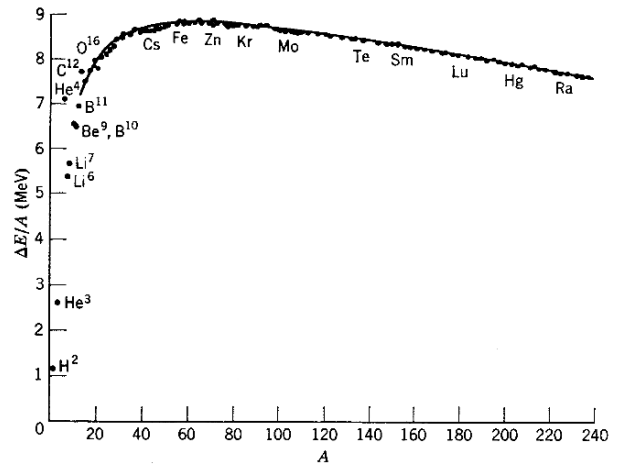


FIGURE 17.3. The average binding energy per nucleon for stable nuclei. From R. Eisberg and R. Resnick, *Quantum Physics of Atoms, Molecules, Solids, Nuclei, and Particles*, 2nd ed., New York, John Wiley & Sons, 1985, p. 524. Reprinted with permission of John Wiley & Sons.

neutral atom, while  $m$  stands for the mass of a bare nucleus. For the neutron,  $m = M$ . In Eq. 17.5, we can add  $Zm_e c^2$  to the first term and add  $Zm_e c^2$  to the last term, to obtain the binding energy in terms of the masses of the corresponding neutral particles:

$$\text{BE} = ZM_p c^2 + (A - Z)M_n c^2 - M_{\text{atom}} c^2. \quad (17.6)$$

This is fortunate, because neutral masses (or those for ions carrying one or two charges) are the quantities actually measured in mass spectroscopy.

Masses are measured in *unified mass units*  $u$ , defined so that the mass of neutral  $^{12}\text{C}$  is exactly 12  $u$ . Carbon is used for the standard because hydrocarbons can be made in combinations to give masses close to any desired mass. The carbon standard replaced one based on the naturally occurring mixture of oxygen isotopes in the early 1960s. (One of the troubles with the earlier standard was that the relative abundance of the various oxygen isotopes varies with time and with location on the earth.) The earlier unit was called the atomic mass unit,  $amu$ . One still finds confusion in the literature about which standard is being used, and the carbon standard is sometimes called an  $amu$ .

One unified mass unit is related to the kilogram, the joule, and the electron volt by

$$1 \text{ u} = 1.66054 \times 10^{-27} \text{ kg}, \\ (1 \text{ u})(c^2) = \begin{cases} 1.49241 \times 10^{-10} \text{ J} \\ 931.49 \text{ MeV}. \end{cases} \quad (17.7)$$

If one plots the binding energy per nucleon versus mass number as in Fig. 17.3, one sees that the binding energy per nucleon has a maximum near  $A = 60$ , and that the average binding energy (except for light elements) is about 8 MeV per nucleon. For less stable nuclei on either side of the stable line plotted in Fig. 17.2, the binding energy is less than that for the nuclei shown here.

The maximum near  $A = 60$  is what makes both *fission* and *fusion* possible sources of energy. A heavy nucleus with  $A$  near 240 can split roughly in half, giving two fission products. Since the nucleons in each of the products are more tightly bound on the average than in the original nucleus, energy is released. This energy difference comes almost entirely from the  $Z^2$  dependence of the Coulomb repulsion of the protons in the nuclei. In fusion, two nuclei of very low  $A$  combine to give a nucleus of higher  $A$ , for which the binding energy per nucleon is greater.

## 17.2 Nuclear Decay: Decay Rate and Half-Life

If a nucleus has more energy than it would if it were in its ground state, it can decay. If the nucleus has sufficient energy, it can emit a proton, neutron, or cluster of nucleons [ $\alpha$  particle ( ${}^4_2\text{He}$ ), deuteron ( ${}^2_1\text{H}$ ), etc.]. When a nucleus has enough excitation energy to decay by nuclear emission it usually does so in such an extremely short time that the nuclei could never be introduced in the body after they were produced. An exception is the  $\alpha$  decay of a few elements near the upper (high- $Z$ ) end of the periodic table. They are found in nature, either because their lifetimes are very long or because they are formed as the result of some other decay process that has a long lifetime.

If a nucleus has just a small amount of excess energy, it emits a  $\gamma$  ray, a photon analogous to the x ray or visible photons emitted by an excited atom. Another process that can occur is the emission of a positive or negative electron, with the conversion of a proton to a neutron, or vice versa. This is called  $\beta$  decay. Both  $\gamma$  and  $\beta$  decay will be described in detail in the next two sections.

Each excited nucleus has a probability  $\lambda dt$  of decaying in time  $dt$ . When there are  $N$  nuclei present, the average number decaying in time  $dt$  is<sup>1</sup>

$$-dN = N\lambda dt.$$

The rate of change of  $N$  is the *activity*,  $A(t)$ , the number of decays per second:

$$A(t) = \frac{dN}{dt} = -\lambda N.$$

This leads to the familiar exponential decay of Chapter 2:

$$N = N_0 e^{-\lambda t}.$$

The half-life  $T_{1/2}$  is related to  $\lambda$  by Eq. 2.10:

$$T_{1/2} = \frac{0.693}{\lambda}. \quad (17.8)$$

<sup>1</sup>The decay constant is called  $\lambda$  in this chapter to conform to the usage in nuclear medicine.

## 17.3 Gamma Decay and Internal Conversion

When a nucleus is in an excited state, it can lose energy by photon emission. The energy levels of the nucleus are characterized by certain quantum numbers, and  $\gamma$  emission is subject to selection rules analogous to those for x-ray emission by atoms. Half-lives for  $\gamma$  emission range from  $10^{-20}$  to  $10^{+8}$  s.

Figure 17.4 shows an energy level diagram for  ${}^{99}_{43}\text{Tc}$  (technetium), an isotope widely used in nuclear medicine, along with some tabular material that we will need as we progress through this chapter. There are two important levels to consider in  ${}^{99}_{43}\text{Tc}$ . The ground state is not stable but decays by  $\beta$  decay, considered in the next section. However, its decay rate is so small (half-life of  $2.12 \times 10^5$  years) that we can ignore its decay. There is a level at an excitation of 0.143 MeV above the ground state that has a half-life of 6 h for  $\gamma$  decay. This is an unusually long half-life; we call it a *metastable state* and denote it by  ${}^{99m}\text{Tc}$ . Looking at the table labeled input data, we see that there are two modes of decay of the nucleus from this state. The first is the emission of a 0.0021-MeV  $\gamma$  ray followed by a 0.1405-MeV  $\gamma$  ray. It occurs 0.986 of the time. The other possibility is the emission of one  $\gamma$  ray, of energy 0.1426 MeV, which happens in 0.014 of the decays.

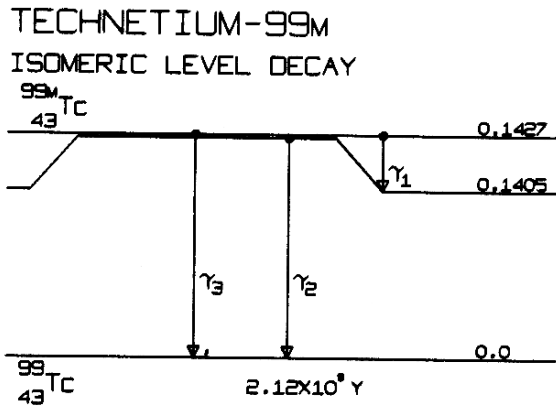
The notations  $E3$ ,  $M1$ , and  $M4$  in the last column of the input data refer to the selection rules and quantum number changes in the transitions. We will not need the details, although they can be used to estimate the decay rates. The labels  $E1$ ,  $E2$ , and  $E3$  are called *electric dipole*, *electric quadrupole*, and *electric octupole*, respectively.  $M1$  means *magnetic dipole*, and  $M4$  means magnetic  $2^4$  or *magnetic hexadecapole*.

Whenever a nucleus loses energy by  $\gamma$  decay, there is a competing process called *internal conversion*. The energy to be lost in the transition,  $E_\gamma$ , is transferred directly to a bound electron (usually a  $K$  or  $L$  electron), which is then ejected with a kinetic energy

$$T = E_\gamma - B, \quad (17.9)$$

where  $B$  is the binding energy of the electron.

The *mean number per disintegration* in the table of input data is the mean number of times that the indicated transition between energy levels takes place. In the table of output data, on the other hand, it means the mean number of times that radiation is emitted. To see the distinction, compare the  $\gamma_2$  entries in the input data and output data of Fig. 17.4. The  $\gamma_2$  transition from the 0.1405-MeV level to the ground state occurs 0.9860 times per disintegration. From the output data, we see that this transition takes place by emission of a photon ( $\gamma_2$ ) 0.8787 times, by  $K$  internal conversion 0.0913 times, by  $L$  internal conversion 0.0118 times, and by  $M$  internal conversion 0.0039 times (the sum is 0.9857, which agrees with the value 0.9860 times per disintegration).



\*\*INPUT DATA\*\*

43 TECHNETIUM 99M    HALF LIFE = 6.03 HOURS

DECAY MODE- ISOMERIC LEVEL

TRANSITION	MEAN NUMBER/DISINTEGRATION	TRANSITION ENERGY (MEV)	OTHER NUCLEAR DATA
GAMMA 1	0.9860	0.0021	E3
GAMMA 2	0.9860	0.1405	M1, AK = 0.104 K/L = 7.70
GAMMA 3	0.0140	0.1426	M4, AK=23.0 AL1I1 = 9.21

REF.- LEDERER, C.M. ET AL, TABLE OF ISOTOPES, 6TH ED.  
LEGRAND, J. ET AL, INT. J. APPL. RAD. AND ISOTOPES 21, 139 (1970).

\*\*OUTPUT DATA\*\*

43 TECHNETIUM 99M    HALF LIFE = 6.03 HOURS

DECAY MODE- ISOMERIC LEVEL

RADIATION	MEAN NUMBER/DISINTEGRATION	MEAN ENERGY/PARTICLE	EQUI-LIBRIUM DOSE CONSTANT
	$n_i$	$\bar{E}_i$ (MeV)	$\Delta_i$ (g-rad/uCi-h)
GAMMA 1	0.0000	0.0021	0.0000
M INT CON ELECT	0.9860	0.0016	0.0035
GAMMA 2	0.8787	0.1405	0.2630
K INT CON ELECT	0.0913	0.1194	0.0232
L INT CON ELECT	0.0118	0.1377	0.0034
M INT CON ELECT	0.0039	0.1400	0.0011
GAMMA 3	0.0003	0.1426	0.0001
K INT CON ELECT	0.0088	0.1215	0.0022
L INT CON ELECT	0.0035	0.1398	0.0010
M INT CON ELECT	0.0011	0.1422	0.0003
K ALPHA-1 X-RAY	0.0441	0.0183	0.0017
K ALPHA-2 X-RAY	0.0221	0.0182	0.0008
K BETA-1 X-RAY	0.0105	0.0206	0.0004
KLL AUGER ELECT	0.0152	0.0154	0.0005
KLM AUGER ELECT	0.0055	0.0178	0.0002
LMM AUGER ELECT	0.1093	0.0019	0.0004
MMY AUGER ELECT	1.2359	0.0004	0.0011

FIGURE 17.4. Energy levels and decay data for the isotope <sup>99m</sup>Tc. The various features are discussed in the text. Reprinted by permission of the Society of Nuclear Medicine from Dillman, L. T., and F. C. Von der Lage. MIRD Pamphlet No. 10. *Radionuclide Decay Schemes and Nuclear Parameters for Use in Radiation Dose Estimation*, 1974, p. 62.

To calculate the mean number of times a radiation is emitted from the mean number of transitions, we need numbers  $f$  that are the fraction of transitions involving a particular radiation. The fraction associated with  $\gamma$  decay is  $f_r$ , the fraction with  $K$  internal conversion is  $f_K$ , and so forth. The sum of all these fractions is unity:

$$f_r + f_K + f_L + f_M + \dots = 1. \quad (17.10)$$

Often these fractions are not listed in the literature. Instead, one finds the *internal conversion coefficient*  $\alpha$ . For conversion of a  $K$  electron, it is  $\alpha_K = f_K/f_r$ . For the  $L$  shell it is  $\alpha_L = f_L/f_r$ , and so on. One also finds in the literature the ratio

$$\frac{K}{L} = \frac{f_K}{f_L} = \frac{\alpha_K}{\alpha_L}.$$

A useful empirical relationship is that  $f_M \approx f_L/3$ . In the input data of Fig. 17.4,  $\alpha_K$  is called AK.

Once internal conversion has created a hole in the electronic structure of the atom, characteristic x rays and Auger electrons will be emitted. They must also be considered in calculating the total dose from the nuclear decay.

## 17.4 Beta Decay and Electron Capture

Nuclei that are not on the line of stability in Fig. 17.2 have greater internal energy and are susceptible to some kind of decay. They can lose energy by  $\gamma$  emission. In addition, nuclei above the line of stability have too many protons relative to the number of neutrons; nuclei below the line have relatively too many neutrons.

Two modes of decay allow a nucleus to approach the stable line. In *beta* ( $\beta^-$  or electron) *decay*, a neutron is converted into a proton. This keeps  $A$  constant, lowering  $N$  by one and raising  $Z$  by one. In *positron* ( $\beta^+$ ) *decay*, a proton is converted into a neutron. Again  $A$  remains unchanged,  $Z$  decreases and  $N$  increases by 1. We find  $\beta^+$  decay for nuclei above the line of stability and  $\beta^-$  decay for nuclei below the line. Figure 17.5 shows a portion of the line of stability, a line of constant  $A$  ( $Z = A - N$ ), and the regions for  $\beta^+$  and  $\beta^-$  decay.

We can plot the energy of the neutral atom for different nuclei along the line of constant  $A$ . Since there are one or two stable nuclei, there is some value of  $Z$  and  $N$  for which the energy is a minimum. The energy increases in either direction from this minimum. The first approximation to a curve with a minimum is a parabola, as shown in Fig. 17.6 for a nucleus of odd  $A$ .<sup>2</sup> When  $Z$  is too small, a neutron is converted to a proton by  $\beta^-$  decay. If  $Z$  is too large, a proton changes to a neutron by  $\beta^+$  decay or electron capture (to be described below).

<sup>2</sup>This parabola and the general behavior of the binding energy with  $Z$  and  $A$  can be explained remarkably well by the semiempirical

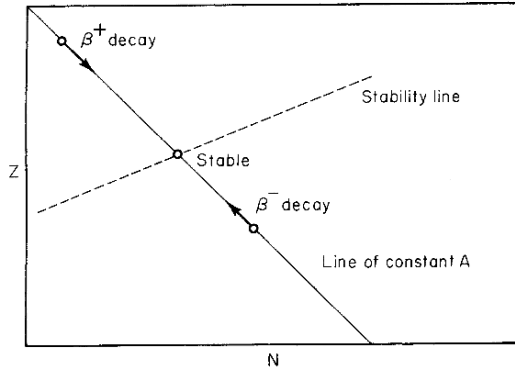


FIGURE 17.5.  $\beta^-$  decay and  $\beta^+$  decay do not change  $A$ . They do change  $N$  and  $Z$  to bring the nucleus closer to the stability line.

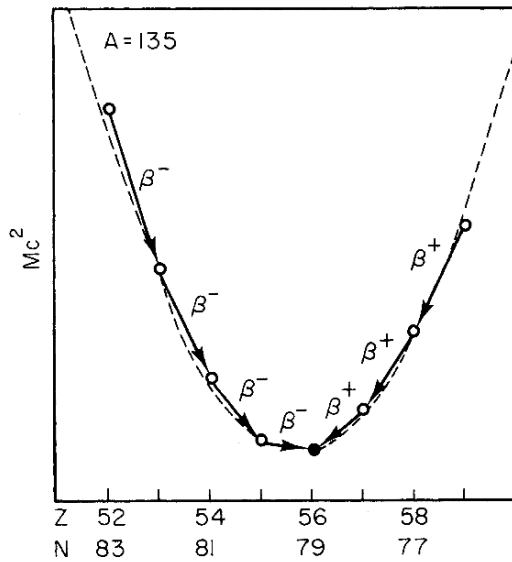


FIGURE 17.6. Energy of nuclei as a function of  $Z$  for an odd value of  $A$  ( $A = 135$ ). The only stable nucleus is  ${}_{56}^{135}\text{Ba}$ ; nuclei of lower  $Z$  undergo  $\beta^-$  emission; those of higher  $Z$  undergo  $\beta^+$  emission or electron capture.

When  $A$  is odd, there are an even number of protons and an odd number of neutrons (even-odd) or vice versa (odd-even). When we plot the energies of even- $A$  nuclei, we find that the masses lie on two different parabolas (Fig. 17.7). The one for which both  $Z$  and  $N$  are odd (odd-odd) has greater energy than the parabola for which both are even. The reason is that nucleons have lower energy when they are paired with one another in such a way that their spins are antiparallel. In the even-even case, the neutrons and the protons are all paired off and have this lower energy; in the odd-odd case there are both an unpaired proton and an unpaired neutron, and the en-

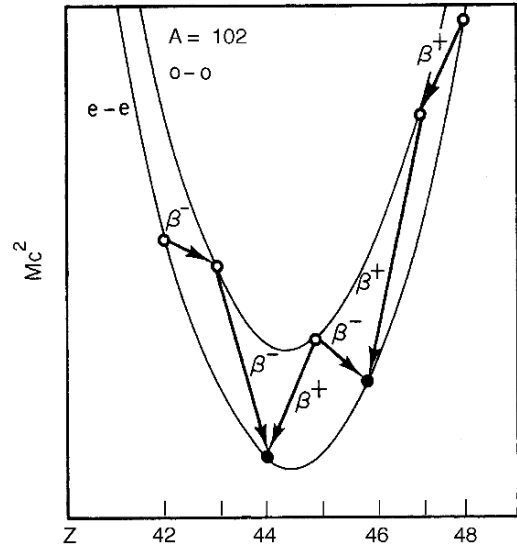


FIGURE 17.7. Energy of even- $A$  nuclei as a function of  $Z$ . Nuclei with an odd number of protons and neutrons have higher energies than those with an even number of each. This makes it possible for the same nucleus to decay by either  $\beta^-$  or  $\beta^+$  emission.

ergy is higher. As we change  $Z$  by one, we jump back and forth between the odd-odd and the even-even parabolas. For odd- $A$  nuclei, either the neutrons are paired and one proton is not, or vice versa. There is always one unpaired nucleon as  $Z$  changes, so there is only one parabola.

The existence of the two parabolas means that there are usually (but not always) two stable nuclei with an odd-odd nucleus between them that can decay by either  $\beta^-$  or  $\beta^+$  emission.

The emission of a  $\beta^-$  particle is accompanied by the emission of a *neutrino* (strictly speaking, an antineutrino):

$${}^A_Z X \rightarrow {}^A_{Z+1} Y + \beta^- + \bar{\nu}. \quad (17.11)$$

The neutrino has no charge and no rest mass,<sup>3</sup> so that like a photon, it travels with velocity  $c$  and its energy and momentum are related by  $E = pc$ . Neutrinos hardly interact with matter at all, so they are quite difficult to detect. Nevertheless they have been detected through certain specific nuclear reactions that take place on the rare occasions when a neutrino does interact with a nucleus. A particle that seemed originally to be an invention to conserve energy and angular momentum now has a strong experimental basis.

Suppose that  $\beta$  decay consisted of the ejection of only a  $\beta$  particle. If the original nucleus  $X$  were at rest,<sup>4</sup> then nucleus  $Y$  would recoil in the direction opposite the  $\beta$

<sup>3</sup>Recent measurements indicate that the neutrino may have a rest mass, but it is less than 3 eV. [S. Eidelman *et al.* (Particle Data Group), *Phys. Lett. B* **592**: 1 (2004) (URL: <http://pdg.lbl.gov>)]

<sup>4</sup>Its thermal energy of about  $\frac{1}{40}$  eV is negligible compared to the energy released in decay.

ical mass formula [Evans (1955, Chapter 11); Eisberg and Resnick, (1985, p. 528)].

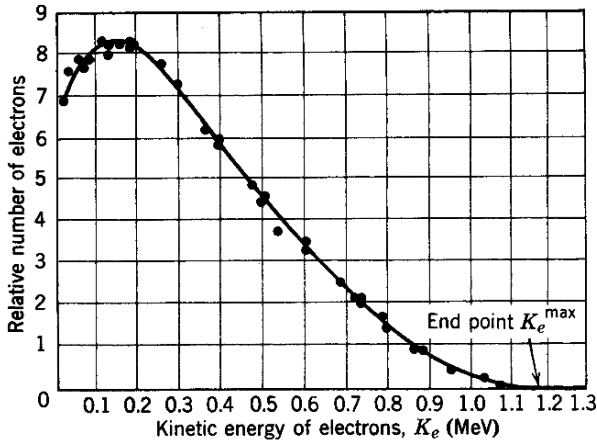


FIGURE 17.8. A typical spectrum of  $\beta$  particles. In this case it is for the  $\beta$  decay of  $^{210}_{83}\text{Bi}$ . From Robert Eisberg and Robert Resnick. *Quantum Physics of Atoms, Molecules, Solids, Nuclei, and Particles*, 2nd ed., p. 566. Copyright ©1985 John Wiley & Sons. Reproduced by permission of John Wiley & Sons.

particle to conserve momentum; the ratio of its velocity to that of the  $\beta$  particle would be given by their mass ratio. The recoil nucleus and the  $\beta$  particle would each have a definite fraction of the total energy available from the decay, and the  $\beta$  particles would all have the same energy. However, the observed  $\beta$ -particle energy spectrum is not a line spectrum but a continuum ranging from zero to the expected energy, as shown in Fig. 17.8. The missing energy is carried by the neutrino. The different energies correspond to different angles of emission of the neutrino relative to the direction of the  $\beta$  particle. This kind of spectrum is characteristic of three bodies emerging from the reaction.

The total kinetic energy for the three emerging particles is

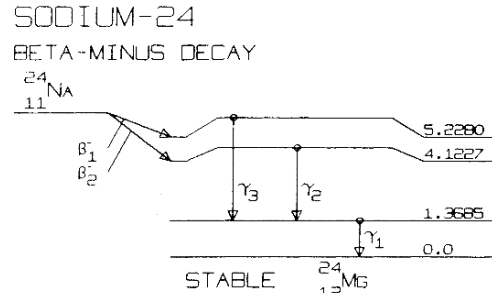
$$E_{\text{decay}} = m_{Z,A}c^2 - m_{Z+1,A}c^2 - m_e c^2.$$

If we add and subtract  $Zm_e c^2$ , the result is unchanged:

$$\begin{aligned} E_{\text{decay}} &= (m_{Z,A}c^2 + Zm_e c^2) - (m_{Z+1,A}c^2 + Zm_e c^2) + Zm_e c^2 + m_e c^2 \\ &= M_{Z,A}c^2 - M_{Z+1,A}c^2. \end{aligned} \quad (17.12)$$

The energy released in the decay is given by the difference in rest energies of the initial and final neutral atoms. This energy is shared in different amounts by the three particles; it is shared mainly by the neutrino and electron, since the nucleus is so massive and its kinetic energy is  $p^2/2m$ . The maximum or end-point energy of the  $\beta$  spectrum in Fig. 17.8 corresponds to  $E_{\text{decay}}$ .

Figure 17.9 shows data for the decay of  $^{24}\text{Na}$ , an isotope that has been used in nuclear medicine. The transition labeled  $\beta_2$  is overwhelmingly the most common. The  $\beta_2$  emission is followed by two  $\gamma$  rays, and the end-point energy of the  $\beta$  decay is 1.392 MeV. On the other hand,



\*\*INPUT DATA\*\*

11 SODIUM 24      HALF LIFE = 15.0 HOURS

DECAY MODE- BETA MINUS

TRANSITION	MEAN NUMBER/DISINTEGRATION	TRANSITION ENERGY (MEV)	OTHER NUCLEAR DATA
BETA MINUS 1	0.0008	0.1860*	ALLOWED
BETA MINUS 2	0.9992	1.3920*	ALLOWED
GAMMA 1	1.0000	1.3685	E <sub>2</sub> , AK=0.000010
GAMMA 2	0.9992	2.7539	E <sub>2</sub> , AK=0.000010
GAMMA 3	0.0008	3.8595	M <sub>1</sub> , AK(I) = 0.000001

\*ENDPOINT ENERGY

REF.- ENDT, P.M. AND VAN DER LEUN, C., NUCL. PHYS. A105, 261 (1967).

\*\*OUTPUT DATA\*\*

11 SODIUM 24      HALF LIFE = 15.0 HOURS

DECAY MODE- BETA MINUS

RADIATION	MEAN NUMBER/DISINTEGRATION	MEAN ENERGY/PARTICLE (MeV)	EQUI-LIBRIUM DOSE CONSTANT (g-rad/ $\mu\text{Ci-h}$ )
	$n_i$	$\bar{E}_i$	$d_i$
BETA MINUS 2	0.9992	0.5547	1.1805
GAMMA 1	0.9999	1.3685	2.9149
GAMMA 2	0.9991	2.7539	5.8610
GAMMA 3	0.0008	3.8595	0.0065

FIGURE 17.9. Energy levels and data for the  $\beta$  decay of  $^{24}\text{Na}$ . Reprinted by permission of the Society of Nuclear Medicine from L. T. Dillman and F. C. Von der Lage. MIRD Pamphlet No. 10. *Radionuclide Decay Schemes and Nuclear Parameters for Use in Radiation Dose Estimation*, p. 19.

the average energy of the  $\beta$  particle is only 0.5547 MeV, about 40% of the end-point energy.

Emission of a positron converts a proton into a neutron, and  $Z$  decreases by one. A neutrino is also emitted:

$${}^A_Z X \rightarrow {}^A_{Z-1} Y + \beta^+ + \nu. \quad (17.13)$$

The decay energy is again given by

$$E_{\text{decay}} = m_{Z,A}c^2 - m_{Z-1,A}c^2 - m_e c^2.$$

However, this time, when we add  $Zm_e c^2$  to the first term and subtract  $(Z-1)m_e c^2$  from the second term to convert



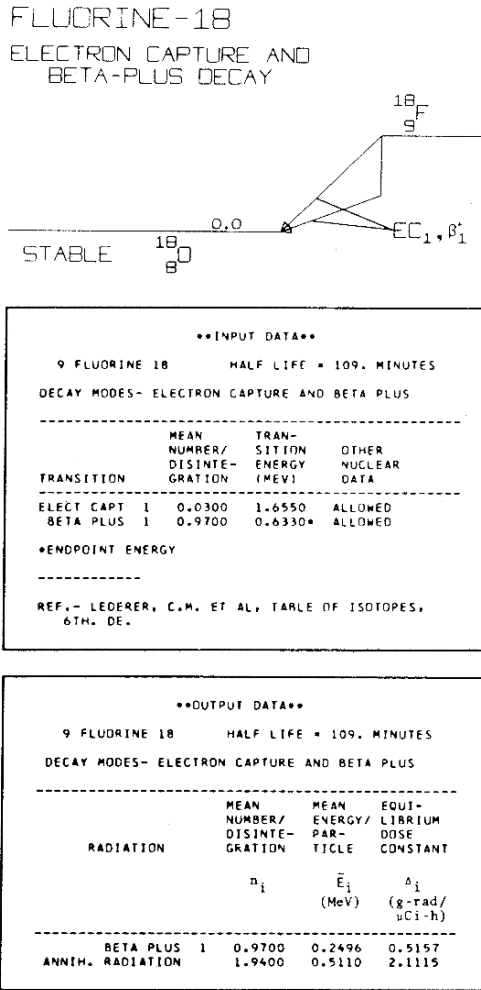


FIGURE 17.10. Energy levels and data for the  $\beta^+$  decay of  $^{18}\text{F}$ . Reprinted by permission of the Society of Nuclear Medicine from L. T. Dillman and F. C. Von der Lage. MIRD Pamphlet No. 10. *Radionuclide Decay Schemes and Nuclear Parameters for Use in Radiation Dose Estimation* p. 18.

these to atomic masses, the electron masses do not cancel. Instead, we get

$$E_{\text{decay}} = M_{Z,A}c^2 - M_{Z-1,A}c^2 - 2m_e c^2. \quad (17.14)$$

Positron emission will not occur unless the initial neutral atomic mass exceeds the final neutral atomic mass by at least  $2m_e c^2$ . We remind ourselves of this by drawing a vertical line of length  $2m_e c^2$  before drawing the slanted line for the  $\beta^+$  decay, as in Fig. 17.10, the decay scheme for  $^{18}\text{F}$ .

The first entry in the table of input data in Fig. 17.10 is for *electron capture*. The transition energy listed is  $2m_e c^2$  more than for  $\beta^+$  decay. Some of the inner electrons of the atom are close enough to the nucleus (quantum-mechanically, the electron wave functions overlap the nucleus enough) so that the electron is captured by the nucleus, and a neutrino is emitted. In terms of nuclear masses, an electron rest energy is added to the parent

nucleus (we ignore its kinetic energy):

$$E_{e.c.} = m_e c^2 + m_{Z,A}c^2 - m_{Z-1,A}c^2.$$

If we add and subtract  $(Z - 1)m_e c^2$ , we have

$$E_{e.c.} = M_{Z,A}c^2 - M_{Z-1,A}c^2. \quad (17.15)$$

A *K* electron<sup>5</sup> is usually captured. The energy from the nuclear transition is given to a neutrino. No electron emerges, but there are *K* x rays and Auger electrons,<sup>6</sup> as there are any time a vacancy in the *K* shell occurs, and these contribute to the radiation dose. They are not listed in the output data of Fig. 17.10 because the *K* x rays only have an energy of about 530 eV. We now understand that Auger electrons can be very important in the dose in some cases.

There is also an entry under output data labeled *annihilation radiation*. Once a positron has been emitted, it slows down like any other charged particle. At some point it combines with an electron (since the positron and electron constitute a particle-antiparticle pair), and all of the rest energy of both particles goes into two photons.<sup>7</sup> The energy conservation equation is

$$2m_e c^2 = 2h\nu. \quad (17.16)$$

For each original positron emitted, two photons are produced, each of energy  $m_e c^2 = 0.511$  MeV.

## 17.5 Calculating the Absorbed Dose from Radioactive Nuclei within the Body

When a radiopharmaceutical is given to a patient for either diagnosis or therapy, the nuclei end up in different organs in varying amounts; for example,  $^{99m}\text{Tc}$ -labeled albumin microspheres injected intravenously lodge in the lungs. The problem is to calculate the whole-body absorbed dose, the dose to the lungs, and the dose to other organs.

The dose calculation is carried out in the following way:<sup>8</sup>

1. Calculate the total number of nuclear transformations or disintegrations in organ *h*. It is called the *cumulated activity*  $\tilde{A}_h$  or  $N_h$ .
2. Calculate the mean energy emitted per unit cumulated activity for each type of photon or particle emitted.

<sup>5</sup>See Chapter 14.

<sup>6</sup>See Chapter 14.

<sup>7</sup>Three photons are occasionally emitted.

<sup>8</sup>Dose calculations in this chapter follow the technique and notation recommended by the MIRD Committee of the Society of Nuclear Medicine [Loevinger *et al.* (1988) and Stabin *et al.* (2005)].

- (a) If the radioactive nucleus can emit several types of particles or photons per transformation, call  $n_i$  the mean number of particles or photons of type  $i$  emitted per transformation. These include  $\gamma$  rays, electrons, x rays and Auger electrons. [In the “output data” of Dillman and Von der Lage (1974),  $n_i$  is called the *mean number per disintegration*. In the more recent report of Weber *et al.* (1989) it is called *particles per transition*. We have continued to show the older tables here because the newer ones contain only the output data.] The data are also available in electronic form [Eckerman *et al.* (1994); Stabin and da Luz (2002); RADAR (the Radiation Group Assessment Resource), www.doseinfo-radar.com; and the National Nuclear Data Center, www.nndc.bnl.gov/mird/].
- (b) For each type  $i$  determine  $E_i$ , the *mean energy per particle or photon*.
- (c) Calculate  $\Delta_i = n_i E_i$ , the *mean energy emitted per unit cumulated activity*, for each type of particle or photon emitted. (In earlier MIRD literature, this was called the *equilibrium absorbed dose constant*.)
3. Calculate  $\phi_i(r_k \leftarrow r_h)$ , the fraction of the radiation of type  $i$  emitted in source region  $r_h$  that is absorbed in target region  $r_k$ , and divide by the mass of the target region to get the *specific absorbed fraction*

$$\Phi_i(r_k \leftarrow r_h) = \frac{\phi_i(r_k \leftarrow r_h)}{m_k}.$$

( $\Phi$  has the units of inverse mass.)

4. The *mean absorbed dose* in organ  $k$  due to activity in organ  $h$ ,  $\bar{D}$  (in  $\text{J kg}^{-1}$  or Gy) is

$$\begin{aligned} \bar{D}(r_k \leftarrow r_h) &= \tilde{A}_h \sum_i n_i E_i \Phi_i(r_k \leftarrow r_h), \\ \bar{D}(r_k \leftarrow r_h) &= \tilde{A}_h \sum_i \Delta_i \Phi_i(r_k \leftarrow r_h). \end{aligned} \quad (17.17)$$

5. If several organs are radioactive, a sum must be taken over each organ:

$$\bar{D}(r_k) = \sum_h \tilde{A}_h \sum_i \Delta_i \Phi_i(r_k \leftarrow r_h). \quad (17.18)$$

The next three sections show how to determine  $\tilde{A}$ ,  $\Delta_i$ , and  $\Phi_i$ . Some tables [Snyder *et al.* (1969, 1976)] give values of  $\Phi_i$  for photons of various energies. It is necessary to multiply by  $\Delta_i$  and sum for the isotope of interest. These sums must be repeated over and over again for common radionuclides. The sum is called the *mean absorbed dose per unit cumulated activity*:

$$S(r_k \leftarrow r_h) = \sum_i \Delta_i \Phi_i(r_k \leftarrow r_h), \quad (17.19)$$

$$\bar{D}(r_k \leftarrow r_h) = \tilde{A}_h S(r_k \leftarrow r_h), \quad (17.20)$$

$$\bar{D}(r_k) = \sum_h \tilde{A}_h S(r_k \leftarrow r_h). \quad (17.21)$$

A table of  $S$  for many common radionuclides is available [Snyder *et al.* (1975)]. The tables cannot be summed over  $h$  because the values of  $\tilde{A}_h$  depend on how the isotope is administered. A computer program OLINDA/EXM is most commonly used for these calculations [Stabin, Sparks and Crowe (2005)]. These authors call  $S$  the *dose factor*.

To discuss units, imagine there is only one type of radiation. In SI units the dose is simply

$$D(\text{Gy}) = [\tilde{A}(\text{dimensionless})] [\Delta_i(\text{J})] [\Phi_i(\text{kg}^{-1})]. \quad (17.22a)$$

In day-to-day calculations, it is often easier to use mixed units and write

$$\begin{aligned} D(\text{Gy}) &= k \left( \frac{\text{Gy kg}}{\text{MBq s MeV}} \right) [\tilde{A}(\text{MBq s})] \\ &\times [\Delta_i(\text{MeV})] [\Phi_i(\text{kg}^{-1})] \end{aligned} \quad (17.22b)$$

In an older system of units, where the dose is in rad and the total number of transitions is in microcurie-hour (see below), the equation is

$$D(\text{rad}) = [\tilde{A}(\mu\text{Ci h})] [\Delta_i(\text{g rad } \mu\text{Ci}^{-1} \text{ h}^{-1})] [\Phi_i(\text{g}^{-1})]. \quad (17.22c)$$

The next three sections discuss cumulated activity, the mean energy emitted, and the absorbed fraction of the energy. Then all of these concepts are combined with examples of absorbed dose calculations.

## 17.6 Activity and Cumulated Activity

The activity  $A(t)$  is the number of radioactive transitions (or transformations or disintegrations) per second. The SI unit of activity is the *becquerel* (Bq):

$$1 \text{ Bq} = 1 \text{ transition s}^{-1}. \quad (17.23)$$

The earlier unit of activity, which is still used occasionally, is the *curie* (Ci):

$$\begin{aligned} 1 \text{ Ci} &= 3.7 \times 10^{10} \text{ Bq}, \\ 1 \mu\text{Ci} &= 3.7 \times 10^4 \text{ Bq}. \end{aligned} \quad (17.24)$$

The cumulated activity  $\tilde{A}$  is the total number of transitions that take place. The SI unit of cumulated activity is the transition or the Bq s. Both are dimensionless. The old unit of cumulated activity is the  $\mu\text{Ci h}$ :

$$1 \mu\text{Ci h} = 1.332 \times 10^8 \text{ Bq s}. \quad (17.25)$$

Consider a sample of  $N_0$  radioactive nuclei at time  $t = 0$ . The total number of nuclei remaining at time  $t$  is  $N(t) = N_0 e^{-\lambda t}$ , and the total activity is  $A(t) = \lambda N(t) =$

$A_0 e^{-\lambda t}$ . The cumulated activity between times  $t_1$  and  $t_2$  is

$$\begin{aligned} \tilde{A}(t_1, t_2) &= \int_{t_1}^{t_2} A(t) dt = \frac{A_0}{\lambda} (e^{-\lambda t_1} - e^{-\lambda t_2}) \quad (17.26) \\ &= N(t_1) - N(t_2). \end{aligned}$$

If all times are considered,  $t_1 = 0$  and  $t_2 = \infty$ ,

$$\tilde{A} = \tilde{A}(0, \infty) = \frac{A_0}{\lambda} = \frac{A_0 T_{1/2}}{0.693} = 1.443 A_0 T_{1/2}. \quad (17.27)$$

This is, as we would expect,  $N_0$ .

### 17.6.1 The General Distribution Problem: Residence Time

Suppose that a radioactive substance is introduced in the body by breathing, ingestion, or injection. It may move into and out of many organs before decaying, and it may even leave the body. The details of how it moves depend on the pharmaceutical to which it is attached.

The cumulated activity in organ  $h$  is the total number of disintegrations in that organ:

$$N_h = \tilde{A}_h = \int_0^\infty A_h(t) dt. \quad (17.28)$$

The dose to organ  $k$  is then

$$D_k = \sum_h N_h S(r_k \leftarrow r_h). \quad (17.29)$$

The units of  $N_h$  are disintegrations (dimensionless) or Bq s. If initial activity  $A_0$  (Bq) is administered to the patient, the ratio  $N_h/A_0$  is called the *residence time* in organ  $h$ :

$$\tau_h = \frac{N_h}{A_0} = \frac{\tilde{A}_h}{A_0} = \frac{\tilde{A}_h(0, \infty)}{A_0}. \quad (17.30)$$

The residence time is the length of time that activity at a constant rate  $A_0$  would have to reside in the organ to give that cumulated activity. The residence time for a given substance and organ must be determined by measurement, guided by the use of appropriate models. Many residence times have been determined and published. The presence of an abnormality in some organ can drastically alter the residence time.

We now calculate the cumulated activity and residence time for some simple situations.

### 17.6.2 Immediate Uptake with No Biological Excretion

This is the simplest example. A certain fraction of the radiopharmaceutical is taken up very rapidly in some organ, and it stays there. This is a good model for  $^{99m}\text{Tc}$ -sulfur colloid, which is used for liver imaging. About 85% is trapped in the liver; the remainder goes to the spleen

and elsewhere [Loevinger *et al.* (1988), p. 23]. The activity in the organ is  $A_h(t) = A_h e^{-\lambda t}$ . [Note the difference between the activity in organ  $h$  as a function of time,  $A_h(t)$ , the initial activity in organ  $h$ ,  $A_h$ , and the cumulated activity in organ  $h$ ,  $N_h = \tilde{A}_h$ .] Let the fraction of the activity in the organ be  $F_h$ . The cumulated activity is

$$\tilde{A}_h = A_h \int_0^\infty e^{-\lambda t} dt = \frac{A_h}{\lambda} = \frac{F_h A_0}{\lambda}.$$

The residence time is

$$\tau_h = \frac{\tilde{A}_h}{A_0} = \frac{F_h}{\lambda} = 1.443 F_h T_{1/2}. \quad (17.31)$$

### 17.6.3 Immediate Uptake with Exponential Biological Excretion

Suppose that in addition to physical decay with decay constant  $\lambda$ , the pharmaceutical moves to another organ while it is still radioactive. Such a process can be complicated, perhaps involving storage in the gut or bladder. In other cases, the disappearance from a particular organ may be close to exponential with a biological disappearance constant  $\lambda_j$ . (Assume for now that all the radioactive nuclei can disappear biologically. If some are bound in different chemical forms, this might not be true.) If  $N$  is the number of radioactive nuclei in the organ (not the total number originally administered), then the rate of change of  $N$  is

$$\frac{dN}{dt} = -(\lambda + \lambda_j)N,$$

the solution to which is  $N(t) = N_0 e^{-(\lambda + \lambda_j)t}$ . The activity is  $\lambda N$ , not  $-dN/dt$ . Since it is proportional to  $N$ , we can again write

$$A_h(t) = A_h e^{-(\lambda + \lambda_j)t} = \lambda N_0 e^{-(\lambda + \lambda_j)t}. \quad (17.32)$$

Again,  $N_0 = A_h/\lambda$ . The decay constant  $\lambda + \lambda_j$  is larger than the physical decay constant. The effective half-life is

$$(T_j)_{\text{eff}} = \frac{0.693}{\lambda + \lambda_j}. \quad (17.33)$$

In terms of the physical and biological half-lives  $T$  and  $T_j$ , this is

$$\frac{1}{(T_j)_{\text{eff}}} = \frac{1}{T} + \frac{1}{T_j} \quad (17.34)$$

or

$$(T_j)_{\text{eff}} = \frac{TT_j}{T + T_j}. \quad (17.35)$$

The cumulated activity is

$$\begin{aligned} \tilde{A}_h(t_1, t_2) &= A_h \int_{t_1}^{t_2} e^{-(\lambda + \lambda_j)t} dt \\ &= \frac{A_h}{\lambda + \lambda_j} (e^{-(\lambda + \lambda_j)t_1} - e^{-(\lambda + \lambda_j)t_2}). \end{aligned} \quad (17.36)$$

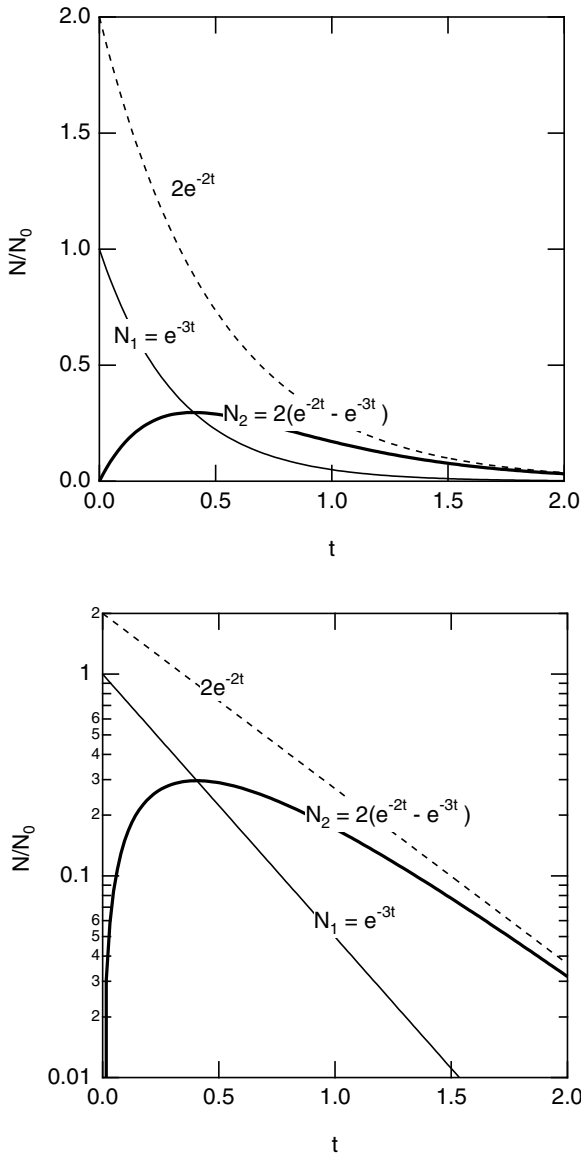


FIGURE 17.11. An example of two-compartment transfer when  $\lambda = 1$ ,  $\lambda_1 = 2$ , and  $\lambda_2 = 1$ .

The cumulated activity for all time is

$$\tilde{A}_h = \frac{A_h}{\lambda + \lambda_j} = 1.443 (T_j)_{\text{eff}} A_h. \quad (17.37)$$

### 17.6.4 Immediate Uptake Moving through Two Compartments

Consider the simplest two-compartment model. A total of  $N_0$  nuclei are administered that move immediately to the first compartment. They then move exponentially from the first compartment to the second but do not move back. The number in the first compartment is given by

$$\frac{dN_1}{dt} = -(\lambda_1 + \lambda)N_1. \quad (17.38)$$

The radioactive decay constant is  $\lambda$  and the biological disappearance rate is  $\lambda_1$ . In compartment 2, the substance enters from compartment 1 and is biologically removed with constant  $\lambda_2$ :

$$\frac{dN_2}{dt} = +\lambda_1 N_1 - (\lambda + \lambda_2)N_2. \quad (17.39)$$

Suppose we start with no nuclei in either compartment and inject  $N_0$  nuclei in compartment 1 at  $t = 0$ . Then one can show (see Problem 11) that

$$N_1(t) = N_0 e^{-(\lambda + \lambda_1)t} \quad (17.40)$$

so

$$\frac{dN_2}{dt} = \lambda_1 N_0 e^{-(\lambda + \lambda_1)t} - (\lambda + \lambda_2)N_2, \quad (17.41)$$

the solution to which is

$$N_2(t) = N_0 \frac{\lambda_1}{\lambda_1 - \lambda_2} \left( e^{-(\lambda + \lambda_2)t} - e^{-(\lambda + \lambda_1)t} \right). \quad (17.42)$$

These solutions are worth examining. They are plotted in Fig. 17.11 for  $\lambda = 1$ ,  $\lambda_1 = 2$ , and  $\lambda_2 = 1$ . The number of nuclei in compartment 1 is  $N_0 e^{-3t}$ . At first, many of the particles leaving compartment 1 enter compartment 2, and  $N_2$  rises. When there is no more of the substance entering the second compartment from the first,  $N_2$  decays at a rate  $\lambda + \lambda_2 = 2$ . This corresponds to the vanishing of the second term in Eq. 17.42. The larger the value of  $\lambda_1$ , the faster the second term vanishes. For very large values of  $\lambda_1$ , the second term vanishes quickly, the factor  $\lambda_1 / (\lambda_1 - \lambda_2)$  approaches unity, and the decay is nearly  $N_2(t) = N_0 e^{-(\lambda + \lambda_2)t}$ . The case  $\lambda_1 = \lambda_2$  is discussed in Problem 13. The activities are

$$A_1(t) = \lambda N_1(t), \quad A_2(t) = \lambda N_2(t)$$

and the cumulated activities are obtained by integration:

$$\tilde{A}_1 = \frac{A_0}{\lambda + \lambda_1}, \quad (17.43)$$

$$\tilde{A}_2 = \frac{A_0 \lambda_1}{(\lambda + \lambda_1)(\lambda + \lambda_2)}.$$

The residence times are

$$\tau_1 = \frac{1}{\lambda + \lambda_1}, \quad (17.44)$$

$$\tau_2 = \frac{\lambda_1}{(\lambda + \lambda_1)(\lambda + \lambda_2)}.$$

### 17.6.5 More Complicated Situations

A number of more complicated situations are solved by Loevinger *et al.* (1988). These include situations where substances move between compartments in both directions, the experimental data for the activity have been fit with a series of exponentials, and convolution techniques are used. All of these cases are for isotopes and pharmaceuticals used in clinical practice.

### 17.6.6 Activity per Unit Mass

It is sometimes convenient to use the *mean initial activity per unit mass*

$$C_h = \frac{A_h}{m_h} \text{ Bq kg}^{-1} \quad (17.45)$$

and the *cumulated mean activity per unit mass*

$$\tilde{C}_h = \frac{\tilde{A}_h}{m_h} = \frac{\tau_h A_0}{m_h} \text{ kg}^{-1}. \quad (17.46)$$

Earlier units for these were  $\mu\text{Ci g}^{-1}$  and  $\mu\text{Ci h g}^{-1}$ .

## 17.7 Mean Energy Emitted per Unit of Cumulated Activity

The mean energy emitted per unit cumulated activity  $\Delta_i$  is determined by knowing  $n_i$  and  $E_i$  for each particle or photon that is emitted. For a given nuclear transformation, the  $n_i$  and  $E_i$  must include all photons (whether  $\gamma$  rays or x rays) and all electrons (betas, internal conversion electrons, and Auger electrons). In SI units,

$$\Delta_i \text{ (in J)} = n_i E_i \text{ (in J)}. \quad (17.47a)$$

If  $E_i$  is expressed in MeV, we must use the conversion factor  $1 \text{ MeV} = 1.6 \times 10^{-13} \text{ J}$ . In the old system of units, there is the conversion factor:

$$\begin{aligned} \Delta_i \text{ (g rad } \mu\text{Ci}^{-1} \text{ h}^{-1}) &= n_i E_i \text{ (MeV)} \\ &\times (3.7 \times 10^4 \text{ s}^{-1} \mu\text{Ci}^{-1})(1.6 \times 10^{-13} \text{ J MeV}^{-1}) \\ &\times (10^7 \text{ erg J}^{-1})(3.6 \times 10^3 \text{ s h}^{-1})(10^{-2} \text{ rad g erg}^{-1}) \\ \Delta_i &= 2.13 n_i E_i. \end{aligned} \quad (17.47b)$$

Values of  $\Delta_i$  in the old units are found in the “output tables” for each nucleus (see Figs. 17.4, 17.9, and 17.10). We will calculate some values in this section to show how it is done.

Although  $\beta$  particles have a complicated energy spectrum, they are the easiest radiation for which to determine  $\Delta_i$ . Values of  $n_i$  are available in nuclear data tables that show the decay schemes for the nucleus under consideration, and average  $\beta$  energies have usually been measured. For positron decay, there are also two 0.511-MeV annihilation photons to be considered.

Referring to  $^{18}\text{F}$ , Fig. 17.10, we see that 0.97 of the decays are positron emission with an average energy of  $0.2496 \text{ MeV} = 4.00 \times 10^{-14} \text{ J}$ . Therefore,  $\Delta_i$  is  $0.97 \times 4.00 \times 10^{-14} = 3.87 \times 10^{-14} \text{ J}$ . For the old units, multiply by  $2.13/1.6 \times 10^{-13} = 1.33 \times 10^{13}$ , to get  $\Delta_i = 0.516 \text{ g rad } \mu\text{Ci}^{-1} \text{ h}^{-1}$ , which agrees with the entry under output data of Fig. 17.10. There are two annihilation photons for each nuclear transition, so  $n_i = 1.94$  and  $E_i = 0.511 \text{ MeV}$  for the annihilation radiation. This gives  $\Delta_i = 1.59 \times 10^{-13} \text{ J}$  or  $2.11 \text{ g rad } \mu\text{Ci}^{-1} \text{ h}^{-1}$ .

TABLE 17.2. Additional properties of  $^{99}\text{Tc}$  for calculation of  $\Delta_i$ .

Fluorescence yield <sup>a</sup>	$W_K$	0.74
$K$ -shell binding energy <sup>b</sup>	$B_K$	0.021 04 MeV
$L$ -shell binding energy	$B_L$	0.0028 MeV
$M$ -shell binding energy	$B_M$	0.0005 MeV
$\frac{K_\alpha}{K_\alpha + K_\beta} = 0.863$ (ratio of x rays emitted)		
$\frac{K_\beta}{K_\alpha + K_\beta} = 0.137$ (ratio of x rays emitted)		

<sup>a</sup>Estimated using Fig. 17.14.

<sup>b</sup>Binding energies are from *Handbook of Chemistry and Physics*, 51st ed., Cleveland, The Chemical Rubber Co., 1966, p. E-186.

Since electron capture competes with positron emission, it is also listed in the input data for  $^{18}\text{F}$  as occurring 3% of the time. Most of the energy is taken away by the neutrino, and it does not contribute to the absorbed dose. The x rays emitted by the residual  $^{18}\text{O}$  have such low energies that they are not listed in the output data. For a nucleus of higher  $Z$ , however, they would be important.

We turn now to  $\gamma$  emission, which often occurs after  $\beta$  emission because the resulting nucleus is not in its ground state. Internal conversion competes with the  $\gamma$  emission. Let us use the specific example  $^{99m}\text{Tc}$ , whose decay scheme is shown in Fig. 17.4. The 6-h half-life is associated with a metastable state, and the decay produces three possible  $\gamma$  rays. The “ground state” is actually not stable, but decays by emission with a half-life of  $2.1 \times 10^5$  yr. The problems will show that this can be neglected.

In addition to the data in the “input data” table of Fig. 17.4, we need some information about the x-ray characteristics of  $^{99}\text{Tc}$ . These are listed in Table 17.2. The subscripts of  $n_i$ ,  $E_i$ , and  $\Delta_i$  in the following all refer to the line in the output data of Fig. 17.4.

Consider  $\gamma_1$ . Its energy (0.0021 MeV) is less than the binding energy of either a  $K$  or  $L$  electron, so there is no  $K$  or  $L$  internal conversion. However,  $\alpha_M$  is very large, and we will assume that all of the  $\gamma_1$  transitions are  $M$ -shell internal conversions. In the output table (Fig. 17.4), this means that  $\Delta_1$  for  $\gamma_1$  is zero. The energy of the internal-conversion electron is the decay energy minus  $B_M$ :  $E_2 = 0.0021 - 0.0005 = 0.0016 \text{ MeV}$ . Then

$$\begin{aligned} \Delta_2 &= n_2 E_2 = (0.9860)(0.0016)(1.6 \times 10^{-13}) \\ &= 2.52 \times 10^{-16} \text{ J}. \end{aligned}$$

The remaining 0.0005 MeV is taken care of by  $M$  Auger electrons.

Now consider  $\gamma_2$ . There can be  $\gamma$  rays of this energy and internal conversion electrons from the  $K$ ,  $L$ , or  $M$  shells. We are told (input data) that  $\alpha_K = 0.104$ , and that  $\alpha_K = 7.7\alpha_L$ . It is also known empirically that

$\alpha_L \approx 3\alpha_M$ . Therefore, we can write

$$\begin{aligned}\alpha_K &= 0.104, \\ \alpha_L &= 0.0135, \\ \alpha_M &= 0.0045.\end{aligned}$$

Now Eq. 17.10 combined with the definition of  $\alpha$  gives

$$\begin{aligned}f_r + \alpha_K f_r + \alpha_L f_r + \alpha_M f_r &= 1, \\ f_r(1 + \alpha_K + \alpha_L + \alpha_M) &= 1, \\ f_r &= \frac{1}{1.122} = 0.8913, \\ f_K = \alpha_K f_r &= 0.0927, \\ f_L = \alpha_L f_r &= 0.0120, \\ f_M = \alpha_M f_r &= 0.0040.\end{aligned}\tag{17.48}$$

Each of these must be multiplied by  $n_{\gamma_2} = 0.9860$  to get the overall number of photons or internal-conversion electrons per decay associated with  $\gamma_2$ :

$$\begin{aligned}n_3 = n_{\gamma_2} f_r &= (0.9860)(0.8913) = 0.8788, \\ n_4 = n_{\gamma_2} f_K &= (0.9860)(0.0927) = 0.0914, \\ n_5 = n_{\gamma_2} f_L &= (0.9860)(0.0120) = 0.0118, \\ n_6 = n_{\gamma_2} f_M &= (0.9860)(0.0040) = 0.0039.\end{aligned}\tag{17.49}$$

The energies are calculated as follows:

$$\begin{aligned}E_3 = E_{\gamma_2} &= 0.1405 \text{ MeV}, \\ E_4 = E_{\gamma_2} - B_K &= 0.1405 - 0.0210 = 0.1195 \text{ MeV}, \\ E_5 = E_{\gamma_2} - B_L &= 0.1405 - 0.0028 = 0.1377 \text{ MeV}, \\ E_6 = E_{\gamma_2} - B_M &= 0.1405 - 0.0005 = 0.1400 \text{ MeV}.\end{aligned}\tag{17.50}$$

The values of  $\Delta_i$  are the products of these:

$$\begin{aligned}\Delta_3 &= 1.976 \times 10^{-14} \text{ J} = 0.2627 \text{ g rad } \mu\text{Ci}^{-1} \text{ h}^{-1}, \\ \Delta_4 &= 1.748 \times 10^{-15} \text{ J} = 0.0232 \text{ g rad } \mu\text{Ci}^{-1} \text{ h}^{-1}, \\ \Delta_5 &= 2.600 \times 10^{-16} \text{ J} = 0.0035 \text{ g rad } \mu\text{Ci}^{-1} \text{ h}^{-1}, \\ \Delta_6 &= 8.736 \times 10^{-17} \text{ J} = 0.0012 \text{ g rad } \mu\text{Ci}^{-1} \text{ h}^{-1}.\end{aligned}$$

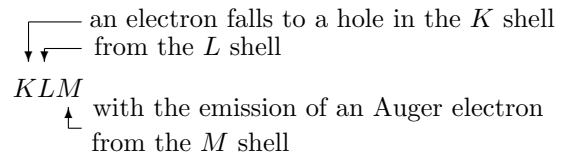
Similar calculations for the third  $\gamma$  ray are left to the problems.

We must next consider x-ray and Auger electron emission. A  $K$ -shell hole can be produced by a  $K$  internal-conversion electron from either  $\gamma_2$  ( $n_4 = 0.0913$ ) or  $\gamma_3$  ( $n_8 = 0.0088$ ). The total number of holes per nuclear transition is 0.1001. Of these, a fraction  $W_K = 0.74$  give x rays. The total number per transition is 0.074. Of these, a fraction  $K_\alpha/(K_\alpha + K_\beta) = 0.863$  go to  $K_\alpha$  x rays. These are listed as lines 11 and 12 in the output data of Fig. 17.4. Our calculation gives  $n_{11} + n_{12} = 0.0639$ .

The table gives 0.0662 for this sum. Considering that our value of  $W_K$  was obtained independently of the table, this is good agreement. For  $K_\beta$  x rays, we get  $n_{13} = (0.1001)(0.74)(0.137) = 0.0101$ . The energies of the x rays are obtained by subtracting the binding energies:

$$\begin{aligned}E_{11}(K_{\alpha_1}) &= B_K - B_L = 0.0210 - 0.0028 = 0.0182 \text{ MeV}, \\ E_{13}(K_\beta) &= B_K - B_M = 0.0210 - 0.0005 = 0.0205 \text{ MeV}.\end{aligned}$$

Of the holes in the  $K$  shell, a fraction  $1 - W_K = 0.26$  decay by emission of Auger electrons. The total number of  $K$  holes is 0.1001; the total number of  $K$  Auger electrons should therefore be  $(0.1001)(0.26) = 0.0260$ . The notation of the “output data” table is of the form



The sum of  $n_i$  for  $KLL$  and  $KLX$  ( $X$  denoting shells above the  $L$  shell) is 0.0207, in good agreement with the 0.0260 we calculated.

## 17.8 Calculation of the Absorbed Fraction

The remaining part of the dose determination problem is the most difficult: the calculation of  $\phi(r_k \leftarrow r_h)$ , the fraction of the radiation of a certain type emitted in region  $r_h$  that is absorbed in region  $r_k$ . A lot has been published on this problem; this section provides only an introduction.

### 17.8.1 Nonpenetrating Radiation

The simplest case is for charged particles or photons of very low energy that lose all their energy after traveling a short distance. If the source volume is much larger than this distance, we can say that the target volume is the same as the source volume:

$$\phi(r_k \leftarrow r_h) = \begin{cases} 0, & r_k \neq r_h \\ 1 & r_k = r_h. \end{cases}\tag{17.51}$$

### 17.8.2 Infinite Source in an Infinite Medium

Suppose that a radioactive source is distributed uniformly throughout a region that is so large that edge effects can be neglected. The activity per unit mass is  $C$ , so the total activity is  $\tilde{A} = M\tilde{C}$ , where  $M$  is the mass of the material. The energy released is  $\tilde{A}\Delta$ .

This is absorbed in mass  $M$ , so the fractional absorbed energy is 1, as in case 1. The dose is

$$D = \frac{M\tilde{C}\Delta}{M} = \tilde{C}\Delta.\tag{17.52}$$

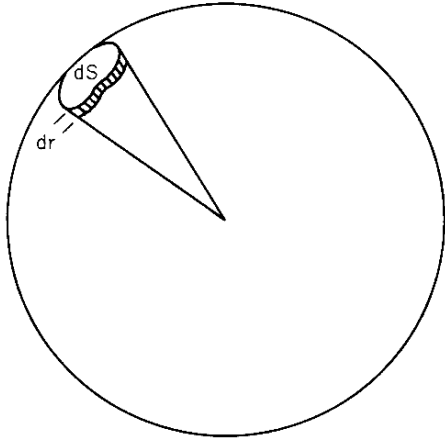


FIGURE 17.12. A small volume of absorbing material is introduced at distance  $r$  from a point source of  $\gamma$  rays.

(This is why  $\Delta$  used to be called the *equilibrium absorbed dose constant*.)

### 17.8.3 Point Source of Monoenergetic Photons in Empty Space

Another simple case is a point source of monoenergetic photons in empty space. The total amount of energy released by the source is  $\tilde{A}\Delta_i$ . If the energy of the radiation is  $E_i$ , the number of photons is  $\tilde{A}\Delta_i/E_i$ . At distance  $r$  the number per unit area is  $\tilde{A}\Delta_i/4\pi r^2 E_i$ . If a small amount of substance of area  $dS$ , density  $\rho$ , thickness  $dr$ , and energy absorption coefficient  $\mu_{en}$  is introduced as in Fig. 17.12, the amount of energy absorbed in it is  $E_i$  times the number of photons absorbed:  $\delta E = \tilde{A}\Delta_i dS \mu_{en} dr / 4\pi r^2$ . Therefore, the absorbed fraction is

$$\phi = \frac{\delta E}{\tilde{A}\Delta_i} = \frac{\mu_{en} dr dS}{4\pi r^2}. \quad (17.53)$$

This is exactly what we expect from the definition of  $\phi$ . If the source radiates its energy isotropically, the fraction passing through  $dS$  is  $dS/(4\pi r^2)$ . The fraction of that energy absorbed in  $dr$  is  $\mu_{en} dr$ . The specific absorbed fraction is

$$\Phi = \frac{\phi}{M} = \frac{\phi}{\rho dS dr} = \frac{\mu_{en}}{4\pi r^2 \rho}. \quad (17.54)$$

### 17.8.4 Point Source of Monoenergetic Photons in an Infinite Isotropic Absorber

If the source is not in empty space but in an infinite, homogeneous, isotropic absorbing medium, the number of photons at distance  $r$  from the source is modified by the factor  $e^{-\mu_{atten}r} B(r)$ , where the *buildup factor*  $B(r)$  accounts for secondary photons. Therefore,

$$\phi = \frac{\mu_{en} dr dS e^{-\mu_{atten}r}}{4\pi r^2} B(r) \quad (17.55)$$

and

$$\Phi = \frac{\mu_{en}}{\rho} \frac{e^{-\mu_{atten}r}}{4\pi r^2} B(r). \quad (17.56)$$

The buildup factor has been tabulated for photons of various energies in water [Berger (1968)].

### 17.8.5 More Complicated Cases—the MIRD Tables

For more realistic geometries, the calculation of  $\phi$  is quite complicated. Tables for humans of average build have been prepared by the MIRD Committee [Snyder *et al.* (1969, 1975, 1976)]. A “Monte Carlo” computer calculation was used. The description below shows how it works in principle; the actual calculations, though equivalent, are different in detail to save computer time.

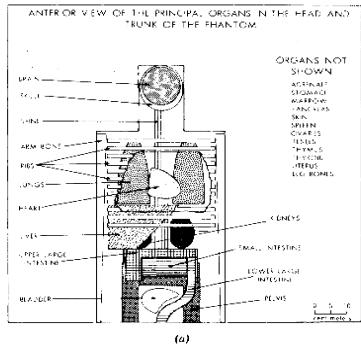
The radioactive nuclei are assumed to be distributed uniformly throughout the source organ. A point within the source organ is picked. The model emits a photon of energy  $E$  in some direction, picked at random from all possible directions. This photon is followed along its path; for every element  $ds$  of its path, the probability of its interacting,  $\mu_{atten} ds$ , is calculated. The computer program then “flips a coin” with this probability of having heads. If a head occurs, the photon is considered to interact at that point. If the interaction is Compton scattering, the angle is picked at random with a relative probability given by the differential cross section. The energy of a recoil electron for that scattering angle is calculated and deposited at the interaction site. Similar procedures are followed for the photoelectric effect and pair production. The scattered photon is then followed in the same way. If a tail occurred on the first flip, the photon is allowed to travel another distance  $ds$  and the probability of interaction is again calculated. This procedure is repeated until all the energy has been absorbed.

To determine what kind of material the photons are traveling through, a model of the body called a phantom is used. An example of a phantom is shown in Fig. 17.13. This entire procedure is repeated many times for each organ, until one has a map of the radiation deposited in all organs by  $\gamma$  rays leaving that point in the source organ.

The procedure is described in much greater detail by Snyder *et al.* (1969, 1976). Table 17.3 shows a portion of a table for  $\phi$ . Note that for each photon energy there are two columns:  $\phi$  and  $100\sigma_\phi/\phi$ , which is the percent fractional standard deviation in  $\phi$ , related to the square root of the number of photons absorbed in the target organ.

A computer code (OLINDA/EXM) is usually used to make the calculations [Stabin *et al.* (2005)].

Arqueros and Montesinos (2003) provide a pedagogical discussion of Monte Carlo simulation of  $\gamma$ -ray transport. A pedagogical program for whole-body Monte Carlo calculations has been developed by Hunt *et al.* (2004). It is



**HEART**  
 The heart is half an ellipsoid capped by a hemisphere which is cut by a plane. A rotation and translation are then effected. The heart (Fig. 4) is represented by  

$$x_1 = 0.6943(x + 1) - 0.3237(y + 3) - 0.6428(z - 51),$$

$$y_1 = 0.4226(x + 1) + 0.9063(y + 3),$$

$$z_1 = 0.5826(x + 1) - 0.2717(y + 3) + 0.7660(z - 51),$$

$$\left(\frac{x_1}{8}\right)^2 + \left(\frac{y_1}{5}\right)^2 + \left(\frac{z_1}{5}\right)^2 \leq 1,$$

$$x_1^2 + y_1^2 + z_1^2 \leq (5)^2 \quad \text{if } x_1 < 0,$$

$$\frac{x_1}{3} + \frac{z_1}{5} \geq -1 \quad \text{if } x_1 < 0$$
 and has a volume of 603.1 cm<sup>3</sup>.

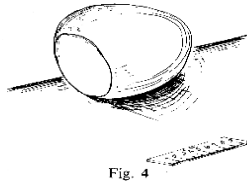


Fig. 4

FIGURE 17.13. The phantom used by the MIRD Committee for calculations of the absorbed fraction. (a) A view of the whole body. (b) Details of the heart boundaries. Reprinted by permission of the Society of Nuclear Medicine from W. S. Snyder, M. R. Ford, G. G. Warner, and H. L. Fisher. MIRD Pamphlet No. 5. Estimates of Absorbed Fractions for Monoenergetic Photon Sources Uniformly Distributed in Various Organs of a Heterogeneous Phantom. *J. Nucl. Med.* 1969; **10** (Suppl. 3): 5–52, Figs. 4 and 5.

available through the RADAR web site: [www.doseinfo-radar.com](http://www.doseinfo-radar.com).

Often most of the isotope is taken up in one or two organs, and the rest of it distributes fairly uniformly through the rest of the body. Using the subscript  $h$  for the organs with the greatest activity, TB to mean total body, and RB to mean the rest of the body,

$$\tilde{A}_{RB} = \tilde{A}_{TB} - \sum_h \tilde{A}_h. \quad (17.57)$$

The dose is then

$$D_k = \sum_h \tilde{A}_h S(r_k \leftarrow r_h) + \tilde{A}_{RB} S(r_k \leftarrow RB). \quad (17.58)$$

The quantity  $S(r_k \leftarrow RB)$  cannot easily be tabulated, since it depends on what organs are included in the sum over  $h$ . Substituting the tabulated quantity  $S(r_k \leftarrow TB)$  introduces errors because the “hot” organs that have significant activity are included a second time. One solution to this problem is to modify the cumulated activities [Coffey and Watson (1979)]. First, define a uniform total body cumulated activity that has the same cumulated activity per unit mass as the rest of the body:

$$\tilde{A}_u = \frac{m_{TB}}{m_{RB}} \tilde{A}_{RB}. \quad (17.59)$$

This activity in the total body would give a dose

$$D_k = \tilde{A}_u S(r_k \leftarrow TB).$$

Then define for each organ of interest the quantity  $\tilde{A}_h^*$ , which is the difference between the actual activity in organ  $h$  and that assuming the substance is uniformly distributed in the total body:

$$\tilde{A}_h^* = \tilde{A}_h - \frac{m_h}{m_{RB}} \tilde{A}_{RB}. \quad (17.60)$$

Then the dose to organ  $k$  is

$$D_k = \sum_h \tilde{A}_h^* S(r_k \leftarrow r_h) + \tilde{A}_u S(r_k \leftarrow TB). \quad (17.61)$$

Problem 32 shows that Eqs. 17.59–17.61 are consistent with Eqs. 17.57 and 17.58 if

$$\frac{m_{RB}}{m_{TB}} S(r_k \leftarrow RB) + \sum_h \frac{m_h}{m_{TB}} S(r_k \leftarrow r_h) = S(r_k \leftarrow TB), \quad (17.62)$$

which is consistent with a uniform source  $\tilde{A}_u$  distributed throughout the body. The dose can be determined either by calculating the modified activities and using the total body  $S$  in Eq. 17.61, or by calculating  $S$  for the rest of the body from Eq. 17.62 and using the unmodified activities. Problem 33 shows how these reformulations work in a simple case.

## 17.9 Radiopharmaceuticals and Tracers

A radioactive nucleus by itself is not very useful. It must usually be attached to some substance that will give it the desired biological properties, for example, to be preferentially absorbed in the region of interest. It must also be prepared in a sterile form, free of toxins that produce a fever (pyrogens) so that it can be injected in the patient. This section surveys some of the properties of *radiopharmaceuticals*.

### 17.9.1 Physical Properties

The half-life must be short enough so that a reasonable fraction of the radioactive decays take place during the diagnostic procedure; any decays taking place later give the patient a dose that has no benefit. (This requirement can be relaxed if the biological excretion is rapid.) On the other hand, the lifetime must be long enough so that the radiopharmaceutical can be prepared and delivered to the patient.

For diagnostic work, the decay scheme should minimize the amount of nonpenetrating radiation. Such radiation provides a dose to the patient but never reaches the detector. This means that there should be as few charged particles ( $\beta$  particles) as possible. The ideal source then is a  $\gamma$  source, which means that the nucleus is in an excited state (an isomer). Such states are usually very short-lived. Not only should the nucleus be a  $\gamma$  emitter, but the internal conversion coefficient should be small, since internal



TABLE 17.3. Absorbed fractions for a uniform source in the lungs, calculated using the MIRD phantom, for photon energies from 10 to 200 keV, with percent errors.

Target organ	Photon energy <i>E</i> (MeV)									
	0.010	0.015	0.020	0.030	0.050	0.100	0.200	Target organ	$\frac{100\sigma_\phi}{\phi}$	$\frac{100\sigma_\phi}{\phi}$
Adrenals	$\phi$	$\phi$	$\phi$	$\phi$	$\phi$	$\phi$	$\phi$	Adrenals	$\frac{100\sigma_\phi}{\phi}$	$\frac{100\sigma_\phi}{\phi}$
Bladder								Bladder		
GI(stomach)								GI(stomach)		
GI(SI)								GI(SI)		
GI(ULI)								GI(ULI)		
GI(LLI)								GI(LLI)		
Heart								Heart		
Kidneys								Kidneys		
Liver								Liver		
Lungs								Lungs		
Marrow								Marrow		
Pancreas								Pancreas		
Sk.(rib)								Sk.(rib)		
Sk.(pelvis)								Sk.(pelvis)		
Sk.(spine)								Sk.(spine)		
Sk.(skull)								Sk.(skull)		
Skeleton (total)								Skeleton (total)		
Skin								Skin		
Spleen								Spleen		
Thyroid								Thyroid		
Uterus								Uterus		
Trunk								Trunk		
Legs								Legs		
Head								Head		
Total body								Total body		

Source: Reprinted by permission of the Society of Nuclear Medicine from W. S. Snyder, M. R. Ford, G. G. Warner, and H. L. Fisher. MIRD Pamphlet No. 5. Estimates of Absorbed Fractions for Monoenergetic Photon Sources Uniformly Distributed in Various Organs of a Heterogeneous Phantom. *J. Nucl. Med.* 1969 **10** (Suppl 3): 5-52. Table pp. 30-31, with permission of the publisher.

conversion produces nonpenetrating electrons. Positron emitters are more desirable than are  $\beta^-$  emitters because the positrons produce 0.5-MeV radiation that can reach an external detector. For therapy, on the other hand, nonpenetrating radiation is ideal.

It is also necessary that the decay product have no undesirable radiations. If the decay is a  $\beta^-$  or  $\beta^+$  decay, the product has different chemical properties from the parent and may be taken up selectively by a different organ. If it is also radioactive, this can confuse a diagnosis and give an undesirable dose to the other organ.

Ease of chemical separation of the radioactive substance from whatever carrier it is produced with is also important. It is necessary to remove the radioactive isotope from stable isotopes of the same element, because the chemicals are usually toxic. This toxicity is avoided by giving the chemical in minute amounts, which can only be done if the specific activity is high.

### 17.9.2 Biological Properties

For diagnostic work, a pharmaceutical is needed that is taken up more by the diseased tissue to give a "hot spot" or taken up less to give a "cold spot." The former is easier to see with small amounts of radioactivity, but both techniques are used. For therapy one wishes to have selective absorption of the pharmaceutical so that the radiations will destroy the target organ but not the rest of the body. There are several mechanisms by which a pharmaceutical may be localized.

1. *Active transport.* The drug is concentrated by a specific organ against a concentration gradient. Examples are the selective concentration of iodine in the thyroid, salivary, and gastric glands. (It is rapidly excreted from the last two but is retained in the thyroid). This technique is also effective for certain drugs in the kidney.
2. *Phagocytosis.* Particles in the size range 1–1,000 nm may be phagocytized—taken up by specialized cells of the reticuloendothelial system. This can take place in liver, bone marrow, and spleen. Particles of size 1 nm go to the Kupfer cells of the liver and to the marrow, while larger particles (100–1,000 nm) are gathered by phagocytes in the liver and spleen.
3. *Sequestration.* Still larger particles, such as red blood cells that have been denatured by heat, are gathered in the spleen or liver by the process called sequestration. The particles are trapped as the blood percolates through the pulp of the spleen and are later phagocytized.
4. *Capillary blockade.* The capillaries have a diameter of 7–10  $\mu\text{m}$ . Particles from 20 to 40  $\mu\text{m}$  diameter injected into a vein will find progressively larger vessels as they work their way through the right heart and will be stopped in the capillaries of the lung.

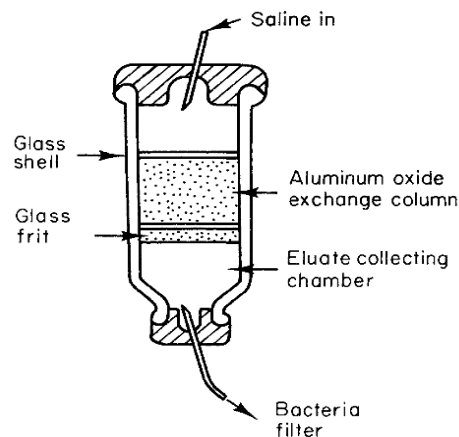


FIGURE 17.14. A  $^{99}\text{Mo}$ - $^{99\text{m}}\text{Tc}$  generator system. Molybdenum is trapped in the aluminum oxide layer. Eluant introduced at the top flows through and is collected at the bottom.

5. *Diffusion.* It is also possible for a pharmaceutical to move through a membrane to a region of lower concentration. There is a blood–brain barrier between the blood and the central nervous system that is relatively impermeable even to small ions. In a brain scan the chemical is not concentrated in normal brain tissue but leaks into tissue where the blood–brain barrier is compromised by a lesion.
6. *Compartmental localization.* A suitable pharmaceutical injected in the blood may remain there a long time, mixing well and allowing the blood volume to be determined.

The most widely used isotope is  $^{99\text{m}}\text{Tc}$ . As its name suggests, it does not occur naturally on earth, since it has no stable isotopes. We consider it in some detail to show how an isotope is actually used. Its decay scheme has been discussed above. There is a nearly monoenergetic 140-keV  $\gamma$  ray. Only about 10% of the energy is in the form of nonpenetrating radiation. The isotope is produced in the hospital from the decay of its parent,  $^{99}\text{Mo}$ , which is a fission product of  $^{235}\text{U}$  and can be separated from about 75 other fission products. The  $^{99}\text{Mo}$  decays to  $^{99\text{m}}\text{Tc}$ .

Tchnetium is made available to hospitals through a "generator" that was developed at Brookhaven National Laboratories in 1957 and is easily shipped. Isotope  $^{99}\text{Mo}$ , which has a half-life of 67 h, is adsorbed on an alumina substrate in the form of molybdate ( $\text{MoO}_4^{2-}$ ). From 8 to 100 GBq of  $^{99}\text{Mo}$  can be provided. The heart of such a generator (without the lead shielding) is shown in Fig. 17.14. As the  $^{99}\text{Mo}$  decays, it becomes pertechnetate ( $\text{TcO}_4^-$ ). Sterile isotonic eluting solution is introduced under pressure above the alumina and passes through after filtration into an evacuated eluate container. After removal of the technetium, the continued decay of  $^{99}\text{Mo}$  causes the  $^{99\text{m}}\text{Tc}$  concentration to build up again. A generator lasts about a week.

Several steps must be taken to prepare the pertechnetate as a radiopharmaceutical. First, it must be checked for breakthrough of the <sup>99</sup>Mo. The Nuclear Regulatory Commission allows  $1.5 \times 10^{-4}$  Bq of <sup>99</sup>Mo per Bq of <sup>99m</sup>Tc. The purity is checked by placing the eluate in a lead sleeve that attenuates the <sup>99m</sup>Tc  $\gamma$  ray much more than the  $\approx 750$ -keV  $\gamma$  rays from <sup>99</sup>Mo and measuring the activity. It is also checked with a colorimetric test for the presence of aluminum ion.

The eluate can be used directly for imaging brain, thyroid, salivary gland, urinary bladder, and blood pool, or it can be combined with phosphate, albumin or aggregated albumin, colloidal sulfur, or FeCl<sub>3</sub>. Commercial kits are available for making these preparations.

For example, kits for labeling aggregated human albumin are commercially available. A vial containing 10 ml of saline solution is enough for ten doses. The aggregated albumin particles are 10–70  $\mu$ m in diameter. Each milliliter of solution contains  $(4 - 8) \times 10^5$  particles. Tin is attached to the microspheres and serves to bind technetium. Up to 10<sup>9</sup> Bq of technetium pertechnetate is added to the vial by the user. A typical adult dose is 10–40 MBq ( $3.51 \times 10^5$  albumin particles). The problems consider attaching Tc to the microspheres and what fraction of the capillaries are blocked by this kind of study.

Other common isotopes are <sup>201</sup>Tl, <sup>67</sup>Ga, and <sup>123</sup>I. Thallium, produced in a cyclotron, is chemically similar to potassium and is used in heart studies, though it is being replaced by <sup>99m</sup>Tc–sestamibi and <sup>99m</sup>Tc–tetrofosmin. Gallium is used to image infections and tumors. Iodine is also produced in a cyclotron and is used for thyroid studies.

### 17.10 Sample Dose Calculation

We pull this discussion together by making a simplified calculation of the dose to various organs from <sup>99m</sup>Tc-labeled microspheres used in a lung scan. We assume that 37 MBq of <sup>99m</sup>Tc is injected, that it all lodges in the capillaries of the lung, and that it remains there long enough so that the half-life is the physical half-life.<sup>9</sup> The residence time is then  $\tau_h = 1.443T_{1/2} = (1.443)(6) = 8.658$  h, so the cumulated activity is  $\bar{A}_{\text{lung}} = (3.7 \times 10^7)(8.658 \times 60 \times 60) = 1.153 \times 10^{12}$  Bq s.

The steps in calculating  $S$  and the dose are summarized in Table 17.4, which combines information on  $\Delta_i$  with values of  $\phi$  for lung, heart, liver, head, and the whole body. The values of  $\Delta_i$  are from Fig. 17.15, which is a more

<sup>9</sup>The last is not a good assumption. The <sup>99m</sup>Tc leaches from the microspheres into the general circulation. A more accurate calculation requires measurements and the use of a convolution integral, as described in Loevinger *et al.* (1988, pp. 79–81). The principle residence times are 4.3 h in the lung, 1.8 h in the extravascular space, 0.83 h in the urine, 0.7 h in the kidney, and 0.6 h in the blood.

43-TECHNETIUM-99M

HALF-LIFE = 6.01 HOURS  
DECAY MODE(S):  $\beta^-$ , IT

11-AUG-86

RADIATION	PARTICLES/ TRANSITION n(i)	ENERGY/ PARTICLE E(i) MeV	ENERGY/TRANSITION	
			$\Delta(i)$ rad g/ $\mu$ Ci h	$\Delta(i)$ Gy kg/Bq s
ce-M, $\gamma$ 1	9.16E-01	1.748E-03†	3.41E-03	2.56E-16
ce-N <sup>+</sup> , $\gamma$ 1	7.58E-02	2.173E-03†	3.51E-04	2.64E-17
$\gamma$ 2	8.91E-01	1.405E-01	2.67E-01	2.00E-14
ce-K, $\gamma$ 2	8.84E-02	1.195E-01	2.25E-02	1.70E-15
ce-L <sub>1</sub> , $\gamma$ 2	9.72E-03	1.375E-01	2.85E-03	2.15E-16
ce-L <sub>2</sub> , $\gamma$ 2	6.32E-04	1.377E-01	1.85E-04	1.40E-17
ce-L <sub>3</sub> , $\gamma$ 2	3.29E-04	1.378E-01	9.66E-05	7.26E-18
ce-M, $\gamma$ 2	1.94E-03	1.401E-01†	5.79E-04	4.36E-17
ce-N <sup>+</sup> , $\gamma$ 2	3.74E-04	1.405E-01†	1.12E-04	8.43E-18
ce-K, $\gamma$ 3	5.53E-03	1.216E-01	1.43E-03	1.08E-16
ce-L <sub>1</sub> , $\gamma$ 3	9.34E-04	1.396E-01	2.78E-04	2.08E-17
ce-L <sub>2</sub> , $\gamma$ 3	1.94E-04	1.398E-01	5.78E-05	4.34E-18
ce-L <sub>3</sub> , $\gamma$ 3	5.92E-04	1.400E-01	1.77E-04	1.33E-17
ce-M, $\gamma$ 3	3.35E-04	1.422E-01†	1.02E-04	7.64E-18
K $\alpha$ , x-ray	3.99E-02	1.837E-02	1.56E-03	1.17E-16
K $\beta$ , x-ray	2.10E-02	1.825E-02	8.17E-04	6.14E-17
K $\beta$ , x-ray	6.82E-03	2.062E-02	3.00E-04	2.26E-17
Auger-KL <sub>1</sub> L <sub>1</sub>	1.23E-03	1.487E-02	3.90E-05	2.95E-18
Auger-KL <sub>1</sub> L <sub>2</sub>	2.14E-03	1.512E-02	6.90E-05	5.17E-18
Auger-KL <sub>1</sub> L <sub>3</sub>	1.64E-03	1.524E-02	5.33E-05	4.00E-18
Auger-KL <sub>2</sub> L <sub>1</sub>	6.44E-03	1.547E-02	2.12E-04	1.60E-17
Auger-KL <sub>2</sub> L <sub>2</sub>	2.43E-03	1.559E-02	8.07E-05	6.07E-18
Auger-KL <sub>2</sub> L <sub>3</sub>	1.80E-03	1.755E-02†	6.73E-05	5.05E-18
Auger-KL <sub>3</sub> X	1.42E-03	1.780E-02†	5.39E-05	4.05E-18
Auger-KL <sub>3</sub> X	2.49E-03	1.792E-02†	9.51E-05	7.13E-18
Auger-L <sub>2</sub> MM	1.98E-02	2.125E-03†	8.97E-05	6.74E-18
Auger-L <sub>2</sub> MX	8.37E-03	2.538E-03†	4.53E-05	3.40E-18
Auger-L <sub>3</sub> MX	4.81E-02	2.009E-03†	2.06E-04	1.55E-17
Auger-L <sub>3</sub> MX	2.07E-02	2.422E-03†	1.07E-04	8.03E-18
Auger-MXY	1.11E+00	4.092E-04†	9.68E-04	7.27E-17
Listed x, $\gamma$ and $\gamma_{\pm}$ radiations			2.69E-01	2.02E-14
Omitted x, $\gamma$ and $\gamma_{\pm}$ radiations†			3.22E-04	2.42E-17
Listed $\beta$ , ce and Auger radiations			3.43E-02	2.58E-15
Omitted $\beta$ , ce and Auger radiations†			1.22E-04	9.20E-18
Listed radiations			3.03E-01	2.27E-14
Omitted radiations†			4.45E-04	3.35E-17

† Average energy  
‡ Each omitted transition contributes <0.100% to  $\Sigma\Delta(i)$  in its category.  
RUTHENIUM-99 daughter, yield 3.70E-05, is stable.  
TECHNETIUM-99 daughter, yield 9.9996E-01, is radioactive.

FIGURE 17.15. The values of  $\Delta_i$  for <sup>99m</sup>Tc used in Table 17.4 to calculate the dose from a source in the lungs. These are more recent values than those in Fig. 17.4. The reference at the bottom to ruthenium-99 is because <sup>99m</sup>Tc undergoes  $\beta$  decay in  $3.7 \times 10^{-5}$  of transitions. This does not affect any of the entries in the table. Reprinted by permission of the Society of Nuclear Medicine from D. A. Weber, K. F. Eckerman, L. T. Dillman, and J. C. Ryman. *MIRD: Radionuclide Data and Decay Schemes*. New York, Society of Nuclear Medicine, 1989: 178–179.

recent version of the output table of Fig. 17.4. Table 17.4 refers to the line number for the entry in both Fig. 17.15 and Fig. 17.4. It is worth taking time to compare the entries with the lines in Fig. 17.4 to see the variations with more recent information. Values of  $\phi_i(r_k \leftarrow r_h)$  are taken to be 1 in the lung and the whole body when the radiations are nonpenetrating, that is, photons with energy less than 25 keV or electrons. For the high-energy photons (line 3) the values of  $\phi$  are obtained by interpolation to 140 keV from the values in Table 17.3 for 100 and 200 keV. The sum  $S_k = \sum \Delta_i \phi_i$ , the mass of each organ, and the dose for the cumulated activity of  $1.153 \times 10^{12}$  Bq

TABLE 17.4. Values of  $\Delta_i$ ,  $E_i$ , and  $\phi_i$  for  $^{99m}\text{Tc}$  in the lung.

$i$ , Line in Fig. 17.15	$\Delta_i$ (Gy kg <sup>-1</sup> Bq <sup>-1</sup> s <sup>-1</sup> )	$E_i$ (keV) (e denotes an electron)	$\phi_i$					Line in Fig. 17.4	$\Delta_i$ (g rad $\mu\text{Ci}^{-1}$ h <sup>-1</sup> )
			Lung	Heart	Liver	Head	Whole Body		
1	$2.56 \times 10^{-16}$	e	1	0	0	0	1	0.0000	
2	$2.64 \times 10^{-17}$	e	1	0	0	0	1	0.0034	
3	$2.00 \times 10^{-14}$	140.5	0.0495	0.0135	0.0166	0.0077	0.3785	0.0004	
4	$1.70 \times 10^{-15}$	e	1	0	0	0	1	0.2670	
5-7	$2.15 \times 10^{-16}$	e	1	0	0	0	1	0.0252	
8	$4.36 \times 10^{-17}$	e	1	0	0	0	1	0.0031	
9	$8.43 \times 10^{-18}$	e	1	0	0	0	1	0.0006	
10	$1.08 \times 10^{-16}$	142.6	0.0495	0.0135	0.0166	0.0077	0.3785	0.0001	
11-13	$3.84 \times 10^{-17}$	e	1	0	0	0	1	0.0000	
14	$7.64 \times 10^{-18}$	e	1	0	0	0	1	0.0014	
15	$1.17 \times 10^{-16}$	18.37	1	0	0	0	1	0.0005	
16	$6.14 \times 10^{-17}$	18.25	1	0	0	0	1	0.0001	
17	$2.26 \times 10^{-17}$	20.62	1	0	0	0	1	0.0016	
18-22	$3.419 \times 10^{-17}$	e	1	0	0	0	1	0.0008	
23-25	$1.623 \times 10^{-17}$	e	1	0	0	0	1	0.0003	
26-28	$3.367 \times 10^{-17}$	e	1	0	0	0	1	0.0005	
29	$7.27 \times 10^{-17}$	e	1	0	0	0	1	0.0002	
$\sum \Delta_i \phi_i$			$3.75 \times 10^{-15}$	$2.70 \times 10^{-16}$	$3.32 \times 10^{-16}$	$1.54 \times 10^{-16}$	$1.03 \times 10^{-14}$	0.0045	
$m$ (kg)			0.999	0.603	1.833	5.278	70.036	0.0010	
$S = \sum \Delta_i \phi_i / m$			$3.76 \times 10^{-15}$	$4.48 \times 10^{-16}$	$1.81 \times 10^{-16}$	$2.92 \times 10^{-17}$	$1.48 \times 10^{-16}$		
Dose (Gy) $A_0 = 37$ MBq			$4.33 \times 10^{-3}$	$5.16 \times 10^{-4}$	$2.09 \times 10^{-4}$	$3.36 \times 10^{-5}$	$1.70 \times 10^{-4}$		

TABLE 17.5. Some typical doses for nuclear medicine procedures.

Study and agent	$A_0$ (MBq)	Organ and highest dose (mSv)	Total body dose (mSv)	Effective dose (mSv)
Bone $^{99m}\text{Tc}$ -pyrophosphate	555	Bladder wall 51	2.0	4.4
Heart $^{201}\text{Tl}$ -chloride	55	Kidneys 20	3.6	13
Liver $^{99m}\text{Tc}$ -sulfur colloid	185	Bladder wall 17	0.9	2.6

Source: Adapted from Table 9-3 in P. B. Zanzonico, A. B. Brill, and D. V. Becker, Radiation dosimetry, Chapter 9 in H. N. Wagner, Jr., Z. Szabo, and J. W. Buchanan, eds. *Principles of Nuclear Medicine*, 2nd. ed. Philadelphia, Saunders (1995).

s are shown on the bottom lines. The dose to the lungs is  $4.3 \times 10^{-3}$  Gy. The whole body dose is much less because the absorbed energy is divided by the mass of the entire body. The value of  $\phi$  shows that about 38% of the photon energy is absorbed in the body.

The dose to the lungs is considerably greater than in a chest x ray; however, a chest x ray is almost useless for diagnosing a pulmonary embolus. The whole body dose is not unreasonable.

Table 17.5 shows some typical doses from various nuclear medicine procedures. The effective dose is defined on p. 468.

## 17.11 Auger Electrons

In Sec. 15.9 we discussed the deexcitation of atoms, including the emission of Auger and Coster-Kronig electrons. The Auger cascade means that several of these electrons are emitted per transition. If a radionuclide is in a compound that is bound to DNA, the effect of several electrons released in the same place is to cause as much damage per unit dose as high-LET radiation. Linear energy transfer was defined in Chapter 15. A series of reports on this effect have been released by the American Association of Physicists in Medicine (AAPM) [Sastry (1992); Howell (1992); Humm *et al.* (1994)].

Many electrons (up to 25) can be emitted for one nuclear transformation, depending on the decay scheme [Howell (1992)]. The electron energies vary from a few eV to a few tens of keV. Corresponding electron ranges are from less than 1 nm to 15  $\mu\text{m}$ . The diameter of the DNA double helix is about 2 nm. A number of experiments [reviewed in the AAPM reports, also Kassis (2004)] show that when the radioactive substance is in the cytoplasm the cell damage is like that for low-LET radiation in Fig. 15.32 with relative biological effectiveness (RBE) = 1. When it is bound to the DNA, survival curves are much steeper, as with the  $\alpha$  particles in Fig. 15.32 (RBE  $\approx$  8). When it is in the nucleus but not bound to DNA the RBE

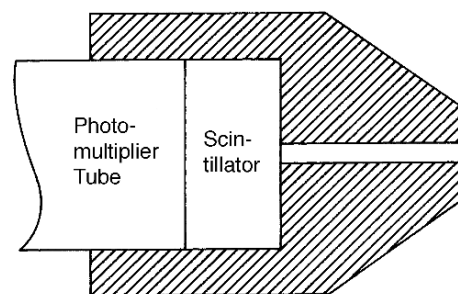


FIGURE 17.16. A scintillator with a lead collimator to give directional sensitivity.

is about 4. The fraction of the Auger emitter that binds to the DNA depends on the chemical agent to which the nuclide is attached. There is also a significant bystander effect [Kassis (2004)].

## 17.12 Detectors; The Gamma Camera

Nuclear medicine images do not have the inherent spatial resolution of diagnostic x-ray images; however, they provide functional information: the increase and decrease of activity as the radiopharmaceutical passes through the organ being imaged.

Early measurements were done with single detectors such as the scintillation detector<sup>10</sup> shown in Fig. 17.16. Directional sensitivity is provided by a collimator, which can be cylindrical or tapered. Single detectors are still used for in vitro measurements and for thyroid uptake studies.

Two-dimensional images can be taken with the *scintillation camera* or *gamma camera* shown in Figs. 17.17 and 17.18. The scintillator is 6–12 mm thick and about 60 cm across. Modern scintillators are rectangular. The scintillator is viewed by an array of 50–100 photomultiplier tubes arranged in a hexagonal array. The tube nearest

<sup>10</sup>Scintillation detectors were discussed in Sec. 16.3.

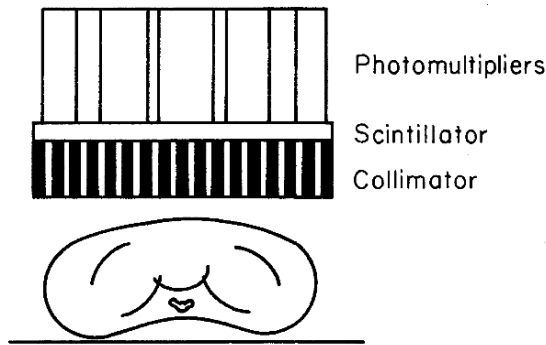


FIGURE 17.17. Side view of a scintillation camera. A collimator allows photons from the patient to strike the scintillator directly above the source. An array of photomultiplier tubes records the position and energy of the detected photon.

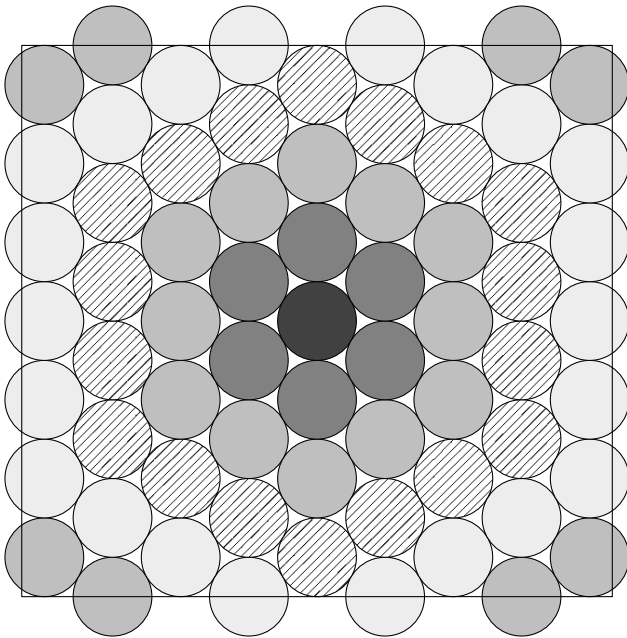


FIGURE 17.18. A square scintillator viewed by an array of 67 photomultiplier tubes. The hexagonal arrangement of the tubes above the scintillator gives the closest spacing between tubes.

where the photon interacts receives the greatest signal. Signals from each tube are combined to give the total energy signal and  $x$  and  $y$  position signals.

The collimator is a critical component of the gamma camera. The channels are usually hexagonal, with walls just thick enough to stop most of the photons which do not pass down the collimator opening. The collimator usually has parallel channels; single pinholes, diverging, and converging channels are sometimes used and can lead to geometric distortions of the image [Cherry *et al.* (2003), p. 221, 239ff]. The spatial resolution depends on the distance from the source to the collimator, as shown for one collimator in Fig. 17.19. There are trade-offs between sensitivity and resolution [Links and Eng-

dahl (1995)]. Some of the aspects of collimator design are discussed in Problems 48–50.

Figure 17.20 shows a bone scan of a child taken with a gamma camera. The  $^{99m}\text{Tc}$ -diphosphonate is taken up in areas of rapid bone growth. Bone growth at the epiphyses at the end of each bone can be seen. There are also hot spots at the injection site, in one kidney, and in the bladder.

Nuclear medicine can show physiologic function. For example, if the isotope is uniformly distributed in the blood, viewing the heart and synchronizing the data accumulation with the electrocardiogram (gating) allows one to measure blood volume in the heart when it is full and contracted, and to calculate the *ejection fraction*, the fraction of blood in the full left ventricle that is pumped out. Fig. 17.21, shows pictures and contours of the heart at end-systole and end-diastole. The imaging agent was  $^{99m}\text{Tc}$ -labeled human red blood cells.

Figure 17.22 shows a series of images taken at six different angles around a patient who has had a lung transplant. The left lung is new and shows considerably more activity than the diseased right lung.

## 17.13 Single-Photon Emission Computed Tomography

Still another detection scheme, *single-photon emission computed tomography* (SPECT), is analogous to computed tomography (CT). The detector is sensitive to all radioactivity along a line passing through the patient. The counting rate is thus proportional to a projection through the patient, and a cross-sectional slice can be reconstructed from a series of projections, just as was done with x-ray CT using the techniques in Ch. 12. A series of images like those in Fig. 17.22, but at more angles, are used to reconstruct a three-dimensional image that can then be viewed from any direction, with slices at any desired depth. A SPECT scan is shown in Fig. 17.23. There are five reconstructed slices in planes parallel to the long axis of the heart. The left ventricle is prominent, and the right ventricle can be seen faintly in the last few slices.

One of the problems with SPECT is photon attenuation along the projection line. This is shown in Fig. 17.24 for a cylindrical source with uniform activity throughout. Let  $A_V$  be the activity per unit volume, and ignore variations in  $1/r^2$ . The projection  $F(x)$  is

$$F(x) = \int_{-a}^a A_V(x, y) \Delta x \Delta z e^{-\mu(y+a)} dy, \quad (17.63)$$

where  $dy \Delta x \Delta z$  is the volume detected. When  $A_V(x, y)$  is constant (a uniform activity distribution), this can be integrated to give

$$F = \frac{A_V \Delta x \Delta z}{\mu} \left( 1 - e^{-2\mu(R^2 - x^2)^{1/2}} \right). \quad (17.64)$$

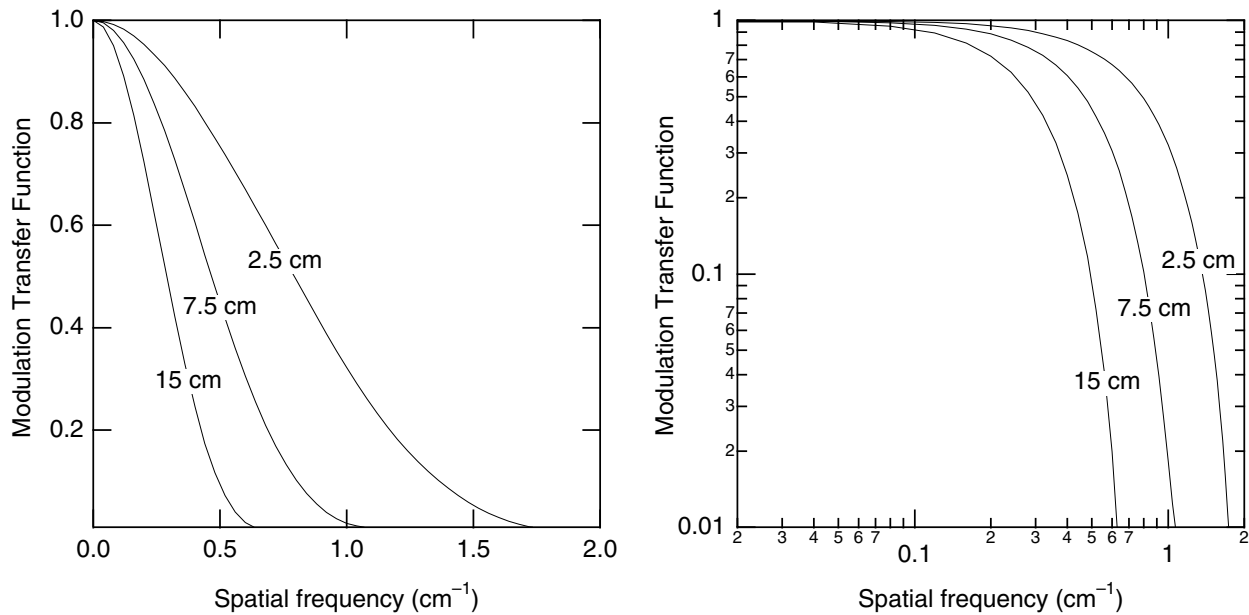


FIGURE 17.19. Modulation transfer function curves for a typical parallel-hole collimator for different source-to-collimator distances. Both linear and log-log plots are shown. The source-to-collimator distances are 2.5, 7.5, and 15 cm. Data are from J. C. Erhardt, L. W. Oberly, and J. M. Cuevas, *Imaging Ability of Collimators in Nuclear Medicine*, Rockville, MD, U.S. Dept. HEW, Publ. No. (FDA)79-8077 (1978), p. 39.

This is plotted in Fig. 17.25 for  $\mu = 0$ ,  $\mu = 10 \text{ m}^{-1}$  (511-keV annihilation radiation) and  $\mu = 15 \text{ m}^{-1}$  (140 keV  $^{99m}\text{Tc}$ ). When  $\mu = 0$ ,  $F(x) = A_V(2a\Delta x\Delta z)$ , where  $2a$  is the thickness of the source along the projection. Corrections for attenuation are made in a number of ways.<sup>11</sup> Other nuclides used besides  $^{99m}\text{Tc}$  are  $^{81m}\text{Kr}$ ,  $^{133}\text{Xe}$ ,  $^{131}\text{I}$ ,  $^{67}\text{Ga}$ ,  $^{123}\text{I}$ , and  $^{201}\text{Tl}$ .

TABLE 17.6. Positron emitters used in nuclear medicine.

Nuclide	Half-life
$^{11}_6\text{C}$	20.3 min
$^{13}_7\text{N}$	10.0 min
$^{15}_8\text{O}$	2.1 min
$^{18}_9\text{F}$	109.7 min

## 17.14 Positron Emission Tomography

If a positron emitter is used as the radionuclide, the positron comes to rest and annihilates an electron, emitting two annihilation photons back to back. In *positron emission tomography* (PET) these are detected in coincidence. This simplifies the attenuation correction, because the total attenuation for both photons is the same for all points of emission along each  $\gamma$  ray through the body (see Problem 54). Positron emitters are short-lived, and it is necessary to have a cyclotron for producing them in or near the hospital. This is proving to be less of a problem than initially imagined. Commercial cyclotron facilities deliver isotopes to a number of nearby hospitals. Patterson and Mosley (2005) found that 97% of the people in the United States live within 75 miles of a clinical PET facility.

We have mentioned that nuclear medicine procedures have the potential to measure function, as the molecules to which the isotopes are bound move from or-

gan to organ in the body. This is particularly true for some of the lighter positron emitters, which have the advantage of being natural constituents of molecules in the body or similar to them (Table 17.6). PET can provide a *functional image* with information about metabolic activity. A very common positron agent is  $^{18}\text{F}$  fluorodeoxyglucose—glucose in which a hydroxyl group has been replaced with  $^{18}\text{F}$ . The PET signal is largest in those cells that have taken up the  $^{18}\text{F}$  because they are actively metabolizing glucose. PET has become particularly important in studies of brain function, where active neurons are detected by an increase in their metabolism, and in locating metastatic cancer. The number of installed PET scanners is growing very rapidly. Most of them have built-in CT scanners to provide accurate fused PET/CT images.

A PET scan overlaid on a magnetic resonance (MRI) image is shown in Fig. 17.26 The positron emitter is  $^{15}\text{O}$ -labeled water. The views are described in the caption. The subject is sequentially touching each finger of the left hand with the thumb. Activity can be seen in the

<sup>11</sup>See Cherry *et al.* (2003, pp. 305–312); Larsson (1980).



FIGURE 17.20. A scintillation camera “bone scan” of a 7-year-old male who received a  $^{99m}\text{Tc}$ -diphosphonate injection. An anterior view is on the left, and a posterior view is on the right. The scan shows an area of decreased uptake surrounded by a dark ring in the right anterior skull, consistent with an *eosinophilic granuloma*. Identifiable hot regions are the injection site in the right elbow, an attempted injection site in the right hand, the bladder, and the left kidney, which is probably not remarkable on this exam, along with the ends of the long bones. Photograph courtesy of B. Hasselquist, Ph.D., Department of Diagnostic Radiology, University of Minnesota.

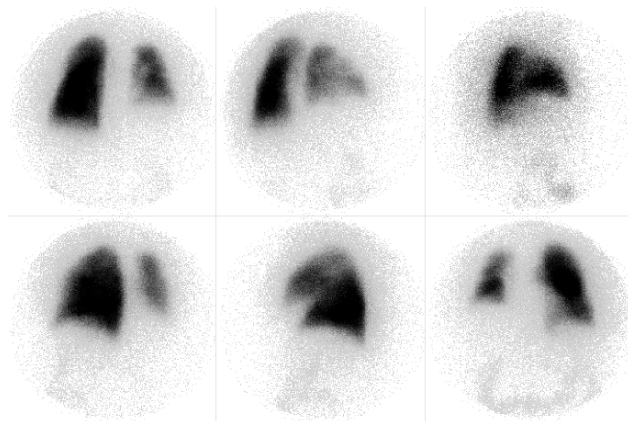


FIGURE 17.22. Lung scans of a patient who has received a lung transplant. The upper left is a posterior view; each successive view is rotated about the patient, ending with an anterior view on the lower right. The left lung is the transplant. It has much more activity than the diseased right lung. Photograph courtesy of B. Hasselquist, Ph.D., Department of Diagnostic Radiology, University of Minnesota.



FIGURE 17.23. Single photon emission computed tomographic (SPECT) slices of the heart. The patient was injected with  $^{99m}\text{Tc}$ -tetrofosmin, an agent that is taken up by myocardium. The images have been reconstructed in planes parallel to the axis of the heart. The dark myocardium surrounds the blood in the left ventricle. Photograph courtesy of B. Hasselquist, Ph.D., Department of Diagnostic Radiology, University of Minnesota.

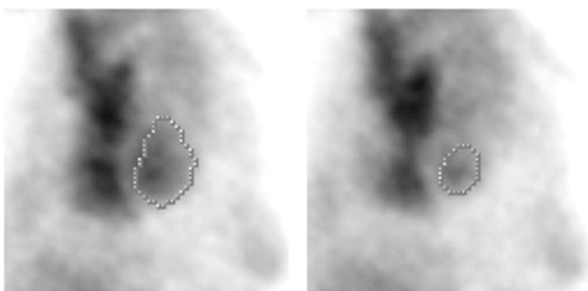


FIGURE 17.21. Two gated-scintillation camera views of the heart, imaged with  $^{99m}\text{Tc}$ -labeled red blood cells. The dots outline the left ventricle. On the left is end diastole (left ventricle filled with blood). On the right is end systole (left ventricle at smallest volume). The ejection fraction is 66%. Photograph courtesy of B. Hasselquist, Ph.D., Department of Diagnostic Radiology, University of Minnesota.

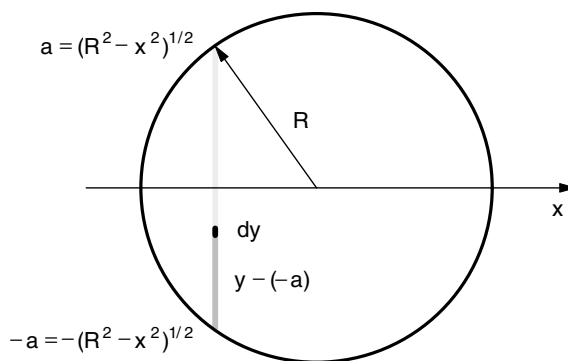


FIGURE 17.24. Projection perpendicular to the  $x$  axis for a radioactive source of uniform concentration, including the effect of photon attenuation.

right cerebral sensorimotor cortex (slice, upper right) and in the left cerebellum (slice, lower left). The technique is described by Rehm *et al.* (1994) and Strother *et al.* (1995).

### 17.15 Brachytherapy and Internal Radiotherapy

*Brachytherapy* (*brachy* means short) involves implanting in a tumor sources for which the radiation falls off



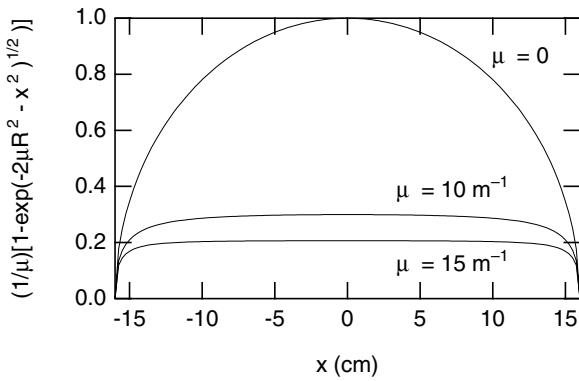


FIGURE 17.25. Plot of the projection including attenuation, Eq. 17.64, for  $\mu = 0$ ,  $\mu = 10 \text{ m}^{-1}$  (corresponding to 511-keV annihilation radiation) and  $\mu = 15 \text{ m}^{-1}$  (corresponding to the photons from  $^{99m}\text{Tc}$ ). The radius of the circle is 16 cm.

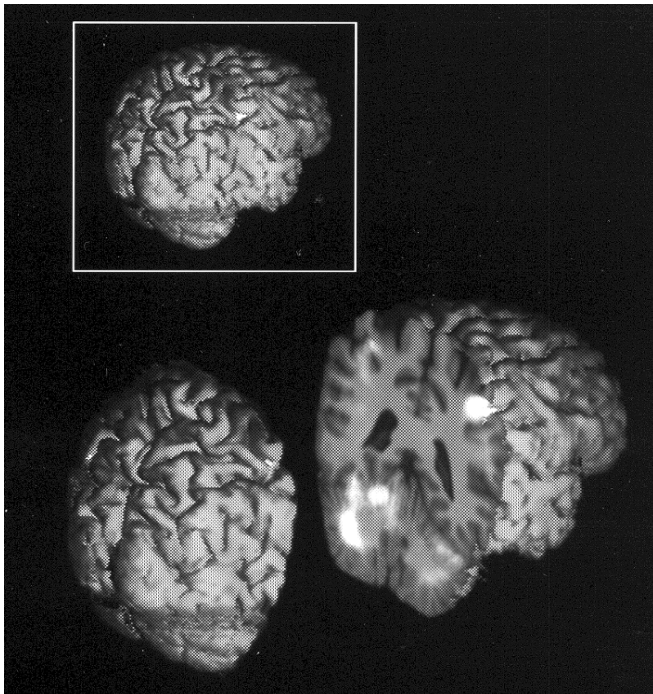


FIGURE 17.26. A positron emission tomography (PET) scan is overlaid on an MR image. At the upper left is a three-dimensional MRI of the brain viewed from above and to the right. At the bottom the image has been sliced through the motor strip and cerebellum, and the two pieces are separated. The PET image has been overlaid on the slice. The positron emitter is  $^{15}\text{O}$ -labeled water. The subject is sequentially touching each finger of the left hand with the thumb. Activity can be seen in the right cerebral sensorimotor cortex (slice, upper right) and in the left cerebellum (slice, lower left). Image courtesy of Prof. Kelly Rehm, University of Minnesota and the PET Imaging Service, Veterans Administration Medical Center, Minneapolis.

rapidly with distance because of attenuation, short range, or  $1/r^2$ . Originally the radioactive sources (seeds) were implanted surgically, resulting in high doses to the oper-

ating room personnel. In the *afterloading* technique, developed in the 1960s, hollow catheters are implanted surgically and the sources inserted after the surgery. Remote afterloading, developed in the 1980s, places the sources by remote control, so that only the patient receives a radiation dose.

We saw in Chapter 16 that fractionation of the dose results in better sparing of normal tissue for a given probability of killing the tumor. Afterloading allows the sources to be placed and removed, but it is often difficult for the patient to tolerate the catheters for long periods of time. This has led to the development of *high-dose-rate brachytherapy* (HDR), in which the dose is given in one or a few fractions over the course of a day or two [Nag (1994)]. Though this is much easier for the patient, tissue sparing is not as great as with a longer treatment. Current practice seeks to compensate for this by meticulous treatment planning based on an extended version of the linear-quadratic model, and by making sure that the tumor receives much higher doses than the surrounding normal tissue.

Radium was the first brachytherapy source, but it has been replaced by a number of nuclei that decay by  $\beta^-$  emission or electron capture. Conventional low-dose-rate brachytherapy is delivered at  $0.4\text{--}1.0 \text{ Gy hr}^{-1}$ . High dose rates are about  $1 \text{ Gy min}^{-1}$ .

Patients with coronary artery disease are often treated with *balloon angioplasty*, in which a coronary artery is dilated by inserting a balloon on the end of a catheter into the femoral artery in the leg and from there through the aorta and into the coronary artery. One problem is *restenosis* or reclosure of the artery. Restenosis can be reduced by placing a *stent*—a helical coil of wire—in the artery at the time of the angioplasty. Restenosis sometimes occurs within a stent, though the rate of recurrence is reduced by using a stent which elutes (gives off) a restenosis-inhibiting drug. If restenosis does occur, it can be treated by placing a string of radioactive seeds in the stent. Treatments may use either a gamma emitter,  $^{192}\text{Ir}$ , for 20 minutes, or a beta emitter ( $^{90}\text{Sr}/^{90}\text{Y}$ ) for 3 minutes [Kaluza and Raizner (2004); Fox (2002)].

*Internal radiotherapy* treats the patient with a radionuclide in a chemical that is selectively taken up by the tumor. The classic example is the administration by mouth of capsules containing  $^{131}\text{I}$  for treatment of hyperthyroidism and thyroid cancer. Other nuclides are being used experimentally for breast and neuroendocrine tumors and melanoma [Fritzberg and Wessels (1995)]. A radionuclide for this purpose should emit primarily nonpenetrating radiation, have a physical half-life long compared to the biological half-life, have a large activity per unit mass, and exhibit a high degree of specificity for the tumor. If the nuclide can be delivered within the cell, then Auger electrons can be exploited. One way to achieve high concentrations in the tumor is *radioimmunotherapy*: monoclonal antibodies are tagged with the radionuclide [see the special issue of *Medical Physics* edited by Buchsbaum

and Wessels (1993)]. It turns out that double-strand DNA breaks from Auger cascades occur more often than had been expected, and that the bystander effect is important. The use of Auger electrons from nuclides attached to the appropriate antibodies for cancer therapy is under active development; see Kassis (2004). The MIRD formulation can be adapted to the dose calculations [Watson *et al.* (1993)]. Radionuclide therapy is described for a general audience by Coursey and Nath (2000).

## 17.16 Radon

The naturally occurring radioactive nuclei are either produced continuously by cosmic  $\gamma$  ray bombardment, or they are the products in a decay chain from a nucleus whose half-life is comparable to the age of the earth. Otherwise they would have already decayed. There are three naturally occurring radioactive decay chains near the high- $Z$  end of the periodic table. One of these is the decay products from  $^{238}\text{U}$ , shown in Fig. 17.27. The half-life of  $^{238}\text{U}$  is  $4.5 \times 10^9$  yr, which is about the same as the age of the earth. A series of  $\alpha$  and  $\beta$  decays lead to radium,  $^{226}\text{Ra}$ , which undergoes  $\alpha$  decay with a half-life of 1620 yr to radon,  $^{222}\text{Rn}$ .

Uranium, and therefore radium and radon, are present in most rocks and soil. Radon, a noble gas, percolates through grainy rocks and soil and enters the air and water in different concentrations. Although radon is a noble gas, its decay products have different chemical properties and attach to dust or aerosol droplets which can collect in the lungs. High levels of radon products in the lungs have been shown by both epidemiological studies of uranium miners and by animal studies to cause lung cancer [Committee on the Biological Effects of Ionizing Radiations, BEIR IV (1988); BEIR VI (1999)]. The deposition process is quite complicated. A certain fraction of the decay products attach to aerosol droplets. That fraction is an important parameter in estimating the dose, because the unattached particles are deposited in the airways; those that have attached to aerosols also are also deposited in the airways, the site depending on the droplet size. The rate at which natural mucus clearing from the lungs removes them is also variable.

The  $^{222}\text{Rn}$  decay scheme is shown in Fig. 17.28. (Alternate branches that occur very rarely are not shown.) The shaded nuclides are the greatest contributors to the dose. Radon is a noble gas; once it decays the other shaded nuclides decay shortly after. Radon dosimetry is described on pp. 137–158 of BEIR IV (1988) and in BEIR VI (1999). Typical uranium activities in soil are  $20 \text{ Bq kg}^{-1}$  (range 7–40), leading to radon concentrations in the air over average soil of about  $4 \text{ Bq m}^{-3}$ .

The *working level* (WL) has been defined to be any combination of the shaded isotopes in Fig. 17.28 in 1 liter of air at ambient temperature and pressure that results in the ultimate emission of  $1.3 \times 10^5 \text{ MeV}$  of  $\alpha$ -particle

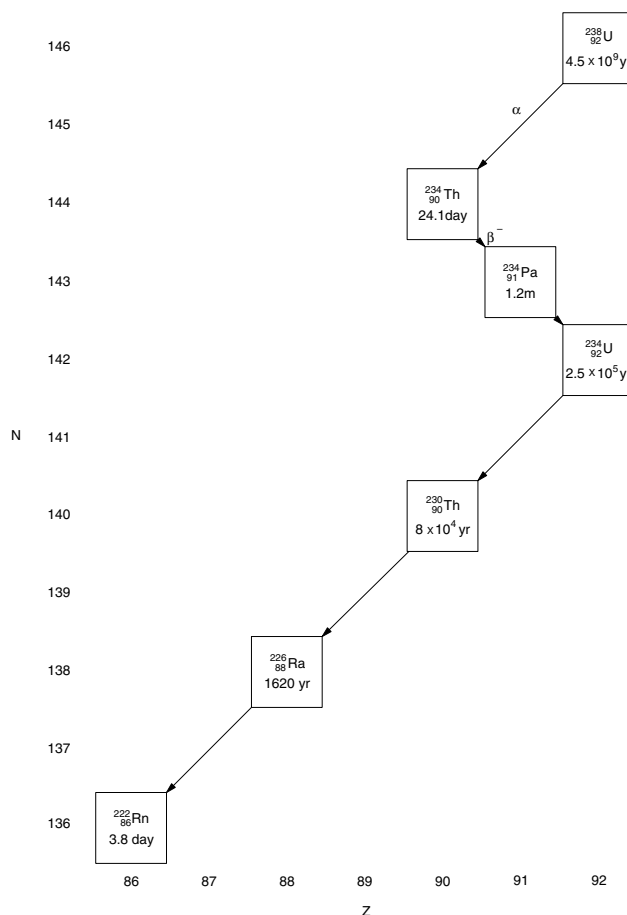


FIGURE 17.27. Decay of  $^{238}\text{U}$  to radon.

energy. This is about the energy liberated by the decay products in equilibrium with 100 pCi (3.7 Bq) of radon. Thus, 1 WL corresponds to  $3.7 \text{ Bq l}^{-1}$  or  $3700 \text{ Bq m}^{-3}$ . More recently, the activity of radon and its decay products has been described by the *Potential Alpha Energy Concentration* (PAEC) [BEIR VI (1999), p. 179]. Its units are  $\text{J m}^{-3}$ .

The *working-level month* (WLM) measures the total radon exposure and is 1 WL for 170 h (1 month of 40-h work weeks). Another unit is the PAEC multiplied by the number of hours exposure, measured in  $\text{J h m}^{-3}$ . There are  $3.5 \times 10^{-3} \text{ J h m}^{-3}$  per WLM.

Dose estimates for the miners and for the general population require models of aerosol size, unattached fraction, target cells, exercise level, and occupancy factors that are described in BEIR IV (1988). Averaging over all of these variables shows a dose in the lungs of about 6 mGy per WLM, with a factor-of-2 uncertainty because of these variables.

The report uses a time-since-exposure model to estimate the risk of lung cancer on the basis of four studies of groups of miners. The model predicts a relative risk ratio that is unity for no exposure and increases linearly to 3.5 for a continuous exposure of 5 WLM per year

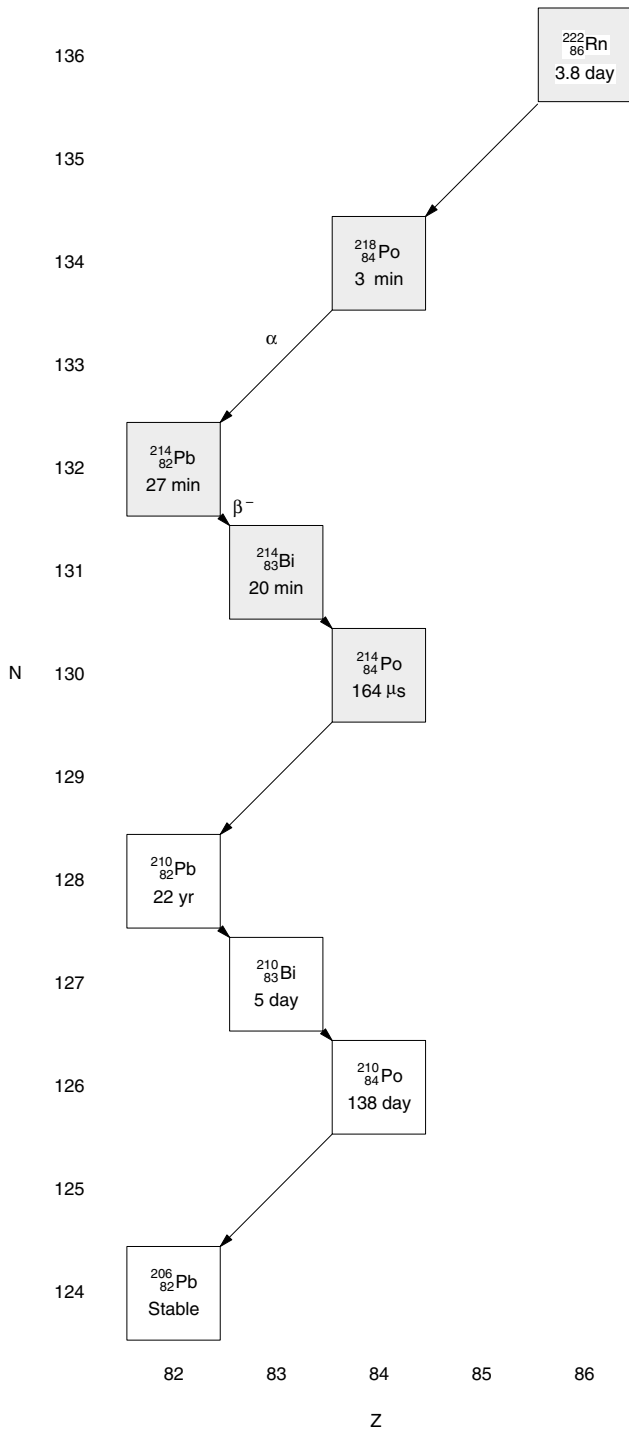


FIGURE 17.28. Decay of radon. The decay of the shaded nuclides is most significant in determining dose.

over a lifetime.<sup>12</sup> The report uses the linear-non-threshold model to estimate risks to the general population at small exposures. The issue of applying the linear-no-threshold model was discussed in Sec. 16.13. See particularly the

<sup>12</sup>BEIR IV (1988), Fig. 2.2. This is averaged by BEIR over smokers and nonsmokers and by me over sex.

data from the Cohen study in Fig. 16.57. Typical radon concentrations in houses are usually less than  $4r_0$  or  $4 \text{ pCi l}^{-1}$  ( $128 \text{ Bq m}^{-3}$ ) or 0.04 WL. (We saw in Sec. 16.13 that  $r_0 = 37 \text{ Bq m}^{-3} = 1 \text{ pCi l}^{-1}$ ). Exposure to  $r_0$  for 24 h per day for one year gives 0.5 WLM. The miners had exposures of 5–100 WLM per year, over periods of 3–20 years.

### Symbols Used in Chapter 17

Symbol	Use	Units	First used on page
$a$	Distance	m	501
$b$	Source to collimator distance	m	511
$c$	Speed of light	$\text{m s}^{-1}$	482
$d$	Width of collimator channel	m	511
$e$	Electron charge	C	482
$f_r$	Fraction of transition energy released as photons		485
$f_K, f_L$	Fraction of transition energy released in $K$ - or $L$ -shell internal conversion		485
$g$	Detector efficiency		511
$h$	Planck's constant	J s	488
$h, k$	Denote specific organs		489
$l$	Collimator thickness	m	511
$m_0$	Rest mass	kg	482
$m_x$	Rest mass of particle type $x$	kg	483
$n_i$	Mean number (fraction) of emissions of type $i$ per transition		489
$p$	Momentum	$\text{kg m s}^{-1}$	486
$r_h, r_k$	Source and target regions		489
$r$	Distance	m	494
$r_0$	Radon concentration unit	$\text{Bq m}^{-3}$	506
$s$	Path length	m	494
$t$	Time	s	484
$t$	Collimator septum thickness	m	511
$v$	Speed	$\text{m s}^{-1}$	482
$w$	Distance across collimator wall in the direction of photon travel	m	511
$x, y, z$	Position	m	501
$A$	Mass number		482
$A, A_0$	Activity	Bq	484
$\bar{A}_h$	Cumulated activity in organ $h$	$\text{Bq s}$	489
$B$	Buildup factor		494
$B, B_K, B_L$	Binding energy	eV	484
$C_h, \bar{C}_h$	Activity and cumulated activity per unit mass in organ $h$	$\text{Bq kg}^{-1}; \text{kg}^{-1}$	492
$D$	Dose	J $\text{kg}^{-1}$ (Gy)	489
$E, E_\gamma$	Energy	J, eV	482
$F_h$	Fraction of activity in organ $h$		490

Symbol	Use	Units	First used on page
$F_h$	Fraction of activity in organ $h$		490
$F$	Projection	Bq	501
$K$	Geometric factor		511
$M, M_X$	Mass	kg	487
$N$	Neutron number		482
$N, N_0$	Number of nuclei		484
$R, R_0$	Nuclear radius	m	482
$R$	Radius of disk	m	501
$R_t, R_o$	True and observed counting rates	$s^{-1}$	510
$S$	Mean absorbed dose per unit cumulated activity	$J\ kg^{-1}$	489
$S$	Area	$m^2$	494
$T$	Kinetic energy	J, eV	482
$T$	Time	s	508
$T_{1/2}$	Half-life	s	484
$T_j$	Half-life for $j$ th biological disappearance process	s	490
$W_K$	Fluorescence yield for $K$ shell		493
$Z$	Atomic number (number of protons)		482
$\alpha_K, \alpha_L$	Internal conversion coefficient		485
$\alpha_h$	Fraction of total activity in organ $h$		508
$\beta^-, \beta^+$	Electron and positron (in $\beta$ decay)		485
$\lambda$	Physical decay constant	$s^{-1}$	484
$\lambda_j$	Decay constant for $j$ th biological process	$s^{-1}$	490
$\mu$	Attenuation coefficient	$m^{-1}$	501
$\mu_{en}$	Energy absorption coefficient	$m^{-1}$	494
$\nu, \bar{\nu}$	Neutrino, antineutrino		486
$\nu$	Photon frequency	Hz	488
$\rho$	Density	$kg\ m^{-3}$	494
$\sigma_\phi$	Standard deviation of $\phi$		494
$\phi_i$	Absorbed fraction		489
$\tau$	Detector dead time	s	510
$\tau_h$	Residence time in organ $h$	s	490
$\Delta_i$	Mean energy emitted in radiation type $i$	J	489
$\Phi_j$	Specific absorbed fraction	$kg^{-1}$	489

trons in each shell are

Shell	Number of electrons	BE per electron (eV)
$K$	2	69,525
$L$	8	11,023
$M$	18	2,125
$N$	32	215
$O$	12	35
$P$	2	1

Calculate the atomic rest energy of tungsten.

### Section 17.4

**Problem 4** Refer to Figs. 17.2 and 17.5. Uranium splits roughly in half when it undergoes nuclear fission. Will the fission fragments decay by  $\beta^+$  or  $\beta^-$  emission?

**Problem 5** The following nuclei of mass 15 are known:  ${}^{15}_6C$ ,  ${}^{15}_7N$ , and  ${}^{15}_8O$ . Of these,  ${}^{15}_7N$  is stable. How do the others decay?

**Problem 6** Look up the decay schemes of the following isotopes (for example, in the Handbook of Chemistry and Physics, CRC Press, or at [www.nndc.bnl.gov/](http://www.nndc.bnl.gov/)). Comment on their possible medical usefulness:  ${}^3H$ ,  ${}^{15}O$ ,  ${}^{13}N$ ,  ${}^{18}F$ ,  ${}^{22}Na$ ,  ${}^{68}Ga$ ,  ${}^{64}Cu$ ,  ${}^{11}C$ ,  ${}^{123}I$ , and  ${}^{56}Ni$ .

**Problem 7** Look up the half-lives of the isotopes in Fig. 17.6 (for instance in the Handbook of Chemistry and Physics, CRC Press or at [www.nndc.bnl.gov/](http://www.nndc.bnl.gov/)). Relate qualitatively the half life to the position of the isotope on the parabola.

### Section 17.5

**Problem 8** Calculate the conversion factor  $k$  of Eq. 17.22b.

### Section 17.6

**Problem 9** Show that  $1\ Ci\ h = 1.332 \times 10^8$  disintegrations or Bq s.

**Problem 10** Obtain a numerical value for the residence time for  ${}^{99m}Tc$ -sulfur colloid in the liver if 85% of the drug injected is trapped in the liver and remains there until it decays.

**Problem 11** Derive Eqs. 17.40–17.42.

**Problem 12** Calculate numerical solutions of Eqs. 17.40 and 17.42 and plot them on semilog paper. Use  $\lambda = 2, \lambda_1 = 0.5, \lambda_2 = 3$ .

**Problem 13** Eq. 17.42 is not valid if  $\lambda_1 = \lambda_2$ . In that case, try a solution of the form  $N_2 = Bte^{-\lambda t}$  and obtain a solution.

**Problem 14** Derive Eqs. 17.43 and 17.44.

## Problems

### Section 17.1

**Problem 1** The best current (2002) value for the mass of the proton is  $1.007276467\ u$ . The mass of the electron is  $5.485799095 \times 10^{-4}\ u$ . The binding energy of the electron in the hydrogen atom is  $13.6\ eV$ . Calculate the mass of the neutral hydrogen atom.

**Problem 2** Solve Eq. 17.1 for the kinetic energy,  $T$ . Show that when  $v \ll c$ , it reduces to the familiar  $T = m_0v^2/2$ .

**Problem 3** The rest energy of the  ${}^{184}_{74}W$  nucleus is  $171,303\ MeV$ . The average binding energies of the elec-

**Problem 15** The biological half-life of iodine in the thyroid is about 25 days.  $^{125}\text{I}$  has a half-life of 60 days.  $^{132}\text{I}$  has a half-life of 2.3 h. Find the effective half-life in each case.

**Problem 16** For Sec. 17.6.4, with  $\lambda = 0.05 \text{ h}^{-1}$ ,  $\lambda_1 = 1 \text{ h}^{-1}$ , and  $\lambda_2 = 0.1 \text{ h}^{-1}$ , find  $\tilde{A}_1$  and  $\tilde{A}_2$  in terms of the initial activity  $A_0$  and in terms of the initial number of nuclei  $N_0$ .

**Problem 17**  $N_0$  radioactive nuclei with physical decay constant  $\lambda$  are injected in a patient at  $t = 0$ . The nuclei move into the kidney at a rate  $\lambda_1$ , so that the number in the rest of the body falls exponentially:  $N(t) = N_0 e^{-(\lambda + \lambda_1)t}$ . Suppose that the nuclei remain in the kidney for a time  $T$  before moving out in the urine. (This is a crude model for the radioactive nuclei being filtered into the glomerulus and then passing through the tubules before going to the bladder.)

(a) Calculate the cumulated activity and the residence time in the kidney by finding the total number of nuclei entering the kidney and multiplying by the probability that a nucleus decays during the time  $T$  that it is in the kidney.

(b) Calculate the cumulated activity and residence time in the bladder, assuming that the patient does not void.

**Problem 18** Suppose that at  $t = 0$ ,  $^{99m}\text{Tc}$  with an activity of 370 kBq enters a patient's bladder and stays there for 2 h, at which time the patient voids, eliminating all of it. What is the cumulated activity? What is the cumulated activity if the time is 4 h?

**Problem 19** Suppose that the  $^{99m}\text{Tc}$  of the previous problem does not enter the bladder abruptly at  $t = 0$ , but that it accumulates linearly with time. At the end of 2 h the activity is 370 kBq and the patient voids, eliminating all of it. What is the cumulated activity?

**Problem 20** A radioactive substance has half-life  $T_{1/2}$ . It is excreted from the body with biological half-life  $T_1$ .  $N_0$  radioactive nuclei are introduced in the body at  $t = 0$ . Find the total number that decay inside the body.

**Problem 21** The fractional distribution function  $\alpha_h$  is the fraction of the total activity which is in organ  $h$ :  $\alpha_h(t) = A_h(t)/A(t) = A_h(t)/A_0 e^{-\lambda t}$ .

(a) Show that  $\tau_h = \int_0^\infty \alpha_h(t) e^{-\lambda t} dt$ .

(b) Calculate  $\alpha_1(t)$  and  $\alpha_2(t)$  for Eqs. 17.40 and 17.42 and show that integration of these expressions leads to Eqs. 17.44.

**Problem 22** Suppose that the fractional distribution function (defined in the previous problem) is  $\alpha(t) = 1, t < T$ ;  $\alpha(t) = b, t > T$ ; ( $b < 1$ ). Find the residence time. This is a simple model for the situation where a bolus (a fixed amount in a short time) of some substance passes through an organ once and is then distributed uniformly in the blood.

**Problem 23** The distribution function  $q_h(t)$  is defined to be the activity in organ  $h$  corrected for radioactive decay to a reference time. If the correction is from time  $t$  to time 0, find an expression for  $q_h(t)$  in terms of  $A_h(t)$ .

**Problem 24** The "official" definition of the fractional distribution function  $\alpha_h(t)$  is the ratio of the distribution function  $q_h(t)$  produced by a bolus administration to the patient, divided by the activity  $A_0$  in the bolus. Show that this is equivalent to the definition in Problem 21.

**Problem 25** Show that if the uptake in a compartment is not instantaneous but exponential, with subsequent exponential decay, the cumulated activity is  $\tilde{A} = 1.443 A_0 (T_e T_{ue} / T_u)$ , where  $T_e$  is the effective half-life for excretion, and  $T_{ue} = T_u T_{1/2} / (T_u + T_{1/2})$ . Hint: See Eq. 17.43.

### Section 17.7

**Problem 26** Use the output data of Fig. 17.4 to estimate values for  $W_K$ ,  $K_\alpha / (K_\alpha + K_\beta)$ , and  $K_\beta / (K_\alpha + K_\beta)$ . Compare your values to those used in Table 17.2.

**Problem 27** Rearrange the output data of Fig. 17.4. Find the total  $\Delta$  for emission of photons below 30 keV and charged particles. Rank the radiations in the order they contribute to the dose.

**Problem 28** Calculate the entries in the output data of Fig. 17.4 for  $\gamma_3$ , using the same techniques that were used in the text for  $\gamma_1$  and  $\gamma_2$ .

**Problem 29** The isotope  $^{133}_{54}\text{Xe}$  is used for studies of pulmonary function by inhalation. It decays by  $\beta$  emission with a half-life of 5.3 days to  $^{133}_{55}\text{Cs}$ . The maximum  $\beta$  energy is 0.346 MeV; the average is 0.100 MeV. The cesium then emits a 0.081-MeV  $\gamma$  ray. The Cs has the following properties:

$$\alpha_K = 1.46, \quad \alpha_L = 2.35, \quad \alpha_M = 0.078$$

$$E_K = 0.031 \text{ MeV}, B_K = 0.036 \text{ MeV}, B_L = 0.006 \text{ MeV}.$$

Calculate  $\Delta_i$  for the  $\beta$  particle, the  $\gamma$  ray,  $K$  and  $L$  internal conversion electrons, and  $K_\alpha$  x rays. Assume that all x rays are  $K_\alpha$ .

**Problem 30** Nitrogen-13 has a half-life of 10 min. All of the disintegrations emit a positron with end point energy 1.0 MeV (average energy 0.488 MeV). There is no electron capture. Make a table of radiations that must be considered for calculating the absorbed dose and determine  $E_i$  and  $\Delta_i$  for each one.

**Problem 31** A patient swallows  $3.5 \times 10^9 \text{ Bq}$  of  $^{131}\text{I}$ . The half-life of the iodine is 8 days. Ten minutes later the patient vomits all of it. If none had yet left the stomach and all was vomited, determine the cumulated activity and residence time in the stomach.

## Section 17.8

**Problem 32** Derive Eq. 17.61 by substituting Eqs. 17.59 and 17.60 in Eq. 17.58. You will also have to justify and use Eq. 17.62.

**Problem 33** The body consists of two regions. Region 1 has mass  $m_1$  and cumulated activity  $\tilde{A}_1$ . It is completely surrounded by region 2 of mass  $m_2$  and cumulated activity  $\tilde{A}_2 = \tilde{A}_0 - \tilde{A}_1$ . We can say that the mass of the total body is  $m_{TB} = m_1 + m_2 = m_1 + m_{RB}$ . A single radiation is emitted with disintegration energy  $\Delta$ . The radiation is nonpenetrating so that

$$\phi(1 \leftarrow 1) = \phi(2 \leftarrow 2) = 1,$$

$$\phi(1 \leftarrow 2) = \phi(2 \leftarrow 1) = 0.$$

- What are  $\phi(TB \leftarrow 1)$  and  $\phi(TB \leftarrow 2)$ ?
- What are the corresponding values of  $\Phi$  and  $S$ ?
- Show that directly from the definition, Eq. 17.58

$$D_1 = \tilde{A}_1 \Delta / m_1,$$

$$D_2 = D_{RB} = \tilde{A}_2 \Delta / m_2,$$

$$D_{TB} = \tilde{A}_0 \Delta / (m_1 + m_2)$$

- Calculate  $\tilde{A}_u$  and  $\tilde{A}_1^*$ .
- What is  $S(1 \leftarrow TB)$ ? Remember that  $\phi$  is calculated for activity uniformly distributed within the source region.
- Calculate the dose to region 1 using Eq. 17.61 and show that it agrees with (c).
- Evaluate  $S(1 \leftarrow RB)$  using Eq. 17.62 and show that it agrees with  $S(1 \leftarrow 2)$ .

**Problem 34** The body consists of two regions. Region 1 has mass  $m_1$  and cumulated activity  $\tilde{A}_1$ . It is completely surrounded by region 2 of mass  $m_2$  and cumulated activity  $\tilde{A}_2$ . A single radiation is emitted with disintegration energy  $\Delta$ . The characteristics of the radiation are such that

$$\phi(1 \leftarrow 1) + \phi(2 \leftarrow 1) = 1,$$

$$\phi(1 \leftarrow 2) + \phi(2 \leftarrow 2) + \phi(0 \leftarrow 2) = 1,$$

where  $\phi(0 \leftarrow 2)$  represents energy from region 2 that has escaped from the body. Obtain expressions for the dose to each region and the whole body dose.

## Section 17.9

**Problem 35** Consider the decay of a parent at rate  $\lambda_1$  to an offspring that decays with rate  $\lambda_2$ .

- Write a differential equation for the amount of offspring present.
- Solve the equation.
- Discuss the solution when  $\lambda_2 > \lambda_1$ .
- Discuss the solution when  $\lambda_2 < \lambda_1$ .
- Plot the solution for a technetium generator that is eluted every 24 h.

**Problem 36**  $N_0$  nuclei of  $^{99m}\text{Tc}$  are injected into the body. What is the maximum activity for the decay of the metastable state? When does the maximum activity for decay of the ground state occur if no Tc atoms are excreted? What is the ratio of the maximum metastable state activity to the maximum ground-state activity?

**Problem 37** If 1  $\mu\text{Ci}$  of  $^{99m}\text{Tc}$  is injected in the blood and stays there, relate the activity in a sample drawn time  $t$  later to the volume of the sample and the total blood volume. If the gamma rays are detected with 100% efficiency, what will be the counting rate for a 10-ml sample of blood if the blood volume is 5 liters? (Using non-SI units was intentional.)

**Problem 38** Assume that aggregated human albumin is in the form of microspheres. A typical dose of albumin microspheres is 0.5 mg of microspheres containing 80 MBq of  $^{99m}\text{Tc}$  and 15  $\mu\text{g}$  of tin. There are  $1.85 \times 10^6$  microspheres per mg.

- How many  $^{99m}\text{Tc}$  atoms are there per microsphere?
- How many tin atoms per microsphere?
- How many technetium atoms per tin atom?
- What fraction of the surface of a microsphere is covered by tin? Assume the sphere has a density of  $10^3 \text{ kg m}^{-3}$ .

**Problem 39** It is estimated that the total capillary surface area in the lung is  $90 \text{ m}^2$ . Assume each capillary has 50 segments, each 10  $\mu\text{m}$  long, and a radius of 5  $\mu\text{m}$ .

- How many capillaries are there in the lung?
- There are about  $3 \times 10^8$  alveoli in both lungs. How many capillaries per alveolus are there?
- An alveolus is 150–300  $\mu\text{m}$  in diameter. Are the above answers consistent?
- A typical dose of albumin microspheres is 0.5 mg with an average diameter of 25  $\mu\text{m}$ . There are  $1.85 \times 10^6$  spheres per mg. What fraction of the capillaries are blocked if there is good mixing?

## Section 17.10

**Problem 40** The half-life of  $^{99m}\text{Tc}$  is 6.0 h. The half-life of  $^{131}\text{I}$  is 8.07 day. Assume that the same initial activity of each is given to a patient and that all of the substance remains within the body.

- Find the ratio of the cumulated activity for the two isotopes.
- $^{99m}\text{Tc}$  emits 0.141-MeV photons. For each decay of  $^{131}\text{I}$  the most important radiations are 0.89  $\beta^-$  of average energy 0.192 MeV and 0.81 photons of 0.365 MeV. If all of the decay energy were absorbed in the body, what would be the ratio of doses for the same initial activity?

**Problem 41** A patient is given an isotope which spreads uniformly through the lungs. It emits a single radiation: a  $\gamma$  ray of energy 50 keV. There are no internal-conversion

electrons. The cumulated activity is 40 GBq s. Find the absorbed dose in the liver ( $m = 1.83$  kg).

**Problem 42** The decay of  $^{99m}\text{Tc}$  can be approximated by lumping all of the decays into two categories:

Radiation	$E_i$ (MeV)	$\Delta_i$ (J)
$\gamma$	0.14	$2 \times 10^{-14}$
Electrons and soft x rays		$2.76 \times 10^{-15}$

Sulfur colloid labeled with 100 MBq of  $^{99m}\text{Tc}$  is given to a patient and is taken up immediately by the liver. Assume it stays there. Find the dose to the liver, spleen, and whole body. Use the following information:

Target organ	Mass (kg)	Absorbed fraction for a source in the liver	
		$E(\gamma) = 0.1$ MeV	$E(\gamma) = 0.2$ MeV
Liver	1.833	0.165	0.158
Spleen	0.176	0.000606	0.000645
Whole body	70.0	0.454	0.415

**Problem 43** An ionization-type smoke detector contains 4.4  $\mu\text{Ci}$  of  $^{241}\text{Am}$ . This isotope emits  $\alpha$  particles (which we will ignore) and a 60-keV  $\gamma$  ray, for which  $n = 0.36$ . The half-life is 458 yr.

- (a) How many moles of  $^{241}\text{Am}$  are in the source?
- (b) Ignoring attenuation, backscatter, and buildup in any surrounding material (such as the cover of the smoke detector), what is the absorbed dose in a small sample of muscle located 2 m away, if the muscle is under the detector for 8 h per day for 1 year?

**Problem 44** One mCi of a radioactive substance lodges permanently in a patient's lungs. The substance emits a single 80-keV  $\gamma$  ray. It has a half-life of 12 h. Find the cumulated activity and the dose to the liver (mass 1833 g).

**Problem 45** The dose calculation for microspheres in the lung was an oversimplification because technetium leaches off the spheres. The footnote in Section 17.10 lists some more realistic residence times. If none of the technetium is excreted from the body, the sum of all the residence times will still be 8.7 h. Assume that the residence time in the lungs is 4.3 h and the residence time in the rest of the body is 4.4 h.

- (a) Show that  $\tilde{A}_u = 4.46 \times 3,600 \times A_0$  and  $\tilde{A}_{\text{lung}}^* = 4.24 \times 3,600 \times A_0$ .
- (b) For a source distributed uniformly throughout the total body, the absorbed fractions for 140-keV photons are  $\phi(\text{lung} \leftarrow \text{TB}) = 0.0053$ ,  $\phi(\text{TB} \leftarrow \text{TB}) = 0.3572$ . Split the radiation into penetrating and nonpenetrating components:

$$S(\text{lung} \leftarrow \text{TB}) = (\phi_{\text{nonpen}} \Delta_{\text{nonpen}} + \phi_{\text{penetrating}} \Delta_{\text{penetrating}}) / m_{\text{lung}}$$

Remember that for activity uniformly distributed in the total body,  $\phi(\text{lung} \leftarrow \text{TB}) = m_{\text{lung}} / m_{\text{TB}}$  and use some of the information in Table 17.4 to show that

$$S(\text{lung} \leftarrow \text{TB}) = 1.463 \times 10^{-16} \text{ J kg}^{-1},$$

$$S(\text{TB} \leftarrow \text{TB}) = 1.414 \times 10^{-16} \text{ J kg}^{-1}.$$

- (c) Calculate the dose to the lungs and the total body dose for an initial activity of 37 MBq. Compare the values to those in Table 17.4.

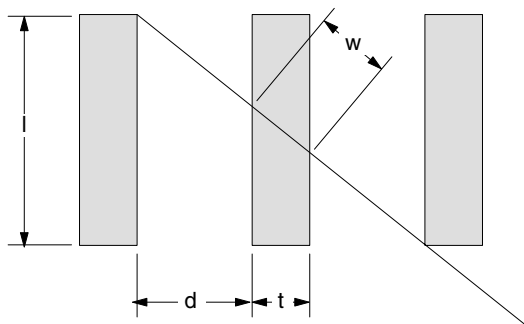
### Section 17.12

**Problem 46** Nuclear counting follows Poisson statistics. Show that for a fixed average counting rate  $R$  (counts per second) the standard deviation of a sum of  $N$  measurements each of length  $T$  is the same as a single measurement of duration  $NT$ . (Hint: You will first have to consider the situation where one measures  $y = x_1 + x_2 + \dots$  and find the variance of  $y$  in terms of the variances of the  $x_i$  when there is no correlation between the  $x_i$ .)

**Problem 47** The interaction of a photon in a nuclear detector (an "event") initiates a process in the detector that lasts for a certain length of time. A second event occurring within a time  $\tau$  of the first event is not recorded as a separate event. Suppose that the true counting rate is  $R_t$ . A counting rate  $R_o$  is observed.

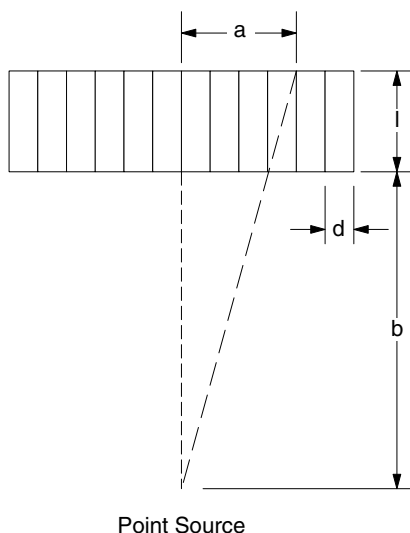
- (a) A nonparalyzable counting system is "dead" for a time  $\tau$  after each recorded event. Additional events that occur during this dead time are not recorded but do not prolong the dead time. Show that  $R_t = R_o / (1 - R_o \tau)$  and  $R_o = R_t / (1 + R_t \tau)$ .
- (b) A paralyzable counting system is unable to record a second event unless a time  $\tau$  has passed since the last event. In other words, an event occurring during the dead time is not only not recorded, it prolongs the dead time. Show that in this case  $R_o = R_t e^{-R_t \tau}$ . (Hint: Use the Poisson distribution of Appendix J to find the fraction of events separated by a time greater than  $\tau$ . The probability that the next event occurs between  $t$  and  $t + dt$  is the probability of no event during time  $t$  multiplied by the probability of an event during  $dt$ .)
- (c) Plot  $R_o$  vs.  $R_t$  for the two cases when  $\tau$  is fixed. The easiest way to do this is to plot  $R_o \tau$  vs.  $R_t \tau$ .

**Problem 48** Two channels of a collimator for a gamma camera are shown in cross section, along with the path of a photon that encounters the minimum thickness of collimator septum (wall).



- (a) Show that if  $(d + t)/l \ll 1$ , then  $w/t = l/(2d + t)$ .
- (b) If transmission through the septum is to be less than 5%, what is the relationship between  $t$ ,  $d$ ,  $l$ , and  $\mu$ ? Evaluate this for  $^{99m}\text{Tc}$  and for a positron emitter.

**Problem 49** Photons from a point source a distance  $b$  below a collimator pass through channels out to a distance  $a$  from the perpendicular to the collimator passing through the source.



- (a) Find an expression for  $a$  in terms of  $b$ ,  $d$ , and  $l$ .
- (b) Assume that  $a$  is related to the spatial frequency  $k$  for which the modulation transfer function (MTF) = 0.5 in Fig. 17.19 by  $a = K/k$ , where  $K$  is a constant. Calculate the thickness  $l$  of the collimator.

**Problem 50** The collimator efficiency of a gamma camera is defined to be the fraction of the  $\gamma$  rays emitted isotropically by a point source that pass through the collimator into the scintillator.

(a) Consider a circular channel of diameter  $d$  in the collimator directly over the source. Show that the fraction of the photons striking the scintillator after passing through that channel is  $d^2/16(l + b)^2$ . (Assume that any photons that strike the septum are lost).

(b) Use the result of the previous problem to estimate the number of channels through which at least some photons from the point source pass. Assume that the fraction of collimator area that is occupied by channels rather than lead is  $[d/(d + t)]^2$ .

(c) Calculate the geometric efficiency  $g$  assuming that all channels that pass any photons have the same efficiency as the one on the perpendicular from the source. Show that it is of the form

$$g = K^2 \left(\frac{d}{l}\right)^2 \left(\frac{d}{d+t}\right)^2$$

and evaluate  $K$ . More detailed calculations show that  $K$  is about 0.24 for a hexagonal array of round holes and 0.26 for hexagonal holes.<sup>13</sup>

(d) How does the detector efficiency relate to the collimator resolution?

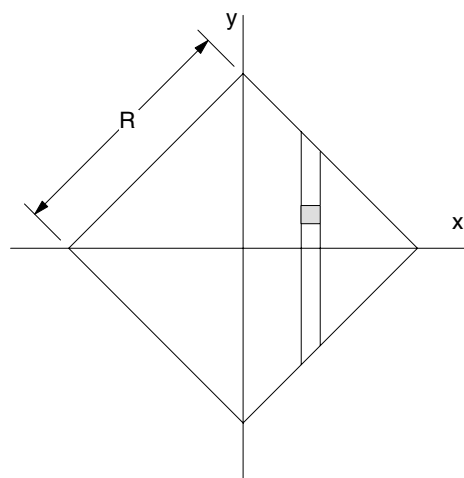
Section 17.13

**Problem 51** (a) Derive Eq. 17.64 from Eq. 17.63.

(b) Calculate the limit of Eq. 17.64 when there is no attenuation.

**Problem 52** The attenuation distortion for SPECT can be reduced by making measurements on opposite sides of the patient and taking the geometric mean. The geometric mean of variables  $x_1$  and  $x_2$  is  $(x_1 x_2)^{1/2}$ . Calculate the geometric mean of two SPECT measurements on opposite sides of the patient. Ignore possible  $1/r^2$  effects.

**Problem 53** Consider a radioactive source having a uniform activity per unit volume  $A_V$  and the square geometry shown below.



(a) Calculate the projection  $F(x)$  including the effects of attenuation with coefficient  $\mu$ .

(b) Plot  $F(x)$  for  $\mu = 0$  and for  $\mu R = 3$ .

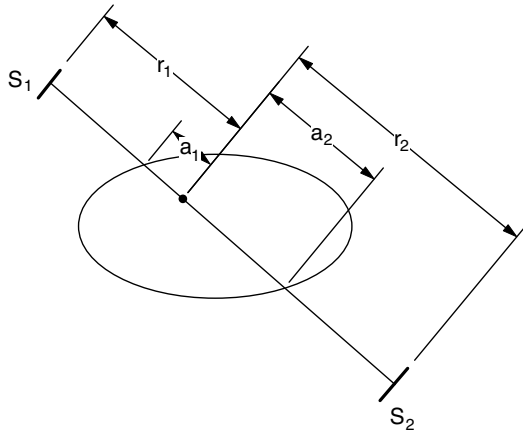
Section 17.14

**Problem 54** Suppose that  $A$  positrons are emitted from a point per second. They come to rest and annihilate

<sup>13</sup>Cherry et al. (2003, p. 242); R. P. Grenier, M. A. Bender, and R. H. Jones (1974). A computerized multicrystal scintillation gamma camera, Chapter 3 in H. G. Hine and J. A. Sorenson, eds. *Instrumentation in Nuclear Medicine*. New York, Academic, Vol. 2.



within a short distance of their source. When a positron annihilates, two photons are emitted in opposite directions. Two photon detectors are set up on opposite sides of the source. The source is distance  $r_1$  from the first detector, of area  $S_1$ , and  $r_2$  from the second detector of area  $S_2$ . The area  $S_2$  is large enough so that the second photon will definitely enter detector 2 if the first photon enters detector 1. Assume that both detectors count with 100% efficiency.



(a) Show that the number of counts in the first detector would be  $2AS_1/4\pi r_1^2$  if there were no attenuation between source and detector, and that it is  $(2AS_1/4\pi r_1^2)e^{-\mu a_1}$  if attenuation in a thickness  $a_1$  of the body is considered.

(b) Detector 2 detects the second photon for every photon that strikes detector 1. Assuming a uniform attenuation coefficient and body thickness  $a_2$ , find an expression for the number of events in which both photons are detected.

**Problem 55** Positron emission tomography relies on simultaneous detection of the back-to-back annihilation gamma rays (a “coincidence”). In addition to true coincidences, there can be “scatter coincidences” in which annihilation photons coming from a point that is not on the line between the two detectors enter both detectors. There can also be “random coincidences” which arise from photons from completely independent decays that occur nearly simultaneously. Consider a ring of detectors around a patient. Make three drawings showing true coincidences, scatter coincidences and random coincidences.

### Section 17.16

**Problem 56** The half-life of  $^{235}\text{U}$  is  $7 \times 10^8$  yr. The age of the earth is 4.5 billion years. What fraction of the  $^{235}\text{U}$  that existed on the earth when it was first formed is present now?

**Problem 57** There are three naturally occurring decay series beginning with three long-lived isotopes:  $^{238}\text{U}$  (Figs. 17.27 and 17.28),  $^{235}\text{U}$ , and  $^{232}\text{Th}$ . The  $^{232}\text{Th}$  series begins with the  $\alpha$  decay of  $^{232}\text{Th}$  (half-life =  $1.4 \times 10^{10}$  yr) to

nucleus A which undergoes  $\beta^-$  decay to nucleus B which undergoes  $\beta^-$  decay to nucleus C which undergoes  $\alpha$  decay to nucleus D which undergoes  $\alpha$  decay to nucleus E, etc. Make a chart like Fig. 17.27 showing the first five steps in the series, and identify the five nuclei A–E.

**Problem 58** One way to determine the age of biological remains is “carbon-14 dating.” The common isotope of carbon is stable  $^{12}\text{C}$ . The rare isotope  $^{14}\text{C}$  decays with a half-life of 5,370 yr.  $^{14}\text{C}$  is constantly created in the atmosphere by cosmic rays. The equilibrium between production and decay results in about 1 of every  $10^{12}$  atoms of carbon in the atmosphere being  $^{14}\text{C}$ , mostly as part of a  $\text{CO}_2$  molecule. As long as the organism is alive, the ratio of  $^{12}\text{C}$  to  $^{14}\text{C}$  in the body is the same as in the atmosphere. Once the organism dies, it no longer incorporates  $^{14}\text{C}$  from the atmosphere, and the number of  $^{14}\text{C}$  nuclei begins to decrease. Suppose the remains of an organism have one  $^{14}\text{C}$  for every  $10^{13}$   $^{12}\text{C}$  nuclei. How long has it been since the organism died?

**Problem 59** Consider a fictitious two-step decay series analogous to the more complex series shown in Fig. 17.27. The series starts with isotope A which decays at rate  $\lambda_1$  to isotope B. Isotope B decays to isotope C with rate  $\lambda_2$ . Isotope C is stable.

(a) Derive the differential equation governing the number of nuclei  $N_A$ ,  $N_B$ , and  $N_C$ . Where else in this chapter have you seen the same equations?

(b) Solve the differential equations using the initial conditions  $N_A(0) = N$ ,  $N_B(0) = N_C(0) = 0$ . Make sure your solutions make sense for  $t \rightarrow 0$  and  $t \rightarrow \infty$ .

(c) Find  $N_B/N_A$  in the limit  $\lambda_2 \gg \lambda_1$ . Ignore short times. Also find activities  $A_A$  and  $A_B$ . Explain physically how such a small number of nuclei  $N_B$  can contribute so much to the total activity.

## References

Arqueros, F., and G. D. Montesinos (2003). A simple algorithm for the transport of gamma rays in a medium. *Amer. J. Phys.* **71**(1): 38–45.

BEIR IV (1988). Committee on the Biological Effects of Ionizing Radiations. *Health Risks of Radon and Other Internally Deposited Alpha-Emitters*. Washington, D.C., National Academy Press.

BEIR VI (1999). Committee on Health Risks of Exposure to Radon. *Health Effects of Exposure to Radon*. Washington, D.C., National Academy Press.

Berger, M. J. (1968). *Energy Deposition in Water by Photons from Point Isotropic Sources*. NM/MIRD Pamphlet 2. New York, Society of Nuclear Medicine.

Buchsbaum, D., and B. W. Wessels (1993). Introduction: Radiolabeled antibody tumor dosimetry. *Med. Phys.* **20**(2, Pt. 2): 499–501.

- Cherry, S. R., J. A. Sorenson, and M. E. Phelps (2003). *Physics in Nuclear Medicine*, 3rd ed. Philadelphia, Saunders.
- Coffey, J. L., and E. E. Watson (1979). Calculating the dose from remaining body activity: A comparison of two methods. *Med. Phys.* **6**(4): 307–308.
- Coursey, B. M. and R. Nath (2000). Radionuclide therapy. *Physics Today* **53**(4): 25–30.
- Dillman, L. T., and F. C. Von der Lage (1974). *Radionuclide Decay Schemes and Nuclear Parameters for Use in Radiation Dose Estimation*. NM/MIRD Pamphlet 10. New York, Society of Nuclear Medicine.
- Eckerman K. F., R. J. Westfall, J. C. Ryman, and M. Cristy (1994). Availability of nuclear decay data in electronic form, including beta spectra not previously published. *Health Phys.* **67**(4): 338–345.
- Eisberg, R., and R. Resnick (1985). *Quantum Physics of Atoms, Molecules, Solids, Nuclei, and Particles*, 2nd ed. New York, Wiley.
- Evans, R. D. (1955). *The Atomic Nucleus*. New York, McGraw-Hill.
- Fox, R. A. (2002). Intravascular brachytherapy of the coronary arteries. *Phys. Med. Biol.* **47**: R1–R30.
- Fritzberg, A. R., and B. W. Wessels (1995). Therapeutic radionuclides. In H. N. Wagner, Jr., Z. Szabo, and J. W. Buchanan, eds. *Principles of Nuclear Medicine*, 2nd ed. Philadelphia, Saunders, pp. 229–234.
- Howell, R. W. (1992). Radiation spectra for Auger-emitting radionuclides: Report No. 2 of the AAPM Nuclear Medicine Task Group No. 6. *Med. Phys.* **19**(6): 1371–1383.
- Humm, J. L., R. W. Howell, and D. V. Rao (1994). Dosimetry of Auger-electron-emitting radionuclides: Report No. 3 of the AAPM Nuclear Medicine Task Group No. 6. *Med. Phys.* **12**(12): 1901–1915.
- Hunt J.G., F. C. da Silva and C. L. Mauricio (2004). The validation of organ dose calculations using voxel simulators and Monte Carlo methods applied to point and water immersion sources. *Rad. Prot. Dosimetry* **108**(1): 85–89.
- Kaluza, G. L., and A. E. Raizner (2004). Brachytherapy for stenosis after stenting for coronary artery disease: its role in the drug-eluting stent era. *Current Opinion in Cardiol.* **19**: 601–607.
- Kassis, A. I. (2004). The amazing world of Auger electrons. *Int. J. Rad. Biol.*, **80**(11-12): 789–803.
- Larsson, S. A. (1980). Gamma camera emission tomography: Development and properties of a multisectional emission computed tomography system. *Acta Radiol.* (Suppl. 363).
- Links, J. M., and J. C. Engdahl (1995). Planar imaging. Chapter 17 in H. N. Wagner, Jr., Z. Szabo, and J. W. Buchanan, eds. *Principles of Nuclear Medicine*, 2nd ed. Philadelphia, Saunders.
- Loevinger, R., T. F. Budinger, and E. E. Watson (1988). *MIRD Primer for Absorbed Dose Calculations*. New York, Society of Nuclear Medicine.
- Nag, S. ed. (1994). *High Dose Rate Brachytherapy: A Textbook*. Armonk, NY, Futura.
- Patterson, J. C., and M. L. Mosley (2005). How available is positron tomography in the United States? *Mol. Imaging Biol.* **7**(3): 197–200.
- Rehm, K., S. C. Strother, J. R. Anderson, K. A. Schaper, and D. A. Rottenberg (1994). Display of merged multimodality brain images using interleaved pixels with independent color scales. *J. Nucl. Med.* **35**: 1815–1821.
- Sastry, K. S. R. (1992). Biological effects of the Auger emitter iodine-125: A review. Report No. 1 of the AAPM Nuclear Medicine Task Group No. 6. *Med. Phys.* **19**(6): 1361–1370.
- Snyder, W. S., M. R. Ford, and G. G. Warner (1976). *Specific Absorbed Fractions for Radiation Sources Uniformly Distributed in Various Organs of a Heterogeneous Phantom*. NM/MIRD Pamphlet 5, revised. New York, Society of Nuclear Medicine.
- Snyder, W. S., M. R. Ford, G. G. Warner, and H. L. Fisher (1969). *Estimates of Absorbed Fractions for Monoenergetic Photon Sources Uniformly Distributed in Various Organs of a Heterogeneous Phantom*. NM/MIRD Pamphlet 5. New York, Society of Nuclear Medicine.
- Snyder, W. S., M. R. Ford, G. G. Warner, and S. B. Watson (1975). *S, Absorbed Dose per Unit Cumulated Activity for Selected Radionuclides and Organs*. NM/MIRD Pamphlet 11. New York, Society of Nuclear Medicine.
- Stabin, M. G., and L. C. Q. P. da Luz (2002). Decay data for internal and external dose assessment. *Health Phys.* **83**(4): 471–475.
- Stabin, M. G., R. B. Sparks, and E. Crowe (2005). OLINDA/EXM: The second-generation personal computer software for internal dose assessment in nuclear medicine. *J. Nucl. Med.* **46**(6): 1023–1027.
- Strother, S. C., J. R. Anderson, Jr., K. A. Schaper, J. J. Sidtis, J. S. Liow, R. P. Woods, and D. A. Rottenberg (1995). Principal component analysis and the scaled subprofile model compared to intersubject averaging and statistical parametric mapping: I. Functional connectivity of the human motor system studied with <sup>15</sup>O-water PET. *J. Cerebral Blood Flow Metab.* **15**(5): 738–753.
- Watson, E. E., M. G. Stabin, and J. A. Siegel (1993). MIRD formulation. *Med. Phys.* **20**(2, Pt. 2): 511–514.
- Weber, D. A., K. F. Eckerman, L. T. Dillman, and J. C. Ryman (1989). *MIRD: Radionuclide Data and Decay Schemes*. New York, Society of Nuclear Medicine.

# Magnetic Resonance Imaging

Magnetic resonance imaging (MRI) (formerly called nuclear magnetic resonance imaging) provides very-high-resolution images without ionizing radiation. There is also the potential for more elaborate imaging, including flow, diffusion, and the signature of particular atomic environments.

Magnetic resonance phenomena are more complicated than x-ray attenuation or photon emission by a radioactive nucleus. MRI depends upon the behavior of atomic nuclei in a magnetic field, in particular, the orientation and motion of the nuclear magnetic moment in the field. The patient is placed in a strong static magnetic field (typically 1–4 T). This is usually provided by a hollow cylindrical (solenoidal) magnet, though some machines use other configurations so that the physician can carry out procedures on the patient while viewing the MRI image. Other coils apply time-varying spatial gradients to the magnetic field, along with radio-frequency signals that cause the magnetization changes described below. Still other coils detect the very weak radio-frequency signals resulting from these changes.

First, we must understand the property that we are measuring. Section 18.1 describes the behavior of a magnetic moment in a static magnetic field, and Sec. 18.2 shows how the nuclear spin is related to the magnetic moment. Section 18.3 introduces the concept of the magnetization vector, which is the magnetic moment per unit volume, while Sec. 18.4 develops the equations of motion for the magnetic moment. In order to describe the motion of the magnetization, it is convenient—in fact, almost essential—to use the rotating coordinate system described in section 18.5.

To make a measurement, the nuclear magnetic moments originally aligned with the static magnetic field are made to rotate or precess in a plane perpendicular to the static field, after which the magnetization gradually returns to its original value. This relaxation phenomenon

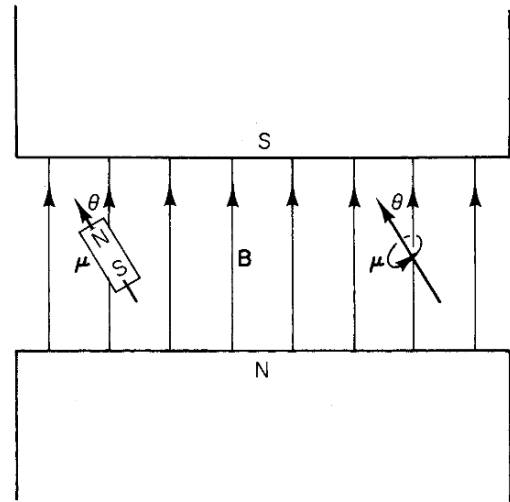


FIGURE 18.1. A magnetic dipole in a magnetic field. The dipole can be either a bar magnet or a current loop.

is described in Sec. 18.6. Sections 18.7 and 18.8 describe ways in which the magnetization can be manipulated for measurement or imaging.

Imaging techniques are finally introduced in Sec. 18.9. Sections 18.10 and 18.11 describe how chemical shifts and blood flow can affect the image or can themselves be imaged. The last two sections describe functional MRI (fMRI) and diffusion effects.

## 18.1 Magnetic Moments in an External Magnetic Field

Magnetic resonance imaging detects the magnetic dipoles in the nuclei of atoms in the human body. We saw in Chapter 8 that isolated magnetic monopoles have never

been observed [see Eq. 8.6], and that magnetic fields are produced by moving charges or electric currents. In some cases, such as bar magnets, the external field is the same as if there were magnetic charges occurring in pairs or *dipoles*.<sup>1</sup> The strength of a dipole is measured by its *magnetic dipole moment*  $\boldsymbol{\mu}$ . (In Chapter 8 the magnetic dipole moment was called  $\mathbf{m}$  to avoid confusion with  $\mu_0$ . In this chapter we use  $\boldsymbol{\mu}$  to avoid confusion with the quantum number  $m$  and to be consistent with the literature in the field.) The magnetic dipole moment is analogous to the electric dipole moment of Chapter 7; however, it is produced by a movement of charge, such as charge moving in a circular path. The units of  $\boldsymbol{\mu}$  are  $\text{J T}^{-1}$  or  $\text{A m}^2$ . We saw that when a magnetic dipole is placed in a magnetic field as in Fig. 18.1, it is necessary to apply an external torque  $\boldsymbol{\tau}_{\text{ext}}$  to keep it in equilibrium. This torque, which is required to cancel the torque exerted by the magnetic field, vanishes if the dipole is aligned with the field. The torque exerted on the dipole by the magnetic field  $\mathbf{B}$  is

$$\boldsymbol{\tau} = \boldsymbol{\mu} \times \mathbf{B} \quad (18.1)$$

(This is Eq. 8.4.)

The potential energy of the dipole is the work that must be done by  $\boldsymbol{\tau}_{\text{ext}}$  to change the dipole's orientation in the magnetic field without changing any kinetic energy it might have. To increase angle  $\theta$  by an amount  $d\theta$  requires that work be done on the dipole-magnetic field system. This work is the increase in potential energy of the system:

$$dU = \mu B \sin \theta d\theta. \quad (18.2)$$

This can be integrated to give the change in potential energy when the angle changes from  $\theta_1$  to  $\theta_2$ :

$$U(\theta_2) - U(\theta_1) = -\mu B (\cos \theta_2 - \cos \theta_1).$$

If the energy is considered to be zero when the dipole is at right angles to  $\mathbf{B}$ , then the potential energy is

$$U(\theta) = -\mu B \cos \theta = -\boldsymbol{\mu} \cdot \mathbf{B}. \quad (18.3)$$

In many cases the moving charges that give rise to the magnetic moment of an object possess angular momentum  $\mathbf{L}$ . Often the magnetic moment is parallel to and proportional to the angular momentum:  $\boldsymbol{\mu} = \gamma \mathbf{L}$ . The proportionality factor  $\gamma$  is called the *gyromagnetic ratio* (sometimes called the magnetogyric ratio). When such an object is placed in a uniform magnetic field, the resulting motion can be quite complicated. The torque on the object is  $\boldsymbol{\tau} = \boldsymbol{\mu} \times \mathbf{B} = \gamma \mathbf{L} \times \mathbf{B}$ . It is not difficult to show (Problem 1) that the torque is the rate of change of the

<sup>1</sup>Dipoles can be arranged so that their fields nearly cancel, giving rise to still higher order moments such as the quadrupole moment or the octupole moment. (See Chapter 7). A configuration for which the quadrupole moment is important is two magnets in a line arranged as N-S-S-N.

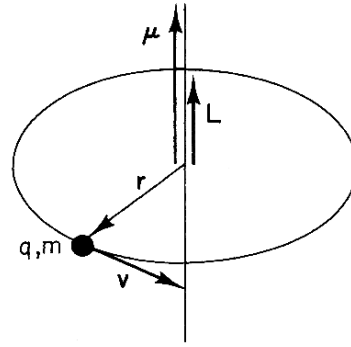


FIGURE 18.2. A particle of charge  $q$  and mass  $m$  travels in a circular orbit. It has a magnetic moment  $\boldsymbol{\mu}$  and angular momentum  $\mathbf{L}$ . If the charge is positive,  $\boldsymbol{\mu}$  and  $\mathbf{L}$  are parallel; if it is negative they are in opposite directions.

angular momentum,  $\boldsymbol{\tau} = d\mathbf{L}/dt$ . Therefore the equation of motion is

$$\gamma(\mathbf{L} \times \mathbf{B}) = \frac{d\mathbf{L}}{dt} \quad (18.4a)$$

or

$$\gamma(\boldsymbol{\mu} \times \mathbf{B}) = \frac{d\boldsymbol{\mu}}{dt}. \quad (18.4b)$$

Solutions to these equations are discussed in Sec. 18.4.

## 18.2 The Source of the Magnetic Moment

Atomic electrons and the protons and neutrons in the atomic nucleus can possess both angular momentum and a magnetic moment. The magnetic moment of a particle is related to its angular momentum. We can derive this relationship for a charged particle moving in a circular orbit. We saw in Chapter 8 that the magnitude of the magnetic moment of a current loop is the product of the current  $i$  and the area of the loop  $S$ :

$$|\boldsymbol{\mu}| = \mu = iS. \quad (18.5)$$

The direction of the vector is perpendicular to the plane of the loop. Its direction is defined by a right-hand rule: curl the fingers of your right hand in the direction of current flow and your thumb will point in the direction of  $\boldsymbol{\mu}$  (see the right-hand part of Fig. 18.1). This is the same right-hand rule that relates the circular motion of a particle to the direction of its angular momentum.

Suppose that a particle of charge  $q$  and mass  $m$  moves in a circular orbit of radius  $r$  as in Fig. 18.2. The speed is  $v$  and the magnitude of the angular momentum is  $L = mvr$ . The effective current is the charge  $q$  multiplied by the number of times it goes past a given point on the circumference of the orbit in one second:  $i = qv/2\pi r$ . The magnetic moment has magnitude  $\mu = iS = i\pi r^2 = qvr/2$ . Since the angular momentum is  $L = mvr$  and  $\boldsymbol{\mu}$  and  $\mathbf{L}$  are both perpendicular to the plane of the orbit, we can write

$$\boldsymbol{\mu} = \left( \frac{q}{2m} \right) \mathbf{L} = \gamma \mathbf{L}. \quad (18.6)$$

TABLE 18.1. Values of the spin and gyromagnetic ratio for a free electron and various nuclei of interest.

Particle	Spin	$\gamma = \omega_{\text{Larmor}}/B$ ( $\text{s}^{-1} \text{T}^{-1}$ )	$\nu/B$ (MHz $\text{T}^{-1}$ )
Electron	$\frac{1}{2}$	$1.7608 \times 10^{11}$	$2.8025 \times 10^4$
Proton	$\frac{1}{2}$	$2.6753 \times 10^8$	42.5781
Neutron	$\frac{1}{2}$	$1.8326 \times 10^8$	29.1667
$^{23}\text{Na}$	$\frac{3}{2}$	$0.7076 \times 10^8$	11.2618
$^{31}\text{P}$	$\frac{1}{2}$	$1.0829 \times 10^8$	17.2349

The quantity  $\gamma = q/2m$  is the gyromagnetic ratio for this system. The units  $\gamma$  of are  $\text{T}^{-1} \text{s}^{-1}$  (see Problem 2). The magnetic moment and the orbital angular momentum are parallel for a positive charge and antiparallel for a negative charge.

An electron or a proton also has an intrinsic magnetic moment quite separate from its orbital motion. It is associated with and proportional to the intrinsic or “spin” angular momentum  $\mathbf{S}$  of the particle. We write

$$\boldsymbol{\mu} = \gamma \mathbf{S}. \quad (18.7)$$

The value of  $\gamma$  for a spin is *not* equal to  $q/2m$ .

Two kinds of spin measurements have biological importance. One is associated with electron magnetic moments and the other with the magnetic moments of nuclei. Most neutral atoms in their ground state have no magnetic moment due to the electrons. Exceptions are the transition elements that exhibit paramagnetism. Free radicals, which are often of biological interest, have an unpaired electron and therefore have a magnetic moment. In most cases this magnetic moment is due almost entirely to the spin of the unpaired electron.

Magnetic resonance imaging is based on the magnetic moments of atomic nuclei in the patient. The total angular momentum and magnetic moment of an atomic nucleus are due to the spins of the protons and neutrons, as well as any orbital angular momentum they have inside the nucleus. Table 18.1 lists the spin and gyromagnetic ratio of the electron and some nuclei of biological interest.

If the nuclear angular momentum is  $\mathbf{I}$  with quantum number  $I$ , the possible values of the  $z$  component of  $\mathbf{I}$  are  $m\hbar$ , where  $m = -I, (-I + 1), \dots, I$ . For  $I = \frac{1}{2}$ , the values are  $-1/2$  and  $1/2$ , while for  $I = \frac{3}{2}$  they are  $-3/2, -1/2, 1/2$  and  $3/2$ . The direction of the external magnetic field defines the  $z$  axis, and the energy of a spin is given by  $-\boldsymbol{\mu} \cdot \mathbf{B} = -\gamma \mathbf{I} \cdot \mathbf{B} = -\gamma m\hbar B$ . The difference between adjacent energy levels is  $\gamma B\hbar$ , and the angular frequency of a photon corresponding to that difference is  $\omega_{\text{photon}} = \gamma B$ .

## 18.3 The Magnetization

The MR image depends on the *magnetization* of the tissue. The magnetization of a sample,  $\mathbf{M}$ , is the average magnetic moment per unit volume. In the absence of an external magnetic field to align the nuclear spins, the magnetization is zero. As an external magnetic field  $\mathbf{B}$  is applied, the spins tend to align in spite of their thermal motion, and the magnetization increases, proportional at first to the external field. If the external field is strong enough, all of the nuclear magnetic moments are aligned, and the magnetization reaches its saturation value.

We can calculate how the magnetization depends on  $\mathbf{B}$ . Consider a collection of spins of a single nuclear species in an external magnetic field. This might be the hydrogen nuclei (protons) in a sample. The spins do not interact with each other but are in thermal equilibrium with the surroundings, which are at temperature  $T$ . We do not consider the mechanism by which they reach thermal equilibrium. Since the magnetization is the average magnetic moment per unit volume, it is the number of spins per unit volume,  $N$ , times the average magnetic moment of each spin:  $\mathbf{M} = N \langle \boldsymbol{\mu} \rangle$ .

To obtain the average value of the  $z$  component of the magnetic moment, we must consider each possible value of quantum number  $m$ . We multiply the value of  $\mu_z$  corresponding to each value of  $m$  by the probability that  $m$  has that value. Since the spins are in thermal equilibrium with the surroundings, the probability is proportional to the Boltzmann factor of Chapter 3,  $e^{-(U/k_B T)} = e^{\gamma m\hbar B/k_B T}$ . The denominator in Eq. 18.8 normalizes the probability:

$$\langle \mu_z \rangle = \frac{\gamma \hbar \sum_{m=-I}^I m e^{\gamma m\hbar B/k_B T}}{\sum_{m=-I}^I e^{\gamma m\hbar B/k_B T}}. \quad (18.8)$$

At room temperature  $\gamma \hbar B/k_B T \ll 1$  (see Problem 4), and it is possible to make the approximation  $e^x \approx 1 + x$ . The sum in the numerator then has two terms:

$$\sum_{m=-I}^I m + \frac{\gamma \hbar B}{k_B T} \sum_{m=-I}^I m^2.$$

The first sum vanishes. The second is  $I(I+1)(2I+1)/3$ . The denominator is

$$\sum_{m=-I}^I 1 + \frac{\gamma \hbar B}{k_B T} \sum_{m=-I}^I m.$$

The first term is  $2I+1$ ; the second vanishes. Therefore we obtain

$$\langle \mu_z \rangle = \frac{\gamma^2 \hbar^2 I(I+1)}{3k_B T} B. \quad (18.9)$$

The  $z$  component of  $\mathbf{M}$  is

$$M_z = N \langle \mu_z \rangle = \frac{N \gamma^2 \hbar^2 I(I+1)}{3k_B T} B, \quad (18.10)$$

which is proportional to the applied field.

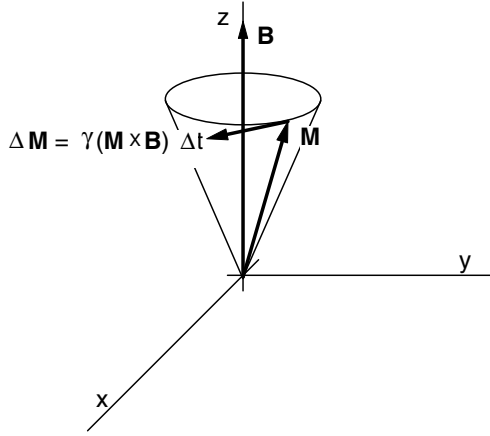


FIGURE 18.3. The system with initial magnetization  $\mathbf{M}$  has been given just enough additional angular momentum to precess about the direction of the static magnetic field  $\mathbf{B}$ . The rate of change of  $\mathbf{M}$  is perpendicular to both  $\mathbf{M}$  and  $\mathbf{B}$ . For short time intervals,  $\Delta\mathbf{M} = \gamma(\mathbf{M} \times \mathbf{B}) \Delta t$ .

## 18.4 Behavior of the Magnetization Vector

A remarkable result of quantum mechanics is that the average or expectation value of a spin obeys the classical Equation 18.4b:

$$\frac{d\langle\boldsymbol{\mu}\rangle}{dt} = \gamma(\langle\boldsymbol{\mu}\rangle \times \mathbf{B}) \quad (18.11)$$

whether or not  $\mathbf{B}$  is time dependent [Slichter (1978), p. 20]. Multiplying by the number of spins per unit volume we obtain

$$\frac{d\mathbf{M}}{dt} = \gamma(\mathbf{M} \times \mathbf{B}). \quad (18.12)$$

This equation can lead to many different behaviors of  $\mathbf{M}$ , some of which are quite complicated.

The simplest motion occurs if  $\mathbf{M}$  is parallel to  $\mathbf{B}$ , in which case  $\mathbf{M}$  does not change because there is no torque. Another relatively simple motion, called *precession*, is shown in Figure 18.3. With the proper initial conditions  $\mathbf{M}$  (and  $\langle\boldsymbol{\mu}\rangle$ ) precess about the direction of  $\mathbf{B}$ . That is, they both rotate about the direction of  $\mathbf{B}$  with a constant angular velocity and at a fixed angle  $\theta$  with the direction of  $\mathbf{B}$ . Since  $\mathbf{M} \times \mathbf{B}$  is always at right angles to  $\mathbf{M}$ ,  $d\mathbf{M}/dt$  is at right angles to  $\mathbf{M}$ , and the angular momentum does not change magnitude. The analytic solution can be investigated by writing Eq. 18.12 in Cartesian coordinates when  $\mathbf{B}$  is along the  $z$  axis:

$$\begin{aligned} \frac{dM_x}{dt} &= \gamma M_y B_z, \\ \frac{dM_y}{dt} &= -\gamma M_x B_z, \\ \frac{dM_z}{dt} &= 0. \end{aligned} \quad (18.13)$$

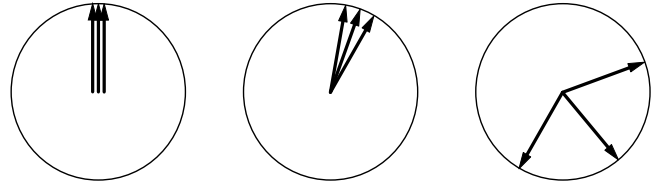


FIGURE 18.4. If several spins precess in the  $xy$  plane at slightly different rates, the total spin amplitude decreases due to dephasing.

One possible solution to these equations is

$$\begin{aligned} M_z &= M_{\parallel} = \text{const}, \\ M_x &= M_{\perp} \cos(-\omega t), \\ M_y &= M_{\perp} \sin(-\omega t). \end{aligned} \quad (18.14)$$

You can verify that these are a solution for arbitrary values of  $M_{\perp}$  and  $M_{\parallel}$  as long as  $\omega = \omega_0 = \gamma B_z$ . This is called the *Larmor precession frequency*. The minus sign means that for positive  $\gamma$  the rotation is clockwise in the  $xy$  plane. The classical Larmor frequency is equal to the frequency of photons corresponding to the energy difference given by successive values of  $\boldsymbol{\mu} \cdot \mathbf{B}$ . For this solution the initial values of  $\mathbf{M}$  at  $t = 0$  are  $M_x(0) = M_{\perp}$ ,  $M_y(0) = 0$ , and  $M_z(0) = M_{\parallel}$ .

We need to modify the equation of motion, Eq. 18.12, to include changes in  $\mathbf{M}$  that occur because of effects other than the magnetic field. Suppose that  $\mathbf{M}$  has somehow been changed so that it no longer points along the  $z$  axis with the equilibrium value given by Eq. 18.10. Thermal agitation will change the populations of the levels so that  $M_z$  returns to the equilibrium value, which we call  $M_0$ . We *postulate* that the rate of exchange of energy with the reservoir is proportional to how far the value of  $M_z$  is from equilibrium:

$$\frac{dM_z}{dt} = \frac{1}{T_1} (M_0 - M_z).$$

The quantity  $T_1$ , which is the inverse of the proportionality constant, is called the *longitudinal relaxation time* or *spin-lattice relaxation time*.

We also *postulate* an exponential disappearance of the  $x$  and  $y$  components of  $\mathbf{M}$  with a *transverse relaxation time*  $T_2$  (sometimes called the *spin-spin relaxation time*). (This assumption is often not a good one. For example, the decay of  $M_x$  and  $M_y$  in ice is more nearly Gaussian than exponential.) The equations are

$$\frac{dM_x}{dt} = -\frac{M_x}{T_2}, \quad \frac{dM_y}{dt} = -\frac{M_y}{T_2}.$$

The transverse relaxation time is always shorter than  $T_1$ . Here is why. A change of  $M_z$  requires an exchange of energy with the reservoir. This is not necessary for changes confined to the  $xy$  plane, since the potential energy ( $\boldsymbol{\mu} \cdot \mathbf{B}$ ) does not change in that case.  $M_x$  and  $M_y$  can change as  $M_z$  changes, but they can also change by

other mechanisms, such as when individual spins precess at slightly different frequencies, a process known as *dephasing*. The angular velocity of precession can be slightly different for different nuclear spins because of local variations in the static magnetic field; the angular velocity can also fluctuate as the field fluctuates with time. These variations and fluctuations are caused by neighboring atomic or nuclear magnetic moments or by inhomogeneities in the external magnetic field. Figure 18.4 shows how dephasing occurs if several magnetic moments precess at different rates.

Combining these approximate equations for relaxation in the absence of an applied magnetic field with Eq. 18.12 for the effect of a magnetic field gives the *Bloch equations*:<sup>2</sup>

$$\begin{aligned}\frac{dM_z}{dt} &= \frac{1}{T_1} (M_0 - M_z) + \gamma (\mathbf{M} \times \mathbf{B})_z, \\ \frac{dM_x}{dt} &= -\frac{M_x}{T_2} + \gamma (\mathbf{M} \times \mathbf{B})_x, \\ \frac{dM_y}{dt} &= -\frac{M_y}{T_2} + \gamma (\mathbf{M} \times \mathbf{B})_y.\end{aligned}\quad (18.15)$$

While these equations are not rigorous and there is no reason for the relaxation to be strictly exponential, they have proven to be quite useful in explaining many facets of nuclear spin magnetic resonance.

One can demonstrate by direct substitution the following solution to Eqs. 18.15 for a static magnetic field  $\mathbf{B}$  along the  $z$  axis:

$$\begin{aligned}M_x &= M_0 e^{-t/T_2} \cos(-\omega_0 t), \\ M_y &= M_0 e^{-t/T_2} \sin(-\omega_0 t), \\ M_z &= M_0 (1 - e^{-t/T_1}),\end{aligned}\quad (18.16)$$

where  $\omega_0 = \gamma B$ . This solution corresponds to what happens if  $\mathbf{M}$  is somehow made to precess in the  $xy$  plane. (We will see how to accomplish this in Sec. 18.5.) The magnetization in the  $xy$  plane is initially  $M_0$ , and the amplitude decays exponentially with time constant  $T_2$ . The initial value of  $M_z$  is zero, and it decays back to  $M_0$  with time constant  $T_1$ . A perspective plot of the trajectory of the tip of vector  $\mathbf{M}$  is shown in Fig. 18.5.

## 18.5 A Rotating Coordinate System

### 18.5.1 Transforming to the Rotating Coordinate System

It is *much* easier to describe the motion of  $\mathbf{M}$  in a coordinate system that is rotating about the  $z$  axis at the Larmor frequency. Figure 18.6 shows a vector  $\mathbf{M}$  and two

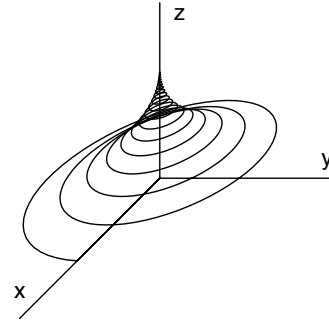


FIGURE 18.5. The locus of the tip of the magnetization  $\mathbf{M}$  when it relaxes according to Eqs. 18.16.

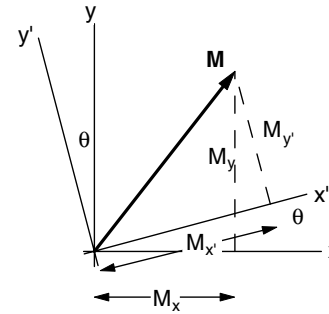


FIGURE 18.6. The vector  $\mathbf{M}$  can be represented by components along  $x$  and  $y$  or along  $x'$  and  $y'$ .

coordinate systems,  $xy$  and  $x'y'$ . The  $z$  component of  $\mathbf{M}$  is unchanged. By considering the other components in Fig. 18.6, we see that

$$\begin{aligned}M_x &= M_{x'} \cos \theta - M_{y'} \sin \theta, \\ M_y &= M_{x'} \sin \theta + M_{y'} \cos \theta \\ M_z &= M_{z'}.\end{aligned}\quad (18.17a)$$

This can also be written in matrix form. A rotation through angle  $\theta$  around the  $z$  axis gives

$$\mathbf{M} = \begin{pmatrix} M_x \\ M_y \\ M_z \end{pmatrix} = \begin{pmatrix} \cos \theta & -\sin \theta & 0 \\ \sin \theta & \cos \theta & 0 \\ 0 & 0 & 1 \end{pmatrix} \begin{pmatrix} M_{x'} \\ M_{y'} \\ M_{z'} \end{pmatrix} = \mathbf{R}\mathbf{M}'.\quad (18.17b)$$

Rotations about the other axes are discussed in Problem 12. Note that rotating the coordinate system that describes a fixed vector is equivalent to rotating the vector in the opposite direction, so the results quoted in Problem 12 apply to both situations.

For a three-dimensional coordinate system rotating clockwise around the  $z$  axis,  $\theta = -\omega t$ , the  $z$ -component of  $\mathbf{M}$  is unchanged, and the transformation equations are

$$\begin{aligned}M_x &= M_{x'} \cos(-\omega t) - M_{y'} \sin(-\omega t), \\ M_y &= M_{x'} \sin(-\omega t) + M_{y'} \cos(-\omega t), \\ M_z &= M_{z'}.\end{aligned}\quad (18.18)$$

<sup>2</sup>Felix Bloch and Edward Purcell shared the 1952 Nobel Prize in Physics for their discovery of nuclear magnetic resonance.

The time derivative of  $\mathbf{M}$  is obtained by differentiating each component and remembering that  $\mathbf{M}'$  can also depend on  $t$ :

$$\begin{aligned} \frac{dM_x}{dt} &= \frac{dM_{x'}}{dt} \cos(-\omega t) - \frac{dM_{y'}}{dt} \sin(-\omega t) \\ &\quad + \omega M_{x'} \sin(-\omega t) + \omega M_{y'} \cos(-\omega t), \\ \frac{dM_y}{dt} &= \frac{dM_{x'}}{dt} \sin(-\omega t) + \frac{dM_{y'}}{dt} \cos(-\omega t) \\ &\quad - \omega M_{x'} \cos(-\omega t) + \omega M_{y'} \sin(-\omega t), \\ \frac{dM_z}{dt} &= \frac{dM_{z'}}{dt}. \end{aligned} \quad (18.19)$$

We can use these expressions to write the equations of motion in the rotating frame. First consider a system without relaxation effects and with a static field  $B_z$  along the  $z$  axis. We will show that the components of  $\mathbf{M}$  in a system rotating at the Larmor frequency are constant. The equations of motion are given in Eqs. 18.13. In terms of variables in the rotating frame, the equation for  $dM_x/dt$  becomes

$$\begin{aligned} \frac{dM_{x'}}{dt} \cos(-\omega t) - \frac{dM_{y'}}{dt} \sin(-\omega t) \\ + \omega M_{x'} \sin(-\omega t) + \omega M_{y'} \cos(-\omega t) \\ = \gamma [M_{x'} \sin(-\omega t) + M_{y'} \cos(-\omega t)] B_z. \end{aligned}$$

If the frame rotates at the Larmor frequency  $\omega_0 = \gamma B_z$ , the third and fourth terms on the left are equal to the right-hand side. The equation becomes

$$\frac{dM_{x'}}{dt} \cos(-\omega_0 t) - \frac{dM_{y'}}{dt} \sin(-\omega_0 t) = 0.$$

Under the same circumstances, the equation for  $dM_y/dt$  gives

$$\frac{dM_{x'}}{dt} \sin(-\omega_0 t) + \frac{dM_{y'}}{dt} \cos(-\omega_0 t) = 0.$$

Solving these simultaneously shows that  $dM_{x'}/dt = 0$  and  $dM_{y'}/dt = 0$ . Therefore in the rotating system  $M_{x'}$  and  $M_{y'}$  are constant. Equation 18.13 showed that  $M_{z'}$  is constant, so the components of  $\mathbf{M}$  are constant in the frame rotating at the Larmor frequency. Using Eqs. 18.18 to transform back to the laboratory system gives the solution Eq. 18.14.<sup>3</sup>

<sup>3</sup>For those familiar with vector analysis, the general relationship between the time derivative of any vector  $\mathbf{M}$  in the laboratory system and a system rotating with angular velocity  $\boldsymbol{\Omega}$  is

$$\left( \frac{d\mathbf{M}}{dt} \right)_{\text{lab}} = \left( \frac{\partial \mathbf{M}}{\partial t} \right)_{\text{rot}} + \boldsymbol{\Omega} \times \mathbf{M}.$$

This can be applied to the magnetization combined with Eq. 18.12 to give

$$\left( \frac{\partial \mathbf{M}}{\partial t} \right)_{\text{rot}} = \gamma(\mathbf{M} \times \mathbf{B}) - \boldsymbol{\Omega} \times \mathbf{M} = \gamma \mathbf{M} \times \left( \mathbf{B} + \frac{\boldsymbol{\Omega}}{\gamma} \right),$$

which vanishes if  $\gamma \mathbf{B} = -\boldsymbol{\Omega}$ .

### 18.5.2 An Additional Oscillating Field

The next problem we consider in the rotating coordinate system is the addition of an oscillating magnetic field  $B_1 \cos(\omega t)$  along the  $x$  axis, fixed in the laboratory system. We will show that if the applied field is at the Larmor frequency, the equations of motion in the rotating system, Eqs. 18.25, are quite simple but very important. They are given below.

They are derived as follows. From the  $x$  component of Eq. 18.12,

$$\frac{dM_x}{dt} = \gamma(M_y B_z - M_z B_y),$$

we obtain (remembering that the  $x'y'$  system is rotating at the Larmor frequency  $\omega_0$ )

$$\begin{aligned} \frac{dM_{x'}}{dt} \cos(-\omega_0 t) - \frac{dM_{y'}}{dt} \sin(-\omega_0 t) + \omega_0 M_{x'} \sin(-\omega_0 t) \\ + \omega_0 M_{y'} \cos(-\omega_0 t) \\ = \gamma B_z [M_{x'} \sin(-\omega_0 t) + M_{y'} \cos(-\omega_0 t)]. \end{aligned}$$

Since  $\omega_0 = \gamma B_z$ , the last two terms on the left cancel the terms on the right, leaving

$$\frac{dM_{x'}}{dt} \cos(-\omega_0 t) - \frac{dM_{y'}}{dt} \sin(-\omega_0 t) = 0. \quad (18.20)$$

Similarly, the  $y$ -component of Eq. 18.12,

$$\frac{dM_y}{dt} = \gamma(M_z B_x - M_x B_z),$$

transforms and reduces to (remembering that  $M_z = M_{z'}$ )

$$\frac{dM_{x'}}{dt} \sin(-\omega_0 t) + \frac{dM_{y'}}{dt} \cos(-\omega_0 t) = \gamma B_1 M_{z'} \cos(-\omega t). \quad (18.21)$$

The  $z$ -component of Eq. 18.12 is

$$\frac{dM_z}{dt} = \gamma(M_x B_y - M_y B_x), \quad (18.22)$$

which transforms to

$$\begin{aligned} \frac{dM_{z'}}{dt} &= -\gamma B_1 M_{x'} \cos(\omega t) \sin(-\omega_0 t) \\ &\quad - \gamma B_1 M_{y'} \cos(\omega t) \cos(-\omega_0 t). \end{aligned}$$

It is possible to eliminate  $M_{x'}$  from Eqs. 18.20 and 18.21 by multiplying Eq. 18.20 by  $-\sin(-\omega_0 t)$ , multiplying Eq. 18.21 by  $\cos(-\omega_0 t)$ , and adding. The result is

$$\frac{dM_{y'}}{dt} = \gamma B_1 M_{z'} \cos(\omega t) \cos(-\omega_0 t). \quad (18.23)$$

A similar technique can be used to eliminate  $M_{y'}$  from these two equations:

$$\frac{dM_{x'}}{dt} = \gamma B_1 M_{z'} \cos(\omega t) \sin(-\omega_0 t). \quad (18.24)$$



### 18.5.3 Nutation

Equations 18.22–18.24 are the equations of motion for the components of  $\mathbf{M}$  in the rotating system. If  $\omega \neq \omega_0$ , the motion is complicated, but averaged over many Larmor periods the right-hand side of each equation is zero. If the applied field oscillates at the Larmor frequency,  $\omega = \omega_0$ , then the  $\cos^2(-\omega_0 t)$  factors average to  $\frac{1}{2}$  while factors like  $\sin(-\omega_0 t) \cos(-\omega_0 t)$  average to zero.

The averaged equations are a very important result:

$$\frac{dM_{x'}}{dt} = 0, \quad (18.25a)$$

$$\frac{dM_{y'}}{dt} = \frac{\gamma B_1}{2} M_{z'}, \quad (18.25b)$$

$$\frac{dM_{z'}}{dt} = -\frac{\gamma B_1}{2} M_{y'}. \quad (18.25c)$$

The first equation says that if  $M_{x'}$  is initially zero, it remains zero. Let us define a new angular frequency

$$\omega_1 = \frac{\gamma B_1}{2}. \quad (18.26)$$

It is the frequency of nutation or rotation caused by  $B_1$  oscillating at the Larmor frequency. It is much lower than the Larmor frequency because  $B_1 \ll B_z$ . In terms of  $\omega_1$ , Eqs. 18.25b and 18.25c become

$$\frac{dM_{z'}}{dt} = -\omega_1 M_{y'}, \quad \frac{dM_{y'}}{dt} = \omega_1 M_{z'}.$$

These are a pair of coupled linear differential equations with constant coefficients. Differentiating one and substituting it in the other gives

$$\frac{d^2 M_{z'}}{dt^2} = -\omega_1 \frac{dM_{y'}}{dt} = -\omega_1^2 M_{z'}, \quad (18.27)$$

which has a solution ( $a$  and  $b$  are constants of integration)

$$M_{z'} = a \sin(\omega_1 t) + b \cos(\omega_1 t). \quad (18.28)$$

From Eq. 18.25c we get

$$M_{y'} = -\frac{1}{\omega_1} \frac{dM_{z'}}{dt} = -a \cos(\omega_1 t) + b \sin(\omega_1 t). \quad (18.29)$$

The values of  $a$  and  $b$  are determined from the initial conditions. For example, if  $\mathbf{M}$  is initially along the  $z$  axis,  $a = 0$  and  $b = M_0$ . Then

$$\begin{aligned} M_{x'} &= 0, \\ M_{y'} &= M_0 \sin(\omega_1 t), \\ M_{z'} &= M_0 \cos(\omega_1 t). \end{aligned} \quad (18.30)$$

This kind of motion—precession about the  $z$  axis combined with a change of the projection of  $\mathbf{M}$  on  $z$ —is called *nutation*.

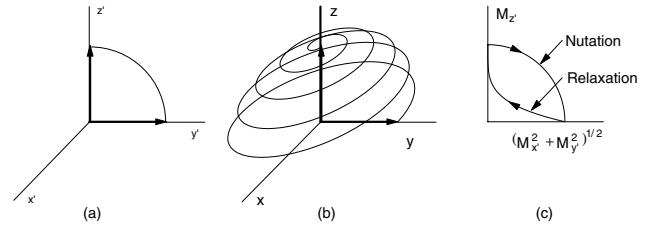


FIGURE 18.7. The locus of the tip of the magnetization  $\mathbf{M}$  when an oscillating magnetic field  $B_1$  is applied for a time  $t$  such that  $\omega_1 t = \pi/2$ . This is often called a “ $\pi/2$ ” pulse. (a) The rotating frame. (b) The laboratory frame. (c) Plots of  $M_{z'}$  vs  $(M_{x'}^2 + M_{y'}^2)^{1/2}$  showing the difference between nutation and relaxation.

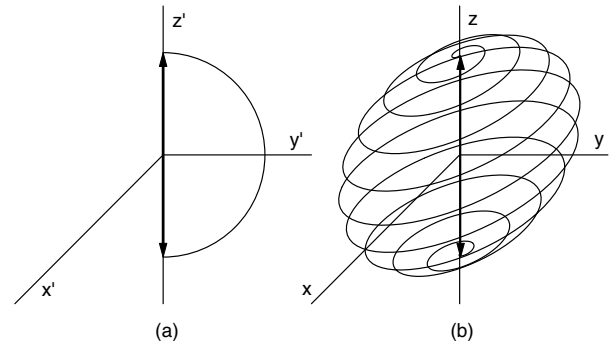


FIGURE 18.8. A “ $\pi$  pulse.”  $B_1$  is applied for a time  $t = \pi/\omega_1$  and rotates  $\mathbf{M}$  to point along the  $-z$  axis. (a) The rotating frame. (b) The laboratory frame.

### 18.5.4 $\pi$ and $\pi/2$ Pulses

From Eqs. 18.30 it is easy to see that turning  $B_1$  on for a quarter of a period of  $\omega_1$  (a  $90^\circ$  pulse or  $\pi/2$  pulse,  $t = T/4 = \pi/2\omega_1$ ) nutates  $\mathbf{M}$  into the  $x'y'$  plane, while a  $180^\circ$  or  $\pi$  pulse nutates  $\mathbf{M}$  to point along the  $-z$  axis.  $\mathbf{M}$  nutates about the rotating  $x'$  axis. Shifting the phase of  $B_1$  changes the axis in the  $x'y'$  plane about which  $\mathbf{M}$  nutates. It may seem strange that an oscillating magnetic field pointing along an axis fixed in the laboratory frame causes rotation about an axis in the rotating frame. The reason is that  $B_1$  is also oscillating at the Larmor frequency, so that its amplitude changes in just the right way to cause this behavior of  $\mathbf{M}$ . Figures 18.7 and 18.8 show this nutation in both the rotating frame and the laboratory frame for a  $\pi/2$  pulse and a  $\pi$  pulse.

Figure 18.7(c) emphasizes the difference between nutation and relaxation by plotting  $M_{z'}$  vs the projection of  $\mathbf{M}$  in the  $x'y'$  plane. For nutation the components of  $\mathbf{M}$  are given by Eqs. 18.30, the magnitude of  $\mathbf{M}$  is unchanged, and the locus is a circle. For relaxation the components are given by Eqs. 18.16.

Another interesting solution is one for which the initial value of  $\mathbf{M}$  is

$$\begin{aligned} M_{x'}(0) &= M_0 \cos \alpha, \\ M_{y'}(0) &= M_0 \sin \alpha, \end{aligned}$$

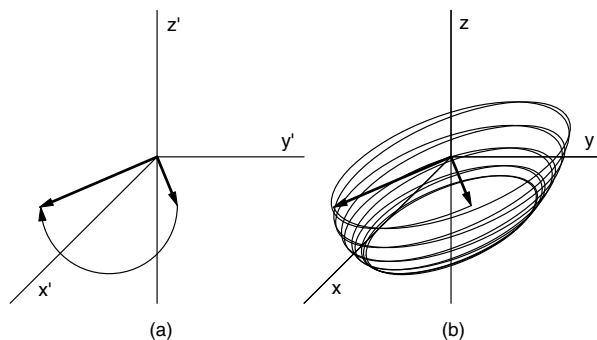


FIGURE 18.9. A magnetic field  $B_1$  pointing along the laboratory  $x$  axis and oscillating at the Larmor frequency causes nutation of  $\mathbf{M}$  through an angle  $\pi$  around the rotating  $x'$  axis. In this case  $\mathbf{M}$  was initially in the  $x'y'$  plane. The motion shown here is plotted from Eqs. 18.30 in (a) the rotating and (b) the laboratory frames.

$$M_{z'}(0) = 0.$$

This corresponds to an  $\mathbf{M}$  that has already been nutated into the  $x'y'$  plane. Substituting these values in Eqs. 18.28 and 18.29 shows that  $b = 0$  and  $a = M_0 \sin \alpha$ . Then the solution is

$$\begin{aligned} M_{x'}(t) &= M_0 \cos \alpha, \\ M_{y'}(t) &= M_0 \sin \alpha \cos(\omega_1 t), \\ M_{z'}(t) &= -M_0 \sin \alpha \sin(\omega_1 t). \end{aligned} \quad (18.31)$$

This solution is plotted in Fig. 18.9 in both the rotating frame and the laboratory frame for the case of a  $\pi$  pulse (a pulse of duration  $\pi/\omega_1$ ). The effect is to nutate  $\mathbf{M}$  about the  $x'$  axis in the rotating coordinate system. We will see later that this is a very useful pulse.

## 18.6 Relaxation Times

Since longitudinal relaxation changes the value of  $M_z$  and hence  $\boldsymbol{\mu} \cdot \mathbf{B}$ , it is associated with a change of energy of the nucleus. The principal force that can do work on the nuclear spin and change its energy arises from the fact that the nucleus is in a fluctuating magnetic field due to neighboring nuclei and the electrons in paramagnetic atoms.

One way to analyze the effect of this magnetic field is to say that the change of spin energy  $E$  is accompanied by the emission or absorption of a photon of frequency  $\nu_{\text{photon}} = E/h$ , or  $\omega_{\text{photon}} = \omega_0$ . An increase of spin energy requires the absorption of a photon at the Larmor frequency (*stimulated absorption*). This will have a high probability if the fluctuating magnetic field has a large Fourier component at the Larmor frequency. A decrease of spin energy is accompanied by the emission of a photon. This can happen spontaneously in a vacuum (*spontaneous emission*), or it can be stimulated by the presence of other photons at the Larmor frequency (*stimu-*

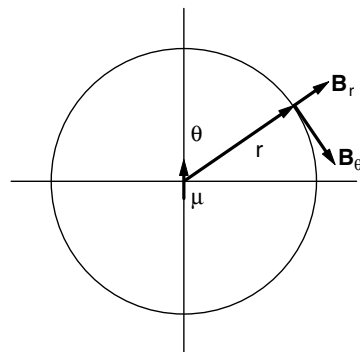


FIGURE 18.10. The magnetic field components of a dipole in spherical coordinates point in the directions shown.

lated emission). These relative probabilities can be calculated using quantum mechanics. Stimulated emission or absorption is much more probable than is spontaneous emission.

The random magnetic field at a nucleus fluctuates because of the movement of the nucleus in the magnetic field of nearby atoms and nuclei. If the field changes rapidly enough, it will have Fourier components at the Larmor frequency that can induce transitions that cause  $M_z$  to change by absorption or stimulated emission. To get an idea of the strength of the field involved, consider the field at one hydrogen nucleus in a water molecule due to the other hydrogen nucleus. The field due to a magnetic dipole is given by

$$\begin{aligned} B_r &= \frac{\mu_0}{4\pi} \frac{2\mu}{r^3} \cos \theta, \\ B_\theta &= \frac{\mu_0}{4\pi} \frac{\mu}{r^3} \sin \theta, \\ B_\phi &= 0, \end{aligned} \quad (18.32)$$

where angle  $\theta$  is defined in Fig. 18.10. (The factor  $\mu_0/4\pi \equiv 10^{-7} \text{ T m A}^{-1}$  is required in SI units.) The magnetic field at one hydrogen nucleus in a water molecule due to the other hydrogen nucleus is about  $(3-4) \times 10^{-4} \text{ T}$  (see Problem 14). Consider the water molecule shown in Fig. 18.11. We refer to each hydrogen nucleus as a proton. The  $z$  components of the proton magnetic moments are shown. If the water molecule is oriented as in Fig. 18.11(a), the field at one proton due to the other has a certain value. If the water molecule remains fixed in space, as in ice, the field is constant with time. If the molecule is tumbling as in liquid water, the orientation changes as in Fig. 18.11(b), and the field changes with time.

When the molecules are moving randomly, the fluctuating magnetic field components are best described by their autocorrelation functions. The simplest assumption one can make<sup>4</sup> is that the autocorrelation function  $\phi_{11}$

<sup>4</sup>A more complete model recognizes that different atoms experience fluctuating fields with different correlation times and that frequency components at twice the Larmor frequency also contribute.

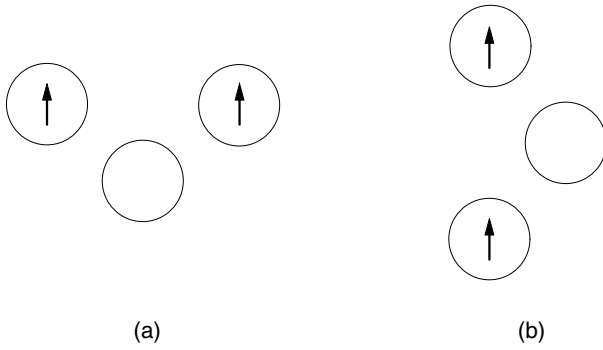


FIGURE 18.11. The  $z$  components of the magnetic moments of two protons in a water molecule are shown for two different molecular orientations, (a) and (b). When the water molecule is fixed in space, as in ice, the magnetic field that one proton produces in the neighborhood of the other is static. When the water molecule tumbles, as in a liquid or gas, the field that one proton produces at the other changes with time.

TABLE 18.2. Approximate relaxation times at 20 MHz.

	$T_1$ (ms)	$T_2$ (ms)
Whole blood	900	200
Muscle	500	35
Fat	200	60
Water	3,000	3,000

of each magnetic field component is exponential and that each field component has the same correlation time  $\tau_C$ :

$$\phi_{11}(\tau) \propto e^{-|\tau|/\tau_C}. \quad (18.33)$$

The Fourier transform of the autocorrelation function gives the power at different frequencies. It has only cosine terms because the autocorrelation is even. Comparison with the Fourier transform pair of Eq. 11.100 shows that the power at frequency  $\omega$  is proportional to  $\tau_C/(1+\omega^2\tau_C^2)$ . With the assumption that the transition rate, which is  $1/T_1$ , is proportional to the power at the Larmor frequency, we have [see also Slichter (1978), p. 167, or Dixon *et al.* (1985)]

$$\frac{1}{T_1} = \frac{C\tau_C}{1 + \omega_0^2\tau_C^2}, \quad (18.34)$$

where  $C$  is the proportionality constant.

The correlation time in a solid is much longer than in a liquid. For example, in liquid water at 20°C it is about  $3.5 \times 10^{-12}$  s; in ice it is about  $2 \times 10^{-6}$  s. Figure 18.12 shows the behavior of  $T_1$  as a function of correlation time, plotted from Eq. 18.34 with  $C = 5.43 \times 10^{10} \text{ s}^{-2}$ . For short correlation times  $T_1$  does not depend on the Larmor frequency. At long correlation times  $T_1$  is proportional to the Larmor frequency, as can be seen from Eq. 18.34. The minimum in  $T_1$  occurs when  $\omega_0 = 1/\tau_C$  in this model.

Table 18.2 shows some typical values of the relaxation times for a Larmor frequency of 20 MHz. Neighboring

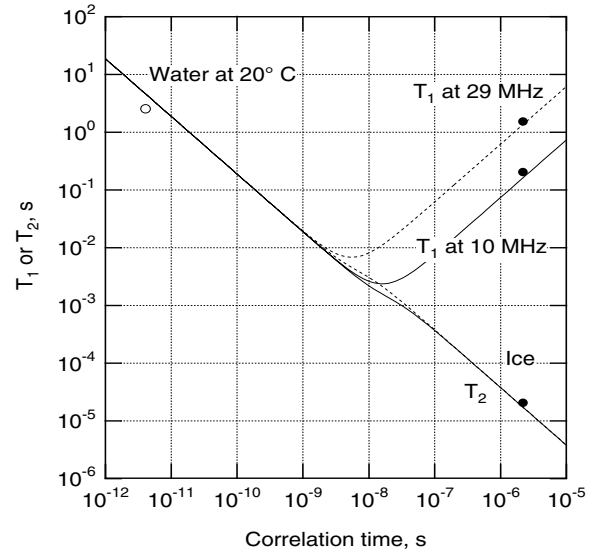


FIGURE 18.12. Plot of  $T_1$  and  $T_2$  vs correlation time of the fluctuating magnetic field at the nucleus. The dashed lines are for a Larmor frequency of 29 MHz; the solid lines are for 10 MHz. Experimental points are shown for water (open dot) and ice (solid dots).

paramagnetic atoms reduce the relaxation time by causing a fluctuating magnetic field. For example, adding 20 ppm of  $\text{Fe}^{3+}$  to pure water reduces  $T_1$  from 3,000 to 20 ms.

Differences in relaxation time are easily detected in an image. Different tissues have different relaxation times. A contrast agent containing gadolinium ( $\text{Gd}^{3+}$ ), which is strongly paramagnetic, is often used in magnetic resonance imaging. It is combined with many of the same pharmaceuticals used with  $^{99m}\text{Tc}$ , and it reduces the relaxation time of nearby nuclei.

The hemoglobin that carries oxygen in the blood exists in two forms: oxyhemoglobin and deoxyhemoglobin. The former is diamagnetic and the latter is paramagnetic, so the relaxation time in blood depends on the amount of oxygen in the hemoglobin. The imaging technique that exploits this is called BOLD (blood oxygen level dependent).

The same model for the fluctuating fields which led to Eq. 18.34 gives an expression for  $T_2$ :

$$\frac{1}{T_2} = \frac{C\tau_C}{2} + \frac{1}{2T_1}, \quad (18.35)$$

$$T_2 = \frac{2}{C\tau_C} \left[ \frac{1 + \omega_0^2\tau_C^2}{2 + \omega_0^2\tau_C^2} \right].$$

There is a slight frequency dependency to  $T_2$  for values of the correlation time close to the reciprocal of the Larmor frequency.

Another effect that causes the magnetization to rapidly decrease is dephasing. Dephasing across the sample occurs because of inhomogeneities in the externally-applied field. Suppose that the spread in Larmor frequency and

the transverse relaxation time are related by  $T_2\Delta\omega = K$ . (Usually  $K$  is taken to be 2.) The spread in Larmor frequencies  $\Delta\omega$  is due to a spread in magnetic field  $\Delta B$  experienced by the nuclear spins in different atoms. The total variation in  $B$  is due to fluctuations caused by the magnetic field of neighbors and to variation in the applied magnetic field across the sample:

$$\Delta B_{\text{tot}} = \Delta B_{\text{internal}} + \Delta B_{\text{external}}.$$

Therefore

$$\Delta\omega_{\text{tot}} = \Delta\omega_{\text{internal}} + \Delta\omega_{\text{external}}.$$

The total spread is associated with the experimental relaxation time,  $T_2^* = K/\Delta\omega_{\text{tot}}$ . The “true” or “non-recoverable” relaxation time  $T_2 = K/\Delta\omega_{\text{internal}}$  is due to the fluctuations in the magnetic field intrinsic to the sample. Therefore

$$\frac{1}{T_2^*} = \frac{1}{T_2} + \frac{\gamma\Delta B_{\text{external}}}{K}. \quad (18.36)$$

$T_2$  is called the nonrecoverable relaxation time because various experimental techniques can be used to compensate for the external inhomogeneities, but not the internal atomic ones.

### 18.7 Detecting the Magnetic Resonance Signal

We have now seen that a sample of nuclear spins in a strong magnetic field has an induced magnetic moment; that it is possible to apply a sinusoidally varying magnetic field and nutate the magnetic moment to precess at any arbitrary angle with respect to the static field; and that the magnetization then relaxes or returns to its original state with two characteristic time constants, the longitudinal and transverse relaxation times. We next consider how a useful signal can be obtained from these spins. This is done by measuring the weak magnetic field generated by the magnetization as it precesses in the  $xy$  plane.

Suppose that a sample is at the origin. The motions plotted in Fig. 18.7 suggest that one way to produce a magnetization rotating in the  $xy$  plane is to have a static field along the  $z$  axis, combined with a coil in the  $yz$  plane (perpendicular to the  $x$  axis) connected to a generator of alternating current at frequency  $\omega_0$ . Turning on the generator for a time  $\Delta t = \pi/2\omega_1 = \pi/\gamma B_1$  rotates the magnetization into the  $xy$  plane (a  $90^\circ$  or  $\pi/2$  pulse). If the generator is then turned off, the same coil can be used to detect the changing magnetic flux due to the rotating magnetic moments. The resulting signal, an exponentially damped sine wave, is called the *free induction decay* (FID).

To estimate the size of the signal induced in the coil, imagine a magnetic moment  $\boldsymbol{\mu} = M\boldsymbol{\Delta V}$  rotating in the  $xy$  plane as shown in Fig. 18.13. The voltage  $v$  induced

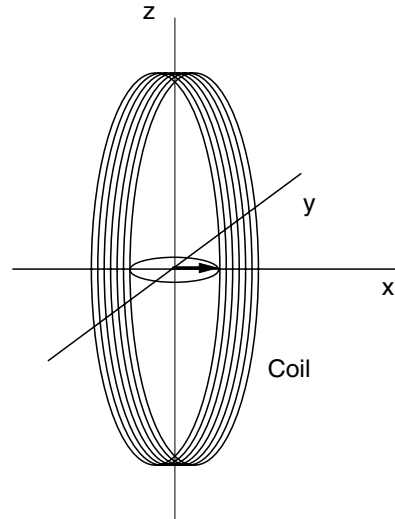


FIGURE 18.13. A magnetic moment rotating in the  $xy$  plane induces a voltage in a pickup coil in the  $yz$  plane. The coil is viewed from slightly to the right of the coil.

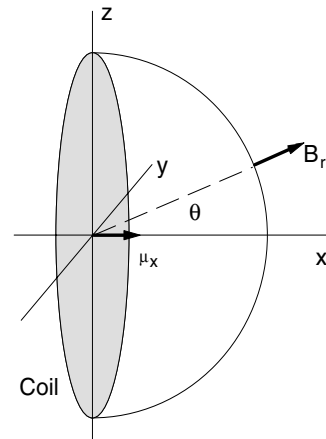


FIGURE 18.14. A dipole along the  $x$  axis generates a flux through the shaded circle in the  $yz$  plane that is equal and opposite to that through the hemispherical cap. The drawing is viewed from slightly to the right of the  $yz$  plane.

in a one-turn coil in the  $yz$  plane is the rate of change of the magnetic flux through the coil:

$$v = -\frac{\partial\Phi}{\partial t} = -\frac{\partial}{\partial t} \iint \mathbf{B} \cdot d\mathbf{S}.$$

The magnetic field far from a magnetic dipole can be written most simply in spherical coordinates [Eqs. 18.32]. We need the flux through the coil of radius  $a$  in the  $yz$  plane. However, Eqs. 18.32 are not valid close to the dipole. Since a fundamental property of the magnetic field is that for a closed surface  $\iint \mathbf{B} \cdot d\mathbf{S} = 0$ , the flux through the coil in Fig. 18.13 is the negative of the flux  $\Phi$  through

the hemispherical cap in Fig. 18.14:

$$\begin{aligned} \Phi &= - \int B_r 2\pi a^2 \sin \theta d\theta = - \frac{\mu_0}{4\pi} \frac{4\pi \mu_x}{a} \int_0^{\pi/2} \cos \theta \sin \theta d\theta \\ &= - \frac{\mu_0}{4\pi} \frac{2\pi \mu_x}{a}. \end{aligned} \tag{18.37}$$

At any instant  $\boldsymbol{\mu}$  can be resolved into components along  $x$  and  $y$ . The component pointing along  $y$  contributes no net flux through the spherical cap of Fig. 18.14. Therefore, the flux for a magnetic moment  $\boldsymbol{\mu} = \mathbf{M}\Delta V$ , where  $\mathbf{M}$  is given by Eqs. 18.16, is

$$\Phi = - \frac{\mu_0}{4\pi} \frac{2\pi M_0 \Delta V}{a} e^{-t/T_2} \cos(-\omega_0 t).$$

The induced voltage is  $-\partial\Phi/\partial t$ :

$$v = \frac{\mu_0}{4\pi} \frac{2\pi M_0 \Delta V}{a} e^{-t/T_2} \left( -\frac{1}{T_2} \cos(-\omega_0 t) + \omega_0 \sin(-\omega_0 t) \right).$$

Since  $1/T_2 \ll \omega_0$ , this can be simplified to

$$v = - \frac{\mu_0}{4\pi} \frac{\omega_0}{a} 2\pi M_0 \Delta V e^{-t/T_2} \sin(-\omega_0 t).$$

If the value of  $M_z$  which exists at thermal equilibrium has been nutated into the  $xy$  plane, then  $M_0$  is given by the  $M_z$  of Eq. 18.10. For a spin- $\frac{1}{2}$  particle (and using the fact that  $\omega_0 = \gamma B_0$ ) we obtain

$$v = - \frac{\mu_0}{4\pi} \frac{\pi N \Delta V}{2k_B T a} \gamma^3 \hbar^2 B_0^2 e^{-t/T_2} \sin(-\omega_0 t). \tag{18.38}$$

Here  $N \Delta V$  is the total number of nuclear spins involved,  $B_0$  is the field along the  $z$  axis, and  $a$  is the radius of the coil that detects the free-induction-decay signal. For a volume element of fixed size, as in magnetic resonance imaging, the sensitivity is inversely proportional to the coil radius. If the sample fills the coil, as in most laboratory spectrometers, then  $\Delta V \propto a^3$  and the sensitivity is proportional to  $a$ .

## 18.8 Some Useful Pulse Sequences

Many different ways of applying radio-frequency pulses to generate  $B_1$  have been developed by nuclear magnetic resonance spectroscopists for measuring relaxation times. There are five “classic” sequences, which also form the basis for magnetic resonance imaging.

### 18.8.1 Free-Induction-Decay (FID) Sequence

Free induction decay was described in Sec. 18.7. A  $\pi/2$  pulse nutates  $\mathbf{M}$  into the  $xy$  plane, where its precession induces a signal in a pickup coil. The signal is of the form  $e^{-(t/T_2^*)} \sin(-\omega_0 t)$ , where  $T_2^*$  is the experimental transverse relaxation time, including magnetic field inhomogeneities due to the apparatus as well as those intrinsic

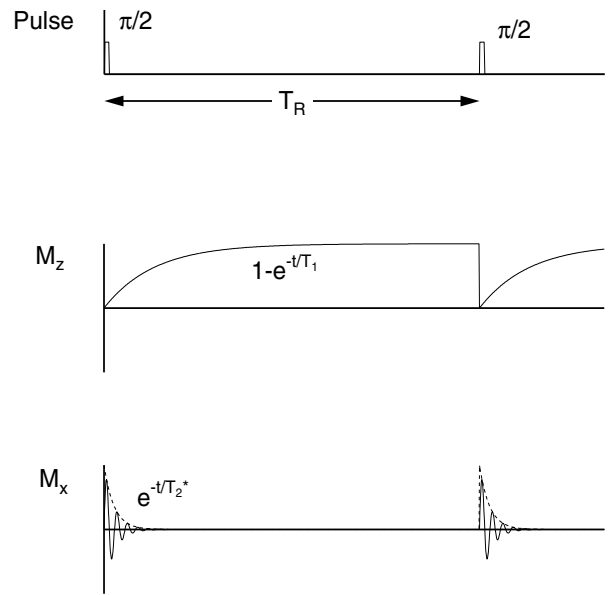


FIGURE 18.15. Pulse sequence and signal for a free-induction-decay measurement.

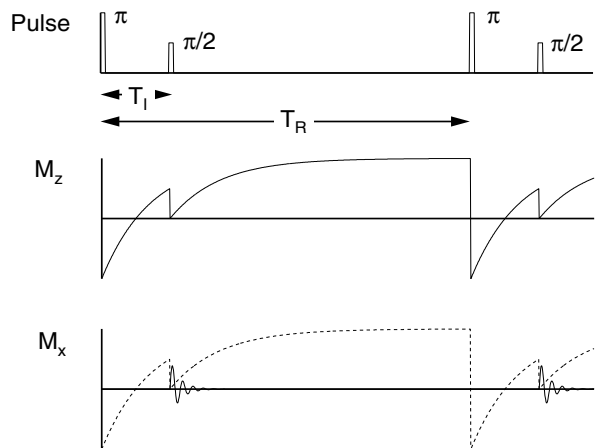


FIGURE 18.16. The inversion recovery sequence allows determination of  $T_1$  by making successive measurements at various values of the interrogation time  $T_1$ .

to the sample. Figure 18.15 shows the pulse sequence, the value of  $M_x$ , and the value of  $M_z$ . The signal is proportional to  $M_x$ . The pulses can be repeated after time  $T_R$  for signal averaging. It is necessary for  $T_R$  to be greater than, say,  $5T_1$  in order for  $M_z$  to return nearly to its equilibrium value between pulses.

### 18.8.2 Inversion-Recovery (IR) Sequence

The inversion-recovery sequence allows measurement of  $T_1$ . A  $\pi$  pulse causes  $\mathbf{M}$  to point along the  $-z$  axis. There

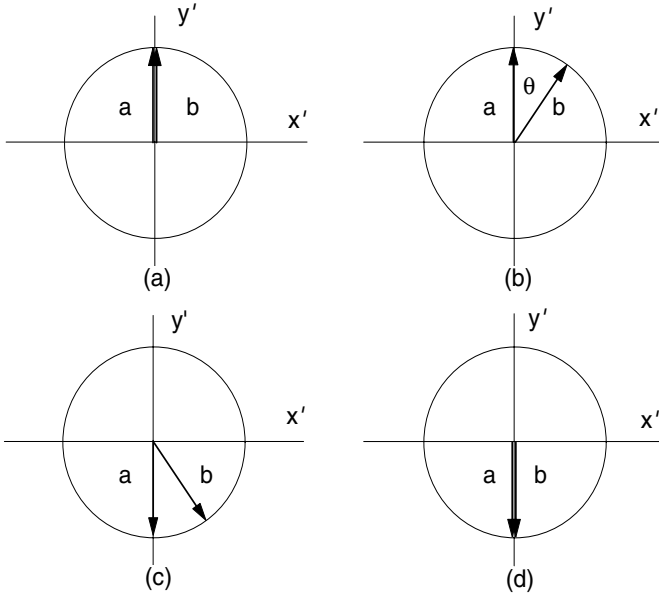


FIGURE 18.17. Two magnetic moments are shown in the  $x'y'$  plane in the rotating coordinate system. Moment **a** rotates at the Larmor frequency and remains aligned along the  $y'$  axis. Moment **b** rotates clockwise with respect to moment **a**. (a) Both moments are initially in phase. (b) After time  $T_E/2$  moment **b** is clockwise from moment **a**. (c) A  $\pi$  pulse nutates both moments about the  $x'$  axis. (d) At time  $T_E$  both moments are in phase again.

is not yet any signal at this point.  $M_z$  returns to equilibrium according to  $M_z = M_0 [1 - 2e^{-(t/T_1)}]$ . A  $\pi/2$  interrogation pulse at time  $T_I$  rotates the instantaneous value of  $M_z$  into the  $xy$  plane, thereby giving a signal proportional to  $M_0 [1 - 2e^{-(T_I/T_1)}]$ , as shown in Fig. 18.16. The process can be repeated; again the repeat time must exceed  $5T_1$ .

You can see from Fig. 18.16 that there will be no signal at all if  $T_I/T_1 = 0.693$ . If  $T_I$  is less than this, the  $M_x$  signal will be inverted (negative). Unless special detector circuits are used which allow one to determine that  $M_x$  is negative, the results can be confusing.

Inversion recovery images take a long time to acquire and there is ambiguity in the sign of the signal. There are also problems with the use of a  $\pi$  pulse for slice selection [defined in Sec. 18.9; the details of the problems are found in Joseph and Axel (1984)].

### 18.8.3 Spin-Echo (SE) Sequence

The pulse sequence shown in Fig. 18.17 can be used to determine  $T_2$  rather than  $T_2^*$ . Initially a  $\pi/2$  pulse nutates  $\mathbf{M}$  about the  $x'$  axis so that all spins lie along the rotating  $y'$  axis. Figure 18.17(a) shows two such spins. Spin **a** continues to precess at the same frequency as the rotating coordinate system; spin **b** is subject to a slightly smaller magnetic field and precesses at a slightly lower frequency, so that at time  $T_E/2$  it has moved clockwise in the rotat-

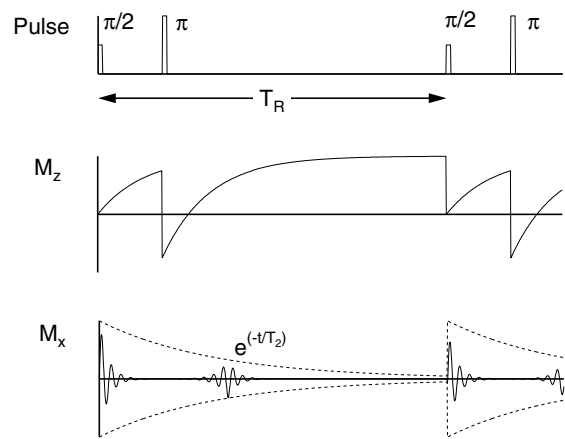


FIGURE 18.18. The pulse sequence and magnetization components for a spin-echo sequence.

ing frame by angle  $\theta$ , as shown in Fig. 18.17(b). At this time a  $\pi$  pulse is applied that rotates all spins around the  $x'$  axis. Spin **a** then points along the  $-y'$  axis; spin **b** rotates to the angle shown in Fig. 18.17(c). If spin **b** still experiences the smaller magnetic field, it continues to precess clockwise in the rotating frame. At time  $T_E$  both spins are in phase again, pointing along  $-y'$  as shown in Fig. 18.17(d). The resulting signal is called an echo, and the process for producing it is called a spin-echo sequence. The formation of an echo depends only on the fact that the magnetic field at the nucleus remained the same before and after the  $\pi$  pulse; it does not depend on the specific value of the dephasing angle. Therefore, all of the spin dephasing that has been caused by a time-independent magnetic field is reversed in this process. There remains only the dephasing caused by fluctuating magnetic fields. Figure 18.18 shows the pulse sequence and signal.

### 18.8.4 Carr-Purcell (CP) Sequence

When a sequence of  $\pi$  pulses that nutate  $\mathbf{M}$  about the  $x'$  axis are applied at  $T_E/2, 3T_E/2, 5T_E/2, \text{etc.}$ , a sequence of echoes are formed, the amplitudes of which decay with relaxation time  $T_2$ . This is shown in Fig. 18.19. Referring to Fig. 18.17, one can see that the echoes are aligned alternately along the  $-y'$  and  $+y'$  axes. One advantage of the Carr-Purcell sequence is that it allows one to determine rapidly many points on the decay curve. Another advantage relates to diffusion. The molecules that contain the excited nuclei may diffuse. If the external magnetic field  $B_0$  is not uniform, the molecules can diffuse to another region where the magnetic field is slightly different. As a result the rephasing after a pulse does not completely cancel the initial dephasing. This effect is reduced by the Carr-Purcell sequence (see Problem 38).

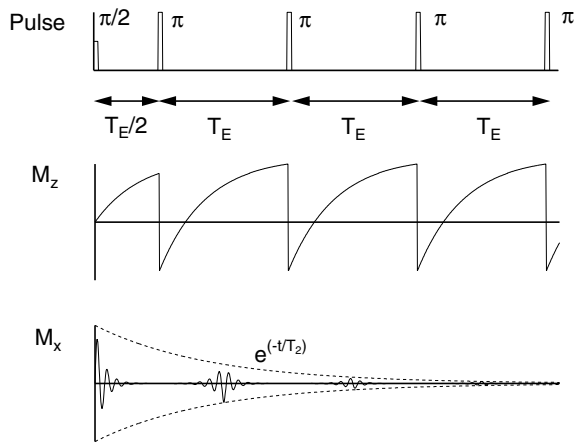


FIGURE 18.19. The Carr–Purcell pulse sequence. All pulses nutate about the  $x'$  axis. Echoes alternate sign. The envelope of echoes decays as  $e^{-t/T_2}$ , where  $T_2$  is the unrecoverable transverse relaxation time.

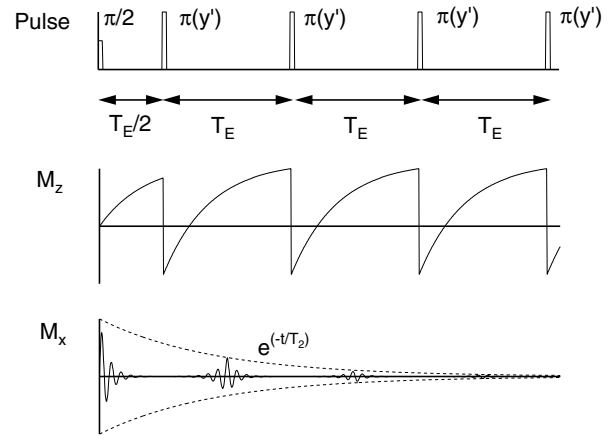


FIGURE 18.21. The CPMG pulse sequence.

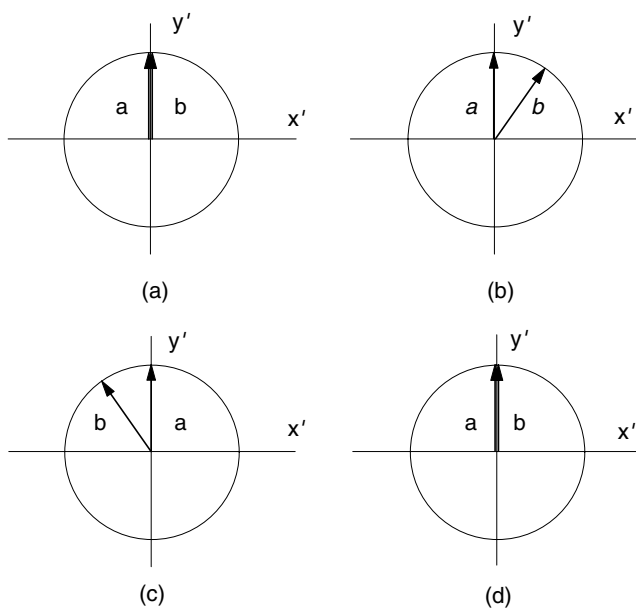


FIGURE 18.20. The effect of the Carr–Purcell–Meiboom–Gill pulse sequence on the magnetization. This is similar to Fig. 18.17 except that the  $\pi$  pulses rotate around the  $y'$  axis. Moment  $\mathbf{b}$  rotates clockwise in the  $x'y'$  plane. (a) Both moments are initially in phase. (b) After time  $T_E/2$  moment  $\mathbf{b}$  is clockwise from moment  $\mathbf{a}$ . (c) A  $\pi$  pulse rotates both moments about the  $y'$  axis. (d) At time  $T_E$  both moments are in phase again.

### 18.8.5 Carr–Purcell–Meiboom–Gill (CPMG) Sequence

One disadvantage of the CP sequence is that the  $\pi$  pulse must be very accurate or a cumulative error builds up in successive pulses. The Carr–Purcell–Meiboom–Gill se-

quence overcomes this problem. The initial  $\pi/2$  pulse nutates  $\mathbf{M}$  about the  $x'$  axis as before, but the subsequent pulses are shifted a quarter cycle in time, which causes them to rotate about the  $y'$  axis. This is shown in Fig. 18.20. To see why this pulse sequence is less sensitive to errors in the duration of the  $\pi$  pulses, consider moment  $\mathbf{a}$ . In the CP sequence, Fig. 18.17, a  $\pi$  pulse that is too long will nutate  $\mathbf{a}$  too far, and it will have a smaller component in the  $x'y'$  plane. The next pulse will nutate it even further. In Fig. 18.20, the  $\pi$  pulses will not affect moment  $\mathbf{a}$  at all. This is explored further in Problems 26 and 27.

## 18.9 Imaging

Many more techniques are available for imaging with magnetic resonance than for x-ray computed tomography. They are described by Joseph (1985), by Cho *et al.* (1993), by Vlaardingerbroek and den Boer (2002), and by Liang and Lauterbur (2000). One of these authors, Paul C. Lauterbur, shared with Sir Peter Mansfield the 2003 Nobel Prize in Physiology or Medicine for the discovery of magnetic resonance imaging.

Creation of the images requires the application of gradients in the static magnetic field  $B_z$  which cause the Larmor frequency to vary with position. The first gradient is applied in the  $z$  direction during the  $\pi/2$  pulse so that only the spins in a slice in the patient are *selected* (nutated into the  $xy$  plane). Slice selection is followed by gradients of  $B_z$  in the  $x$  and  $y$  directions. These also change the Larmor frequency. If the gradient is applied during the readout, the Larmor frequency of the signal varies as  $B_z$  varies with position. If the gradient is applied before the readout, it causes a position-dependent phase shift in the signal which can be detected.

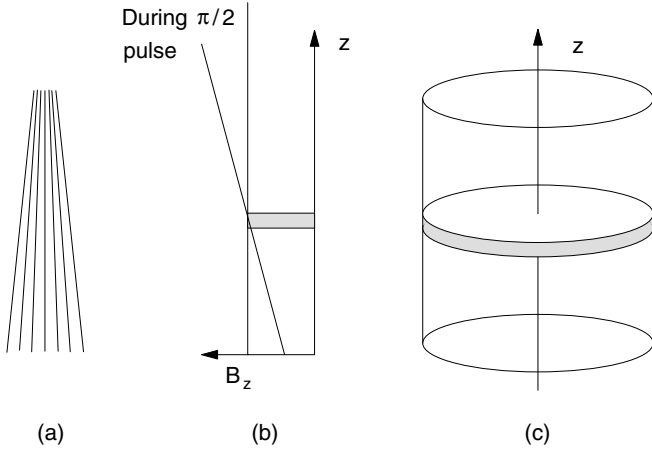


FIGURE 18.22. (a) Magnetic field lines for a magnetic field that increases in the  $z$  direction. (b) A plot of  $B_z$  vs  $z$  with and without a gradient. (c) After application of a field gradient in the  $z$  direction during the specially shaped rf pulse, all of the spins in the shaded slice are excited, that is, they are precessing in the  $xy$  plane.

We discuss several reconstruction methods here. *Projection reconstruction* is similar to CT reconstruction, but is slow and rarely used. A two-dimensional Fourier technique known as *spin warp* or *phase encoding* forms the basis of the techniques used in most machines. We also describe briefly some techniques that are even faster. Finally, we discuss how the image contrast can be modified by changing the pulse sequence parameters.

Our initial discussion is based on a spin-echo pulse sequence, repeated with a repetition time  $T_R$  as shown in Fig. 18.18.

### 18.9.1 Slice Selection

First, suppose we simply apply a  $\pi/2$  pulse to the entire sample in a 1.5-T machine ( $\omega_0 = 401 \times 10^6 \text{ s}^{-1}$ ;  $\nu_0 = 63.9 \text{ MHz}$ ). If the duration of this pulse is to be, say, 5 ms, it requires a constant amplitude of the radio-frequency magnetic field

$$B_1 = \pi/\gamma\Delta t = 2.35 \times 10^{-6} \text{ T.} \quad (18.39)$$

The pulse lasts for  $3 \times 10^5$  cycles at the Larmor frequency. The frequency spread of the pulse is about 200 Hz. This excites all the proton spins in the entire sample.

For MR imaging, we want to select a thin slice in the sample. In order to select a thin slice (say  $\Delta z = 1 \text{ cm}$ ) we apply a magnetic field gradient in the  $z$  direction while applying a specially shaped  $B_1$  signal. In a static magnetic field  $B_0$ , the field lines are parallel. The field strength is proportional to the number of lines per unit area and does not change. With the gradient applied in the volume of interest, the field lines converge, and the field increases linearly with  $z$  as shown in Figs. 18.22(a)

and 18.22(b):

$$B_z(z) = B_0 + G_z z. \quad (18.40)$$

We adopt a notation in which  $\mathbf{G}$  represents a partial derivative of the  $z$  component of the magnetic field:

$$\mathbf{G} = \begin{pmatrix} G_x \\ G_y \\ G_z \end{pmatrix} = \begin{pmatrix} \partial B_z/\partial x \\ \partial B_z/\partial y \\ \partial B_z/\partial z \end{pmatrix}. \quad (18.41)$$

In a typical machine,  $G_z = 5 \times 10^{-3} \text{ T m}^{-1}$ . For a slice thickness  $\Delta z = 0.01 \text{ m}$ , the Larmor frequency across the slice varies from  $\omega_0 - \Delta\omega$  to  $\omega_0 + \Delta\omega$ , where  $\Delta\omega = \gamma G_z \Delta z/2 = 6.68 \times 10^3 \text{ s}^{-1}$  ( $\Delta f = 1.064 \text{ kHz}$ ).

It is possible to make the signal  $B_x(t)$  consist of a uniform distribution of frequencies between  $\omega_0 - \Delta\omega$  and  $\omega_0 + \Delta\omega$ , so that all protons are excited in a slice of thickness  $\Delta z$  from  $-\Delta z/2$  to  $+\Delta z/2$ . Let the amplitude of  $B_x$  in the interval  $(\omega, d\omega)$  be  $A$ . Using Eq. 11.55,  $B_x(t)$  is given by

$$\begin{aligned} B_x(t) &= \frac{A}{2\pi} \int_{\omega_0 - \Delta\omega}^{\omega_0 + \Delta\omega} \cos(\omega t) d\omega \\ &= \frac{A\Delta\omega}{\pi} \frac{\sin(\Delta\omega t)}{\Delta\omega t} \cos(\omega_0 t). \end{aligned} \quad (18.42)$$

This has the form  $B_1(t) \cos(\omega_0 t)$ , where  $B_1(t) = (A\Delta\omega/\pi) \sin(\Delta\omega t)/(\Delta\omega t)$ . The function  $\sin(x)/x$  has its maximum value of 1 at  $x = 0$ . It is also called the  $\text{sinc}(x)$  function. The angle  $\phi$  through which the spins are nutated is

$$\begin{aligned} \phi &= \int_{-\infty}^{\infty} \omega_1(t) dt = \frac{\gamma}{2} \int_{-\infty}^{\infty} B_1(t) dt \\ &= \frac{\gamma A \Delta\omega}{2\pi} \int_{-\infty}^{\infty} \frac{\sin(\Delta\omega t)}{\Delta\omega t} dt \\ &= \frac{\gamma A}{2}. \end{aligned}$$

For a  $\pi/2$  pulse,  $A = \pi/\gamma$ . The maximum value of  $B_1$  is therefore  $\Delta\omega/\gamma = G_z \Delta z/2$ , as shown in Fig. 18.23. The  $B_x$  pulse does not have an abrupt beginning; it grows and decays as shown. In practice, it is truncated at some distance from the peak where the lobes are small.

While the gradient is applied, the transverse components of spins at different values of  $z$  precess at different rates (see Problem 32). Therefore it is necessary to apply a gradient  $G_z$  of opposite sign after the  $\pi/2$  pulse is finished in order to bring the spins back to the phase they had at the peak of the slice selection signal. The gradient is removed when all of the spins in the slice shown in Fig. 18.22(c) are back in phase. They then continue to precess in the  $xy$  plane at the Larmor frequency. This gives the first  $M_x$  pulse in Fig. 18.24. This initial free-induction-decay pulse is not used for imaging.

The voltage induced in the pickup coil surrounding the sample is proportional to the free induction decay of  $\mathbf{M}$  in the entire slice. That is, the voltage signal induced in



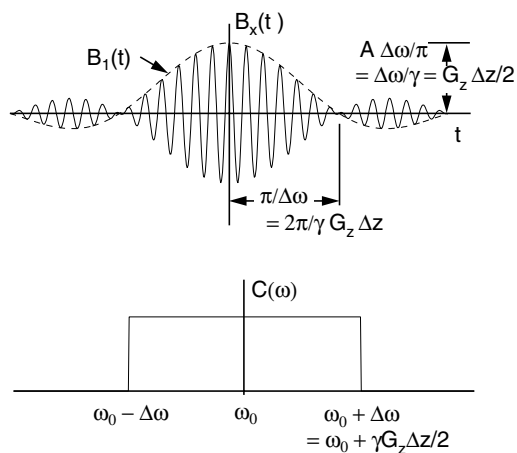


FIGURE 18.23. (a) The  $B_x(t)$  signal shown is used to selectively excite a slice. It consists of  $\cos(\omega_0 t)$  modulated by a  $\text{sinc}(x)$  or  $\sin(x)/x$  pulse  $B_1(t)$ . (b) The frequency spectrum contains a uniform distribution of frequencies.

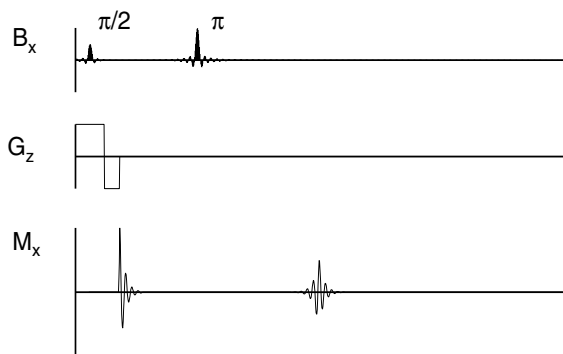


FIGURE 18.24. A slice selection pulse sequence. While a gradient  $G_z$  is applied, a  $\pi/2$   $B_x$  (rf) pulse nutates the spins in a slice of thickness  $z$  into the  $xy$  plane. A negative  $G_z$  gradient restores the phase of the precessing spins. The echo after the  $\pi$  pulse is from the entire slice.

the pickup coil is proportional to  $\int M(x, y, z) \cos(-\omega_0 t) f(t) dV$ , where  $M(x, y, z)$  is the magnetization per unit volume that was nutated into the  $xy$  plane,  $\cos(-\omega_0 t)$  represents the change in signal as  $\mathbf{M}$  rotates in the  $xy$  plane at the Larmor frequency, and  $f(t)$  represents relaxation, signal buildup during an echo, and so on. Figure 18.24 shows the echo after a subsequent  $\pi$  pulse.

We assume that changes in  $f(t)$  are slow compared to the Larmor frequency and neglect them here. Then the signal from an element  $dx dy$  in the slice is

$$v(t) = A dx dy \Delta z M(x, y, z) \cos(-\omega_0 t). \quad (18.43)$$

Constant  $A$  includes all the details of the detecting coils and receiver.

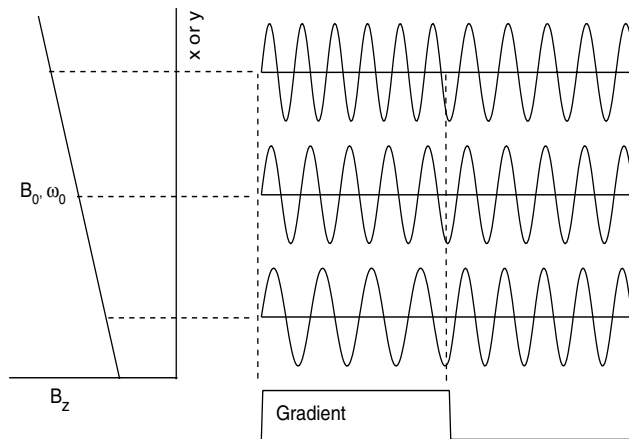


FIGURE 18.25. A gradient in  $B_z$  causes the Larmor frequency to vary with position. If the signal is measured while the gradient is applied, the Larmor frequency varies with position. If the signal is measured after the gradient has been applied and removed, a position-dependent phase shift remains.

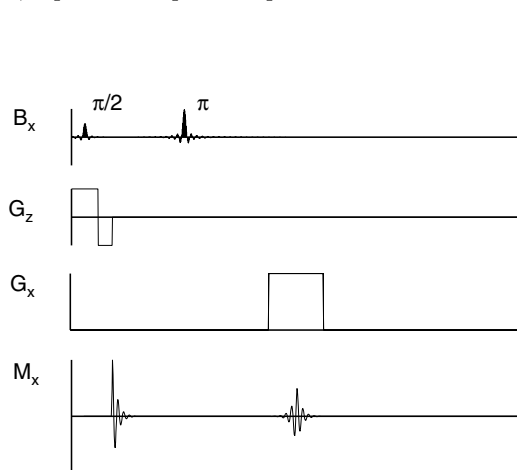


FIGURE 18.26. A gradient  $G_x$  is applied during  $x$  readout. The echo signal between  $\omega$  and  $\omega + d\omega$  is proportional to the magnetization in a strip between  $x$  and  $x + dx$ , integrated over all values of  $y$ .

### 18.9.2 Readout in the $x$ Direction

We now need to extract  $x$  and  $y$  position information from  $v(t)$ . This is done by creating gradients of  $B_z$  in the  $x$  or  $y$  directions. As shown in Fig. 18.25, if the signal is measured while a gradient is applied, the Larmor frequency varies with position. Suppose that  $B_z$  is given a gradient  $G_x$  in the  $x$  direction during the echo signal readout, as shown in Fig. 18.26. The spins that echo in the shaded slice between  $x$  and  $x + dx$  in Fig. 18.27 will be precessing with a Larmor frequency between  $\omega$  and  $\omega + d\omega$ , where

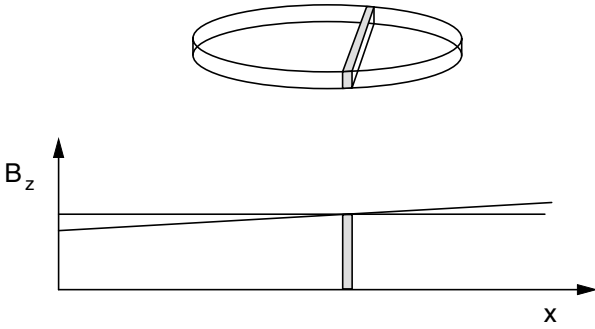


FIGURE 18.27. Because the gradient  $G_x$  is applied during readout, the Larmor frequency of all spins in the shaded slice is between  $\omega$  and  $\omega + d\omega$ .

$\omega = \omega_0 + \gamma G_x x$ . The signal from the entire slice is

$$v(t) = A\Delta z \int dx \left( \int dy M(x, y, z) \right) \cos[-\omega(x)t]. \quad (18.44)$$

We use the fact that  $\omega(x) = \omega_0 + \gamma G_x x$  to write the signal as

$$v(t) = A\Delta z \int dx \left[ \left( \int dy M(x, y, z) \right) \cos(-\omega_0 t - \gamma G_x x t) \right]. \quad (18.45)$$

Since the  $z$  slice has already been selected, let us simplify the notation by dropping the  $z$  dependence of  $\mathbf{M}$ . The electronics in the detector multiply  $v(t)$  by  $\cos(\omega_0 t)$  or  $\sin(\omega_0 t)$  and average over many cycles at the Larmor frequency. The results are two signals that form the basis for constructing the image:

$$\begin{aligned} s_c(t) &= \overline{v(t) \cos(\omega_0 t)} \propto \iint dx dy M(x, y) \cos(-\gamma G_x x t), \\ s_s(t) &= \overline{v(t) \sin(\omega_0 t)} \propto \iint dx dy M(x, y) \sin(-\gamma G_x x t). \end{aligned} \quad (18.46)$$

The time average is over many cycles at the Larmor frequency but a time short compared to  $2\pi/\gamma G_x x_{\max}$ .

### 18.9.3 Projection Reconstruction

By inspecting Eq. 18.46 and remembering the relationship between  $\omega$  and  $x$ , we see that the Fourier transforms of  $s_c(t)$  and  $s_s(t)$  are both proportional to  $\int M(x, y) dy$ . (Of course, the signals are digitized and one actually deals with discrete transforms.) This means that  $s_c$  or  $s_s$  can be Fourier analyzed to determine the amount of signal in the frequency interval  $(\omega, d\omega)$  corresponding to  $(x, dx)$ , which is proportional to the projection  $\int M(x, y) dy$  along the shaded strip. In Sec. 12.5 we learned how to reconstruct an image from a set of projections. The entire readout process can therefore be repeated with the gradient rotated slightly in the  $xy$  plane (that is, with a combination of  $G_x$  and  $G_y$  during readout). This is indicated in Fig. 18.28, which indicates many scans, with different values of  $G_x$  and  $G_y$ , related by  $G_x/G_y = \tan \theta$ , where  $\theta$  is

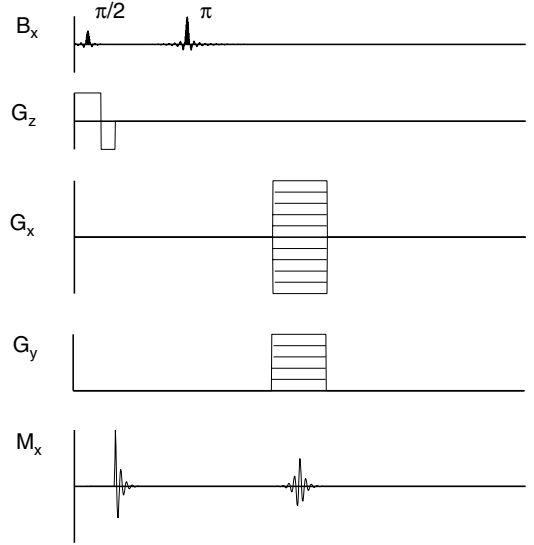


FIGURE 18.28. Projection reconstruction techniques can be used to form an image. A series of measurements are taken, each with simultaneous gradients  $G_x$  and  $G_y$ .

the angle between the projection and the  $x$  axis. All of the techniques for reconstruction from projections that were developed for computed tomography can be used to reconstruct  $M(x, y)$ . Sending the proper combination of currents through the  $x$  and  $y$  gradient coils rotates the gradient; no rotating mechanical components are needed.

### 18.9.4 Phase Encoding

Techniques are available for magnetic resonance imaging that are not available for computed tomography. They are based on determining directly the Fourier coefficients in two or three dimensions. The basic technique is called *spin warp* or *phase encoding*. We saw in Fig. 18.25 that if a gradient is applied after the  $\pi/2$  slice-selection pulse, a position-dependent phase shift remains even after the gradient is turned off. Let us make this quantitative. We wish to construct an image of  $M(x, y)$ , modified by the function  $f(t)$  that accounts for relaxation, etc. For simplicity of notation we again assume  $f$  is unity and suppress the  $z$  dependence, since slice selection has already been done. We will construct  $M(x, y)$  from its Fourier transform. The Fourier transform of  $M(x, y)$  is given by Eqs. 12.9:

$$\begin{aligned} M(x, y) &= \left( \frac{1}{2\pi} \right)^2 \int_{-\infty}^{\infty} dk_x \int_{-\infty}^{\infty} dk_y \\ &\quad \times [C(k_x, k_y) \cos(k_x x + k_y y) \\ &\quad + S(k_x, k_y) \sin(k_x x + k_y y)]. \end{aligned} \quad (18.47a)$$

with the coefficients given by

$$C(k_x, k_y) = \int_{-\infty}^{\infty} dx \int_{-\infty}^{\infty} dy M(x, y) \cos(k_x x + k_y y), \quad (18.47b)$$

$$S(k_x, k_y) = \int_{-\infty}^{\infty} dx \int_{-\infty}^{\infty} dy M(x, y) \sin(k_x x + k_y y). \quad (18.47c)$$

Our problem is to determine  $C$  and  $S$  and from them construct the image.

The information from the  $x$  readout gives us  $C(k_x, 0)$  and  $S(k_x, 0)$  directly. We show this for the cosine transform. From Eq. 18.47b

$$C(k_x, 0) = \int_{-\infty}^{\infty} dx \left( \int_{-\infty}^{\infty} dy M(x, y) \right) \cos(k_x x). \quad (18.48)$$

Comparing this to the expression for  $s_c(t)$  in Eq. 18.46, we see that

$$C(k_x, 0) \propto s_c(k_x/\gamma G_x). \quad (18.49a)$$

Similarly,

$$S(k_x, 0) \propto s_s(k_x/\gamma G_x). \quad (18.49b)$$

The times at which  $s_c$  and  $s_s$  are measured and therefore the values of  $k_x$  are, of course, discrete. The discussion in Sec. 12.3 shows that the values of  $k_x$  are multiples of the lowest spatial frequency:  $k_x = m \Delta k = m k_0 = 2\pi m/L_x$ . The corresponding times to measure the signal are  $t_m = 2\pi m/L_x \gamma G_x$ . The spatial extent of the image in the  $x$  direction or “field of view”  $L_x$  determines the spacing  $\Delta k_x$ . The desired pixel size determines the maximum value of  $k_x$  or  $m$ :  $\Delta x = \pi/k_{\max} = L_x/2m_{\max}$ . The discrete values of  $k_x$  are shown in Fig. 18.29(a).

The next problem is to make a similar determination for nonzero values of  $k_y$ . To do so, a gradient  $G_y = \partial B_z/\partial y$  is applied at some time between slice selection and readout. This makes the Larmor frequency vary in the  $y$  direction. If the phase-encoding pulse is due to a uniform gradient that lasts for a time  $T_p$ , the total phase change is

$$\Delta\phi = \int \omega(t) dt = \gamma G_y T_p y = k_y y. \quad (18.50)$$

The readout signal, Eq. 18.44, is replaced by

$$v(t) = A \Delta z \int dx \int dy M(x, y) \cos[\omega(x)t + k_y y]. \quad (18.51)$$

Note that the added phase does not depend on  $t$ . However, the cosine term must now be included in both the  $x$  and  $y$  integrals. Carrying through the mathematics of the detection process shows that temporal Fourier transformation of the signals determines  $C(k_x, k_y)$  and  $S(k_x, k_y)$  for all values of  $k_x$  and for the particular value of  $k_y$  determined by the  $G_y$  phase selection pulse. Different values of the  $G_y$  pulse give the coefficients for different values of  $k_y$ , as shown in Fig. 18.29. Both positive and negative gradients are used to give both positive and negative

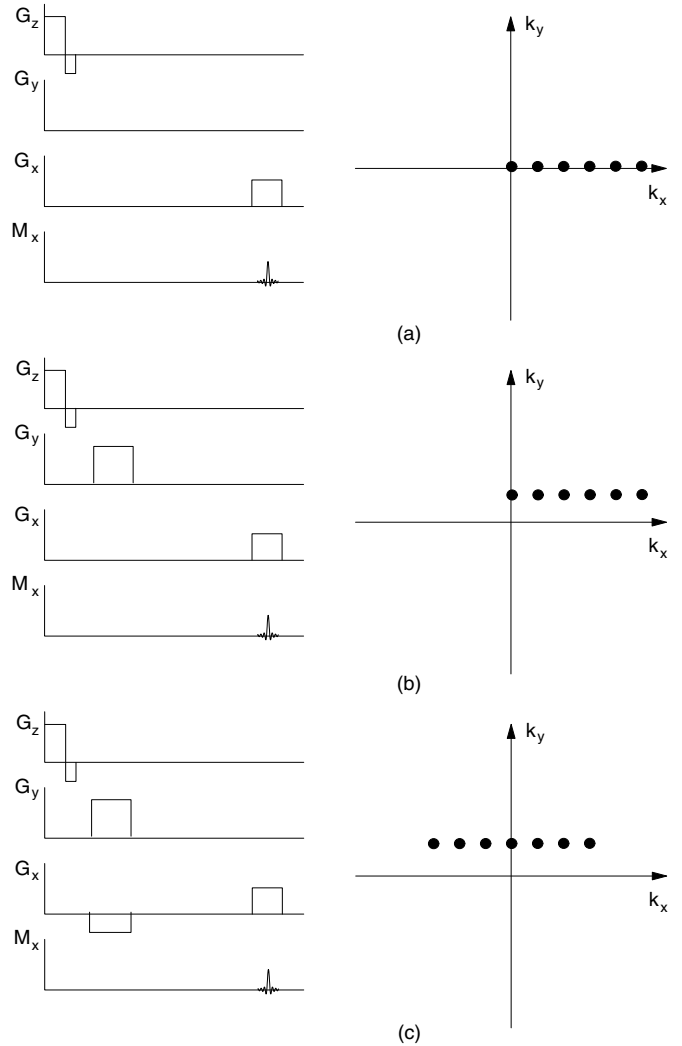


FIGURE 18.29. (a) The signal measured while the  $x$  gradient is applied gives the spatial Fourier transform of the image along the  $k_x$  axis. (b) The addition of a phase-encoding gradient sets a nonzero value for  $k_y$  so that the readout determines the spatial Fourier transform along a line parallel to the  $k_x$  axis. (c) Phase encoding along the  $x$  axis as well shifts the line along which the coefficients are determined.

values of  $k_y$ . Application of a gradient  $G_x$  during the phase-encoding time (in addition to the readout gradient) changes the starting value of  $k_x$ . This allows one to determine the coefficients for negative values of  $k_x$ . This figure has been drawn without taking into account that the application of a  $\pi$  pulse changes  $k_x$  to  $-k_x$  and  $k_y$  to  $-k_y$ . The gradients and signals for this spin-echo determination are shown in Fig. 18.30. The coefficients are substituted in Eq. 18.47a to reconstruct  $M(x, y, z)$  for the  $z$  slice in question.

### 18.9.5 Other Pulse Sequences

Dozens of other pulse sequences have been invented, all of which are based on the fundamentals presented here.

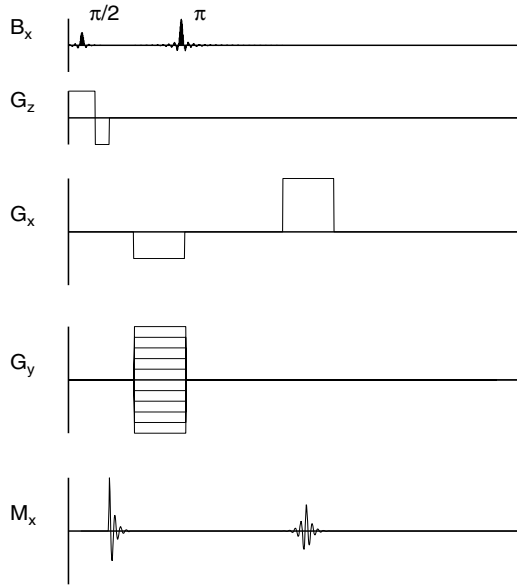


FIGURE 18.30. The signals in a standard phase encoding. The pulse sequence is repeated for each value of  $k_y$ .

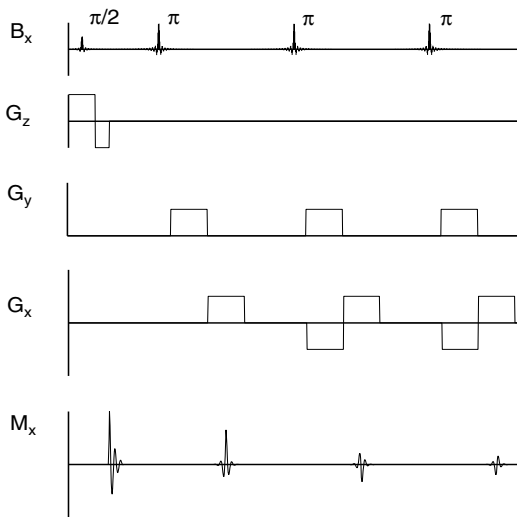


FIGURE 18.31. A fast spin echo sequence uses a single  $\pi/2$  slice selection pulse followed by multiple echo rephasing pulses. A correction must be made for the transverse decay.

We mention only a few, and there are many variations of these. For details, see Bernstein *et al.* (2004).

*Fast spin echo* or *turbo spin echo* uses a single  $\pi/2$  pulse, followed by a series of  $\pi$  pulses, as shown in Fig. 18.31. Each  $\pi$  pulse produces an echo, though the echo amplitudes decay and a correction for this must be made in the image reconstruction. Each  $G_y$  pulse increments or “winds” the phase by a fixed amount. A negative  $G_x$  pulse resets the positions of the  $k_x$  values. Faster image acquisition sequences not only save time, but they may allow the image to be obtained while the patient’s breath is held, thereby eliminating motion artifacts.

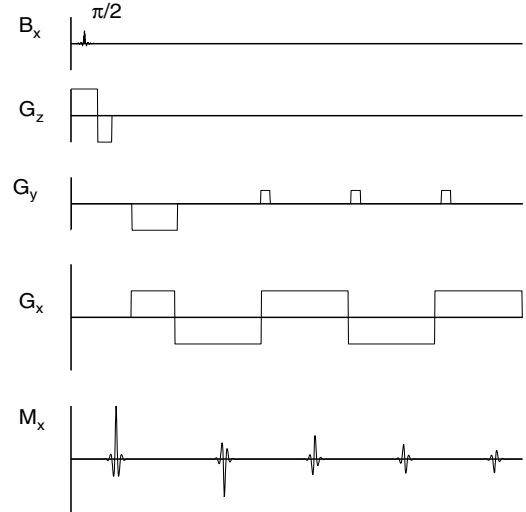


FIGURE 18.32. Echo planar imaging uses a very uniform magnet and eliminates the rephasing  $\pi$  pulses.

The major problem with conventional spin echo is that one must wait a time  $T_R \gg T_1$  between measurements for different values of  $k_y$ . One way to speed things up is to use the intervening time to make measurements in a slice at a different value of  $z$ . Another technique is to use a flip angle smaller than  $\pi/2$ . Suppose the flip angle is  $\alpha = 20^\circ$ . This gives a transverse magnetization proportional to  $\sin 20^\circ = 0.34$  while reducing the longitudinal magnetization to  $\cos 20^\circ = 0.94$ . Thus,  $k$  space can be sampled until the transverse signal has decayed and another  $\alpha$  flip pulse can immediately be applied to restore the transverse magnetization.

*Echo-planar imaging* (EPI) eliminates the  $\pi$  pulses. It requires a magnet with a very uniform magnetic field, so that  $T_2$  (in the absence of a gradient) is only slightly greater than  $T_2^*$ . The gradient fields are larger, and the gradient pulse durations shorter, than in conventional imaging. The goal is to complete all the  $k$ -space measurements in a time comparable to  $T_2^*$ . In EPI the echoes are not created using  $\pi$  pulses. Instead, they are created by dephasing the spins at different positions along the  $x$  axis using a  $G_x$  gradient, and then reversing that gradient to rephase the spins, as shown in Fig. 18.32. Whenever the integral of  $G_x(t)$  is zero, the spins are all in phase and the signal appears. A large negative  $G_y$  pulse sets the initial value of  $k_y$  to be negative; small positive  $G_y$  pulses (“blip”) then increase the value of  $k_y$  for each successive  $k_x$  readout. Echo-planar imaging requires strong gradients—at least five times those for normal studies—so that the data can be acquired quickly. Moreover, the rise- and fall-times of these pulses are short, which induces large voltages in the coils. Eddy currents are also induced in the patient, and it is necessary to keep these below the threshold of sensitivity. These problems can be reduced by using sinusoidally varying gradient currents. Image reconstruction takes longer, because the sample

points in  $k$ -space are not on a rectangular grid. The engineering problems are discussed in Schmitt *et al.* (1998), in Vlaardingerbroek and den Boer (2002) and in Bernstein *et al.* (2004).

High spatial frequencies give the sharp edge detail in an image; the lowest spatial frequencies give the overall contrast. (We saw this in Figs. 12.9 and 12.10.) Changing the order of sampling points in  $k$  space can be useful. For example, when the image may be distorted by blood flow (see Sec. 18.11), it is possible to change the gradients in such a way that the values of  $k$  near zero are measured right after the excitation. This gives the proper signal within the volume of the vessel. The higher spatial frequencies, which show vessel edges, are less sensitive to blood flow and are acquired later.

A three-dimensional Fourier transform of the image can be obtained by selecting the entire sample and then phase encoding in both the  $y$  and  $z$  directions while doing frequency readout along  $x$ . One must step through all values of  $k_y$  for each value of  $k_z$ . This forms the basis for imaging very small samples with very high resolution (MRI microscopy).

### 18.9.6 Image Contrast and the Pulse Parameters

The appearance of an MR image can be changed drastically by adjusting the repetition time and the echo time. Problem 24 derives a general expression for the amplitude of the echo signal when a series of  $\pi/2$  pulses are repeated every  $T_R$  seconds. The magnetic moment in the sample at the time of the measurement, considering both longitudinal and transverse relaxation, is

$$M(T_R, T_E) = M_0 \left( 1 - 2e^{-T_R/T_1 + T_E/2T_1} + e^{-T_R/T_1} \right) \times e^{-T_E/T_2}. \quad (18.52)$$

If  $T_R \gg T_E$ , this simplifies to

$$M(T_R, T_E) = M_0(1 - e^{-T_R/T_1})e^{-T_E/T_2}, \quad (18.53)$$

where  $M_0$  is proportional to the number of proton spins per unit volume  $N$ , as shown in Eq. 18.10. We consider an example that compares muscle ( $M_0 = 1.02$  in arbitrary units,  $T_1 = 500$  ms, and  $T_2 = 35$  ms) with fat ( $M_0 = 1.24$ ,  $T_1 = 200$  ms, and  $T_2 = 60$  ms).

Figure 18.33 shows two examples where  $T_R$  is relatively long and  $M_0$  returns nearly to its initial value between pulses. If the echo time is short, then the image is nearly independent of both  $T_1$  and  $T_2$  and it is called a *density-weighted image*. If  $T_E$  is longer, then the transverse decay term dominates and it is called a  *$T_2$ -weighted image*. The signal is often weak and therefore noisy because there has been so much decay.

Figure 18.34 shows what happens if the repetition time is made small compared to  $T_1$ . This is a  *$T_1$ -weighted image* because the differences in  $T_1$  are responsible for most of

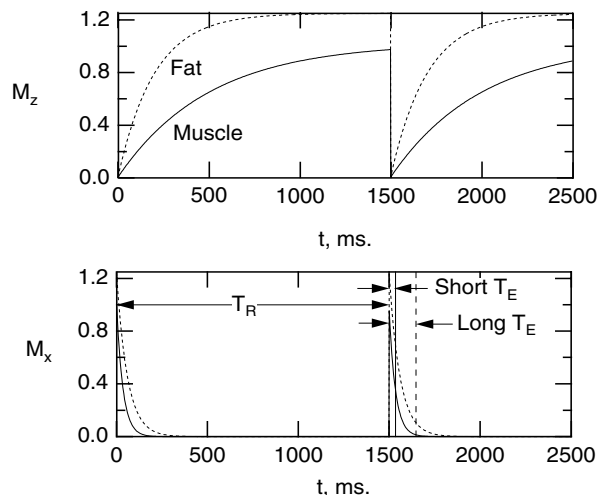


FIGURE 18.33. The intensity of the signal from different tissues depends on the relationship between the repetition time and echo times of the pulse sequence, and the relaxation times of the tissues being imaged. This figure and the next show the magnetization curves for two tissues: muscle (relative proton density 1.02,  $T_1 = 500$  ms,  $T_2 = 35$  ms) and fat (relative proton density 1.24,  $T_1 = 200$  ms,  $T_2 = 60$  ms). The repetition time is 1,500 ms, which is long compared to the longitudinal relaxation times. A long echo time gives an image density that is very sensitive to  $T_2$  values. A short echo time (even shorter than shown) gives an image that depends primarily on the spin density.

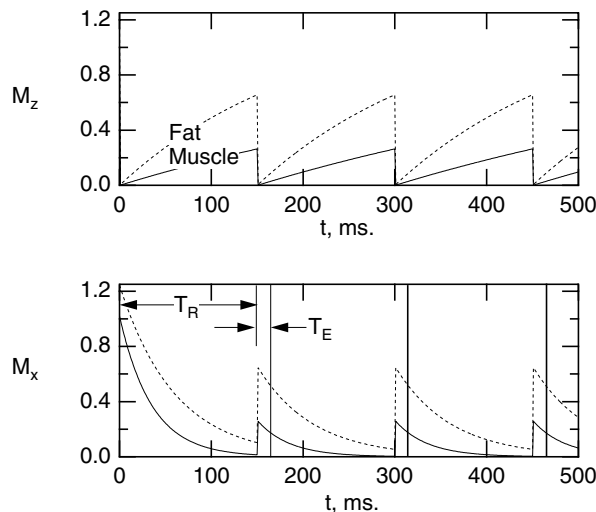


FIGURE 18.34. The tissue parameters are the same as in Fig. 18.33. The repetition time is short compared to the longitudinal relaxation time. As a result, the first echo must be ignored. With a short  $T_E$ , the image density depends strongly on the value of  $T_1$ .

the difference in signal intensity. Notice also that the very first pulse nutates the full  $M_0$  into the transverse plane, so an echo after the first pulse would give an anomalous reading. Echoes are measured only for the second and later pulses.

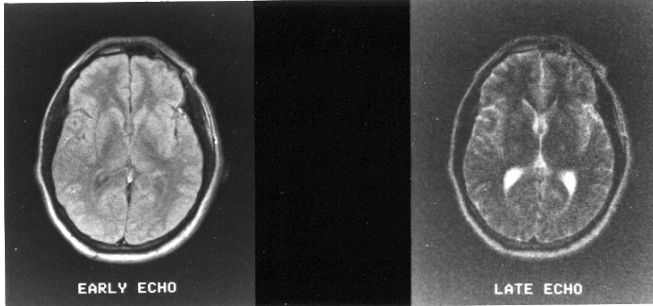


FIGURE 18.35. Spin-echo images taken with short and long values of  $T_E$ , showing the difference in  $T_2$  values for different parts of the brain. Photograph courtesy of R. Morin, Ph.D., Department of Diagnostic Radiology, University of Minnesota.

Suppose that the value of  $T_2$  for fat had been shorter than the value for muscle. Then there would have been a value of  $T_E$  for which the two transverse magnetization curves crossed, and the two tissues would have been indistinguishable in the image. At larger values of  $T_E$ , their relative brightnesses would have been reversed. Figure 18.35 shows spin-echo images taken with two different values of  $T_E$ , for which the relative brightnesses are quite different.

### 18.9.7 Safety

Safety issues in MRI include forces on magnetic objects in and around the patient such as aneurysm clips, hairpins, pacemakers, wheel chairs, and gas cylinders [Shellock (2002), Kanal *et al.* (2002)], absorbed radio-frequency energy (Problem 19), and induced currents from rapidly changing magnetic field gradients. The rapid changes of magnetic field can stimulate nerves and muscles, cause heating in electrical leads and certain tattoos, and possibly induce ventricular fibrillation. Induced fields are reviewed by Schaefer *et al.* (2000).

## 18.10 Chemical Shift

If the external magnetic field is very homogeneous, it is possible to detect a shift of the Larmor frequency due to a reduction of the magnetic field at the nucleus because of diamagnetic shielding by the surrounding electron cloud. The modified Larmor frequency can be written as

$$\omega = \gamma B_0(1 - \sigma). \tag{18.54}$$

Typical values of  $\sigma$  are in the range  $10^{-5} - 10^{-6}$ . They are independent of  $B_0$ , as expected for a diamagnetic effect proportional to  $B_0$ . Measurements are made by Fourier transformation of the free-induction-decay signal, averaged over many repetitions if necessary to provide the resolution required to detect the shift.

A great deal of work has been done with  $^{31}\text{P}$ , because of its presence in adenosine triphosphate and adenosine

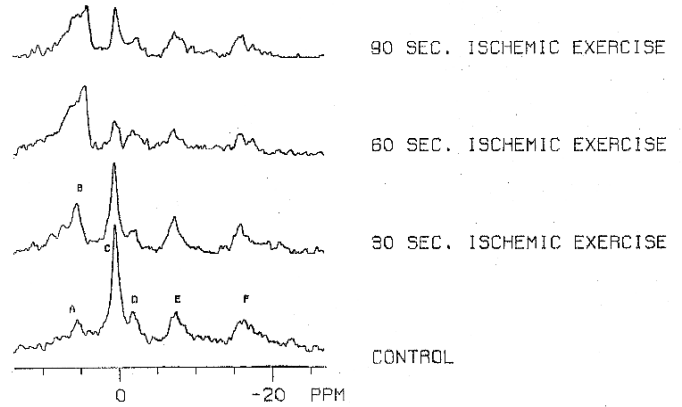


FIGURE 18.36. A series of  $^{31}\text{P}$  NMR spectra from the forearm of a normal adult showing the change in various chemical-shift peaks with exercise. Peak A is inorganic phosphate; C is phosphocreatine; D, E, and F are from the three phosphates in ATP. One can see the disappearance of ATP and phosphocreatine with exercise, accompanied by the buildup of inorganic phosphate. From R. L. Nunnally (1985). NMR spectroscopy for in vivo determination of metabolism; an overview, in S. R. Thomas and R. L. Dixon, eds. *NMR in Medicine: The Instrumentation and Clinical Applications*, College Park, MD, AAPM. Used by permission.

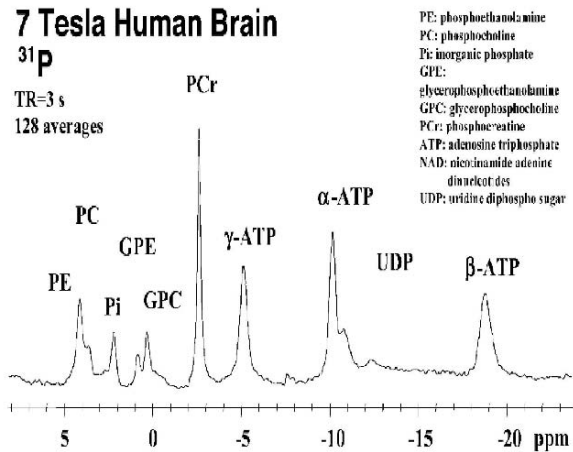


FIGURE 18.37. A chemical shift spectrum for  $^{31}\text{P}$  taken from the visual cortex at the back of the brain using a 7-tesla machine. From H. Lei, X.-H. Zhu, X.-L. Zhang and K. Ugurbil. In vivo  $^{31}\text{P}$  magnetic resonance spectroscopy of the human brain at 7 T: An initial experience. *Magn. Reson. Med.* **49**:199–205 (2003). Used by permission. Image courtesy of Professor Kamil Ugurbil.

diphosphate (ATP and ADP). Free energy is supplied for many processes in the body by the conversion of ATP to ADP. Figure 18.36 shows shifts in the  $^{31}\text{P}$  peaks due to metabolic changes. With exercise the ATP and phosphocreatine peaks diminish and the inorganic phosphate peak increases. Fig. 18.37 shows a very high resolution chemical shift spectrum from the human visual cortex taken with a 7-tesla machine.

### 3D-CSI of $^{31}\text{P}$ MRS and $^1\text{H}$ images acquired using the coil at 7T

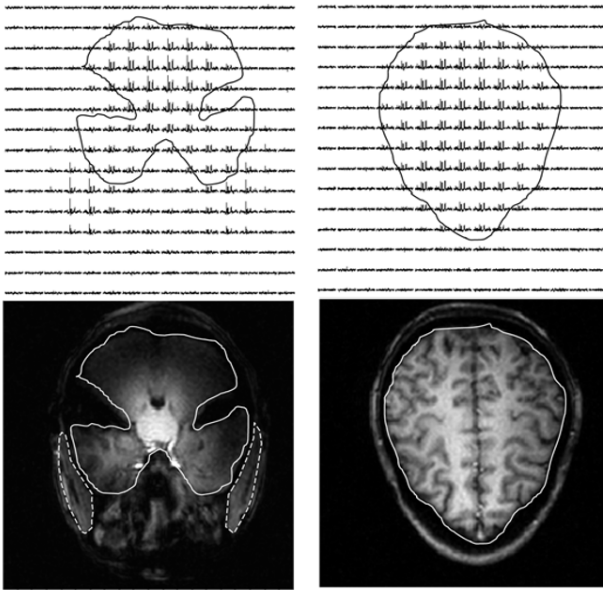


FIGURE 18.38. The image on the left displays  $^{31}\text{P}$  chemical shift data as spectra from individual voxels. The image of the slice from which these data are obtained is shown below the spectra. The slice cuts through the cerebellum and temporal lobes of the brain (solid outline). The dashed lines mark skeletal muscle which also contains phosphorylated metabolites, with a higher creatine phosphate level (PCr) compared to brain. The slice on the right is through brain only. Image courtesy of Prof. Kamil Ugurbil.

It is also possible to make chemical shift images. Figure 18.38 shows a series of  $^{31}\text{P}$  spectra from the brain. An image of the slice from which these data are obtained is shown below the spectra. The slice on the left cuts through the cerebellum and temporal lobes of the brain. It also includes some skeletal muscle. The slice on the right is through brain only.

## 18.11 Flow Effects

Flow effects can distort a magnetic resonance image. Spins initially prepared with one value of  $\mathbf{M}$  can flow out of a slice before the echo and be replaced by spins that had a different initial value of  $\mathbf{M}$ . This is called *washout*. Spins that have been shifted in phase by a field gradient can flow to another location before the readout pulse is applied. Axel (1985) reviews the effect on images. This technique has also been used to measure blood flow [Battocletti *et al.* (1981)].

To understand the washout effect consider a simple model in which a blood vessel is perpendicular to the slice, as shown in Fig. 18.39. To simplify further, assume

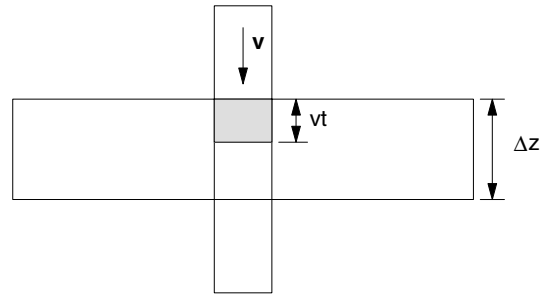


FIGURE 18.39. A blood vessel is perpendicular to the slice. The model developed in the text assumes plug flow, that is, all of the blood is flowing with the same speed  $v$ .

that all the blood flows with the same speed  $v$ , independent of where it is in the vessel. This is called *plug flow*.

First consider washout of the excited spins. Suppose that at time  $T_E/2$  a  $\pi$  pulse is applied to the slice in Fig. 18.39 and that the echo is measured at time  $T_E$ . The shaded area in the vessel represents new blood that flows in during time  $t$ . If the flow velocity is zero, no new blood flows in, all of the blood in the slice was excited, and the signal has full strength. If the velocity is greater than  $2\Delta z/T_E$ , all of the spins that were flipped by the pulse will leave the sensitive region by the time of the echo, and there will be no signal. Because we assume plug flow, the fraction washed out is a linear function of velocity up to the critical value of  $v$ . The fraction of excited spins remaining at  $T_E$  is given by

$$f = \begin{cases} 1 - \frac{vT_E}{2\Delta z}, & v < 2\Delta z/T_E \\ 0, & v \geq 2\Delta z/T_E. \end{cases} \quad (18.55)$$

Now consider washout of spins between pulses. We saw that the effect of repetition and echo times on the MRI signal is given by Eq. 18.52, which, if  $T_R \gg T_E$ , simplifies to Eq. 18.53. For low velocities ( $v < \Delta z/T_R$ ) there is an enhancement of the signal because blood with a larger value of  $M_z$  flows into the sensitive region. For  $vT_R < \Delta z$ , the factor in parentheses in Eq. 18.53 is replaced by

$$\frac{vT_R}{\Delta z} + \left(1 - \frac{vT_R}{\Delta z}\right) \left(1 - e^{-T_R/T_1}\right).$$

The first term represents spins that flow in and the second those that still remain and that are still affected by the previous pulse. This can be rearranged as

$$\left(1 - e^{-T_R/T_1}\right) + \frac{vT_R}{\Delta z} e^{-T_R/T_1}. \quad (18.56)$$

This factor has the value  $1 - e^{-T_R/T_1}$  for small  $v$  and is proportional to  $v$  when  $v \gg T_R/\Delta z$ . More complicated models can be developed. Phase changes because the blood flows through magnetic field gradients are also important.

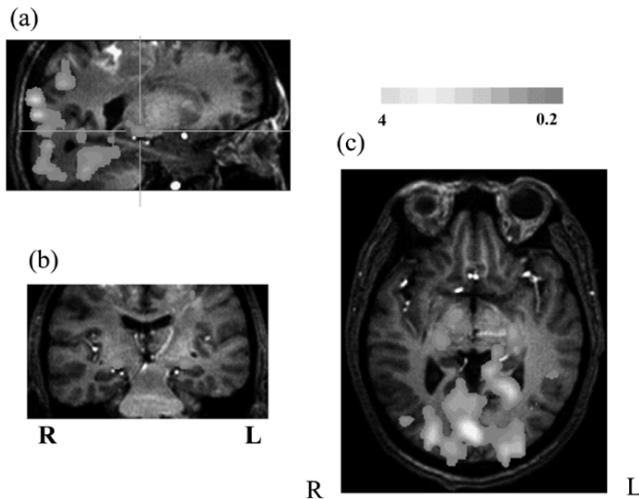


FIGURE 18.40. Functional MRI in three planes: (a) sagittal (side) view; (b) coronal (front) view; (c) axial view. The layers viewed in (b) and (c) are indicated by the lines in (a). Bright spots superimposed on the image show activity in the visual cortex and in some structures between the eye and the visual cortex. The magnetic field is 4 T. Adapted from Chen *et al.* (1998). Image supplied by Professor Kamil Ugurbil.

## 18.12 Functional MRI

Magnetic resonance imaging provides excellent structural information. Various contrast agents can provide information about physiologic function. For example, various contrast agents containing gadolinium are injected intravenously. They leak through a damaged blood-tissue barrier and accumulate in the damaged region. At small concentrations  $T_1$  is shortened.

One can also inject a contrast agent and watch its first pass through the circulatory system. Such an agent typically changes the magnetic susceptibility and shortens  $T_2$ .

The term *functional magnetic resonance imaging* (fMRI) usually refers to a technique developed in the 1990s that allows one to study structure and function simultaneously. The basis for fMRI is inhomogeneities in the magnetic field caused by the differences in the magnetic properties of oxygenated and deoxygenated hemoglobin. No external contrast agent is required. Oxygenated hemoglobin is less paramagnetic than deoxyhemoglobin. If we make images before and after a change in the blood flow to a small region of tissue (perhaps caused by a change in its metabolic activity), the difference between the two images is due mainly to changes in the blood oxygenation. One usually sees an increase in blood flow to a region of the brain when that region is active. This blood oxygenation level dependent (BOLD) contrast in the two images provides information about the metabolic state of the tissue, and therefore about the tissue function [Ogawa *et al.* (1990); Price *et al.* (2002)]. A recent image of the brain during visual stimulation is

shown in Fig. 18.40. In addition to the visual cortex in (c), activity is seen in the lateral geniculate nucleus [(b) and (c)], which is on the pathway from the eye to the visual cortex. Functional MRI provides functional information similar to that from PET (Sec. 17.14), but without the need for radionuclides.

Another recent technique that can be classified as functional is the detection of prostate cancer that has metastasized to a lymph node when the metastasis is not yet apparent by other imaging techniques. Monocrystalline iron oxide particles injected in the blood will be taken up by normal lymph nodes but not those with metastases. The technique is effective for lymph nodes larger than 5 mm [Harisinghani *et al.* (2003); see also the commentary by Koh *et al.* (2003)].

## 18.13 Diffusion and Diffusion Tensor MRI

Our analysis of MRI so far assumes that the nuclei are stationary except for rotation of their spin axis. In practice, these nuclei are free to diffuse throughout the tissue (Chapter 4). The magnetization  $\mathbf{M}$  depends on the total number of particles per unit volume with average spin components  $\langle \mu_x \rangle$ ,  $\langle \mu_y \rangle$ , and  $\langle \mu_z \rangle$ . In the rotating coordinate system there is no precession. In the absence of relaxation effects  $\langle \boldsymbol{\mu} \rangle$  does not change. In that case changes in  $\mathbf{M}$  depend on changes in the concentration of particles with particular components of  $\langle \boldsymbol{\mu} \rangle$ , so the rate of change of each component of  $\langle \boldsymbol{\mu} \rangle$  is given by a diffusion equation. For example, for  $M_x$ ,

$$\frac{\partial M_x}{\partial t} = D \nabla^2 M_x.$$

If the processes are linear, this diffusion term can be added to the other terms in the Bloch equations. The details are given in Problem 38.

In a spin-echo pulse sequence, the amplitude of the echo will be smaller if the spins have diffused to different locations within the tissue between the time of the excitation pulse and the echo. This artifact degrades the signal during traditional MRI, but can be valuable if one wants to measure the diffusion constant. The rate of diffusion depends sensitively on temperature, so measurements of the diffusion constant provide a way to monitor internal temperatures noninvasively [Delannoy *et al.* (1991)]. Moseley *et al.* (1990) showed that diffusion MRI is valuable for detecting regional cerebral ischemia, and it has become a useful tool in stroke research.

Diffusion can be monitored during a spin-echo sequence by applying magnetic field gradients of the same magnitude and duration before and after the  $\pi$  pulse, as shown in Fig. 18.41. If a spin is stationary, these gradients have no effect: they shift the phase of the spins in one direction before the  $\pi$  pulse, but shift the phase in the other direction after the  $\pi$  pulse, restoring the original phase.



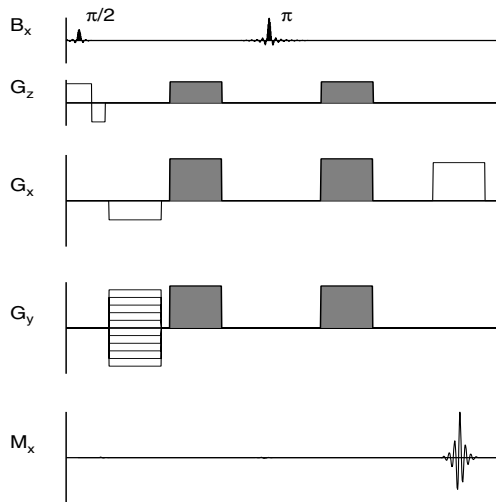


FIGURE 18.41. A simplified pulse sequence for diffusion tensor imaging. The sequence is similar to that shown in Fig. 18.30, for 2-D imaging using phase encoding. The first FID signal is not seen because the  $G_x$  and  $G_y$  gradients dephase the spins. The diffusion gradients, shown in gray, are applied before and after the  $\pi$  pulse. For stationary spins, any phase shift produced by the first diffusion gradient is canceled by an opposite phase shift produced by the second diffusion gradient. Spins that diffuse during this pulse sequence are affected differently by the first and second diffusion gradients, which affects the signal. For diffusion tensor imaging the gradients must be applied in all three directions. For more details, see Mattiello *et al.* (1994).

However, for spins that diffuse from one location to another between the application of the gradients, the phase shift of the first gradient is not cancelled by an opposite phase shift in the second, so the gradients introduce a net phase shift. This shift lowers the echo amplitude, with the reduction depending on the square of the gradient and the diffusion constant (Problem 38).

In some tissues, such as nerve fibers, diffusion is anisotropic, meaning that the diffusion constant depends on direction. In such cases the effect of diffusion depends on the direction of the magnetic field gradient. Basser *et al.* (1994) extended diffusion MRI so that the entire diffusion tensor is measured. The diffusion tensor (or matrix) is similar to the conductivity tensor discussed in Sec. 7.9. Using matrix notation, the fluence rate of diffusing particles with aligned nuclear spins is related to the particle concentration by

$$\begin{pmatrix} j_x \\ j_y \\ j_z \end{pmatrix} = - \begin{pmatrix} D_{xx} & D_{xy} & D_{xz} \\ D_{yx} & D_{yy} & D_{yz} \\ D_{zx} & D_{zy} & D_{zz} \end{pmatrix} \begin{pmatrix} \frac{\partial C}{\partial x} \\ \frac{\partial C}{\partial y} \\ \frac{\partial C}{\partial z} \end{pmatrix} \quad (18.57)$$

One can show that the diffusion matrix is always symmetric:  $D_{yx} = D_{xy}$ , etc.

Diffusion is usually greater along the direction of the nerve or muscle fibers. Since the orientation of the fibers change throughout the body, the elements of the diffusion tensor vary as well. However, some features of the diffusion tensor, such as the trace (see Problem 40), are independent of the fiber direction, and are particularly useful when monitoring diffusion in anisotropic tissue, such as the white matter of the brain. In addition, the diffusion tensor contains information about the fiber direction, allowing one to map fiber tract trajectories noninvasively using MRI [Basser *et al.* (2000)]. See also the review by Thomas *et al.* (2000).

### Symbols Used in Chapter 18

Symbol	Use	Units	First used on page
$a$	Loop radius	m	525
$a, b$	Constants	$J T^{-1} m^{-3}$	521
$f$	Fraction		535
$h$	Planck's constant	J s	522
$\hbar$	Planck's constant (reduced)	J s	517
$i$	Current	A	516
$j_x, j_y, j_z$	fluence rate	$m^{-2} s^{-1}$	537
$k_B$	Boltzmann constant	$J K^{-1}$	517
$k_x, k_y, k_z$	Spatial frequency	$m^{-1}$	530
$m$	Mass	kg	516
$m$	Azimuthal quantum number		517
$m$	Integer		531
$q$	Electric charge	C	516
$r$	Radius	m	516
$s$	Signal	V	530
$t$	Time	s	516
$v$	Velocity	$m s^{-1}$	516
$v$	Voltage difference	V	524
$x$	Dimensionless variable		528
$x, y, z$	Axes	m	518
$x', y', z'$	Axes (rotating)	m	519
$\Delta z$	Slice thickness	m	528
$A$	Amplitude	T s	529
$A$	Constant	$V T J^{-1}$	530
$B, \mathbf{B}$	Magnetic field	T	516
$B_1$	Oscillating magnetic field	T	520
$C$	Constant in expression for relaxation time	$s^{-2}$	523
$E$	Energy	J	522
$G_x, G_y, G_z$	Gradient of $B_z$ in the $x, y,$ or $z$ direction	$T m^{-1}$	528
$\mathbf{I}$	Nuclear angular momentum	$kg m^2 s^{-1}$	517
$I$	Nuclear angular momentum quantum number		517
$K$	Constant		524

Symbol	Use	Units	First used on page
$L, \mathbf{L}$	Orbital angular momentum	$\text{kg m}^2 \text{s}^{-1}$	516
$M, \mathbf{M}$	Magnetization	$\text{J T}^{-1} \text{m}^{-3}$	517
$N$	Number of spins per unit volume	$\text{m}^{-3}$	517
$\mathbf{R}$	Rotation matrix		519
$S$	Area	$\text{m}^2$	516
$\mathbf{S}$	Spin angular momentum	$\text{kg m}^2 \text{s}^{-1}$	517
$T$	Temperature	K	517
$T$	Period	s	521
$T_E$	Time of echo	s	526
$T_I$	Interrogation time	s	526
$T_R$	Repetition time between pulse sequences	s	528
$T_1$	Longitudinal relaxation time	s	518
$T_2$	Transverse relaxation time	s	518
$T_2^*$	Experimental transverse relaxation time	s	524
$T_p$	Length of gradient pulse	s	531
$U$	Potential energy	J	516
$V$	Volume	$\text{m}^3$	525
$\alpha$	Arbitrary angle		522
$\gamma$	Gyromagnetic ratio	$\text{T}^{-1} \text{s}^{-1}$	516
$\mu, \boldsymbol{\mu}$	Magnetic moment	$\text{J T}^{-1}$	516
$\mu_0$	Magnetic permeability of space	$\text{T m A}^{-1}$	516
$\nu$	Frequency	Hz	517
$\theta$	Angle		516
$\sigma$	Chemical shift factor		534
$\tau, \boldsymbol{\tau}$	Torque	N m	516
$\tau$	Shift time for autocorrelation	s	523
$\tau_C$	Correlation time	s	523
$\omega$	Angular frequency	$\text{s}^{-1}$	517
$\omega_1$	Angular frequency for $B_1$ rotation	$\text{s}^{-1}$	521
$\omega_0$	Larmor angular frequency	$\text{s}^{-1}$	519
$\phi$	Azimuthal angle		522
$\phi$	Phase		531
$\phi_{11}$	Autocorrelation function		523
$\Phi$	Magnetic flux	weber (T m <sup>2</sup> )	525
$\boldsymbol{\Omega}$	Angular velocity vector	$\text{s}^{-1}$	520

## Problems

### Section 18.1

**Problem 1** Show that for a particle of mass  $m$  located at position  $\mathbf{r}$  with respect to the origin, the torque about the origin is the rate of change of the angular momentum about the origin.

### Section 18.2

**Problem 2** Show that the units of  $\gamma$  are  $\text{T}^{-1} \text{s}^{-1}$ .

**Problem 3** Find the ratio of the gyromagnetic ratio in Table 18.1 to the value  $q/2m$  for the electron and proton.

### Section 18.3

**Problem 4** Evaluate the quantity  $\gamma m \hbar B / k_B T$  and the Larmor frequency for electron spins and proton spins in magnetic fields of 0.5 and 4.0 T at body temperature (310 K).

**Problem 5** Verify that  $\sum 1 = 2I + 1$ ,  $\sum m = 0$ , and  $\sum m^2 = I(I + 1)(2I + 1)/3$ , when the sums are taken from  $-I$  to  $I$ , in the cases that  $I = \frac{1}{2}$ , 1, and  $\frac{3}{2}$ .

**Problem 6** Obtain an expression for the magnetization analogous to Eq. 18.10 in the case  $I = \frac{1}{2}$  when one cannot make the assumption  $\gamma \hbar B / k_B T \ll 1$ .

**Problem 7** Calculate the coefficient of  $B$  in Eq. 18.10 for a collection of hydrogen nuclei at 310 K when the number of hydrogen nuclei per unit volume is the same as in water.

### Section 18.4

**Problem 8** Verify that Eqs. 18.16 are a solution of Eqs. 18.15.

**Problem 9** Calculate the value of  $M_x^2 + M_y^2 + M_z^2$  for relaxation Eqs. 18.16 when  $T_1 = T_2$ .

**Problem 10** Equations 18.16 correspond to a solution of the Bloch equations in the presence of a static field  $B$ . What would be the solutions if initially  $M_x = 0$ ,  $M_y = 0$ , and  $M_z = -M_0$ ?

### Section 18.5

**Problem 11** (a) Use Fig. 18.6 to derive Eq. 18.18.

(b) Show that

$$M_{x'} = M_x \cos \theta + M_y \sin \theta,$$

$$M_{y'} = -M_x \sin \theta + M_y \cos \theta.$$

(c) Combine these equations with the equations for  $M_x$  and  $M_y$  to show that the application of both transformations brings one back to the starting point.

**Problem 12** Equation 18.17 shows how to transform the components of a vector in the primed system (rotated an angle  $\theta$  clockwise from the unprimed system) into the unprimed system. Use the arguments of Section 18.5 to derive the following transformation matrices for counter-clockwise rotations.

(a) Angle  $\alpha$  about the  $x$  axis:

$$\begin{pmatrix} 1 & 0 & 0 \\ 0 & \cos \alpha & \sin \alpha \\ 0 & -\sin \alpha & \cos \alpha \end{pmatrix}$$

(b) Angle  $\beta$  about the  $y$  axis:

$$\begin{pmatrix} \cos \beta & 0 & -\sin \beta \\ 0 & 1 & 0 \\ \sin \beta & 0 & \cos \beta \end{pmatrix},$$

(c) Angle  $\theta$  about the  $z$  axis:

$$\begin{pmatrix} \cos \theta & \sin \theta & 0 \\ -\sin \theta & \cos \theta & 0 \\ 0 & 0 & 1 \end{pmatrix}.$$

Why are the minus signs different from those in Eq. 18.17b?

**Problem 13** Calculate  $M^2 = M_x^2 + M_y^2 + M_z^2$  for the solution of Eqs. 18.30 and compare it to the results of Problem 9.

### Section 18.6

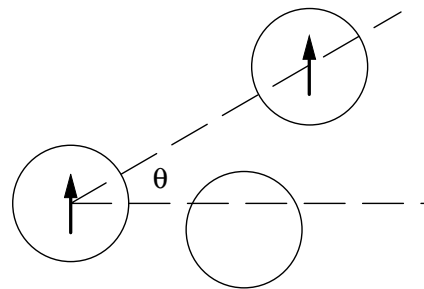
**Problem 14** Use Eqs. 18.32 to find the magnetic field at one proton due to the other proton in a water molecule when both proton spins are parallel to each other and perpendicular to the line between the protons. The two protons form an angle of  $104.5^\circ$  and are each  $96.5 \times 10^{-12}$  m from the oxygen.

**Problem 15** The magnetic field at a distance of 0.15 nm from a proton is  $4 \times 10^{-4}$  T. What change in Larmor frequency does this  $\Delta B$  cause? How long will it take for a phase difference of  $\pi$  radians to occur between a precessing spin feeling this extra field and one that is not?

**Problem 16** Consider a collection of spins that are aligned along the  $x$  axis at  $t = 0$ . They precess in the  $xy$  plane with different angular frequencies spread uniformly between  $\omega - \Delta\omega/2$  and  $\omega + \Delta\omega/2$ . If the total magnetic moment per unit volume is  $M_0$  at  $t = 0$ , show that at time  $T = 4/\Delta\omega$  it is  $M_0 \sin(2)/2 = 0.455M_0$ .

**Problem 17** What is the contribution to the transverse relaxation time for a magnetic field of 1.5 T with a uniformity of 1 part per million? The nonrecoverable relaxation time of brain is about 2.5 ms. What dominates the measured transverse relaxation in brain?

**Problem 18** Suppose the two dipoles of the water molecule shown below point in the  $z$  direction while the line between them makes an angle  $\theta$  with the  $x$  axis. Determine the angle  $\theta$  for which the magnetic field of one dipole is perpendicular to the dipole moment of the other. For this angle the interaction energy is zero. This  $\theta$  is called the “magic angle” and is used when studying anisotropic tissue such as cartilage [Xia (1998)].



### Section 18.7

**Problem 19** In solving this problem, you will develop a simple model for estimating the radio-frequency energy absorption in a patient undergoing an MRI procedure.

(a) Consider a uniform conductor with electrical conductivity  $\sigma$ . If it is subject to a changing magnetic field  $B_1(t) = B_1 \cos(\omega_0 t)$ , apply Eq. 8.19 to a circular path of radius  $R$  at right angles to the field to show that the electric field at radius  $R$  has amplitude  $E_0 = R\omega_0 B_1/2$ . (Because this is proportional to  $R$ , the model gives the skin dose, along the path for which  $R$  is largest.)

(b) Use Ohm’s law in the form  $j = \sigma E$  to show that the time average power dissipated per unit volume of material is  $p = \sigma E_0^2/2 = \sigma R^2 \omega_0^2 B_1^2/8$  and that if the mass density of the material is  $\rho$ , the specific absorption rate (SAR) or dose rate is  $SAR = \sigma R^2 \omega_0^2 B_1^2/8\rho$ .

(c) If the radio-frequency signal is not continuous but is pulsed, show that this must be modified by the “duty cycle” factor  $\Delta t/T_R$ , where  $\Delta t$  is the pulse duration and  $T_R$  is the repetition period.

(d) Combine these results with the fact that rotation through an angle  $\theta$  (usually  $\pi$  or  $\pi/2$ ) in time  $\Delta t$  requires  $B_1 = 2\theta/\gamma\Delta t$  and that  $\omega_0 = \gamma B_0$ , to obtain  $SAR = (1/T_R\Delta t)(\sigma/2\rho)(R^2/4)B_0^2\theta^2$ .

(e) Use typical values for the human body— $R = 0.17$  m,  $\sigma = 0.3$  S  $m^{-1}$ —to evaluate this expression for a  $\pi/2$  pulse.

(f) For  $B_0 = 0.5$  T and  $SAR < 0.4$  W  $kg^{-1}$  determine the minimum value of  $\Delta t$  for  $T_R = 1$  s. Also find  $B_1$ .

(g) For  $180^\circ$  pulses, what is the dose in Gy? (This should not be compared to an x-ray dose because this is nonionizing radiation.)

**Problem 20** Use Eq. 18.38 to calculate the initial amplitude of a signal induced in a one-turn coil of radius 0.5 m for protons in a 1-mm cube of water at 310 K in a magnetic field of 1.0 T. (The answer will be too small a signal to be useful; multiple-turn coils must be used.)

### Section 18.8

**Problem 21** Plot the maximum amplitude of an inversion recovery signal vs. the interrogation time if the detector is sensitive to the sign of the signal and if it is not.

**Problem 22** (a) Obtain an analytic expression for the maximum value of the first and second echo amplitudes in a Carr–Purcell pulse sequence in terms of  $T_2$  and  $T_E$ .

(b) Repeat for a CPMG pulse sequence.

**Problem 23** Consider the behavior of  $M_z$  in Figs. 18.19 and 18.21. The general equation for  $M_z$  is  $M_z = M_0 + Ae^{-t/T_1}$ . After several  $\pi$  pulses, the value of  $M_z$  is flipping from  $-b$  to  $b$ . Find the value of  $b$ .

**Problem 24** Consider a spin–echo pulse sequence (Fig. 18.18). Find

(a)  $M_z$  just before the  $\pi$  pulse at  $T_E/2$ ,

(b)  $M_z$  just after the  $\pi$  pulse at  $T_E/2$ ,

(c)  $M_z$  just before the  $\pi/2$  pulse at  $T_R$ , and

(d) the first and second echo amplitudes as a function of  $T_E$ ,  $T_R$ ,  $T_1$  and  $T_2$ . (The second amplitude is the same as all subsequent amplitudes.)

**Problem 25** This problem uses matrices to analyze the spin–echo pulse sequence. Use the rotation matrices given in Problem 12. Start with  $\mathbf{M} = (0, 0, M_0)$ . Rotate  $\mathbf{M}$  about  $x'$  by  $\pi/2$ , then about  $z'$  by  $\theta$ , then about  $x'$  by  $\pi$ , and finally about  $z'$  by  $\theta$ . What are the final components of  $\mathbf{M}$ ? Identify what pulse sequence or physical process corresponds to each rotation. Why would  $\theta$  be nonzero in the rotating reference frame? What would be the significance if the final  $\mathbf{M}$  is independent of  $\theta$ ?

**Problem 26** (a) Make a three-dimensional sketch of Fig. 18.17. Assume spin  $a$  is initially aligned with the  $y'$  axis and spin  $b$  is  $30^\circ$  clockwise from spin  $a$ . Then make similar sketches for a Carr–Purcell sequence that rotates the spins about the  $x'$  axis at the following times: just before the  $\pi$  pulse at  $T_E/2$ , just after the  $\pi$  pulse at  $T_E/2$ , at  $T_E$ , just before the  $\pi$  pulse at  $3T_E/2$ , just after the  $\pi$  pulse at  $3T_E/2$ , and at  $2T_E$ . Assume that the  $\pi$  pulse rotates the spins exactly  $180^\circ$ . Then make sketches when the  $\pi$  pulses rotate the spins by  $185^\circ$ .

(b) Repeat for a CPMG pulse sequence that rotates spin  $a$  and spin  $b$  around the  $y'$  axis. Again, consider two cases: the  $\pi$  pulses rotate by  $180^\circ$  and  $185^\circ$ . Your sketches will show the advantage of the CPMG pulse sequence when there is an error in the duration of the  $\pi$  pulse.

**Problem 27** This problem uses the matrices introduced in Problem 12 to examine the difference between the Carr–Purcell and the Carr–Purcell–Meiboom–Gill pulse sequences.

(a) Start with  $\mathbf{M} = (0, 0, M_0)$ . Rotate about  $x'$  by  $\pi/2$ , about  $z'$  by  $\theta$ , about  $x'$  by  $\pi$ , about  $z'$  by  $\theta$  again, about  $x'$  by  $\pi$ , and about  $z'$  by  $\theta$ . What is the final result? This process corresponds to the first two echoes produced by a Carr–Purcell pulse sequence.

(b) Repeat the analysis of part (a), but change the two  $\pi$  rotations about  $x'$  to two  $\pi + \delta$  rotations about  $x'$ . Assume  $\delta \ll \pi$  and use the approximations  $\cos(\pi + \delta) = -\cos \delta \approx -1$  and  $\sin(\pi + \delta) = -\sin \delta \approx -\delta$  to simplify your result. Keep only terms in order  $\delta$ . What is your final result?

This process corresponds to the first two echoes produced by a Carr–Purcell pulse sequence in which the  $\pi$  pulses have slightly wrong amplitudes.

(c) Repeat the analysis of part (b) but change the rotations about  $x'$  to be rotations about  $y'$ . What are the differences between the CP and CPMG pulse sequences? Explain why the CPMG pulse sequence is superior to the CP pulse sequence.

## Section 18.9

**Problem 28** Show that an alternative expression for the field amplitude required for a  $\pi/2$  pulse is  $B_1 = B_0\pi/\omega_0\Delta t = B_0/2\nu\Delta t$ .

**Problem 29** A certain MRI machine has a static magnetic field of 1.0 T. Spins are excited by applying a field gradient of  $3 \text{ mT m}^{-1}$ . If the slice is to be 5 mm thick, what is the Larmor frequency and the spread in frequencies that is required?

**Problem 30** Consider a pair of gradient coils of radius  $a$  perpendicular to the  $z$  axis and located at  $z = \pm\sqrt{3}a/2$ . The current flows in the opposite direction in each single-turn coil.

(a) Use the results of Problem 8.9 to obtain an expression for  $B_z$  along the  $z$  axis.

(b) For a gradient of  $5 \text{ mT m}^{-1}$  at the origin and  $a = 10 \text{ cm}$ , find the current required in a single-turn coil.

**Problem 31** Find a linear approximation for Eq. 18.53 for very small values of  $T_E$  and  $T_R$ , and discuss why it is called a  $T_1$ -weighted image.

**Problem 32** The slice selection gradient  $G_z$  must be applied for a time  $\tau$  which is at least as long as the duration of the  $B_1$  pulse. Suppose that  $\tau = 6 \times 2\pi/(\gamma G_z \Delta z)$  (see Fig. 18.23). How much has the phase at the top of the slice ( $z = \Delta z$ ) changed with respect to the middle of the slice ( $z = 0$ )?

**Problem 33** Relate the resolution in the  $y$  direction to  $G_y$  and  $T_p$ .

**Problem 34** Discuss the length of time required to obtain a  $256 \times 256$  image in terms of  $T_R$  and  $T_E$ . The field of view is 15 cm square. Consider both projection reconstruction and spin warp images. Introduce any other parameters you need.

**Problem 35** The limiting noise in a well-designed machine is due to thermal currents in the body. The noise is proportional to  $B_0$  and the volume  $V_n$  sampled by the radio-frequency pickup coil. The noise is also proportional to  $T^{-1/2}$ , where  $T$  is the time it takes to acquire the image. Show that the signal-to-noise ratio is proportional to  $B_0 T^{1/2} V_v / V_n$ , where  $V_v$  is the volume of the picture element.

Section 18.10

**Problem 36** The chemical shift difference between water and fat is  $\Delta\sigma = 3.5$  ppm. This can cause a spatial shift of the images from fat and water if the readout gradients are large. Estimate this shift for a 1.5 T machine and a gradient of  $5 \text{ mT m}^{-1}$ .

Section 18.11

**Problem 37** Use the model of Sec. 18.11 to plot the flow correction as a function of velocity for  $T_E = 10 \text{ ms}$ ,  $T_1 = 900 \text{ ms}$ , and  $T_2 = 400 \text{ ms}$ , when (a)  $T_R = 50 \text{ ms}$ , (b)  $T_R = 200 \text{ ms}$ .

Section 18.13

**Problem 38** This problem shows how to extend the Bloch equations to include the effect of diffusion of the molecules containing the nuclear spins in an inhomogeneous external magnetic field. Since  $\mathbf{M}$  is the magnetization per unit volume, it depends on the total number of particles per unit volume with average spin components  $\langle\mu_x\rangle$ ,  $\langle\mu_y\rangle$ , and  $\langle\mu_z\rangle$ . In the rotating coordinate system there is no precession. In the absence of relaxation effects  $\langle\boldsymbol{\mu}\rangle$  does not change. In that case changes in  $\mathbf{M}$  depend on changes in the concentration of particles with particular components of  $\langle\boldsymbol{\mu}\rangle$ , so the rate of change of each component of  $\langle\boldsymbol{\mu}\rangle$  is given by a diffusion equation. For example, for  $M_x$ ,

$$\frac{\partial M_{x'}}{\partial t} = D\nabla^2 M_{x'}.$$

If the processes are linear this diffusion term can be added to the other terms in the Bloch equations. Suppose that there is a uniform gradient in  $B_z$ ,  $G_z$ , and that the coordinate system rotates with the Larmor frequency for  $z = 0$ . When  $z$  is not zero, the rotation term does not quite cancel the  $(\mathbf{M} \times \mathbf{B})_z$  term.

(a) Show that the  $x$  and  $y$  Bloch equations become

$$\begin{aligned} \frac{\partial M_{x'}}{\partial t} &= +\gamma G_z z M_{y'} - \frac{M_{x'}}{T_2} + D\nabla^2 M_{x'}, \\ \frac{\partial M_{y'}}{\partial t} &= -\gamma G_z z M_{x'} - \frac{M_{y'}}{T_2} + D\nabla^2 M_{y'}. \end{aligned}$$

(b) Show that in the absence of diffusion

$$\begin{aligned} M_{x'} &= M(0)e^{-t/T_2} \cos(\gamma G_z z t), \\ M_{y'} &= M(0)e^{-t/T_2} \sin(\gamma G_z z t). \end{aligned}$$

(c) Suppose that  $\mathbf{M}$  is uniform in all directions. At  $t = 0$  all spins are aligned. Spins that have been rotating faster in the plane at  $z + \Delta z$  will diffuse into plane  $z$ . Equal numbers of slower spins will diffuse in from plane  $z - \Delta z$ . Show that this means that the phase of  $\mathbf{M}$  will not change but the amplitude will.

(d) It is reasonable to assume that the amplitude of the diffusion-induced decay will not depend on  $z$  as long as we are far from boundaries. Therefore try a solution of the form

$$\begin{aligned} M_{x'} &= M(0)e^{-t/T_2} \cos(\gamma G_z z t) A(t), \\ M_{y'} &= M(0)e^{-t/T_2} \sin(\gamma G_z z t) A(t), \end{aligned}$$

and show that  $A$  must obey the differential equation

$$\frac{1}{A} \frac{dA}{dt} = -D\gamma^2 G_z^2 t^2,$$

which has a solution  $A(t) = \exp(-D\gamma^2 G_z^2 t^3/3)$ .

(e) Show that if there is a rotation about  $y'$  at time  $T_E/2$ , then at time  $T_E$   $M_x$  is given by

$$M_x(T_E) = -M_0 \exp(-T_E/T_2) \exp(-D\gamma^2 G_z^2 T_E^3/12).$$

Hint: This can be done formally from the differential equations. However, it is much easier to think physically about the meaning of each factor in the expressions shown in (d) for  $M_{x'}$  and  $M_{y'}$ . This result means that a CPMG sequence with short  $T_E$  intervals can reduce the effect of diffusion when there is an external gradient.

**Problem 39** A commercial MRI machine is operated with a magnetic gradient of  $3 \text{ mT m}^{-1}$  while a slice is being selected. What is the effect of diffusion? Use the diffusion constant for self-diffusion in water and the results of Problem 38. Compare the correction factor to  $\exp(-T_E/T_2)$  when  $T_2 = 75 \text{ ms}$ .

**Problem 40** When a coordinate system is rotated as in Fig. 18.6, the diffusion tensor or diffusion matrix, which is always symmetric, transforms as

$$\begin{aligned} \begin{pmatrix} D_{x'x'} & D_{x'y'} \\ D_{x'y'} & D_{y'y'} \end{pmatrix} &= \begin{pmatrix} \cos\theta & \sin\theta \\ -\sin\theta & \cos\theta \end{pmatrix} \\ &\times \begin{pmatrix} D_{xx} & D_{xy} \\ D_{xy} & D_{yy} \end{pmatrix} \begin{pmatrix} \cos\theta & -\sin\theta \\ \sin\theta & \cos\theta \end{pmatrix}. \end{aligned}$$

We have not proved this; note that the rightmost matrix is the same one that would be seen if Eq. 18.17 were written in matrix form:

$$\begin{pmatrix} M_x \\ M_y \end{pmatrix} = \begin{pmatrix} \cos\theta & -\sin\theta \\ \sin\theta & \cos\theta \end{pmatrix} \begin{pmatrix} M_{x'} \\ M_{y'} \end{pmatrix}.$$

(a) Perform the matrix multiplication and find expressions for  $D_{x'x'}$ ,  $D_{x'y'}$ , and  $D_{y'y'}$  in terms of  $D_{xx}$ ,  $D_{xy}$ ,  $D_{yy}$ , and  $\theta$ .

(b) Find the angle  $\theta$  such that  $D_{x'y'}$  is zero (the diffusion tensor is diagonal). This is equivalent to finding the orientation of the fibers in the tissue.

(c) The trace of a matrix is the sum of its diagonal elements. Show that the trace of the diffusion matrix in the rotated coordinates,  $D_{x'x'} + D_{y'y'}$ , is equal to the trace of the diffusion matrix in the original coordinates,  $D_{xx} + D_{yy}$ . Thus, the trace of the diffusion tensor is independent of fiber direction.

## References

- Axel, L. (1985). Flow effects in magnetic resonance imaging, in S. R. Thomas and R. L. Dixon, eds. *NMR in Medicine: The Instrumentation and Clinical Applications*. College Park, MD, AAPM.
- Basser, P. J., J. Mattiello, and D. LeBihan (1994). MR diffusion tensor spectroscopy and imaging. *Biophys. J.*, **66**: 259–267.
- Basser, P. J., S. Pajevic, C. Pierpaoli, J. Duda, and A. Aldroubi (2000). In vivo fiber tractography using DT-MRI data. *Magn. Reson. Med.*, **44**: 625–632.
- Battocletti, J. H., R. E. Halbach, and S. X. Salles-Cunha (1981). The NMR blood flow meter—Theory and history. *Med. Phys.* **8**: 435–443.
- Bernstein, M. A., K. F. King and X.-h. Joe Zhou (2004). *Handbook of MRI Pulse Sequences*. Amsterdam, Elsevier Academic Press.
- Chen, W., T. Kato, X.-H. Zhu, J. Strupp, S. Ogawa and K. Ugurbil (1998). Mapping of lateral geniculate nucleus activation during visual stimulation in the human brain using fMRI. *Magn. Reson. Med.* **39**(1): 89–96.
- Cho, Z.-H., J. P. Jones, and M. Singh (1993). *Foundations of Medical Imaging*. New York, Wiley-Interscience.
- Delannoy, J., C. N. Chen, R. Turner, R. L. Levin, and D. LeBihan (1991). Noninvasive temperature imaging using diffusion MRI. *Magn. Reson. Med.* **19**: 333–339.
- Dixon, R. L., K. E. Ekstrand, and P. R. Moran (1985). The physics of proton NMR: Part II—The microscopic description. In S. R. Thomas and R. L. Dixon, eds. *NMR in Medicine: The Instrumentation and Clinical Applications*. College Park, MD, AAPM.
- Harisinghani, M. G., J. Barentsz, P. F. Hahn, W. M. Deserno, S. Tabatabaei, C. H. van de Kaa, J. de la Rosette, and R. Weissleder (2003). Noninvasive detection of clinically occult lymph-node metastases in prostate cancer. *New Engl. J. Med.* **348**(25): 2491–2499.
- Joseph, P. M. (1985). Pulse sequences for magnetic resonance imaging. In S. R. Thomas and R. L. Dixon, eds. *NMR in Medicine: The Instrumentation and Clinical Applications*. College Park, MD, AAPM.
- Joseph, P. M., and L. Axel (1984). Potential problems with selective pulses in NMR imaging systems. *Med. Phys.* **11**(6): 772–777.
- Kanal, E., J. P. Borgstede, A. J. Barkovich, C. Bell, W. G. Bradley, J. P. Felmlee, J. W. Froelich, E. M. Kaminiski, E. K. Keeler, J. W. Lester, E. A. Scoumis, L. A. Zaremba, and M. D. Zininger (2002). American College of Radiology white paper on MR safety. *AJR Amer. J. Roentg.* **178**(6): 1335–1347. [See also the comment by F. G. Shellock and J. V. Crues, pp. 1349–1352.]
- Koh, D.-M., G. J. R. Cook, and J. E. Husband (2003). New horizons in oncologic imaging. *New Engl. J. Med.* **348**(25): 2487–2488.
- Lei, H., X.-H. Zhu, X.-L. Zhang, K. Ugurbil and W. Chen (2003). In vivo  $^{31}\text{P}$  magnetic resonance spectroscopy of human brain at 7 T: An initial experience. *Magn. Reson. Med.* **49**: 199–205.
- Liang, Z.-P., and P. C. Lauterbur (2000). *Principles of Magnetic Resonance Imaging: A Signal Processing Perspective*. New York, IEEE Press.
- Mattiello, J., P. J. Basser and D. LeBihan (1994). Analytical expressions for the B-matrix in NMR diffusion imaging and spectroscopy. *J. Magn. Reson. Ser. A*, **108**: 131–141.
- Moseley, M. E., Y. Cohen, J. Mintorovitch, L. Chileuitt, H. Shimizu, J. Kucharczyk, M. F. Wendland, and P. R. Weinstein (1990). Early detection of regional cerebral ischemia in cats: comparison of diffusion- and  $T_2$ -weighted MRI and spectroscopy. *Magn. Reson. Med.* **14**: 330–346.
- Ogawa, S., T. M. Lee, A. R. Kay, and D. W. Tank. (1990). Brain magnetic resonance imaging with contrast dependent on blood oxygenation. *Proc Natl. Acad. Sci. USA*, **87**: 9868–9872.
- Price, R. R., J. Allison, R. J. Massoth, G. D. Clarke, and D. J. Drost (2002). Practical aspects of functional MRI (NMR Task Group #8). *Med. Phys.* **29**(8): 1892–1912.
- Schaefer, D. J., J. D. Bourland, and J. A. Nyenhuis (2000). Review of patient safety in time-varying gradient fields. *J. Mag. Res. Imaging* **12**: 20–29.
- Schmitt, F., M. K. Stehling, and R. Turner (1998). *Echo-Planar Imaging*. Berlin, Springer.
- Shellock, F. G. (2002). Magnetic resonance safety update 2002: Implants and devices. *J. Mag. Res. Imaging* **16**: 485–496.
- Slichter, C. P. (1978). *Principles of Magnetic Resonance*. New York, Springer.
- Thomas, D. L., M. F. Lythgoe, G. S. Pell, F. Calamante, and R. J. Ordidge (2000). The measurement of diffusion and perfusion in biological systems using magnetic resonance imaging. *Phys. Med. Biol.* **45**: R97–R138.
- Vlaardingerbroek, M. T., and J. A. den Boer (2002). *Magnetic Resonance Imaging: Theory and Practice*. 2nd ed. Berlin, Springer.
- Xia, Y. (1998). Relaxation anisotropy in cartilage by NMR microscopy ( $\mu\text{MRI}$ ) at 14- $\mu\text{m}$  resolution. *Magn. Reson. Med.* **39**: 941–949.

# Appendix A

## Plane and Solid Angles

### A.1 Plane Angles

The angle  $\theta$  between two intersecting lines is shown in Fig. A.1. It is measured by drawing a circle centered on the vertex or point of intersection. The arc length  $s$  on that part of the circle contained between the lines measures the angle. In daily work, the arc length is marked off in degrees.

In some cases, there are advantages to measuring the angle in *radians*. This is particularly true when trigonometric functions have to be differentiated or integrated. The angle in radians is defined by

$$\theta = \frac{s}{r}. \quad (\text{A.1})$$

Since the circumference of a circle is  $2\pi r$ , the angle corresponding to a complete rotation of  $360^\circ$  is  $2\pi r/r = 2\pi$ . Other equivalences are

Degrees	Radians
360	$2\pi$
57.2958	1
1	0.01745

(A.2)

Since the angle in radians is the ratio of two distances, it is dimensionless. Nevertheless, it is sometimes useful to

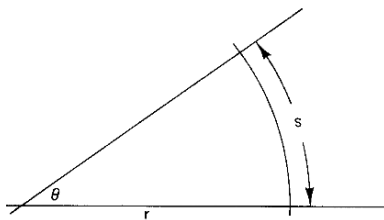


FIGURE A.1. A plane angle  $\theta$  is measured by the arc length  $s$  on a circle of radius  $r$  centered at the vertex of the lines defining the angle.

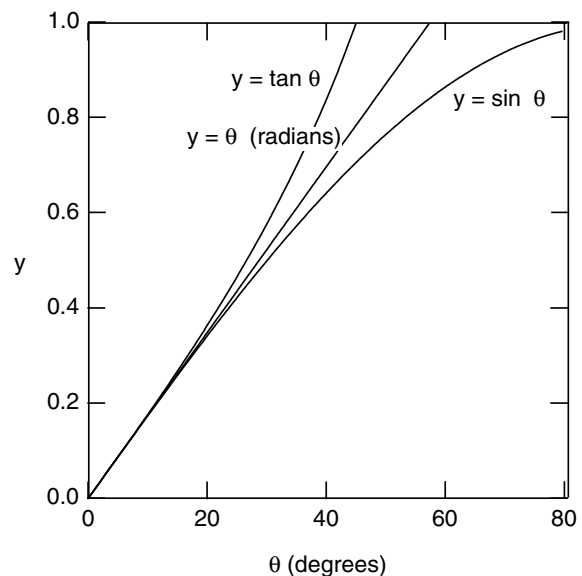


FIGURE A.2. Comparison of  $y = \tan \theta$ ,  $y = \theta$  (radians), and  $y = \sin \theta$ .

specify that something is measured in radians to avoid confusion.

One of the advantages of radian measure can be seen in Fig. A.2. The functions  $\sin \theta$ ,  $\tan \theta$ , and  $\theta$  in radians are plotted vs angle for angles less than  $80^\circ$ . For angles less than  $15^\circ$ ,  $y = \theta$  is a good approximation to both  $y = \tan \theta$  (2.3% error at  $15^\circ$ ) and  $y = \sin \theta$  (1.2% error at  $15^\circ$ ).

### A.2 Solid Angles

A plane angle measures the diverging of two lines in two dimensions. Solid angles measure the diverging of a cone of lines in three dimensions. Figure A.3 shows a series of

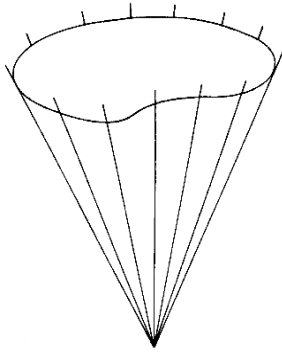


FIGURE A.3. A cone of rays in three dimensions.

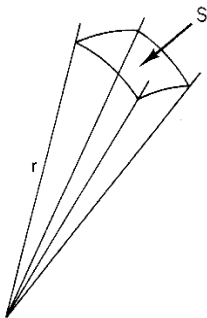


FIGURE A.4. The solid angle of this cone is  $\Omega = S/r^2$ .  $S$  is the surface area on a sphere of radius  $r$  centered at the vertex.

rays diverging from a point and forming a cone. The solid angle  $\Omega$  is measured by constructing a sphere of radius  $r$  centered at the vertex and taking the ratio of the surface area  $S$  on the sphere enclosed by the cone to  $r^2$ :

$$\Omega = \frac{S}{r^2}. \tag{A.3}$$

This is shown in Fig. A.4 for a cone consisting of the planes defined by adjacent pairs of the four rays shown. The unit of solid angle is the *steradian* (sr). A complete

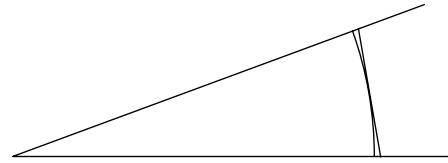


FIGURE A.5. For small angles, the arc length is very nearly equal to the length of the tangent to the circle.

sphere subtends a solid angle of  $4\pi$  steradians, since the surface area of a sphere is  $4\pi r^2$ .

When the included angle in the cone is small, the difference between the surface area of a plane tangent to the sphere and the sphere itself is small. (This is difficult to draw in three dimensions. Imagine that Fig. A.5 represents a slice through a cone; the difference in length between the circular arc and the tangent to it is small.) This approximation is often useful. A  $3 \times 5$ -in. card at a distance of 6 ft (72 in.) subtends a solid angle which is approximately

$$\frac{3 \times 5}{72^2} = 2.9 \times 10^{-3} \text{ sr.}$$

It is not necessary to calculate the surface area on a sphere of 72 in. radius.

## Problems

**Problem 1** Convert 0.1 radians to degrees. Convert  $7.5^\circ$  to radians.

**Problem 2** Use the fact that  $\sin \theta \approx \theta \approx \tan \theta$  to estimate the sine and tangent of  $3^\circ$ . Look up the values in a table and see how accurate the approximation is.

**Problem 3** What is the solid angle subtended by the pupil of the eye (radius = 3 mm) at a source of light 30 m away?



# Appendix B

## Vectors; Displacement, Velocity, and Acceleration

### B.1 Vectors and Vector Addition

A *displacement* describes how to get from one point to another. A displacement has a magnitude (how far point 2 is from point 1 in Fig. B.1) and a direction (the direction one has to go from point 1 to get to point 2). The displacement of point 2 from point 1 is labeled **A**. Displacements can be added: displacement **B** from point 2 puts an object at point 3. The displacement from point 1 to point 3 is **C** and is the sum of displacements **A** and **B**:

$$\mathbf{C} = \mathbf{A} + \mathbf{B}. \quad (\text{B.1})$$

A displacement is a special example of a more general quantity called a *vector*. One often finds a vector defined as a quantity having a magnitude and a direction. However, the complete definition of a vector also includes the requirement that vectors add like displacements. The rule for adding two vectors is to place the tail of the second vector at the head of the first; the sum is the vector from the tail of the first to the head of the second.

A displacement is a change of position so far in such a direction. It is independent of the starting point. To know where an object is, it is necessary to specify the starting point as well as its displacement from that point.

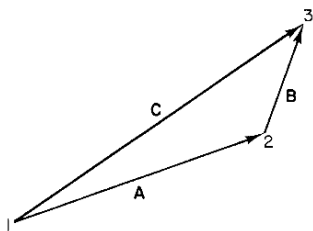


FIGURE B.1. Displacement **C** is equivalent to displacement **A** followed by displacement **B**:  $\mathbf{C} = \mathbf{A} + \mathbf{B}$ .

Displacements can be added in any order. In Fig. B.2, either of the vectors **A** represents the same displacement. Displacement **B** can first be made from point 1 to point 4, followed by displacement **A** from 4 to 3. The sum is still **C**:

$$\mathbf{C} = \mathbf{A} + \mathbf{B} = \mathbf{B} + \mathbf{A}. \quad (\text{B.2})$$

The sum of several vectors can be obtained by first adding two of them, then adding the third to that sum, and so forth. This is equivalent to placing the tail of each vector at the head of the previous one, as shown in Fig. B.3. The sum then goes from the tail of the first vector to the head of the last.

The negative of vector **A** is that vector which, added to **A**, yields zero:

$$\mathbf{A} + (-\mathbf{A}) = 0. \quad (\text{B.3})$$

It has the same magnitude as **A** and points in the opposite direction.

Multiplying a vector **A** by a *scalar* (a number with no associated direction) multiplies the magnitude of vector **A** by that number and leaves its direction unchanged.

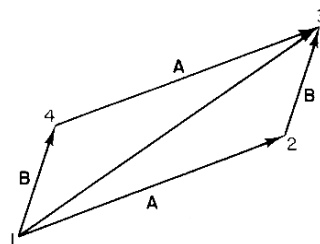


FIGURE B.2. Vectors **A** and **B** can be added in either order.

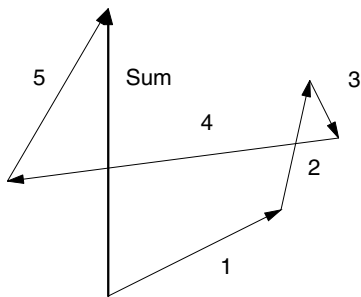


FIGURE B.3. Addition of several vectors.

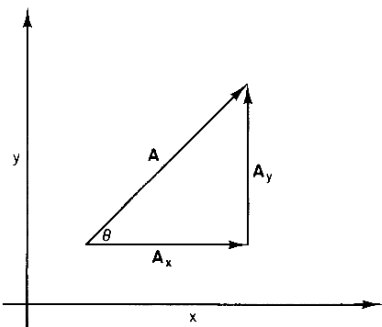


FIGURE B.4. Vector  $\mathbf{A}$  has components  $\mathbf{A}_x$  and  $\mathbf{A}_y$ .

## B.2 Components of Vectors

Consider a vector in a plane. If we set up two perpendicular axes, we can regard vector  $\mathbf{A}$  as being the sum of vectors parallel to each of these axes. These vectors,  $\mathbf{A}_x$  and  $\mathbf{A}_y$  in Fig. B.4, are called the *components* of  $\mathbf{A}$  along each axis<sup>1</sup>. If vector  $\mathbf{A}$  makes an angle  $\theta$  with the  $x$  axis and its magnitude is  $A$ , then the magnitudes of the components are

$$\begin{aligned} A_x &= A \cos \theta, \\ A_y &= A \sin \theta. \end{aligned} \tag{B.4}$$

The sum of the squares of the components is  $A_x^2 + A_y^2 = A^2 \cos^2 \theta + A^2 \sin^2 \theta = A^2(\sin^2 \theta + \cos^2 \theta)$ . Since, by Pythagoras' theorem, this must be  $A^2$ , we obtain the trigonometric identity

$$\cos^2 \theta + \sin^2 \theta = 1. \tag{B.5}$$

In three dimensions,  $\mathbf{A} = \mathbf{A}_x + \mathbf{A}_y + \mathbf{A}_z$ . The magnitudes can again be related using Pythagoras' theorem, as shown in Fig. B.5. From triangle  $OPQ$ ,  $A_{xy}^2 = A_x^2 + A_y^2$ . From triangle  $OQR$ ,

$$A^2 = A_{xy}^2 + A_z^2 = A_x^2 + A_y^2 + A_z^2. \tag{B.6}$$

In our notation,  $\mathbf{A}_x$  means a vector pointing in the  $x$  direction, while  $A_x$  is the magnitude of that vector. It can

<sup>1</sup>Some texts define the component to be a scalar, the magnitude of the component defined here.

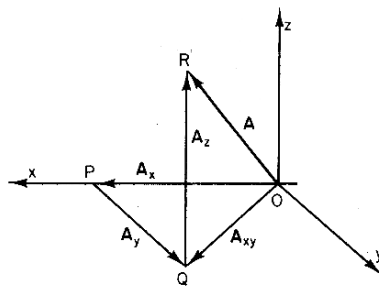


FIGURE B.5. Addition of components in three dimensions.

become difficult to keep the distinction straight. Therefore, it is customary to write  $\hat{x}$ ,  $\hat{y}$ , and  $\hat{z}$  to mean vectors of unit length pointing in the  $x$ ,  $y$ , and  $z$  directions. (In some books, the unit vectors are denoted by  $\hat{i}$ ,  $\hat{j}$ , and  $\hat{k}$  instead of  $\hat{x}$ ,  $\hat{y}$ , and  $\hat{z}$ .) With this notation, instead of  $\mathbf{A}_x$ , one would always write  $A_x \hat{x}$ .

The addition of vectors is often made easier by using components. The sum  $\mathbf{A} + \mathbf{B} = \mathbf{C}$  can be written as

$$\begin{aligned} A_x \hat{x} + A_y \hat{y} + A_z \hat{z} + B_x \hat{x} + B_y \hat{y} + B_z \hat{z} \\ = C_x \hat{x} + C_y \hat{y} + C_z \hat{z}. \end{aligned}$$

Like components can be grouped to give

$$\begin{aligned} (A_x + B_x) \hat{x} + (A_y + B_y) \hat{y} + (A_z + B_z) \hat{z} \\ = C_x \hat{x} + C_y \hat{y} + C_z \hat{z}. \end{aligned}$$

Therefore, the magnitudes of the components can be added separately:

$$\begin{aligned} C_x &= A_x + B_x, \\ C_y &= A_y + B_y, \\ C_z &= A_z + B_z. \end{aligned} \tag{B.7}$$

## B.3 Position, Velocity, and Acceleration

The *position* of an object at time  $t$  is defined by specifying its displacement from an agreed-upon origin:

$$\mathbf{R}(t) = x(t)\hat{x} + y(t)\hat{y} + z(t)\hat{z}.$$

The *average velocity*  $\mathbf{v}_{av}(t_1, t_2)$  between times  $t_1$  and  $t_2$  is defined to be

$$\mathbf{v}_{av}(t_1, t_2) = \frac{\mathbf{R}(t_2) - \mathbf{R}(t_1)}{t_2 - t_1}.$$

This can be written in terms of the components as

$$\begin{aligned} \mathbf{v}_{av} &= \left( \frac{x(t_2) - x(t_1)}{t_2 - t_1} \right) \hat{x} + \left( \frac{y(t_2) - y(t_1)}{t_2 - t_1} \right) \hat{y} \\ &+ \left( \frac{z(t_2) - z(t_1)}{t_2 - t_1} \right) \hat{z}. \end{aligned}$$

The *instantaneous velocity* is

$$\begin{aligned}\mathbf{v}(t) &= \frac{d\mathbf{R}}{dt} = \frac{dx}{dt}\hat{\mathbf{x}} + \frac{dy}{dt}\hat{\mathbf{y}} + \frac{dz}{dt}\hat{\mathbf{z}} \\ &= v_x(t)\hat{\mathbf{x}} + v_y(t)\hat{\mathbf{y}} + v_z(t)\hat{\mathbf{z}}.\end{aligned}\tag{B.8}$$

$$\mathbf{a}(t) = \frac{d\mathbf{v}}{dt} = \frac{dv_x}{dt}\hat{\mathbf{x}} + \frac{dv_y}{dt}\hat{\mathbf{y}} + \frac{dv_z}{dt}\hat{\mathbf{z}}.$$

## Problems

The  $x$  component of the velocity tells how rapidly the  $x$  component of the position is changing.

The *acceleration* is the rate of change of the velocity with time. The instantaneous acceleration is

**Problem 1** At  $t = 0$ , the position of an object is given by  $\mathbf{R} = 10\hat{\mathbf{x}} + 5\hat{\mathbf{y}}$ , where  $R$  is in meters. At  $t = 3$  s, the position is  $\mathbf{R} = 16\hat{\mathbf{x}} - 10\hat{\mathbf{y}}$ . What was the average velocity between  $t = 0$  and 3 s?



# Appendix D

## Taylor's Series

Consider the function  $y(x)$  shown in Fig. D.1. The value of the function at  $x_1$ ,  $y_1 = y(x_1)$ , is known. We wish to estimate  $y(x_1 + \Delta x)$ .

The simplest estimate, labeled approximation 0 in Fig. D.1, is to assume that  $y$  does not change:  $y(x_1 + \Delta x) \approx y(x_1)$ . A better estimate can be obtained if we assume that  $y$  changes everywhere at the same rate it does at  $x_1$ . Approximation 1 is

$$y(x_1 + \Delta x) \approx y(x_1) + \left. \frac{dy}{dx} \right|_{x_1} \Delta x.$$

The derivative is evaluated at point  $x_1$ .

An even better estimate is shown in Fig. D.2. Instead of fitting the curve by the straight line that has the proper first derivative at  $x_1$ , we fit it by a parabola that matches both the first and second derivatives. The approximation

is

$$y(x_1 + \Delta x) \approx y(x_1) + \left. \frac{dy}{dx} \right|_{x_1} \Delta x + \frac{1}{2} \left. \frac{d^2y}{dx^2} \right|_{x_1} (\Delta x)^2.$$

That this is the best approximation can be derived in the following way. Suppose the desired approximation is more general and uses terms up to  $(\Delta x)^n = (x - x_1)^n$ :

$$y_{\text{approx}} = A_0 + A_1(x - x_1) + A_2(x - x_1)^2 + \dots + A_n(x - x_1)^n \quad (\text{D.1})$$

The constants  $A_0, A_1, \dots, A_n$  are determined by making the value of  $y_{\text{approx}}$  and its first  $n$  derivatives agree with the value of  $y$  and its first  $n$  derivatives at  $x = x_1$ . When  $x = x_1$ , all terms with  $x - x_1$  in  $y_{\text{approx}}$  vanish, so that

$$y_{\text{approx}}(x_1) = A_0.$$

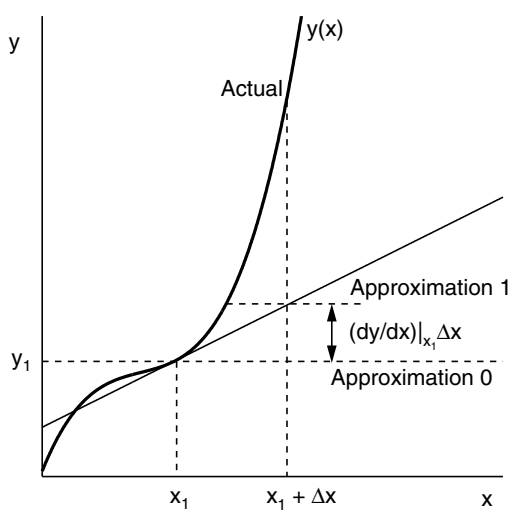


FIGURE D.1. The zeroth-order and first-order approximations to  $y(x)$ .

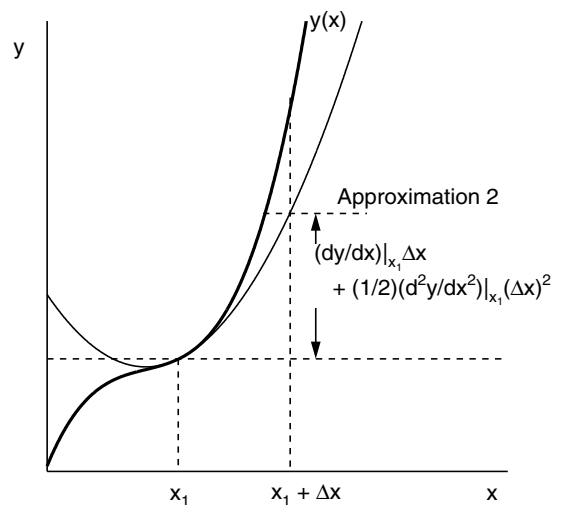


FIGURE D.2. The second-order approximation fits  $y(x)$  with a parabola.

TABLE D.1.  $y = e^{2x}$  and its derivatives.

Function or derivative	Value at $x_1 = 0$
$y = e^{2x}$	1
$\frac{dy}{dx} = 2e^{2x}$	2
$\frac{d^2y}{dx^2} = 4e^{2x}$	4
$\frac{d^3y}{dx^3} = 8e^{2x}$	8

TABLE D.2. Values of  $y$  and successive approximations.

$x$	$y = e^{2x}$	$1 + 2x$	$1 + 2x + 2x^2$	$1 + 2x + 2x^2 + \frac{4}{3}x^3$
-2	0.0183	-3.0	5.0	-5.67
-1.5	0.0498	-2.0	2.5	-2.0
-1	0.1353	-1.0	1.0	-0.33
-0.4	0.4493	0.2000	0.5200	0.4347
-0.2	0.6703	0.6000	0.6800	0.6693
-0.1	0.8187	0.8000	0.8200	0.8187
0	1.0000	1.0000	1.0000	1.0000
0.1	1.2214	1.2000	1.2200	1.2213
0.2	1.4918	1.4000	1.4800	1.4907
0.4	2.2255	1.8000	2.1200	2.2053
1.0	7.389	3.0000	5.0000	6.33
2.0	54.60	5.0	13.0	23.67

The first derivative of  $y_{\text{approx}}$  is

$$\frac{d(y_{\text{approx}})}{dx} = A_1 + 2A_2(x-x_1) + 3A_3(x-x_1)^2 + \dots + nA_n(x-x_1)^{n-1}.$$

The second derivative is

$$2A_2 + 3 \times 2A_3(x-x_1) + \dots + n(n-1)A_n(x-x_1)^{n-2},$$

and the  $n$ th derivative is

$$n(n-1)(n-2) \dots 2A_n = n!A_n.$$

Evaluating these at  $x = x_1$  gives

$$\left. \frac{d(y_{\text{approx}})}{dx} \right|_{x_1} = A_1,$$

$$\left. \frac{d^2(y_{\text{approx}})}{dx^2} \right|_{x_1} = 2 \times 1 \times A_2,$$

$$\left. \frac{d^3(y_{\text{approx}})}{dx^3} \right|_{x_1} = 3 \times 2 \times 1 \times A_3,$$

$$\left. \frac{d^n(y_{\text{approx}})}{dx^n} \right|_{x_1} = n!A_n.$$

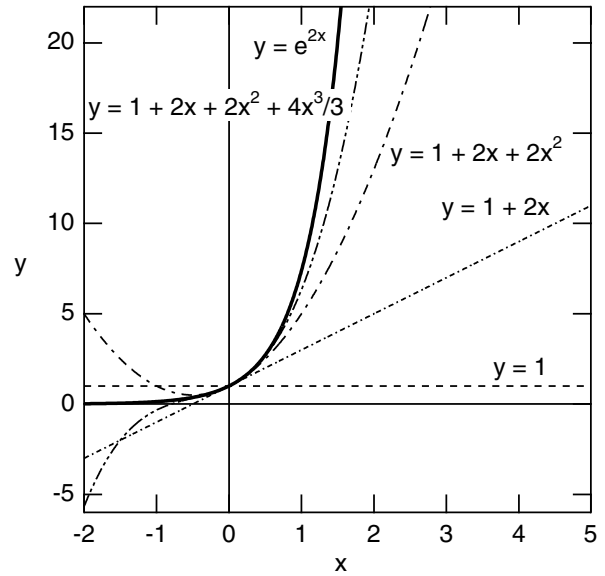


FIGURE D.3. The function  $y = e^{2x}$  with Taylor's series expansions about  $x = 0$  of degree 0, 1, 2, and 3.

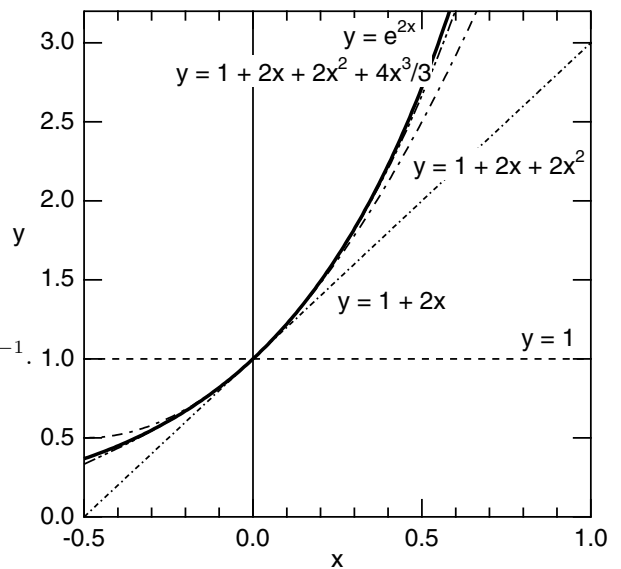


FIGURE D.4. An enlargement of Fig. D.3 near  $x = 0$ .

Combining these expressions for  $A_n$  with Eq. D.1, we get

$$y(x_1 + \Delta x) \approx y(x_1) + \sum_{n=1}^N \frac{1}{n!} \left. \frac{d^n y}{dx^n} \right|_{x_1} (\Delta x)^n. \quad (\text{D.2})$$

Tables D.1 and D.2 and Figs. D.3 and D.4 show how the Taylor's series approximation gets better over a larger and larger region about  $x_1$  as more terms are added. The function being approximated is  $y = e^{2x}$ . The derivatives

are given in Table D.1. The expansion is made about  $x_1 = 0$ .

Finally, the Taylor's series expansion for  $y = e^x$  about  $x = 0$  is often useful. Since all derivatives of  $e^x$  are  $e^x$ , the value of  $y$  and each derivative at  $x = 0$  is 1. The series is

$$e^x = 1 + x + \frac{1}{2!}x^2 + \frac{1}{3!}x^3 + \cdots = \sum_{m=0}^{\infty} \frac{x^m}{m!}. \quad (\text{D.3})$$

(Note that  $0! = 1$  by definition.)

## Problems

**Problem 1** Make a Taylor's series expansion of  $y = a + bx + cx^2$  about  $x = 0$ . Show that the expansion exactly reproduces the function.

**Problem 2** Repeat the previous problem, making the expansion about  $x = 1$ .

**Problem 3** (a) Make a Taylor's series expansion of the cosine function about  $x = 0$ . Remember that  $d(\sin x)/dx = \cos x$  and  $d(\cos x)/dx = -\sin x$ .

(b) Make a Taylor's series expansion of the sine function.

# Appendix E

## Some Integrals of Sines and Cosines

The average of a function of  $x$  with period  $T$  is defined to be

$$\langle f \rangle = \frac{1}{T} \int_{x'}^{x'+T} f(x) dx. \quad (\text{E.1})$$

The sine function is plotted in Fig. E.1(a). The integral over a period is zero, and its average value is zero. The area above the axis is equal to the area below the axis. Figure E.1(b) shows a plot of  $\sin^2 x$ . Since  $\sin x$  varies between  $-1$  and  $+1$ ,  $\sin^2 x$  varies between  $0$  (when  $\sin x = 0$ ) and  $+1$  (when  $\sin x = \pm 1$ ). Its average value, from inspection of Fig. E.1(b) is  $\frac{1}{2}$ . If you do not want to trust the drawing to convince yourself of this, recall the identity  $\sin^2 \theta + \cos^2 \theta = 1$ . Since the sine function and the cosine function look the same, but are just shifted along the axis, their squares must also look similar. Therefore,  $\sin^2 \theta$  and  $\cos^2 \theta$  must have the same average. But if their sum is always  $1$ , the sum of their averages must be  $1$ . If the two averages are the same, then each must be  $\frac{1}{2}$ .

These same results could have been obtained analytically by using the trigonometric identity

$$\sin^2 x = \frac{1}{2} - \frac{1}{2} \cos 2x. \quad (\text{E.2})$$

The integrals of  $\sin x$  and  $\cos x$  are

$$\begin{aligned} \int \sin ax dx &= -\frac{1}{a} \cos ax, \\ \int \cos ax dx &= \frac{1}{a} \sin ax. \end{aligned} \quad (\text{E.3})$$

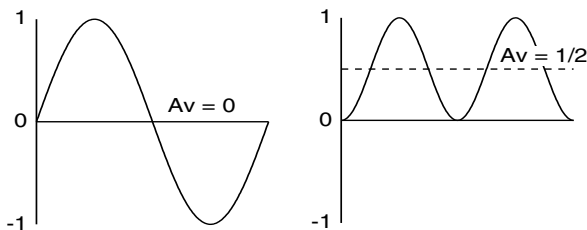


FIGURE E.1. (a) Plot of  $y = \sin x$ . (b) Plot of  $y = \sin^2 x$ .

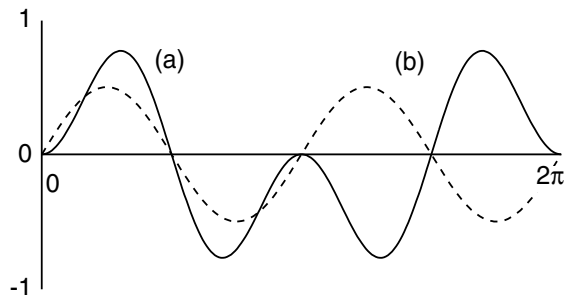


FIGURE E.2. Plot of one period of (a)  $y = \sin x \sin 2x$ ; (b)  $y = \sin x \cos x$ .

These could be used to show that the average value of  $\sin x$  or  $\cos x$  is zero. Then Eq. E.2 could be used to show that the average of  $\sin^2 x$  is  $\frac{1}{2}$ .

The integral of  $\sin^2 x$  over a period is its average value times the length of the period:

$$\int_0^T \sin^2 x dx = \int_0^T \cos^2 x dx = \frac{T}{2}. \quad (\text{E.4})$$

We will also encounter integrals like

$$\begin{aligned} \int_0^T \sin mx \sin nx dx, \quad m \neq n, \\ \int_0^T \cos mx \cos nx dx, \quad m \neq n, \\ \int_0^T \cos mx \sin nx dx, \quad m = n, \quad m \neq n. \end{aligned} \quad (\text{E.5})$$

All these integrals are zero. This can be shown using integral tables. Or, you can see why the integrals vanish by considering the specific examples plotted in Fig. E.2. Each integrand has equal positive and negative contributions to the total integral.



# Appendix F

## Linear Differential Equations with Constant Coefficients

The equation

$$\frac{dy}{dt} + by = a \quad (\text{F.1})$$

is called a *linear differential equation* because each term involves only  $y$  or its derivatives [not  $y(dy/dt)$  or  $(dy/dt)^2$ , etc.]. A more general equation of this kind has the form

$$\frac{d^N y}{dt^N} + b_{N-1} \frac{d^{N-1} y}{dt^{N-1}} + \cdots + b_1 \frac{dy}{dt} + b_0 y = f(t). \quad (\text{F.2})$$

The highest derivative is the  $N$ th derivative, so the equation is of order  $N$ . It has been written in standard form by dividing through by any  $b_N$  that was there originally, so that the coefficient of the highest term is one. If all the  $b$ 's are constants, this is a linear differential equation with constant coefficients. The right-hand side may be a function of the independent variable  $t$ , but *not* of  $y$ . If  $f(t) = 0$ , it is a *homogeneous* equation; if  $f(t)$  is not zero, it is an *inhomogeneous* equation.

Consider first the homogeneous equation

$$\frac{d^N y}{dt^N} + b_{N-1} \frac{d^{N-1} y}{dt^{N-1}} + \cdots + b_1 \frac{dy}{dt} + b_0 y = 0. \quad (\text{F.3})$$

The exponential  $e^{st}$  (where  $s$  is a constant) has the property that  $d(e^{st})/dt = se^{st}$ ,  $d^2(e^{st})/dt^2 = s^2 e^{st}$ ,  $d^n(e^{st})/dt^n = s^n e^{st}$ . The function  $y = Ae^{st}$  satisfies Eq. F.3 for any value of  $A$  and certain values of  $s$ . The equation becomes

$$A(s^N e^{st} + b_{N-1} s^{N-1} e^{st} + \cdots + b_1 s e^{st} + b_0 e^{st}) = 0,$$

$$A(s^N + b_{N-1} s^{N-1} + \cdots + b_1 s + b_0) e^{st} = 0.$$

This equation is satisfied if the polynomial in parentheses is equal to zero. The equation

$$s^N + b_{N-1} s^{N-1} + \cdots + b_1 s + b_0 = 0 \quad (\text{F.4})$$

is called the *characteristic equation* of this differential equation. It can be written in a much more compact form using summation notation:

$$\sum_{n=0}^N b_n s^n = 0, \quad (\text{F.5})$$

with  $b_N = 1$ .

For Eq. F.1, the characteristic equation is  $s + b = 0$  or  $s = -b$ , and a solution to the homogeneous equation is  $y = Ae^{-bt}$ .

If the characteristic equation is a polynomial, it can have up to  $N$  roots. For each distinct root  $s_n$ ,  $y = A_n e^{s_n t}$  is a solution to the differential equation. (The question of solutions when there are not  $N$  distinct roots will be taken up below.) This is still not the solution to the equation we need to solve. However, one can prove<sup>1</sup> that the most general solution to the inhomogeneous equation consists of the homogeneous solution,

$$y = \sum_{n=1}^N A_n e^{s_n t},$$

plus *any* solution to the inhomogeneous equation. The values of the arbitrary constants  $A_n$  are picked to satisfy some other conditions that are imposed on the problem. If we can guess the solution to the inhomogeneous equation, that is fine. However we get it, we need only one such solution to the inhomogeneous equation. We will not prove this assertion, but we will apply it to the first- and second-order equations and see how it works.

---

<sup>1</sup>See, for example, G. B. Thomas. *Calculus and Analytic Geometry*, Reading, MA, Addison-Wesley (any edition).

### F.1 First-order Equation

The homogeneous equation corresponding to Eq. F.1 has solution  $y = Ae^{-bt}$ . There is one solution to the inhomogeneous equation that is particularly easy to write down: when  $y$  is constant, with the value  $y = a/b$ , the time derivative vanishes and the inhomogeneous equation is satisfied. The most general solution is therefore of the form

$$y = Ae^{-bt} + \frac{a}{b}.$$

If the initial condition is  $y(0) = 0$ , then  $A$  can be determined from  $0 = Ae^{-b0} + a/b$ . Since  $e^0 = 1$ , this gives  $A = -a/b$ . Therefore

$$y = \frac{a}{b} (1 - e^{-bt}). \tag{F.6}$$

A physical example of this is given in Sec. 2.7.

### F.2 Second-order Equation

The second-order equation

$$\frac{d^2y}{dt^2} + b_1 \frac{dy}{dt} + b_0y = 0 \tag{F.7}$$

has a characteristic equation  $s^2 + b_1s + b_0 = 0$  with roots

$$s = \frac{-b_1 \pm \sqrt{b_1^2 - 4b_0}}{2}. \tag{F.8}$$

This equation may have no, one, or two solutions.

If it has two solutions  $s_1$  and  $s_2$ , then the general solution of the homogeneous equation is  $y = A_1e^{s_1t} + A_2e^{s_2t}$ .

If  $b_1^2 - 4b_0$  is negative, there is no solution to the equation for a real value of  $s$ . However, a solution of the form  $y = Ae^{-\alpha t} \sin(\omega t + \phi)$  will satisfy the equation. This can be seen by direct substitution. Differentiating this twice shows that

$$\begin{aligned} \frac{dy}{dt} &= -\alpha Ae^{-\alpha t} \sin(\omega t + \phi) + \omega Ae^{-\alpha t} \cos(\omega t + \phi), \\ \frac{d^2y}{dt^2} &= \alpha^2 Ae^{-\alpha t} \sin(\omega t + \phi) - 2\alpha\omega Ae^{-\alpha t} \cos(\omega t + \phi) \\ &\quad - \omega^2 Ae^{-\alpha t} \sin(\omega t + \phi). \end{aligned}$$

If these derivatives are substituted in Eq. F.7, one gets the following results. The terms are written in two columns. One column contains the coefficients of terms with  $\sin(\omega t + \phi)$ , and the other column contains the coefficients of terms with  $\cos(\omega t + \phi)$ . The rows are labeled on the left by which term of the differential equation they came from.

Term	Coefficients	
	$\sin(\omega t + \phi)$	$\cos(\omega t + \phi)$
$d^2y/dt^2$	$\alpha^2 - \omega^2$	$-2\alpha\omega$
$b_1(dy/dt)$	$-b_1\alpha$	$b_1\omega$
$b_0y$	$b_0$	$0$

The only way that the equation can be satisfied for all times is if the coefficient of the  $\sin(\omega t + \phi)$  term and the coefficient of the  $\cos(\omega t + \phi)$  term separately are equal to zero. This means that we have two equations that must be satisfied (call  $b_0 = \omega_0^2$ ):

$$2\alpha\omega = b_1\omega,$$

$$\alpha^2 - \omega^2 - b_1\alpha + \omega_0^2 = 0.$$

From the first equation  $2\alpha = b_1$ , while from this and the second,  $\alpha^2 - \omega^2 - 2\alpha^2 + \omega_0^2 = 0$ , or  $\omega^2 = \omega_0^2 - \alpha^2$ . Thus, the solution to the equation

$$\frac{d^2y}{dt^2} + 2\alpha \frac{dy}{dt} + \omega_0^2 y = 0 \tag{F.9}$$

is

$$y = Ae^{-\alpha t} \sin(\omega t + \phi) \tag{F.10a}$$

where

$$\omega^2 = \omega_0^2 - \alpha^2, \quad \alpha < \omega_0. \tag{F.10b}$$

Solution F.10 is a decaying exponential multiplied by a sinusoidally varying term. The initial amplitude  $A$  and the phase angle  $\phi$  are arbitrary and are determined by other conditions in the problem. The constant  $\alpha$  is called the damping. Parameter  $\omega_0$  is the undamped frequency, the frequency of oscillation when  $\alpha = 0$ .  $\omega$  is the damped frequency.

When the damping becomes so large that  $\alpha = \omega_0$ , then the solution given above does not work. In that case, the solution is given by

$$y = (A + Bt)e^{-\alpha t}, \quad \alpha = \omega_0. \tag{F.11}$$

This case is called *critical damping* and represents the case in which  $y$  returns to zero most rapidly and without multiple oscillations. The solution can be verified by substitution.

If  $\alpha > \omega_0$ , then the solution is the sum of the two exponentials that satisfy Eq. F.8:

$$y = Ae^{-at} + Be^{-bt}, \tag{F.12a}$$

where

$$a = \alpha + \sqrt{\alpha^2 - \omega_0^2}, \tag{F.12b}$$

$$b = \alpha - \sqrt{\alpha^2 - \omega_0^2}. \tag{F.12c}$$

When  $\alpha = 0$ , the equation is

$$\frac{d^2y}{dt^2} + \omega_0^2 y = 0. \tag{F.13}$$

The solution may be written either as

$$y = C \sin(\omega_0 t + \phi) \tag{F.14a}$$

or as

$$y = A \cos(\omega_0 t) + B \sin(\omega_0 t). \tag{F.14b}$$

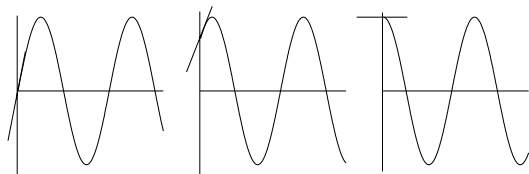


FIGURE F.1. Different starting points on the sine wave give different combinations of the initial position and the initial velocity.

The simplest physical example of this equation is a mass on a spring. There will be an equilibrium position of the mass ( $y = 0$ ) at which there is no net force on the mass. If the mass is displaced toward either positive or negative  $y$ , a force back toward the origin results. The force is proportional to the displacement and is given by  $F = -ky$ . The proportionality constant  $k$  is called the spring constant. Newton's second law,  $F = ma$ , is  $m(d^2y/dt^2) = -ky$  or, defining  $\omega_0^2 = k/m$ ,

$$\frac{d^2y}{dt^2} + \omega_0^2 y = 0.$$

This (as well as the equation with  $\alpha \neq 0$ ) is a second-order differential equation. Integrating it twice introduces two constants of integration:  $C$  and  $\phi$ , or  $A$  and  $B$ . They are usually found from two initial conditions. For the mass on the spring, they are often the initial velocity and initial position of the mass.

The equivalence of the two solutions can be demonstrated by using Eqs. F.14a and a trigonometric identity to write  $C \sin(\omega_0 t + \phi) = C[\sin \omega_0 t \cos \phi + \cos \omega_0 t \sin \phi]$ . Comparison with Eq. F.14b shows that  $B = C \cos \phi$ ,  $A = C \sin \phi$ . Squaring and adding these gives  $C^2 = A^2 + B^2$ , while dividing one by the other shows that  $\tan \phi = A/B$ .

Changing the initial phase angle changes the relative values of the initial position and velocity. This can be seen from the three plots of Fig. F.1, which show phase angles  $0$ ,  $\pi/4$ , and  $\pi/2$ . When  $\phi = 0$ , the initial position is zero, while the initial velocity has its maximum value. When  $\phi = \pi/4$ , the initial position has a positive value, and so does the initial velocity. When  $\phi = \pi/2$  the initial position has its maximum value and the initial velocity is zero. The values of  $A$  and  $B$  are determined from the initial position and velocity. At  $t = 0$ , Eq. F.14b and its derivative give  $y(0) = A$ ,  $dy/dt(0) = \omega_0 B$ .

The term in the differential equation equal to  $2\alpha(dy/dt)$  corresponds to a drag force acting on the mass and damping the motion. Increasing the damping coefficient  $\alpha$  increases the rate at which the oscillatory behavior decays. Figure F.2 shows plots of  $y$  and  $dy/dt$  for different values of  $\alpha$ .

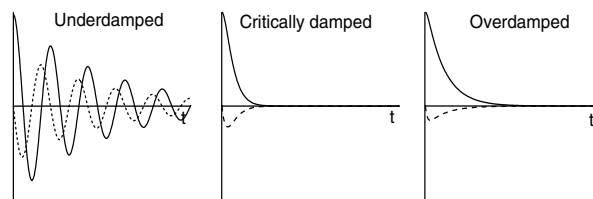


FIGURE F.2. Plot of  $y(t)$  (solid line) and  $dy/dt$  (dashed line) for different values of  $\alpha$ .

TABLE F.1. Solutions of the harmonic oscillator equation.

$\frac{d^2y}{dt^2} + 2\alpha \frac{dy}{dt} + \omega_0^2 y = 0$		
Case	Criterion	Solution
Underdamped	$\alpha < \omega_0$	$y = Ae^{-\alpha t} \sin(\omega t + \phi)$ $\omega^2 = \omega_0^2 - \alpha^2$
Critically damped	$\alpha = \omega_0$	$y = (A + Bt)e^{-\alpha t}$
Overdamped	$\alpha > \omega_0$	$y = Ae^{-at} + Be^{-bt}$ $a = \alpha + (\alpha^2 - \omega_0^2)^{1/2}$ $b = \alpha - (\alpha^2 - \omega_0^2)^{1/2}$

The second-order equation we have just studied is called the *harmonic oscillator* equation. Its solution is needed in Chap. 8 and is summarized in Table F.1.

## Problems

**Problem 1** From Eq. F.14 with  $\omega_0 = 10$ , find  $A$ ,  $B$ ,  $C$ , and  $\phi$  for the following cases:

- (a)  $y(0) = 5$ ,  $(dy/dt)(0) = 0$ .
- (b)  $y(0) = 5$ ,  $(dy/dt)(0) = 5$ .
- (c)  $y(0) = 0$ ,  $(dy/dt)(0) = 50$ .

(d) What values of  $A$ ,  $B$ , and  $C$  would be needed to have the same  $\phi$  as in case (b) and the same amplitude as in case (a)?

**Problem 2** Verify Eq. F.11 in the critically damped case.

**Problem 3** Find the general solution of the equation

$$\frac{d^2y}{dt^2} + 2\alpha \frac{dy}{dt} + \omega_0^2 y = \begin{cases} 0, & t \leq 0 \\ \omega_0^2 y_0, & t \geq 0 \end{cases}$$

subject to the initial conditions  $y(0) = 0$ ,  $(dy/dt)(0) = 0$

- (a) for critical damping,  $\alpha = \omega_0$ ,
- (b) for no damping, and
- (c) for overdamping,  $\alpha = 2\omega_0$ .

# Appendix G

## The Mean and Standard Deviation

TABLE G.1. Quiz scores.

Student No.	Score	Student No.	Score
1	80	16	71
2	68	17	83
3	90	18	88
4	72	19	75
5	65	20	69
6	81	21	50
7	85	22	81
8	93	23	94
9	76	24	73
10	86	25	79
11	80	26	82
12	88	27	78
13	81	28	84
14	72	29	74
15	67	30	70

In many measurements in physics or biology there may be several possible outcomes to the measurement. Different values are obtained when the measurement is repeated. For example, the measurement might be the number of red cells in a certain small volume of blood, whether a person is right-handed or left-handed, the number of radioactive disintegrations of a certain sample during a 5-min interval, or the scores on a test.

Table G.1 gives the scores on an examination administered to 30 people. These results are also plotted as a histogram in Fig. G.1.

The table and the histogram give all the information that there is to know about the experiment unless the result depends on some variable that was not recorded, such as the age of the student or where the student was sitting during the test.

In many cases the frequency distribution gives more information than we need. It is convenient to invent some quantities that will answer the questions: Around what values do the results cluster? How wide is the distribution of results? Many different quantities have been invented for answering these questions. Some are easier to calculate or have more useful properties than others.

The *mean* or *average* shows where the distribution is centered. It is familiar to everyone: add up all the scores and divide by the number of students. For the data given above the mean is  $\bar{x} = 77.8$ .

It is often convenient to group the data by the value obtained, along with the frequency of that value. The data of Table G.1, are grouped this way in Table G.2. The mean is calculated as

$$\bar{x} = \frac{1}{N} \sum_i f_i x_i = \frac{\sum_i f_i x_i}{\sum_i f_i},$$

where the sum is over the different values of the test scores that occur. For the example in Table G.2, the sums are  $\sum_i f_i = 30$ ,  $\sum_i f_i x_i = 2335$ , so  $\bar{x} = 2335/30 = 77.8$ . If a large number of trials are made,  $f_i/N$  can be called the

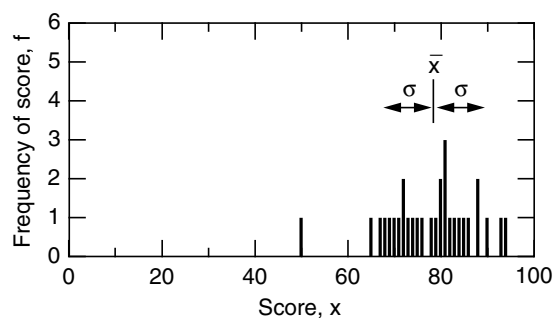


FIGURE G.1. Histogram of the quiz scores in Table G.1

TABLE G.2. Quiz scores grouped by score

Score number $i$	Score $x_i$	Frequency of score, $f_i$	$f_i x_i$
1	50	1	50
2	65	1	65
3	67	1	67
4	68	1	68
5	69	1	69
6	70	1	70
7	71	1	71
8	72	2	144
9	73	1	73
10	74	1	74
11	75	1	75
12	76	1	76
13	78	1	78
14	79	1	79
15	80	2	160
16	81	3	243
17	82	1	82
18	83	1	83
19	84	1	84
20	85	1	85
21	86	1	86
22	88	2	176
23	90	1	90
24	93	1	93
25	94	1	94

probability  $p_i$  of getting result  $x_i$ . Then

$$\bar{x} = \sum_i x_i p_i. \quad (\text{G.1})$$

Note that  $\sum p_i = 1$ .

The average of some function of  $x$  is

$$\overline{g(x)} = \sum_i g(x_i) p_i. \quad (\text{G.2})$$

For example,

$$\overline{x^2} = \sum_i (x_i)^2 p_i.$$

The width of the distribution is often characterized by the *dispersion* or *variance*:

$$\overline{(\Delta x)^2} = \overline{(x - \bar{x})^2} = \sum_i p_i (x_i - \bar{x})^2. \quad (\text{G.3})$$

This is also sometimes called the mean square variation: the mean of the square of the variation of  $x$  from the mean. A measure of the width is the square root of this, which is called the *standard deviation*  $\sigma$ . The need for taking the square root is easy to see since  $x$  may have units associated with it. If  $x$  is in meters, then the variance has the units of square meters. The width of the distribution in  $x$  must be in meters.

A very useful result is

$$\overline{(x - \bar{x})^2} = \overline{x^2} - \bar{x}^2.$$

To prove this, note that  $(x_i - \bar{x})^2 = x_i^2 - 2x_i \bar{x} + \bar{x}^2$ . The variance is then

$$\overline{(\Delta x)^2} = \sum_i p_i x_i^2 - 2 \sum_i x_i \bar{x} p_i + \sum_i p_i \bar{x}^2.$$

The first sum is the definition of  $\overline{x^2}$ . The second sum has a number  $\bar{x}$  in every term. It can be factored in front of the sum, to make the second term  $-2\bar{x} \sum_i x_i p_i$ , which is just  $-2(\bar{x})^2$ . The last term is  $(\bar{x})^2 \sum_i p_i = (\bar{x})^2$ . Combining all three sums gives Eq. G.4. In summary,

$$\sigma = \sqrt{\overline{(\Delta x)^2}}, \quad (\text{G.4})$$

$$\sigma^2 = \overline{(\Delta x)^2} = \overline{(x - \bar{x})^2} = \overline{x^2} - \bar{x}^2.$$

This equation is true as long as the  $p_i$ 's are accurately known. If the  $p_i$ 's have only been estimated from  $N$  experimental observations, the best estimate of  $\sigma^2$  is  $N/(N-1)$  times the value calculated from Eq. G.4.

For the data of Fig. G.1,  $\sigma = 9.4$ . This width is shown along with the mean at the top of the figure.

## Problems

**Problem 1** Calculate the variance and standard deviation for the data in Table G.2.

# Appendix H

## The Binomial Probability Distribution

Consider an experiment with two mutually exclusive outcomes that is repeated  $N$  times, with each repetition being independent of every other. One of the outcomes is labeled “success”; the other is called “failure.” The experiment could be throwing a die with success being a three, flipping a coin with success being a head, or placing a particle in a box with success being that the particle is located in a subvolume  $v$ .

In a single try, call the probability of success  $p$  and the probability of failure  $q$ . Since one outcome must occur and both cannot occur at the same time,

$$p + q = 1. \quad (\text{H.1})$$

Suppose that the experiment is repeated  $N$  times. The probability of  $n$  successes out of  $N$  tries is given by the *binomial probability distribution*, which is stated here without proof.<sup>1</sup> We can call the probability  $P(n; N)$ , since it is a function of  $n$  and depends on the parameter  $N$ . Strictly speaking, it depends on two parameters,  $N$  and  $p$ :  $P(n; N, p)$ . It is<sup>2</sup>

$$P(n; N) = P(n; N, p) = \left( \frac{N!}{n!(N-n)!} \right) p^n (1-p)^{N-n}. \quad (\text{H.2})$$

The factor  $N!/[n!(N-n)!]$  counts the number of different ways that one can get  $n$  successful outcomes; the probability of each of these ways is  $p^n(1-p)^{N-n}$ . In the example of three particles in Sec. 3.1, there are three ways to have one particle in the left-hand side. The particle can be either particle  $a$  or particle  $b$  or particle  $c$ . The factor

gives directly

$$\left( \frac{N!}{n!(N-n)!} \right) = \frac{3!}{1!2!} = \frac{3 \times 2 \times 1}{(1)(2 \times 1)} = \frac{6}{2} = 3.$$

The remaining factor,  $p^n(1-p)^{N-n}$ , is the probability of taking  $n$  tries in a row and having success and taking  $N-n$  tries in a row and having failure.

The binomial distribution applies if each “try” is independent of every other try. Such processes are called *Bernoulli processes* (and the binomial distribution is often called the Bernoulli distribution). In contrast, if the probability of an outcome depends on the results of the previous try, the random process is called a *Markov process*. Although such processes are important, they are more difficult to deal with and are not discussed here.

Some examples of the use of the binomial distribution are given in Chap. 3. As another example, consider the problem of performing several laboratory tests on a patient. In the 1970s it became common to use automated machines for blood-chemistry evaluations of patients; such machines automatically performed (and reported) 6, 12, 20, or more tests on one small sample of a patient’s blood serum, for less cost than doing just one or two of the tests. But this meant that the physician got a large number of results—many more than would have been asked for if the tests were done one at a time. When such test batteries were first done, physicians were surprised to find that patients had many more abnormal tests than they expected. This was in part because some tests were not known to be abnormal in certain diseases, because no one had ever looked at them in that disease. But there still was a problem that some tests were abnormal in patients who appeared to be perfectly healthy.

We can understand why by considering the following idealized situation. Suppose that we do  $N$  independent tests, and suppose that in healthy people, the probability that each test is abnormal is  $p$ . (In our vocabulary,

<sup>1</sup>A detailed proof can be found in many places. See, for example, F. Reif (1964). *Statistical Physics*. Berkeley Physics Course, Vol. 5, New York, McGraw-Hill, p. 67.

<sup>2</sup> $N!$  is  $N$  factorial and is  $N(N-1)(N-2)\cdots 1$ . By definition,  $0! = 1$ .

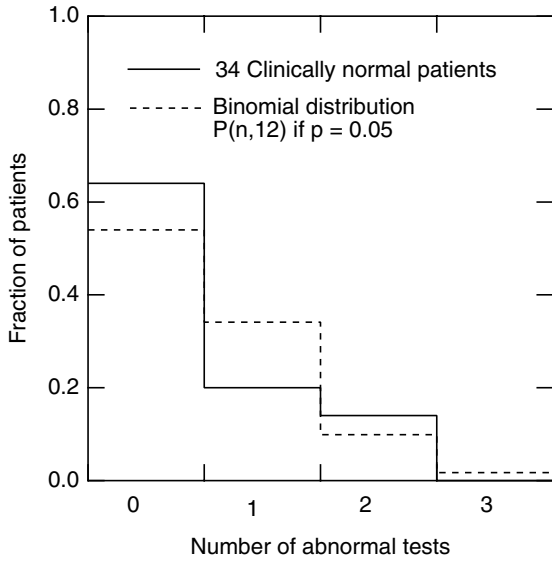


FIGURE H.1. Measurement of the probability that a clinically normal patient having a battery of 12 tests done has  $n$  abnormal tests (solid line) and a calculation based on the binomial distribution (dashed line). The calculation assumes that  $p = 0.05$  and that all 12 tests are independent. Several of the tests in this battery are not independent, but the general features are reproduced.

having an abnormal test is “success”!). The probability of not having the test abnormal is  $q = 1 - p$ . In a perfect test,  $p$  would be 0 for healthy people and would be 1 in sick people; however, very few tests are that discriminating. The definition of normal vs abnormal involves a compromise between false positives (abnormal test results in healthy people) and false negatives (normal test results in sick people). Good reviews of this problem have been written by Murphy and Abbey<sup>3</sup> and by Feinstein.<sup>4</sup> In many cases,  $p$  is about 0.05. Now suppose that  $p$  is the same for all the tests and that the tests are independent. Neither of these assumptions is very good, but they will show what the basic problem is. Then, the probability for all of the  $N$  tests to be normal in a healthy patient is given by the binomial probability distribution:

$$P(0; N, p) = \frac{N!}{0!N!} p^0 q^N = q^N.$$

If  $p = 0.05$ , then  $q = 0.95$ , and  $P(0; N, p) = 0.95^N$ . Typical values are  $P(0; 12) = 0.54$ , and  $P(0; 20) = 0.36$ . If the assumptions about  $p$  and independence are right, then only 36% of healthy patients will have all their tests normal if 20 tests are done.

Figure H.1 shows a plot of the number of patients in a series who were clinically normal but who had abnormal

tests. The data have the general features predicted by this simple model.

We can derive simple expressions to give the mean and standard deviation if the probability distribution is binomial. The mean value of  $n$  is defined to be

$$\bar{n} = \sum_{n=0}^N nP(n; N) = \sum_{n=0}^N \frac{N!n}{n!(N-n)!} p^n (1-p)^{N-n}.$$

The first term of each sum is for  $n = 0$ . Since each term is multiplied by  $n$ , the first term vanishes, and the limits of the sum can be rewritten as

$$\sum_{n=1}^N \frac{N!n}{n!(N-n)!} p^n (1-p)^{N-n}.$$

To evaluate this sum, we use a trick. Let  $m = n - 1$  and  $M = N - 1$ . Then we can rewrite various parts of this expression as follows:

$$\frac{n}{n!} = \frac{1}{(n-1)!} = \frac{1}{m!},$$

$$p^n = pp^m,$$

$$N! = (N)(N-1)!,$$

$$(N-n)! = [N-1-(n-1)]! = (M-m)!.$$

The limits of summation are  $n = 1$  or  $m = 0$ , and  $n = N$  or  $m = M$ . With these substitutions

$$\bar{n} = Np \sum_{m=0}^M \frac{M!}{m!(M-m)!} p^m (1-p)^{M-m}.$$

This sum is exactly the sum of a binomial distribution over all possible values of  $m$  and is equal to one. We have the result that, for a binomial distribution,

$$\bar{n} = Np. \tag{H.3}$$

This says that the average number of successes is the total number of tries times the probability of a success on each try. If 100 particles are placed in a box and we look at half the box so that  $p = \frac{1}{2}$ , the average number of particles in that half is  $100 \times \frac{1}{2} = 50$ . If we put 500 particles in the box and look at  $\frac{1}{10}$  of the box, the average number of particles in the volume is also 50. If we have 100 000 particles and  $v/V = p = 1/2000$ , the average number is still 50.

For the binomial distribution, the variance  $\sigma^2$  can be expressed in terms of  $N$  and  $p$  using Eq. G.4. The average of  $n^2$  is

$$\overline{n^2} = \sum_n P(n; N) n^2 = \sum_{n=0}^N \frac{N!}{n!(N-n)!} n^2 p^n (1-p)^{N-n}.$$

The trick to evaluate this is to write  $n^2 = n(n-1) + n$ . With this substitution we get two sums:

$$\begin{aligned} \overline{n^2} &= \sum_{n=0}^N \frac{N!}{n!(N-n)!} n(n-1) p^n q^{N-n} \\ &+ \sum_{n=0}^N \frac{N!n}{n!(N-n)!} p^n q^{N-n}. \end{aligned}$$

<sup>3</sup>E. A. Murphy and H. Abbey (1967). The normal range—a common misuse. *J. Chronic Dis.* **20**: 79.

<sup>4</sup>A. R. Feinstein (1975). Clinical biostatistics XXVII. The derangements of the normal range. *Clin. Pharmacol. Therap.* **15**: 528.

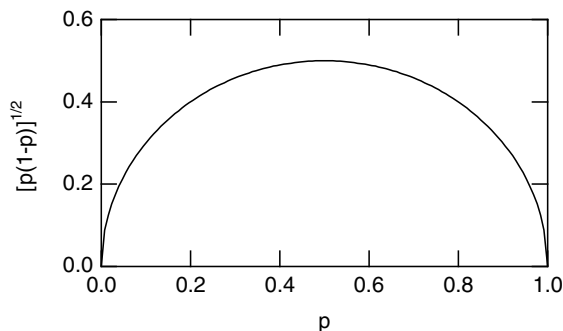


FIGURE H.2. Plot of  $[p(1 - p)]^{1/2}$ .

The second sum is  $\bar{n} = Np$ . The first sum is rewritten by noticing that the terms for  $n = 0$  and  $n = 1$  both vanish. Let  $m = n - 2$  and  $M = N - 2$ :

$$\begin{aligned} \overline{n^2} &= Np + N(N - 1) \sum_{m=0}^M \frac{M!}{m!(M - m)!} p^2 p^m q^{M-m} \\ &= Np + N(N - 1)p^2 = Np + N^2 p^2 - Np^2. \end{aligned}$$

Therefore,

$$(\Delta n)^2 = \overline{n^2} - \bar{n}^2 = Np - Np^2 = Np(1 - p) = Npq.$$

For the binomial distribution, then,

$$\sigma = \sqrt{Npq} = \sqrt{\bar{n}q}.$$

The standard deviation for the binomial distribution for fixed  $p$  goes as  $N^{1/2}$ . For fixed  $N$ , it is proportional to  $\sqrt{p(1 - p)}$ , which is plotted in Fig. H.2. The maximum value of  $\sigma$  occurs when  $p = q = \frac{1}{2}$ . If  $p$  is very small, the event happens rarely; if  $p$  is close to 1, the event nearly always happens. In either case, the variation is reduced. On the other hand, if  $N$  becomes large while  $p$  becomes small in such a way as to keep  $\bar{n}$  fixed, then  $\sigma$  increases to a maximum value of  $\sqrt{\bar{n}}$ . This variation of  $\sigma$  with  $N$  and  $p$  is demonstrated in Fig. H.3. Figures H.3(a)–H.3(c) show how  $\sigma$  changes as  $N$  is held fixed and  $p$  is varied. For  $N = 100$ ,  $p$  is 0.05, 0.5, and 0.95. Both the mean and  $\sigma$  change. Comparing Fig. H.3(b) with H.3(d) shows two different cases where  $\bar{n} = 50$ . When  $p$  is very small because  $N$  is very large in Fig. H.3(d),  $\sigma$  is larger than in Fig. H.3(b).

## Problems

**Problem 1** Calculate the probability of throwing 0, 1, . . . , 9 heads out of a total of nine throws of a coin.

**Problem 2** Assume that males and females are born with equal probability. What is the probability that a couple will have four children, all of whom are girls? The couple has had three girls. What is the probability that they will have a fourth girl? Why are these probabilities so different?

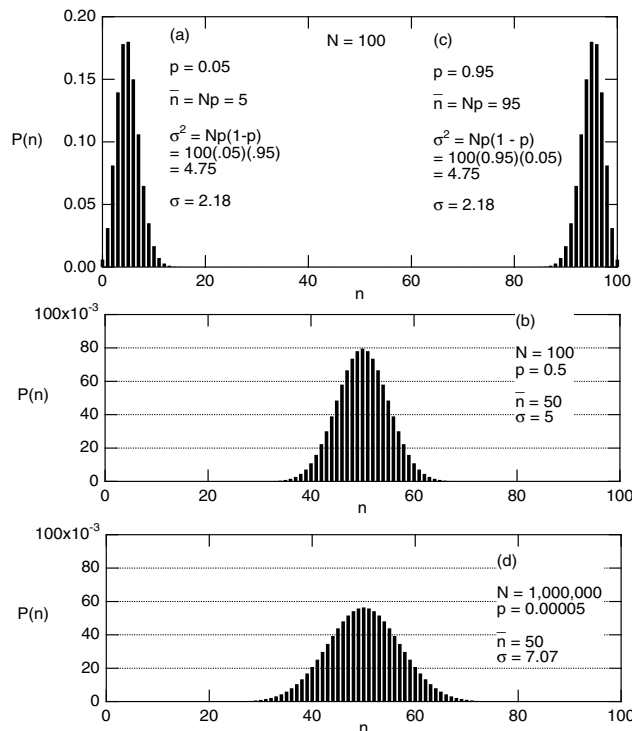


FIGURE H.3. Examples of the variation of  $\sigma$  with  $N$  and  $p$ . (a), (b), and (c) show variations of with  $p$  when  $N$  is held fixed. The maximum value of  $\sigma$  occurs when  $p = 0.5$ . Note that (a) and (c) are both in the top panel. Comparison of (b) and (d) shows the variation of  $\sigma$  as  $p$  and  $N$  change together in such a way that  $\bar{n}$  remains equal to 50.

**Problem 3** The Mayo Clinic reported that a single stool specimen in a patient known to have an intestinal parasite yields positive results only about 90% of the time [R. B. Thomson, R. A. Haas, and J. H. Thompson, Jr. (1984). *Intestinal parasites: The necessity of examining multiple stool specimens. Mayo Clin. Proc.* 59: 641–642]. What is the probability of a false negative if two specimens are examined? Three?

**Problem 4** The Minneapolis Tribune on October 31, 1974 listed the following incidence rates for cancer in the Twin Cities greater metropolitan area, which at that time had a total population of 1.4 million. These rates are compared to those in nine other areas of the country whose total population is 15 million. Assume that each study was for one year. Are the differences statistically significant? Show calculations to support your answer. How would your answer differ if the study were for several years?

Type of cancer	Incidence per 100 000 population per year	
	Twin Cities	Other
Colon	35.6	30.9
Lung (women)	34.2	40.0
Lung (men)	63.6	72.0
Breast (women)	81.3	73.8
Prostate (men)	69.9	60.8
Overall	313.8	300.0



**Problem 5** *The probability that a patient with cystic fibrosis gets a bad lung illness is 0.5% per day. With treatment, which is time consuming and not pleasant, the daily probability is ten times less.<sup>5</sup> Show that the probability of not having an illness in a year is 16% without treatment and 83% with treatment.*

---

<sup>5</sup>These numbers are from W. Warwick, MD, private communication. See also A. Gawande, The bell curve. *The New Yorker*, December 6, 2004, pp. 82–91.

# Appendix I

## The Gaussian Probability Distribution

Appendix H considered a process that had two mutually exclusive outcomes and was repeated  $N$  times, with the probability of “success” on one try being  $p$ . If each try is independent, then the probability of  $n$  occurrences of success in  $N$  tries is

$$P(n; N, p) = \frac{N!}{(n!)(N - n)!} p^n (1 - p)^{N - n}. \quad (\text{I.1})$$

This probability distribution depends on the two parameters  $N$  and  $p$ . We have seen two other parameters, the mean, which roughly locates the center of the distribution, and the standard deviation, which measures its width. These parameters,  $\bar{n}$  and  $\sigma$ , are related to  $N$  and  $p$  by the equations

$$\begin{aligned} \bar{n} &= Np, \\ \sigma^2 &= Np(1 - p). \end{aligned}$$

It is possible to write the binomial distribution formula in terms of the new parameters instead of  $N$  and  $p$ . At best, however, it is cumbersome, because of the need to evaluate so many factorial functions. We will now develop an approximation that is valid when  $N$  is large and which allows the probability to be calculated more easily.

The procedure is to take the log of the probability,  $y = \ln(P)$  and expand it in a Taylor’s series (Appendix D) about some point. Since there is a value of  $n$  for which  $P$  has a maximum and since the logarithmic function is monotonic,  $y$  has a maximum for the same value of  $n$ . We will expand about that point; call it  $n_0$ . Then the form of  $y$  is

$$y = y(n_0) + \left. \frac{dy}{dn} \right|_{n_0} (n - n_0) + \frac{1}{2} \left. \frac{d^2y}{dn^2} \right|_{n_0} (n - n_0)^2 + \dots$$

Since  $y$  is a maximum at  $n_0$ , the first derivative vanishes and it is necessary to keep the quadratic term in the expansion.

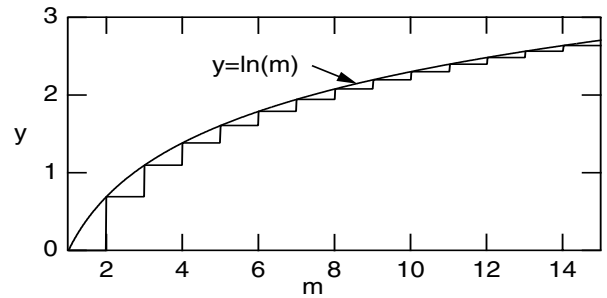


FIGURE I.1. Plot of  $y = \ln m$  used to derive Stirling’s approximation.

To take the logarithm of Eq. I.1, we need a way to handle the factorials. There is a very useful approximation to the factorial, called *Stirling’s approximation*:

$$\ln(n!) \approx n \ln n - n. \quad (\text{I.2})$$

To derive it, write  $\ln(n!)$  as

$$\ln(n!) = \ln 1 + \ln 2 + \dots + \ln n = \sum_{m=1}^n \ln m.$$

The sum is the same as the total area of the rectangles in Fig. I.1, where the height of each rectangle is  $\ln m$  and the width of the base is one. The area of all the rectangles is approximately the area under the smooth curve, which is a plot of  $\ln m$ . The area is approximately

$$\int_1^n \ln m \, dm = [m \ln m - m]_1^n = n \ln n - n + 1.$$

This completes the proof of Eq. (I.2). Table I.1 shows values of  $n!$  and Stirling’s approximation for various values of  $n$ . The approximation is not too bad for  $n > 100$ .

TABLE I.1. Accuracy of Stirling's approximation.

$n$	$n!$	$\ln(n!)$	$n \ln n - n$	Error	% Error
5	120	4.7875	3.047	1.74	36
10	$3.6 \times 10^6$	15.104	13.026	2.08	14
20	$2.4 \times 10^{18}$	42.336	39.915	2.42	6
100	$9.3 \times 10^{157}$	363.74	360.51	3.23	0.8

We can now return to the task of deriving the binomial distribution. Taking logarithms of Eq. I.1, we get

$$y = \ln P = \ln(N!) - \ln(n!) - \ln(N - n)! + n \ln p + (N - n) \ln(1 - p).$$

With Stirling's approximation, this becomes

$$y = N \ln N - n \ln n - N \ln(N - n) + n \ln(N - n) + n \ln p + (N - n) \ln(1 - p). \tag{I.3}$$

The derivative with respect to  $n$  is

$$\frac{dy}{dn} = -\ln n + \ln(N - n) + \ln p - \ln(1 - p).$$

The second derivative is

$$\frac{d^2y}{dn^2} = -\frac{1}{n} - \frac{1}{N - n}.$$

The point of expansion  $n_0$  is found by making the first derivative vanish:

$$0 = \ln \frac{(N - n_0)p}{n_0(1 - p)}.$$

Since  $\ln 1 = 0$ , this is equivalent to  $(N - n_0)p = n_0(1 - p)$  or  $n_0 = Np$ . The maximum of  $y$  occurs when  $n$  is equal to the mean. At  $n = n_0$  the value of the second derivative is

$$\frac{d^2y}{dn^2} = -\frac{1}{Np} - \frac{1}{N(1 - p)} = -\frac{1}{Np(1 - p)}.$$

It is still necessary to evaluate  $y_0 = y(n_0)$ . If we try to do this by substitution of  $n = n_0$  in Eq. I.3, we get zero. The reason is that the Stirling approximation we used is too crude for this purpose. (There are additional terms in Stirling's approximation that make it more accurate.) The easiest way to find  $y(n_0)$  is to call it  $y_0$  for now and determine it from the requirement that the probability be normalized. Therefore, we have

$$y = y_0 - \frac{1}{2Np(1 - p)}(n - Np)^2$$

so that, in this approximation,

$$P(n) = e^y = e^{y_0} e^{-(n - Np)^2/[2Np(1 - p)]}.$$

With  $Np = \bar{n}$ ,  $e^{y_0} = C_0$ , and  $Np(1 - p) = \sigma^2$ , this is

$$P(n) = C_0 e^{-(n - \bar{n})^2/2\sigma^2}.$$

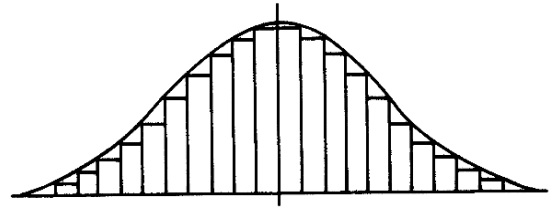


FIGURE I.2. Evaluating the normalization constant.

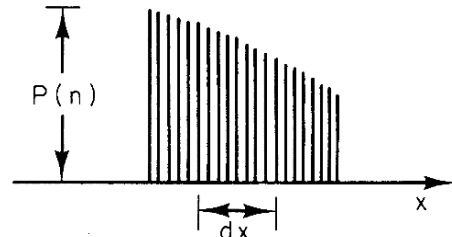


FIGURE I.3. The allowed values of  $x$  are closely spaced in this case.

To evaluate  $C_0$ , note that the sum of  $P(n)$  for all  $n$  is the area of all the rectangles in Fig. I.2. This area is approximately the area under the smooth curve, so that

$$1 = C_0 \int_{-\infty}^{\infty} e^{-(n - \bar{n})^2/2\sigma^2} dn.$$

It is shown in Appendix K that half of this integral is

$$\int_0^{\infty} dx e^{-bx^2} = \frac{1}{2} \sqrt{\frac{\pi}{b}}.$$

Therefore the normalization integral is (letting  $x = n - \bar{n}$ )

$$\int_{-\infty}^{\infty} e^{-x^2/2\sigma^2} dx = \sqrt{2\pi\sigma^2}.$$

The normalization constant is  $C_0 = 1/\sqrt{2\pi\sigma^2}$ , so that the Gaussian or normal probability distribution is

$$P(n) = \frac{1}{\sqrt{2\pi\sigma^2}} e^{-(n - \bar{n})^2/2\sigma^2}. \tag{I.4}$$

It is possible, as in the case of the random-walk problem, that the measured quantity  $x$  is proportional to  $n$  with a very small proportionality constant,  $x = kn$ , so that the values of  $x$  appear to form a continuum. As shown in Fig. I.3, the number of different values of  $n$  [each with about the same value of  $P(n)$ ] in the interval  $dx$  is proportional to  $dx$ . The easiest way to write down the Gaussian distribution in the continuous case is to recognize that the mean is  $\bar{x} = k\bar{n}$ , and the standard deviation is  $\sigma_x^2 = \overline{(x - \bar{x})^2} = \overline{x^2} - \bar{x}^2 = k^2\overline{n^2} - k^2\bar{n}^2 = k^2\sigma^2$ . The term  $P(x)dx$  is given by  $P(n)$  times the number of different values of  $n$  in  $dx$ . This number is  $dx/k$ .

Therefore,

$$\begin{aligned}
 P(x)dx &= P(n)\frac{dx}{k} = dx \frac{1}{k\sqrt{2\pi\sigma^2}} e^{-(x/k - \bar{x}/k)^2 / 2\sigma^2} \\
 &= dx \frac{1}{\sqrt{2\pi}\sigma_x} e^{-(x - \bar{x})^2 / 2\sigma_x^2}. \tag{I.5}
 \end{aligned}$$

To recapitulate: the binomial distribution in the case of large  $N$  can be approximated by Eq. I.4, the Gaussian or normal distribution, or Eq. I.5 for continuous variables. The original parameters  $N$  and  $p$  are replaced in these approximations by  $\bar{n}$  (or  $\bar{x}$ ) and  $\sigma$ .

# Appendix J

## The Poisson Distribution

Appendix H discussed the binomial probability distribution. If an experiment is repeated  $N$  times, and has two possible outcomes, with “success” occurring with probability  $p$  in each try, the probability of getting that outcome  $x$  times in  $N$  tries is

$$P(x; N, p) = \frac{N!}{x!(N-x)!} p^x (1-p)^{N-x}.$$

The distribution of possible values of  $x$  is characterized by a mean value  $\bar{x} = Np$  and a variance  $\sigma^2 = Np(1-p)$ . It is possible to specify  $\bar{x}$  and  $\sigma^2$  instead of  $N$  and  $p$  to define the distribution.

Appendix I showed that it is easier to work with the Gaussian or normal distribution when  $N$  is large. It is specified in terms of the parameters  $\bar{x}$  and  $\sigma^2$  instead of  $N$  and  $p$ :

$$P(x; \bar{x}, \sigma^2) = \frac{1}{(2\pi\sigma^2)^{1/2}} e^{-(x-\bar{x})^2/2\sigma^2}.$$

The *Poisson distribution* is an approximation to the binomial distribution that is valid for large  $N$  and for small  $p$  (when  $N$  gets large and  $p$  gets small in such a way that their product remains finite). To derive it, rewrite the binomial probability in terms of  $p = \bar{x}/N$ :

$$\begin{aligned} P(x) &= \frac{N!}{x!(N-x)!} (\bar{x}/N)^x (1-\bar{x}/N)^{N-x} \\ &= \frac{N!}{x!(N-x)!} \frac{1}{N^x} \bar{x}^x \left(1 - \frac{\bar{x}}{N}\right)^N \left(1 - \frac{\bar{x}}{N}\right)^{-x}. \end{aligned} \quad (\text{J.1})$$

It is necessary next to consider the behavior of some of these factors as  $N$  becomes very large. The factor  $(1 - \bar{x}/N)^N$  approaches  $e^{-\bar{x}}$  as  $N \rightarrow \infty$ , by definition (see p. 32). The factor  $N!/(N-x)!$  can be written out as

$$\frac{N(N-1)(N-2)\cdots 1}{(N-x)(N-x-1)\cdots 1} = N(N-1)(N-2)\cdots(N-x+1).$$

If these factors are multiplied out, the first term is  $N^x$ , followed by terms containing  $N^{x-1}$ ,  $N^{x-2}$ , ..., down to  $N^1$ . But there is also a factor  $N^x$  in the *denominator* of the expression for  $P$ , which, combined with this gives

$$1 + (\text{something})N^{-1} + (\text{something})N^{-2} + \cdots.$$

As long as  $N$  is very large, all terms but the first can be neglected. With these substitutions, Eq. J.1 takes the form

$$P(x) = \frac{1}{x!} \bar{x}^x e^{-\bar{x}} \left(1 - \frac{\bar{x}}{N}\right)^{-x}. \quad (\text{J.2})$$

The values of  $x$  for which  $P(x)$  is not zero are near  $\bar{x}$ , which is much less than  $N$ . Therefore, the last term, which is really  $[1/(1-p)]^x$ , can be approximated by one, while such a term raised to the  $N$ th power had to be approximated by  $e^{-x}$ . If this is difficult to understand, consider the following numerical example. Let  $N = 10\,000$  and  $p = 0.001$ , so  $\bar{x} = 10$ . The two terms we are considering are  $(1 - 10/10\,000)^{10\,000} = 4.517 \times 10^{-5}$ , which is approximated by  $e^{-10} = 4.54 \times 10^{-5}$ , and terms like  $(1 - 10/10\,000)^{-10} = 1.001$ , which is approximated by 1.

With these approximations, the probability is  $P(x) = [(\bar{x})^x/x!]e^{-\bar{x}}$  or, calling  $\bar{x} = m$ ,

$$P(x) = \frac{m^x}{x!} e^{-m}. \quad (\text{J.3})$$

This is the Poisson distribution and is an approximation to the binomial distribution for large  $N$  and small  $p$ , such that the mean  $\bar{x} = m = Np$  is defined (that is, it does not go to infinity or zero as  $N$  gets large and  $p$  gets small).

This probability, when summed over all values of  $x$ , should be unity. This is easily verified. Write

$$\sum_{x=0}^{\infty} P(x) = e^{-m} \sum_{x=0}^{\infty} \frac{m^x}{x!}.$$

TABLE J.1. Comparison of the binomial, Gaussian, and Poisson distributions.

Binomial	$P(x; N, p) = \frac{N!}{x!(N-x)!} p^x (1-p)^{N-x}$ $\bar{x} = m = Np$ $\sigma^2 = Np(1-p) = m(1-p)$
Gaussian	$P(x; m, \sigma) = \frac{1}{(2\pi\sigma^2)^{1/2}} e^{-(x-m)^2/2\sigma^2}$
Poisson	$P(x; m) = \frac{m^x}{x!} e^{-m}$ $m = Np$ $\sigma^2 = m$

But the sum on the right is the series for  $e^m$ , and  $e^{-m}e^m = 1$ . The same trick can be used to verify that the mean is  $m$ :

$$\sum_{x=0}^{\infty} xP(x) = \sum_{x=0}^{\infty} x \frac{m^x}{x!} e^{-m} = \sum_{x=1}^{\infty} x \frac{m^x}{x!} e^{-m}.$$

The index of summation can be changed from  $x$  to  $y = x - 1$ :

$$\sum_{x=0}^{\infty} xP(x) = \sum_{y=0}^{\infty} \frac{(y+1)}{(y+1)!} m^y m e^{-m} = m \sum_{y=0}^{\infty} \frac{m^y}{y!} e^{-m} = m.$$

One can show that the variance for the Poisson distribution is  $\sigma^2 = (x - m)^2 = m$ .

Table J.1 compares the binomial, Gaussian, and Poisson distributions. The principal difference between the binomial and Gaussian distributions is that the latter is valid for large  $N$  and is expressed in terms of the mean and standard deviation instead of  $N$  and  $p$ . Since the Poisson distribution is valid for very small  $p$ , there is only one parameter left, and  $\sigma^2 = m$  rather than  $m(1-p)$ .

The Poisson distribution can be used to answer questions like the following:

1. How many red cells are there in a small square in a hemocytometer? The number of cells  $N$  is large; the probability  $p$  of each cell falling in a particular square is small. The variable  $x$  is the number of cells per square.
2. How many gas molecules are found in a small volume of gas in a large container? The number of tries is each molecule in the larger box. The probability that an individual molecule is in the smaller volume is  $p = V/V_0$ , where  $V$  is the small volume and  $V_0$  is the volume of the entire box.
3. How many radioactive nuclei (or excited atoms) decay (or emit light) during a time  $dt$ ? The probability of decay during time  $dt$  is proportional to how long  $dt$  is:  $p = \lambda dt$ . The number of tries is the  $N$  nuclei that might decay during that time.

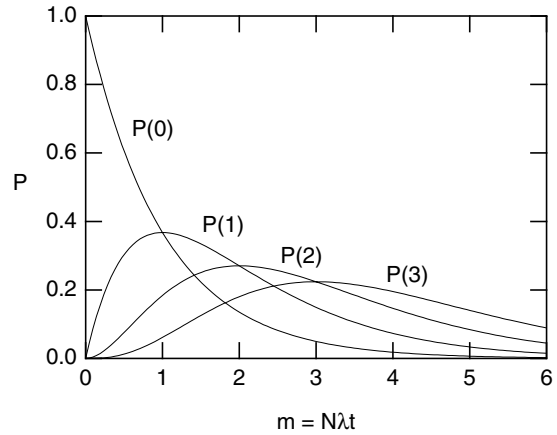


FIGURE J.1. Plot of  $P(0)$  through  $P(3)$  vs  $N\lambda t$ .

The last example is worth considering in greater detail. The probability  $p$  that each nucleus decays in time  $dt$  is proportional to the length of the time interval:  $p = \lambda dt$ . The average number of decays if many time intervals are examined is

$$m = Np = N\lambda dt.$$

The probability of  $x$  decays in time  $dt$  is

$$P(x) = \frac{(N\lambda dt)^x}{x!} e^{-N\lambda dt}.$$

As  $dt \rightarrow 0$ , the exponential approaches one, and

$$P(x) \rightarrow \frac{(N\lambda dt)^x}{x!}.$$

The overwhelming probability for  $dt \rightarrow 0$  is for there to be no decays:  $P(0) \approx (N\lambda dt)^0/0! = 1$ . The probability of a single decay is  $P(1) = N\lambda dt$ ; the probability of two decays during  $dt$  is  $(N\lambda dt)^2/2$ , and so forth.

If time interval  $t$  is finite, it is still possible for the Poisson criterion to be satisfied, as long as  $p = \lambda t$  is small. Then the probability of no decays is

$$P(0) = e^{-m} = e^{-N\lambda t}.$$

The probability of one decay is

$$P(1) = (N\lambda t)e^{-N\lambda t}.$$

This probability increases linearly with  $t$  at first and then decreases as the exponential term begins to decay. The reason for the lowered probability of one decay is that it is now more probable for two or more decays to take place in this longer time interval. As  $t$  increases, it is more probable that there are two decays than one or none; for still longer times, even more decays become more probable. The probability that  $n$  decays occur in time  $t$  is  $P(n)$ . Figure J.1 shows plots of  $P(0)$ ,  $P(1)$ ,  $P(2)$ , and  $P(3)$ , vs  $m = N\lambda t$ .

## Problems

**Problem 1** In the United States one year, 400 000 people were killed or injured in automobile accidents. The total population was 200 000 000. If the probability of being killed or injured is independent of time, what is the probability that you will escape unharmed from 70 years of driving?

**Problem 2** Large proteins consist of a number of smaller subunits that are stuck together. Suppose that an error is made in inserting an amino acid once in every  $10^5$  tries;  $p = 10^{-5}$ . If a chain has length 1000, what is the probability of making a chain with no mistakes? If the chain length is  $10^5$ ?

**Problem 3** The muscle end plate has an electrical response whenever the nerve connected to it is stimulated. I. A. Boyd and A. R. Martin [The end plate potential in mammalian muscle. *J. Physiol.* **132**: 74–91 (1956)]

found that the electrical response could be interpreted as resulting from the release of packets of acetylcholine by the nerve. In terms of this model, they obtained the following data:

Number of packets reaching the end plate	Number of times observed
0	18
1	44
2	55
3	36
4	25
5	12
6	5
7	2
8	1
9	0

Analyze these data in terms of a Poisson distribution.

# Appendix K

## Integrals Involving $e^{-ax^2}$

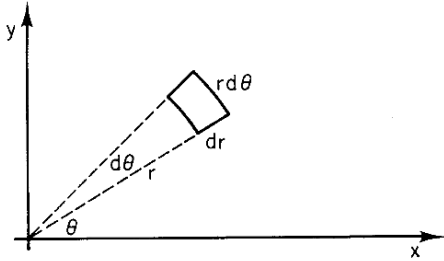


FIGURE K.1. An element of area in polar coordinates.

Integrals involving  $e^{-ax^2}$  appear in the Gaussian distribution. The integral

$$I = \int_{-\infty}^{\infty} e^{-ax^2} dx$$

can also be written with  $y$  as the dummy variable:

$$I = \int_{-\infty}^{\infty} e^{-ay^2} dy.$$

These can be multiplied together to get

$$I^2 = \int_{-\infty}^{\infty} \int_{-\infty}^{\infty} dx dy e^{-ax^2} e^{-ay^2} = \int_{-\infty}^{\infty} \int_{-\infty}^{\infty} dx dy e^{-a(x^2+y^2)}.$$

A point in the  $xy$  plane can also be specified by the polar coordinates  $r$  and  $\theta$  (Fig. K.1). The element of area  $dx dy$  is replaced by the element  $r dr d\theta$ :

$$I^2 = \int_0^{2\pi} d\theta \int_0^{\infty} r dr e^{-ar^2} = 2\pi \int_0^{\infty} r dr e^{-ar^2}.$$

To continue, make the substitution  $u = ar^2$ , so that  $du = 2ardr$ . Then

$$I^2 = 2\pi \int_0^{\infty} \frac{1}{2a} e^{-u} du = \frac{\pi}{a} [-e^{-u}]_0^{\infty} = \frac{\pi}{a}.$$

The desired integral is, therefore,

$$I = \int_{-\infty}^{\infty} e^{-ax^2} dx = \sqrt{\frac{\pi}{a}}. \quad (\text{K.1})$$

This integral is one of a general sequence of integrals of the general form

$$I_n = \int_0^{\infty} x^n e^{-ax^2} dx.$$

From Eq. K.1, we see that

$$I_0 = \frac{I}{2} = \frac{1}{2} \sqrt{\frac{\pi}{a}}. \quad (\text{K.2})$$

The next integral in the sequence can be integrated directly with the substitution  $u = ax^2$ :

$$I_1 = \int_0^{\infty} x e^{-ax^2} dx = \frac{1}{2a} \int_0^{\infty} e^{-u} du = \frac{1}{2a}. \quad (\text{K.3})$$

A value for  $I_2$  can be obtained by integrating by parts:

$$I_2 = \int_0^{\infty} x^2 e^{-ax^2} dx.$$

Let  $u = x$  and  $dv = x e^{-ax^2} dx = -(1/2a)d(e^{-ax^2})$ . Since  $\int u dv = uv - \int v du$ ,

$$\int_0^{\infty} x^3 e^{-ax^2} dx = -\frac{x e^{-ax^2}}{2a} + \frac{1}{2a} \int e^{-ax^2} dx.$$

This expression is evaluated at the limits 0 and  $\infty$ . The term  $x e^{-ax^2}$  vanishes at both limits. The second term is  $I_0/2a$ . Therefore,

$$I_2 = \frac{1}{2 \times 2a} \sqrt{\frac{\pi}{a}}.$$



This process can be repeated to get other integrals in the sequence. The even members build on  $I_0$ ; the odd members build on  $I_1$ . General expressions can be written. Note that  $2n$  and  $2n + 1$  are used below to assure even and odd exponents:

$$\int_0^\infty x^{2n} e^{-ax^2} dx = \frac{1 \times 3 \times 5 \times (2n-1)}{2^{n+1} a^n} \sqrt{\frac{\pi}{a}}, \quad (\text{K.4})$$

$$\int_0^\infty x^{2n+1} e^{-ax^2} dx = \frac{n!}{2a^{n+1}}, \quad (a > 0). \quad (\text{K.5})$$

The integrals in Appendix I are of the form

$$\int_{-\infty}^\infty e^{-x^2/2\sigma^2} dx.$$

This integral is  $2I_0$  with  $a = 1/(2\sigma^2)$ . Therefore, the integral is  $\sqrt{2\pi\sigma^2}$ .

Integrals of the form

$$J = \int_0^\infty x^n e^{-ax} dx,$$

can be transformed to the forms above with the substitution  $y = x^{1/2}$ ,  $x = y^2$ ,  $dx = 2y dy$ . Then

$$J = \int_0^\infty y^{2n} e^{-ay^2} 2y dy = 2 \int_0^\infty y^{2n+1} e^{-ay^2} dy.$$

Therefore

$$\int_0^\infty x^n e^{-ax} dx = \frac{n!}{a^{n+1}} = \frac{\Gamma(n+1)}{a^{n+1}}. \quad (\text{K.6})$$

The gamma function  $\Gamma(n) = (n-1)!$  if  $n$  is an integer. Unlike  $n!$ , it is also defined for noninteger values. Although we have not shown it, Eq. K.6 is correct for noninteger values of  $n$  as well, as long as  $a > 0$  and  $n > -1$ .

## Problems

**Problem 1** Use integration by parts to evaluate

$$I_3 = \int_0^\infty x^3 e^{-ax^2} dx.$$

Compare this result to Eq. K.5.

**Problem 2** Show that  $\int_{-\infty}^\infty x e^{-ax^2} dx = 0$ . Note the lower limit is  $-\infty$ , not 0. There is a hard way and an easy way to show this. Try to find the easy way.

# Appendix L

## Spherical and Cylindrical Coordinates

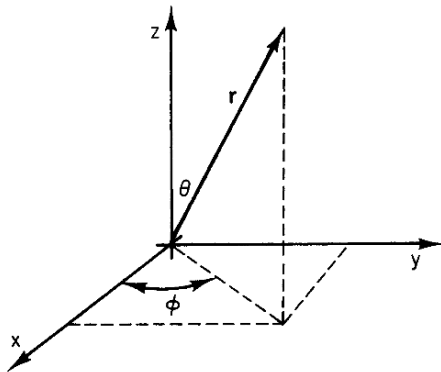


FIGURE L.1. Spherical coordinates.

It is possible to use coordinate systems other than the rectangular (or Cartesian)  $(x, y, z)$ : In spherical coordinates (Fig. L.1) the coordinates are radius  $r$  and angles  $\theta$  and  $\phi$ :

$$\begin{aligned} x &= r \sin \theta \cos \phi, \\ y &= r \sin \theta \sin \phi, \\ z &= r \cos \theta. \end{aligned} \quad (\text{L.1})$$

In Cartesian coordinates a volume element is defined by surfaces on which  $x$  is constant (at  $x$  and  $x + dx$ ),  $y$  is constant, and  $z$  is constant. The volume element is a cube with edges  $dx$ ,  $dy$ , and  $dz$ . In spherical coordinates, the cube has faces defined by surfaces of constant  $r$ , constant  $\theta$ , and constant  $\phi$  (Fig. L.2). A volume element is then

$$dV = (dr)(r d\theta)(r \sin \theta d\phi) = r^2 \sin \theta d\theta d\phi dr. \quad (\text{L.2})$$

To calculate the divergence of vector  $\mathbf{J}$ , resolve it into components  $\mathbf{J}_r$ ,  $\mathbf{J}_\theta$ , and  $\mathbf{J}_\phi$ , as shown in Fig. L.2. These components are parallel to the vectors defined by small displacements in the  $r$ ,  $\theta$ , and  $\phi$  directions. A detailed

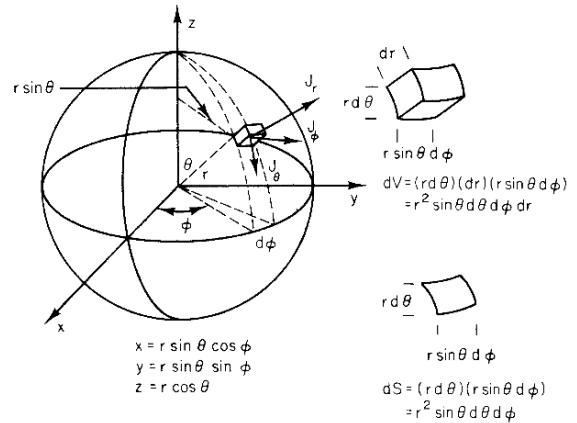


FIGURE L.2. The volume element and element of surface area in spherical coordinates.

calculation<sup>1</sup> shows that the divergence is

$$\begin{aligned} \text{div } \mathbf{J} = \nabla \cdot \mathbf{J} &= \frac{1}{r^2} \frac{\partial}{\partial r} (r^2 J_r) + \frac{1}{r \sin \theta} \frac{\partial}{\partial \theta} (\sin \theta J_\theta) \\ &+ \frac{1}{r \sin \theta} \frac{\partial}{\partial \phi} (J_\phi). \end{aligned} \quad (\text{L.3})$$

The gradient, which appears in the three-dimensional diffusion equation (Fick's first law), can also be written in spherical coordinates. The components are

$$\begin{aligned} (\nabla C)_r &= \frac{\partial C}{\partial r}, \\ (\nabla C)_\theta &= \frac{1}{r} \frac{\partial C}{\partial \theta}, \\ (\nabla C)_\phi &= \frac{1}{r \sin \theta} \frac{\partial C}{\partial \phi}. \end{aligned} \quad (\text{L.4})$$

<sup>1</sup>H. M. Schey (2005). *Div, Grad, Curl, and All That*. 4th. ed. New York, Norton.

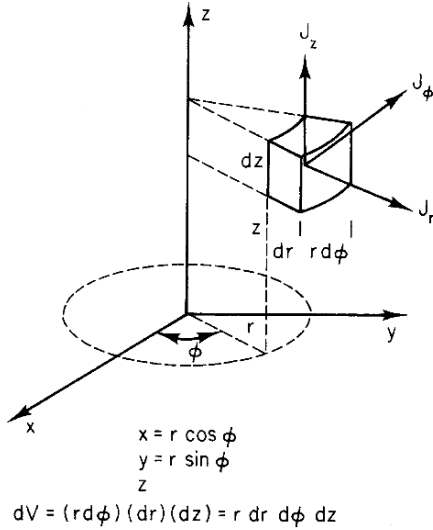


FIGURE L.3. A cylindrical coordinate system.

Figure L.2 also shows that the element of area on the surface of the sphere is  $(r d\theta)(r \sin \theta d\phi) = r^2 \sin \theta d\theta d\phi$ . The element of solid angle is therefore

$$d\Omega = \sin \theta d\theta d\phi.$$

This is easily integrated to show that the surface area of a sphere is  $4\pi r^2$  or that the solid angle is  $4\pi$  sr.

$$\begin{aligned} S &= r^2 \int_0^\pi \sin \theta d\theta \int_0^{2\pi} d\phi = 2\pi r^2 \int_0^\pi \sin \theta d\theta \\ &= 2\pi r^2 [-\cos \theta]_0^\pi = 4\pi r^2. \end{aligned}$$

Similar results can be written down in cylindrical coordinates  $(r, \phi, z)$ , shown in Fig. L.3.

Table L.1 shows the divergence, gradient and curl in rectangular, cylindrical, and spherical coordinates, along with the Laplacian operator  $\nabla^2$ .

TABLE L.1. The vector operators in rectangular, cylindrical and spherical coordinates.

Rectangular, $x, y, z$	Cylindrical $r, \phi, z$	Spherical $r, \theta, \phi$
Gradient		
$(\nabla C)_x = \frac{\partial C}{\partial x}$	$(\nabla C)_r = \frac{\partial C}{\partial r}$	$(\nabla C)_r = \frac{\partial C}{\partial r}$
$(\nabla C)_y = \frac{\partial C}{\partial y}$	$(\nabla C)_\phi = \frac{1}{r} \frac{\partial C}{\partial \phi}$	$(\nabla C)_\theta = \frac{1}{r} \frac{\partial C}{\partial \theta}$
$(\nabla C)_z = \frac{\partial C}{\partial z}$	$(\nabla C)_z = \frac{\partial C}{\partial z}$	$(\nabla C)_\phi = \frac{1}{r \sin \theta} \frac{\partial C}{\partial \phi}$
Laplacian		
$\nabla^2 C = \frac{\partial^2 C}{\partial x^2}$	$\nabla^2 C = \frac{1}{r} \frac{\partial}{\partial r} \left( r \frac{\partial C}{\partial r} \right)$	$\nabla^2 C = \frac{1}{r^2} \frac{\partial}{\partial r} \left( r^2 \frac{\partial C}{\partial r} \right)$
$+ \frac{\partial^2 C}{\partial y^2}$	$+ \frac{1}{r^2} \frac{\partial^2 C}{\partial \phi^2} + \frac{\partial^2 C}{\partial z^2}$	$+ \frac{1}{r^2 \sin \theta} \frac{\partial}{\partial \theta} \left( \sin \theta \frac{\partial C}{\partial \theta} \right)$
$+ \frac{\partial^2 C}{\partial z^2}$		$+ \frac{1}{r^2 \sin^2 \theta} \frac{\partial^2 C}{\partial \phi^2}$
Divergence		
$\nabla \cdot \mathbf{j} = \frac{\partial j_x}{\partial x}$	$\nabla \cdot \mathbf{j} = \frac{1}{r} \frac{\partial(rj_r)}{\partial r}$	$\nabla \cdot \mathbf{j} = \frac{1}{r^2} \frac{\partial(r^2 j_r)}{\partial r}$
$+ \frac{\partial j_y}{\partial y} + \frac{\partial j_z}{\partial z}$	$+ \frac{1}{r} \frac{\partial j_\phi}{\partial \phi} + \frac{\partial j_z}{\partial z}$	$+ \frac{1}{r \sin \theta} \frac{\partial(\sin \theta j_\theta)}{\partial \theta}$
		$+ \frac{1}{r \sin \theta} \frac{\partial j_\phi}{\partial \phi}$
Curl		
$(\nabla \times \mathbf{j})_x = \frac{\partial j_z}{\partial y}$	$(\nabla \times \mathbf{j})_r = \frac{1}{r} \frac{\partial j_z}{\partial \phi}$	$(\nabla \times \mathbf{j})_r = \frac{1}{r \sin \theta}$
$- \frac{\partial j_y}{\partial z}$	$- \frac{\partial j_\phi}{\partial z}$	$\times \left[ \frac{\partial(\sin \theta j_\phi)}{\partial \theta} - \frac{\partial(j_\theta)}{\partial \phi} \right]$
$(\nabla \times \mathbf{j})_y = \frac{\partial j_x}{\partial z}$	$(\nabla \times \mathbf{j})_\phi = \frac{\partial j_r}{\partial z}$	$(\nabla \times \mathbf{j})_\theta = \frac{1}{r \sin \theta}$
$- \frac{\partial j_z}{\partial x}$	$- \frac{\partial j_z}{\partial r}$	$\times \left[ \frac{\partial j_r}{\partial \phi} - \frac{\sin \theta \partial(rj_\phi)}{\partial r} \right]$
$(\nabla \times \mathbf{j})_z = \frac{\partial j_y}{\partial x}$	$(\nabla \times \mathbf{j})_z = \frac{1}{r} \frac{\partial(rj_\phi)}{\partial r}$	$(\nabla \times \mathbf{j})_\phi$
$- \frac{\partial j_x}{\partial y}$	$- \frac{1}{r} \frac{\partial j_r}{\partial \phi}$	$= \frac{1}{r} \left[ \frac{\partial(rj_\theta)}{\partial r} - \frac{\partial j_r}{\partial \theta} \right]$

# Appendix M

## Joint Probability Distributions

In both physics and medicine, the question often arises of what is the probability that  $x$  has a certain value  $x_i$  while  $y$  has the value  $y_j$ . This is called a *joint probability*. Joint probability can be extended to several variables. This appendix derives some properties of joint probabilities for discrete and continuous variables.

### M.1 Discrete Variables

Consider two variables. For simplicity assume that each can assume only two values. The first might be the patients health, with values *healthy* and *sick*; the other might be the results of some laboratory test, with results *normal* and *abnormal*. Table M.1 shows the values of the two variables for a sample of 100 patients. The joint probability that a patient is healthy *and* has a normal test result is  $P(x = 0, y = 0) = 0.6$ ; the probability that a patient is sick and has an abnormal test is  $P(1, 1) = 0.15$ . The probability of a false positive test is  $P(0, 1) = 0.20$ ; the probability of a false negative is  $P(1, 0) = 0.05$ .

The probability that a patient is healthy regardless of the test result is obtained by a summing over all possible test outcomes:  $P(x = 0) = P(0, 0) + P(0, 1) = 0.6 + 0.2 = 0.8$ .

In a more general case, we can call the joint probability  $P(x, y)$ , the probability that  $x$  has a certain value

TABLE M.1. The results of measurements on 100 patients showing whether they are healthy or sick and whether a laboratory test was normal or abnormal.

	Healthy ( $x = 0$ )	Sick ( $x = 1$ )
Normal test ( $y = 0$ )	60	5
Abnormal test ( $y = 1$ )	20	15

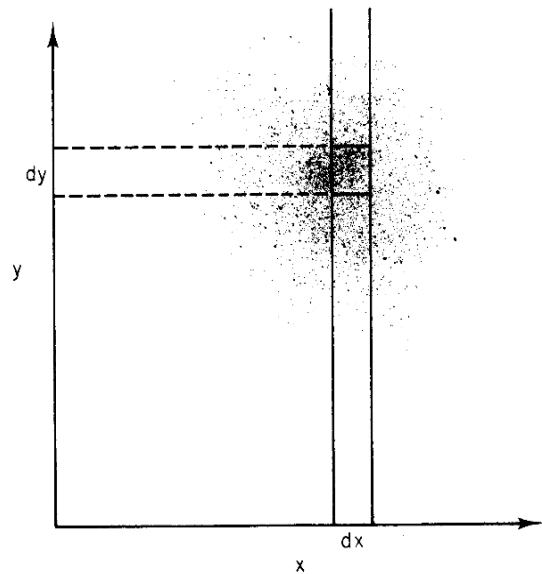


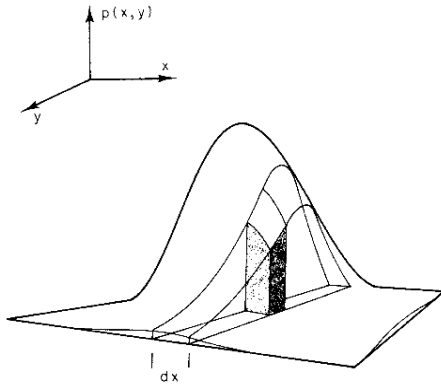
FIGURE M.1. The results of measuring two continuous variables simultaneously. Each experimental result is shown as a point.

independent of  $y$   $P_x(x)$ , and so forth. Then

$$\begin{aligned} P_x(x) &= \sum_y P(x, y) \\ P_y(y) &= \sum_x P(x, y). \end{aligned} \tag{M.1}$$

Since any measurement must give some value for  $x$  and  $y$ , we can write

$$\begin{aligned} 1 &= \sum_x P_x(x) = \sum_x \sum_y P(x, y), \\ 1 &= \sum_y P_y(y) = \sum_y \sum_x P(x, y). \end{aligned} \tag{M.2}$$

FIGURE M.2. Perspective drawing of  $p(x, y)$ .

## M.2 Continuous Variables

When a variable can take on a continuous range of values, it is quite unlikely that the variable will have *precisely* the value  $x$ . Instead, there is a probability that it is in the interval  $(x, dx)$ , meaning that it is between  $x$  and  $x + dx$ . For small values of  $dx$ , the probability that the value is in the interval is proportional to the width of the

interval. We will call it  $p_x(x)dx$ . The extension to joint probability in two dimensions is  $p(x, y)dxdy$ . This is the probability that  $x$  is in the interval  $(x, dx)$  and  $y$  is in the interval  $(y, dy)$ . Figure M.1 shows each outcome of a joint measurement as a dot in the  $xy$  plane. The probability that  $x$  is in  $(x, dx)$  regardless of the value of  $y$  is

$$p_x(x)dx = \left( \int p(x, y)dy \right) dx. \quad (\text{M.3})$$

It is proportional to the total number of dots in the vertical strip in Fig. M.1. Normalization requires that

$$1 = \int p_x(x)dx = \int dx \int dy p(x, y). \quad (\text{M.4})$$

The first strip could be taken horizontally:

$$1 = \int p_y(y)dy = \int dy \int dx p(x, y).$$

Figure M.2 shows a perspective drawing of  $p(x, y)$ . The volume of the shaded column is  $p(x, y)dxdy$ . The volume of the slice is  $p_x(x)dx$ . The entire volume under the surface is equal to one.

# Appendix N

## Partial Derivatives

When a function depends on several variables, we may want to know how the value of the function changes when one or more of the variables is changed. For example, the volume of a cylinder is

$$V = \pi r^2 h.$$

How does  $V$  change when  $r$  is changed while the height of the cylinder is kept fixed?

$$V(r + \Delta r) = \pi(r + \Delta r)^2 h = \pi(r^2 + 2r\Delta r + \Delta r^2)h.$$

Subtracting the original volume, we have

$$\Delta V = \pi(2r\Delta r + \Delta r^2)h.$$

In the limit of small  $\Delta r$ , this is

$$dV = 2\pi h r dr.$$

This is the same answer we would have gotten if  $h$  had been regarded as a constant. The *partial derivative* of  $V$  with respect to  $r$  is defined to be

$$\left(\frac{\partial V}{\partial r}\right)_h = \lim_{\Delta r \rightarrow 0} \left(\frac{V(r + \Delta r, h) - V(r, h)}{\Delta r}\right) = 2\pi r h.$$

The subscript  $h$  in the partial derivative symbol means that  $h$  is held fixed during the differentiation. Sometimes it is omitted; when it is not there, it is understood that all variables except the one following the  $\partial$  are held fixed.

If the cylinder radius is held fixed while the height is varied, we can write

$$\Delta V = V(r, h + \Delta h) - V(r, h) = \pi r^2 \Delta h.$$

The partial derivative is

$$\left(\frac{\partial V}{\partial h}\right)_r = \lim_{\Delta h \rightarrow 0} \left(\frac{V(r, h + \Delta h) - V(r, h)}{\Delta h}\right) = \pi r^2.$$

Suppose now that we allow small changes in both  $r$  and  $h$ . The difference in volume is

$$\Delta V = V(r + \Delta r, h + \Delta h) - V(r, h).$$

We can add and subtract the term  $V(r, h + \Delta h)$ :

$$\begin{aligned} \Delta V &= V(r + \Delta r, h + \Delta h) - V(r, h + \Delta h) \\ &\quad + V(r, h + \Delta h) - V(r, h) \\ &= \frac{V(r + \Delta r, h + \Delta h) - V(r, h + \Delta h)}{\Delta r} \Delta r \\ &\quad + \frac{V(r, h + \Delta h) - V(r, h)}{\Delta h} \Delta h. \end{aligned}$$

In the limit as  $\Delta r$  and  $\Delta h \rightarrow 0$ , the first term is

$$\left(\frac{\partial V}{\partial r}\right)_h \Delta r$$

evaluated at  $h + \Delta h$ . If the derivatives are continuous at  $(r, h)$ , the derivative evaluated at  $(r, h + \Delta h)$  is negligibly different from the derivative evaluated at  $(r, h)$ . Therefore, we can write

$$dV = \left(\frac{\partial V}{\partial r}\right)_h dr + \left(\frac{\partial V}{\partial h}\right)_r dh.$$

This result is true for several variables. For a function  $w(x, y, z)$

$$dw = \left(\frac{\partial w}{\partial x}\right)_{y,z} dx + \left(\frac{\partial w}{\partial y}\right)_{x,z} dy + \left(\frac{\partial w}{\partial z}\right)_{x,y} dz. \quad (\text{N.1})$$

The derivatives are evaluated as though the variables being held fixed were ordinary constants. If  $w = 3x^2yz^4$ ,

$$\left(\frac{\partial w}{\partial x}\right)_{y,z} = 6xyz^4,$$

$$\left(\frac{\partial w}{\partial y}\right)_{x,z} = 3x^2z^4,$$

$$\left(\frac{\partial w}{\partial z}\right)_{x,y} = 12x^2yz^3.$$

It is also possible to take higher derivatives, such as  $\partial^2 w/\partial x^2$  or  $\partial^2 w/\partial x\partial y$ . One important result is that the order of differentiation is unimportant, if the function, its first derivatives, and the derivatives in question are continuous at the point where they are evaluated. Without filling in all the details of a rigorous proof, we will simply note that

$$f = \frac{\partial w}{\partial x} = \lim_{\Delta x \rightarrow 0} \left( \frac{w(x + \Delta x, y) - w(x, y)}{\Delta x} \right)$$

$$g = \frac{\partial w}{\partial y} = \lim_{\Delta y \rightarrow 0} \left( \frac{w(x, y + \Delta y) - w(x, y)}{\Delta y} \right).$$

The mixed partials are

$$\begin{aligned} \frac{\partial^2 w}{\partial y \partial x} &= \frac{\partial f}{\partial y} = \lim_{\Delta y \rightarrow 0} \left( \frac{f(x, y + \Delta y) - f(x, y)}{\Delta y} \right) = \lim_{\substack{\Delta x \rightarrow 0 \\ \Delta y \rightarrow 0}} \\ &\times \left( \frac{w(x + \Delta x, y + \Delta y) - w(x, y + \Delta y) - w(x + \Delta x, y) + w(x, y)}{\Delta x \Delta y} \right) \end{aligned}$$

$$\begin{aligned} \frac{\partial^2 w}{\partial x \partial y} &= \frac{\partial g}{\partial x} = \lim_{\substack{\Delta y \rightarrow 0 \\ \Delta x \rightarrow 0}} \\ &\times \left( \frac{w(x + \Delta x, y + \Delta y) - w(x + \Delta x, y) - w(x, y + \Delta y) + w(x, y)}{\Delta x \Delta y} \right). \end{aligned}$$

The right side of each of these equations is the same, except for the order of the terms. Thus

$$\frac{\partial}{\partial x} \frac{\partial w}{\partial y} = \frac{\partial}{\partial y} \frac{\partial w}{\partial x}$$

## Problems

**Problem 1** If  $w = 12x^3y + z$ , find the three partial derivatives  $\partial w/\partial x$ ,  $\partial w/\partial y$ , and  $\partial w/\partial z$ .

**Problem 2** If  $V = xyz$  and  $x = 5$ ,  $y = 6$ ,  $z = 2$ , find  $dV$  when  $dx = 0.01$ ,  $dy = 0.02$ , and  $dz = 0.03$ . Make a geometrical interpretation of each term.

# Appendix O

## Some Fundamental Constants and Conversion Factors

The values of the fundamental constants are from the 2002 least-squares adjustment, available at [physics.nist.gov/PhysRefData/contents-constants.html](http://physics.nist.gov/PhysRefData/contents-constants.html).

Symbol	Constant	Value	SI units
$c$	Velocity of light in vacuum	$2.997\,925 \times 10^8$	$\text{m s}^{-1}$
$e$	Elementary charge	$1.602\,177 \times 10^{-19}$	C
$F$	Faraday constant	$9.648\,53 \times 10^4$	$\text{C mol}^{-1}$
$g$	Standard acceleration of free fall	9.806 65	$\text{m s}^{-2}$
$h$	Planck's constant	$6.626\,069 \times 10^{-34}$	J s
$\hbar$	Planck's constant (reduced)	$1.054\,572 \times 10^{-34}$	J s
$k_B$	Boltzmann's constant	$6.582\,119 \times 10^{-16}$ $1.380\,651 \times 10^{-23}$ $8.617\,343 \times 10^{-5}$	eV s J K <sup>-1</sup> eV K <sup>-1</sup>
$m_e$	Electron rest mass	$9.109\,382 \times 10^{-31}$	kg
$m_e c^2$	Electron rest energy	$8.187\,105 \times 10^{-14}$ $5.109\,99 \times 10^5$	J eV
$m_p$	Proton rest mass	$1.672\,622 \times 10^{-27}$	kg
$N_A$	Avogadro's number	$6.022\,142 \times 10^{23}$	$\text{mol}^{-1}$
$r_e$	Classical electron radius	$2.817\,940 \times 10^{-15}$	m
$R$	Gas constant	8.314 47	$\text{J mol}^{-1}$ K <sup>-1</sup>
$u$	Mass unit ( <sup>12</sup> C standard)	$1.660\,538 \times 10^{-27}$	kg
$u c^2$	Mass unit (energy units)	$9.314\,94 \times 10^8$	eV
$\epsilon_0$	Electrical permittivity of space	$8.854\,19 \times 10^{-12}$	$\text{C}^2 \text{N}^{-1}$ $\text{m}^{-2}$
$1/4\pi\epsilon_0$		$8.987\,55 \times 10^9$	$\text{N m}^2 \text{C}^{-2}$
$\sigma_{SB}$	Stefan Boltzmann constant	$5.670\,40 \times 10^{-8}$	$\text{W m}^{-2}$ K <sup>-4</sup>
$\lambda_C$	Compton wavelength of electron	$2.426\,31 \times 10^{-12}$	m
$\mu_B$	Bohr magneton	$9.274\,009 \times 10^{-24}$	J T <sup>-1</sup>
$\mu_0$	Magnetic permeability of space	$4\pi \times 10^{-7}$	T m A <sup>-1</sup>
$\mu_N$	Nuclear magneton	$5.050\,783 \times 10^{-27}$	J T <sup>-1</sup>

Some of the more useful conversion factors for converting from older units to SI units are listed. They are taken from *Standard for Metric Practice*, ASTM E 380-76, Copyright 1976 by the American Society for Testing and Materials, Philadelphia.

To convert from	To	Multiply by
angstrom	meter	$1.000\,000 \times 10^{-10}$
atmosphere (standard)	pascal	$1.013\,250 \times 10^5$
bar	pascal	$1.000\,000 \times 10^5$
barn	meter <sup>2</sup>	$1.000\,000 \times 10^{-28}$
calorie (thermochemical)	joule	4.184 000
centimeter of mercury (0 °C)	pascal	$1.333\,22 \times 10^3$
centimeter of water (4 °C)	pascal	$9.806\,38 \times 10^1$
centipoise	pascal second	$1.000\,000 \times 10^{-3}$
curie	becquerel	$3.700\,000 \times 10^{10}$
dyne	newton	$1.000\,000 \times 10^{-5}$
electron volt	joule	$1.602\,18 \times 10^{-19}$
erg	joule	$1.000\,000 \times 10^{-7}$
fermi (femtometer)	meter	$1.000\,000 \times 10^{-15}$
gauss	tesla	$1.000\,000 \times 10^{-4}$
liter	meter <sup>3</sup>	$1.000\,000 \times 10^{-3}$
mho	siemens	1.000 000
millimeter of mercury	pascal	$1.333\,22 \times 10^2$
poise	pascal second	$1.000\,000 \times 10^{-1}$
roentgen	coulomb per kilogram	$2.58 \times 10^{-4}$
torr	pascal	$1.333\,22 \times 10^2$



# Index

- A scan, 352
- AAPM, 383, 384, 397, 445, 500
- Abbey, H., 564
- Abductor muscle, 7
- Aberration
  - chromatic, 389
  - spherical, 389
- Ablation, 381
- Able, K. P., 217, 224
- Able, M. A., 217, 224
- Abramowitz, M., 199, 201, 250, 253, 338, 340
- Absolute temperature, 57
- Absorbed dose, 427
- Absorption coefficient, 365
- Absorption edge, 404
- Acceleration, 547
- Accommodation, 389
- Acetabulum, 7
- Acetylcholine, 104, 137, 185, 573
- ACHD, 376
- Achilles tendon, 6
- Acoustic impedance, 346
- Actinometry, 383
- Action potential, 135
  - foot, 174
  - Gaussian approximation, 182
  - propagating, 159
  - space-clamped, 158
- Activating function, 200
- Active transport, 497
- Activity, 76, 484, 489
  - cumulated, 488, 489
- Activity vector, 180
- Adair, R. K., 244, 247, 253, 317, 323
- Adenosine triphosphate (ATP), 3
- Adiabatic approximation, 416
- Adiabatic process, 54
- ADP, 67, 534
- Afterloading, 504
- Ahlen, S. P., 418, 420, 423, 434
- Aine, C., 225
- Air
  - acoustic impedance, 346
  - attenuation, 350
  - density and specific heat, 61
  - speed of sound, 345
- Alberts, B., 459
- Albumin, 129, 130
- Aldroubi, A., 542
- Algae, 217
- Aliasing, 294, 309
  - in an image, 331
- Allen, A. P., 47
- Allen, R. D., 103
- Allison, J., 542
- Allos, S. H., 225
- $\alpha$  particle, 424, 484, 505
- Alternans, 282
- Alveoli, 1, 19, 77, 104, 256
- American Association of Physicists in Medicine, *see* AAPM
- American Heart Association, 195
- Ampere, 145
- Ampere's law, 206, 213, 216
  - and Biot-Savart law, 220
- Amplitude attenuation coefficient, 350
- Ampullae of Lorenzini, 244, 252
- Anaplasia, 378
- Anderka, M., 293, 323
- Anderson, H. L., 357
- Anderson, J. R., 513
- Anesthetic, 163
- Angelakos, J. D., 175
- Angiography, 376, 453

- Angioplasty, 504  
 Angioscopy, 376  
 Angstrom, 3  
 Angular momentum, 516  
 Anisotropy, 191, 192  
 Annihilation radiation, 414, 488  
 Anode, 193  
 Anode break excitation, 173  
 Anomalous rectification, 251  
 Antineutrino, 486  
 Antiscatter grid, 450  
 Antonini, E., 76  
 Antzelevitch, C., 185, 201  
 Anumonwo, J. B., 165, 175  
 Aorta, 20, 456  
 Apoptosis, 458  
 Aquaspirillum magnetotacticum, 217  
 Aqueous, 388  
 Arai, S., 224  
 Armstrong, B. K., 380, 397  
 Arqueros, F., 425, 434, 494, 512  
 Arteriole, 20  
 Artificial insemination, 72  
 Artificial kidney, 120  
 Ascites, 116  
 Ashley, J. C., 435  
 Astigmatism, 389  
 Astumian, R. D., 244, 247, 252–254, 317–319, 323  
 Ataxia-tangliectasia, 461  
 Athens, J. W., 323  
 Atherosclerosis, 376  
 Atkins, P. W., 70, 79  
 Atmosphere, 43  
     pressure variation, 60, 75  
 Atmosphere (pressure unit), 14  
 Atomic deexcitation, 410  
 Atomic energy levels, 402  
 Atomic number, 482  
 Atoms per unit volume, 366  
 ATP, 67, 534  
 Atrioventricular node, *see see* AV node  
 Attenuation  
     of sound wave, 349  
     water, 350  
 Attenuation coefficient, 365  
     amplitude, 350  
     effective, 368  
     intensity, 350  
     linear, 409  
     mass, 409  
 Attenuator  
     ladder, 171  
 Attix, F. H., 407, 414, 420, 422, 426, 429, 430, 434,  
     440, 445, 467, 477  
 Attractor, 262, 269  
 Auditory evoked response, 308  
 Auger electron, 410, 425, 485, 500, 504  
     cascade, 411, 438  
 Augmented limb leads, 188  
 Austin-Seymour, M., 478  
 Autocorrelation function, 299, 522  
     of exponential pulse, 305  
     and energy spectrum, 305  
     and power spectrum, 301  
     of noise, 314  
     of sine wave, 300  
     of square wave, 300  
 AV node, 185, 194  
 Average, 561  
     ensemble, 52  
     time, 52  
 Average reference recording, 196, 201  
 Avogadro's number, 59, 85, 409  
     definition in SI units, 366  
 Axel, L., 526, 535, 542  
 Axelrod, D., 96, 108, 109  
 Axon, 2, 135  
     cable model, 149  
     electric field, 148  
     membrane capacitance, 149, 163  
     membrane capacitance and conductance, 150  
     membrane equivalent circuit, 155  
     membrane time constant, 150  
     myelinated, 136, 160  
     potassium gate, 157  
     potassium Nernst potential, 155  
     potential outside, 177  
     sodium conductance, 157  
     sodium gate, 158  
     sodium Nernst potential, 155  
     space-clamped, 154, 158  
     surface charge density, 149  
     unmyelinated, 136, 160  
     voltage-clamped, 154  
 Axoplasm, 136  
 Ayotte, P., 473, 477  
  
 B scan, 352, 356  
 Background  
     natural, 470  
 Backscatter  
     factor, 430  
 Backx, P. H., 202  
 Bacteria, 2  
     magnetotactic, 217, 222  
     orientation in a magnetic field, 223  
 Bacteriophage, 2  
 Badeer, H. S., 18, 29  
 Bainton, C. R., 261  
 Balduzzi, A., 398  
 Balloon angioplasty, 504  
 Bambynek, W., 411, 434  
 Banavar, J. R., 41, 47  
 Bank, R. A., 133

- Bar, 12  
 Barach, J. P., 212, 218, 221, 224  
 Barentsz, J., 542  
 Barium, 449  
 Barium fluorobromide, 446  
 Barker, A. T., 214, 224  
 Barkovich, A. J., 542  
 Barlow, H. B., 392, 397  
 Barn (unit), 404  
 Barnes, F. S., 244, 253  
 Barneston, R. StC., 399  
 Barold, S. S., 194, 201  
 Barr, G., 87, 108  
 Barr, R. C., 154, 160, 175  
 Barrett, H. H., 325, 333, 341  
 Barrett, J. N., 240  
 Barth, R. F., 467, 477  
 Bartlett, A. A., 39, 47, 274, 283  
 Basal cell, 378, 381  
 Basal cell carcinoma, 464  
 Basal cell carcinoma (BCC), 380, 381  
 Basal metabolic rate, 61  
 Base, 549  
 Basilar membrane, 349  
 Basin of attraction, 266  
 Bass, M., 397, 399  
 Basser, P. J., 104, 108, 130, 133, 537, 542  
 Bastian, J., 243, 253  
 Battocletti, J. H., 535, 542  
 Baum, M. J., 398  
 Baumgartner, C., 225  
 Baylor, D. A., 392, 399  
 Bazylnski, D. A., 217, 224  
 Beam hardening, 448  
 Bean, C. P., 87, 108, 123, 127, 128, 133  
 Beaurepaire, E., 399  
 Beck, R. E., 128, 133  
 Becker, D. V., 500  
 Becklund, O. A., 328, 341  
 Becquerel (unit), 472, 489  
 Bee, 217, 222  
 Beer's law, 365  
 Begon, M., 266, 283  
 BEIR, 471–473, 477, 505, 506, 512  
 Bell, C., 542  
 Bell, G. I., 313  
 Bellon, E. M., 224  
 Belousov–Zhabotinsky reaction, 275  
 Bender, M. A., 511  
 Benedek, G. B., 10, 29, 90, 91, 100, 108  
 Bennison, L. J., 44  
 Berg, H. C., 96, 108  
 Berg, M. J., 44, 47  
 Berger, M. J., 494, 512  
 Berggren, K-F., 434  
 Bergmanson, J. P. G., 381, 397  
 Berlinger, W. G., 47  
 Berne, B. J., 372, 397  
 Bernoulli equation, 18  
 Bernoulli process, 563  
 Bernstein, M. A., 532, 533, 542  
 Berry, E., 398, 399  
 Berson, A. S., 225  
 Bessel function, 250, 338, 340, 352  
   modified, 199  
 Beta decay, 484, 485  
   spectrum, 487  
 Bethe, H., 418  
 Bethe–Bloch formula, 420  
 Bevington, P. R., 289, 323  
 Beyer, R. T., 350, 357  
 Bianchi, A. M., 308, 310, 323  
 Bicudo, C. E. M., 224  
 Bidomain model, 191, 192, 195, 199, 221  
 Bieber, M. T., 107, 108  
 Biersack, J. P., 415, 418–423, 435  
 Bifocal lenses, 389  
 Bifurcation, 266  
   diagram, 270  
 Bilirubin, 377  
 Binding energy  
   electronic, 484  
   nuclear, 483  
   per nucleon, 483  
 Binomial probability distribution, 51, 101, 563  
 Bioheat equation, 382  
 Biot-Savart law, 206  
   and Ampere's law, 220  
   and magnetic field around an axon, 208  
   current in, 207  
 Bipolar electrode, 194  
 Birch, R., 439, 477  
 Bird, R. B., 90  
 Birds, 217  
 Birefringence, 371  
 Births, 321  
   spontaneous, 293, 294  
 Bishop, C. R., 323  
 Blackbody, 372  
 Blackbody radiation  
   and heat loss, 375  
   vs. frequency, 375  
   vs. wavelength, 373  
 Blackford, B., 225  
 Blackman, R. B., 295, 323  
 Blackman-Tukey method, 309  
 Blair, D. F., 96, 109  
 Blakemore, N., 217  
 Blakemore, R. P., 217, 224  
 Blank, M., 253, 254  
 Bloch equations, 519  
 Bloch, F., 418, 519  
 Blood flow  
   pulmonary artery, 296

- Blood pressure, 255  
 Blood-brain barrier, 116  
 Blount, W. P., 10  
 Blume, S., 376, 397  
 Boas, D. A., 398  
 Boccara, A. C., 399  
 Bockris, J. O'M., 234, 253  
 Bodenschatz, E., 283  
 Bohr, N., 418  
 Boice, J. D., 468, 477  
 BOLD (Blood Oxygen Level Dependent), 523, 536  
 Boltzmann factor, 54, 58–62, 85, 227, 372, 517  
 Boltzmann's constant, 57  
 Bone scan, 501  
 Boone, J. M., 414, 434  
 Borgstede, J. P., 542  
 Born charging energy, 144, 234  
 Born, C. G., 466  
 Boron neutron capture therapy (BNCT), 467  
 Borthakur, A., 254  
 Bostrom, R. G., 480  
 Bouma, B. E., 370, 397, 399  
 Boundary-element method, 191  
 Bourland, J. D., 193, 201, 202, 534, 542  
 Boyd, I. A., 573  
 Bracewell, R. N., 295, 323  
 Brachytherapy, 461, 467, 503  
   high-dose-rate, 504  
 Bradley, W. G., 542  
 Bradshaw, L. A., 225  
 Bradshaw, P., 23, 29  
 Bradycardia, 194  
 Bragg peak, 466, 477  
 Bragg rule, 422  
 Bragg-Gray relationship, 468  
 Bramson, M. A., 373, 397  
 Brandts, B., 225  
 Brauer, F., 225  
 Braun, T. J., 274, 283  
 Breathing  
   energy loss due to, 61  
 Bremsstrahlung, 413, 417, 437  
   energy fluence, 438  
 Bren, S. P. A., 245, 253  
 Brennan, J. N., 224  
 Brenner, D. J., 472, 477  
 Březina, V., 295  
 Březina, V., 294, 323  
 Briggs, E. A., 434  
 Brightness contrast, 451  
 Brill, A. B., 500  
 Brittenham, G. N., 217, 224  
 Broad, W. J., 455, 477  
 Broad-beam geometry, 408  
 Bronzino, J. D., 308, 310, 323  
 Brooks, A. L., 471, 478  
 Brooks, R. A., 455, 457, 478  
 Brown, B., 225  
 Brown, J. H., 42, 47, 79  
 Brown, J. H. U., 399  
 Brown, R., 85  
 Brown, R. T., 434  
 Brownian motion, 61, 85, 312  
 Bruglio, A., 398  
 Bub, G., 275, 283  
 Buchanan, J. W., 500, 513  
 Buchsbaum, D., 505, 512  
 Bucky, G., 450  
 Budd, T., 425, 434  
 Budinger, T. F., 488, 490, 491, 498, 513  
 Buffer  
   calcium, 104  
 Buildup factor, 429, 494  
 Buka, R.L., 380, 397  
 Bundle branch block, 189  
 Bundle of His, 185  
 Buoyancy, 14  
 Burch, W. M., 103  
 Burnes, J. E., 191, 202  
 Bush, D. A., 479  
 Bystander effect, 460, 500  
 Cable equation, 152  
   and ladder attenuator, 171  
 Cable model, 149  
 Cabral, J. M., 253  
 Cadene, M., 254  
 Calamante, F., 542  
 Calcaneus, 6  
 Calcium, 279  
   -induced calcium release, 105  
   diffusion, 105  
   waves, 105  
 Calland, C. H., 120, 133  
 Calore, E., 398  
 Calorie, 54, 75  
   dietary, *see* Kilocalorie  
 Calorimetry, 475  
 Cameron, J. R., 348, 349, 378, 397  
 Campbell, D. L., 185, 201  
 Cancer  
   prostate, 536  
 Cancer and power-line-frequency fields, 244  
 Candle (unit), 387  
 Capacitance, 143  
   concentric cylinders, 169  
   cylindrical membrane, 174  
   membrane, 163  
   resistance and diffusion, 165  
 Capillary, 2, 20, 104, 115  
 Capillary blockade, 497  
 Carbohydrate, 3  
<sup>11</sup>C, 502  
<sup>14</sup>C dating, 512

- Carbon dioxide
  - production, 256
  - regulation, 257, 259, 261
- Carbon monoxide, 74
- Carbonyl group, 240
- Carcinoma
  - basal cell, 380, 464
  - squamous cell, 380
- Cardiac arrest, 72
- Cardiac cell, 2
- Cardiac output, 21
- Carlsson, C. A., 434
- Carlsson, G. A., 407, 434
- Caro, C. G., 23, 29
- Carr–Purcell (CP) Sequence, 526
- Carr–Purcell–Meiboom–Gill (CPMG) Sequence, 527
- Carslaw, H. S., 91, 94, 100, 106, 108
- Carstensen, E. L., 245, 253
- Cartilage
  - articular, 130
- Casper, B. M., 68, 79
- Castelli, W. P., 47
- Catalyst, 74
- Catfish, 243
- Catheter, 376
- Cathode, 194
  - virtual, 194
    - “dog bone”, 196
- Cathode-ray tube, 203
- Cavitation, 353
- Cavity radiation, *see* Blackbody radiation
- Cebeci, T., 23, 29
- Cell
  - eukaryotic, 2
  - membrane, 3
  - producing or absorbing a substance, 96
  - prokaryotic, 2
  - size, 2
- Cell culture, 458
- Cell sorting, 223
- Cell survival
  - fractionation curve, 460
- Cella, L., 479
- Cellular automata, 275, 282
- Center of gravity, 3
- Center of mass, 362
- Central slice theorem, 331
- Centrifuge, 26, 75
- Cerebral cortex, 212
- Cerutti, S., 308, 310, 323
- Cesaro, S., 398
- Cesium iodide, 446
- Chait, B. T., 253, 254
- Chamberlain, J. M., 398, 399
- Chance, B., 367–369, 398, 399
- Chand, B., 435
- Chandler, W. K., 250, 253
- Chang, S-B. R., 225
- Chang, W., 398
- Channel
  - selectivity, 240
- Channels
  - calcium, 238
  - chloride, 238
  - delayed rectifier, 238
  - potassium, 238
  - sodium, 238
  - two-state model, 240
- Chaos, 316
  - deterministic, 264, 270
  - in heart cells, 276
- Chaotic behavior, 269
- Characteristic x rays, 438, 485
- Charcoal, activated, 44
- Charge
  - free and bound, 144
- Charge distribution
  - cylindrically symmetric, 139
  - line, 139
  - on cell membrane, 141
  - plane sheet, 139
  - point, 139
  - spherically symmetric, 139
- Charge screening, 403
- Charged-particle equilibrium, 428, 440
- Charman, W. N., 390, 397
- Charnov, E. L., 79
- Charra, B., 133
- Chavez, A. E., 414, 434
- Cheeseman, J., 380, 397
- Chemical dosimeter, 445
- Chemical potential, 62, 88, 114, 115
  - ideal gas, 62
  - solute, 62, 69
  - water, 69
- Chemical shift, 534, 541
  - images, 535
- Chemotaxis, 94, 96
- Chemotherapy, 42
- Chen, C. N., 542
- Chen, J., 254
- Chen, P.-S., 283
- Chen, W., 536, 542
- Cherry, S. R., 501, 502, 511, 513
- Cheyne–Stokes respiration, 274
- Chick embryo, 213
- Chick, W. L., 279
- Chien, A., 478
- Chileuitt, L., 542
- Chittka, L., 398
- Cho, Z. H., 335
- Cho, Z.-H., 331, 341, 455, 478, 527, 542
- Cholesterol
  - Raman spectrum, 372

- Christodolou, E., 478  
 Chromatic aberration, 389  
 Chromosome, 458, 459  
 Chronaxie, 171, 193  
 Chronic granulocytic leukemia, 275  
 Chung, S-H., 254  
 CIE, 379, 387  
 Cilia, 349  
 Circulation, 20, 278  
 Circulatory system, 20  
 Clark, J., 182, 183, 191, 199, 201, 209  
 Clark, J. W., 175  
 Clark, V. A., 36, 47  
 Clarke, G. D., 542  
 Clarke, J., 218, 224  
 Classical electron radius, 406, 419  
 Clausius-Clapeyron equation, 78  
 Clearance, 36, 278, 382  
 Clostridium, 146  
 Cloud chamber, 425  
 Cocco, C., 398  
 Cochlea, 349  
 Cochlear duct, 349  
 Cochlear implant, 192  
 Cochran, W. W., 217, 224  
 Coffey, J. L., 495, 513  
 Cohen, A., 309, 310, 323  
 Cohen, B. L., 472, 473, 478, 506  
 Cohen, D., 216, 224  
 Cohen, L., 478  
 Cohen, L. G., 214, 224, 225  
 Cohen, S. L., 253  
 Cohen, Y., 542  
 Coherence, 370  
 Coherent scattering, 403, 407  
 Cokelet, G. R., 133  
 Collagen, 130  
 Collective dose, 471  
 Collimator, 447  
     gamma camera, 501, 510, 511  
     multi-leaf, 464  
 Collision kerma, 440  
 Collision time, 86  
 Color blindness, 72  
 Colton, C. K., 133  
 Colyvan, M., 281, 283  
 Comer, M. B., 201  
 Commission Internationale de l'Eclairage, *see* CIE  
 Common bundle, 185  
 Compass  
     in birds, 217  
 Competitive binding assay, 481  
 Complex exponential, 291  
 Complex notation, 303  
 Complex numbers, 291  
 Compound interest, 32  
 Compound microscope, 396  
 Compounds and mixtures, 410  
 Compressibility, 15, 344  
 Compressive strength, 12  
 Compton scattering, 403, 405, 442  
     cross section, 406  
     differential cross section, 406  
 Compton wavelength, 405  
 Computed radiography, 450  
 Computed tomography  
     spiral, 455  
 Concentration  
     and potential difference, 228  
 Concentration work, 63  
 Conductance, 145  
 Conduction system, 185, 194  
 Conduction velocity  
     myelinated, 160, 162  
     unmyelinated, 160, 162  
 Conductivity  
     anisotropic, 191, 192  
     interior and exterior, 181  
     non-uniform, 191  
     tensor, 191  
 Conductor, 142  
 Cones (retinal), 387, 390  
 Conformal radiation therapy  
     three-dimensional, 465  
 Congestive heart failure, 35  
 Conjunctivitis, 381  
 Constant-field model, 235  
 Contact lens, 107, 381  
 Continuity equation, 82  
     differential form, 84  
     integral form, 83  
     with creation or destruction, 85  
 Continuous slowing down approximation, 423  
 Contrast  
     brightness, 451  
     exposure, 451  
     film, 441  
     noise brightness, 451  
     noise exposure, 451  
 Contrast agent, 448  
 Convection coefficient, 76  
 Conversion factors, 583  
 Convolution, 326, 327  
     theorem, 326, 328  
 Cook, G., 77, 79  
 Cook, G. J. R., 536, 542  
 Cooley, J. W., 295, 323  
 Coordinate system  
     rotating, 519  
<sup>64</sup>Cu, 44  
 Cormack, A. M., 455, 478  
 Cornea, 107, 381, 388  
 Cornsweet, T. N., 390, 397  
 Correlation function, 298

- Corry, B., 254  
 Cortisol, 321  
 Cosset, J. M., 478  
 Coster-Kronig transition, 411, 500  
 Cotton, P., 376, 397  
 Coulomb, 137  
 Coulomb's Law, 137  
 Countercurrent exchange  
   and heat loss, 132  
 Countercurrent transport, 121  
 Coupling medium, 355  
 Coursey, B. M., 505, 513  
 Covino, B. G., 163, 175  
 Cox, J. D., 464  
 Crank, J., 91, 100, 108  
 Crasemann, B., 434  
 Creatinine clearance test, 44  
 Cristy, M., 513  
 Critical damping, 558  
 Cromer, D. T., 434  
 Cross correlation  
   and signal averaging, 309  
 Cross product, 5  
 Cross section, 86, 365  
   differential, 366  
   energy transfer, 407  
   scattering, 366  
   total, 366  
 Cross-correlation function, 298  
 Crouzy, S. C., 243, 253  
 Crowder, S. W., 136, 175  
 Crowe, E., 488, 489, 494, 513  
 Crowell, J. W., 274, 284  
 Crues, J. V., 542  
 CSDA, 423  
 CT, 455  
 Cuevas, J. M., 502  
 Cuffin, B. N., 224  
 Cumulated activity, 488, 489  
 Cumulated mean activity per unit mass, 492  
 Curie (unit), 489  
 Curie temperature, 216  
 Curl, 213  
   in different coordinate systems, 578  
 Curran, P. F., 120, 133  
 Current  
   bound, 216  
   electric, 145  
   free, 216  
   total, 16  
   volume, 16, 81  
 Current density, 16  
   electric, 145  
 Current dipole, 179  
   electric and magnetic measurements compared,  
     210  
   in spherical conductor, 221  
 Current dipole moment, 180  
   of the heart, 186  
 Current source, 178  
   potential due to, 178  
 Cyclic GMP, 392  
 Cylindrical coordinates, 578  
 Cystic fibrosis, 566  
 Cytokinesis, 459  
  
 da Luz, L. C. Q. P., 489, 513  
 da Silva, F. C., 495, 513  
 Dainty, J. C., 452, 478  
 Dall'Amico, R., 398  
 Damage, *see* Radiation damage  
 Danish, E. H., 224  
 Dasari, R. R., 371, 398  
 Data  
   surrogate, 316, 317  
 Davidenko, J. M., 186, 201  
 Davidson, H., 399  
 Davis, L., 153, 175, 284  
 de Araujo, F. F., 217, 224  
 De Boer, J. F., 371, 397  
 De Kepper, P., 283  
 de la Rosette, J., 542  
 De Stefano, P., 398  
 Dead-time correction, 510  
 Death rate, 35, 38, 43  
 Debye, 168  
 Debye length, 230  
 Debye-Hückel model, 231  
 Decay  
   constant, 33  
   exponential, 33  
   Multiple paths, 37  
   rate, 33  
   variable, 35  
   with constant input, 38  
 Decibel, 311, 347  
 Declercq, E. R., 323  
 Deexcitation  
   atomic, 410  
 DeFelice, L. J., 242, 253, 307, 323  
 Deffeyes, K. S., 217, 224  
 Defibrillation, 72  
 Defibrillator, 192, 195  
 Degeneracy, 59  
 Degrees of freedom, 53, 55, 265  
 Del Fante, C., 398  
 Delaney, C., 332, 341  
 Delannoy, J., 536, 542  
 Delay-differential equation, 272, 275  
 Delayed rectifier channels, 238  
 Delmar, M., 184, 201  
 Delta function, 304  
 Delta rays, 424  
 Demand pacemaker, 200

- den Boer, J. A., 527, 533, 542
- Dendrites, 135  
in cerebral cortex, 212
- Denier van der Gon, J. J., 195
- Denk, W., 243, 253
- Dennis, S. S., 158, 165, 175
- Denny, E. W., 480
- Denny, M. W., 15, 29, 61, 75–77, 79, 107, 108, 345, 346, 350, 357, 394, 397
- Density  
current, 16  
optical, 441
- Density effect, 420, 422
- Density gradient separation, 26
- Density of states factor, 59
- Density-weighted image, 533
- Denyer, J. C., 175
- Deoxyribonucleic acid (DNA), 3, 24
- Department of Energy, 471
- Dephasing, 519, 523
- Depolarization, 136
- Depth of field, 390
- Derivative, partial, 57
- Dermis, 380
- Deserno, W. M., 542
- Detecting weak magnetic fields, 218
- Detective quantum efficiency (DQE), 452
- Detector  
thin-film transistor, 450
- Detriment, 468
- Deuteron, 484
- DeVita, V. T., 463, 478
- DeWerd, L. A., 446
- Dextrose, 130
- Di Diego, J. M., 201
- Diabetes, 312
- Dialysis, 116  
renal, 120
- Diamagnetism, 215, 216
- Diamantopoulos, L., 399
- Diastole, 20
- Diastolic interval, 282
- Diathermy, 350
- Diatomic molecule, 362
- DiChiro, G., 455, 457, 478
- Dickerson, R. H., 77, 79
- Dielectric, 143  
saturation, 233
- Dielectric constant, 144  
lipid, 144  
lipid bilayer, 163  
water, 144
- Diem, M., 372, 397
- Differential equation  
characteristic equation, 557  
homogeneous and inhomogeneous, 557  
linear, 557  
non-linear, 263  
second order, 558
- Diffey, B. L., 378–380, 397, 398
- Diffusion, 85, 119, 541  
and capacitance, 165  
and chemical reaction, 105  
and drift, 98  
and electrotonus, 171  
anisotropic, 104  
as random walk, 100  
between concentric spheres, 166  
between two spheres, 166  
circular disk, 166  
constant, 88  
in one dimension, 93  
in three dimensions, 93, 101  
in two dimensions, 93, 101  
of photons, 367  
of spins in MRI, 536  
self, 90  
sphere to infinity, 166  
tensor, 104, 537  
time-dependent, 368  
to a cell producing or absorbing a substance, 96  
to or from a disk, 94, 106  
to or from a spherical cell, 94  
trace (of tensor), 537, 541  
with a buffer, 105
- Diffusion constant  
and viscosity, 89  
determination of, 100  
effective, 105  
photon, 367  
vs. molecular weight, 90
- Diffusion equation, 91  
general solution, 99
- DiFrancesco, D., 165, 175
- Digital detector, 446  
storage phosphor, 446  
thin-film transistor, 446
- Digital subtraction angiography, 453
- Dillman, L. T., 485, 487–489, 498, 513
- Dimethylchlortetracycline, 379
- Dini, G., 398
- Diopter (unit), 389
- Dipole  
electric, 484  
energy in a magnetic field, 516  
magnetic, 484, 516
- Dipole moment  
electric, 168, 233
- Dirac, P. A. M., 304
- Direct radiography, 450
- Discrete Fourier transform, 291
- Disease, incidence and prevalence, 44
- Dispersion, 562
- Displacement, 3, 545



- Displacement current, 207
- Ditto, W. L., 276, 283, 284
- Diuresis, 117
- Divergence, 84
  - in different coordinate systems, 578
- Dixon, R. L., 523, 534, 542
- Dizon, A. E., 225
- DNA, 74, 459, 461, 500
- Dobson unit, 378
- Dog bone, 196
- Dogfish, 244
- Doi, K., 442, 451, 478, 479
- Donnan equilibrium, 227
- Doppler effect, 353, 370
- Dose
  - absorbed, 427
  - effective, 469
  - entrance, 441
  - equivalent, 468
  - exit, 441
- Dose equivalent, 468
- Dose factor, 489
- Dose fractions, 461
- Dose rate
  - in photochemistry, 395
- Dot product, 11
- Doubling time, 34
- Douglas, J. G., 467, 478
- Doyle, D. A., 239, 253
- Drift, 85
  - and diffusion, 98
- Driving force, 88, 90
- Driving pressure, 114, 118
- Droplet keratopathy, 381
- Drosophila melanogaster*, 239
- Drost, D. J., 542
- Dubois, A., 399
- Ducros, M. G., 397
- Duda, J., 542
- Duderstadt, J. J., 368, 398
- Duffy, H. S., 201
- Duncan, W., 467, 478
- Dunn, R. A., 225
- Durbin, R. P., 127, 128, 133
- Dye
  - voltage-sensitive, 196
- Dyer, A. G., 398
- Dynamical system, 265
- Dysplasia, 378
- e*, definition of, 33
- Eames, C. and R., 29
- Ear, 348
  - canal, 348
  - drum, 348
  - external, middle, inner, 348
  - inner, 243
  - mechanoreceptors, 243
  - ossicles, 348
  - sensitivity, 347
- Early-responding tissue, 461, 462
- Echo planar imaging (EPI), 532
- Eckerman, K. F., 489, 498, 513
- Eddy currents, 214
- Edema, 116
  - and osmotic pressure, 116
  - cerebral, 116, 129
  - pulmonary, 119
- Edge-spread function, 329
- Edwards, F. M., 477, 479
- EEG, 196, *see* Electroencephalogram
  - average reference recording, 196
- Effective dose, 469
- Eidelman, S., 486
- Einstein (unit), 393
- Einthoven's triangle, 188
- Eisberg, R., 216, 218, 224, 364, 483, 486, 487, 513
- Eisberg, R. M., 364
- Eisenman, G., 108
- Ejection fraction, 501
- Ekstrand, K. E., 542
- Elastography, 376
- Electric dipole moment, 233
- Electric displacement, 207
- Electric field
  - definition, 138
- Electrical potential, 141
- Electrical stimulation, 192
- Electrocardiogram, 177
  - and solid angle theorem, 198
  - leads, 187
  - left ventricular hypertrophy, 189
  - normal, 189
  - R-R interval, 199
  - right bundle branch block, 189
  - right ventricular hypertrophy, 189
- Electrode
  - anodal, 194, 200
  - cathodic, 194, 200
  - pacing, 194, 199
  - spherical, 170
- Electrode heating
  - during magnetic stimulation, 222
  - in a changing magnetic field, 222
- Electroencephalogram, 177, 196, 201, 212, 309
- Electromagnetic spectrum, 360
- Electromagnetic wave, 360
- Electromotive force, 214
- Electromyogram, 177, 192, 310
- Electron
  - Auger, 410
  - classical radius, 406
  - for radiation therapy, 465
  - rest energy, 407

- rest mass, 407
- Electron capture, 488
- Electron volt, 57, 144, 360
- Electroporation, 244
- Electrosurgery, 170
- Electrotonus, 153, 161
- Eller, M. S., 398
- Elliott, D. M., 27, 29
- Elliston, C. D., 472, 477
- Elson, H. R., 466
- Embedding, 316
  - dimension, 316
  - time lag, 316
- Emission
  - spontaneous and stimulated, 522
- Emissivity, 373, 375
  - of skin, 375
- Emmetropia, 389
- End-plate potential, 573
- Endocardial and epicardial membrane currents, 184
- Endoplasmic reticulum, 105
- Energy
  - equipartition theorem, 60
  - fluence, 382, 384, 385
  - fluence rate, 384, 385
  - imparted, 426, 427
  - ionization, 362, 403
  - kinetic, 10
  - lost and imparted, 423
  - radiant, 383
  - transferred, 426
    - net, 428
- Energy exchange, 56
- Energy level, 53
- Energy levels, 56, 361
  - atomic electron, 402
  - band, 372
  - hydrogen atom, 361
  - rotational, 363
  - splitting, 372
  - vibrational, 364
- Energy spectrum
  - of a pulse, 304
  - of exponential pulse, 305
- Energy-momentum relationship
  - relativistic, 405
- Engdahl, J. C., 501, 513
- Englehardt, R., 224
- Enquist, B. J., 47
- Ensemble, 50
- Ensemble and time averages, 56
- Ensemble average, 52
- Enthalpy, 68
- Entrainment, 266, 281
- Entropy, 58, 64
  - ideal gas, 76, 77
  - of mixing, 67
- Entry region, 22
- Enzyme, 74
- Eosinophilic granuloma, 503
- Epicardium, 191
- Epidemiological studies, 245
- Epidermis, 378
- Epiphysis, 7, 9, 501
- Epstein, A. E., 275, 276, 283
- Epstein, I. R., 283
- Equal anisotropy ratios, 192
- Equilibrium
  - approach to, 259
  - charged-particle, 428
    - transient, 429
  - diffusive, 62
  - in volume exchange, 63
  - particle, 62
  - radiation, 428
  - rotational, 4
  - thermal, 56, 62
  - translational, 3
- Equilibrium absorbed dose constant, 489, 494
- Equilibrium and steady state
  - distinction, 55
- Equilibrium constant, 67
- Equilibrium state, 52
- Equipartition of energy, 60, 61
- Equivalent dose, 468
- Ergodic hypothesis, 56
- Erhardt, J. C., 502
- Erne, S. N., 225
- Error
  - mean square, 286
- Error function, 100, 154, 171, 193, 199
- Erythema, 379, 395
- Erythrocyte, 2, 117
- Escape peak, 442
- Escherichia coli*, 2, 96
- Esenaliev, R. O., 371, 398
- Esselle, K. P., 214, 224
- Essenpreis, M., 398
- Ethanol, 44
- Eukaryotes, 2
- Eustachian tube, 348
- Evans, R. D., 438, 478, 486, 513
- Evans, S. J., 284
- Even function, 290
- Evoked response, 196, 212, 308
- Excess absolute risk, 470
- Excess relative risk, 470
- Excitable media, 282
  - waves in, 275
- Exit dose, 441
- Exitance, 384, 385
- Expectation value, 367
- Exponent, 549
- Exponential

- complex, 291
  - decay, 33
  - function, 32
  - growth, 31
- Exponentials, fitting, 38
- Exposure, 440
- Exposure contrast, 451
- Extensive variables, 64
- Exterior potential
  - and electrocardiogram, 180
  - and solid angle, 181
  - arbitrary pulse, 182
  - cardiac depolarization, 179
  - from action potential, 181
  - from depolarization, 180
  - general case far from axon, 183
  - nerve impulse, 179
  - ratio to interior, 180
- Extinction coefficient, 394
- Extracellular fluid, 136
- Extracorporeal photopheresis, 381
- Eye
  - emmetropic (normal), 389
  - human, 388
  - hypermetropic (farsighted), 389
  - insect, 387
  - myopic (near-sighted), 389
  - resolution, 390
  - under water, 397
- Factorial, 563
- Fainting, 194
- False negative, 564, 579
- False positive, 564, 579
- Far field, 352
- Faraci, M., 398
- Farad, 143
- Faraday constant, 60
- Faraday induction law, 213, 524
- Farmer, J., 369, 398
- Farr, P. M., 379, 398
- Farrell, D. E., 224
- Farrell, T. J., 398
- Fast Fourier Transform (FFT), 295, 321
- Fatt, I., 107, 108
- Fédération CECOS, 72
- Feedback
  - carbon dioxide regulation, 256
  - loop, 255
  - negative, 255
  - one time constant, 259
  - positive, 255
  - steady-state conditions, 256
  - summary, 273
  - time constant and fixed delay, 272
  - two time constants, 262
- Feinstein, A. R., 564
- Feld, M. S., 371, 398
- Feldman, E. S., 224
- Felmlee, J. P., 542
- Femur, 7
- Fenton, F. H., 284
- Ferrimagnetism, 216
- Ferromagnetism, 216
- Ferrous sulfate, 445
- Feynman's ratchet, 318
- Feynman, R., 318, 323
- Fibrillation
  - ventricular, 195
- Fibula, 6
- Fick tracer method, 103
- Fick's law, 88, 91, 99
- Fick's second law, 230, 367, 382
- Field
  - radiation treatment, 464
- Field of view, 329
- Film
  - as x-ray detector, 440
  - gamma, 441
  - graininess, 452
  - speed, 441
- Film-screen combination, 450
- Filtration
  - of x-rays, 446
- Filtration coefficient, 117
- Finite-element method, 191
- Fink, R. W., 434
- First law of thermodynamics, 53
- Fischer, R., 224
- Fish
  - breathing, 76
- Fish gills, 122
- Fisher, H. L., 495, 496, 513
- Fishman, H. M., 244, 252, 254
- Fishman, R. A., 116, 133
- Fission
  - nuclear, 484, 497
- Fit
  - linear, 287
  - polynomial, 287
- Fitzgerald, A. J., 372, 398, 399
- FitzHugh–Nagumo model, 281
- Fitzmaurice, M., 371, 398
- Fixed point
  - stable, 262
  - unstable, 262
- Flannery, B. P., 109, 202, 225, 323, 341
- Flotte, T., 398
- Flounder
  - ocean, 244
- Flow
  - laminar, 15
  - Poiseuille, 17
  - total, 16

- Flow (mathematical), one dimensional, 262  
 Flow effects (in MRI), 535  
 Flow rate, 81  
 Fluence  
   energy, 382, 412  
   particle, 81, 367, 412  
   photon, 367  
   volume, 81  
 Fluence rate, 81, 367  
   volume, 16, 117  
 Fluid  
   Newtonian, 15, 87  
 Fluorescein, 380  
 Fluorescence, 196, 364, 403, 410  
 Fluorescence yield, 411, 413, 492  
 $^{18}\text{F}$ , 488, 492, 502  
   fluorodeoxyglucose, 502  
 Fluoroscopy, 454  
   for fitting shoes, 475  
 Flux, 81  
   total, 16  
   volume, 81  
 Flux density, 81  
   volume, 16  
 Flux transporter (magnetic), 218  
 Flynn, E., 225  
 Focal length, 388  
 Follicle-stimulating hormone, 322  
 Food consumption, 40  
 Force, 3  
   generalized, 64  
   nuclear, 483  
   surface, 12  
 Ford, C. A., 119, 133  
 Ford, M. R., 495, 496, 513  
 Foster, K. R., 245, 246, 253, 254  
 Fourier integral, 301, 303  
   complex, 303  
 Fourier series, 290  
   complex, 292  
   discrete, equally-spaced data, 291  
   for piecewise continuous function, 295  
   for square wave, 296  
   sample duration not a period, 293  
   square wave, 292  
 Fourier transform, 301, 303, 523, 530  
   complex, 303  
   discrete, 291  
   discrete (2-d), 332  
   fast, 295  
   of exponential pulse, 303  
 Fourtanier, A. M., 380, 398  
 Fovea, 390  
 Fowler, P. H., 424, 425, 435  
 Fox, J. J., 277, 283  
 Fox, R. A., 504, 513  
 Fractional distribution function, 508  
 Fractional rate of growth or decay, 35  
 Fractionation curve, 460  
 Fraden, J., 376, 398  
 Framingham study, 36  
 Francis, J. E., 443  
 Frankel, R. B., 217, 220, 224  
 Fraunhofer zone, 352  
 Freake, M., 225  
 Free body diagram, 7  
 Free energy  
   Gibbs, 66  
 Free expansion, 73  
 Free induction decay (FID), 524, 525  
 Free radical, 445, 458  
 Freeston, I. L., 214, 224  
 Freier, S., 68, 79  
 Frequency, 289  
   angular, 289  
   half-power, 311  
   spatial, 326, 329  
 Frequency response, 280, 310  
   glucose and insulin, 312  
 Fresnel zone, 352  
 Freund, H. U., 434  
 Fricke dosimeter, 445  
 Friedman, R. N., 212, 224, 225  
 Fritzberg, A. R., 504, 513  
 Froelich, J. W., 542  
 Fruit fly, 239  
   shaker mutant, 239  
 Fuchs, A. F., 29, 133, 175, 284  
 Fujimoto, J. G., 370, 398  
 Function  
   piecewise continuous, 295  
 Functional MRI, 536  
 Fundamental constants, 583  
 Fundamental equation of thermodynamics, 65  
 Fung, Y. C., 12, 13, 29  
 Furocoumarins, 380  
 Fusion  
   nuclear, 484  
 Fuster, V., 398  
 Gabbe, E. E., 224  
 Gadolinium, 523, 536  
 Gadolinium oxysulfide, 441  
 Gain, 258  
   open-loop, 258  
 Galanski, M., 479  
 Galletti, P. M., 120, 133  
 $^{67}\text{Ga}$ , 498, 502  
 Gamma (film), 441  
 Gamma camera, 500  
 Gamma decay, 484  
 Gamma function, 576  
 Gammiatoni, L., 317, 323  
 Gangrene, 146

- Gans, D. S., 399
- Gap junctions, 184
- Gap phase, 459
- Gardner, M. J., 225
- Garfinkel, A., 276, 282–284
- Garg, M. L., 435
- Garg, R. R., 435
- Garrard, C. L., 225
- Gas
- ideal, 60, 61
- Gas constant, 60
- Gas multiplication, 444
- Gasiorowicz, S., 374, 398
- Gaskill, J. D., 329, 341
- Gastric juice, 63
- Gastrocnemius, 6
- Gating current, 241
- Gatland, I. R., 288, 323
- Gauss, 204
- Gauss's law, 138
- for magnetic field, 205
  - free and bound charge, 144
- Gaussian distribution, 91, 99, 568
- Gauvin, D., 477
- Gawande, A., 566
- Geddes, L. A., 136, 175, 193, 201, 202
- Geetha, J., 284
- Geiger counter, 444
- Geiger's rule, 477
- Geise, R., 451, 453, 454
- Gel dosimeter, 445
- Geller, A. C., 398
- Genant, H. K., 442, 478
- General thermodynamic relationship, 65
- Generalized force, 64
- Gennari, F. J., 117, 133
- Germanium, 445
- Gevins, A., 212, 226
- Giasson, C. J., 381, 398
- Gibbs factor, 76
- Gibbs free energy, 65, 66
- Gibbs paradox, 68
- Gibbs phenomenon, 296
- Gielen, F. L. H., 212, 223, 224
- Gilchrist, B. A., 380, 398
- Giles, W. R., 175
- Gillooly, J. F., 47, 74, 79
- Gilmour, R. F., 283
- Gimm, H. A., 404, 434
- Gingl, Z., 318, 323
- Gingras, S., 477
- Ginzburg, L., 281, 283
- Giorgiani, G., 398
- Gittelsohn, K., 284
- Glass, L., 264, 266–268, 271, 273–276, 283, 284, 316, 317, 323
- Globulin, 129
- Glomerulus, 17, 27, 116
- Glucose, 3, 67, 117
- Glucose regulation, 279
- Glucose tolerance, 312
- Glutamate, 137
- Gluteus medius, 7
- Gluteus minimus, 7
- Glycine, 137
- Glycoaminoglycans, 249
- GMP, cyclic, 392
- Goiter, 277
- Goldberg, M. J., 47
- Goldman–Hodgkin–Katz equations, 236
- Golzarian, J., 225
- Gompertz mortality function, 44
- Goodsell, D. S., 3, 29
- Goodsitt, M., 457, 478
- Gorby, Y., 217
- Gou, S.-y., 96, 109
- Gougoutas, A., 254
- Gould, J. L., 217, 224, 225
- Gouy–Chapman model, 229
- Gradient, 88, 142
- diffusion, 537
  - in different coordinate systems, 578
  - magnetic, 528
  - phase-encoding, 529
  - readout, 529
  - slice-selection, 528
- Gradiometer, 219
- Granger, H. J., 115, 133
- Grant, R. M., 348, 349
- Gras, J. L., 103
- Grass, Inc., 196
- Gray (unit), 427, 468
- Gray body, 373
- Gray, D. E., 357
- Green's function, 100
- Gregory, K., 398
- Greigite, 217
- Grenier, R. P., 511
- Grid
- antiscatter, 450
- Grievenkamp, J. E., 390, 398
- Grimes, D. I. F., 212, 224
- Grossweiner, L., 364, 367, 368, 381–383, 398
- Grove, R. I., 479
- Growth rate
- variable, 35
- Grundfest, H., 182, 202, 209
- Guevara, M. R., 276, 283
- Gulbis, J. M., 253
- Gulrajani, R. M., 177, 191, 201
- Guttman, R., 43
- Guyton, A. C., 20, 115, 117, 122, 133, 137, 175, 261, 274, 284, 321, 323
- Gyromagnetic ratio, 516, 517

- h* gate, 157, 173  
 Haas, R. A., 565  
 Habrand, J. L., 467, 478  
 Haddad, J. G., 381, 398  
 Hademenos, G. J., 26, 29  
 Hafemeister, D., 244, 253  
 Hahn, P. F., 542  
 Haie, C., 478  
 Hair cells, 243, 349  
 Halbach, R. E., 542  
 Halberg, F., 293, 321, 323  
 Haldane, J. B. S., 45, 47  
 Half-life, 34, 484  
     effective, 490  
 Half-power frequency, 311  
 Half-value layer, 476  
 Hall, E. J., 457–462, 472, 478  
 Hall, J. E., 175  
 Hall, K., 283  
 Hall, M. A., 270, 271  
 Hallett, M., 214, 224, 225  
 Halliday, D., 7, 29, 142, 175, 363, 373, 375, 398  
 Halliday, G. M., 399  
 Hämäläinen, M., 212  
 Hämäläinen, R., 212, 213, 218, 224, 315  
 Hamblen, D. P., 443  
 Hamill, O. P., 238, 243, 253  
 Hamilton, L. J., 368, 398  
 Hänggi, P., 323  
 Hanlon, E. B., 371, 372, 398  
 Harisinghani, M. G., 536, 542  
 Harmonic images, 353  
 Harmonic oscillator, 263, 363, 559  
 Harmonics, 289  
 Harri, R., 213, 224, 315  
 Harris, C. C., 443  
 Harris, J. W., 181, 184, 202, 224  
 Hart, H., 35, 36, 47  
 Hasselquist, B., 503  
 Hastings, H. M., 277, 282, 284  
 Hawkes, D. J., 407, 435  
 Hayes, N. D., 273, 284  
 HCl, 393  
 Heald, M. A., 387, 398  
 Heart block, 194  
     intermittent, 200  
     second degree, 200  
     sinus exit, 200  
 Heart failure, 116, 194  
 Heart rate, 46  
 Heat capacity, 61, 278  
     air, 61, 76  
     at constant volume, 61  
     ideal gas, 61  
     specific, 61  
     water, 75  
 Heat conduction, 103, 106, 382  
 Heat engine, 70  
 Heat flow, 54, 61  
 Heat loss  
     and countercurrent exchange, 132  
 Heat stroke, 274  
 Heaton, C. L., 378  
 Hecht, S., 390, 391, 398  
 Hee, M. R., 370, 398  
 Helfre, S., 478  
 Helical CT, 455  
 Heller, L., 214, 224  
 Hellman, L., 35, 36, 47  
 Helmholtz, 136  
 Hematocrit, 23  
 Hemmingsen, A. M., 41, 47  
 Hemochromatosis, 217  
 Hemoglobin, 24, 369, 523, 536  
 Hemosiderosis, 217  
 Hempelmann, L. H., 475  
 Hende, W. R., 343, 352, 355, 357, 446, 447, 450, 454,  
     477–479  
 Henderson, L. W., 119, 133  
 Henriquez, C. S., 184, 191, 192, 202  
 Hereditary spherocytosis, 117  
 Hermann, M., 398  
 Herrick, J. F., 17, 29  
 Hertz (unit of frequency), 289  
 Hexadecapole  
     magnetic, 484  
 Hidajat, N., 479  
 Hielscher, A., 369, 398  
 Higson, D. J., 471, 478  
 Hilborn, R. C., 263–265, 271, 284  
 Hildebrand, J. H., 67, 79, 87, 108, 114, 133  
 Hill, B. C., 196, 202  
 Hille, B., 29, 133, 155, 175, 235, 238, 243, 253, 284  
 Hinds, M., 202  
 Hine, H. G., 511  
 Hip, 7, 8  
 Hobbie, R. K., 185, 188, 189, 425, 434  
 Hodgkin's disease, 463  
 Hodgkin, A., 136, 148, 153, 154, 171, 175, 253  
 Hodgkin–Huxley model, 268, 275  
 Hoke, M., 225  
 Hole, 438  
 Holmes, T. W., 465, 478  
 Honig, B., 231, 254  
 Horacek, B. M., 224, 225  
 Hormesis, 472  
 Horowitz, P., 175  
 Hosaka, H., 211, 224  
 Hot tub, 274  
 Hotomaroglu, O., 284  
 Hounsfield (unit), 456  
 Hounsfield, G. N., 455, 478  
 Howell, R. W., 500, 513  
 Howerton, R. J., 434

- Hu, X-p., 330, 331  
 Huang, D., 370, 398  
 Hubbell, J. H., 404, 407, 408, 411, 414, 434, 435, 448, 478  
 Huda, W., 457, 478  
 Human immunodeficiency virus (HIV), 2  
 Humm, J. L., 500, 513  
 Hunt, D. C., 454, 478  
 Hunt, J. G., 495, 513  
 Husband, J. E., 536, 542  
 Huxley, A. F., 136, 154, 175  
 HVL, 476  
 Hydraulic permeability, 117  
   pore model, 123  
 Hydrogen  
   spectrum, 361  
 Hydrogen peroxide, 458  
 Hydroxyl free radical, 458  
 Hyperbolic functions, 166  
 Hypermetropia, 389  
 Hyperplasia, 378  
 Hyperpolarization, 173  
 Hyperthermia, 381  
 Hyperthyroidism, 504  
 Hypertrophy, 378  
 Hypoproteinemia, 116  
 Hysteresis, 13, 19  
   magnetic, 216  
  
 Ice ages, 317  
 ICRP, 468, 469, 478  
 ICRU, 350, 352, 357, 367, 414, 415, 417, 420–424, 426, 435, 437, 439, 440, 447, 448, 450, 478  
 Ideal gas, 73  
 Ideal gas law, 60, 63  
 Ideal solution, 114  
 Ideker, R. E., 196, 202, 276, 283  
 Illuminance, 384  
 Ilmoniemäki, R. J., 213, 214, 224, 315  
 Image  
   density-weighted, 533  
    $T_1$ -weighted, 533  
    $T_2$ -weighted, 533  
 Image contrast  
   and MR pulse parameters, 533  
 Image intensifier tube, 454  
 Image quality, 450  
 Imaginary number, 292  
 Impact parameter, 418  
 Impedance  
   acoustic, 346  
   characteristic, 346  
   reactive component, 346  
   transformation in middle ear, 349  
 IMPT, 467  
 Impulse approximation, 416, 419  
 Impulse function, 304  
  
 Impulse response, 312, 326  
 Incidence, 380  
 Incidence of disease, 44  
 Incoherent scattering, 403, 406  
 Incremental-signal transfer factor, 442  
 Incubator  
   neonatal, 376  
 Incus, 348  
 Index of refraction, 359, 364  
   of aqueous, 388  
   of crystalline lens, 388  
   of vitreous, 388  
 Inelastic scattering, 403  
 Inflammatory response, 116, 378  
 Influence function, 100  
 Infrared  
   photography, 376  
   radiation, 360, 375  
   spectroscopy, 368  
 Ingard, K. U., 343, 357  
 Inman, V. T., 7, 9, 29  
 Inner ear, 349  
 Insulin, 312  
 Integrals  
   trigonometric, 555  
 Intensifying screen, 441  
 Intensity  
   of sound, 347  
   radiant, 383  
   reference, 347  
 Intensity attenuation coefficient, 350  
 Intensity-modulated proton therapy, 467  
 Intensity-modulated radiation therapy, 465  
 Interferometer, 370  
 Internal conversion, 484, 492  
   coefficient, 485  
   electron, 492  
 Internal radiotherapy, 504  
 International Commission on Radiation Units and Measurements, *see* ICRU  
 International Commission on Radiological Protection, *see* ICRP  
 Interstitial fluid, 115  
 Intestinal parasites, 565  
 Intestinal villi, 122  
 Intracellular fluid, 136  
 Intravascular ultrasound, 376  
 Inulin, 393  
 Inverse problem, 198  
 Inversion recovery (IR), 525  
 Iodine, 449  
    $^{123}\text{I}$ , 498  
    $^{131}\text{I}$ , 502, 504  
 Iodine deficiency, 277  
 Ion  
   Born charging energy, 144  
 Ionization chamber, 444, 468

- Ionization energy, 362, 403  
     average, 420  
<sup>192</sup>Ir, 504  
 Iris, 388  
 Iron stores  
     in the body, 217  
 Irradiance, 384, 385  
 Isodose contours, 464  
 Isosbestic point, 369  
 Isotonic saline, 130  
 Isotope, 482  
 Isotropic radiation, 386  
 Itoh, M., 399  
 Itzkan, I., 371, 398  
 Izatt, J. A., 370, 371, 399
- J. H. Brown, 47  
 Jabinsek, V., 225  
 Jabola, B. R., 479  
 Jackson, D. F., 407, 435  
 Jacques, S. L., 398  
 Jaeger, J. C., 91, 94, 100, 106, 108  
 Jalife, J., 165, 175, 194–196, 201, 202, 212, 225, 268,  
     275, 283, 284  
 Jalinous, R., 214, 224  
 James, R. B., 445, 479  
 Jang, I-K., 398  
 Janka, G. E., 224  
 Jaramillo, F., 317, 323  
 Jaundice, neonatal, 377  
 Jeffrey, K., 194, 200, 202  
 Jeffreys, B. S., 153, 175  
 Jeffreys, H., 153, 175  
 Jejunum, 170  
 Jiang, D., 200, 202  
 Jiang, Y., 239, 254  
 Johnson noise, 242, 312, 314  
 Johnson, G. F., 47  
 Johnson, J. B., 314  
 Joint probability distribution, 579  
 Jones, J. P., 341, 455, 478, 527, 542  
 Jones, R. H., 511  
 Jongsma, H. J., 175  
 Joseph, P. M., 526, 527, 542  
 Josephson junction, 218  
 Joule, 11  
 Jung, P., 323
- K edge  
     in contrast agent, 448  
 K shell, 438  
 Köhler, T., 25, 29  
 Kagan, A. R., 463, 479  
 Kaiser, I. H., 293, 321, 323  
 Kalender, W. A., 455, 456, 478, 479  
 Kalmijn, Ad. J., 243, 254  
 Kaluza, G. L., 504, 513  
 Kaminski, E. M., 542  
 Kanal, E., 534, 542  
 Kane, B. J., 136, 175  
 Kannel, W. B., 47  
 Kaplan, D., 264, 271, 275, 284, 316, 317, 323  
 Karagueuzian, H. S., 283  
 Karhu, J., 214, 224  
 Kassirer, J. P., 117, 133  
 Kassis, A. I., 458, 461, 479, 500, 505, 513  
 Katchalsky, A., 120, 133  
 Kathren, R. L., 472, 479  
 Katila, T., 225  
 Kato, T., 542  
 Katz, B., 135, 137, 154, 175  
 Kaufman, L., 224, 225  
 Kavanagh, K. M., 284  
 Kay, A. R., 542  
 Kazerooni, E., 478  
 Keeler, E. K., 542  
 Keener, J. P., 275, 284  
 Keizer, J., 105, 109  
 Kelvin, 57  
 Kempe, C. H., 41, 47  
 Keratin, 378  
 Keratitis, 381  
 Keratopathy, 381  
 Keriakes, J. G., 466  
 Kerma, 427  
     collision, 428, 429  
     radiative, 428  
 Kernicterus, 377  
 Ketcham, D., 449  
 Kevan, P. G., 387, 398  
 Keynes, R. D., 239, 254  
 Khan, F. M., 464–467, 479  
 Khoo, M. C. K., 256, 284  
 Kidney, 37, 116, 278  
     artificial, 120  
     glomerulus, 17  
 Kil, J. R., 283  
 Kilocalorie, 54, 75  
 Kim, Y.-H., 283  
 Kimlin, M. G., 380, 398  
 Kinetic energy, 10  
 King, K. F., 532, 533, 542  
 Kirby, S. S., 454, 478  
 Kirchhoff's laws, 147  
 Kirschvink, J. L., 217, 224, 225, 247, 248, 254  
 Kiss, L. B., 318, 323  
 Kissel, L. H., 407, 435  
 Kleiber, M., 41  
 Klein, L. S., 195, 202  
 Klein-Nishina  
     factor, 432  
     formula, 406  
 Kligman, L. H., 380, 398  
 Knisley, S. B., 196, 202



- Knobler, E., 381, 398  
 Knuutila, J., 213, 224, 315  
 Kobayashi, A. K., 247, 254  
 Kobayashi-Kirschvink, A., 254  
 Koh, D.-M., 536, 542  
 Koh, W. J., 478  
 Koizumi, H., 399  
 Konarzewski, M., 42, 47  
 Kondo, S., 472, 479  
 Koo, T.-W., 371, 398  
 Kovacs, G. T. A., 136, 175  
 Kozłowski, J., 42, 47  
 Krämer, U., 398  
 Kramer, J. R., 371, 398  
 Krane, K. S., 7, 29, 142, 175, 363, 373, 375, 398  
 Kricke, A., 380, 397  
 Kripke, M. L., 380, 398  
<sup>81m</sup>Kr, 502  
 Kucharczyk, J., 542  
 Kuo, A., 253  
 Kupfer cells, 497  
 Kustin, K., 283  
 Kuyucak, S., 254
- Laüger, P., 148, 175  
 LaBarbera, M., 27, 29  
 Lakshminarayanan, A. V., 335, 341  
 Lamb, H., 248, 254  
 Lambert's law, 386  
 Laminar flow, 15, 16  
 Lamothe, M. J. R., 225  
 Lanchester, F. W., 280  
 Langevin equation, 87  
 Lanino, E., 398  
 Lopicque, L., 193, 202  
 Laplacian, 91  
 Laramore, G. E., 478  
 Large-signal transfer factor, 442  
 Larin, K. V., 398  
 Larina, I. V., 398  
 Larmor precession frequency, 518, 522  
 Larsson, S. A., 502, 513  
 Laser surgery, 381  
 Late-responding tissue, 461, 462  
 Latent heat of vaporization, 75  
 Lateral geniculate nucleus, 536  
 Latitude, 441  
 Lauterbur, P. C., 527, 542  
 Law of Laplace, 26, 77  
 Lawrence, C. M., 380, 398  
 Le, A., 254  
 Le, T. H., 330, 331  
 Lead zirconate titanate, 351  
 Leads  
   ECG, 187  
   limb, 187  
     augmented, 188  
     precordial, 188  
 Least squares, 201, 285  
   linear, 287  
   nonlinear, 288  
   polynomial, 288  
 Lebec, M., 399  
 LeBihan, D., 108, 542  
 Lee, M.-H., 283  
 Lee, T. M., 542  
 Left and right bundles, 185  
 Left ventricular hypertrophy, 189, 190  
 Legendre polynomial, 181, 184  
 Lei, H., 534, 542  
 Leigh, J., 399  
 Leighton, R. B., 323  
 Leiter, D., 284  
 Lenir-Cohen-Solal, C., 478  
 Lennard, R. F., 212, 224  
 Lens, 388  
 Lenz's law, 214, 215  
 Lester, J. W., 542  
 LET, 423  
 Létourneau, E. G., 477  
 Leuchtag, H. R., 236, 254  
 Leukemia, 42, 275  
 Levenberg-Marquardt method, 289  
 Lever, L. R., 380, 398  
 Lévesque, B., 477  
 Levin, R. L., 542  
 Levitt, D., 87, 98, 109, 124, 127, 133  
 Levy, R. P., 479  
 Lewis number, 104  
 Lewis, C. A., 238, 254  
 Li, T. K., 44  
 Liang, Z.-P., 527, 542  
 Light  
   photon properties, 360  
   polarized, 371  
   speed, 359  
   wave nature, 360, 370  
 Lightfoot, E. N., 90  
 Lighthill, J., 15, 29  
 Lighthill, M. J., 304, 323  
 Likavek, M. J., 116, 133  
 Limb leads, 187  
 Lime peel, 380  
 Limit cycle  
   bifurcation of, 266  
   stable, 266  
   unstable, 266  
 Lin, C. P., 370, 398  
 Lindemans, F. W., 195, 202  
 Lindhard, J., 418, 420  
 Lindner, A., 120, 133  
 Lindsay, R. B., 350, 357  
 Line approximation, 184  
 Line integral, 142

- Line-spread function, 329
- Linear energy transfer, 423, 458
- Linear least squares
  - weighted, 288
- Linear regression, 287
- Linear system, 325
- Linear-nonthreshold model, 471, 472, 506
- Linear-quadratic model, 460
- Links, J. M., 501, 513
- Liow, J. S., 513
- Lipid bilayer, 163
- Lissner, H. R., 7, 29
- Lithotripsy, 350, 353
- Littmark, U., 415, 418–423, 435
- Liu, D-W., 201
- Liu, H., 369, 398
- Liver, 116, 217
- Local control of tumor, 463
- Locatelli, F., 398
- Loevinger, R., 488, 490, 491, 498, 513
- Log-log graph paper, 39
- Logarithm
  - definition, 549
  - natural, 549
- Logistic equation, 39, 265, 266
- Logistic map, 269
- Lomax, A., 479
- Longitudinal wave, 344, 346
- Lopatin, A. N., 254
- Lorente de Nó, R., 153, 175
- Lorentz force, 204, 222
- Lotka-Volterra equations, 46
- Lounasmaa, O. V., 213, 224, 315
- Lowe, H. C., 398
- Lu, J., 244, 252, 254
- Lubin, J. H., 473, 479
- Lukas, A., 201
- Lumen, 376
- Lumen (unit), 387
- Luminance, 384
- Luminous
  - efficacy, 387
  - energy, 384
  - exitance, 384
  - exposure, 384
  - flux, 384, 387
  - intensity, 384, 387
- Lung transplant, 503
- Luo, C. H., 158, 175
- Lutz, G., 445, 479
- LVH, *see* Left ventricular hypertrophy
- Lybanon, M., 288, 323
- Lynch, D. K., 387, 399
- Lysaght, M. J., 119, 120, 133
- Lythgoe, M. F., 542
- m* gate, 157
- M mode, 353
- Maccaferri, G., 165, 175
- MacDose, 434
- Maciel, H. S., 254
- Mackay, J., 398
- Mackenzie, D., 47
- Mackey, M. C., 264, 266–268, 273–275, 283, 284
- Mackie, T. R., 465, 478
- MacKinnon, R., 239, 240, 253, 254
- Macklem, P. T., 13, 29
- MacNeill, B. D., 376, 398
- Macovski, A., 451, 479
- Macrophage, 216
- Macrostate, 52, 55
  - disordered, 52
  - nonrandom, 52
  - ordered, 52
  - random, 52
- Maddock, J. R., 96, 109
- Madronich, S., 377, 378, 398
- Maer, W., 479
- Magleby, K. L., 240
- Magnetic dipole, 215
  - field far from, 522
- Magnetic field, 203, 205
  - crayfish axon, 208
  - detection, 218
  - earth, 218
  - from a current dipole in a conducting sphere, 212
  - from axon, 208
  - from depolarizing cell, 210
  - from point source of current, 207
  - lines, 205
  - of a current dipole in a conducting sphere, 221
  - remanent, 216
- Magnetic field intensity, 216
- Magnetic moment, 204, 516
  - and angular momentum, 516
  - nuclear, 517
  - torque, 205
- Magnetic monopole
  - absence of, 205
- Magnetic permeability, 216
- Magnetic resonance imaging
  - intravascular, 377
- Magnetic shielding, 214
- Magnetic stimulation, 222
- Magnetic susceptibility, 203, 216
- Magnetism
  - and special relativity, 203
- Magnetite, 216, 217, 222
- Magnetization, 216, 517
- Magnetocardiogram, 209, 211
- Magnetoencephalogram, 209, 212, 314
- Magnetopneumography, 216
- Magnetosome, 217, 222, 247, 248
- Magnetotactic bacteria, 217

- Magnification, 327  
 Magnifying glass, 396  
 Magnoni, D. M., 175  
 Magnoni, M., 165  
 Mainardi, L. T., 308–310, 323  
 Makhina, E. N., 254  
 Maki, A., 399  
 Makita, S., 399  
 Malleus, 348  
 Malmivuo, J., 177, 202  
 Mammography, 453  
 Mannitol, 116, 129  
 Manoharan, R., 371, 398  
 Manoyan, J. M., 422, 435  
 Mansfield, P., 527  
 Mansfield, T. A., 96, 109  
 Maor, E., 33, 47  
 Marchesoni, F., 323  
 Maris, M., 399  
 Maritan, A., 47  
 Mark, H., 434  
 Markov process, 563  
 Maroudas, A., 133  
 Marshall, M., 425, 434, 439, 477  
 Martel, R., 477  
 Martin, A. R., 175, 573  
 Marty, A., 253  
 Mass attenuation coefficient, 409  
   tissue, 447  
 Mass energy absorption coefficient, 413  
   table (on the web), 441  
 Mass energy transfer coefficient, 413  
 Mass fraction, 410  
 Mass number, 482  
 Mass stopping power, 414  
 Mass unit  
   atomic, 483  
   unified, 483  
 Massoth, R. J., 542  
 Mattiello, J., 108, 537, 542  
 Maughan, W. Z., 295, 323  
 Mauricio, C. L., 495, 513  
 Mauro, A., 229, 230, 254  
 Maxwell's equations, 222  
 May, R. M., 269, 284  
 Mayaux, M. J., 72  
 Mazal, A., 478  
 Mazumdar, J. N., 15, 20, 22, 29  
 McCollough, C. H., 468, 469, 479  
 McDonagh, A. F., 377, 398  
 McGrayne, S. B., 217, 224  
 McGregor, R. G., 477  
 McKee, P. A., 36, 47  
 McMahan, T., 41, 47  
 McNamara, P. M., 47  
 Meadowcroft, P. M., 23, 29  
 Mean, 561  
 Mean absorbed dose, 489  
 Mean absorbed dose per unit cumulated activity, 489  
 Mean energy emitted per unit cumulated activity, 489  
 Mean energy per ion pair, 439  
 Mean energy per unit cumulated activity, 488  
 Mean free path, 85  
 Mean initial activity per unit mass, 492  
 Mean number per disintegration, 484, 489  
 Mean square error, 286  
 Meandering waves, 276  
 Mechanoreceptors, 243  
 Medical Internal Radiation Dose, *see* MIRD  
 MEG, 209  
 Mehta, D., 435  
 Meidner, H., 96, 109  
 Melanin, 378  
 Melanocyte, 378  
 Melanoma, 380, 381  
 Mellinger, M. D., 398  
 Membrane, 111  
   force on, 128  
   permeable, 111  
   semipermeable, 111  
 Membrane capacitance, 163  
 Membrane permeability, 120  
 Mercader, M. A., 275, 284  
 Messina, C., 381, 398  
 Metabolic rate, 41, 256  
 Metaplasia, 378  
 Metastable state, 484  
 Metastases, 463  
 Metric prefixes, 1  
 Metric system, 1  
 Metz, C. E., 451, 479  
 Meves, H., 253  
 Michaels, D. C., 284  
 Microscope, 396  
 Microstate, 52, 55  
 Microstates, 64  
   energy dependence, 57  
 Microwave radiation, 360  
 Mielczarek, E. V., 217, 224, 275, 284  
 Miles, W. M., 194, 195, 202  
 Miller, B., 398  
 Miller, B. D., 202  
 Miller, C. E., 191, 202  
 Miller, J. M., 398  
 Milner, T. E., 397  
 Milnor, W. R., 20, 23, 29, 296, 297, 323  
 Milonni, P. W., 364, 398  
 Miners, 216  
 Mines, G. R., 275, 284  
 Minimum auditory field (MAF), 347  
 Minimum auditory pressure (MAP), 347  
 Minimum erythema dose, 379  
 Mintorovitch, J., 542  
 Miralbell, R., 467, 479

- MIRD, 481, 489, 494–496, 505  
 Mitochondria, 2  
 Mitosis, 458, 459  
 Mitrani, R. D., 195, 202  
 Mixing  
   entropy of, 67  
   heat of, 68  
 Modulation transfer function, 328, 390, 450  
 Modulus  
   shear, 13  
   Young's, 12  
 Moe, G. K., 268  
 Mole, 366  
 Mole fraction, 69  
 Moller, J. H., 189, 190  
 Moller, W., 216, 225  
<sup>99</sup>Mo, 497, 498  
 Molybdenum target x-ray tube, 454  
 Moment arm, 5, 10  
 Moment of inertia, 363  
 Monte Carlo calculation, 367, 369, 425, 494  
 Montesinos, G. D., 425, 434, 494, 512  
 Moore, J. W., 274, 284  
 Moran, J., 120, 133  
 Moran, P. R., 542  
 Morin, R., 534  
 Morrison, P., 3, 29  
 Morrow, M. N., 202  
 Morse, P. M., 343, 357  
 Mortality function, 44  
 Mortimer, J. T., 202  
 Mortimer, M., 266, 283  
 Moseley, H., 380, 398, 474  
 Moseley, M. E., 536, 542  
 Moses, H. W., 194, 202  
 Moskowitz, B. M., 217, 224  
 Mosley, M. L., 502, 513  
 Moss, F., 317–319, 323  
 Moss, W. T., 464  
 Mossman, K. L., 472, 479  
 Motamedi, M., 398  
 Mottle, 452  
 Motz, J. T., 371, 398  
 Moulder, J. E., 244, 245, 254, 458, 479  
 Moulton, K. P., 202  
 Mouritsen, H., 217, 224  
 Moy, G., 231, 254  
 Moyal, D. D., 380, 398  
 Moyers, M., 466, 467, 479  
 MR Image  
   and pulse parameters, 533  
 Muir, W. A., 224  
 Multipole expansion, 184  
 Murphy, C. R., 175  
 Murphy, E. A., 564  
 Murphy, M. R., 377, 398  
 Murray's law, 27  
 Murray, J. D., 39, 46, 47  
 Muscle  
   gastrocnemius, 6  
   gluteus medius, 7  
   gluteus minimis, 7  
   soleus, 6  
 Mutual inductance, 223  
 Myelinated fiber  
   time and space constants, 161  
 Myers, K. J., 325, 333, 341  
 Myocardial cells  
   and nerve cells compared, 184  
   repolarization, 179  
 Myocardial infarct, 36, 44, 211, 376  
 Myoglobin, 76  
 Myopia, 389  
  
*n* gate, 157  
 Nag, S., 504, 513  
 Nagai, Y., 283  
 Nagel, H. D., 457, 458, 479  
 Narrow-beam geometry, 408  
 Nath, R., 505, 513  
 National Institute of Standards and Technology, *see*  
   NIST  
 National Nuclear Data Center, 489  
 National Research Council, 245, 254  
 Nattel, S., 283  
 Natural background, 470  
 Natural logarithm, 549  
 Navier-Stokes equation, 27  
 NCRP, 454, 470, 471, 479  
 Near field, 352  
 Near-infrared radiation, 369  
 Near-infrared spectroscopy, 377  
 Nedbal, L., 294, 295, 323  
 Negative resistance, 252  
 Neher, E., 238, 253, 254  
 Nelson, J. S., 397  
 Nemoto, I., 224  
 Neonatal jaundice, 377  
 Neper, 350  
 Nephron, 116  
 Nephrotic syndrome, 116  
 Nernst equation, 60, 148, 228  
   sodium, 155  
 Nernst potential  
   calcium, 170  
   potassium, 155  
   sodium, 155  
 Nernst-Planck equation, 235  
 Nerve cell, 75  
 Nerves  
   Sympathetic and parasympathetic, 185  
 Nesson, M. H., 247, 254  
 Nesterenko, V. V., 201  
 Neunlist, M., 196, 202

- Neurotransmitter, 137
- Neutrino, 486
  - rest mass, 486
- Neutron therapy, 467
- Newhauser, W. D., 466, 467
- Newman, E. B., 349, 357
- Newton's law of cooling, 76
- Newton's second law, 10, 49
- Newton's third law, 12
- Newton, I., 359
- Newtonian fluid, 15, 23, 87
- Nicholls, A., 231, 254
- Nichols, C. G., 251, 254
- Nickel skin allergy, 380
- Nickell, S., 367, 398
- Nielsen, P., 217, 224
- Nijsten, T. E., 381, 399
- Nilson, J., 284
- Nioka, S., 399
- NIST, 410, 414, 423, 441
- $^{13}\text{N}$ , 502
- Noble, D., 165, 175
- Nodal escape beats, 185
- Node of Ranvier, 136, 160
- Noise, 75, 242, 306, 308
  - 1/f, 315
  - autocorrelation function, 314
  - Johnson, 242, 312, 314
  - pink, 315
  - power spectrum, 314
  - quantum, 451
  - shot, 242, 312, 451
  - source, 313
  - white, 314
- Noise brightness contrast, 451
- Noise equivalent quanta, 452
- Noise exposure contrast, 451
- Nolte, J., 137, 175
- Noninvasive electrocardiographic imaging, 191
- Nonlinear least squares, 288
- Nonmelanoma skin cancer (NMSC), 380
- Norepinephrine, 185
- Normal distribution, 568
- Normoneva, D. A., 29
- Northern Hemisphere, 217
- Nuclear force, 483
- Nuclear scattering, 421
- Nunally, R. L., 534
- Nunez, P. L., 196, 202
- Nutation, 521, 528
- Nyenhuis, J. A., 534, 542
- Nyquist frequency, 310
- Nyquist sampling criterion, 290
- Nyquist, H., 314, 323
  
- O'Brien, D., 41, 47
- O'Meara, N. M., 313
  
- OATZ, 217
- Oberly, L. W., 502
- Ocean flounder, 244
- Octupole
  - electric, 484
- Odd function, 290
- Oellrich, R. G., 377, 398
- Oersted, H. C., 203
- Ogawa, S., 536, 542
- Ohm, 145
- Ohm's law, 145, 182, 190
  - and current density, 146
  - anisotropic medium, 191
- Okada, T. C., 225
- Okada, Y., 225
- Oldendorf, W., 455
- OLINDA/EXM, 489, 494
- One-dimensional flow (mathematical), 262
- Open-loop gain, 258
- Operating point, 257
  - approach to, 259
- Optical coherence microscopy, 371
- Optical coherence tomography, 370, 376
- Optical density, 441
  - and exposure, 475
- Optical transfer function, 328
- Orban, M., 283
- Orbital quantum number, 402
- Ordidge, R. J., 542
- Orear, J., 288, 323
- Organelle, 2
- Orthogonality relations
  - for trigonometric functions, 296
- Orton, C., 458, 462, 479
- Osmolality, 115
- Osmolarity, 115
- Osmosis
  - in ideal gas, 112
  - in liquid, 114, 117
  - reverse, 119
- Osmotic diuresis, 116
- Osmotic flow
  - difference from diffusion, 111
- Osmotic fragility, 117
- Osmotic pressure
  - and capillaries, 115
  - and chemical potential, 114
  - and driving pressure, 114
  - and interstitial fluid, 115
  - in ideal gas, 114
  - in liquid, 114
- Ossicles, 348
- Osteoarthritis, 130, 249
- Othmer, J. G., 105, 109
- Oudit, G. Y., 185, 202
- Oval window, 348, 349
- Øverbø, I., 404, 434

- Oxic-anoxic transition zone, 217  
 $^{15}\text{O}$ , 502  
 Oxygen consumption, 256  
 Ozone, 377
- P wave, 186, 194  
 $^{31}\text{P}$ , 534  
 Pacemaker, 192, 194, 267  
 Pacing electrode, 194  
 Page, C. H., 214, 224  
 Paine, P. L., 87, 109  
 Pair production, 403, 407  
   free electron, 407  
 Pajevic, S., 542  
 Paliwal, B., 478  
 Palotta, B. S., 240  
 Panfilov, A. V., 275, 284  
 Paramagnetism, 215, 216  
 Paramecium, 1  
 Parasympathetic nerves, 185  
 Parathyroid hormone, 279  
 Parisi, A. V., 380, 398  
 Parkinson, J. S., 96, 109  
 Parseval's theorem, 305  
 Partial derivative, 57  
 Partial derivatives  
   order of differentiation, 582  
 Particle Data Group, 486  
 Particle exchange  
   equilibrium, 62  
 Particles per transition, 489  
 Pascal, 12  
 Pascual-Leone, A., 225  
 Patch-clamp recording, 238  
 Patterson, J. C., 502, 513  
 Patterson, M. S., 368, 369, 398, 399  
 Patton, H. D., 20, 29, 116, 122, 133, 135, 137, 148, 175,  
   257, 284  
 Paul, C. F., 381, 399  
 Pauli exclusion principle, 362, 421  
 Pauli promotion, 421  
 Payne, J. T., 337  
 Pearson, W. L., 254  
 Pecora, R., 372, 397  
 Pedley, T. J., 29  
 Pell, G. S., 542  
 Penetration depth  
   thermal, 383  
 Penkoske, P. A., 284  
 Perfumes, 380  
 Perfusion, 382  
 Period doubling, 269  
   in heart cells, 276  
 Periodogram, 309  
 Perkins, D. H., 424, 425, 435  
 Permeability  
   hydraulic, 117  
   magnetic, 216  
   membrane, 120  
 Perotti, C., 398  
 Perrin, J. E., 85  
 Pertsov, A. M., 275, 284  
 PET, 502, 536  
 Peters, R. H., 41, 47  
 Petrie, R. J., 213, 225  
 Pfuetzner, R. A., 253  
 Phagocytosis, 497  
 Phantom, 494  
 Phase, 289  
   resetting, 264–267  
   singularity, 283  
   space, 263  
 Phase encoding, 528, 530  
 Phase transfer function, 328  
 Phased array, 353  
 Phelps, M. E., 501, 502, 511, 513  
 Phenobarbital, 44  
 Phenothiazines, 379  
 Phlebotomy, 119  
 Phosphate, 278  
 Phosphorescence, 364  
 Photochemotherapy, 381  
 Photoelectric effect, 403, 404  
 Photographic emulsion, 424  
 Photometry, 383  
 Photomultiplier tube, 500  
 Photon, 360  
   attenuation coefficient, 409  
   characteristic, 410  
   diffusion constant, 367  
   exitance, 384  
   fluence, 384  
   fluence rate, 384  
   fluorescence, 410  
   flux, 384  
   flux exposure, 384  
   flux intensity, 384  
   flux irradiance, 384  
   flux radiance, 384  
   secondary, 413, 429  
 Photon absorption, 365  
 Photon scattering, 365  
 Photons, 244  
 Photopheresis, 381  
 Photopic vision, 387  
 Photosynthesis, 67, 294  
   in aquatic plants, 394  
 Physiological recruitment, 200  
 Pi pulse, 521  
 Pi/2 pulse, 524  
 Pickard, W. F., 244, 254  
 Pierpaoli, C., 542  
 Piezoelectric transducer, 350  
 Pigeon, 217, 222

- Pilkington, T. C., 202  
 Pillon, M., 398  
 Pillsbury, D. M., 378  
 Pinna, 348  
 Pirene, M. H., 390, 391, 398, 399  
 Pires, M. A., 224  
 Pituitary, 256, 277  
 Planck's constant, 244, 360  
 Plane wave, 344, 386  
 Plaque, 376  
     vulnerable, 376  
 Plasma, 37  
 Plasmon, 418  
 Plasticity, 196  
 Platt, J., 478  
 Platzman, R. L., 440, 479  
 Plonsey, R., 20, 153, 154, 160, 175, 177, 182–184, 191,  
     193, 199, 201, 202, 209, 284  
 Plug flow, 535  
 Pneumothorax, 448  
 Pogue, B. W., 369, 399  
 Poincaré, J. H., 263  
 Point charge, 139  
 Point-spread function, 327, 390  
     for an ideal imaging system, 327  
 Poise (unit of viscosity), 15  
 Poiseuille flow, 17, 20, 123  
     departures from, 22  
 Poiseuille, J. L. M., 17  
 Poisson distribution, 366, 391, 571  
     and shot noise, 242  
 Poisson equation, 230  
 Poisson statistics  
     in cancer incidence, 471  
     in cell survival, 463  
     in image, 451  
     in photon fluence, 457  
     in radiation damage, 460  
 Poisson's ratio, 27  
 Poisson-Boltzmann equation, 230  
     analytic solution, 250  
     linearized, 230  
 Polacin, A., 479  
 Polarization, 372  
     electric, 234  
     of dielectric, 143  
 Polarized light, 371  
 Polk, C., 244, 247, 248, 254  
 Polonsky, K. S., 313  
 Polynomial  
     regression, 288  
 Pontvert, D., 478  
 Poon, T. S. C., 380, 399  
 Positron, 403, 407, 414  
     decay, 485  
 Positron emission tomography, 502  
 Postow, E., 254  
 Postulates of statistical mechanics, 55  
 Potassium channels  
     shaker, 241  
     slow, 185  
 Potassium conductance, 156  
 Potassium gate, 157  
 Potassium Nernst potential, 155  
 Potential  
     electric, 141  
     outside axon, 177  
     transmembrane, 196  
 Potential Alpha Energy Concentration (PEAC) (unit),  
     505  
 Potential difference, 142  
     and ion concentration, 228  
 Potential energy, 141  
 Potish, R. A., 479  
 Potts, T. J., 398  
 Powell, C. F., 424, 425, 435  
 Power, 10, 11, 146  
 Power law, 39  
 Power spectral density (PSD), 309  
     Blackman-Tukey method, 309  
     magnetic noise, 314  
     periodogram, 309  
 Power spectrum, 297  
 Power, average, 304  
 Pratt, R. H., 407, 435  
 Prausnitz, J. M., 67, 79, 87, 108  
 Precession, 518  
 Precordial leads, 188  
 Predator-prey problem, 46  
 Press, W. H., 105, 109, 182, 201, 202, 208, 209, 225,  
     285, 289, 295, 308, 309, 323, 339, 341  
 Pressure, 13  
     diastolic, 20  
     systolic, 20  
 Preston, W., 479  
 Prevalence of disease, 44  
 Price, R. E., 434  
 Price, R. R., 536, 542  
 Prickle layer, 378  
 Principal quantum number, 402  
 Probability, 50  
     binomial, 51  
 Product  
     cross, 5  
     dot, 11  
     scalar, 11  
     vector, 5  
 Projection, 501  
 Projection reconstruction, 528, 530  
 Projection theorem, 331  
 Projections, 331  
 Prokaryotes, 2  
 Proportional counter, 444  
 Protein, 2

- Proton therapy, 466  
 Protoplast, 2  
 Protozoans, 1  
 PRU (peripheral resistance unit), 20  
 Pryde, J. A., 87, 109  
 Pryor, T. A., 323  
 Psoralen, 381  
 Psoriasis, 381  
 Pterygium, 381  
 Puliafito, C. A., 370, 398  
 Pulmonary embolus, 500  
 Pulse echo techniques, 352  
 Pulse oximeter, 369  
 Punske, B. B., 211, 225  
 Pupil, 388  
 Pupil size, 274  
 Purcell, C. J., 211, 225  
 Purcell, E. M., 22, 29, 96, 107–109, 203, 207, 215, 225, 519  
 Puri, S., 435  
 Purkinje fibers, 185, 268  
 PUVA, 381  
 Pyramidal cells, 221
- $Q_{10}$ , 74, 157, 159  
 QRS wave, 186, 194  
 Qu, Z., 283  
 Quadrupole  
   electric, 484  
   magnetic, 516  
 Quality factor, 468  
 Quantum mottle, 452  
 Quantum number, 53  
 Quantum numbers  
   atomic electrons, 361  
   rotational, 363  
   vibrational, 364  
 Quasiperiodicity, 271  
 Quatrefoil pattern, 211  
 Québec, 473  
 Quinine water, 379
- RADAR (Radiation Group Assessment Resource), 489, 495  
 Radial isochron clock, 265, 266, 281  
 Radian, 543  
 Radiance, 384, 386  
 Radiant  
   energy, 383, 384  
   exposure, 384  
   flux, 384  
   intensity, 383, 384  
   power, 383, 384  
 Radiation  
   biological effects, 457  
   electromagnetic, 244  
   natural background, 470  
   risk, 468  
   weighting factor, 468  
 Radiation chemical yield, 439  
 Radiation damage  
   type A, 460, 462  
   type B, 460, 462  
 Radiation equilibrium, 428  
 Radiation risk model  
   hormesis, 472  
   linear non-threshold, 471  
   threshold, 472  
 Radiation therapy, 464  
   conformal, 465  
   electron, 465  
   intensity-modulated, 465  
 Radiation yield, 424, 437  
 Radiative transition, 410  
 Radiobiology, 457  
 Radiochromic film, 445  
 Radiograph, 446  
 Radiographic signal, 451  
 Radioimmunoassay, 481  
 Radioimmunotherapy, 504  
 Radiometry, 383  
 Radiopharmaceuticals, 495  
 Radiotherapy  
   internal, 504  
 $^{226}\text{Ra}$ , 505  
 Radius  
   atomic, 482  
   nuclear, 482  
 Radon, 469, 470, 472  
 $^{222}\text{Rn}$ , 505  
 Radon transformation, 333  
 Railroad tracks, 42  
 Raizner, A. E., 504, 513  
 Ramachandran, G. N., 335, 341  
 Raman scattering, 371  
 Raman spectroscopy, 377  
 Ramirez, R. J., 202  
 Random walk, 100  
 Range, 414, 423  
 Ranvier  
   node of, 136  
 Rao, D. V., 513  
 Rao, P. Y., 434  
 Rappoport, S. I., 117  
 Rardon, D. P., 194, 195, 202  
 Rasmusson, R. L., 201  
 Ratchet and pawl, 318  
 Rattay, F., 200, 202  
 Rayleigh scattering, 407  
 RBE, 468  
 Reactance, 346  
 Reaction-diffusion process, 105  
 Receptor  
   mechanical, 136



- stretch, 135
- temperature, 135
- Receptor field, 390
- Reckwerdt, P., 465, 478
- Reconstruction from projections
  - filtered back projections, 332
  - Fourier transform, 331
- Recruitment
  - physiological, 200
- Rectification
  - anomalous, 251
- Rectifier channels, 236
- Red blood cell, 3, 24
- Red cells, 117
- Reddy, A. K. N., 234, 253
- Reddy, R., 254
- Reduced mass, 363
- Reduced scattering coefficient, 367
- Reentrant circuit, 186, 195, 198
- Reference action spectrum, 379
- Reflection, 388
  - total internal, 396
- Reflection at a boundary, 347
- Reflection coefficient, 118, 120, 347
  - pore model, 127
- Refraction, 388
- Refractory period, 158, 173, 186
- Regression
  - linear, 287
  - polynomial, 288
- Rehm, K., 503, 504, 513
- Reich, P., 46, 47
- Reif, F., 50, 53, 55, 64, 79, 86, 109, 563
- Relative biological effectiveness, 468
- Relative risk, 245
- Relativity
  - special, 482
- Relaxation oscillator, 185
- Relaxation time
  - experimental, 524
  - longitudinal, 518, 523
  - non-recoverable, 524
  - spin-lattice, *see* Relaxation time, longitudinal
  - spin-spin, *see* Relaxation time, transverse
  - thermal, 382
  - transverse, 518, 523
- rem (unit), 468
- Remanent magnetic field, 216
- Renal arteries, 456
- Renal dialysis, 116
- Renal tubules, 122
- Repeller, 262
- Repolarization, 136, 185
- Reservoir, 58, 65
- Residence time, 490
- Residuals, 286
- Resistance, 145
  - parallel and series, 147
  - vascular, 20
- Resnick, R., 7, 29, 142, 175, 216, 218, 224, 363, 364, 373, 375, 398, 483, 486, 487, 513
- Resolution
  - and spatial frequency, 329
- Respiration of glucose, 67
- Response
  - impulse, 326
- Rest energy, 482
- Rest mass, 405
- Restenosis, 504
- Resting potential, 136
  - atrial and ventricular cells, 184
- Restitution, 282
- Restricted linear collision stopping power, 423
- Retina, 381, 388
- Reversal potential, 237, 238, 251
- Reverse osmosis, 119
- Reversible process, 65
- Reynolds number, 22, 29, 45
- Rheobase, 171, 193
- Ribberfors, R., 434
- Richards, W. O., 213, 225
- Rieke, F., 392, 399
- Riggs, D. S., 39, 47, 256, 278, 279, 284
- Right ventricular hypertrophy, 189
- Rinaldo, A., 47
- Risk
  - excess, 470
  - models, 471
  - relative, 245
- Ritchie, R. H., 435
- Ritenour, E. R., 343, 352, 355, 357, 446, 447, 450, 454–456, 478
- Rivabella, L., 398
- Robinson, D. K., 289, 323
- Rodriguez, J., 332, 341
- Rods (retinal), 387, 390
- Roentgen (unit), 440, 475
- Roll-off, 312
- Rollins, A. M., 371, 399
- Romani, G.L., 225
- Romberg integration, 182, 209
- Romer, R. H., 42, 214, 225
- Rose, A., 392, 399
- Rosenbaum, D. S., 196, 202
- Rossi, B., 406, 435
- Rossi, C. J., 479
- Rossi-Fanelli, A., 76
- Rossmann, K., 442, 478
- Rotating coordinate system, 519
- Rotation matrices, 519, 538
- Roth, B. J., 192, 195, 202, 208, 212, 214, 218, 221–226
- Rottenberg, D. A., 513
- Round window, 349
- Rowlands, J. A., 446, 450, 454, 478, 479

- Roy, S.C., 435  
 Rudy, Y., 158, 175, 191, 202  
 Ruohonen, J., 214, 224  
 Rushton, W. A. H., 153, 160, 171, 175  
 Ruta, V., 254  
 RVH, *see* Right ventricular hypertrophy  
 Ryman, J. C., 498, 513
- SA node, 164, 185, 194  
 Safety in MRI, 534  
 Saint-Jalmes, H., 371, 399  
 Sakane, K. K., 254  
 Sakitt, B., 392, 399  
 Sakmann, B., 238, 253, 254  
 Salles-Cunha, S. X., 542  
 Saltatory conduction, 160  
 Sands, M., 323  
 Sap flow, 27  
 SAR, *see* Specific absorption rate  
 Sarcoplasmic reticulum, 105  
 Sarvas, J., 221, 225  
 Sastry, K. S. R., 500, 513  
 Sato, S., 224, 225  
 Saturation, 216  
 Savage, V. M., 41, 47, 79  
 Savannah sparrow, 217  
 Scalar, 545  
 Scalar product, 11  
 Scaling, 40  
 Scattering  
   coherent, 403, 407  
   Compton, 403, 405  
   incoherent, 403, 406  
   inelastic, 403  
   nuclear, 421  
   Raman, 403  
   Rayleigh, 407  
   Thomson, 406  
 Scattering coefficient  
   reduced, 367  
 Scattering cross section, *see* Cross section  
 Schaefer, B. E., 378, 399  
 Schaefer, D. J., 534, 542  
 Schaper, K. A., 513  
 Scher, A. M., 29, 133, 175, 278, 284  
 Scherr, P., 87, 109  
 Schey, H. M., 84, 89, 97, 109, 138, 175, 577  
 Schlaer, S., 390, 391, 398  
 Schlesinger, T. E., 445, 479  
 Schlienger, P., 478  
 Schmidt, T., 479  
 Schmidt-Nielsen, K., 46, 47, 122, 131, 133  
 Schmitt, F., 533, 542  
 Schmitt, J. M., 370, 399  
 Schmitt, O. H., 245, 254  
 Schneider, J. A., 202  
 Schneider, U., 479  
 Schneidermann, R., 133  
 Schrödinger equation, 49  
 Schroter, S. T., 29  
 Schueler, B. A., 468, 469, 479  
 Schultz, J. S., 128, 133  
 Schulz, R. J., 463, 479  
 Schuman, J. S., 370, 398  
 Schwan, H. P., 246, 253  
 Schwartz, D., 72  
 Schwartz, L., 478  
 Schwiegerling, J., 398  
 Scintillation camera, 500  
 Scintillation detector, 442, 500  
 Scotopic vision, 387, 390, 454  
 Scott, A. C., 150, 154, 175  
 Scott, R. L., 67, 79, 87, 108, 114, 133  
 Scoumis, E. A., 542  
 Screen  
   intensifying, 441  
 Screening  
   atomic electron (charge), 403  
 Scribner, B. H., 133  
 Second law of thermodynamics, 70  
 Sedimentation velocity, 26  
 Seed, W. A., 29  
 Seibert, J. A., 446, 479  
 Selection rules, 362–364, 438, 484  
 Self-diffusion, 90  
 Self-similarity, 270  
 Seltzer, S. M., 414, 434, 435, 448, 478  
 Semicircular canals, 349  
 Semiconductor detector, 445  
 Semilog paper, 34  
 Semipermeable membrane, 111  
 Sepulveda, N. G., 195, 202  
 Sequestration, 497  
 Serruys, P. W., 399  
 Setton, L. A., 29  
 Sevick, E. M., 369, 399  
 Seymour, R. S., 41, 47  
 Sha, Q., 254  
 Shabashon, L., 458, 479  
 Shadley, J. D., 458, 479  
 Shadowitz, A., 207, 225  
 Shafer, K. E., 371, 398  
 Shaker channels, 239  
 Shani, G., 445, 479  
 Shapiro, E. M., 250, 254  
 Shapiro, L., 96, 109  
 Shark  
   and earth's magnetic field, 220  
 Shaw, R., 329, 341, 452, 478  
 Shear modulus, 13  
 Shear rate, 15  
 Shellock, F. G., 534, 542  
 Shells  
   atomic, 402

- Sherrard, D. J., 133  
 Sherwood number, 107  
 Sherwood, B. A., 364, 399  
 Shimizu, H., 542  
 Shot noise, 242, 312  
 Shrier, A., 276, 283  
 Sick sinus syndrome, 194, 200  
 Sicouri, S., 201  
 Sidtis, J. J., 513  
 Siegel, J. A., 505, 513  
 Siemens, 145  
 Sievert (unit), 468  
 Signal, 75, 306  
   and noise, 308  
   radiographic, 451  
 Signal averaging, 308  
 Signal-to-noise ratio, 452  
 Sigworth, F. J., 239, 241, 243, 253, 254  
 Silicon, 445  
 Silver halide, 441  
 Silver, H. K., 41, 47  
 Silver, S., 175  
 Silverstein, M. E., 119, 133  
 Sinc function, 528  
 Singh, M., 341, 455, 478, 527, 542  
 Singh, N., 435  
 Singh, S., 435  
 Single-channel recording, 238  
 Single-photon emission computed tomography, 501  
 Sink, 262  
 Sinoatrial node, *see see* SA node  
 Sinogram, 333  
 Sinus exit block, 200  
 Skofronick, J. G., 348, 349  
 Slater, J. D., 467, 479  
 Slater, J. M., 479  
 Slice selection, 527, 528  
 Slichter, C. P., 518, 523, 542  
 Slide projector, 396  
 Small intestine, 213  
 Smith, M. A., 398  
 Smith, W., 323  
 Smye, S. W., 372, 399  
 Smythe, W. R., 166, 175  
 Snell's law, 388  
 Snow blindness, 381  
 Snyder, W. S., 489, 494–496, 513  
 Sobol, W. T., 446, 479  
 Söderberg, P. G., 381, 397  
 Sodium  
   -potassium pump, 148  
   Nernst potential, 155  
<sup>24</sup>Na, 487  
 Sodium gate, 157  
 Sodium spectral line, 372  
 Soffer, B. H., 387, 399  
 Solar constant, 377, 395  
 Soleus, 6  
 Solid angle, 181, 366, 544  
   defined, 543  
   theorem, 198  
 Solute, 67, 69  
 Solute permeability, 120  
   pore model, 128  
 Solute transport, 119, 122  
   pore model, 127  
 Solution  
   ideal, 114  
 Solvent, 67  
 Solvent drag, 85, 119  
   in an electric field, 235  
 Sorenson, J. A., 501, 502, 511, 513  
 Sorgen, P. L., 201  
 Sound level measurement  
   weighting, 347  
 Source, 262  
 Space invariance, 327  
 Spano, M. L., 276, 283, 284  
 Sparks, R. B., 488, 489, 494, 513  
 Spatial frequency, 326, 329  
   and field of view, 329  
   and resolution, 329  
 Special relativity, 203, 220, 222, 405, 482  
 Specific absorbed fraction, 489  
 Specific absorption rate, 534, 539  
 Specific heat  
   water, 75  
 Specific heat capacity, 61, 382  
 Specific metabolic rate, 46  
 SPECT, 501  
 Spector, R., 47  
 Spectral efficiency function, 387  
 Spectroscopy  
   infrared, 368  
 Spectrum  
   beta decay, 487  
   Wiener, 452  
 Spherical aberration, 389  
 Spherical coordinates, 577  
 Spherocytosis, 117  
 Spheroid degeneration of the eye, 381  
 Sphincter, pre-capillary, 20  
 Spider's thread, 25  
 Spin  
   electron, 215, 361  
 spin  
   nuclear, 517  
 Spin echo (SE), 526, 528  
   fast or turbo, 532  
 Spin quantum number, 402  
 Spin warp encoding, 528  
 Spiral CT, 455  
 Spiral wave, 186, 275, 283  
 Spontaneous births, 294

- Spontaneous emission, 522
- Spray, D. C., 201
- Squamous cell carcinoma (SCC), 380, 381
- SQUID, 218, 223
- Squid, 2
  - giant axon, 154
- SRIM, 415, 422, 423
- Srinivas, S. M., 397
- Srinivasan, R., 196, 202
- Stabin, M. G., 488, 489, 494, 505, 513
- Stahlhofen, W., 216, 225
- Standard deviation, 562
- Standing wave, 345
- Stanley, P. C., 191, 202
- Stapes, 348
- Stark, L., 256, 275, 284
- Stark, L. C., 390, 399
- State space, 263
- Stationarity, 327
- Stationary random process, 307
- Stationary system, 326
- Statistical mechanics, 50
  - postulates, 55
- Staton, D. J., 211, 212, 225
- Steady state and equilibrium
  - distinction, 55
- Steel, G. G., 458, 459, 479
- Stefan-Boltzmann law, 374
- Stegun, I. A., 199, 201, 250, 253, 338, 340
- Stehling, M. K., 533, 542
- Steiner, R., 29
- Steiner, R. F., 133, 175, 284
- Steinmuller, D. R., 130, 133
- Steketee, J., 375, 399
- Stenosis, 376
- Stent, 504
  - drug-eluting, 504
- Steradian, 544
- Stereocilia, 243
- Steric factor, 120, 127
- Stern, R. S., 381, 399
- Steroid-eluting electrode, 195
- Stewart, W. E., 90
- Stimulated emission, 522
- Stimulus
  - brain, 196
  - current density, 165
  - strength-duration curve, 171
  - strength-interval curve, 173
- Stinson, W. G., 398
- Stirling's approximation, 567
- Stochastic resonance, 317
- Stocker, H., 181, 184, 202
- Stokes' law, 87, 90, 248
- Stopping cross section, 415
- Stopping interaction strength, 420
- Stopping number
  - per atomic electron, 420
- Stopping power, 414
  - electronic, 416
  - for compounds, 422
  - for electrons and positrons, 422
  - mass, 414
  - nuclear, 416
  - radiative, 416
- Storment, C. W., 136, 175
- Stragglings, 423
- Straight-line fit, 285, 287
- Strain, 344
  - normal, 12
  - shear, 13
- Stratum corneum, 378
- Stratum granulosum, 378
- Strauss, H. C., 201
- Streamline, 15, 18
- Strength-duration curve, 171, 193
- Strength-interval curve, 173
- Stress, 12, 344
  - normal, 12
  - shear, 13
- Strogatz, S. H., 262–265, 271, 284
- Stroink, G., 211, 214, 216, 225
- Stroke volume, 21
- <sup>90</sup>Sr, 504
- Strother, S. C., 503, 513
- Strouse, P., 478
- Structure mottle, 452
- Strupp, J., 542
- Stuchly, M. A., 214, 224
- Studniberg, H. M., 381, 399
- Sturis, J., 313
- Subexcitation, 440
- Subshells
  - atomic, 402
- Suess, C., 477, 479
- Suit, H., 467, 479
- Sulfides, 217
- Sulfonamides, 379
- Sulfonureas, 379
- Sun protection factor (SPF), 380
- Superconducting quantum interference device, 218
- Superconductor, 218
- Superposition, 325
- Surface tension, 65, 77
- Surface-to-volume ratio, 191
- Surfactant, 77
- Surrogate data, 316, 317
- Surroundings, 52
- Survival curve, 458
- Susceptibility
  - electric, 144
- Sutoh, Y., 399
- Svedberg, 26
- Swanson, E. A., 370, 398

- Sweating, 278  
 Sweeney, J. D., 202  
 Swift, C. D., 434  
 Swihart, C. J., 236, 254  
 Swinney, K. R., 208, 209, 225  
 Swithenby, S. J., 212, 224, 225  
 Sympathetic nerves, 185  
 Synapse, 104, 135, 136  
 Syncope, 194  
 Syncytium, 184  
 Synolakis, C. E., 18, 29  
 Synthesis, 459  
 System, 52  
   linear, 325  
   stationary, 326  
 System dynamics, 265  
 Systole, 18, 20  
 Szabo, A., 96, 109  
 Szabo, Z., 500, 513
- T rays, 372  
 T wave, 186  
 $T_1$ -weighted image, 533  
 $T_2$ -weighted image, 533  
 Tabatabaei, S., 542  
 Taccardi, B., 211, 225  
 Tachycardia  
   ventricular, 186  
 Taffet, S. M., 201  
 Tai, C., 200, 202  
 Takano, M., 398  
 Talajic, M. T., 283  
 Talus, 6, 7  
 Tan, G. A., 211, 225  
 Tanaka, A., 479  
 Tanelian, D. L., 136, 175  
 Tang, Y-h., 105, 109  
 Tank, D. W., 542  
 Target entity, 365  
 Taylor's series, 551  
   of exponential function, 553  
 Taylor, A. E., 115, 133  
 Tearney, G. J., 370, 397, 399  
 $^{99m}\text{Tc}$ , 33, 484, 492, 497, 498, 502  
   albumin, 498  
   diphosphonate, 501, 503  
   generator, 497  
   pertechnetate, 497  
   pyrophosphate, 500  
   red blood cells, 501  
   sestamibi, 498  
   sulfur colloid, 490, 500, 510  
   tetrofosmin, 498, 503  
 Tectorial membrane, 349  
 Telegrapher's equation, 152  
 Temperature  
   absolute, 57  
   celsius, 58  
   negative, 73  
 Temperature regulation, 278  
 "10-20" system for EEG leads, 196  
 Tendon  
   Achilles, 6  
 Tenforde, T. S., 244, 245, 254  
 Tensile strength, 12  
 Terahertz radiation, 361, 372  
 Tesla, 204  
 Tetley, I. J., 103  
 Tetrodotoxin, 238  
 Teukolsky, S. A., 109, 202, 225, 323, 341  
 $^{201}\text{Tl}$ , 498, 500, 502  
 Theodoris, G. C., 390, 399  
 Thermal conductivity, 103, 382  
 Thermal equilibrium, 56, 57  
 Thermal noise  
   retinal, 392  
 Thermal penetration depth, 383  
 Thermal relaxation time, 382  
 Thermodynamic identity, 65  
 Thermodynamic relationship, general, 65  
 Thermodynamics  
   first law, 53  
   second law, 70  
 Thermography, 376  
 Thermoluminescent dosimeter, 445  
 Thiazide diuretics, 379  
 Thin-film transistor, 450  
 Thin-lens equation, 388  
 Thomas, D. L., 537, 542  
 Thomas, G. B., 557  
 Thomas, I. M., 213, 225  
 Thomas, L., 120, 133  
 Thomas, S. R., 534  
 Thompson, D. J., 266, 283  
 Thompson, J. H., 565  
 Thompson, W. J., 288, 323  
 Thomson scattering, 406  
 Thomson, R. B., 565  
 $^{232}\text{Th}$ , 512  
 Three-dimensional conformal radiation therapy, 465  
 Threshold detection, 317  
 Threshold stimulus strength, 173  
 Thyroid, 256  
   stimulating hormone (TSH), 256, 277  
 Thyroid hormone, 278  
   Thyroxine (T4), 256, 277  
   Tri-iodothyronine (T3), 256  
 Tibia, 6  
 Tissue weighting factor, 469  
 Tittel, F. K., 398  
 TMS, 214  
 Tobacco, photosynthesis, 294  
 Tomanaga, M., 479  
 Tomography

- computed, 455
  - optical coherence, 370
- Tomotherapy, 465
- Tondury, P., 224
- Tooby, P. F., 26, 29
- Torque, 4, 516
  - on rotating sphere, 248
- Torr, 20
- Total angular momentum quantum number, 402
- Total internal reflection, 396
- Total linear attenuation coefficient, *see* Attenuation coefficient
- Trace of a matrix, 104
- Transcranial magnetic stimulation, 214
- Transducer, 135
  - piezoelectric, 350
- Transfer factor, 442
- Transfer function, 311
  - modulation, 328
  - optical, 328
  - phase, 328
- Transient charged-particle equilibrium, 429
- Transition
  - Coster-Kronig, 411
  - nonradiation, 410
  - radiationless, 410
  - radiative, 410
- Transmission at a boundary, 347
- Transmission coefficient, 347, 355
- Transmittance, 441
- Transport
  - countercurrent, 121
  - solute, 119, 122
  - volume, 122
- Transvenous pacing, 194
- Transverse relaxation time
  - recoverable and non-recoverable, 524
- Transverse wave, 346
- Traveling wave, 345
- Trayanova, N., 184, 191, 202
- Tree, 27
- Trehan, P. N., 435
- Trigonometric integrals, 555
- Triplet production, 407
- Tripp, J. H., 224
- Trochanter, greater, 7
- Trontelj, Z., 212, 225
- Trowbridge, E. A., 23, 29
- TTX, 238
- Tucker, R. D., 245, 254
- Tukey, J. W., 295, 323
- Tumor eradication, 463
- Tuna, 217, 222
- Tung, C. J., 423, 435
- Tung, L., 196, 202
- Turbidity, 367
- Turbulence, 22
- Turnbull, G., 225
- Turner, J. S., 284
- Turner, R., 533, 542
- Tympanic chamber, 349
- Uderzo, C., 398
- Uehara, M., 227, 254
- Ugurbil, K., 534–536, 542
- Ultracentrifuge, 75
- Ultrafiltration, 119
- Ultrasound
  - diagnostic, 350
  - intravascular, 376
- Ultraviolet spectrum, 377
- Ungar, I. J., 200, 202
- Units of “power” and “energy”, 309
- Upton, A. C., 471, 480
- $^{235}\text{U}$ , 497, 512
- $^{238}\text{U}$ , 505
- Urea, 116
- Urie, M., 467, 479
- Urruchi, W. I., 254
- UVA, 377, 380, 381
- UVB, 377, 380, 381
- UVC, 377, 381
- van de Kaa, C. H., 542
- van der Gon, J. J. D., 202
- van der Pol oscillator, 316
- van Eijk, C. W. E., 444, 480
- van Ginnekin, A. C. G., 175
- van Hulsteyn, D. B., 214, 224
- Van Langenhove, G., 399
- van Leeuwen, P., 225
- van't Hoff's law, 115, 118
- Vapor pressure, 75, 78
- Variable rate of growth or decay, 35
- Variables
  - extensive, 64
  - electric charge, 64
  - Length, 64
  - Surface area, 64
  - volume, 64
- Variance, 562
- Vascular resistance, 20
- Vasodilation, 116
- Vector, 3, 545
  - addition, 545
  - components, 546
  - unit, 546
- Vector operators
  - in different coordinate systems, 578
- Vector product, 5
- Veigele, W. J., 434
- Veldhuyzen van Zanten, S. J. O., 225
- Velocity
  - average, 546

- instantaneous, 547
- root-mean-square, 85
- Velocity gradient, 15
- Vena cava, 20
- Ventilation rate, 256
- Ventricular fibrillation, 195, 275, 276, 282
- Ventricular tachycardia, 186, 195, 275
- Venules, 20
- Vergence, 389
- Verheye, S., 376, 399
- Vestibular chamber, 349
- Vetterling, W. T., 109, 202, 225, 323, 341
- Villars, F. M. H., 10, 29, 90, 91, 100, 108
- Virtual cathode, 194
  - “dog-bone”, 196
- Virtual image, 396
- Virus, 2
- Viscoelasticity, 13
- Viscosity, 13, 15, 87
  - of water, 90
- Viscous torque on a rotating sphere, 248
- Vision
  - scotopic, 454
- Visscher, P. B., 295, 323
- Visual cortex, 534, 536
- Visual evoked response, 308
- Vitamin D, 381
- Vitreous, 388
- Vlaardingerbroek, M. T., 527, 533, 542
- Vogel, S. V., 15, 20, 29
- Vollrath, F., 25, 29
- Volt, 142
- Voltage difference, 141
- Voltage divider, 147
- Voltage source
  - ideal, 313
- Voltage-sensitive dye, 196
- Volume transport, 122
  - pore model, 127
  - through a membrane, 117
- Von der Lage, F. C., 485, 487–489, 513
- Voorhees, C. R., 193, 202
- Voorhees, W. D., 202
- Voroshilovsky, O., 283
  
- Wachtel, E., 133
- Wagner, H. N., 443, 500, 513
- Wagner, J., 105, 109
- Wagner, R. F., 451, 452, 478, 480
- Walcott, C. J., 217, 225
- Walker, G. C., 398
- Walker, M. M., 217, 225
- Walker, W. B., 477
- Wang, D., 96, 109
- Wang, L., 398
- Wang, M. D., 108
- Warburg equation, 106
  
- Warmuth, I., 398
- Warner, G. G., 495, 496, 513
- Warwick, W., 566
- Washout (in MRI), 535
- Watanabe, A., 182, 202, 209
- Water
  - acoustic impedance, 346
  - compressibility, 345
  - density, 345
  - dielectric constant, 144
  - speed of sound, 345
  - transmission vs. wavelength, 387
- Water molecule
  - dipole moment, 233
- Watson, E. E., 488, 490, 491, 495, 498, 505, 513
- Watson, S. B., 513
- Watt, 11
- Wave
  - longitudinal, 344
  - plane, 344
  - standing, 345
  - traveling, 345
- Wave equation, 173, 343, 344
- Wave number, 345
- Weaver, J. C., 244, 247, 252–254, 317, 323
- Weaver, K. E., 480
- Weaver, W., 50, 79
- Weaver, W. D., 72
- Web site for this book, xvi
- Webb, S., 465, 480
- Webb, W. W., 243, 253
- Weber, D. A., 489, 498, 513
- Webster, J., 369, 398, 399
- Webster, J. G., 170, 176
- Weighting factor
  - radiation, 468
- Weinberg, H., 225
- Weinstein, P. R., 542
- Weinstock, H., 225
- Weiss, G., 193
- Weiss, J. N., 276, 283
- Weiss-Fogh, T., 107, 109
- Weissleder, R., 542
- Welder’s flash, 381
- Weller, P., 381, 399
- Wendland, M. F., 542
- Wessels, B. W., 504, 505, 512, 513
- West, G. B., 41, 42, 47, 79
- Westfall, R. J., 513
- Whinnery, J. R., 175
- White noise, 314
- White, C. R., 41, 47
- White, R. J., 116, 133
- White-blood-cell count, 275
- Wick, G. L., 26, 29
- Wieben, O., 369, 399
- Wiener spectrum, 452

- Wiener theorem for random signals, 309  
Wiesenfeld, K., 317, 323  
Wikelski, M., 217, 224  
Wikswow, J. P., 195, 202, 208, 209, 211, 212, 217, 218, 221, 223–226  
Wilders, R., 158, 165, 175  
Wiley, J. D., 170, 176  
Williams, C. R., 475  
Williams, C. S., 328, 341  
Williams, M., 7, 29  
Williamson, S. J., 212, 226  
Wilson, B. C., 368, 399  
Winfrey, A. T., 267, 268, 275, 276, 282, 284  
Winsor, R., 446, 480  
Witkowski, F. X., 276, 284  
Wolfe, R. S., 217, 224  
Woodford, B. J., 254  
Woods, C., 225  
Woods, M. C., 221  
Woods, R. P., 513  
Woodruff, W. H., 47  
Woosley, J. K., 208, 223, 225, 226  
Work, 10, 54  
    concentration, 63  
    pressure-volume, 19, 21  
Working level, 505  
    month, 505  
Worthington, C. R., 164, 176  
Wortman, R. J., 398  
  
X radiation, 360  
X-ray absorption edge, 404  
X-ray spectrum  
    bremsstrahlung, 437  
    characteristic, 437, 438  
    thick target, 439  
    thin target, 438  
X-ray tube, 446  
  
Xenon, 477  
 $^{133}\text{Xe}$ , 502, 508  
Xia, Y., 539, 542  
Xylem, 27  
  
Yaar, M., 398  
Yamashita, Y., 369, 399  
Yasuno, Y., 371, 399  
Yatagai, T., 399  
Yazdanfar, S., 370, 371, 399  
Yield  
    fluorescence, 411  
Yodh, A., 367, 369, 398, 399  
Yonas, H., 479  
Yonemoto, L. T., 479  
Young's modulus, 12, 344  
Young, A. C., 278  
Young, A. R., 378, 398  
Young, T., 359  
  
Zacchello, G., 398  
Zalewski, E. F., 383, 387, 399  
ZanESCO, L., 398  
Zanzonico, P. B., 500  
Zaremba, L. A., 542  
Zaret, B. L., 225  
Zecca, M., 398  
Zhang, X-C., 372, 399  
Zhang, X-L., 542  
Zhang, Y., 398  
Zhou, X-H., 532, 533, 542  
Zhu, X-H., 542  
Ziegler, J. F., 415, 418–423, 435  
Zininger, M. D., 542  
Zinonev, N. N., 398  
Zipes, D. P., 194, 195, 201, 202, 212, 225, 283, 284  
Zorec, R., 225  
Zumoff, B., 35, 36, 47  
Zwanzig, R., 96, 109